Lawrence Berkeley National Laboratory
LBL Publications

Title
Cool - Color Roofing Material PIER Final Project Report

Permalink
https://escholarship.org/uc/item/9484d9wr

Authors
Hashem, Akbari
Berdahl, Paul
Wiel, Steve
et al.

Publication Date
2006-08-01

Peer reviewed

eScholarship.org Powered by the California Digital Library
University of California

Arnold Schwarzenegger
Governor

COOL-COLOR ROOFING MATERIAL

PIER FINAL PROJECT REPORT

Prepared For:
California Energy Commission
Public Interest Energy Research Program

Prepared By:
Lawrence Berkeley National Laboratory
and Oak Ridge National Laboratory

ERNEST ORLANDO LAWRENCE
BERKELEY NATIONAL LABORATORY

August 2006
CEC-500-2006-067

Prepared By:
Lawrence Berkeley National Laboratory
Hashem Akbari
Berkeley, California
Contract No. 500-01-021

Oak Ridge National Laboratory
William Miller
Oak Ridge, Tennessee

Prepared For:
California Energy Commission
Public Interest Energy Research (PIER) Program

Chris Scruton
Contract Manager

Ann Peterson
Building End-Use Energy Efficiency Team Leader

Nancy Jenkins
PIER Energy Efficiency Research Office Manager

Martha Krebs, Ph.D.
Deputy Director
ENERGY RESEARCH AND DEVELOPMENT DIVISION

B. B. Blevins
Executive Director

DISCLAIMER

This report was prepared as the result of work sponsored by the California Energy Commission. It does not necessarily represent the views of the Energy Commission, its employees or the State of California. The Energy Commission, the State of California, its employees, contractors and subcontractors make no warrant, express or implied, and assume no legal liability for the information in this report; nor does any party represent that the uses of this information will not infringe upon privately owned rights. This report has not been approved or disapproved by the California Energy Commission nor has the California Energy Commission passed upon the accuracy or adequacy of the information in this report.

Disclaimer

This document was prepared as an account of work sponsored by the United States Government. While this document is believed to contain correct information, neither the United States Government nor any agency thereof, nor The Regents of the University of California, nor any of their employees, makes any warranty, express or implied, or assumes any legal responsibility for the accuracy, completeness, or usefulness of any information, apparatus, product, or process disclosed, or represents that its use would not infringe privately owned rights. Reference herein to any specific commercial product, process, or service by its trade name, trademark, manufacturer, or otherwise, does not necessarily constitute or imply its endorsement, recommendation, or favoring by the United States Government or any agency thereof, or The Regents of the University of California. The views and opinions of authors expressed herein do not necessarily state or reflect those of the United States Government or any agency thereof or The Regents of the University of California.

Acknowledgments

This work was supported by the California Energy Commission through its Public Interest Energy Research Program (PIER), by the Laboratory Directed Research and Development (LDRD) program at Lawrence Berkeley National Laboratory (LBNL), and by the Assistant Secretary for Renewable Energy under Contract No. DE-AC02-05CH11231. The authors wish to thank CEC Commissioner Arthur Rosenfeld and PIER managers Nancy Jenkins and Chris Scruton for their support and advice. Special thanks go also to Mark Levine, Director of the Environmental Energy Technologies Division at LBNL for his encouragement and support in the initiation of this project.

This work has been collaborative research among Oak Ridge National Laboratory (ORNL), LBNL, and the industry. We acknowledge the contributions of Tony Chiovare (Custom-Bilt Metals); Lou Hahn (Elk Corporation); Ingo Joedicke (ISP Minerals); Chris Gross, Jeff Jacobs and Frank Klink (3M Company); Scott Kriner (Akzo Nobel Coatings); James Dunn and Kenneth Loye (Ferro); David Mirth (Owens Corning); Jeffrey Nixon (Shepherd Color Company); Joe Reilly (American Rooftile Coatings); Robert Scichili (initially BASF Industrial Coatings; currently a consultant to the coated metal industry); Ming L. Shiao (CertainTeed); Krishna Srinivas (GAF); Yoshihiro Suzuki (MCA Clay Tile); Jerry Vandewater (Monier Lifetile); Michelle Vondran (Steelscape); and Lou Zumpano (Hanson Roof Tile).

We also acknowledge the guidance, support, and directives of the Project Advisory Committee (PAC) members: Gregg Ander (Southern California Edison Company); Aaron Becker (Dupont Titanium Technologies); Carl Blumstein (California Institute for Energy and Environment);Tom Bollnow (National Roofing Contractors Association); Jack Colbourn and Kathy Diehl (US Environmental Protection Agency, San Francisco office); Steven Harris (Quality Auditing Institute); Noah Horowitz (Cool Roof Rating Council and National Resource Defense Council); Scott Kriner (Cool Metal Roofing Coalition); Shari Litow (DuPont Titanium Technologies); Archie Mulligan (Habitat for Humanity); Mike Evans (Evans Construction); Jerry Wager (Ochoa & Shehan); Rick Olson (Roof Tile Institute); Mike Rothenberg (Bay Area Air Quality Management District); Steven Ryan (US EPA); Thomas Shallow (Asphalt Roofing Manufacturers Association); Peter Turnbull (Pacific Gas and Electric Company; and Jessica C Yen (DuPont Titanium Technologies).

Please cite this report as follows:

Hashem Akbari, Paul Berdahl, Ronnen Levinson, Steve Wiel, William Miller, and Andre Desjarlais 2006. *Cool-Color Roofing Material.* California Energy Commission, PIER Building End-Use Energy Efficiency Program. CEC-500-2006-067.

Preface

The Public Interest Energy Research (PIER) Program supports public interest energy research and development that will help improve the quality of life in California by bringing environmentally safe, affordable, and reliable energy services and products to the marketplace.

The PIER Program, managed by the California Energy Commission (Energy Commission) conducts public interest research, development, and demonstration (RD&D) projects to benefit the electricity and natural gas ratepayers in California. The Energy Commission awards up to $62 million annually in electricity-related RD&D, and up to $15 million annually for natural gas RD&D.

The PIER program strives to conduct the most promising public interest energy research by partnering with RD&D organizations, including individuals, businesses, utilities, and public or private research institutions.

PIER funding efforts are focused on the following RD&D program areas:

- Buildings End-Use Energy Efficiency
- Industrial/Agricultural/Water End-Use Energy Efficiency
- Renewable Energy Technologies
- Environmentally Preferred Advanced Generation
- Energy-Related Environmental Research
- Energy Systems Integration

Cool-color Roofing Material is the final report for the Cool Roofs project, contract number 500-02-021, conducted by Lawrence Berkeley National Laboratory and Oak Ridge National Laboratory. The information from this project contributes to PIER's Buildings End-Use Energy Efficiency program.

For more information on the PIER Program, please visit the Energy Commission's website at www.energy.ca.gov/pier or contact the Energy Commission at (916) 654-5164.

Table of Contents

Preface iii
Abstract vi
Executive Summary 1
1.0 Introduction 6
1.1. Background 6
1.2. Project Objectives 8
1.3. Report Organization 10
2.0 Technical Tasks 11
2.1. Task 2.4: Development of Cool-Colored Coatings 11
2.2. Task 2.5: Development of Prototype Cool-Colored Roofing Materials 21
2.3. Task 2.6: Field-Testing and Product Useful Life Testing 33
2.4. Task 2.7: Technology Transfer and Market Plan 41
3.0 Conclusions and Recommendations 48
3.1. Recommendations 49
4.0 References 51
5.0 List of Attachments 52

List of Figures

Figure 1. (a) Spectral solar power distribution and (b) solar spectral reflectances of cool and standard brown surfaces 6

Figure 2. Value of potential annual residential energy savings from cool roofs in 11 U.S. metropolitan areas 8

Figure 3. Illustration of the team's pigment characterization activities 13

Figure 4. Pinwheel™ screen shot 15

Figure 5. Solar spectral reflectance of a Pinwheel™-formulated cool coating 16

Figure 6. Description of an iron oxide red pigment in the LBNL pigment database 18

Figure 7. First index page of the LBNL pigment database, ... 19

Figure 8. Application of the two-layer technique to manufacture cool-colored materials 22

Figure 9. Development of "super-white" shingles 23

Figure 10. White roofs and walls are used in Bermuda and Santorini, Greece 23

Figure11. Development of a cool black shingle by industrial partner ISP Minerals 24

Figure 12. Examples of standard and prototype cool shingles; R is solar reflectance 25

Figure 13. Application of cool-colored roofing shingles on two houses advertised by Elk Corp.25

Figure14. Palette of color-matched cool (top row) and conventional (bottom row) roof tile coatings developed by industrial partner American Rooftile Coatings....26

Figure 15. Simulated roofing products made from metal....29

Figure 16. Some of the cool-colored coatings for metal roofing products available from BASF Industrial Coatings)....30

Figure 17. (a) Solar reflectance (b) and total color change of asphalt shingles exposed to accelerated direct fluorescent UV radiation....32

Figure 18. Daily air-conditioning energy consumption and savings, measured during the daylight hours from June through September 2005....34

Figure 19. Solar reflectance of light-gray concrete tile coupons (19a) and painted metal coupons (19b) exposed to climatic soiling at each of the seven CA weathering sites....36

Figure 20. Integrated heat flow measured through the roof deck (heat loss to the sky during the day and during the night) and the attic floor....38

Figure 21. Oxidation (carbonyl) profiles measured during accelerated UV aging of polypropylene....40

Figure 22. Spectral reflectance of new and weathered western red cedar roofing shingles. The solar reflectance is 0.46 when new and declines to 0.21 after 6 years exposure....40

List of Tables

Table ES1. A comparison of the attributes of cool-colored and standard roofing products* 5

Table 1. Projected residential roofing market in the U.S. western region surveyed by Western Roofing (2002)....7

Table 2. Pigment properties tabulated in the LBNL pigment database....20

Table 3. Sample cool-colored clay tiles and their solar reflectances....27

Table 4: Cool Team articles published or presented in industry magazines, conferences, and journals....41

Table 5. Industry needs to successfully market their cool roof products....44

Table 6. Estimates of annual cooling electricity savings (kWh) and heating energy penalties (therms) from installing cool-colored roofs on pre-1980 single-family detached homes....46

Table 7. Estimates of annual cooling electricity savings (kWh) and heating energy penalties (therms) from installing cool-colored roofs on post-1980 single-family detached homes....47

Abstract

Solar reflective, thermally emissive (cool) roofs decrease demand for building air conditioning power, lower the ambient air temperature, and, by promoting lower ambient air temperatures, retard the formation of smog. For example, raising the solar reflectance of a roof from 0.10 (typical of a conventional dark roof) to 0.35 (typical of a cool dark roof) can reduce building cooling energy use by more than 10 percent. In 2002, suitable cool *white* materials were available for most products, with the notable exception of asphalt shingles, the most widely used roofing material. However, cooler *colored* (nonwhite) materials were needed for all types of roofing, especially in the residential market. The California Energy Commission engaged Lawrence Berkeley National Laboratory and Oak Ridge National Laboratory to work with the roofing industry to develop cool-colored roofing products, with the goal of bringing to market within three to five years roofs that meet the ENERGY STAR qualifying solar reflectance of 0.25. This project led to the development of prototype colored asphalt shingles with solar reflectances of up to 0.35. One manufacturer currently markets colored asphalt shingles with solar reflectance of 0.25. Colored metal, clay tile, and concrete tile roofing materials with solar reflectances of 0.30 to 0.60 are currently sold in California.

Keywords: cool roof, reflectance, building energy, cool-color, energy efficiency, albedo, roofing material manufacture, pigment

Executive Summary

Introduction

Coatings colored with conventional pigments tend to absorb the invisible near-infrared (NIR) radiation that bears more than half of the power in sunlight. Replacing conventional pigments with "cool" pigments that absorb less NIR radiation can yield roofing coatings similar in color to those used in conventional roofs with higher solar reflectance. These cool coatings lower roof surface temperature, which in turn reduces the need for cooling energy in conditioned buildings and makes unconditioned buildings more comfortable. For example, raising the solar reflectance of a residential roof from 0.10 (the typical reflectance of a conventional dark color, to 0.35 (the reflectance of cool dark color) can decrease building cooling-energy use by 7 percent to 15 percent.

In 2002, suitable cool *white* materials were available for most roofing products, with the notable exception of asphalt shingles[1]. To respond to the consumer preference for colored roofs, cool *nonwhite* materials are needed for all types of roofing—and especially for asphalt shingles, which account for about 54 percent of the total residential roof market in the western United States.

Purpose

The California Energy Commission engaged Lawrence Berkeley National Laboratory (LBNL) and Oak Ridge National Laboratory (ORNL)—hereafter called the Cool Team—to work with the roofing industry to develop cool-colored roofing products, with the goal of bringing cool roofing products that meet the ENERGY STAR qualifying solar reflectance of 0.25 to market with within three to five years.

Project Objectives

- Characterize the optical properties of common and innovative pigments
- Develop a software tool to maximize the solar reflectance of color-specified roofing material
- Work with roofing manufacturers to design innovative cool roofing material production methods
- Measure the energy savings of the cool roofs on demonstration houses and test the performance of conventional and cool roofing systems at ORNL's steep-slope assembly testing facility
- Characterize the effects of weathering and aging on the cool roofs
- Estimate the energy and demand savings of the new cool roof materials
- Help bring cool roofing products to market within three to five years

Project Outcomes

---

1 Shingles marketed as "white" are gray in color with a typical solar reflectance of about 0.25.

Pigment characterization and manufacturing partnership

The Cool Team developed complex inorganic dark colored pigments that are highly reflective in the near-infrared portion of the solar spectrum. The team also created a software tool for designing high-reflectance coatings that match the colors of conventional colored roofing products. The team then worked with a consortium of 16 industry partners—representing most of the major and several minor U.S. roofing manufacturers—to develop novel manufacturing methods, which industry partners then used to manufacture cool roof prototypes and products.

To date and as the direct result of this collaborative effort, manufacturers of roofing materials have introduced cool shingles, cool concrete tile coatings, and cool concrete tiles and have significantly expanded the production of cool clay tiles and cool metal roofs. The manufacturing partners of the two national labs have raised the solar reflectance of commercially available concrete tile, clay tile, and metal roofing products to 0.30–0.45 (up from 0.05–0.25) by reformulating their pigmented coatings.

Test results

Tests of roofs at residential sites that compared the energy performance of cool and conventional roofs yielded these findings:

- The attic air temperature beneath a cool chocolate brown concrete tile roof (solar reflectance 0.41) was 3 to 5 K (5.4 to 9°F) cooler than that below a the same color and type conventional roof (solar reflectance 0.10)
- The attic air temperature beneath the cool brown metal shake roof (solar reflectance 0.31) was 5 to 7 K (9 to 12.6°F) cooler than a similar color and type conventional roof (solar reflectance 0.08).

Material testing showed that long-term change in the solar reflectance of cool roofs—which could compromise the benefits—appears to be driven by particulate matter that sticks to the roofs and resists being washed off by wind or rain.

Steep-slope assembly testing at ORNL suggests that sub-tile venting is just as important as the increase in solar reflectance in reducing the heat flow into the conditioned space of a house. Further, these tests revealed that sub-time venting reduces the small winter heating loss associated with cool-color roofs.

Finally, the accelerated and product useful life testing were promising, showing that novel cool pigmented concrete, clay, painted metal, and asphalt shingle roofs maintain their solar reflectance as well as do their standard production counterparts.

Technology transfer

The Cool Team, in conjunction with respective industry partners, presented research results at appropriate trade shows, and published their results in each industry's appropriate trade magazines. More than 20 journal articles have been published by the Cool Team over the course of the project.

In collaboration with the roofing industry partners, the Cool Team prepared a market plan outlining industry/national lab collaborative efforts that would help the Energy Commission

deploy cool-colored roofing. The plan focuses on six parallel initiatives: regulate; increase product selection; label; educate; provide incentives; and demonstrate performance.

Cool Team estimates of energy and peak demand savings showed that increasing roof solar reflectance from a conventional dark roof of 0.10 to a cool-colored roof of 0.30 yields net savings in the range of 100–600 kWh per 100 m^2 per year. These data can be used to prepare a protocol for updating the state's Title 24 building energy code to include cool-colored roofing materials.

Conclusions

By enlisting the partnership of most of the major roofing manufacturers in the United States, the Cool Team exceeded the initial goal of creating dark asphalt shingles with solar reflectances of at least 0.25 and other nonwhite roofing products—including tiles and painted metals—with solar reflectances not less than 0.35.

Many of the products resulting from this work are already in the marketplace. For example, BASF industrial Coatings has launched a line of cool-colored siliconized-polyester coating, MCA Clay Tile is selling 11 products with solar reluctances about 0.25, and Elk Corporation has introduced its Prestique Cool-color Series, a line of light-gray and light-brown asphalt shingle with solar reflectances at or above 0.25. The Cool Team therefore met its commercialization goal of helping to bring products to market in three to five years.

Recommendations

Near the end of the project, the Cool Team's 16 industrial partners discussed their needs to further develop and successfully market their residential cool roofing products. Their recommendations, summarized below, were used to develop a deployment proposal.

- First and foremost, residential cool roofs need to be credited and recommended in the state's Title 24 standards that primarily determine what products are used in the construction of new houses and in major remodels.
- More cool materials for all residential (and commercial) sloped roofing systems must be available and appropriately labeled.
- The cool roofing pigment database should be maintained and expanded with new materials to assist the industry in developing new and advanced materials at competitive prices.
- The aging and weathering of cool roofing materials and their effects on the useful life of roofs need to be further studied.
- Appropriate labels on roofing products must be universally applied.
- Architects, designers, builders, roofing material distributors and retailers, and consumers need to learn of the availability and benefits of using cool roofing materials.
- California's utilities and government can further influence the selection of cool roofs through innovative incentive and rebate programs to accelerate their market penetration.
- For utilities to develop incentive programs and for manufacturers to coordinate their materials development with their marketing efforts, they need to have an industry-consensus calculator to accurately estimate energy and peak demand of cool-colored

roofs. The calculator should account for both the cooling energy savings and potential heating energy penalties of cool roofs.

- Market penetration can be accelerated by enhancing the credibility of retailer and utility marketing claims through large-scale demonstrations of cool roofs to consumers, developer, designers, and roofing contractors.

Benefits to California

Regional climate modeling suggests that the widespread application of cool roofs can reduce urban air temperatures, decreasing cooling peak power demand and smog production. For example, on a warm afternoon in Los Angeles, each 1 K (1.8°F) decrease in the daily maximum temperature lowers peak demand for electric power by about 2 percent to 4 percent and each 1 K (1.8°F) decrease down to 21°C (70°F) reduces smog (specifically, the probability that the maximum concentration of ozone will exceed the California standard of 90 parts per billion) by 5%. A 3 K (5.4°F) reduction in the air temperature of the Los Angeles basin could reduce peak power demand by 200 MW, offer cooling energy savings worth $21 M/year, and yield a 12%reduction in ozone worth $104 M/year [Rosenfeld et al. 1998]. More than 450 U.S. counties (including some of the most heavily populated areas of California) had ozone levels that exceeded federal eight-hour standards as of 2004. Widespread adoption of cool roofs could help cities in many of these areas reduce the magnitude of their air quality problem. Table ES1 summarizes many of the benefits of cool roofing, based on findings from a single-family home.

The principal application of cool-color roofing is to provide roofing manufacturers with the tools they need to develop energy-efficient products that benefit their customers and improve the competitive advantage of these U.S roofing products in the marketplace. Cool-color roofing materials provide clear, measured advantages and dollar savings compared to conventional roofing materials at a small cost premium that is paid back within a few years through reduced energy bills.

Table ES1. A comparison of the attributes of cool-colored and standard roofing products*

Feature	Glazed clay tile roofing	Polymer–coated concrete tile roofing	Polymer–coated metal roofing	Asphalt shingle roofing with ceramic–coated granules
Example of conventional roofing product (manufacturer/model/color name)	MCA Clay Tile/Corona Tapered Mission/Burnt Sienna	American Rooftile Coatings/Warm Earthtone Rooftile Coating /Onyx	Custom–Bilt Metals/Titan Select Vail Shingle/ Musket Brown	Elk/Prestique Plus High Definition/ Weatherwood
Example of cool roofing product (manufacturer/model/color)	MCA Clay Tile/Corona Tapered Mission/ Tobacco	American Rooftile Coatings/Cooltile IR Coating™/IR Onyx topcoat over plaster white basecoat	Custom–Bilt Metals/Titan Cool Roof Vail Shingle /Musket Brown	Elk/Prestique Cool-color Series/Cool Weatherwood
Solar reflectance of conventional roofing product sample	0.18	0.04	0.08	0.09
Solar reflectance of cool roofing product sample	0.37	0.38	0.27	0.25
Solar reflectance increase (cool product reflectance–conventional product reflectance) for dark colors (range reflects difference in reflectance for different colors)**	0.18–0.25	0.18–0.34	0.17–0.25	0.10–0.16
Reduction in peak surface temperature on a summer afternoon of the cool roof (K)	10–12	10–17	10–12	7–9
Peak power demand savings of the cool roof (W)	300–400	300–400	400–600	300–350
Annual cooling energy savings of the cool roof (kWh)	150–400	150–400	250–650	190–490
Annual cooling energy savings at $0.15/kWh of the cool roof ($)	22–60	22–60	37–97	28–73
Annual heating energy penalty of the cool roof (therms)	1–4	1–4	2–8	1–5
Annual heating energy penalty at $1.5/therm of the cool roof ($)	2–6	2–6	3–12	2–7
Net savings provided by the cool roof ($)	20 –54	20–54	35–85	26–66
Cost premium of the cool roof compared with conventional roof ($)†	nil	100–500	nil	500
15–year net present value of net energy savings at 3% discount ($)	240–650	240–650	420–1020	310–790
Simple payback time of the cool roof (years)	0	2–10	0	8–19

* Only the solar reflectances of the cool and conventional products are compared; all other rows enumerate the energy, power, or money saved by the cool roof as compared to a conventional roof on a single-story electrically heated and cooled 200 m^2 (2,150 ft^2) home built after 1980 in Sacramento, CA.

**A dark-colored surface is defined as one that reflects no more than 20% of visible sunlight. Smooth, flat surfaces reflect about 5% of visible sunlight when black; about 10% when dark brown; and about 10–20% when dark red, dark green, or dark blue.

† The cost premium of cool roofs is a matter of industry debate. Specifically, the industry lacks consensus on whether replacing conventional pigments with cool pigments in an existing manufacturing process would introduce a significant cost premium.

1.0 Introduction

1.1. Background

The world is facing disruptive global climate change from greenhouse gas emissions and increasingly expensive and scarce energy supplies. Energy efficiency reduces those emissions and mitigates the rising cost of energy. Cool-color roofing—a new technology that uses solar-reflective pigments to reduce a home's energy and peak demand—promises a significant leap in energy efficiency.

Coatings colored with conventional pigments tend to absorb the invisible near-infrared (NIR) radiation that bears more than half of the power in sunlight. Replacing conventional pigments with "cool" pigments that absorb less NIR radiation can yield colored coatings similar in color to conventional roofing materials, but with higher solar reflectance (see Figure 1). These cool coatings lower roof surface temperature, which in turn reduces the need for cooling energy in conditioned buildings and makes unconditioned buildings more comfortable.

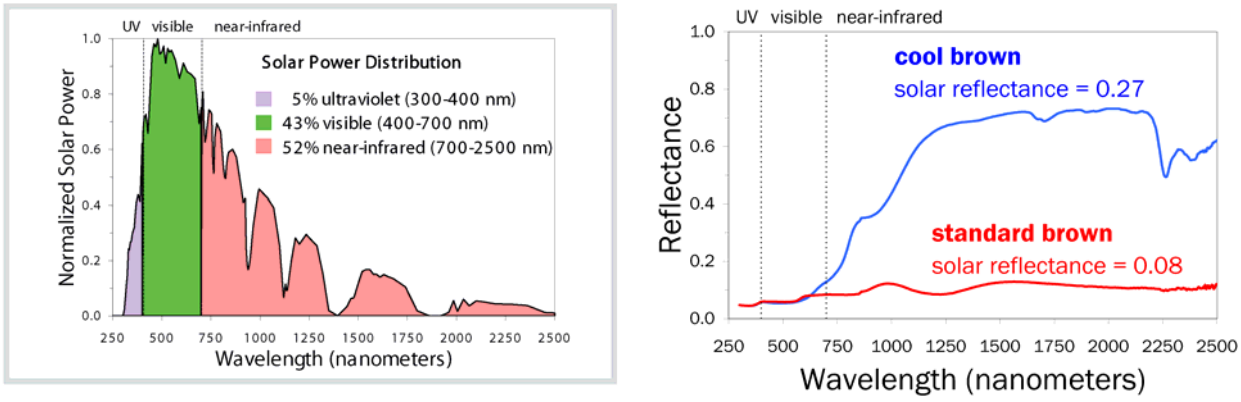

(a) (b)

Figure 1. (a) Spectral solar power distribution and (b) solar spectral reflectances of cool and standard brown surfaces

1.1.1. Potential energy and indirect benefits of cool roofs

Field studies in California and Florida have demonstrated cooling energy savings in excess of 20% upon raising the solar reflectance of a roof from the 10–0.20 reflectances typical of conventional roofs to 0.60 (Konopacki and Akbari, 2001; Konopacki et al. 1998; Parker et al. 2002). Energy savings are particularly pronounced in older houses that have little or no attic insulation, especially if the attic contains the air distribution ducts. At 8¢/kWh, the value of potential U.S. net commercial and residential energy savings (cooling savings minus heating penalties) exceeds $750 million per year (Akbari et al. 1999). Cool roofs also significantly reduce peak electric demand in summer (Akbari et al. 1997; Levinson et al. 2005a).

Further, the widespread installation of cool roofs can lower the ambient air temperature in a neighborhood or city, decreasing the need for air conditioning, retarding smog formation, and improving environmental comfort. These "indirect" benefits of reduced ambient air temperatures have roughly the same economic value as the direct energy savings (Rosenfeld et

al. 1998). Lower surface temperatures may also increase the lifetime of roofing products particularly asphalt shingles), reducing replacement and disposal costs.

1.1.2. The size and value of the western U.S. roofing market

According to *Western Roofing Insulation and Siding* magazine (2002), the total value of the 2002 projected residential roofing market in 14 western U.S. states (AK, AZ, CA, CO, HI, ID, MT, NV, NM, OR, TX, UT, WA, and WY) was about $3.6 billion (B). The research team estimated that 40% ($1.4B) of that amount was spent in California. The lion's share of residential roofing expenditure was for fiberglass asphalt shingle (hereafter, simply "shingle"), which accounted for $1.7B, or 47% of sales. Concrete and clay roof tiles made up $0.95B (27%), while wood, metal, and slate roofing collectively represented another $0.55B (15%). The value of all other roofing projects was about $0.41B (11%). The team estimates that the roofing market area distribution was 54–58% fiberglass shingle, 8–10% concrete tile, 8–10% clay tile, 7% metal, 3% wood shake, and 3% slate (see Table 1).

Table 1. Projected residential roofing market in the U.S. western region surveyed by Western Roofing (2002). The Western region includes AK, AZ, CA, CO, HI, ID, MT, NV, NM, OR, TX, UT, WA, and WY.

Roofing Type	Market share by $		Estimated market share by roofing area
	$B	%	%
Fiberglass Shingle	1.70	47.2	53.6-57.5
Concrete Tile	0.50	13.8	8.4-10.4
Clay Tile	0.45	12.6	7.7-9.5
Metal/Architectural	0.21	5.9	6.7-7.2
Wood Shingle/Shake	0.17	4.7	2.9-3.6
Slate	0.17	4.7	2.9-3.6
Other	0.13	3.6	4.1-4.4
SBC Modified	0.08	2.1	2.4-2.6
APP Modified	0.07	1.9	2.2-2.3
Metal/Structural	0.07	1.9	2.2-2.3
Cementitious	0.04	1.1	1.2-1.3
Organic Shingles	0.02	0.5	0.6
Total	**3.60**	**100**	**100**

The research team estimated that applying cool-colored roofs to houses could achieve a net energy savings in the U.S. worth over $400 million per year (Konopacki et al. 1997). The

estimated savings in California (in 2005 $) is about $100 million per year. Figure 2 shows potential savings of cool-colored residential roofing materials in 11 U.S. metropolitan areas.

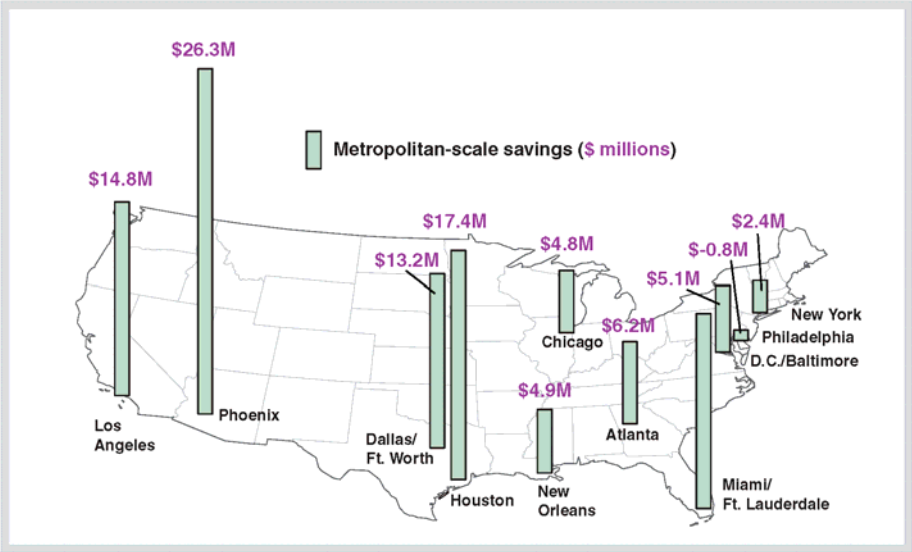

Figure 2. Value of potential annual residential energy savings from cool roofs in 11 U.S. metropolitan areas

1.1.3. The need for cool-color roofing

In 2002, suitable cool *white* materials were available for most roofing products, with the notable exception of asphalt shingles[2]. However, white residential roofing products sell poorly in California, where homeowners prefer the aesthetics of dark-colored roofs. To respond to this market preference, cool nonwhite materials are needed for all types of roofing. Cool color roofing technology makes solar-reflective roofing available in any color (dark or light) by selectively reflecting the invisible component of sunlight in the NIR spectrum.

On a summer day, the peak daily surface temperature of a cool dark roof of solar reflectance 0.35 is about 14 K (25°F) lower than that of a conventional dark roof of solar reflectance 0.10. The cool dark roof conducts about 20–40% less heat into a home's conditioned space than does a conventional dark roof, reducing the home's demand for cooling power by about 7–15% in the late afternoon. During these afternoon hours, demand for air conditioning strains the electrical grid and requires utilities to produce additional power using less efficient, more expensive, and more polluting "peak" generators.

1.2. Project Objectives

In May 2002, the California Energy Commission (Energy Commission) sponsored a research project to develop cool nonwhite roofing products that could revolutionize the residential roofing industry. This project—which brought together Lawrence Berkeley National Laboratory (LBNL) and Oak Ridge National Laboratory (ORNL)—aimed to develop complex inorganic color pigments that are dark in color but highly reflective in the NIR portion of the solar

2 Shingles marketed as "white" are gray in color with a typical solar reflectance of about 0.25.

spectrum. The high NIR reflectance of coatings formulated with these and other cool pigments—e.g., chromium oxide green, cobalt blue, phthalocyanine blue, Hansa yellow—can be exploited to manufacture roofing materials that reflect more sunlight than conventionally pigmented roofing products.

The cool-color program at LBNL has three elements:

- Measuring the rates at which many common pigmented coatings absorb (convert to heat) and backscatter (reflect) light at wavelengths in the ultraviolet (UV), visible, and NIR spectra
- Using these rates to develop a software tool for the design of color-matched coatings with high solar reflectance
- Working with the roofing industry to develop novel manufacturing methods and encourage the manufacture of cool roof prototypes and products

ORNL was charged with demonstrating the new material to measure both the residential energy savings achieved by use of cool-colored roofing and the extent to which exposure changes the appearance and performance of cool-colored roofing. ORNL also tested several cool roofing products at their facilities at Oak Ridge. In this report, this national labs partnership is referred to as the "Cool Team."

To complete the project goals, the cool team developed a strong relationship with industry, forming a consortium that included most of the major roofing manufacturers, as well as many smaller manufacturers:

- 3M Company (St. Paul, MN);
- Akzo Nobel (Columbus, OH);
- American Rooftile Coatings (Fullerton, CA);
- BASF Industrial Coatings (Southfield, MI);
- CertainTeed Corporation (Valley Forge, PA);
- Custom-Bilt Metals (Chino, CA);
- Elk Corporation (Ennis, TX);
- Ferro Corporation (Cleveland, OH);
- GAF Materials (Wayne, NJ);
- Hanson Roof Tile (Fontana, CA);
- ISP Minerals (Hagerstown, MD);
- MCA Clay Tile (Corona, CA);
- Monier Lifetile (Thousand Oaks, CA);
- Owens Corning (Granville, OH);
- Shepherd Color Company (Cincinnati, OH); and
- Steelscape Inc. (Kalama, WA).

These partners were needed to help develop new manufacturing processes, develop and eventually commercialize new products, and help develop a commercialization plan.

1.3. Report Organization

This report will summarize the Cool Team activities within each of the project tasks, listed below:

Task 2.4:	**Development of Cool-colored Coatings**
Task 2.4.1	Identify and Characterize Pigments with High Solar Reflectance
Task 2.4.2	Develop a Computer Program for Optimal Design of Cool Coatings
Task 2.4.3	Develop a Database of Cool-Colored Pigments
Task 2.5	**Development of Prototype Cool Colored Roofing Materials**
Task 2.5.1	Review of Roofing Materials Manufacturing Methods
Task 2.5.2	Design Innovative Methods for Application of Cool Coatings to Roofing Materials
Task 2.5.3	Accelerated Weathering Testing
Task 2.6	**Field-Testing and Product Useful Life Testing**
Task 2.6.1	Building Energy-Use Measurements at California Demonstration Sites
Task 2.6.2	Materials Testing at Weathering Farms in California
Task 2.6.3	Steep-slope Assembly Testing at ORNL
Task 2.6.4	Product Useful Life Testing
Task 2.7	**Technology Transfer and Market Plan**
Task 2.7.1	Technology Transfer
Task 2.7.2	Market Plan
Task 2.7.3	Title 24 Code Revisions

The report ends with a summary of conclusions, recommendations, and benefits of the work to California. Attachments to this report provide additional details on the tasks listed above.

2.0 Technical Tasks

The following is a summary of the work accomplished in each task.

2.1. Task 2.4: Development of Cool-Colored Coatings

To determine how to optimize the solar reflectance of a pigmented coating matching a particular color, and how the performance of a cool-colored roofing material compares to that of a standard material, the Cool Team

- Characterized the optical properties of over 80 single-pigment coatings
- Created a database of pigment characteristics
- Developed a computer model to maximize the solar reflectance of roofing materials for a choice of visible color

2.1.1. Task 2.4.1: Identify and characterize pigments with high solar reflectance

The project team examined pigments in widespread use, with particular emphasis on those that may be useful for formulating nonwhite materials that can reflect the near-infrared portion of sunlight, such as the complex inorganic color pigments (mixed metal oxides).

Pigment characterization begins with measuring the reflectance r and transmittance t of a thin coating (e.g., a 25-µm thick paint film) colored by single pigment, such as iron oxide red. These "spectral," or wavelength-dependent, properties of the pigmented coating are measured at 441 evenly spaced wavelengths spanning the solar spectrum (300 to 2500 nanometers). Inspection of the film's spectral absorptance (calculated as $1-r-t$) reveals whether a pigmented coating is "cool" (has low NIR absorptance) or "hot" (has high NIR absorptance).

The spectral reflectance and transmittance measurements are used to compute spectral rates of light absorption K and backscattering (reflection) S per unit depth of film. A cool-color is defined by a small absorption coefficient K in the near infrared. For cool-colors, the backscattering coefficient S is small in the visible spectral range for formulating dark colors (or large in the visible spectral land for light colors), and preferably large in the NIR. (Weak backscattering in the NIR is acceptable when a basecoat or the substrate provide high NIR reflectance.) Calculations of S and K employ a variant of the Kubelka-Munk two-flux continuum model of light propagation through a pigmented coating that Berkeley Lab has adapted to account for the reflectance of incompletely diffused light at the air-coating interface. Such "interface reflectances" can significantly alter the reflectance and transmittance of the optically thin pigmented coatings applied to roofing materials.

As a check, the Cool Team found that values of S computed from the Kubelka-Munk model for generic titanium dioxide (rutile) white pigment were in rough agreement with values computed from the Mie theory, supplemented by a simple multiple scattering model.

The optical properties of 87 single-pigment films—4 white, 21 black or brown, 14 blue or purple, 11 green, 9 red or orange, 14 yellow, and 14 pearlescent—were characterized by computing spectral Kubelka-Munk coefficients from spectral measurements of film reflectance and transmittance. Twenty-six polyvinylidene fluoride (PVDF) resin paint films were provided by a manufacturer of coil-coating paints. Another 34 acrylic paints were purchased as artist colors,

and the remaining 27 coatings were acrylic-base letdowns (dilutions) of cool (primarily metal-oxide) pigment dispersions from pigment manufacturers.

The team identified cool pigments in the white, yellow, black/brown, red/orange, blue/purple, and pearlescent color groupings with NIR thin-film absorptances less than 0.1, as well as other pigments in the black/brown, blue/purple, green, red/orange, yellow and pearlescent groupings with NIR absorptances less than 0.2. Most are NIR transmitting and require an NIR-reflecting background to form a cool coating. Over an opaque white background, some pigments in the pearlescent, white, yellow, black/brown red/orange, green, and blue/purple families offer NIR reflectances of at least 0.7, while other pigments in the blue/purple, black/brown, and green color families have NIR reflectances of at least 0.5. A few members of the white, yellow, black/brown, pearlescent, red/orange, and green color families have NIR scattering sufficiently strong to yield NIR reflectances of at least 0.3 (and up to 0.64) over a black background.

Use of pigments with NIR absorptances approaching unity (e.g., nonselective blacks) should be minimized in cool coatings, as might be the use of certain pearlescent, blue/purple, red/orange, and brown/black pigments with NIR absorptances exceeding 0.5.

Figure 3 illustrates the team's pigment characterization activities, showing (a) images over white and black backgrounds of the 87 single-pigment films; (b) coupons of a pigmented polymer film (an organic red) over white and black backgrounds; and (c) the measured and computed solar spectral reflectances of a pigmented polymer film (an inorganic cool black). The three charts show, from top to bottom, (i) measured reflectance, measured transmittance, and computed absorptance of a free film; (ii) Kubelka-Munk backscattering and absorption coefficients computed from the measured reflectance and transmittance of the free film; and (iii) the measured and computed reflectances of the film over black and white backgrounds, which are used to validate the accuracy of the backscattering and absorption coefficients computed from the free-film properties.

The team has published two milestone papers published in the academic journal *Solar Energy Materials & Solar Cells* (Attachment 1). Feedback from the journal's referees was extremely positive. To wit:

> Referee #1: "Great work with extensive detail, I have not seen such detail on pigments since work in the 1960s by the aerospace companies. It is nice to see such a seminal work in one location and with one set of testing methodologies. Please publish."
>
> Referee #2: "...Very nice work, uniform and detailed—the beginnings of a handbook. Very valuable to my industry (paint formulation). If Elsevier puts together a Materials Property Handbook, the results of this work should be in it."

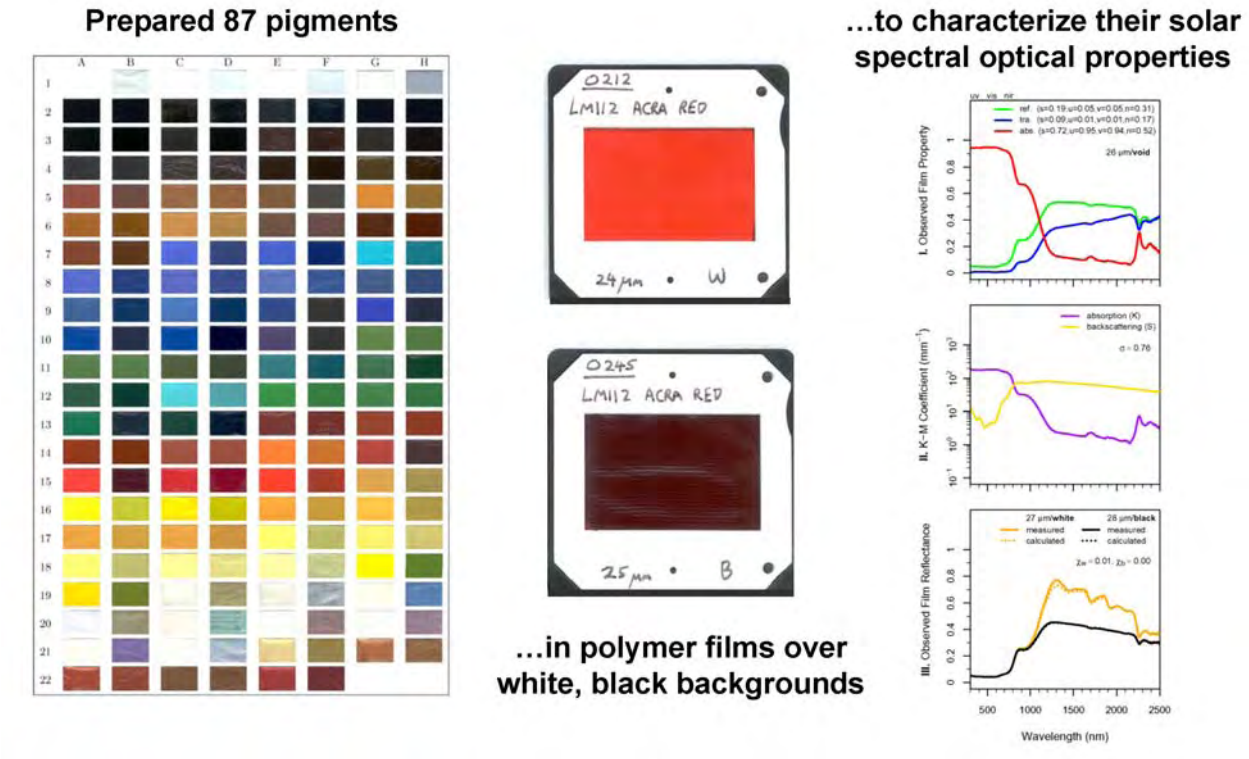

(a) (b) (c)

Figure 3. Illustration of the team's pigment characterization activities, showing (a) images over white and black backgrounds of the 87 characterized single-pigment coatings; (b) coupons of a pigmented polymer paint film (an organic red) over white and black backgrounds; and (c) measured and computed solar spectral optical properties of a characterized pigmented paint film (an inorganic black)

2.1.2. Task 2.4.2: Develop a computer program for optimal design of cool coatings

The radiative properties of the pigmented coatings characterized in Task 2.4.1 serve as inputs to Pinwheel™, a software tool for the design of color-matched cool coatings that the LBNL team has developed and shared with its industrial partners.

Pinwheel™ formulates color-matched coatings with high solar reflectance. It models a coated surface with two or three layers: an opaque substrate, an optional basecoat, and a topcoat. The solar spectral reflectance of the substrate; the thickness and colorant composition of the optional basecoat; and the thickness of the topcoat are specified by the coating designer. Pinwheel™ then seeks the topcoat colorant composition that maximizes the solar reflectance of the coated surface while acceptably matching a target visible spectral reflectance. The solar spectral reflectance of a coated surface, and hence its solar reflectance and visible spectral reflectance, are computed by applying to the solar spectral absorption and backscattering coefficients of colorants (a) a two-flux, two-constant model of light propagation through a film and (b) a colorant mixture model. Pinwheel™ has a large library of over 80 colorants whose solar spectral properties have been characterized by LBNL.

This tool differs in three major respects from conventional coating formulation software. First, it predicts solar spectral reflectance (300 to 2500 nm), rather than just visible spectral reflectance (400 to 700 nm). Second, it does not require that coatings be opaque. This permits design of thin coatings that transmit both visible and near-infrared light, as well as thicker coatings that stop visible light but transmit near-infrared light. Third, it contains the solar (and not just visible) spectral properties of the 80+ colorants.

Pinwheel™ executes in R, an interpreted programming environment available as free software for the Windows, Mac OS X, and Unix platforms. The following Pinwheel™ code designs a cool coating that matches a known color (“emerald green”) and combines up to three colorants:

```
design(
     target="emerald-green",
     topcoat.colorants=list("U08, G", "W", "Y01, Y10, Y14")
)
```

The first colorant is to be chosen from the set “U08, G”, where “U08” is a particular blue and “G” can be any of 11 characterized green pigments. The second colorant is to be “W”, which represents any of four characterized white pigments. The third colorant is to be chosen from the set of three characterized yellow pigments “Y01, Y10, Y14”. Each colorant can be present in a volume concentration ranging (by default) from 0 to 30%. The allowable concentrations are among many specifiable parameters with default values.

Figure 4 shows Pinwheel™ seeking the three-colorant combination that will produce the coating with maximum solar reflectance that matches the desired target color to within an acceptable tolerance. Chart a (upper right-hand corner) shows the visible spectral reflectance achieved by a particular set of colorants in a certain vector of concentrations. Chart b (upper left-hand corner) shows the visible spectral reflectance of all acceptable solutions found with all concentration vectors of that particular set of colorants. Chart c (lower left-hand corner) shows the solar reflectance versus match error of all acceptable solutions. The text (lower-right hand corner) shows some of the parameters used in the formulation of this coating.

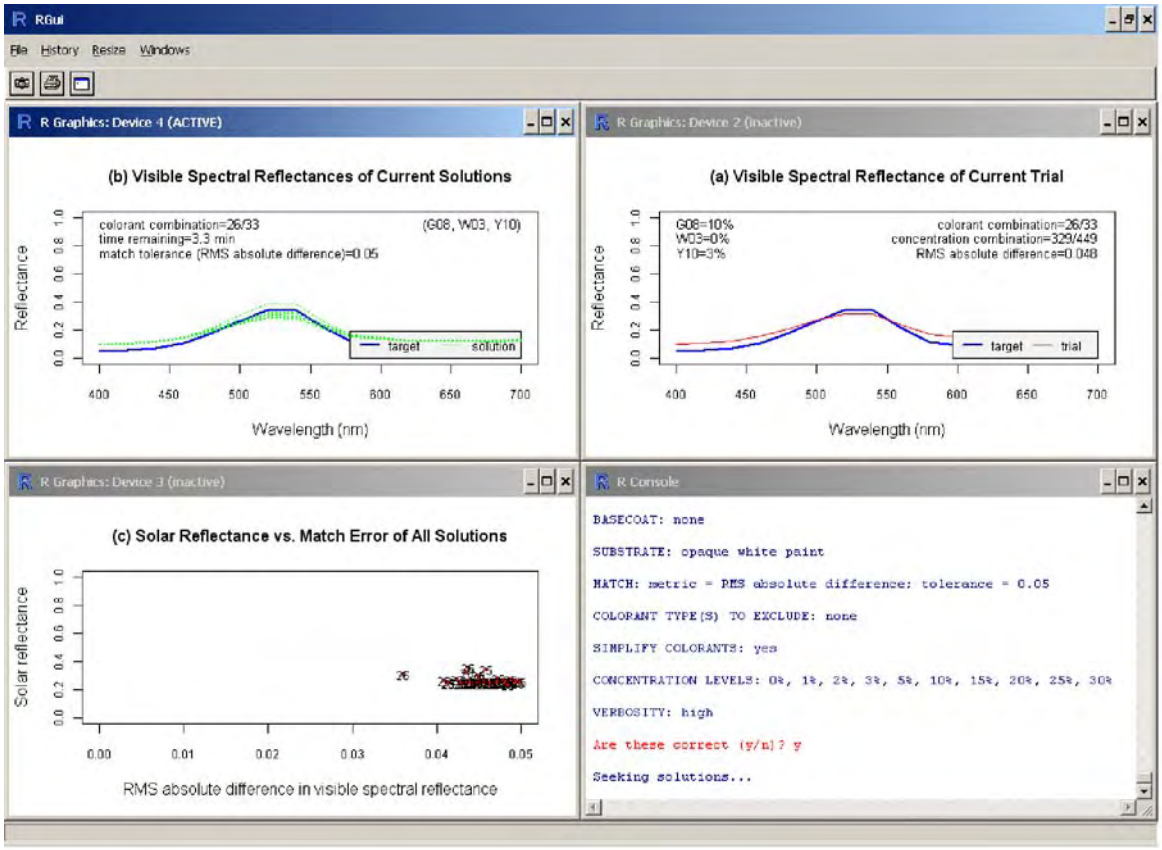

Figure 4. Pinwheel™ screen shot

Figure 5 shows one of 163 acceptable solutions found by Pinwheel™. Solutions are ordered by descending solar reflectance, so solution 2 (shown here) is that with the second highest solar reflectance. It achieves a solar reflectance of 0.38 using volume concentrations of 1% phthalocyanine green and 1% iron oxide yellow in an otherwise clear 25-µm coating over an opaque white substrate.

Pinwheel™ is currently being tested by five manufacturers. Its user manual can be found in Attachment 2.

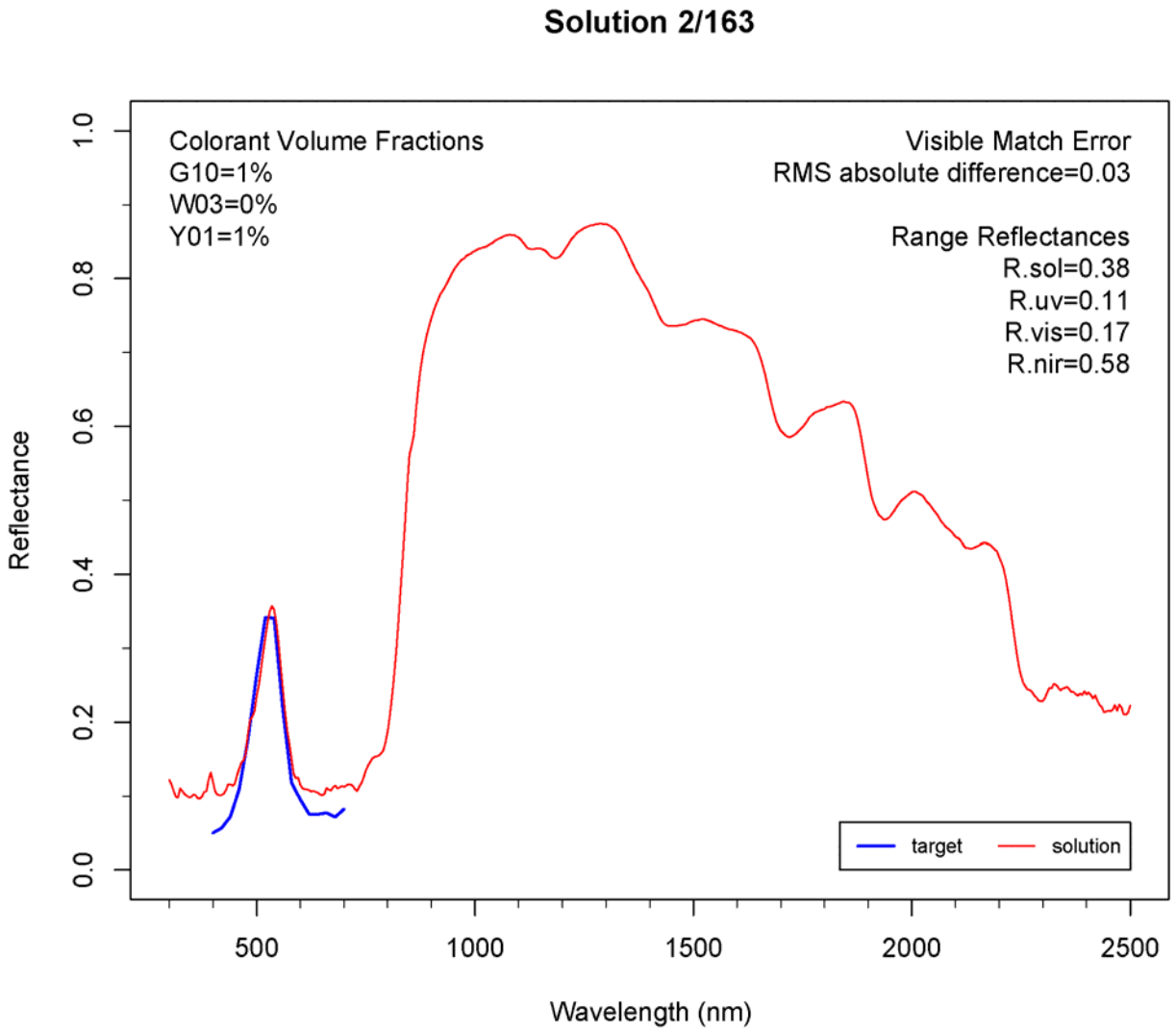

Figure 5. Solar spectral reflectance of a Pinwheel™-formulated cool coating (solution) designed to match the visible spectral reflectance of a particular shade of green (target)

2.1.3. Task 2.4.3: Develop a database of cool-colored pigments

To help the roofing industry identify cool pigments to use and hot pigments to avoid in their coatings, the LBNL researchers have produced a browsable HTML database detailing the solar spectral optical properties of 87 single-colorant ("masstone") pigmented coatings. It also includes the solar spectral optical properties of 104 tints (mixtures of single colors with white) and 32 binary mixtures of nonwhite colors. The database charts the solar spectral reflectance, transmittance, absorptance, backscattering coefficient, and absorption coefficient of each pigmented coating, and also presents images, commentary, and a chemical description of each pigment (Figure 6). Machine-readable datafiles are also included.

Figure 7 shows the first index page of the online database, including links to detail pages for four white pigments and 21 black/brown pigments. A typical detail page includes the following:

- Links to a datasheet from the pigment's manufacturer; commentary about the pigment from the LBNL articles produced for Task 2.4.1
- Large images of the pigment's masstone, tint, and binary nonwhite mixture films
- Charts and tables of the solar spectral properties of these films (Figure 6)

The tabular information available for each pigment is detailed in Table 2. The database is online at http://Coolcolors.LBL.gov.

The database summary can be found in Attachment 3.

[R03] Red Iron Oxide (iii)

Paint Code	**R03**
Paint Name	Red Iron Oxide (iii)
Pigment Name	Ferro Red V-13810 (PR 101)
Color Family	Red/Orange
Color Subfamily	iron oxide red
Mean Particle Size (microns)	0.27
Dry Film PVC	3%
Pigment Datasheet	available
Paint Datasheet	unavailable
LBNL Commentary	available

Masstone and Mixtures with White (Tints)

[R03] Red Iron Oxide (iii) +
[W03] Titanium White (i)

image over white				
image over black				
spectral datafile	R03 masstone	R03 tint 1:4	R03 tint 1:9	W03 masstone

guide to reading spectral datafiles

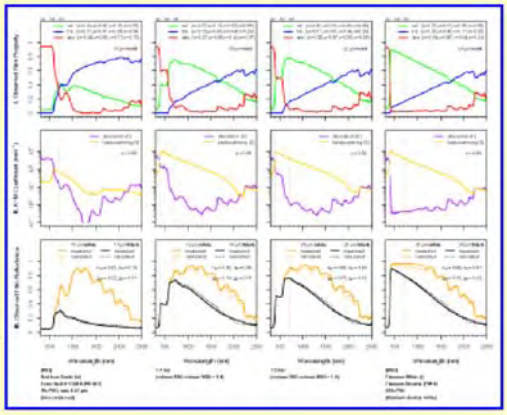

Mixtures with Nonwhite Colors

[R03] Red Iron Oxide (iii) +
[B16] Iron Titanium Brown Spinel (i)

image over white			
image over black			
spectral datafile	R03 masstone	R03+B16 mixture 1:1	B16 masstone

guide to reading spectral datafiles

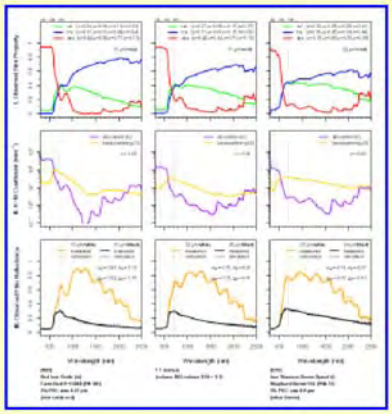

Figure 6. Description of an iron oxide red pigment in the LBNL pigment database

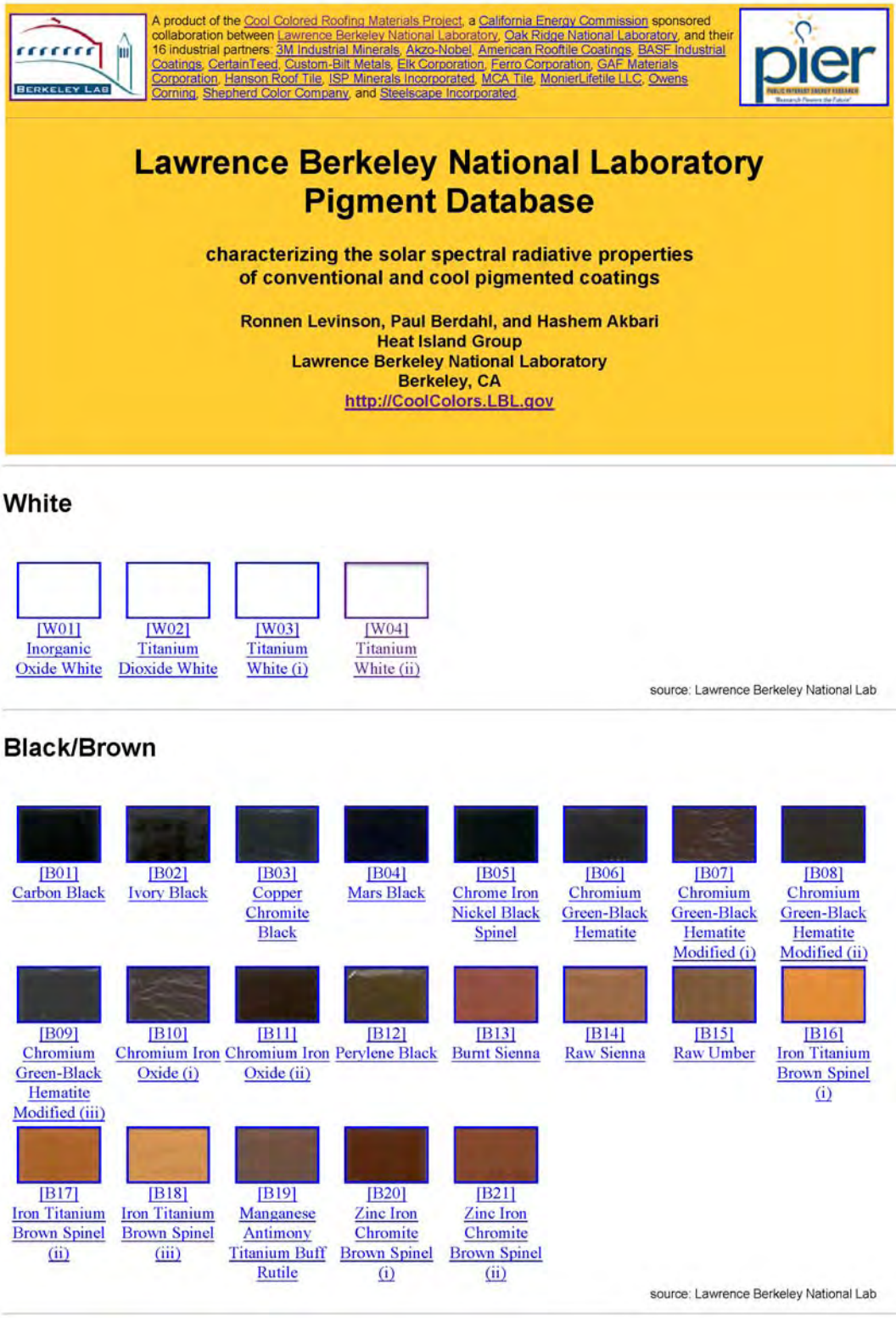

Figure 7. First index page of the LBNL pigment database, including links to the detail pages of 4 white pigments and 21 black/brown pigments. The remaining index pages link to the detail pages of 62 more pigments.

Table 2. Pigment properties tabulated in the LBNL pigment database

instructions	how to view and interpret this datafile
comments	authorship and disclaimer
computation date	when K-M coefficients were calculated
color family	white, black/brown, blue/purple, green, red/orange, yellow, or pearlescent
pigment category	pigment chemistry or characteristic (e.g., cobalt titanate green or non-selective black)
code	used to identify this pigment in our pigment characterization paper (note: this value likely to be replaced)
paint name	assigned by the paint manufacturer
pigment name	assigned by the pigment manufacturer
internal description	LBNL's description of masstone, tint, or mixture
component names	LBNL's description of the paint's components
component ratios	parts by volume of each component
dry-film PVC	pigment volume concentration (volume pigment:volume paint) in dry film
delta.v (microns)	thickness of film sample over void background [exclusive of substrate, if present] (μm)
delta.w (microns)	thickness of film sample over opaque white background [exclusive of background and substrate, if present] (μm)
delta.b (microns)	thickness of film sample over opaque black background [exclusive of background and substrate, if present] (μm)
sigma	non-spectral forward scattering ratio
spectral ranges	definitions of solar, ultraviolet, visible, and near-infrared ranges used in spectral averaging
R.tilde.fv averages	spectrally averaged, irradiance-weighted values of the measured reflectance of the film over a void background
T.tilde.fv averages	spectrally averaged, irradiance-weighted values of the measured transmittance of the film over a void background
A.tilde.fv averages	spectrally averaged, irradiance-weighted values of the measured absorptance of the film over a void background
R.tilde.fw averages	spectrally averaged, irradiance-weighted values of the measured reflectance of the film over an opaque white background
R.tilde.fb averages	spectrally averaged, irradiance-weighted values of the measured reflectance of the film over an opaque black background
R.tilde.ow averages	spectrally averaged, irradiance-weighted values values of the measured reflectance of the opaque white background
lambda (nm)	wavelengths at which spectral values are presented
insolation (W/m^2/nm)	air-mass 1.5 hemispherical solar spectral irradiance (W m^{-2} nm^{-1})
R.tilde.fv	measured spectral reflectance of the film over a void background
T.tilde.fv	measured spectral transmittance of the film over a void background
A.tilde.fv	measured spectral absorptance of the film over a void background
R.tilde.fw	measured spectral reflectance of the film over an opaque white background
R.tilde.fb	measured spectral reflectance of the film over an opaque black background
K (1/mm)	Kubelka-Munk (K-M) spectral absorption coefficient (mm^{-1})
S (1/mm)	K-M spectral backscattering coefficient (mm^{-1})
R.inf	continuous refractive index (CRI) spectral reflectance of an opaquely thick film
R.tilde.inf	observed spectral reflectance of an opaquely thick film
R.tilde.fw.calc	observed spectral reflectance of the film over an opaque white background, as computed from the K-M coefficients
R.tilde.fb.calc	observed spectral reflectance of the film over an opaque black background, as computed from the K-M coefficients
T.v	internal transmittance of the film
q.i.at.zero	diffuse fraction q of the downflux i exiting the bottom of the film ($z = 0$)
q.j.at.delta	diffuse fraction q of the upflux j exiting the top of the film ($z = \delta$)
omega.i.at.zero	interface reflectance ω to the downflux i exiting the bottom of the film ($z = 0$)
omega.j.at.delta	interface reflectance ω to the upflux j exiting the top of the film ($z = \delta$)

2.2. Task 2.5: Development of Prototype Cool-Colored Roofing Materials

The Cool Team estimates that roofing shingles, tiles, and metal panels comprise more than 80% (by roof area) of the residential roofing market in the western United States. In this project, the Cool Team collaborated with manufacturers of many roofing materials to evaluate the best ways to increase the solar reflectance of these products. The results of this research have been utilized by the manufacturers to produce cool roofing materials. To date and as the direct result of this collaborative effort, manufacturers of roofing materials have introduced cool shingles, cool concrete tile coatings, and cool concrete tiles; and significantly expanded the production of cool clay tiles and cool metal roofs.

2.2.1. Task 2.5.1: Review of roofing material manufacturing methods

The objective of this subtask was to compile information on roofing material manufacturing methods. The Cool Team contacted several representative manufacturers of various roofing materials to obtain information on the processes used to color their products. The team also reviewed literature on the fabrication and coloration of roofing materials.

This analysis suggested that cool-colored roofing materials can be manufactured using the existing equipment in production and manufacturing plants. The three principle ways to improve the solar reflectance of roofing materials include using raw materials with high solar reflectance; using cool pigments in the coating; and applying a two-layered coloring technique using pigmented materials with high solar reflectance as an under-layer. Although all these options are in principle easy to implement, they may require changes to current production techniques that could increase the cost and reduce the market competitiveness of the finished products.

The results of this study were published as a two-part article in *Western Roofing Insulation and Siding* magazine. A copy of the final report for this study is enclosed in Attachment 4.

2.2.2. Task 2.5.2: Design innovative methods for applying cool coatings to roofing materials

In addition to using NIR reflective pigments in the manufacture of cool roofing materials, applying novel engineering techniques can provide a cost-effective way to further enhance the solar reflectance of colored roofing materials. Cool-colored pigmented coatings are partly transparent to NIR light; thus, any NIR light not reflected by the cool pigmented coating is transmitted to its substrate, where it can be absorbed. A reflective basecoat can be used to increase the system's NIR and solar reflectance. This method is referred as a two-layer, or bilayer, technique.

The project team has detailed the innovative engineering methods in an article in press in the academic journal *Solar Energy Materials & Solar Cells*. A prepress draft of this article is included in Attachment 5.

Figure 8 demonstrates the application of the two-layered technique to manufacture cool-colored materials. A thin layer of dioxazine purple (14–27 μm) is applied on four substrates: (a) aluminum foil (~ 25 μm), (b) opaque white paint (~ 1000 μm), (c) non-opaque white paint (~ 25 μm), and (d) opaque black paint (~ 25 μm). As can be seen (and confirmed by the visible reflectance spectrum), the color of the material is black. However, the solar reflectance of the

sample exceeds 0.40 when applied to an opaque white or aluminum foil substrate, while its solar reflectance over a black substrate is only 0.05.

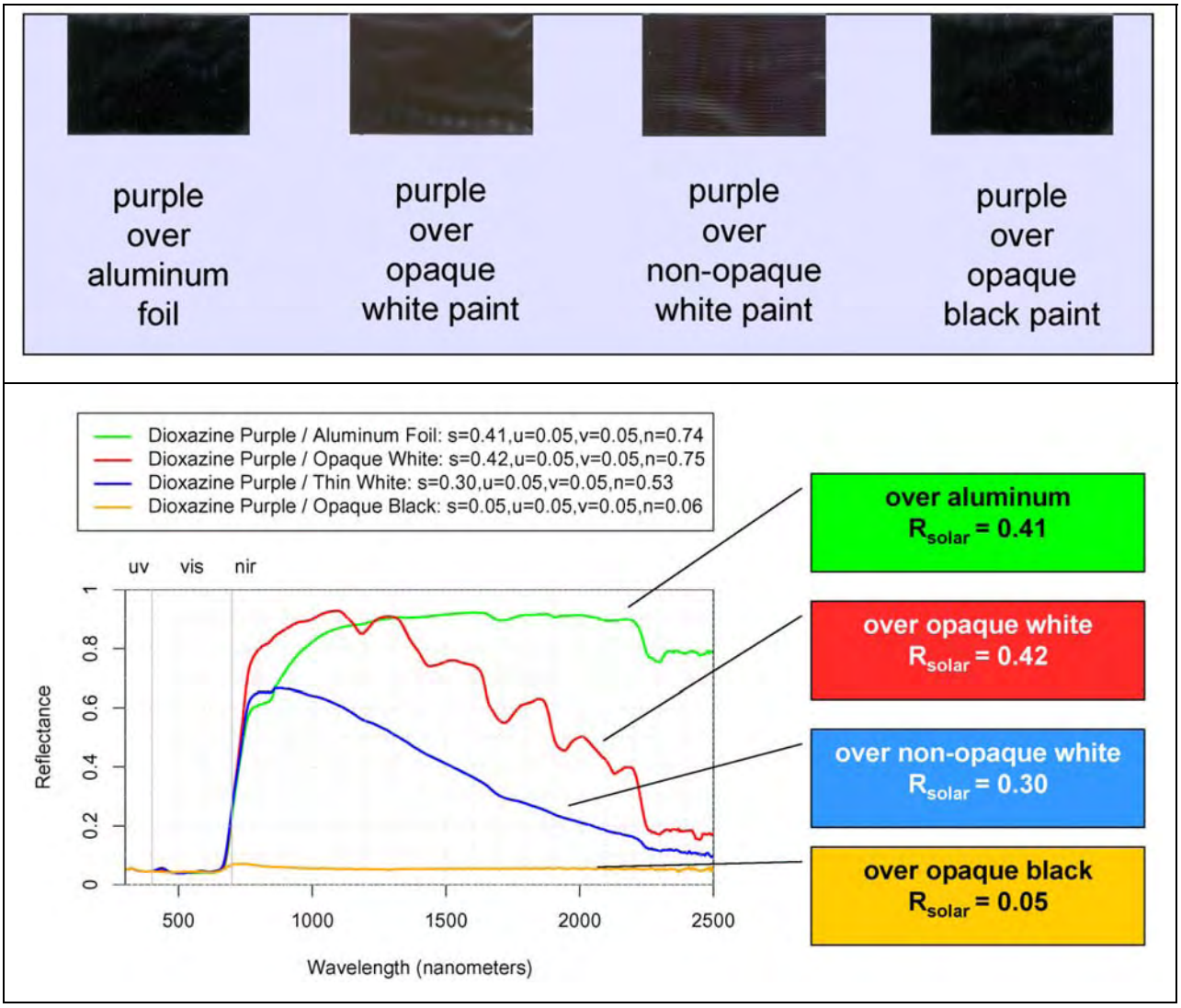

Figure 8. Application of the two-layer technique to manufacture cool-colored materials

2.2.2.1. Shingles

The solar reflectance of a new shingle is, by design, dominated by the solar reflectance of its granules, which cover over 97% of its surface. Until recently, manufacturers produced granules with high solar reflectance by using a coating pigmented with titanium dioxide (TiO_2) rutile white. Because a thin TiO_2-pigmented coating is reflective but not opaque in the NIR, multiple layers are needed to obtain high solar reflectance. This technique has been used to produce "super-white" (meaning truly white, rather than gray) granulated shingles with solar reflectances exceeding 0.5 (see Figure 9).

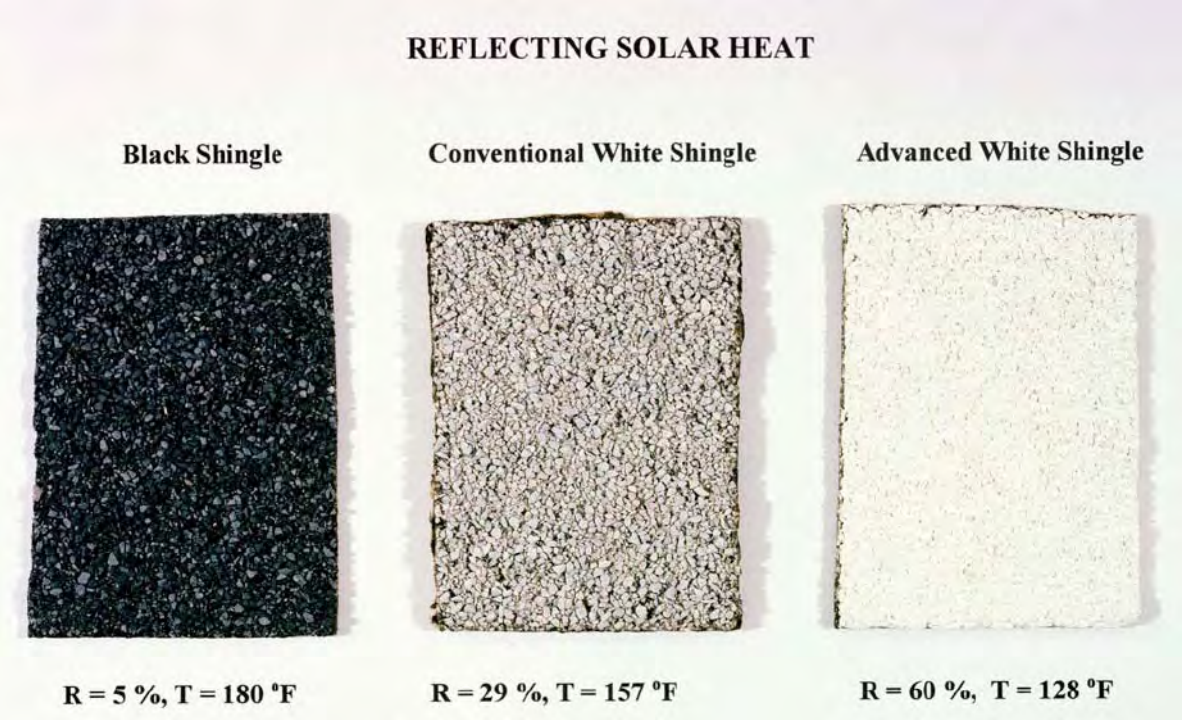

Figure 9. Development of "super-white" shingles

Although white roofing materials are popular in some areas, such as Greece and Bermuda (see Figure 10), many consumers prefer aesthetically pleasing nonwhite roofs. Manufacturers have tried to produce colored granules with high solar reflectance by using nonwhite pigments with high NIR reflectance. To increase the solar reflectance of colored granules with cool pigments, multiple color layers, a reflective undercoating, and/or reflective aggregate should be used. Obviously, each additional coating increases the cost of production.

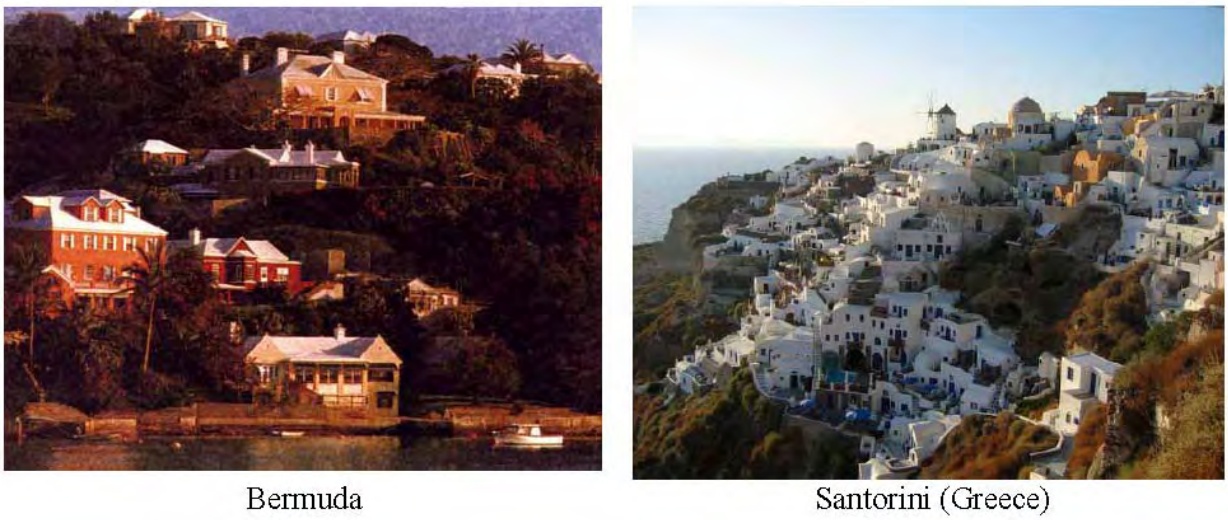

Figure 10. White roofs and walls are used in Bermuda and Santorini, Greece

In close collaboration with partners at ISP Minerals, 3M Company, Elk, GAF, and CertainTeed, the labs have developed more than 100 single and multiple-color shingle prototypes. Figure 11 illustrates the iterative development of a cool black shingle prototype by industrial partner ISP Minerals. A conventional black roof shingle has a solar reflectance of about 0.04. Replacing the granule's standard black pigment with a cool NIR-scattering black pigment (prototype 1) increases the solar reflectance of the shingle to 0.12. Incorporating a thin white sublayer (prototype 2) raises the shingle's solar reflectance to 0.16; using a thicker white sublayer (prototype 3) increases the shingle's solar reflectance to 0.18. The figure also shows an approximate performance limit (solar reflectance 0.25) obtained by applying 25-micron NIR-reflective black topcoat over an opaque white background.

Several cool shingles have been developed within the last year. Figure 12 shows examples of prototype cool shingles and compares the solar reflectance of each with a conventionally pigmented counterpart of the same color.

In parallel to the above efforts, two partners (3M and Elk) have developed cool-colored shingles for three popular colored products. On March 2005, Elk announced the availability of the three cool-colored shingles. The Cool Team is currently testing the performance of these cool shingles in two demonstration houses in Redding, CA. Figure 13 shows two houses with cool-colored roofing shingles from Elk.

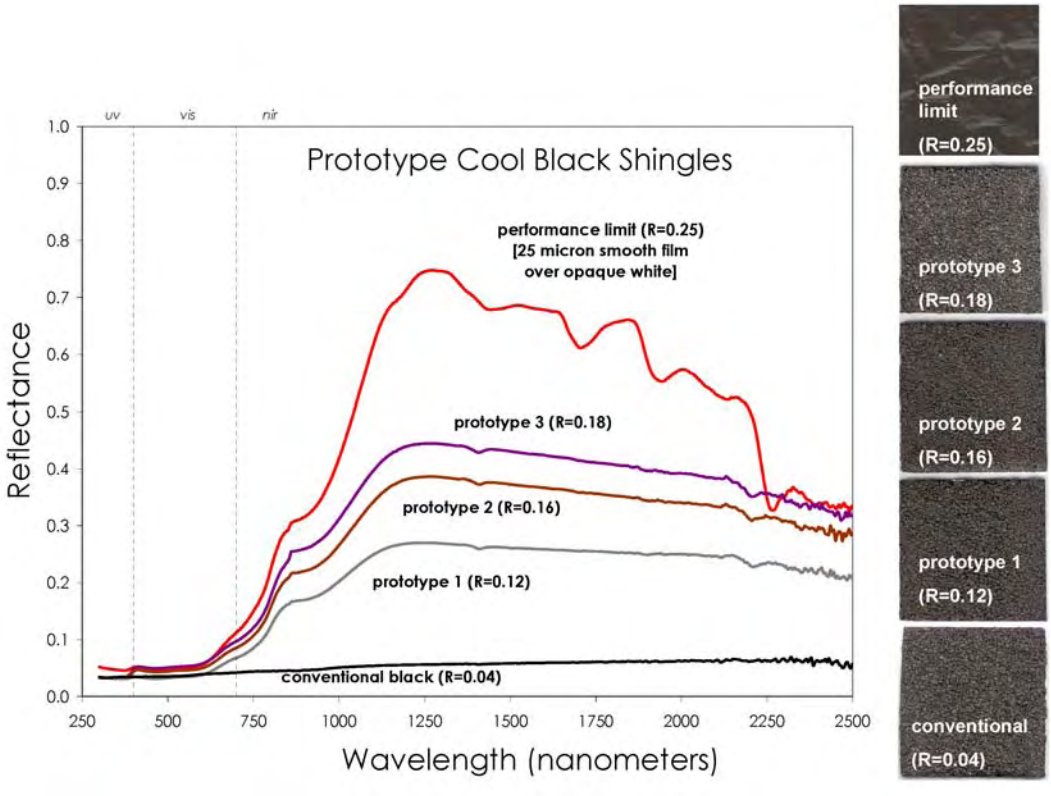

Figure11. Development of a cool black shingle by industrial partner ISP Minerals. Shown are the solar spectral reflectances, images, and solar reflectances (R) of a conventional black shingle, three prototype cool black shingles, and a smooth cool black film over an opaque white background.

Figure 12. Examples of standard and prototype cool shingles; R is solar reflectance

Figure 13. Application of cool-colored roofing shingles on two houses advertised by Elk Corp.

2.2.2.2. Tiles and tile coatings

Clay and concrete tiles are used in many areas around the world. In the United States, clay and concrete tiles are more popular in the hot climate regions. Three methods improve the solar reflectance of colored tiles: (1) use clay or concrete with low concentrations of light-absorbing impurities, such as iron oxides and elemental carbon; (2) color the tile with cool pigments contained in a surface coating or mixed integrally; and/or (3) include an NIR-reflective (e.g., white) basecoat beneath an NIR-transmitting colored topcoat. Although all these options are in principle easy to implement, they may require changes to current production techniques that can increase the cost of the finished products. Colorants can be included throughout the body of the tile, or used in a surface coating. Both methods need to be addressed.

Consortium member American Rooftile Coatings has developed a palette of cool nonwhite coatings for concrete tiles. Each of the COOL TILE IR COATINGS™ shown in the top row of Figure 14 has a solar reflectance better than 0.40. The solar reflectance of each cool coating exceeds that of a color-matched, conventionally pigmented coating by 0.15 (terracotta) to 0.37 (black).

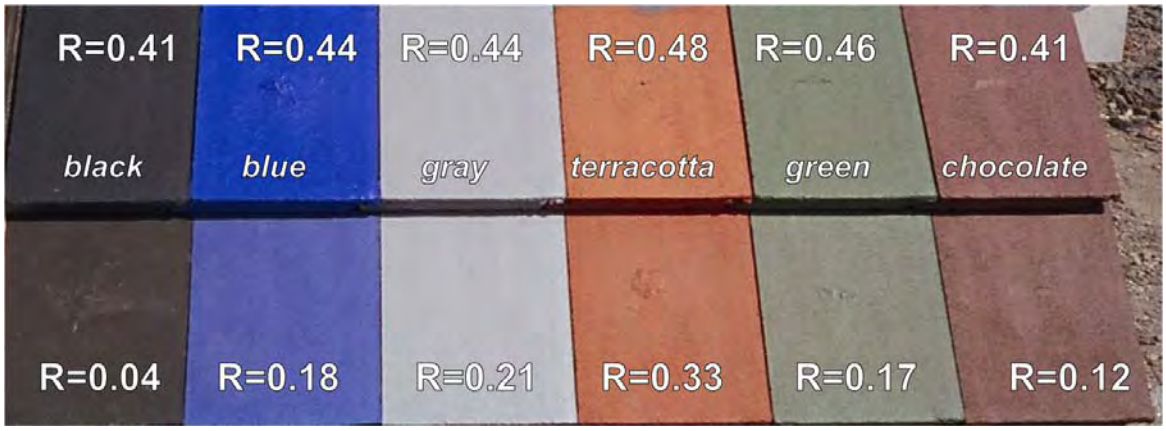

Figure14. Palette of color-matched cool (top row) and conventional (bottom row) roof tile coatings developed by industrial partner American Rooftile Coatings. Shown on each coated tile is its solar reflectance R.

MCA Clay Tile is producing several cool nonwhite clay tile products (Table 3), and MonierLifetile has developed several cool nonwhite concrete tile prototypes. The Cool Team is currently testing a cool-colored concrete tile on a demonstration house in Sacramento and a cool-colored clay tile on the attic test assembly at ORNL.

Table 3. Sample cool-colored clay tiles and their solar reflectances (Source: http://www.MCA-Tile.com)

Model	Color	Initial solar reflectance	Solar reflectance after 3 years
Weathered Green Blend		0.43	0.49
Natural Red		0.43	0.38
Brick Red		0.42	0.40
White Buff		0.68	0.56
Tobacco		0.43	0.41
Peach Buff		0.61	0.48
Regency Blue		0.38	0.34
Light Cactus Green		0.51	0.52

2.2.2.3. Metal Panels

Metal roofing materials are installed on a small (but growing) fraction of the U.S. residential roofs. Historically metal roofs have had only about 3% of the residential market. However, the architectural appeal, flexibility, and durability, due in part to the cool-colored pigments, has steadily increased the sales of painted metal roofing, and as of 2002 its sales volume has increased to 8.9% of the residential market, making it the fastest growing residential roofing product (F.W. Dodge 2005). Metal roofs are available in many colors and can simulate the shape and form of many other roofing materials (see Figure 15). Applying cool-colored pigments in metal roofing materials may require fewer production processes changes (and in many cases no changes) than in any other roofing material. In fact, cool pigments have been incorporated into paint systems used for metal roofing since 2002. For example, the BASF Industrial Coatings line of cool coatings for metal includes over 20 cool-colored products (Figure 16).

As in the cases of tile and asphalt shingle, cool pigments can be applied to metal via a single or two-layered technique. If the metal substrate is highly reflective, a single-layered technique may suffice. The coatings for metal shingles are thin, durable polymer materials. These thin layers use materials efficiently, but limit the maximum amount of pigment present. However, the metal substrate can provide some NIR reflectance if the coating is transparent in the NIR. Several manufacturers have developed cool-colored metal roof products.

Cool nonwhite coatings have been enthusiastically adopted by premium coil coaters and metal roofing manufacturers. Metal panels and clay tiles were the first types of roofing to be produced in cool-colors. BASF Industrial Coatings (Southfield, MI) has launched a line of cool-colored siliconized-polyester coatings that is quickly replacing their conventional siliconized-polyester coatings. Steelscape Inc. (Kalama, WA) has recently introduced a cool polyvinylidene fluoride coating for the metal building industry. Custom-Bilt Metals (Chino, CA) has switched more than 250 of its metal roofing products to cool-colors. The Cool Team is currently testing a cool-colored metal roof on a demonstration house in Sacramento.

(a) (b) (c)

(d) (e) (f)

(g) (h) (i)

(j) (k) (l)

Figure 15. Simulated roofing products made from metal: (a) Advanta Shingles; (b) Bermuda Shakes; (c) Castle Top; (d) Dutch Seam Panel; (e) Granutile; (f) Perma Shakes; (g) Scan Roof Tile; (h) Snap Seam Tile; (i) Techo Tile; (j) Verona Tile; (k) Oxford Shingles; and (l) Timbercreek Shakes. Products a through j are manufactured by ATAS International, Inc., while products k and l are manufactured by Classic Products, Inc. (Photos courtesy of ATAS International and Classic Products).

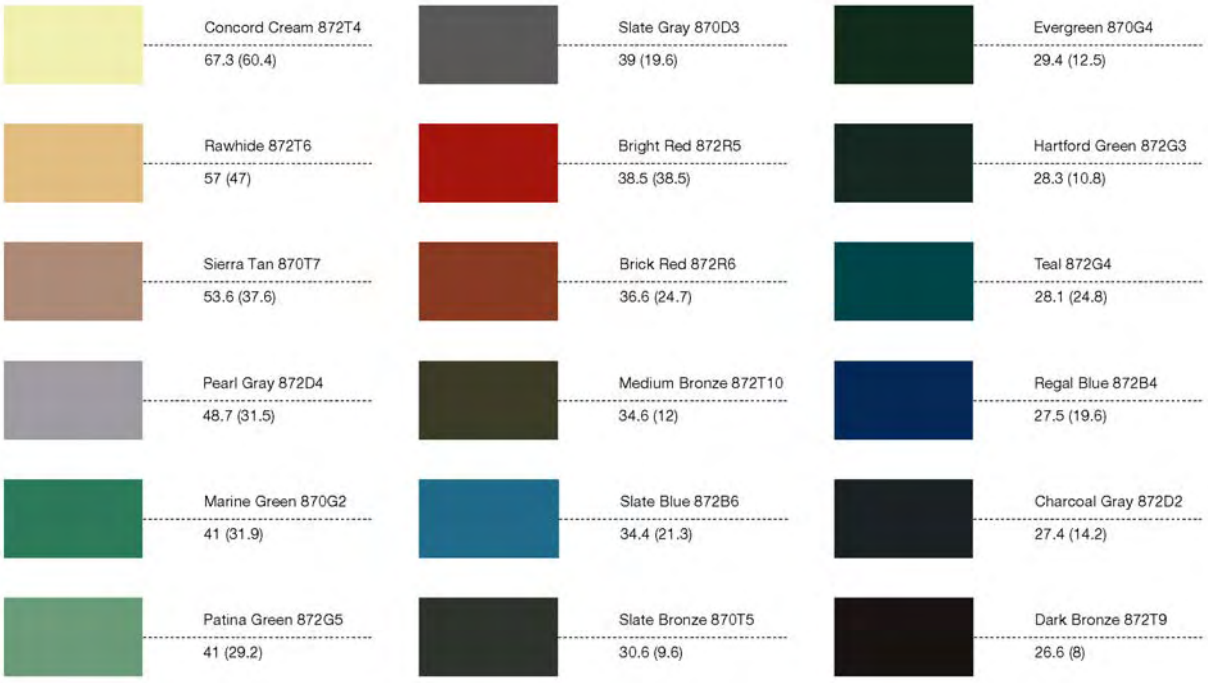

Figure 16. Some of the cool-colored coatings for metal roofing products available from BASF Industrial Coatings. To the right of each color swatch is shown the solar reflectance of the cool formulation, followed (in parentheses) by the solar reflectance of a color-matched standard formulation. (Source: http://www.basf.com/pdfs/ULTRA-Cool.pdf).

2.2.3. Task 2.5.3: Accelerated weathering testing (durability of cool nonwhite coatings)

Roofing materials fail mainly because of three processes:

- Gradual changes to physical and chemical composition induced by the absorption of UV light
- Aging and weathering (e.g., loss of plasticizers in polymers and low-molecular-weight components in asphalt), which may accelerate as temperature increases
- Diurnal thermal cycling, which stresses the material by expansion and contraction

The project goal was to clarify the material degradation effects due to UV absorption and to heating. Durability performance must be demonstrated to persuade homebuilders to adopt cool-colored tile and asphalt shingle roof products.

Shepherd Color Company and 3M provided the Cool Team access to their weatherometers for evaluating the effect of fluorescent (UV) light exposure and xenon-arc exposure on the solar reflectance, fading and gloss retention of clay, concrete, painted metal and asphalt shingle roof products. Clay tiles were provided by MCA Clay Tile. Painted PVDF metal samples with and without cool pigmented colors were provided by BASF and Steelscape. Shingles were provided by U.S. companies that wish their products' identities to remain confidential; however, the data for shingles with and without cool pigments are provided in coded format. Details of the accelerated and natural sunlight test results are provided in the Task 2.5.3 report, Attachment 6.

Results of accelerated fluorescent (UV) light exposures show that pigment stability and discoloration resistance of the painted metals, concrete tiles and clay tiles with cool pigments are as good as those of commercially available conventionally pigmented products. Independent UV testing by BASF produced similar findings. They proved that cool pigmented colors retained their gloss just as well as standard production pigments. The fade resistance of painted metal cool-colored blue and yellow masstones is much improved over the respective standard colors. Blue, especially a blue tint, is well known to fade; however, the cool-colored masstone blue shows excellent fade resistance.

Results for asphalt shingles were just as promising and showed no deleterious effects on solar reflectance or total color change after being subjected to 5000 hours of fluorescent or xenon-arc exposures (see Figure 17). Total color change (ΔE) less than 1 is almost indistinguishable and is considered quite good by the industry. Cool-pigmented shingles coded A and E had a total color change (ΔE) less than 1.5 after 5000 hours of UV exposure. In contrast, their conventionally pigmented counterparts had ΔE's that were 50% higher for Code A and 100% higher for Code E. The ΔE for the Code C shingle with cool-pigments exceeded 2.0 after 1000 hours then dropped below 1.0 after 5000 hours. Reasons for the behavior are unknown; however, overall the data clearly shows that the cool-pigmented shingles when subjected to simulated direct solar UV radiation from a UVB-340 lamp perform just as well as standard products accepted on the open market. The asphalt shingles with cool pigments do not lose solar reflectance, and they remain fade resistant.

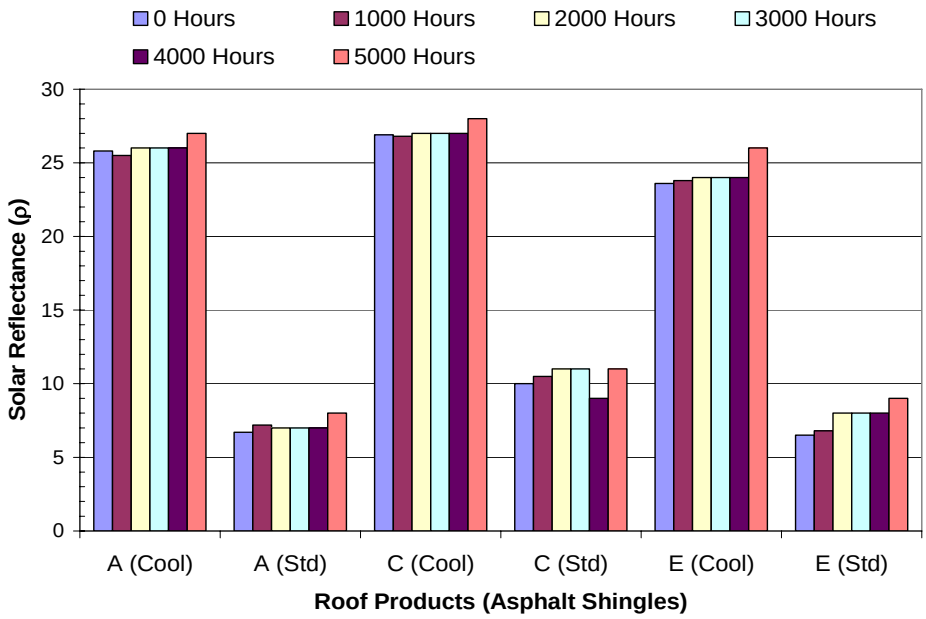

a) Solar reflectance of cool-pigmented and standard production shingles.

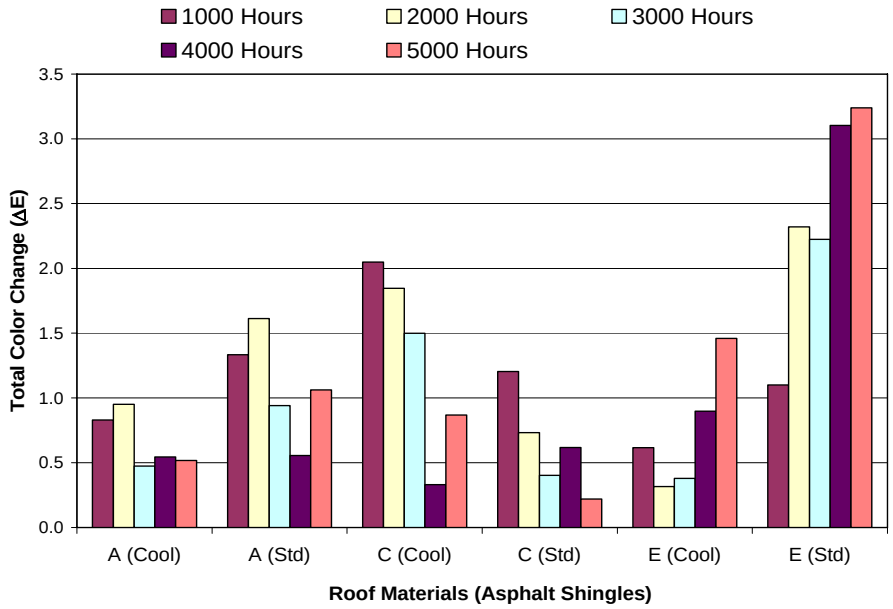

b) Total color change ΔE for cool-pigmented and standard production shingles.

Figure 17. (a) Solar reflectance (b) and total color change of asphalt shingles exposed to accelerated direct fluorescent UV radiation simulating solar's short-wave irradiance (data courtesy of Shepherd Color Company)

2.3. Task 2.6: Field-Testing and Product Useful Life Testing

2.3.1. Task 2.6.1: Building energy-use measurements at California demonstration sites

The Cool Team set up a residential demonstration site in Fair Oaks, California (near Sacramento), consisting of two pairs of single-family, detached houses roofed with painted metal shakes and concrete tile. The team also set up two houses in Redding, California to demonstrate asphalt shingles. The demonstration pairs each include one building roofed with a cool-pigmented product and a second building roofed with a conventionally pigmented product of nearly the same color. The paired homes are adjacent, and share the same floor plan, roof orientation, and level of blown ceiling insulation (3.4 m^2K/W, a.k.a. R-19). All have air-handlers and air-delivery duct work in the attic. Demonstration homes in Fair Oaks have soffit and gable vents, while the homes in Redding are equipped with soffit and ridge vents. The Redding demonstration homes each use two 3½-ton air conditioners for comfort cooling. The homes will be monitored through at least summer 2006.

A data acquisition system continuously logs temperatures at the roof surface, on the underside of the roof deck, in the mid-attic air, at the top of the insulation, on the interior ceiling's sheet-rock surface, and inside the building. Relative humidity in the attic air and the residence are also measured. Heat flux transducers are embedded in the sloped roofs and the attic floor to measure the roof heat flows and the ceiling heat leakage. The Cool Team has instrumented the building to measure the total house and air-conditioning power demands. A fully instrumented meteorological weather station is set up to collect the ambient dry bulb temperature, relative humidity, solar irradiance, and wind speed and direction.

One of the Fair Oaks homes roofed with low-profile concrete tile was colored with a conventional chocolate brown coating (solar reflectance 0.10), while the other was colored with a matching cool chocolate brown with solar reflectance 0.41. The attic air temperature beneath the cool brown tile roof has been measured to be 3 to 5 K (5.4 to 9°F) cooler than that below the conventional brown tile roof during a typical hot summer afternoon. The results for the pair of Fair Oaks homes roofed with painted metal shakes are even more promising. There the attic air temperature beneath the cool brown metal shake roof (solar reflectance 0.31) was measured to be 5 to 7 K (9 to 12.6°F) cooler than that below the conventional brown metal shake roof (solar reflectance 0.08). Attic air temperature below the cool shingle (solar reflectance 0.26) was about 3 K (5.4°F) cooler than the temperature below the conventional pigmented shingle roof (solar reflectance 0.09).

The application of cool-colored coatings reduced the surface temperature of the cool-pigmented roofs, which in turn reduced the average daytime heat flows through the roof deck by 20% for cool pigmented tile, by 32% for cool pigmented painted metal shakes, and by 30% for cool pigmented asphalt shingle roofs as compared to each roof type's conventional counterpart.

The thermal data demonstrated drops in the heat penetrating into the conditioned space, which yields cooling electrical energy savings. Cool pigmented tile and cool pigmented metal shakes reduced the daytime cooling electrical energy by about 2 kWh per day.

As the temperature difference from the outdoor air to the home's interior air (return air) increases, the cooling savings also increase for the pair of shingle-roofed demonstration homes

(Figure 18). At an outdoor air-to-indoor air temperature difference of 10 K (about 32°C outdoor air temperature) the home with cool pigmented asphalt shingles uses about 6.3 kWh per day less electricity than does the other home with conventional shingles. This represents savings of about 0.90 kWh per day per ton of cooling capacity.

It is interesting to note that the hotter the outdoor air temperature, the greater the energy savings for the air-conditioners operating in all demonstration homes with cool pigmented roofs. This small trend could be important in terms of Time Dependent Valuation of energy that places a premium cost on energy consumed during the hottest portion of the day.

The report for Task 2.6.1 documenting the thermal performance and electrical energy savings is provided in Attachment 7.

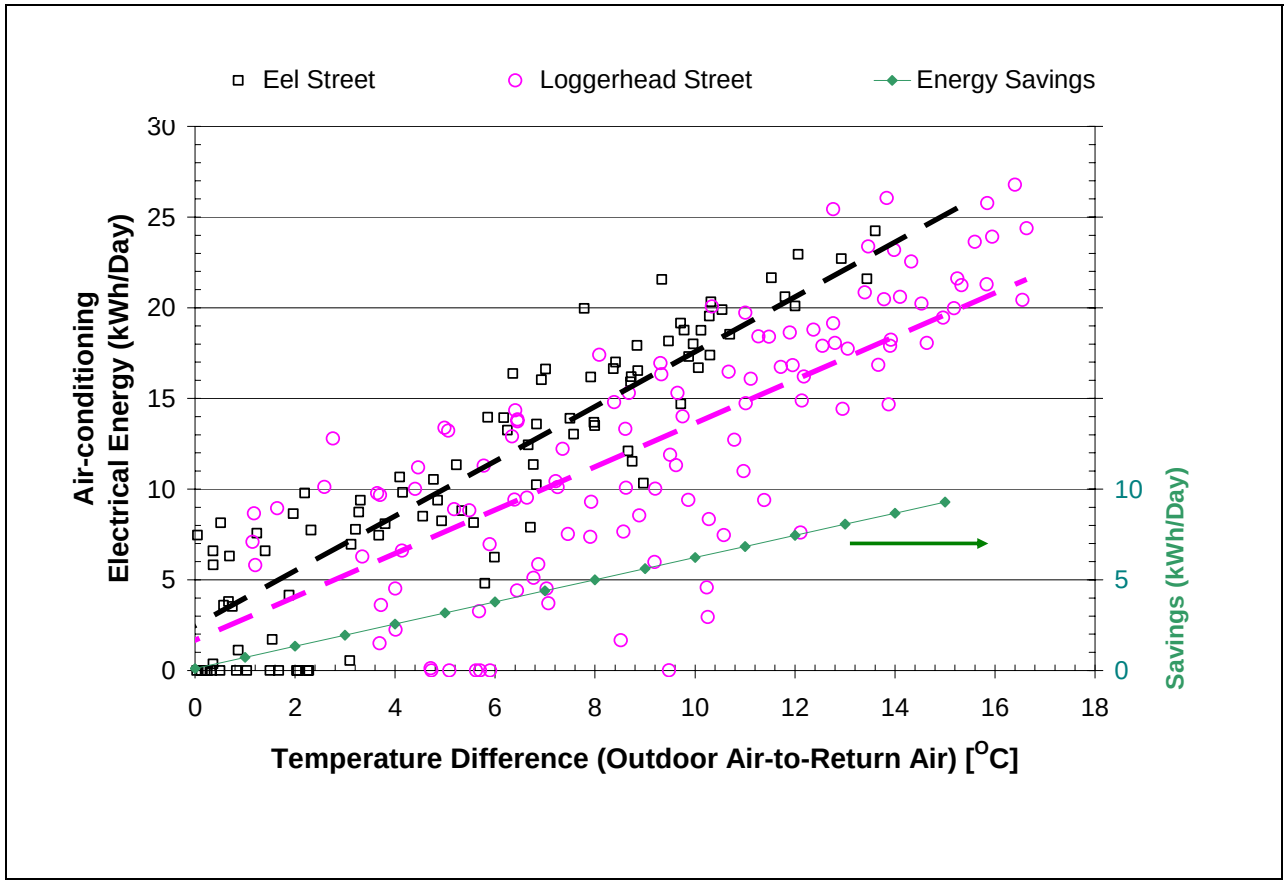

Figure 18. Daily air-conditioning energy consumption and savings, measured during the daylight hours from June through September 2005, for demonstrations with asphalt shingle roofs with and without cool pigments. The Redding demonstration homes each use two 3½ ton air-conditioners for comfort

2.3.2. Task 2.6.2: Materials testing at weathering farms in California

In addition to conducting the laboratory accelerated testing reported in Task 2.5.3, the Cool Team naturally weathered various types of conventional- and cool-pigmented roofing products at seven California sites. (Note that the concrete coupons were placed in the field about 6 months later than were the painted metal and clay coupons.) The final report is contained in Attachment 8 and has been submitted for journal review and publication to document the effect of soiling on the solar reflectance of the conventional- and cool-pigmented roof products.

Airborne particulate matter that settles on a roof can either reflect or absorb incoming solar radiation, depending on the chemistry and size of the particles. These light scattering and absorption processes occur within a few microns of the surface and can affect the solar reflectance of the roof. The long-term change in reflectance appears driven by the ability of the particulate matter to cling to the roof and resist being washed off by wind and or rain.

Contaminants collected from samples of roof products exposed at the seven California weathering sites were analyzed to characterize the chemical and/or biological nature of the soil layer on each roof sample and to identify contaminants that degrade or enhance solar reflectance.

The chemical composition of particles deposited on the roof samples was very similar across the state of California; there was no clear distinction from one region to another. Organic and elemental carbon (soot) was detected. However, the elemental carbon was present in concentrations too small to contribute significantly to the loss of solar reflectance. Dust particles (characterized by Ca and Fe) and organic carbon raised the reflectance of low-reflectance samples and lowered the reflectance of the high-reflectance samples.

During this 2½ year time-limited study, the initial solar reflectance for the concrete tile, clay and painted metal coupons dropped about 6% (Figure 19). The solar reflectance of the cool pigmented metal coupons always exceeded that of the standard pigmented coupons (Figure 19b). Climatic soiling did not cause the cool pigmented roof coupons to lose any more solar reflectance points than their standard pigmented counterparts. Figure 19b shows that the reflectance of the samples had decreased significantly by August 2004, toward the end of the dry California summer. By the following April, after winter rains, less soil is present and much of the reflectance has been restored. Increasing the roof slope from 9.5° (2 in 12) to 33.7° (8 in 12) appears to diminish the effect of climatic soiling. Precipitation and or wind sweeping occurring during the winter months helps restore most of the initial solar reflectance. The thermal emittance remained invariant with time and location and was therefore not affected by climatic soiling.

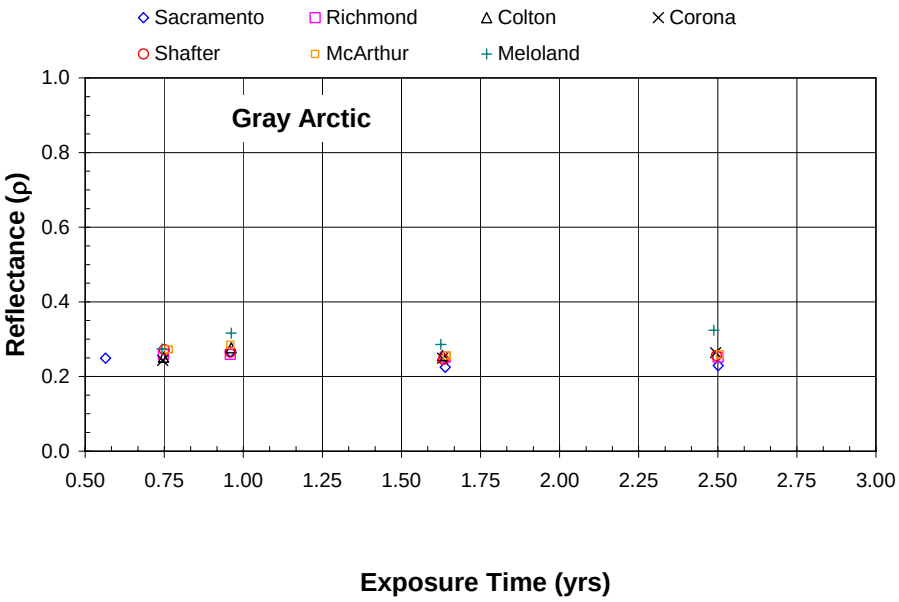

19a) Cool-color light-gray concrete coupons placed in field 6 months later than metal coupons in Figure 19b

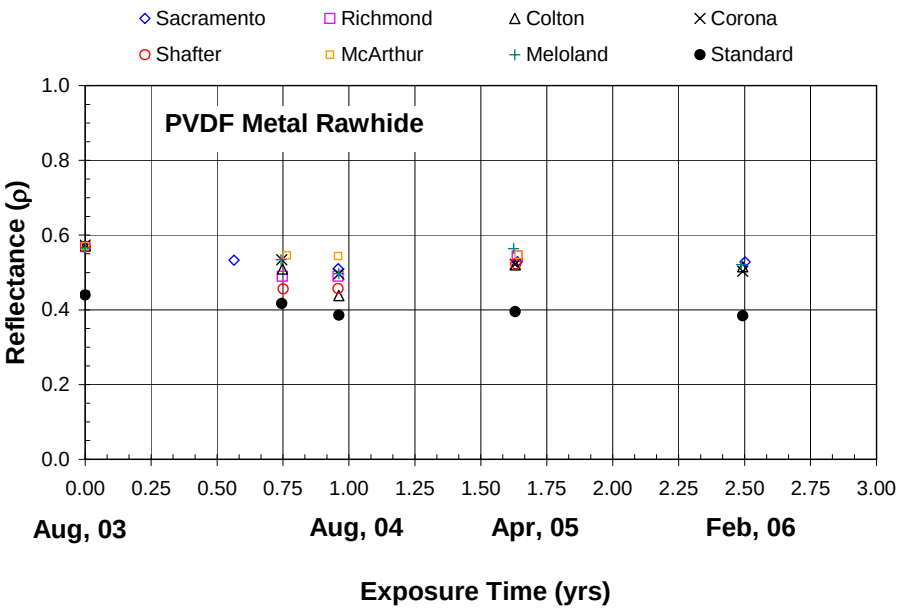

19b) Painted PVDF metal coupons (off-white cool-color and standard off-white color)

Figure 19. Solar reflectance of light-gray concrete tile coupons (19a) and painted metal coupons (19b) exposed to climatic soiling at each of the seven CA weathering sites

2.3.3. Task 2.6.3: Steep-slope assembly testing at ORNL

Cool-color pigments and sub-tile venting of clay and concrete tile roofs—achieved by direct nailing or attaching tile roofs to a deck with batten or batten and counter-batten construction—significantly impact the heat flow crossing the roof deck of a steep-sloped roof. The Tile Roofing Institute (TRI) and its affiliate members are keenly interested in documenting the magnitude of the drop in heat flow to obtain solar reflectance credits with state and federal cool roof building efficiency standards. To examine this issue, the Cool Team at ORNL installed S-Misson clay and concrete tile roofs, a medium-profile concrete tile roof, and a flat slate tile roof on fully instrumented attic test assemblies. The team recorded temperature measures of the roof, deck, attic, and ceiling, heat flows, solar reflectance, thermal emittance, and the ambient weather for each of the tile roofs and an adjacent attic cavity covered with a conventional pigmented and direct-nailed asphalt shingle roof. ORNL measured the tile's underside temperature and the bulk air temperature and heat flows just underneath the tile for batten and counter-batten tile systems and compared the results to the conventional asphalt shingle.

The team's measurements showed that the combination of improved solar reflectance afforded by cool pigmented colors and sub-tile venting reduced the peak heat flow crossing the roof deck at noontime for the clay tile roof (solar reflectance 0.54) by 70% compared to the flow crossing the conventional shingle roof (solar reflectance of 0.09). The slate and medium-profile concrete roofs, having nearly the same surface properties as the conventional shingle, reduced the deck heat flow ~45% compared to that crossing the shingle roof because of sub-tile venting. Opening the ridge vent of the attics to allow both attic and sub-tile ventilation caused more heat to be exhausted out the ridge for both the S-Mission clay (solar reflectance 0.54) and the slate tile (solar reflectance 0.13) systems and therefore further improved the performance of the two tile roofs. The effect was more pronounced for the slate tile than for the S-Mission tile because the slate tile has less air leakage between tiles.

Sub-tile venting and use of cool pigments reduce the summertime heat penetrating into the conditioned space; however, in the winter the air gap adds an additional radiation heat transfer resistance. Subsequently, the tile's thermal mass and sub-tile venting have limited the wintertime heat loss to about the same loss observed for the direct nailed asphalt shingle in East Tennessee's climate (Figure 20). Sub-tile venting therefore can lessen the heating penalty associated with cool roof products. The improved summer performance coupled with the reduced heat losses during the winter as compared to a shingle roof show that offset-mounting roofs can provide the roof industry the opportunity to market cool pigmented roofs in climates that are predominated more by heating loads. Typically, the monetary breakeven point for cool roofs occurs where the ratio (cooling degree days/heating degree dates [CDD/HDD])$_{65}$ is about 0.4; however, sub-tile venting can move this climatic boundary of affordable energy cost savings farther north.

A report summarizing and analyzing the experimental data is enclosed in Attachment 9.

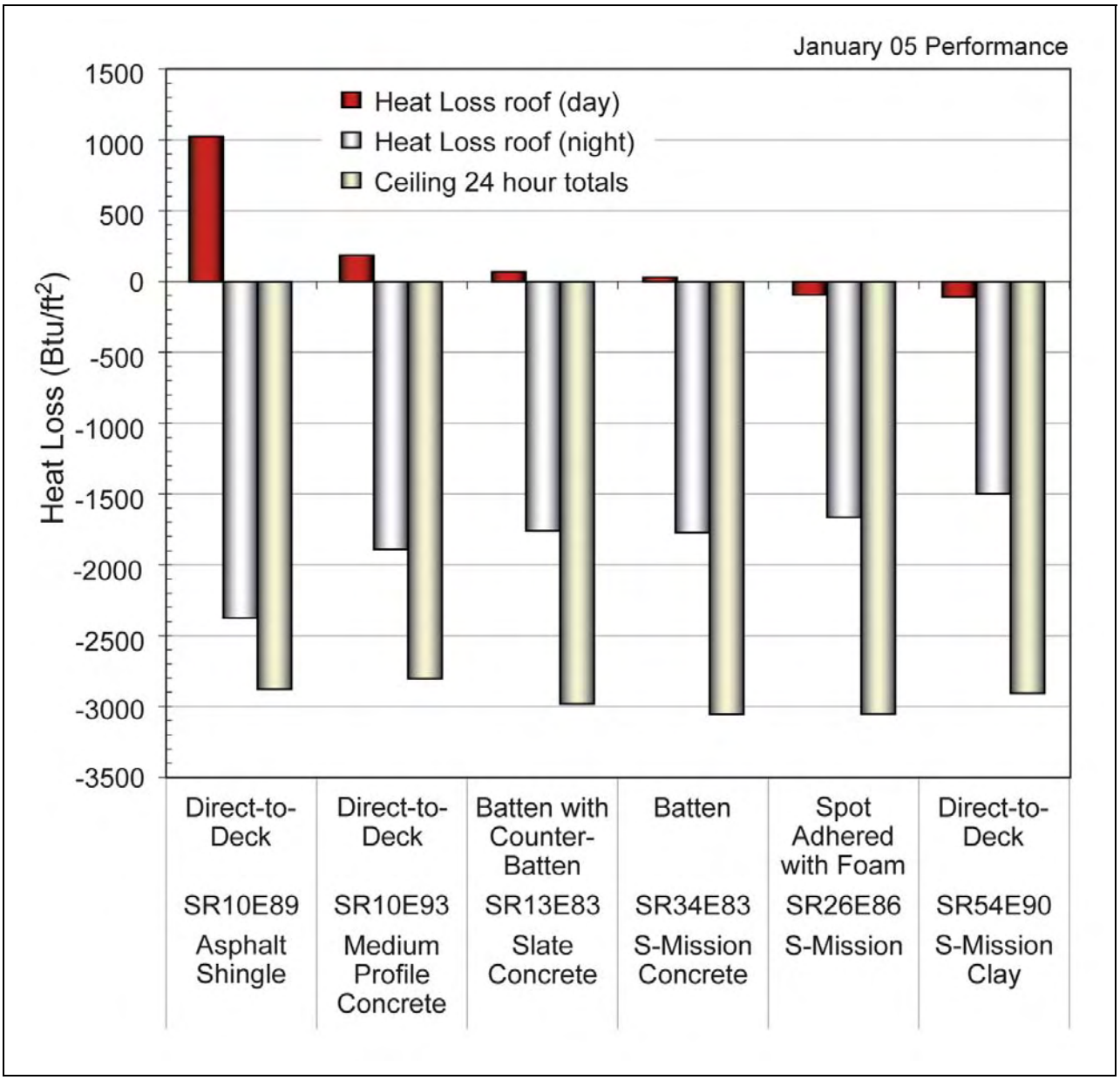

Figure 20. Integrated heat flow measured through the roof deck (heat loss to the sky during the day and during the night) and the attic floor (ceiling 24 hour total heat flow from conditioned space through ceiling into the attic) for all tile and shingle roofs field tested in East Tennessee during the month of January 2005. SR10E89 represents a solar reflectance of 0.10 and a thermal emittance of 0.89.

2.3.4. Task 2.6.4: Product useful life testing

In this task, the project team reviewed several aspects of the weathering of roofing materials. Degradation of materials initiated by ultraviolet radiation affects plastics used in roofing, as well as wood and asphalt. Elevated temperatures accelerate many deleterious chemical reactions and hasten diffusion of material components. Effects of moisture include decay of wood, acceleration of corrosion of metals, staining of clay, and freeze-thaw damage. Soiling of roofing materials causes objectionable stains and reduces the solar reflectance of reflective materials. (Soiling of non-reflective materials can also increase solar reflectance.) Soiling can be attributed to biological growth (e.g., cyanobacteria, fungi, algae), deposits of organic and mineral particles, and to the accumulation of fly ash, hydrocarbons, and soot from combustion. The Cool Team summarized the results of this work in a review article submitted to the journal *Construction and Building Materials*. A copy of the paper is enclosed **in** Attachment 10. Two specific examples illustrating weathering behavior are given below, taken from this paper.

Most of the ultraviolet-light-induced degradation mechanisms of polymeric roofing materials involve oxidation. That is, the absorption of an UV photon initiates material breakdown, but chemical combination with oxygen is also an essential step. Figure 21 shows how oxygen penetrates polypropylene during photo-oxidation, as evidenced by the carbonyl (C=O) group identified by spectroscopy. After 1200 hours of exposure, it's clear that oxygen has penetrated about 0.3 mm into this plastic. This oxygenated surface region becomes brittle and cracks (crazes). While this specific example utilizes polypropylene, similar behavior is seen in other organic building materials including asphalt, other plastics, and wood.

Ideally, roofing materials are engineered to be impervious to sunlight, moisture, and other elements of the weather. Thus, robust inorganic materials such as metal oxide pigments, minerals (such as the crushed stone for roofing granules), concrete, and clay are employed. Among organic materials, a few fluorinated polymers stand out as durable, and others, such as asphalt, can be used when an overlying ultraviolet-absorbing material provides UV protection. Wood is an example of an organic material that can even be used without a UV-absorbing overlayer. Wood does photo-oxidize, changes color, crazes, and is gradually eroded as it weathers. However, the rate of erosion of durable wood species, when kept dry, is very slow, so the lifetime is measured in decades. Figure 22 documents how the spectral reflectance of western red cedar roofing shingles changes as it ages. The color gradually becomes less red. It is interesting that the near-infrared reflectance of wood is larger than the visual (400 to 700 nm) reflectance; wood is naturally cool.

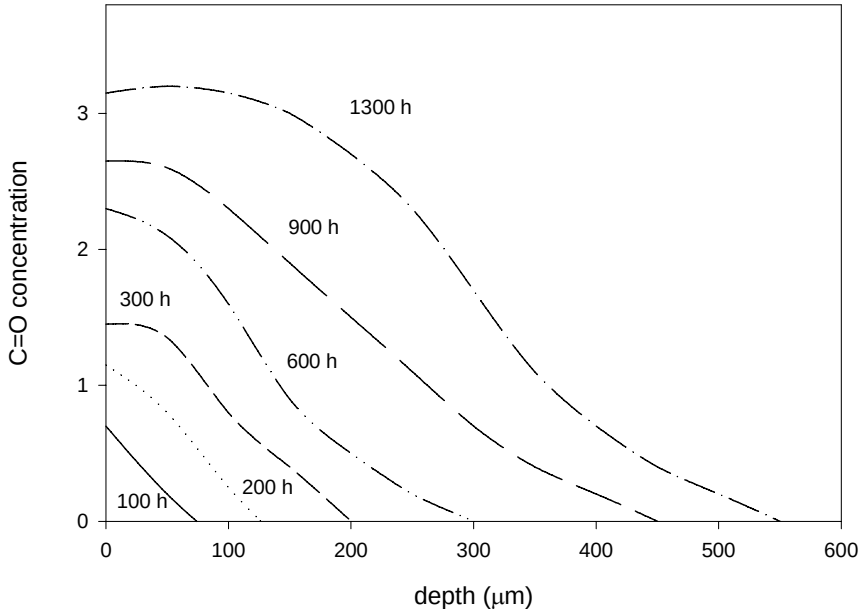

Figure 21. Oxidation (carbonyl) profiles measured during accelerated UV aging of polypropylene

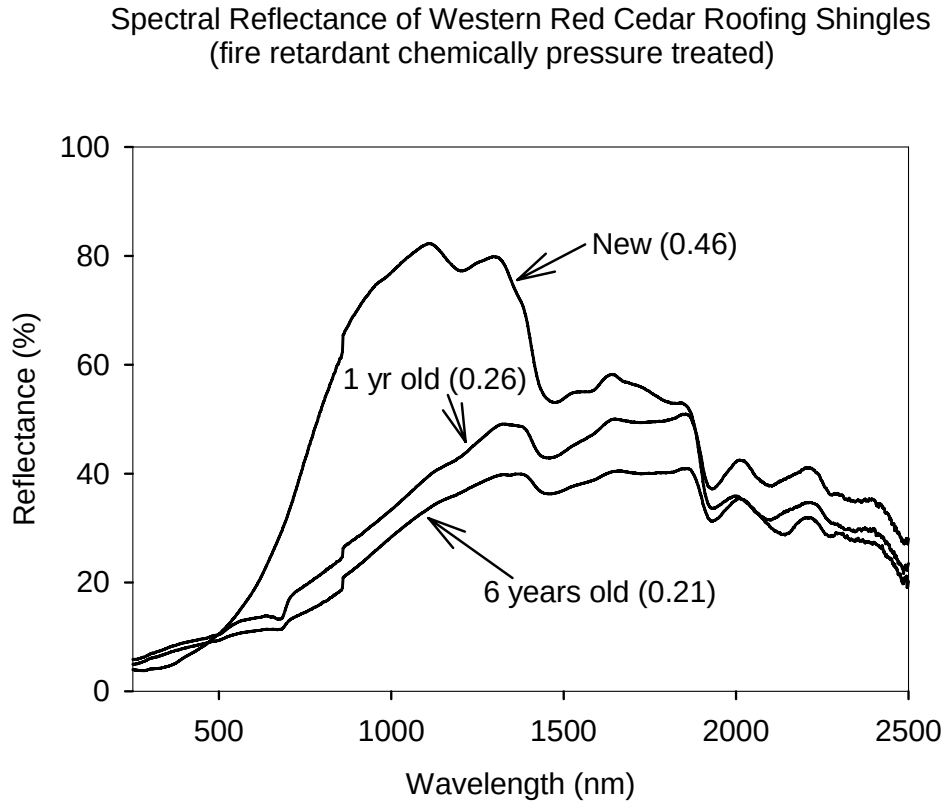

Figure 22. Spectral reflectance of new and weathered western red cedar roofing shingles. The solar reflectance is 0.46 when new and declines to 0.21 after 6 years exposure.

2.4. Task 2.7: Technology Transfer and Market Plan

LBNL, ORNL, color pigment manufacturers and granule manufacturers worked and supported the roofing manufacturers to penetrate the roofing market with new more reflective cool-colored roofing materials. The project team worked with roofing component manufacturers and color pigment manufacturers to introduce prototype cool-colored asphalt shingles, clay and concrete tiles, metal roofing, and wood shake roof products.

2.4.1. Task 2.7.1: Technology transfer

The objective of this task was to support the roofing industry by promoting and accelerating the market penetration of cool-color pigmented roof products. Both laboratories, in conjunction with their respective industry partners, presented research results at appropriate trade shows, and published their results in each industry's appropriate trade magazine. Table 4 below lists articles presented in various trade magazines, conferences, and journals; a copy of each publication can be found in Attachment 11 (or in an earlier attachment).

Table 4: Cool Team articles published or presented in industry magazines, conferences, and journals

Akbari, H. and A. Desjarlais. 2005. Cooling down the house: Residential roofing products soon will boast "cool"surfaces. *Professional Roofing*, March.
Akbari, H., R. Levinson, and P. Berdahl. 2005. A review of methods for the manufacture of residential roofing materials, Part I." *Western Roofing Insulation and Siding*. Jan/Feb, p. 54.
Akbari, H., R. Levinson, and P. Berdahl. 2005. A review of methods for the manufacture of residential roofing materials, Part II. *Western Roofing Insulation and Siding*. Mar/Apr, p. 52.
Akbari, H., R. Levinson, W. Miller, and P. Berdahl. 2005. Cool-colored roofs to save energy and improve air quality. *Proceedings of the 1st International Passive and Low Energy Cooling for the Built Environment*, *Palenc 2005, Vol 1*. pp. 89. 19-21 May, Santorini, Greece.
Akbari, H. 2005. Potentials of urban heat island mitigation. *Proceedings of the 1st International Passive and Low Energy Cooling for the Built Environment*, *Palenc 2005, Vol 1*. pp. 11. 19-21 May, Santorini, Greece.
Akbari, H., A.A. Berhe, R. Levinson, S. Graveline, K. Foley, A. Delgado, and R. Paroli. 2005. Aging and weathering of cool roofing membranes. Proceedings of *Cool Roofing … Cutting through the Glare.* Atlanta GA, May 12-13, RCI Foundation.
Akbari, H., P. Berdahl, R. Levinson, S. Wiel, A. Desjarlais, W. Miller, N. Jenkins, A. Rosenfeld, and C. Scruton. 2004. Cool-colored materials for roofs. *Proceedings of the 2004 ACEEE Summer Study on Energy Efficiency in Buildings, Vol. 1.* p. 1. Pacific Grove, CA.
Akbari, H., P. Berdahl, R. Levinson, S. Wiel, A. Desjarlais, W. Miller, N. Jenkins, A. Rosenfeld, and C. Scruton. 2004. Cool-colors: a roofing study is developing cool products for residential roofs, *Eco-Structure*. Sep/Oct, pp. 50-56.
Levinson, R., P. Berdahl, A.A. Berhe, and H. Akbari. 2005. Effects of soiling and cleaning on the reflectance and solar heat gain of a light-colored roofing membrane. *Atmospheric Environment*, **39**, 7807-7824.

Levinson, R., P. Berdahl, H. Akbari, W. Miller, I. Joedicke, J. Reilly, Y. Suzuki, and M. Vondran. 2005. Methods of creating solar-reflective nonwhite surfaces and their application to residential roofing materials. *Solar Energy Materials & Solar Cells* (in press).

Levinson, R., P. Berdahl, and H. Akbari. 2005. Solar spectral optical properties of pigments, part I: Model for deriving scattering and absorption coefficients from transmittance and reflectance measurements. *Solar Energy Materials & Solar Cells*. 89(4), 319-349.

Levinson, R., P. Berdahl, and H. Akbari. 2005. Solar spectral optical properties of pigments, part II: Survey of common colorants. *Solar Energy Materials & Solar Cells, Vol 89*. 4 pp. 351-389.

Levinson, R., P. Berdahl, and H. Akbari. 2005. Solar spectral optical properties of pigments. Proceedings of *Cool Roofing … Cutting through the Glare*. Atlanta GA, May 12-13, RCI Foundation.

Levinson, R., H. Akbari ,and J. Reilly. 2004. Cooler tile-roofed buildings with near-infrared-reflective nonwhite coatings. Accepted by *Building & Environment*.

Miller, W.A., W.M. MacDonald, A.O. Desjarlais, J.A. Atchley, M. Keyhani, R. Olson, and J. Vandewater. 2005. Experimental analysis of the natural convection effects observed within the closed cavity of tile roofs. Proceedings of *Cool Roofing … Cutting through the Glare*. Atlanta GA, May 12-13, RCI Foundation.

Miller, W. A., S. Kriner, and D.S.Parker. 2005. Cool metal roofing is topping the building envelope with energy efficiency and sustainability. Proceedings of *Cool Roofing … Cutting through the Glare*. Atlanta GA, May 12-13, RCI Foundation.

Miller, W. A., A.O. Desjarlais, H. Akbari, R. Levinson, P. Berdahl, and R.G. Scichili. 2004. Special IR reflective pigments make a dark roof reflect almost like a white roof. *Thermal Performance of the Exterior Envelopes of Buildings*, *IX*, proceedings of ASHRAE THERM IX. Clearwater, FL., Dec.

Miller, W. A., A.O. Desjarlais, D.S. Parker, and S. Kriner. 2004. Cool metal roofing tested for energy efficiency and sustainability, *International Conference on Building Envelope Systems and Technologies (ICBEST)*, proceedings of National Research Council Canada. Toronto Canada, May 2-7.

Miller, W.A., K.T. Loye, A.O. Desjarlais, and R.P. Blonski, 2003. PVDF coatings with special IR reflective pigments. *Fluorine in Coatings V*, proceedings of Paint Research Association. Orlando, FL., Jan.

Miller, W.A., K.T. Loye, A.O. Desjarlais, and R.P. Blonski. 2002. Cool-color roofs with complex inorganic color pigments. *ACEEE Summer Study on Energy Efficiency in Buildings,* proceedings of American Council for an Energy Efficient Economy. Asilomar Conference Center in Pacific Grove, CA., Aug.

2.4.2. Task 2.7.2: Market plan

The objective of this subtask was to develop and initiate actions to facilitate the market adoption of cool-pigmented reflective roofing products.

The Energy Commission through this project has dramatically advanced the technology of nonwhite cool roofs that help save energy by exploiting complex inorganic paint pigments to

boost the solar reflectance of clay and concrete tile, painted metal, and asphalt shingle roofing. The project has successfully developed several nonwhite cool-colored roof products for sloped roofs over the past three years and has shown positive energy savings in residential field tests demonstrating pairs of homes roofed in concrete tile, painted metal and asphalt shingles with and without cool pigmented materials. Without further efforts, the accomplishments achieved by the Energy Commission in its Cool Roofs PIER project will creep into the marketplace over the next several decades, slowly bringing the significant energy, cost, smog and carbon savings that the technology promises.

Near the end of the project, the team's 16 industrial partners discussed their needs to further develop and successfully market their residential cool roofing products. Their recommendations and requests, summarized in Table 5, include the following points.

- First and foremost, residential cool roofs need to be credited and recommended in California's Title 24 standards that primarily determine what products are used in the construction of new houses and major remodels.
- More cool materials for all residential (and commercial) sloped roofing systems must be available and appropriately labeled.
- Appropriate labels on roofing products must be universally applied.
- Architects, designers, builders, roofing material distributors and retailers, and consumers need to learn of the availability and benefits of using cool roofing materials.
- California's utilities and government can further influence the selection of cool roofs through innovative incentive and rebate programs to accelerate their market penetration.
- Market penetration can be accelerated by enhancing the credibility of retailer and utility marketing claims through large-scale demonstrations of cool roofs to consumers, developers, designers, and roofing contractors.

In collaboration with the roofing industry partners, the Cool Team prepared a market plan that outlines industry/national labs collaborative efforts to help the CEC in deploying cool-colored roofing. The plan focuses on six parallel initiatives: (1) regulate; (2) increase product selection; (3) label; (4) educate; (5) provide incentives; and (6) demonstrate performance. This market plan is enclosed in Attachment 12.

Table 5. Industry needs to successfully market their cool roof products

Assistance requested in marketing cool roofs	Industry partner requesting assistance
Continuing education for design build firms, architects, utility consumers, construction professionals, and homeowners integrated into seminars offered by the California Association of Building Energy Consultants (CABEC)	Steelscape, BASF, Custom-Bilt, Shepherd
Software to estimate the cooling energy savings and peak demand reduction achieved by installing cool roofs on specific buildings	Steelscape, BASF, Custom-Bilt, Ferro, Elk, ARC
Monitoring of solar reflectance and color change of the materials installed at the California weathering sites	Steelscape, BASF, Custom-Bilt, ISP, Ferro, Elk, ARC
Monitoring of solar reflectance, color change, and thermal performance of materials at ORNL test facilities and the Sacramento test homes	Steelscape, BASF, Custom-Bilt, ISP, Elk, Ferro, ARC
Expansion of the cool coating database	Steelscape, BASF, Custom-Bilt, ISP, Ferro, Shepherd, 3M
Large-scale demonstration of cool roofs	Steelscape, BASF, Custom-Bilt, ISP, Ferro, Elk, ARC
Predictive software for designing cool coatings	Steelscape, BASF, Custom-Bilt, ISP, Ferro, 3M
Research to increase roof material reflectivity and reduce costs	ISP, Ferro, Elk, 3M, Shepherd, ARC
Tools to accurately measure roofing material solar reflectance	ISP, Elk, 3M, ARC
Calculations of weathering benefits of cool roofing	ISP
Identification of new materials and techniques	ISP, Ferro, 3M
Determination of the relationship between granule and ultimate shingle reflectances	3M
Acceleration of cool roof rating criteria by the Cool Roof Rating Council (CRRC) and ENERGY STAR	3M

2.4.3. Task 2.7.3: Title 24 code revisions

The objective of this task was to prepare a preliminary document of energy and peak demand savings for installing cool roofs in various California climates. This data can be further developed to prepare a proposal for updating the Title 24 building energy code to include cool-colored roofing materials.

To estimate the energy savings of cool-colored roofing materials, the project team calculated the annual cooling energy use of a prototypical house for all 16 California climate zones. The team used a simplified model that correlates the cool energy savings to annual cooling degree days (base 18°C ≈ 65°F) (CDD18). The model is developed by regression of simulated cooling energy use against CDD18. The Cool Team performed parametric analysis and simulated the cooling and heating energy use of a prototypical house with varying level of roof insulation (R-0, R-1, R-3, R-5, R-7, R-11, R-19, R-30, R-38, and R-49) and roof reflectance (0.05, 0.1, 0.2, 0.4, 0.6, and 0.8) in more than 250 climate regions, using the DOE-2 building energy use simulation program. For each prototypical analysis, the parametric analysis led to 15,000 DOE-2 simulations. Then the resulting cooling and heating energy use was correlated to CDD18.

The prototypical house used in these calculations is assumed to have roofing insulation of 0.88 to 5.3 m^2K/W (R-5 to R-30 insulation). The estimates of savings are for an increase in roof solar reflectance by about 0.2 (change of the roof reflectance from 0.1 to 0.3 for shingles; change of the roof reflectance from 0.2 to 0.4 for clay and concrete tiles). These calculations present the variation in energy savings in 16 California climate zones. This document only reports cooling energy savings and does not account for potential wintertime heating energy penalties. Tables 6 and 7 below show potential cooling energy savings in kWh per year for a house with $100m^2$ of roof area for stock of pre-1980 and post-1980 houses, respectively. The savings can be linearly adjusted for houses with larger or smaller roof areas. For most California climates, the application of cool-colored roof yields net savings in the range of 100–600 kWh per 100 m^2 per year. The savings are obviously smaller for buildings with higher roof insulation. For houses that are not air conditioned, cool-colored roofing materials offer comfort, typically at very reasonable costs.

Attachment 13 contains the technical document discussing the potential energy savings in a greater detail.

Table 6. Estimates of annual cooling electricity savings (kWh) and heating energy penalties (therms) from installing cool-colored roofs on pre-1980 single-family detached homes with gas furnace heating systems. All savings and penalties are per 100 m^2 of roof area. Solar reflectance change is 0.2 (shingle roof reflectance change is from 0.1 to 0.3; clay and concrete tiles roof reflectance change is from 0.2 to 0.4). The savings and penalties can be linearly adjusted for other values of changes in solar reflectance.

Roof Insulation	R-5		R-7		R-11		R-19		R-30	
Climate Zone	Cooling (kWh)	Heating (therms)	Cooling (kWh)	Heating (therms)	Cooling (kWh)	Heating (therms)	Cooling (kWh)	Heating (therms)	Cooling (kWh)	Heating (therms)
CTZ1	110	-11	90	-9	67	-7	47	-5	35	-5
CTZ2	172	-9	149	-7	120	-6	93	-4	76	-3
CTZ3	117	-8	97	-6	73	-5	52	-4	39	-3
CTZ4	155	-7	133	-6	106	-5	80	-3	65	-3
CTZ5	116	-8	96	-6	73	-5	51	-3	39	-3
CTZ6	160	-5	137	-4	110	-3	84	-2	68	-2
CTZ7	181	-5	157	-4	127	-3	99	-2	82	-1
CTZ8	214	-5	188	-4	156	-3	124	-2	104	-1
CTZ9	244	-5	215	-4	180	-3	146	-2	124	-1
CTZ10	286	-6	255	-5	216	-3	177	-2	152	-2
CTZ11	292	-8	260	-7	221	-5	182	-4	156	-3
CTZ12	223	-8	196	-7	162	-5	130	-4	110	-3
CTZ13	372	-7	336	-6	289	-4	241	-3	209	-2
CTZ14	350	-9	315	-7	270	-6	225	-4	195	-3
CTZ15	646	-4	593	-3	521	-2	445	-1	393	-1
CTZ16	148	-14	126	-12	99	-10	75	-8	60	-6

Table 7. Estimates of annual cooling electricity savings (kWh) and heating energy penalties (therms) from installing cool-colored roofs on post-1980 single-family detached homes with gas furnace heating systems. All savings and penalties are per 100 m^2 of roof area. Solar reflectance change is 0.2 (shingle roof reflectance change is from 0.1 to 0.3; clay and concrete tiles roof reflectance change is from 0.2 to 0.4). The savings and penalties can be linearly adjusted for other values of changes in solar reflectance.

Roof Insulation	R-11		R-19		R-30		R-38		R-49	
Climate Zone	Cooling (kWh)	Heating (therms)	Cooling (kWh)	Heating (therms)	Cooling (kWh)	Heating (therms)	Cooling (kWh)	Heating (therms)	Cooling (kWh)	Heating (therms)
CTZ1	43	-4	29	-3	21	-2	18	-2	15	-2
CTZ2	73	-3	54	-2	42	-2	38	-2	34	-1
CTZ3	46	-3	32	-2	23	-1	20	-1	17	-1
CTZ4	65	-3	47	-2	36	-1	33	-1	29	-1
CTZ5	46	-3	32	-2	23	-1	20	-1	17	-1
CTZ6	67	-2	49	-1	38	-1	34	-1	30	0
CTZ7	77	-2	58	-1	45	-1	41	0	37	0
CTZ8	93	-2	71	-1	57	-1	51	-1	47	0
CTZ9	107	-2	83	-1	67	-1	61	0	55	0
CTZ10	127	-2	100	-1	81	-1	74	-1	68	-1
CTZ11	130	-3	102	-2	83	-1	76	-1	70	-1
CTZ12	97	-3	74	-2	59	-1	54	-1	49	-1
CTZ13	168	-2	134	-2	111	-1	102	-1	94	-1
CTZ14	158	-3	125	-2	103	-2	95	-1	87	-1
CTZ15	300	-1	244	-1	206	0	190	0	176	0
CTZ16	61	-6	44	-4	34	-3	30	-3	27	-3

3.0 Conclusions and Recommendations

Raising roof reflectivity from an existing 0.10 (conventional dark roof) to about 0.35 (cool dark roof) can reduce cooling energy use in buildings by more than 10%. Cool roofs also result in a lower ambient temperature that further decreases the need for air conditioning and retards smog formation. In 2002, suitable cool *white* materials were available for most roof products, with the notable exception of asphalt shingles; cooler *colored* materials are needed for all types of roofing. To help to fill this gap, the California Energy Commission engaged LBNL and ORNL to work on a three-year project with the roofing industry to develop and produce reflective, colored roofing products. The intended outcome of this project was to make cool-colored roofing materials a market reality within three to five years. For residential shingles, the project team has developed prototype colored-shingles with solar reflectances of up to 0.35. One manufacturer currently markets colored shingles with the ENERGY STAR qualifying solar reflectance of 0.25. Colored metal and clay tile roofing materials with solar reflectances of 0.30 to 0.60 are currently available in the California market.

LBNL and ORNL performed research and development in conjunction with pigment manufacturers and worked with roofing materials manufacturers to reduce the sunlit temperatures of nonwhite asphalt shingles, clay tiles, concrete tiles, metal products, and wood shakes. A significant portion of the effort was devoted to identification and characterization of pigments to include and exclude in cool coating systems, and to the development of engineering methods for effective and economic incorporation of cool pigments in roofing materials. The project also measured and documented the laboratory and in-situ performances of roofing products. The Cool Team also established and monitored three pairs of demonstration homes to measure and showcase the energy-saving benefits of cool roofs. In collaboration with the Energy Commission, the Cool Team convened a Project Advisory Committee, composed of 15 to 20 diverse professionals, to provide strategic guidance to the project.

In order to determine how to optimize the solar reflectance of a pigmented coating matching a particular color, and how the performance of cool-colored roofing products compares to that of a standard material, the project team (1) measured and characterized the optical properties of many standard and innovative pigmentation materials; (2) developed a computer model to maximize the solar reflectance of roofing materials for a choice of visible colors; and (3) created a database of characteristics of cool pigments.

In order to help manufacturers design innovative methods to produce cool-colored roofing materials, the team (1) compiled information on roofing materials manufacturing methods; (2) worked with roofing manufacturers to design innovative production methods for cool-colored materials; and (3) tested the performance of materials in weather-testing facilities.

One of the project objectives was to demonstrate, measure, and document the building energy savings, improved durability, and sustainability attained by use of cool-colored roof materials for key stakeholders (consumers, roofing manufacturers, roofing contractors, and retail home improvement centers). In order to do this, the team (1) monitored buildings at California demonstration sites to measure and document the energy savings of cool-colored roof materials; (2) conducted materials testing at weathering farms in California; (3) conducted thermal testing

at the ORNL Steep-slope Assembly Testing Facility; and (4) performed a detailed study to investigate the effect of solar reflectance on product useful life.

The Cool Team also developed partnerships with various members of the roofing industry. The Cool Team worked through the trade associations to communicate and advertise to their membership new cool-color roof technology and products. This collaboration induced the manufacturers to develop a market plan for California and to provide technical input and support for this activity. Through the industry partners, many California housing developers and contractors have been convinced to install the new cool-colored roofing products.

Re-roofing houses with cool products when roofs are due for replacement and specifying cool roofs in new construction are economically sensible ways to significantly increase energy efficiency. The small price premium of cool roofs is paid back in air conditioning savings within a few years. When a sufficiently large number of home and commercial building owners adopt cool roofs regionally, earlier modeling and field experiments show that urban air temperatures decrease, slowing the rate of smog formation. This improves public health and helps cities meet federally mandated clean air requirements. Finally, cool roofs decrease peak electrical demand on hot summer afternoons, reducing strain on the electrical grid and helping to avoid blackouts and brownouts.

If applied to cars, cool-color technology could improve fuel economy by allowing manufacturers to downsize air conditioning units. These savings could help further reduce greenhouse gas emissions and enhance U.S. energy security by reducing reliance on imported petroleum. For all of these reasons, cool colors on roofs and in other applications have tremendous potential to contribute to the solution of major global problems within a short time, at a reasonable cost.

3.1. Recommendations

The Energy Commission has dramatically advanced the technology of nonwhite cool roofs that exploit cool pigments to boost the solar reflectance of clay tile, concrete tile, painted metal, and shingle roofing. The project has successfully developed several nonwhite cool-colored roof products for sloped roofs over the past three and a half years and has shown positive energy savings in residential field tests demonstrating pairs of homes roofed in concrete tile, painted metal, and asphalt shingles with and without cool pigmented materials. Without further efforts, the accomplishments achieved by the Energy Commission in this project will creep into the marketplace over the next several decades, slowly bringing the significant energy, cost, smog and carbon savings that the technology promises.

The team recommends the following step to rapidly accelerate the uptake of cool roofing materials:

- First and foremost, residential cool roofs need to be credited and recommended in California's Title 24 standards, which primarily determine what products are used in the construction of new houses and major remodels.
- More cool materials for all residential (and commercial) sloped roofing systems must be available and appropriately labeled.
- The cool roofing pigment database should be maintained and expanded with new materials in help the industry develop new and advanced materials at competitive prices.

- The aging and weathering of cool roofing materials and their effects on the useful life of roofs need to be further studied.
- Appropriate labels on roofing products must be universally applied.
- Architects, designers, builders, roofing material distributors and retailers, and consumers need to learn of the availability and benefits of using cool roofing materials.
- California's utilities and government can further influence the selection of cool roofs through innovative incentive and rebate programs to accelerate their market penetration.
- For utilities to develop incentive programs and for manufacturers to coordinate their materials development with their marketing efforts, they need to have an industry-consensus calculator to accurately estimate energy and peak demand of cool-colored roofs. The calculator should account for both the cooling energy savings and potential heating energy penalties of cool roofs.
- Finally, market penetration can be accelerated by enhancing the credibility of retailer and utility marketing claims through large-scale demonstrations of cool roofs to consumers, developers, designers, and roofing contractors.

4.0 References

Akbari. H, P. Berdahl, R. Levinson, S. Wiel, A. Desjarlais, W. Miller, N. Jenkins, A. Rosenfeld, and C. Scruton. 2004. "Cool-colored materials for roofs." *Proceedings of the 2004 ACEEE Summer Study on Energy Efficiency in Buildings, Vol. 1.* p. 1. Pacific Grove, CA.

Akbari, H., S. Konopacki, and M. Pomerantz. 1999. "Cooling energy savings potential of reflective roofs for residential and commercial buildings in the United States." *Energy.* 24, 391-407.

Akbari, H., S. Bretz, H. Taha, D. Kurn, and J. Hanford. 1997. "Peak power and cooling energy savings of high-albedo roofs." *Energy and Buildings – Special Issue on Urban Heat Islands and Cool Communities*. 25(2), 117–126.

F.W. Dodge. 2005. *Construction Outlook Forecast*. F.W. Dodge Market Analysis Group, 24 Hartwell Avenue, Lexington, MA 02421.

F.W. Dodge. 2003. *Construction Outlook Forecast*. F.W. Dodge Market Analysis Group, 24 Hartwell Avenue, Lexington, MA 02421.

Konopacki, S. and H. Akbari. 2001. *Measured energy savings and demand reduction from a reflective roof membrane on a large retail store in Austin*. Lawrence Berkeley National Laboratory Report No. LBNL-47149. Berkeley, CA.

Konopacki, S., L. Gartland, H. Akbari, and L. Rainer. 1998. *Demonstration of energy savings of cool roofs.* Lawrence Berkeley National Laboratory Report No. LBNL-40673. Berkeley, CA.

Konopacki, S., H. Akbari, M. Pomerantz, S. Gabersek, and L. Gartland. 1997. *Cooling energy savings potential of light-colored roofs for residential and commercial buildings in 11 U.S. metropolitan areas.* Lawrence Berkeley National Laboratory Technical Report LBNL-39433. Berkeley, CA.

Levinson, R., H. Akbari, S. Konopacki, and S. Bretz. 2005a. "Inclusion of cool roofs in nonresidential Title 24 prescriptive requirements." *Energy Policy*. 33(2): 151-170.

Levinson, R., P. Berdahl, and H. Akbari. 2005b. "Spectral solar optical properties of pigments part I: Model for deriving scattering and absorption coefficients from transmittance and reflectance measurements." *Solar Energy Materials & Solar Cells.* 89(4), 319-349.

Levinson, R., P. Berdahl, and H. Akbari. 2005c. "Spectral solar optical properties of pigments, part II: Survey of common colorants." *Solar Energy Materials & Solar Cells.* 89(4), 351-389.

Parker, D.S., J.K. Sonne, and J.R. Sherwin. 2002. "Comparative evaluation of the impact of roofing systems on residential cooling energy demand in Florida." *Proceedings of the 2002 ACEEE Summer Study on Energy Efficiency in Buildings, Vol. 1.* p. 219. Pacific Grove, CA.

Rosenfeld, A.H., J.J. Romm, H. Akbari, and M. Pomerantz. 1998. "Cool communities: strategies for heat islands mitigation and smog reduction." *Energy and Buildings*. 28(1), 51–62.

Western Roofing. 2005. Online at http://WesternRoofing.net .

5.0 List of Attachments

Attachment Name	Publication Number
Attachment 1: Task 2.4.1 Reports: : Identify and Characterize Pigments with High Solar Reflectance	CEC-500-2006-067-AT1
Attachment 2: Task 2.4.2 Reports: Develop a Computer Program for Optimal Design of Cool Coatings	CEC-500-2006-067-AT2
Attachment 3: Task 2.4.3 Reports: Develop a Database of Cool-Colored Pigments	CEC-500-2006-067-AT3
Attachment 4: Task 2.5.1 Reports: Review of Roofing Materials Manufacturing Methods	CEC-500-2006-067-AT4
Attachment 5: Task 2.5.2 Reports: Design Innovative Methods for Application of Cool Coatings to Roofing Materials	CEC-500-2006-067-AT5
Attachment 6: Task 2.5.3 Reports: Accelerated Weathering Testing	CEC-500-2006-067-AT6
Attachment 7: Task 2.6.1 Reports: Building Energy-Use Measurements at California Demonstration Sites	CEC-500-2006-067-AT7
Attachment 8: Task 2.6.2 Reports: Materials Testing at Weathering Farms in California	CEC-500-2006-067-AT8
Attachment 9: Task 2.6.3 Reports: Steep-slope Assembly Testing at ORNL	CEC-500-2006-067-AT9
Attachment 10: Task 2.6.4 Reports: Product Useful Life Testing	CEC-500-2006-067-AT10
Attachment 11: Task 2.7.1 Reports: Technology Transfer	v CEC-500-2006-067-AT11
Attachment 12: Task 2.7.2 Reports: Market Plan	CEC-500-2006-067-AT12
Attachment 13: Task 2.7.3 Reports: Title 24 Code Revisions	CEC-500-2006-067-AT13

Arnold Schwarzenegger
Governor

COOL-COLOR ROOFING MATERIAL ATTACHMENT 1: TASK 2.4.1 REPORTS – IDENTIFY AND CHARACTERIZE PIGMENTS WITH HIGH SOLAR REFLECTANCE

PIER FINAL PROJECT REPORT

Prepared For:
California Energy Commission
Public Interest Energy Research Program

Prepared By:
Lawrence Berkeley National Laboratory
and Oak Ridge National Laboratory

ERNEST ORLANDO LAWRENCE
BERKELEY NATIONAL LABORATORY

June 2006
CEC-500-2006-067-AT1

Prepared By:
Lawrence Berkeley National Laboratory
Hashem Akbari
City, State
Contract No. 500-01-021
Work Authorization (if applicable)

Oak Ridge National Laboratory
William Miller
Oak Ridge, Tennessee

Prepared For:

California Energy Commission

Public Interest Energy Research (PIER) Program

Chris Scruton
Contract Manager

Ann Peterson
Building End-Use Energy Efficiency Program Team Leader

Nancy Jenkins
PIER Energy Efficiency Research Office Manager

Martha Krebs, Ph. D.
Deputy Director
ENERGY RESEARCH AND DEVELOPMENT DIVISION

B.B. Blevins
Executive Director

DISCLAIMER

This report was prepared as the result of work sponsored by the California Energy Commission. It does not necessarily represent the views of the Energy Commission, its employees or the State of California. The Energy Commission, the State of California, its employees, contractors and subcontractors make no warrant, express or implied, and assume no legal liability for the information in this report; nor does any party represent that the uses of this information will not infringe upon privately owned rights. This report has not been approved or disapproved by the California Energy Commission nor has the California Energy Commission passed upon the accuracy or adequacy of the information in this report.

Available online at www.sciencedirect.com
SCIENCE DIRECT®
Solar Energy Materials & Solar Cells
ELSEVIER
Solar Energy Materials & Solar Cells 89 (2005) 319–349
www.elsevier.com/locate/solmat

Solar spectral optical properties of pigments—Part I: model for deriving scattering and absorption coefficients from transmittance and reflectance measurements

Ronnen Levinson*, Paul Berdahl, Hashem Akbari

Lawrence Berkeley National Laboratory, 1 Cyclotron Road, Berkeley, CA 94720, USA

Received 15 June 2004; received in revised form 5 November 2004; accepted 12 November 2004
Available online 24 February 2005

Abstract

The suitability of a pigment for inclusion in "cool" colored coatings with high solar reflectance can be determined from its solar spectral backscattering and absorption coefficients. Pigment characterization is performed by dispersing the pigment into a transparent film, then measuring spectral transmittance and reflectance. Measurements of the reflectance of film samples on black and white substrates are also used. A model for extracting the spectral backscattering coefficient S and absorption coefficient K from spectrometer measurements is presented. Interface reflectances complicate the model. The film's diffuse reflectance and transmittance measurements are used to determine S and K as functions of a wavelength-independent model parameter σ that represents the ratio of forward to total scattering. σ is used to estimate the rate at which incident collimated light becomes diffuse, and is determined by fitting the measured film reflectance backed by black. A typical value is $\sigma = 0.8$. Then, the measured film reflectance backed by white is compared with a

*Corresponding author. Tel.: +1 510 486 7494; fax: +1 425 955 1992.
E-mail addresses: RMLevinson@LBL.gov (R. Levinson), PHBerdahl@LBL.gov (P. Berdahl), H_Akbari@LBL.gov (H. Akbari).

0927-0248/$ - see front matter Published by Elsevier B.V.
doi:10.1016/j.solmat.2004.11.012

Nomenclature

English symbols

a	defined as $(S+K)/S$
b	defined as $(a^2-1)^{1/2}$
f	film
g	background
i	intensity of total downflux
i_c	intensity of collimated downflux (incident direction is downward)
i_d	intensity of diffuse downflux
j	intensity of total upflux
j_c	intensity of collimated upflux
j_d	intensity of diffuse upflux
K	absorption coefficient
m	relative refractive index or wavelength index
M	total number of wavelengths
n	refractive index
N	observed near-infrared reflectance
q	fraction of total flux that is diffuse
R	reflectance
$\tilde{R}_c$	observed reflectance of collimated light
R_f	CRI (continuous refractive index) reflectance of film (absent interface reflectances)
$\tilde{R}_f$	observed reflectance of film
$R_{f,\ell}$	CRI reflectance of film with background ℓ
$\tilde{R}_{f,\ell}$	observed reflectance of film with background ℓ = b (black), w (white), or v (void)
R_g	CRI reflectance of background
$\tilde{R}_g$	observed reflectance of background
$R_{g,\ell}$	CRI reflectance of background ℓ
$\tilde{R}_{g,\ell}$	observed reflectance of background ℓ
R^i	reflectance to downflux
R^j	reflectance to upflux
R_u	CRI reflectance of opaque undercoat
$\tilde{R}_u$	observed reflectance of opaque undercoat
$R^\star$	intermediate value used in computation of reflectance of complex backgrounds
S	backscattering coefficient (scattering into opposite hemisphere)
T	internal transmittance
$\tilde{T}$	observed transmittance
T^i	downflux transmittance
T^j	upflux transmittance
$\tilde{T}_c$	observed collimated flux transmittance
z	distance from bottom of film

Greek symbols

α, β, γ	components of multi-layer system
δ	film thickness
Δ	error in intensity gradient or reflectance
ε	global error in predicted reflectance
η	average pathlength parameter
λ	wavelength (in vacuum)
μ	maximum absolute error in predicted reflectance
ρ	density
σ	forward scattering ratio (fraction of scattered light directed into forward hemisphere)
τ	internal film transmittance
τ_c	internal film collimated transmittance
χ	root-mean-square error in predicted reflectance
ω	reflectance at interface of media with different refractive indices
ω^i	reflectance of interface to downflux
ω^j	reflectance of interface to upflux
ω_c^i	reflectance of interface to collimated downflux
ω_c^j	reflectance of interface to collimated upflux

computed value as a self-consistency check. Measurements on several common pigments are used to illustrate the method.
Published by Elsevier B.V.

Keywords: Pigment characterization; Solar spectral optical properties; Kubelka-Munk theory; Refractive-index discontinuity; Cool roofs

1. Introduction

Nonwhite pigments with high near-infrared (NIR) reflectance historically have been used to camouflage military surfaces (by mimicking foliage) and to minimize solar heating of dark exterior architectural surfaces, such as colored vinyl siding and gray battleship hulls [1–3]. In recent years roofing manufacturers have incorporated NIR-reflecting pigments in coatings applied to a variety of nonwhite roofing products, such as metal panels and clay tiles [4–9]. The work we present here develops and validates a model for computation of solar spectral absorption and backscattering coefficients (current article), which is then applied to wide variety of pigments that may be used in architectural coatings (companion article, [10]).

Visible light (400–700 nm) accounts for only 43% of the energy in the air-mass 1.5 global solar irradiance spectrum (300–2500 nm) typical of North-American insolation [11]; the remainder arrives as near-infrared (700–2500 nm, 52%) or ultraviolet (300–400 nm, 5%) radiation (Fig. 1). Hence, replacing NIR-absorbing (“conventional”) roofing with visually similar, NIR–reflecting (“cool”) roofing can significantly reduce building heat gain. A recent study found that increasing the solar

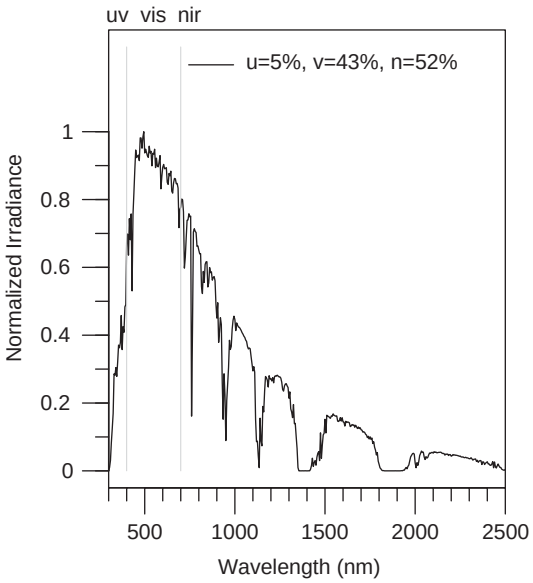

Fig. 1. Air mass 1.5 hemispherical solar spectral irradiance typical of North American insolation (5% ultraviolet, 43% visible, 52% near-infrared) [11].

reflectance of the roof of a prototypical California nonresidential building from 0.20 (conventional medium gray) to 0.55 (soiled white) yields statewide average annual source energy savings per unit roof area of 30 MJ/m^2; peak power demand savings of 2.1 W/m^2; and cost savings (15-year net present value of energy, plus savings achieved by downsizing cooling equipment) of \$6/m^2 [12,13]. A *cool* medium-gray roof with an initial near-infrared reflectance of 0.80 might have a weathered solar reflectance of about 0.42 [12,14]. Since energy, power, and cost savings are approximately proportional to change in weathered solar reflectance [15], using this cool medium-gray roof (weathered solar reflectance 0.42) in place of a standard medium gray roof (weathered solar reflectance 0.20) would yield about 60% of the white-roof savings, or 18 MJ/m^2 source energy, 1.3 W/m^2 peak power, and \$3.5/m^2 energy and equipment cost. Installing such cool colored roofing on nonresidential new construction in California could yield annual statewide savings of 84 TJ source energy, 5.5 MW peak power, and \$17 M energy and equipment cost.

A cool coating must have low visible transmittance to hide its background and low NIR absorptance to minimize NIR heat gain. Cool films may be subclassified as either "NIR-reflecting" or "NIR-transmitting." An NIR-reflecting film is always cool, while an NIR-transmitting film requires an NIR-reflecting background (e.g., a shiny metal or a white coating) to form a colored NIR-reflecting composite [1,16].

A paint is a dispersion of pigment particles (e.g., titania) in a clear binder, such as acrylic. The propagation of light through pigmented coatings is of natural interest to the coating and colorant industries, and has been extensively studied over the past century. The optical properties of a freely suspended film (i.e., reflectance,

transmittance, and absorptance) depend on (a) the real and imaginary refractive indices of the pigment and the binder; (b) the size, shape, and concentration of the pigment particles; and (c) the thickness of the film. These optical properties may be determined either *microscopically* or *macroscopically*.

The microscopic approach applies the principles of electromagnetism to analyze the interaction of light with pigment particles, including interparticle effects (i.e., multiple scattering). Mie theory [17] applies well to spherical pigment particles separated by distances large compared to the light wavelength, but is less useful when particles are closely packed or exhibit either geometric or electromagnetic anisotropy. Knowledge of the detailed scattering cross sections of the pigment particles is useful but not sufficient for the simulation for the reflectance of paint-type coatings [18,19]. Most practical colored coatings contain strongly scattering pigments and/or have strongly scattering substrates, making it essential to include multiple scattering effects from the outset. Furthermore, the pigment particles are often close enough together to make the scattering by neighboring particles electromagnetically interdependent [20].

The macroscopic approach treats the coating as a continuous medium with bulk abilities to absorb and scatter light. One of the simplest and most popular continuum models is the two-flux theory introduced by Schuster in 1905 [21] and popularized by Kubelka and Munk [22–26]. The Kubelka–Munk (K–M) model describes the one-dimensional, bidirectional propagation of diffuse light through a film by parameterizing the rates at which the film absorbs and/or backscatters light. Details of the angular dependence of the radiative transfer are neglected, as are polarization effects. Only two spectral optical measurements (reflectances over two different backgrounds, or one reflectance and one transmittance) are needed to compute the two parameters (spectral absorption and backscattering per unit length) that predict the spectral reflectance and spectral transmittance of a coating of arbitrary thickness and background. The utility of this model is limited by its assumption that light is diffuse throughout the film, which fails when a weakly-scattering film is illuminated by collimated light from a spectrometer or the sun.

More sophisticated models track both diffuse and collimated fluxes. Three-flux models [27] track two diffuse fluxes and one collimated flux, while four-flux models [28,29] track two diffuse and two collimated beams. Compared to the K–M model, three- and four-flux theories require additional spectral measurements and spectral parameters, and yield significantly more complex expressions for film reflectance and transmittance. However, they are more accurate than the K–M two-flux model, particularly when applied to films that are both weakly backscattering and weakly absorbing [30].

Color and pigment references [31–33] and pigment manufacturers [5,6] typically report the spectral reflectance of a well-hiding (i.e., visibly opaque, or ''masstone'') coating, and sometimes also that of a tint (mixture with white). This description of the coating's masstone (and tint, if given) is insufficient to determine solar spectral absorption and backscattering coefficients. First, spectral reflectance is typically reported over only the visible spectrum, though manufacturers marketing cool pigments usually report spectral reflectance over the entire solar spectrum. Second, the coating is often NIR-transmitting, making its NIR reflectance dependent on that

of its background (typically a primed metal panel). Third, knowledge of a film's opaque reflectance yields only the ratio of its absorption and backscattering coefficients. Determination of both coefficients requires measurements of either (a) the reflectances of a non-opaque film over two different backgrounds, or (b) the reflectance and transmittance of a non-opaque film.

References sometimes also report the ratio of the absorption and scattering coefficients [23,34], which is equivalent to reporting opaque reflectance. However, our review of the optics and colorant literature identified only a few published spectra of absorption and backscattering coefficients, such as two for titanium dioxide white [35,20] and one for quinacridone red [36]. Vendors of propriety color-formulation software [37–40] have further unpublished K–M coefficient data for the visible spectrum.

A straightforward and useful way to characterize the optical properties of a pigmented coating is to measure its spectral reflectance and transmittance, then calculate its spectral absorptance as $1-\text{reflectance}-\text{transmittance}$. Pigments with weak or strong NIR absorption can be identified by inspection of the spectral absorptance curve. However, knowledge of the spectral reflectance and transmittance of two differently pigmented films is not sufficient to predict the spectral reflectance and transmittance of a film colored with a mixture of the two pigments. Computation of a mixture's optical properties requires the knowledge of the bulk properties of each component pigment (in vehicle), such as the K–M backscattering and absorption coefficients. The simplest such mixture model approximates the backscattering and absorption coefficients of a mixture as the volume-weighted averages of the backscattering and absorption coefficients of its constituents [41].

We balance accuracy and simplicity by introducing a variant of the K–M two-flux model that, while less detailed than true four-flux models, does consider the extent to which incident collimated light has been scattered by passage through the film. This article sets out the theory needed to compute absorption and backscattering coefficients from spectrometer measurements of film reflectance and transmittance, then applies it to several commonly used single-pigment coatings. Model accuracy is checked by comparing the predicted and measured reflectances of each film over various backgrounds. A companion article [10] considers these characterizations pigment-by-pigment, identifying both cool pigments—i.e., those that can be used to make NIR-reflecting or NIR-transmitting cool coatings—and pigments that should be excluded from cool coatings. Our goal is to provide complete solar spectral absorption and backscattering coefficients describing a large palette of pigments usable for architectural coatings.

2. Theory

We present the theory required to compute K–M coefficients from spectrometer measurements in seven stages. Specifically, we

1. Review the standard K–M two-flux model and identify the errors that stem from its assumption that light in the film is fully diffuse.

2. Summarize the K–M solutions that relate film reflectance and transmittance to absorption and backscattering coefficients.
3. Develop the theory needed to adjust the film reflectance and transmittance measured by a spectrometer to correct for "interface" reflectances that occur when light passes to a medium of differing refractive index.
4. Show how to calculate the reflectance of a composite background, such as a clear substrate with an opaque undercoat.
5. Present a technique for computing the magnitude of interface reflectance to incompletely diffused light, to account for the geometry of light striking the interface.
6. Develop a method for estimating the extent to which collimated light is diffused by passage through a scattering film.
7. Summarize our computational algorithm.

The purpose of our measurements and model of radiant transfer in single-pigment coatings is to obtain backscattering and absorption coefficients S and K that approximately characterize the pigment. High precision is not the goal, but a reliable general characterization of each individual pigment is. We cover the solar spectral region from 300 to 2500 nm at 5-nm intervals. Each wavelength is treated independently of all others except for the use of the forward scattering ratio. Since the K–M model applies to diffuse illumination, whereas we are using collimated radiation, the treatment may be expected to be more accurate in strongly scattering films in which a fully diffuse radiation field quickly develops. However, we have used a formulation in which a non-scattering pigment (e.g., a dye) is assigned a K value approximating Beer's law for diffuse radiation traversing a slab. In summary, we are not expecting precise characterization, but expect to extract consistent, reliable, and practical information for each pigment.

2.1. *Two-flux Kubelka–Munk model vs. four-flux Maheu–Letoulouzan–Gouesbet model*

The one-dimensional propagation of light through a coating is approximated by the two-flux K–M theory, in which downward and upward beams can be absorbed and/or backscattered as they traverse the film. All light in the film is assumed to be diffuse (subscript d), either because the film is diffusely illuminated, or because the film is strongly scattering. The downward diffuse flux $i_d(z)$ and upward diffuse flux $j_d(z)$ within the film are modelled by

$$-\frac{di_d}{dz} = -(K+S)i_d + Sj_d, \tag{1}$$

$$\frac{dj_d}{dz} = -(K+S)j_d + Si_d, \tag{2}$$

where K and S are coefficients of absorption and backscattering, respectively. The fluxes and coefficients are wavelength-specific.

The *Maheu–Letoulouzan–Gouesbet* (M–L–G) four-flux model [28,29] removes the K–M assumption that all light in the film is diffuse by tracking two collimated fluxes (i_c,j_c) and two diffuse fluxes (i_d,j_d). Denoting the intensities of the total downwelling flux and total upwelling flux by $i(z) = i_c(z) + i_d(z)$ and $j(z) = j_c(z) + j_d(z)$, respectively, the M–L–G model may be expressed in the form

$$-\left(\frac{di_c}{dz}\right)_{M-L-G} = -\eta^{-1}[K + (1-\sigma)^{-1}S]i_c, \tag{3}$$

$$\left(\frac{dj_c}{dz}\right)_{M-L-G} = -\eta^{-1}[K + (1-\sigma)^{-1}S]j_c, \tag{4}$$

$$-\left(\frac{di}{dz}\right)_{M-L-G} = -(K+S)(\eta^{-1}i_c + i_d) + S(\eta^{-1}j_c + j_d), \tag{5}$$

$$\left(\frac{dj}{dz}\right)_{M-L-G} = -(K+S)(\eta^{-1}j_c + j_d) + S(\eta^{-1}i_c + i_d). \tag{6}$$

The average pathlength parameter η is the ratio of the diffuse beam pathlength to the collimated beam pathlength, which equals 2 for perfectly diffuse light [22,23]. The forward scattering ratio σ is the ratio of light scattered into the forward hemisphere to total scattering. Here, following M–L–G, we have made the simplifying assumption that σ is the same for both collimated and diffuse light.

Applying the K–M model to total fluxes i and j (rather than to the purely diffuse fluxes i_d and j_d) yields flux gradients

$$-\left(\frac{di}{dz}\right)_{K-M} = -(K+S)i + Sj = -(K+S)(i_c + i_d) + S(j_c + j_d), \tag{7}$$

$$\left(\frac{dj}{dz}\right)_{K-M} = -(K+S)j + Si = -(K+S)(j_c + j_d) + S(i_c + i_d), \tag{8}$$

with errors

$$\Delta\left(-\frac{di}{dz}\right) \equiv \left(-\frac{di}{dz}\right)_{K-M} - \left(-\frac{di}{dz}\right)_{M-L-G} = -(K+S)(1-\eta^{-1})i_c + S(1-\eta^{-1})j_c, \tag{9}$$

$$\Delta\left(\frac{dj}{dz}\right) \equiv \left(\frac{dj}{dz}\right)_{K-M} - \left(\frac{dj}{dz}\right)_{M-L-G} = -(K+S)(1-\eta^{-1})j_c + S(1-\eta^{-1})i_c, \tag{10}$$

that arise because the pathlength of collimated light is shorter than that of diffuse light by a factor of η. Since $1-\eta^{-1} > 0$, applying the K–M model to light that is partially collimated and partially diffuse tends to overestimate both (a) attenuation by absorption and backscattering, and (b) intensification by opposite-beam backscattering.

This study relies mainly on the total-flux K–M model [Eqs. (7) and (8)] because it offers relatively compact solutions for film reflectance and transmittance. However, the M–L–G relations for the collimated fluxes [Eqs. (3) and (4)] are used to

estimate the extent to which initially collimated light is diffused by passage through the film.

2.2. K–M model solutions for film reflectance and transmittance

Consider a film of thickness δ illuminated from above at $z = \delta$. If illumination comes from a medium of refractive index equal to that of the film, and both K and S are independent of z, the reflectance of the film's upper surface to downward illumination is

$$R_f \equiv \left(\frac{j}{i}\right)_{z=\delta} = \frac{1 - R_g(a - b\coth bS\delta)}{a - R_g + b\coth bS\delta}, \tag{11}$$

where

$$a \equiv (S + K)/S, \tag{12}$$

$$b \equiv (a^2 - 1)^{1/2} \tag{13}$$

and $R_g \equiv (j_d/i_d)_{z=0}$ is the reflectance of the film's background at $z = 0$. We refer to R_f as the film's "continuous refractive index" (CRI) reflectance, since it assumes that incident light passes to a medium of the same refractive index. The film's *internal transmittance* is

$$\tau \equiv \frac{i_{z=0}}{i_{z=\delta}} = \frac{b}{a\sinh bS\delta + b\cosh bS\delta}. \tag{14}$$

2.3. Determining backscattering and absorption coefficients from film reflectance and transmittance

A film with CRI reflectance $R_{f,0}$ over a black background ($R_{g,0} = 0$) and CRI reflectance $R_{f,1}$ over a non-black background ($R_{g,1} > 0$) has backscattering and absorption coefficients

$$S = \frac{1}{b\delta}\left(\operatorname{arccoth}\frac{1 - aR_{f,0}}{bR_{f,0}}\right) \tag{15}$$

and

$$K = (a - 1)S, \tag{16}$$

where

$$a = \frac{1}{2}\left[R_{f,1} + \frac{R_{f,0} - R_{f,1} + R_{g,1}}{R_{f,0}R_{g,1}}\right]. \tag{17}$$

The value of $R_{f,0}$ (and hence those of S and K) may also be obtained from CRI film reflectances $R_{f,1}$ and $R_{f,2}$ over dissimilar, nonzero background reflectances $R_{g,1}$

and $R_{g,2}$:

$$R_{f,0} = \frac{R_{f,1}R_{g,2} - R_{f,2}R_{g,1}}{R_{g,2} + R_{g,1}(R_{f,1}R_{g,2} - R_{f,2}R_{g,2} - 1)}. \tag{18}$$

A third approach is to determine $R_{f,0}$ and the K–M coefficients from $R_{f,1}$ and τ:

$$R_{f,0} = \frac{1 + R_{f,1}R_{g,1} - \sqrt{(1 - R_{f,1}R_{g,1})^2 + 4(R_{g,1}\tau)^2}}{2R_{g,1}}. \tag{19}$$

Using $R_{f,1}$ and τ to determine K and S can improve accuracy when $R_{f,1} - R_{f,0} \ll 1$ (i.e., $\tau \ll 1$ and/or $R_{g,1} \ll 1$).

The preceding solutions [Eqs. (11)–(19)] may be found in multiple references [22–26].

If the film is weakly absorbing ($K \to 0$), then $a \to 1$; $b \to 0$; and Eqs. (11), (14) and (15) may be evaluated in the non-absorbing limit:

$$\lim_{K\to 0} R_f = \frac{R_g + (1 - R_g)S\delta}{1 + (1 - R_g)S\delta}, \tag{20}$$

$$\lim_{K\to 0} \tau = \frac{1}{1 + S\delta} \tag{21}$$

and

$$\lim_{K\to 0} S = \frac{R_{f,0}}{(1 - R_{f,0})\delta}. \tag{22}$$

Similarly, if the film is weakly scattering ($S \to 0$), we obtain

$$\lim_{S\to 0} R_f = \tau^2 R_g = \exp(-2K\delta)R_g, \tag{23}$$

$$\lim_{S\to 0} \tau = \exp(-K\delta) \tag{24}$$

and

$$\lim_{S\to 0} K = -\frac{\ln \tau}{\delta}. \tag{25}$$

Note that absorption coefficients smaller than $K_{min} \approx 0.1\,mm^{-1}$ or greater than $K_{max} \approx 200\,mm^{-1}$ are difficult to resolve because reducing K below K_{min} or increasing K above K_{max} yields changes in film transmittance and reflectance too small to be accurately measured. For example, Eq. (25) predicts that at these lower and upper absorption-coefficient bounds, a 25-μm-thick non-scattering film would have internal transmittances of 0.998 and 0.007, respectively. The range of resolvable scattering coefficients has the same lower bound ($S_{min} \approx 0.1\,mm^{-1}$) and a significantly higher upper bound ($S_{max} \approx 4000\,mm^{-1}$). At these lower and upper scattering-coefficient bounds, Eq. (21) predicts that a 25-μm-thick nonabsorbing film would have internal transmittances of 0.998 and 0.010, respectively. Thus, computed

K–M coefficients will tend to be clipped to within the ranges $K_{\min} \leqslant K \leqslant K_{\max}$ and $S_{\min} \leqslant S \leqslant S_{\max}$.

2.4. Correcting spectrometer measurements of film reflectance and transmittance for refractive-index discontinuities

Film reflectance measured by an air-filled spectrometer will differ from CRI film reflectance predicted by the K–M model due to the change in refractive index at the air-film interface $z = \delta$. The Saunderson correction [42] relates the film's "observed" reflectance $\tilde{R}_f$—i.e., the value of reflectance that would be observed by an air-filled spectrometer or a pyranometer—to its CRI reflectance R_f:

$$\tilde{R}_f = \omega^i + \frac{(1-\omega^i)(1-\omega^j)R_f}{1-\omega^j R_f}. \tag{26}$$

ω^i and ω^j denote the reflectances of the interface to the downward flux ("downflux") $i(z)$ and upward flux ("upflux") $j(z)$, respectively. Inverting this relationship yields the CRI film reflectance R_f described by the K–M model:

$$R_f = \frac{\omega^i - \tilde{R}_f}{\omega^i + \omega^j(1-\tilde{R}_f) - 1}. \tag{27}$$

Computing the internal transmittance τ from spectrometer measurements is appreciably more complicated. The reflectance $R^i_{1,2}$ and transmittance $T^i_{1,2}$ of downwelling light by a two-layer system $\{1,2\}$ are

$$R^i_{1,2} = R^i_1 + \frac{T^i_1 T^j_1 R^i_2}{1-R^j_1 R^i_2}, \tag{28}$$

$$T^i_{1,2} = \frac{T^i_1 T^i_2}{1-R^j_1 R^i_2}, \tag{29}$$

where T^i_1 and T^i_2 are the upper and lower layers' transmittances of downwelling light, R^i_1 and R^i_2 are their reflectances to downwelling light, and R^j_1 is the upper layer's reflectance to upwelling light [23, p. 124]. The transmittance of downwelling light by a three-layer system $\{1,2,3\}$ is obtained by applying Eq. (29) first to layer 2 over layer 3, and then to layer 1 over the combined layer $\{2,3\}$:

$$T^i_{1,2,3} = \frac{T^i_1 T^i_{2,3}}{1-R^j_1 R^i_{2,3}} = \frac{T^i_1 T^i_2 T^i_3}{(1-R^j_1 R^i_{2,3})(1-R^j_2 R^i_3)}, \tag{30}$$

where the reflectance of the lower system $\{2,3\}$ is given by Eq. (28):

$$R^i_{2,3} = R^i_2 + \frac{T^i_2 T^j_2 R^i_3}{1-R^j_2 R^i_3}. \tag{31}$$

A free-film system (that is, a film surrounded above and below by air) may be considered to have three layers: α, the air-film interface at $z = \delta$; β, the film occupying $0 < z < \delta$; and γ, the film-air interface at $z = 0$. The film's internal

transmittance is non-directional—i.e.,

$$\tau = T_\beta = T^i_\beta = T^j_\beta. \tag{32}$$

If the film has uniform absorption and backscattering coefficients (i.e., $dK/dz = dS/dz = 0$), its reflectance is also non-directional [23, pp. 123–127]:

$$R_\beta = R^i_\beta = R^j_\beta. \tag{33}$$

It can be shown by comparing the bilayer film reflectances R_f and $R^i_{\alpha,\beta}$ predicted by Eqs. (11) and (28) that

$$R_\beta = R_{f,0}. \tag{34}$$

Since the interfaces are non-absorbing,

$$T^i_\alpha = 1 - R^i_\alpha, \tag{35}$$

$$T^i_\gamma = 1 - R^i_\gamma. \tag{36}$$

Eqs. (30)–(36) can be solved to obtain the film's internal transmittance τ from the film's *observed transmittance* $\tilde{T} = T^i_{\alpha,\beta,\gamma}$, yielding

$$\tau = \frac{-(1-R^i_\alpha)(1-R^i_\gamma) + \sqrt{[(1-R^i_\alpha)(1-R^i_\gamma)]^2 + 4R^j_\alpha R^i_\gamma (1 - R_{f,0}R^i_\gamma)(1 - R^j_\alpha R_{f,0})\tilde{T}^2}}{2R^j_\alpha R^i_\gamma \tilde{T}}, \tag{37}$$

where $R^i_\alpha = \omega^i_\delta$, $R^j_\alpha = \omega^j_\delta$, and $R^i_\gamma = \omega^i_0$.

A film that lies on a clear substrate with air above the film and below the substrate is equivalent to a free-film system in which the film-substrate interface, γ_a, and the substrate-air interface, γ_b, comprise the third layer γ. We obtain τ by evaluating Eq. (37) with R^i_γ given by Eq. (28):

$$R^i_\gamma = R^i_{\gamma_a,\gamma_b} = R^i_{\gamma_a} + \frac{T^i_{\gamma_a} T^j_{\gamma_a} R^i_{\gamma_b}}{1 - R^j_{\gamma_a} R^i_{\gamma_b}} = R^i_{\gamma_a} + \frac{(1-R^i_{\gamma_a})(1-R^j_{\gamma_a})R^i_{\gamma_b}}{1 - R^j_{\gamma_a} R^i_{\gamma_b}}, \tag{38}$$

where $R^i_{\gamma_a} = \omega_{\text{film}\to\text{substrate}}$, $R^j_{\gamma_a} = \omega_{\text{substrate}\to\text{film}}$, and $R^i_{\gamma_b} = \omega_{\text{substrate}\to\text{air}}$.

Eq. (19) expresses film reflectance over black, $R_{f,0}$, in terms of internal transmittance τ, while Eq. (37) expresses τ in terms of $R_{f,0}$. Simultaneous solution yields

$$R_{f,0} = \frac{A - B\sqrt{C}}{D}, \tag{39}$$

where

$$A = (1-R^i_\alpha)^2(1-R^i_\gamma)^2(1 + R_{f,1}R_{g,1})R_{g,1} + 2(R_{g,1} - R^j_\alpha R^i_\gamma R_{f,1})([(1 + R_{f,1}R_{g,1})R^i_\gamma - R_{g,1}]R^j_\alpha - R^i_\gamma R_{g,1})\tilde{T}^2,$$

$$B = (1-R^i_\alpha)(1-R^i_\gamma)R_{g,1},$$

$$C = (1 - R^i_\alpha)^2(1 - R^i_\gamma)^2(1 + R_{f,1}R_{g,1})^2 + 4(1 - R^j_\alpha R_{f,1})(1 - R^i_\gamma R_{f,1})(R^j_\alpha - R_{g,1})(R^i_\gamma - R_{g,1})\tilde{T}^2,$$

$$D = 2[(1 - R^i_\alpha)^2(1 - R^i_\gamma)^2 R^2_{g,1} - (R^i_\gamma R_{g,1} - R^j_\alpha[(1 + R_{f,1}R_{g,1})R^i_\gamma - R_{g,1}])\tilde{T}^2].$$

The internal transmittance is obtained by substituting the result of Eq. (39) into Eq. (37).

2.5. Computing background reflectance

The film's background reflectance R_g naturally depends on what lies below the film. There are four configurations relevant to this study, depending on the presence or absence of (a) a transparent substrate below the film and (b) an opaque undercoat below the film or film-substrate system.

1. *No substrate or undercoat*. R_g equals the reflectance of the film-air interface at the film bottom $z = 0$:

$$R_g = \omega_{film\to air}. \tag{40}$$

2. *Undercoat only*. R_g equals the undercoat's CRI reflectance

$$R_u = \frac{\omega^i - \tilde{R}_u}{\omega^i + \omega^j(1 - \tilde{R}_u) - 1}, \tag{41}$$

where $\omega^i = \omega_{air\to undercoat}$, $\omega^j = \omega_{undercoat\to air}$, and $\tilde{R}_u$ is the undercoat's observed reflectance.

3. *Substrate with undercoat*. We compute R_g in two stages. First, we apply the Saunderson correction [Eq. (26)] to R_u to account for the substrate-undercoat interface:

$$R^\star = \omega^i + \frac{(1 - \omega^i)(1 - \omega^j)R_u}{1 - \omega^j R_u}, \tag{42}$$

where $\omega^i = \omega_{substrate\to undercoat}$ and $\omega^j = \omega_{undercoat\to substrate}$. Next, we apply the Saunderson correction to $R^\star$ to account for the film-substrate interface:

$$R_g = \omega^i + \frac{(1 - \omega^i)(1 - \omega^j)R^\star}{1 - \omega^j R^\star}, \tag{43}$$

where $\omega^i = \omega_{film\to substrate}$ and $\omega^j = \omega_{substrate\to film}$.

4. *Substrate only*. Replacing the undercoat in the previous configuration with a substrate–air interface,

$$R^\star = \omega_{substrate\to air}. \tag{44}$$

We then evaluate Eq. (43) as before to obtain R_g.

2.6. Estimating interface reflectance resulting from change in refractive index

Light striking a smooth boundary separating a medium of refractive index n_0 from a medium of another refractive index n_1 will be partly reflected. The magnitude of this "interface reflectance" ω depends on n_0, n_1, and the angular distribution of the light. If the light is perfectly *collimated* (indicated by subscript c), the normal interface reflectance will be

$$\omega_{c,n_0\to n_1} = \left(\frac{n_1 - n_0}{n_1 + n_0}\right)^2. \tag{45}$$

If the light is perfectly *diffuse* (subscript d), the reflectance depends on whether the light is passing from low index to high index ($n_0 < n_1$), or vice-versa ($n_0 > n_1$). Let

$$f(m) = \frac{1}{2} + \frac{(m-1)(3m+1)}{6(m+1)^2} + \left[\frac{m^2(m^2-1)^2}{(m^2+1)^3}\right] \ln\frac{m-1}{m+1} - \frac{2m^3(m^2+2m-1)}{(m^2+1)(m^4-1)} + \left[\frac{8m^4(m^4+1)}{(m^2+1)(m^4-1)^2}\right] \ln m. \tag{46}$$

Then [27], [23, pp. 11–15]

$$\omega_{d,n_0\to n_1} = \begin{cases} f(n_1/n_0), & n_0 < n_1, \\ 1 - (n_1/n_0)^2[1 - f(n_0/n_1)], & n_0 > n_1. \end{cases} \tag{47}$$

An initially collimated beam (say, that generated by a spectrometer) that has passed through a scattering medium will be partially diffuse. We propose approximating the interface reflectance to light with diffuse fraction q by

$$\omega_{n_0\to n_1}(q) = (1-q) \times \omega_{c,n_0\to n_1} + q \times \omega_{d,n_0\to n_1}. \tag{48}$$

Perfectly collimated light has $q = 0$, while perfectly diffuse light has $q = 1$.

Light downwelling through a film system passes from air ($n = 1$) to a paint resin (e.g., acrylic or polyvinylidene fluoride [PVDF], $n = 1.5$); to a transparent substrate, if present (e.g., polyester, $n = 1.65$); and to either an opaque paint undercoat ($n = 1.5$) or a void—i.e., an air-filled black body cavity ($n = 1$). Upwelling light undergoes an analogous series of interface reflections. Interface reflectances are minor when light is perfectly collimated (e.g., $\omega_{c,\text{air}\leftrightarrow\text{resin}} = 0.04$) and when light is perfectly diffuse but passes to a medium of higher n (e.g., $\omega_{d,\text{air}\to\text{resin}} = 0.09$). However, total internal reflectance of rays that strike the interface at supercritical angles ($\theta > \arcsin[n_0/n_1]$) yields large reflectances when diffuse light passes to a medium of lower n (Table 1). For example, $\omega_{d,\text{resin}\to\text{air}}$ has a theoretical value of about 0.60 when light is perfectly diffuse. It should be noted that there is significant uncertainty in the true magnitude of this partial total internal reflectance. For example, studies of light diffused by opal glasses ($n = 1.5$) have measured glass–air interface reflectances ranging from 0.3 to 0.6 [43,44].

Since a spectrometer illuminates a film with collimated light, the diffuse fraction of downwelling light striking the air–film interface at ($z = \delta$) is $q^i_\delta = 0$. The diffuse

Table 1
Reflection due to change in refractive index at a smooth interface

Collimated Light ($q = 0$) From	To $n = 1$ (air)	$n = 1.5$ (paint resin)	$n = 1.65$ (polyester substrate)
$n = 1$ (air)	0	0.04	0.06
$n = 1.5$ (paint resin)	0.04	0	0.002
$n = 1.65$ (polyester substrate)	0.06	0.002	0
Diffuse Light ($q = 1$) From	To $n = 1$ (air)	$n = 1.5$ (paint resin)	$n = 1.65$ (polyester substrate)
$n = 1$ (air)	0	0.09	0.11
$n = 1.5$ (paint resin)	0.60	0	0.03
$n = 1.65$ (polyester substrate)	0.67	0.19	0

fractions at the other interfaces depend on the nature of the film and its background. For example, consider the following three cases for a film system *without substrate*:

1. *Non-scattering film without undercoat*. If $S = 0$ and the film has no undercoat, the downflux and upflux will be fully collimated at all interfaces.
2. *Scattering film without undercoat*. If $S > 0$, the downwelling light striking the film–air interface at the bottom of the film will be partly diffuse. Since this interface ($n = 1.5$ to $n = 1$) preferentially reflects diffuse light, the upwelling light striking the film–air interface at the top of the film will be almost perfectly diffuse unless the scattering is very weak.
3. *Scattering or non-scattering film with undercoat*. If the film has an opaque, diffusely reflecting undercoat (e.g., black or white paint), upwelling light striking the film–air interface at the top of the film will be perfectly diffuse. There is no refractive-index change at the bottom of the film, and hence no interface reflection to consider.

The above description applies also to a film that has a substrate (e.g., glass) with refractive index equal to that of the film. A similar but somewhat more complex accounting is required when the film has a substrate (e.g., polyester) with refractive index different from that of the film.

The diffuse fraction of light striking the various refractive-index interfaces of a film that does not have an undercoat can be estimated by comparing the intensities of the collimated and total fluxes at these interfaces. The diffuse fraction of downwelling light striking the film–air or film–(substrate + air) interface at the

bottom of the film is

$$q_0^i = 1 - i_c(0)/i(0) \tag{49}$$

and that of upwelling light striking the film–air interface at the top of the film is

$$q_\delta^j = 1 - j_c(\delta)/j(\delta). \tag{50}$$

Since the film's observed transmittance—i.e., the ratio of flux leaving the bottom of the film to the *unit* flux incident on the top of the film—is $\tilde{T} = (1 - \omega_0^i)i(0)$ and its observed reflectance is $\tilde{R}_f = \omega_\delta^i + (1 - \omega_\delta^j)j(\delta)$, the total downflux at the bottom of the film and upflux at the top of the film may be expressed in terms of the film measurements as

$$i(0) = \tilde{T}/(1 - \omega_0^i) \tag{51}$$

and

$$j(\delta) = (\tilde{R}_f - \omega_\delta^i)/(1 - \omega_\delta^j). \tag{52}$$

We take the following approach to determine $i_c(0)$ and $j_c(\delta)$—i.e., the collimated downflux just inside the bottom of the film, and the collimated upflux just inside the top of the film. In the K–M and M–L–G models, the film's CRI reflectance of collimated light is zero, because backscattering is assumed to convert collimated light into oppositely directed diffuse light. The film's *observed* reflectance and transmittance of collimated light, $\tilde{R}_c$ and $\tilde{T}_c$, can be determined by applying Eqs. (28) and (29) to the system's three layers—air-film interface, film, and film-air or film-(substrate + air) interface. This yields

$$i_c(0) = \tilde{T}_c/(1 - \omega_{c,0}^i) = \frac{(1 - \omega_{c,\delta}^i)\tau_c}{1 - \tau_c^2 \omega_{c,\delta}^j \omega_{c,0}^i} \tag{53}$$

and

$$j_c(\delta) = (\tilde{R}_c - \omega_{c,\delta}^i)/(1 - \omega_{c,\delta}^j) = \frac{(1 - \omega_{c,\delta}^i)\omega_{c,0}^i \tau_c^2}{1 - \tau_c^2 \omega_{c,\delta}^j \omega_{c,0}^i}. \tag{54}$$

We estimate the internal transmittance of collimated light, τ_c, from Eq. (3), yielding

$$\tau_c = \exp\{-[K + (1 - \sigma)^{-1} S]\delta/\eta\}, \tag{55}$$

where the average pathlength parameter η is assumed to be 2. The forward scattering ratio σ is a fitted parameter, as described in the next section.

2.7. Algorithms

Spectral K–M coefficients can be computed from either (A) observed spectral reflectance and transmittance over a void background; or (B) observed spectral reflectances over two different backgrounds (e.g., opaque black and opaque white). In Method A, we must determine the internal transmittance and CRI reflectance of a film with a void background, which in turn requires estimation of the forward

scattering ratio σ, spectral diffuse fractions, and spectral interface reflectances. This is much more complex than Method B, in which we need only calculate CRI film reflectances with the assumption that light exiting the film-air interface is fully diffuse. However, there are several advantages to Method A. First, the two optical measurements are made on the same specimen, which ensures that the film properties used to compute the K–M coefficients are based on samples of the same thickness. Second, measuring both reflectance and transmittance yields absorptance, which directly indicates whether a film is hot or cool. Third, since light reflected from a film's background makes two passes through the film, it is more accurate to characterize a film with one reflectance and one transmittance than with two reflectances. This is important when the film is nearly opaque, and/or the two backgrounds have similar reflectance (e.g., in the ultraviolet, where a white background is poorly reflecting). Hence, we use Method A.

Taking as inputs the observed spectral reflectance and transmittance of a film with a void background, we seek (a) spectral values of the K–M coefficients, $K(\lambda)$ and $S(\lambda)$; and (b) a wavelength-independent value of σ that minimizes the global error in the predicted value of a third observed spectral film reflectance, such as that over a black background. Algorithm I describes the process for seeking the spectral coefficients given σ; Algorithm II, which calls Algorithm I, describes the optimization of σ.

I. Determining spectral K– M coefficients given a non-spectral forward scattering ratio. We perform the following at each wavelength of interest. If the film is opaque, we report only its CRI reflectance, since in this case it is not possible to calculate both K and S. Otherwise, we compute initial values of interface reflectances by assuming that the light is everywhere collimated. Let subscripts v, b, and w refer to void, opaque black, and opaque white backgrounds, respectively. We iterate the following six steps until either (a) the fractional changes in K and S fall below some threshold (e.g., 1%), or (b) reaching an iteration limit (say, 5).

1. Use the inverse Saunderson correction [Eq. (27)] to calculate CRI film reflectances $R_{f,v}$ and $R_{f,b}$ from their corresponding observed values.
2. Calculate background reflectances $R_{g,v}$ and $R_{g,b}$ from Eqs. (40)–(44).
3. Calculate $R_{f,0}$ and τ from Eqs. (39) and (37), respectively.
4. If $R_{f,0} > 0$:
   (a) Calculate a from Eq. (17).
   (b) If $a > 1$, calculate b, S, and K from Eqs. (13), (15), and (16), respectively.
   (c) If $a \leqslant 1$, assume that $K = 0$ and evaluate S from Eq. (22).
5. If $R_{f,0} \leqslant 0$, assume that $S = 0$ and evaluate τ and K from Eqs. (24) and (25), respectively.
6. Calculate new values of the interface reflectances ω_δ^j and ω_0^i by applying Eqs. (49)–(55) to the current values of S, K, ω_δ^j and ω_0^i.

When the iterations finish, we calculate the CRI film reflectance over each background (void, black, and white) from K and/or S using Eq. (11), (20), or (23).

We then calculate the corresponding observed reflectances via the Saunderson correction [Eq. (26)].

II. Determining non-spectral forward scattering ratio. We choose the value of σ between 0 and 1 that minimizes the difference between the measured and calculated observed values of the film's reflectance over black. We seek a wavelength-independent value of σ to keep the model simple. Specifically, we minimize the global error $\varepsilon = \chi + \mu$ over M wavelengths, where

$$\chi = \left(\frac{1}{M} \sum_{m=1}^{M} \Delta_m^2 \right)^{1/2}, \tag{56}$$

$$\mu = \max |\Delta_m|, m = 1 \ldots M \tag{57}$$

and

$$\Delta_m = \tilde{R}_{\mathrm{f,calc}}(\lambda_m) - \tilde{R}_{\mathrm{f,meas}}(\lambda_m). \tag{58}$$

Our choice of global error norm ε helps avoid values of σ that yield a small RMS error χ but generate large Δ_m at one or more wavelengths.

3. Experiment

The optical properties of 87 pigmented films—4 white, 21 black or brown, 14 blue or purple, 11 green, 9 red or orange, 14 yellow, and 14 pearlescent—were characterized by computing spectral K–M coefficients and non-spectral forward scattering ratios from spectral measurements of film reflectance and transmittance.

3.1. Sample preparation

Twenty-six PVDF resin paint films were provided by a manufacturer of coil-coating paints. Another 34 acrylic paints were purchased as artist colors, and the remaining 27 coatings were acrylic-base letdowns (dilutions) of cool (primarily metal-oxide) pigment dispersions from pigment manufacturers. The PVDF and acrylic resins in these coatings each have refractive index $n = 1.5$.

Each PVDF film was prepared by (a) using a wirewound rod (a long cylindrical rod covered with a single winding of tightly wrapped wire) to coat an aluminum substrate; (b) baking and quenching the coating; (c) dissolving the aluminum with hydrochloric acid; and then (d) rinsing the film with water. We prepared a substrated film of each acrylic paint by coating a 25-μm thick sheet of clear Mylar-D® polyester ($n = 1.65$; non-scattering; absorptance <0.02 at $400-2100$ nm, <0.07 at $325-400$ nm and 2100–2500 nm; strongly absorbing below 325 nm, approaching 0.9 absorptance at 300 nm) with a wirewound rod, then allowing the paint to dry overnight at room temperature. Film thicknesses (excluding substrate, if any) ranged from 10 to 37 μm.

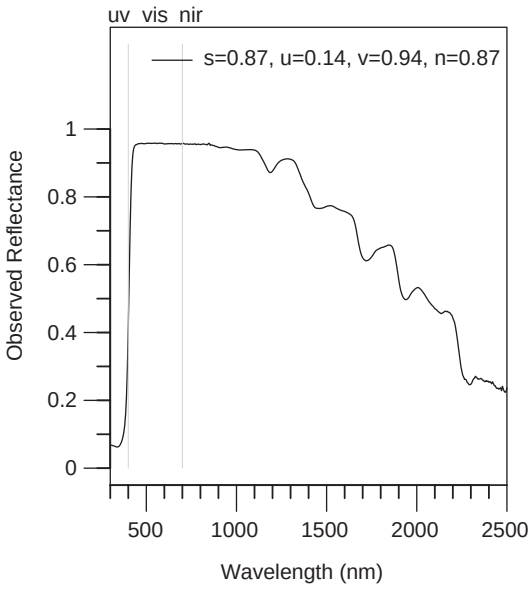

Fig. 2. Observed spectral reflectance of an opaque white background (1.5-mm thick TiO_2-white acrylic paint film).

Three 35-mm × 40-mm samples of each film were placed in glassless slide mounts, and the central thickness of each sample measured with a micrometer (accuracy ±2 μm). The back of the first sample was coated with an opaque layer of black paint (synthetic black iron oxide, 0.9 ± 0.2 mm, non-reflecting); the back of the second sample was coated with an opaque layer of white paint (titanium dioxide, 1.6 ± 0.4 mm; spectral reflectance shown in Fig. 2); and the back of the third sample was not coated. These film backgrounds are denoted "black," "white," and "void," respectively. The final term refers to the state of having no undercoating, in which case light passing through the film enters an air-filled light trap when the film's reflectance is measured in a spectrometer.

3.2. Optical measurements and corrections

A Perkin–Elmer Lambda-900 UV-VIS-NIR spectrometer equipped with a 150-mm Labsphere integrating sphere was used to measure each paint film's reflectance over black, reflectance over white, reflectance over void, and transmittance. The specular components of both reflectance and transmittance were included. Optical measurements were performed at 5-nm intervals over the solar spectrum (300–2500 nm), and were subject to two corrections.

A. Removing thin-film interference. First, thin-film interference induced by the uniform thickness of the polyester substrate creates noticeable ripples in the measured reflectance and transmittance of acrylic paints at wavelengths where

the paint film is highly transmitting. Hence, the measured spectral reflectance and transmittance of films with substrates were smoothed by convolution with a discrete Gaussian filter when the measured spectral transmittance exceeded a threshold. The filter width (±10 wavelengths), spread (half width/3), and transmittance threshold (0.7) were sized to remove as much of the thin-film interference as possible while minimizing distortion of true spectral features.

B. Removing detector-transition discontinuities. The spectrometer has two adjacent light detectors at the bottom of its integrating sphere: a UV–VIS photomultiplier tube for wavelengths below 860 nm, and a lead-sulfide NIR sensor for wavelengths of 860 nm and greater. It is common to observe a blip (i.e., a small but spectrally rapid change) in measured reflectance and/or transmittance near this detector transition. Since some films with blips also exhibited several slightly negative values of absorptance (1-reflectance–transmittance) in the NIR, we concluded that the NIR detector's signal was more likely in error.

We suspect that this discontinuity stems from the design of the integrating sphere. First, the baffle that shields the UV–VIS sensor from beam radiation may imperfectly shield the neighboring NIR sensor. Second, the efficiency of integrating sphere varies with the exact location of the reflected specular spot, which in turn depends on target texture and curvature [45]. Errors are roughly ±1% of the reflected specular component in most of the solar spectrum, and closer to ±2% beyond 2000 nm where the reflectance of the sphere's Spectralon® surface is a little lower. (These estimates are based on the reflectance of a mirror that is tipped slightly to move the specular spot by several millimeters.) Since the phototube detector used for the UV and visible measurements and the lead-sulfide detector covering the infrared beyond 860 nm are not in exactly the same position within the integrating sphere, the integrating sphere efficiency errors can be different, resulting in small discontinuities near 860 nm.

We adjusted the reflectances and transmittances measured by the NIR detector by first extrapolating a "corrected" value at 860 nm from the values at 850 and 855 nm, then adding the difference between the corrected and measured 860-nm values to measured values at all wavelengths greater than 860 nm. This correction eliminated the slightly negative absorptances.

Observations of negative absorbance may also result if the spot at which the film transmittance is measured is thinner than the spot at which film reflectance is measured. Consider a non-absorbing sample with exactly 0.5 transmittance and 0.5 reflectance. If the transmittance measurement is made on a part of the sample that is 5% thinner than the spot at which reflectance is measured, the transmittance measurement may be too large by about 0.025, and sample absorptance (1-reflectance–transmittance) may appear to be negative.

3.3. Computing pigment volume concentration

The pigment volume concentration (PVC) of each dry coating was computed either from the specific gravities of paint, pigment, and binder, or from pigment-load information supplied by the manufacturer.

4. Results

Model performance was gauged by examining (a) spectral characterizations of six representative pigments and (b) the accuracy with which computed K–M coefficients predict film reflectance over black and white backgrounds. The six sample results are presented below. Spectral characterizations of all 87 pigmented films are reported in a companion article [10].

4.1. Detailed spectral analyses of six representative pigments

The measured and computed spectral properties of films colored with each of six pigments—(a) titanium dioxide white, (b) carbon black, (c) iron oxide red, (d) phthalo blue, (e) phthalo green, and (f) mica flakes coated with titanium dioxide—are shown in Fig. 3. Charted for each coating are (I) measured optical properties of a film over void; (II) computed K–M coefficients; (III) computed diffuse fractions and interface reflectances; and (IV) measured and computed values of reflectance over black and white backgrounds.

Chart I shows the film's measured reflectance $\tilde{R}_{f,v}(\lambda)$ and measured transmittance $\tilde{T}(\lambda)$ over void, which are used to compute K–M coefficients; and computed absorptance, $\tilde{A}(\lambda) = 1 - \tilde{R}_{f,v}(\lambda) - \tilde{T}(\lambda)$. Its legend tabulates solar ("s"), UV ("u"), visible ("v"), and NIR ("n") spectrally integrated values computed by weighting each property with the air-mass 1.5 solar spectral irradiance shown in Fig. 1.

Chart II presents backscattering and absorption coefficients $S(\lambda)$ and $K(\lambda)$, along with the non-spectral forward scattering ratio σ that minimizes the error in predicted reflectance over black. In this graph, non-zero K–M coefficients are assigned a minimum value of $0.1\,\mathrm{mm}^{-1}$, which is an estimate of the smallest resolvable non-zero value for K and S (cf. Section 2.3). At wavelengths where only S is shown, K was assumed to be zero, and vice versa. Where the film is opaque, neither S nor K is shown.

Chart III shows a few of the ancillary properties computed in the process of generating K–M coefficients, namely the diffuse fraction q and the interface reflectance ω for fluxes exiting the top and bottom of the void-backed film. These interface reflectances are used to correct the measured values of film reflectance and transmittance during computation of K and S (cf. Section 2.4).

Chart IV compares values of over-black and over-white observed reflectances $\tilde{R}_{f,b}(\lambda)$ and $\tilde{R}_{f,w}(\lambda)$ computed from the K–M coefficients to values measured with the spectrometer. The computed reflectance over black (ROB) is fitted to its corresponding measured value by the choice of the non-spectral forward scattering ratio. However, the computed reflectance over white (ROW) is independent of the measured ROW, since the latter property is not used to calculate K–M coefficients. Hence, the error in ROW serves as a strong check for the accuracy of K and S, while the error in ROB serves as a weaker check. Also shown in this chart are the RMS errors χ_w and χ_b in predictions of ROW and ROB, and the measured over-white and over-black NIR reflectances N_w and N_b.

A. Titanium Dioxide White. Titanium dioxide white (Fig. 3a) scatters strongly in most of the solar spectrum but absorbs strongly in the UV (below 400 nm). In most of the visible and infrared spectra there is little absorption. The inferred scattering coefficient S declines by two orders of magnitude between 400 and 2500 nm, which is typical behavior for scattering pigments. For generic TiO_2 (rutile) we have 200-nm particles of refractive index ≈ 2.7. For well-dispersed particles that are much smaller than the wavelength, we expect Rayleigh behavior in which the scattering cross section decreases as λ^{-4}. Thus we might expect S to decline by more than three orders of magnitude between 400 and 2500 nm. On a log–log plot (not shown), the slope of the scattering curve is increasingly negative at longer wavelengths, reaching about -3 at 2500 nm, so that the Rayleigh limit is not quite reached. The "background" or minimum absorption coefficient here of $0.5\,mm^{-1}$, multiplied by film thickness, is about 0.015. Since, as mentioned earlier, absorptance measurement uncertainties are on the order of 0.01, no definite conclusion can be reached about the actual minimum absorptance. In fact, the underprediction of reflectance over white from 600 to 1400 nm suggests that the film absorptance may be slightly overestimated.

The absorption and backscattering curves are interrupted at four wavelengths in the UV where the 29-μm thick film is opaque.

Chart I shows a small upward shift in reflectance near 860 nm, where the spectrometer switches from its UV–VIS sensor to its NIR sensor. This indicates that the algorithm to remove such discontinuities (cf. Section 3.2) is imperfect. The small peaks in absorptance (Chart I) and absorption coefficient (Chart II) at 1700 nm are a feature of the binder, since they appear in many differently pigmented films, including some without substrates. Most polymers have significant IR absorption due to hydrogen vibrations of C–H structures in the 2000–2400 nm range [46]. Weaker overtones appear in the 1600–1800 nm regions. Thus, some of the NIR absorptance features seen here are due to the polymer binder. However, it is not unusual for TiO_2 pigments to be coated with metal hydroxides, and hydrogen vibrations in H_2O and OH groups may sometimes appear as well.

Chart III indicates that the computed scattering is strong enough to fully diffuse light exiting the bottom of the film ($q_0^i = 1$) at wavelengths <1200 nm, and to fully diffuse the light exiting the top of the film ($q_\delta^i = 1$) at all wavelengths (cf. Section 2.6). The non-spectral FSR $\sigma = 0.69$ is in agreement with the theoretical prediction of about 0.65 obtained by assuming a particle diameter of 200 nm, a relative refractive index of $(2.75 + 0i)/1.5$, a PVC of 5%, and a free-space wavelength of 550 nm [47, Fig. 1].

Fig. 3. (ii/ii) Measurements and model calculations for six coatings: (a) titanium dioxide white, (b) carbon black, (c) iron oxide red, (d) phthalo blue, (e) phthalo green, and (f) mica flakes coated with titanium dioxide. Shown from top to bottom are (I) measured reflectance, transmittance, and absorptance of film with void background; (II) Kubelka–Munk backscattering and absorption coefficients S and K, and non-spectral forward scattering ratio σ; (III) computed diffuse fraction and interface reflectance of fluxes exiting top and bottom of film; and (IV) measured and computed film reflectances over white [w] and black [b] backgrounds, measured NIR reflectance N, and the RMS error χ.

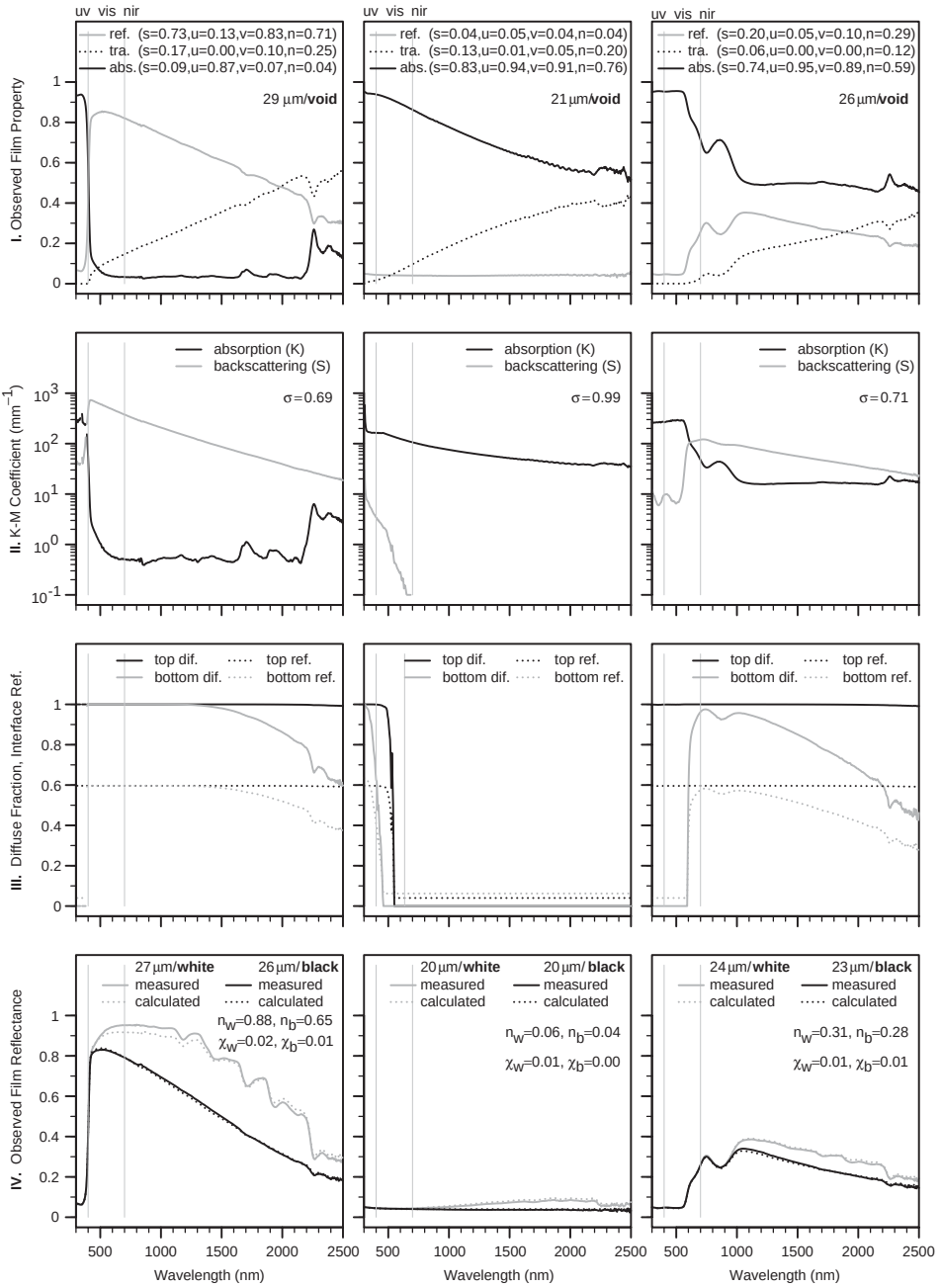

(a)
Inorganic Oxide White
Ishihara Tipaque CR-90 (PW 6)
15% PVC
{titanium dioxide white}

(b)
Carbon Black
Amorphous Carbon Black (PBk 7)
0.4% PVC
{carbon black}

(c)
Red Iron Oxide (i)
Bayer Bayferrox 6622 Iron Oxide (PR 101)
9% PVC
{iron oxide red}

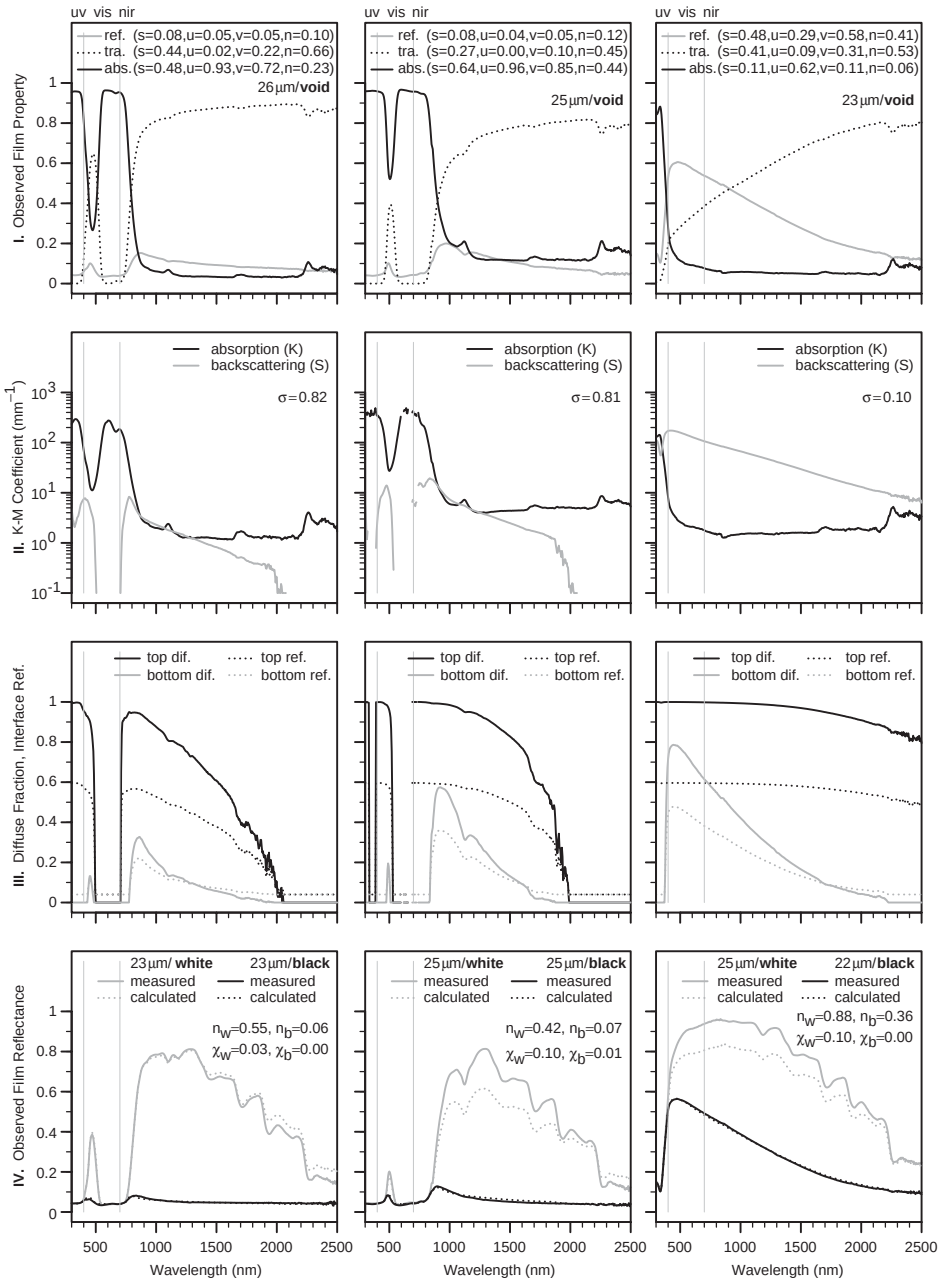

(d)
Phthalo Blue (ii)
Toyo Lionel BF-28201 (PB 15)
5% PVC
{phthalocyanine blue}

(e)
Phthalo Green (ii)
Clariant GT-674-D Endurophthal
Green B (PG 7)
4% PVC
{phthalocyanine green}

(f)
Bright White (Pearlescent)
Engelhard Exterior Mearlin 139X Bright White
11% PVC
{mica + titanium dioxide}

Fig. 3. (ii/ii)

The computed ROB closely matches the measured ROB, but the calculated ROW is about 0.04 low over the range 600–1300 nm (Chart IV). We consider three possible explanations.

1. *Inaccurate K– M coefficients.* Underprediction of film reflectance suggests that the algorithm may have overestimated K and/or underestimated S. At 1000 nm, $K \approx 0.5\,\mathrm{mm}^{-1}$, $S \approx 200\,\mathrm{mm}^{-1}$, the CRI reflectance of the opaque white background is 0.98, and the observed reflectances over black and white are underpredicted by 0.01 and 0.04, respectively. Eq. (11) indicates that reducing K to zero while leaving S unchanged would increase the over-black and over-white reflectances by 0.007 and 0.02, respectively. Alternately, increasing S fivefold to $1000\,\mathrm{mm}^{-1}$ while leaving K unchanged would yield corresponding increases of 0.15 and 0.02. Setting K to zero—which assumes that neither the pigment nor the binder absorb any light whatsoever—would match the over-black reflectances, but leave the ROW underpredicted by 0.02. Setting $S = 1000\,\mathrm{mm}^{-1}$ would yield the same underprediction of ROW, while wildly overpredicting ROB. Of these, the mostly likely explanation is that we have overpredicted K.
2. *Inaccurate film-air interface reflectance*. We may have misestimated the film-air interface reflectance used in the Saunderson correction [Eq. (26)] to the predicted reflectances over black and white. We use the theoretical value $\omega_{\mathrm{film}\to\mathrm{air}} = 0.6$ because light exiting the top of a diffusely undercoated film should be fully diffuse. However, since reflectances as low as 0.3 have been observed for diffuse light passing from $n = 1.5$ to $n = 1$ [44], we consider the effects of changing ω. The CRI ROB and ROW at 1000 nm are 0.84 and 0.95, respectively. When $\omega = 0.60$, the corresponding observed film reflectances are 0.69 and 0.91. Reducing ω to 0.5 increases the observed reflectances by 0.05 and 0.01, respectively; increasing ω to 0.7 decreases them by 0.06 and 0.03. Hence decreasing ω would aggravate the ROB error much more than it would reduce the ROW error, and increasing ω would increase both ROB and ROW errors.
3. *Inaccurate background reflectance*. The reflectance of the sample's opaque white background might be higher than assumed. This is unlikely because the layer of opaque white paint whose reflectance is charted in Fig. 2 is about 1.5-mm thick, and has a spectral transmittance less than 0.01 over virtually the entire solar spectrum. Thus, while making the white undercoating too thin could reduce the reflectance of the sample over white, making the white undercoating too thick should not measurably increase the over-white reflectance.

B. Carbon black. Carbon black (Fig. 3b) is a strongly absorbing pigment with an exponentially-decreasing absorption coefficient that falls half a decade over the solar spectrum (Chart II). It has weak scattering in the UV and visible spectra typical of soot [48], and is essentially non-scattering in the NIR. We note that its measured reflectance over black is approximately 0.04 in the visible and NIR spectra (Chart IV), which is the result expected for a collimated beam passing from air ($n = 1$) to a non-scattering paint ($n = 1.5$). In these spectra, the CRI ROB $R_{\mathrm{f},0}$ computed from Eq. (39) is slightly negative (mean value −0.003); hence, the film is assumed to be

non-scattering, the top and bottom diffuse fractions are set to zero (Chart III), and the absorption coefficient is computed in the non-scattering limit from Eq. (25).

The 21-μm thick film prepared from a diluted carbon black artist paint is quite transparent (Chart I), making it easy to compute K from its transmittance. The forward scattering ratio $\sigma = 0.99$ has little meaning because $S = q = 0$ in the NIR. The near-perfect matches between calculated and measured reflectances over black and white match (Chart IV) likely arise from the film's strong absorption, possibly because absorptive attenuation reduces the influence of scattering on film reflectance.

C. Iron oxide red. Iron oxide red (Fig. 3c) has very strong absorption at wavelengths below 600 nm, and strong scattering at wavelengths longer than 660 nm (Chart II), leading to its dark red appearance over either a white or black background (Chart IV). At wavelengths below 600 nm, the bottom diffuse fraction is forced to zero because the high absorptance ($K > 200\,\mathrm{mm}^{-1}$) generates small values of $i_c(0)$ and $i(c)$, which in turn yield an unphysical (i.e., negative) estimate of diffuse fraction. The matches between predicted and measured reflectances (Chart IV) are quite good, probably because the absorption is never small ($K > 20\,\mathrm{mm}^{-1}$). Other iron oxide red pigments showed less NIR absorption than this pigment [10].

D, E. Phthalocyanine blue and green. Phthalocyanine blue (Fig. 3d) and phthalocyanine green (Fig. 3e) are weakly scattering, dyelike pigments with strong absorption in parts of the visible and NIR. Their strong absorptances in the reddish potions of the visible spectrum (Chart I) give each a dark blue or green appearance over a white background, and almost black appearances over a black background (Chart IV). Both of these PVDF-based free films are about 25-μm thick, have a PVC of about 5%, are fitted with $\sigma \approx 0.8$, and show excellent agreement between measured and calculated reflectances over black. However, the error in ROW is much larger for the green than it is for the blue. At 1280 nm (peak green ROW error), the measured reflectances of green over white and blue over white are each 0.81, but the green film's K and S are each three times larger than those of the blue film. Thus, while the model closely estimates the reflectance of blue over white (error 0.01), its underpredicts the reflectance of green over white by 0.20.

F. Mica flakes coated with titanium dioxide. This pearlescent white film (Fig. 3f) containing mica flakes coated with titanium dioxide is strongly scattering and weakly absorbing in the visible and NIR spectra. Its absorption and backscattering curves are shaped like those of titanium dioxide (Fig. 3a), but K and S are about half an order of magnitude higher and lower, respectively (Chart II). The K–M model is not expected to accurately describe pearlescent films. Since these platelike pigment particles tend to align with the plane of the films, the collimated light that they scatter is unlikely to be uniformly diffuse. This particular pearlescent exhibits one of the poorest fits to ROW, second only to that of the aforementioned phthalo green. The very low $\sigma = 0.1$ may result from specular reflection by the flakes.

4.2. Accuracy of K–M model vs. backscattering and absorption thicknesses

Fig. 4 charts errors in predicted ROW and ROB vs. backscattering thickness $S\delta$ and absorption thickness $K\delta$ using about 38,000 measurements (87 pigments × 441

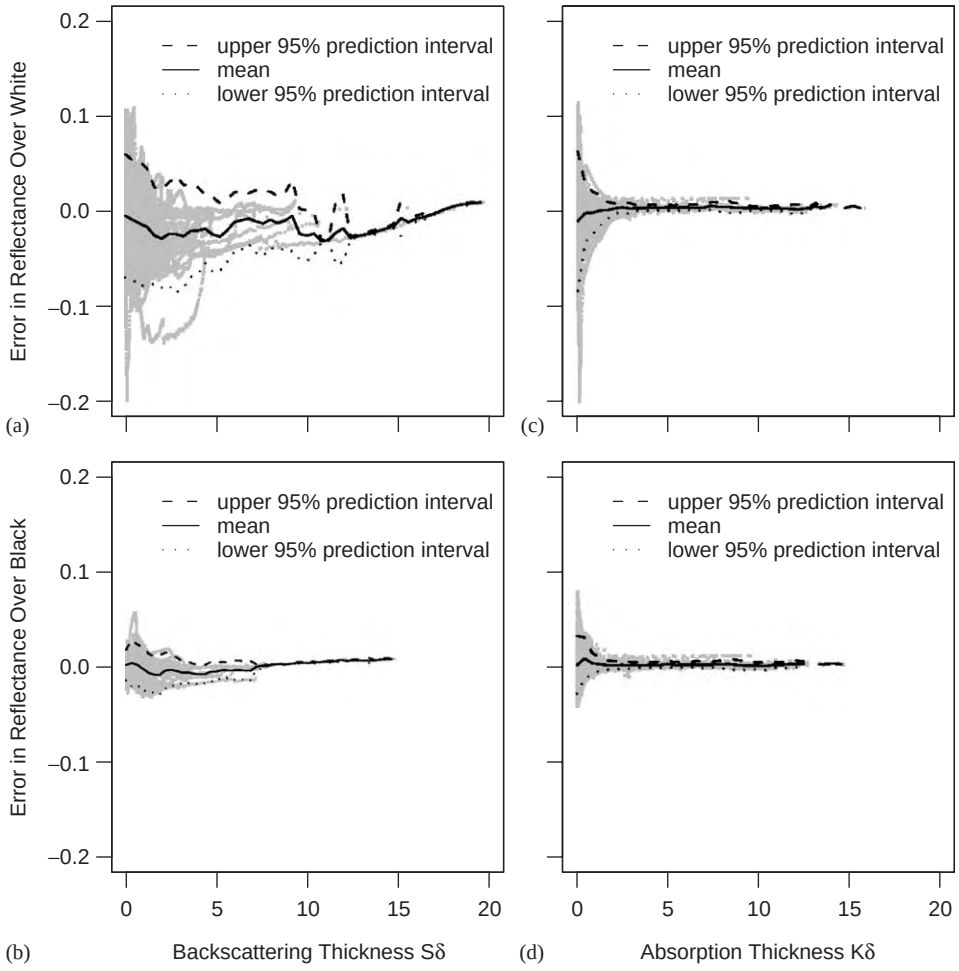

Fig. 4. Errors in reflectances computed from Kubelka–Munk coefficients. Shown are (a, b) computed − measured values of observed film reflectance over (white, black) backgrounds vs. backscattering thickness $S\delta$; and (c, d) the same errors vs. absorption thickness $K\delta$.

wavelengths/pigment). On average (as indicated by the mean error curves in charts [a] and [b]), the model underpredicts both ROW and ROB. As suggested by a prior theoretical error analysis of the K–M model [30], prediction errors are greatest when the film is weakly scattering and/or weakly absorbing. Typical errors ranges (that is, the 95% prediction interval limits) are −0.07 to +0.06 (ROW) and −0.02 to +0.02 (ROB) for weakly scattering films; −0.08 to +0.06 (ROW) and −0.02 to +0.02 (ROB) for weakly absorbing films; −0.04 to +0.01 (ROW) and −0.01 to +0.01 (ROB) for strongly scattering films; and less than ±0.01 (ROW and ROB) for strongly absorbing films.

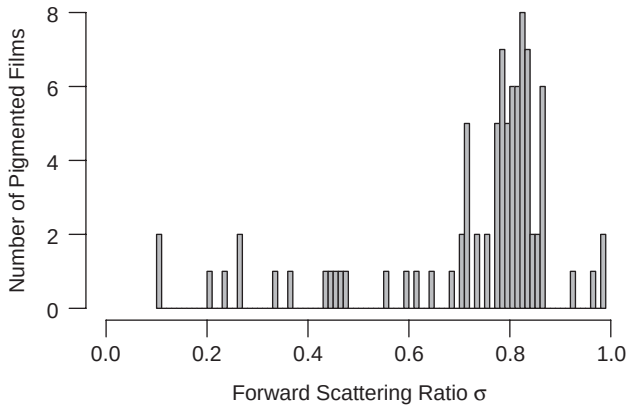

Fig. 5. Frequency distribution of non-spectral forward scattering ratio σ. Most pigmented films characterized were strongly forward scattering.

4.3. Fitted forward scattering ratio

The distribution of forward scattering ratios computed for the 87 coatings shown in Fig. 5 indicates that most of the tested paints are strongly forward scattering ($0.7 \leqslant \sigma \leqslant 0.9$).

5. Conclusions

We have presented a variant of the two-flux K–M model that determines backscattering and absorption coefficients primarily from the reflectance and transmittance of a film over a void background, using the reflectance over black to obtain an estimate of the forward scattering ratio. Detailed spectral analyses of six representative pigments combined with statistical analyses of about 38,000 spectral measurements indicate several strengths and weaknesses of the model.

1. The K–M coefficients appear qualitatively correct, in the sense that the absorption coefficient reproduces the spectral features of the film's absorptance, and the backscattering coefficient exhibits those of the film's reflectance over black.
2. The film reflectances over white and black backgrounds computed from K–M coefficients closely match corresponding measured values for the first four representative pigments—titanium dioxide white, carbon black, iron oxide red, and phthalo blue—with RMS errors in ROW and ROW not exceeding 0.03 and 0.01, respectively. The last two representative pigments—phthalo green and pearlescent bright white—exhibit large errors (RMS 0.10) in predicted ROW.
3. The model on average underpredicts both ROB and ROW, with errors on the order of about ± 0.07 for ROW and ± 0.02 for ROB when a film is weakly

scattering and/or weakly absorbing. The latter feature suggests that the model is likely to underestimate the NIR reflectance of cool (weakly NIR absorbing) films.

Acknowledgements

This work was supported by the California Energy Commission (CEC) through its Public Interest Energy Research Program (PIER), by the Laboratory Directed Research and Development (LDRD) program at Lawrence Berkeley National Laboratory (LBNL), and by the Assistant Secretary for Renewable Energy under Contract No. DE-AC03-76SF00098. The authors wish to thank CEC Commissioner Arthur Rosenfeld and PIER program managers Nancy Jenkins and Chris Scruton for their support and advice. Special thanks go also to Mark Levine, director of the Environmental Energy Technologies Division at LBNL, and Stephen Wiel, head of the Energy Analysis Department at LBNL, for their encouragement and support in the initiation of this project. We also wish to thank the following people for their assistance: Kevin Stone and Melvin Pomerantz, LBNL; Michelle Vondran, John Buchko, and Robert Scichili, BASF Corporation; Richard Abrams, Robert Blonski, Ivan Joyce, Ken Loye, and Ray Wing, Ferro Corporation; Tom Steger and Jeffrey Nixon, Shepherd Color Company; and Robert Anderson, Liquitex Artist Materials.

References

[1] R.F. Brady, L.V. Wake, Principles and formulations for organic coatings with tailored infrared properties, Prog. Org. Coat. 20 (1) (1992) 1–25.
[2] G. Burkhart, T. Detrie, D. Swiler, When black is white, Paint and Coatings Industry Magazine, January 2001.
[3] T.R. Sliwinski, R.A. Pipoly, R.P. Blonski, Infrared reflective color pigment, US Patent 6,174,360 B1, January 16, 2001.
[4] J.D. Nixon, The chemistry behind 'Cool Roofs', eco-structure 1 (1) (2003) 63–65.
[5] Ferro Corporation, Cool Colors™ and Eclipse™ pigments, http://ferro.com.
[6] Shepherd Color Company, Arctic infrared-reflecting pigments, http://shepherdcolor.com.
[7] BASF Industrial Coatings, Ultra-Cool™: the new heat reflective coatings from BASF, http://www.ultra-cool.basf.com.
[8] Custom–Bilt Metals, Ultra-Cool™ coating saves energy and money on Custom-Bilt metals roofing systems, http://www.custombiltmetals.com.
[9] MCA Tile, MCA Tile ENERGY STAR roof products, http://www.mcatile.com.
[10] R. Levinson, P. Berdahl, H. Akbari, Solar spectral optical properties of pigments – Part II: survey of common colorants, Sol. Energy Mater. Sol. Cells 89 (4) (2005) 351–389, this issue; doi:10.1016/j.solmat.2004.11.013.
[11] ASTM, ASTM G 173-03: standard tables for reference solar spectral irradiance at air mass 1.5: direct normal and hemispherical on 37° tilted surface, Technical report, American Society for Testing and Materials, 2003.
[12] R. Levinson, H. Akbari, S. Konopacki, S. Bretz, Inclusion of cool roofs in nonresidential Title 24 prescriptive requirements, Report LBNL-50451, Lawrence Berkeley National Laboratory, Berkeley, CA, 2002.
[13] R. Levinson, H. Akbari, S. Konopacki, S. Bretz, Inclusion of cool roofs in nonresidential Title 24 prescriptive requirements, J. Energy Policy 33 (2005) 151–170.

[14] P. Berdahl, H. Akbari, L.S. Rose, Aging of reflective roofs: soot deposition, Appl. Opt. 41 (12) (2002) 2355–2360.
[15] S. Konopacki, H. Akbari, M. Pomerantz, S. Gabersek, L. Gartland, Cooling energy savings potential of light-colored roofs for residential and commercial buildings in 11 US metropolitan areas, Report LBNL-39433, Lawrence Berkeley National Laboratory, Berkeley, CA, 1997.
[16] Yasuhiro Genjima, Haruhiko Mochizuki, Infrared radiation reflector and infrared radiation transmitting composition, US Patent 6,366,397 B1, April 16, 2002.
[17] M. Born, E. Wolf, Principles of Optics, seventh ed., Cambridge University Press, Cambridge, 1999.
[18] H.C. van de Hulst, Light Scattering by Small Particles, Dover Publications, New York, 1981.
[19] C.F. Bohren, D.R. Huffman, Absorption and Scattering of Light by Small Particles, Wiley, New York.
[20] L.E. McNeil, R.H. French, Multiple scattering from rutile TiO_2 particles, Acta Mater. 48 (2001) 4571–4576.
[21] A. Schuster, Radiation through a foggy atmosphere, Astrophys. J. 21 (1) (1905) 1.
[22] P. Kubelka, New contributions to the optics of intensely light-scattering materials, part I, J. Opt. Soc. Am. 38 (1948) 448–457.
[23] G. Kortum, Reflectance Spectroscopy: Principles, Methods, Applications, Springer, Berlin, 1969.
[24] C.F. Bohren, Multiple scattering of light and some of its observable consequences, Am. J. Phys. 55 (6) (1987) 524–533.
[25] D.B. Judd, Color in Business, Science, and Industry, Wiley, New York, 1952.
[26] R.M. Johnston, Pigment Handbook, vol. III, Color Theory, Wiley, New York, 1988, pp. 229–288, (Chapter D–b).
[27] J.W. Ryde, The scattering of light by turbid media: part I, Proceedings of the Royal Society of London: Series A, vol. 131 (817), May 1931, pp. 451–464.
[28] B. Maheu, J.N. Letoulouzan, G. Gouesbet, Four-flux models to solve the scattering transfer equation in terms of Lorenz–Mie parameters, Appl. Opt. 23 (19) (1984) 3353–3362.
[29] W.E. Vargas, Generalized four-flux radiative transfer model, Appl. Opt. 37 (13) (1998) 2615–2623.
[30] W.E. Vargas, G.A. Niklasson, Applicability conditions of the Kubelka–Munk theory, Appl. Opt. 36 (22) (1997) 5580–5586.
[31] Y.S. Touloukian, D.P. DeWitt, R.S. Hernicz, Thermal Radiative Properties: Coatings, vol. 9, Thermophysical Properties of Matter, IFI/Plenum, New York, 1972.
[32] P.A. Lewis, Pigment Handbook, vol. 1, Wiley, New York, 1988.
[33] R. Mayer, The Artist's Handbook of Materials and Techniques, fifth ed., Viking Penguin, 1991.
[34] R.S. Berns, Billmeyer and Saltzman's Principles of Color Technology, third ed., Wiley, New York, 2000.
[35] W.E. Vargas, G.A. Niklasson, Generalized method for evaluating scattering parameters used in radiative transfer models, J. Opt. Soc. Am. A 14 (9) (1997) 2243–2252.
[36] L.E. McNeil, R.H. French, Light scattering from red pigment particles: multiple scattering in a strongly absorbing system, J. Appl. Phys. 89 (1) (2001) 283–293.
[37] Avantes, Mix2Match color matching software, http://avantes.com.
[38] Color-Tec, Color formulation software, http://color-tec.com.
[39] Datacolor, Paintmaker laboratory software, http://datacolor.com.
[40] GretagMacbeth, ProPalette® plastics/coatings color formulation and quality control software,http://gretagmacbeth.com.
[41] E. Allen, Optical Radiation Measurements, vol. 2, Colorant Formulation and Shading, Academic Press, New York, 1980, pp. 289–336 (Chapter 7).
[42] J.L. Saunderson, Calculation of the color of pigmented plastics, J. Opt. Soc. Am. 32 (12) (1942) 727–736.
[43] J.W. Ryde, B.S. Cooper, The scattering of light by turbid media: part II, Proc. R. Soc. London. Ser. A 131 (817) (1931) 464–475.
[44] D. Spitzer, J.J. Ten Bosch, A simple method for determination of the reflection coefficient at the internal surfaces of turbid slabs, Opt. Commun. 9 (3) (1973) 311–314.

[45] A. Roos, C.G. Ribbing, M. Bergkvist, Anomalies in integrating sphere measurements on structured samples, Appl. Opt. 27 (18) (1988) 3828–3832.
[46] R.T. Conley, Infrared Spectroscopy, second ed., Allyn and Bacon Inc., Boston, 1972.
[47] W.E. Vargas, G.A. Niklasson, Forward-scattering ratios and average pathlength parameter in radiative transfer models, J. Phys: Condens. Matter 9 (1997) 9083–9096.
[48] M.Y. Choi, G.W. Mulholland, A. Hamins, T. Kashiwagi, Comparisons of the soot volume fraction using gravimetric and light extinction techniques, Combust. Flame 102 (1995) 161–169.

Available online at www.sciencedirect.com
SCIENCE DIRECT®
Solar Energy Materials & Solar Cells
ELSEVIER
Solar Energy Materials & Solar Cells 89 (2005) 351–389
www.elsevier.com/locate/solmat

Solar spectral optical properties of pigments—Part II: survey of common colorants

Ronnen Levinson*, Paul Berdahl, Hashem Akbari

Lawrence Berkeley National Laboratory, 1 Cyclotron Road, Berkeley, CA 94720, USA

Received 15 June 2004; received in revised form 5 November 2004; accepted 12 November 2004
Available online 11 March 2005

Abstract

Various pigments are characterized by determination of parameters S (backscattering) and K (absorption) as functions of wavelength in the solar spectral range of 300–2500 nm. Measured values of S for generic titanium dioxide (rutile) white pigment are in rough agreement with values computed from the Mie theory, supplemented by a simple multiple scattering model. Pigments in widespread use are examined, with particular emphasis on those that may be useful for formulating non-white materials that can reflect the near-infrared (NIR) portion of sunlight, such as the complex inorganic color pigments (mixed metal oxides). These materials remain cooler in sunlight than comparable NIR-absorbing colors. NIR-absorptive pigments are to be avoided. High NIR reflectance can be produced by a reflective metal substrate, an NIR-reflective underlayer, and/or by the use of a pigment that scatters strongly in the NIR.
Published by Elsevier B.V.

Keywords: Pigment characterization; Solar spectral optical properties; Kubelka-Munk absorption and backscattering coefficients; Cool roofs; Titanium dioxide

*Corresponding author. Tel.: +1 510 486 7494; fax: +1 425 955 1992.
E-mail addresses: RMLevinson@LBL.gov (R. Levinson), PHBerdahl@LBL.gov (P. Berdahl), H_Akbari@LBL.gov (H. Akbari).

0927-0248/$ - see front matter Published by Elsevier B.V.
doi:10.1016/j.solmat.2004.11.013

1. Introduction

A companion article [1] presented a theoretical framework and experimental procedure that can be used to determine the Kubelka–Munk backscattering and absorption coefficients of a pigmented film. The current article applies this model to each of 87 predominantly single-pigment films, with special attention paid to characterizing the near-infrared (NIR) properties that determine whether a pigment is "hot" or "cool." These pigments include (but are not limited to) inorganic colorants conventionally used for architectural purposes, such as titanium dioxide white and iron oxide black; spectrally selective organics, such as dioxazine purple; and spectrally selective inorganics developed for cool applications, such as selective blacks that are mixed oxides of chromium and iron.

Several pigment handbooks [2–6] provide valuable supplemental information on the properties, synthesis methods, and applications of many of the pigments characterized in this study. Naturally, as far as optical properties are concerned, these references provide data mainly in the visible spectral range (an exception is [5]).

2. Pigment classification

For convenience in presentation, the pigments were grouped by color "family" (e.g., green) and then categorized by chemistry (e.g., chromium oxide green). Some families span two colors (e.g., black/brown) because it is difficult to consistently identify color based on pigment name and color index (convention for identifying colorants [7]). For example, a dark pigment may be marketed as "black," but carry a "pigment brown" color index designation and exhibit red tones more characteristic of brown than of black. The following list shows in parentheses a mnemonic single-letter abbreviation assigned to each color family, and in braces the population of each color family and pigment category. Pigment categories are presented in the order of simpler inorganics, more complex inorganics, and then finally organics. Each member of a color family is assigned an identification code X*nn*, where X is the color family abbreviation and *nn* is a serial number. For example, the 11 members of the green color family ("G") have identification codes G01 through G11. The same pigment may be present in more than one pigmented film. For example, our survey includes four titanium dioxide white films (W01–W04). However, the concentration of pigment, pigment particle size, and/or source of the pigment (manufacturer) may vary from film to film.

1. White (W) {4}
   (a) titanium dioxide white {4}.
2. Black/brown (B) {21}
   (a) carbon black {2},
   (b) other non-selective black {2},
   (c) chromium iron oxide selective black {7},
   (d) other selective black {1},

(e) iron oxide brown {3},
(f) other brown {6}.

3. Blue/purple (U) {14}
   (a) cobalt aluminate blue {4},
   (b) cobalt chromite blue {5},
   (c) iron blue {1},
   (d) ultramarine blue {1},
   (e) phthalocyanine blue {2},
   (f) dioxazine purple {1}.
4. Green (G) {11}
   (a) chromium oxide green {2},
   (b) modified chromium oxide green {1},
   (c) cobalt chromite green {3},
   (d) cobalt titanate green {3},
   (e) phthalocyanine green {2}.
5. Red/orange (R) {9}
   (a) iron oxide red {4},
   (b) cadmium orange {1},
   (c) organic red {4}.
6. Yellow (Y) {14}
   (a) iron oxide yellow {1},
   (b) cadmium yellow {1},
   (c) chrome yellow {1},
   (d) chrome titanate yellow {4},
   (e) nickel titanate yellow {4},
   (f) strontium chromate yellow + titanium dioxide {1},
   (g) Hansa yellow {1},
   (h) diarylide yellow {1}.
7. Pearlescent (P) {14}
   (a) mica + titanium dioxide {9},
   (b) mica + titanium dioxide + iron oxide {5}.

3. Pigment properties by color and category

Table 1 summarizes some relevant bulk properties of the pigmented films in each category, such as NIR reflectances over black and white backgrounds. The measured and computed spectral properties of each pigmented film are shown in Fig. 1. Each film has a column of charts of the type presented in the companion article [1] with the omission of the chart of ancillary parameters (diffuse fractions and interface reflectances). Color images of the films are shown in Fig. 2.

When examining spectral optical properties, it is worth noting that most of the NIR radiation in sunlight arrives at the shorter NIR wavelengths. Of the 52% of solar energy delivered in the NIR spectrum (700–2500 nm), 50% lies within

Table 1
Ranges of NIR reflectance over white (ROW_{nir}), NIR reflectance over black (ROB_{nir}), visible transmittance (T_{vis}), and thickness (δ) measured for pigmented films in each pigment category

Category	ROW_{nir}	ROB_{nir}	T_{vis}	δ (μm)	Film Codes
Titanium dioxide white	0.87–0.88	0.24–0.65	0.10-0.42	17–29	W01-W04
Carbon black	0.05–0.06	0.04–0.04	0.03–0.07	16–19	B01–B02
Other non-selective black	0.04–0.05	0.04–0.05	0.00–0.07	20–24	B03–B04
Chromium iron oxide selective black	0.23–0.48	0.11–0.35	0.00–0.15	19–26	B05–B11
Organic selective black	0.85	0.10	0.01	23	B12
Iron oxide brown	0.47–0.61	0.06–0.27	0.03–0.24	14–26	B13–B15
Other brown	0.50–0.74	0.22–0.40	0.01–0.24	17–28	B16–B21
Cobalt aluminate blue	0.62–0.71	0.09–0.20	0.16–0.28	16–23	U01–U05
Cobalt chromite blue	0.55–0.70	0.10–0.25	0.05–0.28	16–26	U06–U09
Iron blue	0.25	0.05	0.27	12	U10
Ultramarine blue	0.52	0.05	0.20	23	U11
Phthalocyanine blue	0.55–0.63	0.06–0.08	0.21–0.22	14–26	U12–U13
Dioxazine purple	0.82	0.05	0.21	10	U14
Chromium oxide green	0.50–0.57	0.33–0.40	0.00–0.01	12–26	G01–G02
Modified chromium oxide green	0.71	0.22	0.22	23	G03
Cobalt chromite green	0.58–0.64	0.14–0.18	0.17–0.28	13–23	G04–G06
Cobalt titanate green	0.37–0.73	0.21–0.30	0.04–0.22	10–24	G07–G09
Phthalocyanine green	0.42–0.45	0.06–0.07	0.10–0.20	13–25	G10–G11
Iron oxide red	0.31–0.67	0.19–0.38	0.00–0.08	13–26	R01–R04
Cadmium orange	0.87	0.26	0.18	10	R05
Organic red	0.83–0.87	0.06–0.14	0.15–0.32	11–27	R06–R09
Iron oxide yellow	0.70	0.21	0.16	19	Y01
Cadmium yellow	0.87	0.29	0.25	11	Y02
Chrome yellow	0.83	0.34	0.18	24	Y03
Chrome titanate yellow	0.80–0.86	0.26–0.62	0.05–0.23	17–26	Y04–Y07
Nickel titanate yellow	0.77–0.87	0.22–0.64	0.09–0.51	17–27	Y08–Y11
Strontium chromate yellow + titanium dioxide	0.86	0.38	0.21	19	Y12
Hansa yellow	0.87	0.06	0.43	11	Y13
Diarylide yellow	0.87	0.08	0.35	12	Y14
Mica + titanium dioxide	0.88–0.90	0.35–0.54	0.31–0.54	17–37	P01–P09
Mica + titanium dioxide + iron oxide	0.27–0.85	0.25–0.44	0.02–0.42	20–24	P10–P14

700–1000 nm; 30% lies within 1000–1500 nm; and 20% lies within 1500–2500 nm (Fig. 3). We refer to the 700–1000 nm region containing half the NIR solar energy (and a quarter of the total solar energy) as the "short" NIR.

In the discussions below, black and white *backgrounds* are assumed to be opaque, with observed NIR reflectances of 0.04 and 0.87, respectively. Note that in the absence of the air-film interface, the continuous refractive index (CRI) NIR reflectances of the black and white backgrounds are 0.00 and 0.94, respectively.

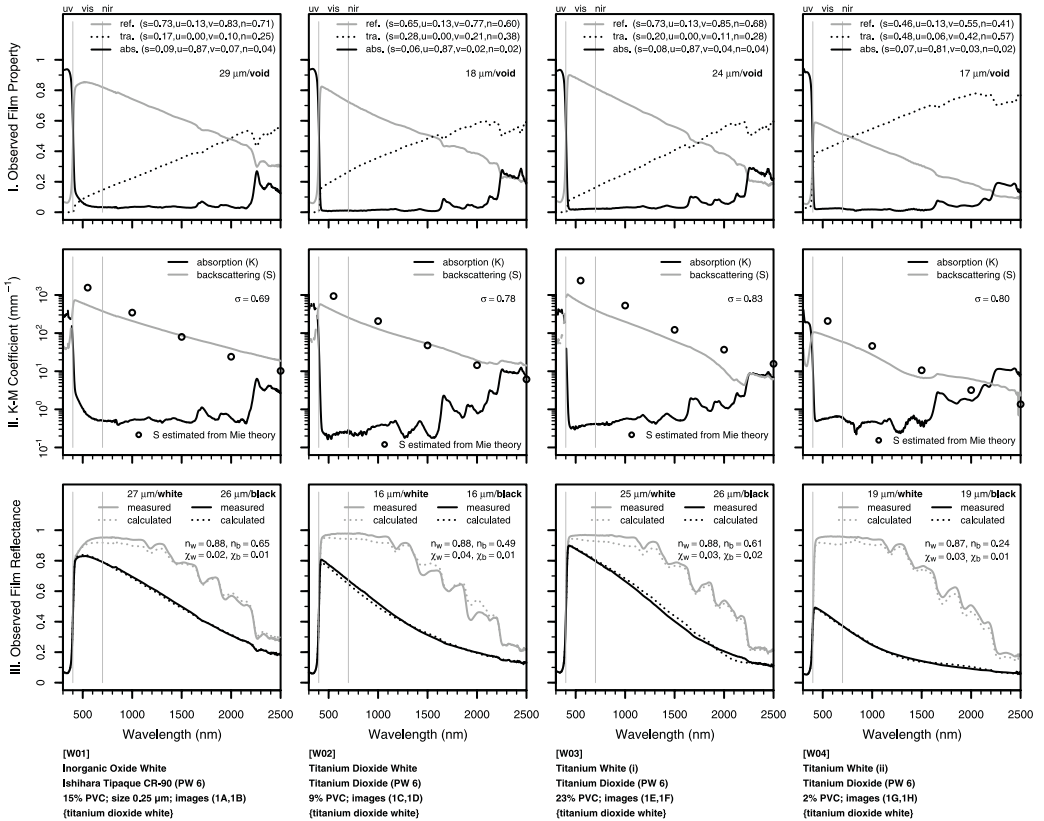

Fig. 1. (i/xxii) Measurements and model calculations for 87 predominately single-pigment films. Shown from top to bottom are (I) measured reflectance, transmittance, and absorptance of film with void background; (II) Kubelka–Munk backscattering and absorption coefficients S and K, and non-spectral forward scattering ratio σ; and (III) measured and computed film reflectances over white [w] and black [b] backgrounds, along with measured NIR reflectance n and RMS error χ. Also listed are pigment identification code; paint name; pigment name; PVC; pigment particle size, if known; and location of images in Fig. 2.

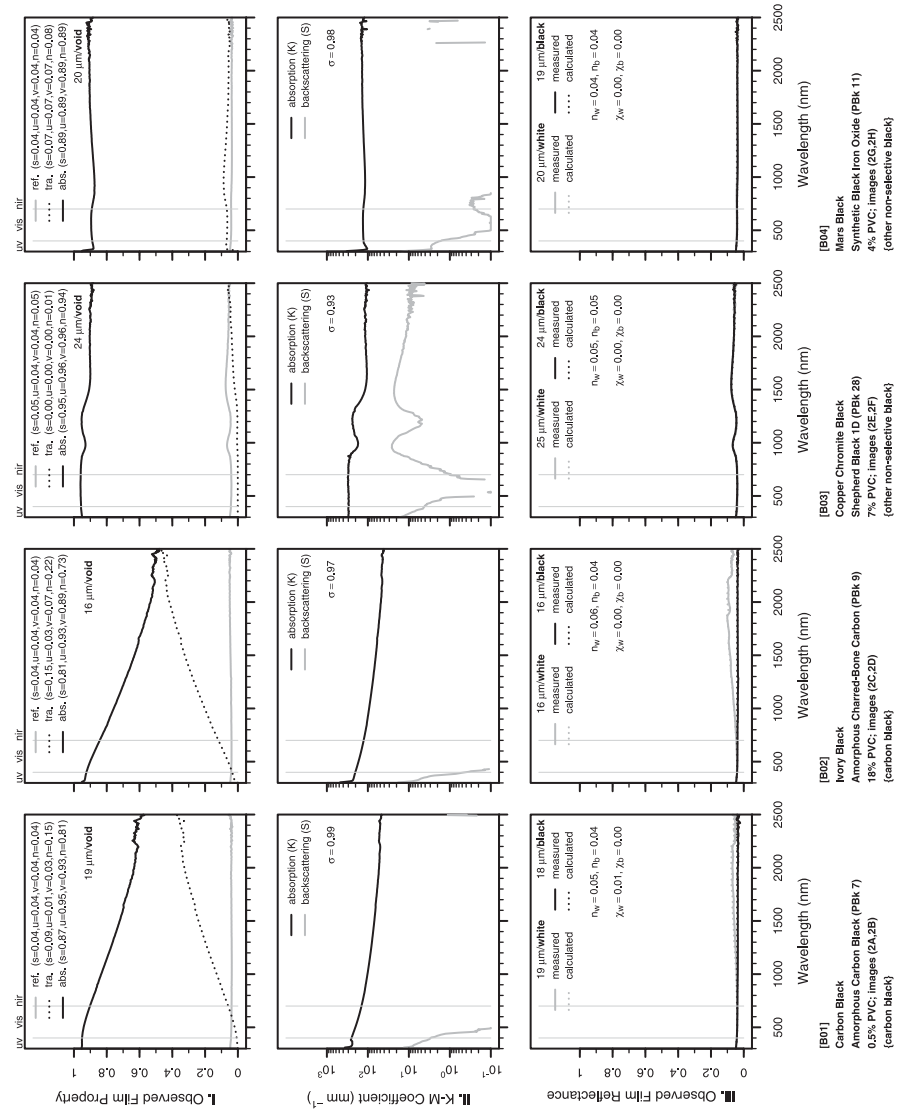
I. Observed Film Property
II. K-M Coefficient (mm⁻¹)
III. Observed Film Reflectance
uv vis nir
ref. (s=0.04,u=0.04,v=0.04,n=0.04)
trns. (s=0.09,u=0.01,v=0.03,n=0.15)
abs. (s=0.87,u=0.93,v=0.89,n=0.81)
19 µm/void
ref. (s=0.04,u=0.04,v=0.04,n=0.04)
trns. (s=0.15,u=0.03,v=0.07,n=0.22)
abs. (s=0.81,u=0.93,v=0.89,n=0.73)
16 µm/void
ref. (s=0.05,u=0.04,v=0.04,n=0.05)
trns. (s=0.00,u=0.00,v=0.00,n=0.01)
abs. (s=0.95,u=0.96,v=0.96,n=0.94)
24 µm/void
ref. (s=0.04,u=0.04,v=0.04,n=0.04)
trns. (s=0.07,u=0.07,v=0.07,n=0.09)
abs. (s=0.89,u=0.89,v=0.89,n=0.89)
20 µm/void
absorption (K)
backscattering (S)
σ = 0.99
σ = 0.97
σ = 0.93
σ = 0.98
19 µm/white
measured
calculated
18 µm/black
nW = 0.05, nb = 0.04
χW = 0.01, χb = 0.00
16 µm/white
16 µm/black
nW = 0.06, nb = 0.04
χW = 0.00, χb = 0.00
25 µm/white
24 µm/black
nW = 0.05, nb = 0.05
χW = 0.00, χb = 0.00
20 µm/white
19 µm/black
nW = 0.04, nb = 0.04
χW = 0.00, χb = 0.00
Wavelength (nm)
[B01]
Carbon Black
Amorphous Carbon Black (PBk 7)
0.5% PVC; images (2A,2B)
(carbon black)
[B02]
Ivory Black
Amorphous Charred-Bone Carbon (PBk 9)
18% PVC; images (2C,2D)
(carbon black)
[B03]
Copper Chromite Black
Shepherd Black 1D (PBk 28)
7% PVC; images (2E,2F)
(other non-selective black)
[B04]
Mars Black
Synthetic Black Iron Oxide (PBk 11)
4% PVC; images (2G,2H)
(other non-selective black)

Fig. 1. (ii/xxii)

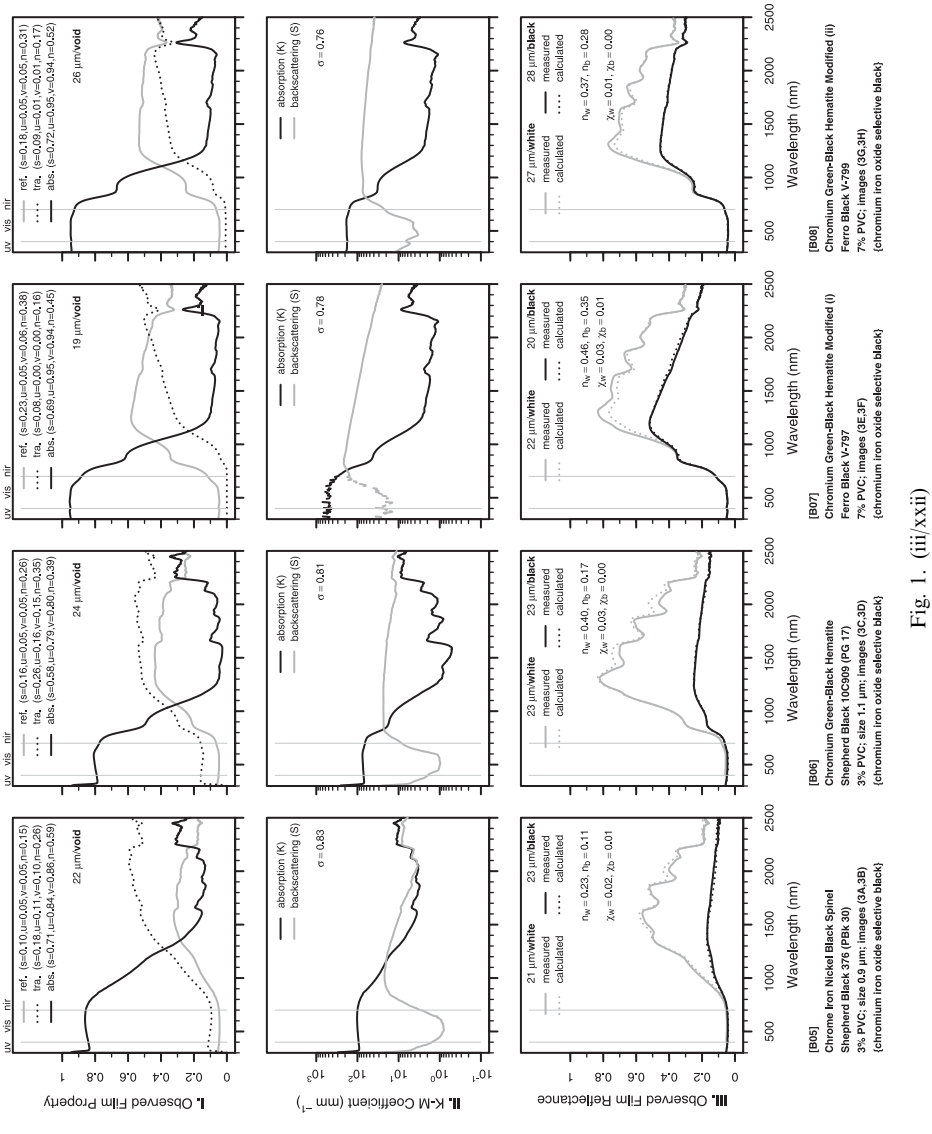

Fig. 1. (iii/xxii)

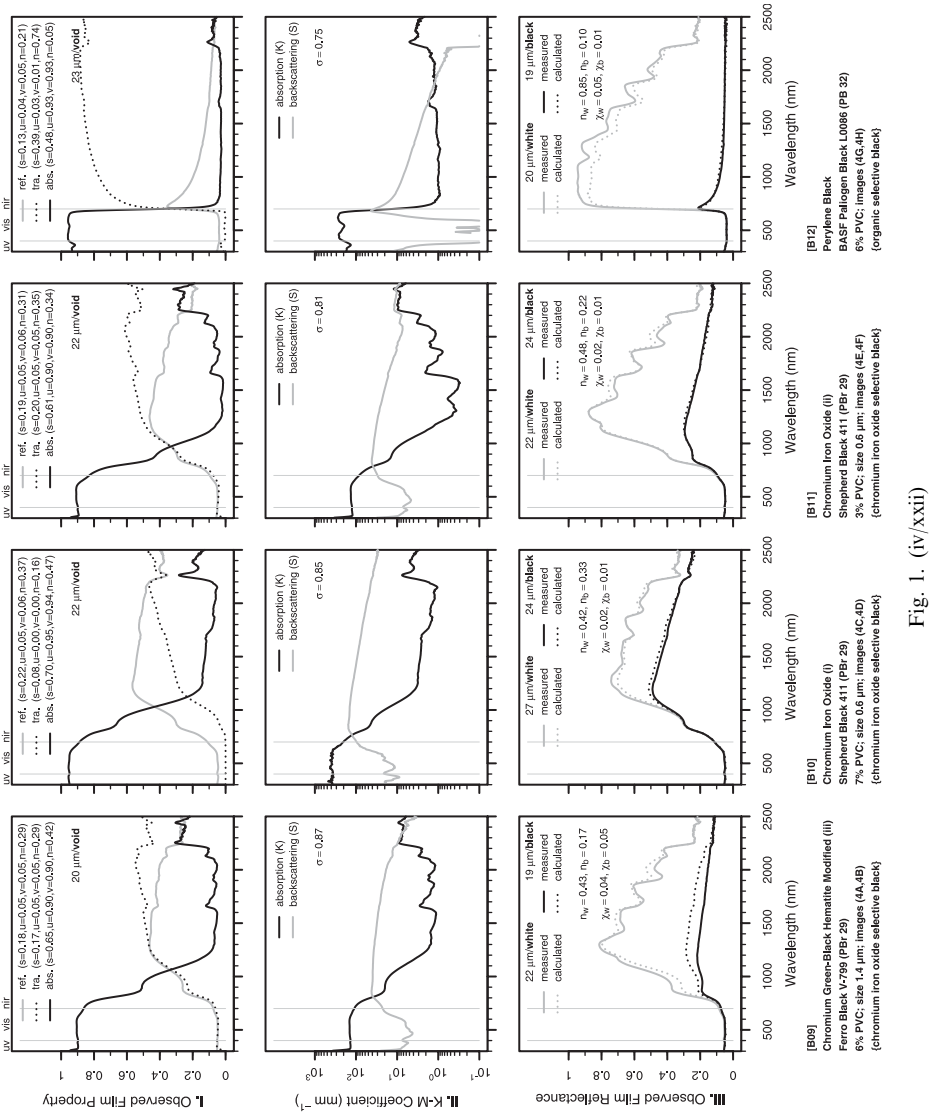
I. Observed Film Property
II. K-M Coefficient (mm⁻¹)
III. Observed Film Reflectance
Wavelength (nm)
uv vis nir
[B09]
Chromium Green-Black Hematite Modified (iii)
Ferro Black V-799 (PBr 29)
6% PVC; size 1.4 μm: images (4A,4B)
(chromium iron oxide selective black)
[B10]
Chromium Iron Oxide (i)
Shepherd Black 411 (PBr 29)
7% PVC; size 0.6 μm: images (4C,4D)
(chromium iron oxide selective black)
[B11]
Chromium Iron Oxide (ii)
Shepherd Black 411 (PBr 29)
3% PVC; size 0.6 μm: images (4E,4F)
(chromium iron oxide selective black)
[B12]
Perylene Black
BASF Fallogen Black L0086 (PB 32)
6% PVC: images (4G,4H)
(organic selective black)

Fig. 1. (iv/xxii)

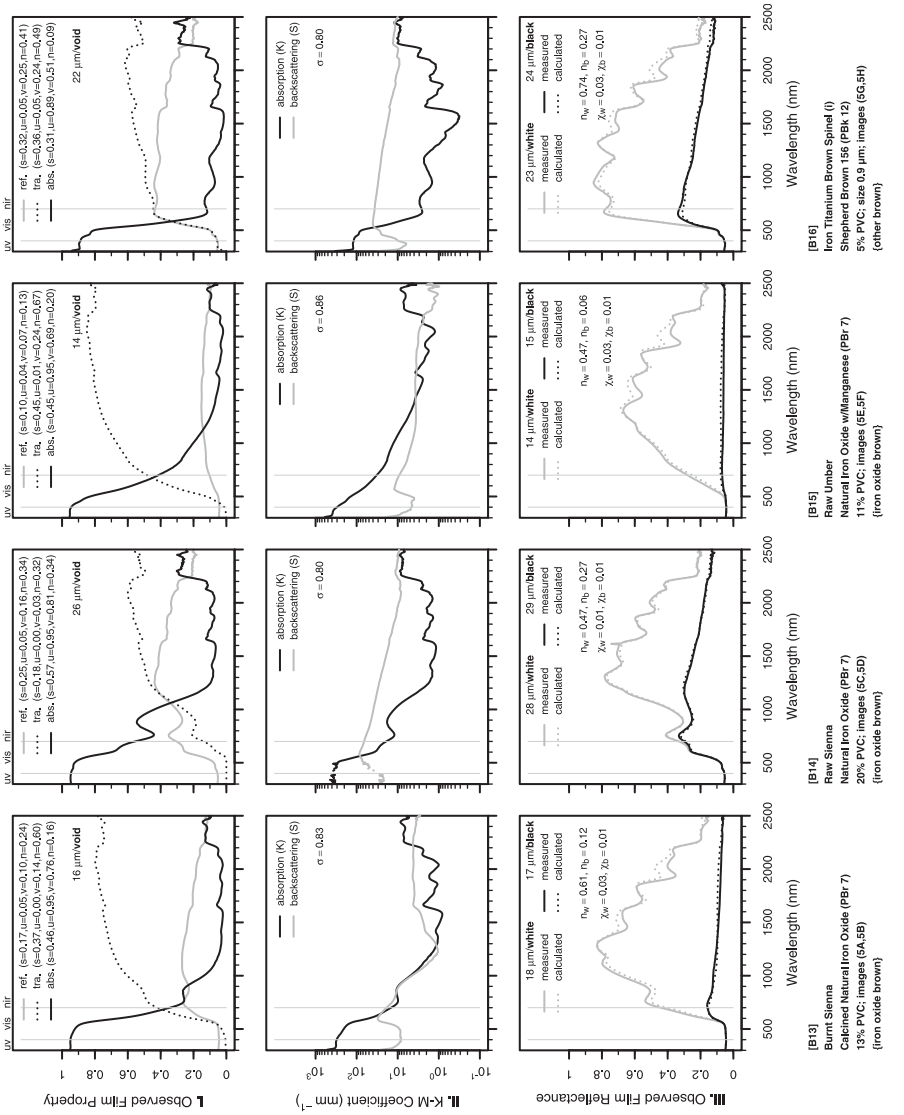
I. Observed Film Property
II. K-M Coefficient (mm⁻¹)
III. Observed Film Reflectance
uv vis nir
ref. (s=0.17,μ=0.05,v=0.10,n=0.24)
tra. (s=0.37,μ=0.00,v=0.14,n=0.60)
abs. (s=0.46,μ=0.95,v=0.76,n=0.16)
16 μm/void
ref. (s=0.25,μ=0.05,v=0.16,n=0.34)
tra. (s=0.18,μ=0.00,v=0.03,n=0.32)
abs. (s=0.57,μ=0.95,v=0.81,n=0.34)
26 μm/void
ref. (s=0.10,μ=0.04,v=0.07,n=0.13)
tra. (s=0.45,μ=0.01,v=0.24,n=0.67)
abs. (s=0.45,μ=0.95,v=0.69,n=0.20)
14 μm/void
ref. (s=0.32,μ=0.05,v=0.25,n=0.41)
tra. (s=0.36,μ=0.05,v=0.24,n=0.49)
abs. (s=0.31,μ=0.89,v=0.51,n=0.09)
22 μm/void
absorption (K)
backscattering (S)
σ = 0.83
σ = 0.80
σ = 0.86
σ = 0.80
18 μm/white
17 μm/black
28 μm/white
29 μm/black
14 μm/white
15 μm/black
23 μm/white
24 μm/black
measured
calculated
n_w = 0.61 , n_b = 0.12
χ_w = 0.03, χ_b = 0.01
n_w = 0.47 , n_b = 0.27
χ_w = 0.01, χ_b = 0.01
n_w = 0.47 , n_b = 0.06
χ_w = 0.03, χ_b = 0.01
n_w = 0.74 , n_b = 0.27
χ_w = 0.03, χ_b = 0.01
Wavelength (nm)
[B13]
Burnt Sienna
Calcined Natural Iron Oxide (PBr 7)
13% PVC; images (5A,5B)
{iron oxide brown}
[B14]
Raw Sienna
Natural Iron Oxide (PBr 7)
20% PVC; images (5C,5D)
{iron oxide brown}
[B15]
Raw Umber
Natural Iron Oxide w/Manganese (PBr 7)
11% PVC; images (5E,5F)
{iron oxide brown}
[B16]
Iron Titanium Brown Spinel (i)
Shepherd Brown 156 (PBk 12)
5% PVC; size 0.9 μm; images (5G,5H)
{other brown}

Fig. 1. (v/xxii)

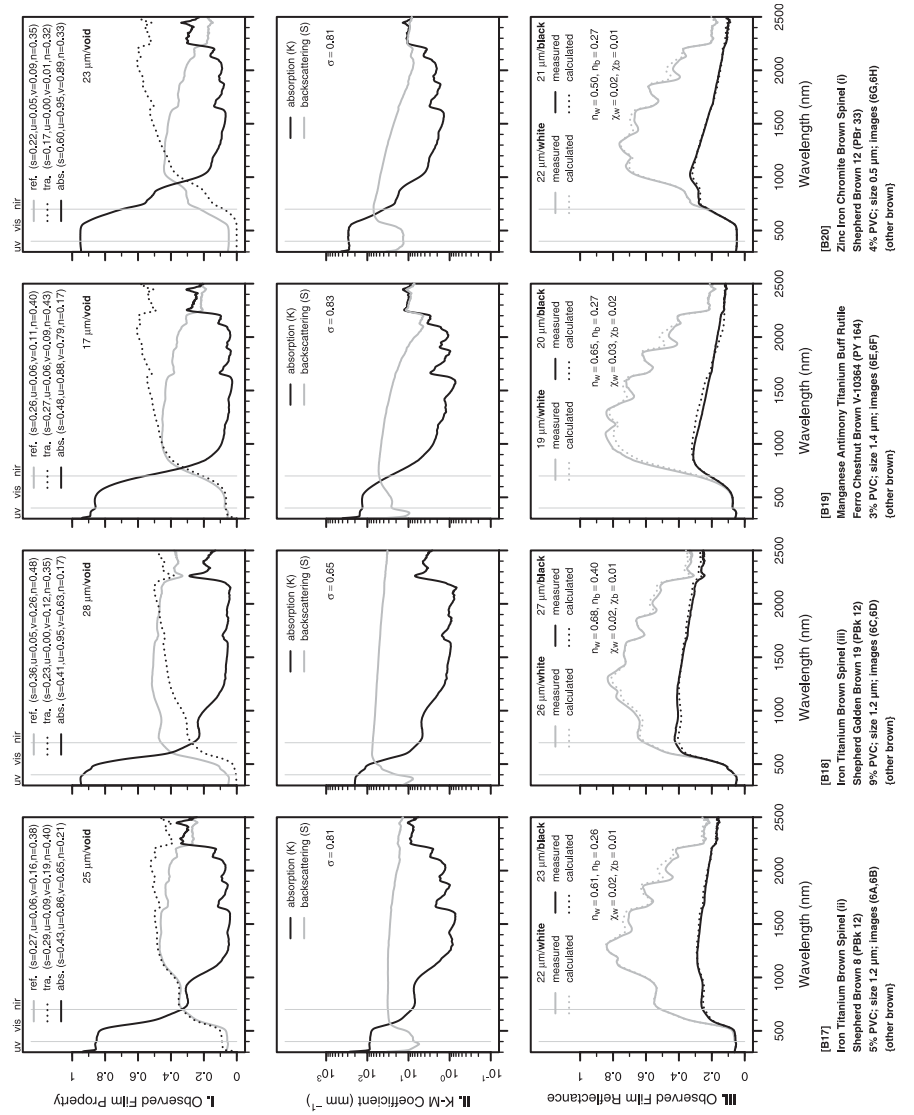

[B17] Iron Titanium Brown Spinel (ii) Shepherd Brown 8 (PBk 12) 5%; PVC; size 1.2 μm; images (6A,6B) (other brown)

[B18] Iron Titanium Brown Spinel (iii) Shepherd Golden Brown 19 (PBk 12) 9%; PVC; size 1.2 μm; images (6C,6D) (other brown)

[B19] Manganese Antimony Titanium Buff Rutile Ferro Chestnut Brown V-10364 (PY 164) 3%; PVC; size 1.4 μm; images (6E,6F) (other brown)

[B20] Zinc Iron Chromite Brown Spinel (i) Shepherd Brown 12 (PBr 33) 4% PVC; size 0.5 μm; images (6G,6H) (other brown)

Fig. 1. (vi/xxii)

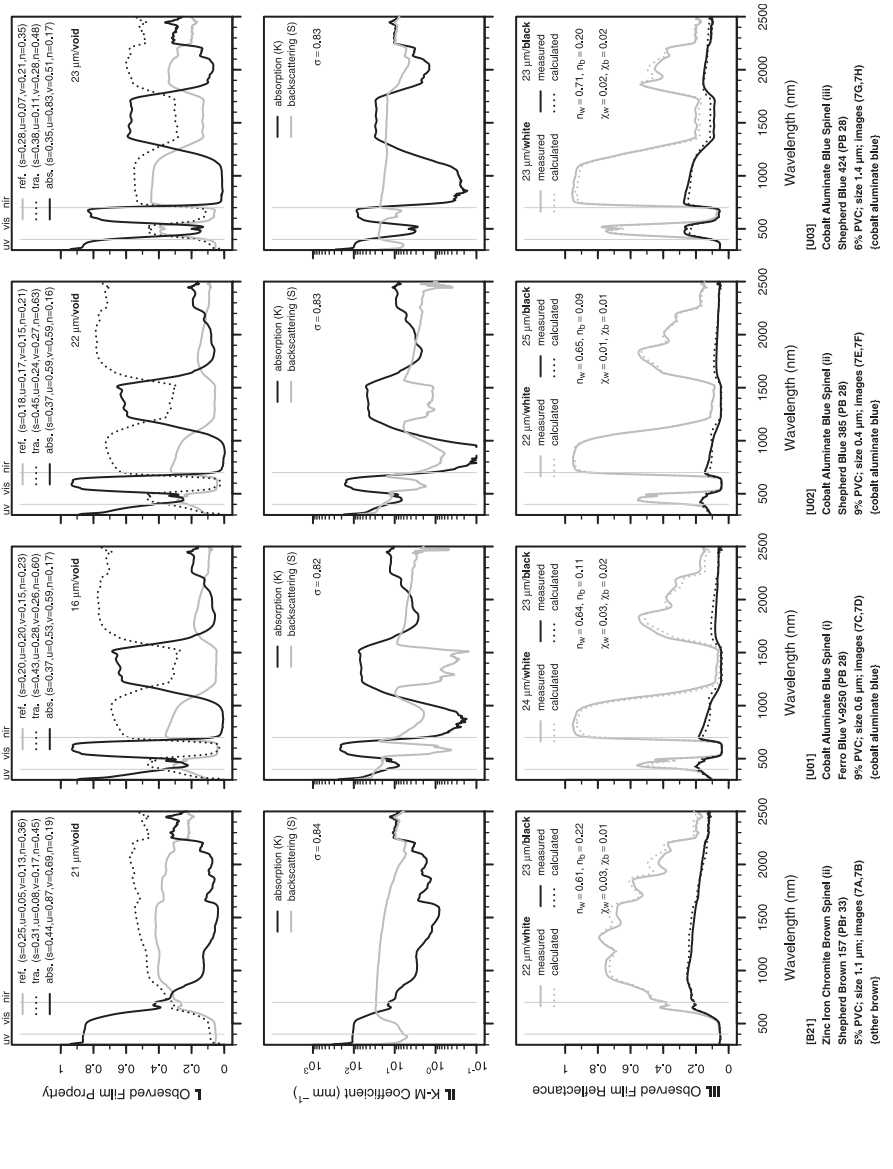

Fig. 1. (vii/xxii)

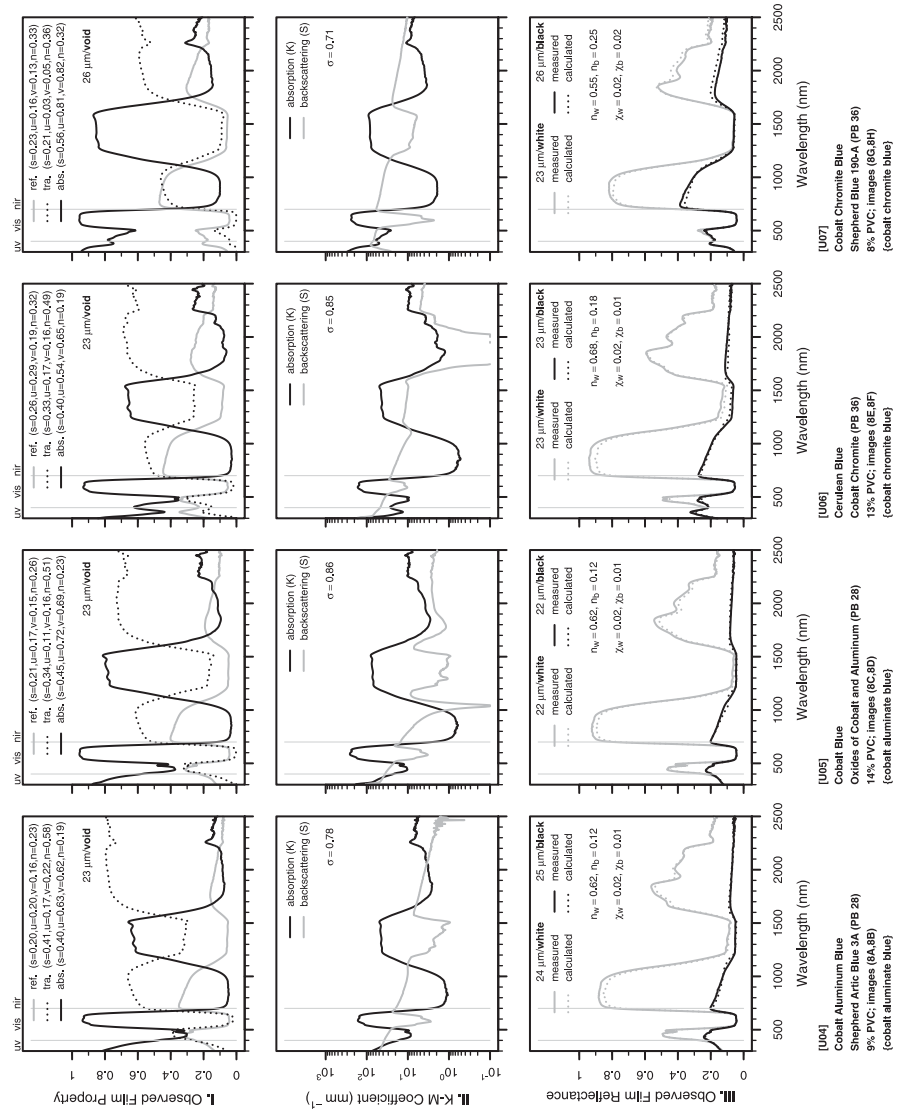

Fig. 1. (viii/xxii)

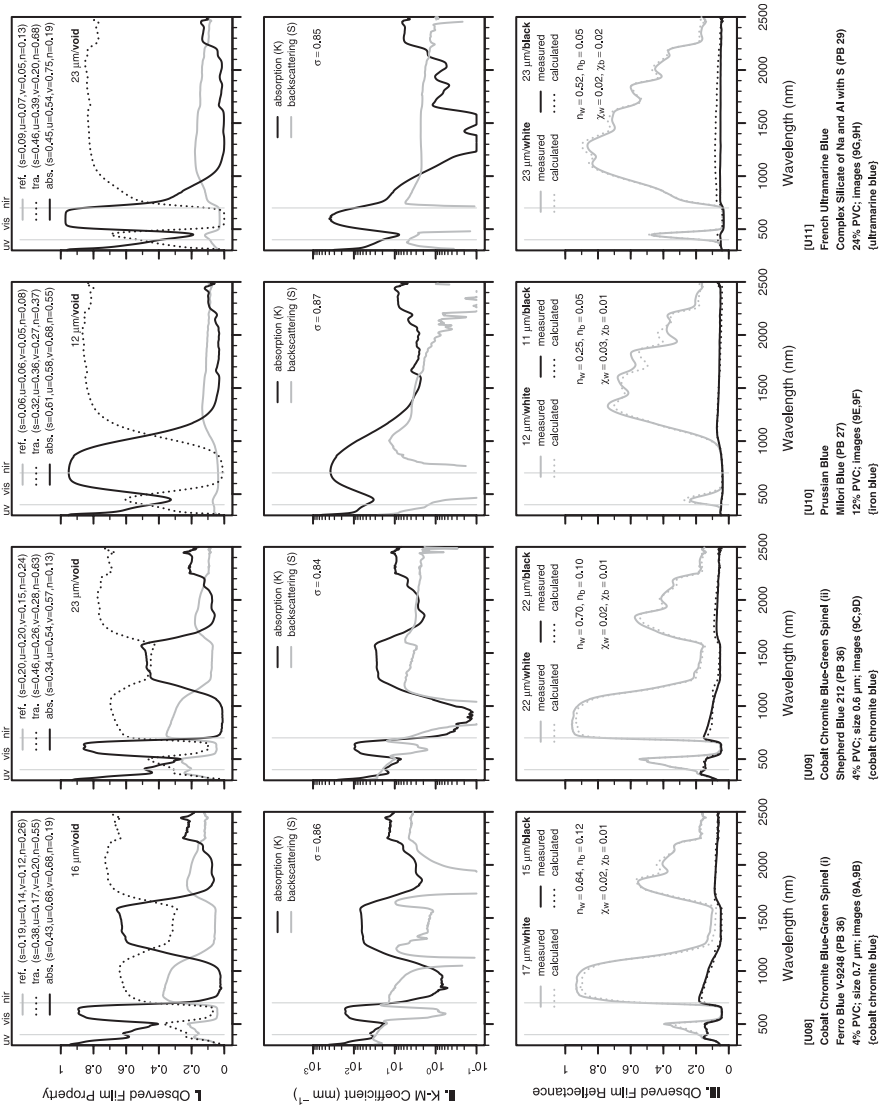
uv vis nir
I. Observed Film Property
II. K-M Coefficient (mm⁻¹)
III. Observed Film Reflectance
Wavelength (nm)
[U08]
Cobalt Chromite Blue-Green Spinel (i)
Ferro Blue V-9248 (PB 36)
4% PVC; size 0.7 μm; images (9A,9B)
{cobalt chromite blue}
[U09]
Cobalt Chromite Blue-Green Spinel (ii)
Shepherd Blue 212 (PB 36)
4% PVC; size 0.6 μm; images (9C,9D)
{cobalt chromite blue}
[U10]
Prussian Blue
Milori Blue (PB 27)
12% PVC; images (9E,9F)
{iron blue}
[U11]
French Ultramarine Blue
Complex Silicate of Na and Al with S (PB 29)
24% PVC; images (9G,9H)
{ultramarine blue}

Fig. 1. (ix/xxii)

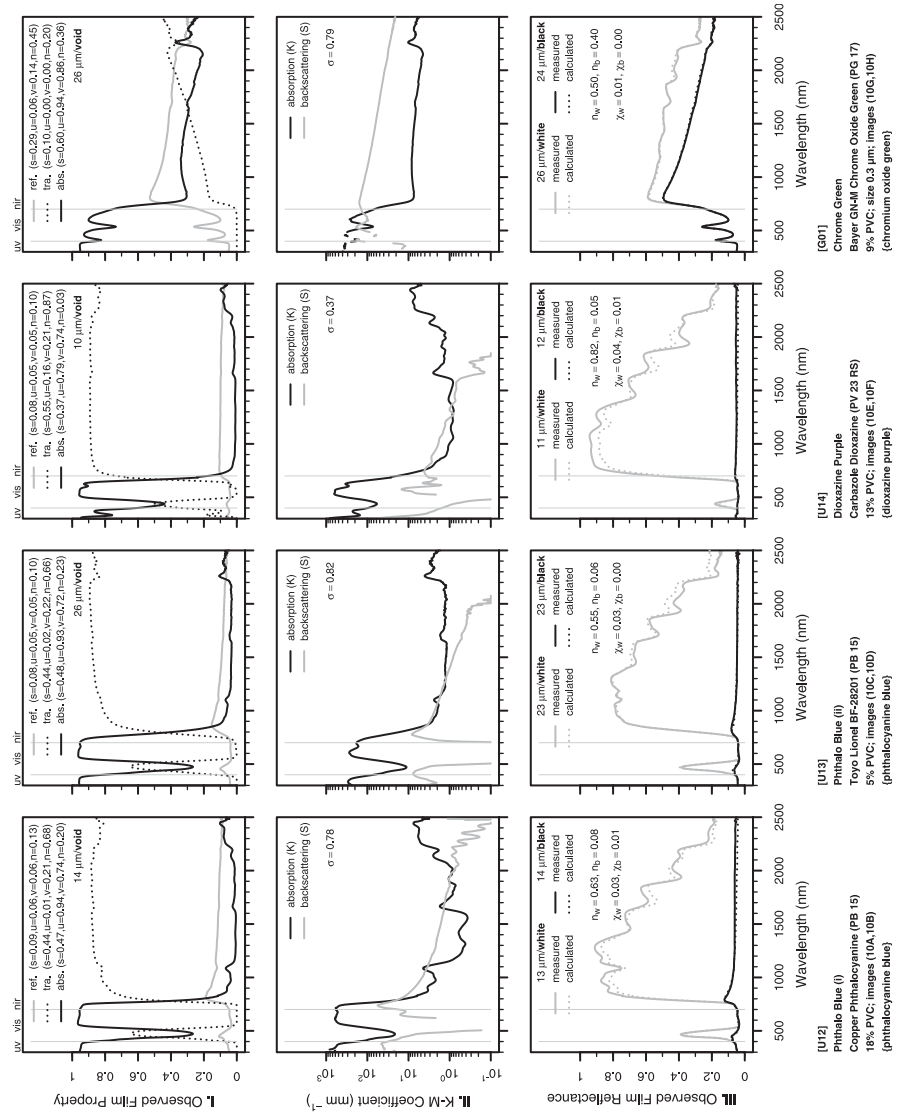
I. Observed Film Property
II. K-M Coefficient (mm⁻¹)
III. Observed Film Reflectance
uv vis nir
Wavelength (nm)
ref. (s=0.09,μ=0.06,ν=0.06,π=0.13)
tra. (s=0.44,μ=0.01,ν=0.27,π=0.68)
abs. (s=0.47,μ=0.94,ν=0.74,π=0.20)
14 μm/void
ref. (s=0.08,μ=0.05,ν=0.05,π=0.10)
tra. (s=0.44,μ=0.02,ν=0.22,π=0.66)
abs. (s=0.48,μ=0.93,ν=0.72,π=0.23)
26 μm/void
ref. (s=0.08,μ=0.05,ν=0.05,π=0.10)
tra. (s=0.55,μ=0.15,ν=0.21,π=0.87)
abs. (s=0.37,μ=0.79,ν=0.74,π=0.03)
10 μm/void
ref. (s=0.29,μ=0.06,ν=0.14,π=0.45)
tra. (s=0.10,μ=0.00,ν=0.00,π=0.20)
abs. (s=0.60,μ=0.94,ν=0.86,π=0.36)
26 μm/void
absorption (K)
backscattering (S)
σ = 0.78
σ = 0.82
σ = 0.37
σ = 0.79
13 μm/white
14 μm/black
measured
calculated
$n_W = 0.63$, $n_B = 0.08$
$\chi_W = 0.03$, $\chi_B = 0.01$
23 μm/white
23 μm/black
$n_W = 0.55$, $n_B = 0.06$
$\chi_W = 0.03$, $\chi_B = 0.00$
11 μm/white
12 μm/black
$n_W = 0.82$, $n_B = 0.05$
$\chi_W = 0.04$, $\chi_B = 0.01$
26 μm/white
24 μm/black
$n_W = 0.50$, $n_B = 0.40$
$\chi_W = 0.01$, $\chi_B = 0.00$
[U12]
Phthalo Blue (i)
Copper Phthalocyanine (PB 15)
18% PVC; images (10A,10B)
{phthalocyanine blue}
[U13]
Phthalo Blue (ii)
Toyo Lionel BF-28201 (PB 15)
5% PVC; images (10C,10D)
{phthalocyanine blue}
[U14]
Dioxazine Purple
Carbazole Dioxazine (PV 23 RS)
13% PVC; images (10E,10F)
{dioxazine purple}
[G01]
Chrome Green
Bayer GN-M Chrome Oxide Green (PG 17)
9% PVC; size 0.3 μm; images (10G,10H)
{chromium oxide green}

Fig. 1. (x/xxii)

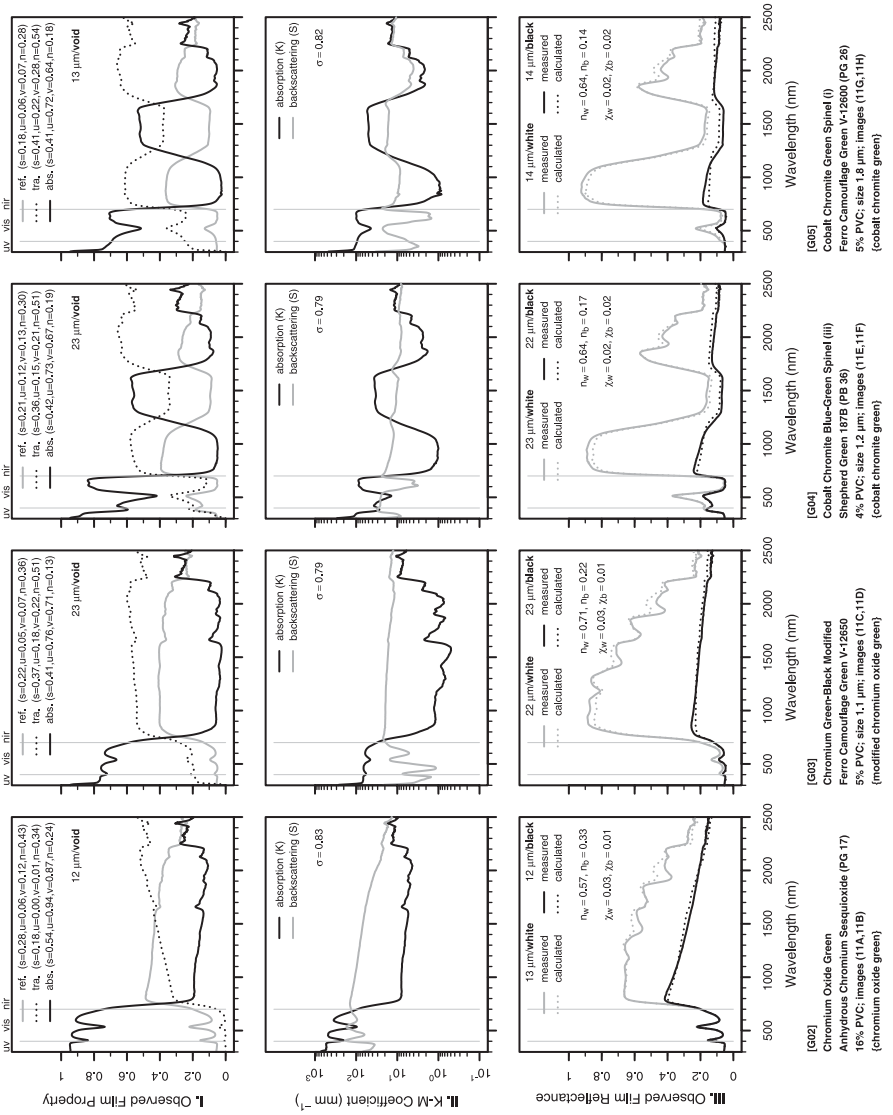
I. Observed Film Property
II. K-M Coefficient (mm⁻¹)
III. Observed Film Reflectance
uv vis nir
ref. (s=0.28,μ=0.06,v=0.12,n=0.43)
trns. (s=0.18,μ=0.06,v=0.01,n=0.34)
abs. (s=0.54,μ=0.94,v=0.87,n=0.24)
12 μm/void
absorption (K)
backscattering (S)
σ = 0.83
13 μm/white
12 μm/black
measured
calculated
nW = 0.57, nb = 0.33
χW = 0.03, χb = 0.01
Wavelength (nm)
[G02]
Chromium Oxide Green
Anhydrous Chromium Sesquioxide (PG 17)
16% PVC; images (11A,11B)
(chromium oxide green)
ref. (s=0.22,μ=0.05,v=0.07,n=0.36)
trns. (s=0.37,μ=0.18,v=0.22,n=0.51)
abs. (s=0.41,μ=0.76,v=0.71,n=0.19)
23 μm/void
σ = 0.79
23 μm/white
23 μm/black
nW = 0.71, nb = 0.22
χW = 0.03, χb = 0.01
[G03]
Chromium Green-Black Modified
Ferro Camouflage Green V-12650
5% PVC; size 1.1 μm; images (11C,11D)
(modified chromium oxide green)
ref. (s=0.21,μ=0.12,v=0.13,n=0.30)
trns. (s=0.36,μ=0.15,v=0.21,n=0.51)
abs. (s=0.42,μ=0.73,v=0.67,n=0.19)
σ = 0.79
22 μm/white
22 μm/black
nW = 0.64, nb = 0.17
χW = 0.02, χb = 0.02
[G04]
Cobalt Chromite Blue-Green Spinel (iii)
Shepherd Green 187B (PB 36)
4% PVC; size 1.2 μm; images (11E,11F)
(cobalt chromite green)
ref. (s=0.18,μ=0.06,v=0.07,n=0.28)
trns. (s=0.41,μ=0.22,v=0.28,n=0.54)
abs. (s=0.41,μ=0.72,v=0.64,n=0.18)
13 μm/void
σ = 0.82
14 μm/white
14 μm/black
nW = 0.64, nb = 0.14
χW = 0.02, χb = 0.02
[G05]
Cobalt Chromite Green Spinel (i)
Ferro Camouflage Green V-12600 (PG 26)
5% PVC; size 1.8 μm; images (11G,11H)
(cobalt chromite green)

Fig. 1. (xi/xxii)

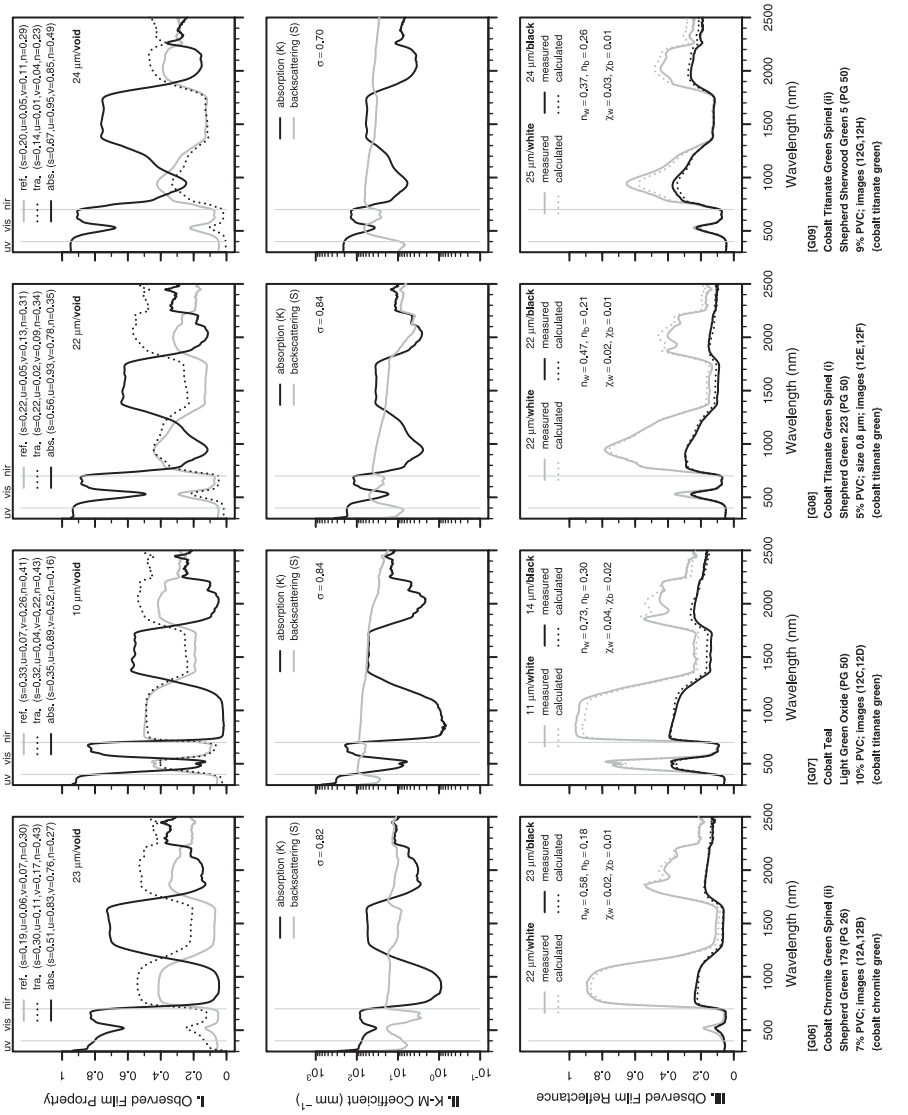

Fig. 1. (xii/xxii)

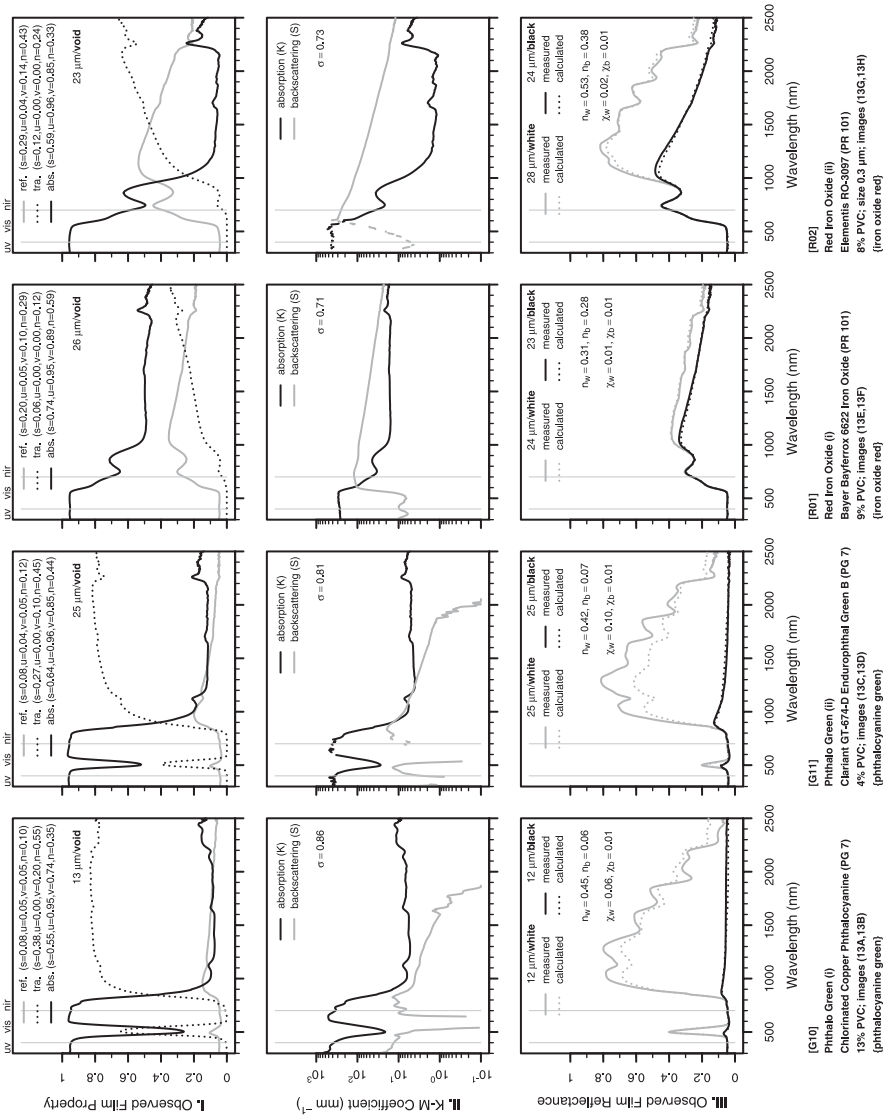

Fig. 1. (xiii/xxii)

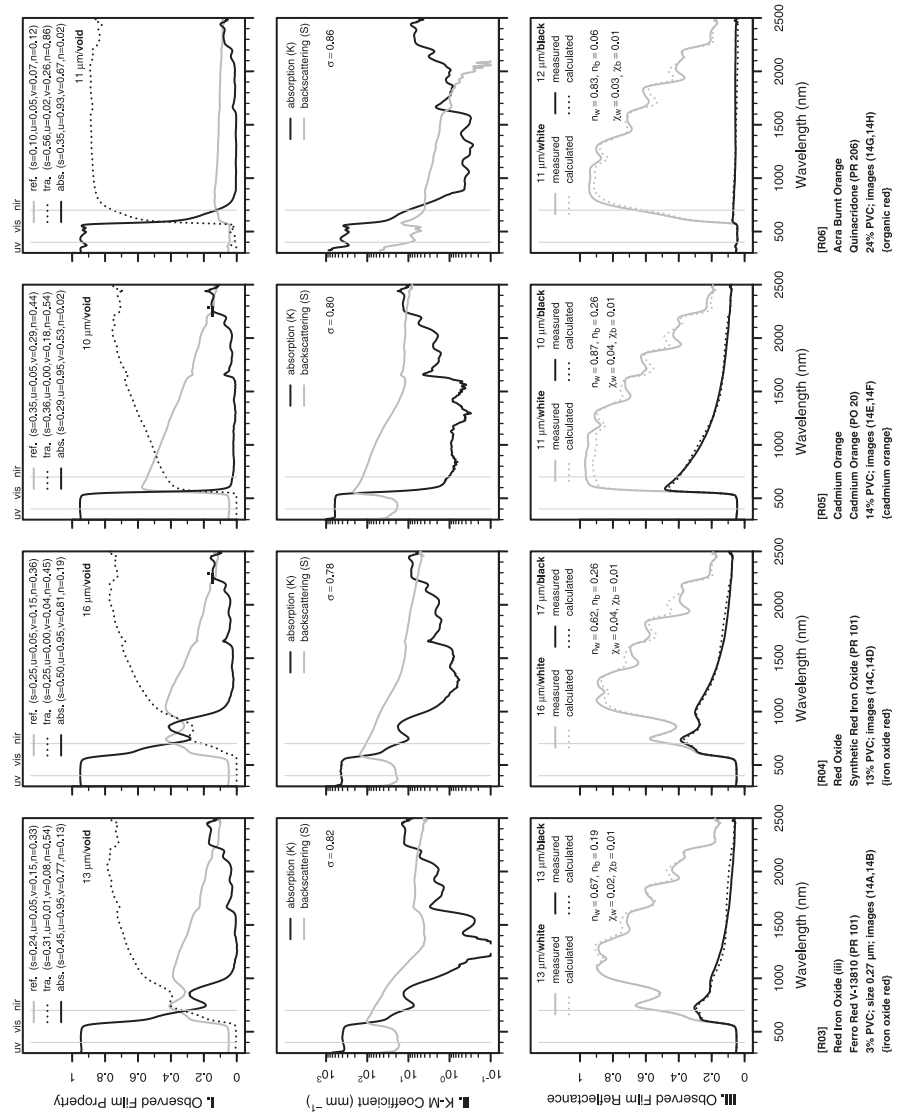

[R03]
Red Iron Oxide (iii)
Ferro Red V-13810 (PR 101)
3% PVC; size 0.27 µm; images (14A,14B)
(iron oxide red)

[R04]
Red Oxide
Synthetic Red Iron Oxide (PR 101)
13% PVC; images (14C;14D)
(iron oxide red)

[R05]
Cadmium Orange
Cadmium Orange (PO 20)
14% PVC; images (14E;14F)
(cadmium orange)

[R06]
Acra Burnt Orange
Quinacridone (PR 206)
24% PVC; images (14G;14H)
(organic red)

Fig. 1. (xiv/xxii)

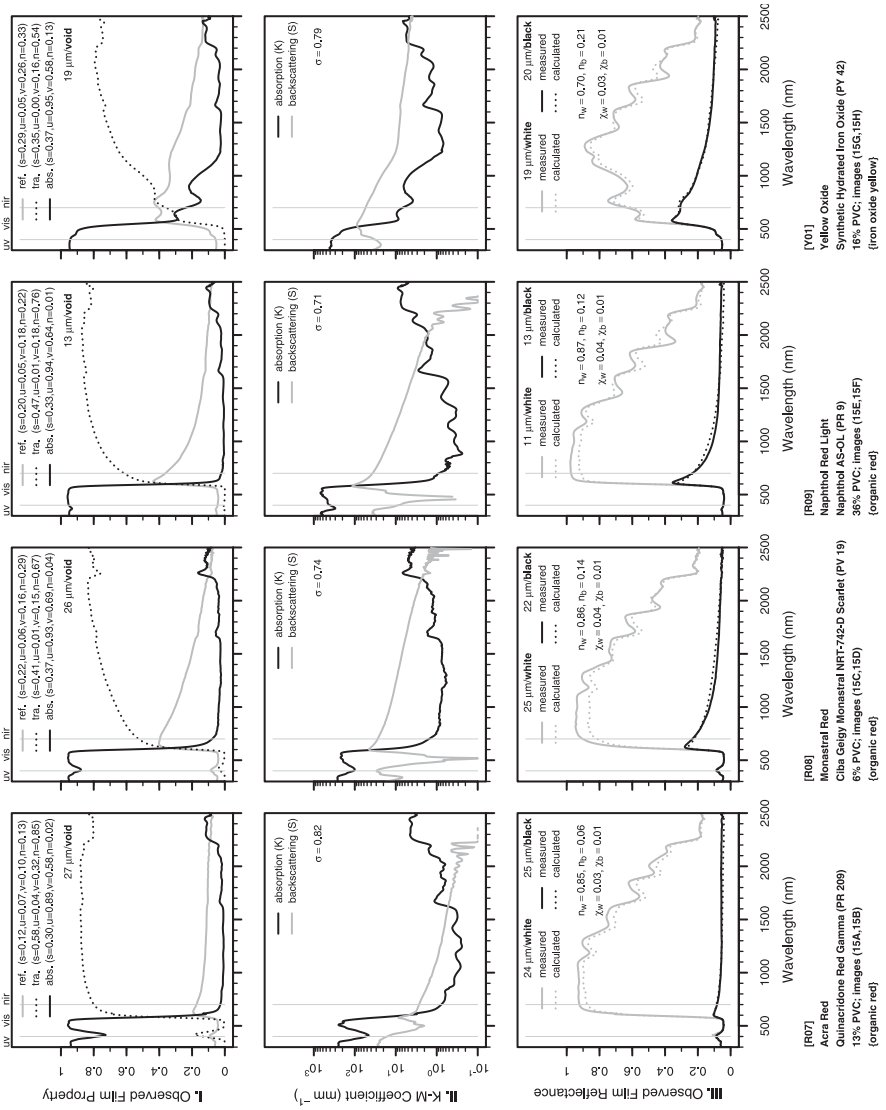
I. Observed Film Property
II. K-M Coefficient (mm⁻¹)
III. Observed Film Reflectance
uv vis nir
ref. (s=0.12,u=0.07,v=0.10,n=0.13)
trns. (s=0.58,u=0.04,v=0.22,n=0.85)
abs. (s=0.30,u=0.89,v=0.58,n=0.02)
27 µm/void
ref. (s=0.22,u=0.06,v=0.16,n=0.29)
trns. (s=0.44,u=0.01,v=0.15,n=0.67)
abs. (s=0.37,u=0.93,v=0.69,n=0.04)
26 µm/void
ref. (s=0.20,u=0.05,v=0.18,n=0.22)
trns. (s=0.47,u=0.01,v=0.18,n=0.76)
abs. (s=0.33,u=0.94,v=0.64,n=0.01)
13 µm/void
ref. (s=0.29,u=0.05,v=0.26,n=0.33)
trns. (s=0.35,u=0.00,v=0.16,n=0.54)
abs. (s=0.37,u=0.95,v=0.58,n=0.19)
19 µm/void
absorption (K)
backscattering (S)
σ = 0.82
σ = 0.74
σ = 0.71
σ = 0.79
24 µm/white
25 µm/black
measured
calculated
n_W = 0.85, n_b = 0.06
χ_W = 0.03, χ_b = 0.01
25 µm/white
22 µm/black
n_W = 0.86, n_b = 0.14
χ_W = 0.04, χ_b = 0.01
11 µm/white
13 µm/black
n_W = 0.87, n_b = 0.12
χ_W = 0.04, χ_b = 0.01
19 µm/white
20 µm/black
n_W = 0.70, n_b = 0.21
χ_W = 0.03, χ_b = 0.01
Wavelength (nm)
[R07]
Acra Red
Quinacridone Red Gamma (PR 209)
13% PVC; images (15A.15B)
(organic red)
[R08]
Monastral Red
Ciba Geigy Monastral NRT-742-D Scarlet (PV 19)
6% PVC; images (15C.15D)
(organic red)
[R09]
Naphthol Red Light
Naphthol AS-OL (PR 9)
36% PVC; images (15E.15F)
(organic red)
[Y01]
Yellow Oxide
Synthetic Hydrated Iron Oxide (PY 42)
16% PVC; images (15G.15H)
(iron oxide yellow)

Fig. 1. (xv/xxii)

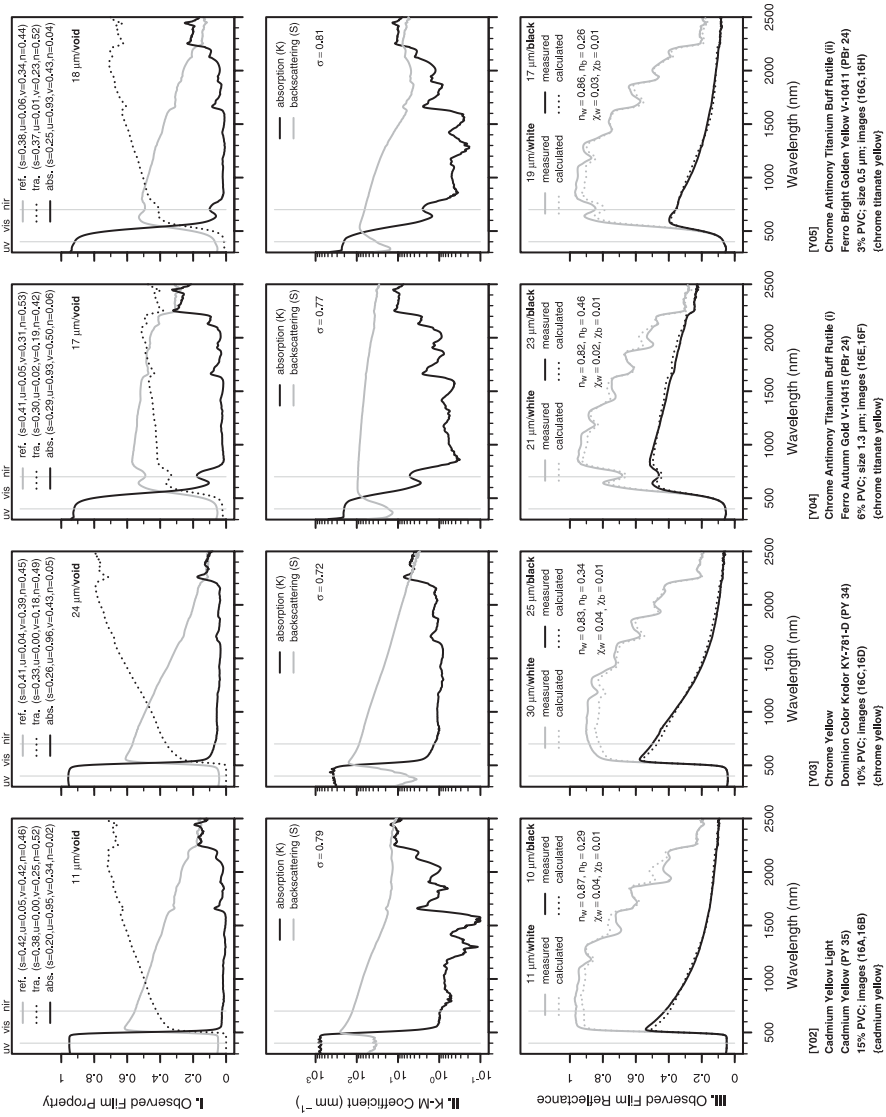

Fig. 1. (xvi/xxii)

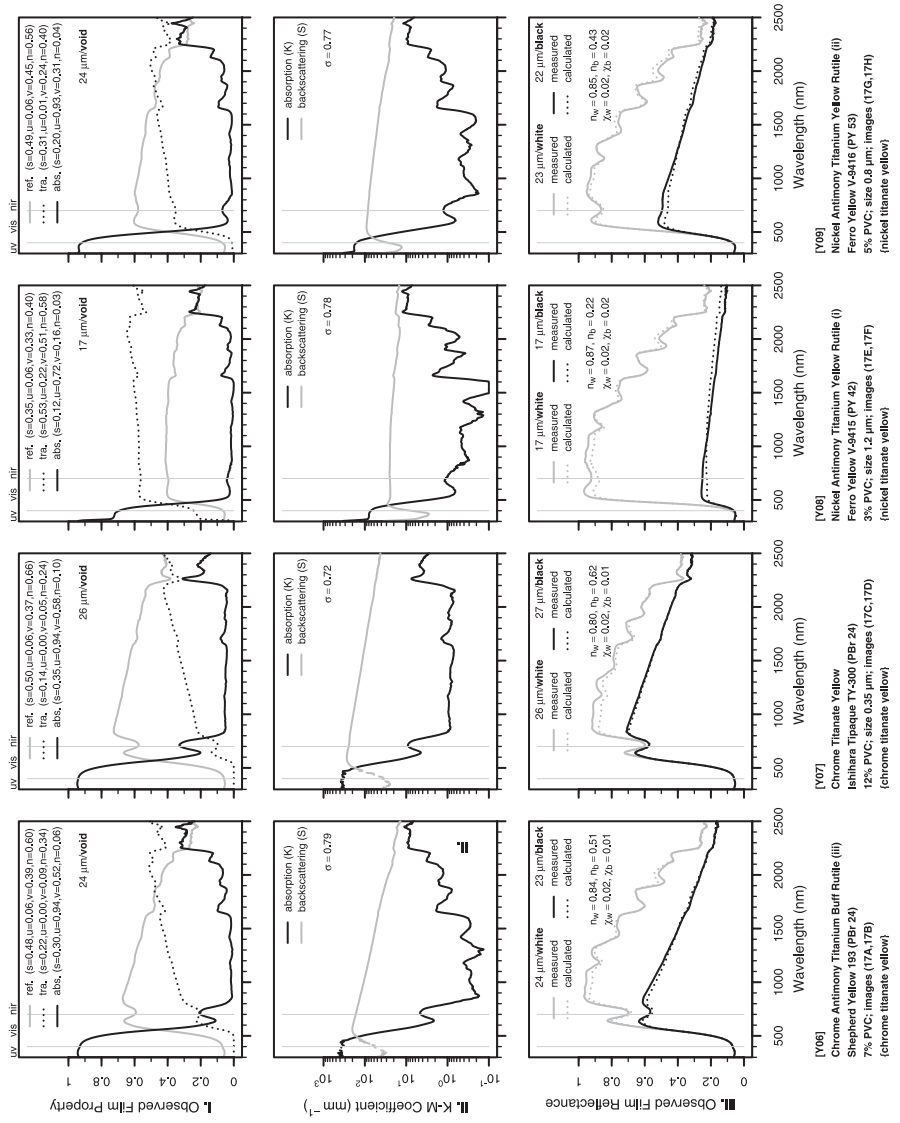

Fig. 1. (xvii/xxii)

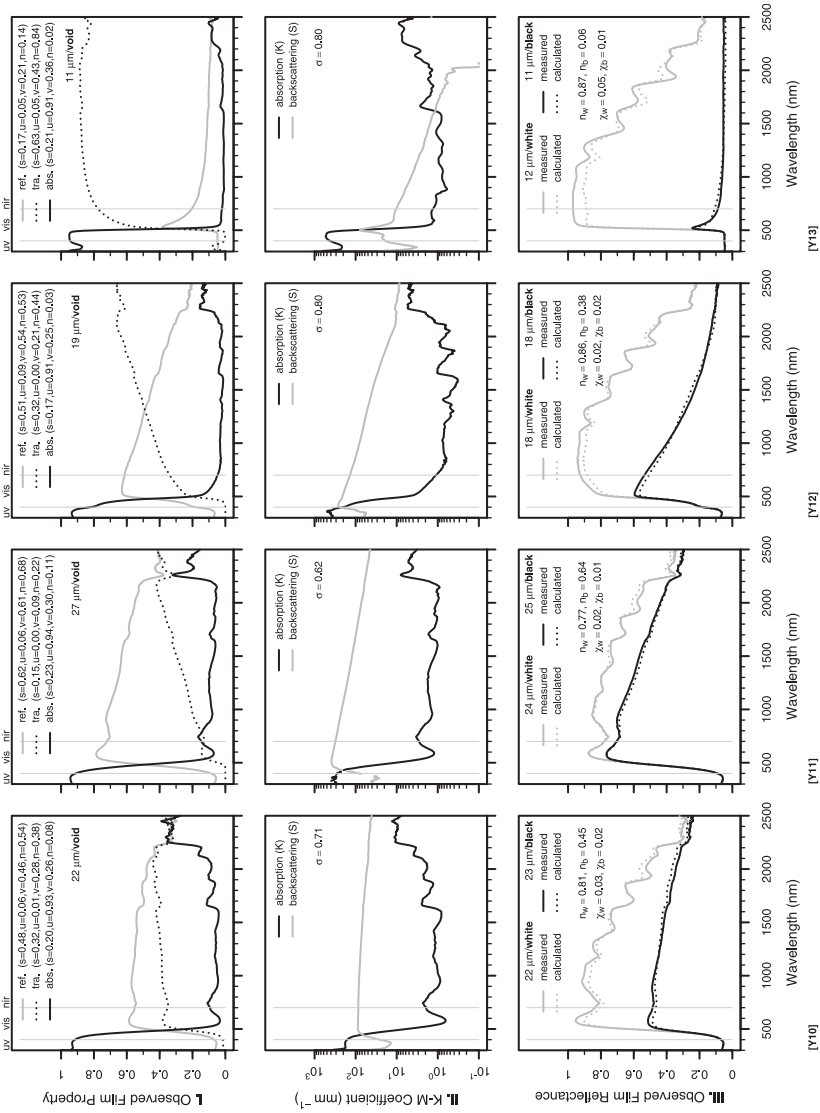

Fig. 1. (xviii/xxii)

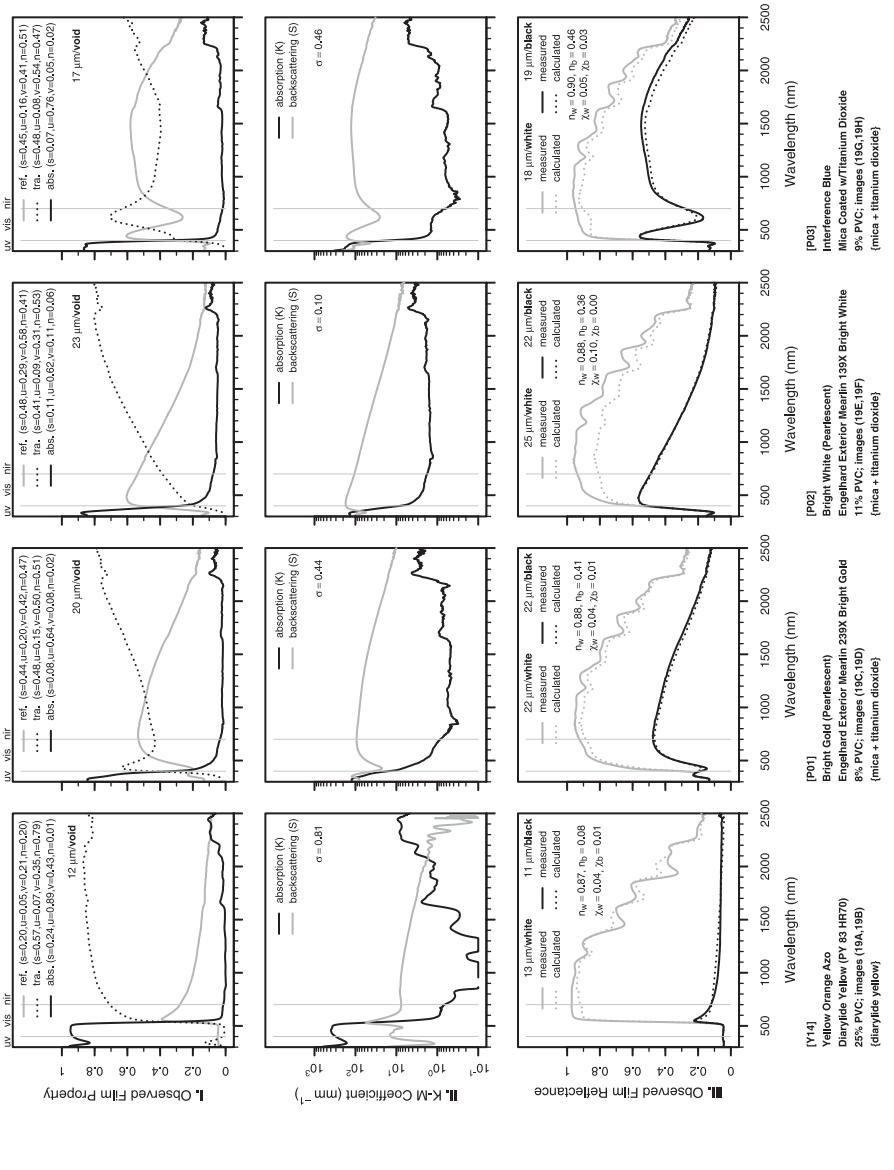

Fig. 1. (xix/xxii)

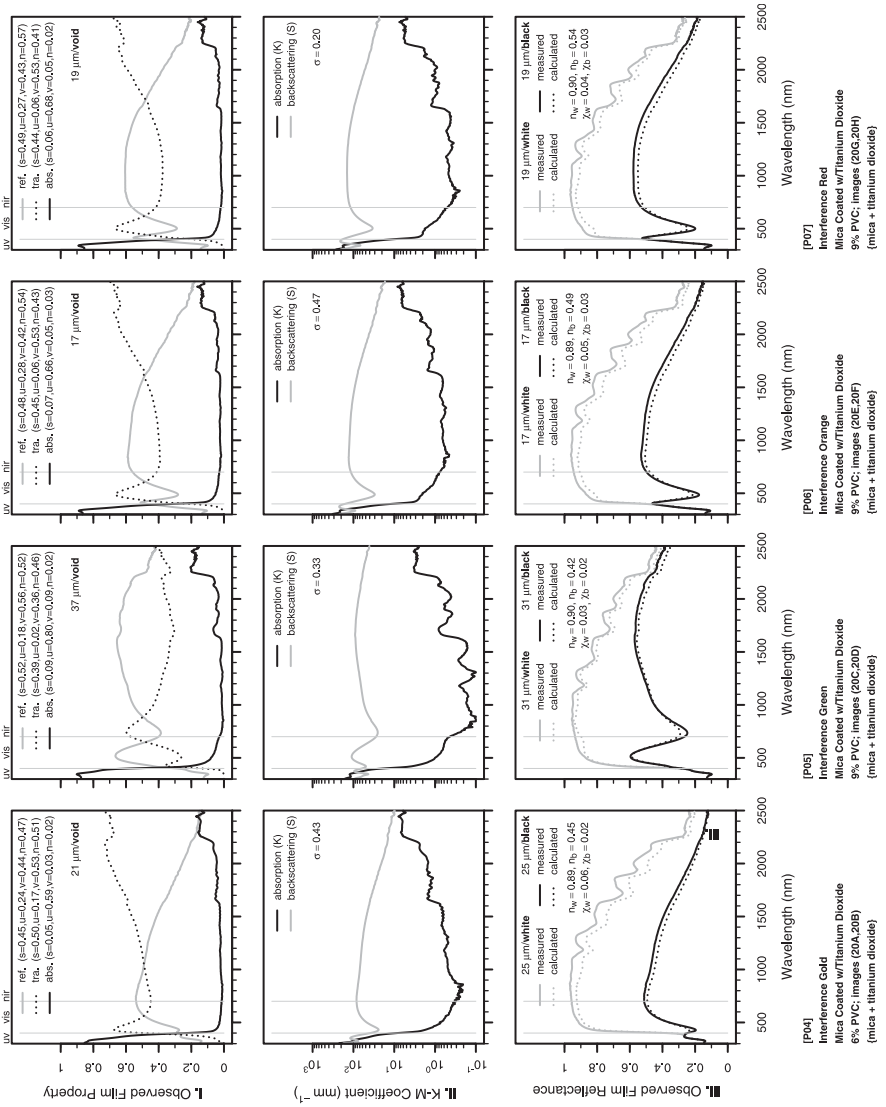
I. Observed Film Property
II. K-M Coefficient (mm⁻¹)
III. Observed Film Reflectance
uv vis nir
ref. (s=0.45,μ=0.24,v=0.44,n=0.47)
trn. (s=0.50,μ=0.17,v=0.53,n=0.51)
abs. (s=0.05,μ=0.59,v=0.03,n=0.02)
21 μm/void
ref. (s=0.52,μ=0.18,v=0.56,n=0.52)
trn. (s=0.39,μ=0.02,v=0.36,n=0.46)
abs. (s=0.09,μ=0.80,v=0.09,n=0.02)
37 μm/void
ref. (s=0.48,μ=0.28,v=0.42,n=0.54)
trn. (s=0.45,μ=0.06,v=0.53,n=0.40)
abs. (s=0.07,μ=0.66,v=0.05,n=0.03)
17 μm/void
ref. (s=0.49,μ=0.27,v=0.43,n=0.57)
trn. (s=0.44,μ=0.06,v=0.53,n=0.41)
abs. (s=0.06,μ=0.68,v=0.05,n=0.02)
19 μm/void
absorption (K)
backscattering (S)
σ = 0.43
σ = 0.33
σ = 0.47
σ = 0.20
25 μm/white
measured
calculated
25 μm/black
nW = 0.89, nb = 0.45
χW = 0.06, χb = 0.02
31 μm/white
31 μm/black
nW = 0.90, nb = 0.42
χW = 0.03, χb = 0.02
17 μm/white
17 μm/black
nW = 0.89, nb = 0.49
χW = 0.05, χb = 0.03
19 μm/white
19 μm/black
nW = 0.90, nb = 0.54
χW = 0.04, χb = 0.03
Wavelength (nm)
[P04]
Interference Gold
Mica Coated w/Titanium Dioxide
6% PVC; images (20A,20B)
(mica + titanium dioxide)
[P05]
Interference Green
Mica Coated w/Titanium Dioxide
9% PVC; images (20C,20D)
(mica + titanium dioxide)
[P06]
Interference Orange
Mica Coated w/Titanium Dioxide
9% PVC; images (20E,20F)
(mica + titanium dioxide)
[P07]
Interference Red
Mica Coated w/Titanium Dioxide
9% PVC; images (20G,20H)
(mica + titanium dioxide)

Fig. 1. (xx/xxii)

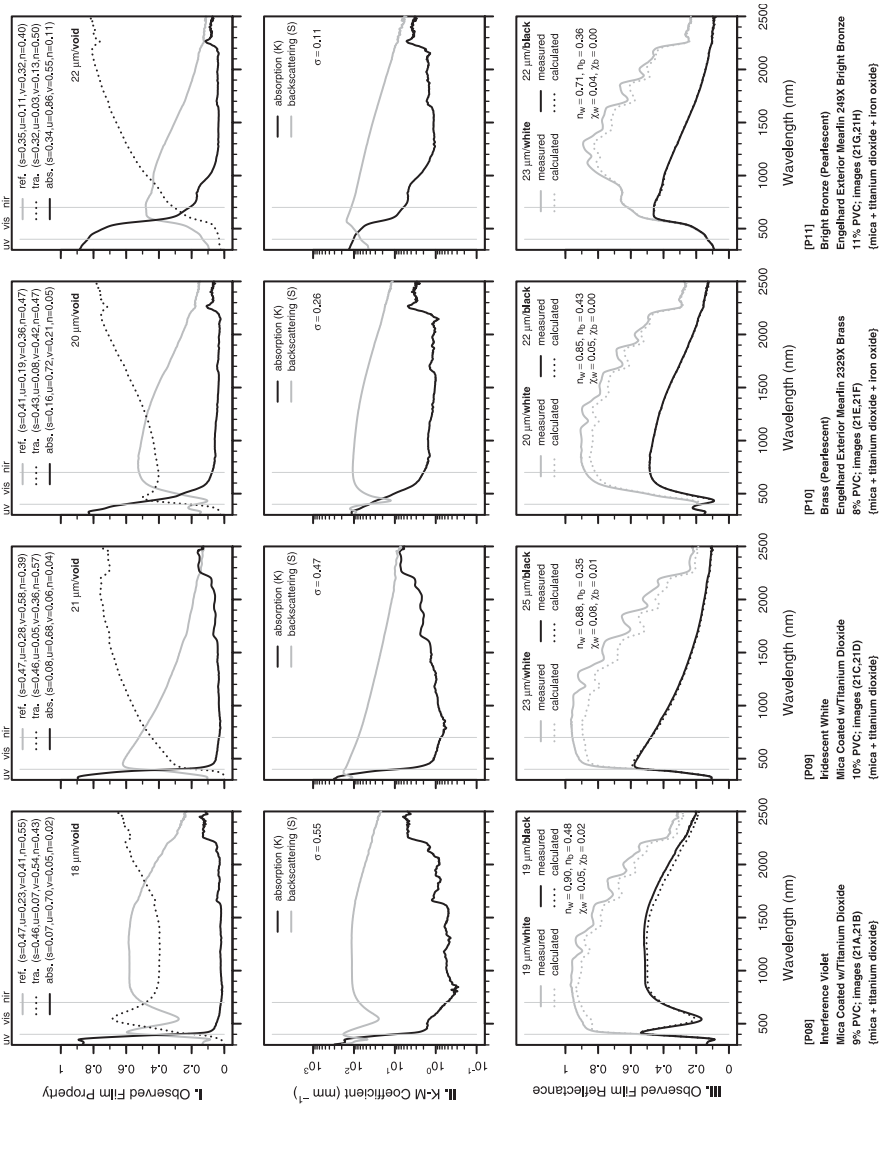

Fig. 1. (xxi/xxii)

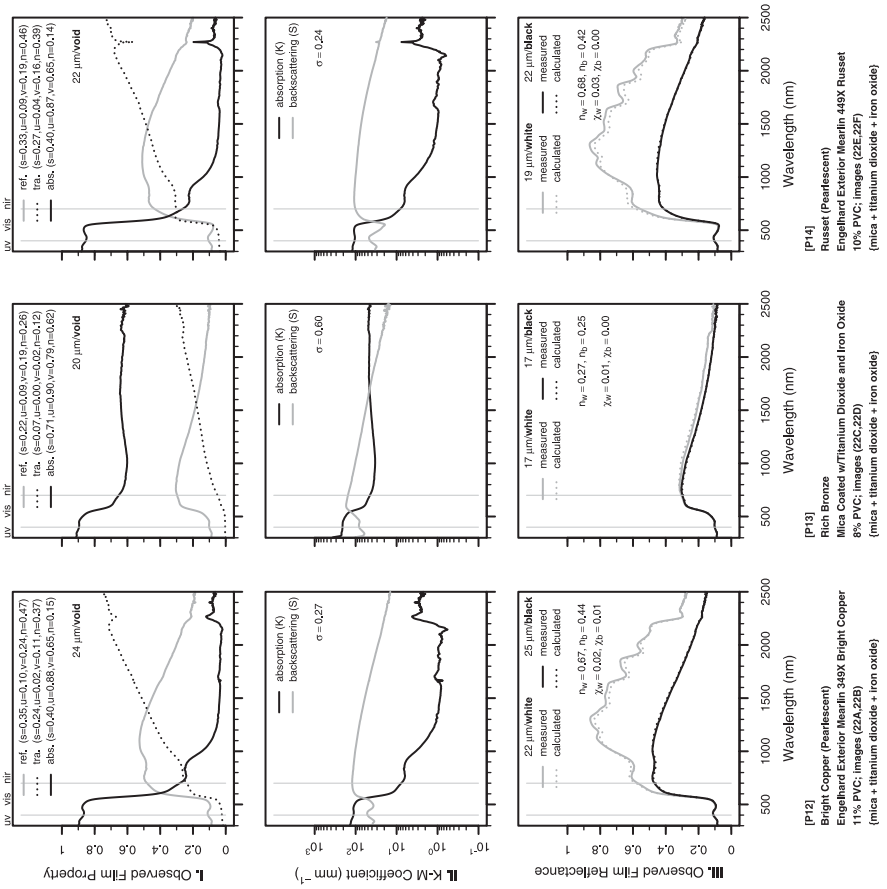

Fig. 1. (xxii/xxii)

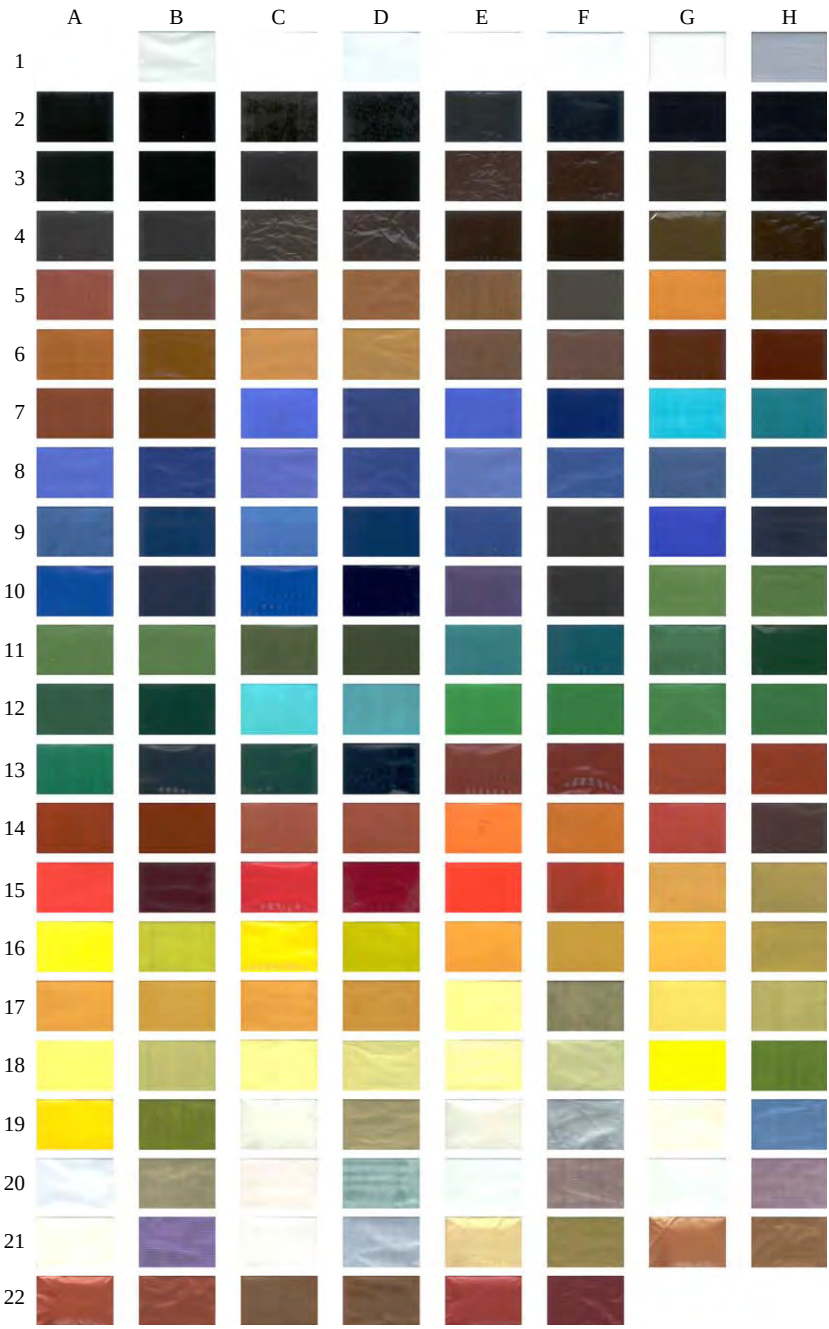

Fig. 2. Color images of paint films cited in Fig. 1. Shown for each paint film is its appearance over a white background, followed by its appearance over a black background.

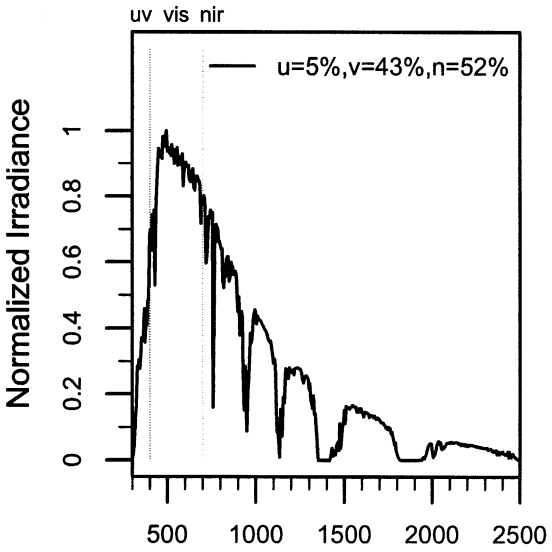

Fig. 3. Air mass 1.5 hemispherical solar spectral irradiance typical of North American insolation (5% ultraviolet, 43% visible, 52% NIR) [27].

3.1. White

All four whites were titanium dioxide (TiO_2) rutile. Other white pigments (not characterized in this study) include zinc oxide, zinc sulfide, antimony oxide, zirconium oxide, zirconium silicate (zircon), and the anatase phase of TiO_2.

TiO_2 rutile is a strongly scattering, weakly absorbing, stable, inert, nontoxic, inexpensive, and hence extremely popular white pigment [2]. TiO_2 whites W01–W04 exhibit similar curves of strong backscattering and weak absorption in the visible and NIR, except for drops in backscattering around 1500–2000 nm seen for W03 and W04. These last two samples are undiluted and 12:1 diluted versions of the same artist color.

Of the available white pigments, the rutile phase of TiO_2 has the highest refractive index in the visible (about 2.7) and therefore has the strongest visible light scattering power at the optimum particle size of about 0.2 μm. Its angle-weighted scattering coefficient s is estimated from the Mie scattering theory to be about $12\,\mu m^{-1}$ for the center of the visible spectrum at 550 nm, assuming 0.22 μm diameter particles suspended in a clear binder with refractive index 1.5 [8,9]. Based on the same method as [8], one of us [10, Fig. 1 and Eq. (1)] has obtained angle-weighted scattering coefficient $s \approx 10.4\,\mu m^{-1}$ at 550 nm, using slightly different values for the refractive index of TiO_2. Thus there is good general agreement among different authors on this basic result from the Mie theory.

The question arises, what is the relation between the Mie theory result for s and the Kubelka–Munk backscattering coefficient S? Palmer et al. [8] give an equation

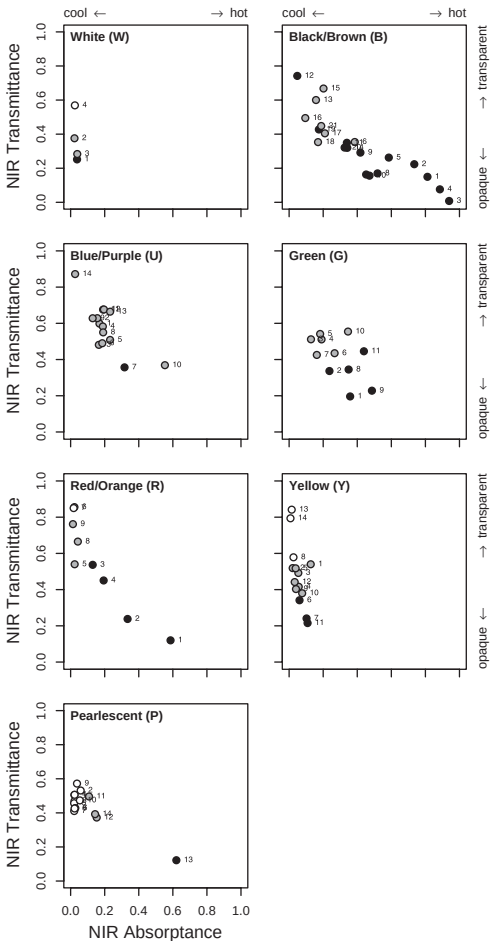

Fig. 4. NIR absorptances and transmittances of 87 pigmented films. A pigment with low NIR-absorptance is cool, but a cool pigment with high NIR transmittance requires an NIR-reflecting background. The color of each circle's interior indicates visible transmittance: black, less than 0.1; gray, between 0.1 and 0.3; white, over 0.3.

for the film reflectance of a non-absorbing layer as $R = (sf\delta)/(2 + sf\delta)$, where f is the pigment volume concentration and δ is the film thickness. The corresponding Kubelka–Munk equation is $R = S\delta/(1 + S\delta)$, which suggests that S should be identified with $\frac{1}{2}fs$. For clarification, we consider the special case of isotropic scattering, and examine the limit of weak scattering. Then s is just the total scattering cross section. In this limit the result of Palmer et al. is then exact if the incident radiation is a normally incident collimated beam; half the scattering is into the forward hemisphere, and half into the backward hemisphere. However, we are more interested in the reflectance for completely diffuse radiation, which is twice as large in this limit. Thus we identify S with fs. Superimposed on the backscattering curves

for samples W01–W04 are additional Mie-theory estimates for backscattering coefficient S as a function of wavelength, based on Ref. [10, Fig. 1 and Eq. (1)]. The measurements and theoretical estimates are in reasonable, but not precise, agreement. (If we had assumed $S = (1/2)fs$, agreement would be better in the visible region.)

At the longer infrared wavelengths, the measured backscattering declines more slowly than the theoretical values. (The theoretical values are approaching a Rayleigh regime in which S is proportional to the inverse fourth power of wavelength.) A plausible reason is the clumping of pigment particles. It is known that such clumping can raise the NIR reflectance [11].

Physically, the light scattering is due to the difference between the refractive index of the rutile particles (2.7) and that of the surrounding transparent medium (1.5). At high pigment volume concentrations, the presence of numerous nearby rutile particles raises the effective refractive index of the surrounding medium, and thereby reduces the efficiency of scattering. This fall in scattering efficiency is termed pigment crowding [12].

Rutile is a direct bandgap semiconductor and therefore has a very abrupt transition from low absorption to high absorption that occurs at 400 nm, the boundary between the visible and ultraviolet regions. For wavelengths below 400 nm (photon energies above 3.1 eV), the absorption is so strong that our data saturate, except in the case of the highly dilute (2% PVC) sample W04. At wavelengths above 400 nm, absorption is weak; most of the spectral features may be attributed to the binders used. One of the four white pigments (W01) does have a slightly less abrupt transition at 400 nm—there is an absorption "tail" near the band edge. This type of behavior is likely due to impurities in the TiO_2.

The sharp rise in absorptance near 300 nm shown for some films such as W04 is an artifact due to the use of a polyester substrate.

3.2. Black/brown

3.2.1. Carbon black, other non-selective black

Carbon black, bone black (10% carbon black + 84% calcium phosphate), copper chromite black ($CuCr_2O_4$), and synthetic iron oxide black (Fe_3O_4 magnetite) (B01–B04) are weakly scattering pigments with strong absorption across the entire solar spectrum. Carbon black B01 is the most strongly absorbing, but all four are "hot" pigments.

Most non-selective blacks are metallic in nature, with free electrons permitting many different allowed electronic transitions and therefore broad absorption spectra. Carbon black is a semi-metal that has many free electrons, but not as many as present in highly conductive metals. Both the iron oxide (magnetite) and copper chromite blacks are (electrically conducting) metals.

3.2.2. Chromium iron oxide selective black

Chromium iron oxide selective blacks (B05–B11) are mixed metal oxides (chromium green–black hematite, chromium green–black hematite modified,

chromium iron oxide, or chromium iron nickel black spinel) formulated to have NIR reflectance significantly higher than carbon and other non-selective blacks. Some, such as chromium green–black hematite B06, appear more brown than black. While these pigments have good scattering in the NIR, with a backscattering coefficient at 1000 nm about half that of TiO_2 white, they are also quite absorbing ($K \approx 50\,mm^{-1}$) in the short NIR. These pigments are visibly hiding (opaque to visible radiation) and NIR transmitting, so use of a white background improves their NIR reflectances without significantly changing their appearances.

Pure chromium oxide green (Cr_2O_3; color index designation pigment green 17), has the hematite crystal structure and will be discussed further together with other green pigments. When some of the chromium atoms are replaced by iron, a dark brownish black with the same crystal structure is obtained—i.e., a traditional cool black pigment (e.g., B06–B11; B05 differs because it contains nickel and has a spinel structure). It is sometimes designated as Cr-Fe hematite [13] or chromium green–black hematite [14], and has been used to formulate infrared-reflective vinyl siding since about 1984 [15]. A number of modern recipes for modified versions of this basic cool black incorporate minor amounts of a variety of other metal oxides. One example is the use of a mixture of 93.5 g of chromium oxide, 0.94 g of iron oxide, 2.38 g of aluminum oxide, and 1.88 g of titanium oxide [16]. The mixture is calcined at about 1100 °C to form hematite-structure crystallites of the resulting mixed metal oxide.

3.2.3. *Organic selective black*

Perylene black (B12) is a weakly scattering, dyelike organic pigment that absorbs strongly in the visible and very weakly in the NIR. Its sharp absorption decrease at 700 nm gives this pigment a jet black appearance and an exceptionally high NIR reflectance (0.85) when applied over white. Perylene pigments exhibit excellent lightfastness and weatherfastness, but their basic compound (dianhydride of tetracarboxylic acid) may or may not be fast to alkali; Refs. [4] and [2] disagree on the latter point.

3.2.4. *Iron oxide brown*

Iron oxide browns (B13–B15) such as burnt sienna, raw sienna, and raw umber exhibit strong absorption in part of the visible spectrum and low absorption in the NIR. These can provide effective cool brown coatings if given a white background, though this will make some (e.g., burnt sienna B13) appear reddish. These browns are "natural" and can be expected to contain various impurities.

3.2.5. *Other brown*

Other browns characterized (B16–B21) include iron titanium (Fe–Ti) brown spinel, manganese antimony titanium buff rutile, and zinc iron chromite brown spinel. These mixed-metal oxides have strong absorption in most or all of the visible spectrum, plus weak absorption and modest scattering in the NIR. A white undercoating improves the NIR reflectance of all browns, but brings out red tones in Fe–Ti brown spinels B16 and B17.

The cool Fe–Ti browns (B16–B18) have spinel crystal structure and basic formula Fe_2TiO_4 [14,17]. Despite the presence of Fe^{2+} ions, the infrared absorption of this material is weak. (In many materials, the Fe^{2+} ion is associated with infrared absorption [18,19]; see also our data for Fe_3O_4. The current data demonstrate that the absorption spectra also depend on the environment of the Fe^{2+} ion.) We also note that while B17 and B18 are nominally the same material, the details of the absorption are different.

We have not yet characterized a synthetic iron oxide hydrate brown (e.g., FeOOH).

3.3. Blue/purple

3.3.1. Cobalt aluminate blue, cobalt chromite blue

Cobalt aluminate blue (nominally $CoAl_2O_4$, but usually deficient in Co [3]; U01–U05) and cobalt chromite blue ($Co[Al,Cr]_2O_4$; U06–U09) derive their appearances from modest scattering ($S \approx 30\,mm^{-1}$) in the blue (400–500 nm) and strong absorption ($K \approx 150\,mm^{-1}$) in the rest of the visible spectrum. They have very low absorption in the short NIR, but exhibit an undesirable absorption band in the 1200–1600 nm range, which contains 17% of the NIR energy. A white background dramatically increases NIR reflectance but makes some (e.g., cobalt aluminum blue spinel U02) much lighter in color.

3.3.2. Iron blue

Iron (a.k.a. Prussian or Milori) blue (U10) is a weakly scattering pigment with strong absorption in the visible and short NIR, and weak absorption at longer wavelengths. It appears black and has little NIR reflectance over a black background, but looks blue and has a modest NIR reflectance (0.25) over a white background. Iron blue is not ideal for cool coating formulation.

3.3.3. Ultramarine blue

Ultramarine blue (U11), a complex silicate of sodium and aluminum with sulfur, is a weakly scattering pigment with some absorption in the short NIR. If sparingly used, it can impart absorption in the yellow spectral region without introducing a great deal of NIR absorption. This is a durable inorganic pigment with some sensitivity to acid [2].

While most colored inorganic pigments contain a transition metal such as Fe, Cr, Ni, Mn, or Co, ultramarine blue is unusual. It is a mixed oxide of Na, Si, and Al, with a small amount of sulfur ($Na_{7.5}Si_6Al_6O_{24}S_{4.5}$). The metal oxide skeleton forms an open clathrate sodalite structure that stabilizes S_3^- ions in cages to form the chromophores [3, Section 3.5] [20]. Thus isolated S_3 molecules with an attached unpaired electron cause the light absorption in the 500–700 nm range, producing the blue color. The refractive index of ultramarine blue is not very different from the typical matrix value of 1.5 [3, Section 3.5], so the pigment causes little scattering.

3.3.4. Phthalocyanine blue

Copper phthalocyanine blue (U12–U13) is a weakly scattering, dyelike pigment with strong absorption in the 500–800 nm range and weak absorption in the rest of the visible and NIR. Phthalo blue appears black and has minimal NIR reflectance over a black background, but looks blue and achieves a high NIR reflectance (0.63) over a white background (U12). It is durable and lightfast, but as an organic pigment it is less chemically stable than (high temperature) calcined mixed metal oxides such as the cobalt aluminates and chromites. General information on the structure and properties of phthalocyanines is available in Ref. [21]. The refractive index varies with wavelength, and exceeds 2 in the short wavelength part of the infrared spectrum [22]. Therefore the weak scattering we observe in our samples indicates that the particle size is quite small. The pigment handbook indicates a typical particle diameter of 120 nm [2], which is consistent with our data.

3.3.5. Dioxazine purple

Dioxazine purple (U14) is an organic optically similar to phthalo blue, but even more absorbing in the visible and less absorbing in the NIR. It is nearly ideal for formulation of dark NIR-transparent layers, but is subject to the chemical stability considerations noted above for phthalo blue.

3.4. Green

3.4.1. Chromium oxide green, modified chromium oxide green

Chromium oxide green Cr_2O_3 (G01–G02) exhibits strong scattering alternating with strong absorption across the visible spectrum, and strong scattering and mild absorption in the NIR. Since the pigment is almost opaque in the visible, a thin layer of chromium oxide green over a white background yields a medium-green coating with good NIR reflectance (0.57 for 13-μm thick film G02). The modified chromium oxide green (G03) is mostly chromium oxide, with small amounts of iron oxide, titanium dioxide, and aluminum oxide [16]. A layer of the modified chromium oxide green over a white background produces a medium green with excellent NIR reflectance (0.71).

Cr_2O_3 green is often mentioned as an infrared-reflective pigment that is useful for simulating the high infrared reflectance of plant leaves. Indeed, a high NIR reflectance is observed. However, our data for sample films G01 and G02 do show that there is a broadband absorption of about $10\,mm^{-1}$ in the near-infrared. While our measurements of absorptance coefficient are not precise for low absorptances, this value is clearly distinct from zero. Pure Cr_2O_3, fired in air, tends to become slightly rich in oxygen, which results in p-type semiconducting behavior [23,24]. Thus it is possible that the broadband IR absorption of Cr_2O_3 is due to free carrier absorption by mobile holes. Ref. [23] also reports that doping with Al can reduce the p-type conductivity in Cr_2O_3, so it seems likely that doping with Al and/or certain other metals can also reduce the IR absorption.

The modified chromium oxide green G03 is similar to G01 and G02 Cr_2O_3. However its green reflectance peak at 550 nm is somewhat smaller and its infrared absorption is clearly much smaller than those of samples G01 and G02.

3.4.2. Cobalt chromite green

Cobalt chromite green (G04–G06) is similar to cobalt chromite blue, and is commonly used for military camouflage.

3.4.3. Cobalt titanate green

Cobalt titanate green (G07–G09) is similar to cobalt chromite green, but scatters more strongly across the entire solar spectrum and has a pronounced absorption trough around 500 nm. A white background makes cobalt teal G07 very NIR reflective (0.73) but also appear light blue (hence, the name teal). The other two cobalt titanate greens (G08, G09) have respectable NIR reflectances (0.47, 0.37) over white and appear medium green.

3.4.4. Phthalocyanine green

Phthalocyanine green (G10–G11) is similar to phthalocyanine blue, but absorbs more strongly in the short NIR. Hence, the NIR reflectance of a thin phthalo green film over white, while good, is only 70% of that achieved by a thin layer of phthalo blue over white (0.45 for G10 vs. 0.63 for U12). Note also that the error in predicted reflectance over white for G11 is large, as discussed in the companion article [1].

3.5. Red/orange

3.5.1. Iron oxide red

Iron oxide red (R01–R04) derives its appearance from weak scattering and very strong absorption in the 400–600 nm band. One of the iron oxide reds (R01) exhibits moderate absorption across the NIR that may be due to doping of the Fe_2O_3 hematite crystals with impurities or result from broadband absorbing impurity phases such as Fe_3O_4; it is not a cool pigment. However, the remaining three iron oxide reds weakly absorb in the NIR and present both a dark red appearance and good NIR reflectance (0.53–0.67) over a white background. R02 also has a respectable NIR reflectance (0.38) over a black background, and has backscattering S comparable with TiO_2 white in the NIR.

3.5.2. Cadmium orange

Cadmium orange (R05) has weak scattering and very strong absorption in the 400–600 nm band, followed by strong scattering and virtually no absorption at longer wavelengths. Applied over a white background, it appears bright orange and has very high NIR reflectance (0.87)—essentially the same as that of the white background. Cadmium orange (and cadmium yellow, below) are Cd(S,Se) direct bandgap semiconductors. They exhibit sharp transitions between absorbing and non-absorbing regions, and have high refractive indices (e.g., 2.5 for CdS) that lead to large scattering coefficients. However, sensitivity to acid and the toxicity of cadmium limit their applications.

3.5.3. Organic red

Organic red pigments (R06–R09) such as acra burnt orange, acra red, monastral red, and naphthol red light have weak scattering and strong (sometimes very strong) absorption up to 600 nm, followed by very weak absorption and moderate-to-weak scattering at longer wavelengths. As a result they yield a medium-red color and a very high NIR reflectance (0.83–0.87) when applied over a white background. Masstones of acra burnt orange, acra red, and naphthol red light are all lightfast; their tints are slightly less so [2].

3.6. Yellow

3.6.1. Iron oxide yellow

Iron oxide yellow FeOOH (Y01) is a brownish yellow similar to iron oxide red. It appears tan and has a high NIR reflectance (0.70) when applied over a white background.

3.6.2. Cadmium yellow

Cadmium yellow (Y02) is similar to cadmium orange. It appears bright yellow and has very high NIR reflectance (0.87) over white.

3.6.3. Chrome yellow

Chrome yellow $PbCrO_4$ (Y03) is optically similar to cadmium yellow but exhibits a more gradual reduction in absorptance. It appears bright yellow and achieves a high NIR reflectance (0.83) over white. In some applications, the presence of lead and/or the Cr(VI) ion impose limitations.

3.6.4. Chrome titanate yellow

Chrome titanate yellow (Y04–Y07) is similar to chrome yellow, but scatters more strongly in the NIR. Its scattering coefficient can exceed 100 mm^{-1} in the short NIR, suggesting that this pigment might be used in place of titanium dioxide white to provide a background of high NIR reflectance. Over a black background, chrome titanate yellow appears brown to green and has moderate to high NIR reflectance (0.26–0.62). Over white, it appears orange to yellow and has very high NIR reflectance (0.80–0.86). Y07 over black produces a medium brown with NIR reflectance 0.62.

The curves for Y04 and Y05 illustrate how the backscattering coefficient S varies with particle size (manufacturer data). For smaller particles, the decrease in S with increasing wavelength is more dramatic.

3.6.5. Nickel titanate yellow

Nickel titanate yellow (Y08–Y11) is similar to chrome titanate yellow. Note that these compounds usually also contain antimony in their formulation. Over white, it appears a muted yellow and yields very high NIR reflectance (0.77–0.87); over black, it appears yellowish green and achieves moderate to high NIR reflectance (0.22–0.64). Y11 is a particularly good candidate to use over black.

3.6.6. Strontium chromate yellow + titanium dioxide

Strontium chromate yellow (solids mass fraction 11%) mixed with titanium dioxide (solids mass fraction 9%) in a paint primer (Y12) appears greenish brown over a black background, and pale yellow over a white background. It has very low absorption (order $1\,mm^{-1}$) and strong scattering (order $100\,mm^{-1}$) at 1000 nm, giving it a good NIR reflectance over black (0.38) and a very high NIR reflectance over white (0.86).

3.6.7. Hansa yellow, diarylide yellow

Hansa yellow (Y13) and diarylide yellow (Y14) are weakly scattering, dyelike organic pigments with high absorption below 500 nm and very weak absorption elsewhere. Over white, they typically (though not always) appear bright yellow and orange–yellow, respectively, and yield very high NIR reflectance (0.87).

3.7. Pearlescents

3.7.1. Mica + titanium dioxide

Mica flakes coated with titanium dioxide (P01–P09) exhibit strong scattering and weak absorption, producing their colors (e.g., gold, blue, green, orange, red, violet, or bright white) via thin-film interference. Some have scattering coefficients exceeding $100\,mm^{-1}$ in the near infrared. Over white, they appear white and have very high NIR reflectance (0.88–0.90); over black, they typically (though not always) achieve their named colors and have high NIR reflectance (0.35–0.54). The NIR reflectance of a pearlescent film over an opaque white background can exceed that of the background.

3.7.2. Mica + titanium dioxide + iron oxide

Mica flakes coated with titanium dioxide and iron oxide (P10–P14) are in most cases similar to mica flakes coated with only titanium dioxide, but are more absorbing, less scattering, darker, and somewhat less reflecting in the NIR. The exception is rich bronze P13, which has very high absorption and would not make a suitable cool pigment.

3.8. Aluminum + iron oxide + silicon oxide

While not characterized in the current study, the solar spectral reflectances of single-layer (iron oxide Fe_2O_3) or double layer (Fe_2O_3 on silicon dioxide SiO_2) interference coatings on aluminum flakes are presented in Refs. [25,26].

3.9. Cool and hot pigments

A simple way to evaluate the utility of a pigmented coating for "cool" applications is to consider its NIR absorptance and NIR transmittance. If the NIR absorptance is low, the pigment is cool. However, a cool pigment that has high NIR transmittance will require an NIR-reflective background (typically white or metallic) to produce an

NIR-reflecting coating. Charts of the NIR absorptance and transmittance of the members of each color family are shown in Fig. 4. An ideal cool pigment would appear near the lower left corner of the chart, indicating that it is weakly absorbing, weakly transmitting, and thus strongly reflecting in the NIR. Pigments appearing higher on the left side of the chart will form a cool coating if given an NIR-reflective background. Use of pigments appearing toward the right side of the chart (i.e., those with strong NIR absorption) should be avoided in cool applications. It should be noted that these charts do not provide perfect comparisons of "cool" performance because they show the NIR properties of films of varying thickness (10–37 μm) and visible hiding (visible transmittance 0–0.43 for non-pearlescents, and 0.02–0.54 for the pearlescents). Black-filled circles indicate visible transmittance less than 0.1; gray-filled circles, between 0.1 and 0.3; and white-filled circles, above 0.3.

There are cool films in the white, yellow, brown/black, red/orange, blue/purple, and pearlescent families with NIR absorptance less than 0.1. These films have moderate to high NIR transmittances (0.25–0.85), indicating than they would require an NIR-reflective background to perform well. There are also other slightly less cool black/brown, blue/purple, green, red/orange, yellow and pearlescent films with NIR absorptance less than 0.2. These have somewhat lower NIR transmittances (0.20–0.70), but are still far from NIR-opaque. A handful of pearlescent, blue/purple and red/orange films, along with half a dozen brown/black films, have NIR absorptances exceeding 0.5 and may be considered warm. A few nonselective blacks with NIR absorptance approaching unity may be considered hot.

Other useful metrics for "coolness" are NIR reflectances over white and black backgrounds (Table 1). Over a white background, the coolest pigments—i.e., those with NIR reflectances of at least 0.7—include members of the pearlescent, white, yellow, black/brown, red/orange, and blue/purple color families: mica coated w/ titanium dioxide (0.88–0.90), titanium dioxide white (0.87–0.88), cadmium yellow (0.87), cadmium orange (0.87), Hansa yellow (0.87), diarylide yellow (0.87), organic selective black (0.85), organic red (0.83–0.87), dioxazine purple (0.82), chrome titanate yellow (0.80–0.86), nickel titanate yellow (0.77–0.87), modified chromium oxide green (0.71), and iron oxide yellow (0.70). Other pigments with NIR reflectances of at least 0.5 include members of the blue/purple, black/brown, and green color families: cobalt aluminum blue (0.62–0.70), cobalt chromite blue (0.55–0.70), phthalo blue (0.55–0.63), cobalt chromite green (0.58–0.64), ultramarine blue (0.52), chromium oxide green (0.50–0.57), and other brown (0.50–0.74). Over a black background, the coolest pigments—in this case, those with NIR reflectances of at least 0.3—include members of the white, yellow, black/brown, red/orange, pearlescent, and green color families: titanium dioxide white (0.24–0.65), nickel titanate yellow (0.22–0.64), chrome titanate yellow (0.26–0.62), mica coated w/ titanium dioxide (0.35–0.54), mica + titanium dioxide + iron oxide (0.25–0.44), chromium oxide green (0.33–0.40), other brown (0.22–0.40), strontium chromate yellow + titanium dioxide (0.38), iron oxide red (0.19–0.38), chromium iron oxide selective black (0.11–0.35), and cobalt titanate green (0.21–0.30).

4. Conclusions

Our characterizations of the solar spectral optical properties of 87 predominately single-pigment paint films with thicknesses ranging from 10 to 37 μm have identified cool pigments in the white, yellow, brown/black, red/orange, blue/purple, and pearlescent color groupings with NIR absorptances less than 0.1, as well as other pigments in the black/brown, blue/purple, green, red/orange, yellow and pearlescent groupings with NIR absorptances less than 0.2. Most are NIR transmitting and require an NIR-reflecting background to form a cool coating. Over an opaque white background, some pigments in the pearlescent, white, yellow, black/brown, red/orange, green, and blue/purple families offer NIR reflectances of at least 0.7, while other pigments in the blue/purple, black/brown, and green color families have NIR reflectances of at least 0.5. A few members of the white, yellow, black/brown, red/orange, pearlescent, and green color families have NIR scattering sufficiently strong to yield NIR reflectances of at least 0.3 (and up to 0.64) over a black background.

Use of pigments with NIR absorptances approaching unity (e.g., nonselective blacks) should be minimized in cool coatings, as might be the use of certain pearlescent, blue/purple, red/orange, and brown/black pigments with NIR absorptances exceeding 0.5.

Acknowledgements

This work was supported by the California Energy Commission (CEC) through its Public Interest Energy Research Program (PIER), by the Laboratory Directed Research and Development (LDRD) program at Lawrence Berkeley National Laboratory (LBNL), and by the Assistant Secretary for Renewable Energy under Contract No. DE-AC03-76SF00098. The authors wish to thank CEC Commissioner Arthur Rosenfeld and PIER program managers Nancy Jenkins and Chris Scruton for their support and advice. Special thanks go also to Mark Levine, director of the Environmental Energy Technologies Division at LBNL, and Stephen Wiel, head of the Energy Analysis Department at LBNL, for their encouragement and support in the initiation of this project. We also wish to thank the following people for their assistance: Kevin Stone and Melvin Pomerantz, LBNL; Michelle Vondran, John Buchko, and Robert Scichili, BASF Corporation; Richard Abrams, Robert Blonski, Ivan Joyce, Ken Loye, and Ray Wing, Ferro Corporation; Tom Steger and Jeffrey Nixon, Shepherd Color Company; and Robert Anderson, Liquitex Artist Materials.

References

[1] R. Levinson, P. Berdahl, H. Akbari, Solar spectral optical properties of pigments – Part I: model for deriving scattering and absorption coefficients from transmittance and reflectance measurements, Sol. Energy Mater. Sol. Cells 89 (4) (2005) 319–349, this issue; doi:10.1016/j.solmat.2004.11.012.

[2] P.A. Lewis, Pigment Handbook, vol. I, Wiley, New York, 1988.

[3] G. Buxbaum, Industrial Inorganic Pigments, second ed., Wiley-VCH, 1998.

[4] W. Herbst, K. Hunger, Industrial Organic Pigments, VCH, 1993.
[5] Y.S. Touloukian, D.P. DeWitt, R.S. Hernicz, Thermal Radiative Properties: Coatings, Thermophysical Properties of Matter, vol. 9, IFI/Plenum, New York, 1972.
[6] R. Mayer, The Artist's Handbook of Materials and Techniques, fifth ed., Viking Penguin, 1991.
[7] Society of Dyers and Colourists and American Association of Textile Chemists and Colorists, Colour index international: fourth online edition, http://www.colour-index.org.
[8] B.R. Palmer, P. Stamatakis, C.G. Bohren, G.C. Salzman, A multiple-scattering model for opacifying particles in polymer films, J. Coat. Technol. 61 (779) (1989) 41–47.
[9] E.S. Thiele, R.H. French, Computation of light scattering by anisotropic spheres of rutile titania, Adv. Mater. 10 (15) (1998) 1271–1276.
[10] P. Berdahl, Pigments to reflect the infrared radiation from fire, J. Heat Transfer 117 (1995) 355–358.
[11] D.J. Rutherford, L.A. Simpson, Use of a flocculation gradient monitor for quantifying titanium dioxide pigment dispersion in dry and wet paint films, J. Coat. Technol. 57 (724) (1985) 75–84.
[12] R.R. Blakey, J.E. Hall, Pigment Handbook, Titanium Dioxide, vol. I, Wiley, New York, 1988, pp. 1–42 (Chapter A).
[13] D.R. Swiler, Manganese vanadium oxide pigments, US Patent 6,485,557 B1, November 26, 2002.
[14] Dry Color Manufacturer's Association (DCMA), Classification and chemical description of the complex inorganic color pigments, Dry Color Manufacturer's Association, Alexandria, VA 22320, 1991.
[15] E.B. Rabinovitch, J.W. Summers, Infrared reflecting vinyl polymer compositions, US Patent 4,424,292, 1984.
[16] T.R. Sliwinski, R.A. Pipoly, R.P. Blonski, Infrared reflective color pigment, US Patent 6,174,360 B1, January 16, 2001.
[17] V.A.M. Brabers, The electrical conduction of titanomagnetites, Physica B 205 (1995) 143–152.
[18] L.B. Glebov, E.N. Boulos, Absorption of iron and water in the Na_2O–CaO–MgO–SiO_2 glasses, II. Selection of intrinsic, ferric, and ferrous spectra in the visible and UV regions, J. Non-Cryst. Solids 242 (1998) 49–62.
[19] R.N. Clark, Manual of Remote Sensing, Remote Sensing for the Earth Sciences, Spectroscopy of Rocks and Minerals, and Principles of Spectroscopy, vol. 3, Wiley, New York, 1999, pp. 3–58 (Chapter 1), http://speclab.cr.usgs.gov, Fig. 5.
[20] R.J.H. Clark, D.G. Cobbold, Characterization of sulfur radical anions in solutions of alkali polysulfides in dimethylformamide and hexamethylphosphoramide and in the solid state in ultramarine blue, green, and red, Inorg. Chem. 17 (1978) 3169–3174.
[21] N.B. Mckeown, Phthalocyanine Materials: Synthesis, Structure and Function, Cambridge University Press, Cambridge, UK, 1998.
[22] S. Wilbrandt, O. Stenzel, A. Stendal, U. Beckers, C. von Borczyskowski, The linear optical constants of thin phthalocyanine and fullerite films from the near infrared to the UV spectral regions: estimation of electronic oscillator strength values, J. Phys. B 29 (1996) 2589–2595.
[23] D. de Cogan, G.A. Lonergan, Electrical conduction in Fe_2O_3 and Cr_2O_3, Solid State Commun. 15 (1974) 1517–1519.
[24] H. Goodenough, Landolt–Bornstein Numerical Data and Functional Relationships in Science and Technology, New Series, Group III: Crystal and Solid-State Physics, vol. 17g (Semiconductors: Physics of Non-Tetrahedrally Bonded Binary Compounds III), Oxides of Chromium, Springer, Berlin, 1984, pp. 242–247, 548–551 (Chapter 9.15.2.5.1).
[25] G.B. Smith, A. Gentle, P. Swift, A. Earp, N. Mronga, Coloured paints based on coated flakes of metal as the pigment, for enhanced solar reflectance and cooler interiors: description and theory, Sol. Energy Mater. Sol. Cells 79 (2) (2003) 163–177.
[26] G.B. Smith, A. Gentle, P. Swift, A. Earp, N. Mronga, Coloured paints based on iron oxide and silicon oxide coated flakes of aluminium as the pigment, for energy efficient paint: optical and thermal experiments, Sol. Energy Mater. Sol. Cells 79 (2) (2003) 179–197.
[27] ASTM, ASTM G 173-03: standard tables for reference solar spectral irradiance at air mass 1.5: direct normal and hemispherical on 37° tilted surface, Technical Report, American Society for Testing and Materials, 2003.

Arnold Schwarzenegger
Governor

COOL-COLOR ROOFING MATERIAL ATTACHMENT 2: TASK 2.4.2 REPORTS - DEVELOP A COMPUTER PROGRAM FOR OPTIMAL DESIGN OF COOL COATINGS

PIER FINAL PROJECT REPORT

Prepared For:
California Energy Commission
Public Interest Energy Research Program

Prepared By:
Lawrence Berkeley National Laboratory
and Oak Ridge National Laboratory

ERNEST ORLANDO LAWRENCE
BERKELEY NATIONAL LABORATORY

June 2006
CEC-500-2006-067-AT2

Prepared By:
Lawrence Berkeley National Laboratory
Hashem Akbari
Berkeley, California
Contract No. 500-01-021

Oak Ridge National Laboratory
William Miller
Oak Ridge, Tennessee

Prepared For:
California Energy Commission
Public Interest Energy Research (PIER) Program

Chris Scruton
Contract Manager

Ann Peterson
Building End-Use Energy Efficiency Team Leader

Nancy Jenkins
PIER Energy Efficiency Research Office Manager

Martha Krebs, Ph.D.
Deputy Director
ENERGY RESEARCH AND DEVELOPMENT DIVISION

B. B. Blevins
Executive Director

DISCLAIMER

This report was prepared as the result of work sponsored by the California Energy Commission. It does not necessarily represent the views of the Energy Commission, its employees or the State of California. The Energy Commission, the State of California, its employees, contractors and subcontractors make no warrant, express or implied, and assume no legal liability for the information in this report; nor does any party represent that the uses of this information will not infringe upon privately owned rights. This report has not been approved or disapproved by the California Energy Commission nor has the California Energy Commission passed upon the accuracy or adequacy of the information in this report.

Pinwheel (version 0.1.1): a tool for the design of color-matched coatings with high solar reflectance

Ronnen Levinson*, Paul Berdahl, and Hashem Akbari
Lawrence Berkeley National Laboratory
Berkeley, CA

May 19, 2005

1 Introduction

Slightly over half of the power in ground-level solar radiation arrives in the invisible "near-infrared" spectrum (700 to 2500 nm). Pinwheel is an application for the design of color-matched coatings with high near-infrared reflectance. Surfaces with such coatings will stay cooler in the sun than conventionally colored surfaces, which is advantageous in warm climates.

*e-mail RMLevinson@LBL.gov; tel. 510/486-7494

We model a coated surface with two or three layers: an opaque substrate, an optional basecoat, and a topcoat. The solar spectral reflectance of the substrate; the thickness and colorant composition of the optional basecoat; and the thickness of the topcoat are specified by the coating designer. Pinwheel then seeks the topcoat colorant composition that maximizes the solar reflectance of the coated surface while acceptably matching a target visible spectral reflectance. Since the visible spectral reflectance is fixed (to within a tolerance), this process is essentially equivalent to maximizing near-infrared reflectance.[1]

The solar spectral reflectance of a coated surface, and hence its solar reflectance and visible spectral reflectance, are computed by applying to the solar spectral absorption and backscattering coefficients of colorants (a) a two-flux, two-constant model of light propagation through a film and (b) a colorant mixture model. Pinwheel has a large library of over 80 colorants (i.e., pigments and dyes) whose solar spectral properties have been characterized by LBNL.

Our tool differs in three major respects from conventional coating formulation software. First, it predicts solar spectral reflectance (300 - 2500 nm), rather than just visible spectral reflectance (400 - 700 nm). Second, it does not require that coatings be opaque. This permits design of thin coatings that transmit both visible and near-infrared light, as well as thicker coatings that stop visible light but transmit near-infrared light. Third, it contains the solar (and not just visible) spectral properties of many colorants.

2 Installation

Pinwheel executes in R, an interpreted programming environment available as free software for the Windows, Mac OS X, and Unix platforms. It has not yet been tested on non-Windows platforms.

2.1 Windows

1. Download the R base-package installer (version 2.1.0 or later; current name `rw2010.exe`) from `http://r-project.org`. Install R to its default directory (`C:\\Program Files\R`).

2. Download `Pinwheel-installer.exe` from `http://CoolColors.LBL.gov/pinwheel`, then run (i.e., double-click) the installer to create the folder `Pinwheel` (Table 1). Note that a password (available from the author) is required to install Pinwheel.

3. If R was installed in a directory other than `C:\\Program Files\R`, or if its version number exceeds 2.1.0, modify the target of the shortcut `Pinwheel/Launch Pinwheel` (original value: '`"C:\\Program Files\R\rw2010\bin\Rgui.exe" --no-restore --no-save`)' to point to the installed executable `RGui.exe`.

[1] In North America, 43% of ground-level global (direct + diffuse) solar radiation arrives in the visible spectrum (400 - 700 nm); 52% arrives in the near-infrared spectrum (700 - 2500 nm), and 5% in the ultraviolet spectrum (300 - 400 nm).

Table 1: Contents of the top-level folder `Pinwheel`.

item	type	contents
`Application Code`	folder	the Pinwheel application R code file
`Colorant Data`	folder	tab-delimited text files detailing the solar spectral radiative properties of 87 colorants
`Documentation`	folder	user's manual (this document)
`Reports`	folder	tabular (tab-delimited text) and graphical (PDF) solution reports generated by Pinwheel
`Substrate Reflectances`	folder	tab-delimited text files specifying the solar spectral reflectances (300 - 2500 nm @ 5-nm intervals) of several substrates
`Target Reflectances`	folder	user-defined, tab-delimited text files specifying the visible spectral reflectances (400 - 700 nm @ 20-nm intervals) of the design targets
`User Code`	folder	user-defined R code files that call the Pinwheel routines
`Launch Pinwheel`	file	shortcut that launches the R environment and sets the R working directory to the folder `Pinwheel`
`.RProfile`	file	R code that is automatically loaded when the R environment is launched via the `Launch Pinwheel` shortcut; `.RProfile` code loads the actual Pinwheel code in the subfolder `Application Code`
`ReadMe.txt`	file	Release notes (text).
`License.pdf`	file	License document (PDF).

2.2 Other platforms

To be written after testing.

3 Operation

The Pinwheel function `design()` inputs the specifications of the coated surface, such its desired visible spectral reflectance and a list of possible colorants, and outputs visually acceptable coating designs sorted in order of descending solar reflectance. There are five steps to this process.

1. Prepare a tabular datafile specifying the desired ("target") visible spectral reflectance of the coated surface.
2. Compose an R-code file consisting of a single `design()` function call whose arguments specify the coating system, the target reflectance datafile, and the colorants to try.
3. Launch Pinwheel.
4. Execute your design code within R after Pinwheel has loaded.
5. Review the solutions.

Table 2: Format of visible spectral reflectance table. Note that each reflectance r is a value between 0 and 1, and that the header row is required.

wavelength (nm)	reflectance
400	r_{400}
420	r_{420}
440	r_{440}
460	r_{460}
480	r_{480}
500	r_{500}
520	r_{520}
540	r_{540}
560	r_{560}
580	r_{580}
600	r_{600}
620	r_{620}
640	r_{640}
660	r_{660}
680	r_{680}
700	r_{700}

3.1 Preparing a visible spectral reflectance file

The target visible spectral reflectance of the coated surface is specified by reflectances (values 0 to 1) at 16 wavelengths from 400 to 700 nm at 20-nm intervals. Use a text editor or spreadsheet application to create a 17-row, two-column table of the form shown in Table 2. Save the table to the folder `Pinwheel/Target Reflectances` as a tab-delimited text file with a descriptive name of the form *`color`*`.txt`, such as `emerald-green.txt`.

3.2 Composing a `design()` call

The `design()` call arguments specify several physical characteristics of the coating system, including

- the candidate colorants for the topcoat (*required*)
- the desired visible spectral reflectance of the coated surface (*required*)
- the thickness of the topcoat (*optional*—defaults to 25 μm)
- the colorants to use in the basecoat (if present), and their volume concentrations (*optional*—defaults to no basecoat)
- the thickness of the basecoat, if present (*optional*—defaults to no basecoat)
- the substrate (*optional*—defaults to opaque white paint)

The arguments also specify several parameters for the coating design algorithm and its output, including

- the volume concentration levels at which to try each topcoat colorant (*optional*—defaults to 0%, 1%, 2%, 3%, 5%, 10%, 15%, 20%, 25%, and 30%)
- the metric used to measure the error in the match of visible spectral reflectance (*optional*—defaults to root mean square of the difference)
- the tolerance (i.e., allowable error) in the match of visible spectral reflectance (*optional*—defaults to 0.05)
- categories of colorants to exclude from the topcoat, such as those that are organic (*optional*—defaults to none)
- whether to simplify the candidate colorants for the topcoats by removing redundant colorants (*optional*—defaults to yes)
- whether to compute colorant absorption coefficients from tints (mixtures of colorants with white), rather than from masstones (pure colorants) (*optional*—defaults to yes)
- a limit to the number of solutions to retain for each topcoat colorant combination (*optional*—defaults to no limit)
- whether to output tabular and/or graphical solution reports (*optional*—each defaults to yes)
- whether to return the solutions for use in R code that calls `design()` (*optional*—defaults to no)
- whether to skip confirmation of the design parameters (*optional*—defaults to no)
- level of on-screen charting to occur during the design process (*optional*—defaults to high)

The syntax of a `design()` function call is

```
design(arg1=val1, arg2=val2, ...)
```

where each *`arg`* is a named argument, and *`val`* is its value.

3.2.1 Required `design()` arguments

The value of `topcoat.colorants` must be specified. Also note that either `target` or `target.mixture`, but not both, must be specified.

`topcoat.colorants` The candidate colorants for the topcoat, specified as a list of colorant vectors. A colorant vector is a set of one or more colorants, of which only one member will appear in the topcoat. If given a list of n colorant vectors, the design function will specify a topcoat

with n colorants, one from each colorant vector.
A colorant vector may take the conventional R form `c("col1", "col2", ...)`, or the convenience form `"col1, col2, ..."`. The list of colorant vectors takes the conventional R form `list(vect1, vect2, ...)`, and must contain at least colorant vector. A colorant `col` is specified by its three-character code of the form `Fnn` (e.g., G03, representing Ferro Camouflage Green V-12650 {modified chromium oxide green in paint Chromium Green-Black Modified}. All 87 colorants are listed in Appendix A. The convenience form `F` represents all members of color family `F`; for example, `"W, G03"` is equivalent to `"W01, W02, W03, W04, G03"`).

Example: `topcoat.colorants=list("U01, U02, U03", "Y03, Y06", "R")` specifies that the topcoat will have three colorants, of which the first will be one of three blues (U01, U02, U03); the second will be one of two yellows (Y03, Y06); and the third will be one of the nine members of the red color family (R01, R02, ..., R09).

3.2.2 Optional `design()` arguments

The following arguments have default values (shown) which may be overridden by specifying `arg=val` in the function call. Note that either `target` or `target.mixture`, but not both, must be specified by the user; the other should be left NULL.

`target=NULL` The name of a target visible spectral reflectance file whose path is `Pinwheel/Target Reflectances/target.txt`. The default value of NULL indicates that the target visible spectral reflectances is to be obtained instead from a target mixture specified by the argument `target.mixture`. Note that the ".txt" suffix is omitted when defining `target`.

Example: `target="emerald-green"` specifies that the target visible spectral reflectance file is `Pinwheel/Target Reflectances/emerald-green.txt`.

`target.mixture=NULL` The name of an LBNL-prepared mixture from which to obtain the target visible spectral reflectance.[2] The default value of NULL indicates that the target visible spectral reflectance is to be obtained instead from the target spectral reflectance file specified by the argument `target`. Note: if a target mixture is used, the argument `target.mixture.background` must also be specified.

Example: `target.mixture="U11+G03[1:1]"` specifies that the target visible spectral reflectance should be obtained from mixture U11+G03[1:1].

`target.mixture.background=NULL` If `"white"`, use for the target visible spectral reflectance that of mixture `target.mixture` measured over a background of clear polyester + opaque white paint. If `"black"`, use that measured over a background of clear polyester + opaque black

[2]These mixtures are useful targets for testing Pinwheel because their compositions are known to and reported by `design()`. Enter '`mixtures`' at the R prompt to see the names of all LBNL-prepared mixtures.

paint. Note this argument is relevant only when a target mixture is specified.

Example: `target.mixture.background="white"` sets the background of the target mixture to clear polyester + opaque white paint.

`topcoat.thickness=25` Thickness of the topcoat in microns.

Example: `topcoat.thickness=15` specifies that the topcoat is 15 μm thick.

`basecoat.colorants=NULL` Colorants and their volume concentrations in the basecoat, if one exists. These are specified as a list of colorant-named concentrations of the form `list(`*`col1=c1, col2=c2, ...`*`)`, where *`c1`* is the concentration (value 0-1) of colorant *`col1`*. The default value of NULL indicates the absence of a basecoat.

Example: `basecoat.colorants=list("Y01"=0.15, "P04"=0.05)` specifies that the basecoat will contain yellow Y01 (concentration 15%) and pearlescent P04 (concentration 5%).

`basecoat.thickness=NULL` Thickness of the basecoat in microns. The default value of NULL indicates the absence of a basecoat.

Example: `basecoat.thickness=10` specifies that the basecoat is 10 μm thick.

`substrate="opaque white paint"` The name of the substrate, the solar spectral reflectance of which is stored in the file `Pinwheel/Substrate Reflectances/`*`substrate`*`.txt`. Measured solar spectral reflectances data is supplied for six substrates—`"opaque white paint"`, `"opaque black paint"`, `"aluminum foil"`, `"bare zincalume"`, `"treated zincalume"`, `"bare HDG"`, and `"treated HDG"`. Also, a theoretical "gray" substrate having reflectance $R/100$ at all wavelengths in the solar spectrum may be specified as `"gray`*`R`*`"` for any integer value of R between 0 and 100. There are no actual spectral datafiles for the reflectances of the gray substrates.

Example 1 (real substrate): `substrate="aluminum foil"` specifies that the substrate solar spectral reflectance file is `Pinwheel/Substrate Reflectances/aluminum foil.txt`.
Example 2 (theoretical substrate): `substrate="gray7"` specifies a hypothetical gray substrate with a uniform 7% solar spectral reflectance.

`concentration.levels=c(0,1,2,3,5,10,15,20,25,30)/100` The volume concentrations at which to try each topcoat colorant. Note the division by 100, because concentrations are expressed on a scale of 0 to 1, not 0 to 100. Concentrations may also be specified in the convenience form `"`*`c1, c2, c3, ...`*`"`, but in this form the concentrations values must be written as decimals (e.g., `"0, 0.01, 0.02, ..."`).

Table 3: Categories of colorants that can be excluded from the topcoat design, and the codes and descriptions of the members of each category.

hot		toxic		organic	
code	*description*	*code*	*description*	*code*	*description*
B01	carbon black	R05	cadmium orange	B12	perylene black
B02	bone black	Y02	cadmium yellow	U12	phthalo blue
B03	copper chromite black			U13	phthalo blue
B04	synthetic iron oxide black			U14	dioxazine purple
U10	iron blue			G10	phthalocyanine green
R01	iron oxide red			G11	phthalocyanine green
P13	mica + titanium dioxide + iron oxide			R06	acra burnt orange
				R07	acra red
				R08	monastral red
				R09	napthol red light
				Y13	yellow medium azo
				Y14	yellow orange azo

Example: `concentration.levels=c(0,1,2,3,4,5,6,7,8,9,10)/100` specifies test concentrations of 0%, 1%, 2%, 3%, 4%, 5%, 6%, 7%, 8%, 9%, and 10%.

`match.metric="rms.absolute"` The metric used to measure the error in the match of visible spectral reflectance. `"rms.absolute"` is the root mean square of the absolute difference between the visible spectral reflectances of the trial mixture and the target; `"max.absolute"` is the maximum absolute difference between these two spectra. Other metrics may be implemented in future versions of Pinwheel.

Example: `match.metric="max.absolute"` specifies the match metric should be maximum absolute difference.

`match.tolerance=0.05` The maximum acceptable error in the match of visible spectral reflectance (value 0-1).

Example: `match.tolerance=0.03` specifies a match tolerance of 0.03.

`exclude=NULL` A vector of the conventional R form `c(`*`cat1, cat2, ...`*`)` or the convenience form `"`*`cat1, cat2, ...`*`"` specifying the categories of colorants not to use in the topcoat. Excludable categories include `"hot"` (strongly NIR-absorbing), `"toxic"` (containing cadmium), and `"organic"` (Table 3). The default value of `NULL` indicates that no categories are to be excluded.

Example: `exclude="hot, toxic"` will exclude from the topcoat any hot or toxic colorants.

`compute.k.from.tint=TRUE` Whether to use, if available,[3] the solar spectral absorption coefficient

[3]Tint-based absorption coefficients are available for the 56 colorants that were characterized in acrylic films

Table 4: Sets of similar colorants that can be represented in topcoat design by a single colorant.

similar colorants	representative colorant	colorant description
W01, W02, W03, W04	W03	titanium dioxide white
B08, B09	B08	Ferro Black V-799
B10, B11	B11	Shepherd Black 411
U12, U13	U13	phthalocyanine blue
G10, G11	G10	phthalocyanine green

K of a colorant computed from its tint, rather than from its masstone. Tint-based absorption coefficients are more accurate at wavelengths where the masstone is strongly absorbing and the masstone-based absorption coefficient is likely to be underestimated.

Example: `compute.k.from.tint=FALSE` prevents the use of tint-based absorption coefficients.

`simplify=TRUE` Whether to simplify (when possible) the candidate colorants for the topcoat by reducing similar colorants in a colorant vector to a single representative colorant (Table 4).

Example: `simplify=FALSE` turns off simplification.

`solutions.per.combination=NULL` The (integer) limit to the number of solutions to retain for each topcoat colorant combination. The default value of NULL indicates that all solutions will be retained. When a limit is specified, the solutions with the highest solar reflectance are retained.

Example: `solutions.per.combination=5` will limit to five the number of solutions retained for each topcoat colorant combination.

`verbosity="high"` The level of on-screen charting to take place during the design process. When `"high"`, three charts will be shown: (a) the visible spectral reflectance of the current trial; (b) the visible spectral reflectance of all solutions (current colorant combination); and (c) the solar reflectance vs. visible match error for all solutions (all colorant combinations). When `"medium"`, graph (a) is omitted; when `"low"`, all three graphs are omitted. Mode `"medium"` is much faster than mode `"high"`, while mode `"low"` is slightly faster than mode `"medium"`.

Example: `verbosity="medium"` displays only charts (b) and (c) during the design process.

`output.graphical.report=TRUE` Whether to generate a graphical report charting and describing each solution.

Example: `output.graphical.report=FALSE` prevents the generation of a graphical report.

prepared by LBNL, but not for the 31 colorants that were characterized in PVDF films prepared by one of LBNL's industrial partners.

`output.tabular.report=TRUE` Whether to generate a tabular report detailing each solution.
Example: `output.tabular.report=FALSE` prevents the generation of a tabular report.

`return.solutions=FALSE` Whether to return the `design()` solutions to R at the conclusion of the function call. This is not necessary if tabular and/or graphic reports are generated, but may be useful if `design()` is called within another algorithm. For example, the R code `x <- design(`*`arg1=val1, arg2=val2,`* `return.solutions=TRUE, ...)` would assign the solutions to the variable `x`. The default value of FALSE causes no value to be returned. textitExample: `return.solutions=TRUE` causes `design()` to return its solutions to R at the conclusion of the function call.

`confirm.parameters=TRUE` Whether to display and confirm the coating system parameters [i.e., the values of the arguments to `design()`] before designing a topcoat. Confirmation is useful when running Pinwheel interactively, but should be turned off for unattended operation.

Example: `confirm.parameters=FALSE` turns off parameter confirmation.

3.2.3 `design()` call examples

1. Using default physical and process parameters.

```
design(
    target="emerald-green",
    topcoat.colorants=list("U08, G", "W", "Y01, Y10, Y14"),
)
```

This minimalist call designs a system that has the substrate `"opaque white paint"`, no basecoat, and a topcoat of thickness 25 μm that contains three colorants: the first, either cobalt chromite blue U08 or a member of the green color family (G); the second, a member of the white color family (W); and the third, either iron oxide yellow Y01, nickel titanate yellow Y10, or diarylide yellow Y14. The colorants will be simplified by eliminating four redundant colorants: titanium dioxide whites W01, W02, and W04 (similar to titanium dioxide white W03); and phthalo green G11 (similar to phthalo green G10). It will try to match the target visible spectral reflectance specified by the file `Pinwheel/Target Reflectances/emerald-green.txt` to within an RMS absolute difference of 0.05. Each colorant will be considered at volume concentrations of 0%, 1%, 2%, 3%, 5%, 10%, 15%, 20%, 25%, and 30%. All solutions will be retained, and both tabular and graphical reports will be generated. The input parameters will be confirmed before the design begins, and many details of the design process will be charted on-screen. No value will be returned as a result of this call.

2. Changing physical parameters.

```
design(
    target="emerald-green",
    topcoat.colorants=list("U08, G", "W", "Y01, Y10, Y14"),
    exclude="organic, hot",
    topcoat.thickness=20,
    basecoat.colorants=list("Y01"=0.15, "P04"=0.05),
    basecoat.thickness=15,
    substrate="treated zincalume"
)
```

This call reduces the topcoat thickness to 20 μm; changes the substrate to treated zincalume; adds a 15-μm basecoat composed of 15% iron oxide yellow Y01 and 5% interference gold pearlescent P04; and excludes from consideration in the topcoat any organic or hot colorants.

3. Changing physical and process parameters.

```
design(
    target="emerald-green",
    topcoat.colorants=list("U08, G", "W", "Y01, Y10, Y14"),
    topcoat.thickness=20,
    basecoat.colorants=list("Y01"=0.15, "P04"=0.05),
    basecoat.thickness=15,
    substrate="treated zincalume",
    concentration.levels=c(0,1,2,3,4,5,6,7,8,9,10)/100,
    match.metric="max.absolute",
    match.tolerance=0.03,
    verbosity="low"
)
```

This call uses topcoat colorant concentration levels of 0%, 1%, 2%, 3%, 4%, 5%, 6%, 7%, 8%, 9%, and 10%, and accepts trial mixtures whose visible spectral reflectances matches that of the target to within a maximum absolute difference of 0.03. It does not generate any on-screen charts during the design processes, greatly reducing the time needed to complete the design. This call reduces the topcoat thickness to 20 μm, changes the substrate to treated zincalume, and adds a 15-μm basecoat composed of 15% iron oxide yellow Y01 and 5% interference gold pearlescent P04.

4. Calibrating `design()` using a mixture of known composition.

```
design(
    target.mixture="U14+Y01[1:1]",
    target.mixture.background="white",
```

```
    topcoat.colorants=list("U14", "Y01"),
    topcoat.thickness=22,
    substrate="opaque white paint",
    match.tolerance=0.04
)
```

This call tests `design()` on an LBNL-prepared mixture of two paints—one colored with dioxazine purple U14, and the other colored with iron oxide yellow Y01. The goal is to find among the solutions one in which the concentrations of colorants U14 and Y01 approximately match their known concentrations in the mixture (which is reported).

3.2.4 Preparing design code

While a `design()` call may be entered at the R prompt, it is typically easier to compose the call in a text editor, such as EditPad Pro (`http://editpadpro.com`) or Notepad, and save it to the folder `Pinwheel/User Code`. It is helpful to give your file a meaningful name of the form *`design`*`.R`. For example, a call that will design an emerald green coated surface might be saved as `Pinwheel/User Code/emerald-green-design01.R`.

3.3 Launching Pinwheel

Open (double-click) the shortcut `Pinwheel/Launch Pinwheel` to launch R and load Pinwheel into the R environment. The startup process may take a few minutes as Pinwheel loads the colorant data and makes a series of one-time calculations.

3.4 Executing design code

Once Pinwheel has finished loading, it will display the message '`PINWHEEL is ready`'. Load and execute your design code either by entering

```
source("User Code/design.R")
```

at the R prompt or by using the menu command `File>Source R Code...` to select your code file. The Windows keyboard shortcut for the latter command is `ALT-f s`.

The `design()` call typically creates multiple windows within R. These windows, which tend to overlap, can be neatly placed side by side using the menu command `Windows>Tile` or keyboard shortcut `ALT-w t` (Figure 1). Note that a screen resolution of 1152 × 864 pixels or greater is required for proper rendering of the on-screen graphics.

When done, exit R by entering quit() or using the menu command `File>Exit`.

3.5 Reviewing solutions

Unless configured otherwise, `design()` will generate both tabular and graphical solution reports.

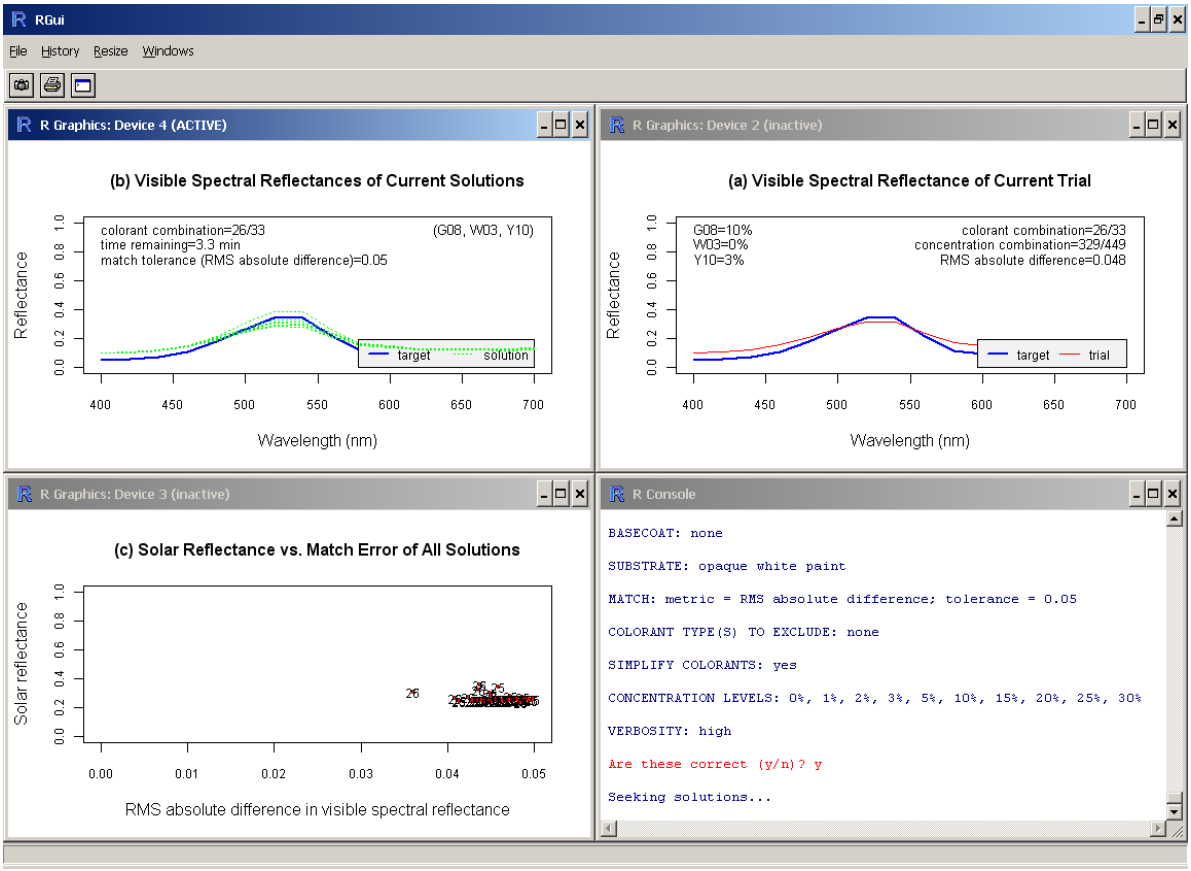

Figure 1: Pinwheel windows neatly tiled using the R menu command `Windows>Tile`.

The tabular report is a tab-delimited text file written to `Pinwheel/Reports/`*`target`*`-tabular-report.txt`. It will not load properly in Excel (at least not in Excel 2000) because the 441-element solar spectral reflectances in the report require more than 256 columns. However, you can view it in any text editor, or parse it with any programming language.

The graphical report is a PDF file written to `Pinwheel/Reports/`*`target`*`-graphical-report.pdf`. It shows one solution per page in order of descending solar reflectance (Figure 2). It is best to view this file in a standalone version of Acrobat or Acrobat Reader, rather than with the Acrobat Reader browser plug-in. Set the View options to Fit in Window and Single Page, then use the Page Up/Down keys to flip through the solutions.

4 Expandability

Substrate solar spectral reflectances files named *`substrate`*`.txt` can be added to the folder `Pinwheel/Substrate Reflectances`. Quit and restart Pinwheel after adding a new substrate reflectance file.

References

[1] Ronnen Levinson, Paul Berdahl, and Hashem Akbari. Lawrence Berkeley National Laboratory Pigment Database. `http://CoolColors.LBL.gov/LBNL-Pigment-Database/database.html`.

[2] Ronnen Levinson, Paul Berdahl, and Hashem Akbari. Solar spectral optical properties of pigments, Part I: model for deriving scattering and absorption coefficients from transmittance and reflectance measurements. *Solar Energy Materials & Solar Cells*, (in press), 2005.

[3] Ronnen Levinson, Paul Berdahl, and Hashem Akbari. Solar spectral optical properties of pigments, Part II: survey of common colorants. *Solar Energy Materials & Solar Cells*, (in press), 2005.

A Colorants

Tables A-1 through A-7 list the 87 colorants grouped into the white, black/brown, blue/purple, green, red/orange, yellow, and pearlescent families. The colorants are fully described in LBNL's pigment database [1] and articles [2, 3].

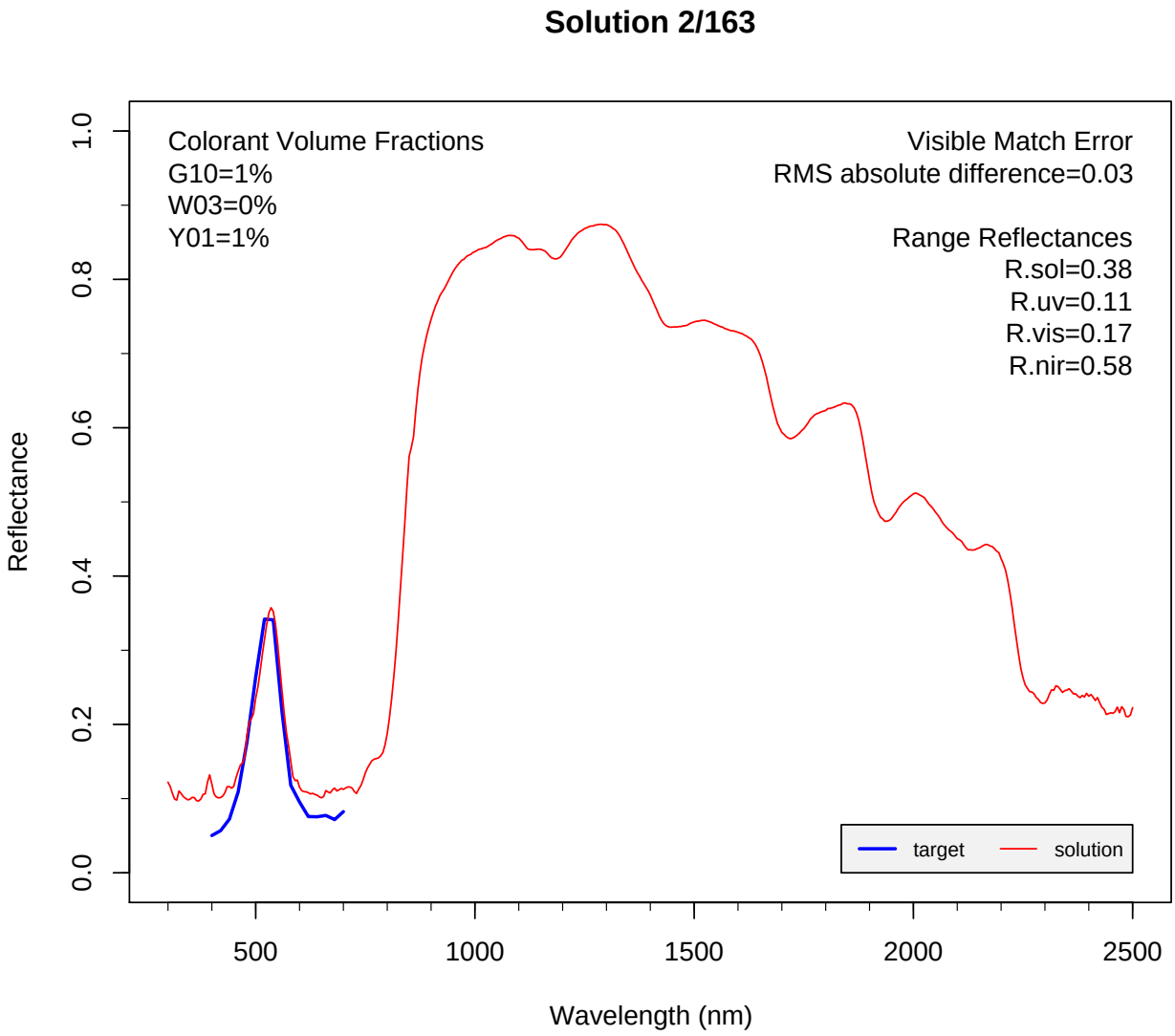

TARGET: emerald−green

TOPCOAT: thickness = 25 µm; colorants = G10 (1%), W03 (0%), Y01 (1%)

BASECOAT: none

SUBSTRATE: opaque white paint

G10 = Chlorinated Copper Phthalocyanine (PG 7) {phthalocyanine green in paint Phthalo Green (i)}
W03 = Titanium Dioxide (PW 6) {titanium dioxide white in paint Titanium White (i)}
Y01 = Synthetic Hydrated Iron Oxide (PY 42) {iron oxide yellow in paint Yellow Oxide}

Figure 2: A solution shown in a graphical report.

Table A-1: White colorants

code	description
W01	Ishihara Tipaque CR-90 (PW 6) {titanium dioxide white in paint Inorganic Oxide White}
W02	Titanium Dioxide (PW 6) {titanium dioxide white in paint Titanium Dioxide White}
W03	Titanium Dioxide (PW 6) {titanium dioxide white in paint Titanium White (i)}
W04	Titanium Dioxide (PW 6) {titanium dioxide white in paint Titanium White (ii)}

Table A-2: Black/brown colorants

code	description
B01	Amorphous Carbon Black (PBk 7) {carbon black in paint Carbon Black}
B02	Amorphous Charred-Bone Carbon (PBk 9) {carbon black in paint Ivory Black}
B03	Shepherd Black 1D (PBk 28) {other non-selective black in paint Copper Chromite Black}
B04	Synthetic Black Iron Oxide (PBk 11) {other non-selective black in paint Mars Black}
B05	Shepherd Black 376 (PBk 30) {chromium iron oxide selective black in paint Chrome Iron Nickel Black Spinel}
B06	Shepherd Black 10C909 (PG 17) {chromium iron oxide selective black in paint Chromium Green-Black Hematite}
B07	Ferro Black V-797 {chromium iron oxide selective black in paint Chromium Green-Black Hematite Modified (i)}
B08	Ferro Black V-799 {chromium iron oxide selective black in paint Chromium Green-Black Hematite Modified (ii)}
B09	Ferro Black V-799 (PBr 29) {chromium iron oxide selective black in paint Chromium Green-Black Hematite Modified (iii)}
B10	Shepherd Black 411 (PBr 29) {chromium iron oxide selective black in paint Chromium Iron Oxide (i)}
B11	Shepherd Black 411 (PBr 29) {chromium iron oxide selective black in paint Chromium Iron Oxide (ii)}
B12	BASF Paliogen Black L0086 (PB 32) {organic selective black in paint Perylene Black}
B13	Calcined Natural Iron Oxide (PBr 7) {iron oxide brown in paint Burnt Sienna}
B14	Natural Iron Oxide (PBr 7) {iron oxide brown in paint Raw Sienna}
B15	Natural Iron Oxide w/Manganese (PBr 7) {iron oxide brown in paint Raw Umber}
B16	Shepherd Brown 156 (PBk 12) {other brown in paint Iron Titanium Brown Spinel (i)}
B17	Shepherd Brown 8 (PBk 12) {other brown in paint Iron Titanium Brown Spinel (ii)}
B18	Shepherd Golden Brown 19 (PBk 12) {other brown in paint Iron Titanium Brown Spinel (iii)}
B19	Ferro Chestnut Brown V-10364 (PY 164) {other brown in paint Manganese Antimony Titanium Buff Rutile}
B20	Shepherd Brown 12 (PBr 33) {other brown in paint Zinc Iron Chromite Brown Spinel (i)}
B21	Shepherd Brown 157 (PBr 33) {other brown in paint Zinc Iron Chromite Brown Spinel (ii)}

Table A-3: Blue/purple colorants

code	description
U01	Ferro Blue V-9250 (PB 28) {cobalt aluminate blue in paint Cobalt Aluminate Blue Spinel (i)}
U02	Shepherd Blue 385 (PB 28) {cobalt aluminate blue in paint Cobalt Aluminate Blue Spinel (ii)}
U03	Shepherd Blue 424 (PB 28) {cobalt aluminate blue in paint Cobalt Aluminate Blue Spinel (iii)}
U04	Shepherd Artic Blue 3A (PB 28) {cobalt aluminate blue in paint Cobalt Aluminum Blue}
U05	Oxides of Cobalt and Aluminum (PB 28) {cobalt aluminate blue in paint Cobalt Blue}
U06	Cobalt Chromite (PB 36) {cobalt chromite blue in paint Cerulean Blue}
U07	Shepherd Blue 190-A (PB 36) {cobalt chromite blue in paint Cobalt Chromite Blue}
U08	Ferro Blue V-9248 (PB 36) {cobalt chromite blue in paint Cobalt Chromite Blue-Green Spinel (i)}
U09	Shepherd Blue 212 (PB 36) {cobalt chromite blue in paint Cobalt Chromite Blue-Green Spinel (ii)}
U10	Milori Blue (PB 27) {iron blue in paint Prussian Blue}
U11	Complex Silicate of Na and Al with S (PB 29) {ultramarine blue in paint French Ultramarine Blue}
U12	Copper Phthalocyanine (PB 15) {phthalocyanine blue in paint Phthalo Blue (i)}
U13	Toyo Lionel BF-28201 (PB 15) {phthalocyanine blue in paint Phthalo Blue (ii)}
U14	Carbazole Dioxazine (PV 23 RS) {dioxazine purple in paint Dioxazine Purple}

Table A-4: Green colorants

code	description
G01	Bayer GN-M Chrome Oxide Green (PG 17) {chromium oxide green in paint Chrome Green}
G02	Anhydrous Chromium Sesquioxide (PG 17) {chromium oxide green in paint Chromium Oxide Green}
G03	Ferro Camouflage Green V-12650 {modified chromium oxide green in paint Chromium Green-Black Modified}
G04	Shepherd Green 187B (PB 36) {cobalt chromite green in paint Cobalt Chromite Blue-Green Spinel (iii)}
G05	Ferro Camouflage Green V-12600 (PG 26) {cobalt chromite green in paint Cobalt Chromite Green Spinel (i)}
G06	Shepherd Green 179 (PG 26) {cobalt chromite green in paint Cobalt Chromite Green Spinel (ii)}
G07	Light Green Oxide (PG 50) {cobalt titanate green in paint Cobalt Teal}
G08	Shepherd Green 223 (PG 50) {cobalt titanate green in paint Cobalt Titanate Green Spinel (i)}
G09	Shepherd Sherwood Green 5 (PG 50) {cobalt titanate green in paint Cobalt Titanate Green Spinel (ii)}
G10	Chlorinated Copper Phthalocyanine (PG 7) {phthalocyanine green in paint Phthalo Green (i)}
G11	Clariant GT-674-D Endurophthal Green B (PG 7) {phthalocyanine green in paint Phthalo Green (ii)}

Table A-5: Red/orange colorants

code	description
R01	Bayer Bayferrox 6622 Iron Oxide (PR 101) {iron oxide red in paint Red Iron Oxide (i)}
R02	Elementis RO-3097 (PR 101) {iron oxide red in paint Red Iron Oxide (ii)}
R03	Ferro Red V-13810 (PR 101) {iron oxide red in paint Red Iron Oxide (iii)}
R04	Synthetic Red Iron Oxide (PR 101) {iron oxide red in paint Red Oxide}
R05	Cadmium Orange (PO 20) {cadmium orange in paint Cadmium Orange}
R06	Quinacridone (PR 206) {organic red in paint Acra Burnt Orange}
R07	Quinacridone Red Gamma (PR 209) {organic red in paint Acra Red}
R08	Ciba Geigy Monastral NRT-742-D Scarlet (PV 19) {organic red in paint Monastral Red}
R09	Naphthol AS-OL (PR 9) {organic red in paint Naphthol Red Light}

Table A-6: Yellow colorants

code	description
Y01	Synthetic Hydrated Iron Oxide (PY 42) {iron oxide yellow in paint Yellow Oxide}
Y02	Cadmium Yellow (PY 35) {cadmium yellow in paint Cadmium Yellow Light}
Y03	Dominion Color Krolor KY-781-D (PY 34) {chrome yellow in paint Chrome Yellow}
Y04	Ferro Autumn Gold V-10415 (PBr 24) {chrome titanate yellow in paint Chrome Antimony Titanium Buff Rutile (i)}
Y05	Ferro Bright Golden Yellow V-10411 (PBr 24) {chrome titanate yellow in paint Chrome Antimony Titanium Buff Rutile (ii)}
Y06	Shepherd Yellow 193 (PBr 24) {chrome titanate yellow in paint Chrome Antimony Titanium Buff Rutile (iii)}
Y07	Ishihara Tipaque TY-300 (PBr 24) {chrome titanate yellow in paint Chrome Titanate Yellow}
Y08	Ferro Yellow V-9415 (PY 42) {nickel titanate yellow in paint Nickel Antimony Titanium Yellow Rutile (i)}
Y09	Ferro Yellow V-9416 (PY 53) {nickel titanate yellow in paint Nickel Antimony Titanium Yellow Rutile (ii)}
Y10	Shepherd Yellow 195 (PY 53) {nickel titanate yellow in paint Nickel Antimony Titanium Yellow Rutile (iii)}
Y11	Ishihara Tipaque TY-50 (PY 53) {nickel titanate yellow in paint Nickel Titanate Yellow}
Y12	Strontium Chromate Yellow + Titanium Dioxide {strontium chromate yellow + titanium dioxide in paint Primer}
Y13	Arylide Yellow 5GX (PY 74 LF) {Hansa yellow in paint Yellow Medium Azo}
Y14	Diarylide Yellow (PY 83 HR70) {diarylide yellow in paint Yellow Orange Azo}

Table A-7: Pearlescent colorants

code	description
P01	Engelhard Exterior Mearlin 239X Bright Gold {mica + titanium dioxide in paint Bright Gold (Pearlescent)}
P02	Engelhard Exterior Mearlin 139X Bright White {mica + titanium dioxide in paint Bright White (Pearlescent)}
P03	Mica Coated w/Titanium Dioxide {mica + titanium dioxide in paint Interference Blue}
P04	Mica Coated w/Titanium Dioxide {mica + titanium dioxide in paint Interference Gold}
P05	Mica Coated w/Titanium Dioxide {mica + titanium dioxide in paint Interference Green}
P06	Mica Coated w/Titanium Dioxide {mica + titanium dioxide in paint Interference Orange}
P07	Mica Coated w/Titanium Dioxide {mica + titanium dioxide in paint Interference Red}
P08	Mica Coated w/Titanium Dioxide {mica + titanium dioxide in paint Interference Violet}
P09	Mica Coated w/Titanium Dioxide {mica + titanium dioxide in paint Iridescent White}
P10	Engelhard Exterior Mearlin 2329X Brass {mica + titanium dioxide + iron oxide in paint Brass (Pearlescent)}
P11	Engelhard Exterior Mearlin 249X Bright Bronze {mica + titanium dioxide + iron oxide in paint Bright Bronze (Pearlescent)}
P12	Engelhard Exterior Mearlin 349X Bright Copper {mica + titanium dioxide + iron oxide in paint Bright Copper (Pearlescent)}
P13	Mica Coated w/Titanium Dioxide and Iron Oxide {mica + titanium dioxide + iron oxide in paint Rich Bronze}
P14	Engelhard Exterior Mearlin 449X Russet {mica + titanium dioxide + iron oxide in paint Russet (Pearlescent)}

Arnold Schwarzenegger
Governor

COOL-COLOR ROOFING MATERIAL ATTACHMENT 3: TASK 2.4.3 REPORTS - DEVELOP A DATABASE OF COOLCOLORED PIGMENTS

PIER FINAL PROJECT REPORT

Prepared For:
California Energy Commission
Public Interest Energy Research Program

Prepared By:
Lawrence Berkeley National Laboratory and Oak Ridge National Laboratory

ERNEST ORLANDO LAWRENCE
BERKELEY NATIONAL LABORATORY

June 2006
CEC-500-2006-067-AT3

Prepared By:
Lawrence Berkeley National Laboratory
Hashem Akbari
Berkeley, California
Contract No. 500-01-021

Oak Ridge National Laboratory
William Miller
Oak Ridge, Tennessee

Prepared For:
California Energy Commission
Public Interest Energy Research (PIER) Program

Chris Scruton
Contract Manager

Ann Peterson
Building End-Use Energy Efficiency Team Leader

Nancy Jenkins
PIER Energy Efficiency Research Office Manager

Martha Krebs, Ph.D.
Deputy Director
ENERGY RESEARCH AND DEVELOPMENT DIVISION

B. B. Blevins
Executive Director

DISCLAIMER

This report was prepared as the result of work sponsored by the California Energy Commission. It does not necessarily represent the views of the Energy Commission, its employees or the State of California. The Energy Commission, the State of California, its employees, contractors and subcontractors make no warrant, express or implied, and assume no legal liability for the information in this report; nor does any party represent that the uses of this information will not infringe upon privately owned rights. This report has not been approved or disapproved by the California Energy Commission nor has the California Energy Commission passed upon the accuracy or adequacy of the information in this report.

Lawrence Berkeley National Laboratory Pigment Database: Guide to Reading Spectral Datafiles

Ronnen Levinson*, Paul Berdahl, and Hashem Akbari
Heat Island Group
Lawrence Berkeley National Laboratory
Berkeley, CA

February 13, 2005

Each pigmented coating is described by a tab-delimited text file that provides one column of data per pigment property. It can be read by nearly any spreadsheet application, charting utility, text editor, word processor, or custom program. One easy way to view its contents is to open the file with Microsoft Excel, select all cells, and execute Format/Column/Autofit Selection for best display.

The first row of each column names the property, and the remaining rows give its value(s). Pigment properties are detailed in Table 1.

Note: each spectral datafile is stored in the LBNL Pigment database as a ZIP archive with AES 128-bit encryption. The archives can be unzipped with any modern file compression/expansion utility, such as WinZip 9.0 or later (http://WinZip.com). Members and industrial partners of the Cool Colors project may obtain the decryption key via fax by contacting Ronnen Levinson and providing a fax number.

References

1. R. Levinson, P. Berdahl, and H. Akbari. 2005. Solar spectral optical properties of pigments, Part I: Model for deriving scattering and absorption coefficients from transmittance and reflectance measurements. *Solar Energy Materials & Solar Cells* (in press).

2. R. Levinson, P. Berdahl, and H. Akbari. 2005. Solar spectral optical properties of pigments, Part II: Survey of common colorants. *Solar Energy Materials & Solar Cells* (in press).

*E-mail RMLevinson@LBL.gov; tel. 510/486-7494

instructions	how to view and interpret this datafile
comments	authorship and disclaimer
computation date	when K-M coefficients were calculated
color family	white, black/brown, blue/purple, green, red/orange, yellow, or pearlescent
pigment category	pigment chemistry or characteristic (e.g., cobalt titanate green or non-selective black)
code	used to identify this pigment in our pigment characterization paper (note: this value likely to be replaced)
paint name	assigned by the paint manufacturer
pigment name	assigned by the pigment manufacturer
internal description	LBNL's description of masstone, tint, or mixture
component names	LBNL's description of the paint's components
component ratios	parts by volume of each component
dry-film PVC	pigment volume concentration (volume pigment:volume paint) in dry film
delta.v (microns)	thickness of film sample over void background [exclusive of substrate, if present] (μm)
delta.w (microns)	thickness of film sample over opaque white background [exclusive of background and substrate, if present] (μm)
delta.b (microns)	thickness of film sample over opaque black background [exclusive of background and substrate, if present] (μm)
sigma	non-spectral forward scattering ratio
spectral ranges	definitions of solar, ultraviolet, visible, and near-infrared ranges used in spectral averaging
R.tilde.fv averages	spectrally averaged, irradiance-weighted values of the measured reflectance of the film over a void background
T.tilde.fv averages	spectrally averaged, irradiance-weighted values of the measured transmittance of the film over a void background
A.tilde.fv averages	spectrally averaged, irradiance-weighted values of the measured absorptance of the film over a void background
R.tilde.fw averages	spectrally averaged, irradiance-weighted values of the measured reflectance of the film over an opaque white background
R.tilde.fb averages	spectrally averaged, irradiance-weighted values of the measured reflectance of the film over an opaque black background
R.tilde.ow averages	spectrally averaged, irradiance-weighted values values of the measured reflectance of the opaque white background
lambda (nm)	wavelengths at which spectral values are presented
insolation (W/m^2/nm)	air-mass 1.5 hemispherical solar spectral irradiance (W m^{-2} nm^{-1})
R.tilde.fv	measured spectral reflectance of the film over a void background
T.tilde.fv	measured spectral transmittance of the film over a void background
A.tilde.fv	measured spectral absorptance of the film over a void background
R.tilde.fw	measured spectral reflectance of the film over an opaque white background
R.tilde.fb	measured spectral reflectance of the film over an opaque black background
K (1/mm)	Kubelka-Munk (K-M) spectral absorption coefficient (mm^{-1})
S (1/mm)	K-M spectral backscattering coefficient (mm^{-1})
R.inf	continuous refractive index (CRI) spectral reflectance of an opaquely thick film
R.tilde.inf	observed spectral reflectance of an opaquely thick film
R.tilde.fw.calc	observed spectral reflectance of the film over an opaque white background, as computed from the K-M coefficients
R.tilde.fb.calc	observed spectral reflectance of the film over an opaque black background, as computed from the K-M coefficients
T.v	internal transmittance of the film
q.i.at.zero	diffuse fraction q of the downflux i exiting the bottom of the film ($z = 0$)
q.j.at.delta	diffuse fraction q of the upflux j exiting the top of the film ($z = \delta$)
omega.i.at.zero	interface reflectance ω to the downflux i exiting the bottom of the film ($z = 0$)
omega.j.at.delta	interface reflectance ω to the upflux j exiting the top of the film ($z = \delta$)

Table 1: Pigment property definitions.

Arnold Schwarzenegger
Governor

COOL-COLOR ROOFING MATERIAL ATTACHMENT 4: TASK 2.5.1 REPORTS - REVIEW OF ROOFING MATERIALS MANUFACTURING METHODS

PIER FINAL PROJECT REPORT

Prepared For:
California Energy Commission
Public Interest Energy Research Program

Prepared By:
Lawrence Berkeley National Laboratory and Oak Ridge National Laboratory

ERNEST ORLANDO LAWRENCE
BERKELEY NATIONAL LABORATORY

June 2006
CEC-500-2006-067-AT4

Prepared By:
Lawrence Berkeley National Laboratory
Hashem Akbari
Berkeley, California
Contract No. 500-01-021

Oak Ridge National Laboratory
William Miller
Oak Ridge, Tennessee

Prepared For:
California Energy Commission
Public Interest Energy Research (PIER) Program

Chris Scruton
Contract Manager

Ann Peterson
Building End-Use Energy Efficiency Team Leader

Nancy Jenkins
PIER Energy Efficiency Research Office Manager

Martha Krebs, Ph.D.
Deputy Director
ENERGY RESEARCH AND DEVELOPMENT DIVISION

B. B. Blevins
Executive Director

DISCLAIMER

This report was prepared as the result of work sponsored by the California Energy Commission. It does not necessarily represent the views of the Energy Commission, its employees or the State of California. The Energy Commission, the State of California, its employees, contractors and subcontractors make no warrant, express or implied, and assume no legal liability for the information in this report; nor does any party represent that the uses of this information will not infringe upon privately owned rights. This report has not been approved or disapproved by the California Energy Commission nor has the California Energy Commission passed upon the accuracy or adequacy of the information in this report.

Reports included in this attachment:

- Review of Residential Roofing Materials, Part I
- Review of Residential Roofing Materials, Part II
- A Review of Methods for the Manufacture of Residential Roofing Materials

Review of Residential Roofing Materials, Part I

A Review of Methods for the Manufacture of Residential Roofing Materials

by Hashem Akbari, Ronnen Levinson, and Paul Berdahl, Heat Island Group, Lawrence Berkeley National Laboratory

According to *Western Roofing Insulation and Siding* magazine (2002), the total value of the 2002, residential roofing market in 14 western U.S. states (Alaska, Ariz., Calif., Colo., Hawaii, Idaho, Montana, Nevada, New Mexico, Oregon, Texas, Utah, Wash., and Wyoming) was about $3.6 billion. We estimate that 40% ($1.4 billion) of that amount was spent in California. The lion's share of residential roofing expenditure was for fiberglass shingle, which accounted for $1.7 billion, or 47% of sales. Concrete and clay roof tile made up $0.95 billion (27%), while wood, metal, and slate roofing collectively represented another $0.55 billion (15%). The value of all other roofing projects was about $0.41 billion (11%).

We estimated roofing area market shares by assuming that roofing projects involving concrete tile, clay tile, wood shingle/shake, or slate were 50% to 100% more expensive than those using other roofing materials, such as shingle, metal, or membrane. This suggests that the roofing market area distribution is 54-58% fiberglass shingle, 8-10% concrete tile, 8-10% clay tile, 7% metal, 3% wood shake, and 3% slate.

2002 Project residential roofing market in the U.S. western region[a] surveyed by *Western Roofing* (2002).

Roofing Type	Market share by $		Market share by roofing area (%)	
	$B	%	Estimate 1	Estimate 2
Fiberglass Shingle	1.70	47.2	53.6	57.5
Concrete Tile	0.50	13.8	10.4	8.4
Clay Tile	0.45	12.6	9.5	7.7
Wood Shingle/Shake	0.17	4.7	3.6	2.9
Metal/Architectural	0.21	5.9	6.7	7.2
Slate	0.17	4.7	3.6	2.9
Other	0.13	3.6	4.1	4.4
SBC Modified	0.08	2.1	2.4	2.6
APP Modified	0.07	1.9	2.2	2.3
Metal/Structural	0.07	1.9	2.2	2.3
Cementitious	0.04	1.1	1.2	1.3
Organic Shingles	0.02	0.5	0.6	0.6
Total	**3.6**	**100**	**100**	**100**

a. The 14 states included in the U.S. western region are Alaska, Ariz., Calif., Colo., Hawaii, Idaho, Montana, Nevada, New Mexico, Oregon, Texas, Utah, Wash., and Wyoming.

The functional distribution of the steep-slope roofing market (including both residential and small-commercial buildings) was about 60% replacement, 25% new construction, and 15% repair and maintenance.

This paper examines methods for manufacturing fiberglass shingles, concrete tiles, clay tiles, and metal roofing that constitute over 80% of all roofing materials, by both expenditure and area. We have focused on these four roofing products because they are typically colored with pigmented coatings or additives. We do not discuss production of wood and slate roofing. A better understanding of the current practices for manufacturing colored roofing materials would allow us to develop cool colored materials creatively and more effectively. The paper also discusses innovative methods for increasing the solar reflectance of these roofing materials.

INSPECTING THE FINISHED PRODUCT AT A CLAY TILE PLANT.

Methodology

We reviewed the pertinent literature for production of roofing materials and visited several roofing material manufacturing plants.

Literature Review

The following briefly summarizes several pertinent sources of information about roofing manufacturing methods available from websites, articles, papers, patents, and books. In *The Science and Technology of Traditional and Modern Roofing Systems*, Laaly (1992) provides an overview of the production and application of various roofing materials. A website of the National Park Services (NPS 2003) also provides the historical backgrounds of several roofing materials, including asbestos-cement shingle, asphalt shingle, clay tile, composition (built-up roofing), metal, slate, and wood shingle.

The Department of Health and Human Services (DHHS 2001) and the Environmental Protection Agency

(EPA 1995) have each prepared extensive documents discussing various manufacturing methods for asphalt roofing products. These focus on environmental pollution, and do not address the effects of roof reflectivity and its effects on heating-and-cooling energy use and on roof durability.

Brown (1960) and Jewett et al. (1994) detail the manufacture of colored roofing granules in chapters of 1960 and 1994 editions of *Industrial Mineral and Rocks*. Though these texts cover a wide range of technical and marketing issues related to the manufacture and production of colored granules, they provide limited information on granule coloring techniques. Joedicke (1997 and 2002) discusses this topic in greater detail.

Finally, Paris and Chusid (1997, 1999) briefly describe methods for coloring concrete products using powder, liquid, and granulated pigments. They also discuss issues related to the durability of colored concrete.

Plant Visits

We visited a shingle plant, a metal roofing plant, and a clay tile plant in southern California; and a granule production plant and a concrete tile plant in northern California.

- ***Asphalt Shingle:*** Asphalt is a dark-brown-to-black cementitious material, solid or semisolid, in which the predominant constituents are naturally-occurring or petroleum-derived bitumens. It is used as a weatherproofing agent. The term asphalt shingle is generically used for both fiberglass and organic shingles. There are two grades of asphalt shingles: (1) standard, a.k.a. 3-tab; and (2) architectural, a.k.a. laminated or

(Continued on Page 56)

Circle #72 on Reader Service Card

WESTERN COLLOID PRODUCTS

THE EMULSION TECHNOLOGY COMPANY

COLD PROCESS ROOFING SYSTEMS

- Water Based Systems
- Seamless, Tough, Flexible
- Manufacturer's Warranties
- U.L. Ratings
- Standard or Elastomeric
- 25+ Year Track Record
- Polyester & Chopped Fiberglass Reinforced
- Recover - No Need For Tear Off
- Energy Saving Reflective Surfacing

PROTECTIVE & REFLECTIVE COATING & MAINTENANCE PRODUCTS

- Elastomeric Reflective Coatings
  Energy Saving - Fire Rated - White & Colors
- Water Based Aluminum Coating
  Energy Saving - Prolongs Roof life - Economical
- Asphalt Emulsion ASTM D 1227-III
- Elastomeric Asphalt Emulsion
- Elastomeric Flashing Compound
  Water Based - Permanently Elastomeric
- Metal Roofing Systems
- Polyester Fabrics
- Bulk Delivery Service

WESTERN COLLOID PRODUCTS

OAKLAND
PORTLAND
LOS ANGELES

For Information Call:

OAKLAND (510) 430-0270
LOS ANGELES (800) 464-8292

www.westerncolloidnc.com

Circle #71 on Reader Service Card

Review of Residential Roofing Material, Part I

(Continued from Page 55)

dimensional. Asphalt shingles come in various colors.

Examples: Fiberglass shingles, commonly known as "asphalt shingles," consist of fiber mats that are coated with asphalt and then covered with granules. Granules, a.k.a. mineral granules or ceramic granules, are opaque naturally- or synthetically-colored aggregates commonly used to surface-cap sheets and shingles.

Organic shingles have a thick cellulose base that is saturated in soft asphalt. This saturation makes them heavier than fiberglass shingles, and less resistant to heat and humidity, but more durable in freezing conditions.

- ***Tile:*** Usually made of concrete or clay. Concrete tile is a combination of sand, cement, and water; the water fraction depends on the manufacturing process. Concrete tiles are either air-cured or auto-claved. Color is added to the surface of the tile with a slurry coating process, or added to the mixture during the manufacturing process.

Clay tile is a combination of various clays and water. Color is added to the surface of the tile with a slurry coating process before the tile is kiln-fired.

- ***Metal:*** Metal roofs can be classified as architectural or structural.

Examples: Architectural (hydrokinetic-watershedding) standing-seam roof systems are typically used on steep slopes with relatively short panel lengths. They usually do not have sealant in the seam because they are designed to shed water rapidly. They do not provide structural capacity or load resistance, and their installation is less labor-intensive because they have a solid substrate platform that makes installation easier..

FIBERGLASS ENTERING THE SHINGLE PRODUCTION MACHINERY.

Structural (hydrostatic-watershedding) standing-seam roof systems are versatile metal panel systems that can be used on both steep- and low-slope roofs and are designed to be water-resistant. Most structural standing-seam systems include a factory-applied sealant in the standing seams to help ensure water tightness. These panel systems provide structural capacity and load resistance.

Manufacturing Methods - Shingles

- *Production of colored granules.* Granules cover over 97% of the surface of a typical asphalt-soaked fiberglass shingle. Granules are applied to asphalt shingles for several reasons, including UV protection, col-

Circle #70 on Reader Service Card

oration, ballasting, impact resistance, and fire resistance.

Granule manufacturing plants are typically sited near a quarry of suitable base rocks, including andesite, coal slag, diabase, metabasalt, nephaline syenite, quartzite, rhyodacite, rhyolite, and/or river gravel. The essential characteristics of the base rock include: opacity to ultraviolet light, to protect the asphalt from ultraviolet damage; chemical and physical inertness, to provide resistance to acid rain, leaching, freeze/thaw, wet/dry cycling, oxidation and rusting; low porosity, to improve physical strength, binding between coating and rock, and efficiency with which the pigment coating covers the surface; and resistance to high firing temperatures. Other necessary characteristics include moderate hardness, to remain intact during the granule coloring process; moderate density (to weight the shingle against wind lift); uniformity, and crush equidimensionality (to prevent directional embedment in the shingle manufacturing process, which changes shingle appearance).

In a roofing-granule manufacturing plant, rocks blasted from quarries are crushed in several stages to reduce the rock to granule-size aggregate (0.5 to 2 mm). In this process, the larger aggregates are recycled to the crushing system and the smaller debris is separated for other usage.

Once the granules are milled to the right size, they are transferred to the coloring plant. In the coloring plant, in a continuous process they are mixed with a semi-ceramic color coating. The coating is a mix of color pigments in a sodium silicate, hydrated kaolin clay, and water. The preheated granules are mixed and tumbled with coating sufficient to cover the surface. The wet coated granules are then transferred to a rotary kiln where they are gradually heated to 250-550°C (500-1,000°F). This dehydrates and polymerizes the coating, forming an insoluble pigmented ceramic layer. The granule is then gradually cooled in a rotary cooler by sprayed water and circulated air. Finally, the pigmented granules are coated with mineral oil to control dust and to improve asphalt adhesion. The mineral oil typically evaporates within a few months.

The pigments used for colored granules must have certain properties, including stability at high temperature, chemical inertness, ease of dispersion, color consistency, weather stability, non-toxicity, and low cost. Common pigments used in roofing granules include titanium dioxide (white), zinc ferrite (yellow), red iron oxides, carbon black, chrome oxide (green), and ultramarine (blue). Typically, 2.3-2.7 kg (5-6 lb.) of pigment per ton of granules are required to create a single-layer coating. Multiple coatings are needed to increase pigment loading. Some granule manufacturing plants have parallel coloring lines that can be used in series to apply multiple layers of coatings on granules. The granules (both colored and uncolored) are transported to shingle manufacturing companies by road and rail.

(Editor's Note: Next issue, we'll present Part II of this article.)

Circle #69 on Reader Service Card

Review of Residential Roofing Materials, Part II

A Review of Methods for the Manufacture of Residential Roofing Materials

by Hashem Akbari, Ronnen Levinson, and Paul Berdahl, Heat Island Group, Lawrence Berkeley National Laboratory

INSPECTING THE FINISHED PRODUCT AT A CLAY TILE PLANT.

Production of shingles. Fiberglass asphalt shingles have three major components: fiberglass mat, asphalt (with additive fillers), and granules (colored and uncolored). In a typical plant, the fiberglass mat is fed into a roll coater that applies layers of stabilized coating asphalt to the top and bottom surfaces of the webbing sheet. Stabilized coating asphalt is harder and more viscous than straight asphalt, and has a higher softening point. The mineral stabilizer may consist of finely divided limestone, silica, slate dust, dolomite, or other minerals.

The "filled" or "stabilized" coating asphalt applied at the coater is produced in the mixer, which is usually positioned above the manufacturing line at the coater. Coating asphalt, typically at 200-270°C (400-520°F), is piped into the mixer, and the mineral stabilizer is added. To eliminate moisture problems and to help maintain the temperature above 180°C (360°F) for proper coating consistency in the mixer, the mineral stabilizer is dried and preheated before being fed into the mixer.

The weight of the finished product is controlled by the thickness of coating asphalt used. The coating rolls can be moved closer together to reduce the amount of coating applied to the substrate, or separated to increase it. Most modern plants are equipped with automatic scales or profile scanners that monitor the sheets during the manufacturing process and warn the operator when too much or too little coating is being applied.

Colored and uncolored granules are applied in a section of the manufacturing line that usually consists of a multi-compartmented granule hopper, two parting-agent hoppers, and two large press rollers. The hoppers are fed through flexible hoses from one or more machine bins above the line. These machine bins (sometimes called surge bins) provide temporary storage. The granule hopper drops colored granules from its various compartments onto the top surface of the moving sheet of coated web in the sequence necessary to produce the desired color or pattern on the roofing.

Next, the sheet is cooled by passing it over water-cooled rollers; water may also be sprayed directly onto the sheet to speed cooling. The final steps in the production of asphalt roofing shingles are cutting and packaging. After the shingles have been cut by machine they are moved by a roller conveyor to automatic packaging equipment. The packaged shingles are then stacked on pallets and transferred by forklift to storage areas or waiting trucks.

- *Clay tiles.* Clay tile production begins by mixing and crushing various raw clay materials. For example, the raw clays used at MCA include "yellow shell clay" (a highly refractory clay [i.e., having high heat resistance, permitting vertical firing without warping] with medium plasticity); "apple clay" (a weakly refractory clay with high plasticity); and "AAA clay" (a medium refractory, low shrinkage clay with high iron content to make the tile red).

The raw clays are thoroughly mixed with water and aged for 4-5 days. The aging process allows the dry material to absorb the moisture fully, improving plasticity. This increases yields from the extrusion process and thus lowers the unit production cost.

Several extrusion machines and dies are employed to produce clay tiles of various shapes. Prior to extrusion, the clay flows through a vacuum chamber to remove air, preventing cracking of tiles during the firing process. This process is also very important for proper vitrification (conversion to a glassy state), which makes the tile weather-resistant (i.e., resistant to freezing/thawing and salt intrusion) [See Clay Roof Tile Specifications: ASTM C-1167 for more detail]. An automated cutter at the end of each extruder cuts the tile to desired size, and trims the edges. The wet extruded tile is then dried in a sequence of temperature-controlled chambers for about 24 hours. By reducing the excessive moisture in the tiles, this drying process will reduce the probability of cracks when the tile is fired. The drying process typically starts with circulating ambient air at a temperature of about 20-30°C, gradually increasing the temperature to about 90°C using waste heat from the kiln-cooling process. Drying reduces the tile's moisture content from 15% to less than 1%.

(Continued on Page 54)

Review of Residential Roofing Materials, Part II

(Continued from Page 52)

The dry raw tiles are inspected for defects before they are sprayed with glossy or matte glazes. The glazing is a mixture of water, pigments and clay additives. For the glossy finish, frits (glassy silicates), clay, and color-glazed materials are added to the glazing mixture. The glazed tiles are positioned in vertical stacks or in a "standing up" position, with typically 1.25 cm (½") spacers to allow an even heat distribution in the kiln. Even heating yields evenly colored tiles with good mechanical properties.

CONCRETE TILE EXTRUSION MACHINE.

The glazed tiles are then passed through a kiln, fired for 14-20 hours, depending upon the production schedule. The kiln has three stages: preheat, heating, and cooling. In the preheating zone, the tiles are gradually heated to about 700°C by warm drawn air from the heating zone. In the heating zone, the tiles are directly fired for about four hours by gas flame, reaching a maximum temperature of about 1050°C. Then the tiles are gradually cooled to about 300-400°C by drawing outside air through the kiln. The clay tile is ready to ship as soon as it is removed from the kiln - no curing is required. The clay tile colors are permanent and do not fade with exposure to the sun.

■ *Concrete tiles.* Sand, cementitious materials, limestone fillers, and water are the main ingredients (by mass) of concrete tiles. Pigments are added for color and polymers are used as a water-resistant coating on the tile surface. Pigments are typically added to the surface in a slurry coat comprised of pigment, cement, silica and water. Finished concrete tiles may also be painted. The major components contributing to the cost are cementitious materials, sand, polymer coating, and pigments.

Concrete tile production begins by mixing aggregate (sand) and fillers. Sand is pre-washed to remove dirt contaminants. Recycled aggregates and quarry waste are also used in the mixture, and milled calcium carbonate is used as filler (calcium carbonate filler is an inexpensive material that improves the quality of concrete). Then the aggregate and filler mix are mixed with cementitious materials before water is added to the mixture. The percentages of calcium carbonate filler added to the mix vary from facility to facility. At this stage, pigments may be added to color the concrete mix. The ingredients are completely mixed before being fed to the molding machine.

Several machines and molds are employed to produce concrete tiles of various shapes. The mold and the wet concrete tile run on a conveyor where the tiles are partially dried and polymeric coating is applied to the surface before curing. The tiles and the mold are packed in a curing chamber for about four hours, where the concrete tile is cured and dried. The molds and tiles run through a separator that removes the molds from the tiles. The dry raw tiles are inspected for defects before they are sprayed with colored coatings. The tiles are then covered with post-coating polymers. The coating is a mixture of water, pigments, and polymeric additives. The coated tiles are then dried, stacked, and packed for shipment.

■ *Metal Roofing.* Metal production for the roofing industry may be divided into two phases: (1) metallic and/or coil coating plants, where raw metal coils are cleaned, metallic coated, primed, and coated with paint (some facilities can both metallic-coat and paint, while others only apply paint); and (2) metal-forming plants, where the coated coils are either used to produce flat metal panels, or pressed into shapes that simulate non-metal roofing products (e.g., shake, slate, or tile).

Coil Coating Plants. Coil coaters produce rolled metals in the thickness, width, metal-coating type, and color specified by their customers, which include but are not limited to members of the roofing industry. An advanced metal coil plant typically has four major production lines: a *pickle line*, where the hot band coil (hot band coils are the result of steel slabs being elongated and rolled into coiled sheet of finite width and thickness; the temperature and amount of processing determine mechanical properties of the coil) is uncoiled and cleaned of oxides, edges are trimmed to customer requirement, and the coil is oiled in preparation of further processing; a *cold mill line,* where the pickled bands are reduced in thickness 65-80% to meet ordered thickness, and rolled to a suitable shape, and texture is applied to the surface; a *metallic coating line*, where the coils are cleaned again, a layer of metallic coating is applied, and the surface is treated for either painting or bare metal application; and a *paint line* where primer and finish coatings are applied. Many coil coaters consist of only a paint line; they do not process their own substrate. In addition to steel, aluminum can also be coated via the coil process.

Pickle line. The raw material for this industry is typically a thick metal steel coil. The hot-band coil is pickled when it first arrives at the coating plant. There it is

uncoiled and cleaned in a series of acid baths to ensure the proper surface for further processing (cold rolling and galvanizing [coating with zinc] or galvalumizing [coating with a zinc/aluminum alloy]). The steel is then side-trimmed to the customer's specifications for width. At the end of the pickle-line process, the steel is re-coiled and ready to go on to the cold rolling mill. The pickle line is capable of continuous production. One coil is processed while the other is prepared to be fed to the line.

Cold Mill Line. In the cold-reversing mill (CRM) line, the thickness of the metal coil is reduced to specification by repeatedly passing through pressure rolls. Larger-scale cold mills will have four or five "stands" in a row that the strip passes through. This way the full gauge reduction is achieved with one pass.

Metal Coating Line. In the metal coating line, the steel coils are cleaned again, a layer of metallic coating is applied, and the surface is treated either for painting or for use as bare metal. Coils from the cold mill line are fed to the system and welded together for continuous-line operation. The coil then passes through an accumulator tower; the steel coils are cleaned in preparation for the metallic coating before being fed to the annealing furnace to achieve the desired mechanical properties. Coming out of the furnace, the strip is directly dipped into a molten bath of zinc or galvalume. The specified coating weight is achieved by air wiping excess metal before it solidifies. The hot-coated coil is then cooled and treated with a surface-conditioning mill, the process is very similar to the cold mill, but on a much smaller scale as gauge reduction is not the goal, simply a smooth surface. The steel is slightly elongated for uniform flatness by the tension leveler. The surface can also be chemically treated and coated with a resin for bare-metal applications.

Paint Line. The paint line is similar to the metal coating line. In the paint line, a coil from the metal-coating line is fed to the system where coils are welded or stitched together for a continuous operation of the line. Then the coil passes though an accumulator tower and cleaner prior to chemical coating. The chemical coater pre-treats the surface to accept primer or paint and to provide corrosion resistance. A primer is then applied to the steel strip and cured in the prime oven. Then the strip is coated with the finish paint and cured in the finish oven. Paint lines have the ability to paint only one or both sides of the strip, depending on customer requirements. The cured, painted steel is then quenched with water and cooled to room temperature. Finally, rollers remove the excess water, and the steel goes into the exit accumulator before it is taken up onto an exit reel. The finished strip can be sent back through the paint line if additional paint layers are desired. This is often done for print or pattern finishes where the final product consists of multiple colors that can mimic wood shakes, asphalt shingles or aged copper.

Metal Forming Plants. Metal forming plants cut and press painted or unpainted metal coils to form either flat panels or simulations of non-metal roofing products (e.g., shake, shingle, tile, and slate). A very few fabricators

(Continued on Page 56)

CELL-CRETE CORP
Insulating Concrete Roof Deck Specialists

Tired of being held up by rising Polyiso board prices?

Licensed in California, Arizona, Nevada, Utah, Idaho, Alaska, and Hawaii

Ask how Cell-Crete Corporation can help to reduce the cost of your next job!!

Southern CA Office
800-660-8062
FAX 626-357-2537

Northern CA Office
800-696-0433
FAX 510-471-6426

Arizona Office
928-468-2365
FAX 928-468-2365

Nevada Office
702-366-1954
FAX 702-366-9474

www.cell-crete.com
E-mail Info@cell-crete.com

Circle #71 on Reader Service Card

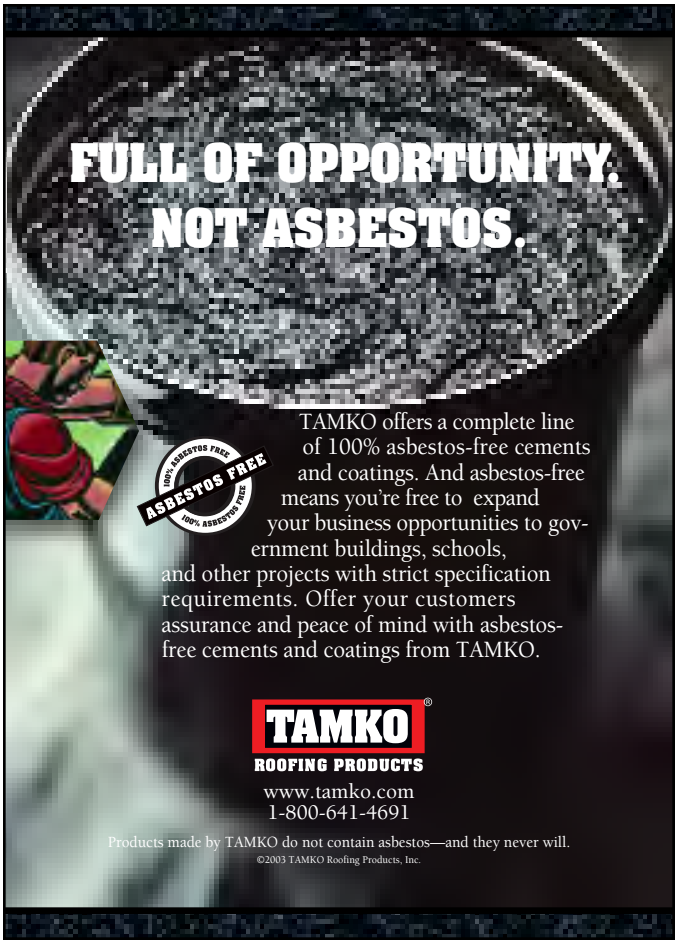

Circle #70 on Reader Service Card

Circle #69 on Reader Service Card

Review of Residential Roofing Materials, Part II

(Continued from Page 55)

apply granulated material to the painted panels in order to simulate asphalt shingles. However, most fabricators of shingle or tile-type profiles use embossing or stamping to achieve the desired look.

Methods to Produce Cool Roofing Materials

■ *Shingles.* The solar reflectance of a new shingle is dominated by the solar reflectance of its granules, since by design the surface of a shingle is well covered with granules. Hence, we focus on the production of cool granules. There are primarily two ways to increase the solar reflectance of the granules: manufacturing granules from highly reflective (e.g., white) rocks, and/or coating the granules with reflective pigments. The use of naturally white rock is limited by local availability of suitable inert rocks, which are often not found in large quarries. Hence, manufacturers usually color the granules.

Until recently, the way to produce granules with high solar reflectance has been to use titanium dioxide (TiO_2) rutile, a white pigment. Since a thin layer of TiO_2 is reflective but not opaque, multiple layers are needed to obtain the desired solar reflectance. This technique has been used to produce "super-white" (meaning truly white, rather than gray) granulated shingles with solar reflectances exceeding 0.5. Manufacturers have also tried to produce colored granules with high solar reflectance by using non-white pigments with high NIR reflectance. However, like TiO_2, cool colored pigments are also partly transparent to NIR light; thus, any NIR light not reflected by the cool pigment is transmitted to the (typically dark) granule underneath, where it can be absorbed. To increase the solar reflectance of colored granules with cool pigments, multiple color layers, a reflective undercoating, and/or reflective aggregate should be used. Obviously, each additional coating increases the cost of production.

A conventional black roof shingle has a reflectance of about 0.04. On the first try to increase the solar reflectance of the shingle, we replaced the standard black pigment on the granules with one that is NIR reflective. That increased the reflectance of the granule to 0.12. On the second try, we used a two-layered technique where we first applied a layer of TiO_2 white base (increasing the solar reflectance of the base granule to 0.28) and then a layer of NIR-reflective black pigment. This increased the reflectance of the black granule to 0.16. On our third prototype, the base granule was coated in ultra-white (reflectance 0.44) and then with a NIR-reflective black pigment. This increased the solar reflectance to 0.18.

The application of pigmented coatings to roofing granules appears to be the critical process step. Several layers of silicate coatings can be involved, and may include not just one or more pigments, but the use of clay additives to control viscosity, biocides to prevent staining, and process

chemistry controls to avoid unreacted dust on the product.

One way to reduce the cost is to produce cool colored granules via a two-step, two-layer process. In the first step, the granule is pre-coated with an inexpensive pigment that is highly reflective to NIR light. In the second step, the cool colored pigment is applied to the pre-coated granules.

Shingles tend to lose some granules as they age and weather, exposing asphalt-coated fiberglass and reducing solar reflectance. Substituting a reflective sealant for the black asphalt could slow this. While developing such a replacement for asphalt may be of long-term interest, we do not see an easy solution to this problem.

It should be noted that the reflectance of an asphalt shingle covered with granules will be less than that of the granule's coating, since some of the light reflected by each granule will strike a neighboring granule and be absorbed. These "multiple reflections" can reduce shingle reflectance by as much as 0.15.

Finally, the granule manufacturing and shingle manufacturing industries have designed their quality-control laboratories to test the visible color of their products. We anticipate that the industry will need to equip itself with additional instruments to test the solar reflectance and the NIR optical properties of their products. It is also envisioned that unified standards have to be developed to address issues related to manufacturing of cool colored granules and shingles.

- *Clay tiles.* Options for production of colored tiles are similar to those of the roofing shingles. The three ways to improve the solar reflectance of clay tiles include: (1) use of raw clay materials with low concentrations of iron oxides and elemental carbon; (2) use of cool pigments in the coating; and (3) application of the two-layered coating technique using pigmented materials with high solar reflectance as an underlayer. Although all these options are in principle easy to implement, they may require changes in the current production techniques that may add to cost of the finished products. Colorants can be included throughout the body of the tile, or used in a surface coating. Both methods need to be addressed.
- *Concrete tiles.* There are three ways to improve the solar reflectance of colored concrete tiles. The first is to whiten the tile by using white cement in concrete mix; using a white cementitious surface coating (during the pre-cure coating); and/or or using white polymeric surface coating (during the post-cure coating). The second method is to use cool color pigments (infrared-scattering colored pigments) in the coating to provide choice of high-reflectance color. Examples of such cool colored pigments include mixed metal complex inorganic pigments. Cool pigments have been used successfully by a few leading and innovative tile-manufacturing companies. The third approach is to use cool pigments over a highly reflective undercoat. The undercoat must be allowed to dry properly before application of the topcoat. For example, phthalocyanines blue can be used in manufacture of

(Continued on Page 58)

We SPECIALIZE in LEISTER Hot Air Tools, it's all we do!

LEISTER

ASC
Authorized Sales & Service Center

At Assembly Supplies, Co, SERVICE isn't an afterthought, it's part of our commitment to keeping you, our customers, up and running with:

- **Quality Products**
- **Guaranteed Supply of Replacement Parts**
- **And Service When You Need It!**

The LEISTER Triac "S" pictured here is a 5 year old machine that came in for service… total cost for the repair was $83 - a new power cord, carbon brushes, air filter and a good , deep cleaning and this tool was ready to weld again!

Always **FREE** Repair Inspections!

It's easy, just ship us your sick Leister tool(s) with your company information and we'll do the rest. We will thoroughly inspect your tool and fax you a FREE repair estimate within 24 hours. Did we say FREE?

Factory Authorized Sales, Service & Training Center
2245 Enterprise Street, #100 - Escondido, CA 92029
Tel (800) 694-1472 – Fax (888) 694-4275 • HotAirTools.com

It's Our Service That Sets Us Apart!

Circle #68 on Reader Service Card

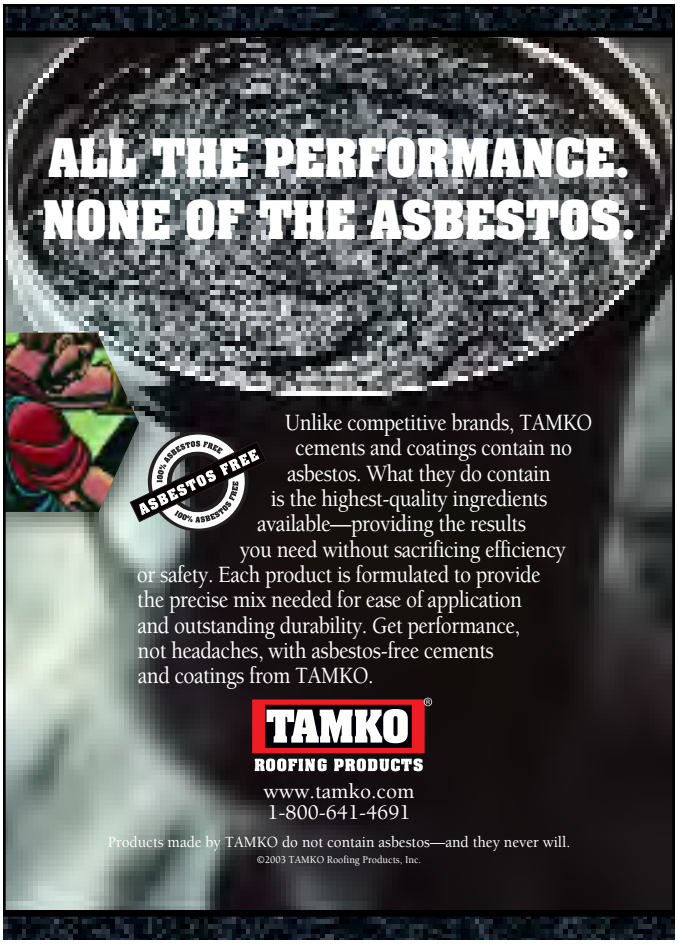

Circle #67 on Reader Service Card

Review of Residential Roofing Materials, Part II

(Continued from Page 57)

blue concrete tiles. In these prototypes, cool colored coatings are applied on a white base coat on concrete tiles.

■ *Metal panels.* Application of cool colored pigments in metal roofing materials may require the fewest number of changes to the existing production processes. As in the cases of tiles and asphalt shingle, cool pigments can be applied to metal via a single- or a double-layered technique. If the raw metal is highly reflective, a single-layered technique may suffice. The coatings for metal shingles are thin, durable, polymer materials. These thin layers use materials efficiently, but limit the maximum amount of pigment present. However, the metal substrate can provide some NIR reflectance if the coating is transparent in the NIR.

■ *Quality control.* The quality-control laboratories of colored roofing manufacturers are typically equipped to test the visual appearance (e.g., color) of their products. We anticipate that the industry will need to acquire instruments for testing the solar reflectance and NIR reflectances of their products. It is also envisioned that unified standards will have to be developed to address the initial reflectance, aged reflectance, mechanical properties, and thermal properties of cool colored roofing materials.

Conclusions

Fiberglass roofing shingles, tiles, and metallic materials comprise over 80% (by roof area) of the U.S. western region residential roofing market. In cooling-dominated regions, increasing the solar reflectance of the roofs lowers air-conditioning use in cooled buildings and improves comfort in unconditioned buildings. Our analysis has suggested that cool colored roofing materials can be manufactured using the existing equipment in production and manufacturing plants. The three principal ways to improve the solar reflectance of roofing materials are: (1) using raw materials with high solar reflectance, (2) using cool pigments in the coating; and (3) applying a two-layered coloring technique using pigmented materials with high solar reflectance as an underlayer. Although all these options are in principle easy to implement, they may require changes in the current production techniques that may add to cost and competitiveness of the finished products. Application of cool colored pigments in metal roofing materials may require the fewest number of changes in the existing production processes. As in the cases of tile and fiberglass shingle, cool pigments can be applied to metal via a single or a double-layered technique. If the raw metal is highly reflective, a single-layered technique may suffice. Additional quality-control measurements may be required to verify that coatings are truly NIR reflective.

Circle #66 on Reader Service Card

LBNL-55574

A Review of Methods for the Manufacture of Residential Roofing Materials

Hashem Akbari, Ronnen Levinson, and Paul Berdahl
Heat Island Group
Lawrence Berkeley National Laboratory
Berkeley, CA 94720

A Report Prepared for:

California Energy Commission PIER Program

Program Manager: Nancy Jenkins

Project Manager: Chris Scruton

June 2003

* This study was supported by funding from the California Energy Commissions (CEC) through the U.S. Department of Energy under contract DE-AC03-76SF00098.

DISCLAIMER

This document was prepared as an account of work sponsored by the United States Government. While this document is believed to contain correct information, neither the United States Government nor any agency thereof, nor The Regents of the University of California, nor any of their employees, makes any warranty, express or implied, or assumes any legal responsibility for the accuracy, completeness, or usefulness of any information, apparatus, product, or process disclosed, or represents that its use would not infringe privately owned rights. Reference herein to any specific commercial product, process, or service by its trade name, trademark, manufacturer, or otherwise, does not necessarily constitute or imply its endorsement, recommendation, or favoring by the United States Government or any agency thereof, or The Regents of the University of California. The views and opinions of authors expressed herein do not necessarily state or reflect those of the United States Government or any agency thereof or The Regents of the University of California.

ACKNOWLEDGEMENTS

This study was supported by funding from the California Energy Commission (CEC) through the U. S. Department of Energy under contract DE-AC03-76SF00098. The authors would like to acknowledge the support and guidance of the CEC project Manager Chris Scruton, as well as the contributions of our industrial partners including Mr. Gus Freshwater (vice president and general manager of the Elk Corporation shingle manufacturing plant in Shafter, CA); Dr. Louis Hahn and Mr. Keith Tellman (both from Elk Corporation, Texas Headquarters); Dr. Christopher Gross (3M Industrial Mineral Division); Dr. Ingo Joedicke (ISP headquarter in Hagerstown MD); Mr. David Carlson (manager of ISP granule plant in Ione, CA); Mr. Steve Perry (the plant shift facilitator at the Steelscape coil-coating plant in Rancho Cucamonga, CA); Ms. Michelle Vondran (formerly with BASF, now with Steelscape), Mr. John Marotta, and Mr. Jay Lewis (both with BASF); Mr. Jerry Vandewater and Mr. Jim Smith (both from MonierLifetile), and Mr. Yoshihiro Suzuki (general manager and director of MCA Tile in Corona, CA).

A Review of Methods for the Manufacture of Residential Roofing Materials*

Hashem Akbari, Ronnen Levinson, and Paul Berdahl
Heat Island Group
Lawrence Berkeley National Laboratory
Berkeley, CA 94720

Abstract

Shingles, tiles, and metal products comprise over 80% (by roof area) of the California roofing market (54-58% fiberglass shingle, 8-10% concrete tile, 8-10% clay tile, 7% metal, 3% wood shake, and 3% slate). In climates with significant demand for cooling energy, increasing roof solar reflectance reduces energy consumption in mechanically cooled buildings, and improves occupant comfort in non-conditioned buildings. This report examines methods for manufacturing fiberglass shingles, concrete tiles, clay tiles, and metal roofing. The report also discusses innovative methods for increasing the solar reflectance of these roofing materials. We have focused on these four roofing products because they are typically colored with pigmented coatings or additives. A better understanding of the current practices for manufacturing colored roofing materials would allow us to develop cool colored materials creatively and more effectively.

* This study was supported by funding from the California Energy Commissions (CEC) through the U.S. Department of Energy under contract DE-AC03-76SF00098.

Introduction

According to *Western Roofing Insulation and Siding* magazine (2002), the total value of the 2002 projected residential roofing market in 14 western U.S. states (AK, AZ, CA, CO, HI, ID, MT, NV, NM, OR, TX, UT, WA, and WY) was about $3.6 billion (B). We estimate that 40% ($1.4B) of that amount was spent in California. The lion's share of residential roofing expenditure was for fiberglass shingle, which accounted for $1.7B, or 47% of sales. Concrete and clay roof tile made up $0.95B (27%), while wood, metal, and slate roofing collectively represented another $0.55B (15%). The value of all other roofing projects was about $0.41B (11%).

We estimated roofing *area* market shares by assuming that roofing projects involving concrete tile, clay tile, wood shingle/shake, or slate were 50% (*Estimate 1*) to 100% (*Estimate 2*) more expensive than those using other roofing materials, such as shingle, metal, or membrane. This suggests that the roofing market area distribution was 54-58% fiberglass shingle, 8-10% concrete tile, 8-10% clay tile, 7% metal, 3% wood shake, and 3% slate (Table 1).

The functional distribution of the *steep-slope* roofing market in 2002 (including both residential and small-commercial buildings) was about 60% replacement, 25% new construction, and 15% repair and maintenance.

This paper examines methods for manufacturing fiberglass shingles, concrete tiles, clay tiles, and metal roofing that constitute over 80% of all roofing materials by both expenditure and area. Table 2 briefly describes each technology. We have focused on these four roofing products because they are typically colored with pigmented coatings or additives. We do not discuss production of wood and slate roofing. A better understanding of the current practices for manufacturing colored roofing materials would allow us to develop cool colored materials creatively and more effectively. The paper also discusses innovative methods for increasing the solar reflectance of these roofing materials.

Methodology

We reviewed the literature for production of roofing materials and visited several roofing material manufacturing plants.

Literature review

The following briefly summarizes several pertinent sources of information about roofing manufacturing methods available from web sites, articles, papers, patents, and books. In *The Science and Technology of Traditional and Modern Roofing Systems*, Laaly (1992) provides an overview of the production and application of various roofing materials. A web site of the National Park Services (NPS 2003) also provides the historical backgrounds of several roofing materials, including asbestos-cement shingle, asphalt shingle, clay tile, composition (built-up roofing), metal, slate, and wood shingle.

The Department of Health and Human Services (DHHS 2001) and the Environmental Protection Agency (EPA 1995) have each prepared extensive documents discussing various manufacturing methods for asphalt roofing products. These focus on environmental pollution, and do not address the effects of roof reflectivity on heating and cooling energy use and on roof durability.

Brown (1960) and Jewett et al. (1994) detail in chapters of 1960 and 1994 editions of *Industrial Mineral and Rocks* the manufacture of the colored roofing granules that are used in fiberglass and organic shingle roofs. Though these texts cover a wide range of technical and marketing issues related to the manufacture and production of colored granules, they provide limited information on granule coloring techniques. Joedicke (1997 and 2002) discusses this topic in greater detail.

Finally, Paris and Chusid (1997, 1999) briefly describe methods for coloring concrete products using powder, liquid, and granulated pigments. They also discuss issues related to the durability of colored concrete.

Plant visits

We visited a shingle plant, a metal roofing plant, and a clay tile plant in southern California; and a granule production plant and a concrete tile plant in northern California. Brief discussions of these plants are provided in the Appendix.

Table 1. 2002 Project residential roofing market in the U.S. western region[a] surveyed by Western Roofing (2002).

Roofing Type	Market share by $		Market share by roofing area (%)	
	$B	%	Estimate 1	Estimate 2
Fiberglass Shingle	1.70	47.2	53.6	57.5
Concrete Tile	0.50	13.8	10.4	8.4
Clay Tile	0.45	12.6	9.5	7.7
Wood Shingle/Shake	0.17	4.7	3.6	2.9
Metal/Architectural	0.21	5.9	6.7	7.2
Slate	0.17	4.7	3.6	2.9
Other	0.13	3.6	4.1	4.4
SBC Modified	0.08	2.1	2.4	2.6
APP Modified	0.07	1.9	2.2	2.3
Metal/Structural	0.07	1.9	2.2	2.3
Cementitious	0.04	1.1	1.2	1.3
Organic Shingles	0.02	0.5	0.6	0.6
Total	**3.60**	**100**	**100**	**100**

a. The 14 states included in the U.S. western region are AK, AZ, CA, CO, HI, ID, MT, NV, NM, OR, TX, UT, WA, and WY.

Table 2. Residential-building roofing technologies and their market shares in the 14-state U.S. western region surveyed by Western Roofing (2002).

Technology	Description	MARKET SHARE[a] Sales	Area[b]
Asphalt Shingle	Asphalt is a dark brown to black cementitious material, solid or semisolid, in which the predominant constituents are naturally occurring or petroleum-derived bitumens. It is used as a weatherproofing agent. The term asphalt shingle is generically used for both fiberglass and organic shingles. There are two grades of asphalt shingles: (1) standard, a.k.a. 3-tab; and (2) architectural, a.k.a. laminated or dimensional. Asphalt shingles come in various colors.	**47.7%**	**58.1%**
Examples	Fiberglass shingles, commonly known as "asphalt shingles," consist of fiber mats that are coated with asphalt and then covered with granules. Granules, a.k.a. mineral granules or ceramic granules, are opaque naturally- or synthetically-colored aggregates commonly used to surface cap sheets and shingles.	47.2%	57.5%
	Organic shingles have a thick cellulose base that is saturated in soft asphalt. This saturation makes them heavier than fiberglass shingles, and less resistant to heat and humidity, but more durable in freezing conditions.	0.5%	0.6%
Tile	Usually made of concrete or clay.	**26.4%**	**16.1%**
	Concrete tile is a combination of sand, cement, and water; the water fraction depends on the manufacturing process. Concrete tiles are either air-cured or auto-claved. Color is added to the surface of the tile with a slurry coating process, or added to the mixture during the manufacturing process.	13.8%	8.4%
	Clay tile is a combination of various clays and water. Color is added to the surface of the tile with a slurry coating process before the tile is kiln-fired.	12.6%	7.7%
Metal	Metal roofs can be classified as *architectural* or *structural*.	**7.8%**	**9.5%**
Examples	Architectural (hydrokinetic-watershedding) standing-seam roof systems are typically used on steep slopes with relatively short panel lengths. They usually do not have sealant in the seam because they are designed to shed water rapidly. They do not provide structural capacity or load resistance, and their installation is less labor-intensive because they have a solid substrate platform that makes installation easier.	5.9%	7.2%
	Structural (hydrostatic-watershedding) standing-seam roof systems are versatile metal panel systems that can be used on both steep- and low-slope roofs and are designed to be water-resistant. Most structural standing-seam systems include a factory-applied sealant in the standing seams to help ensure water tightness. These panel systems provide structural capacity and load resistance.	1.9%	2.3%
Other	All other roofing materials that are not covered under the categories mentioned above.	**18.1%**	**16.3%**

a. California accounts for 38% of the market in the 14 states (AK, AZ, CA, CO, HI, ID, MT, NV, NM, OR, TX, UT, WA, and WY) that make up the western region surveyed by *Western Roofing* magazine.

b. The roof areas fractions are LBNL's estimates and are derived from product costs and market shares.

Manufacturing methods

Shingles

Production of colored granules

Granules cover over 97% of the surface of a typical asphalt-soaked fiberglass shingle. Granules are applied to asphalt shingles for several reasons, including UV protection, coloration, ballasting, impact resistance, and fire resistance.

Granule manufacturing plants are typically sited near a quarry of suitable base rocks, including andesite, coal slag, diabase, metabasalt, nephaline syenite, quartzite, rhyodacite, rhyolite, and river gravel. The essential characteristics of the base rock include (1) opacity to ultraviolet light, to protect the asphalt from ultraviolet damage; (2) chemical and physical inertness, to provide resistance to acid rain, leaching, freeze/thaw, wet/dry cycling, oxidation and rusting; (3) low porosity, to improve physical strength, binding between coating and rock, and efficiency with which the pigment coating covers the surface; and (4) tolerance of high firing temperatures. Other necessary characteristics include moderate hardness, to remain intact during the granule coloring process; moderate density, to weight the shingle against wind lift; uniformity; and crush equidimensionally, to prevent directional embedment in the shingle manufacturing process, which changes shingle appearance.

In a roofing granule manufacturing plant, rocks blasted from quarries are crushed in several stages to create granule-size aggregate (0.5 to 2 mm) (Figure 1). In this process, the larger aggregates are recycled to the crushing system and the smaller debris is separated for other usage.

Once the granules are milled to the right size, they are transferred to the coloring plant. In the coloring plant, they are coated with a semi-ceramic color coating via a continuous process. The coating is a mixture of color pigments, sodium silicate, hydrated kaolin clay, and water. The preheated granules are mixed and tumbled with coating sufficient to cover the surface. The wet coated granules are then transferred to a rotary kiln where they are gradually heated to 250-550 °C (500-1000 °F). This dehydrates and polymerizes the coating, forming an insoluble pigmented ceramic layer. The granules are then gradually cooled in a rotary cooler by sprayed water and circulated air. Finally, the pigmented granules are coated with mineral oil to control dust and to improve asphalt adhesion. The mineral oil typically evaporates within a few months.

The pigments used for colored granules must have certain properties, including stability at high temperature, chemical inertness, ease of dispersion, color consistency, weather stability, non-toxicity, and low cost. Common pigments used in roofing granules include titanium dioxide (white), zinc ferrite (yellow), red iron oxides, carbon black, chrome oxide (green), and ultramarine (blue). Typically, 2.3-2.7 kg (5-6 lb) of pigment is required per tonne of granules to create a single-layer coating. Multiple coatings are needed to increase pigment loading. Some granule manufacturing plants have parallel coloring lines that can also be used in series to apply multiple layers of coatings? to granules.

The granules (both colored and uncolored) are transported to shingle manufacturing companies by road and rail.

Production of shingles

Fiberglass asphalt shingles have three major components: fiberglass mat, asphalt (with additive mineral stabilizer fillers), and granules (colored and uncolored). In a typical plant, the fiberglass mat is fed into a roll coater that applies layers of stabilized coating asphalt to the top and bottom surfaces of the webbing sheet. Stabilized coating asphalt is harder and more viscous than straight asphalt, and has a higher softening point. The mineral stabilizer used in asphalt roofing applications is an inorganic material, typically a crushed rock. It may consist of finely divided limestone, silica, slate dust, dolomite, or other minerals. Because this material is inorganic, it is less susceptible than asphalt to temperature change and fire. These properties are important for shingle manufacturing. Asphalt with stabilizer provides uniform and consistent properties within the climatic temperature range. Essentially, the stabilizer reduces viscosity in colder weather (making the shingle less brittle) and increases viscosity in warmer weather (increasing the softening point). In addition, the mineral stabilizer decreases the flammability of asphalt, thus allowing a higher fire rating of the shingle.

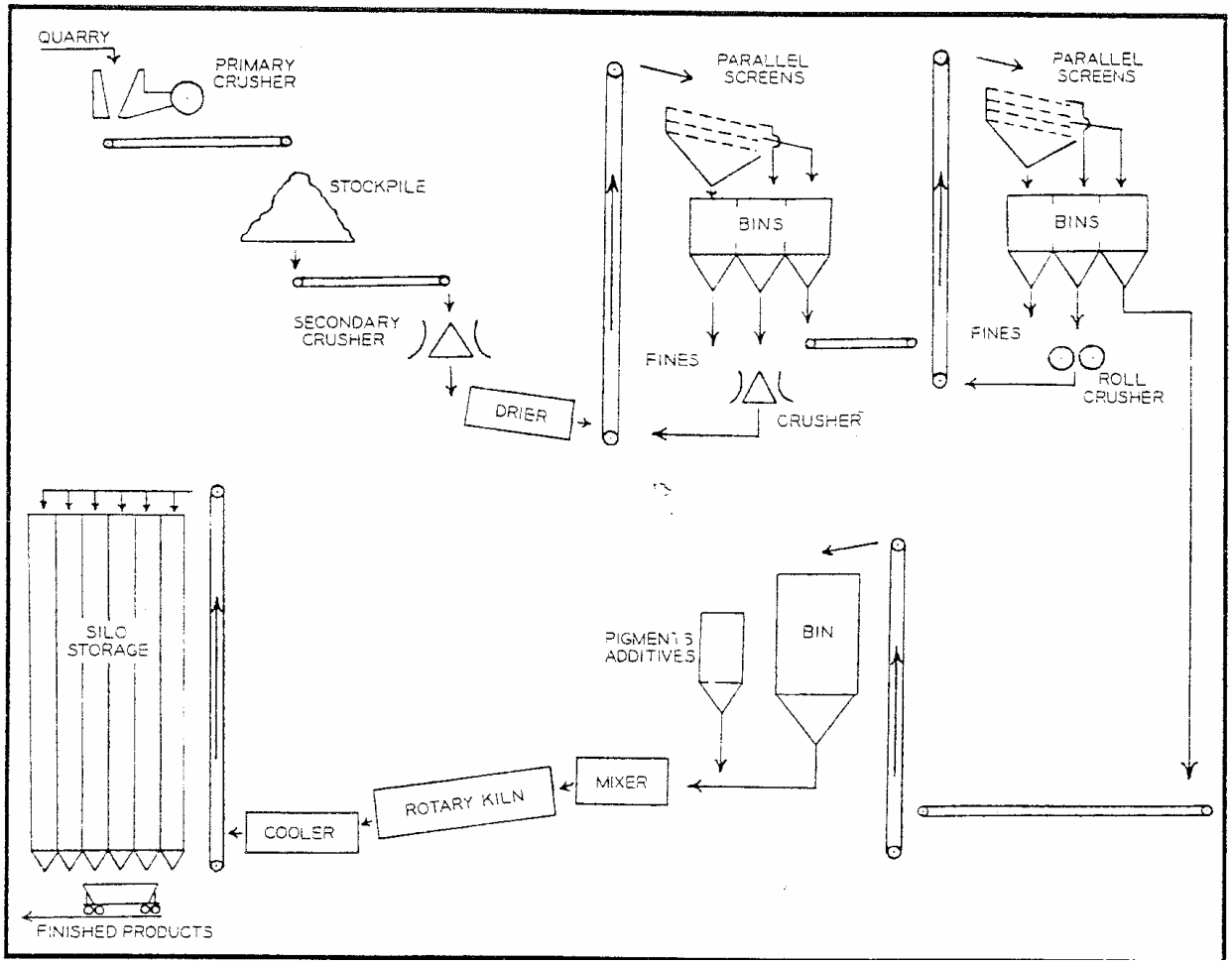

Figure 1. Schematic of a granule production plant. (Figure courtesy of Jewett, C.L., et al. *1994)*

The “filled” or “stabilized” coating asphalt applied at the coater is produced in the mixer, which is usually positioned above the manufacturing line at the coater. Coating asphalt, typically at 200-270 °C (400-520 °F), is piped into the mixer, and the mineral stabilizer is added. To eliminate moisture problems and to help maintain the temperature above 180 °C (360 °F) for proper coating consistency in the mixer, the mineral stabilizer is dried and preheated before it is added.

The weight of the finished product is controlled by the thickness of the asphalt coating. The distance between the coating rolls controls the amount of coating applied to the substrate. Most modern plants are equipped with automatic scales or profile scanners that monitor the sheets during the manufacturing process and warn the operator when too much or too little coating is being applied.

Colored and uncolored granules are applied in a section of the manufacturing line that usually consists of a multi-compartmented granule hopper, two parting agent hoppers, and two large press rollers. The hoppers are fed through flexible hoses from one or more machine bins located above the production line. These machine bins (sometimes called surge bins) provide temporary storage. The granule hopper drops colored granules from its various compartments onto the top surface of the moving sheet of coated web in the sequence necessary to produce the desired color pattern on the roofing.

Next, the sheet is cooled by passing it over water-cooled rollers; water may also be sprayed directly onto the sheet to speed cooling. The final steps in the production of asphalt roofing shingles are cutting and packaging. After the shingles have been cut by machine, they are moved by roller conveyor to automatic packaging equipment. The packaged shingles are then stacked on pallets and transferred by forklift to storage areas or waiting trucks. Photos of various stages of the process and schematic of the total process are shown in Figure 2 and Figure 3.

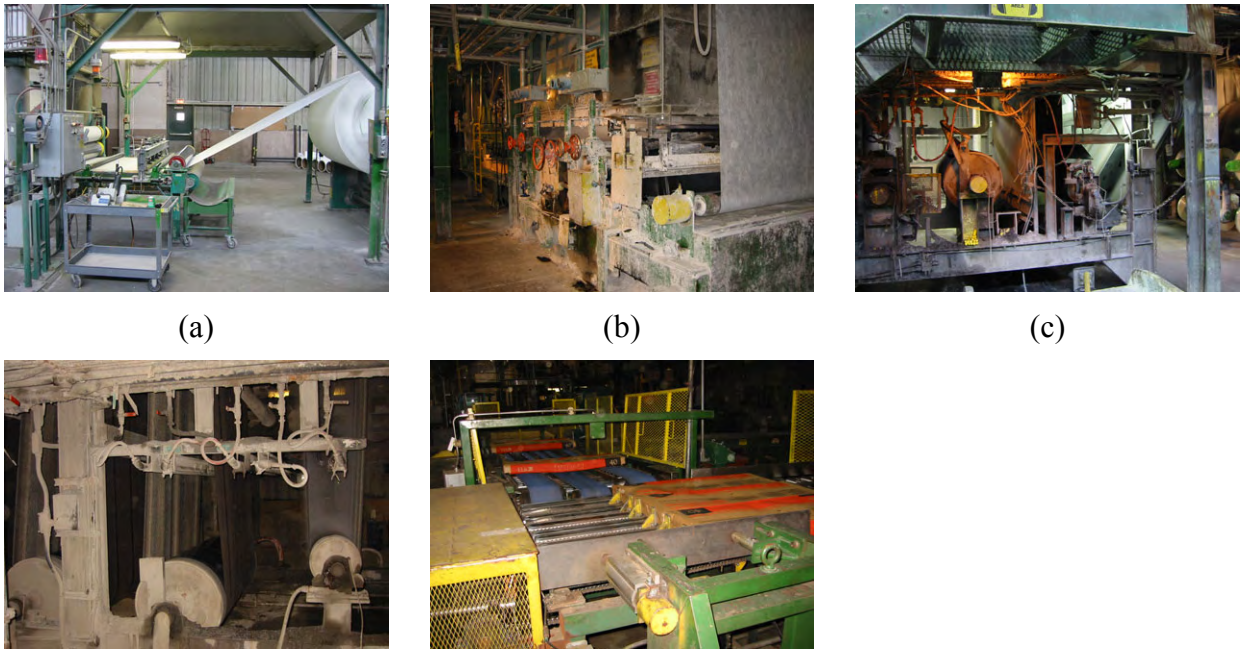

(a) (b) (c)

(d) (e)

Figure 2. Shingle manufacturing processes: (a) fiberglass mat is fed into the line; (b) fiberglass enters the shingle production machinery; (c) fiberglass is soaked in asphalt and filler, then granules are roller-applied to both sides of the shingles; (d) shingle rolls are water-cooled by wet rollers; (e) cut and stacked shingles are packaged for shipping.

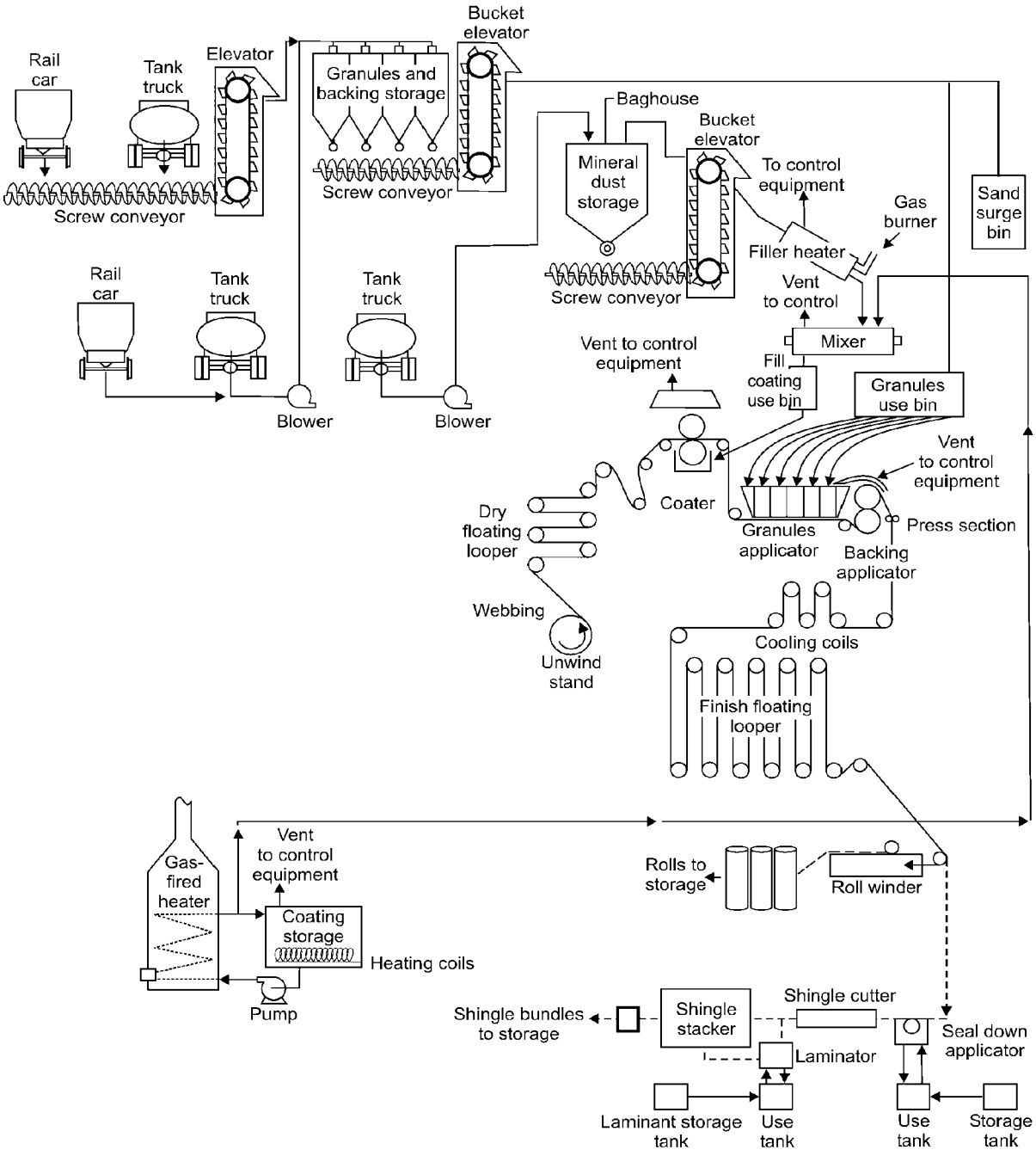

Figure 3. Schematic of a fiberglass shingle production plant. (Figure courtesy of DHHS 2001)

Clay tiles

Clay tile production begins by mixing and crushing various raw clay materials. For example, the raw clays used at MCA Tile, Inc. include “yellow shell clay” (a clay with medium plasticity having high heat resistance, permitting vertical firing without warping); “apple clay” (a clay with high plasticity and low heat resistance); and “AAA clay” (a low shrinkage, medium heat resistance clay, with high iron content to make the tile red).

The raw clays are thoroughly mixed with water and aged for 4-5 days. The aging process allows the dry material to fully absorb the moisture, improving plasticity. This increases yields from the extrusion process and thus lowers the unit production cost.

Several extrusion machines and dies are employed to produce clay tiles of various shapes. Prior to extrusion, the clay flows through a vacuum chamber to remove air, preventing cracking of tiles during the firing process. This process is also very important for proper vitrification (conversion to a glassy state), which makes the tile weather resistant (i.e., resistant to freezing/thawing and salt intrusion; see Standard Specification for Clay Roof Tiles: ASTM C-1167 for more detail). An automated cutter at the end of each extruder cuts the tile to the desired size, and trims the edges. The wet extruded tile is then dried in a sequence of temperature-controlled chambers for about 24 hours. By reducing the excessive moisture in the tiles, this drying process reduces the probability of cracks when the tile is fired. The drying process typically starts with circulating ambient air at a temperature of about 20-30 °C, gradually increasing the temperature to about 90 °C using waste heat from the kiln-cooling process. Drying reduces the tile’s mass moisture content from 15% to less than 1%.

The dry raw tiles are inspected for defects before they are sprayed with glossy or matte glazes. The glazing is a mixture of water, pigments and clay additives. For the glossy finish, frits (glassy silicates), clay and color glazed materials are added to the glazing mixture. The glazed tiles are positioned in vertical stacks or in a “standing up” position, with typically 1.25 cm (1/2”) spacers to allow an even heat distribution in the kiln. Even heating yields evenly colored tiles with good mechanical properties.

The glazed tiles are then passed through a kiln fired for 14-20 hours, depending upon the production schedule. The kiln has three stages: preheat, heating and cooling. In the preheating zone, the tiles are gradually heated to about 700 °C by warm drawn air from the heating zone. In the heating zone, the tiles are directly fired for about 4 hours by gas flame, reaching a maximum temperature of about 1050 °C. Then the tiles are gradually cooled to about 300-400 °C by drawing outside air through the kiln. The clay tile is ready to ship as soon as it is removed from the kiln and cools to ambient temperature—no curing is required. The clay tile colors are permanent and do not fade with exposure to the sun. Photos of several steps in the process are shown in Figure 4.

(a) (b) (c)

(d) (e) (f)

(g) (h) (i)

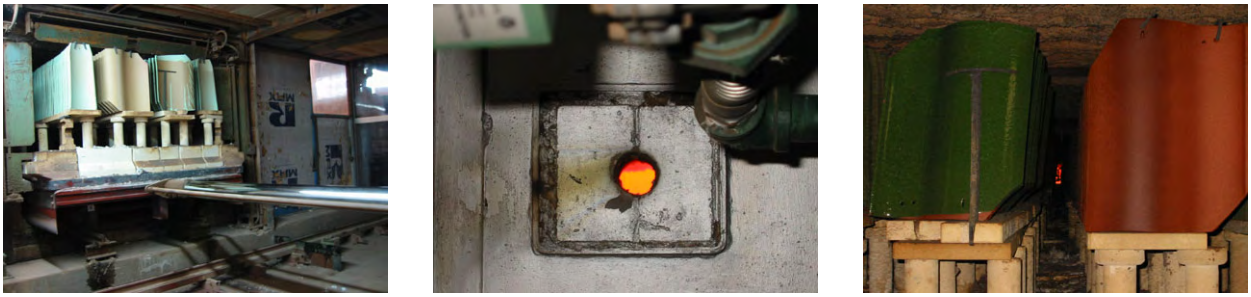

(j) (k) (l)

Figure 4 (I of II).Clay tile manufacturing processes: (a,b) production begins by mixing and crushing raw clay components; (c,d) extrusion machines and molds produce variously shaped tiles; (e) the wet extruded tile is dried in a sequence of temperature- and humidity-controlled drying chambers for about 24 hours; (f,g,h) the dry raw tiles are inspected for defects and sprayed with glossy or mat glazes; (i) the coated tiles are stacked with spacers (typically 1.25 cm) to allow an even heat distribution in the kiln; (j,k,l) the coated tiles are kiln-fired for 14-20 hours.

(m)

(n)

Figure 4 (II of II). Clay tile manufacturing processes: (m) the finished tiles are shipped to customers. Figure (n) shows various tile samples.

Concrete tiles

Sand, cementitious materials, limestone fillers, and water are the main ingredients (by mass) of concrete tiles (see Figure 5). Pigments are added for color and polymers are used as a water resistant coating on the tile surface. Pigments are typically added to the surface in a slurry coat comprised of pigment, cement, silica and water. Finished concrete tiles may also be painted. The major components contributing to the cost are cementitious materials, sand, polymer coating, and pigments. Pigments are typically added to the surface in a slurry coat comprised of pigment, cement, silica and water. Tiles may also be painted.

Concrete tile production begins by mixing aggregate (sand) and fillers (see Figure 6). Sand is pre-washed to remove dirt contaminants. Recycled aggregates and quarry waste are also used in the mixture. Milled calcium carbonate, an inexpensive material that improves the quality of concrete, is used as filler. Then the aggregate and filler are mixed with cementitious materials before water is added to the mixture. At this stage, pigments may be added to color the concrete mix. The ingredients are completely mixed before being fed to the molding machine.

Several machines and molds are employed to produce concrete tiles of various shapes (see Figure 7). The mold and the wet concrete tile run on a conveyor where the tiles are partially dried and polymeric a coating is applied to the surface before curing. The tiles and the mold are packed in a curing chamber for about four hours, where the concrete tile is cured and dried. The molds and tiles run through a separator that removes the molds. The dry raw tiles are inspected for defects before they are sprayed with colored coatings. The tiles are then covered with post-coating polymers. The coating is a mixture of water, pigments, and polymeric additives. The coated tiles are then dried, stacked, and packed for shipment.

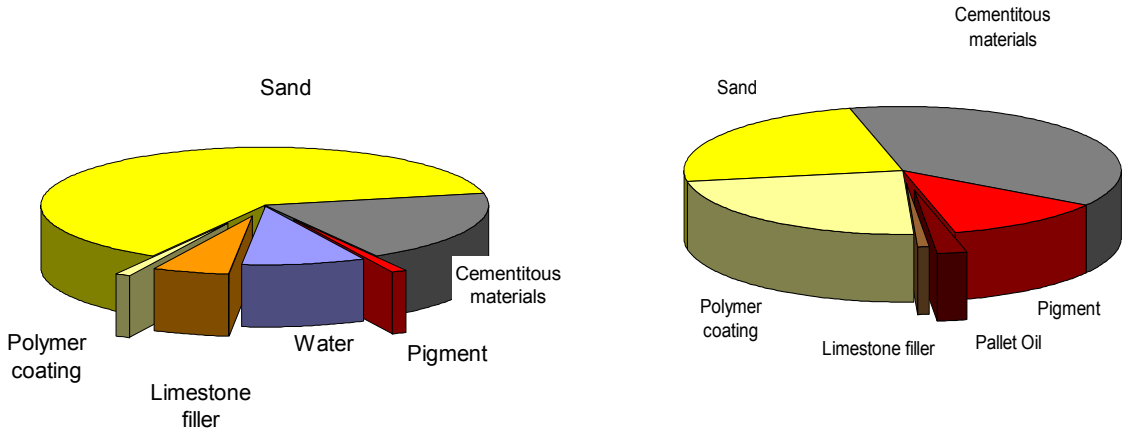

Figure 5. Typical composition of a concrete rooftile, by mass and by cost. (Figure courtesy of MonierLifetile)

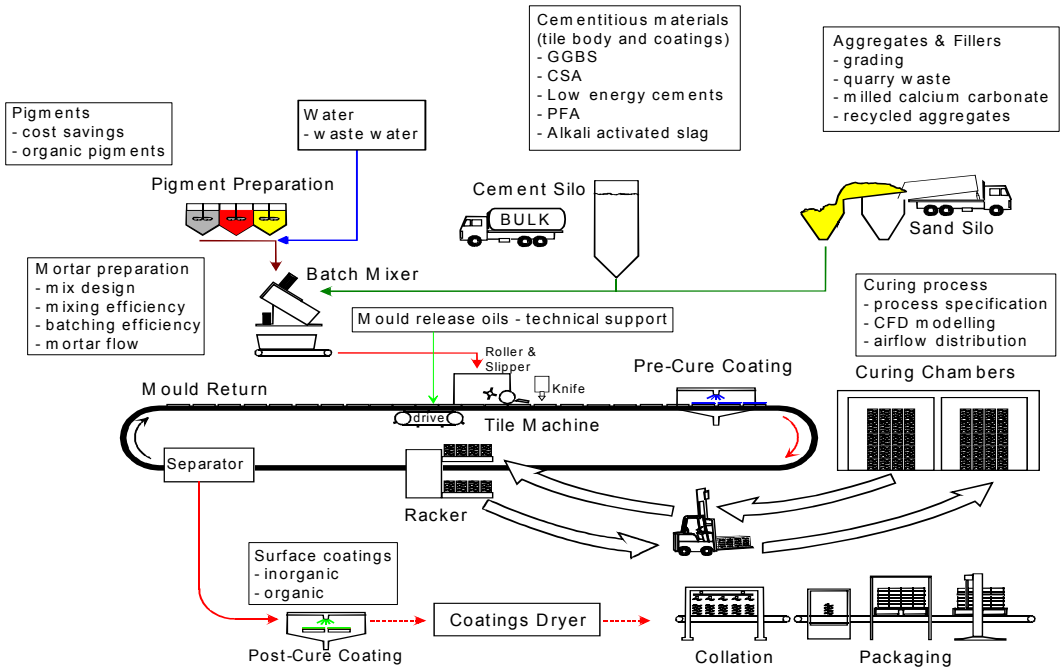

Figure 6. Schematic of a concrete rooftile production plant. (Figure courtesy of MonierLifetile)

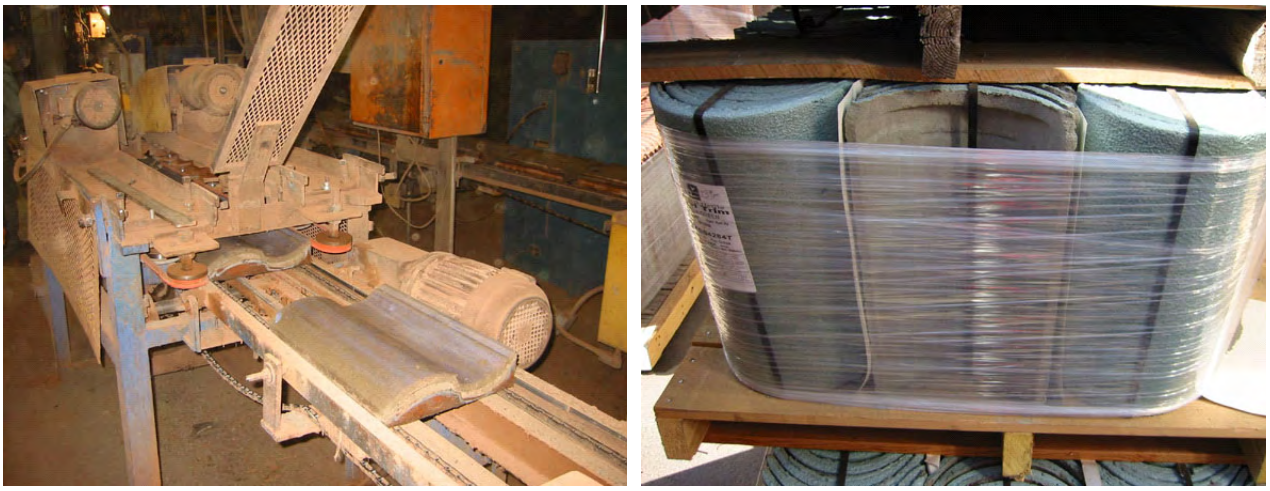

(a) (b)

Figure 7. (a) Concrete tile molding machine and (b) final products ready to ship

Metal roofing

Metal production for the roofing industry may be divided into two phases: (1) coil coating plants, where raw metal coils are cleaned, metallic coated, primed, and paint coated (some facilities can both metallic coat and paint, while others only apply paint); and (2) metal forming plants, where the coated coils are either used to produce flat metal panels, or pressed into shapes that simulate non-metal roofing products (e.g., shake, slate, or tile).

Coil coating plants

Coil coaters produce rolled metals in the thickness, width, metal coating type and color specified by their customers, which include but are not limited to members of the roofing industry. An advanced metal coil plant typically has four major production lines: a *pickle line*, where the hot-band coil[†] is uncoiled, is cleaned of oxides, has its edges trimmed to customer requirement, and is oiled in preparation of further processing; a *cold mill line*, where the pickled bands are reduced in thickness 65-80% to meet ordered thickness, are rolled to a suitable shape, and have texture applied to the surface; a *metallic coating line*, where the coils are cleaned again, a layer of metallic coating is applied, and the surface is treated for either painting or use of the product in a bare metal application; and a *paint line* where primer and finish coatings are applied. Many coil coaters consist of only a paint line; they do not process their own substrate.

PICKLE LINE

The raw material for this industry is typically a thick metal steel coil. The hot-band coil is pickled when it first arrives at the coating plant (Figure 8). There it is uncoiled and cleaned in a series of acid baths (stages 1-4) to ensure the proper surface for further processing, where it may be subjected to cold rolling and galvanizing (coating with zinc) or galvalumizing (coating with a zinc/aluminum alloy). The steel is then side-trimmed for width to the customer's specifications (stage 5). At the end of the pickle line process, the steel is re-coiled (stage 6) and ready to go on

[†] Hot band coils are the result of steel slabs being elongated and rolled into coiled sheet of finite width and thickness; the temperature and amount of processing determine mechanical properties of the coil.

to the cold rolling mill. The pickle line is capable of continuous production. One coil is processed while the other is prepared to be fed to the line.

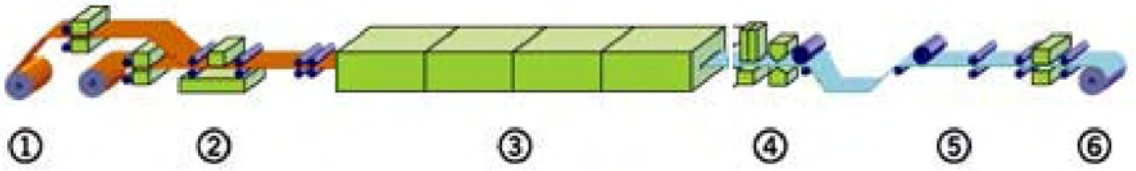

(1) Hot-rolled coil. The hot-rolled coil enters the pickle line.

(2) Stitcher. The end of one coil is joined to the beginning of the next coil.

(3) Acid tank. The band of steel is run through a series of acid tanks to remove rust, then rinsed in hot water.

(4) Side trimmer. The sides of the band are trimmed to the specified width.

(5) Shear. The stitches that connected two coils at the beginning of the line are cuts out.

(6) Tension reel. The steel is recoiled.

Figure 8. Metal coil coating: pickle line. (Figure courtesy of Steelscape 2003)

COLD MILL LINE

In the cold reversing mill (CRM) line, the thickness of the metal coil is reduced to specification by passing through pressure rolls (Figure 9). Larger scale cold mills pass the coil through a series of our or five rollers (Item 3 in Figure 9) to achieve the desired reduction in thickness. This way the full gauge reduction is achieved with one pass.

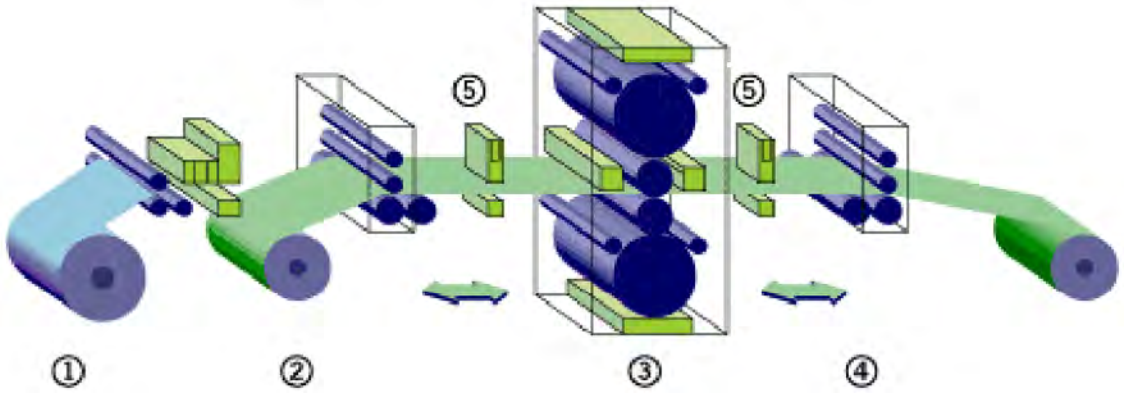

(1) Cold mill entry. The metal is uncoiled and passed forward through the rollers.

(2) Entry tension reel. After its initial pass through the CRM, the coil is prepared for the next pass through the rollers.

(3) Main roller set. Rollers apply pressure to the steel to reduce its thickness. The number of passes depended on the specification for the final thickness.

(4) Delivery tension reel. The steel is re-coiled.

(5) Thickness gauge.

Figure 9. Metal coil coating: cold mill line. (Figure courtesy of Steelscape 2003)

METAL COATING LINE

In the metal coating line, the steel coils are cleaned again, a layer of metallic coating (zinc of zinc/aluminum alloy) is applied, and the surface is treated either for painting or for use as bare metal (Figure 10). Coils from the cold mill line are fed to the entry reel (stage 1) and welded together (stage 2) for continuous line operation. The coil then passes through an accumulator tower (stage 3), after which the steel coils are cleaned in preparation for the metallic coating (stage 4) before being fed to the annealing furnace to achieve the desired mechanical properties (stage 5). Coming out of the furnace the strip is directly dipped into a molten bath of zinc or galvalume. The specified coating weight is achieved by air-wiping excess metal before it solidifies (stage 6). The hot-coated coil is then cooled (stage 7) and treated in a surface-conditioning mill (stage 8). The process is very similar to the cold mill, but on a much smaller scale as the goal is to smooth the surface, not thin the coil. The steel is slightly elongated for uniform flatness by the tension leveler (stage 9). The surface can also be chemically treated (stage 10) and coated with a resin (stage 11) for bare metal applications.

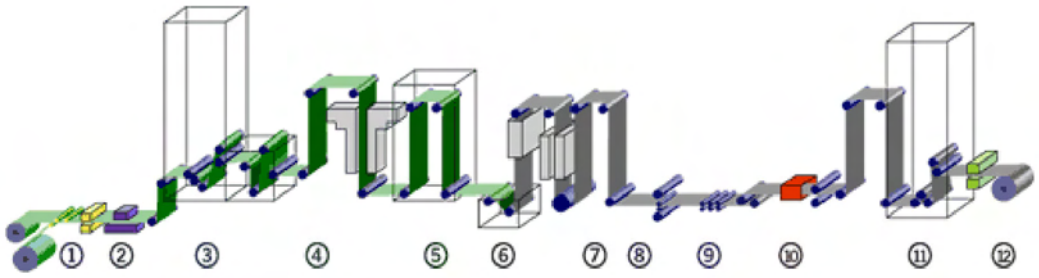

(1) Entry reel.

(2) Welder. The end of one coil is welded to the beginning of another for continuous operation.

(3) Entry accumulator tower.

(4) Cleaning unit. Steel is sprayed with a caustic soltuion, rinsed, and dried.

(5) Furnace. Steel is heat treated for desired mechanical properties.

(6) Coating pot. Steel is coated with either Zn or 55%Al-45%Zn.

(7) Cooling tower. Steel is cooled to near room temperature.

(8) Surface conditioning mill (SCM). Prepares the steel for painting.

(9) Tension leveler. Steel is slightly elongated for uniform flatness.

(10) Chemical treatment. Provides interim protection against coating deterioration during storage.

(11) Resin coater. Provides lubrication for roll forming, suppresses hand/foot prints during installation, and provides some corrosion protection.

(12) Exit accumulator tower.

(13) Exit tension reel.

Figure 10. Metal coil coating: metal coating line. (Figure courtesy of Steelscape 2003)

PAINT LINE

The paint line is similar to the metal coating line. In the paint line (Figure 11), a coil from the metal coating line is fed to the entry reel (stage 1) where coils are welded or stitched together for

continuous operation of the line. The coil then passes though an accumulator tower and cleaner (stage 2) prior to chemical coating. The chemical coater (stage 3) pre-treats the surface to accept primer or paint and to provide corrosion resistance. A primer (stage 4) is then applied to the steel strip and cured in the prime oven. Then the strip is coated with the finish paint (stage 5) and cured in the finish oven. Paint lines can paint one or both sides of the strip, depending on customer requirement. The cured, painted steel is then quenched with water and cooled to room temperature (stage 6). Finally, rollers remove the excess water, and the steel goes into the exit accumulator (stage 7) before it is taken up onto an exit reel (stage 8). The finished strip can be sent back through the paint line if additional paint layers are desired. This is often done for print or pattern finishes where the final product includes multiple colors to mimic wood shakes, asphalt shingles or aged copper.

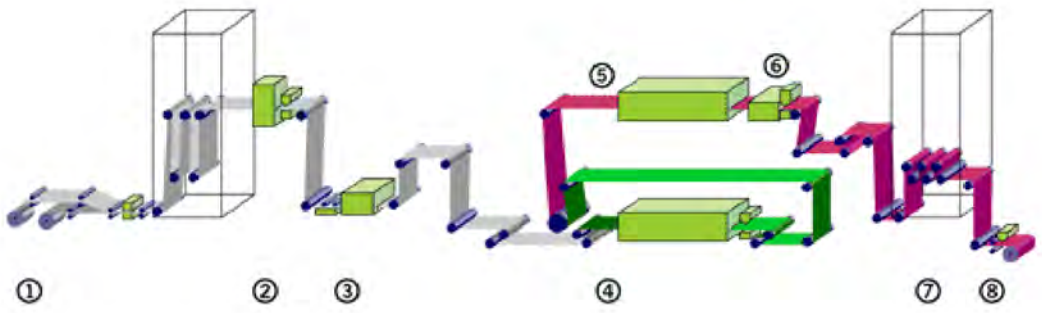

(1) Entry reels.

(2) Cleaning unit.

(3) Chemical coater. Applies an initial coating on the steel.

(4) Prime coater. Coats the steel with the primer.

(5) Finish coater. Coats the steel with the finish paint.

(6) Water quench. Painted steel is cooled down to room temperature.

(7) Exit accumulator.

(8) Exit reel.

Figure 11. Metal coil coating: paint. (Figure courtesy of Steelscape 2003)

Metal forming plants

Metal forming plants cut and press painted or unpainted metal coils to form either flat panels or simulations of non-metal roofing products (e.g., shake, shingle, tile, and slate). A very few fabricators apply granulated material to the painted panels in order to simulate asphalt shingles. However, most fabricators of shingle or tile type profiles use embossing or stamping to achieve the desired look. Some examples of metal roofing products are shown in Figure 12.

(a) (b) (c)

(d) (e) (f)

(g) (h) (i)

(j) (k) (l)

Figure 12. Simulated roofing products made from metal: (a) Advanta Shingles; (b) Bermuda Shakes; (c) Castle Top; (d) Dutch Seam Panel; (e) Granutile; (f) Perma Shakes; (g) Scan Roof Tile; (h) Snap Seam Tile; (i) Techo Tile; (j) Verona Tile; (k) Oxford Shingles; and (l) Timbercreek Shakes. Products a-j are manufactured by ATAS International, Inc., while products k and l are manufactured by Classic Products, Inc. (Photos courtesy of ATAS International and Classic Products)

Methods to Produce Cool Roofing Materials

Shingles

The solar reflectance of a new shingle is dominated by the solar reflectance of its granules, since by design, the surface of a shingle is well covered with granules. Hence, we focus on the production of cool granules. There are primarily two ways to increase the solar reflectance of the granules: manufacturing granules from highly reflective (e.g., white) rocks, and/or coating the granules with reflective pigments. The use of naturally white rock is limited by local availability of suitable inert rocks, which are often not found in large quarries. Hence, manufacturers usually color the granules.

Until recently, the way to produce granules with high solar reflectance has been to use titanium dioxide (TiO_2) rutile, a white pigment. Since a thin layer of TiO_2 is reflective but not opaque, multiple layers are needed to obtain the desired solar reflectance. This technique has been used to produce "super-white" (meaning truly white, rather than gray) granulated shingles with solar reflectance exceeding 0.5. Manufacturers have also tried to produce colored granules with high solar reflectance by using nonwhite pigments with high near-infrared (NIR) reflectance. However, like TiO_2, cool-colored pigments are also partly transparent to NIR light; thus, any NIR light not reflected by the cool pigment is transmitted to the (typically dark) granule underneath, where it can be absorbed. To increase the solar reflectance of colored granules with cool pigments, multiple color layers, a reflective undercoating, and/or reflective aggregate should be used. Obviously, each additional coating increases the cost of production.

Figure 13 shows the iterative development of a cool black shingle. A conventional black roof shingle has a reflectance of about 0.04. On the first try to increase the solar reflectance of the shingle, we replaced the standard black pigment on the granules with one that is NIR reflective. That increased the reflectance of the granule to 0.12. On the second try, we used a two-layered technique where we first applied a layer of TiO_2 white base (increasing the solar reflectance of the base granule to 0.28) and then a layer of NIR-reflective black pigment. This increased the reflectance of the black granule to 0.16. On our third prototype, the base granule was coated in ultra-white (reflectance 0.44) and then with an NIR-reflective black pigment. This increased the solar reflectance to 0.18. Figure 13 also shows the performance limit (reflectance 0.25) where a 25-μm thick layer of NIR-reflective black coating is applied on an opaque white background.

The application of pigmented coatings to roofing granules appears to be the critical process step. Several layers of silicate coatings can be involved, and may include not just one or more pigments, but the use of clay additives to control viscosity, biocides to prevent staining, and process chemistry controls to avoid unreacted dust on the product.

One way to reduce the cost is to produce cool-colored granules via a two-step, two-layer process. In the first step, the granule is pre-coated with an inexpensive pigment that is highly reflective to NIR light. In the second step, the cool-colored pigment is applied to the pre-coated granules.

Shingles tend to lose some granules as they age and weather, exposing asphalt-coated fiberglass and reducing solar reflectance. Substituting a reflective sealant for the black asphalt could slow this. While developing such a replacement for asphalt may be of long-term interest, we do not see an easy or short-term solution to this problem.

It should be noted that the reflectance of an asphalt shingle covered with granules will always be less than that of the granule's coating, since some of the light reflected by each granule will strike a neighboring granule and be absorbed. These "multiple reflections" can reduce shingle reflectance by as much as 0.15.

Finally, the granule manufacturing and shingle manufacturing industries have designed their quality-control laboratories to test the visible color of their products. We anticipate that the industry will need to equip itself with additional instruments to test the solar reflectance and the NIR optical properties of their products. It is also envisioned that unified standards have to be developed to address issues related to manufacturing of cool-colored granules and shingles.

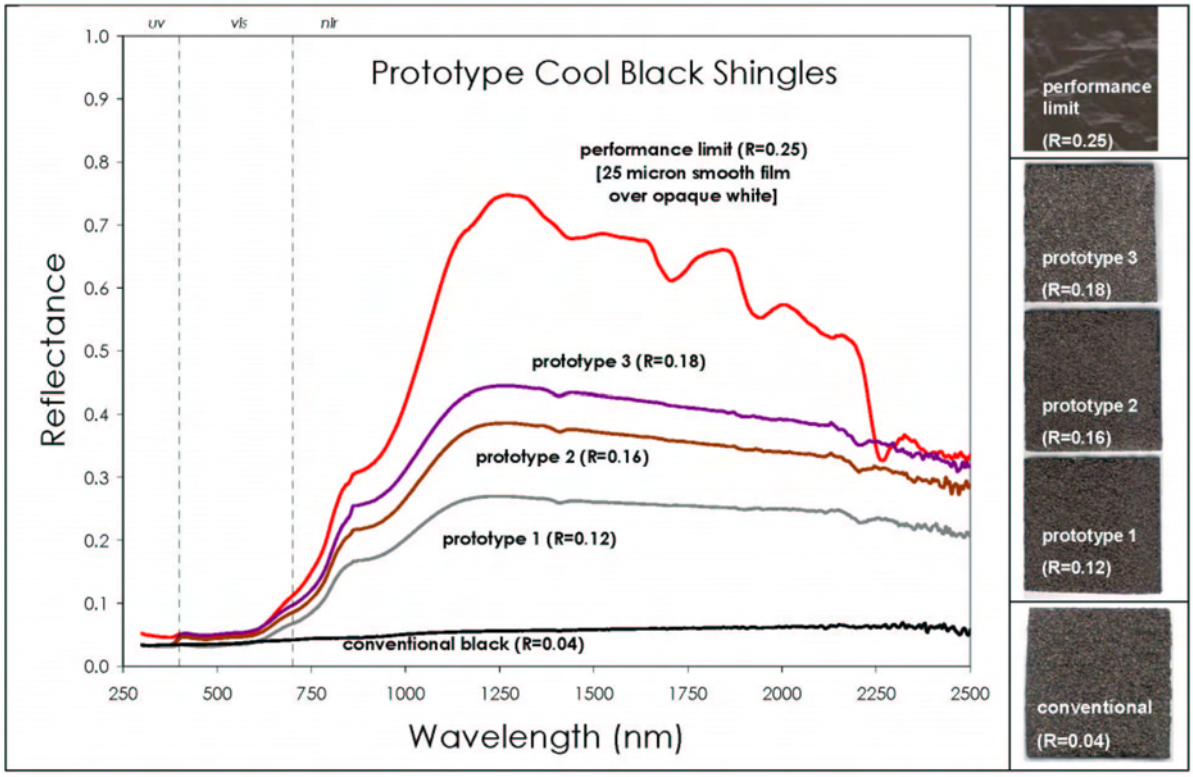

Figure 13. Development of a cool black shingle. R = Solar reflectance.

Clay tiles

Considerations for production of cooler colored tiles are similar to those of the roofing shingles. Three ways to improve the solar reflectance of clay tiles are: (1) use of raw clay materials with low concentrations of iron oxides and elemental carbon; (2) use of cool pigments in the coating; and (3) application of the two-layered coating technique using pigmented materials with high solar reflectance as an underlayer. Although all these options are in principle easy to implement, they may require changes to current production techniques that may add to cost of the finished products. Colorants can be included throughout the body of the tile, or used in a surface coating. Both methods need to be addressed.

Concrete tiles

There are three ways to improve the solar reflectance of colored concrete tiles. The first is to whiten the tile by using white cement in the concrete mix; using a white cementitious surface coating (during the pre-cure coating); and/or using white polymeric surface coating (during the post-cure coating). The second method is to use cool color pigments (infrared-scattering colored pigments) in the coating to provide choice of high-reflectance color. Examples of such cool colored pigments include mixed metal complex inorganic pigments. Cool pigments have been used successfully by a few leading and innovative tile-manufacturing companies. The third approach is to use cool pigments over a highly reflective undercoat. The undercoat must be allowed to properly dry before application of the topcoat. For example, near-infrared transparent phthalocyanine blue can be applied over a white undercoat to produce a cool blue tile.

Figure 14 shows the results of an effort to develop coatings for concrete tile roofs. Various coatings yielded a palette of cool colors each with solar reflectance exceeding 0.4. In some of these prototypes (the blue and the black), cool colored coatings are applied over a white base coat.

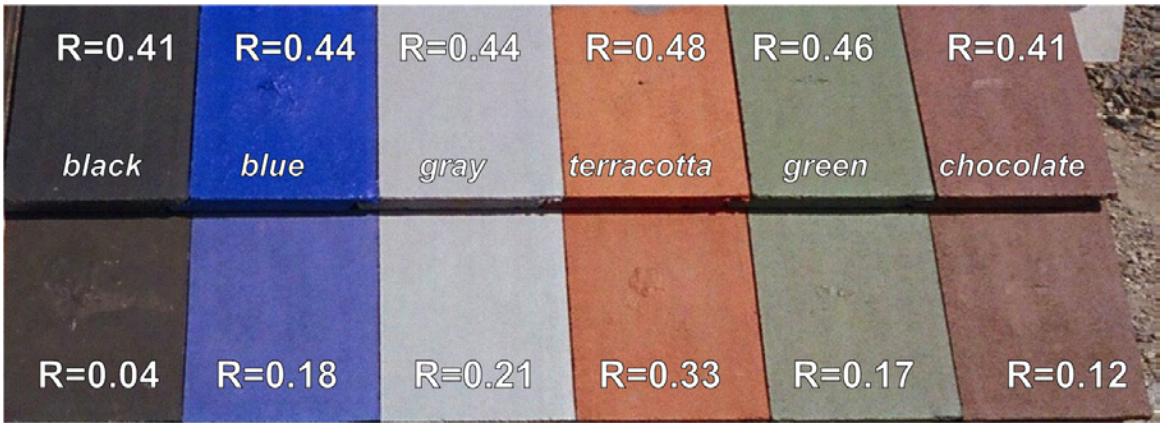

Figure 14. Solar reflectance (R) of several prototype cool coatings for concrete tile roofs. (Image courtesy of American Rooftile Coatings)

Metal panels

Application of cool-colored pigments in metal roofing materials may require the least change to the existing production processes. As in the cases of tiles and asphalt shingle, cool pigments can be applied to metal via a single or a double-layered technique. If the raw metal is highly reflective, a single-layered technique may suffice. The coatings for metal shingles are thin, durable polymer materials. These thin layers use materials efficiently, but limit the maximum amount of pigment present. However, the metal substrate can provide some NIR reflectance if the coating is transparent in the NIR.

Quality control

The quality-control laboratories of colored roofing manufacturers are typically equipped to test the visual appearance (e.g., color) of their products. We anticipate that the industry will need to acquire instruments for testing the solar reflectance and NIR reflectances of their products. It is also envisioned that unified standards will have to be developed to address the initial reflectance,

aged reflectance, mechanical properties, and thermal properties of cool-colored roofing materials.

Conclusions

Fiberglass roofing shingles, tiles, and metallic materials comprise over 80% (by roof area) of the U.S. western region residential roofing market. In cooling-dominated regions, increasing the solar reflectance of the roof lowers air-conditioning use in a cooled building and improves comfort in an unconditioned building.

Our analysis has suggested that cool-colored roofing materials can be manufactured using the existing equipment in production and manufacturing plants. The three principle ways to improve the solar reflectance of roofing materials including: (1) using of raw materials with high solar reflectance, (2) using cool pigments in the coating; and (3) applying a two-layered coloring technique using pigmented materials with high solar reflectance as an underlayer. Although all these options are in principle easy to implement, they may require changes to current production techniques that may add to cost and market competitiveness of the finished products.

Application of cool-colored pigments in metal roofing materials may require the least change to the existing production processes. As in the cases of tile and fiberglass shingle, cool pigments can be applied to metal via a single or a double-layered technique. If the raw metal is highly reflective, a single-layered technique may suffice.

Additional quality control measurements may be required to verify that coatings are truly NIR-reflective.

References

ARMA. 1997. “Residential Asphalt Roofing Manual.” Asphalt Roofing Manufacturers Association, 4041 Power Mill Rd., Suite 404. Calverton, MD 20705. (301) 348-2002 FAX: (301) 348-2020. www.asphaltroofing.org

ASTM C 1167. 2003. "Standard Specification for Clay Roof Tiles," ASTM International. For referenced ASTM standards, visit the ASTM website, www.astm.org.

Brown, J.A. 1960. Granules. Chapter 19 of *Industrial Mineral and Rocks*. Ed. J.L. Gillson. American Institute of Mining, Metallurgical, and Petroleum Engineers. This reference provides a detailed overview of the manufacturing methods of colored granules.

DHHS (NIOSH). 2001. Publication No. 2001-127. Asphalt fume exposure during the manufacture of asphalt roofing products. United States Department of Health and Human Services (National Institute for Occupational Safety and Health). August. http://www.cdc.gov/niosh/pdfs/2001-127.pdf
This document in detail describes various manufacturing methods for asphalt roofing products.

EPA. 1995. Compilation of Air Pollutant Emission Factors, AP-42, Fifth Edition, Volume I: *Stationary Point and Area Sources*. Chapter 11. United States Environmental Protection Agency. http://www.epa.gov/ttn/chief/ap42/ch11/final/c11s02.pdf
This document in detail describes various manufacturing methods and emissions from plants for asphalt roofing manufacturers.

Jewett, C.L., Collins, R.C., Weaver, L.W., and McShea, T. 1994. Roofing Granules. In *Industrial Mineral and Rocks (Nonmetallics other than Fuels)*. Senior Ed. Donald D. Carr, American Institute of Mining,

Metallurgical, and Petroleum Engineers. Society for Mining, Metallurgy, and Exploration, Littleton, CO. This reference provides a detailed overview of colored granules manufacturing methods.

Joedicke, I. 1997. Iron oxides in roofing granules manufacture. Intertech Conferences. Iron Oxides 97 for Colorant & Chemical Applications.
The paper discusses the production and coloring of roofing granules.

Joedicke, I. 2002. Roofing granules with a decorative metallic appearance. United States Patent Application Publications: US 2002/0187306 A1.
The patent briefly discusses the colored roofing granules and methods for preparation of granules with decorative metallic appearance.

Laaly, H.O. 1992. *The Science and Technology of Traditional and Modern Roofing Systems*. Laaly Scientific Publishing, Los Angeles, CA. This book provides an overview of the production and application of various roofing materials.

NPS. 2003. From asbestos to zinc, Roofing of Historic Buildings, National Park Services.
http://www.cr.nps.gov/hps/tps/roofingexhibit/introduction.htm
This site provides a historical background of several roofing materials including: asbestos-cement shingles, asphalt shingles, clay tile, composition (built-up roofing), metals, slate, and wood shingles.

Paris, N. and Chusid, M. 1999. Color in concrete: Beauty and Durability. (Reprint from *Concrete International* Magazine and the American Concrete Institute.
http://www.daviscolors.com/literature/pdf/Durability.PDF
The document discusses the color durability and cleaning methods for concrete.

Paris, N. and Chusid, M. 1997. Coloring systems.
http://www.daviscolors.com/literature/pdf/COLORING.PDF
This document briefly describes methods for coloring concrete products using powder, liquid, and granules, and pigments.

Steelscape. 2003. http://www.steelscape.com/aboutsteelscape/phototour.html.

Western Roofing. 2002. 2002 Market Survey. pp 62-63, July/August.

Western Roofing. 2003. Roofing Up in the West. pp 61-67, January/February.

Appendix: Factories Visited for This Study

We visited several California facilities that produce roofing materials of interest, including a fiberglass shingle factory, a roofing granule plant, a clay roofing tile factory, a concrete roofing tile factory, and a metal coil coating plant.

Fiberglass shingle plant

Elk Corporation, California Division
6200 Zerker Road, Shafter, CA 93263

This advanced, fully automated plant was built in 1993 and become operational in 1995. Elk buys and mixes 15 different colors of granules to produce roofing shingles in a variety of colors. At the Shafter plant, about 1200 tons of colored and 500 tons of uncolored granules are consumed each day in shingle production.

In addition to its main production line, the Shafter plant has a pilot line for limited production of special-order shingles. This pilot line may be useful when we wish to manufacture limited quantities of cool-colored roofing shingles for field testing.

The plant has a quality control laboratory to test the visual and mechanical properties of the shingles.

A virtual tour of the Elk plant is available online at <http://roofing.elkcorp.com/new_virtual_tours.cfm>.

Roofing granule plant

ISP Granule Products, Inc.
1900 Highway 104, Ione, CA 95640

ISP acquired this plant in 2002. The plant is located near rock quarries, and can make both single-coat and multi-coat products.

The plant has a quality control laboratory to test the visual and mechanical properties of the granules.

Metal coil coating

Steelscape, Inc.
11200 Arrow Route, Rancho Cucamonga, CA 91730

Steelscape has four major production lines: a *pickle line*, where hot-band metal is uncoiled, cleaned and trimmed to a desired width; a *cold mill line*, where the coil is thinned to a desired thickness; a *metallic coating line*, where the coils are recleaned, a layer of metallic coating (zinc or zinc/aluminum alloy) is applied, and the surface is treated for painting or for use as a bare metal; and a *paint line*, where primer and finish layers are applied.

The plant has a quality control laboratory to test the visual, mechanical, and chemical properties of the painted and unpainted products.

A virtual tour of the Steelscape plant is available online at <http://www.steelscape.com/aboutsteelscape/phototour.html>.

Clay roofing tile plant

Maruhachi Ceramics of America, Inc. (MCA)

1985 Sampson Avenue, Corona, CA 92879

MCA Tile is a modern clay tile manufacturing plant that supplies tiles to the western U.S. The facility and has five major operations: (1) mixing raw clay materials and preparing clay batt (dough); (2) extrusion molding of clay batt to form tiles; (3) air drying of raw tiles; (4) coloring tiles; and (5) kiln-firing colored tiles. MCA manufactures both glazed and unglazed colored tiles.

There is a quality control laboratory at the plant to test the visual and mechanical properties of the tiles. MCA has also a solar spectrum reflectometer (Devices & Services) to measure the solar reflectance of the tiles.

More information on MCA Tile products is available online at <http://www.mca-tile.com>.

Concrete roofing tile plant

MonierLifetile

342 Roth Road, Lathrop, CA 95330

Monier Lifetile is a major manufacturer of concrete roof tiles with 12 plants spread throughout the country. The facility at Lathrop operates in three shifts—and has five major operations: (1) mixing raw sand and filler materials, (2) mixing the concrete mixture and colorants, (3) molding of concrete to form tiles, (4) pre-cure coating of the tiles, (5) air drying of tiles, (6) and post cure-coating and coloring of tiles.

There is a quality control laboratory at the plant to test the visual and mechanical properties of the concrete tiles. The plant at the Lathrop did not have instruments to measure the solar reflectance of the tiles.

More information on MonierLifetile products is available at < **http://www.monierlifetile.com/**>.

Arnold Schwarzenegger
Governor

COOL-COLOR ROOFING MATERIAL ATTACHMENT 5: TASK 2.5.2 REPORTS - DESIGN INNOVATIVE METHODS FOR APPLICATION OF COOL COATINGS TO ROOFING MATERIALS

PIER FINAL PROJECT REPORT

Prepared For:
California Energy Commission
Public Interest Energy Research Program

Prepared By:
Lawrence Berkeley National Laboratory and Oak Ridge National Laboratory

ERNEST ORLANDO LAWRENCE
BERKELEY NATIONAL LABORATORY

June 2006
CEC-500-2006-067-AT5

Prepared By:
Lawrence Berkeley National Laboratory
Hashem Akbari
Berkeley, California
Contract No. 500-01-021

Oak Ridge National Laboratory
William Miller
Oak Ridge, Tennessee

Prepared For:
California Energy Commission
Public Interest Energy Research (PIER) Program

Chris Scruton
Contract Manager

Ann Peterson
Building End-Use Energy Efficiency Team Leader

Nancy Jenkins
PIER Energy Efficiency Research Office Manager

Martha Krebs, Ph.D.
Deputy Director
ENERGY RESEARCH AND DEVELOPMENT DIVISION

B. B. Blevins
Executive Director

DISCLAIMER

This report was prepared as the result of work sponsored by the California Energy Commission. It does not necessarily represent the views of the Energy Commission, its employees or the State of California. The Energy Commission, the State of California, its employees, contractors and subcontractors make no warrant, express or implied, and assume no legal liability for the information in this report; nor does any party represent that the uses of this information will not infringe upon privately owned rights. This report has not been approved or disapproved by the California Energy Commission nor has the California Energy Commission passed upon the accuracy or adequacy of the information in this report.

In press at *Solar Energy Materials & Solar Cells* (accepted August 2005)

Methods of Creating Solar-Reflective Nonwhite Surfaces and their Application to Residential Roofing Materials

Ronnen Levinson*, Lawrence Berkeley National Laboratory
1 Cyclotron Road, MS 90R2000, Berkeley, CA 94720
phone 510/486-7494; RMLevinson@LBL.gov

Paul Berdahl, Lawrence Berkeley National Laboratory
1 Cyclotron Road, MS 70R0108B, Berkeley, CA 94720
phone 510/486-5278; PHBerdahl@LBL.gov

Hashem Akbari, Lawrence Berkeley National Laboratory
1 Cyclotron Road, MS 90R2000, Berkeley, CA 94720
phone 510/486-4287; H_Akbari@LBL.gov

William Miller, Oak Ridge National Laboratory
PO Box 2008, MS6070, Oak Ridge, TN 37831
phone 865/574-2013; wml@ORNL.gov

Ingo Joedicke, ISP Mineral Products, Inc.
34 Charles St., Hagerstown, MD 21740
phone 301/733-4000; IJoedicke@ispcorp.com

Joseph Reilly, American Rooftile Coatings
250 Viking Avenue, Brea, CA 92821
phone 877/919-2727; jcreilly@adelphia.net

Yoshi Suzuki, MCA Clay Tile
1985 Sampson Avenue, Corona, CA 92879
phone 800/736-6221; YSuzuki@mca-tile.com

Michelle Vondran, Steelscape Inc.
1200 Arrow Rt; Rancho Cucamonga, CA 91730
phone 909/484-4623; michelle.vondran@steelscape.com

Abstract

We describe methods for creating solar-reflective nonwhite surfaces and their application to a wide variety of residential roofing materials, including metal, clay tile, concrete tile, wood, and asphalt shingle. Reflectance in the near-infrared (NIR) spectrum (0.7 – 2.5 μm) is maximized by

* Contact author.

coloring a topcoat with pigments that weakly absorb and (optionally) strongly backscatter NIR radiation and adding an NIR-reflective basecoat (e.g., titanium dioxide white) if both the topcoat and the substrate weakly reflect NIR radiation. Coated steel and glazed clay tile roofing products achieved NIR reflectances of up to 0.50 and 0.75, respectively, using only cool topcoats. Gray concrete tiles achieved NIR reflectances as high as 0.60 with coatings colored by NIR-scattering pigments. Such tiles could attain NIR reflectances of up to 0.85 by overlaying a white basecoat with a topcoat colored by NIR-transparent organic pigments. Granule-surfaced asphalt shingles achieved NIR reflectances as high as 0.45 when the granules were covered with a white basecoat and a cool color topcoat.

Introduction

A roof with high solar reflectance (ability to reflect sunlight) and high thermal emittance (ability to radiate heat) stays cool in the sun, reducing demand for cooling power in conditioned buildings and increasing occupant comfort in unconditioned buildings. Nonmetallic surfaces and most polymer-coated metal surfaces have high thermal emittance. Hence, a cool roofing surface may be described as a nonmetal or polymer-coated metal with high solar reflectance.

Visible light (0.4 – 0.7 μm) [1] contains 43% of the power in the air-mass 1.5 global solar irradiance spectrum (0.3 – 2.5 μm) typical of North-American ground-level insolation; the remainder arrives as near-infrared (NIR) radiation (0.7 – 2.5 μm, 52%) or ultraviolet (UV) radiation (0.3 – 0.4 μm, 5%) (ASTM 2003). A clean, smooth, and solar-opaque white surface strongly reflects both visible and NIR radiation, achieving a solar reflectance of about 0.85. This is the coolest type of roofing surface, and is ideal for low-slope roofs visible neither from ground level nor from taller buildings.

The solar reflectance of a roofing surface (especially that on a home) may be constrained by (a) desire for a nonwhite appearance, which limits visible reflectance; (b) NIR transparency of a thin and/or sparsely pigmented coating; and/or (c) curvature, which can cause light reflected from one face to be absorbed by another face. Nonwhite surfaces can be made as cool as possible by maximizing reflectance in the NIR spectrum, which does not affect color. Smoothing rough surfaces can increase reflectance at all wavelengths.

This study describes the engineering principles for creating a solar-reflective coated surface, and their application to a wide variety of residential roofing materials, including metal, clay tile, concrete tile, wood, and asphalt shingle.

Literature Review

Brady and Wake (1992) present the basic method for creating a coating with high NIR reflectance: color an otherwise transparent topcoat with pigments that weakly absorb and (optionally) strongly backscatter NIR radiation, adding an NIR-reflective basecoat (e.g., titanium

[1] The spectrum of visible light is typically specified as either 0.38 – 0.78 μm, or 0.40 – 0.70 μm. We choose the simpler range 0.40 to 0.70 μm because phototropic responses to light in the tails (0.38 – 0.40 μm and 0.70 – 0.78 μm) are low (ASTM 2001).

dioxide white) if both the topcoat and the substrate weakly reflect NIR radiation (Figure 1). This technique is reprised in whole or in part by U.S. patents and patent applications for creating generic NIR-reflectors (Genjima and Haruhiko 2002; Hugo 2002) and for creating NIR-reflective granules and/or granule-surfaced asphalt shingles (Gross and Graham 2005; Joedicke 2003; Ming et al. 2005a,b).

The authors reviewed current methods of manufacturing metal, clay tile, concrete tile, and asphalt shingle roofing materials in a earlier pair of articles (Akbari et al. 2005a,b).

Methodology

Maximizing solar reflectance of a colored surface

The fraction R of solar radiation incident at wavelengths between λ_0 and λ_1 that is reflected by a surface is the irradiance-weighted average of the surface's spectral reflectance r(λ). That is,

$$R_{\lambda_0 \to \lambda_1} = \left(\int_{\lambda_0}^{\lambda_1} r(\lambda)\, i(\lambda)\, d\lambda \right) \Big/ \int_{\lambda_0}^{\lambda_1} i(\lambda)\, d\lambda \,, \tag{1}$$

where i(λ) is the solar spectral irradiance (power per unit area per unit wavelength). Average reflectances of interest include solar reflectance *S* (0.3 – 2.5 μm), UV reflectance *U* (0.3 – 0.4 μm), visible reflectance *V* (0.4 – 0.7 μm), and NIR reflectance *N* (0.7 – 2.5 μm).

It follows from Eq. (1) that the solar reflectance of a surface may be computed as the weighted average of its UV, visible, and NIR reflectances. The aforementioned distribution of solar power (5% UV, 43% visible, and 52% NIR) yields

$$S = 0.05\ U + 0.43\ V + 0.52\ N \,. \tag{2}$$

Strong UV absorption by surface-layer pigments (e.g., titanium dioxide rutile white) or aggregate (e.g., granules) is usually desirable to prevent UV damage to lower components of the roofing product, such as the primer layer in a coated metal system or the asphalt in a granule-surfaced asphalt shingle. High UV reflectance would be even better, but is difficult to achieve with nonmetallic surfaces. Hence, we maximize solar reflectance by establishing high reflectances in the visible and NIR spectra that contain 95% of the incident solar radiation.

Since there is usually more than visible spectral reflectance curve (reflectance versus wavelength in the visible spectrum) that will yield a desired color under a particular illuminant, it is possible to maximize visible reflectance by designing to a color, rather than to a visible spectral reflectance curve. However, this may yield metamerism, in which the color of the coated surface matches that of another surface under one illuminant (e.g., early morning sun) but not another (e.g., noon sun). Maximizing only NIR reflectance avoids this problem.

Creating a coated surface with high NIR reflectance

When appearance and hence visible reflectance are constrained by design, a "cool" surface is one with high NIR reflectance. Consider a substrate (opaque structural material) with a uniformly

pigmented coating. The spectral (wavelength-specific) reflectance of this system depends on the spectral reflectance of the substrate, the thickness of the coating, and on the extent to which light passing through the coating is absorbed (converted to heat) and/or backscattered (reversed in direction) at that wavelength by suspended pigment particles. Reflectance is also influenced by the refractive index of the otherwise-clear coating vehicle. For example, the passage of normally incident collimated light from air (refractive index 1) to a smooth polymer or silicate coating (refractive index 1.5) induces a 4% "first surface" reflection.

Backscattering usually has less effect than does absorption on the reflectance of a substrate with a pigmented coating because some of the light backscattered toward the surface is later backscattered away from the surface. Consider a 25-μm-thick pigmented coating applied to a substrate of reflectance 0.50. Neglecting first surface effects, a nonabsorbing coating with a Kubelka-Munk backscattering coefficient of 5 mm^{-1} will increase system reflectance by 0.03; of 10 mm^{-1}, by 0.06; of 50 mm^{-1}, by 0.19; of 100 mm^{-1}, by 0.28; and of 200 mm^{-1}, by 0.36. A nonscattering coating with a Kubelka-Munk absorption coefficient of 0.5 mm^{-1} will decrease system reflectance by 0.01; of 1 mm^{-1}, by 0.02; of 5 mm^{-1}, by 0.11; of 10 mm^{-1}, by 0.20; and of 20 mm^{-1}, by 0.32 (Levinson et al. 2005a). That is, the reflectance decrease induced by absorption can be comparable to the reflectance increase caused by backscattering an order of magnitude larger. Hence, we classify the backscattering by a pigmented coating as "weak" if its backscattering coefficient is less than 10 mm^{-1}, "moderate" if between 10 and 100 mm^{-1}, or "strong" if greater than 100 mm^{-1}. Absorption by a pigmented coating is labeled "weak" if its absorption coefficient is less than 1 mm^{-1}, "moderate" if between 1 and 10 mm^{-1}, or "strong" if greater than 10 mm^{-1}.

A pigmented coating will typically be designed to exhibit strong absorption and/or strong backscattering in the visible spectrum to hide (and thereby color) the substrate. We describe a pigmented coating as "cool" if it has weak NIR absorption, and "hot" if it has strong NIR absorption.

Our survey of the solar spectral radiative properties of common colorants (Levinson et al. 2005b) determined that only a few pigments—e.g., titanium dioxide rutile white, nickel and chrome titanate yellows, aluminum flakes, and mica flakes coated with titanium dioxide—exhibit both strong NIR backscattering and weak NIR absorption when suspended in a vehicle of refractive index 1.5 (Table 1). Some of the nominally cool pigments, such as mixed-metal oxide selective blacks, exhibited both moderate-to-strong backscattering and moderate-to-strong absorption in the NIR. These do not meet our strict requirement (weak NIR absorption) for cool pigments, but may nonetheless be useful for cool applications so long as the coating's NIR reflectance (increased by backscattering, decreased by absorption) is sufficiently high. We note that the manufacturer-reported solar spectral reflectance of a thin (order 25 μm) pigmented coating on an aluminum substrate (N=0.90) tends to exaggerate the solar spectral reflectance that a similar coating will achieve when applied to a poor NIR reflector, such as a gray-cement concrete tile (N=0.15).

Most cool pigments surveyed exhibited weak-to-moderate backscattering in a vehicle of refractive index 1.5. A thin (but visibly hiding) coating colored with such pigments may be applied directly over a substrate of high NIR reflectance to produce a colored surface with high

NIR reflectance. Some bare roofing materials have NIR reflectances of 0.55 or higher[2], including wood, treated ZINCALUME® steel, treated hot-dipped galvanized (HDG) steel, and natural red clay tile (Table 2). The application of a cool coating to any of these substrates will yield a cool roofing surface with a solar reflectance of at least 0.30. System NIR reflectance will be further increased by NIR backscattering in the cool coating.

Other bare roofing materials, such as gray-cement concrete tiles and gray-rock-surfaced asphalt shingles, have NIR reflectances in the range of 0.10 to 0.15. These substrates with low NIR reflectance can achieve high NIR reflectance via the application of a 25- to 100-μm thick cool coating pigmented with a moderate-to-strong NIR backscatterer. For example, a smooth, flat, dark gray substrate (N=0.10) with a 25-μm thick polymer or silicate coating pigmented with titanium dioxide rutile white (backscattering coefficient about 200 mm^{-1} and absorption coefficient about 0.5 mm^{-1} at wavelength 1 μm) achieves an NIR reflectance of about 0.65. N can be increased to over 0.80 by making the coating at least 100-μm thick (Table 3; Figure 2). A visibly hiding cool topcoat may be applied over this layer to produce an arbitrarily colored system with high NIR reflectance.

Pigmented coatings with moderate-to-high NIR absorption and backscattering tend to yield moderate NIR reflectance over any surface, since the coating is usually NIR opaque. For example, the same gray substrate with a 25-μm thick coating pigmented with an iron oxide red (backscattering coefficient about 100 mm^{-1} and absorption coefficient about 10 mm^{-1} at wavelength 1 μm) achieves an NIR reflectance of about 0.40. Increasing the coating thickness to 100 μm (or greater) yields an NIR reflectance limited to about 0.50.

Creating a color-matched cool coated surface

A cool coated surface of a particular color may be created by using a mixture of cool pigments in the topcoat. The topcoat must exhibit strong visible absorption and/or backscattering to hide the substrate (and basecoat, if present). It is crucial to not to adjust the color with pigments that strongly absorb light across the entire solar spectrum, such as carbon black, lampblack, iron oxide black, or copper chromite black. The inclusion of any of these NIR-absorbing pigments in the topcoat or basecoat will tend to make the coated surface hot.

Effect of surface curvature on reflectance

Absorption of multiply reflected light can make the net absorptance of a curved, opaque surface exceed the "local" absorptance that would be observed were the surface flat. We plan to quantify in future research the effect of surface curvature on the reflectances of non-flat roofing surfaces, such as S-shaped clay tiles and granule-covered asphalt shingles.

[2] Most NIR reflectances presented in this paper are rounded to the nearest 0.05 to avoid unnecessary detail.

Application to Residential Roofing Materials

Metal

A manufacturer of pigmented polyvinylidene fluoride (PVDF) coatings (BASF Industrial Coatings; Colton, CA) provided (a) four types of steel substrate; (b) seven conventionally coated and seven nominally cool-coated ZINCALUME® steel coupons; (c) a free film of the polyurethane primer layer used between the metal and the color coat; and (d) 27 free films of PDVF coatings colored with different pigments, one pigment per film.

We measured the solar spectral reflectance of each sample from 0.3 to 2.5 μm at 5-nm intervals in accordance with ASTM Standard E903 (ASTM 1996), using a PerkinElmer Lambda 900 UV/visible/NIR spectrometer with a Labsphere 150-mm integrating sphere.

The bare and treated samples of HDG steel (steel coated with zinc) and ZINCALUME® steel (steel coated with an alloy of 55% aluminum, 43.4% zinc, and 1.6% silicon by mass [Steelscape 2005]) had NIR reflectances ranging from about 0.55 to 0.80 (Table 2; Figure 3). We hypothesize that bare ZINCALUME® steel (N=0.80) is appreciably more NIR-reflective than bare HDG steel (N=0.60) because aluminum is more NIR reflective than zinc. Metal treatment—a.k.a. "pretreatment," since it occurs prior to painting—includes cleaning, roughening, and the application of a "conversion layer" to help bind the primer layer to the metal. Treatment decreases the NIR reflectance of ZINCALUME® steel by about 0.10 (to N=0.70) and that of HDG steel by about 0.05 (to N=0.55) (Figure 4). This suggests that cool coatings on treated ZINCALUME® steel will tend to better reflect NIR radiation than will those on treated HDG steel (N up to 0.15 higher).

Conversion coatings are thin (typically less than 1-μm thick) and contain mostly transparent, non-absorbing inorganic phosphate compounds and polymers of refractive index 1.5 (Roland et al. 1998; Hamacher 1994; Mady and Seidel 1996). Mady and Seidel show Auger depth profiles indicating that two such coatings (one on galvanized steel, and the other on aluminum) are each less than 100 nm thick. One possible reason for the reflectance reduction induced by treatment is that the conversion coating may act as a non-absorbing anti-reflection layer (Born and Wolf, 1999). The reflectance of a coated metal is a function of the ratio of coating thickness to wavelength. Since this ratio approaches the same value (zero) as the film becomes very thin and/or the wavelength grows very large, we expect the effect of the coating on system reflectance to vanish at long wavelengths. We observe in Figure 4 that the reflectance reduction induced by treatment of the two steel samples generally diminishes with increasing wavelength.

The reflectance reduction might also stem from surface roughness induced by etching. For example, a polished aluminum surface, while mirror-like, actually has many submicron grooves produced by the polishing-powder particles, and is less reflective than a smooth aluminum film prepared by evaporation in ultrahigh vacuum (Smith et al. 1985).

The NIR absorptance of the 19-μm thick sample of primer (polyurethane pigmented with strontium chromate and titanium dioxide) was about 0.03. Since the primer thickness in the 14 coated ZINCALUME® samples was only about 5 μm, any NIR absorption in the coating systems (primer plus PDVF topcoat) occurred almost entirely in the pigmented PDVF layer.

The NIR reflectances of the seven conventionally coated ZINCALUME® coupons ranged from about 0.05 to 0.25, while those of the seven cool-coated ZINCALUME® coupons ranged from about 0.40 to 0.50 (Figure 5a). This indicates that the nominally cool coatings, while certainly less NIR-absorptive than their color-matched conventional coatings, increased system NIR absorptance by 0.20 to 0.30.

To better understand the nature of the NIR absorptance in the nominally cool pigmented PVDF coatings, and to identify any other pigmented coatings in the manufacturer's product line that might happen to be cool, we characterized the solar spectral radiative properties (reflectance, transmittance, absorptance, backscattering coefficient, and absorption coefficient) of the 27 single-pigment PVDF coatings (Levinson et al. 2005a,b). Many of the nominally cool inorganic pigments exhibited bands of absorption in the NIR induced by the presence of particular elements. For example, pigments that include cobalt were found to have absorption bands centered near wavelength 1.5 μm that cause a 20-μm thick pigmented PVDF coating to absorb about 15 to 40% of NIR radiation. The nominally cool inorganic black pigments containing chromium iron oxide exhibit a gradual, rather than sharp, reduction in absorption from the visible spectrum (where it is desirable) to the NIR spectrum (where it is not), causing a 20-μm thick coating to absorb 35 to 50% of NIR radiation.

A coating pigmented with an organic cool black (perylene black) was found to absorb about 95% of visible radiation, but only about 5% of NIR radiation. When applied in a coating over ZINCALUME® steel (N=0.70), this weakly scattering pigment can produce a black surface with an NIR reflectance of about 0.65 and a solar reflectance of about 0.35. These values well exceed the NIR (0.35) and solar (0.20) reflectances achieved by ZINCALUME® steel with a cool inorganic black PVDF coating.

The total thickness of the coating system (primer plus topcoat) on a metal substrate is typically limited by the need to keep the metal formable without breaking the coating. This tends to make it difficult to significantly increase the NIR reflectance of the system with a basecoat, since the basecoat would have to be quite thin. The additional pass required to apply a basecoat would also increase the cost and reduce the throughput of coil coating processes originally configured for only two layers (primer plus topcoat).

Clay tile

A manufacturer of clay tile roofing (MCA Clay Tile; Corona, CA) supplied 18 clay tile chips (small cut pieces of tile). The NIR reflectance of bare terracotta (natural red) tile was 0.55, while that of glazed tiles ranged from 0.25 (burnt sienna) to 0.75 (white buff). Only two tiles (glazed with burnt sienna and carbon, respectively) had NIR reflectances less than 0.40, and only four tiles had NIR reflectances less than 0.50 (Figure 5b).

Clay tile is typically composed of transparent crystalline particles (size order 10 μm) with anisotropic (directional) refractive indices. Light propagating through the material is scattered when light passes between two differently oriented crystallites that present different indices of refraction. Bare white tile has high reflectance across the NIR spectrum (N=0.85), while bare terracotta tile contains iron oxide (hematite) and therefore exhibits some NIR absorption (Figure 6).

The high NIR reflectance of bare clay tile and the ability to apply thick glazes aid the creation of NIR-reflective glazed clay tiles. It may be possible to modestly increase the NIR reflectance of a glazed tile system by applying and firing a basecoat glaze of white buff before applying and firing the topcoat color glaze. However, it is most important to avoid the use of carbon and other NIR-absorbing pigments in the glaze.

In principle, the solar spectral radiative properties of tile glazes can be characterized in a manner analogous to that used for polymer coatings—i.e., by measurement of the spectral reflectance and transmittance of a glaze applied to a clear substrate, such as quartz, that can withstand firing at 1000ºC. However, since the thermal expansion rate of quartz is several times smaller than that of a silicate glaze, a glaze fired on quartz (rather than on clay) will tend to crack. We continue to seek a substrate that is transparent to sunlight, can be fired at high temperature, and thermally expands at a rate comparable to that of the glaze.

We measured the solar spectral reflectances of 20 single-pigment glazes provided at various concentrations on white clay tiles by a manufacturer of tile glazes (Ferro Corporation Frit/Color Division; Los Angeles, CA). These data will be used in our future efforts to improve the NIR reflectances of glazed clay tiles.

Concrete tile

Lawrence Berkeley National Laboratory (LBNL) collaborated with a manufacturer of concrete-tile coatings (American Rooftile Coatings; Brea, CA) to design 25 prototype acrylic coatings on gray-cement concrete tile chips (N=0.15). We divide these into four sets: (A) six conventionally pigmented, 100-µm thick coatings applied directly to tile; (B) a matching set of six nominally cool-pigmented, 100-µm thick coatings also applied directly to tile; (C) the same six nominally cool-pigmented coatings applied at a thickness of 50 µm over a 100-µm thick acrylic white basecoat (N=0.85); and (D) seven "experimental, " 50- to 150-µm thick topcoats applied over the white basecoat.

The NIR reflectances of the six conventionally coated chips (set A) ranged from 0.05 to 0.55, while those of the nominally cool coatings applied directly to tile (set B) ranged from 0.35 to 0.60. The conventional blue and all the nominally cool coated chips except the black (N=0.35) had NIR reflectances exceeding 0.50 (Figure 5c).

The white basecoat used in set C increased the NIR reflectances of the six nominally cool coatings by less than 0.05, suggesting that the original line of cool topcoats was essentially NIR opaque. However, some of the seven experimental coatings in set D were NIR transparent, and show potential to achieve high NIR reflectance when applied over a white basecoat. For example, a 50-µm thick perylene black topcoat applied over the white basecoat achieved an NIR reflectance of 0.55. We note that a 25-µm thick perylene-black PVDF free film with an opaque white background (N=0.85) prepared in the course of our pigment characterization activities exhibited an NIR reflectance of 0.85. Hence, it is likely that the NIR reflectance of a gray concrete tile with a white basecoat and a perylene black topcoat can be increased from 0.55 to about 0.85 by reformulating the perylene black topcoat.

Wood shake

Light incident on plant material is backscattered as it passes alternately through cell walls of refractive index 1.4 and intracellular air of refractive index 1 (Knipling 1970). This gives plant material high reflectance at all wavelengths, except in those visible bands where lignin and/or chlorophyll absorb light, and in those NIR bands where water absorbs light (Figure 6). Moderately dark bare wood typically has a visible reflectance of 0.20, an NIR reflectance of about 0.70, and a solar reflectance of about 0.45. Hence, bare wood (and wood shakes treated with an NIR-transmissive fire retardant) can be both cool and dark.

A pigment manufacturer (Ferro Corporation Frit/Color Division; Los Angeles, CA) provided 16 samples of wood (N=0.70) with acrylic coatings colored by NIR-scattering inorganic pigments. Each of four pigments (two yellows, one green, and one black) was applied individually to wood in coatings with coverage rates of 150, 125, 100, and 75 ft^2/gal, corresponding to mean thicknesses of 270, 235, 405, and 545 μm, respectively. The thickest yellow coatings increased NIR reflectance to 0.80, while the thickest green coating increased NIR reflectance to 0.75. The thickest black coating reduced NIR reflectance to about 0.55.

When a manufacturer of fire retardants for wood products (Galchem Chemical Inc.; Payson, AZ) added metal-oxide pigments to a fire retardant solution that was pressure-applied to wood shakes, the pigments and some of the fire retardant precipitated out of the solution. Further work in this area is needed to investigate the compatibility of pigments with fire retardants.

Asphalt shingle

Over 97% of the surface of a typical asphalt-soaked fiberglass roofing shingle is covered with a layer of crushed rocks, or "granules," that are about 0.5 to 2 mm in diameter (Akbari et al. 2005a). Hence, the NIR reflectance of an asphalt shingle is determined by that of its granule layer. The NIR reflectance of the granule layer is in turn is limited by (a) the low NIR reflectance of typical gray-rock granules (about 0.10 – 0.15); (b) the low mean thickness of a typical granule coating (about 5 to 10 μm); and (c) weak to moderate NIR backscattering by most pigments.

The simplest way to increase the NIR reflectance of individual granules is to use a naturally white (or otherwise light-colored) aggregate. However, some light-colored rocks such as quartz transmit UV light, and would fail to shield the asphalt from UV radiation in sunlight. If a UV-opaque, NIR-reflective aggregate is not available, an NIR-reflective basecoat pigmented with a titanate white, a titanate yellow, titanium-dioxide coated mica flakes, or aluminum flakes can be applied to an NIR-absorbing aggregate to produce an NIR-reflective granule. For example, a 5-μm thick coating of refractive index 1.5 that is pigmented with titanium dioxide white can increase the NIR reflectance of a smooth, dark gray surface (N=0.10) to 0.35. A 10-μm thick coating will increase NIR reflectance to 0.50; a 25-μm thick coating, to 0.65 (Table 3; Figure 2). A cool, visibly hiding topcoat can provide color and, optionally, additional NIR backscattering.

The thickness of the coating applied to a granule is limited by the coating process, in which granules are preheated in a tumbler; transferred hot to a rotary mixer for application of the wet pigmented coating (pigments in sodium silicate, hydrated kaolin clay, and water); and then fired in a rotary kiln. If the volume ratio of liquid coating to granules is too high, the granules will

tend to fuse together. Multiple passes increase the total coating thickness, but reduce system throughput and increase cost.

LBNL collaborated with a manufacturer of roofing granules (ISP Mineral Products; Hagerstown, MD) to develop approximately 90 prototype shingle coupons (40 cm^2) and 10 prototype shingle boards (0.5 m^2). The shingles were surfaced with (a) bare rock granules; (b) granules with thin or thick white coatings; (c) granules with a thin aluminum coating; (d) granules with cool-pigment topcoats over bare rock, rock with an aluminum basecoat, rock with a thin white basecoat, or rock with a thick white basecoat; (e) salt-and-pepper blends of bright-white granules (rock with a thick white coating) and some of the granules described in (d); and (f) blends of granules of varying sizes.

The NIR reflectance of a shingle surface covered with bare granules was about 0.10. Adding a topcoat colored with a black, brown, green, or blue cool pigment increased NIR reflectance to 0.10 – 0.30. A thin (about 15 μm) aluminum basecoat (granulated surface N=0.35) increased NIR reflectances of the colored granules to about 0.25; a thin (about 15 μm) white basecoat (granulated surface N=0.25), to 0.25 – 0.35; and a thick (about 25 μm) white basecoat (granulated surface N=0.45), to 0.30 – 0.45 (Figure 5d).

Adding a basecoat tended to increase both visible and NIR reflectances unless the topcoat was opaque to visible light. For example, a coating colored with a cool inorganic brown pigment produced a shingle with V=0.15 and N=0.28 when applied over a bare granule. Adding a thin white basecoat yielded V=0.22 and N=0.35; adding a thick white basecoat yielded V=0.26 and N=0.43. The increases in the visible reflectance of this shingle were comparable to its increases in NIR reflectance—that is, the shingle became lighter in color. However, the shingle was not spectrally gray, in the sense that its NIR reflectance well exceeded its visible reflectance.

Figure 7 illustrates the development of cool black asphalt shingle colored with an inorganic cool black pigment. The granules on a conventional shingle are pigmented with carbon—a hot black colorant with strong absorption across the entire solar spectrum—and have no basecoat. In prototype 1, the carbon is replaced by a cool inorganic black, increasing NIR reflectance from 0.05 to 0.19 and solar reflectance from 0.04 to 0.12. Prototype 2 adds a thin white basecoat below the cool inorganic black topcoat, increasing N to 0.26 and S to 0.16. Prototype 3 replaces the thin white basecoat with a thick white basecoat, increasing N to 0.30 and S to 0.18. The top curve ("performance limit") corresponds to a smooth, 25-μm-thick PDVF film (N=0.43, S=0.25) pigmented with this cool black and backed by an opaque white (N=0.85). Roughness and limits to the thicknesses of the basecoat and topcoat are expected to make the reflectance of any granule-surfaced shingle pigmented with this cool inorganic black less than that achieved by the white-backed smooth film.

The prototype salt-and-pepper blends replaced thinly coated white granules with thickly coated white granules; some also replaced standard color granules with cool color granules. Unsurprisingly, using whiter granules increased both visible and NIR reflectances, resulting in a lighter-colored shingle with higher solar reflectance.

Blending various sizes of granules to make the granule layer smoother did not noticeably increase reflectance.

It may be possible to increase the NIR reflectance of granule-surfaced asphalt shingles by applying the pigmented coating to the shingle after bare granules have been pressed into the asphalt, then baking the granulated surface with radiant heat. This approach would coat only the exposed faces of the granules and might mitigate thickness limits associated with the tumble-coating/kiln-drying processes.

We note that several other roofing manufacturers, including CertainTeed (Valley Forge, PA), 3M Industrial Minerals (St. Paul, MN), and Elk Corporation (Dallas, TX) are engaged in analogous efforts to produce cool nonwhite asphalt shingles. The CertainTeed process applies cool pigments to both the roofing granules and the asphalt substrate (Shiao et al. 2005a,b), while the 3M process applies a solar-reflective basecoat and a cool colored topcoat to the granules (Gross and Graham 2005). The Elk process has not been disclosed.

Summary

Surfaces with high thermal emittance (i.e., nonmetals, and most polymer-coated metals) stay cool in the sun when they have high solar reflectance. When strong UV absorptance is required to shield a substrate and visible spectral reflectance is fixed to yield a particular color, maximizing NIR reflectance is equivalent to maximizing solar reflectance. The NIR reflectance of a substrate with a pigmented coating generally depends on NIR absorption and backscattering in the pigmented coating, and on the NIR reflectance of the uncoated substrate. Cool coatings should exhibit low NIR absorption. However, some NIR absorption may be acceptable in a coating that also exhibits strong NIR backscattering. A substrate with high NIR reflectance (e.g., metal, clay tile, or wood) can be colored with any cool coating, while a substrate with low NIR reflectance (such as gray-cement concrete tile or gray aggregate) requires significant NIR backscattering in either the cool topcoat or a cool basecoat.

Coated metal and glazed clay tile roofing products achieved NIR reflectances of up to 0.50 and 0.75, respectively, using only a cool topcoat. Topcoats colored with NIR-transparent organic pigments could yield coated metal systems with NIR reflectances as high as 0.65. Gray-cement concrete tiles have low NIR reflectance, but achieved NIR reflectances as high as 0.60 when thickly coated with NIR-scattering pigments. Coated gray-cement concrete tiles with NIR reflectances as high as 0.85 could be obtained by overlaying a titanium-dioxide basecoat with a topcoat colored by NIR-transparent organic pigments. Granule-surfaced asphalt shingles achieved NIR reflectances as high as 0.45 when a cool color topcoat was applied to granules with a thick white basecoat. Bare wood has an NIR reflectance of about 0.70; the application of certain pigments (e.g., metal oxides) may remove fire retardants from wood roofing products, and is not recommended.

Acknowledgements

This work was supported by the California Energy Commission (CEC) through its Public Interest Energy Research Program (PIER), by the Laboratory Directed Research and Development (LDRD) program at Lawrence Berkeley National Laboratory (LBNL), and by the Assistant Secretary for Renewable Energy under Contract No. DE-AC03-76SF00098. The authors wish to thank CEC Commissioner Arthur Rosenfeld and PIER managers Nancy Jenkins and Chris Scruton for their support and advice. Special thanks go also to Mark Levine, director

of the Environmental Energy Technologies Division at LBNL, and Stephen Wiel, former head of the Energy Analysis Department at LBNL, for their encouragement and support in the initiation of this project. We also wish to thank Jim Dunn of Ferro Corporation for supplying ceramic tiles with pigmented glazes and wood samples with pigmented coatings, and Anthony Galo of Galchem Chemical Inc. for testing the interaction of metal oxide pigments with fire retardants.

References

Akbari, H., R. Levinson and P. Berdahl. 2005a. Review of residential roofing materials, Part I: a review of methods for the manufacture of residential roofing materials. *Western Roofing Insulation and Siding*. Jan/Feb, 54-57.

Akbari, H., R. Levinson, and P. Berdahl. 2005b. Review of residential roofing materials, Part II: a review of methods for the manufacture of residential roofing materials. *Western Roofing Insulation and Siding*. Mar/Apr, 52-58.

ASTM. 1996. ASTM E 903-96: Standard test method for solar absorptance, reflectance, and transmittance of materials using integrating spheres. Annual Book of ASTM Standards, Vol. 12.02. Philadelphia, PA; American Society for Testing and Materials.

ASTM. 2001. ASTM E 308-01: Standard practice for computing the colors of objects by using the CIE system. Annual Book of ASTM Standards, Vol. 06.01. Philadelphia, PA; American Society for Testing and Materials.

ASTM. 2003. ASTM G 173-03: Standard tables for reference solar spectral irradiance at air mass 1.5: direct normal and hemispherical on 37º tilted surface. Annual Book of ASTM Standards, Vol. 14.04. Philadelphia, PA; American Society for Testing and Materials.

Born, M. and E. Wolf 1999, *Principles of Optics*, Sec. 14.4.2, A transparent film on an absorbing substrate, 7th ed., Cambridge University Press, Cambridge, UK.

Brady, R.F. Jr. and L.V. Wake. 1992. Principles and formulations for organic coatings with tailored infrared properties. *Progress in Organic Coatings* (20), 1-25.

Genjima, Y. and H. Mochizuki. 2002. Infrared radiation reflector and infrared radiation transmitting composition. U.S. Patent 6,366,397 B1, Apr. 2.

Gross, C.L. and J. Graham. 2005. Non-white construction surface. U.S. Patent Application Publication US2005/0074580 A1, Apr. 7.

Hamacher, M. 1994. Ecologically safe pretreatments of metal surfaces. Henkel-Referate 30/1994. Abridged version of a paper presented at the European Coating/s Show '93, Nuremberg, Germany, 16 March 1993. Online at http://www.henkel.com/int_henkel/hst/binarydata/en/pdf/ACFJIA0EBp0m.pdf .

Hugo, G. 2002. Coating with spectral selectivity. U.S. Patent Application Publication US2002/0188051 A1, Dec. 12.

Joedicke, I.B. 2003. Roofing granules with a decorative metallic appearance. U.S. Patent 6,548,145 B2, Apr. 15.

Knipling, E.B. 1970. Physical and physiological basis for the reflectance of visible and near-infrared radiation from vegetation. *Remote Sensing of Environment* (1), 155-159.

Levinson, R., P. Berdahl and H. Akbari. 2005a. Solar spectral optical properties of pigments—Part I: model for deriving scattering and absorption coefficients from transmittance and reflectance measurements. *Solar Energy Materials & Solar Cells* (in press).

Levinson, R., P. Berdahl and H. Akbari. 2005b. Solar spectral optical properties of pigments—Part II: survey of common colorants. *Solar Energy Materials & Solar Cells* (in press).

Mady, R. and R. Seidel. 1996. Chromium-free pretreatment processes for coil coating. Henkel-Referate 32/1996. Abridged version of an article in JOT 1995/7 (1995) 46. Online at http://www.henkel.com/int_henkel/hst/binarydata/en/pdf/32_147-151e.pdf .

Roland, W., W. Lorenz and W. Wichelhaus. 1998. Chemical pretreatment in coil coating. Henkel-Referate 34/1998. Abridged version of a paper presented at the ECCA General Meeting in Cascais, Portugal, 25-28 May 1997. Online at http://www.henkel.com/int_henkel/hst/binarydata/en/pdf/34_152-155e.pdf .

Shiao, M.L., G.F. Jacobs, H.M. Kalkanoglu and K.C. Hong. 2005a. Mineral-surfaced roofing shingles with increased solar heat reflectance, and process for producing same. U.S. Patent Application Publication US2005/0072110, Apr. 7.

Shiao, M.L., H.M. Kalkanoglu and K.C. Hong. 2005b. Colored roofing granules with increased solar heat reflectance, solar heat-reflective shingles, and process for producing same. U.S. Patent Application Publication US2005/0072114 A1, Apr. 7.

Smith, D.Y., E. Shiles and M. Inokuti. 1985. The optical properties of metallic aluminum. In *Handbook of Optical Constants of Solids,* Academic Press, New York, pp. 369-406.

Steelscape. 2005. ZINCALUME®: the ideal steel. Online at http://www.steelscape.com/products/brochures/ZincalumeBrochure.pdf .

Table 1. Classification of cool pigments (those with low NIR absorption) according to strength of NIR backscattering in a vehicle of refractive index 1.5.

Strong NIR backscattering (coefficient > 100 mm^{-1} at 1 μm)	Moderate NIR backscattering (coefficient 10 - 100 mm^{-1} at 1 μm)	Weak NIR backscattering (coefficient < 10 mm^{-1} at 1 μm)
chrome titanate yellow	cadmium orange, yellow	cobalt aluminate blue
chromium iron oxide black*	cobalt chromite blue, green*	diarylide yellow
nickel titanate yellow	cobalt titanate green	dioxazine purple
titanium dioxide (rutile) on mica flakes (interference colors)	iron titanium brown spinel	Hansa yellow
	modified chromium oxide green	perylene black
titanium dioxide rutile white	monastral red	phthalocyanine blue, green
	red, brown iron oxides	quinacridone red
		ultramarine blue

***** These pigments exhibit moderate absorption in the NIR and hence are not strictly cool, but have sufficient NIR backscattering to be useful in cool coatings.

Table 2. Typical NIR reflectances (rounded to nearest 0.05) of various uncoated substrates.

Uncoated substrate	NIR reflectance
fresh asphalt	0.05
layer of gray-rock granules	0.10
gray-cement concrete tile	0.15
treated* hot-dipped galvanized steel	0.55
bare hot-dipped galvanized steel	0.60
natural red clay tile	0.70
wood	0.70
treated* ZINCALUME® steel	0.70
bare ZINCALUME® steel	0.80
white ceramic tile	0.85
aluminum foil	0.90

*cleaned and coated with a very thin (about 1 μm) “conversion layer” that helps the primer layer adhere to the metal

Table 3. NIR reflectances (rounded to nearest 0.05) of white[*] and aluminum-flake[**] coatings on a smooth, dark gray substrate (N=0.10).

Coating	NIR reflectance of coated substrate
none	0.10
white, 5 μm	0.35
white, 10 μm	0.50
white, 25 μm	0.65
white, 50 μm	0.75
aluminum flake, 25 μm	0.80
white, 100 μm	0.80
white, 200 μm	0.85

[*] Polyvinylidene fluoride (PVDF) pigmented with titanium dioxide rutile (mean particle size 0.25 μm) at 15% volume concentration. Comparison of measured and computed values of the NIR reflectance of coatings pigmented with titanium dioxide white suggests that these computed values may be slightly (as much as 0.05) too low.

[**] Silicone pigmented with aluminum flakes. It may be possible to achieve a comparable NIR reflectance with a thinner coating because the aluminum flake coating was NIR opaque at a thickness of about 25 μm.

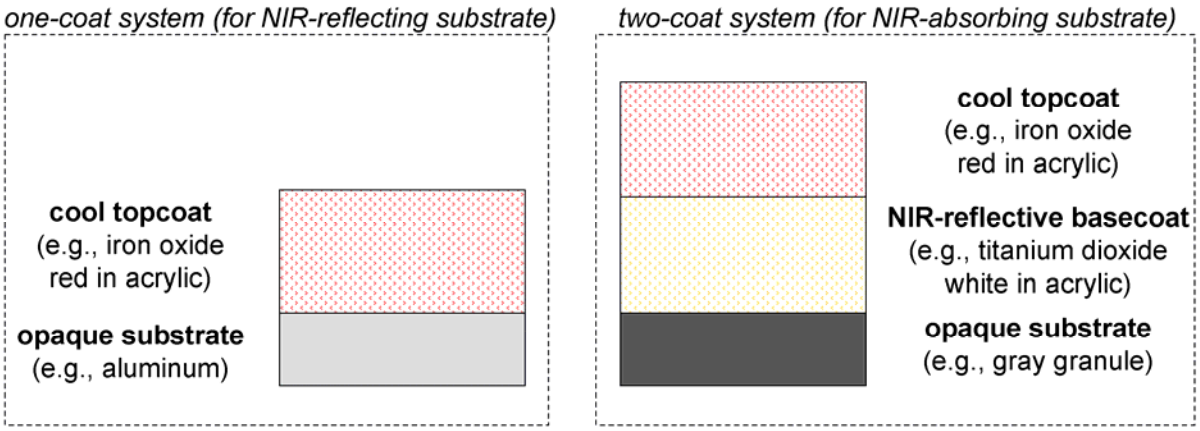

Figure 1. Schematics of one-coat (substrate + topcoat) and two-coat (substrate + basecoat + topcoat) systems. The one-coat system can also be applied over an NIR-absorbing substrate if the topcoat has at least moderate NIR backscattering and is sufficiently thick.

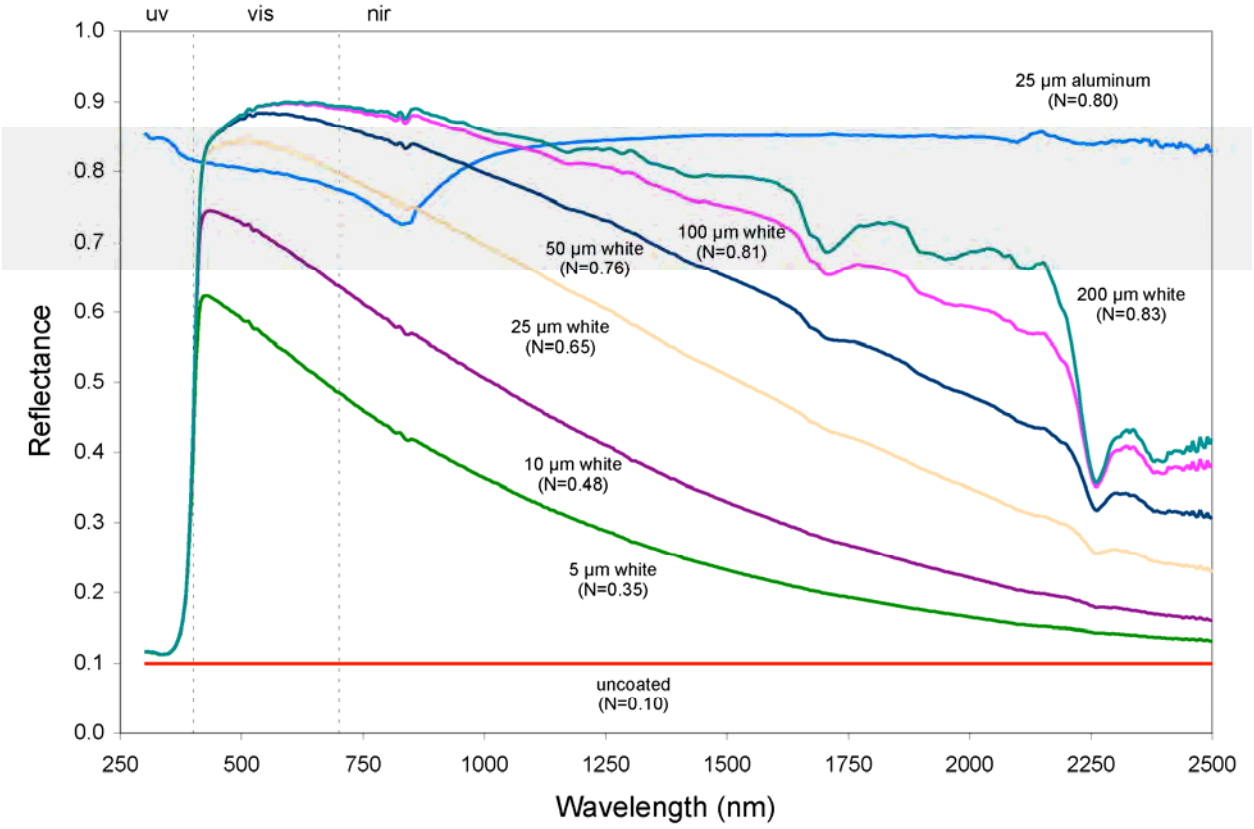

Figure 2. Solar spectral reflectances and NIR reflectances (*N*) of a smooth, dark gray substrate (reflectance 0.10 at all solar wavelengths) with (a) 5, 10, 25, 50, 100, and 200-µm thick PVDF coatings pigmented with titanium dioxide rutile white at 15% pigment volume concentration; and (b) a 25-µm thick silicone coating pigmented with aluminum flakes (pigment volume concentration unknown). The spectral reflectances of the white-coated surfaces were estimated from absorption and backscattering coefficients computed by Levinson et al. (2005a), while that of the aluminum-flake coated surface was measured.

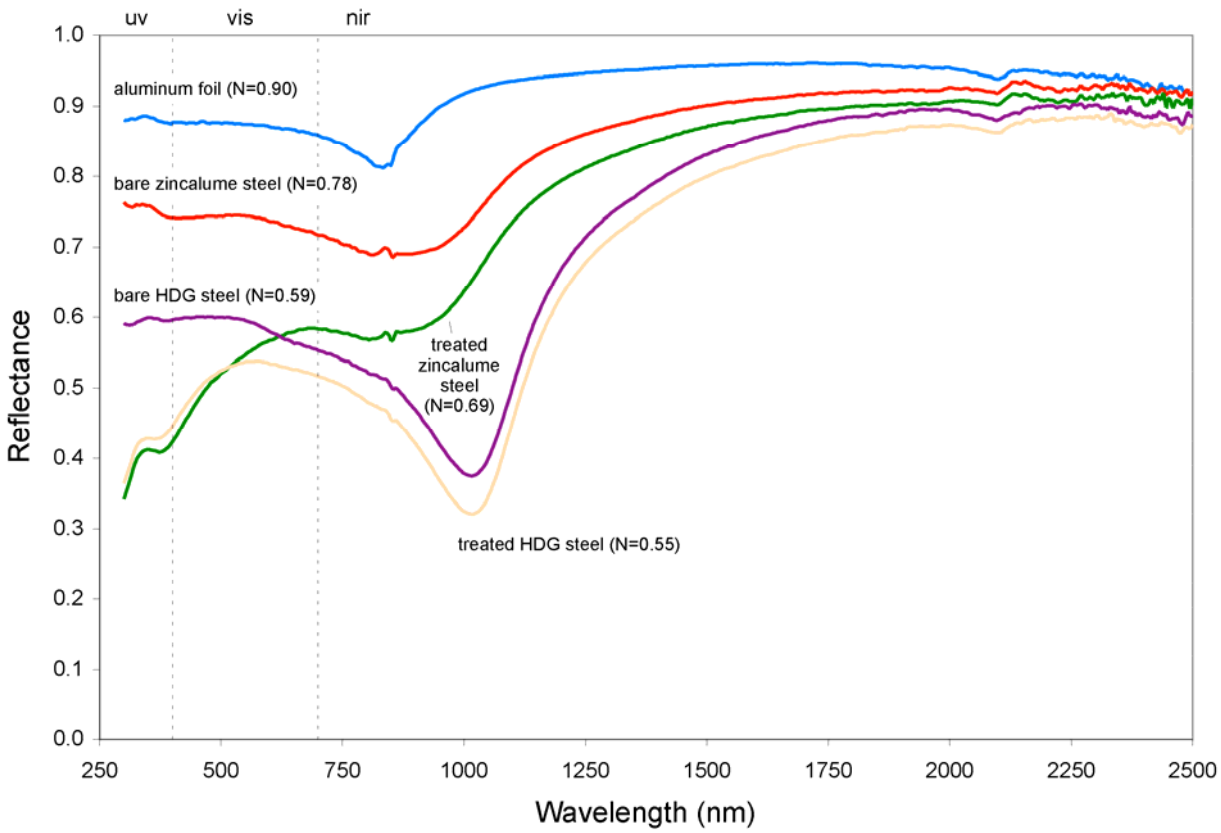

Figure 3. Solar spectral reflectances and NIR reflectances (*N*) of five uncoated, metallic substrates: aluminum foil, bare and treated ZINCALUME® steels, and bare and treated hot-dipped galvanized (HDG) steels.

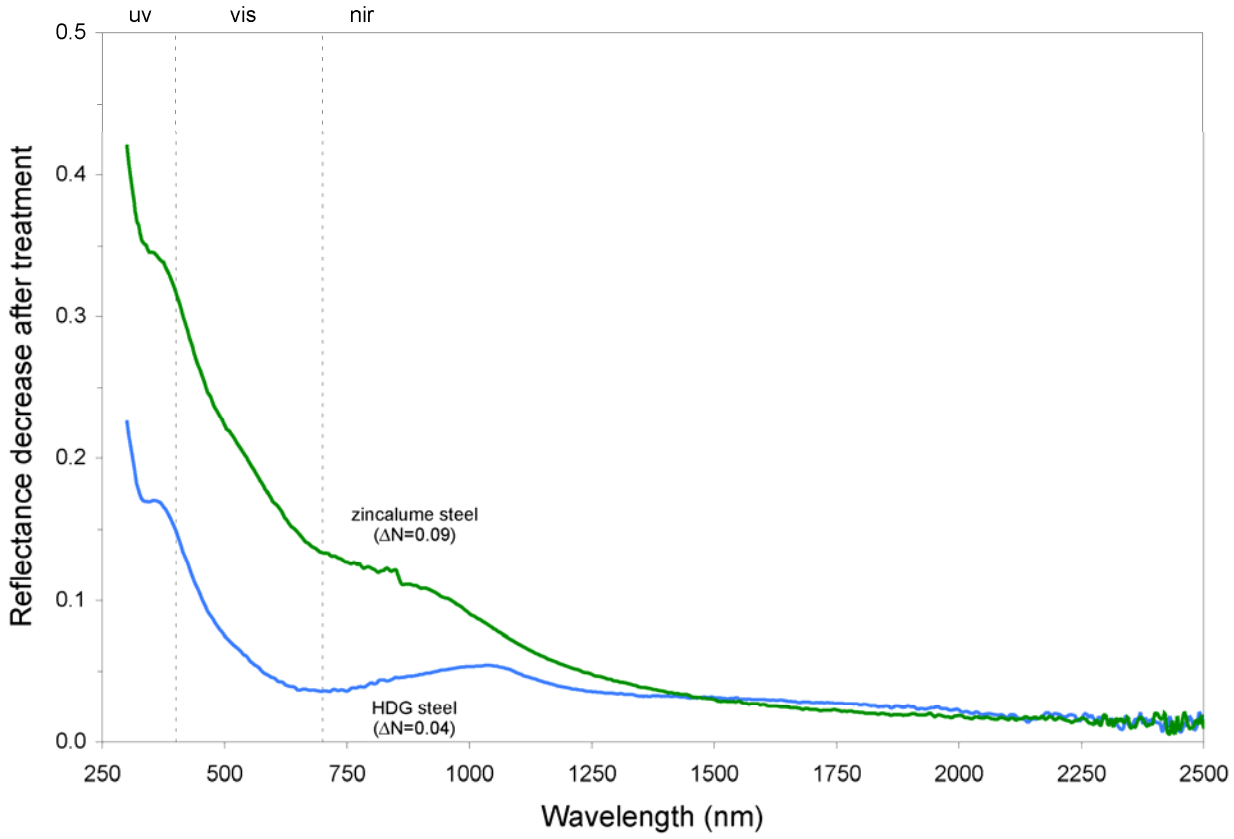

Figure 4. Decreases in spectral reflectance induced by treating ZINCALUME® and hot-dipped galvanized (HDG) steels. Shown also is the decrease ΔN in NIR reflectance.

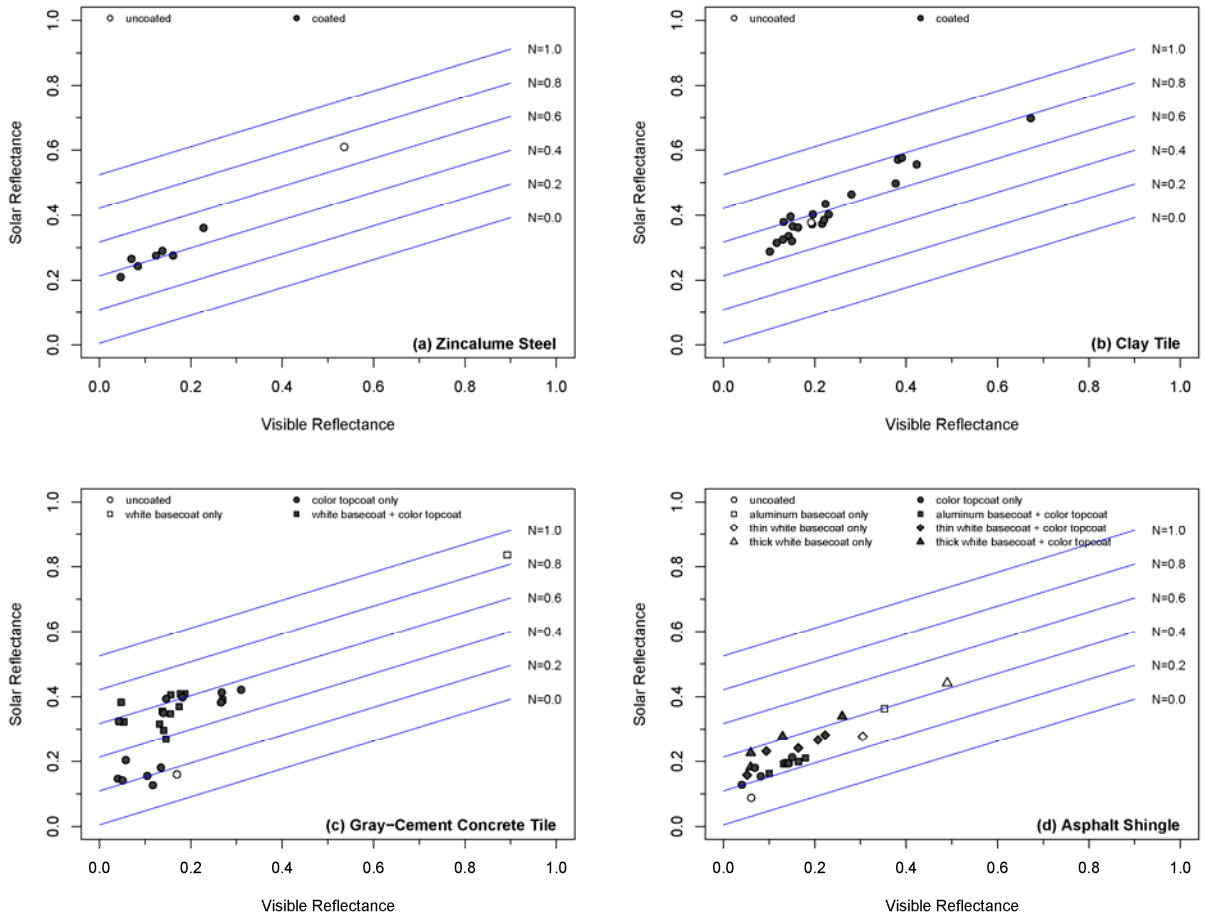

Figure 5. Solar vs. visible reflectances of uncoated and cool-coated samples of (a) treated ZINCALUME® steel, (b) clay tile, (c) gray-cement concrete tile, and (d) granule-surfaced asphalt shingles. Lines of constant NIR-reflectance *N* assume a UV reflectance of 0.1.

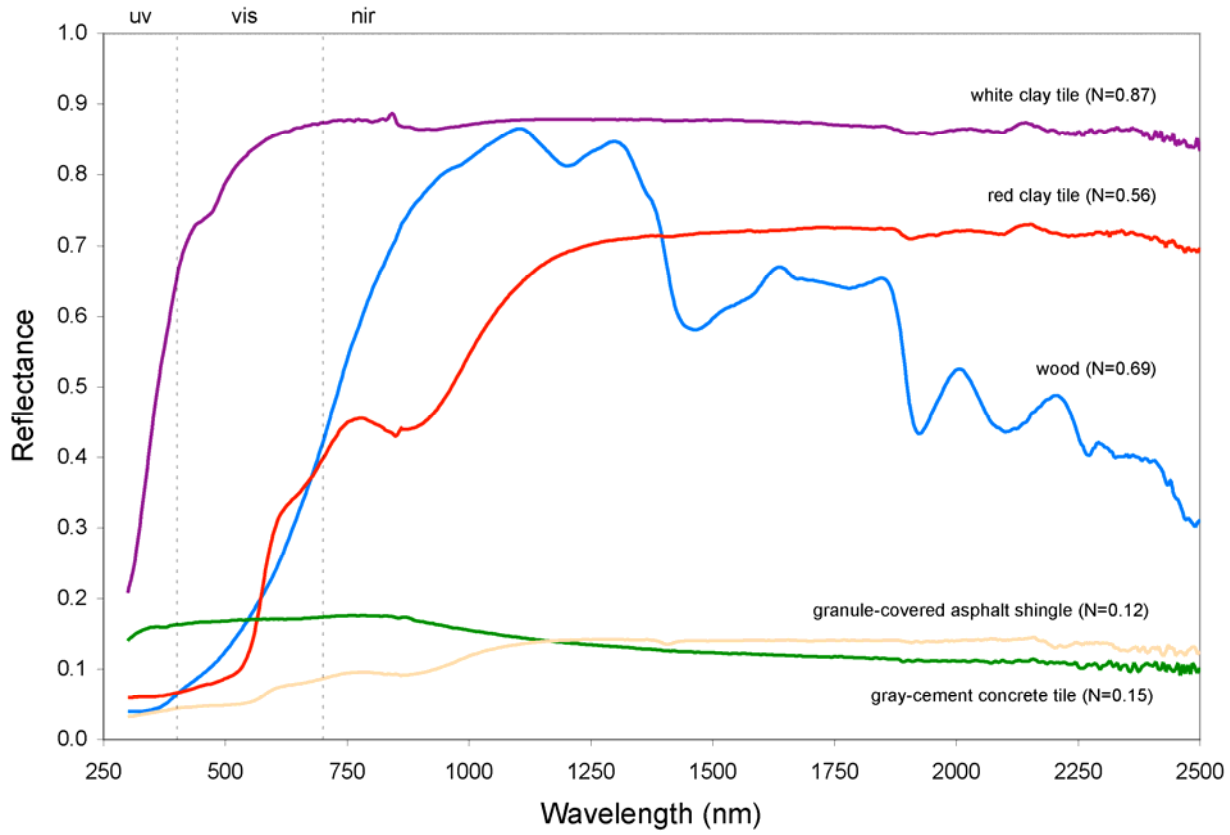

Figure 6. Solar spectral reflectances and NIR reflectances (*N*) of five uncoated, nonmetallic substrates: white clay tile, red clay tile, wood, granule-covered asphalt shingle, and gray-cement concrete tile.

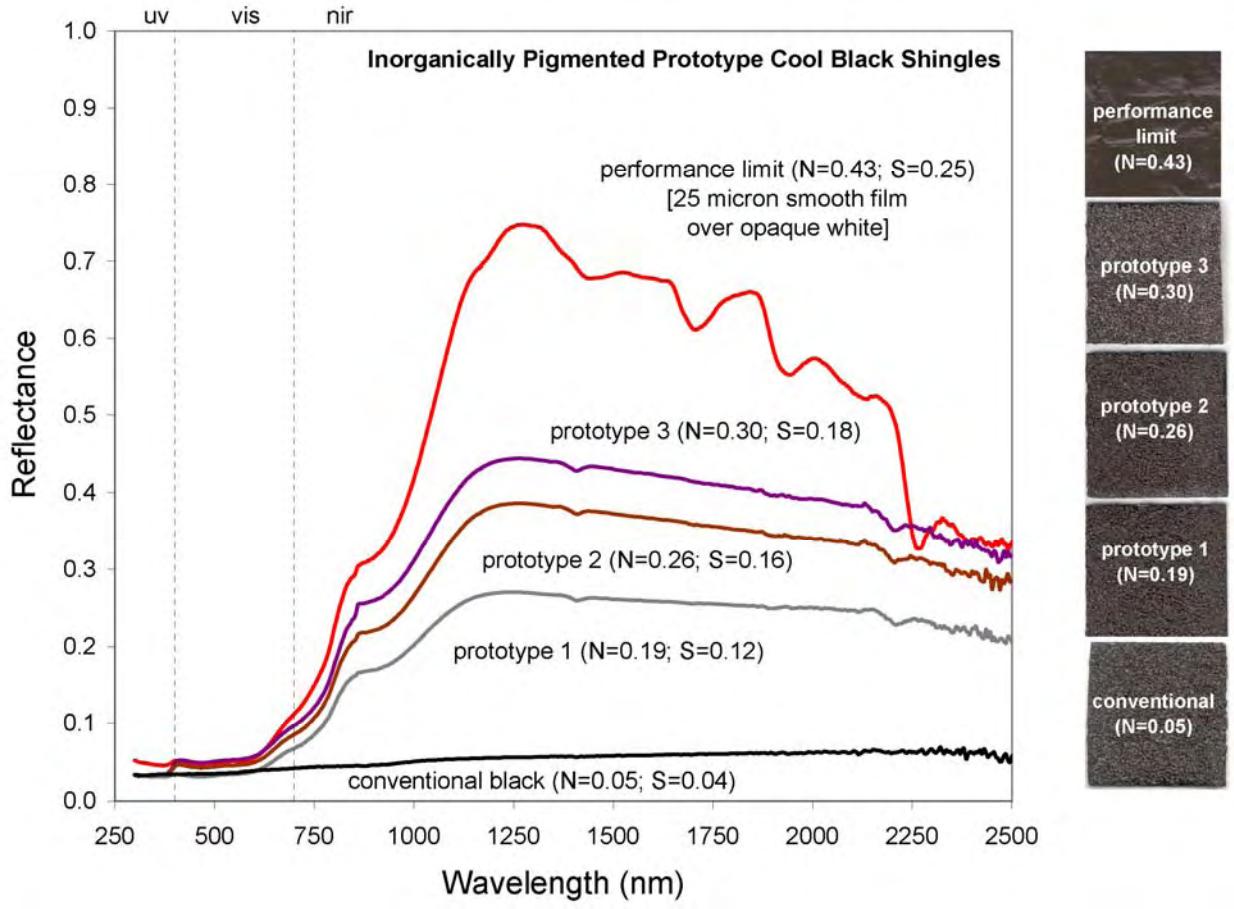

Figure 7. Development of an inorganically pigmented cool black asphalt shingle (*N*=near-infrared reflectance; *S*=solar reflectance).

Arnold Schwarzenegger
Governor

COOL-COLOR ROOFING MATERIAL ATTACHMENT 6: TASK 2.5.3 REPORTS - ACCELERATED WEATHERING TESTING

PIER FINAL PROJECT REPORT

Prepared For:
California Energy Commission
Public Interest Energy Research Program

Prepared By:
Lawrence Berkeley National Laboratory and Oak Ridge National Laboratory

ERNEST ORLANDO LAWRENCE
BERKELEY NATIONAL LABORATORY

June 2006
CEC-500-2006-067-AT6

Prepared By:
Lawrence Berkeley National Laboratory
Hashem Akbari
Berkeley, California
Contract No. 500-01-021

Oak Ridge National Laboratory
William Miller
Oak Ridge, Tennessee

Prepared For:
California Energy Commission
Public Interest Energy Research (PIER) Program

Chris Scruton
Contract Manager

Ann Peterson
Building End-Use Energy Efficiency Team Leader

Nancy Jenkins
PIER Energy Efficiency Research Office Manager

Martha Krebs, Ph.D.
Deputy Director
ENERGY RESEARCH AND DEVELOPMENT DIVISION

B. B. Blevins
Executive Director

DISCLAIMER

This report was prepared as the result of work sponsored by the California Energy Commission. It does not necessarily represent the views of the Energy Commission, its employees or the State of California. The Energy Commission, the State of California, its employees, contractors and subcontractors make no warrant, express or implied, and assume no legal liability for the information in this report; nor does any party represent that the uses of this information will not infringe upon privately owned rights. This report has not been approved or disapproved by the California Energy Commission nor has the California Energy Commission passed upon the accuracy or adequacy of the information in this report.

Accelerated Weathering of Roofing Materials Having New Solar-Reflective Cool Colors

William Miller and Andre Desjarlais
Oak Ridge National Laboratory
PO Box 2008
Oak Ridge, TN 37831

Hashem Akbari and Paul Berdahl
Lawrence Berkeley National Laboratory
Berkeley, CA 94720

and

Brian Schwer and Dave Ziemnik
The Shepherd Color Company
PO Box 20084539 Dues Drive
Cincinnati, Ohio 45246

Jeff Jacobs
3M Company
3M Center, Building 209-1W-14
St. Paul, MN 55144-1000

ABSTRACT

Accelerated weathering tests are used to obtain a "quick look" at material durability at a much faster rate than outdoor weathering. Since the primary stresses on roofing are solar ultraviolet radiation, moisture, and heat, these elements are incorporated into industry standard tests. We describe some of these standard tests, and outline their strengths and weaknesses. New solar-reflective cool roofing materials are emerging, that are non-white or even dark in color. These materials have enhanced reflectance in the near-infrared portion of the solar spectrum when compared with older standard materials. Accelerated testing of the new materials suggests that the durability will be similar to conventional materials in maintenance of color, gloss, and solar reflectance. The new solar-reflective cool roofing materials showed low variability in fade resistance and mechanical properties.

INTRODUCTION

Cool nonwhite pigmented coatings with high reflectance in the near infrared (NIR) spectrum have been enthusiastically adopted by premium coil coaters and metal roofing manufacturers. BASF Industrial Coatings launched "Superl SP II™ ULTRA-Cool®," a line of cool colored silicone modified polyester coatings. Coil-coater Steelscape recently introduced Spectrascape MBM, a cool Kynar coating for the metal building industry. A third industrial partner, Custom-Bilt, switched the majority of its metal roofing products from conventional pigmented colors to infrared reflective cool color pigments. In just a few years, infrared reflective pigments have helped premium coil coated metal roofing double sales and capture 8 percent of the roofing market (F. W. Dodge 2002). However other roof products like clay and concrete tile and especially asphalt shingle products can also exploit the use of infrared reflective pigments termed from here on as cool roof color materials (CRCMs). 3M Company recently introduced 3M™ Cool Roofing Granules for use in the shingle industry which allow asphalt shingle manufacturers to offer products which take advantage of infrared reflective cool color pigments. Our goal is to demonstrate that CRCMs offer a wide range of durable colors that can provide the larger asphalt shingle market and also the clay and concrete tile markets with a solution to the dual roofing demands for the aesthetics of darker colors and the energy efficiency of white. However,

durability performance of shingle and tile products must be demonstrated for homebuilders to adopt tile and asphalt shingle roof products.

Roof products typically undergo degradation from oxidation reactions that result from any combination of the following processes: melt degradation, thermal degradation, and photo-degradation. Of these processes, photo-degradation due to ultraviolet (UV) light and/or xenon-arc exposure is of primary importance for roofing systems. Our objective for this task is to conduct accelerated fluorescent and xenon-arc testing and report on the photo-stability of painted metal, clay and concrete tile and asphalt shingle products.

Fade resistance of roof products with CRCMs

The color of a roof product must remain fade resistant or the product will not sell. Industry judges fade resistance by measuring the spectral reflectance and transmittance of a painted or coated surface and converting the measures to color-scale values based on the procedures in ASTM E308-02 (ASTM 2001). The color-scale values for CRCMs (L_{CRCM}, a_{CRCM} and b_{CRCM}) are compared to standard colors ($L_{Standard}$, $a_{Standard}$ and $b_{Standard}$) and the color differences (ΔL, Δa, and Δb), which represent the luminance of color, are calculated from:

- $\Delta L = L_{CRCM} - L_{Standard}$ where $\Delta L > 0$ is lighter and a $\Delta L < 0$ is darker;
- $\Delta a = a_{CRCM} - a_{Standard}$, where $\Delta a > 0$ is redder and a $\Delta a < 0$ is greener; and
- $\Delta b = b_{CRCM} - b_{Standard}$, where $\Delta b > 0$ is more yellow and $\Delta b < 0$ is bluer.

Manufacturers of premium coil coated metal use a total color difference (ΔE) to specify the permissible color change between a test specimen and a known standard. The total color difference value is described in ASTM D 2244-02 (ASTM 2002), and is a method adopted by the paint industry to numerically identify variability in color over periods of time; it is calculated by the formula:

$$\Delta E = \left[(\Delta L)^2 + (\Delta a)^2 + (\Delta b)^2 \right]^{1/2} \qquad (1)$$

Typically, premium coil-coated metal roofing is warranted for 20 years or more to have a ΔE of 5 units or less for that period. ΔE color changes of 1 unit or less are almost indistinguishable from the original color, and depending on the hue of color, ΔE of 5 or less is considered very good.

Gloss retention of roof products with CRCMs

Gloss is a measure of the percent of specular reflectance resulting from incident visible light. Specular reflectance makes a surface appear shiny or mirror-like as opposed to having a matte type finish which results from diffuse reflectance. The higher the gloss the greater is the percentage of incident light that is reflected specularly. However, it is important to note that gloss is strictly an aesthetic characteristic indicating the form in which visible light is being reflected; it is not a measure of solar reflectance. One of the aesthetic features of asphalt shingles is that they provide primarily diffuse reflectance which eliminates the glare that tends to make any color roof appear white from certain angles in direct sunlight.

A roofing product must also retain its luster or the product will not sell. Industry judges gloss retention by measuring the initial gloss of a painted surface as compared to the same painted surface weathered at a selected time interval at a selected angle.

$$\Delta Gloss = G_{initial} - G_{weathered}$$

where $\Delta G > 0$ is a loss of luster
and a $\Delta G < 0$ is a gain of luster

Ultraviolet radiation can degrade the binder and pigment of a coating system causing it to look "washed out" or "chalked" and lose its gloss. While all types of paint systems will lose some degree of gloss over time, the lower quality systems generally lose their luster much earlier than superior grades. The binder in top quality acrylic latex paint systems will be more resistant to UV radiation than paint systems containing oil or alkyds which absorb radiation causing their binder to break down.

INDUSTRY EXPOSURE DATA —PVDF WITH CRCMS

BASF shared their data for accelerated fluorescent exposure testing of their new line of cool-colored coatings. Masstones[1] with and without CRCMs and of the same color were applied to polyvinylidene fluoride (PVDF) galvanized steel samples and exposed to UV irradiance to observe differences in fading and gloss retention. Samples were exposed to upwards of 10,000 hours of fluorescent UV light using the ASTM G154-04 protocol with a UVB-313 lamp that emits significantly more irradiance below 300 nm than does sunlight. The sample color, hours of exposure and the value of the total color change and the present reduction in gloss are shown in Figure 1. The results show that pigment stability and discoloration resistance of the cool pigments are as good as those commercially available (Fig. 1). The fade resistance of the cool-colored blue and yellow masstones is much improved over the respective standard color. Blue, especially a blue tint, has historically been known to fade; however, the cool colored masstone blue shows excellent fade resistance. The retention of gloss from the original color is also shown to verify performance of the larger-sized cool pigments as compared to standard production pigments. A higher gloss paint is often preferred because it provides a homeowner greater wear and therefore reduced maintenance costs. The gloss retention findings are very important because, the larger the particle, the greater is its effect on film smoothness, which affects the scattering of light. The larger the size of a pigment particle the greater is the drop in gloss of a paint finish; however, the cool pigments actually show a slightly higher retention in gloss as compared to their counterparts and they therefore again perform as well as if not better than present production-painted metals.

Painted metals were also exposed to three years of natural sunlight in Florida following ASTM G7-97 (ASTM 1997). Test data showed excellent light fastness of the CRCM masstones[1] exposed in the field. For the CRCM black masstone the fade resistance is much improved over the standard color. Tints (especially blue) have historically been known to fade; however, 50/50 tints of the CRCMs field tested in Florida also showed excellent fade resistance (Table 1). The highest total color change was observed for the CRCM black tint, which is still indistinguishable from the original color. As example, a standard black had a $\Delta E \sim 3.5$ as compared to the CRCM black which had only a 1.51 ΔE.

[1] Masstones represents the full color of the pigment while tints are blends of colors.

Table 1. Color Difference for 50/50 tints of the CRCMs exposed to natural sunlight for three years in Florida. (ΔE based on International Commission on Illumination (CIE L*A*B) Index)

	Total color difference (ΔE)				
Years	Green	Yellow	Brown	Black	Marine Blue
1	0.55	0.21	0.47	0.19	0.46
2	0.42	0.25	0.70	0.67	0.50
3	0.53	0.14	0.99	1.51	0.76

The xenon-arc accelerated weathering tests were previously reported by Miller et al. (2002) and showed that after 5000 hours of xenon-arc exposure all PVDF metal painted with CRCMs clustered together with $\Delta E<1.5$, which is considered a very good result. The Florida exposure data, fluorescent light exposure data by BASF and the xenon-arc results are promising and show that premium coil-coated metals with CRCMs fade less than do the conventional pigmented paints of the same color whose performance is well characterized. Therefore it is easily understood why CRCMs have been so successfully introduced into the market by the metal roof industry. Painted metal has an excellent opportunity to exploit the use of cool pigments; however, further study is needed to understand the light absorbing processes which may lead researchers to develop even better coating processes with even higher fade resistance for premium coil-coated metals.

EXPOSURE TESTING OF TILE, METAL AND ASPHALT SHINGLE WITH CRCMS

Shepherd Color Company and 3M Company provided time in their weatherometers for evaluating the effect of ultraviolet light exposure and xenon-arc exposure on the fading of various CRCM roof products. Clay tiles were provided by Maruhachi Ceramics of America; no conventional pigmented clay colors were available for test comparisons. Painted PVDF metal samples with and without CRCMs were provided by BASF and Steelscape. Shingles were provided by U.S. companies preferring that their products' identity remain confidential; however, the data for shingles with and without CRCMs is provided in coded format.

Sample Preparation and Weatherometer Protocol

The asphalt shingle samples were cut to a size of 0.07m x 0.07 m (2.75" x 2.75") from each of the different regions of the shingle. The metal and tile samples were 3½ in by 3½ in and were used as received. The samples were placed in sample holders for mounting in a xenon arc and a fluorescent UV light weatherometer and subjected for 5000 hours of accelerated weathering. The weatherometers maintain the temperature, moisture, and light. 3M conducted the xenon-arc accelerated weathering in accordance with ASTM G-155 using cycle 1 as described in G-155 in Table X3.1 Common Exposure Conditions. The Shepherd Color Company conducted the fluorescent accelerated weathering in accordance with ASTM G154-04 using cycle 4 as described in G 154 in Table X2.1 Common Exposure Conditions. A UVB-340 lamp was used for simulating direct solar UV radiation; it has no UV output below 300 nm, which is the cutoff wavelength for terrestrial sunlight.

Samples were measured for color, solar reflectance and gloss initially and after every 1000 hours of exposure. These data are provided in Appendix A.

Solar Reflectance (SR) Instruments

Solar reflectance was measured using a Device and Services Solar Spectrum Reflectometer Model SSR-ER. The instrument uses a tungsten halogen lamp to diffusely illuminate the sample and measures the radiation reflected at a 20 degree angle from normal with four filtered detectors covering the solar spectrum. The relative response of the detectors to the light source is designed to approximate the solar spectrum. The four signals are weighted in appropriate proportions to yield the air-mass 1.5 near-normal-hemispherical solar reflectance, or more simply "solar reflectance."

Color Measurements

3M measured color using a Hunterlab Labscan XE model LSXE colorimeter set up with D65 illuminant and a 10 degree observer. The CIELab scale was used and results recorded as L*, a*, and b* luminance measures. Shepherd Color Company used a MacBeth Color Eye (CE 7000) setup for CIELab scale readings with D65 illuminant and a 10 degree observer.

Gloss Meter

Shepherd and 3M both used BYK Gardner Micro-TRI-gloss 4520 instruments for gloss measurements. Gloss was measured at a 60 degree angle for all samples and the reflected light was measured photo-electrically using the BYK 4520 reflectometer. The instrument conforms to the standards DIN 67530, ISO 2813 and ASTM D 523.

FLUORESCENT UV LIGHT EXPOSURE RESULTS

The solar reflectance, total color change, and gloss of clay and concrete tile and painted metal coupons were measured after 1000 hour increments of fluorescent UV exposure (Fig. 2, 3 and 4 respectively). The red clay and dark brown clay (ironwood) and the terracotta concrete and chocolate brown concrete all showed marginal drops in solar reflectance over the 5000 hour duration of UV exposure (Fig. 2). The chocolate brown and terracotta concrete tiles have CRCM coatings provided by American Rooftile Coatings. The solar reflectances of these samples are much higher than those of their conventional pigmented counterparts having the same color, and their reflectance is just as stable as those of their counterparts after the 5000 hours of UV exposure. Also the total color change of the concrete tiles with CRCMs shows them as fade resistant as their conventional counterparts (Fig. 3). A noticeable drop in gloss (indicative of a loss of luster) is however observed after 3000 hours of UV exposure for the concrete coupons with CRCMs (Fig. 4). Results for the painted metal coupons are very similar to the independent testing conducted by BASF (Fig. 1). The total color change measured at 2000 hours for the brick red metal with CRCMs (Fig. 3) appears spurious because later measures at 3000, 4000 etc hours follow trends observed in the standard brick red coupon (Fig. 3).

Asphalt Shingle Exposure Results

The asphalt shingles with CRCMs had an initial solar reflectance of about 0.26 and a thermal emittance of 0.90. Their counterparts with conventional color pigments had initial solar reflectance values ranging from 0.06 to 0.11 (see Appendix A) and the thermal emittance was 0.89. The fluorescent light exposures did not adversely affect the solar reflectance of the shingles with CRCMs and they maintained their reflectance just as well as the standard production shingles (Fig.5). The CRCM shingles coded A and E had a total color change (ΔE) less than 1.5

after the 5000 hours of UV exposure (Fig. 6). In contrast, their conventionally pigmented counterparts had ΔE's that were 50% higher for Code A and 100% higher for Code E. The ΔE for the Code C shingle with CRCMs exceeded ΔE of 2 after 1000 hours, then it dropped below 1.0 after 5000 hours. Reasons for the behavior are unknown; however, overall the data clearly shows that the shingles with CRCMs when subjected to direct solar UV radiation perform just as well as standard products accepted on the open market. The CRCM asphalt shingles do not lose solar reflectance, and they remain fade resistant.

A granule manufacturer forwarded some data for roofing granules applied on an asphalt-coated panel and exposed to natural weathering at a south Florida exposure site. Table 2 lists the pigment, months of exposure, the initial granule color and the total color change after exposure. The results again show the cool pigments perform as well as or even outperform the conventional pigments. The ΔE for the Ferro pigments is roughly half that measured for the standard production pigments, which indicates that the cool colored coatings have improved retention of color over the 2 to 4 years of natural exposure testing.

Table 2. Granules exposed to natural sunlight in south Florida and painted with and without cool colored coatings.

Pigment	Exposure (months)	Initial Color of Asphalt-Coated Panel			Color Change after Exposure ΔE
		L*	a*	b*	
Carbon Black	18	22.0	0.4	-0.2	**2.4**
Black Iron Oxide	42.5	22.9	2.7	3.6	**1.6**
Ferro V-778	58	26.0	2.1	2.6	**0.8**
Ferro O-1765B	23.5	22.7	1.5	0.7	**0.9**

XENON-ARC EXPOSURE RESULTS

The solar reflectance, total color change and gloss of clay and concrete tile and painted metal coupons were measured after 1000 hour increments of xenon-arc exposure (Fig. 7, 8 and 9 respectively). There is no noticeable loss in solar reflectance in the painted metal and concrete samples. The BASF Ultra-Cool samples held their own against the painted metals with conventionally-pigmented colors (Fig. 7). The terracotta and chocolate brown coatings applied by American Rooftile Coating also maintained their high level of solar reflectance (Fig. 7). An exception occurs with the red clay and ironwood (brown) clay tiles. Here solar reflectance is observed to drop but then begins to increase as exposure continues past about 3000 hours (Fig. 7). The change in total color with time for the red clay tile does not seem consistent and may be spurious. It shows ΔE values exceeding 5.0[2]. The painted metal yielded the lowest total color changes (ΔE < 2.0 after 5000 hours). Total color changes of the concrete tile with CRCM coatings was not very different from the standard pigmented tile (Fig., 8) and the CRCM tile showed comparable fade resistance under xenon-arc exposure. Conventional and CRCM painted metal samples both showed similar losses in gloss (loss of luster). Gloss of the coated concrete

[2] Typically, coil-coated metal roofing panels are warranted for 20 years or more and specify ΔE of 5 units or less for that period.

coupons is all well-behaved (Fig. 9). The terracotta and chocolate brown coatings applied by American Rooftile Coating maintained their luster.

Asphalt Shingle Exposure Results

Xenon-arc testing of the CRCM asphalt shingles showed slight increases in solar reflectance through 3000 hours of exposure (Fig. 10). Solar reflectance increased from 0.27 to 0.29 before leveling at about 0.28 for the Code A shingle with CRCMs. The standard shingles are also showing slight increases in solar reflectance as exposure progresses. Some oxidation of hydrocarbons in the shingles is evidently occurring and is possibly affecting surface reflectance in a positive manner. Total color change of the shingles with CRCMs are very comparable to their standard production counterparts and again show the CRCM shingles perform just as well (Fig. 11). The total color change is less than 3.0 after 5000 hours of exposure, which can be visually distinguished yet is still considered good.

CONCLUSIONS

Xenon-arc and fluorescent light exposures were conducted to judge the effectiveness of CRCMs in painted metal, clay tile, concrete tile and asphalt shingle roof products. Test results were very promising and showed that new cool pigmented concrete, clay, painted metal and asphalt shingle roofs maintain their solar reflectance as well as their standard production counterparts. Total color change is reduced or at least similar and the new cool pigmented products have similar if not improved fade resistance and gloss retention.

The asphalt shingles when heated will undergo chemical changes and changes in visible and solar reflectance. Elevated temperature, for example as provided by solar absorption in dark materials, can accelerate deleterious chemical reactions and hasten the diffusion of low molecular weight components. Since photo-degradation is a complex process that depends upon material type, including additives and impurities, it is difficult to generalize about how photo-degradation should be altered by increased temperatures. Intuitively, one would expect that higher temperatures would assist photo-degradation. However, photo-degradation of the asphalt shingle products was not observed for these accelerated exposure test results. Solar reflectance of the asphalt shingles with and without CRCMs showed slight increases in solar reflectance. Note that increases were larger for the cool pigmented shingles. Total color change among cool pigmented and conventional pigmented shingles was very similar indicating once again that the new infrared reflective products are ready for market.

ACKNOWLEDGEMENTS

The Shepherd Color Company and 3 M Company conducted the weatherometer testing. The efforts of Brian Schwer, Dave Ziemnik of Shepherd Color Company and Jeff Jacobs of 3M Company are greatly appreciated. Hashem Akbari of LBNL, A. Desjarlais of ORNL, S. Wiel of Lawrence Berkeley National Laboratory and C. Scruton of the California Energy Commision provided technical and management advice. J. Reilly, R. Sypowics, American Rooftile Coatings provided concrete tile samples with and without high reflectance coatings; M. Vondran, Steelscape, R. Schichili, BASF and consultant to Custom-Bilt Metals provided the BASF metal samples; Y. Suzuki, MCA Clay Tile provided the clay tile samples; K. Loye, D. Swiler, Ferro Corp. and I. Joedicke, ISP Minerals Corp. provided the natural exposure data of granules. The advice of Lou Hahn of Elk, M. Desouto, K. Srinivasan of GAF Materials Corp., Chris Gross of

3M Company, I. Joedicke, ISP Minerals Corp. and M. Shiao, L. Terrenzio of CertainTeed Corp. also helped with the accelerated testing of asphalt shingle products.

REFERENCES

American Society for Testing and Materials (ASTM). 2002. Designation D2244-02: Standard Practice for Calculation of Color Tolerances and Color Differences from Instrumentally Measured Color Coordinates. West Conshohocken, Pa.: American Society for Testing and Materials.

———. 1997b. Designation G7-97: Standard Practice for Atmospheric Environmental Exposure Testing of Nonmetallic Materials. West Conshohocken, Pa.: American Society for Testing and Materials.

———.2001. Designation E 308-02: Standard Practice for Computing the Colors of Objects by using the CIE System. West Conshohocken, Pa.: American Society for Testing and Materials.

———.. 2002. Designation G 154-04: Standard Practice for Operating Fluorescent Light Apparatus for UV Exposure of Nonmetallic Materials. West Conshohocken, Pa.: American Society for Testing and Materials.

———. 1997b. Designation G7-97: Standard Practice for Atmospheric Environmental Exposure Testing of Nonmetallic Materials. West Conshohocken, Pa.: American Society for Testing and Materials.

———. 2000. Designation G155-00a: Standard Practice for Arc Operating Xenon Arc Light Apparatus for Exposure on Non-metallic Materials. West Conshohocken, Pa.: American Society for Testing and Materials.

F.W. Dodge. 2002. Construction Outlook Forecast, F.W. Dodge Markert Analysis Group, 24 Hartwell Avenue, Lexington, MA 02421. Telephone 800-591-4462, FAX 781-860-6884, URL:www.FWDodge.com.

Miller, W.A., Loye, K. T., Desjarlais, A. O., and Blonski, R.P. 2002. "Cool Color Roofs with Complex Inorganic Color Pigments," in ACEEE Summer Study on Energy Efficiency in Buildings, proceedings of American Council for an Energy Efficient Economy, Asilomar Conference Center in Pacific Grove, CA., Aug. 2002.

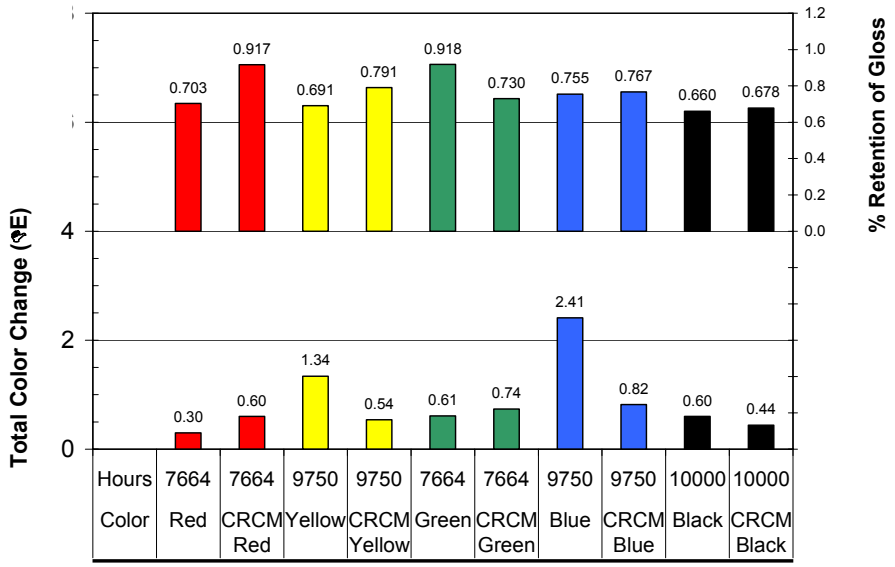

Figure 1. The total color change and the retention of gloss for masstones tested under fluorescent UV light using ASTM G154 protocol. (Data courtesy of BASF).

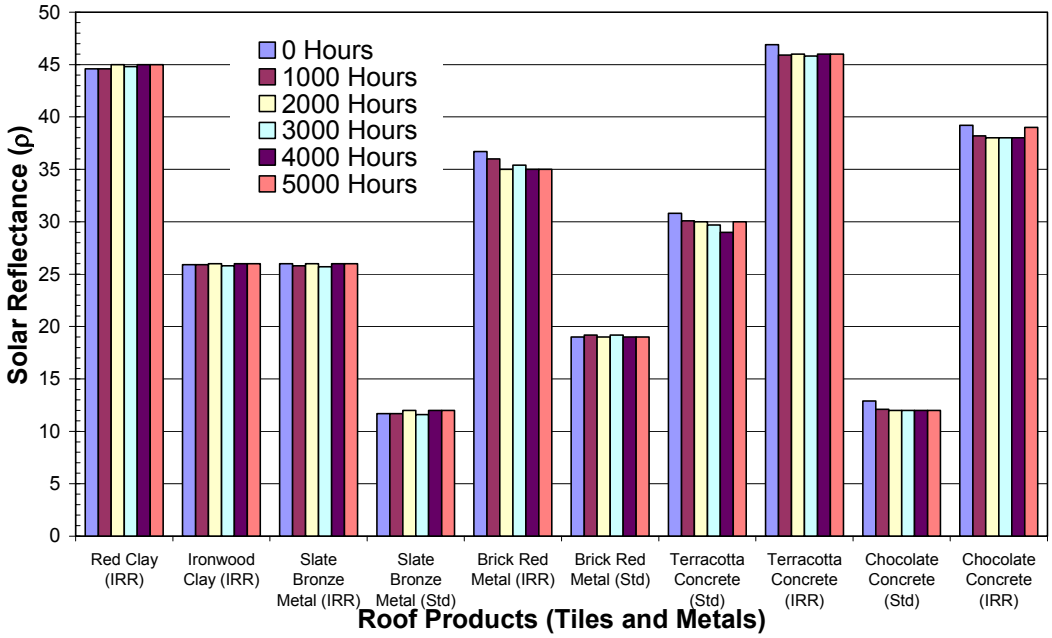

Figure 2. The solar reflectance of tiles and painted metals under fluorescent UV light using ASTM G154-04 protocol. (Data by Shepherd Color Company).

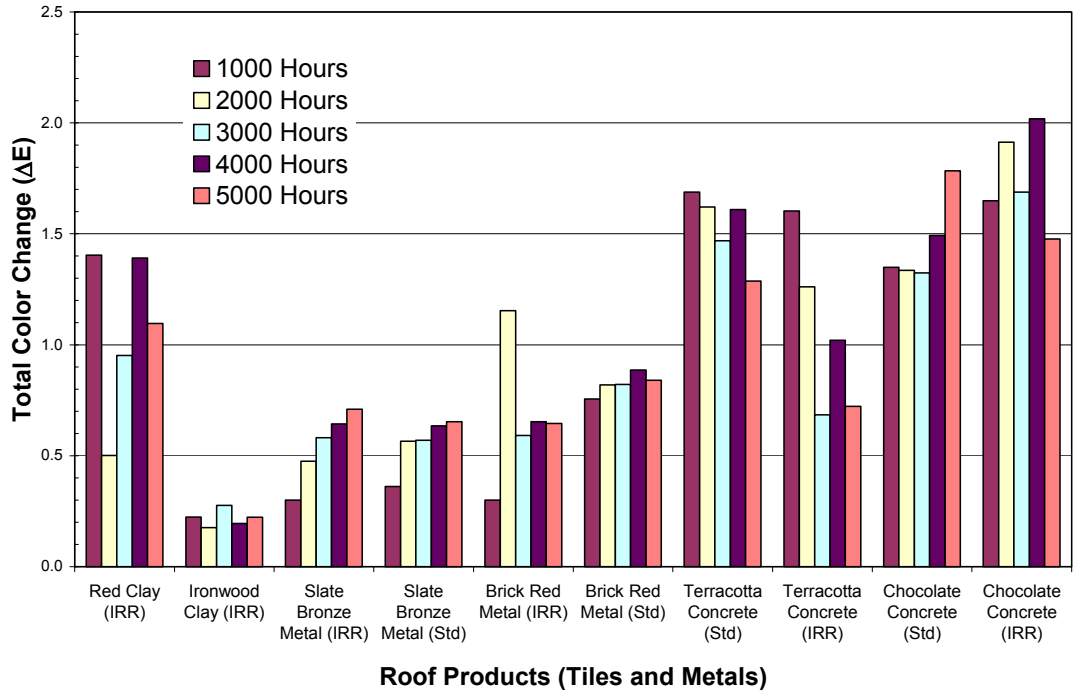

Figure 3. The total color change of tiles and painted metals under fluorescent UV light using ASTM G154-04 protocol. (Data by Shepherd Color Company).

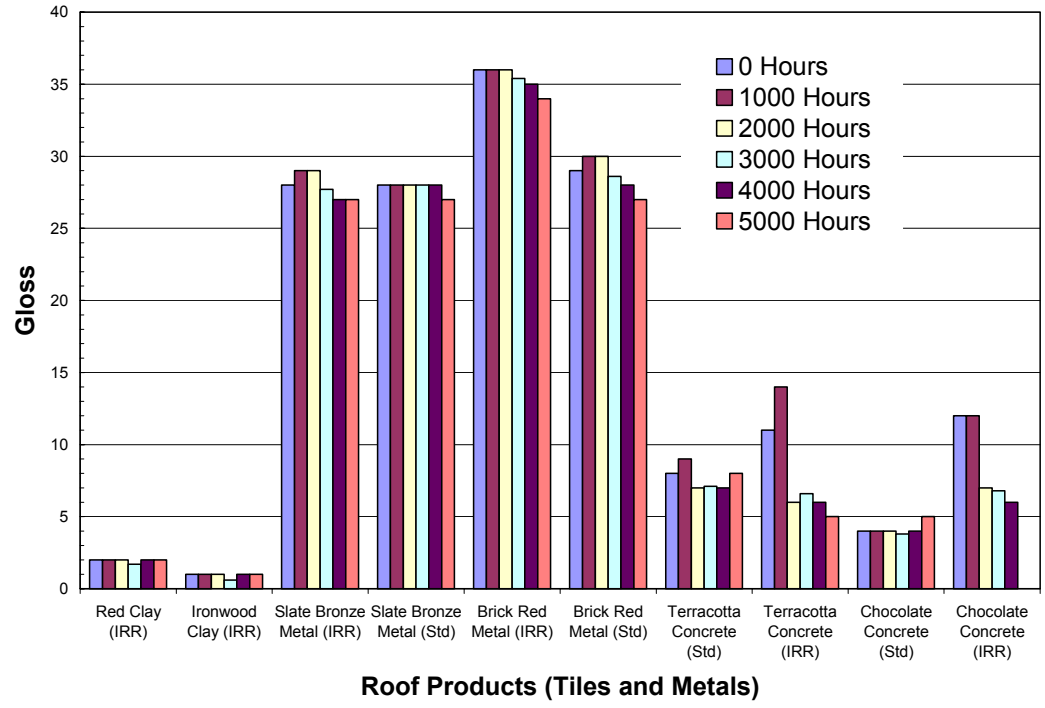

Figure 4. The gloss of tiles and painted metals under fluorescent UV light using ASTM G154-04 protocol. (Data by Shepherd Color Company).

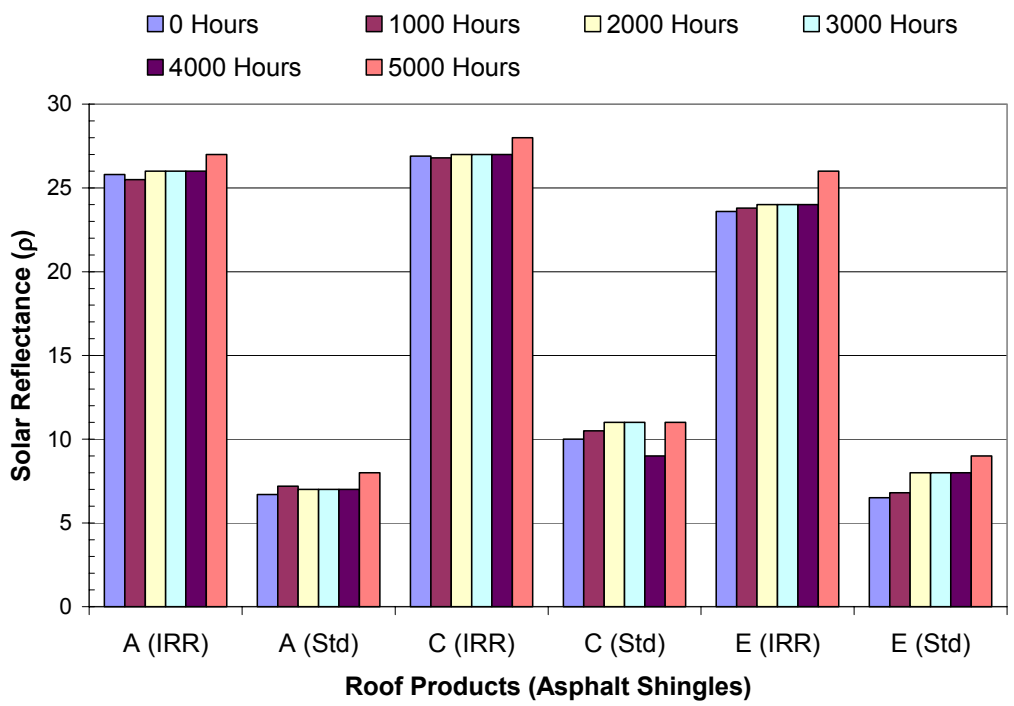

Figure 5. The solar reflectance of asphalt shingles under fluorescent UV light using ASTM G154-04 protocol. (Data by Shepherd Color Company).

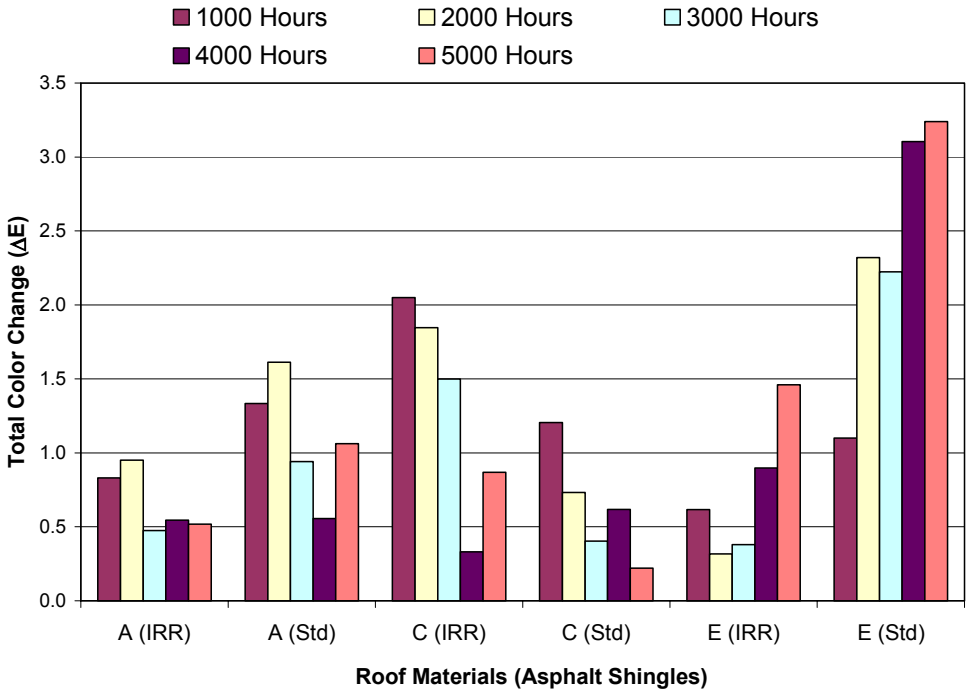

Figure 6. The total color change of asphalt shingles under fluorescent UV light using ASTM G154-04 protocol. (Data by Shepherd Color Company).

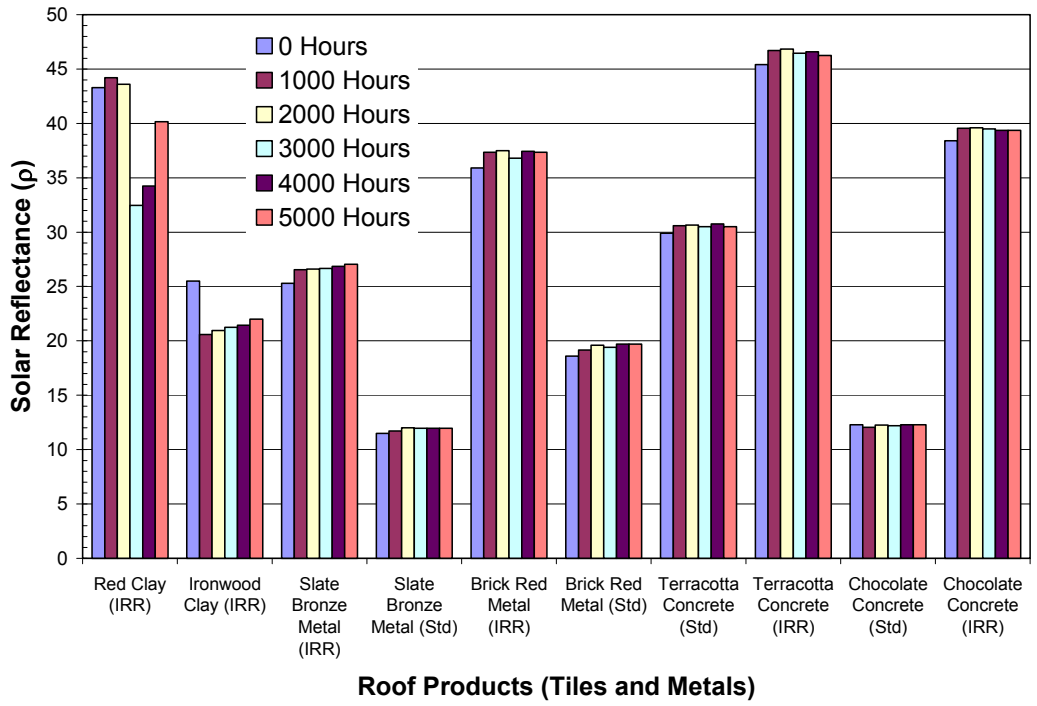

Figure 7. The solar reflectance of tiles and painted metals under xenon-arc light using ASTM G-155 protocol. (Data by 3M Company).

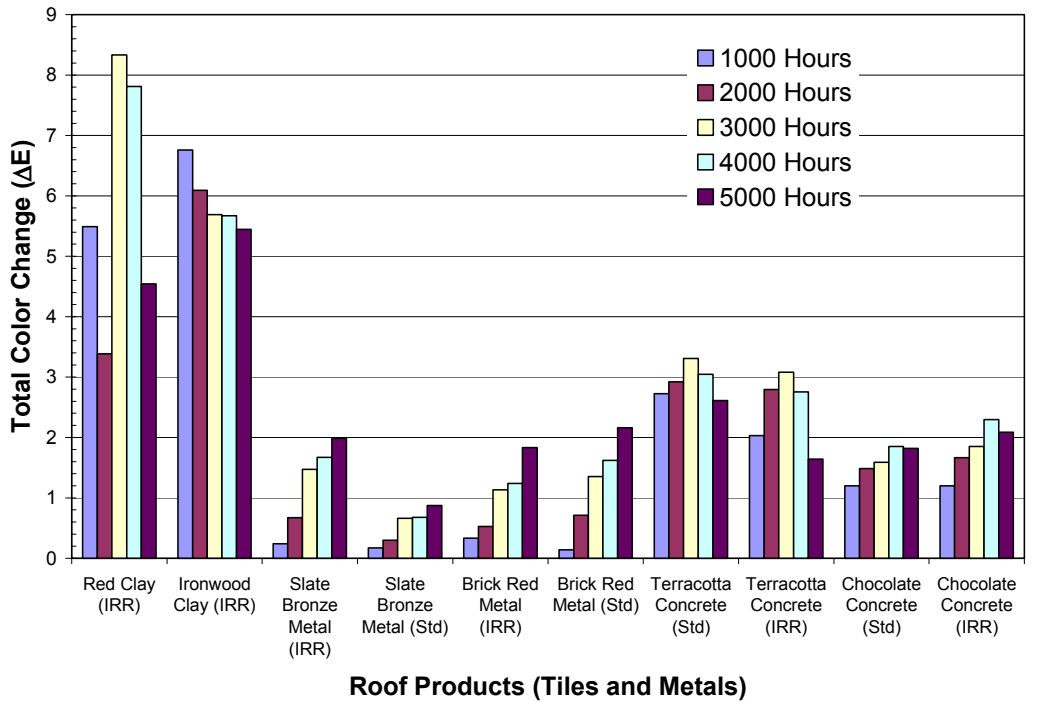

Figure 8. The total color change of tiles and painted metals under xenon-arc light using ASTM G-155 protocol. (Data by 3M Company).

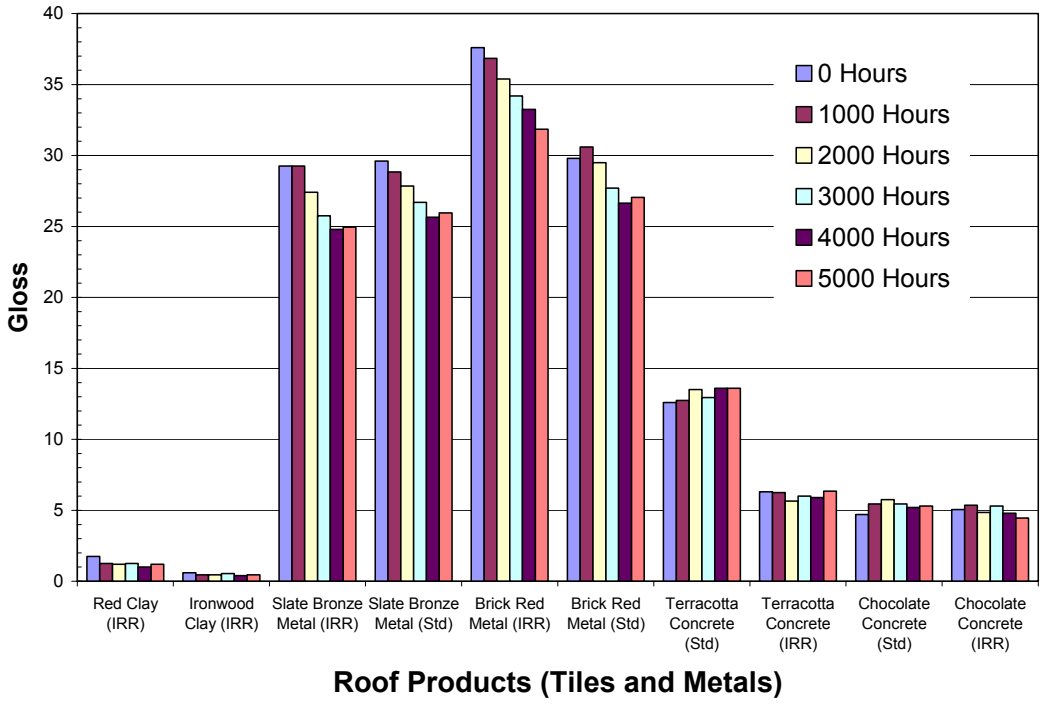

Figure 9. The gloss of tiles and painted metals under xenon-arc light using ASTM G-155 protocol. (Data by 3M Company).

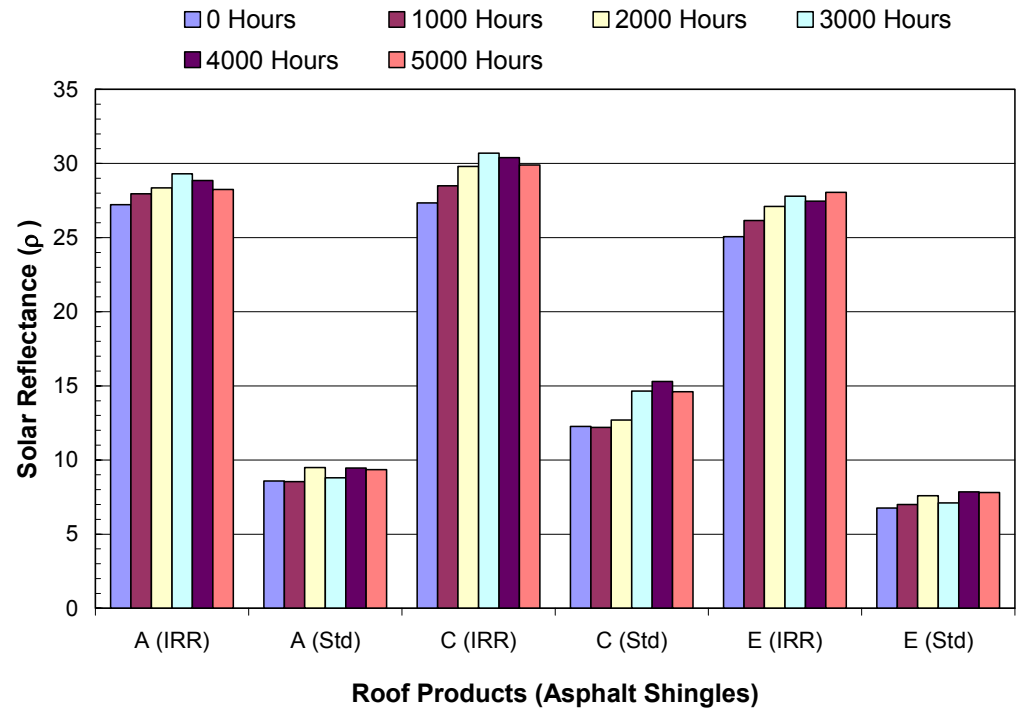

Figure 10. The solar reflectance of asphalt shingles under xenon-arc light using ASTM G-155 protocol. (Data by 3M Company).

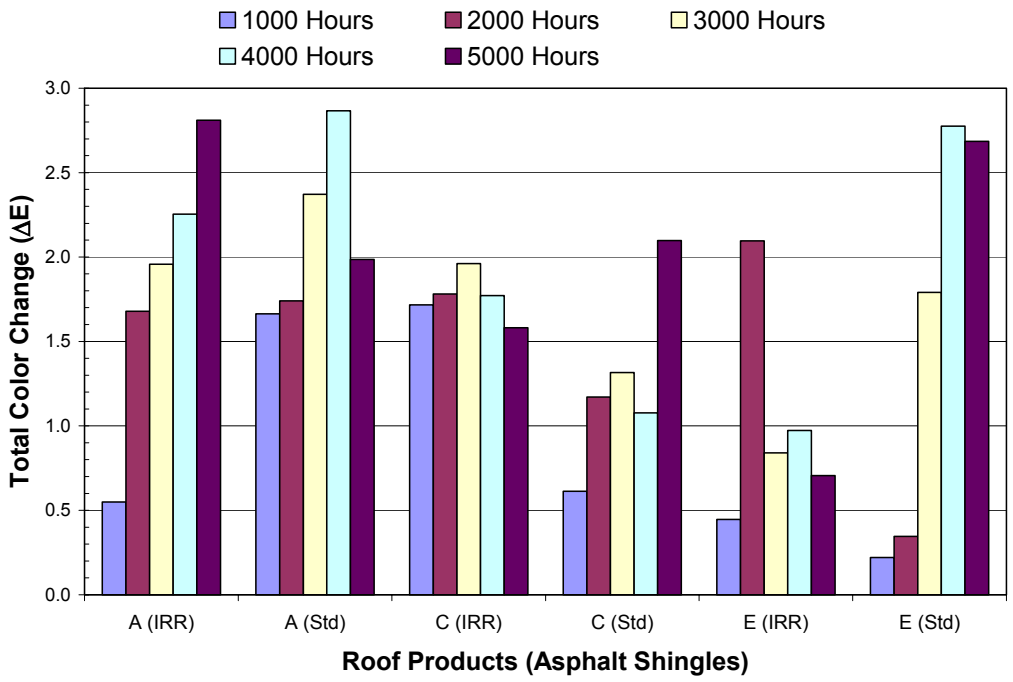

Figure 11. The total color change of asphalt shingles under xenon-arc light using ASTM G-155 protocol. (Data by 3M Company).

Arnold Schwarzenegger
Governor

COOL-COLOR ROOFING MATERIAL ATTACHMENT 7: TASK 2.6.1 REPORTS - BUILDING ENERGY-USE MEASUREMENTS AT CALIFORNIA DEMONSTRATION SITES

PIER FINAL PROJECT REPORT

Prepared For:
California Energy Commission
Public Interest Energy Research Program

Prepared By:
Lawrence Berkeley National Laboratory and Oak Ridge National Laboratory

ERNEST ORLANDO LAWRENCE
BERKELEY NATIONAL LABORATORY

June 2006
CEC-500-2006-067-AT7

Prepared By:
Lawrence Berkeley National Laboratory
Hashem Akbari
Berkeley, California
Contract No. 500-01-021

Oak Ridge National Laboratory
William Miller
Oak Ridge, Tennessee

Prepared For:
California Energy Commission
Public Interest Energy Research (PIER) Program

Chris Scruton
Contract Manager

Ann Peterson
Building End-Use Energy Efficiency Team Leader

Nancy Jenkins
PIER Energy Efficiency Research Office Manager

Martha Krebs, Ph.D.
Deputy Director
ENERGY RESEARCH AND DEVELOPMENT DIVISION

B. B. Blevins
Executive Director

DISCLAIMER

This report was prepared as the result of work sponsored by the California Energy Commission. It does not necessarily represent the views of the Energy Commission, its employees or the State of California. The Energy Commission, the State of California, its employees, contractors and subcontractors make no warrant, express or implied, and assume no legal liability for the information in this report; nor does any party represent that the uses of this information will not infringe upon privately owned rights. This report has not been approved or disapproved by the California Energy Commission nor has the California Energy Commission passed upon the accuracy or adequacy of the information in this report.

California Home Demonstrations Showcasing the Energy Savings of Tile, Painted Metal and Asphalt Shingle Roofs with Cool Color Pigments

William A. Miller, Andre Desjarlais, Phil Childs, Jerry Atchley
Building Envelope Program
Oak Ridge National Laboratory

Hashem Akbari, Ronnen Levinson, Paul Berdahl
Heat Island Group
Lawrence Berkeley National Laboratory

ABSTRACT

Aesthetically pleasing dark roofs can be formulated to reflect like a highly reflective "white" roof in the near infrared portion of the solar spectrum. New paint pigments increase the near infrared reflectance of exterior finishes by minimizing the absorption of near-infrared radiation. The boost in the NIR reflectance drops the surface temperatures of roofs and walls, which in turn reduces cooling-energy use and provides savings for the homeowner and relief for the utilities. The new cool color pigments can potentially reduce emissions of carbon dioxide, which in turn reduces metropolitan heat buildup and urban smog. Energy savings are particularly pronounced in older homes having little or no attic insulation, especially if the attic contains poorly insulated ducts. Cool roofs also result in a lower ambient temperature that further decreases the need for air conditioning, retards smog formation, and improves thermal comfort.

Residential demonstrations consisting of three pairs of single-family, detached houses were set up with concrete tile, painted metal and asphalt shingle roofs to showcase the energy savings of cool-pigmented roofs. For each pair of homes, one was roofed with a cool-pigmented product and the other roofed with a conventionally (warmer) pigmented product of the same color. Measured temperatures and heat flows at the roof surface, within the attic and at the ceiling of the houses are discussed as well as the power usage to help gauge the cost savings afforded by cool-pigmented reflective roof products.

INTRODUCTION

Dark colors are not necessarily dark heat absorbers! Dark colors can be formulated to reflect like a highly reflective "white" color in the NIR portion of the solar spectrum that ranges from 700 to 2,500 nm. Brady and Wake (1992) found that 10 μm particles of TiO_2, when combined with colorants such as red and yellow iron oxides, phthalocyanine blue, and perylene black, could be used to formulate fairly dark colors with near-infrared reflectance of 0.3 and higher. Researchers working with the Department of Defense added complex inorganic color pigments (CICPs) to paints used for military camouflage and matched the reflectance of background foliage in the visible and NIR spectra. The chlorophyll in plants strongly absorbs in the non-green parts of the visible spectrum, giving the leaf a dark green color with high reflectance

elsewhere in the solar spectrum[1] (Kipling 1970). In the NIR the chlorophyll in foliage naturally boosts the reflectance of a plant leaf from 0.1 to about 0.9, which explains why a dark green leaf remains cool on a hot summer day. Tailoring CICPs for high NIR reflectance similar to that of chlorophyll provides an excellent passive energy saving opportunity for exterior residential surfaces such as roofs exposed to the sun's irradiance. A CICP consisting of a mixture of the black pigments chromic oxide (Cr_2O_3) and ferric oxide (Fe_2O_3) increases the solar reflectance of a standard black pigment from 0.05 to 0.26 (Sliwinski, Pipoly & Blonski 2001).

Three pairs of residential demonstrations were established in California for documenting the potential energy savings for single-family detached homes having roofs painted with cool pigmented colors. Two pair of homes were constructed with concrete tile and painted metal roofs with and without cool pigmented colors. Another pair of homes demonstrated asphalt shingles with and without cool pigmented colors.

The California utilities are keenly interested in knowing the amount of electrical energy savings that would occur if roofs with cool pigmented colors, termed here on as cool roof color materials (CRCMs), are adopted in the building market. Our primary objective then is to demonstrate the thermal and potential economic benefits of CRCMs. The reported results also provide the confidence the utilities are seeking for making economic decisions on rebates for cool roof products.

DEMONSTRATION HOMES

It was difficult to estimate the time and effort required to convince a building contractor to accept, install, instrument, and monitor prototype tile, painted metal or asphalt shingle roofs on homes under construction in the Sacramento area. Timing was critical because a six month lead time is typically needed for obtaining city and county building permits. The Sacramento Municipal Utility District (SMUD) was offering through its Advanced Technologies Program to subsidize homes built with insulated concrete form (ICF) walls. LBNL and ORNL were interested in energy efficient roofing and it made good sense to combine the two initiatives and work together on the performance of the building envelope. Evans Construction agreed to partner with ORNL, SMUD, Hanson Roof Tile and Custom-Bilt Metals. A Memorandum of Understanding (MOU) was approved by ORNL, SMUD and Evans Construction for setting up two concrete tile and two painted metal roofs on residential homes built in the Cavalli Hills subdivision of Fair Oaks, CA (Appendix A).

Cavalli Hills is a twelve-lot subdivision having three different house designs (A-, B- and C-style floor plans) with footprints respectively of 120, 130 and 149 square meters (1300, 1400 and 1600 square feet),Fig. 1. A pair of A-style homes each identical in floor plan, layout and equipment design and having 1400 square feet of floor space had identical concrete tile roofs of the same color with and without CRCMs. A second pair of identical C-style homes having 1600 square feet of floor space had identical painted metal shake roofs of the same color with and without CRCMs.

The two pairs of homes in Cavalli Hills constructed with ICF walls also used advanced air-conditioning as part of SMUD's Customer Advanced Technologies field study and rebate program. The ICF walls were made using expanded polystyrene insulation (EPS) forms

[1] except for some bands of radiative absorption by water.

connected with polypropylene ties. Concrete was poured into the erected forms to complete the wall systems. The ICF walls had an overall thermal resistance (R-value) of about 16 hr•ft^2•°F/Btu. Each house is heated by a conventional 90% efficient gas furnace and hot water is supplied by a gas hot water heater. Comfort cooling is provided by split-system FREUS™ air-conditioners. The FREUS™ unit uses water stored in the basin of the outdoor unit and sprays it onto the condenser coils of the outdoor unit (as is commonly done with large commercial cooling equipment). The falling film of water accepts condenser heat and falls back into the reservoir. Any evaporated water is replenished. The evaporative cooling cycle is more efficient than conventional air-cooled equipment.

We intended to field test asphalt shingle roofs at Cavalli Hills as mentioned in the MOU (Appendix A); however, the demand for single-family detached housing caused Evans to accelerate construction and finish all twelve homes before prototype asphalt shingles were available for field testing. SMUD again provided help by trying to win the interest of builders, but the building community in and around Sacramento communicated their preference for concrete tile products. The F. W. Dodge (2002) report revealed that the asphalt shingle industry commands about 86% of the national market; however, in the Pacific Coast region the market share is down at about 75% because of the popularity of concrete and clay tile products. Neither Mercy Housing nor Habitat for Humanity could take advantage of our offer for donated roof materials plus free labor to install.

Elk Corp. had at this point in time developed prototype shingles and worked through their manufacturing representatives to locate a residential site in Redding, CA for demonstrating their new asphalt shingles with and without CRCMs. The firm Ochoa and Shehan Inc. agreed to demonstrate asphalt shingle roofs on two new homes of identical footprint, layout and equipment design. A MOU was written and approved by Elk Corp., Ochoa and Shehan Inc. and ORNL (Appendix B). The Redding site was considered an excellent selection for field testing asphalt shingles because the outdoor ambient air temperature in Redding often peaks at 43.3°C (110°F) during the summer, and winters typically experience sub-freezing outdoor temperatures.

The Cavalli Hill demonstration homes ventilated the attic using soffit and gable vents. R-19 loose fill insulation was blown in the attic space and the indoor air-handler and air-distribution ducting are in the attic. All ducts were wrapped in R-5 insulation. The homes in Redding also have soffit and ridge ventilated attics. For them, R-19 loose fill insulation was blown in the attic space and the indoor air-handler and air-distribution ducting is in the attic. Orineted strand board (OSB) decking facing the attic interior uses a radiant barrier as required by the building codes for the county of Redding.

Homes Showcasing Concrete Tile Roofs

Hanson Roof Tile donated its medium profile Hacienda concrete tile for the two A-style demonstration homes in the Cavalli Hills subdivision (Fig. 1). Evans Construction contracted Dynamic Roofing to install the tile. ORNL personnel worked with Evans and Dynamic Roofing to set up temperature measurements of the roof. Installation included a roof deck made of 5/8 in oriented strand board (OSB); 30-lb saturated asphalt felt paper and 1-in by 1-in battens for offset mounting the tile to the OSB deck (Fig. 2). Evans selected the Hacienda tile with chocolate brown color, which has a solar reflectance of only 0.10 and thermal emittance of 0.93. Ferro worked with Hanson Tile to increase the solar reflectance of the Hacienda tile and observed that

adding cool color pigments to the sand, cement[2], and water mixture during the manufacturing process required excessive amounts of pigment making the product too expensive. The process also diluted the surface color. Ferro developed a slurry coat application that put the reflectance upwards of 0.40. However a parallel initiative by American Rooftile Coating proved to be more successful and economical. They painted their COOL TILE IR COATING™ onto several samples of concrete tiles of different colors (Fig. 3). The solar reflectance of the chocolate brown Hacienda tile exceeded 0.40 and was applied to the second A-style home for demonstrating the benefits of the CRCMs. The application applies a white undercoat followed by a chocolate brown topcoat. Figure 4 shows the completed job of the tile with coating applied by American Rooftile Coating. The vendor provided Evans Construction a 10-year warranty on the paint finish.

Homes Showcasing Painted Metal Roofs

Custom-Bilt donated its Country Manor Shake roof product for field testing at the Cavalli Hills demonstrations (Fig. 5). Evans, at the suggestion of Custom-Bilt Metals, contracted Rinkydink Builders to install the metal roofs. The color of the aluminum shakes with conventional pigments is dark brown and has solar reflectance of 0.08 and thermal emittance of 0.90. Custom-Bilt used BASF's ULTRA-Cool™ pigmented coatings to increase the shake's solar reflectance to 0.31 for the roof of the second demonstration home. Premium coil coated metal roofing probably has an excellent opportunity for applying CRCMs because 1) the metal is already painted 2) the paint coating is reasonably thick (~25 micron) and 3) the substrate has high NIR reflectance (ρ_{NIR} ~ 0.55 to 0.7). The coatings for metal shingles are durable polymer materials, and many metal roof manufacturers have introduced the CRCM pigments in their complete line of painted metal roof products. The additional cost of the pigments is only about 5¢ per square foot of finished metal product (Chiovare 2002). Success of the new CRCM metal products is evident in the market share recently captured by the metal roof industry. Historically metal roofs have had a smaller share of only about 4% in the residential market. The architectural appeal, flexibility, and durability, due in part to the cool color pigments, has steadily increased the sales of painted metal roofing, and as of 2002 its sales volume had doubled since 1999 to 8% of the residential market, making it the fastest growing residential roofing product (F. W. Dodge 2002).

Homes Showcasing Asphalt Shingle Roofs

Elk Corp. donated their Weatherwood Prestique® Cool Color and their conventional Weatherwood Prestique® asphalt shingles for field testing in Redding, CA. The cool color shingle has a solar reflectance of 0.26 and a thermal emittance of 0.90. The conventional Weatherwood shingle has solar reflectance of 0.09 and thermal emittance of 0.89. The cool color shingles are advertised on Elk's web site[3] as the "first energy-efficient cool asphalt shingles offered in a palette of rich, organic colors." Elk offers a 40-year limited warranty with a limited wind warranty of up to 90 mph, and a UL Class "A" fire-rating. The prototype shingles were developed in conjunction with 3M™ to meet initial ENERGY STAR® performance levels.

---

[2] It's difficult to make a cool concrete tile by mixing cool pigments into gray-cement concrete, because the gray cement includes NIR-absorbing iron oxides. A white-cement concrete can be mixed with cool pigments to make a cool product. However, white cement costs about twice as much as gray cement concrete, so tiles are usually made with the latter.

[3] http://www.elkcorp.com/homeowners/products/shingles_prestique_ccs.cfm

The homes demonstrating asphalt shingles are on different cul-de-sacs but within about 100 yards of each other. Both homes have about the same azimuth orientation with respect to the sun which allows direct comparison of the thermal performance of the two roof assemblies. The residences are one-story ranch style homes built on concrete slab. Each house has about 2400 square feet of floor space, and each house uses two split system air-conditioners for comfort cooling.

Instrumentation and Data Acquisition

Instrumentation was added to each demonstration home to catalogue temperatures and heat flows across the roof and attic assembly and the relative humidity of the ambient air in the attic. Sensors were also installed in the living space to measure the indoor ambient return and supply air temperatures and indoor relative humidity. Whole house power, air-conditioner power and compressor cycling rate were measured at homes in Fair Oaks, CA. Only air-conditioner power was monitored at the Redding site.

Roof Deck and Attic Floor (Ceiling)

Heat flux transducers (HFTs) were embedded in the roof decks and the attic floor to measure the heat flows crossing the decks and attic floor of each house. The roof decks are made of 5/8-in OSB. Typical construction uses 15/32-in OSB; however, the 5/8-in OSB was selected because it is of sufficient thickness for embedding a 0.15-in thick HFT in the OSB without compromising accuracy of the heat flow (Fig. 6).

We checked the thermal conductivity of 5/8-in and ¼-in thick boards because OSB is made from various waste wood products and conductivity might vary with thickness. A 2-ft-square section of 5/8-in OSB was placed in a heat flux metering apparatus and calibrated to determine the thermal conductivity of the OSB. Top temperatures of the board were set at 7.2, 23.9, 37.8 and 48.9°C (45, 75, 100 and 120°F), which are typical temperatures observed by Parker, Sonne and Sherwin (2002) for roof decks covered by concrete tile. Results revealed that the thermal conductivity of OSB increased linearly with temperature. A thinner ¼-in OSB board was also tested and found to have thermal conductance within ± 0.5% of the measures obtained for the thicker 5/8-in board. Thermal conductivity of the thinner board varied linearly and had the same slope as the thicker 5/8-in board. The tests verified that the thinner board could be used as a cover plate to hold the heat flux transducer in place (Fig. 6), and would not adversely affect the heat flow.

Shunting due to the differences in thermal conductance of the HFT and the OSB was also accounted for by calibrating the HFT in a 2-ft by 2-ft guard of 5/8-in thick OSB using the ASTM C518 protocol (ASTM 1998). Calibration showed a slight but linear drop in sensitivity as the temperature of the OSB was increased from 4.4 to 48.9°C (40° to 120°F, at temperatures typically observed by Parker in roof decks field tested in Ft. Myers, FL).

The guard became a portion of a sandwich panel equipped with copper/constantan thermocouples and the HFT. Once calibrated the sandwich panels were shipped to the builders and installed in the adjacent roof decks of each demonstration home. The sandwich panel was made of the same material as the deck and was also the same thickness. While the roof products were being installed, the thermocouples attached to the sandwich panels were epoxy glued to the

roof surface[4], taped to the topside of the deck, placed adjacent the HFT embedded in the OSB and taped to the underside of the OSB deck facing the interior of the attic. The thinner ¼-in board attaches to the underside of the deck to provide access for future maintenance (Fig. 7).

A similar procedure was used for setup of the HFT measuring the heat flow crossing the attic floor and entering the conditioned space. Here however, we taped a HFT in the center of a 2-ft by 2-ft piece of gypsum board and covered the device with R-19 batt insulation and proceeded to calibrate the transducer. In the field we simply taped the HFT to ceiling drywall and attached a thermocouple adjacent to the HFT. Later, after insulation was blown into the attic, we placed a thermocouple approximately at the top surface of the blown insulation.

Weather Station

A fully instrumented meteorological weather station was set up at Cavalli Hills to collect the ambient dry bulb temperature, the relative humidity, the wind direction and the wind speed. The station was attached to the back side on the C-style house and extended about 4 feet above the ridge vent. Pyranometers were placed on adjacent sloped roofs of all homes for measuring the morning and afternoon solar irradiance. These measures helped prove that, for instance, the west facing roofs from a pair of homes had the same intensity of solar flux. The instruments also indicated the daylight hours and displayed peak irradiance with time of day.

Power measurements

SMUD installed watt-hour transducers for measuring the cooling energy consumed by the FREUS™ air-conditioners, the whole house power and counters totaling the number of compressor starts of the air-conditioners. Whole house power transducers were checked against electrical energy measures provided by SMUD's revenue meters. Measures were checked at different points in time, and showed the transducer readings within 0.3 to 1.6% of the revenue meter readings (Table 1).

ORNL personnel also made bench top checks of the Rochester model PM 1000 transducers installed by SMUD for measuring air-conditioning power. The transducer was compared to a Wattnode transducer Model WNA-1P-240-P, which ORNL has successfully applied on several applications. Bench top tests showed the SMUD transducer (Rochester model PM 1000) read within 6% of the Wattnode transducer. Further checks of the PM-1000 transducers were made at Cavalli Hills to verify proper polarity of lead wires from each transducer, and to verify the current transducer polarity (i.e., the dot on the front of the CT points toward the house breaker). SMUD personnel conducted field calibrations of all transducers around 02/01/2005 as a check of its instruments.

[4] The painted shakes are made of thin metal of about 26 gauge and we taped the thermocouple to the underside of the shake for measuring surface temperature.

Table 1. Comparison of watt hour transducers to Cavalli Hills Revenue meter readings.						
SMUD Meters	Date		House and Address			
			4979 Mariah Place Tile Roof Standard Color Pigment	4983 Mariah Place Metal Roof Standard Color Pigment	4987 Mariah Place Tile Roof CRCM Pigment	4991 Mariah Place Metal Roof CRCM Pigment
	From	To	kWh	kWh	kWh	kWh
Revenue Meter (kWh)	3/23/2005	4/19/2005	233	421	432	184
Pulse Transducer (kWh)	3/23/2005	4/19/2005	237	422	433	186
Error (%)			**1.63**	**0.32**	**0.30**	**0.98**

Data Acquisition System

Campbell Scientific micro-loggers were used for remote acquisition and recording of field data. Salient features of the micro loggers are provided in Table 2. The loggers were

Table 2. Salient Features of Campbell Scientific data loggers.		
Item	**Item Description**	**CSI Part No.**
1	CR-23x Datalogger with 4 Mbytes memory	CR10X-2M
2	Array based operating system for CR-23X-4m	9801
3	Thermocouple reference thermistor for CR23X Wiring Panel	CR10XTCR
4	12 volt Power supply w/Charging regulator and rechargeable battery	PS100
5	18 volt 1.2 Amp wall charger, 6 ft.	9591
6	16-channel (4-wire) or 32-channel (2-wire) Relay Multiplexer	AM16/32
7	25-Channel Solid-State Multiplexer for Thermocouples	AM25T
8	Data cable, two peripheral connector cable for datalogger, 2 ft.	SC12
9	8-Channel Switch Closure Module	SDM-SW8A
10	Telephone Modem	COM210
11	Phone modem surge protector	6362
12	Enclosure 16/18, weather-resistant	15873

equipped with 4 Mbytes of memory, a 25 channel multiplexer for thermocouples, rechargeable battery, 115Vac-to-24Vdc transformer, modem, modem surge protector, weatherproof enclosure and associated cables.

The mirco logger was programmed to scan every 30 sec and reduce analog signals to the engineering units specified in Table C.1. (Appendix C). Averages of the reduced data were electronically written to an open file every 15-min. The averages were calculated over the 15-min interval and are not running averages; they are reset after each 15-min interval. Electronic format is comma delimited for direct access by spreadsheet programs. Data files consist of one full week of data containing 672 rows of averaged measurements representing the instrument measurements of Table C.1 written every 15-min over the 168 hours of a week. The micro logger automatically closes the existing file and opens a new data file every Friday at midnight for recording the next week of data. A dedicated desktop computer calls the micro logger and acquires the previous week of data over a modem connected to a dedicated phone line.

FIELD RESULTS

The acquisition of field data for the pair of concrete tile roofs started July 2004 while data collection for the pair of painted metal roofs began August 2004. Speculators purchased two of

the four homes in Fair Oaks CA, and the two homes just happened to be one from each of the two pair of homes. Meaningful summer comparisons between homes with and without CRCM roofs did not therefore occur until the summer of 2005. We started collecting field data for the shingle roofs April 2005. Hence the discussions of field results that follow are for the summer of 2005. We intend to continue field acquisition through the summer of 2006 and include any additional insight gained from the field demonstrations in future refereed journal articles.

The attics and roof decks of each demonstration home were instrumented to document the immediate effects of CRCMs on the deck and attic air temperatures and the heat flows crossing the roof deck. Our intent was to demonstrate typical summer performance of CRCMs and to also collect data useful for formulating and validating computer codes capable of calculating the heat transfer occurring within the attic. Once validated, these attic simulations can be coupled to whole house building models for simulating and predicting local, state and national energy savings afforded by roofs with CRCMs.

The results that follow describe temperature and heat flow results for the roofs and attics of the demonstration homes. Afterwards, discussions about the cooling energy and whole house power measures are presented in the section on Cooling Energy Savings.

Concrete Tile Roofs

As stated earlier, the Cool Tile IR COATING™ increased the solar reflectance of the medium profile concrete tile from 0.10 to 0.41. The boost in solar reflectance dropped the surface temperature of the CRCM tiles consistently below those with conventional color pigments. During the afternoon hours for a week in September (Figure 8) the ambient air temperature daily peaked around 30 to 32°C (86 to 90°F). The ridge vent for the tile roofs ran north and south and during the afternoon the sun's irradiance is directly incident on the west facing roof. Surface temperatures of the tile roofs with CRCMs are about 5 to 7.5°C (9 to 13.5°F) cooler during peak irradiance than the conventional pigmented color tile. Similar reductions occur in the attic air temperature, which is about 4°C (7.2°F) cooler than the attic air for the home with conventional pigmented tile. The peak surface temperatures are observed around 3:30 p.m. while the attic air temperature peaks about 1½ hours later at about 5 p.m. P.D.T. (Figure 8), which occurs at about the same time as the peak in outdoor air temperature.

Further inspection of the heat crossing the roof deck and the attic floor reveals 1) that the CRCMs reduce the amount of solar heat penetrating through the deck and the attic floor, and 2) that the peak heat flow crossing the attic floor is delayed similar to the trends in peak attic air temperature and therefore reflects trends that may benefit peak demand reductions for utilities.

About a 25% drop in deck heat flow occurs during times of peak irradiance because of the higher solar reflectance of the tile with CRCMs. An averaged 20% reduction was calculated for daytime[5] exposure during the full month of September. The corresponding drop in heat flow penetrating through the attic floor and into the conditioned space was about 10% of that penetrating the attic floor of the home with conventional color tile (Figure 9). It is important to note that the medium profile tiles were installed on battens and sub-tile venting occurs over the batten and below the tiles. Miller et al. (2005) showed sub-tile venting to further reduce the heat flows crossing the roof deck.

[5] Daytime was defined as the time when the pyranometer measurements on the west facing roof exceeded 250 Watts per square meter, which corresponds to about 10 a.m. through 6:30 p.m.

We observed the heat flow entering the attic floor of the home with CRCM tile as being less than the heat flow in the other home from about noon to well past 8 p.m. The attic floor has code level R-19 blown insulation and the combination of attic insulation, sub-tile venting and thermal mass of the conventional tile most likely caused the continued benefits into the evening hours. The time dependent valuation of energy places a premium on electricity usage from about 1 to 6 p.m. The trends shown for the pair of tile roofs therefore reflect even better potential economic benefits because less air-conditioner power is consumed during the utilities peak summer time demands.

Painted Metal Roofs

The two C-style homes with painted metal roofs are oriented with their respective ridge vents running east-west. Therefore the south facing roofs of each home received both morning and afternoon direct solar irradiance with little or no shading throughout the day (Figure 5). At solar noon for a day of clear skies in September 2005, the painted metal roof with CRCMs had peak surface temperatures that were 10°C (18°F) cooler than the metal roof with conventional paint pigments (Fig. 10). The peak attic air temperature for the home with CRCM metal shakes was 5°C (9°F) cooler (Fig. 10). The drop in surface temperature in turn reduced the heat penetrating into the attic as measured by the heat flux transducer embedded in the OSB decking of the south-facing roof (Fig. 11). Results depict a consistent and sustained reduction in heat flow during the daylight hours. Integrating the heat flow crossing the roof deck for the full month of September showed that the painted metal roof with cool pigments had 32% less heat flow than the deck having the same color painted metal roof but with conventional paint pigments.

CRCMs appeared to provide more thermal benefit for the pair of homes with metal roofs then the pair of homes with tile roofs. We believe the difference is attributable to sub-tile venting of the concrete tile roofs as compared to the metal shake roofs which were direct nailed to the roof deck. Sub-tile venting is more efficient on hotter roofs so it diminishes the effect of the solar reflectance of the cool tiles.

Asphalt Shingle Roofs

July and August ambient air temperatures in Redding, CA often exceed 45°C (110°F). Field data for August 2005 show the conventional shingles exposed in Redding had peak temperatures of about 73°C (163°F) as compared to peak temperatures of about 70°C (158°F) for the shingle with CRCMs. The difference in surface temperature between the conventional and CRCM shingle is not as large as the differences observed for painted metal and or concrete tile simply because the CRCM shingle increased solar reflectance by only 0.17. However, reducing the temperature of shingles has potential benefits for improving the chemical and flexural properties of the shingles. Terrenzio et al. (2002) showed that heating of asphalt shingles promotes the vaporization and diffusion of oils from the asphalt with the subsequent migration of oxygen into the asphalt. Terrenzio noted that as aging progresses, the stiffness of the asphalt increases. Therefore CRCMs may indeed increase the service life of shingles.

Heat flow penetrating the west-facing roof for the pair of homes with asphalt shingles again showed similar trends to the tile and painted metal demonstrations. The deck heat flow is consistently lower when CRCMs are applied to the shingles (Fig. 13). Roughly a 30% drop as compared to the conventionally pigmented shingle was observed over the daylight hours during a week in August 2005.

COOLING ENERGY SAVINGS

Occupancy habits are the Achilles heel of any residential demonstration. It is ironic that while the research conducted in building science targets improved energy efficiency and quality of life, the habits of people often deter energy conserving practices. Testing the homes while unoccupied would certainly help document reductions of whole house energy. As example, Parker et al. (2002) demonstrated that an unoccupied Florida home with a "white reflective" barrel-shaped concrete tile roof reduced the annual cooling energy by 22% of the energy consumed by an identical and adjacent home having an asphalt shingle roof. The cost savings due to the reduced use of comfort cooling energy was about US $120 or about 6.7¢ per square foot per year. Parker's results have become a benchmark in the area of building science. However, Parker's results beg the question. "Are the results realistic when one considers people's occupancy habits?"

The principal focus for the field demonstrations centered on collecting attic and roof data to prove the thermal benefits of the cool pigment technology. But the experiments also included power measurements as well as air-conditioning supply and return air temperatures in an effort to deduce estimates of annual savings despite the effects of occupancy habits or, put differently, corrected for the effects of occupants.

The Sacramento Municipal Utility District (SMUD) forwarded the 2005 summer revenue meter readings for the two pair of demonstration homes in Fair Oaks, CA (Table 3). The kWh use during the 2005 summer for the home with cool color metal shakes was

Table 3. Monthly Energy from Revenue Meter Readings for Demonstration Homes in Fair Oaks CA

	Whole House Monthly Energy (kWh)		Whole House Monthly Energy (kWh)	
Month Ending	Metal Shake Conventional Color	Metal Shake Cool Color	Medium-Profile Tile Conventional Color	Medium-Profile Tile Cool Color
6/18/05	409	552	734	993
7/20/05	1433	749	891	1511
8/18/05	1034	807	884	1412

26% less than that for the same home with conventional metal shakes. However, the cool tile used 56% more energy than did the home with standard tile. Solar reflectance of the cool tile is about 0.41 as compared to 0.08 for the same conventional color tile and should therefore demonstrate some energy savings. Further review of the data and personal discussions with the homeowners revealed that the resident in the home with standard tile roof did not keep the thermostat at 22.2°C (72°F) until after August 19, 2005. The resident is a medical student who spends more time in class and at work than at home. In contrast, the residents in the home with a cool color concrete tile roof utilize their home's amenities more so than their neighbor. We also found out that they dropped the thermostat setting from 22.2° to 21.1°C (72° to 70°F) at night simply for their own sleeping comfort, while the medical student simply crashed in bed.

To correct for these differences in life style, power measurements were reduced into daily electrical energy consumptions. The electrical usage of the whole house and the air-conditioner were plotted against the daily average outdoor air-to-indoor air temperature difference (labeled as OD air-to-Return air in figures 14 - 18). Regression analysis of the reduced data helped to mask the effects of different thermostat settings and occupancy habits. Results for the concrete tile, painted metal and asphalt shingle demonstrations follow.

Cool Concrete Tile Roof

Linear regression of daytime electrical usage against the daytime average outdoor air-to-indoor air temperature difference for both homes with concrete tile roofs shows the home with CRCM concrete tile used more electrical energy than the home with conventional pigmented color tile (view red regression line in Fig. 14). Similar results were also observed in Table 3 from SMUD's revenue meter readings. As stated the one resident hardly lived at home while the other homeowner maintained a more normal lifestyle. Therefore occupancy habits caused the discrepancy and an occupancy habit correction (OHC) is needed. The home with CRCM tile is saving energy but at a different base of comparison than the home with conventional color tile because of miscellaneous plug loads (i.e., lights, electrical cooking, water-pumps in Jacuzzi, etc.).

The field data was searched over the two years of measurements for periods requiring no comfort cooling in hopes of determining miscellaneous plug loads consumed by the resident in the home with the CRCM tile roof. Ample data was found for periods in the early spring and the late fall. The whole house electrical energy use for these days having no compressor energy was compared to the other home and found to use an averaged 12 kWh per day more plug load. We then subtracted 12 kWh from the whole house electrical energy used by the home with CRCM tile to better compare to the whole house usage of the other home (blue regression line in Fig 14). We also plotted the air-conditioner draw again against the daily average outdoor air-to-indoor air temperature difference for both homes (Fig. 15). As the outdoor air-to-indoor air temperature difference increased, the savings in consumed cooling energy also increased (cyan line in Fig. 15). The savings in cooling energy range from about 1 to 2 kWh per day[6], and yield an energy savings of about 9% of the whole house electrical energy consumed per day by the home with conventional pigmented tile (black regression line Fig. 14).

Cool Painted Metal Roof

Linear regressions were again generated for the daily whole house electrical energy and air-conditioning energy consumed as functions of the daily average outdoor air-to-indoor air temperature difference for both homes with painted metal roofing. Recall that the revenue meter readings for the pair of homes with painted metal roofs indicated the home with CRCMs used 26% less electrical energy than the home with a conventional pigmented metal roof. Here we believe occupancy habits skewed the data to favor energy savings. Savings are about 8 kWh of electricity per day (Fig.16); however, air-conditioner usage indicates savings of about 2 kWh per day[7] (Fig. 17). We therefore believe savings are similar to those for the tile roofs and are about 8 to 10% compared to the home having a conventional pigmented metal roof of the same color.

Cool Asphalt Shingle Roof

The electrical energy measured for the air-conditioners operating in demonstration homes in Redding CA (Fig. 18) are more than twice the energy measured for the two pair of homes in Fair Oaks CA. The demonstrations in Redding used two 3½ -ton A/C units, while in Fair Oaks only

[6] Savings do not include the electrical energy used by the indoor blower which pulls about 700 W. Further analysis will include these savings as reflected in reduced compressor on-time for the homes with CRCM roofs.
[7] Savings do not include the power of the indoor blower which consumes about 700 W. Further analysis will include these savings as reflected in reduced compressor on-time for the homes with CRCM roofs.

one 3-ton FREUS™ air-conditioner was needed to provide comfort cooling. Also the homes in Redding were stick-built ranch style homes with 2400 square feet of floor space while the homes in Fair Oaks are two-story homes with 1400 or 1600 square feet of floor space and they also have R-16 ICF walls (see section on Demonstration Home).

When the outdoor air and return air temperatures are about the same, the regression lines for the pair of homes nearly intersect (Fig. 18). This simply means that no cooling is required by the homes, and there is no compressor electrical usage. However, as the temperature difference from the outdoor air to the home's return air increases, the cooling savings also increase for the pair of shingle demonstrations (Fig. 18). At an outdoor air-to-indoor air temperature difference of 10°C (18°F) [about 32.2°C (90°F) outdoor air temperature] the home with CRCM asphalt shingles uses 6.3 kWh per day less electricity[8] than the other home with conventional shingles. The cool pigments are therefore providing savings of roughly 0.90 kWh per day per ton of cooling capacity. The whole house electrical consumption for the homes was gleaned from Redding Electric, and over the summer months (June through September) the revenue meter for the standard home averages to about 55 kWh per day. Therefore, whole house power drops about 11.4% due to the use of CRCMs in asphalt shingles. It is interesting that the hotter the outdoor air temperature the greater are the energy savings for the air-conditioners operating in the homes with CRCM roofs. The trend is slight yet could be important in terms of Time Dependent Valuation of energy that places a premium cost on energy consumed during the hottest portion of the day.

Again it is important to note that revenue meter readings from Redding Electric do not show positive energy saving benefits because of occupancy habits. The one home with a standard shingle roof consumed 1705 kWh from June through September 2005 by revenue meter data from Redding Electric. In comparison, the home with CRCM shingles used 2845 kWh (67% more energy) over the same time period. Occupants in the home with conventional shingles maintained a different lifestyle as compared to the occupants in the home with CRCM shingles.

BENEFICIAL RESULTS OF SHOWCASE HOMES

The field demonstrations turned out to be a powerful way for the tile, metal and asphalt shingle industry participants to showcase and market the performance of new CRCMs to consumers, developers, designers, and roofing contractors. For example, cool nonwhite CRCM coatings have been enthusiastically adopted by premium coil coaters and metal roofing manufacturers. BASF Industrial Coatings launched "ULTRA-Cool™," a line of Kynar coatings that quickly replaced the more conventional silicone modified polyester coatings. Coil-coater Steelscape recently introduced Spectrascape MBM, a cool Kynar coating for the metal building industry. A third industrial partner, Custom-Bilt, switched over 250 of its metal roofing products to cool colors. Tony Chiovare, CEO of Custom-Bilt Metals, stated that the additional cost of the cool-pigments is only about 5¢ per square foot of finished product (Chiovare 2002), which researchers have shown will pay for itself easily within three years because of the building energy savings (Miller et al. 2004).

The new asphalt shingles showcased in Redding have resulted in the demonstrable reduction of heat build up in the roof deck through the use of cool pigments. John McCaskill, Product

[8] Savings do not include the electrical energy used by the indoor blower which pulls about 700 W. Further analysis will include these savings as reflected in reduced compressor on-time for the homes with CRCM roofs

Brand Manager for Elk Corporation, reports the additional finished product cost is roughly 25¢ per square foot which makes this product a reasonable alternative to radiant barriers for the reduction of cooling load. The combined cost effective nature of cool colored asphalt shingles with the potential reduction of Urban Heat Island effects provides a mainstream solution for the residential re-roof market as well as new construction. Elk now offers 4 cool shingle colors across two product lines.

CONCLUSIONS

Thermal performance data proved the superior performance of CRCM in concrete tile, painted metal and asphalt shingle roof products. Surface temperatures are cooler causing average heat flows through the roof deck to drop by 20% for cool pigmented tile, by 32% for cool pigmented painted metal shakes and by 30% for cool pigmented asphalt shingle roofs as compared to conventional roofs. This in turn drops the heat penetrating into the conditioned space which results in cooling and whole house energy savings. Cool pigmented tile and cool pigmented metal shakes reduced whole house electrical energy by about 10%. The asphalt shingle demonstration showed higher savings at about 13%, which we attribute to the difference in construction of the Fair Oaks homes with ICF walls and the Redding homes with conventional 2 by 4 walls. The energy efficient homes with ICF walls in Fair Oaks are providing savings of about 0.67 kWh per day of electrical energy per ton of air-conditioning capacity while in Redding about 0.90 kWh per day is saved per ton of air conditioning capacity.

California's ability to meet peak electricity demand in the future is one of the primary electrical issues confronting its public utility companies. The CEC has stated that hot summer temperatures can drive up peak electrical demand as much as forty-five percent, and California is increasingly relying on out-of-state electrical supplies. Residential air-conditioning loads represent almost 14 percent of the summer peak demand; the equivalent of over 7,000 MW of peak capacity during a hot California summer day. To exacerbate the problem, significant new housing growth in both the near and long term will occur in California's urban areas and hot inland regions. "Cool Roofs" can provide a part (roughly 10%) of the solution to California's dilemma without introducing new complexity (no moving parts). The market opportunity therefore exists for a "cool roofs" business venture. What is needed is the reasoned faith derived from the research and the fortitude to act upon the results.

REFERENCES

Brady, R. F., and L. V. Wake. 1992. "Principles and Formulations for Organic Coatings with Tailored Infrared Properties." Progress in Organic Coatings 20:1–25.

Chiovare, Tony CEO of Custom-Bilt Metals, personal communications with ORNL and LBNL on cost premiums for painted metal roofs having CRCMs. 2004.

F.W. Dodge. 2002. Construction Outlook Forecast, F.W. Dodge Markert Analysis Group, 24 Hartwell Avenue, Lexington, MA 02421. Telephone 800-591-4462, FAX 781-860-6884, URL:www.FWDodge.com.

Kipling, E. B.1970. "Physical and Physiological Basis for the Reflectance of Visible and Near-Infrared Radiation from Vegetation." Remote Sensing of Environment 1 (1970), 1 55-1 59.

Sliwinski, T. R., R. A. Pipoly, and R. P. Blonski. 2001. “Infrared Reflective Color Pigment.” U.S. Patent 6,174,360, January 16.

Miller, W.A., MacDonald, W.M., Desjarlais,A.O., Atchley, J.A.,Keyhani, M., Olson, R., Vandewater, J. 2005. Experimental analysis of the natural convection effects observed within the closed cavity of tile roofs. RCI Foundation conference, “Cool Roofs: Cutting through the glare.” Atlanta GA. May 12-13.

Miller, W. A., Desjarlais, A.O., Akbari, H., Levenson, R., Berdahl, P. and Scichille, R.G. 2004. “Special IR Reflective Pigments Make a Dark Roof Reflect Almost Like a White Roof,” in Thermal Performance of the Exterior Envelopes of Buildings, IX, proceedings of ASHRAE THERM IX, Clearwater, FL., Dec. 2004.

Parker, D.S., Sonne, J. K., Sherwin, J. R. 2002. “Comparative Evaluation of the Impact of Roofing Systems on Residential Cooling Energy Demand in Florida,” in ACEEE Summer Study on Energy Efficiency in Buildings, proceedings of American Council for an Energy Efficient Economy, Asilomar Conference Center in Pacific Grove, CA., Aug. 2002.

ASTM. 1998. Designation C518-98: Standard Test Method for Steady-State Thermal Transmission Properties by Means of the Heat Flow Meter Apparatus. American Society for Testing and Materials, West Conshohocken, PA.

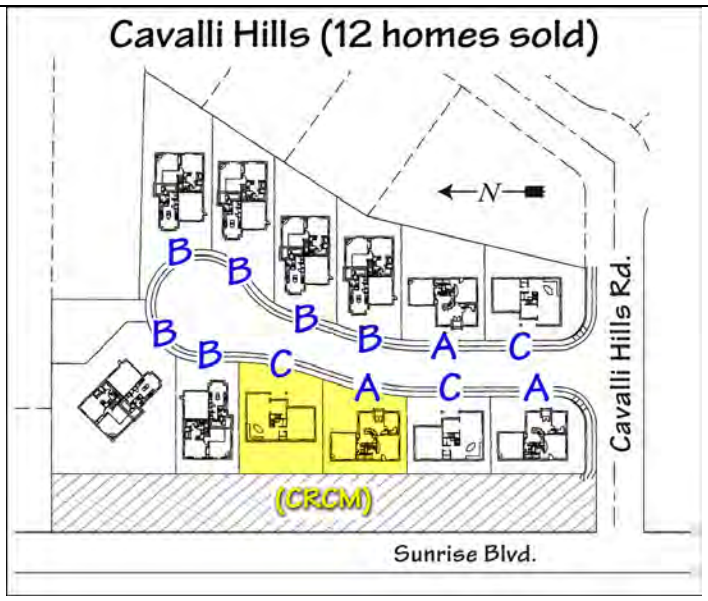

Figure 1. Plan view showing orientation of the demonstration homes in Fair Oaks, CA. The roofs of the A-style homes are Hanson's Hacienda medium profile concrete tile; roofs of the C-style homes are Custom-Bilt Metals Country Manor Shake. All roofs have the same dark brown color.

Figure 2. Hanson's concrete tile loaded onto the roof of one of two A-style homes. The tiles were offset mounted from the roof deck using 1 in by 1 in battens.

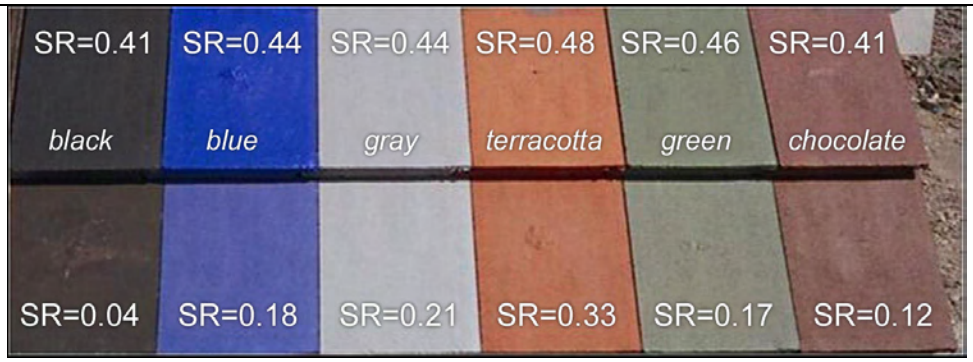

Figure 3. Solar reflectance of concrete tile roofs with CRCMs (top row) and without CRCMs (bottom row). The COOLTILE IR COATING™ technology was developed by Joe Reilly of American Rooftile Coatings.

Figure 4. Finished A-style home demonstrating Hanson Hacienda concrete tile after retrofit painting by American Rooftile Coatings.

Figure 5. Finished C-style home demonstrating Custom-Bilt Metal's painted metal shake having ULTRA-Cool™ pigmented coatings by BASF.

Figure 6. Heat flux transducer embedded in an OSB guard and used to measure heat flow crossing the roof decks of the demonstration homes.

Figure 7. Instrumented sandwich panels contain thermocouples and heat flux transducer for measuring roof temperatures and heat flows.

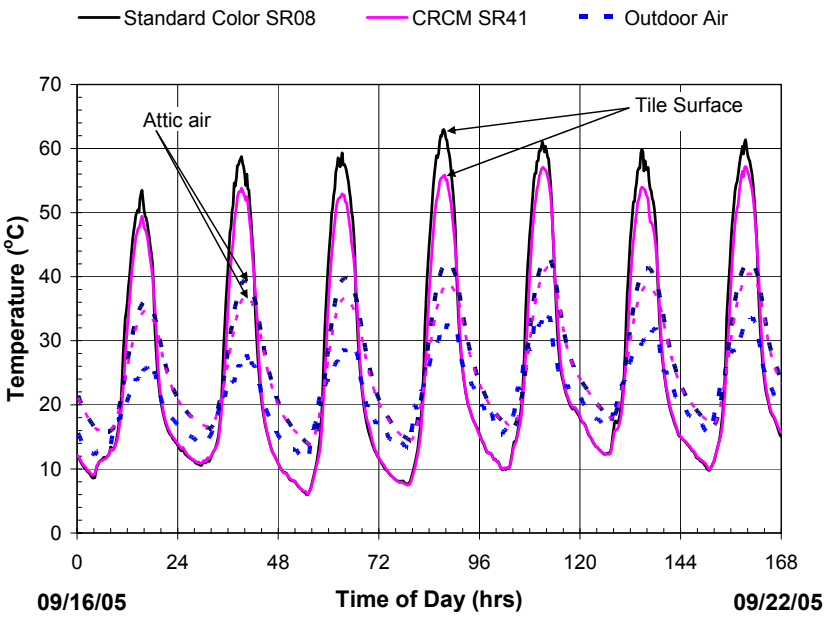

Figure 8. Surface and attic air temperatures for the pair of concrete tile roofs with and without CRCMs for a week of September 2005 data.

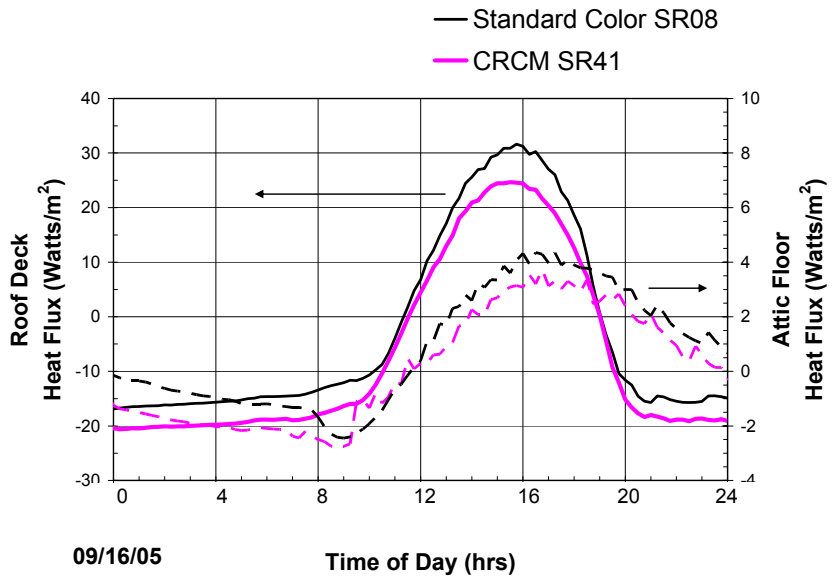

Figure 9. Heat flows penetrating the roof deck and attic floor of the pair of homes with concrete tile roofs with and without CRCMs.

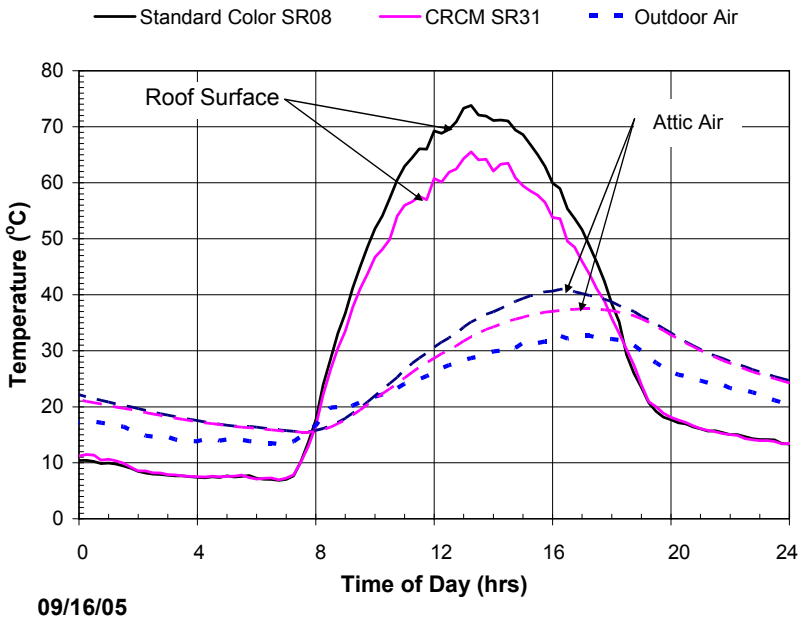

Figure 10. Surface and attic air temperatures for the pair of painted metal shake roofs with and without CRCMs for a week of September 2005 data.

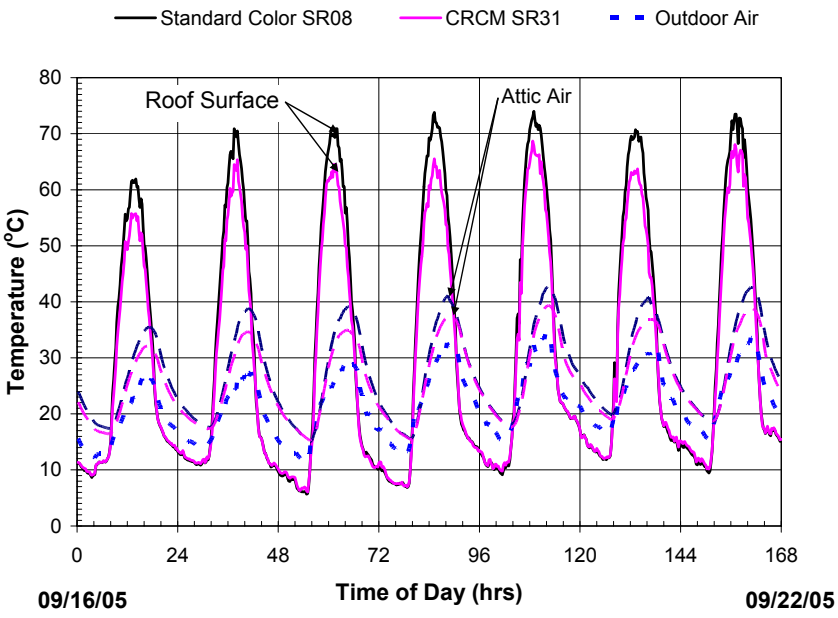

Figure 11 Heat flows penetrating the roof deck for the pair of homes with painted metal shake roofs with and without CRCMs.

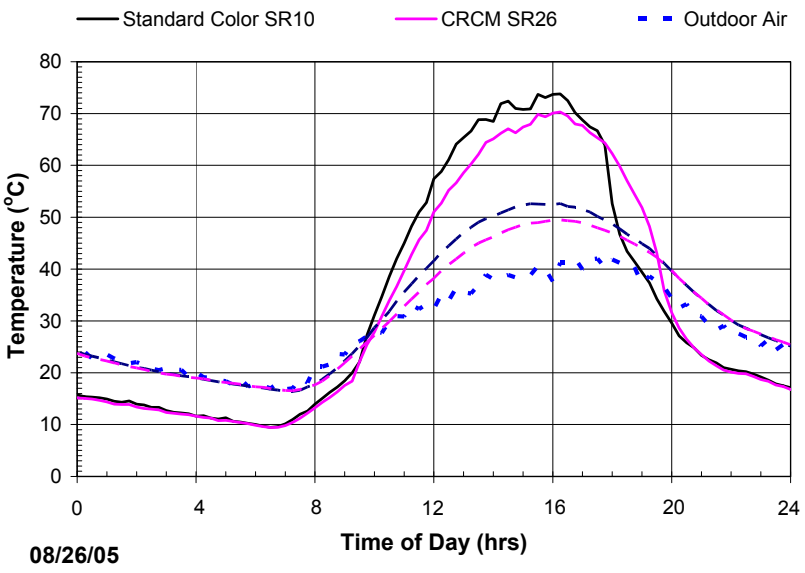

Figure 12. Surface and attic air temperatures for the pair of asphalt shingle roofs with and without CRCMs for a week of August 2005 data.

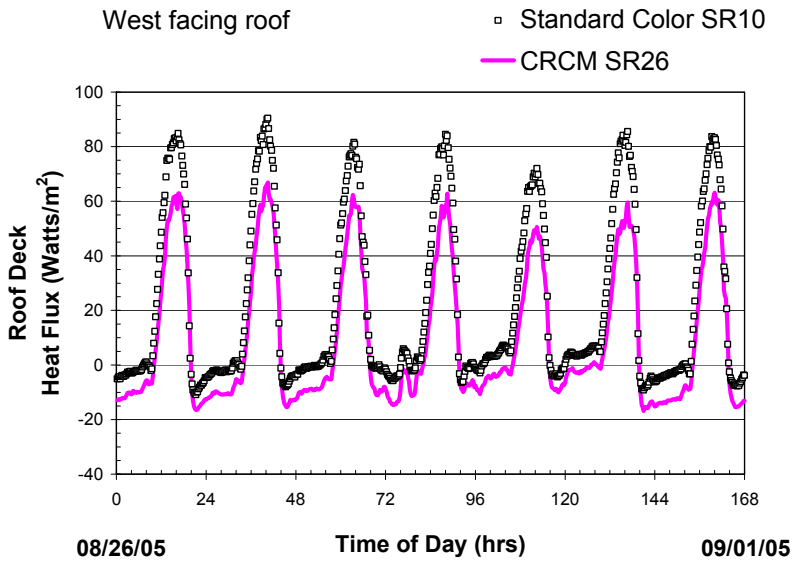

Figure 13 Heat flows penetrating the roof deck for the pair of homes with asphalt shingle roofs with and without CRCMs.

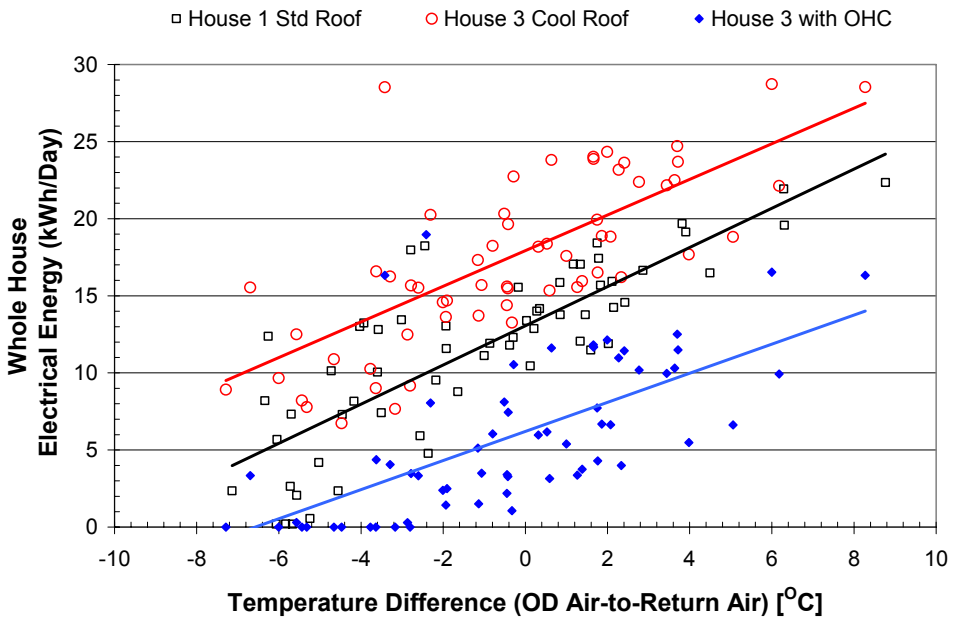

Figure 14. The whole house energy savings, measured during the daylight hours (May through July 2005), for demonstrations with concrete tile roofs with and without CRCMs.

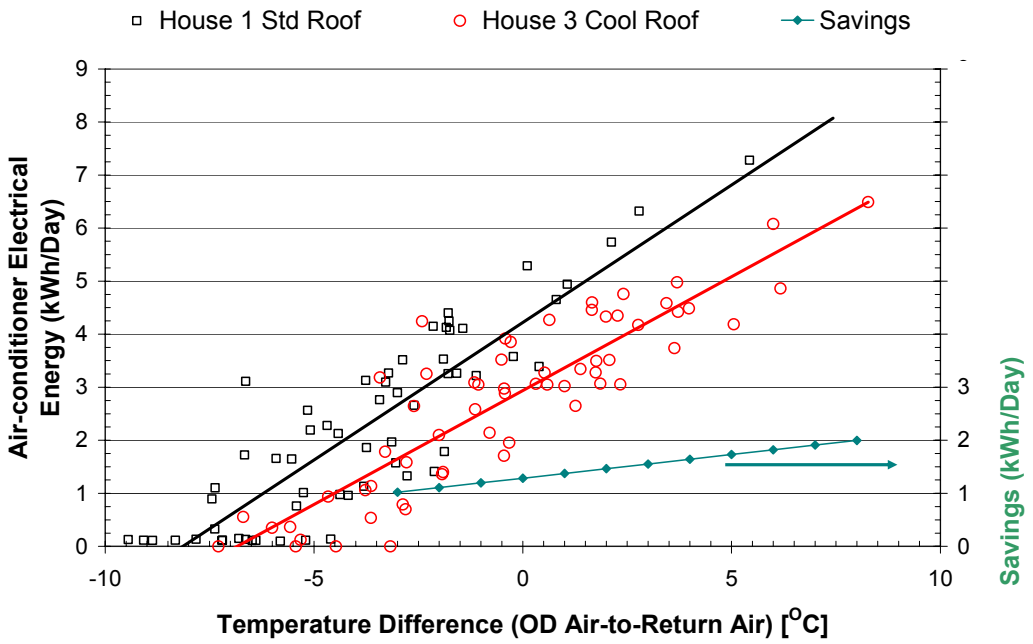

Figure 15. Air-conditioning cooling energy savings, measured during the daylight hours(May through July 2005), for demonstrations with concrete tile roofs with and without CRCMs.

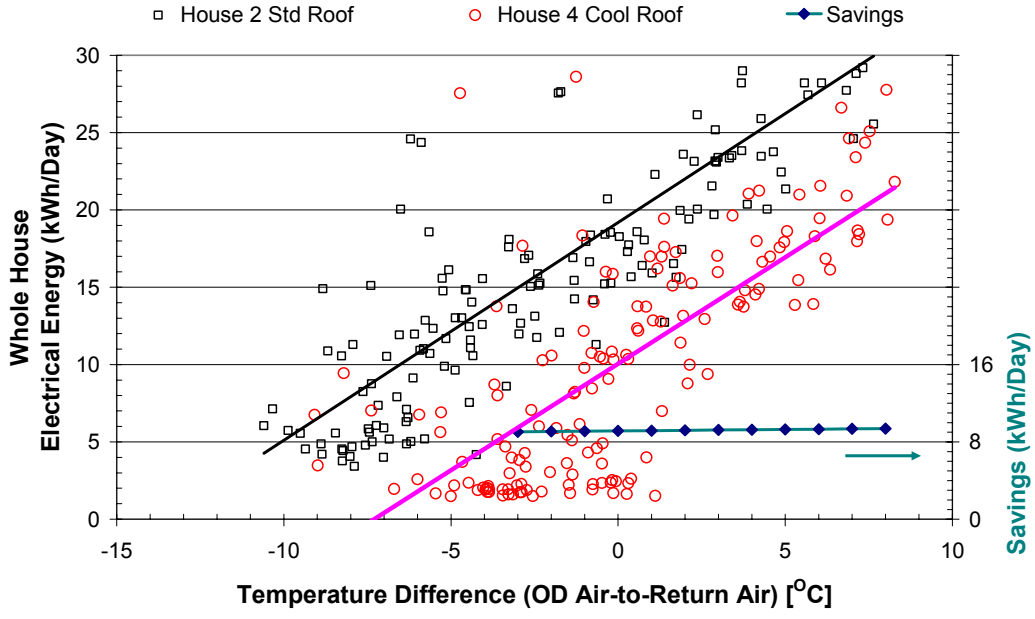

Figure 16. Whole house energy measured during the daylight hours (May through July 2005), for demonstrations with painted metal roof shakes with and without CRCMs.

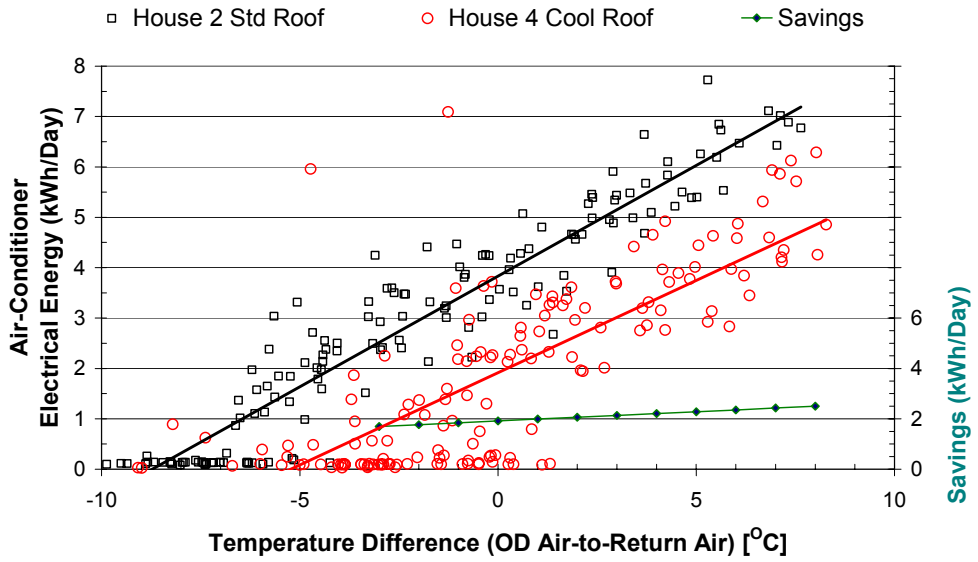

Figure 17. Air-conditioning cooling energy savings, measured during the daylight hours (May through July 2005), for demonstrations with painted metal roof shakes with and without CRCMs.

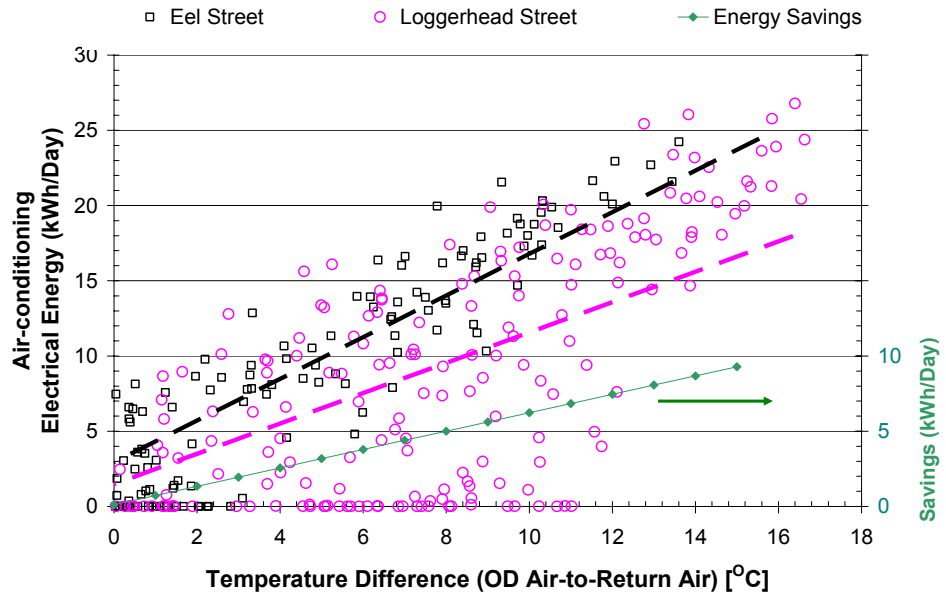

Figure 18. Air-conditioning cooling energy savings, measured during the daylight hours (May through July 2005), for demonstrations with asphalt shingle roofs with and without CRCMs.

MEMORANDUM OF UNDERSTANDING

HOMES IN SACRAMENTO, CA SUBDIVISION FOR DEMONSTRATING CRCM ROOFS AND ICF WALLS

Appendix A

This Memorandum of Understanding represents an agreement by Oak Ridge National Laboratory (ORNL), the Sacramento Municipal Utility District (SMUD) and Mike Evans Construction to cooperate in the development and testing of cool roof colored materials (CRCM).

Whereas, the California Energy Commission (CEC) has contracted the Lawrence Berkeley National Laboratory (LBNL) and the Oak Ridge National Laboratory (ORNL) to develop cool roof colored materials (CRCM) that are visibly dark but can reflect light like a "white" roof in the infrared portion of the solar energy spectrum.

Whereas, LBNL and ORNL are working with the tile, metal and asphalt-shingle roofing industries to accomplish the CEC goal of making CRCM a market reality for all residential roof products within the next five years.

Whereas, the CEC's objectives are 1) to offer consumers information that promotes the development and increased use of highly reflective CRCM and 2) to develop colored composition shingles with solar reflectance of at least 35% and tile and metal materials with reflectance of 50% or more.

Whereas, the Buildings Technology Center (BTC) of the ORNL intends, with support from the Sacramento Municipal Utility District (SMUD) and the cooperation of Mike Evans Construction to set up in March 2003 four residential demonstrations consisting of two pairs of single-family detached homes that have roofs of cool tile (supplied by Hanson Roof Tile) and painted metal materials (supplied by Custom-Bilt Metals) and about March 2004 two additional roofs with composition shingles once CRCM are developed for field-testing.

Whereas, SMUD 's Customer Advanced Technologies program is helping subsidize Evans Construction in exchange for acquiring thermal performance data of insulated concrete form (ICF) walls.

Whereas, it makes good sense to combine the efforts of the parties and work together to measure and document wall, roof and building performance for the 6 demonstration houses. We will instrument four homes during construction slated for March 2003, and will monitor the homes over a three-year period ending about March 2006. The two additional homes with composition shingles are contingent on the development of CRCM shingles.

Whereas, Table 1 lists all the instrument measurements currently proposed by ORNL and SMUD.

Therefore, the parties agree to undertake the activities described below or otherwise agreed in writing during the course of the demonstration project:

DEMONSTRATION HOMES

1. **Evans Construction** will make four demonstration houses available in 2003, and will make available two homes about March 2004 for the activities described below.

INSTRUMENTATION FOR EACH HOME

2. **ORNL** personnel shall make 4-ft by 4-ft sandwich test panels of the same material as used for the roof decks at the demonstration homes, probably oriented strand board (OSB). Each sandwich panel will be made of two sections equaling the same thickness as the rest of the deck. The two panels will sandwich thermocouples and a heat flux transducer for measuring thermal performance of the roofs. A spare thermocouple will be included for possibly measuring the surface temperature of the tile and metal roofs.

3. **Evans Construction** will notify ORNL of the start date for constructing the roof decks, and **ORNL** shall ship eight sandwich test panels to Evans Construction prior to the specified start date.

4. **ORNL** will contract **Dynamic Roofing** (or other firm specified by Evans Construction) to install the sandwich test panels as part of the deck for the test roofs. The north-south orientation of the homes makes it necessary to use two panels per house. The roofing contractor will center and attach one panel to the west-facing roof and center and attach the other to the east-facing roof.

5. **ORNL** personnel under the supervision of **Mike Evans Construction** shall instrument the attic for measuring the attic air temperature and relative humidity and the temperatures around the ceiling insulation as well as the ceiling heat flux. A temperature and relative humidity probe will be mounted in the return duct to measure the return air temperature and relative humidity from the house (see Table 1 for a listing of measurements).

6. SMUD will install two watt-hour meters and meter bases per house. One meter will measure total power consumption; the other will measure the power draw of the HVAC unit. The meters shall be configured with a pulse output device.

7. SMUD will run instrument wires from the two watt-hour meters to the DAS.

8. SMUD in conjunction with ORNL personnel will program the meters for the appropriate watt-hour pulse ratio. SMUD shall have the appropriate hardware and software to program the meters such as the Smartcoupler and MeterMate software used for the GE form 2S kWh-demand kV meter.

9. **ORNL** personnel shall install a pyranometer and an anamometer on the west facing and on the east facing roofs of each house in the vicinity of the heat flux transducers. The instruments have about a 3-in diameter and stand about 2-in off the roof. Instrument wires will be run down the roof and along the soffit to a data acquisition system (DAS).

DATA ACQUISITION SYSTEM

10. **ORNL** personnel under the supervision of Mike Evans Construction shall install a data acquisition system in each house and shall make all instrument connections to the DAS. The DAS can be placed in the attic, and shall have an extended temperature calibration range from -55°C to 85°C for possible attic placement. However, problems do occur even with the best DAS and placement in the garage or on an exterior wall behind the house would cause the least hassle for the technician and the least intrusion for the homeowner.

We will use a Campbell Scientific Model CR23X-4M micro-logger with model AM25T multiplexer for expanded channel capability. The DAS shall be in a NEMA 4 weatherproof and lockable enclosure. The DAS shall have 4 megabytes of extended memory, a phone modem, modem surge protector and rechargeable battery.

11. **ORNL** shall fully program the DAS and shall fully document the data acquisition code for use in later trouble shooting problems by ORNL, LBNL or SMUD personnel. Once operable, ORNL will forward the documentation to LBNL and SMUD.

12. SMUD will direct the phone service to run independent phone lines for hook up to each DAS for transmitting data by modem. These lines will be completely independent of the homeowner's phone system, and shall remain intact for the 3-year field demonstration.

13. SMUD will be responsible for conducting routine maintenance of the DAS systems, and shall support ORNL by trouble-shooting and making operable the DAS.

14. **ORNL** shall weekly check the data string output by the DAS received over the modem, and shall request SMUD to make appropriate corrections to reestablish power, reconnect phone lines or replace backup battery or the backup battery power supply. However, ORNL shall take responsibility for damage to the DAS and instruments, and will either reimburse SMUD for replacement of damaged equipment or ORNL will themselves make appropriate repairs with exception of the watt-hour meters.

AIR TIGHTNESS OF HOUSES

15. **ORNL** personnel under the coordination of Mike Evans Construction shall measure the air tightness of the demonstration homes using a Minneapolis Blower Door test apparatus. A Duct Blaster™ apparatus will be used to check the tightness of the air duct system. Both outside air infiltration and duct leakage will affect air conditioning performance, therefore we will attempt to make all homes about the same tightness. The air tightness of the house and ducting shall be checked after Evans has completed construction but before the homeowner occupies the homes.

16. **ONRL** also requests the opportunity to conduct the air tightness testing at conclusion of the three-year study, and will coordinate the testing with the homeowner.

ONSITE REFLECTANCE MEASURES

17. **ORNL** or **LBNL** personnel will visit the sites quarterly the first year and then semi-annually to measure the reflectance and emittance of the test roofs. The measures will require personnel to climb up a ladder to the roof and make the measurement, which will take only about 15 minutes.

THERMAL SCANS OF HOUSES

18. **ORNL** personnel request the opportunity to make thermal scans of the homes to judge the relative effectiveness of the roofing systems once the homes are built and occupied. As the roof systems age the thermal scans will help document the overall thermal performance of the roof as compared to their starting performance. The scans are taken outside the home and will be conducted yearly.

VISITATION

19. In case of maintenance, repair, routine checks etc, **ORNL** and **SMUD** personnel will coordinate through Evans Construction or the homeowners the permission to egress said property. The homeowners shall allow visitation privileges to ORNL, LBNL or SMUD. However personnel shall schedule visits amenable with the homeowner prior to the actual visit. Visits will be limited to routine maintenance checks and if necessary unscheduled checks to trouble-shoot instruments and or the DAS.

20. At completion of the three-year study **ORNL** will remove the DAS, instruments and wires with exception of those embedded in the roof deck.

CONTACTS

ORNL Building Envelope Group

Andre Desjarlais, Group Leader

Phone: 865-574-0022
FAX: 865-574-9354
E-mail: desjarlaisa@ornl.gov

Sacramento Municipal Utility District

***David Bisbee**, Adv. Technology*

Phone: 916-732-6409
FAX: 916-732-6890
E-mail: dbisbee@smud.org

Evans Construction Company

***Mike Evans**, Owner/Manager*

Phone: 916-939-1854
FAX: 916-939-3419
Email: evansconst@d-web.com

MEMORANDUM OF UNDERSTANDING

DEMONSTRATION OF STANDARD PRODUCTION ASPHALT SHINGLES AND ADVANCED SHINGLES HAVING COOL ROOF COLOR MATERIALS ON HOMES IN REDDING, CA

Appendix B

This Memorandum of Understanding represents an agreement by Oak Ridge National Laboratory (ORNL), the Elk Corporation and *Ochoa and Shehan Inc, a residential construction firm in Redding, CA* to cooperate in the field testing and demonstration of cool roof colored materials (CRCM).

Whereas, the California Energy Commission (CEC) has contracted the Lawrence Berkeley National Laboratory (LBNL) and the Oak Ridge National Laboratory (ORNL) to develop cool roof colored materials (CRCM) that are visibly dark but can reflect light like a "white" roof in the infrared portion of the solar energy spectrum.

LBNL and ORNL are working with the tile, metal and asphalt-shingle roofing industries to accomplish the CEC goal of making CRCM a market reality for all residential roof products within the next five years.

Whereas, the CEC's objectives are 1) to offer consumers information that promotes the development and increased use of highly reflective CRCM and 2) to develop colored composition shingles with solar reflectance of at least 25% and tile and metal materials with reflectance of 50% or more.

Whereas, the Building Envelope Group of the ORNL intends, with support from the Elk Corp. and the cooperation of *Ochoa and Shehan* Construction to set up and monitor for two years (starting Jan 1, 2005 and ending Dec 31, 2006) two residential demonstrations consisting of a pair of single-family detached homes that have composition shingle roofs with and without cool roof color materials.

Whereas, Elk is providing asphalt shingles at no cost for *Ochoa and Shehan* Construction to install on two homes in Redding CA in exchange for acquiring temperature, heat flow and power measurements for the two homes over the course of the two year field study.

ORNL personnel will instrument the two homes during construction slated for November 2004, and will monitor the homes over a two-year period ending Dec 31, 2006.

Whereas, Table 1 lists all the instrument measurements currently proposed by ORNL and Elk

Therefore, the parties agree to undertake the activities described below or otherwise agreed in writing during the course of the demonstration project:

DEMONSTRATION HOMES

1. **Ochoa and Shehan Construction** will make two demonstration houses available in 2004 for the field testing demonstrations described below.

INSTRUMENTATION FOR EACH HOME

2. **ORNL** personnel shall make 2-ft by 2-ft sandwich test panels of the same material as used for the roof decks at the demonstration homes, probably oriented strand board (OSB). Each sandwich panel will be made of two sections equaling the same thickness as the rest of the deck. The two panels will sandwich thermocouples and a heat flux transducer for measuring thermal performance of the roofs. A spare thermocouple will be included for possibly measuring the surface temperature of the shingle roofs.

3. ***Ochoa and Shehan* Construction** will notify ORNL of the start date for constructing the roof decks, and **ORNL** shall ship sandwich test panels to *Ochoa and Shehan* Construction prior to the specified start date.

4. **ORNL** will contract *Ochoa and Shehan* Construction to install the sandwich test panels as part of the deck for the test roofs. The orientation of the homes makes it necessary to use two panels per house.The roofing contractor will center and attach one panel to preferably a south-facing roof and center and attach the other to preferably the north-facing roof.

5. **ORNL** personnel under the supervision of *Ochoa and Shehan* Construction shall instrument the attic for measuring the attic air temperature and relative humidity and the temperatures around the ceiling insulation as well as the ceiling heat flux. A temperature and relative humidity probe will be mounted in the return duct to measure the return air temperature and relative humidity from the house (see Table 1 for a listing of measurements).

6. **ORNL** personnel under the supervision of *Ochoa and Shehan* Construction will install two Model WNA-1P-240-P Wattnode transducers for measuring the power draws of the two HVAC units. The meters shall be housed in weatherproof NEMA enclosures and placed on an exterior wall near the power panel for each home.

7. **ORNL** personnel shall install two pyranometers, one on the south facing roof and the other on the north facing roof of each house in an inconspicuous place near the roof ridge. The instruments have about a 3-in diameter and stand about 2-in off the roof. Instrument wires will be hidden by running them through the ridge or louvered vents into the attic and down inside an exterior wall to a data acquisition system (DAS) housed in a white plastic NEMA enclosure.

DATA ACQUISITION SYSTEM

8. **ORNL** personnel under the supervision of *Ochoa and Shehan* Construction shall install a data acquisition system on an exterior wall of each house (near the power panel) and shall make all instrument connections to the DAS. Placement of the DAS in the attic is not encouraged because problems do occur even with the best DAS and placement on an exterior wall near the power panel would cause the least hassle for the technician and the least intrusion for the homeowner.

   We will use a Campbell Scientific Model CR10X-2M micro-logger with model AM25T multiplexer for expanded channel capability. The DAS shall be in a NEMA 4 weatherproof and lockable enclosure. The DAS shall have 2 megabytes of extended memory, a phone modem, modem surge protector and rechargeable battery. The battery requires a 115 Vac source and therefore ORNL requests the DAS be placed near the power panel for obtaining the necessary instrument power. *Ochoa and Shehan* shall provide an independent phone line for communicating with the DAS.

9. **ORNL** shall fully program the DAS and shall fully document the data acquisition code for use in later trouble shooting problems by ORNL or LBNL personnel.

10. **ORNL** with support from *Ochoa and Shehan* will direct the phone service to run independent phone lines for hook up to each DAS for transmitting data by modem. These lines will be completely independent of the homeowner's phone system, and shall remain intact for the 2-year field demonstration. ORNL shall pay monthly charges incurred by *Ochoa and Shehan* Construction for the phone service to each data logger.

11. **ORNL** shall weekly check the data string output by the DAS received over the modem, and shall take responsibility for damage to the DAS and instruments, and will themselves make appropriate repairs.

AIR TIGHTNESS OF HOUSES (OPTIONAL-DEPENDENT UPON PERMISSION OF HOMEOWNER)

12. **ORNL** under the coordination of *Ochoa and Shehan* Construction and the homeowners shall have the option to measure the air tightness of the demonstration homes using a Minneapolis Blower Door test apparatus. A Duct Blaster™ apparatus will be used to check the tightness of the air duct system. Both outside air infiltration and duct leakage will affect air conditioning performance therefore we will attempt to document the tightness of the two homes. The air tightness of the house and ducting shall be checked after *Ochoa and Shehan* has completed construction but before the homeowner occupies the homes.

13. **ONRL** also requests the opportunity to conduct the air tightness testing at conclusion of the two-year study, and will coordinate the testing per the approval of the homeowner.

ONSITE REFLECTANCE MEASURES

14. **ORNL, LBNL** or Elk personnel will visit the site semiannually to measure the reflectance of the test roofs. The measures will require personnel to climb up a ladder to the roof and make the measurement, which will take only about 15 minutes.

THERMAL SCANS OF HOUSES

15. **ORNL** personnel request the opportunity to make thermal scans of the homes to judge the relative effectiveness of the roofing systems once the homes are built and occupied. As the roof systems age the thermal scans will help document the overall thermal performance of the roof as compared to their starting performance. The scans are taken outside the home and will be conducted yearly.

COMPOSITION SHINGLE RETRIEVAL

16. **ELK** personnel request the opportunity to remove and replace one possibly as many as three shingles from the roof facing the back of each home on an annual basis. Elk will take the field exposed shingles and conduct chemical and mechanical (tensile and flexural) testing to check for changes in the chemical and physical properties of the two different types of shingles. Elk will conduct a Corbett fractionation procedure to show the molecular size of hydrocarbon fractions and will also conduct gel permeation chromatography to show the %weight distribution. Both tests will confirm the loss of naphthenes aromatic oils and the gain of asphaltenes. Results will help confirm that the new shingles with CRCMs perform in a consistent manner with existing standard

production shingles. Appropriate data shall be shared with ORNL for support of the CEC work contracted to ORNL and LBNL.

VISITATION

17. The homeowners shall agree to allow visitation privileges to ORNL, LBNL or ELK personnel in case of maintenance, repair, routine checks of instruments or the DAS. However, all visits will be coordinated through Ochoa and Shehan Construction or the homeowner's permission to egress said property. Therefore personnel shall schedule visits amenable with the homeowner prior to the actual visit. Visits will be limited to field acquisition and or checks to trouble-shoot instruments and or the DAS.

18. At completion of the two-year study **ORNL** will remove the DAS, instruments and wires with exception of those embedded in the roof deck.

CONTACTS

ORNL Building Envelope Group	ELK Group, Inc.	Ochoa and Shehan Construction Company
Andre Desjarlais, Group Leader	**John McCaskill** Product Brand Manager	**Jerry Wagar** Principal Owner
Signature:	Signature:	Signature:
Phone: 865-574-0022 FAX: 865-574-9354 E-mail: desjarlaisa@ornl.gov	Phone: 972-851-0477 FAX: 972-851-0436 E-mail: john.mccaskill@ElkCorp.com	Phone: 530-221-0527 FAX: 530-221-0544 Email: JWagar@OchoaandShehan.com

Appendix C

Table C.1. Instruments specified for measuring the building envelope thermal performance of each house.

INSTRUMENT	*Description*	Location	Attachment	Channel	
South Facing Roof					
Thermocouple (Type T Cu/Con)	26 AWG Unshielded bead	Spare for Roof Surface	Epoxy	8 T	
"	26 AWG Unshielded bead	Deck	Taped	7 T	
"	26 AWG Unshielded bead	In Deck	Embedded between OSBs	6 T	
Heat Flux Transducer	2-in by 2-in by 0.125-in thick	In Deck	Embedded between OSBs	2 Rd^{+}	
Pyranometer Li-Cor	Solar Probe	Near ridge at roof gable	Mounting bracket	4	
Thermocouple (Type T Cu/Con)	26 AWG Unshielded bead	Deck underside	Taped	5 T	
North Facing Roof					
Thermocouple (Type T Cu/Con)	26 AWG Unshielded bead	Spare for Roof Surface	Loctite Epoxy	4 T	
"	26 AWG Unshielded bead	Deck	Taped	3 T	
"	26 AWG Unshielded bead	In Deck	Embedded between OSBs	2 T	
Heat Flux Transducer	2-in by 2-in by 1/8-in thick	In Deck	Embedded between OSBs	1 Rd^{+}	
Pyranometer Li-Cor	Solar Probe	Near ridge at roof gable	Mounting bracket	5	
Thermocouple (Type T Cu/Con)	26 AWG Unshielded bead	Deck underside	Taped	1 T	
Attic interior					
Vaisala 50Y	DB & RH Probe	Attic air 4-ft above insulation	Run along support wire	6	
Thermocouple (Type T Cu/Con)	26 AWG Shielded bead	Top of insulation	Laid atop insulation	10 T	
	26 AWG Unshielded bead	Sheet rock surface facing attic	Taped	9 T	
Heat Flux Transducer	2-in by 2-in by 1/8-in thick	Sheet rock surface facing attic	Sandwiched between insulation and sheet rock	3 Rd^{+}	
House exterior above ridge vent (Not Applicable)					
Vaisala 50Y	DB & RH Probe	Ambient air 3-ft above roof	Mounting bracket	NA	
Anemometer	Wind velocity	Ambient air 3-ft above roof	Mounting bracket	NA	
Wind Vane	Wind direction	Ambient air 3-ft above roof	Mounting bracket	NA	
House interior					
Vaisala 50Y	DB & RH Probe	Entering return grill	Duct mounted	7	
Thermocouple (Type T Cu/Con)	26 AWG Unshielded bead	Leaving evaporator coil	Run along support wire	11 T	
Wattnode transducer	Model WNA-1P-240-P	HVAC Power	NEMA enclosure on exterior wall	8	———
Wattnode transducer	Model WNA-1P-240-P	HVAC Power	NEMA enclosure on exterior wall	9	———

Arnold Schwarzenegger
Governor

COOL-COLOR ROOFING MATERIAL ATTACHMENT 8: TASK 2.6.2 REPORTS - MATERIALS TESTING AT WEATHERING FARMS IN CALIFORNIA

PIER FINAL PROJECT REPORT

Prepared For:
California Energy Commission
Public Interest Energy Research Program

Prepared By:
Lawrence Berkeley National Laboratory and Oak Ridge National Laboratory

ERNEST ORLANDO LAWRENCE
BERKELEY NATIONAL LABORATORY

June 2006
CEC-500-2006-067-AT8

Prepared By:
Lawrence Berkeley National Laboratory
Hashem Akbari
Berkeley, California
Contract No. 500-01-021

Oak Ridge National Laboratory
William Miller
Oak Ridge, Tennessee

Prepared For:
California Energy Commission
Public Interest Energy Research (PIER) Program

Chris Scruton
Contract Manager

Ann Peterson
Building End-Use Energy Efficiency Team Leader

Nancy Jenkins
PIER Energy Efficiency Research Office Manager

Martha Krebs, Ph.D.
Deputy Director
ENERGY RESEARCH AND DEVELOPMENT DIVISION

B. B. Blevins
Executive Director

DISCLAIMER

This report was prepared as the result of work sponsored by the California Energy Commission. It does not necessarily represent the views of the Energy Commission, its employees or the State of California. The Energy Commission, the State of California, its employees, contractors and subcontractors make no warrant, express or implied, and assume no legal liability for the information in this report; nor does any party represent that the uses of this information will not infringe upon privately owned rights. This report has not been approved or disapproved by the California Energy Commission nor has the California Energy Commission passed upon the accuracy or adequacy of the information in this report.

Composition and Effects of Atmospheric Particles on the Performance of Steep-Slope Roofing Materials

Meng-Dawn Cheng* and William A. Miller
Oak Ridge National Laboratory
PO Box 2008
Oak Ridge, TN 37831

and

Paul Berdahl and Hashem Akbari
Lawrence Berkeley National Laboratory
Berkeley, CA 94720

Susan Pfiffner
University of Tennessee, Center for Biomarker Analysis, Knoxville, TN 37916

ABSTRACT

Novel cool color pigments have been developed that are dark in color but weakly absorbing and sometimes strongly scattering in the near infrared portion of the solar spectrum. The high near infrared reflectance of coatings colored with these "cool" pigments is being exploited to manufacture roofing materials that reflect more sunlight than conventional roofing products. The cool pigments result in lower roof surface temperature, which in turn reduces the building's cooling-energy demand. However, determining how weathering affects the solar reflectance and thermal emittance of cool pigmented roofs is of paramount importance for proving sustained thermal performance and thereby accelerating their market penetration in both residential and commercial applications.

Airborne particulate matter that settles on a roof can either reflect or absorb incoming solar radiation, dependent on the chemical content and size of the particles. These light scattering and absorption processes occur within a few microns of the surface, and can affect the solar reflectance of the roof. The long-term change in reflectance appears driven by the ability of the particulate matter to cling to the roof and resist being washed off by wind and or rain. Contaminants collected from samples of roof products exposed at seven California weathering sites were analyzed for elements and types of carbon to characterize the chemical profile of the particles soiling each roof sample and to identify those elements that degrade or enhance solar reflectance. The chemical composition of particles deposited on the roof samples was very similar across California; there was no clear distinction from one region to another. Organic and elemental carbon was detected; however, the amount of elemental carbon was too small to contribute significantly to the loss of solar reflectance. Dust particles (characterized by Ca and Fe) and organic carbon caused a loss of solar reflectance of highly reflective substrates and an increase in reflectance of dark materials.

INTRODUCTION

The long-term benefits of cool pigmented roofing systems (Akbari et al. 2004) can be compromised if a significant loss in solar reflectance occurs during the first few years of service life. Ultraviolet radiation, atmospheric pollution, microbial growths, acid rain, temperature cycling caused by sunlight and sudden thunderstorms, moisture penetration, condensation, wind, hail, and freezing and thawing are all thought to contribute to the loss of a roof's solar

reflectance. Wilkes et al. (2000) completed the testing of 24 different roof coatings on a low-slope test stand and observed about a 25% decrease[1] in the solar reflectance of white-coated and aluminum-coated surfaces as the time of exposure increased; however, the decrease leveled off after 2 years. SPRI Inc. and its affiliates studied the effect of climatic exposure on the surface properties of white thermoplastic single-ply membranes and determined that membranes lose from 30 to 50% of their reflectance over 3 years (Miller et al. 2002). The CMRC and its affiliates AISI, NamZAC, MBMA, MCA and NCCA exposed unpainted and painted metal roofing on both steep- and low-slope test roofs and found that after 3½ years, the painted polyvinylidene fluoride (PVDF) metal roofs lost less than 5% of their original reflectance (Miller et al. 2004). The results of the three different weathering studies are very interesting in terms of their solar reflectance after 3½ years of exposure. The white thermoplastic membrane and white ceramic coating with white topcoat had original reflectance measures that were about 20 percentage points higher than the painted metal; however, after 3-years of field exposure the solar reflectance of the painted metal exceeds that of the thermoplastic membrane and equals that of the coating.

Miller et al. (2002) discovered that aerosol deposition introduced biomass of complex microbial consortia onto the test roofs and the combination of contaminants and biomass accelerated the loss of solar reflectance for the thermoplastic membranes and the roof coatings. Airborne contaminants and biomass were also detected on the painted metal roofs; however, as stated the loss of solar reflectance was less than 5% for the painted metal roofs (Fig. 1). The chemistry of the PVDF paint resin system uses similar organic film bonding to that responsible for Teflon®, making it extremely chemical resistant and dirt shedding. Miller and Rudolph (2003) found the PVDF painted metals maintained solar reflectance even after 30 years of climatic exposure. Therefore the reduction of roof reflectance is closely related to the composition of the roof and to the chemical profile of the contaminants soiling the roof. Field data suggests that the loss of reflectance is due to dust load and or biomass accumulation, which in turn is affected by the climatic conditions. Biomass may be due to the growth of fungi and/or mold species that were transported by airborne particulate matter blown by the wind. Deposition of atmospheric carbon, nitrogen, and moisture accumulation on the roof provide suitable conditions for the colonization of these microbes.

Results published by Berdahl et al. (2002) indicate that the "the long-term change of solar reflectance appears to be determined by the ability of deposited soot to adhere to the roof, resisting washout by rain." Samples studied were bare metal and PVC roofing weathered for 18 years. Berdahl attributed soot, black carbon, and/or elemental carbon to be the primary cause of long-term reflectance loss. However, atmospheric particles are a class of complex mixtures consisting of directly emitted particles such as dusts from road traffics and particles from utility power plant emissions, and indirectly produced particles such as smog that are formed in the atmosphere through photochemical reactions. Deposition of any or all of these particles could cause changes in roof reflectance in addition to soot particles.

A reduction in solar reflectance of a substrate generally requires the presence of light absorbing particles. While soot containing elemental carbon (EC) is an important broadband absorber, two other potentially important absorbers are organic carbon (OC) and iron-containing minerals such as hematite. Organic carbon consists of hydrocarbon substances from combustion, carbon in the form of biomass, and possibly other substances. It is expected to absorb mainly in the short wave part of the visible spectrum (400 - 550 nm) (Kirchstetter et al., 2004). It also

[1] Percentage drops are based on fractional reductions by the formula: $100. * \left(\rho_{initial} - \rho_{aged}\right) / \rho_{initial}$

absorbs in the ultraviolet (UV) range but usually would not reduce the UV reflectance because the typical substrate is also UV absorbing. Hematite also absorbs in the short wave part of the visible range. Thus, hematite rust is reddish in color, due to non-absorbed red light. The details of the hematite absorption (Levinson et al., 2005) are, however, different from OC. It also absorbs in a band in the near infrared (800-900 nm).

An increase in solar reflectance requires the addition of light-scattering particles. For example, a white powder increases the reflectance of a black or gray substrate. The ability of a particle to scatter light is proportional to $(n_{pl}-n_o)^2$, where n_{pl} is the real refractive index of the particle and n_o is the refractive index of the surrounding medium. Many minerals and organic substances have refractive indices in the range of [1.3, 1.8] and therefore in air ($n_o = 1$) cause light scattering. Hematite has quite a high refractive index (~3, Wong and Brus, 2001) and therefore can contribute strongly to light scattering at wavelengths greater than 550 nm.

Suppose a substrate has a clean reflectance denoted R_o, which is coated with a thin soil layer with absorptance a and reflectance r. In view of the assumption that the layer is thin, we take both a and r as small compared to unity. Then, it is not difficult to show that the change in reflectance R of the soiled substrate is given, to first order in r and a, by $R - R_o = -2\,R_o\,a + (1-R_o)^2\,r$. Thus soil absorptance reduces R and soil reflectance increases R. Here we can also see that a will be less important if R_o is small and r will be less important if R_o is close to unity. Anticipating the data to come, we can hypothesize that highly reflective materials tend to lose their reflectance as they are soiled, with the reflectance loss determined by absorption of the soil. Very dark materials tend to become lighter as they are soiled, with the reflectance increase caused by light scattering by soil. It is plausible that the aged solar reflectance of roofs is affected by many factors including atmospheric deposition of soot particles and dusts (e.g., dirt, road dust, and soil particles). To study the issues further, characterization of the chemical and physical attributes of the deposited particles was conducted in the diverse climates of California.

Southern California is densely populated and known for its high volume of almost continuous traffic and emissions. The region is generally low in humidity with certain regions like El Centro having less than 3-in of annual precipitation, therefore making the area an excellent site for studying solar reflectance loss due to dusts and soot. Sufficient moisture is a major environmental condition needed for the growth of microbes such as mold and fungi, which can potentially reduce light reflectance. Under a dry climate, the microbial factor is lessened enabling the field study to focus more on the impacts of physical and chemical factors of aerosols.

The objectives of this study are (1) document the drop in solar reflectance and the change in thermal emittance for roof products having cool color pigments, (2) characterize the particulate matter deposited on roof samples of different materials, (3) establish the relationship between the deposited particulate matter and reduction of solar reflectance, and (4) quantify the contributions of the chemical composition of the particulate matter on the enhancement or loss of solar reflectance on a roof material.

WEATHERING SITES IN CALIFORNIA

Seven sites were selected for exposing painted metal, clay and concrete tile roof products with and without cool color pigments in the diverse climates of California (Table 1). Custom-Bilt Metal, Steelscape, BASF, MonierLifetile, US Tile, Maruhachi Ceramics of America, the Shepherd Color Company, American Rooftile Coatings and Elk Corporation supported the initiative by either field testing roof samples at their respective manufacturing facilities (Table 1) and/or by providing roof products for natural exposure testing. The California population is

expanding rapidly in the Central Valley and around the LA basin, and the sites with Custom-Bilt (Sacramento) and Elk (Shafter) capture the effects of weather, urban pollution and the expanding population. These areas reflect a market with many new homes. Weathering sites with Steelscape, BASF and Maruhachi Ceramics of America are located in existing densely populated areas of San Francisco basin and LA, and represent the market for re-roofing existing homes. Samples were also exposed near weather stations maintained by the California Irrigation Management Information System (CIMIS). Sites in McArthur and El Centro, CA. were selected for acquiring exposure data in the more extreme climates. McArthur is located in the moderate alpine climate of northern California (climate zone 16); El Centro is in the extremely hot desert climate of southern California bordering the Arizona state line (climate zone 15).

The CIMIS web site http://www.cimis.water.ca.gov/ has current weather data that can help estimate through regression analysis the loss of solar reflectance as affected by the climatic elements. In fact, CIMIS has 118 computerized weather stations acquiring hourly, daily, weekly and/or monthly solar irradiance, ambient air temperature and relative humidity as well as wind speed, wind direction and precipitation; Table 2 locates each weathering site and provides the closest CIMIS station to each weathering site. Solar reflectance (SR) of the new and aged samples is also provided for the different samples used for elemental contaminant and also for biomass determinations.

Exposure Racks

All roof samples were installed in exposure rack assemblies, which are 5.5-ft high by 9-ft long, and divided into three sub-frames having respective slopes of 2-, 4- and 8-in of rise for 12-in of run (i.e., slopes of 9.5°, 18.4° and 33.7°). Each sub-frame can hold two "Sure-Grip" sub-assemblies, which are designed to have 6 rows of samples with 34-in of usable space in each row. Sample size is 3.5-in by 3.5-in, a size that LBNL's Perkin-Elmer Lambda 900 spectrophotometer can easily accommodate for measuring the solar reflectance at discrete wavelengths. Finally all exposure rack assemblies were oriented facing south for full exposure to natural sunlight and weathering (Fig. 2).

Table 1. Weathering Sites for exposing roof products with and without cool color pigments.

Company	Contact	City	County	Climate Zone	Roof or Ground Mount
Department of Water Resources CIMIS	Sergio Fierro	El Centro (RS01)	Imperial	15	Ground
Maruhachi Ceramics of America	Yoshihiro Suzuki	Corona (RS02)	Riverside	10	Ground
BASF	Michelle Vondran	Colton (RS03)	San Bernadino	10	Roof
ELK Corporation	Gus Freshwater	Shafter (RS04)	Kern	13	Ground
Steelscape	Bruce Hopkins	Richmond (RS05)	Contra Costa	3	Roof
Custom-Bilt	Dan Bonnington	Sacramento (RS06)	Sacramento	12	Roof
Department of Water Resources CIMIS	Jamie Dubay	McArthur (RS07)	Shasta	16	Ground

Table 2. Identification of Coupons, location nearest CIMIS Station and solar reflectance data..

	El Centro (RS01)	Corona (RS02)	Colton (RS03)	Shafter (RS04)	Richmond (RS05)	Sacramento (RS06)	McArthur (RS07)
CIMIS Site[1]	87	44	44	5	157	131 & 155	43
Latitude	32°48'24"N	33°57'54"N	33°57'54"N	35°31'59"N	37°59'30"N	38°35'58"N	41°03'53"N
Longitude	115°26'46"W	117°20'08"W	117°20'08"W	119°16'52"W	122°28'12"W	121°32'25"W	121°27'16"W
Samples for Element Study	Gray Artic concrete tile	Gray Artic concrete tile	PVDF Metal Charcoal Gray	PVDF Metal Rawhide	PVDF Metal Rawhide	Gray Artic concrete tile	PVDF Metal Rawhide
Sample ID	976	676	517,518,519	704, 705, 706, 707	404,406	378	805,806
Sample Area (m^2)	7.903E-03	7.903E-03	2.371E-02	3.161E-02	1.581E-02	7.903E-03	1.581E-02
SR initial	0.27	0.25	0.31	0.57	0.57	0.27	0.57
SR after 1.63 yrs	0.28	0.23	0.30	0.52	0.55	0.25	0.55
Samples for Biomass Study	PVDF Metal Hartford Green	PVDF Metal Charcoal Gray	Gray Artic concrete tile	Buff Blend Clay tile	PVDF Metal Rawhide	Brown Artic concrete tile	PVDF Metal Rawhide
Sample ID	920, 921, 922, 923	616	576	779,780	405	372	804,807
Sample Area (m^2)	3.161E-02	7.903E-03	7.903E-03	1.581E-02	7.903E-03	7.903E-03	1.581E-02
SR initial	0.27	0.31	0.25	0.53	0.57	0.26	0.57
SR after 1.63 yrs	0.28	0.30	0.24	0.48	0.54	0.25	0.55
	[1] http://wwwcimis.water.ca.gov/cimis/welcome.jsp						

Solar Reflectance (SR) and Thermal Emittance (TE) Instruments

A Device and Services solar spectrum reflectometer was used to measure the solar reflectance (total hemispherical reflectance over spectrum of sun's energy) of the roof samples. The device uses a tungsten halogen lamp to diffusely illuminate a sample. Four detectors, each fitted with differently colored filters, measure the reflected light in different wavelength ranges. The four signals are weighted in appropriate proportions to yield the total hemispherical reflectance. The device was proven accurate to within ±0.003 units (Petrie et al. 2000) through validation against the ASTM E-903 method (ASTM 1996). However, because the CRCMs exhibit high infrared reflectance, some of the field samples were also measured at LBNL using a spectrometer to check the portable reflectometer. The average absolute difference between the Device and Services reflectometer and the spectrometer was about 0.02 points of reflectance with the spectrometer consistently reading lower than the reflectometer (as example, the reflectometer measured a solar reflectance of 0.741 for a IR painted metal while the spectrometer measured 0.73).

The impact of emittance on roof temperature is as important as that of reflectance. A portable Device and Services emissometer was used to measure the thermal emittance using the procedures in ASTM C-1371 (ASTM 1997). The device has a thermopile radiation detector, which is heated to 82.2°C (180°F). The detector has two high-ε and two low-ε elements and is designed to respond only to radiation heat transfer between itself and the sample. Because the device is comparative between the high-ε and the low-ε elements, it must be calibrated in situ using two standards, one having an emittance of 0.89, the other having an emittance of 0.06. Kollie, Weaver, and McElroy (1990) verified the instrument's precision as ±0.008 units and its accuracy as ±0.014 units in controlled laboratory conditions.

SOLAR REFLECTANCE AND THERMAL EMITTANCE

The solar reflectance and the thermal emittance of a roof surface are important surface properties affecting the temperature of a roof which, in turn, drives the heat flow across the roof. Akbari and Konopacki (1998) and Miller et al. (2004) showed that in moderate to predominantly hot climates, an exterior roof surface with a high solar reflectance and high infrared emittance will reduce the exterior temperature and produce savings in comfort cooling. For predominantly heating-load climates, surfaces with moderate reflectance but low infrared emittance save in comfort heating. Determining the affects of climatic soiling on the solar reflectance and infrared emittance of cool color roofs is therefore very important for developing realistic claims of the net energy savings (cooling energy savings less heating penalty).

Coupons of concrete and clay tile and painted metal roof samples were exposed to the elements in six of California's sixteen climate zones. The tabulation of the solar reflectance data for the seven weathering sites is provided in Appendix A. Contaminant samples were collected after 1.6 years of exposure for the coupons identified in Table 2, and the measures of solar reflectance and thermal emittance are reported herein for the Table 2 coupons to view the time dependence of climatic soiling and later, in the contaminants section, the impact of the various contaminants on the loss of solar reflectance.

Affects of Soiling on Solar Reflectance and Thermal Emittance

The painted PVDF coupon having an off-white color (Rawhide) steadily lost solar reflectance over the first year of exposure (Fig. 3). The loss varied from site to site with the least drop observed at McArthur (4%[1] after one year) and the worst occurring in the more desert-like areas of Shafter and Colton (23% after one year). The exposure rack in Colton is roof-mounted while the one in Shafter is ground mounted (Table 1), yet the change in solar reflectance after one year of exposure is very similar between the two sites. Inspection of the off-white painted metal coupon installed in the medium slope rack (4-in rise per 12-in run) at Shafter showed that after one year of exposure the sample was soiled with airborne debris (Fig. 4). However, after an additional 8 months of weathering the samples at all sites regained most of their solar reflectance (average SR loss of only 6% from starting SR value). El Centro and Shafter had less than ½–in of rainfall from Aug 04 through April 05; however, McArthur, Corona, Colton, Sacramento and Richmond had two consecutive months in early 2005 with rains exceeding 5-in per month. The average winds remained steady at about 4 to 5 mph over the entire exposure period at all sites. Hence the results are showing that the loss of reflectance is remedied in part by the combination of precipitation and wind sweeping or simply wind sweeping in the drier climates of El Centro and Shafter.

The darker charcoal gray coupon did not show the same seasonal variations in solar reflectance as the lighter coupon because its solar reflectance is roughly half that of the off-white painted metal (Fig. 5). Dusts tend to lighten darker colors and the soiling of the charcoal gray coupon slightly increased solar reflectance. Coupons of the same color but having conventional pigments (labeled standard in Fig. 3 and 5) have lower solar reflectance than do the cool pigmented colors during the entire exposure period. The result is important because climatic soiling did not cause the cool pigmented colors to degrade more than that observed for the conventional pigmented colors. Therefore the cool pigmented painted metals performed as well as their counterparts. Further, the infrared reflective pigments boost the solar reflectance of a dark more aesthetically pleasing color to about 0.3 to 0.4 (view standard versus cool pigments at start of exposure Fig. 5) and results for the charcoal gray painted metal shows only about a 3% drop in solar reflectance over about 1.6 years of exposure.

Similar findings were observed for the clay and concrete tile coupons (Fig. 6). The coupon had cool pigments added to a glaze coating applied atop the concrete. Results showed that both concrete and clay coupons lost less than 5% of their original solar reflectance (Appendix A). Finally, the effect of roof slope becomes somewhat significant for coupons exceeding an initial solar reflectance of 0.50, as observed for the off-white painted metal coupons displayed in Fig. 7. As stated the coupons collect dust with the worst soiling occurring for samples exposed in Colton (Fig. 7). The crisp and clear alpine climate of McArthur continues to show the lowest loss of reflectance (Fig. 7). Samples at Colton have the greatest amounts of soiling, and show that the drop in solar reflectance diminishes slightly as roof slope increases. However, neither El Centro nor McArthur show this trend with roof slope. Also the darker more aesthetically pleasing roof colors do not show the trend (Fig. 8). The darker charcoal gray coupon shows slight increases in solar reflectance with time in El Centro and in Colton because of the accumulation of dusts that tend to lighten a darker color (Fig. 8). The dusting effect is most evident on the conventional pigmented coupons (Fig. 8). Therefore the effect of roof slope appears more academic and its affect is secondary as compared to the soiling by airborne dust debris. It is also important to again point out that the cool pigmented colors maintain their solar reflectance as well as their conventional pigmented counterparts.

The thermal emittance of the painted metal, clay and concrete tile coupons has not changed much after 1.6 years of exposure in California (Table 3). Miller et al. (2004) and Wilkes et al. (2000) both observed little variation in the thermal emittance of painted and or coated surfaces. Consistent with reported findings, the thermal emittance did not vary from site-to-site nor did it change with time for these painted products. Thermal emittance of metals is strongly dependent on surface properties. Unpainted metals will over time oxidize; the metal oxide surface layer increases the thermal emittance (Miller and Kriner 2001). However, the paint finishes applied to PVDF metal and clay and concrete tile are very durable and there is therefore no adverse weathering effects observed for the thermal emittance of painted roof products.

Table 3. Thermal Emittance measured for roof coupons at different sites over time of exposure.

Roof Sample	Site	Thermal Emittance at Exposure Times (yrs)				
		0.000	0.748	0.962	1.630	2.493
Charcoal Gray PVDF Metal	Corona	0.83			0.82	0.84
	Richmond	0.82	0.82	0.82		
Rawhide PVDF Metal	Corona	0.86			0.84	0.87
	Richmond	0.83	0.84	0.84		
Apricot Buff Clay Tile	Corona					
	Richmond	0.86	0.83	0.83		
Gray Artic Concrete Tile	Corona		0.84			
	Richmond		0.84	0.84		

CONTAMINANTS STUDY

The contaminant study encompassed the identification of elements and carbons for characterizing the chemical profile of the particles soiling each roof sample. The study also included the identification of microbial consortia that might also soil the coupons and degrade the solar reflectance. The procedures used to detect and identify contaminants are reviewed to document the handling of samples and the analysis techniques used to identify particulates.

Procedure for Elemental Contaminants

Contaminants were swabbed from the concrete and painted metal coupons identified in Table 2. The coupons were exposed for about 1.63 years prior to collecting the contaminant samples. Figure 9 shows a cement sample, and three metal samples. The samples from a single site were removed from the exposure racks, wrapped in aluminum foil, stored in a zip plug bag and sent airfreight back to ORNL.

A standard operating procedure was developed for removing the deposited particulate materials from the roof samples. Each sample was placed in a laboratory sonicating[2] bath filled with 800 ml of distilled water held at room temperature (Fig. 10a). After 20 minutes, the sample was removed from the bath using sterilized stainless steel forceps. The water suspension was then poured into a filtration apparatus (shown in Fig. 10b) and vacuum applied to filter the suspended particulate onto the filters. The solution was divided into two 400-mL aliquots. One 400-mL sub-sample was filtered through a 47-mm diameter nylon filter (OSMONIC, Inc., 0.1µm pore size) that was subsequently analyzed for selected metal composition by a certified analytical lab at the Y12 facilities in Oak Ridge, Tennessee. The other 400-mL sub-sample was passed through the same filtration apparatus (Fig. 10b) through a 47-mm diameter glass fiber filter (Whatman 934-GF). About 100 mL of additional deionized water was used to rinse off any particulate matter (PM) that remained on the samples. However, very little was found visually in the rinsed portion indicating the sonicating task was reasonably thorough in the removal of the deposited PM. All the filters were placed in a laboratory dedicator and held overnight at room temperature before being analyzed. As quality control, 400 ml of deionized water was filtered through a nylon filter to create an analytical blank for metal species. A glass fiber blank was created similarly for carbon analysis. The filtration apparatus was rinsed three times using deionized water in between different filtration runs.

Inductively Coupled Plasma (ICP) – Atomic Emission Spectrometry (AES) was used for the analysis by the Y12 lab. The EPA 6010 protocol for filter analysis was followed for analysis of metal content on the filters. We chose to detect the following elements: aluminum, antimony, arsenic, barium, beryllium, boron, cadmium, calcium, chromium, cobalt, copper, iron, lead, lithium, magnesium, manganese, molybdenum, nickel, niobium, phosphorus, potassium, selenium, silicon, silver, sodium, strontium, sulfur, thallium, thorium, titanium, uranium, vanadium, zinc, and zirconium. Most of the elements were below the method's detection limits, indicating their absence in the deposited PM, and are not reported. For those reported, their concentrations are above the blank values which are above or equal to the detection limits. The carbon content was analyzed by a Sunset instrument (the Sunset Laboratory, Inc., Portland, OR) for total, elemental, and organic carbon. Three samples, each 1-square cm, were punched out from a 47-mm diameter quartz filter and analyzed by the instrument, and the average of the triplicate was assigned as the carbon concentration for the sample. If the coefficient of variation of the triplicate concentration is greater than ±5%, the sample is considered as non-uniform

[2] Sonicating agitates the bath using high-frequency sound waves.

deposition and the result may be discarded. In this study all the samples met the precision requirement and were retained in the subsequent data analysis. The Sunset instrument is capable of analyzing carbon content of a filter sample using the temperature and oxidation profiles of particulate carbonaceous species to define organic vs. elemental carbon (i.e., OC vs. EC). The total sum of OC and EC is called the total carbon of a sample.

Procedure for Biomass Detection

Another set of roof tiles and painted metals, separate from samples used in the contaminant study and weathered for 1.6 years in various locations in California, were shipped overnight for biomass analysis. Samples were swapped for lipid and quinone analyses and frozen at -80°C until extraction. Muffled glass fiber filters and sodium phosphate buffer were used to gently rub and retrieve depositional material from the roof samples. The recovered filters were extracted for microbial membrane lipids using a modified Bligh and Dyer extraction and subsequently fractionated into neutral, glyco and polar lipid classes (Bligh and Dyer, 1959; White et. al., 1979). Quinones, present in the neutral lipid fraction, were analyzed on the liquid chromatography-mass spectrometry (Geyer et. al., 2004). Polar lipid fraction was subjected to a sequential saponification/acid hydrolysis/esterification. The resulting PLFA methyl esters were separated, quantified and identified by gas chromatography-mass spectrometry (White and Ringelberg, 1998). Laboratory research was performed by Andrew Parsons (undergraduate), Amanda Smithgall, Maragret Gan and Susan Pfiffner at the University of Tennessee, Center for Biomarker Analysis (Parsons et al. 2005).

Fatty acid nomenclature is based on the fatty acid abbreviated by the number of carbon atoms (a), a colon, the number of unsaturated C-C bonds (b) followed by 'ω' followed by the number of carbons (c) from the methyl end of the molecule to the position of the unsaturation (e.g., a:bωc). For monoenoic fatty acids, the a:bωc molecule is followed by the suffix "c" for the cis- or "t" for trans-configuration. Branched fatty acids are described by iso (i) or anteiso (a), if the methyl branch is one or two carbons from the methyl end or by the position of the methyl group from the carboxylic end of the molecule. Quinones are designated as ubiquinones (UQ) and menaquinones (MK) with a number (4-14) which indicates the number of isoprene units. The PLFA results are presented as biomass in pmol/square cm or as cells/square cm using the conversion factor of 2.5 x 105 cells per pmol (Balkwill et. al. 1988). Community compositions are represented as mole percentage for individual PLFA or for PLFA structural groups. Structural groups are indicated as normal saturates (Nsat), terminally branched saturates (Tbsat), mid-chain branched saturates (Mbsat), monounsaturates (Mono), branched monounsaturates (Bmono), cyclopropyl fatty acids (Cyclo), and polyunsaturates (Poly).

CHEMICAL PROFILE OF ROOF PARTICULATES

Figures 11a-11g individually shows the concentration of each measured chemical species per sample area for the seven sites. At some sites only one sample was pulled, while at another site several samples were pulled just to obtain a sufficient quantity of contaminants (Table 2). All elements shown on the X-axis of each plot are those whose concentrations were higher than the method's detection limits and above the blank values.

Sulfur content in the roof samples was not large, which may be attributed to the absence of coal-fired power plants in California. Calcium is found to be in rather high abundance, except for the remote McArthur site in northeastern California. Due to the small amount of sulfur present, the calcium is likely to be in the form of carbonate (rather than sulfate). Aluminum (Al),

calcium (Ca), iron (Fe), manganese (Mn), and silicon (Si) are the elements consistently found at all seven sites. Potassium (K) was found high at RS02 (Corona), RS03 (Colton), and RS04 (Shafter) sites.

OC values are higher than EC values for all sites. The McArthur site that is located in an alpine climate rather than the industrial and or urban environments of the other sites had the least amount of EC per unit area of pulled sample. Plants and vegetations are excellent sources of emission of organic compounds that could be detected as OC, if the compounds or their reaction products were found on particulate matter. On the other hand, elemental carbons (e.g., soot) emanate from combustion source emissions such as vehicle engine exhausts. We thus attributed the observed higher EC values in Shafter, Richmond and Sacramento to potential contributions by traffics and vehicle emissions at the sites. The traffic volume around the McArthur site area is much less than other areas because of its rural setting, but McArthur is in a forest area where biogenic emissions might be significant. This resulted in higher OC than EC, and the data reported here support this understanding.

To further study the sources of carbon content in aerosol particles, we computed the ratios of EC to OC for the seven sites based on the data shown in Figs 11a-11g. The EC/OC ratio has been successfully used by Appel et al., 1976, Turpin and Huntzicker, 1995, and Strader et al., 1999 to identify whether the carbon in aerosol was primary or secondary in content. If the EC/OC ratio is low and correlation between OC and EC is high, the carbon likely emanates from direct emissions. Average EC/OC value reported by Appel et al., 1976, Turpin and Huntzicker, 1995, and Strader et al., 1999 is about 0.48 in winter, 0.32 in spring, and 0.18 in summer. The EC/OC ratios computed for the seven sites were all smaller than 0.18, much smaller than 0.48. These results suggest, averaged over the 1.6 years, the carbon contents found on PM deposited at these sites were driven primarily by sources such as biogenic emissions and or forest or local brush fire rather than photochemical conversion.

Many of the metals analyzed for all sites are of crustal origins such as road dusts, soil, and or rock debris. The results presented in Fig 11a-11g indicate two major contributors of particulate matter: crustal sources and traffic activities. The importance of these two source categories and their impacts on the performance of roof samples in terms of loss of solar reflectance over time is addressed in the Section “Effect of particulate matter on solar reflectance of roof material”.

Cross correlation of the samples

The pair-wise Spearman rank correlation coefficients among the seven weathering sites were calculated using StatGraphics™ and tabulated in Table 4. The Spearman rank correlation is a nonparametric (distribution-free) rank statistic used as a measure of the strength of the associations between two variables; refer to Lehmann and D'Abrera (1998) for review of the formula used for calculating the Spearman rank correlation coefficient.

The rank correlation yielded coefficients all greater than 0.93 for El Centro, Corona, and Colton. These three sites are in the southern California, and the high ranking indicates particles of similar chemical composition were deposited at these 3 sites. This is reasonable considering that these three sites are in the same region or airshed. Composition of particles deposited at the Shafter site appears to correlate well with the northern and southern sites. The three northern California sites (McArthur, Sacramento, and Richmond), however, do not have strong correlation among themselves similar to the three southern sites. The coefficient for the

Table 4. Spearman Rank Correlation Coefficients for the Seven Sites Included in the Study

	El Centro	Corona	Colton	Shafter	Richmond	Sacramento	Macarthur
El Centro	1.00						
Corona	0.96	1.00					
Colton	0.93	0.97	1.00				
Shafter	0.86	0.92	0.85	1.00			
Richmond	0.92	0.91	0.91	0.83	1.00		
Sacramento	0.62	0.71	0.61	0.88	0.55	1.00	
McArthur	0.75	0.76	0.65	0.86	0.62	0.87	1.00

Sacramento-Richmond pair is 0.55, and the Richmond-McArthur is 0.62. Both values do not suggest strong similarity. The Sacramento-McArthur pair however has a coefficient of value 0.87 that is reasonably high. McArthur, being a rural site in northern California, only mildly correlates with the sites in southern California. The inland site in Sacramento only correlates well with Shafter, and shows statistically weak correlation with any southern sites and Richmond, which is located near the San Francisco bay area.

Effect of particulate matter on solar reflectance of roof materials

The time-integrated (over 1.6 years) solar reflectance measurement data from the seven sites were mapped onto the chemical profiles shown in Figs 11a-11g by a linear function in an attempt to determine important chemical elements that have contributed to the degradation of roof reflectance. The degradation of roof solar reflectance for each site was computed as the difference between the reflectance value measured at 1.6 years and at time zero. The linear function was defined by the formulation:

$$R_{(n,1)} = C_{(n,p)} w_{(p,1)} \qquad (1)$$

where

- R an n by 1 vector of time-integrated reduction of solar reflectance,
- n the number of sites,
- C chemical profiles of deposited particles obtained from the sites using an n by p matrix,
- p number of chemical species in a profile, and
- w weights for the chemical species in a p by 1 vector.

We selected a smaller set of elements containing the following 16 variables: Al, Ca, Cr, Cu, Fe, Mn, Mg, Ni, K, Si, Na, S, V, Zn, OC, and EC for solving Eq. (1) above. We eliminated a variable if the concentration for this variable was zero at each sampling site. We also removed those that we felt unlikely to give us any useful information based on our prior experience in atmospheric aerosol research (e.g., Cheng and Hopke, 1989). We estimated the contribution of each of the selected elements to the 1.6-year integrated solar reflectance reduction values by performing a least-square optimization operation (constrained to go through a zero intercept) in

which the objective is to minimize the square root of the differences between the observed and calculated reflectance values. Table 5 shows the result of the optimization.

Table 5. Least Squares Optimization showing regression coefficients for detected elements.

1	Al (Aluminum)	**-0.0010**	9	K (Potassium)	0.0003
2	Ca (Calcium)	0.0001	10	Si (Silicon)	0.0003
3	Cr (Chromium)	0.0000	11	Na (Sodium)	0.0000
4	Cu (Copper)	0.0000	12	S (Sulfur)	0.0000
5	Fe (Iron)	0.0004	13	V (Vanadium)	0.0000
6	Mn (Manganese)	0.0000	14	Zn (Zinc)	0.0006
7	Mg (Magnesium)	0.0000	15	OC (Organic Carbon)	**-0.0014**
8	Ni (Nickel)	0.0000	16	EC (Elemental Carbon)	0.0000

A positive value in Table 5 indicates the element might contribute to the reduction of solar reflectance, while a negative value indicates the opposite that the element could contribute to the increase of solar reflectance. Results shown in Table 5 indicate, statistically, Cr, Cu, Mn, Mg, Ni, Na, S, V, and EC have no contributions to the change of solar reflectance values. Al and OC contributed to the increase of solar reflectance values found at the sites, and Ca, Fe, K, Si, and Zn could contribute to the degradation of solar reflectance measured on the roof samples. Aluminum oxide has a refractive index of about 1.7, and its particles can thus bereflective in the visible to infrared region. Organic carbon, OC, is a highly complex mixture of materials containing carbon that can be detected in the form of CO_2 when burned. OC is well-known to be a reflective component of aerosol particles (see Novakov and Penner, 1993 in http://eetd.lbl.gov/newsletter/nl17/blackcarbon.html, for example) due to its ability to scatter light. OC absorbs at short wavelengths (UV and blue), but is reflective at longer wavelengths.EC is commonly referred to as black carbon or soot and is believed to be a significant factor in the loss of a roof's solar reflectance (Berdahl et al., 2002). Our regression result here does not indicate the significance of EC in contributing to the degradation of roof solar reflectance.

To obtain a semi-quantitative estimate of the maximum possible optical absorption of the iron, we assume that 70 mg/m^2 are present in the form of small (e.g., 0.27 μm diameter) hematite (Fe_2O_3) pigment particles (Levinson *et al*., 2005). Hematite is a strong absorber of the short wavelength part of the solar spectrum (300 to 550 nm) and a hematite layer could absorb a measurable portion (~28 %) of the short wavelength component. The reported Fe result does support the hypothesis on short-wavelength absorption. A more detailed analysis of solar absorption associated with iron is presented in Appendix B. The complex mixture of atmospheric particles is somewhat confounding the light extinction process as described by the simple linear model of chemical elements. It might be desirable to analyze the crystalline structure of all potential elements in future research.

Discussion of carbon effects on roof solar reflectance

The role of elemental carbon (i.e., soot) if in significant content in aerosols can be dramatic. Fig. 12 shows the expected solar reflectance and visible reflectance as a function of soot concentration, as a fraction of the initial high reflectance R_o (Berdahl et al., 2006). The OC and EC amounts measured in mg per unit area in meter squared at these seven sites are shown in Table 6. The largest EC per unit area was found at Richmond, while the blank filter had virtually no EC. Note that the detection limit for carbon is 0.2 μg. For the sample exposed at Richmond,

Table 6. Derived OC and EC Amounts per Unit Area on the Roof Samples Collected at the seven Sites (Detection Limit of Carbon is 0.2 µg)

Site ID	Organic Carbon (mg/m^2)	Elemental Carbon (mg/m^2)
Blank Filter	**0.257**	0.007
El Centro	8.312	0.237
Corona	5.361	0.240
Colton	6.146	0.165
Shafter	5.591	0.404
Richmond	11.090	1.344
Sacramento	4.461	0.221
McArthur	1.315	0.018

with the largest amount of EC, 1.34 mg per square meter, EC was found to have contributed only 2-3% degradation of its original reflectance. Most of the samples were not greatly affected in reflectance by EC or the soot (< 10%), and the sample from McArthur is virtually unsoiled by soot. In other words, EC was found in too small concentrations to be a significant contributor in reducing surface reflectance at all seven sites in California.

BIOMASS AND COMMUNITY COMPOSITION OF ROOF SAMPLES

Membrane lipids were investigated to gain a better understanding of the microbial community composition and biodensity deposited or residing on these roof samples in the different California environments. Phospholipid fatty acid methyl esters (PLFA) have been used as biomarkers of microbial communities for many years. PLFA analysis is a direct real time monitoring analysis for viable biodensity of microbial communities because they degrade rapidly upon cell death (White et al., 1979). All eukaryote and bacterial cell membranes have PLFA which provide a non-selective means to assay changes in microbial communities (Tunlid and White, 1992, Federle et al., 1986; Findlay and Dobbs, 1993). PLFA ratios may also provide insight on metabolic status and stress of a community (Kieft et al., 1994; Frostagärd et al. 1996). Numerous studies used PLFA analysis to aid in determining microbial community composition and the impact of environmental factors like contamination by hydrocarbons (Pfiffner et al. 1997; Stephens et al., 1998) or metals (Brandt et al. 1999; Bääth et al., 1998).

Biomass PLFA and Quinone

The viable biomass as represent by PLFA composition is shown in Figure 13a. When biomass is converted to cells based on factors described by Balkwill et al. (1988), clay tiles averaged 1.25×10^6 cells per square cm compared to 6.0 and 1.5×10^5 cells per square cm for concrete and metal respectively. We speculate that the biomass may correspond to the texture of the tiles (metals were smooth, while clay tiles were rough). An additional plot (Fig. 13b) shows the average PLFA biomass for each roof material. When comparing biomass estimates based on

quinone composition (Fig. 14a), we did not see a similar trend with the PLFA biomass (Figure 13b and 14b). This may be due to the fact that neutral lipids do not degrade as quickly as PLFA. We speculate that the overall biomass may relate to the material composition of the tiles, i.e. concrete is more alkaline and to surface roughness which may have provided more pockets for particle or bacterial accumulation.

When comparing biomass with solar reflectance, we found that solar reflectance at 1.6 yrs was weakly correlated to increased biomass (R^2=0.51), which is consistent with finding from the contaminant study which showed OC to increase reflectance.

Community Composition

When interpreting the PLFA profiles, 18:2ω6 was the most prominent PLFA ranging from 21-44 mol% (Figure 15). This PLFA is indicative of cyanobacteria and fungi (Weete, 1974). Other major PLFA were 16:0, 18:1ω9c, 18:1ω7c, 18:0 in decreasing relative abundance. The normal saturate PLFA, 16:0 and 18:0, are ubiquitous and are generally seen in all PLFA profiles whereas the 18:1's are indicative of Gram-negative bacteria (Findlay and Dobbs 1993). A15:0 and i16:0 were found in clay and concrete tile, while only clay tiles showed br17:0 and br18:0. These terminally and mid-chain branched saturates are generally found in Gram-positive bacteria. Stress PLFA indicator for Gram-negative bacteria, cy17:0, was seen in the alpine climate (Guckert et al., 1986).

Quinone composition may be used to assess respiratory potential of the microbial community (Geyer et al. 2004). When Gram-negative bacteria and eukaryotes are growing with oxygen, ubiquinones are produced. Under reduced oxygen conditions, Gram-negative and archaeal bacteria produce menaquinones. Gram-positive bacteria produce menaquinones under aerobic and anaerobic conditions. In the figure 16, the quinone profiles are shown. Concrete tiles and the PVDF metal from McArthur had no menaquinones, which suggest an aerobic environment and a lack of Gram-positive bacteria. Clay and PVDF metals from Corona and Meloland showed diverse quinones profiles, which suggest the potential for various microorganisms. Clay and PVDF metal sample from Meloland had UQ/MK ratio of 0.37 to 0.44 and may indicate the presence of microphilic to anaerobic niches.

CONCLUSIONS

Seven sites were selected for exposing painted PVDF metal, clay and concrete tile coupons with and without cool pigmented colors in the arid, alpine, urban populated and also the cool, humid climates of California. The loss in solar reflectance for painted metal and clay and concrete tile coupons was of the order 6% of the initial reflectance for this 2½ year time limited study. Solar reflectance of the cool pigmented coupons always exceeded that of the convention pigmented coupons. Climatic soiling did not cause the cool pigmented roof coupons to lose any more solar reflectance points than their conventional pigmented counterparts. The effect of roof slope appears to have more of an affect on lighter color roofs whose solar reflectance exceeds at least 0.5 and visual shows the accumulation of airborne contaminants. However, precipitation and or wind sweeping helps restore most of the initial solar reflectance. The thermal emittance remained invariant with time and location and was therefore not affected by climatic soiling.

The roof samples collected at seven California sites have been analyzed for elements and carbons by using ICP-AES and Sunset OC/EC instruments following certified analytical procedure. A particle extraction procedure was developed to obtain particles from the roof samples in a consistent manner. The chemical profile of the particles collected by each roof

sample was obtained and reported for the seven sites. Analysis of cross-correlation of the seven chemical profiles shows a clear separation between the rural and urban/industrial sites and correlation among sites in a region; e.g., Southern California. There was also a weak separation between the sites in northern and southern California. We also attempted to identify the elements that contribute to the loss or enhancement of solar reflectance by performing a least-square optimization of the data. The results showed elemental or black carbon did not contribute significantly to the degradation of reflectance, but dust particles (characterized by Al) and organic carbon had a statistically significant effect on balancing the degradation over the course of 1.6 years.

Differences in microbial communities and biomass were seen between the various tile types and climate zones. Abundance of microbial biomass on roof tiles appears to be related to the composition/surface structure of the tile. When examined by PLFA and quinone analyses, some tiles showed diverse microbial communities. Cyanobacteria or fungi represent the dominant player. Future research includes molecular analysis for community composition and phylogenetic identification is ongoing. DNA has been extracted and will be analyzed using selected kingdom gene probes for bacteria and eukaryotes and specific gene probes for cyanobacteria followed by denaturing gradient gel electrophoresis and sequencing of selected bands for phylogenetic identification.

ACKNOWLEDGEMENTS

Funding for this project was provided by the California Energy Commission's Public Interest Energy Research program through the U. S. Department of Energy under contract DE-AC03-76SF00098. The authors acknowledge Doh-Won Lee of Oak Ridge Associated Universities for assistance in analyzing the filter samples for carbon content. The elemental composition of particles was analyzed by the analytical chemistry services at the DOE Y12 complex using ICP-AES instrument. Oak Ridge National Laboratory is managed by UT-Battelle, LLC, for the U.S. Dept. of Energy under contract DE-AC05-00OR22725. The submitted manuscript has been authored by a contractor of the U.S. Government under contract DE-AC05-00OR22725. Accordingly, the U.S. Government retains a nonexclusive, royalty-free license to publish or reproduce the published form of this contribution, or allow others to do so, for U.S. Government purposes.

DISCLAIMERS

Mention of the trade names, instrument model and model number, and any commercial products in the manuscript does not represent the endorsement of the authors nor their employer, the Oak Ridge National Laboratory or the US Department of Energy.

NOMENCLATURE

CIMIS	California Irrigation Management Information System
CMRC	Cool Metal Roof Coalition
AISI	American Institute of Steel Industries
NamZac	Galvalume Sheet Producers of North America
MBMA	Metal Building Manufacturers Association
MCA	Metal Construction Association
NCCA	National Coil Coaters Association
PVC	polyvinylchloride thermoplastic membranes

SR	solar reflectance
TE	thermal emittance
PM	particulate matter
Nsat	terminally branched saturates
Tbsat	mid-chain branched saturates
Mbsat	monounsaturates
Mono	branched monounsaturates
Bmono	cyclopropyl fatty acids
Poly	polyunsaturates

REFERENCES

Akbari,H., P. Berdahl, R. Levinson, R. Wiel, A. Desjarlais, W. Miller, N. Jenkins, A. Rosenfeld, C. Scruton (2004) Cool Colored Materials for Roofs, *ACEEE Summer Study on Energy Efficiency in Buildings.* Proceedings of American Council for an Energy Efficient Economy, Asilomar Conference Center in Pacific Grove, CA, August.

Akbari, H., Konopacki, S.J. 1998. "The Impact of Reflectivity and Emissivity of Roofs on Building Cooling and Heating Energy Use," in Thermal Performance of the Exterior Envelopes of Buildings, VII, proceedings of ASHRAE THERM VIII, Clearwater, FL., Dec. 1998.

ASTM. 1997. Designation C 1371-97: Standard Test Method for Determination of Emittance of Materials Near Room Temperature Using Portable Emissometers. American Society for Testing and Materials, West Conshohocken, PA.

_____. 1996. Designation E903-96: Standard Test Method for Solar Absorption, Reflectance, and Transmittance of Materials Using Integrating Spheres. American Society for Testing and Materials, West Conshohocken, PA.

Appel, B. R., P. Colodny, and J. J. Wesolowski (1976) Analysis of Carbonaceous Materials in Southern California Atmospheric Aerosols, Environ. Sci. Technol., 10: 359-363,

Bååth E, Diaz-Ravina M, Frostegård Å, Campbell CD. 1998. Effect of metal-rich sludge amendments on the soil microbial community. Appl Environ Microbiol 64:238-245.

Balkwill DL, Leach FR, Wilson JT, McNabb JF, White DC. 1988. Equivalence of microbial biodensity measures based on membrane lipid and cell wall components, adenosine triphosphate, and direct counts in subsurface sediments. Microbial Ecol 16:73-84.

Berdahl, P., H. Akbari, and L. S. Rose (2002) Aging of Reflective Roofs: Soot Deposition, *Appl. Opt.*, April 2002 Vol. 41, No. 12, 2355-2360.

Berdahl, P., H. Akbari, R. Levinson, and W. A. Miller (2006) Weathering of Roofing Materials-An Overview, in preparation.

Bligh EG, Dyer WJ. 1959. A rapid method of total lipid extraction and purification. Can J Biochem Phys 37:911-917.

Brandt CC, Schryver JC, Pfiffner SM, Palumbo AV, Macnaughton S. 1999. Using artificial neural networks to assess changes in microbial communities. In: Leeson A, Alleman BC, editors. Bioremediation of Metals and Inorganic Compounds. Columbus: Battelle Press. pp. 1-6.

Cheng, M.-D. and P. K. Hopke (1989) Identification of Markers for Chemical Mass Balance Receptor Model, *Atmos. Environ.*, 23(6): 1,373.

Federle, T.W., Dobbins, D.C., Thornton-Manning, J.R. and Jones, D.D. (1986) Microbial biomass, activity, and community structure in subsurface soils. 24: 365-374.

Findlay RH, Dobbs FC. 1993. Quantitative description of microbial communities using lipid analysis. In: Kemp PF, Sherr BF, Sherr EB, Cole JJ editors. Handbook of Methods in Aquatic Microbial Ecology. Boca Raton, FL. Lewis Publishers. p 271-284.

Frostegård, Å, Tunlid, A, Bååth, E. 1996. Changes in microbial community structure during long-term incubation in two soils experimentally contaminated with metals. Soil Biol Biochem 28:55-63.

Geyer, R., A.D. Peacock, D.C. White, C. Lytle and G.J. Van Berkel. 2004. Atmospheric pressure chemical ionization and atmospheric pressure photoionization for simultaneous mass spectrometric analysis of microbial repiratory ubiquinones and menaquinones. J. Mass Spectrometry 39:922-929.

Guckert JB, Hood MA, White, DC. 1986. Phospholipid, ester-linked fatty acid profile changes during nutrient depletion of Vibrio cholerae: increases in the trans/cis and proportions of cyclopropyl fatty acids. Appl Environ Microbiol 52:794-801.

Kieft, TL, Ringelberg, DB, White, DC. 1994. Changes in ester-linked phospholipid fatty acid profiles of subsurface bacteria during starvation and desiccation in a porous medium. Appl Environ Microbiol 60:3292-3299.

Kirchstetter, T. W., T. Novakov, and P. V. Hobbs (2004) Evidence that the spectral dependence of light absorption by aerosols is affected by organic carbon, J. Geophysical Research-Atmospheres 109, (D21): Art. No. D21208.

Kollie, T. G., F.J. Weaver, D.L. McElroy. 1990. "Evaluation of a Commercial, Portable, Ambient- Temperature Emissometer." Rev. Sci. Instrum., Vol. 61, 1509–1517.

Lehmann, E. L. and D'Abrera, H. J. M. (1998) *Nonparametrics: Statistical Methods Based on Ranks, rev. ed.* Englewood Cliffs, NJ: Prentice-Hall, pp. 292, 300, and 323.

Levinson, R, P. Berdahl, and H. Akbari (2005) Solar spectral optical properties of pigments – part II: survey of common colorants, Sol. Energy Mater. Sol. Cells 89, 351-389 (2005), Fig. 1, Film R03.

Miller, W.A., A. Desjarlais, D.S. Parker and S. Kriner (2004) Cool Metal Roofing Tested for Energy Efficiency and Sustainability, Proceedings of CIB World Building Congress, Toronto, Ontario, May 1-7, 2004.

Miller, W.A., Cheng, M-D., Pfiffner, S., and Byars, N. (2002) *The Field Performance of High-Reflectance Single-Ply Membranes Exposed to Three Years of Weathering in Various U.S. Climates*, Final Report to SPRI, Inc., Aug., 2002.

Miller, W. and B. Rudolph (2003), *Exposure Testing of Painted PVDF Metal Roofing*, Report prepared for the Cool Metal Roof Coalition.

Miller, W. A., and Kriner, S. 2001. "The Thermal Performance of Painted and Unpainted Structural Standing Seam Metal Roofing Systems Exposed to One Year of Weathering," in Thermal Performance of the Exterior Envelopes of Buildings, VIII, proceedings of ASHRAE THERM VIII, Clearwater, FL., Dec. 2001.

Novakov, T. and Penner, J.E. (1993) Large Contribution of Organic Aerosols to Cloud-Condensation-Nuclei Concentrations, *Nature*, 365, 823- 826.

Parsons, A., A. Smithgall, M. Gan, W. Miller, C.D. Cheng, and S.M. Pfiffner. September 2005. Influence of Microbial Deposition on High-Reflectance Roof Tiles. Kentucky-Tennessee Branch of the American Society of Microbiology, Nashville, TN.

Petrie, T. W., A.O. Desjarlais, R.H. Robertson and D.S. Parker. 2000. Comparison of techniques for in-situ, non-damaging measurement of solar reflectance of low-slope roof membrane.

Presented at the 14th Symposium on Thermophysical Properties and under review for publication in International Journal of Thermophysics, Boulder, CO; National Institute of Standards and Technology.

Pfiffner SM, Palumbo, AV, Gibon T, Ringelberg DB, McCarthy JF. 1997. Relating groundwater and sediment chemistry to microbial characterization at BTEX-contaminated site. Appl Biochem Biotech 63-65:775-788.

Stephen JR, Chang Y-J, Gan YD, Peacock A, Pfiffner SM, Barcelona MJ, White DC, Macnaughton SJ. 1998. Microbial characterization of PJ-4 fuel contaminated site using a combined lipid biomarker/PCR-DGGE based approach. Enivron Microbiol 1:231-241.

Strader, R., P. Lurmann, and S. P. Pandis (1999) Evaluation of Secondary Organic Aerosol Formation in Winter, *Atmos. Environ*., 33: 4849-4863.

Tunlid, A, White, DC. 1992. Biochemical analysis of biomass, community structure, nutritional status and metabolic activity of the microbial community in soil. In: Bollag J-M, Stotzky G, editiors. Soil Biochemistry Vol. 7. –. New York: Marcel Dekker Inc., pp. 229-262.

Turprin, B. J. and J. J. Huntzicker (1995) Identification of Secondary Organic Aerosol Episodes and Quantitation of Primary and Secondary Organic Aerosol Concentrations during SCAQS, *Atmos. Environ*., 29: 3527-3544.

Weete JD. 1974. Fungal Lipid Biochemistry: Distribution and Metabolism. New York: Plenum Press.

White DC, Davis WM, Nickels JS, King JD, Bobbie RJ. 1979. Determination of the sedimentary microbial biodensity by extractable lipid phosphate. Oecologia 40: 51-62.

White DC, Ringelberg DB. 1998. Signature Lipid Biomarker Analysis. In Techniques in Microbial Ecology. R. S. Burlage, R. Atlas, D. Stahl, G. Geesey, and G. Sayler, editors. Oxford University Press, New York, NY., pp. 255-272.

Wilkes, K. E., Petrie, T. W., Atchley, J. A., and Childs, P. W. (2000) Roof Heating and Cooling Loads in Various Climates for the Range of Solar Reflectances and Infrared Emittances Observed for Weathered Coatings, pp. 3.361-3.372, *Proceedings, 2000 Summer Study on Energy Efficiency in Buildings.* Washington, D.C.: American Council for an Energy-Efficient Economy.

Wong, S. S. and L. E. Brus (2001) Narrow Mie Optical Cavity Resonances from Individual 100 nm Hematite Crystallites, J. Phys. Chem. B 105, 599-603.

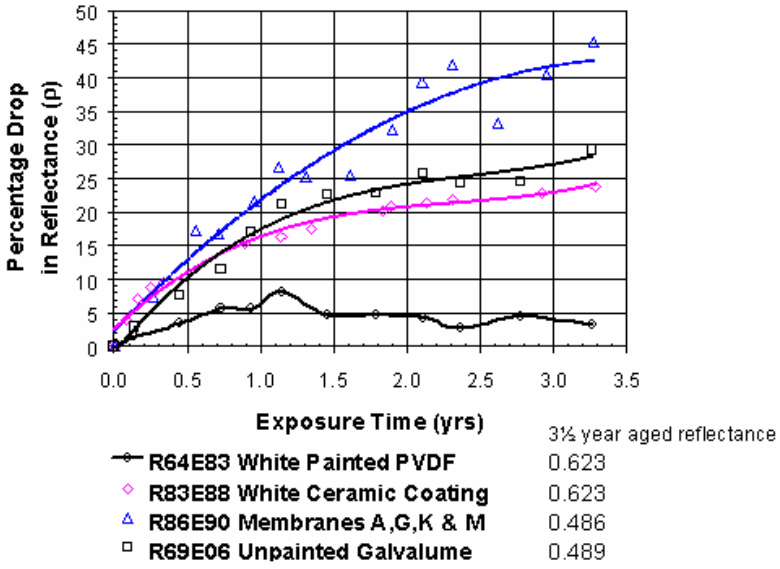

Fig. 1. Loss of solar reflectance for thermoplastic membrane, white ceramic coating and painted PVDF metal and bare Galvalume® roofs after three years of exposure.

Fig. 2. Exposure Rack Assembly used for natural exposure roof samples in seven California climatic zones; site shown is the Elk Manufacturing facility in Shafter, CA.

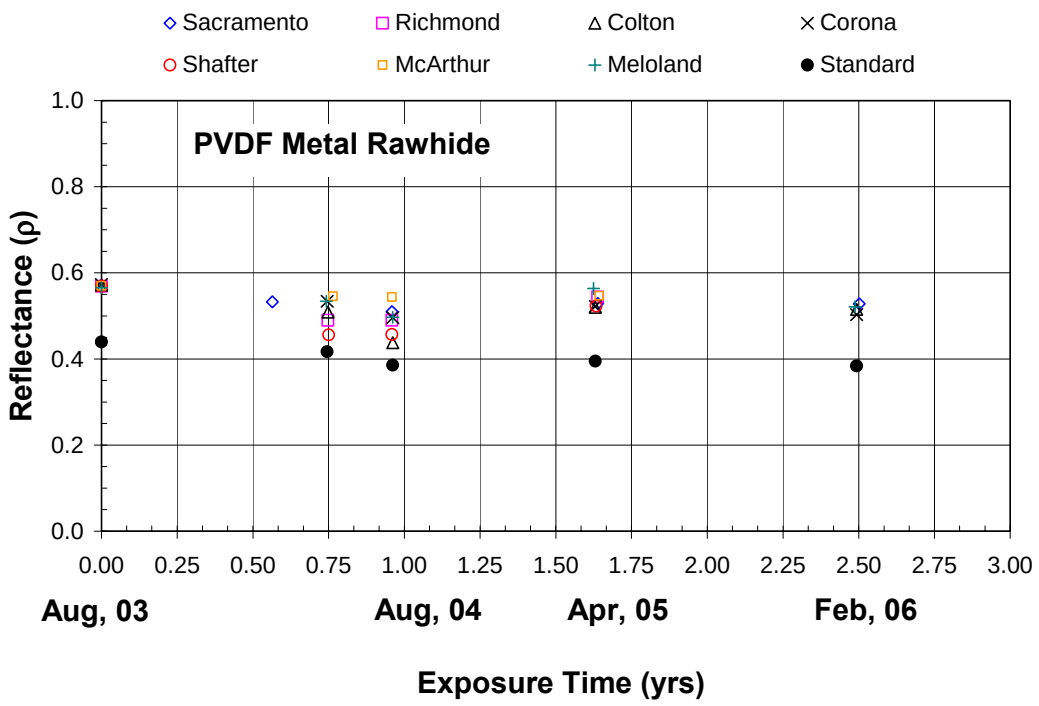

Fig. 3. Solar reflectance of a painted PVDF metal coupon (off-white color) at the seven CA weathering sites.

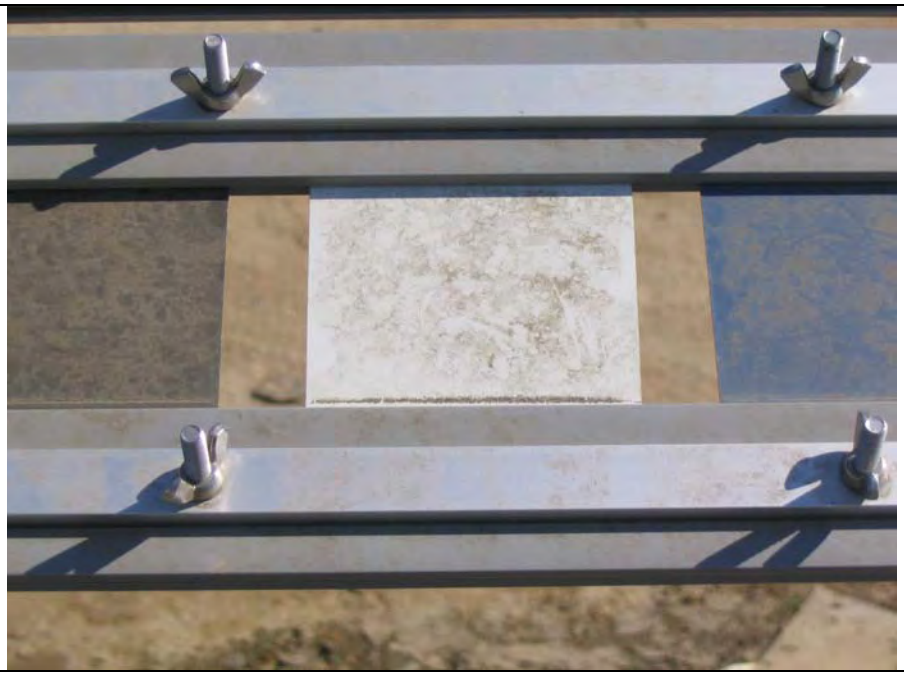

Fig. 4. Painted PVDF metal coupon soiled at the Shafter site after 1 full year of exposure.

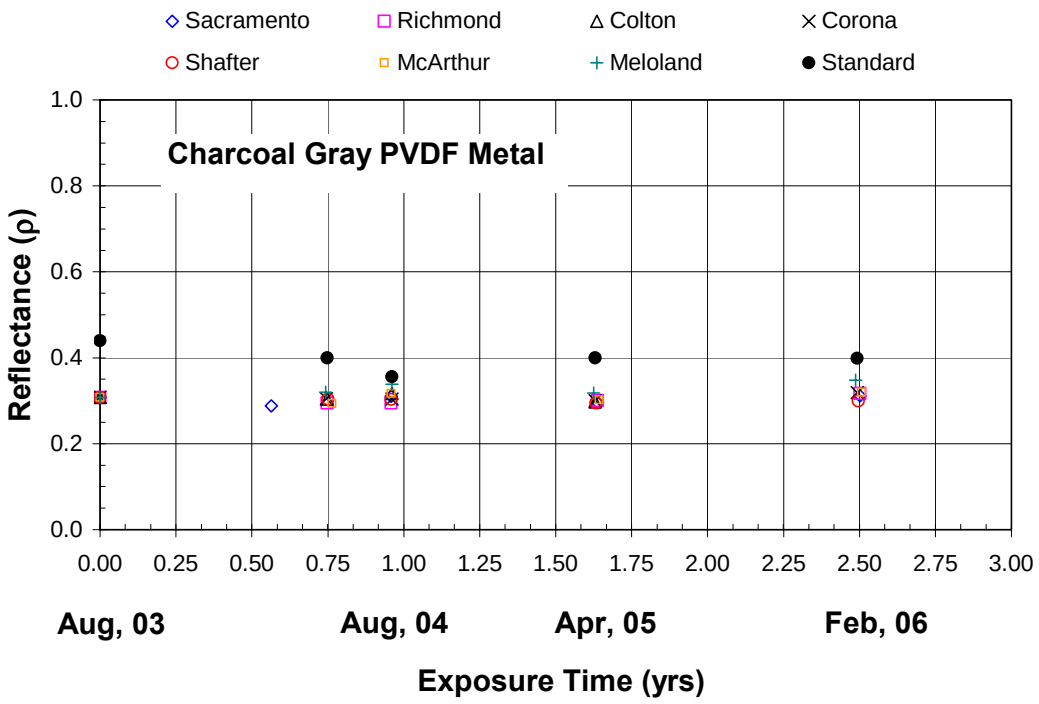

Fig. 5. Solar reflectance of a painted PVDF metal coupon (charcoal gray color) at the seven CA weathering sites.

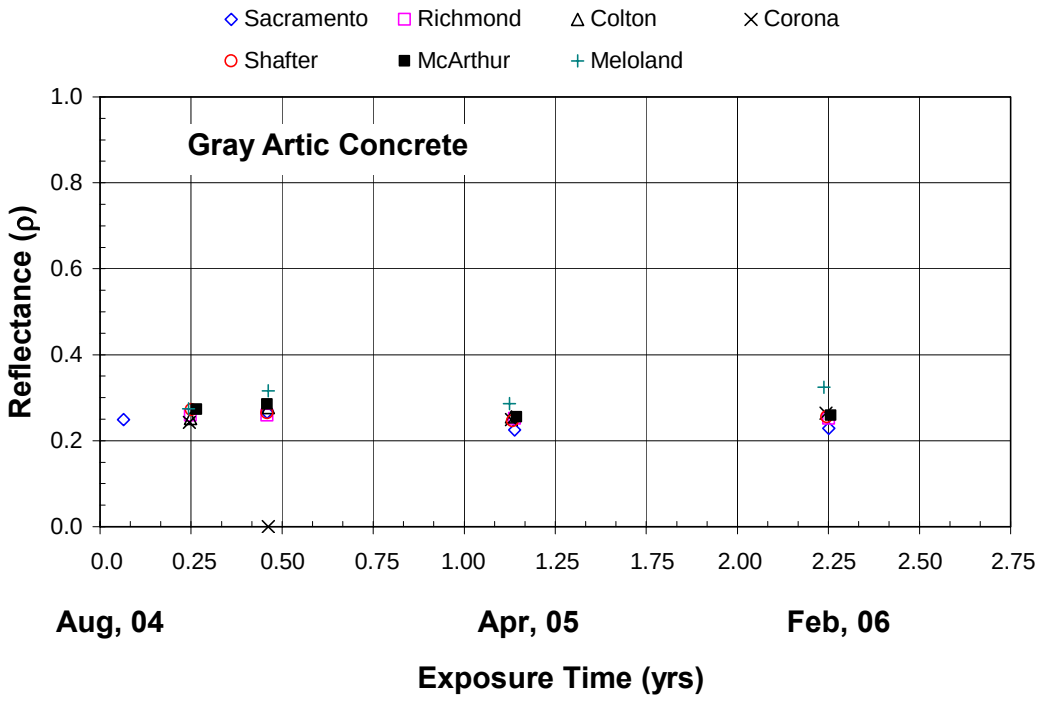

Fig. 6. Solar reflectance of a concrete tile coupon (light gray color) at the seven CA sites.

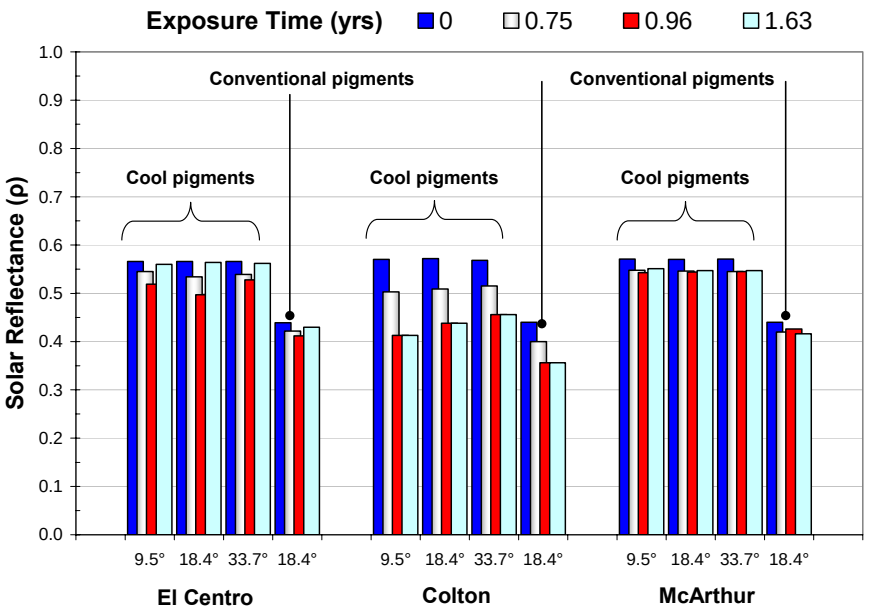

Fig. 7. Off-white (Rawhide) painted polyvinylidene fluoride metal with and without cool pigments. The slopes of 9.5º, 18.4º and 33.7º represent respective exposure settings of 2-in, 4-in and 8-in of rise per 12-in of run.

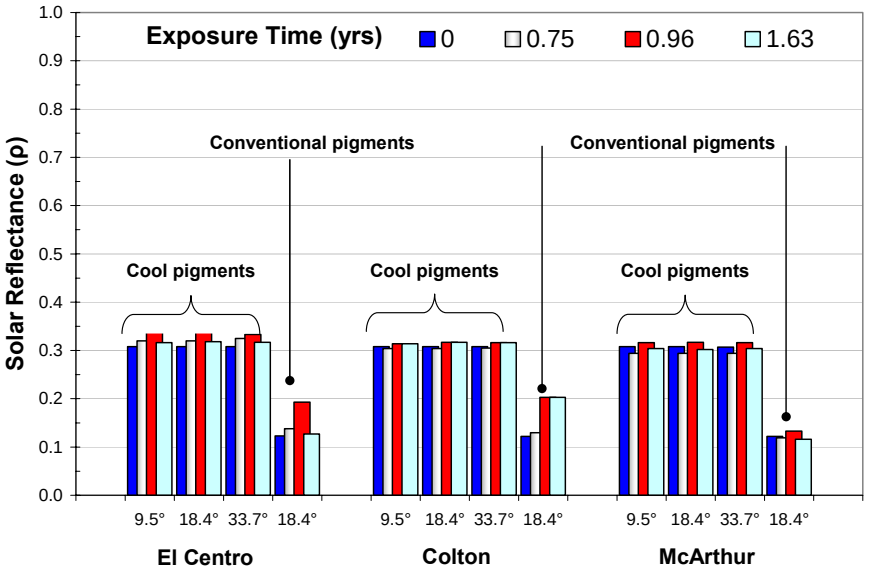

Fig. 8. Charcoal gray painted polyvinylidene fluoride metal with and without cool pigments. The slopes of 9.5º, 18.4º and 33.7º represent respective exposure settings of 2-in, 4-in and 8-in of rise per 12-in of run.

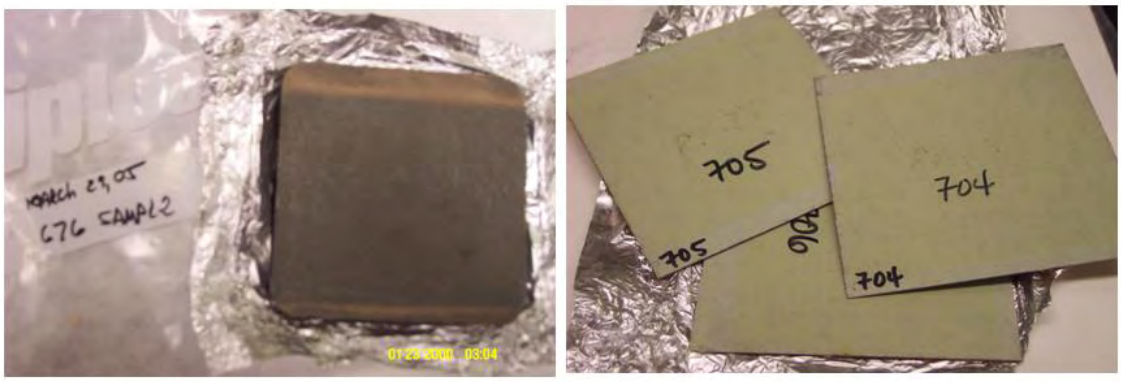

Cement Roof Sample

Metal Roof Sample

Fig. 9. Examples of concrete and painted metal roof samples analyzed for particulate matter and biomass.

Fig. 10a. Sonicating bath of roof samples to extract particulate matter for chemical analysis

Fig. 10b. Filtration of extracted particulate matter for chemical analysis

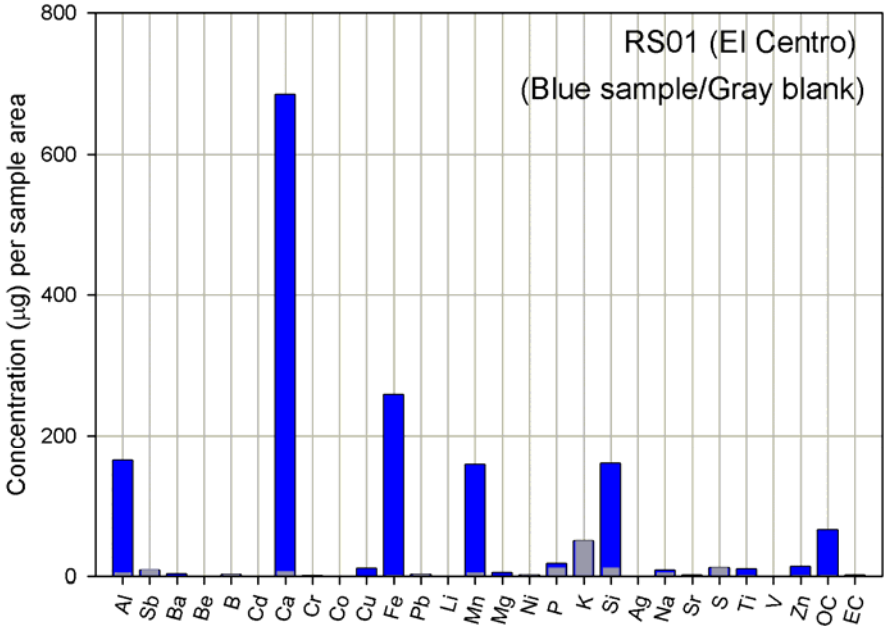

Fig. 11a. Chemical profile of particulate matter deposited on roof sample at El Centro site. Also shown in gray color is the chemical profile of the blank filter.Sample areas provided in Table 2.

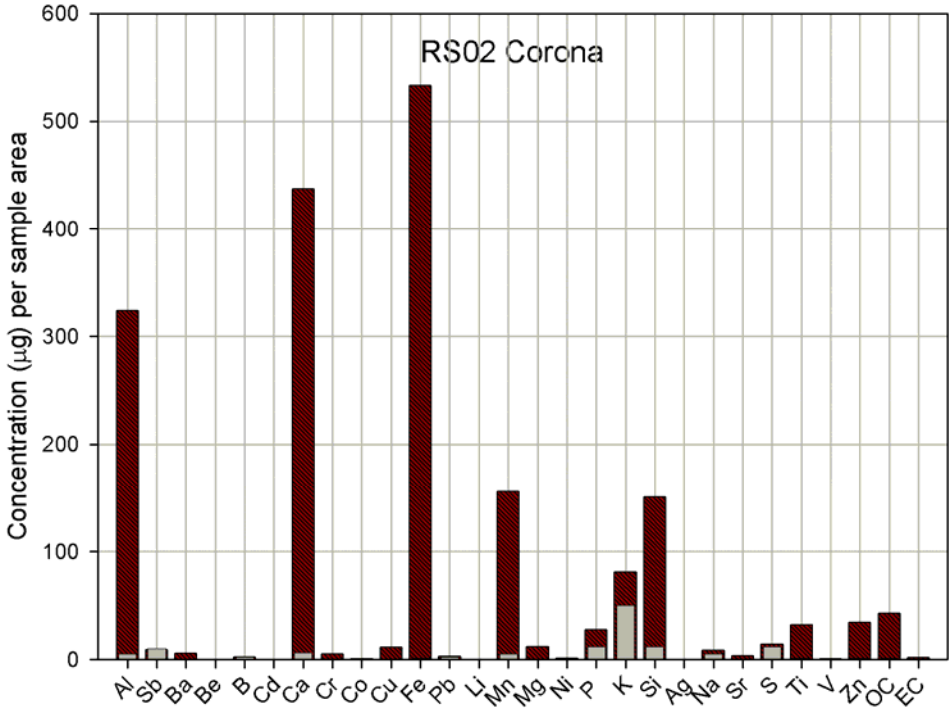

Fig. 11b. Chemical profile of particulate matter deposited on roof sample at Corona site. Also shown in gray color is the chemical profile of the blank filter.

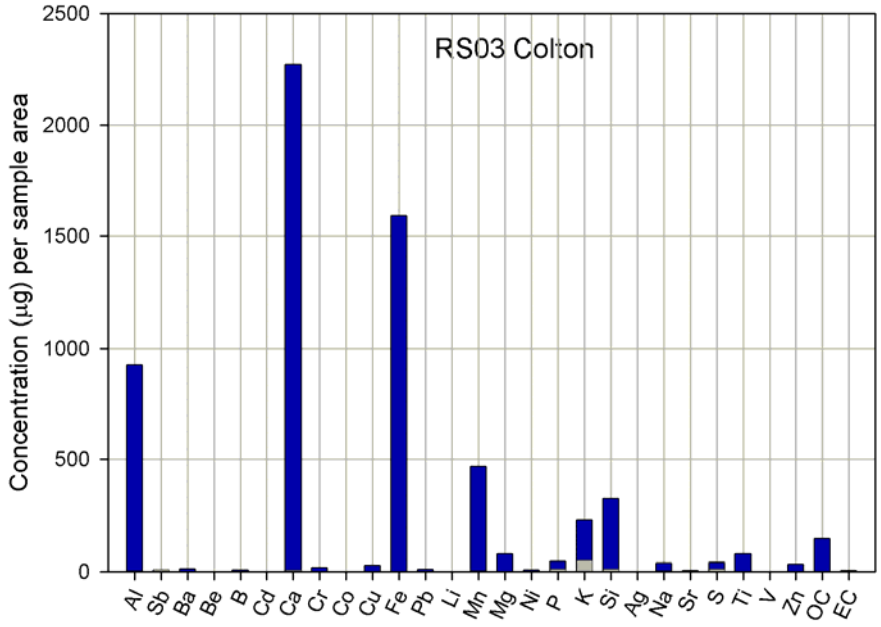

Fig. 11c. Chemical profile of particulate matter deposited on roof sample at Colton site. Also shown in gray color is the chemical profile of the blank filter.

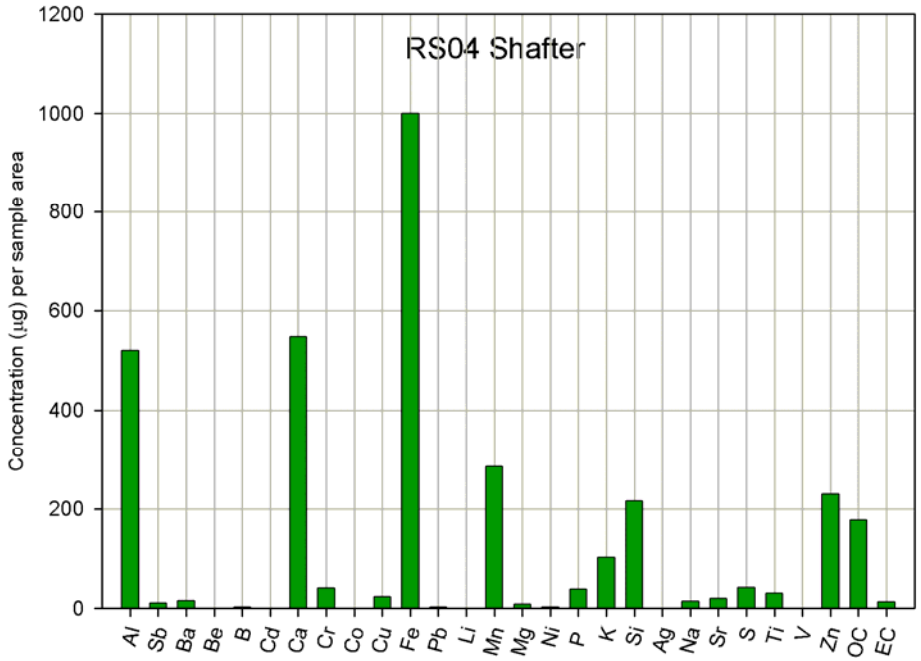

Fig. 11d. Chemical profile of particulate matter deposited on roof sample at Shafter site. Also shown in gray color is the chemical profile of the blank filter.

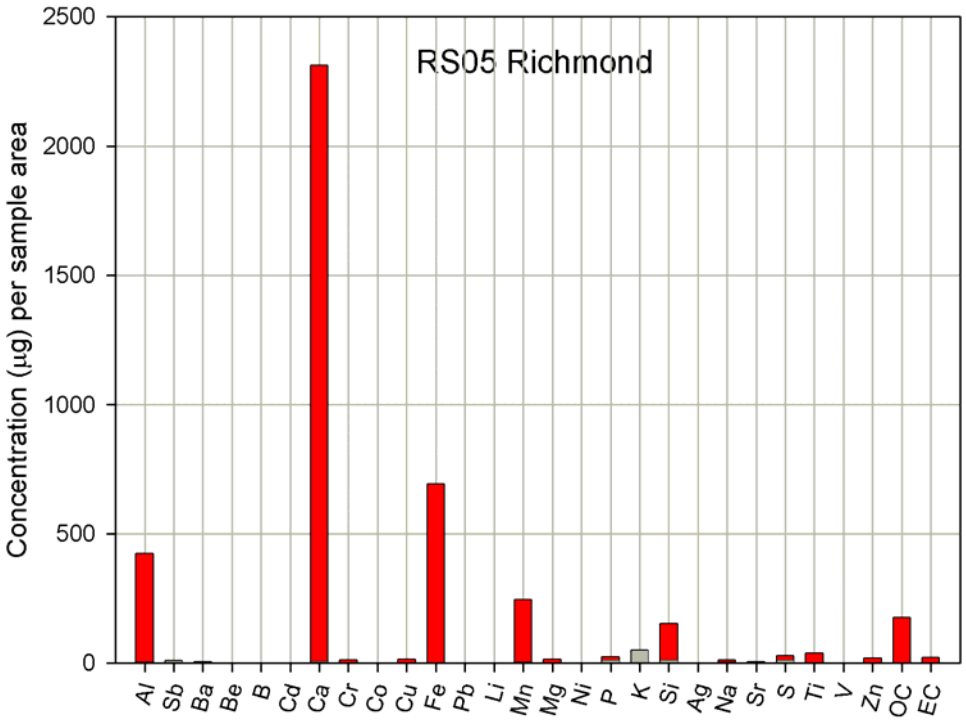

Fig. 11e. Chemical profile of particulate matter deposited on roof sample at Richmond site. Also shown in gray color is the chemical profile of the blank filter.

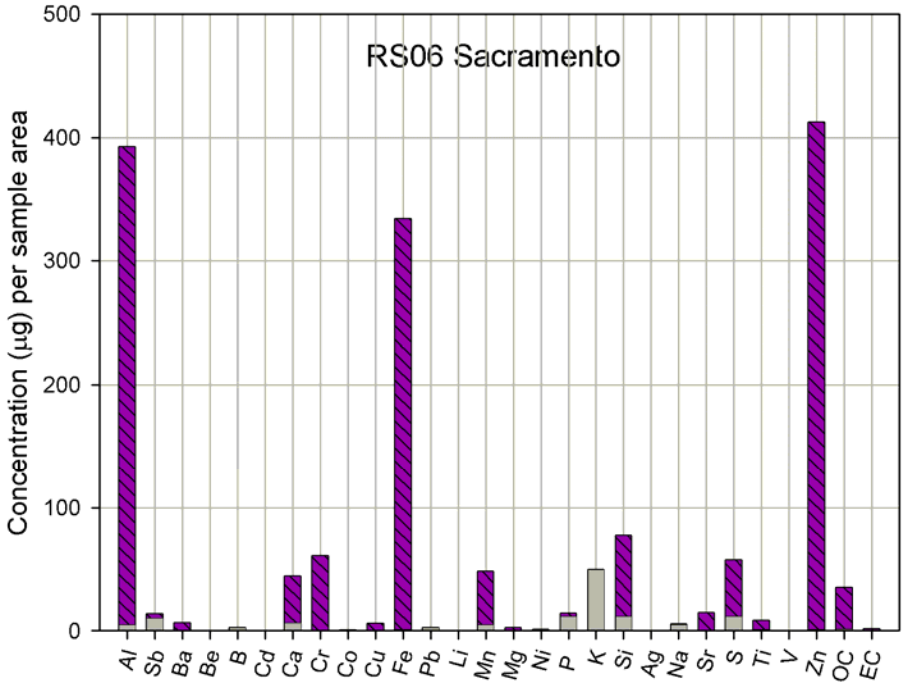

Fig. 11f. Chemical profile of particulate matter deposited on roof sample at Sacramento site. Also shown in gray color is the chemical profile of the blank filter.

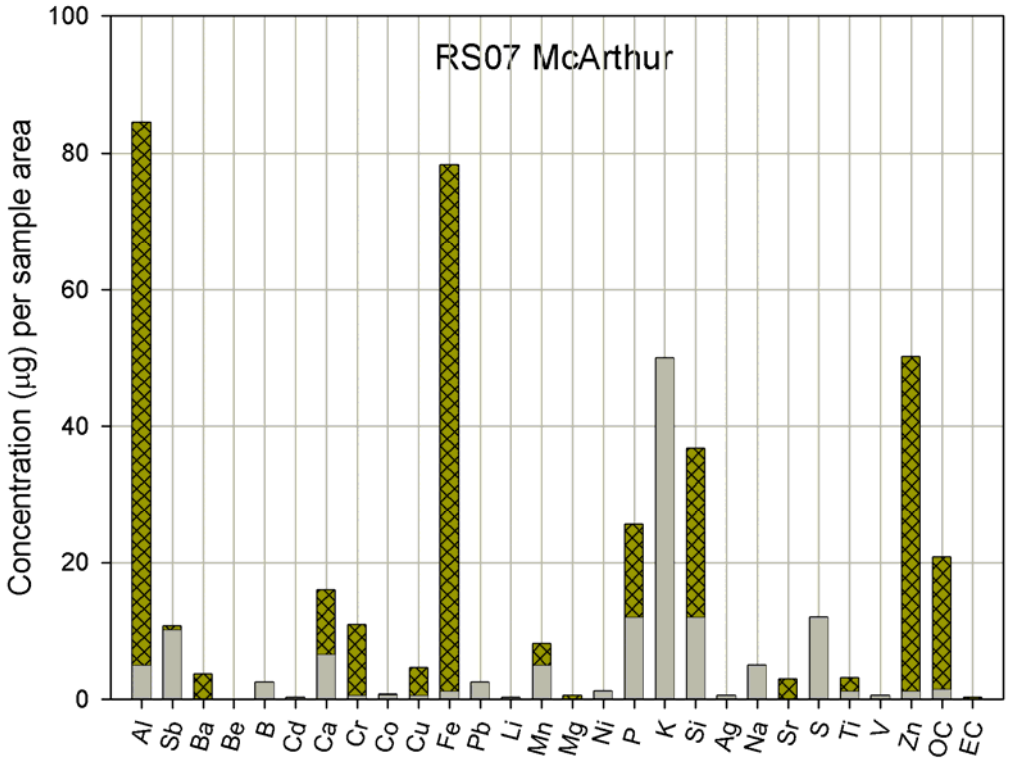

Fig. 11g. Chemical profile of particulate matter deposited on roof sample at McArthur site. Also shown in gray color is the chemical profile of the blank filter.

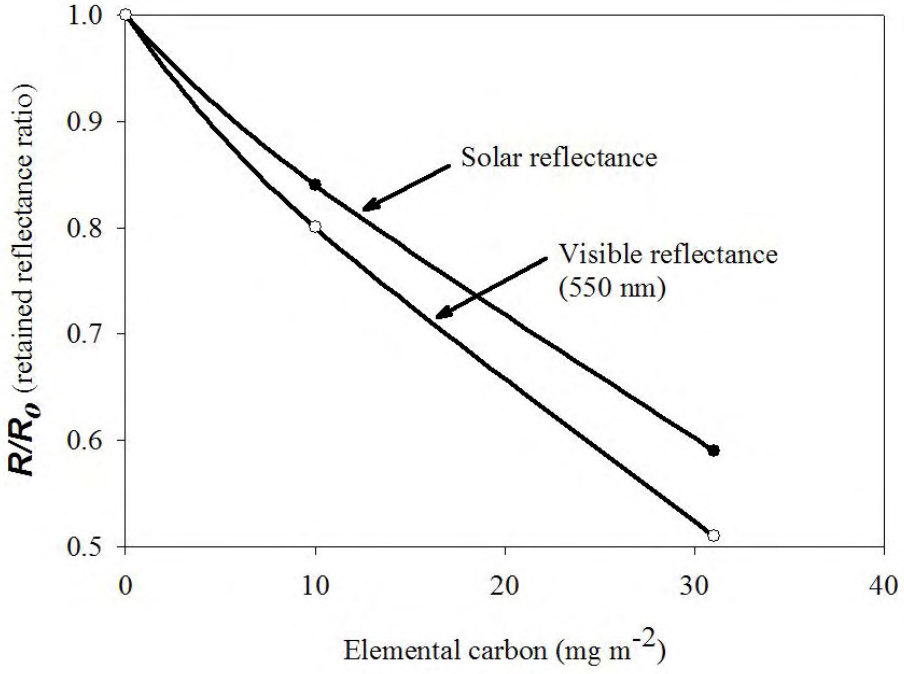

Fig. 12. Expected values for the soiled roof reflectance, divided by the unsoiled reflectance, as a function of elemental carbon (soot) concentration.

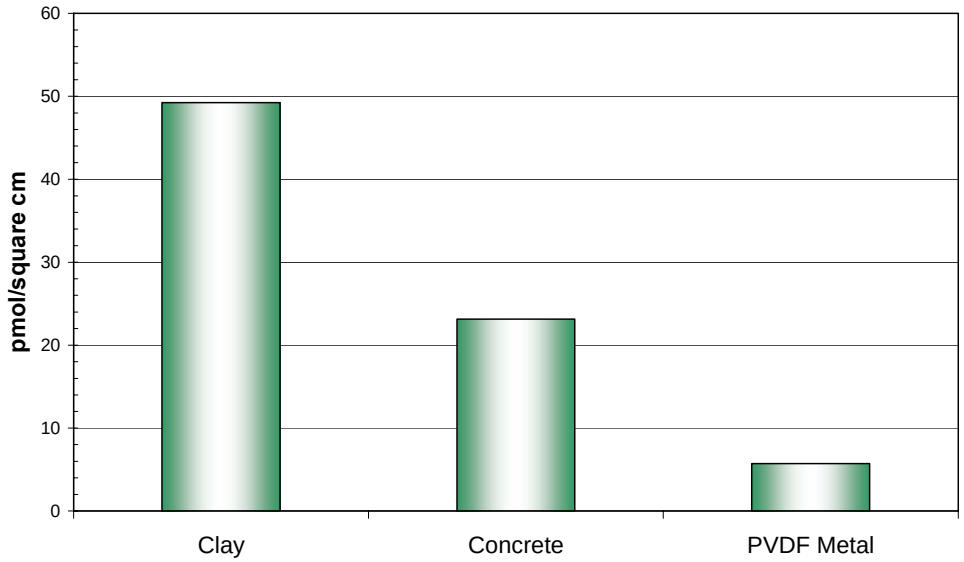

(b) PLFA average by material type

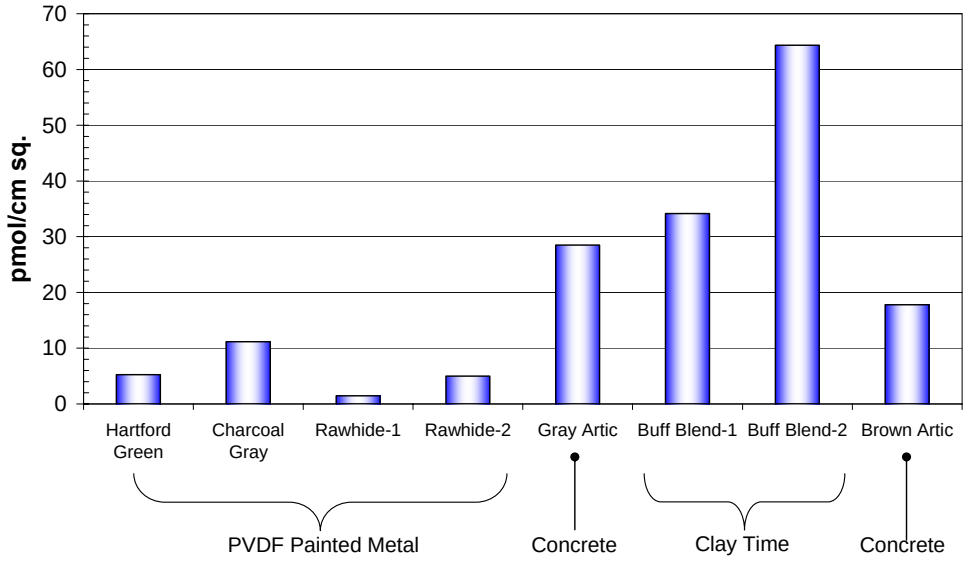

(a) PLFA estimates for each roof sample

Figure 13. Polar Lipid Fatty Acid (PLFA) estimates (a) for all roof samples and (b) averaged for the type of roof material; estimate units are pmol PLFA per square cm.

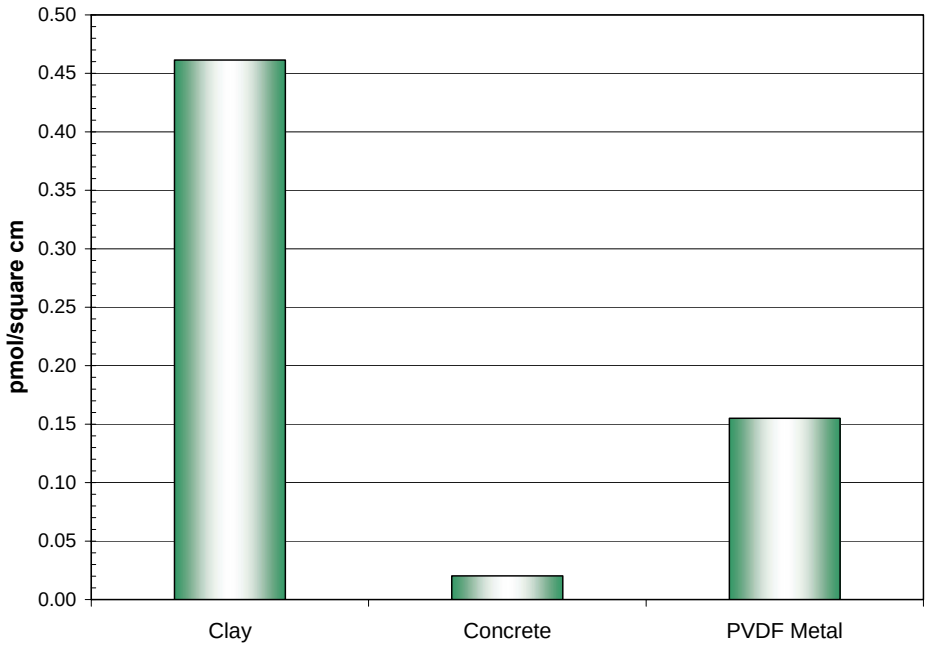

(b) Quinone averaged for type roof material.

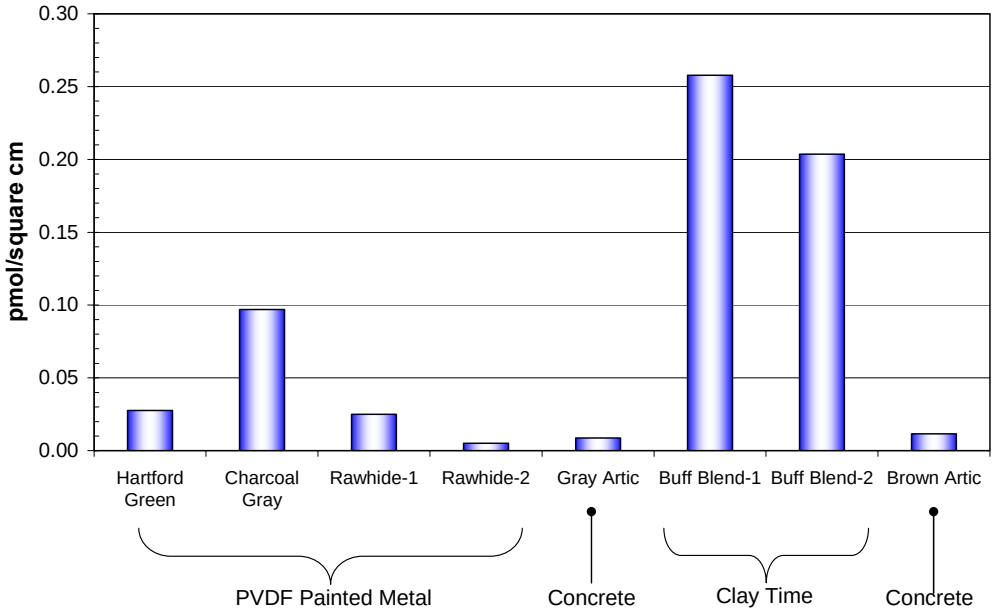

(a) Quinone for all roof samples.

Figure 14. Quinone estimates (a) for all roof samples and (b) averaged for the type of roof material; estimate units are pmol Quinone per square cm.

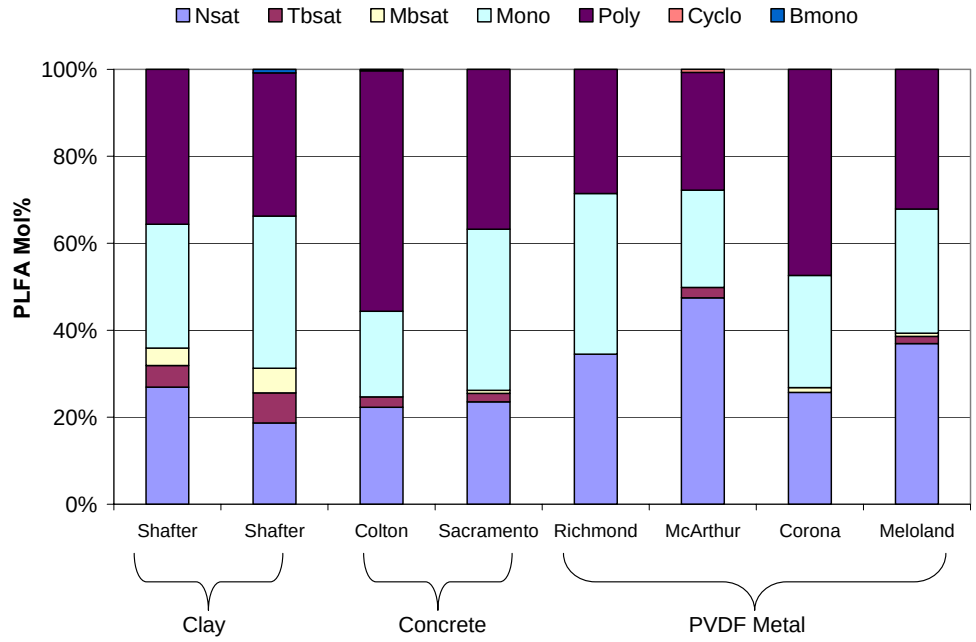

Figure 15. Community structure for the PLFA.

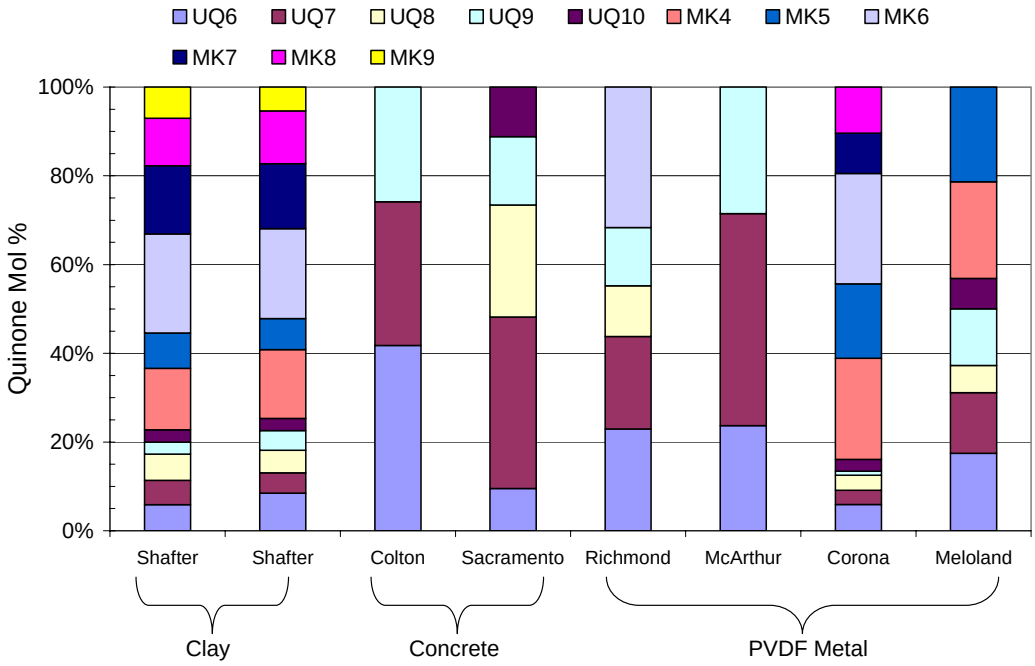

Figure 16. Quinone community composition.

Appendix A

El Centro Exposure Site (RS01)

Painted metal, clay and concrete tile roof products with and without cool color pigments were placed at ground level at the Davis University Agricultural Extension office located in El Centro, CA. Coupons of the roof products were installed in exposure rack assemblies, which are 5.5-ft high by 9-ft long, and divided into three sub-frames having respective slopes of 2-, 4- and 8-in of rise for 12-in of run (i.e., slopes of 9.5°, 18.4° and 33.7°). Each sub-frame can hold two "Sure-Grip" sub-assemblies, which are designed to have 6 rows of samples with 34-in of usable space in each row. Sample size is 3.5-in by 3.5-in. Orientation of the racks was set at 260° CCW and faced south, south-west into the sun. A CIMIS weather station (CIMIS # 87) is adjacent the exposure rack.

Figure A.1. Exposure rack ground mounted at University of Davis Agricultural Extension office, El Centro, CA.

El Centro, CA Solar Reflectance Field Data

Table A.1

				Exposure Time (yrs)				
	Identifier	**Code**	**Slope**	**0.000**	**0.742**	**0.962**	**1.625**	**2.488**
	BASF PVDF Painted Metal							
Regal White	872W2	900	2 in 12	0.740	0.664	0.551	0.724	0.609
	872W2	901	4 in 12	0.741	0.671	0.574	0.724	0.633
	872W2	902	8 in 12	0.740	0.697	0.653	0.722	0.647
	815W98	903	4 in 12	0.685	0.639	0.558	0.673	0.571
Rawhide	872T6	904	2 in 12	0.566	0.545	0.519	0.560	0.513
	872T6	905	4 in 12	0.566	0.534	0.497	0.564	0.521
	872T6	906	8 in 12	0.566	0.539	0.528	0.562	0.525
	836T223	907	4 in 12	0.439	0.422	0.412	0.430	0.410
Slate Blue	872B7	908	2 in 12	0.282	0.296	0.311	0.276	0.319
	872B7	909	4 in 12	0.282	0.297	0.321	0.276	0.308
	872B7	910	8 in 12	0.282	0.286	0.312	0.277	0.305
	815B49	911	4 in 12	0.169	0.192	0.243	0.173	0.240
Brick Red	872R10	912	2 in 12	0.374	0.379	0.384	0.382	0.400
	872R10	913	4 in 12	0.375	0.379	0.389	0.381	0.295
	872R10	914	8 in 12	0.373	0.380	0.389	0.383	0.397
	815R71	915	4 in 12	0.195	0.220	0.254	0.197	0.257
Charcoal Gray	872D6	916	2 in 12	0.308	0.320	0.342	0.316	0.358
	872D6	917	4 in 12	0.308	0.320	0.338	0.318	0.348
	872D6	918	8 in 12	0.308	0.325	0.333	0.317	0.347
	815D119	919	4 in 12	0.123	0.138	0.193	0.127	0.211
Hartford Green	872G16	920	2 in 12	0.270	0.288	0.318	0.276	
	872G16	921	4 in 12	0.272	0.290	0.319	0.276	
	872G16	922	8 in 12	0.274	0.295	0.290	0.280	
	815G37	923	4 in 12	0.088	0.134	0.176	0.094	
Slate Bronze	872T3	924	2 in 12	0.263	0.277	0.312	0.270	0.321
	872T3	925	4 in 12	0.262	0.283	0.304	0.270	0.315
	872T3	926	8 in 12	0.262	0.278	0.314	0.269	0.310
	815T119	927	4 in 12	0.118	0.155	0.250	0.123	0.211
	MCA Clay Tile							
White Buff	2F44	928	2 in 12	0.644	0.574	0.555	0.596	0.544
	2F44	929	4 in 12	0.638	0.567	0.554	0.581	0.539
	2F44	930	8 in 12	0.651	0.593	0.560	0.592	0.551
Apricot Buff	CF50	931	2 in 12	0.620	0.515	0.507	0.543	0.508
	CF50	932	4 in 12	0.598	0.546	0.545	0.574	0.543
	CF50	933	8 in 12	0.607	0.518	0.521	0.539	0.508
Adobe Gray	2F71	934	2 in 12	0.424	0.406	0.412	0.410	0.412
	2F71	935	4 in 12	0.421	0.409	0.414	0.419	0.414
	2F71	936	8 in 12	0.412	0.415	0.432	0.429	0.427
Regency Blue	2F52	937	2 in 12	0.411	0.395	0.398	0.395	0.395
	2F52	938	4 in 12	0.424	0.404	0.413	0.401	0.400
	2F52	939	8 in 12	0.422	0.402	0.409	0.392	0.401
Natural Red	F40	940	2 in 12	0.466	0.441	0.460	0.457	0.450
	F40	941	4 in 12	0.468	0.439	0.450		0.446
	F40	942	8 in 12	0.464	0.445	0.451	0.458	0.453
Weathered Green	B305	943	2 in 12	0.412	0.400	0.413	0.407	0.404
	B305	944	4 in 12	0.400	0.397	0.401	0.397	0.400
	B305	945	8 in 12	0.410	0.402	0.413	0.409	0.409
Ironwood	2F19	946	2 in 12	0.268	0.287	0.313	0.292	0.321
	2F19	947	4 in 12	0.271	0.300	0.315	0.296	0.321
	2F19	948	8 in 12	0.261	0.285	0.300	0.278	0.306
	US Clay Tile							
Buff Blend		979	2 in 12		0.568	0.543	0.568	0.549
Bermuda Blend		980	2 in 12		0.499	0.503	0.508	0.486
	Monierlife Concrete Roof Tile							
Terra Cotta Red	6978	949	2 in 12		0.184	0.268	0.181	0.229
	6978	950	4 in 12					
	6978	951	8 in 12					
Hearthside	3083	952	2 in 12		0.122	0.192	0.145	0.202
	3083	953	4 in 12		0.135	0.219	0.156	0.204
	3083	954	8 in 12		0.141	0.226	0.158	0.200
Riversidepebble	3080	955	2 in 12		0.164	0.225	0.166	0.214
	3080	956	4 in 12		0.131	0.202	0.140	0.189
	3080	957	8 in 12		0.136	0.219	0.154	0.200
Ebony	5047	958	2 in 12		0.133	0.257	0.130	0.188
	5047	959	4 in 12		0.136	0.242	0.156	0.187
	5047	960	8 in 12		0.134	0.219	0.129	0.177
Lincoln Green	4087	961	2 in 12		0.185	0.263	0.181	0.239
	4087	962	4 in 12		0.174	0.233	0.185	0.224
	4087	963	8 in 12		0.174	0.235	0.179	0.217

El Centro, CA Solar Reflectance Field Data

Table A.1

				Exposure Time (yrs)				
	Identifier	**Code**	**Slope**	**0.000**	**0.742**	**0.962**	**1.625**	**2.488**
	Shepherd Artic Match							
Blue Artic		964	2 in 12		0.226	0.285	0.237	0.285
		965	4 in 12		0.234	0.295	0.243	0.277
		966	8 in 12		0.225	0.299	0.235	0.269
Red Artic		967	2 in 12		0.267	0.317	0.279	0.316
		968	4 in 12		0.266	0.318	0.283	0.316
		969	8 in 12		0.309	0.339	0.306	0.338
Brown Artic		970	2 in 12		0.261	0.315	0.283	0.320
		971	4 in 12		0.260	0.315	0.283	0.313
		972	8 in 12		0.251	0.315	0.283	
Black Artic		973	2 in 12		0.260	0.311	0.262	0.298
		974	4 in 12		0.229	0.287	0.229	0.268
		975	8 in 12		0.247	0.299	0.242	0.272
Gray Artic		976	2 in 12		0.265	0.328	0.275	
		977	4 in 12		0.274	0.316	0.286	0.324
		978	8 in 12		0.278	0.323	0.294	
	American Roof Coatings							
NIR3704	Ultra Marine	981	8 in 12		0.389	0.382	0.397	0.396
IR3808	Chocolate	982	8 in 12		0.411	0.408	0.409	0.413
IR3503	Camo Green	983	8 in 12		0.467	0.456	0.460	0.454
IR3108	Light Gray	984	8 in 12		0.432	0.417	0.426	0.421
IR3308	Terracotta	985	8 in 12		0.473	0.455	0.476	0.421
NIR3900	Onyx	986	8 in 12		0.406	0.453	0.467	0.463

Appendix A

Corona Exposure Site (RS02)

Painted metal, clay and concrete tile roof products with and without cool color pigments were placed at ground level adjacent the clay tile manufacturing facility of Maruhachi Ceramics of America, Inc. located in Corona, CA. Coupons of the roof products were installed in exposure rack assemblies, which are 5.5-ft high by 9-ft long, and divided into three sub-frames having respective slopes of 2-, 4- and 8-in of rise for 12-in of run (i.e., slopes of 9.5°, 18.4° and 33.7°). Each sub-frame can hold two "Sure-Grip" sub-assemblies, which are designed to have 6 rows of samples with 34-in of usable space in each row. Sample size is 3.5-in by 3.5-in. Orientation of the racks is 310° CCW from the east and faces south south-east.

Figure A.2. Exposure rack ground mounted at Corona, CA.

Corona, CA Solar Reflectance Field Data

Table A.2

				Exposure Time (yrs)				
	Identifier	**Code**	**Slope**	**0.000**	**0.745**	**0.962**	**1.630**	**2.493**
	BASF PVDF Painted Metal							
Regal White	872W2	600	2 in 12	0.740	0.691	0.542	0.675	0.604
	872W2	601	4 in 12	0.739	0.692	0.605	0.671	0.604
	872W2	602	8 in 12	0.740	0.693	0.651	0.688	0.634
	815W98	603	4 in 12	0.687	0.649	0.566	0.620	0.574
Rawhide	872T6	604	2 in 12	0.573	0.532	0.468	0.518	0.489
	872T6	605	4 in 12	0.573	0.534	0.496	0.522	0.503
	872T6	606	8 in 12	0.569	0.535	0.498	0.524	0.508
	836T223	607	4 in 12	0.440	0.417	0.386	0.395	0.384
Slate Blue	872B7	608	2 in 12	0.282	0.278	0.282	0.259	0.278
	872B7	609	4 in 12	0.281	0.278	0.285	0.259	0.278
	872B7	610	8 in 12	0.282	0.279	0.279	0.262	0.277
	815B49	611	4 in 12	0.172	0.175	0.202	0.165	0.197
Brick Red	872R10	612	2 in 12	0.372	0.363	0.358	0.356	0.365
	872R10	613	4 in 12	0.374	0.364	0.360	0.358	0.368
	872R10	614	8 in 12	0.375	0.363	0.363	0.359	0.370
	815R71	615	4 in 12	0.195	0.198	0.222	0.190	0.223
Charcoal Gray	872D6	616	2 in 12	0.309	0.305	0.314	0.297	
	872D6	617	4 in 12	0.309	0.305	0.304	0.300	0.319
	872D6	618	8 in 12	0.308	0.304	0.305	0.300	0.318
	815D119	619	4 in 12	0.122	0.129	0.164	0.120	0.162
Hartford Green	872G16	620	2 in 12	0.271	0.271	0.289	0.263	0.286
	872G16	621	4 in 12	0.272	0.271	0.280	0.266	0.288
	872G16	622	8 in 12	0.272	0.268	0.274	0.263	
	815G37	623	4 in 12	0.089	0.097	0.142	0.095	0.137
Slate Bronze	872T3	624	2 in 12	0.262	0.261	0.280	0.253	0.278
	872T3	625	4 in 12	0.263	0.263	0.276	0.256	0.280
	872T3	626	8 in 12	0.262	0.262	0.266	0.257	0.278
	815T119	627	4 in 12	0.118	0.124	0.167	0.119	0.161
	MCA Clay Tile							
White Buff	2F44	628	2 in 12	0.640	0.560	0.482	0.526	0.458
	2F44	629	4 in 12	0.651	0.568	0.503	0.536	0.484
	2F44	630	8 in 12	0.632	0.584	0.538	0.550	0.514
Apricot Buff	CF50	631	2 in 12	0.601	0.547	0.482	0.514	0.433
	CF50	632	4 in 12	0.595	0.539	0.477	0.510	0.469
	CF50	633	8 in 12	0.619	0.549	0.558	0.527	0.497
Adobe Gray	2F71	634	2 in 12	0.426	0.414	0.385	0.393	0.366
	2F71	635	4 in 12	0.418	0.420	0.387	0.395	0.383
	2F71	636	8 in 12	0.420	0.400	0.392	0.389	0.380
Regency Blue	2F52	637	2 in 12	0.420	0.395	0.368	0.365	0.338
	2F52	638	4 in 12	0.412	0.388	0.366	0.355	0.350
	2F52	639	8 in 12	0.406	0.396	0.377	0.371	0.361
Natural Red	F40	640	2 in 12	0.449	0.415	0.393	0.395	
	F40	641	4 in 12	0.462	0.430	0.415	0.408	0.394
	F40	642	8 in 12	0.459	0.423	0.430	0.415	0.407
Weathered Green	B305	643	2 in 12	0.411	0.386	0.346	0.357	
	B305	644	4 in 12	0.419	0.378	0.348	0.357	0.340
	B305	645	8 in 12	0.409	0.390	0.385	0.378	0.372
Ironwood	2F19	646	2 in 12	0.267	0.253	0.264	0.240	
	2F19	647	4 in 12	0.273	0.252	0.267	0.245	0.272
	2F19	648	8 in 12	0.270	0.253	0.255	0.257	0.275
	US Clay Tile							
Buff Blend		679	2 in 12		0.536	0.272	0.492	0.436
Bermuda Blend		680	2 in 12		0.456	0.278	0.411	0.396
	Monierlife Concrete Roof Tile							
Terra Cotta Red	6978	649	2 in 12		0.206	0.233	0.197	0.228
	6978	650	4 in 12		0.207	0.209	0.195	0.235
	6978	651	8 in 12		0.178	0.182	0.165	0.212
Hearthside	3083	652	2 in 12		0.143	0.186	0.158	0.196
	3083	653	4 in 12		0.131	0.134	0.166	0.217
	3083	654	8 in 12		0.125	0.138	0.164	0.207
Riversidepebble	3080	655	2 in 12		0.146	0.171	0.164	0.215
	3080	656	4 in 12		0.151	0.142	0.199	0.222
	3080	657	8 in 12		0.151	0.141	0.156	0.200
Ebony	5047	658	2 in 12		0.140	0.186	0.141	0.192
	5047	659	4 in 12		0.131	0.130	0.128	0.176
	5047	660	8 in 12		0.137	0.135	0.125	0.172
Lincoln Green	4087	661	2 in 12		0.169	0.211	0.178	0.227
	4087	662	4 in 12		0.161	0.140	0.174	0.217
	4087	663	8 in 12		0.165	0.164	0.171	0.203

Corona, CA Solar Reflectance Field Data

Table A.2

				Exposure Time (yrs)				
	Identifier	**Code**	**Slope**	**0.000**	**0.745**	**0.962**	**1.630**	**2.493**
	Shepherd Artic Match							
Blue Artic		664	2 in 12		0.255	0.270	0.251	0.257
		665	4 in 12		0.258	0.273	0.249	0.265
		666	8 in 12		0.250	0.262	0.238	0.250
Red Artic		667	2 in 12		0.273	0.283	0.261	0.269
		668	4 in 12		0.270		0.266	0.281
		669	8 in 12		0.276	0.287	0.262	0.279
Brown Artic		670	2 in 12		0.255	0.282	0.253	0.262
		671	4 in 12		0.244	0.268	0.247	0.263
		672	8 in 12		0.258	0.277	0.266	0.278
Black Artic		673	2 in 12		0.230	0.258	0.212	0.249
		674	4 in 12		0.228			0.240
		675	8 in 12		0.234	0.236	0.217	0.238
Gray Artic		676	2 in 12		0.252	0.272	0.233	0.254
		677	4 in 12		0.243		0.249	0.264
		678	8 in 12		0.251	0.278	0.250	0.271
	American Roof Coatings							
NIR3704	Ultra Marine	681	4 in 12		0.383	0.379	0.362	0.367
IR3808	Chocolate	682	4 in 12		0.410	0.395	0.387	0.387
IR3503	Camo Green	683	4 in 12		0.467	0.448	0.435	0.429
IR3108	Light Gray	684	4 in 12		0.438	0.415	0.400	0.395
IR3308	Terracotta	685	4 in 12		0.474	0.463	0.443	0.439
NIR3900	Onyx	686	4 in 12		0.432	0.463	0.434	0.417

Appendix A

Colton Exposure Site (RS03)

Painted metal, clay and concrete tile roof products with and without cool color pigments were placed on top of the low-slope roof at BASF's Research plant in Colton, CA. Coupons of the roof products were installed in exposure rack assemblies, which are 5.5-ft high by 9-ft long, and divided into three sub-frames having respective slopes of 2-, 4- and 8-in of rise for 12-in of run (i.e., slopes of 9.5°, 18.4° and 33.7°). Each sub-frame can hold two "Sure-Grip" sub-assemblies, which are designed to have 6 rows of samples with 34-in of usable space in each row. Sample size is 3.5-in by 3.5-in. Orientation of the racks was set at 270° CCW from the east, so the roof coupons faced directly south to receive full solar exposure.

Figure A.3. Exposure rack mounted on the low-slope roof of BASF's Research facility in Colton, CA.

Colton, CA Solar Reflectance Field Data

Table A.3

				Exposure Time (yrs)				
	Identifier	**Code**	**Slope**	**0.000**	**0.748**	**0.962**	**1.630**	**2.493**
	BASF PVDF Painted Metal							
Regal White	872W2	500	2.628 in 12	0.742	0.646	0.491	0.673	0.639
	872W2	501	4.628 in 12	0.742	0.649	0.537	0.677	0.642
	872W2	502	8.628 in 12	0.743	0.663	0.537	0.681	0.658
	815W98	503	4.628 in 12	0.689	0.602	0.513	0.625	0.602
Rawhide	872T6	504	2.628 in 12	0.570	0.503	0.413	0.521	0.504
	872T6	505	4.628 in 12	0.572	0.509	0.438	0.520	0.515
	872T6	506	8.628 in 12	0.568	0.515	0.456	0.528	0.524
	836T223	507	4.628 in 12	0.440	0.400	0.356	0.400	0.399
Slate Blue	872B7	508	2.628 in 12	0.283	0.276	0.289	0.257	0.272
	872B7	509	4.628 in 12	0.282	0.278	0.290	0.258	0.271
	872B7	510	8.628 in 12	0.283	0.278	0.290	0.257	0.271
	815B49	511	4.628 in 12	0.173	0.185	0.227	0.162	0.181
Brick Red	872R10	512	2.628 in 12	0.375	0.354	0.343	0.353	0.363
	872R10	513	4.628 in 12	0.374	0.355	0.349	0.353	0.365
	872R10	514	8.628 in 12	0.374	0.358	0.349	0.355	0.362
	815R71	515	4.628 in 12	0.195	0.205	0.250	0.186	0.206
Charcoal Gray	872D6	516	2.628 in 12	0.308	0.304	0.314	0.297	0.312
	872D6	517	4.628 in 12	0.308	0.304	0.317	0.297	
	872D6	518	8.628 in 12	0.308	0.305	0.316	0.297	
	815D119	519	4.628 in 12	0.122	0.130	0.203	0.117	
Hartford Green	872G16	520	2.628 in 12	0.272	0.271	0.296	0.254	0.276
	872G16	521	4.628 in 12	0.272	0.273	0.294	0.260	0.277
	872G16	522	8.628 in 12	0.273	0.271	0.294	0.260	0.275
	815G37	523	4.628 in 12	0.089	0.116	0.189	0.088	0.113
Slate Bronze	872T3	524	2.628 in 12	0.262	0.263	0.293	0.251	0.268
	872T3	525	4.628 in 12	0.263	0.264	0.290	0.252	0.270
	872T3	526	8.628 in 12	0.262	0.264	0.287	0.249	0.268
	815T119	527	4.628 in 12	0.118	0.140	0.206	0.115	0.139
	MCA Clay Tile							
White Buff	2F44	528	2.628 in 12	0.647	0.543	0.456	0.559	0.509
	2F44	529	4.628 in 12	0.653	0.554	0.479	0.565	0.523
	2F44	530	8.628 in 12	0.643	0.555	0.482	0.568	0.541
Apricot Buff	CF50	531	2.628 in 12	0.609	0.555	0.472	0.560	0.491
	CF50	532	4.628 in 12	0.611	0.563	0.496	0.576	0.505
	CF50	533	8.628 in 12	0.604	0.519	0.459	0.536	0.506
Adobe Gray	2F71	534	2.628 in 12	0.434	0.361	0.344	0.364	0.352
	2F71	535	4.628 in 12	0.460	0.378	0.359	0.380	0.369
	2F71	536	8.628 in 12	0.449	0.384	0.363	0.386	0.383
Regency Blue	2F52	537	2.628 in 12	0.435	0.379	0.351	0.367	0.351
	2F52	538	4.628 in 12	0.424	0.380	0.355	0.368	0.357
	2F52	539	8.628 in 12	0.430	0.381	0.359	0.369	0.368
Natural Red	F40	540	2.628 in 12	0.461	0.421	0.397	0.423	0.413
	F40	541	4.628 in 12	0.463	0.416	0.389	0.412	0.405
	F40	542	8.628 in 12	0.465	0.418	0.395	0.419	0.417
Weathered Green	B305	543	2.628 in 12	0.405	0.377	0.352	0.377	0.353
	B305	544	4.628 in 12	0.406	0.363	0.341	0.360	0.337
	B305	545	8.628 in 12	0.411	0.358	0.332	0.353	0.336
Ironwood	2F19	546	2.628 in 12	0.270	0.254	0.273	0.240	0.252
	2F19	547	4.628 in 12	0.268	0.253	0.272	0.240	0.252
	2F19	548	8.628 in 12	0.267	0.258	0.271	0.244	0.256
	US Clay Tile							
Buff Blend		579	2.628 in 12		0.514	0.465	0.489	0.471
Bermuda Blend		580	2.628 in 12		0.481	0.455	0.472	0.468
	Monierlife Concrete Roof Tile							
Terra Cotta Red	6978	549	2.628 in 12		0.200	0.230	0.192	0.219
	6978	550	4.628 in 12		0.195	0.222	0.181	0.210
	6978	551	8.628 in 12		0.202	0.226	0.176	0.206
Hearthside	3083	552	2.628 in 12		0.149	0.202	0.178	0.207
	3083	553	4.628 in 12		0.138	0.200	0.158	0.193
	3083	554	8.628 in 12		0.135	0.207	0.161	0.190
Riversidepebble	3080	555	2.628 in 12		0.141	0.195	0.171	0.197
	3080	556	4.628 in 12		0.141	0.201	0.172	0.199
	3080	557	8.628 in 12		0.154	0.196	0.148	0.186
Ebony	5047	558	2.628 in 12		0.139	0.187	0.134	0.167
	5047	559	4.628 in 12		0.130	0.189	0.131	0.160
	5047	560	8.628 in 12		0.143	0.193	0.125	0.155
Lincoln Green	4087	561	2.628 in 12		0.180	0.226	0.172	0.197
	4087	562	4.628 in 12		0.153	0.204	0.152	
	4087	563	8.628 in 12		0.175	0.211	0.169	0.203

Colton, CA Solar Reflectance Field Data

Table A.3

				Exposure Time (yrs)				
	Identifier	**Code**	**Slope**	**0.000**	**0.748**	**0.962**	**1.630**	**2.493**
	Shepherd Artic Match							
Blue Artic		564	2.628 in 12		0.234	0.260	0.222	0.232
		565	4.628 in 12		0.242	0.270	0.229	0.238
		566	8.628 in 12		0.250	0.276	0.242	0.263
Red Artic		567	2.628 in 12		0.265	0.279	0.256	0.254
		568	4.628 in 12		0.276	0.287	0.263	0.264
		569	8.628 in 12		0.311	0.302	0.273	0.289
Brown Artic		570	2.628 in 12		0.250	0.281	0.260	0.263
		571	4.628 in 12		0.265	0.290	0.258	0.266
		572	8.628 in 12		0.266	0.283	0.266	0.276
Black Artic		573	2.628 in 12		0.233	0.265	0.208	0.229
		574	4.628 in 12		0.245	0.264	0.215	0.230
		575	8.628 in 12		0.223	0.255	0.197	0.220
Gray Artic		576	2.628 in 12		0.246	0.277	0.241	
		577	4.628 in 12		0.252	0.277	0.256	
		578	8.628 in 12		0.276	0.286	0.256	0.267
	American Roof Coatings							
NIR3704	Ultra Marine	581	4 in 12		0.369	0.343	0.355	0.358
IR3808	Chocolate	582	4 in 12		0.411	0.365	0.377	0.385
IR3503	Camo Green	583	4 in 12		0.466	0.392	0.426	0.428
IR3108	Light Gray	584	4 in 12		0.433	0.367	0.391	0.392
IR3308	Terracotta	585	4 in 12		0.474	0.403	0.433	0.433
NIR3900	Onyx	586	4 in 12		0.430	0.424	0.426	0.413

Appendix A

Shafter Exposure Site (RS04)

Painted metal, clay and concrete tile roof products with and without cool color pigments were placed at ground level on the premises of Elk Corp.'s manufacturing facility in Shafter, CA. Coupons of the roof products were installed in exposure rack assemblies, which are 5.5-ft high by 9-ft long, and divided into three sub-frames having respective slopes of 2-, 4- and 8-in of rise for 12-in of run (i.e., slopes of 9.5°, 18.4° and 33.7°). Each sub-frame can hold two "Sure-Grip" sub-assemblies, which are designed to have 6 rows of samples with 34-in of usable space in each row. Sample size is 3.5-in by 3.5-in. Orientation of the racks was set at 270° CCW from the east, so the roof coupons faced directly south to receive full solar exposure.

Figure A.4. Exposure rack mounted on the ground at Elk Corp.'s Manufacturing facility in Shafter, CA.

Shafter, CA Solar Reflectance Field Data

Table A.4

				Exposure Time (yrs)				
	Identifier	**Code**	**Slope**	**0.000**	**0.751**	**0.959**	**1.633**	**2.496**
	BASF PVDF Painted Metal							
Regal White	872W2	700	2 in 12	0.739	0.613	0.529	0.687	0.596
	872W2	701	4 in 12	0.742	0.559	0.589	0.685	0.623
	872W2	702	8 in 12	0.737	0.591	0.558	0.689	0.617
	815W98	703	4 in 12	0.688	0.551	0.545	0.638	0.574
Rawhide	872T6	704	2 in 12	0.570	0.490	0.443	0.524	
	872T6	705	4 in 12	0.569	0.456	0.457	0.523	
	872T6	706	8 in 12	0.574	0.469	0.437	0.525	
	836T223	707	4 in 12	0.441	0.378	0.369	0.405	
Slate Blue	872B7	708	2 in 12	0.282	0.278	0.277	0.256	0.256
	872B7	709	4 in 12	0.283	0.279	0.278	0.258	0.261
	872B7	710	8 in 12	0.282	0.278	0.280	0.258	0.262
	815B49	711	4 in 12	0.172	0.199	0.204	0.158	0.176
Brick Red	872R10	712	2 in 12	0.375	0.350	0.340	0.353	0.339
	872R10	713	4 in 12	0.375	0.344	0.347	0.354	0.348
	872R10	714	8 in 12	0.375	0.340	0.338	0.353	0.350
	815R71	715	4 in 12	0.195	0.220	0.218	0.184	0.200
Charcoal Gray	872D6	716	2 in 12	0.308	0.303	0.307	0.295	0.296
	872D6	717	4 in 12	0.308	0.304	0.303	0.295	0.299
	872D6	718	8 in 12	0.308	0.304	0.305	0.297	0.301
	815D119	719	4 in 12	0.122	0.175	0.163	0.116	0.141
Hartford Green	872G16	720	2 in 12	0.270	0.276	0.279	0.258	0.262
	872G16	721	4 in 12	0.272	0.278	0.279	0.260	0.267
	872G16	722	8 in 12	0.271	0.273	0.279	0.260	0.266
	815G37	723	4 in 12	0.088	0.154	0.151	0.086	0.114
Slate Bronze	872T3	724	2 in 12	0.262	0.269	0.273	0.250	0.258
	872T3	725	4 in 12	0.263	0.269	0.273	0.250	0.258
	872T3	726	8 in 12	0.262	0.270	0.277	0.250	0.257
	815T119	727	4 in 12	0.188	0.161	0.180	0.113	0.137
	MCA Clay Tile							
White Buff	2F44	728	2 in 12	0.626	0.503	0.482	0.541	0.476
	2F44	729	4 in 12	0.645	0.487	0.488	0.536	0.473
	2F44	730	8 in 12	0.637	0.505	0.491	0.556	0.488
Apricot Buff	CF50	731	2 in 12	0.644	0.489	0.451	0.513	0.440
	CF50	732	4 in 12	0.652	0.448	0.438	0.505	0.468
	CF50	733	8 in 12	0.606	0.458	0.454	0.522	0.470
Adobe Gray	2F71	734	2 in 12	0.406	0.367	0.358	0.369	0.347
	2F71	735	4 in 12	0.424	0.363	0.359	0.373	0.354
	2F71	736	8 in 12	0.428	0.352	0.358	0.371	0.344
Regency Blue	2F52	737	2 in 12	0.414	0.367	0.366	0.343	0.317
	2F52	738	4 in 12	0.413	0.360	0.367	0.359	0.328
	2F52	739	8 in 12	0.407	0.360	0.382	0.364	0.339
Natural Red	F40	740	2 in 12	0.470	0.415	0.413	0.407	0.368
	F40	741	4 in 12	0.457	0.410	0.429	0.407	0.380
	F40	742	8 in 12	0.460	0.409	0.401	0.414	0.382
Weathered Green	B305	743	2 in 12	0.425	0.362	0.341	0.369	0.345
	B305	744	4 in 12	0.406	0.333	0.328	0.352	0.329
	B305	745	8 in 12	0.401	0.334	0.334	0.364	0.339
Ironwood	2F19	746	2 in 12	0.266	0.260	0.275	0.231	0.240
	2F19	747	4 in 12	0.267	0.267	0.273	0.237	0.247
	2F19	748	8 in 12	0.270	0.262	0.274	0.235	0.241
	US Clay Tile							
Buff Blend		779	2 in 12		0.565	0.486	0.521	
Bermuda Blend		780	2 in 12		0.489	0.436	0.447	
	Monierlife Concrete Roof Tile							
Terra Cotta Red	6978	749	2 in 12		0.202	0.238	0.172	0.189
	6978	750	4 in 12		0.181	0.226	0.154	0.173
	6978	751	8 in 12		0.216	0.235	0.168	0.183
Hearthside	3083	752	2 in 12		0.121	0.196	0.136	0.162
	3083	753	4 in 12		0.125	0.194	0.142	0.184
	3083	754	8 in 12		0.131	0.199	0.144	0.164
Riversidepebble	3080	755	2 in 12		0.142	0.185	0.134	0.167
	3080	756	4 in 12		0.165	0.197	0.164	0.178
	3080	757	8 in 12		0.148	0.187	0.148	0.178
Ebony	5047	758	2 in 12		0.137	0.199	0.112	0.142
	5047	759	4 in 12		0.141	0.197	0.109	0.137
	5047	760	8 in 12		0.141	0.191	0.111	0.137
Lincoln Green	4087	761	2 in 12		0.155	0.210	0.151	0.170
	4087	762	4 in 12		0.177	0.217	0.157	0.189
	4087	763	8 in 12		0.185	0.218	0.161	0.186

Shafter, CA Solar Reflectance Field Data

Table A.4

				Exposure Time (yrs)				
	Identifier	Code	Slope	0.000	0.751	0.959	1.633	2.496
	Shepherd Artic Match							
Blue Artic		764	2 in 12		0.246	0.262	0.238	0.230
		765	4 in 12		0.237	0.249	0.220	0.229
		766	8 in 12		0.226	0.251	0.206	0.217
Red Artic		767	2 in 12		0.312	0.294	0.377	0.279
		768	4 in 12		0.331	0.297	0.313	0.316
		769	8 in 12		0.321	0.297	0.302	0.299
Brown Artic		770	2 in 12		0.251	0.264	0.250	0.242
		771	4 in 12		0.259	0.266	0.253	0.253
		772	8 in 12		0.260	0.263	0.248	0.248
Black Artic		773	2 in 12		0.240	0.256	0.203	0.213
		774	4 in 12		0.231	0.252	0.210	0.221
		775	8 in 12		0.213	0.239	0.196	0.206
Gray Artic		776	2 in 12		0.257	0.260	0.247	0.241
		777	4 in 12		0.272	0.265	0.246	0.256
		778	8 in 12		0.248	0.259	0.238	0.239
	American Roof Coatings							
NIR3704	Ultra Marine	781	4 in 12		0.385	0.338	0.364	0.350
IR3808	Chocolate	782	4 in 12		0.410	0.363	0.378	0.371
IR3503	Camo Green	783	4 in 12		0.464	0.411	0.429	0.408
IR3108	Light Gray	784	4 in 12		0.433	0.377	0.397	0.381
IR3308	Terracotta	785	4 in 12		0.473	0.416	0.443	0.425
NIR3900	Onyx	786	4 in 12		0.422	0.430	0.410	0.392

Appendix A

Richmond Exposure Site (RS05)

Painted metal, clay and concrete tile roof products with and without cool color pigments were placed on top of the steep-slope roof at Steelscape Inc.'s warehouse in Richmond, CA. Coupons of the roof products were installed in exposure rack assemblies, which are 5.5-ft high by 9-ft long, and divided into three sub-frames having respective slopes of 2-, 4- and 8-in of rise for 12-in of run (i.e., slopes of 9.5°, 18.4° and 33.7°). Each sub-frame can hold two "Sure-Grip" sub-assemblies, which are designed to have 6 rows of samples with 34-in of usable space in each row. Sample size is 3.5-in by 3.5-in. Orientation of the racks was set at 235° CCW (facing directly east represents 0° CCW), so the roof coupons faced south, south-west to receive almost full solar exposure.

Figure A.5. Exposure rack mounted on the roof of the Steelscape warehouse in Richmond, CA.

Richmond, CA Solar Reflectance Field Data

Table A.5

				Exposure Time (yrs)				
	Identifier	**Code**	**Slope**	**0.000**	**0.748**	**0.959**	**1.638**	**2.501**
	BASF PVDF Painted Metal							
Regal White	872W2	400	2 in 12	0.742	0.632	0.632	0.718	0.720
	872W2	401	4 in 12	0.742	0.633	0.633	0.716	0.720
	872W2	402	8 in 12	0.742	0.620	0.620	0.713	0.724
	815W98	403	4 in 12	0.688	0.581	0.581	0.661	0.670
Rawhide	872T6	404	2 in 12	0.569	0.492	0.492	0.546	
	872T6	405	4 in 12	0.569	0.490	0.490	0.544	
	872T6	406	8 in 12	0.568	0.484	0.484	0.544	
	836T223	407	4 in 12	0.440	0.381	0.381	0.415	0.429
Slate Blue	872B7	408	2 in 12	0.282	0.257	0.257	0.262	0.265
	872B7	409	4 in 12	0.281	0.259	0.259	0.261	0.275
	872B7	410	8 in 12	0.280	0.256	0.256	0.260	0.275
	815B49	411	4 in 12	0.172	0.172	0.172	0.161	0.174
Brick Red	872R10	412	2 in 12	0.374	0.341	0.341	0.358	0.376
	872R10	413	4 in 12	0.375	0.339	0.339	0.360	0.375
	872R10	414	8 in 12	0.373	0.340	0.340	0.357	0.375
	815R71	415	4 in 12	0.195	0.192	0.192	0.184	0.198
Charcoal Gray	872D6	416	2 in 12	0.308	0.297	0.297	0.301	0.319
	872D6	417	4 in 12	0.308	0.295	0.295	0.300	0.317
	872D6	418	8 in 12	0.308	0.294	0.294	0.299	
	815D119	419	4 in 12	0.122	0.132	0.132	0.115	0.126
Hartford Green	872G16	420	2 in 12	0.272	0.264	0.264	0.262	0.278
	872G16	421	4 in 12	0.273	0.260	0.260	0.261	0.275
	872G16	422	8 in 12	0.272	0.260	0.260	0.258	0.276
	815G37	423	4 in 12	0.088	0.106	0.106	0.084	0.094
Slate Bronze	872T3	424	2 in 12	0.262	0.252	0.252	0.254	0.269
	872T3	425	4 in 12	0.263	0.252	0.252	0.254	0.270
	872T3	426	8 in 12	0.263	0.250	0.250	0.251	0.266
	815T119	427	4 in 12	0.118	0.127	0.127	0.112	0.123
	MCA Clay Tile							
White Buff	2F44	428	2 in 12	0.630	0.585	0.585	0.585	0.583
	2F44	429	4 in 12	0.643	0.585	0.585	0.603	0.601
	2F44	430	8 in 12	0.651	0.564	0.564	0.586	0.590
Apricot Buff	CF50	431	2 in 12	0.602	0.529	0.529	0.539	0.531
	CF50	432	4 in 12	0.599	0.511	0.511	0.535	0.532
	CF50	433	8 in 12	0.607	0.549	0.549	0.566	0.564
Adobe Gray	2F71	434	2 in 12	0.424	0.395	0.395	0.397	0.404
	2F71	435	4 in 12	0.441	0.388	0.388	0.393	0.400
	2F71	436	8 in 12	0.427	0.390	0.390	0.395	0.401
Regency Blue	2F52	437	2 in 12	0.435	0.389	0.389	0.369	0.378
	2F52	438	4 in 12	0.433	0.385	0.385	0.374	0.382
	2F52	439	8 in 12	0.432	0.372	0.372	0.366	0.375
Natural Red	F40	440	2 in 12	0.459	0.408	0.408	0.411	0.418
	F40	441	4 in 12	0.458	0.419	0.419	0.427	0.433
	F40	442	8 in 12	0.461	0.428	0.428	0.428	0.434
Weathered Green	B305	443	2 in 12	0.420	0.362	0.362	0.373	0.373
	B305	444	4 in 12	0.411	0.385	0.385	0.387	0.396
	B305	445	8 in 12	0.413	0.362	0.362	0.374	0.382
Ironwood	2F19	446	2 in 12	0.269	0.258	0.258	0.245	0.259
	2F19	447	4 in 12	0.272	0.259	0.259	0.247	0.263
	2F19	448	8 in 12	0.268	NA	NA	0.249	0.265
	US Clay Tile							
Buff Blend		479	2 in 12		0.585	0.585	0.552	0.577
Bermuda Blend		480	2 in 12		0.489	0.489	0.457	0.467
	Monierlife Concrete Roof Tile							
Terra Cotta Red	6978	449	2 in 12		0.196	0.196	0.177	0.207
	6978	450	4 in 12		0.180	0.180	0.176	0.210
	6978	451	8 in 12		0.194	0.194	0.184	0.219
Hearthside	3083	452	2 in 12		0.125	0.125	0.154	0.159
	3083	453	4 in 12		0.134	0.134	0.142	0.160
	3083	454	8 in 12		0.125	0.125	0.137	0.155
Riversidepebble	3080	455	2 in 12		0.154	0.154	0.175	0.189
	3080	456	4 in 12		0.139	0.139	0.161	0.171
	3080	457	8 in 12		0.143	0.143	0.171	0.166
Ebony	5047	458	2 in 12		0.146	0.146	0.123	0.144
	5047	459	4 in 12		0.145	0.145	0.130	0.151
	5047	460	8 in 12		0.141	0.141	0.128	0.148
Lincoln Green	4087	461	2 in 12		0.157	0.157	0.165	0.193
	4087	462	4 in 12		0.171	0.171	0.174	0.206
	4087	463	8 in 12		0.161	0.161	0.163	0.192

Richmond, CA Solar Reflectance Field Data

Table A.5

				Exposure Time (yrs)				
	Identifier	Code	Slope	0.000	0.748	0.959	1.638	2.501
	Shepherd Artic Match							
Blue Artic		464	2 in 12		0.230	0.230	0.214	0.223
		465	4 in 12		0.234	0.234	0.215	0.237
		466	8 in 12		0.241	0.241	0.219	0.229
Red Artic		467	2 in 12		0.284	0.284	0.266	0.266
		468	4 in 12		0.277	0.277	0.264	0.261
		469	8 in 12		0.270	0.270	0.258	0.260
Brown Artic		470	2 in 12		0.262	0.262	0.252	0.258
		471	4 in 12		0.249	0.249	0.246	0.251
		472	8 in 12		0.247	0.247	0.253	0.251
Black Artic		473	2 in 12		0.229	0.229	0.201	0.206
		474	4 in 12		0.231	0.231	0.196	0.223
		475	8 in 12		0.238	0.238	0.214	0.219
Gray Artic		476	2 in 12		0.262	0.262	0.246	0.243
		477	4 in 12		0.259	0.259	0.252	0.252
		478	8 in 12		0.256	0.256	0.242	0.244
	American Roof Coatings							
NIR3704	Ultra Marine	481	4 in 12		0.371	0.371	0.364	0.378
IR3808	Chocolate	482	4 in 12		0.410	0.410	0.389	0.398
IR3503	Camo Green	483	4 in 12		0.463	0.463	0.438	0.451
IR3108	Light Gray	484	4 in 12		0.434	0.434	0.405	0.422
IR3308	Terracotta	485	4 in 12		0.474	0.474	0.452	0.460
NIR3900	Onyx	486	4 in 12		0.428	0.428	0.445	0.443

Appendix A

Sacramento Exposure Site (RS06)

Painted metal, clay and concrete tile roof products with and without cool color pigments were placed on top of the low-slope roof at Custom-Bilt's warehouse in Sacramento, CA. Coupons of the roof products were installed in exposure rack assemblies, which are 5.5-ft high by 9-ft long, and divided into three sub-frames having respective slopes of 2-, 4- and 8-in of rise for 12-in of run (i.e., slopes of 9.5°, 18.4° and 33.7°). Each sub-frame can hold two "Sure-Grip" sub-assemblies, which are designed to have 6 rows of samples with 34-in of usable space in each row. Sample size is 3.5-in by 3.5-in. Orientation of the racks was set at 270° CCW (facing directly east represents 0° CCW), so the roof coupons faced almost directly south to receive full solar exposure.

Figure A.6. Exposure rack mounted on the low-slope roof of Custom-Bilt Metal's warehouse in Sacramento, CA.

Sacramento, CA Solar Reflectance Field Data

Table A.6

				Exposure Time (yrs)				
	Identifier	Code	Slope	0.000	0.764	0.959	1.644	2.507
	BASF PVDF Painted Metal							
Regal White	872W2	300	1.359 in 12	0.743	0.699	0.646	0.689	0.685
	872W2	301	3.313 in 12	0.742	0.708	0.630	0.699	0.686
	872W2	302	7.122 in 12	0.744	0.706	0.659	0.698	0.688
	815W98	303	3.313 in 12	0.687	0.653	0.601	0.640	0.634
Rawhide	872T6	304	1.359 in 12	0.570	0.533	0.511	0.525	0.529
	872T6	305	3.313 in 12	0.568	0.533	0.510	0.529	0.528
	872T6	306	7.122 in 12	0.568	0.535	0.508	0.531	0.533
	836T223	307	3.313 in 12	0.439	0.410	0.403	0.401	0.408
Slate Blue	872B7	308	1.359 in 12	0.281	0.263	0.282	0.257	0.267
	872B7	309	3.313 in 12	0.282	0.264	0.281	0.256	0.271
	872B7	310	7.122 in 12	0.282	0.264	0.281	0.259	0.270
	815B49	311	3.313 in 12	0.172	0.162	0.194	0.161	0.176
Brick Red	872R10	312	1.359 in 12	0.374	0.348	0.361	0.351	0.362
	872R10	313	3.313 in 12	0.373	0.348	0.361	0.353	0.365
	872R10	314	7.122 in 12	0.374	0.350	0.357	0.354	0.369
	815R71	315	3.313 in 12	0.195	0.182	0.214	0.183	0.196
Charcoal Gray	872D6	316	1.359 in 12	0.309	0.286	0.308	0.293	0.307
	872D6	317	3.313 in 12	0.308	0.288	0.310	0.296	0.311
	872D6	318	7.122 in 12	0.308	0.289	0.308	0.297	0.311
	815D119	319	3.313 in 12	0.123	0.113	0.154	0.116	0.128
Hartford Green	872G16	320	1.359 in 12	0.272	0.253	0.279	0.257	0.270
	872G16	321	3.313 in 12	0.271	0.253	0.279	0.258	0.271
	872G16	322	7.122 in 12	0.271	0.253	0.278	0.259	0.273
	815G37	323	3.313 in 12	0.088	0.084	0.126	0.085	0.097
Slate Bronze	872T3	324	1.359 in 12	0.262	0.244	0.272	0.251	0.261
	872T3	325	3.313 in 12	0.262	0.246	0.274	0.251	0.264
	872T3	326	7.122 in 12	0.262	0.247	0.271	0.251	0.264
	815T119	327	3.313 in 12	0.118	0.111	0.138	0.111	0.123
	MCA Clay Tile							
White Buff	2F44	328	1.359 in 12	0.644	0.597	0.572	0.568	0.583
	2F44	329	3.313 in 12	0.652	0.600	0.578	0.574	0.588
	2F44	330	7.122 in 12	0.630	0.596	0.584	0.585	0.580
Apricot Buff	CF50	331	1.359 in 12	0.600	0.535	0.529	0.520	0.509
	CF50	332	3.313 in 12	0.611	0.557	0.539	0.536	0.534
	CF50	333	7.122 in 12	0.606	0.554	0.545	0.539	0.537
Adobe Gray	2F71	334	1.359 in 12	0.423	0.397	0.404	0.390	0.401
	2F71	335	3.313 in 12	0.418	0.421	0.425	0.415	0.434
	2F71	336	7.122 in 12	0.423	0.412	0.419	0.409	0.419
Regency Blue	2F52	337	1.359 in 12	0.416	0.394	0.408	0.384	0.392
	2F52	338	3.313 in 12	0.428	0.388	0.398	0.375	0.384
	2F52	339	7.122 in 12	0.413	0.397	0.408	0.387	0.398
Natural Red	F40	340	1.359 in 12	0.456	0.409	0.424	0.404	0.414
	F40	341	3.313 in 12	0.457	0.426	0.432	0.427	0.435
	F40	342	7.122 in 12	0.454	0.422	0.433	0.420	0.434
Weathered Green	B305	343	1.359 in 12	0.405	0.367	0.374	0.361	0.372
	B305	344	3.313 in 12	0.405	0.370	0.372	0.361	0.371
	B305	345	7.122 in 12	0.428	0.380	0.381	0.373	0.382
Ironwood	2F19	346	1.359 in 12	0.260	0.242	0.269	0.244	0.257
	2F19	347	3.313 in 12	0.271	0.243	0.264	0.241	0.238
	2F19	348	7.122 in 12	0.269	0.243	0.267	0.241	0.256
	US Clay Tile							
Buff Blend		379	3.313 in 11		0.562	0.567	0.546	0.401
Bermuda Blend		380	3.313 in 11		0.481	0.480	0.465	0.393
	Monierlife Concrete Roof Tile							
Terra Cotta Red	6978	349	1.359 in 12		0.184	0.213	0.183	0.207
	6978	350	3.313 in 12		0.197	0.215	0.173	0.200
	6978	351	7.122 in 12		0.196	0.205	0.174	0.199
Hearthside	3083	352	1.359 in 12		0.151	0.172	0.161	0.175
	3083	353	3.313 in 12		0.125	0.158	0.169	0.164
	3083	354	7.122 in 12		0.142	0.169	0.164	0.164
Riversidepebble	3080	355	1.359 in 12		0.126	0.143	0.140	0.167
	3080	356	3.313 in 12		0.151	0.180	0.149	0.171
	3080	357	7.122 in 12		0.160	0.176	0.161	0.170
Ebony	5047	358	1.359 in 12		0.145	0.152	0.117	0.141
	5047	359	3.313 in 12		0.136	0.156	0.159	0.148
	5047	360	7.122 in 12		0.143	0.150	0.148	0.146
Lincoln Green	4087	361	1.359 in 12		0.169	0.177	0.172	0.200
	4087	362	3.313 in 12		0.173	0.186	0.128	0.193
	4087	363	7.122 in 12		0.179	0.185	0.124	0.192

Sacramento, CA Solar Reflectance Field Data

Table A.6

				Exposure Time (yrs)				
	Identifier	Code	Slope	0.000	0.764	0.959	1.644	2.507
	Shepherd Artic Match							
Blue Artic		364	1.359 in 12		0.244	0.263	0.237	0.241
		365	3.313 in 12		0.251	0.269	0.227	0.239
		366	7.122 in 12		0.246	0.259	0.216	0.217
Red Artic		367	1.359 in 12		0.275	0.286	0.244	0.247
		368	3.313 in 12		0.288	0.298	0.255	0.264
		369	7.122 in 12		0.271	0.284	0.239	0.249
Brown Artic		370	1.359 in 12		0.256	0.278	0.239	0.250
		371	3.313 in 12		0.265	0.287	0.256	0.263
		372	7.122 in 12		0.261	0.273	0.254	
Black Artic		373	1.359 in 12		0.233	0.245	0.205	0.229
		374	3.313 in 12		0.231	0.244	0.199	0.211
		375	7.122 in 12		0.220	0.234	0.187	0.200
Gray Artic		376	1.359 in 12		0.251	0.268	0.225	0.222
		377	3.313 in 12		0.249	0.266	0.225	0.229
		378	7.122 in 12		0.269	0.284	0.248	
	American Roof Coatings							
NIR3704	Ultra Marine	381	3.313 in 12		0.392	0.386	0.386	0.401
IR3808	Chocolate	382	3.313 in 12		0.410	0.395	0.387	0.393
IR3503	Camo Green	383	3.313 in 12		0.463	0.438	0.435	0.446
IR3108	Light Gray	384	3.313 in 12		0.433	0.407	0.403	0.413
IR3308	Terracotta	385	3.313 in 12		0.473	0.452	0.448	0.456
NIR3900	Onyx	386	3.313 in 12		0.417	0.445	0.432	0.423

Appendix A

McArthur Exposure Site (RS07)

Painted metal, clay and concrete tile roof products with and without cool color pigments were placed at ground level in a fenced pasture at McArthur Farms, McArthur, CA. Coupons of the roof products were installed in exposure rack assemblies, which are 5.5-ft high by 9-ft long, and divided into three sub-frames having respective slopes of 2-, 4- and 8-in of rise for 12-in of run (i.e., slopes of 9.5°, 18.4° and 33.7°). Each sub-frame can hold two "Sure-Grip" sub-assemblies, which are designed to have 6 rows of samples with 34-in of usable space in each row. Sample size is 3.5-in by 3.5-in. Orientation of the racks was set at 0° CCW and faced directly east into the rising sun for representing exposure seen on an east facing residential roof.

Figure A.7. Exposure rack ground mounted at McArthur Farms, CA.

McArthur, CA Solar Reflectance Field Data

Table A.7

				Exposure Time (yrs)				
	Identifier	**Code**	**Slope**	**0.000**	**0.764**	**0.959**	**1.644**	**2.507**
	BASF PVDF Painted Metal							
Regal White	872W2	800	2 in 12	0.742	0.720	0.697	0.719	0.725
	872W2	801	4 in 12	0.741	0.723	0.704	0.725	0.729
	872W2	802	8 in 12	0.741	0.725	0.701	0.722	0.726
	815W98	803	4 in 12	0.690	0.665	0.658	0.667	0.667
Rawhide	872T6	804	2 in 12	0.571	0.548	0.543	0.551	
	872T6	805	4 in 12	0.570	0.546	0.544	0.547	
	872T6	806	8 in 12	0.571	0.545	0.545	0.547	
	836T223	807	4 in 12	0.440	0.420	0.426	0.416	
Slate Blue	872B7	808	2 in 12	0.282	0.271	0.277	0.265	0.280
	872B7	809	4 in 12	0.283	0.270	0.277	0.263	0.281
	872B7	810	8 in 12	0.282	0.271	0.227	0.265	0.279
	815B49	811	4 in 12	0.171	0.164	0.176	0.161	0.175
Brick Red	872R10	812	2 in 12	0.375	0.357	0.376	0.366	0.383
	872R10	813	4 in 12	0.375	0.357	0.375	0.364	0.383
	872R10	814	8 in 12	0.376	0.359	0.376	0.366	0.383
	815R71	815	4 in 12	0.195	0.186	0.201	0.184	.277- bird poop
Charcoal Gray	872D6	816	2 in 12	0.308	0.294	0.316	0.304	0.317
	872D6	817	4 in 12	0.308	0.294	0.317	0.302	0.320
	872D6	818	8 in 12	0.307	0.294	0.316	0.304	0.320
	815D119	819	4 in 12	0.122	0.119	0.133	0.116	0.128
Hartford Green	872G16	820	2 in 12	0.272	0.258	0.281	0.264	0.280
	872G16	821	4 in 12	0.272	0.256	0.279	0.261	0.278
	872G16	822	8 in 12	0.270	0.259	0.279	0.266	0.280
	815G37	823	4 in 12	0.088	0.087	0.099	0.084	0.096
Slate Bronze	872T3	824	2 in 12	0.262	0.251	0.268	0.256	0.270
	872T3	825	4 in 12	0.263	0.251	0.270	0.255	0.272
	872T3	826	8 in 12	0.262	0.251	0.269	0.255	0.270
	815T119	827	4 in 12	0.117	0.115	0.128	0.112	0.125
	MCA Clay Tile							
White Buff	2F44	828	2 in 12	0.630	0.612	0.597	0.606	0.608
	2F44	829	4 in 12	0.632	0.612	0.614	0.611	0.617
	2F44	830	8 in 12	0.643	0.619	0.614	0.619	0.626
Apricot Buff	CF50	831	2 in 12	0.617	0.621	0.612	0.615	0.618
	CF50	832	4 in 12	0.597	0.567	0.568	0.567	0.577
	CF50	833	8 in 12	0.607	0.580	0.582	0.582	0.590
Adobe Gray	2F71	834	2 in 12	0.446	0.417	0.430	0.424	0.433
	2F71	835	4 in 12	0.448	0.403	0.419	0.407	0.423
	2F71	836	8 in 12	0.436	0.425	0.441	0.430	0.449
				.				
Regency Blue	2F52	837	2 in 12	0.424	0.413	0.418	0.410	0.418
	2F52	838	4 in 12	0.417	0.415	0.418	0.414	0.425
	2F52	839	8 in 12	0.420	0.400	0.406	0.400	0.405
Natural Red	F40	840	2 in 12	0.457	0.430	0.435	0.427	0.445
	F40	841	4 in 12	0.467	0.420	0.429	0.421	0.441
	F40	842	8 in 12	0.459	0.442	0.451	0.442	0.460
Weathered Green	B305	843	2 in 12	0.405	0.378	0.387	0.376	0.398
	B305	844	4 in 12	0.402	0.396	0.418	0.397	0.413
	B305	845	8 in 12	0.408	0.387	0.399	0.391	0.408
Ironwood	2F19	846	2 in 12	0.261	0.250	0.269	0.253	0.265
	2F19	847	4 in 12	0.263	0.247	0.265	0.251	0.274
	2F19	848	8 in 12	0.263	0.249	0.265	0.250	0.268
	US Clay Tile							
Buff Blend		879	2 in 12		0.578	0.576	0.577	0.563
Bermuda Blend		880	2 in 12		0.493	0.486	0.490	0.496
	Monierlife Concrete Roof Tile							
Terra Cotta Red	6978	849	2 in 12		0.186	0.192	0.176	0.204
	6978	850	4 in 12		0.196	0.200	0.200	0.204
	6978	851	8 in 12		0.186	0.194	0.182	0.213
Hearthside	3083	852	2 in 12		0.140	0.153	0.157	0.175
	3083	853	4 in 12		0.131	0.164	0.146	0.179
	3083	854	8 in 12		0.136	0.150	0.160	0.168
Riversidepebble	3080	855	2 in 12		0.136	0.149	0.148	0.138
	3080	856	4 in 12		0.135	0.139	0.146	0.160
	3080	857	8 in 12		0.143	0.152	0.145	0.155
Ebony	5047	858	2 in 12		0.137	0.145	0.125	0.157
	5047	859	4 in 12		0.140	0.135	0.115	0.133
	5047	860	8 in 12		0.137	0.134	0.117	0.148
Lincoln Green	4087	861	2 in 12		0.171	0.181	0.165	0.193
	4087	862	4 in 12		0.156	0.155	0.155	0.165
	4087	863	8 in 12		0.162	0.161	0.160	0.185

McArthur, CA Solar Reflectance Field Data

Table A.7

				Exposure Time (yrs)				
	Identifier	Code	Slope	0.000	0.764	0.959	1.644	2.507
	Shepherd Artic Match							
Blue Artic		864	2 in 12		0.240	0.258	0.229	0.245
		865	4 in 12		0.236	0.249	0.227	0.239
		866	8 in 12		0.240	0.243	0.227	0.228
Red Artic		867	2 in 12		0.259	0.274	0.247	0.254
		868	4 in 12		0.332	0.320	0.295	0.300
		869	8 in 12		0.267	0.280	0.263	0.266
Brown Artic		870	2 in 12		0.260	0.273	0.254	0.259
		871	4 in 12		0.250	0.273	0.249	0.260
		872	8 in 12		0.256	0.277	0.258	0.265
Black Artic		873	2 in 12		0.230	0.235	0.207	0.209
		874	4 in 12		0.240	0.239	0.208	0.224
		875	8 in 12		0.240	0.239	0.201	0.219
Gray Artic		876	2 in 12		0.269	0.285	0.252	0.230
		877	4 in 12		0.273	0.285	0.256	0.259
		878	8 in 12		0.263	0.282	0.258	0.269
	American Roof Coatings							
NIR3704	Ultra Marine	881	4 in 12		0.391	0.392	0.389	0.401
IR3808	Chocolate	882	4 in 12		0.410	0.410	0.397	0.411
IR3503	Camo Green	883	4 in 12		0.466	0.466	0.451	0.467
IR3108	Light Gray	884	4 in 12		0.434	0.429	0.412	0.426
IR3308	Terracotta	885	4 in 12		0.474	0.477	0.464	0.478
NIR3900	Onyx	886	4 in 12		0.436	0.487	0.464	0.466

Appendix B
Additional notes on soil optical properties

In support of the ORNL/LBNL report to CEC (Task 2.6.2), we show how to compute the absorptance and reflectance of a soil layer from measurements of solar reflectance on light and dark samples. It was shown in the report that winter rains cleaned much of the accumulated dust on PVDF films. Here we make that observation more quantitative. Of the deposits remaining after winter rains, the absorptance and reflectance are positively correlated with measured iron concentrations.

Suppose a substrate has a clean reflectance denoted *Ro*, which is coated with a thin soil layer with absorptance *a* and reflectance *r*. In view of the assumption that the layer is thin, we take both *a* and *r* as small compared to unity. Then, it is not difficult to show that the change in reflectance (*R* - *Ro*) of the soiled substrate is given, to first order in *r* and *a*, by

$$R - Ro = -2Ro\,a + (1 - Ro)2r. \qquad (1)$$

[This equation was derived by summing the different ways a photon can be reflected as $(1\text{-}a\text{-}r)^2\,Ro$ {transmitted twice through the soil layer and reflected from the substrate} plus *r* {reflection from the soil layer}, plus $(1\text{-}a\text{-}r)^2\,r\,Ro^2$ {transmitted twice, reflected once from the underside of the soil layer, and twice from the substrate}]. Thus soil absorptance reduces *R* and soil reflectance increases *R*. Here we can also see that *a* will be less important if *Ro* is small and *r* will be less important if *Ro* is close to unity. Stated another way, for highly reflective materials (*Ro* close to 1), we expect a decline in reflectance due to the soil absorptance *a*. For very dark materials, we expect an increase in reflectance due to the soil reflectance *r*.

The soil parameters *a* and *r* can be determined by fitting if reflectance change measurements are available for two or more substrates with different *Ro*. For fitting purposes it is useful to divide Eq. (1) by *Ro*:

$$(R - Ro)/Ro = -2a + [(1 - Ro)^2/Ro]\,r. \qquad (2)$$

Then a plot of (*R* – *Ro*) /*Ro* versus *Ro* produces a horizontal line at height –2 *a* if *r* is negligible, and increases at decreasing *Ro* if *r* is not negligible. Figure B1 shows an example of the fitting procedure, for Shafter at 1 year. The data are taken from Appendix A of report 2.6.2, using the PVDF samples. The slope chosen is that for which there are both cool and standard samples. The open circles are the fitted curve. A color photograph of a Shafter sample at 1 year is also included in report 2.6.2. Figure B2 shows similar fits for the other 6 sites at 1 year. Figure B3 shows data for Shafter after 1.6 years. At this point it was spring in California and much of the soil deposits have been removed by rain. In this figure the fitted curve was forced to pass through the highest reflectance data point (white) at *Ro* = 0.74 and the non-selective gray at *Ro* = 0.123, because some of the scatter in the data points might be due to spectrally selective interaction between the various substrates and the spectral properties of the soil. Also, in the presence of data scatter, it is desirable to use substrates with widely different *Ro*.

Figure 4 shows similar plots for the other 6 sites. Despite the scatter, in all cases we obtain a non-zero value for *a*. In most cases we obtain a value for *r*, but it is sometimes not distinguishable from zero.

Appendix B
Additional notes on soil optical properties

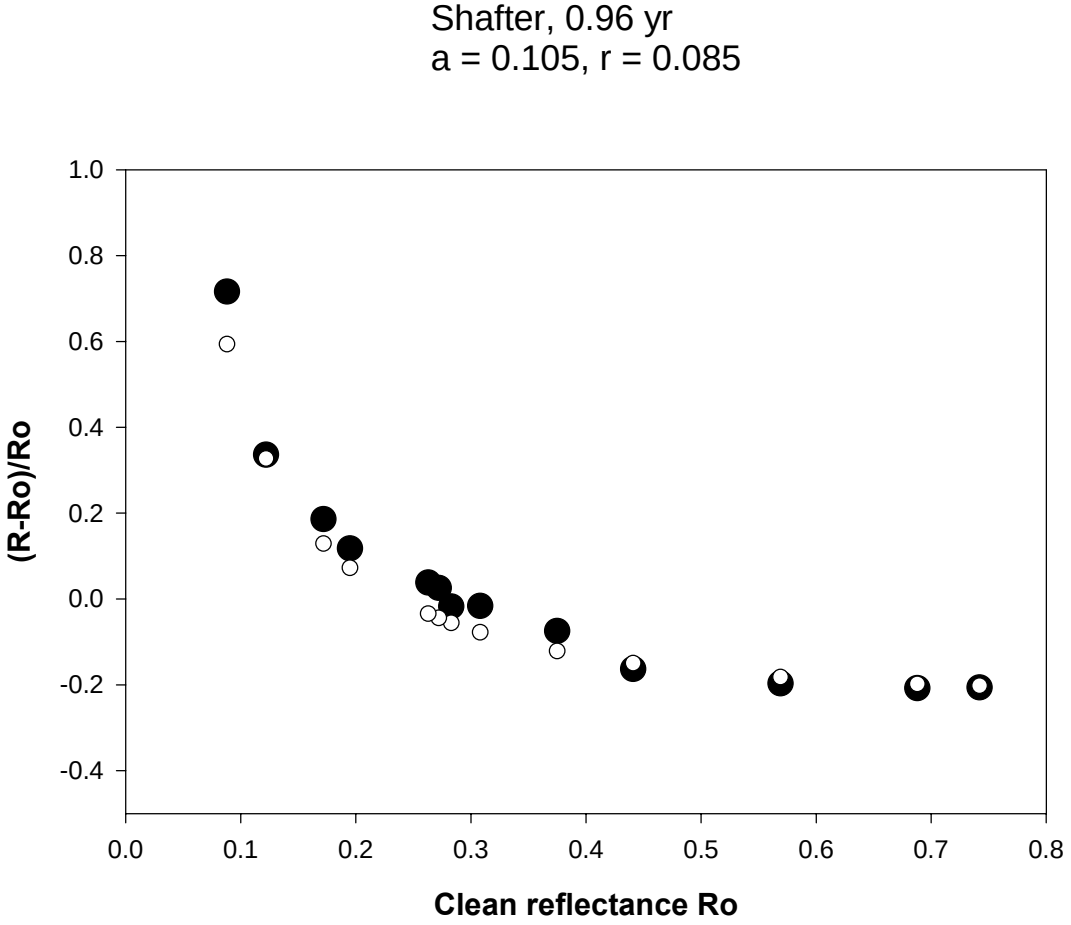

Fig. B1. Measured (solid circles) and fitted (open circles) changes in reflectance due to sample soiling. High reflectance samples lose reflectance; low-reflectance samples gain reflectance.

The results of the curve fitting exercise are collected in Table B1. Judging by the absorptances, the amount of material remaining at 1.6 years is only ½ to ⅛ of that present at 1 year. Thus the weathering, presumably due to dew and rain transport, significantly cleaned the substrates. Note that already even at 1 year, the photograph of the Shafter sample in Fig. B4 of report 2.6.2 shows transport of soil along the surface of the sample to the lower edge. Thus the weathering process significantly alters the original dry atmospheric deposition. Note that the *r*-values were reduced even more than *a*-values at 1.6 years, compared to 1 year. This means that the weathering process not only reduced the quantity of soil originally deposited, but that it altered the composition as well. Of course water-soluble components are expected to be transported by rain, but small and low-density particles are likely to be transported as well. Remaining particles are likely to be larger in size, higher in density, and/or able to adhere to the substrate.

Finally, Table B2 shows the measured concentrations of iron, organic carbon, and elemental carbon at 1.6 years. Plotting *a*- and *r*-values against iron concentration in Fig. B5, we find that higher values of these parameters are associated with higher iron concentrations. The statistical R^2 values are 0.48 for *a* and 0.38 for *r*. Corresponding values for organic carbon (0.03 for *a*) and elemental carbon (0.01 for *a*) were quite low.

Appendix B
Additional notes on soil optical properties

The tentative picture that emerges is that iron-containing mineral dust tends to remain on the Teflon-like PVDF surfaces washed by rain. Concentrations of iron were as large as about 70 mg/m^2. Iron in the ferric 3+ valence state is associated with strong absorption in the short wavelength portion of the solar spectrum (wavelength < 550 nm), as in the case of small hematite particles where the absorption strength is 4 m^2/g. Multiplying these two figures we obtain a crude estimate of 0.28 for short wavelength absorptance. The short wavelength part of the solar spectrum of interest here contains about ¼ of the total solar flux. Thus we estimate that the solar average absorptance due to 70 mg/m^2 of iron could be about 0.07. This number compares well with the ~ 0.05 absorptance at the sites with the highest iron concentration. This rough agreement could be an accident, but at least our picture is consistent.

Table B1. Soil absorptance and reflectance at 1 year, and at 1.6 years. The 1 year data were at the end of the dry summer period, while the 1.6 year data were obtained in the spring, after winter rainfall.

Site	1 year	1 year	1 yr	1.6 years	1.6 years	1.6 yr
	absorptance ***a***	**reflectance** ***r***	***r/a***	**absorptance** ***a***	**Reflectance** ***r***	***r/a***
El Centro	0.10	0.13	1.3	0.012	0.009	0.8
Corona	0.090	0.085	0.9	0.048	0.013	0.3
Colton	0.14	0.15	1.1	0.045	0.008	0.2
Shafter	0.105	0.085	0.8	0.04	0.005	0.1
Richmond	0.075	0.036	0.5	0.025	< 0.003	< 0.1
Sacramento	0.060	0.058	1.0	0.03	< 0.003	< 0.1
McArthur	0.025	0.021	0.8	0.022	< 0.003	< 0.2

Table 2. Concentrations of three substances that could be associated with soil absorptance and reflectance. Iron has a significant correlation (see Fig. B5).

Site	Exposure Time (1.6 years)		
	Iron (mg/m^2)	Organic C (mg/m^2)	Elemental C (mg/m^2)
El Centro	33	8.3	0.2
Corona	68	5.5	0.2
Colton	67	6.1	0.2
Shafter	32	5.6	0.4
Richmond	44	11	1.3
Sacramento	42	4.5	0.2
McArthur	5	1.3	~ 0.02

Appendix B
Additional notes on soil optical properties

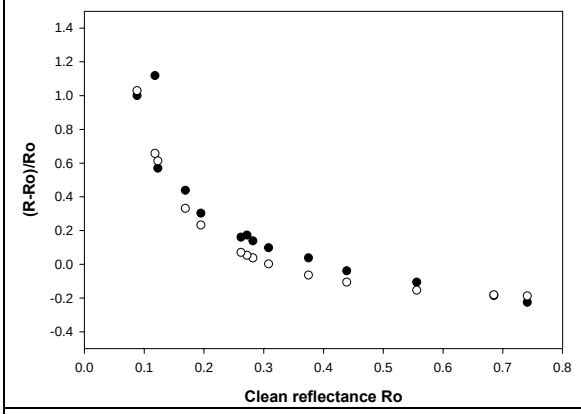

Fig. B2a

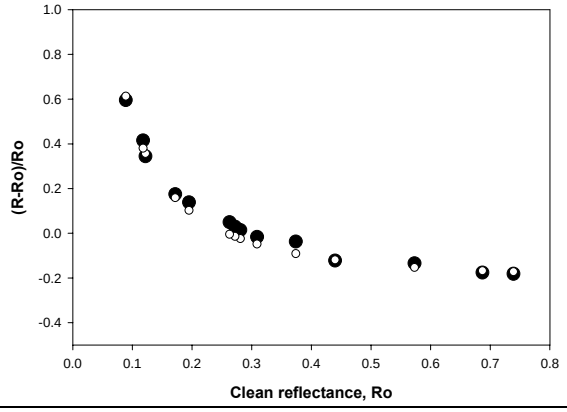

Fig. B2b

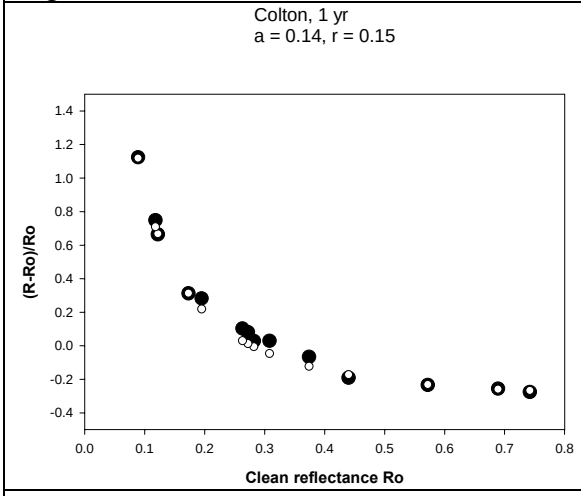

Fig. B2c

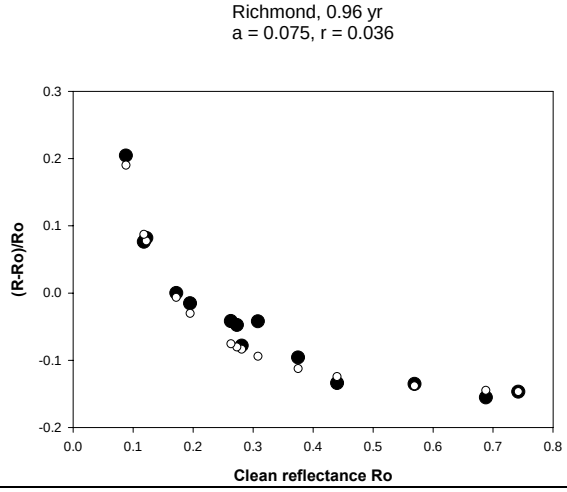

Fig. B2d

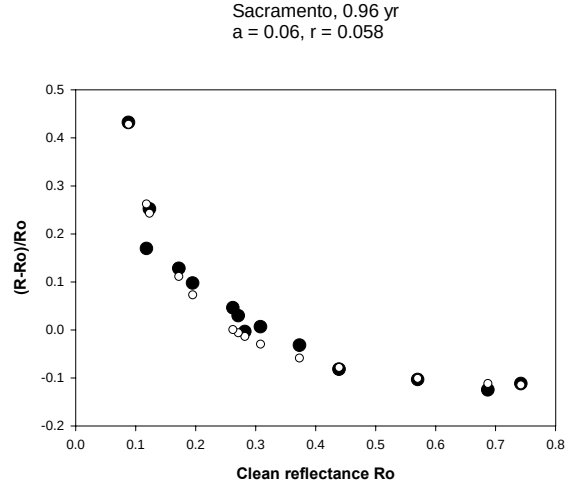

Fig. B2e

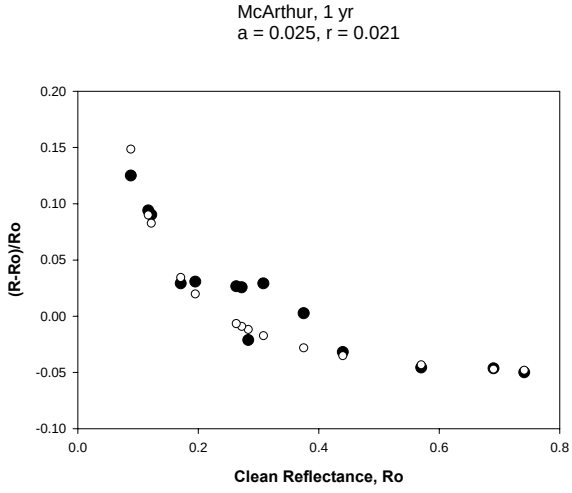

Fig. B2f

Appendix B
Additional notes on soil optical properties

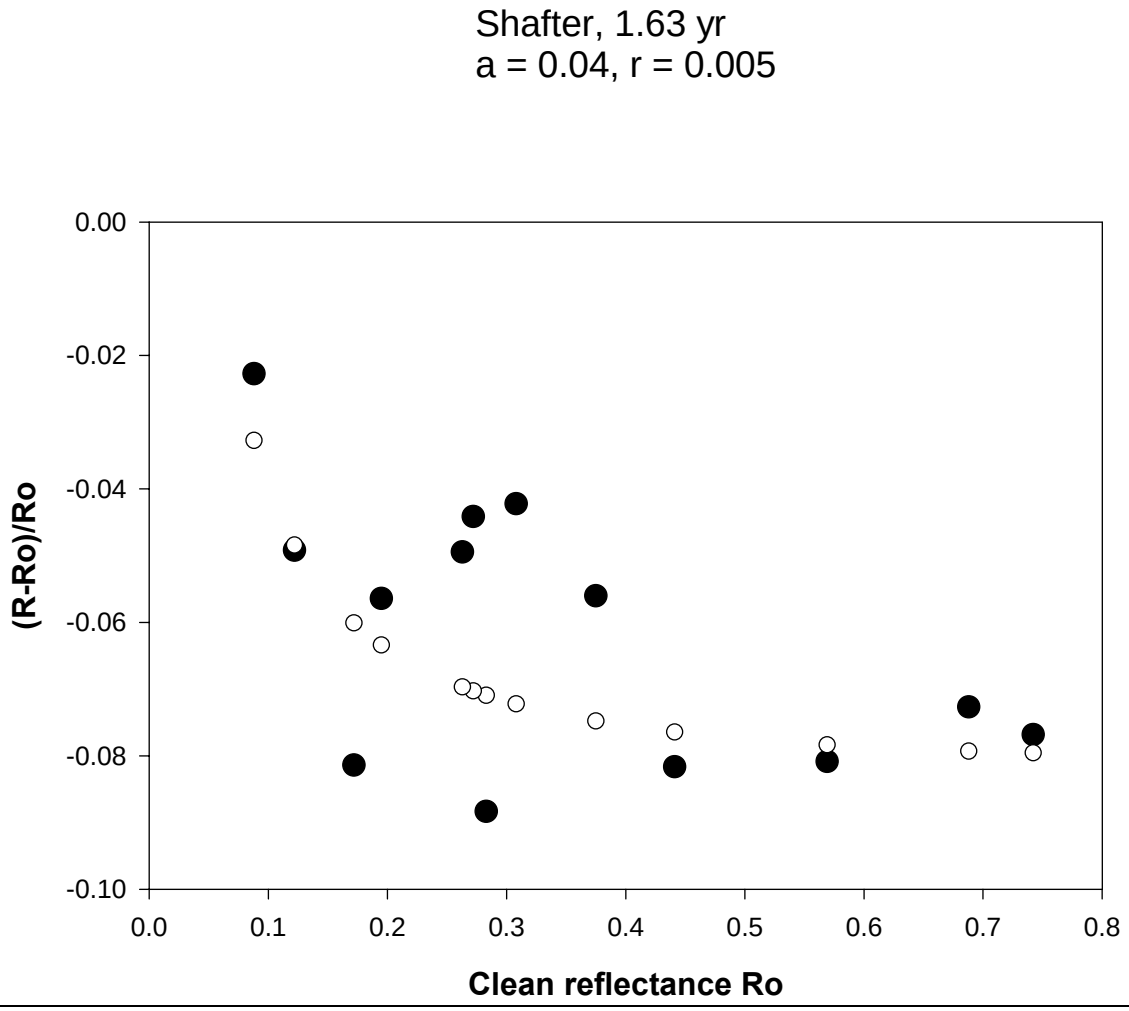

Figure B3. Data for Shafter as in Fig.1, but at 1.6 years rather than 1 year. Smaller values for a and r indicate that less dust is present.

Appendix B
Additional notes on soil optical properties

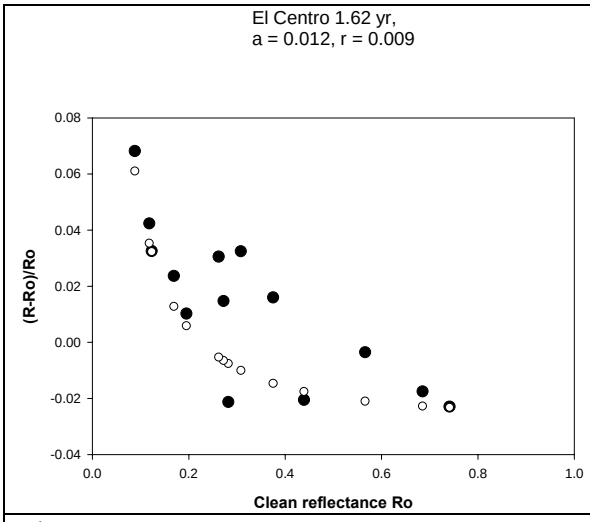

Fig. B4a

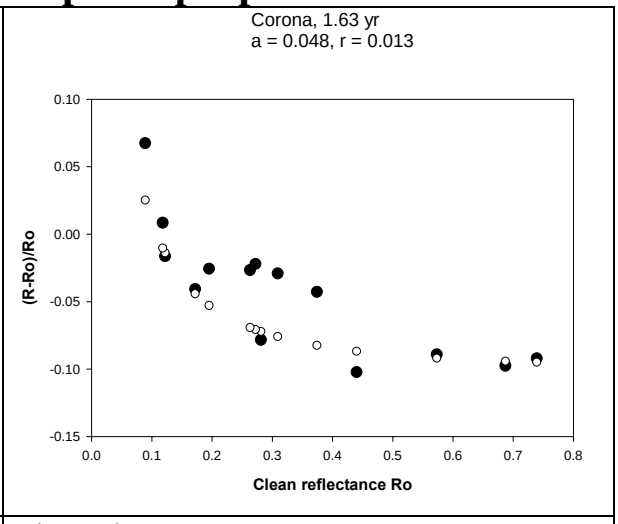

Fig. B4b

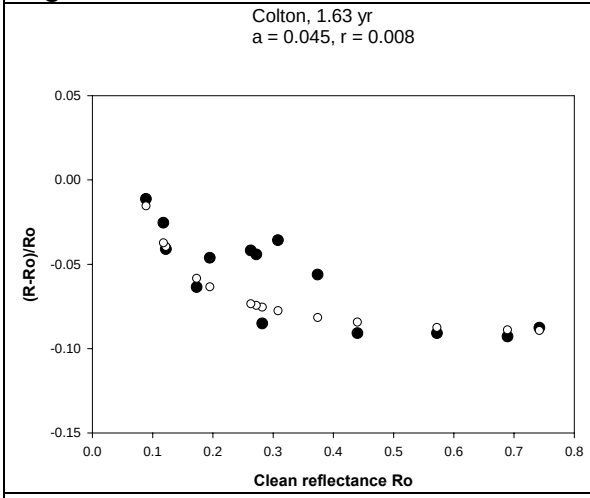

Fig. B4c

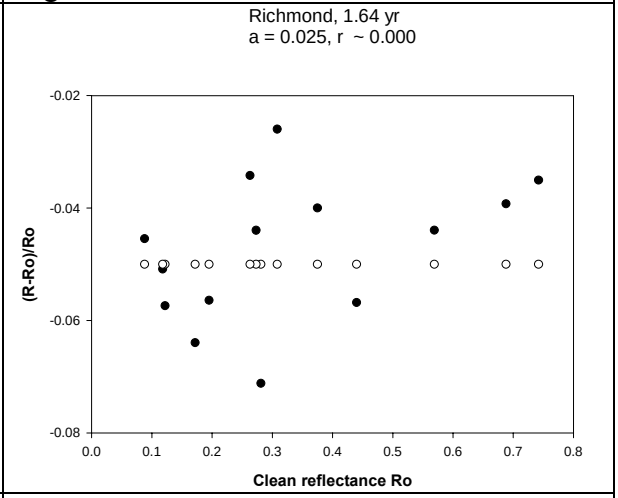

Fig. B4d

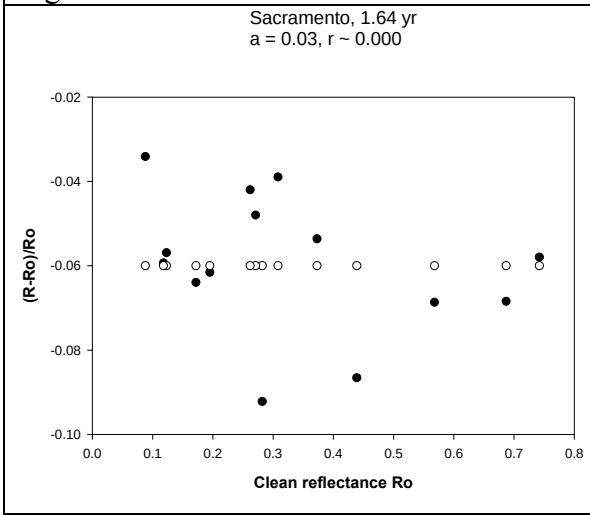

Fig. B4e

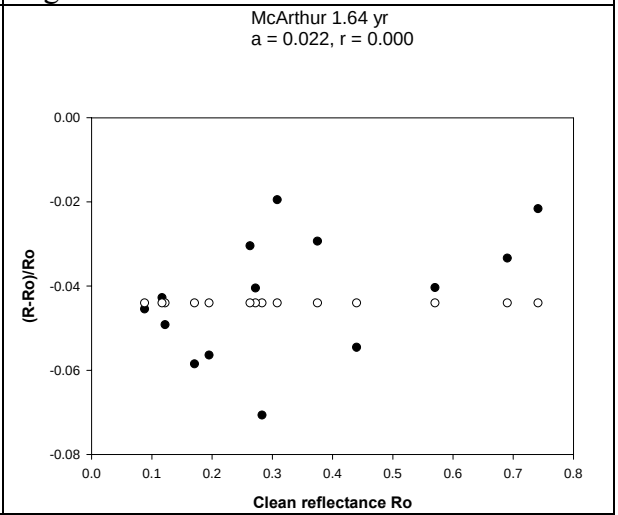

Fig. B4f

Appendix B
Additional notes on soil optical properties

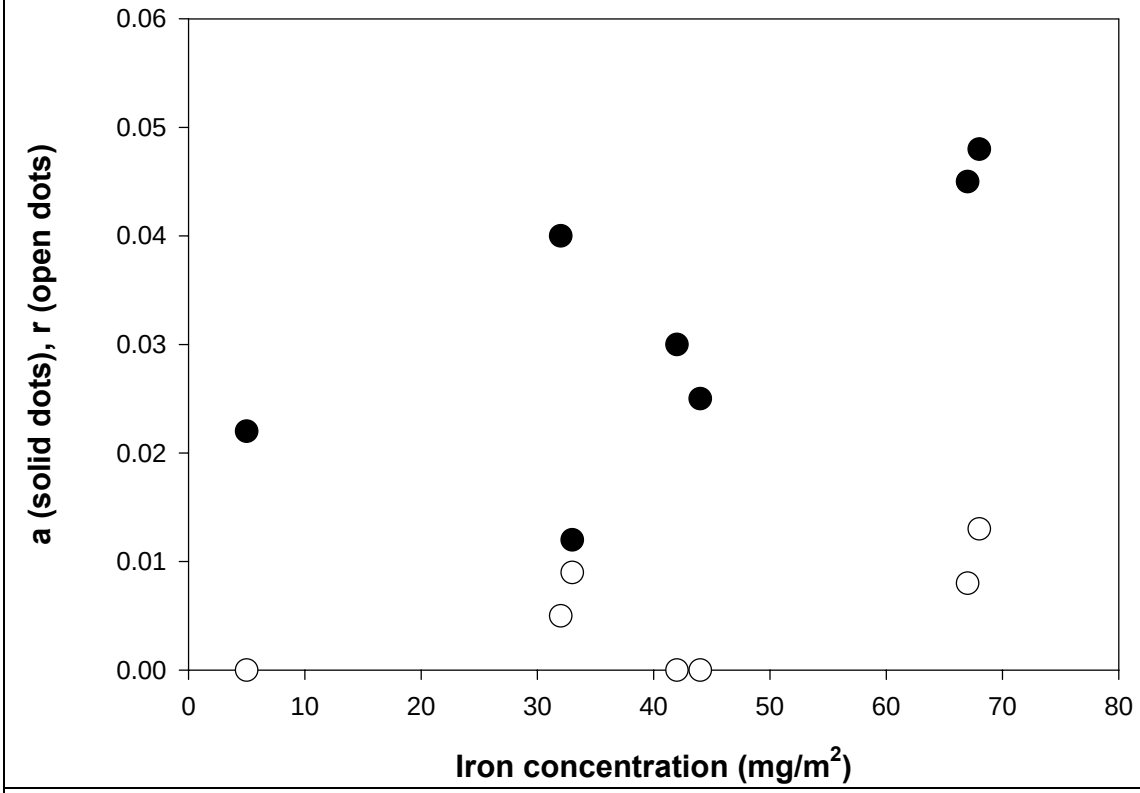

Fig. 5. A plot of data highlighted in Table 1. There are positive correlations of both soil absorptance *a* and soil reflectance *r* with iron concentration.

Arnold Schwarzenegger
Governor

COOL-COLOR ROOFING MATERIAL ATTACHMENT 9: TASK 2.6.3 REPORTS - STEEP-SLOPE ASSEMBLY TESTING AT ORNL

PIER FINAL PROJECT REPORT

Prepared For:
California Energy Commission
Public Interest Energy Research Program

Prepared By:
Lawrence Berkeley National Laboratory and Oak Ridge National Laboratory

ERNEST ORLANDO LAWRENCE
BERKELEY NATIONAL LABORATORY

June 2006
CEC-500-2006-067-AT9

Prepared By:
Lawrence Berkeley National Laboratory
Hashem Akbari
Berkeley, California
Contract No. 500-01-021

Oak Ridge National Laboratory
William Miller
Oak Ridge, Tennessee

Prepared For:
California Energy Commission
Public Interest Energy Research (PIER) Program

Chris Scruton
Contract Manager

Ann Peterson
Building End-Use Energy Efficiency Team Leader

Nancy Jenkins
PIER Energy Efficiency Research Office Manager

Martha Krebs, Ph.D.
Deputy Director
ENERGY RESEARCH AND DEVELOPMENT DIVISION

B. B. Blevins
Executive Director

DISCLAIMER

This report was prepared as the result of work sponsored by the California Energy Commission. It does not necessarily represent the views of the Energy Commission, its employees or the State of California. The Energy Commission, the State of California, its employees, contractors and subcontractors make no warrant, express or implied, and assume no legal liability for the information in this report; nor does any party represent that the uses of this information will not infringe upon privately owned rights. This report has not been approved or disapproved by the California Energy Commission nor has the California Energy Commission passed upon the accuracy or adequacy of the information in this report.

ORNL/TM-2005/265

Steep-Slope Assembly Testing of Clay and Concrete Tile with and without Cool Pigmented Colors

William A. Miller, Ph.D.
Buildings Technology Center
Oak Ridge National Laboratory

Hashem Akbari, Principal Investigator
Heat Island Group
Lawrence Berkeley National Laboratory

Date Published: November 2005

Prepared by the
OAK RIDGE NATIONAL LABORATORY
Oak Ridge, Tennessee 37831-6283
managed by
UT-BATTELLE, LLC
for the
U.S. DEPARTMENT OF ENERGY
under contract DE-AC05-00OR22725

DOCUMENT AVAILABILITY

Reports produced after January 1, 1996, are generally available free via the U.S. Department of Energy (DOE) Information Bridge:

Web site: http://www.osti.gov/bridge

Reports produced before January 1, 1996, may be purchased by members of the public from the following source:

National Technical Information Service
5285 Port Royal Road
Springfield, VA 22161
Telephone: 703-605-6000 (1-800-553-6847)
TDD: 703-487-4639
Fax: 703-605-6900
E-mail: info@ntis.fedworld.gov
Web site: http://www.ntis.gov/support/ordernowabout.htm

Reports are available to DOE employees, DOE contractors, Energy Technology Data Exchange (ETDE) representatives, and International Nuclear Information System (INIS) representatives from the following source:

Office of Scientific and Technical Information
P.O. Box 62
Oak Ridge, TN 37831
Telephone: 865-576-8401
Fax: 865-576-5728
E-mail: reports@adonis.osti.gov
Web site: http://www.osti.gov/contact.html

This report was prepared as an account of work sponsored by an agency of the United States government. Neither the United States government nor any agency thereof, nor any of their employees, makes any warranty, express or implied, or assumes any legal liability or responsibility for the accuracy, completeness, or usefulness of any information, apparatus, product, or process disclosed, or represents that its use would not infringe privately owned rights. Reference herein to any specific commercial product, process, or service by trade name, trademark, manufacturer, or otherwise, does not necessarily constitute or imply its endorsement, recommendation, or favoring by the United States government or any agency thereof. The views and opinions of authors expressed herein do not necessarily state or reflect those of the United States government or any agency thereof.

ACKNOWLEDGEMENTS

Funding for this project was provided by the California Energy Commission's Public Interest Energy Research program through the Lawrewnce Berkeley National Laboratory operated under U. S. Department of Energy under contract DE-AC02-05CH11231. The support and confidence provided by the PIER project managers Chris Scruton and Nancy Jenkins is very much appreciated by the "Cool Roofs" team Hashem Akbari, Paul Berdahl, Ronnen Levinson, and Steve Weil from LBNL and André Desjarlais and William Miller from ORNL. The Tile Roofing Institute and its affiliate members provided the clay and concrete tile. They also provided valuble assistance installing the clay and concrete tile on the respective steep-slope assemblies. Their financial support and guidance are greatly appreciated.

TABLE OF CONTENTS

LIST OF FIGURES vii
LIST OF TABLES ix
ABSTRACT 1
EXECUTIVE SUMMARY 1
OBJECTIVE 3
INTRODUCTION 3
STEEP-SLOPE ATTIC ASSEMBLY 3
Configuration of Clay and Concrete Tile 4
Instrumentation for Attic Assembly 6
Instrumentation for Sub-Tile Venting 8
Data Acquisition System (DAS) 8
Solar Reflectance and Thermal Emittance Instruments 9
SOLAR REFLECTANCE AND THERMAL EMITTANCE 10
Effects of Climatic Soiling 10
Cool Roof Color Materials (CRCMs) 11
FIELD TEST RESULTS 12
Cooling Season Field Performance 13
Effects of Opening the Ridge Vent 15
Heating Season Field Performance 16
Thermal Mass Effects 18
Venting the Underside of Tile Roofs 19
Thermally Induced Airflow Rates 20
Numerical Simulations 21
Airflow Measurements Using Tracer Gas 23
Air Leakage from Tile Systems 24
ATTICSIM MODEL 25
Attic Ventilation 26
Validation Efforts 27
CONCLUSIONS 29
RECOMMENDATIONS 30
NOMENCLATURE 31

REFERENCES 32
APPENDIX A 35
APPENDIX B 39

LIST OF FIGURES

1. Envelope Systems Research Apparatus is a one-story building for testing low- and steep-slope roof products. 4
2. An assembly of steep-slope attics was placed on top of the ESRA and clay and concrete tile were installed by the Tile Roofing Institute. 5
3. Construction of the roof deck showing battens and counter-battens for attaching the slate tile and the parapets used to limit airflows on the underside of the tile to within a given test roof. 6
4. S-Mission clay and concrete tile are designed to have a gap between overlaid tiles. 6
5. The location of temperature, relative humidity, and heat flow measures made on each attic assembly 7
6. Heat flux transducer embedded in the roof deck for measuring the heat flow penetrating through the roof tile and into the attic. 7
7. Setup of attic assembly showing construction materials, instrumentation, and polyisocyanurate insulation used to isolate attic from adjacent attics. 8
8. Instrumentation used on the underside of the tile roofs for validating heat transfer correlations predicting the heat transfer driven by thermally induced airflows. 9
9. Solar reflectance of the clay and concrete tile exposed on the ESRA. 10
10. Solar reflectance of clay tile exposed at weathering sites in California. 11
11. Cooltile IR Coating™ developed by Joe Riley, LBNL, and ORNL. 12
12. Heat penetrating the tile roof of each attic assembly on the ESRA; the ridge vent was closed. 13
13. S-Mission tile reduced the integrated daytime roof heat gain by 50 to 75% of the gain for the asphalt shingle roof. 15
14. Bulk air temperatures underneath the S-Mission clay and the concrete slate tile for two different summer days, one with the ridge vent open and the other with the ridge vent closed. 16
15. Heat penetrating through the roof deck of the S-Mission clay tile and the concrete slate tile with and without venting of the roof deck. 17
16. Roof deck heat flow for two consecutive days in January 2005; ridge vent is closed. 18
17. Integrated heat flow measured through the roof deck for all tile and shingle roofs during the month of January 2005. 19
18. Heat transfer phenomena occurring on the underside of roof tile. 20
19. Numerical simulations for channel flow with and without battens fastened to the underside of tile (the top plate). The channel is at an incline of 30° (5-in. rise for every 12 in. of run), and the top plate is 30°F warmer than the bottom plate. 22
20. Concentration of CO_2 measured under the slate tile roof with batten and counter-battens. 23
21. The leakage of air from the underside of the slate and S-Mission clay tile roofs. 25

22. AtticSim predicted the attic air temperature of the steep-slope attic assembly modeled as a shed roof with and without ridge venting of the shingle roof. 26

23. Validation of AtticSim against field measures of the ceiling heat flux gleaned from the ESRA steep-slope roof assembly with a direct-nailed shingle roof. 27

24. Validation of AtticSim against field measures of the surface temperatures for the asphalt shingles gleaned from the ESRA steep-slope roof assembly. 28

LIST OF TABLES

1. Clay and concrete tile placed on the ESRA's Steep-Slope Attic Assembly. 5

2. Airflow rate and bulk velocity measured at the center of each attic assembly and under the clay and concrete tile roofs using CO_2 as a tracer gas. 24

3. Air infiltration and exfiltration from the S-Mission clay (SR54E90) and the slate concrete (SR13E83) tile roof systems.. 24

4. July 2005 attic temperatures and cumulative heat flows through the roof deck and ceiling of the attic assemblies having both ridge and sub-tile venting 29

5. January 2005 attic temperatures and cumulative heat flows through the roof deck and ceiling of the attic assemblies with the ridge closed to attic and sub-tile ventilation. 30

Steep-Slope Assembly Testing of Clay and Concrete Tile Roofs with and without Cool Pigmented Colors

A new generation of roofing products are being introduced to the market for bringing relief to homeowners and utilities alike. Cool color pigments used to color paints are reducing the amount of energy needed to cool buildings, which in turn helps power companies reduce hot-weather energy consumption. Cool color pigments will also positively impact the environment by helping reduce carbon dioxide emissions, metropolitan heat buildups, and urban smog.

Industry researchers, including those working with the Department of Defense, developed the first prototype cool color pigments for military camouflage to match the visible and the near-infrared reflectance of background foliage. The high infrared reflectance of these pigments can be exploited to manufacture roofing materials that reflect more sunlight than conventional-pigmented roofing products. Therefore, Oak Ridge National Laboratory (ORNL) and the Lawrence Berkeley National Laboratory (LBNL) initiated a three-year "Cool Roof Color Materials" (CRCMs) project to bring cool-colored roofing materials to the roofing market. ORNL, with assistance from LBNL and in conjunction with pigment (colorant) and roof manufacturers, selected appropriate CRCMs, applied them to roofing materials, and field-tested the roof products. Testing occurred at demonstration homes and seven weathering farms in California and at the campus of the Buildings Technology Center (BTC) using the steep-slope attic assembly on the Envelope Systems Research Apparatus (ESRA).

The BTC completed two years of field-testing clay and concrete tile on the ESRA. The center is reporting the results for this phase of work to complete Task 2.6.3 as part of the deliverables for the Public Interest Energy Research (PIER) project "Cool Roof Colored Materials" sponsored by the California Energy Commission (CEC).

ABSTRACT

Cool color pigments and sub-tile venting of clay and concrete tile roofs significantly impact the heat flow crossing the roof deck of a steep-slope roof. Field measures for the tile roofs revealed a 70% drop in the peak heat flow crossing the deck as compared to a direct-nailed asphalt shingle roof. The Tile Roofing Institute (TRI) and its affiliate members are keenly interested in documenting the magnitude of the drop for obtaining solar reflectance credits with state and federal "cool roof" building efficiency standards. Tile roofs are direct-nailed or are attached to a deck with batten or batten and counter-batten construction. S-Misson clay and concrete tile roofs, a medium-profile concrete tile roof, and a flat slate tile roof were installed on fully instrumented attic test assemblies. Temperature measures of the roof, deck, attic, and ceiling, heat flows, solar reflectance, thermal emittance, and the ambient weather were recorded for each of the tile roofs and also on an adjacent attic cavity covered with a conventional pigmented and direct-nailed asphalt shingle roof. ORNL measured the tile's underside temperature and the bulk air temperature and heat flows just underneath the tile for batten and counter-batten tile systems and compared the results to the conventional asphalt shingle.

EXECUTIVE SUMMARY

An assembly of steep-slope attics having shed-type roofs was installed on top of the ESRA for field-testing clay and concrete tile roofs. The attics are adjacent to one another, and their shed roofs face directly south. The footprint for each attic is about 16 ft long by 5 ft wide. Roof slope was set at 4 in. of rise for every 12 in. of run (18.4° pitch). Soffitt and ridge venting are provided with vent openings of 1:300. The steep-slope assembly was field-tested for a summer with the ridge vent closed to simulate

conventional construction in the western states and with the ridge vent open the following summer to observe whether an unimpeded airflow under the tile (sub-tile venting) and attic ventilation would further improve the thermal performance of the tile roofs.

A high-profile S-Mission clay tile with cool pigmented colors, two different styles of high-profile terra-cotta concrete tiles, a medium-profile concrete (the same as that tested in California demonstrations), and a flat concrete slate tile were installed on the attic assemblies by the TRI. The clay S-Mission tile and the medium-profile concrete tile were direct-nailed to the roof deck, a high-profile S-Mission concrete tile was spot-adhered with foam to the roof deck, the flat concrete slate tile was fastened to a batten and counter-batten system, and another concrete S-Mission tile was fastened to battens. A sixth attic assembly has a conventional asphalt shingle roof for comparing roof and ceiling heat flows.

After two full years of exposure to the East Tennessee climate, the clay and concrete tile showed no noticeable loss in solar reflectance. However, two years of exposure in the more dusty California climates of Colton and El Centro caused the solar reflectance for clay tile to drop about 10% of its initial values. Dust and urban pollution in California's urban areas soil the materials more than conditions in the less-populated sections of the state, and the loss of reflectance is most severe for samples exposed at the slope of 2 in. of rise per 12 in. of run. Increasing the slope reduced the soiling because the dust is probably blown away by the strong California winds.Therefore, we believe roof slope affects the loss of reflectance, with the steeper slopes showing less loss in reflectance. Thermal emittance of samples exposed at ORNL and at California sites remained relatively constant at about 0.85.

Field results for the combination of sub-tile venting and improved solar reflectance offered by CRCMs are proving that tile roofs are energy-efficient cool roof products. The Environmental Protection Agency (EPA), the Leadership in Energy and Environmental Design (LEED), and the many state energy offices should therefore offer energy cridits for roofs using sub-tile venting and cool pigmented colors.

The clay tile field tested at ORNL reduced the peak heat transfer penetrating the roof deck at solar noon by about 70% of the heat penetrating through the deck of the attic covered with an asphalt shingle roof. Subsequently, the heat penetrating the ceiling of the non-vented attic assembly was reduced by about 60% of that entering through the ceiling of the non-vented attic assembly with asphalt shingles. The improved performance is due to the tile's high solar reflectance with CRCMs and to the venting occurring on the underside of the clay tile roof.

Field data collected at peak solar loading for concrete tile roofs at ORNL having about the same solar reflectance and thermal emittance as the control asphalt shingle demonstrate that venting the roof deck proportions to about 24 points of solar reflectance. Deck venting caused a significant 50% reduction in the heat penetrating the conditioned space compared to the direct-nailed asphalt shingle roof that is in direct contact with the roof deck. Opening the ridge vent of the attics caused more heat to be exhausted out the ridge for both the S-Mission clay and the slate tile systems and therefore further improved the performance of the two tile roofs. The effect was more pronounced for the slate tile than observed for the S-Mission tile because the slate tile has less air leakage between tiles as determined by tracer gas experiments.

During January winter exposure, the thermal mass and the tile's air channel have reduced the heat loss from the roof to the point that the heat loss from the ceiling of the tile roofs is about the same as the loss for the asphalt shingle roof, implying that the tile roofs are negating the heating penalty associated with a cool roof in Tennessee's moderate climate having 3662 HDD_{65} and 1366 CDD_{65}.

Numerical simulations of the inclined air channel formed by tile roof systems demonstrated that naturally induced flow can be expected at very low roof slopes and very low temperature differences, well below those experienced in roofing systems. The AtticSim computer tool was validated against the steep-slope attic assembly with direct-nailed asphalt shingles. The model effectively predicted the surface temperature of the shingles, the attic air temperature, and, as result, the heat flow penetrating into the

conditioned space. Efforts are continuing to modify the code for predicting the effects of the airflow occurring on the underside of the tile roof. Correlations by McAdams (1954), Brinkworth (2000), and simple boundary layer theory for a constant solar flux are predicting reasonable heat transfer measures within the inclined air channel. The measures of airflow determined from the tracer gas experiments match well the back-calculated values deduced from the McAdams(1954), Brinkworth (2000), and simple boundary layer theory correlations. We therefore have good representative airflow measures for sub-tile venting and are in good position to implement an algorithm formulated after the work by Brinkworth (2000) for use in AtticSim to predict thermal performance of tile roofs.

OBJECTIVE

Thermal performance, solar reflectance, and thermal emittance data were collected from the ESRA to document the energy savings of clay and concrete tile roofs to determine both the benefits of CRCMs and of venting the underside of tile roofs, between the tile and roof deck.

INTRODUCTION

The TRI, ORNL, and LBNL are working together to quantify and report the potential energy savings for concrete and clay tile roofs. TRI and its affiliate members are keenly interested in specifying tile roofs as cool roof products, and they want to know the effects of the tile's solar reflectance and of venting the underside of a tile roof. Parker, Sonne, and Sherwin (2002) demonstrated that a Florida home with a "white reflective" barrel-shaped concrete tile roof used 22% less annual cooling energy than an identical and adjacent home having a dark absorptive asphalt shingle roof. The cost saving due to the reduced use of comfort cooling energy was about $120, or about 6.7¢ per square foot per year.

The venting of the underside of a tile roof also provides thermal benefits for comfort cooling. Residential roof tests by Beal and Chandra (1995) demonstrated a 45% reduction in the daytime heat flux penetrating a counter-batten tile roof as compared to a direct-nailed shingle roof. Parker, Sonne, and Sherwin (2002) observed in their study that a moderate solar reflectance terra cotta barrel-shaped tile reduced the home's annual cooling load by about 8% of the base load measured for an identical home with asphalt shingle roof that was adjacent the home with terra cotta tile. These reported energy savings are attributed in part to thermally driven airflow within the air channel formed by the underside of the tile and the roof deck. The airflow is driven by buoyancy and/or wind driven forces. The air channel also provides an improvement in the insulating effect of the roofing system. Measuring and correctly modeling the heat flow on the underside of a tile roof are key hurdles for predicting the roof's thermal performance. The heat transfer can switch from conduction to single-cell convection to Bénard cell convection dependent on the aspect ratio made by the underside of the tile and the roof deck, the slope of the roof, and the weather. The coexistence and competition of the various modes of heat transfer require experimental measurements and numerical simulations.

Therefore, a combined experimental and analytical approach was conducted with the collection of two years of field data—one year with the ridge vent closed to all attic cavities to mimic conventional construction and the second year with the ridge vent open. Results are shown to report the potential energy savings for residential homes having concrete and clay tile roofs.

STEEP-SLOPE ATTIC ASSEMBLY

The ESRA is a one-story building used to expose large areas of low-slope and steep-slope roofs to East Tennessee's climate. Two sides of the building are mostly below grade, while the other two sides are mostly above grade (Fig. 1). The interior of the ESRA is heated and cooled to a constant temperature of

Fig. 1. Envelope Systems Research Apparatus (ESRA) is a one-story building for testing low- and steep-slope roof products.

70°F year-round. The long axis of the building is oriented east to west, and the test roofs on the ESRA face directly south to receive full exposure from the sun.

Configuration of Clay and Concrete Tile

Members of TRI installed clay and concrete tile on a fully instrumented steep-slope attic assembly (Fig. 2). High-profile S-Mission clay and concrete tile, medium-profile concrete, and a flat concrete slate tile were exposed to East Tennessee's climate for two full years. The clay S-Mission tile and the medium-profile concrete tile were direct-nailed to the roof deck, high-profile S-Mission concrete tile was spot-adhered with foam to the roof deck, the flat concrete slate tile was fastened to a batten and counter-batten system, and another concrete S-Mission tile was fasten to battens (Table 1). The sixth lane (see far left lane in Fig. 2) has a conventional asphalt shingle roof for comparing energy savings. The tile roofs are approximately 5 ft wide with 16 ft of footprint. Table 1 and Appendix A provide the salient features of the test concrete and clay tiles. All tiles, whether direct-nailed or installed on battens, have a sub-tile venting occurring up along the underside of the tile traveling from soffitt to ridge and transversely along the width of the test roofs. Parapet partitions with channel flashing were installed between lanes to keep transverse airflows within a given type of tile (Fig. 3).

Each test roof has its own attic cavity with 11 in. of expanded polystyrene insulation installed between adjacent cavities. This reduces the heat leakage between cavities to less than 0.5% of the solar flux incident at solar noon on a test roof. Therefore, each lane can be tested as a stand-alone entity. Salient features of the ESRA facility are fully discussed by Miller et al. (2002).

Fig. 2. An assembly of steep-slope attics was placed on top of the ESRA and clay and concrete tile were installed by the Tile Roofing Institute.

Table 1. Clay and concrete tile placed on the ESRA's Steep-Slope Attic Assembly

Roof Cover	Attachment to Deck	Reflectance Emittance
		SR*xx*E*yy*[1]
S-Mission Clay	Direct to Deck	SR54E90
Medium-Profile Concrete	Direct to Deck	SR10E93
S-Mission Concrete	Spot Adhered to Deck Using Foam	SR26E86
Slate Concrete	Counter-Batten and Batten	SR13E83
S-Mission Concrete	Batten	SR34E83
Asphalt Shingle	Direct to Deck	SR10E89

[1]SR*xx* states the solar reflectance of a new sample. E*yy* defines the thermal emittance of the new sample. For example, the asphalt-shingle roof is labeled SR10E89; its freshly manufactured surface properties are therefore 0.10-reflectance and 0.89-emittance.

As mentioned, a sub-tile venting occurs up along the underside of the tile roofs because of the design of the tile and the construction of the roof deck. The batten and batten with counter-batten installations provide a unique inclined air channel running from the soffit to the ridge. The bottom surface of the air channel is formed by the roof deck and 30# felt and is relatively in plane and smooth. The top surface is created by the underside of the roofing tiles and is broken at regular intervals by a batten[1] wood furring strip (into which the tiles are fastened). For batten and counter-batten construction, the counter-batten is fastened to the roof deck and run from soffit to ridge, and the batten is nailed on top of the counter-battens (Fig. 3). The underside of the roof tiles establishes the upper surface of the inclined air channel. Tiles are designed with a gap at the respective overlap where one tile lies atop the other. The design allows wind pressures to equalize for reducing wind uplift (Fig. 4). The design further complicates solution of the heat transfer, because an accurate prediction of the airflow is required to predict the heat transfer crossing the roof boundary.

[1] Battens are either fastened directly to roof deck or fastened atop a counter-batten. Battens run parallel to the roof's ridge.

Fig. 3. Construction of the roof deck showing battens and counter-battens for attaching the slate tile and the parapets used to limit airflows on the underside of the tile to within a given test roof.

Fig. 4. S-Mission clay and concrete tile are designed to have a gap between overlaid tiles.

Instrumentation for Attic Assembly

The surface and underside temperatures of the tile, the temperatures of the roof deck on both sides of the oriented strand board (OSB), and the heat flux transmitted through the roof deck are directly measured (Fig. 5) and recorded by a data acquisition system (DAS). All roof decks have a 2-in-square by 0.18-in.-deep routed slot (Fig. 6) with a heat flux transducer (HFT) inserted to measure the heat flow crossing the deck. Each HFT was placed in a guard made of the same OSB material used in construction and calibrated using a FOX 670 Heat Flow Meter Apparatus to correct for shunting effects (i.e., distortion due to three-dimensional heat flow). The attic cavities also have an instrumented area in the ceiling for measuring the heat flows into the conditioned space. The ceiling consists of a metal deck, a 1-in.-thick piece of wood fiberboard lying on the metal deck, and a ½-in.-thick piece of wood fiberboard placed atop the 1-in. piece (Fig. 7). The HFT for measuring ceiling heat flow is embedded between the two pieces of wood fiberboard. It was also calibrated in a guard made of wood fiberboard before being placed in field service.

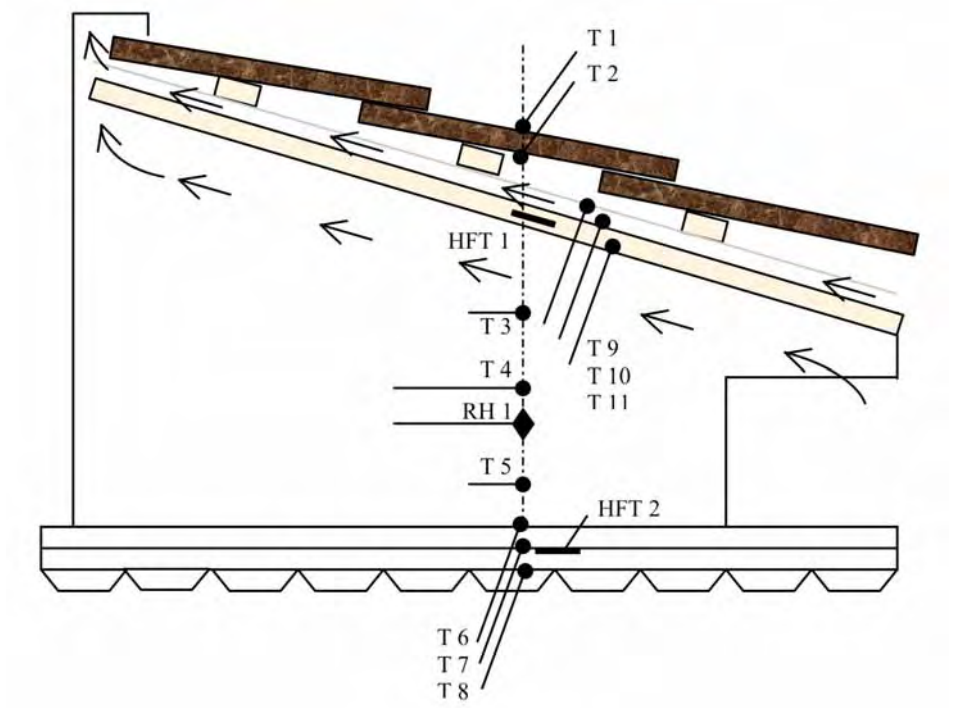

Fig 5. The location of temperature, relative humidity, and heat flow measures made on each attic assembly.

Fig. 6. Heat flux transducer embedded in the roof deck for measuring the heat flow penetrating through the roof tile and into the attic.

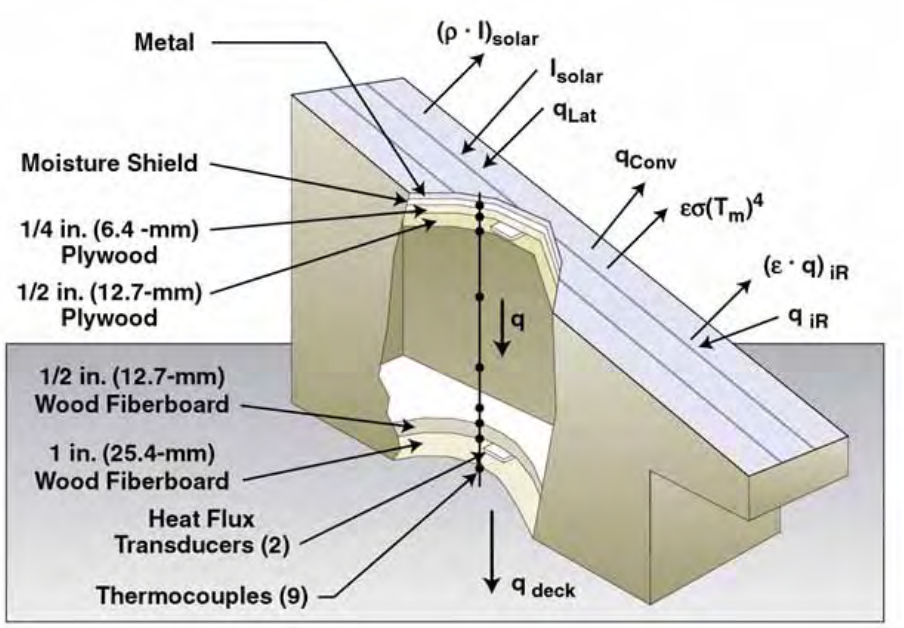

Fig. 7. Setup of attic assembly showing construction materials, instrumentation, and polyisocyanurate insulation used to isolate attic from adjacent attics.

Instrumentation for Sub-Tile Venting

Tile roofs are traditionally offset from the roof deck, and the convection heat transfer in this space may be mixed, being a combination of forced and natural convection heat transfer. Data on the mixed-convection phenomena are sparse because buoyancy effects can cause oscillations in the inertia flow field, which make convergent numerical solutions difficult to obtain. Therefore, the effect of sub-tile venting is a key measurement issue that required added instrumentation.

The S-Mission clay tile and flat slate roofs have thermocouples and HFTs at four stations starting at the soffitt and spaced evenly about 4 ft apart up to the ridge to measure the bulk air temperatures and the heat flux near the underside of the tile (Fig. 8). These measurements are used to gage the convective heat transfer within the air channel made by the underside of the tile and the roof deck. On a typical warm, sunny day, the irradiance from the sun will penetrate the tile roof and will cause a net inflow of heat into the air channel, and a portion of this heat is conducted into the attic space. The penetration of heat into the attic as measured by the HFTs is defined as positive heat flow. Heat leaving the attic or conditioned space is defined as negative heat transfer.

Data Acquisition System

A 700-MHz Pentium III computer collected field data using FIX DMACS version 7.1 software supported by Windows version 2000. The code scanned all instruments every 15 s and electronically recorded averages at 15-min intervals to a historical database within the FIX DMACS hierarchy. Data were retrieved weekly from the historical database and written to a spreadsheet for combination with the weather data and in preparation for later data reduction and analysis.

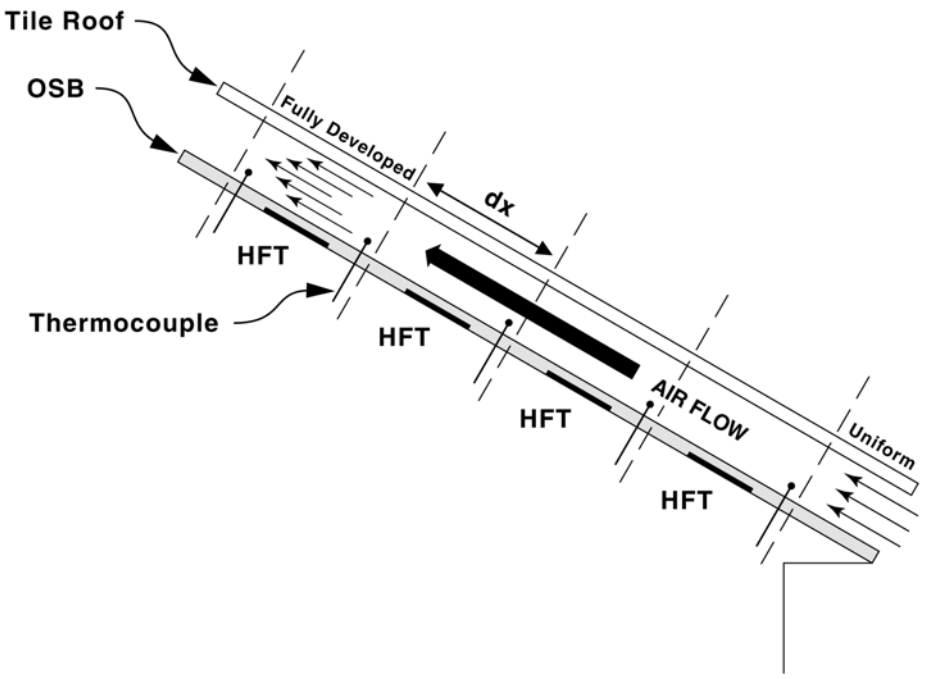

Fig. 8. Instrumentation used on the underside of the tile roofs for validating heat transfer correlations predicting the heat transfer driven by thermally induced airflows.

Solar Reflectance and Thermal Emittance Instruments

A Device and Services solar spectrum reflectometer was used to measure the solar reflectance (total hemispherical reflectance over spectrum of sun's energy) of the roof samples. The device uses a tungsten halogen lamp to diffusely illuminate a sample. Four detectors, each fitted with differently colored filters, measure the reflected light in different wavelength ranges. The four signals are weighted in appropriate proportions to yield the total hemispherical reflectance. The device was proven accurate to within ±0.003 units (Petrie et al. 2000) through validation against the ASTM E-903 method (ASTM 1996). However, because the CRCMs exhibit high infrared reflectance, some of the field samples were also measured at LBNL using a spectrometer to check the portable reflectometer. The average absolute difference between the Device and Services reflectometer and the spectrometer was about 0.02 points of reflectance, with the spectrometer consistently reading lower than the reflectometer. (For example, the reflectometer measured a solar reflectance of 0.741 for a cool pigment painted metal, while the spectrometer measured 0.73.)

The impact of emittance on roof temperature is as important as that of reflectance. A portable Device and Services emissometer was used to measure the thermal emittance using the procedures in ASTM C-1371 (ASTM 1997). The device has a thermopile radiation detector, which is heated to 180°F. The detector has two high-ε and two low-ε elements and is designed to respond only to radiation heat transfer between itself and the sample. Because the device is comparative between the high-ε and the low-ε elements, it must be calibrated in situ using two standards, one having an emittance of 0.89, the other having an emittance of 0.06. Kollie, Weaver, and McElroy (1990) verified the instrument's precision as ±0.008 units and its accuracy as ±0.014 units in controlled laboratory conditions.

SOLAR REFLECTANCE AND THERMAL EMITTANCE

The solar reflectance and the thermal emittance of a roof surface are important surface properties affecting the roof temperature, which, in turn, drives the heat flow through the roof. The solar reflectance (ρ) determines the fraction of the solar radiation incident from all directions that is diffusely reflected by the surface. The thermal emittance (ε) describes how well the surface radiates energy away from itself as compared to a blackbody operating at the same roof temperature. The thermal emittance is the total hemispherical emittance of electromagnetic radiation over all wavelengths with peak irradiance occurring in the far-infrared region for roof temperatures of the order of 150°F.

Effects of Climatic Soiling

Solar reflectance measures of the clay and concrete tile roofs exposed at ORNL were collected quarterly; these data are shown in Fig. 9. The initial solar reflectance and initial thermal emittance are identified for each tile using the abbreviation SRxxEyy described in Table 1. After two years of exposure, the S-Mission tiles (SR54E90, SR26E86 and SR34E83) show little drop in solar reflectance. The medium-profile concrete (SR10E93) and the slate (SR13E83) tiles actually show slight increases in solar reflectance, as does the asphalt shingle roof due to the accumulation of airborne contaminants. Dust tends to lighten these darker colors. Data for clay tile are also shown for field exposure testing in 3 of the 16 climatic zones of California. The clay samples are identical to those tested at ORNL. They show a loss of solar reflectance that occurs because of climatic soiling. The worst soiling observed occurs in the urban area of Colton and the desert area of El Centro (Fig. 10). However, the crisp and clear alpine climate of McArthur shows the lowest loss of solar reflectance, because fewer contaminants pollute the air. Roof

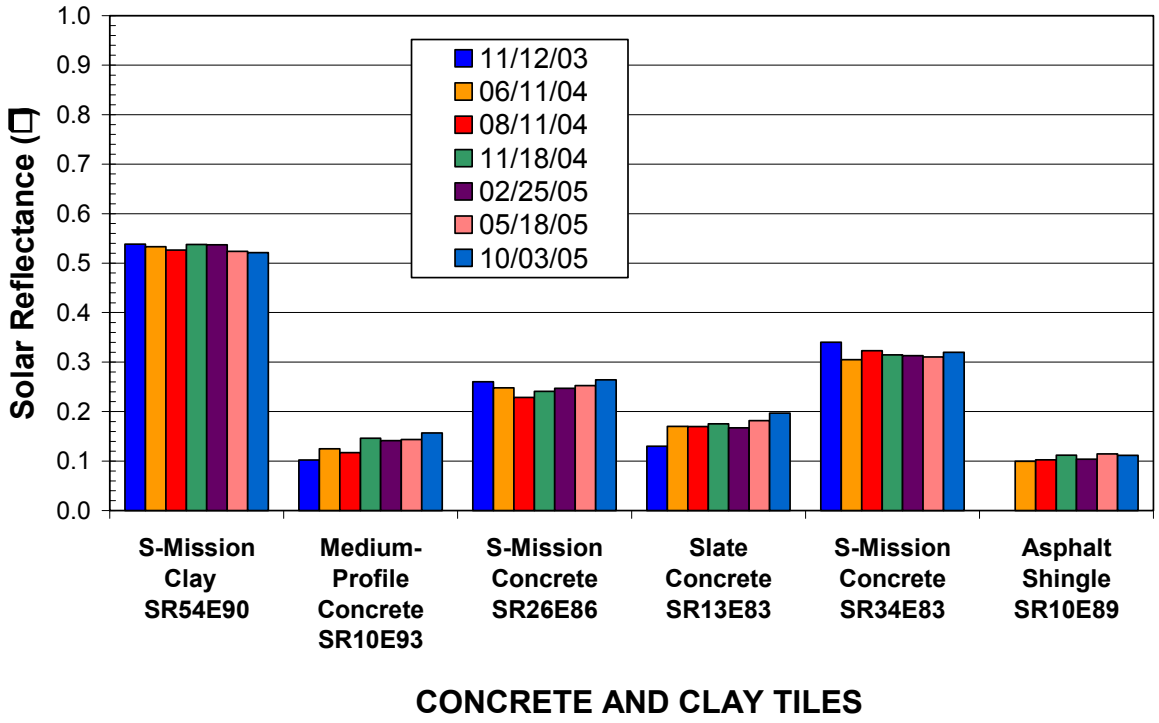

Fig. 9. Solar reflectance of the clay and concrete tile exposed on the ESRA.

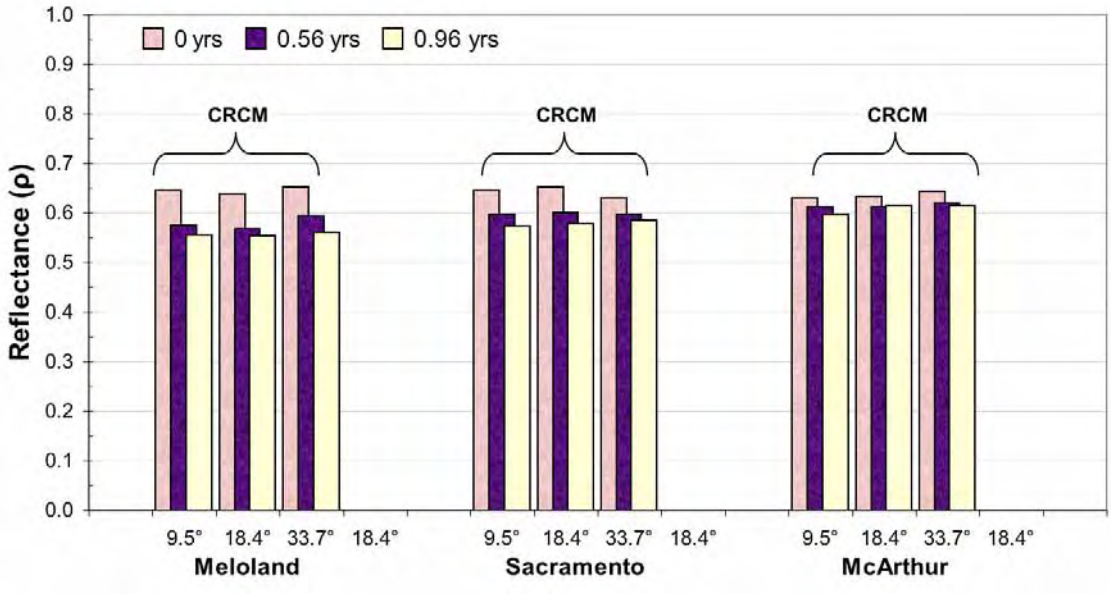

Fig. 10. Solar reflectance of clay tile exposed at weathering sites in California.

slope appears to affect the loss of solar reflectance (Fig. 10). Testing at the slope of 8 in. of rise per 12 in. of run (33.7º slope) has less reflectance loss compared to testing at 2 in. of rise per 12 in. of run (9.5º) for all three exposure sites (Fig. 10). Precipitation is not believed to be the dominant player, especially when one considers that El Centro has less than 3 in. of annual rainfall! Rather, wind may be causing the different losses of solar reflectance as roof slope changes from 9.5º to 33.7º.

Our emphasis on the long-term benefits of cool roofing systems recognizes the potential for a significant loss in solar reflectance in the first few years of service life. Surface contamination and climatic exposure cause the loss. The results in Figs. 9 and 10 show that exposure testing differed between the western and mid-eastern climates of the United States. The samples from the two regions show that California has more airborne dust than does Tennessee, which causes the greater loss of reflectance in California. East Tennessee's climate caused little, if any, soiling of the nonwhite tiles.

The thermal emittance of the clay and concrete tile has not changed much after 2 years of exposure in California. It remains relatively constant at about 0.85.

Cool Roof Color Materials (CRCMs)

The clay tile (SR54E90) tested at ORNL and California exceeds the solar reflectance of all the other tiles (Fig. 9), because it contains complex inorganic color pigments that boost its reflectance in the infrared spectrum. A slurry coating process is used to add color to the surface of a clay tile. Once coated, the clay is kiln-fired, and the firing temperature, the atmosphere, and the pigments affect the final color and solar reflectance [Akbari, et al. (2004a)]. The complex inorganic color pigments, termed here as cool roof color materials, are of paramount importance and will literally revolutionize the roofing industry. The energy and cost savings reported by Parker et al. (2002) for white reflective concrete tile are promising; however, in the residential market, the issues of aesthetics and durability will limit the acceptance of "white" residential roofing. To homeowners, dark roofs simply blend better with the surroundings than their counterpart, a highly reflective "white" roof. What the public is not aware of, however, is that the aesthetically pleasing dark roof can be made to reflect like a "white" roof in the near-infrared spectrum. Miller et al. (2004), Akbari et al. (2004b), and Levinson et al. (2005a and 2005b) provide further details

about the potential energy benefits, identification, and characterization of dark, yet highly reflective, color pigments.

Coating tile with CRCMs has been successfully demonstrated by American Rooftile Coatings, which applied its Cooltile IR Coating™ (Appendix B) to several samples of concrete tiles of different colors (Fig. 11). The solar reflectance for all colors tested exceeded 0.40. Most dramatic is the effect of the dark colors. The black coating increased the solar reflectance from 0.04 to 0.41, while the chocolate brown coating increased from 0.12 to 0.41, a 250% increase in solar reflectance! Because solar heat gain is proportional to solar absorptance, the Cooltile IR Coating™ reduces the solar heat gain by roughly 33%, of that of the standard color, which is very promising. The coating application is a significant advancement for concrete tile, because the alternative is to add the CRCMs to the cement and sand mixture. This requires too much pigment and makes the product too expensive. The coating can certainly help tile roof products comply with legislation being proposed for California's Title 24 building energy efficiency standards for residential buildings. Levinson, Akbari, and Reilly (2004) found that applying the Cooltile IR Coating™ yielded measurable reductions in roof surface temperature, attic air temperature, and ceiling heat flux for scaled buildings field tested in Riverside, Calif. Levinson predicted that the IR coating would save about 92 kWh/year for a 1500-ft^2 Fresno home with R-11 attic insulation and would yield a simple payback for the coating within about 5 years.

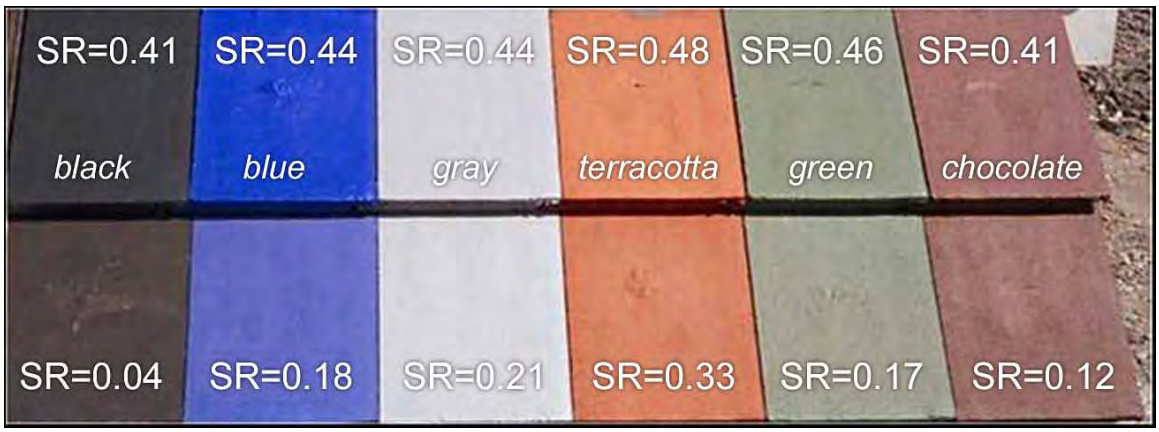

Fig. 11. Cooltile IR Coating™ developed by Joe Riley, LBNL and ORNL.

FIELD TEST RESULTS

The multiple hazard protection provided by concrete and clay tile from fire and wind and the superior aesthetics and durability of tile are making these roof materials the preference of homeowners in western and some southern states. Thermal performance data collected from the attic test assembly at ORNL show tile to be an energy-efficient roof product because of the venting occurring on the underside of the tile and also because of the increase in solar refectance achievable with CRCMs.

Venting of attic spaces, and its effect on heat transmission, moisture, and condensation, has been studied at reasonable length, but little has been studied with regard to the venting and flow patterns observed in the inclined channel created by tile roofs. Rose (1995) gives an overview of the evolution of attic venting, and Romero and Brenner (1998) instrumented a test building for the study of ridge venting procedures and the associated flow within the attic space. Though work is scarce on heat transfer within the narrow air channel in counter-batten installations, insight can be gained from the work done on attic ventilation and on experimental studies of heat transfer in inclined ducts. Ozsunar et. al (2001) studied the effects of inclination on convection within a large aspect ratio duct heated from below. Beal and Chandra (1995) studied heat transfer through direct-nailed tile roofs and counter-batten tile roofs compared to direct-

nailed asphalt shingles. Tile in general reduced heat transmission by 39% for the direct-nailed roof and by 48% for the counter-batten roof.

Cooling Season Field Performance

The clay S-Mission tile (SR54E90), the S-Mission tile spot adhered with foam (SR26E86), and the S-Mission tile on battens (SR34E83) had the least amount of heat penetrating into their respective roof decks (Fig. 12). The roof heat flux data are for two consecutive days of exposure during August 2004 in East Tennessee's hot and humid climate. All three tiles have venting occurring along the underside of the tile's barrel from soffitt to ridge; however, the ridge vent is closed to simulate conventional installations in the western states. Of these three roof systems, the clay tile (SR54E90) had the lowest heat flux through the deck, due primarily to the tile's high solar reflectance. The clay tile reduced the peak heat transfer penetrating the roof deck at solar noon by about 70% of the energy penetrating through the deck of the attic covered with an asphalt shingle roof. Subsequently, the heat penetrating the ceiling of the attic assembly was reduced by about 60% of that entering through the ceiling of the attic assembly with asphalt shingles[2].

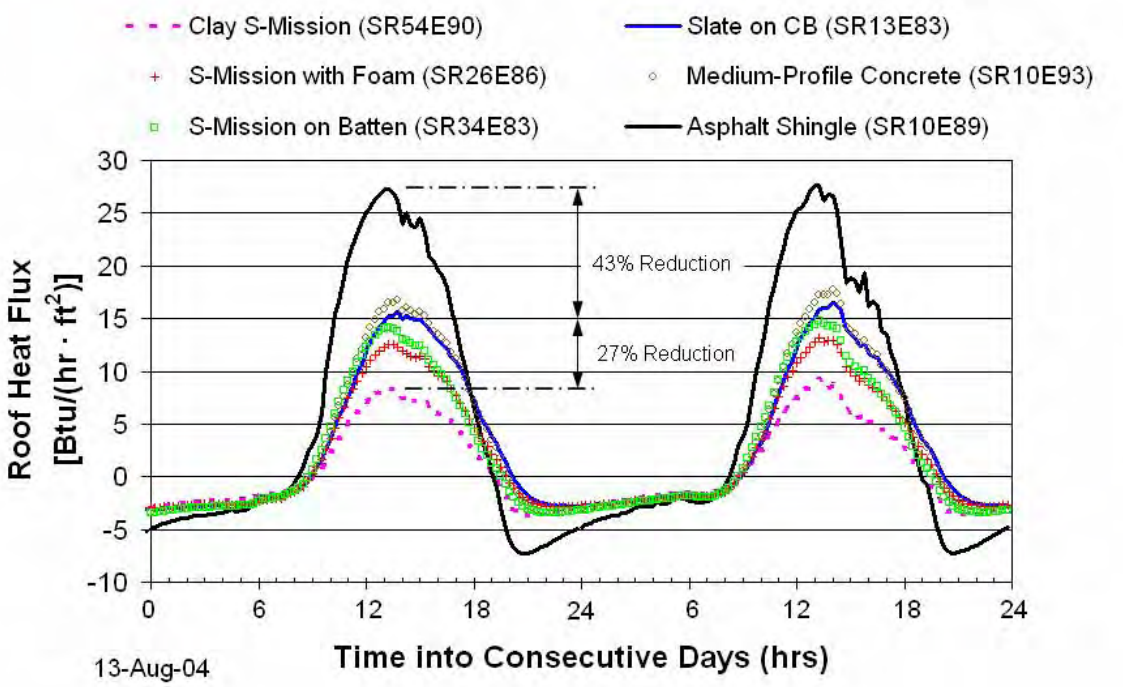

Fig. 12. Heat penetrating the tile roof of each attic assembly on the ESRA; the ridge vent was closed.

The solar reflectance and thermal emittance of the slate roof (SR13E83) and the medium-profile tile (SR10E93) are very similar to that of the asphalt shingle (SR10E89), but the heat transfer through the roof and ceiling of the attic with the slate roof and the medium-profile tile roof are only half that measured for the asphalt shingle roof. The reduction must be due to buoyancy and wind force effects occurring in the inclined air channel that dissipates heat away from the deck. The slate tiles are attached to batten and counter-batten strips, which form the inclined air channel that is about 1½ in. deep. The medium-profile

[2] The ridge vent for the asphalt shingle roof was also closed for the August 2004 comparison to clay and concrete tile roofs field-tested on the ESRA.

tile forms its own half-cylindrical channel of about 0.5 in. radius. It is very interesting that these two dark tile systems (SR13E83 and SR10E91), as compared to the shingle roof (SR10E89), significantly reduce the heat penetrating their respective ceilings. The data in Fig. 12 clearly show the benefit derived from venting the roof deck based solely on the direct comparison of the percent reduction of peak loads (i.e., ~45% reduction for the SR13E83 or SR10E93 and a 70% reduction for the SR54E90 tile as compared to the shingle roof). Proportioning the heat reduction due solely to venting (SR10E93 vs SR10E89) to the heat reduction due to solar reflectance and venting (R54E90 vs SR10E89):

$$\frac{\overbrace{45\%\ \text{due to venting}}^{\text{heat reduction}}}{70\%\ \text{due to venting and SR}} \cdot \left[SR54_{\text{Clay Tile}} - SR10_{\text{Shingle}}\right] \quad (1)$$

yields a venting benefit at solar noon that is equivalent to roughly 30 points of surface reflectance! Hence, the data at peak loading imply that "cool roofing" credits are obtainable through venting the underside of a tile or similarly constructed roof system. The data also clearly show the synergism gained by the solar reflectance of CRCMs (Fig. 12) and the deck venting occurring on the underside of tile roofs. A full month of field data for August 2004 was reduced to better observe the seasonal trends in roof heat transfer for the tile and asphalt shingle roofs. Data for the HFTs embedded in the south-facing roof deck and the ceiling of each attic assembly were integrated over the daylight hours (red bars in Fig. 13), nighttime hours (gray bars in Fig. 13), and the 24-h cycle for HFTs embedded in the ceiling (blue bars in Fig. 13) and summed for the month. Hence, the red and gray bars represent, respectively, the total daytime heat gain and nighttime loss crossing the roof deck during August 2004 exposure. The blue bars represent the total heat transfer into the conditioned space measured from the HFT embedded in the ceiling of each attic assembly.

Results for the unvented attics show that the heat gain entering the asphalt shingle roof is almost double that observed for the medium-profile (SR10E93) and the slate (SR10E83) concrete roofs. Therefore, the effect of venting the underside of the medium-profile and slate tile roofs based on proportioning roof heat transfer (Eq. 1) equates to about 24 points of solar reflectance for the month of August 2004. In other words, an SR34E93 roof with no deck venting would have about the same roof heat transfer as the vented tile (SR10E93) roof.

Again the S-Mission tile roofs have the least amount of heat penetrating the roof deck, with the clay tile (SR54E90) showing best performance. About 4100 Btu/ft^2 of roof surface penetrated the shingle roof as compared to only 1127 Btu/ft^2 for the clay tile roof, representing a 72% reduction in roof heat transfer. This, in turn, leads to the reduction in heat transfer observed crossing the ceiling of the two attic assemblies. The heat transfer penetrating the ceiling of the attic with clay tile was about 75% less than that measured for the heat penetrating the ceiling of the attic with an asphalt shingle roof. It is also interesting to observe that all the tile roofs have less heat loss to the ambient sky as compared to the direct-nailed asphalt shingle roof (Fig. 13). The effect is due in part to the venting occuring on the tile's underside and in part to the thermal mass of the tile. Parker, Sonne, and Sherwin (2002) showed that a white galvanized metal roof slightly outperformed a white S-shaped cement tile roof because the thermal mass of the tile retained more heat that the air-conditioner had to temper earlier in the day than the house with a painted metal roof. However, in more moderate climates, this thermal mass effect is a benefit and will be discussed in the next section on heating seasonal performance.

It is difficult to judge whether venting or surface reflectance is the predominant force dropping the roof flux. However, Beal and Chandra (1995) showed that S-Mission tile on battens reduced the heat penetrating the ceiling by an additional 11% as compared to the same tile of the same color direct-nailed to the deck. Subsequently, sub-tile venting of the tile roofs appears just as important as is the boost in solar reflectance for reducing the heat gain into the attic and conditioned space.

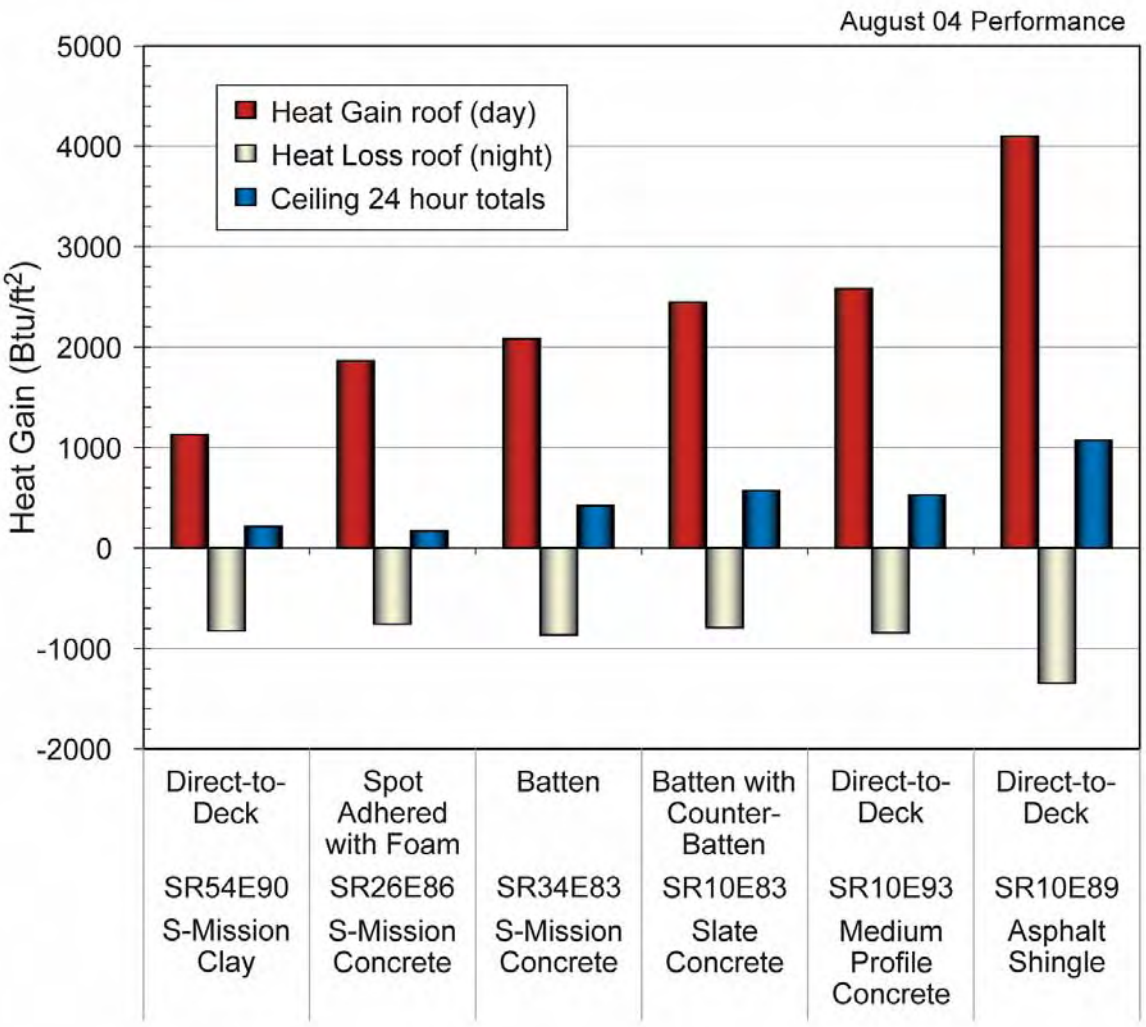

Fig. 13. S-Mission tile reduced the integrated daytime roof heat gain by 50 to 75% of the gain for the asphalt shingle roof.

Effects of Opening the Ridge Vent

As early as 1942, the Federal Housing Administration (FHA) set a 1:300 requirement (i.e., area of soffitt and ridge vent openings to attic footprint) for convective cooling of the attic air and for minimizing condensation on the underside of the roof sheathing as a preventative maintenance measure (FHA 1942). However, the importance of convection cooling of the attic air is controversial. The ridge vents for the tile and asphalt shingle roofs were opened for the summer of 2005 to observe the effects of attic ventilation and, more importantly, the effect of unrestricted airflow within the inclined air gap made by the underside of the tile roofs. Two summer days with very similar outdoor air temperatures and solar irradiance were selected. On one day, the ridge vent was closed; on the other day, it was kept open (Fig. 14). The soffitt vent was open for both summer days of field-testing.

Opening the ridge vent reduced the bulk air temperature within the inclined air channel for the slate (SR10E83) tile and also for the clay (SR54E90) tile (Fig. 14). At solar noon, the bulk air temperature near the underside of the slate tile was 10°F cooler than that observed for the same slate tile with the ridge vent closed during the previous summer. The effect for the S-Mission clay was about a 5°F drop in the bulk air temperature for the two different summer days with very similar weather. Slate tile are laid one atop

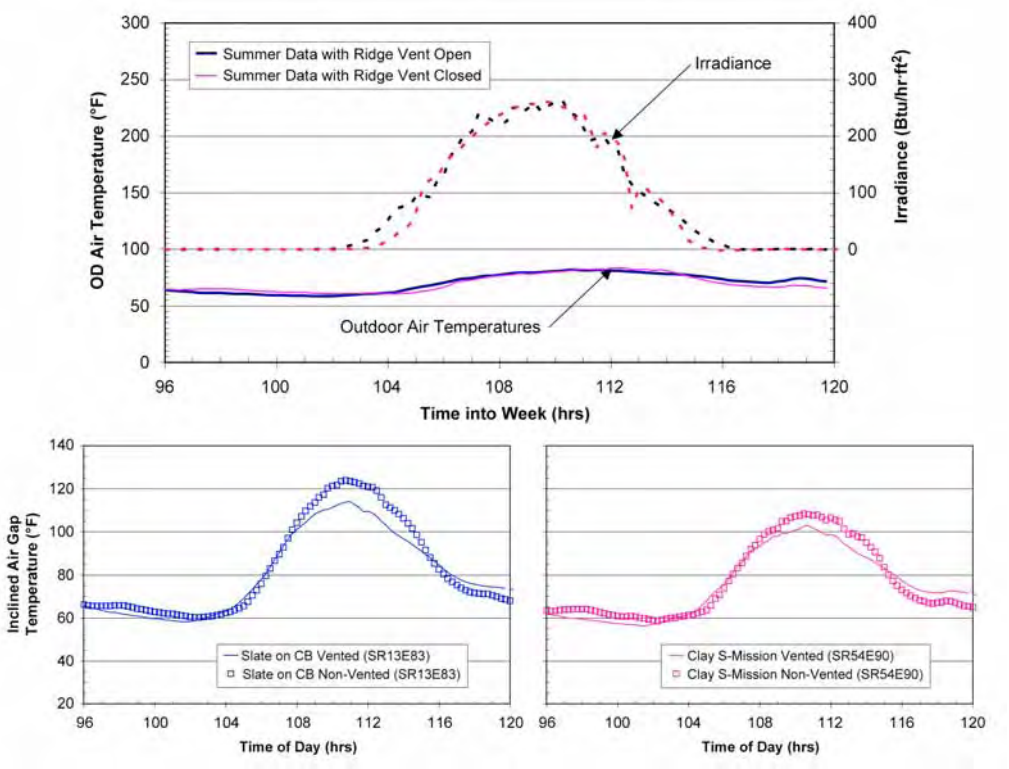

Fig. 14. Bulk air temperatures underneath the S-Mission clay and the concrete slate tile for two different summer days, one with the ridge vent open and the other with the ridge vent closed.

another and have little clearance for the seepage of air between overlapped tile. The S-Mission tile are designed to be porous to minimize wind uplift forces (Fig. 4). Therefore, the clay tile allowed more leakage of air by naturally induced thermal gradiants between overlapped tiles than observed for the slate tile system. As a result, opening the ridge vent caused a more significant drop in heat flow crossing the roof deck for the slate tile roof than for the clay tile roof (Fig. 15). The results imply that opening the ridge caused more heat to be exhausted out the ridge for both the S-Mission clay and the slate tile systems.

Heating Season Field Performance

Cool roofs have received much positive trade press, as well as some state and federal support for installation where comfort cooling is the dominant building energy load. In mixed climates with both significant heating and cooling loads, the wintertime effect reduces the energy benefit because the desirable roof heat gain in winter is diminished somewhat by the higher solar reflectance of the roof. The Achilles' heel of all cool roof systems is therefore the heating penalty that offsets the energy and cost savings associated with the cooling benefit of the reflective roof system. The colder the climate the greater is the penalty, and the trade-off between climate and reflective roofs limits their penetration into predominantly heating-load climates. However, field data for the tile roofs tested in East Tennessee's climate are showing that the tile's mass and sub-tile venting are negating the heating penalty associated with cool roofs.

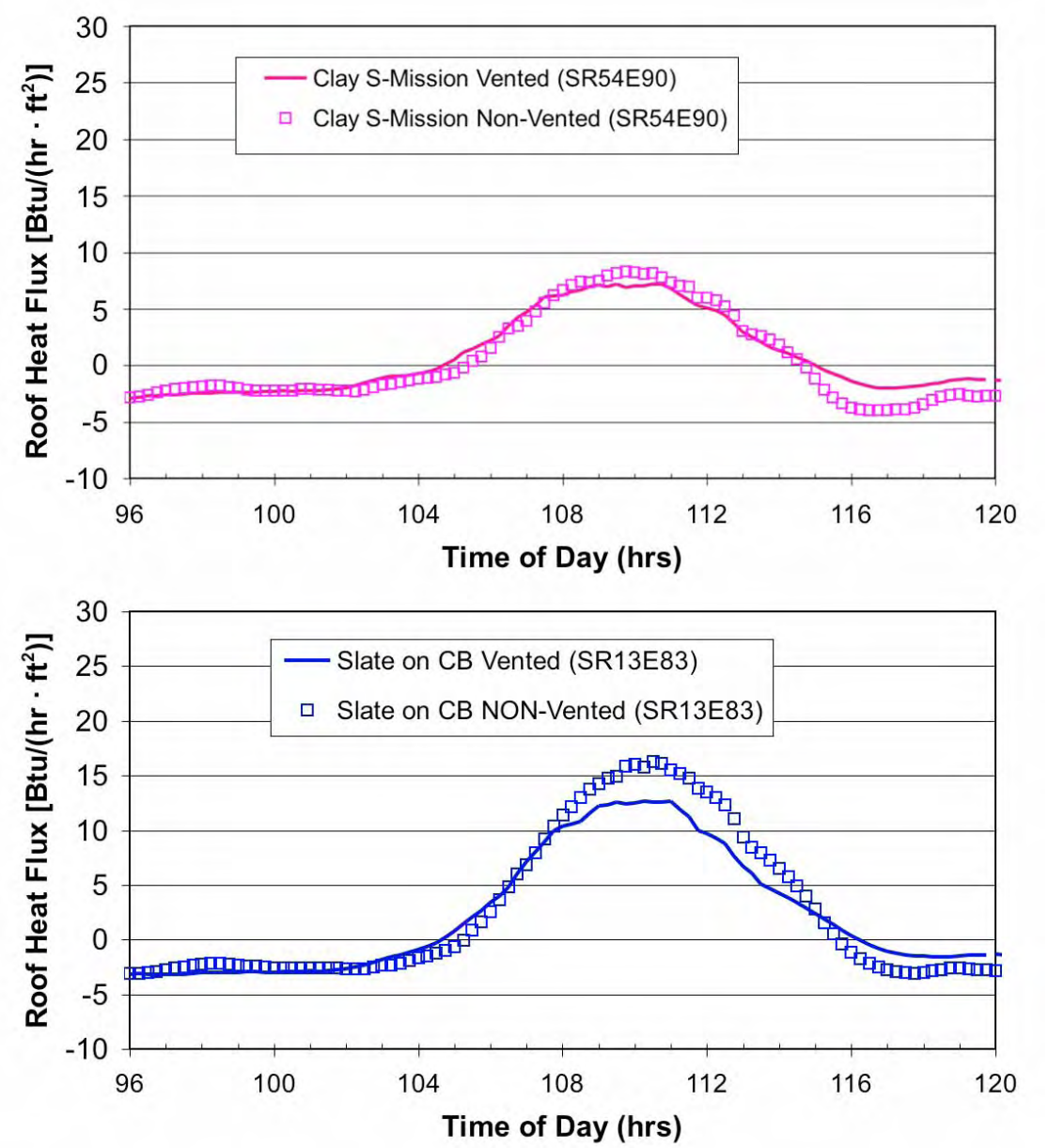

Fig. 15. Heat penetrating through the roof deck of the S-Mission clay tile and the concrete slate tile with and without venting of the roof deck.

Results from two consecutive days with clear Janurary skies are displayed in Fig. 16 to review the thermal performance of the clay and concrete tile roofs compared to that of the dark heat-absorbing asphalt shingle roof. The ridge vents for these tests were closed, and the average ambient air temperature for these two Janurary days was 32°F. At solar noon, the roof deck of the attic with asphalt shingles (SR10E89) absorbed about 15 Btu/h/ft^2 of solar flux, which is almost twice that absorbed by the medium profile (SR10E93) or slate (SR13E83) roofs. The attic assemblies with S-Mission clay and concrete tile

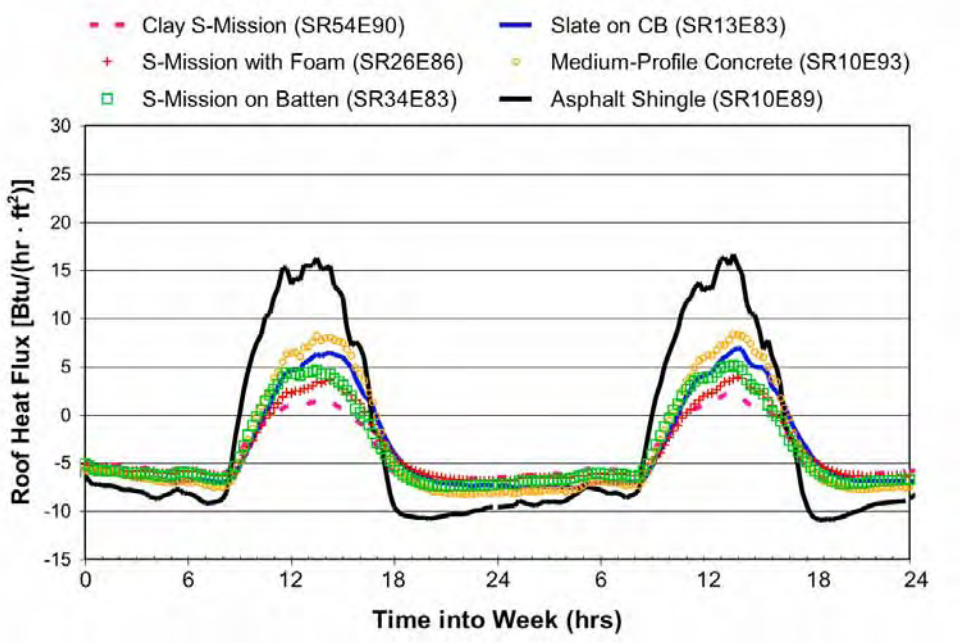

Fig. 16. Roof deck heat flow for two consecutive days in January 2005; the ridge vent is closed.

showed marginal heat gains, with the clay tile showing almost no gain even at solar noon. However, during the evening hours from about 8 p.m. through about 6 a.m., all the tile roofs lose less heat to the night sky than does the asphalt shingle roof (Fig. 16). The tile reach peak day temperatures ranging from 92°F for the SR34E83 S-Mission concrete to 75°F for the S-Mission clay tile (SR54E90). The shingle reaches about 105°F peak temperature. But during the night, the tiles are all warmer than the shingles because of the thermal mass of the tile and because the air channel formed on the underside of the tile adds an additional radiative resistance to night-sky radiations losses as compared to the direct nailed shingle.

Thermal Mass Effects

Results integrated over the month of Janurary 2005, as done similarly for August 2004, show that the thermal mass of the tile roofs nearly counterbalances the heating penalty associated with cool roofing for the moderate climate of Tennessee (Fig. 17). Again, venting the underside of the tile plays a part in the results. The asphalt shingle roof gains about 1000 Btu/ft^2 of roof deck during all January days, while the tile roofs show little gain and some a loss of heat from the roof deck. However, during the evening hours the thermal mass and possibly the tile's air channel have reduced the heat loss from the roof to the point that the heat loss from the ceiling of all roofs is about the same (see blue bars in Fig. 17). These data are very promising, because the tile roofs are negating the heating penalty associated with a cool roof in Tennessee's moderate climate having 3662 HDD_{65} and 1366 CDD_{65}. The fact that the SR54E90 and SR26E86 tile roofs actaully lost heat during the January days implies that the radiative resistance afforded by the inclined air gap on the tile's underside is the primary driver causing the reduction in nighttime heat losses.

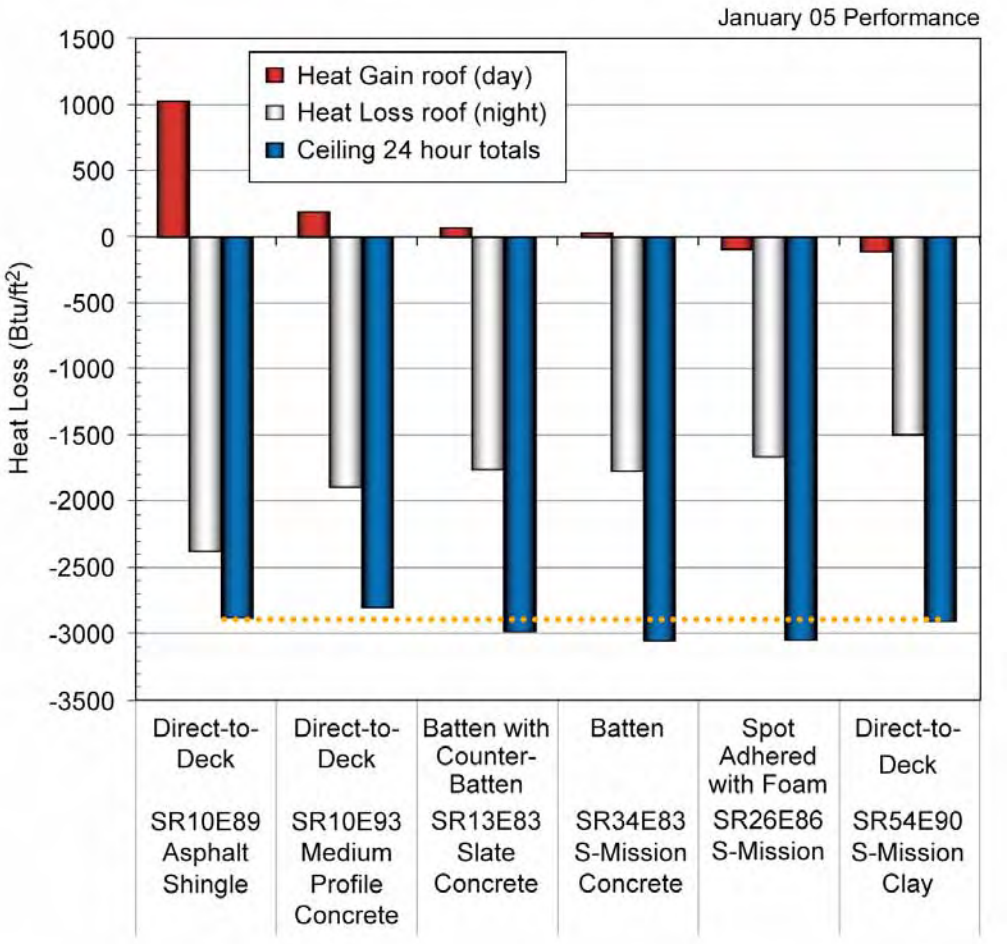

Fig. 17. Integrated heat flow measured through the roof deck for all tile and shingle roofs during the month of January 2005.

Venting the Underside of Tile Roofs

The transfer of heat across the roof tile and roof deck has similar physics to the problem associated with the heat transfer across the inclined air channel formed by roof-mounted solar collectors. Comprehensive reviews of both experimental and theoretical results are available in the literature. Hollands et al. (1976), Arnold et al. (1976), and most recently Brinkworth (2000) studied this situation as applied to flat-plate photovoltaic cladding.

All residential roofs are sloped and make an angle θ with the horizontal plane that ranges from 2 in. of rise per 12 in. of run (9.5º slope) to a steep-sloped roof of 45º. During winter exposure, a roof deck is warmer than the tile and in the inclined air channel, the heated surface is positioned below the cooler tile surface much like the solar panel application studied by Hollands et al. (1976). Here, a more dense air layer near the tile overlays a lighter air adjacent to the roof deck (see θ = 0, Fig. 18). Hollands observed that the heat transfer across the air channel can switch from conduction to single-cell convection to Bénard cell convection, depending on the strength of a non-dimensional parameter called the Rayleigh (Ra) Number. For Rayleigh numbers less than 1708/COS(θ), there is no naturally induced airflow within the cavity, and the heat transfer occurs exclusively by conduction. However, a flow of air occurs if buoyancy forces overcome the resistance imposed by the viscous or frictional forces. As the flow increases due to buoyancy, the heat transfer within the channel can switch to Bénard cell convection,

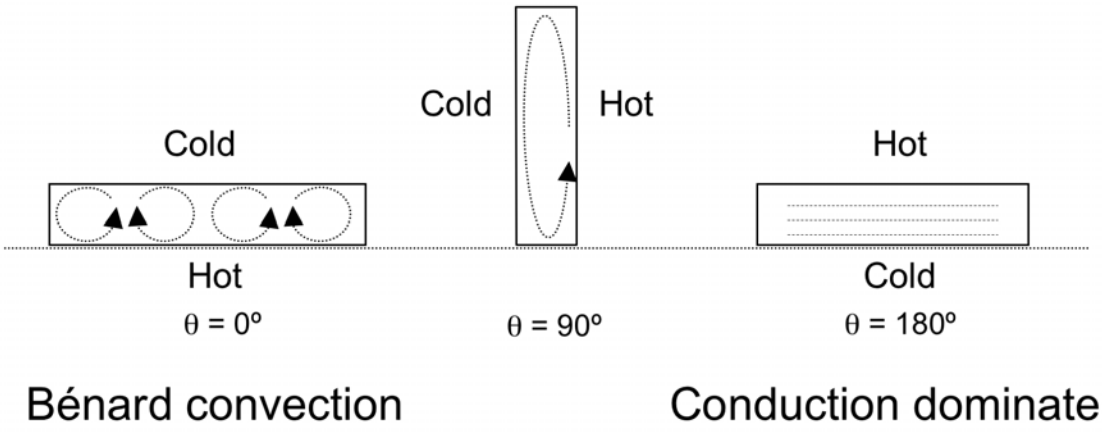

Fig. 18. Heat transfer phenomena occurring on the underside of roof tile.

which has hexagonal cells with flow ascending in the center and descending along the sides of the air channel (see θ = 0, Fig. 18).

Arnold et al. (1976) observed that the channel's aspect ratio and the slope of the solar panel (for our application, a roof) had a major impact on the flow and heat transfer within the air channel. They observed that if the channel was rotated from θ = 180º (summer exposure for a roof) all the way to θ = 0º (winter exposure), the heat transfer rises to a maximum at θ = 90º and then, as θ decreases below 90º, the heat transfer rate first decreases and passes through a local minimum at θ* (Bejan 1984). However, as θ decreases below θ*, the heat transfer rate again rises because of the inception of Bénard cell convection. Arnold et al. (1976) also observed that the aspect ratio of the channel changed the critical angle θ* where the heat transfer across the channel was minimal. The information may be very useful for designing tile to limit ice damming in predominantly cold climates.

During summer exposure, the tile is hotter than the roof deck, and Bénard cell convection does not occur within the inclined channel because the lighter air layer is now atop the denser air layer near the roof deck. The air heated by the underside of the tile tends to rise, and natural convection begins within a boundary layer formed along the underside of the tile (θ = 180, Fig. 18). Brinkworth (2000) studied this situation as applied to flat-plate photovoltaic cladding, and it is this configuration and heat transfer mechanism that are evident in the field experiments discussed for the tile roof systems field-tested on the ESRA.

Thermally Induced Airflow Rates

An integral technique was used to formulate closed form solutions for the thermal boundary layer, the velocity profile and the heat transfer coefficient for the case of natural convection occurring in the inclined channel. Solving the momentum and energy equations for a constant solar flux yielded the following expression for the thermal boundary layer forming on the underside of a tile roof:

$$\delta_T = \frac{(288)^{1/5}}{Pr^{2/5}} \left[\frac{\left\{1 + \frac{5}{4}Pr\right\}^{1/5}}{\left\{\frac{g\beta q_{Tile} SIN(\theta)}{k \cdot \nu^2}\right\}^{1/5}} \right] x^{1/5} \qquad (2)$$

The velocity profile for the thermally induced air movement in the channel becomes:

$$U(x,y) = A(x)\left\{\eta(1-\eta)^2\right\} \tag{3}$$

and the temperature profile for the channel having a constant roof flux becomes:

$$T(x,y) - T_\infty = \frac{q_{roof}\delta_T}{2k_{air}}\left\{1 - 2\eta_T + \eta_T^2\right\} \tag{4}$$

where

$$A(x) = \frac{g\beta\{T_{Roof}(x) - T_\infty\}\delta_T SIN(\theta)}{4\nu}$$

$$\eta = y/\delta$$

$$\eta_T = y/\delta_T$$

The heat transfer coefficient can be determined by taking the temperature profile within the boundary layer and evaluating its gradient at the underside of the tile. Equating the convection to the conduction at the tile's underside yields the expression:

$$h_x = \frac{2k_{air}}{\delta_T} \tag{5}$$

The expressions in Eqs. 2, 3, 4 and 5 are useful for estimating ballpark values for the bulk velocity and heat transfer coefficient within the air channel. After 14 ft of run from the soffitt toward the ridge, the thermal boundary layer has grown to about 0.14 ft. Within this boundary layer the air's maximum velocity is about 1.8 ft/s, and its average velocity is slightly less than 0.8 ft/s. The local heat transfer coefficient is of the order 0.23 Btu/h/°F/ft^2 of tile. These data helped validate bulk velocities obtained from tracer gas measurements; however, the expressions do not account for the obstructions evident in batten and counter-batten roof constructions.

Numerical Simulations

Computer simulations for thermally induced airflow and heat transfer across an inclined air channel were conducted for several different constant-temperature wall boundary conditions and several different inclinations with the horizontal plane to better understand the strength of natural convection forces occurring within the heated channel. The channel was modeled with and without obstructions (battens) on the top plate. The bottom and the two side surfaces of the channel were held at 68°F, and the top surface was fixed at the higher temperature of 98°F to simulate summer exposure of the tile roof. The aspect ratio of the duct was fixed at 0.01, and the inclination was 30° from horizontal (5 in. of rise per 12 in. of run).

The numerical simulations in Fig. 19 are plotted in terms of the isotherms (constant temperature lines shown in color) and the streamlines (lines of constant velocity). The results depicted in Fig. 19a show that with no obstruction a natural convection flow occurs along the underside of the top plate. An exit jet is seen in line with the duct axis indicating a momentum of flow within the boundary layer that carries heat away from the roof deck. In Fig. 19b the obstruction (batten) forces the air to move down and around the batten, causing some mixing of air outside the established boundary layer of the smooth surface. The streamlines of constant velocity are observed penetrating almost to the bottom plate because of the obstructions. The typical gap in a batten and counter-batten slate roof is about 1.5 to 3 in., depending on

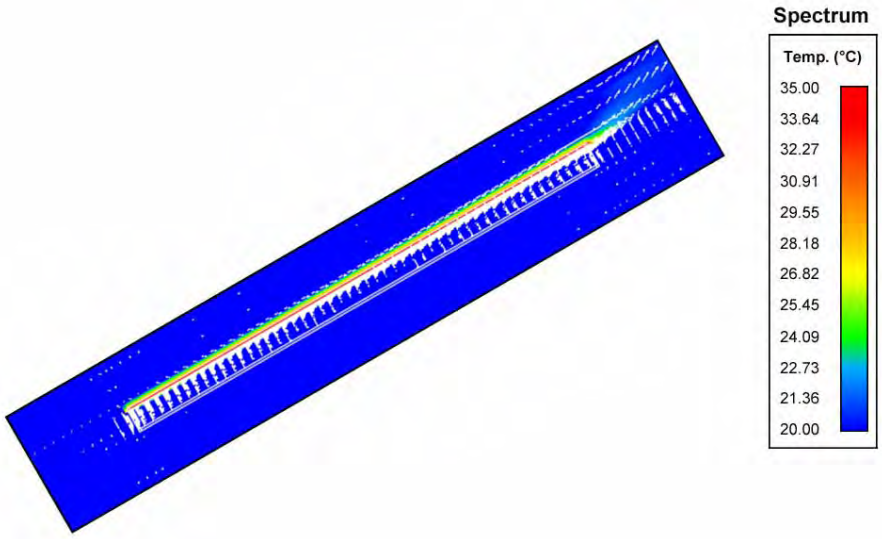

(a) No battens in channel

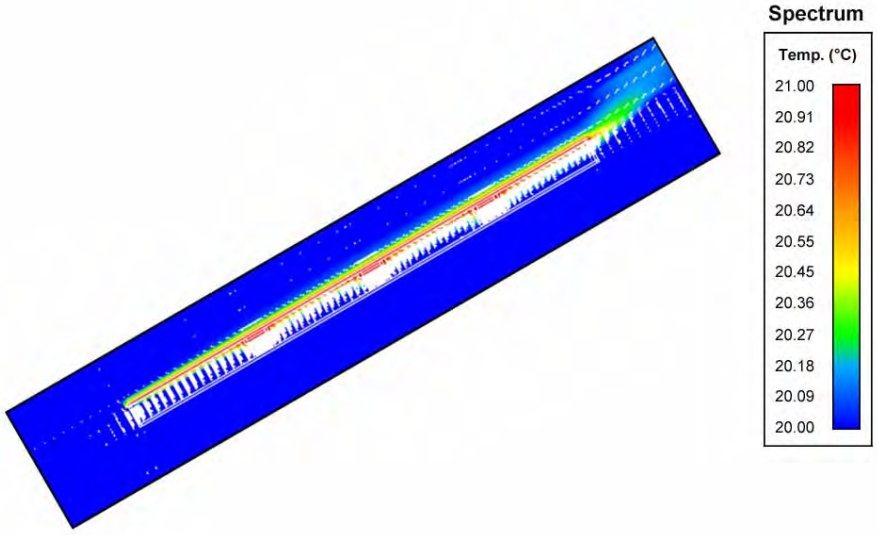

(b) Battens present in channel

Fig. 19. Numerical simulations for channel flow with and without battens fastened to the underside of tile (the top plate). The channel is at an incline of 30° (5-in. rise for every 12 in. of run), and the top plate is 30°F warmer than the bottom plate.

the cross-sectional size of the battens. Recall from the boundary layer (Eq. 2) that after 14 ft from soffitt to ridge, the boundary layer had grown to about 1.4 in. Figure 19b implies that a fully developed flow is established within a shorter distance than occurs in a smooth channel (Fig. 19a). The result is very similar to the stocking of a fireplace. The air in the chimney initially is cold, and the hot air coming from the fire must develop a boundary layer through the colder chimney air to establish a positive pressure gradient for exhausting the hotter air. The inclined channel with battens forms a more developed flow in a shorter distance (i.e., boundary layers on the top and bottom plates meet in a shorter length of run) and a chimney effect occurs, fueling the removal of heat from the roof deck. Hence, the numerical results help to show

qualitatively that the sub-tile venting can be very significant for dissipating heat away from the roof deck, making the tile roof system cooler than conventional direct-nailed systems.

The numerical results do not take into account the effect of a forced-flow component, which may aid or oppose the naturally induced flow, nor is air leakage between the tile overlaps considered. Mixed convection (forced convection driven by wind effects that are accompanied by buoyancy effects) is an additional confounding variable that must be mathematically described a priori the prediction of the heat transfer across the roof deck. The key to the problem is to predict accurately the airflow within the cavity. Once known, the portions of heat penetrating the roof deck and that convected away through the ridge vent can be derived from energy balances.

Airflow Measurements Using Tracer Gas

Measurements were made of the airflow underneath the clay and concrete tile roofs as the buoyancy-driven flow traveled from the soffitt to the ridge of each tile roof. We designed a procedure using tracer gas techniques outlined in ASTM E 741 and also by Lagus et al. (1988). The procedure required monitoring the decay rate of the tracer gas CO_2 with time using the following equation derived from a continuity balance for the concentration of CO_2:

$$\dot{V}_{Air} = -\frac{V_{Channel}}{t} LN\left[\frac{C(t) - C_\infty}{C_i - C_\infty}\right] \tag{6}$$

Three carbon dioxide monitors were placed inside each attic space, and sampling tubes were inserted into the inclined channel from the underside of the OSB decking. The monitors sampled the gas concentration near the soffitt, at the center of the roof and within 2 ft of the ridge vent. We injected the gas into the vent gap of the soffitt and literally saturated the cavity with about 20,000 ppmv of CO_2 gas. The polytropic throttling process occurring during the injection of CO_2 from a pressurized cylinder (i.e., the gas throttles from about 2000 to 20 psi) required the gas to be artificially heated to about 110°F before being injected into the vent cavity. After a substantial buildup of concentration registered on each monitor (i.e., 20,000 ppmv of CO_2) the gas injection was stopped and concentration was recorded at timed intervals (Fig. 20).

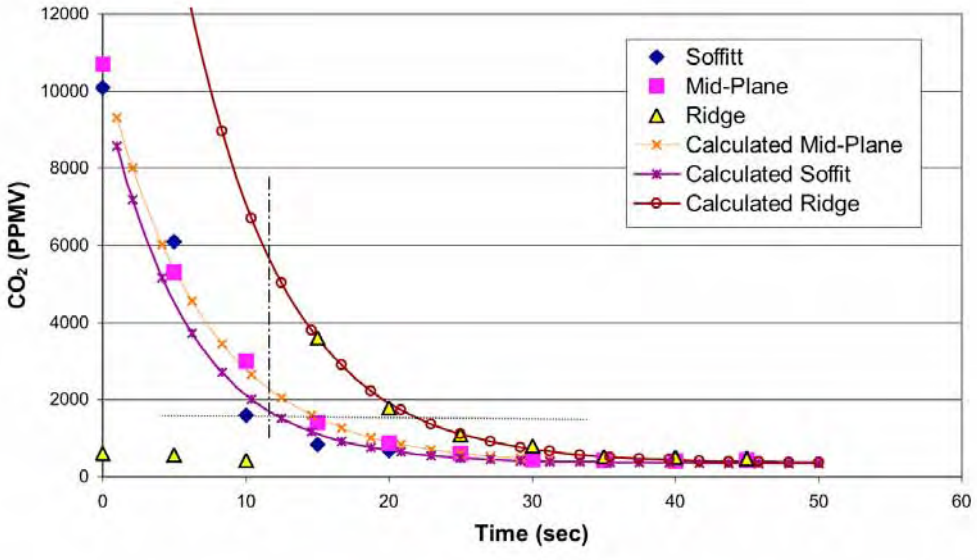

Fig. 20. Concentration of CO_2 measured under the slate tile roof with batten and counter-battens.

Data for the five vented clay and concrete tile roofs were collected (Table 2) and the calculated airflows ranged from about 12 to 33 cfm. The average velocity ranged from about 0.4 to 0.9 ft/s, which is consistent with the average velocity calculated from boundary layer theory.

Table 2. Airflow rate and bulk velocity measured at the center of each attic assembly and under the clay and concrete tile roofs using CO_2 as a tracer gas.

	S-Mission	Medium Profile	S-Mission with foam	Slate on Counter Batten	S-Mission on Batten
	Clay	Concrete Tile			
Volume ($V_{Channel}$ in^3)	7045.1	5600.0	4444.8	5433.1	6669.2
Airflow (cfm)	32.9	11.9	15.5	19.3	22.5
Average Velocity (V_{air} ft/s)	0.88	0.40	0.66	0.67	0.64

All measurements were made around solar noon when the roofs had their highest respective roof temperatures and highest heat flows penetrating into the attic. The clay tile yielded the highest measured buoyancy induced airflow, which is very interesting because the combination of its solar reflectance and sub-tile venting are believed to be the drivers causing the ≈70% reduction in deck heat flow as compared to a direct-nailed shingle roof.

Air Leakage from Tile Systems

Most roof tiles are designed with a gap between the overlapping of tiles placed on the roof. The design equalizes the static air pressure and reduces wind uplift for oceanfront locations occasionally threatened by hurricanes. Kehrer (2005) conducted wind washing studies for tile roofs field tested in Europe during the winter. He observed that the roof pitch facing windward incurred 6–26% more heat loss than the leeward-pitched roof at wind velocities of about 6.7 mph. Using tracer gas experiments Kehrer confirmed that wind washing or the intrusion of outdoor ambient air into the inclined air channel occurs and causes the increased heat loss for windward-facing tile roofs.

Kehrer's (2005) field experiments provide the only open literature data known to the authors that describe the effect of wind washing on the thermal performance of tile roofs. Results from tracer gas testing at ORNL were reduced to leakage rates digressing and egressing the tile roofs in support of modeling and predicting the heat transfer across the tile roof. Data for the S-Mission clay and the slate concrete tiles are listed in Table 3 with measures of airflows near the soffitt and near the ridge from which leakage rates can be viewed for the two styles of tile.

Table 3. Air infiltration and exfiltration from the S-Mission clay (SR54E90) and the slate concrete (SR13E83) tile roof systems.

Tile System	OD Air Temperature	Wind Direction	Wind Speed	Solar Irradiance Horizontal	Air Gap Temperature	Soffitt	Near Ridge	Air Exfiltration (+) Air Infiltration (-)
	°F	North = 0° (CW+)	mph	Btu/hr · ft^2	°F	cfm	cfm	cfm
S-Mission Clay	93.6	175.7	1.57	214.3	111.8	52.6	27.3	25.31
	92.3	190.1	1.63	262.9	118.0	58.4	36.5	21.97
	93.7	187.0	1.13	234.4	118.0	35.3	19.5	15.75
	90.9	255.3	1.42	216.8	104.1	28.5	34.7	-6.20
Slate Concrete	92.0	113.1	1.49	237.6	127.1	32.1	25.5	6.52
	91.8	202.1	1.97	276.6	128.8	22.7	19.5	3.23
A first order error analysis of Eq. 5 showed roughly a 25% uncertainty in airflow measurements.								

The S-Mission clay tile are designed to be more porous than the slate tile and have a greater leakage of air (Table 3). Also, the cross-sectional area on the underside of the clay tile is slightly larger than that of the

slate tile, being 89.5 in.^{2} versus 69 in.^{2} for the slate. Therefore, a slightly larger airflow occurs under the clay tile as compared to the slate tile, even though the underside air temperature is hotter for the slate. The hotter the air temperature, the greater the bouyancy and induced air movement.

The air exfiltration from the clay tile appears to correlate somewhat with wind direction (Fig. 21). Peavy (1979) saw that the air exchange rate for attics correlated with the wind strength and direction incident on the soffitts. Table 3 data for wind direction show the leeward-directed winds possibly reduced the air pressure above the tile while the one more windward point (255.3° for clay) may cause an inleakage of air into the tile. The slate tile does not appear as susceptible to wind effects simply because of its reduced porosity as compared to the S-Mission design (Fig. 21).

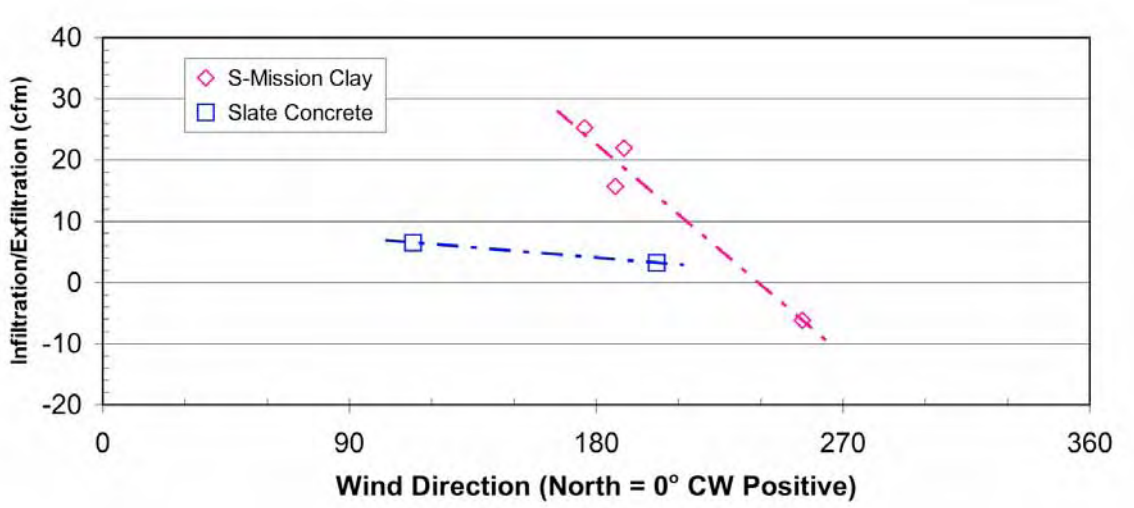

Fig. 21. The leakage of air from the underside of the slate and S-Mission clay tile roofs.

ATTICSIM MODEL

AtticSim is a computer tool for predicting the thermal performance of residential attics. It mathematically describes the conduction through the gables, eaves, roof deck, and ceiling; the convection at the exterior and interior surfaces; the radiosity heat exchange between surfaces within the attic enclosure; the heat transfer to the ventilation air stream; and the latent heat effects due to sorption and desorption of moisture at the wood surfaces. Solar reflectance, thermal emittance, and water vapor permeance of the sundry surfaces are input. The model can account for different insulation R-values and/or radiant barriers attached to the various attic surfaces. It also has an algorithm for predicting the effect of air-conditioning ducts placed in the attic (Petrie et al. 2004). The code reads the roof pitch, length, and width and the ridge orientation (azimuth angle with respect to north) and calculates the solar irradiance incident on the roof. Conduction heat transfer through the two roof decks, two gables, and vertical eaves are modeled using the thermal response factor technique (Kusuda 1969), which requires the thermal conductivity, specific heat, density, and thickness of each attic section for calculating conduction transfer functions.

Heat balances at the interior surfaces (facing the attic space) include the conduction, the radiation exchange with other surfaces, the convection, and the latent load contributions. Heat balances at the exterior surfaces balance the heat conducted through the attic surface to the heat convected to the air, the heat radiated to the surroundings, and the heat stored by the surface. Iterative solution of the simultaneous equations describing the heat balances yields the interior and exterior surface temperatures and the attic air temperature at 1-h time steps. The heat flows at the attic's ceiling, roof sections, gables, and eaves are calculated using the conduction-transfer function equations. The tool was validated by Wilkes (1991)

against field experiments and is capable of predicting the ceiling heat flows integrated over time to within 10% of the field measurement.

Attic Ventilation

Sub-tile venting of tile roofs has been a primary focus of Task 2.6.3; however, modeling the ventilation of the attic is also important for predicting accurately the heat penetrating through the ceiling into the conditioned space. Miller et al. (2004) validated AtticSim's ability to predict reasonable values of attic ventilation against the data of Burch and Treado (1979) and by Walker (1993) and against the data of Parker, Fairey, and Gu (1991). Miller et al. (2004) assumed equal soffit and ridge vent openings with a net free vent area of 1:300.

The steep-slope attic assemblies, however, have shed-type roofs, and the ridge vent was closed for a summer followed by another summer of exposure with the ridge vent open. The code was exercised with and without the ridge vent open and the direct-nailed shingle roof modeled as a shed-type roof. The results show that soffitt and ridge venting (Fig. 22, + symbol for AtticSim prediction) resulted in too much air exchange within the attic cavity because AtticSim under predicted the attic air temperature measured at center of the cavity. The code was then run using measured temperatures for the roof and ceiling boundary conditions to eliminate the confounding variable of weather and enable a check of the attic's radiosity exchange and the air exchange rate. Soffitt venting (ridge modeled as nearly shut) yielded reasonable results (o symbol for AtticSim – BC), as seen in Fig. 22. The results show that a slight adjustment of AtticSim's ventilation algorithm yielded accurate attic air temperatures and ventilation rates.

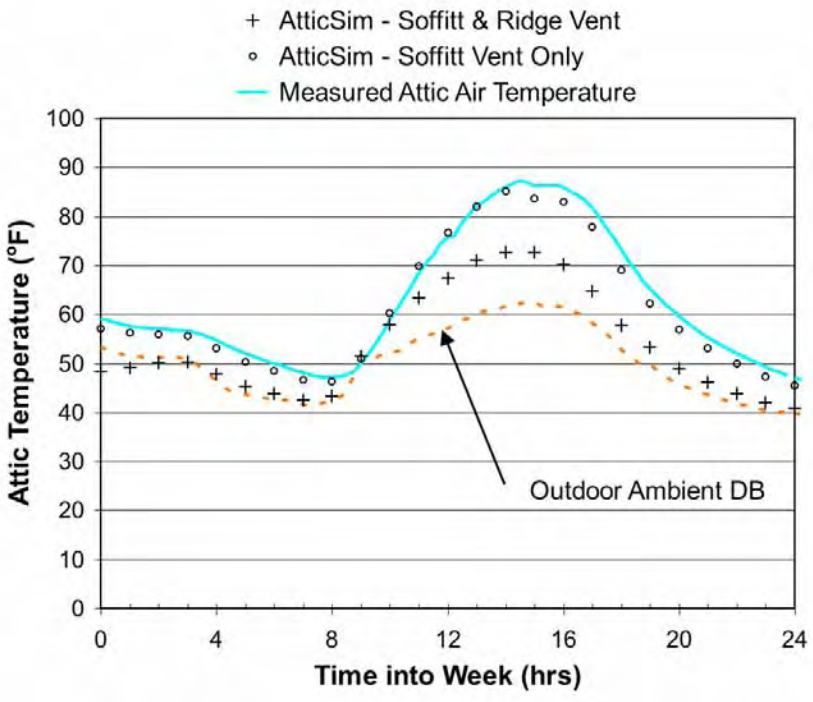

Fig. 22. AtticSim predicted the attic air temperature of the steep-slope attic assembly modeled as a shed roof with and without ridge venting of the shingle roof.

Validation Efforts

Inputs to the AtticSim computer code were developed that describe the geometry and the thermal and moisture characteristics for the attic test lane having a roof with direct-nailed asphalt shingles (SR10E89). Conduction heat transfer through the south-facing roof deck was modeled by developing conduction-transfer functions for a shed roof and for the other five attic surfaces. The transfer functions predict the time-dependent one-dimensional conduction transfer at the interior and exterior surfaces of the attic and couple the results with radiation and convection heat transfer within the attic enclosure to predict the heat flux penetrating into the conditioned space. AtticSim did an excellent job of validating the heat flow penetrating throught the ceiling of the attic assembly having the the direct-nailed shingle roof (Fig. 23).

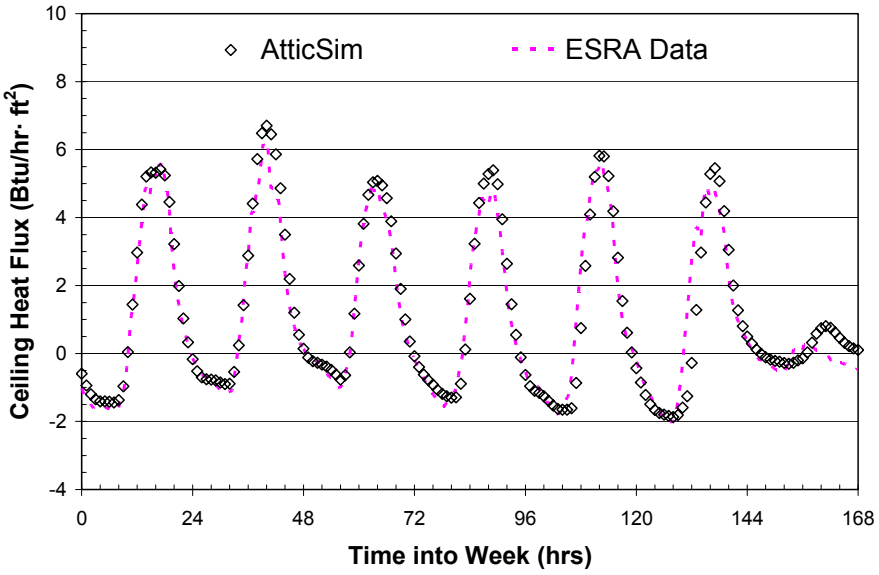

Fig. 23. Validation of AtticSim against field measures of the ceiling heat flux gleaned from the ESRA steep-slope roof assembly with a direct-nailed shingle roof.

The predicted heat flow tracks very well the heat flows measured at solar noon and also during the evening hours. AtticSim tended at solar noon to overpredict the surface temperature of the shingles (Fig. 24), and the heat flux penetrating the roof deck was therefore overpredicted at solar noon. However, the attic air temperature was underpredicted and compensated for the discrepency in Fig. 24 yielding the results shown in Fig. 23 for the ceiling heat flux. Despite these small inconsistencies, the code works well for the case of direct-nailed roof products.

Efforts are continuing to predict the heat flow across a tile roof having a venting occurring along the underside of the roof between the roof deck and the tile. The heat transfer correlations by McAdams (1954) and Nusselt's boundary layer theory were tested against the experimental data for the S-Mission clay and concrete slate tile roofs. McAdams's correlation is for immersed external free convection flows around a vertical isothermal plate and has the form:

$$\overline{NU} = \frac{\bar{h}L}{k} = 0.59\left(Ra_L\right)^{1/4} \qquad (7)$$

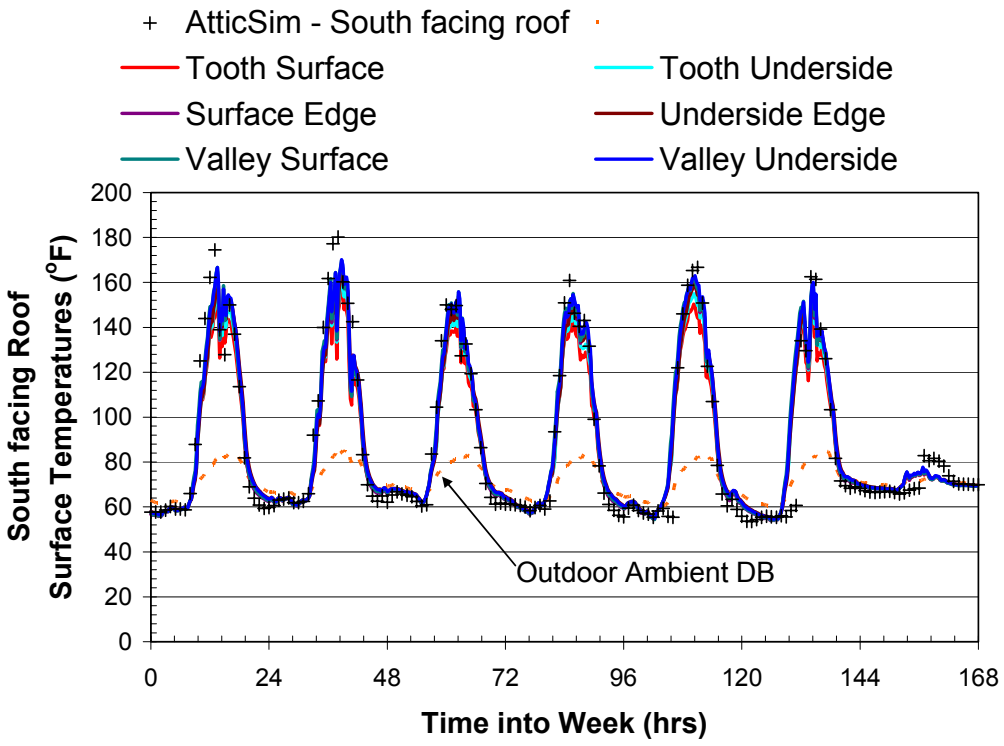

Fig. 24. Validation of AtticSim against field measures of the surface temperatures for the asphalt shingles gleaned from the ESRA steep-slope roof assembly.

The boundary layer correlation for a uniform heat flux has the form:

$$\overline{NU} = \frac{5}{(11520)^{1/5}} \left\{ \frac{Pr \cdot SIN(\theta)}{4/5 + Pr} \right\}^{1/5} (Ra^*)_L \tag{8}$$

Equations 7 and 8 were used to back-calculate the mass flow rate of air moving up the inclined air channel. Energy balances for internal duct flow were derived using constant wall and constant heat flux boundary conditions, and the airflow in the enclosed channel was calculated using the measured temperature and heat flow field data for the five tile roof systems. Using a constant temperature boundary condition yields the expression:

$$LN\left[\frac{T_{Wall} - T_{Air\,out}}{T_{Wall} - T_{Air\,in}} \right] = -\frac{\hbar\{P \cdot L\}}{\dot{m}(C_{P\,Air})} \tag{9}$$

while the constant flux condition yields the expression:

$$\dot{m} \cdot C_{P\,Air} (T_{Air\,out} - T_{Air\,in}) = q''_{solar} (P \cdot L) \tag{10}$$

The constant surface temperature scenario [Eq(s). 7 and 9] yielded volumetric airflow rates of about 24 to 32 cfm. The constant heat flux condition [Eq(s). 8 and 10] yielded flow rates of about 40 to 80 cfm, which is high probably because we used the measured solar irradiance rather than the flux from the underside of

the tile (not known from field data). These back-calculated airflow values are within reason of the airflows determined from the tracer gas experiments (Table 2).

CONCLUSIONS

Clay and concrete tile roofs are energy-efficient cool roof products as verified by field results obtained for East Tennessee's climate. The combination of improved solar reflectance afforded by CRCMs and sub-tile venting reduced the noontime heat flow crossing the roof deck of the clay tile roof by 70% of the flow crossing the conventional shingle roof, which in turn, reduced the heat entering the conditioned space by 60% of the heat flow penetrating the ceiling of the attic assembly with shingle roof. The slate and medium-profile concrete roofs, having nearly the same surface properties as the conventional shingle, reduced the deck heat flow ~45% of that crossing the shingle roof because of sub-tile venting. Proportioning the reduction in deck heat flows due to sub-tile venting to the reducton due to CRCMs and sub-tile venting indicates that sub-tile venting is equivalent to about 30 points of solar reflectance. In other words, the slate tile (SR13E83) on battens and counter-battens is equivalent to a direct-nailed slate roof system with solar reflectance of 0.43 and thermal emittance of 0.83. The results imply that cool roof credits are obtainable for sub-tile venting; the effects of sub-tile venting and CRCMs are synergistic; and subsequently, sub-tile venting of a tile roof is just as important as is the boost in solar reflectance for reducing the heat gain into the conditioned space.

Opening the ridge vent of the attics to allow both attic and sub-tile ventilation caused more heat to be exhausted out the ridge for both the S-Mission clay and the slate tile systems and therefore further improved the performance of the two tile roofs. The effect was more pronounced for the slate tile than observed for the S-Mission tile because the slate tile has less air leakage between tiles.

Tracer gas experiments successfully measured the bouyancy-induced airflows observed for sub-tile venting. These airflows yielded bulk velocities that were within reason of values deduced from first-principle energy balances for the inclined air channel. The sub-tile venting of the S-Mission tile, being designed porous to alleviate wind uplift, was observed to be more susceptible to wind effects than was the slate tile roof.

Summer heat flows for the month of July 2005 were integrated over the daylight and nighttime hours to show seasonal performance of the various roof systems (Table 4). The ridge vent was open for attic and for sub-tile ventilation for all test roofs during July 2005. The best-performing roofs were the direct-nailed S-Mission clay tile and the S-Mission concrete tile spot adhered with foam. Both roofs caused a 50% reduction in the heat penetrating through the ceiling over the full July month. The maximum attic air temperatures for July show the attic of the conventional shingle roof is about 10 to 15°F warmer than any

Table 4. July 2005 attic temperatures and cumulative heat flows through the roof deck and ceiling of the attic assemblies having both ridge and sub-tile venting

Test Roof	SR & TE	Roof Deck Construction	Attic Air (°F)		Roof Deck Heat Flux (Btu/ft²)		Ceiling Heat Flux (Btu/ft²)
			Average	Max	Daytime	Nighttime	24-Hour
Asphalt Shingle	SR10E89	Direct-to-Deck	88.7	116.4	4921	-1085	1999
Slate Concrete	SR13E83	Batten & Counter-batten	84.8	106.4	2915	-543	1366
S-Mission Concrete	SR34E83	Batten	83.7	103.6	2611	-666	1351
Medium Profile Concrete	SR10E93	Direct-to-Deck	84.3	105.5	3172	-522	1200
S-Mission Concrete	SR26E86	Spot Adhered with Foam	83.6	103.2	2316	-603	956
S-Mission Clay	SR54E90	Direct-to-Deck	83.3	101.6	1540	-649	873

of the other tile roofs because of the heat flow crossing the roof deck of the respective tile, which was 35 to 70% less than that crossing the shingle roof (Table 4).

During January 2005 winter exposure (Table 5), sub-tile venting has reduced the heat loss from the tile roofs to the point that it is less than the loss for the asphalt shingle roof. The tile roofs are negating the heating penalty associated with a cool roof in Tennessee's moderate climate having 3662 HDD_{65} and 1366 CDD_{65}. The improved summer performance (Table 4) coupled with the reduced heat losses during the winter (Table 5) show that tile roofs can benefit from CRCMs while at the same time negate the heating penalty associated with a cool roof. Therefore sub-tile venting of tile roofs provides tile manufacturers the opportunity to market high IR reflective tile in more predominant heating load climates.

Table 5. January 2005 attic temperatures and cumulative heat flows through the roof deck and ceiling of the attic assemblies with the ridge closed to attic and sub-tile ventilation

Test	SR & TE	Roof Deck	Nighttime Attic Air (°F)		Roof Deck Heat Flux (Btu/ft²)		Ceiling Heat Flux (Btu/ft²)
Roof		Construction	Average	Min	Daytime	Nighttime	24-Hour
Medium Profile Concrete	SR10E93	Direct-to-Deck	52.8	31.9	185	-1890	-2803
Asphalt Shingle	SR10E89	Direct-to-Deck	49.9	25.6	1024	-2376	-2879
S-Mission Clay	SR54E90	Direct-to-Deck	46.7	25.5	-110	-1499	-2906
Slate Concrete	SR13E83	Batten & Counter-batten	52.5	31.4	69	-1761	-2983
S-Mission	SR26E86	Spot Adhered with Foam	51.1	29.5	-94	-1664	-3054
S-Mission Concrete	SR34E83	Batten	50.1	26.0	30	-1772	-3055

The inclined air channel formed by the tile and the roof deck provides an additional radiative resistance to night-sky heat losses from the tile as compared to the direct-nailed shingle roof. Two of the tile roofs, the clay tile and the S-Mission concrete tile roof spot-adhered to the deck have no net heat gain during the daylight hours for the January exposure (Table 5). Therefore, the reduction in night sky radiation is due more to the decoupling of conduction prevalent in the direct-nailed shingle roof rather than to the thermal mass of the concrete and clay tile roofs. The air channel forces the heat flow from the roof deck to radiate across the air channel rather than conduct from the roof deck through to the surface of the shingle roof.

RECOMMENDATIONS

It is believed that in the simplest case, with no bulk air velocity, the heat transfer within the roof air channel will be dominated by natural convection, but that the more likely case, given some appreciable value of bulk air velocity, will be mixed convection heat transfer. Understanding the regime of heat transfer within the air channel is essential in accurately modeling the overall heat transmission through the roof assembly. The AtticSim computer tool was validated against the steep-slope attic assembly with direct-nailed asphalt shingle. The model predicted well the surface temperature of the shingles, the attic air temperature, and, as a result, the heat flow penetrating into the conditioned space. Efforts are continuing to modify the code for predicting the effects of the airflow occurring on the underside of tile and stone-coated metal roofs. Correlations by McAdams (1954), Brinkworth (2000), and simple boundary layer theory for a constant solar flux are predicting reasonable heat transfer measures within the inclined air channel. The measures of airflow determined from the tracer gas experiments match well the back-calculated values deduced from the correlations provided by McAdams (1954), Brinkworth (2000), and simple boundary layer theory correlations. We therefore have good representative airflow measures for sub-tile venting and are in good position to implement an algorithm fashioned after the work by Brinkworth (2000) for use in AtticSim to predict thermal performance of roofs with underside venting. Once validated, we recommend the code be used for predicting ceiling heat fluxes in the demonstration homes in California.

NOMENCLATURE

δ_t	thermal boundary layer thickness (ft)	δ	momentum boundary layer (ft)
ε or E	thermal emittance	P	wetted perimeter of channel (ft)
ρ or SR	solar reflectance	$\dot{m}$	mass flow rate (lbm/hr)
L	length from soffitt to roof ridge (ft)	C_P	specific heat (Btu/lbm·°R)
T	temperature (°F)	α	thermal diffusivity (ft^2/s)
$\hbar$	convective coefficient (Btu/hr·ft^2·°F)	CDD_{65}, HDD_{65}	cooling and heating degree-days[1]
C	concentration of CO_2 (ppmv)	**Subscripts**	
V	volume of inclined channel	wall	underside of Tile Roof
$\dot{V}$	volumetric flow rate (cfm)	IR	infrared spectrum
β	coefficient of Thermal Expansion (1/°F)	i	initial value
g	gravity (32.2 ft/s^2)	solar	irradiance
q''	Heat flux (Btu/hr·ft^2)	x	x-distance from soffitt to ridge
θ	Roof slope	y	y-distance normal to roof deck
ν	kinematic viscosity (ft^2/s)	roof	tile roof surface or underside
k	thermal conductivity (Btu/hr·ft·°F)	∞	outdoor ambient
η	$= y/\delta_t$	t	time
U(x,y)	velocity (ft/sec)	channel	inclined air gap made by tile and roof deck
$\overline{NU}$	Average Nusselt number $\left(\frac{\hbar L}{k_{air}}\right)$	air	air within inclined channel
Pr	Prandtl number **Error! Objects cannot be created from editing field codes.**	air out	air entering soffitt
Ra	Rayleigh number $= \left(\frac{g\beta(\Delta T)L^3}{\nu \cdot \alpha}\right)$	air in	air leaving ridge
Ra*	Modified Rayleigh number $= \left(\frac{g\beta q'' L^4}{k \cdot \nu \cdot \alpha}\right)$		

[1] A degree-day is the difference between the average daily temperature and the base temperature of 65°F.

REFERENCES

Akbari, H., R. Levinson, P. Berdahl. 2004a. "A Review of Methods for the Manufacture of Residential Roofing Materials." Lawrence Berkeley National Laboratory Report LBNL-55574, Berkeley, CA.

Akbari, H., P. Berdahl, R. Levinson, R. Wiel, A. Desjarlais, W. Miller, N. Jenkins, A. Rosenfeld, C. Scruton. 2004b. "Cool Colored Materials for Roofs." Proceedings of the 2004 ACEEE Summer Study on Energy Efficiency in Buildings, Vol. 1, p. 1, Pacific Grove, CA.

Arnold, J. N., I. Catton, D. K. Edwards. 1976. "Experimental Investigation of Natural Convection in Inclined Rectangular Regions of Differing Aspect Ratios." *Journal of Heat Transfer*. February, 67–71.

ASTM. 2000. *Designation E741-00: Standard Test Method for Determining Air Change in a Single Zone by Means of a Tracer Gas Dilution*. American Society for Testing and Materials, West Conshohocken, Pa.

ASTM. 1997. *Designation C 1371-97: Standard Test Method for Determination of Emittance of Materials Near Room Temperature Using Portable Emissometers*. American Society for Testing and Materials, West Conshohocken, Pa.

ASTM. 1996. *Designation E903-96: Standard Test Method for Solar Absorption, Reflectance, and Transmittance of Materials Using Integrating Spheres*. American Society for Testing and Materials, West Conshohocken, Pa.

Beal, D. and S. Chandra. 1995. "The Measured Summer Performance of Tile Roof Systems and Attic Ventilation Strategies in Hot Humid Climates." *Thermal Performance of the Exterior Envelopes of Buildings VI, U.S. DOE/ORNL/BETEC*, Dec. 4–8, Clearwater, Fla.

Bejan A. 1984. *Convection Heat Transfer*. John Wiley and Sons, New York.

Brinkworth, B. J. 2000. "A Procedure for the Routine Calculation of Laminar Free and Mixed Convection in Inclined Ducts." *International Journal of Heat and Fluid Flow* 21, 456–462.

Burch, D. M. and Treado, S. J. 1979. "Ventilating Residences and Their Attics for Energy Conservation—An Experimental Study." *NBS Special Publication 548: Summer Attic and Whole House Ventilation*. National Bureau of Standards, Washington, D.C.

FHA. 1942 (rev). *Property Standards and Minimum Construction Requirements for Dwellings*. Federal Housing Administration, Washington, D.C.

Hollands, K. G. T., T. E. Unny, G. D. Raithby, and L. Konicek. 1976. "Free Convection Heat Transfer Across Inclined Air Layers*." Journal of Heat Transfer*, May, 189–193.

Kehrer , M. 2005. "*Ventilated versus Compact Roof*." THERMAL PERFORMANCE. 76-108.

Kollie, T. G., F. J. Weaver, D. L. McElroy. 1990. "Evaluation of a Commercial, Portable, Ambient-Temperature Emissometer." *Rev. Sci. Instrum*., Vol. 61, 1509–1517.

Kusuda, T. 1969. "Thermal Response Factors for Multi-Layer Structures of Various Heat Conduction Systems," *ASHRAE Transactions*, Vol. 75, Part 1, 246–271.

Lagus, P. L., V. Kluge, P. Woods, and J. Pearson. 1988. "Tracer Gas Testing within the Palo Verde Nuclear Generating Station Unit 3 Auxiliary Building." *Proceedings of the 20th NRC/DOE Air Cleaning Conference*. Boston, August.

Levinson, R., H. Akbari, and J. Reilly. 2004. "Cooler Tile-Roofed Buildings with Near-Infrared Reflective Nonwhite Coatings." Lawrence Berkeley National Laboratory Report LBNL-54902, Berkeley, CA.

Levinson R., P. Berdahl, and H. Akbari. 2005a. "Solar spectral optical properties of pigments, Part I: model for deriving scattering and absorption coefficients from transmittance and reflectance measurements." *Solar Energy Materials & Solar Cells*, Vol 89/4 pp 319-349.

———. 2005b. "Solar spectral optical properties of pigments, Part II: survey of common colorants." *Solar Energy Materials & Solar Cells*, Vol 89/4 pp 351-389.

McAdams, W. H. 1954. *Heat Transmission*. 3rd ed., McGraw-Hill, New York.

Miller W. A., K. T. Loyle, A. O. Desjarlais, H. Akbari, R. Levenson, P. Berdahl, S. Kriner, S. Weil, and R. G. Scichili. 2004. "Special IR Reflective Pigments Make a Dark Roof Reflect Almost Like a White Roof." *Thermal Performance of the Exterior Envelopes of Buildings, IX. Proceedings of ASHRAE THERM IX*, Clearwater, Fla., December.

Miller, W.A., M. D. Cheng, S. Pfiffner, and N. Byars. 2002. "The Field Performance of High-Reflectance Single-Ply Membranes Exposed to Three Years of Weathering in Various U.S. Climates." *Final Report to SPRI, Inc.,* August.

Ozsunar, A., Baskaya, S., and Sivrioglu, M. 2001. "Numerical Analysis of Grashof Number, Reynolds Number and Inclination Effects on Mixed Convection Heat Transfer in Rectangular Enclosures." *International Communications in Heat and Mass Transfer*, 28, No. 7, September.

Parker, D. S., P. W. Fairey, and L. Gu. 1991. "A Stratified Air Model for Simulation of Attic Thermal Performance." *Insulation Materials: Testing and Applications,* 2nd Volume, ASTM STP 1116, R. S. Graves and D. C. Wysocki, Eds., 44–69, American Society for Testing and Materials, Philadelphia.

Parker, D. S., J. K. Sonne, and J. R. Sherwin. 2002. "Comparative Evaluation of the Impact of Roofing Systems on Residential Cooling Energy Demand in Florida." *ACEEE Summer Study on Energy Efficiency in Buildings*. Proceedings of American Council for an Energy Efficient Economy, Pacific Grove, Calif, August.

Peavy, B. A. 1979. "A Model for Predicting the Thermal Performance of Ventilated Attics." *Summer Attic and Whole House Ventilation, NBS Special Publication 548*, Washington, D.C.

Petrie, T. W., A. O. Desjarlais, R. H. Robertson, and D .S. Parker. 2000. "Comparison of Techniques for In-situ, Non-damaging Measurement of Solar Reflectance of Low-slope Roof Membranes." Presented at the 14th Symposium on Thermophysical Properties. Submitted to *International Journal of Thermophysics*, National Institute of Standards and Technology, Boulder, Colo.

Petrie, T. W., T. K. Stovall, K. E. Wilkes, and A. O. Desjarlais. 2004. "Comparison of Cathedralized Attics to Conventional Attics: Where and When Do Cathedralized Attics Save Energy and Operating Costs?" Presented at ASHRAE THERM VIII, Clearwater, Fla., December. To be published in *Thermal Performance of the Exterior Envelopes of Buildings,* IX.

Romero, M. I., and Brenner, R. J. 1998. “Instrumentation and Measurement of Airflow and Temperature in Attics Fitted with Ridge and Soffitt Vents.” *ASHRAE Transactions* 104.

Rose, W. B. 1995. “The History of Attic Ventilation Regulation and Research.” *Thermal Performance of the Exterior Envelopes of Buildings* VI. American Society of Heating, Refrigeration and Air-Conditioning Engineers, Atlanta.

Walker, I. S. 1993. “Prediction of Ventilation, Heat Transfer and Moisture Transport in Attics.” Ph.D. dissertation, Edmonton, Alberta, Canada.

Wilkes, K. E. 1991.*Thermal Model of Attic Systems with Radiant Barriers*. ORNL/CON-262, Oak Ridge National Laboratory, Oak Ridge, Tenn.

Appendix A

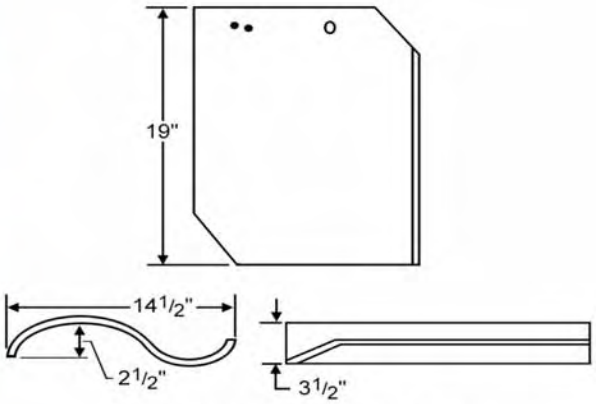

Solar Reflectance SR54
Thermal Emittance E90
Direct-to-Deck

S-Mission clay tile field-tested on the ESRA at the campus of the Buildings Technology Center.

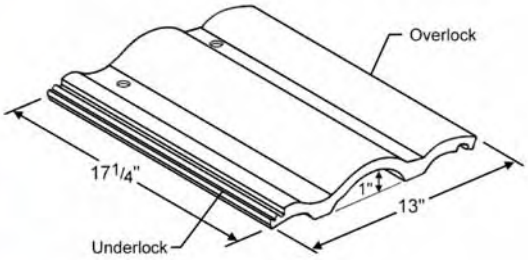

Solar Reflectance SR10
Thermal Emittance E93
Direct-to-Deck

Medium-profile concrete tile used at the Fair Oaks, Calif., demonstrations and also at ORNL.

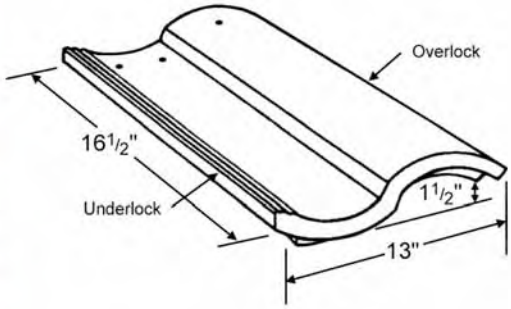

Solar Reflectance SR26
Thermal Emittance E86
Direct-to-Deck with Foam

S-Mission concrete tile spot adhered with foam.

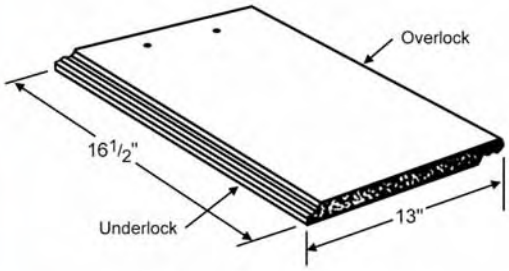

Solar Reflectance SR13
Thermal Emittance E83
Batten & Counter-Batten

Concrete slate tile having solar reflectance and thermal emittance close to that of the asphalt shingle roof.

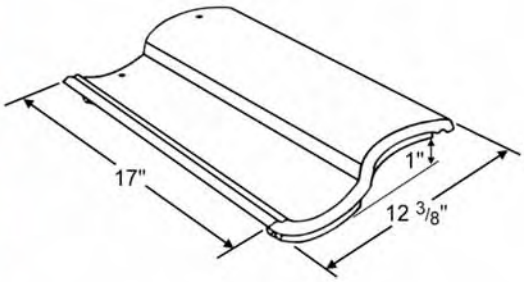

Solar Reflectance SR34
Thermal Emittance E83
Batten

S-Mission Tile Roof attached with battens running parallel to the ridge of the roof.

Appendix B

COOLTILE IR COATINGS™
Conserving energy today for tomorrow's future
Beautiful, durable COOLTILE IR COATINGS™ are developed to meet California energy guidelines for cooltile roofs*. When applied directly to your new or existing tile roof, you can enjoy the latest technology in energy efficiency while saving money on cooling costs. Attractive colors are available to enhance the appearance and life of your roof, adding value to your investment.
R=0.41
R=0.44
R=0.41
R=0.48
R=0.46
R=0.41
BLACK
BLUE
GRAY
TERRACOTTA
GREEN
CHOCOLATE
R=0.04
R=0.18
R=0.21
R=0.33
R=0.17
R=0.12
Comparison of Cooltile IR Coatings (upper row) vs. standard rooftiles demonstrates increased Solar Reflectance R Value.
* Solar reflectance >=0.40 (ASTM C1549) thermal emittance >=0.75 (ASTM C1371)
ENERGY STAR PARTNER
CRRC
COOL ROOF RATING COUNCIL
American Rooftile Coatings
Tile Roof Color Restoration
Tel: 877-919-2727 / Fax: 714-680-6700
www.americanrooftilecoatings.com

Arnold Schwarzenegger
Governor

COOL-COLOR ROOFING MATERIAL ATTACHMENT 10: TASK 2.6.4 REPORTS - PRODUCT USEFUL LIFE TESTING

PIER FINAL PROJECT REPORT

Prepared For:
California Energy Commission
Public Interest Energy Research Program

Prepared By:
Lawrence Berkeley National Laboratory and Oak Ridge National Laboratory

ERNEST ORLANDO LAWRENCE
BERKELEY NATIONAL LABORATORY

June 2006
CEC-500-2006-067-AT10

Prepared By:
Lawrence Berkeley National Laboratory
Hashem Akbari
Berkeley, California
Contract No. 500-01-021

Oak Ridge National Laboratory
William Miller
Oak Ridge, Tennessee

Prepared For:
California Energy Commission
Public Interest Energy Research (PIER) Program

Chris Scruton
Contract Manager

Ann Peterson
Building End-Use Energy Efficiency Team Leader

Nancy Jenkins
PIER Energy Efficiency Research Office Manager

Martha Krebs, Ph.D.
Deputy Director
ENERGY RESEARCH AND DEVELOPMENT DIVISION

B. B. Blevins
Executive Director

DISCLAIMER

This report was prepared as the result of work sponsored by the California Energy Commission. It does not necessarily represent the views of the Energy Commission, its employees or the State of California. The Energy Commission, the State of California, its employees, contractors and subcontractors make no warrant, express or implied, and assume no legal liability for the information in this report; nor does any party represent that the uses of this information will not infringe upon privately owned rights. This report has not been approved or disapproved by the California Energy Commission nor has the California Energy Commission passed upon the accuracy or adequacy of the information in this report.

Deliverable for CEC Task 2.6.4. Report LBNL-59724. Submitted to *Construction and Building Materials,* February, 2006

Weathering of Roofing Materials-An Overview

Paul Berdahl, Hashem Akbari, and Ronnen Levinson
Lawrence Berkeley National Laboratory
Berkeley, CA 94720
and
William A. Miller
Oak Ridge National Laboratory
Oak Ridge, TN 37831

Abstract

An overview of several aspects of the weathering of roofing materials is presented. Degradation of materials initiated by ultraviolet radiation is discussed for plastics used in roofing, as well as wood and asphalt. Elevated temperatures accelerate many deleterious chemical reactions and hasten diffusion of material components. Effects of moisture include decay of wood, acceleration of corrosion of metals, staining of clay, and freeze-thaw damage. Soiling of roofing materials causes objectionable stains and reduces the solar reflectance of reflective materials. (Soiling of non-reflective materials can also increase solar reflectance.) Soiling can be attributed to biological growth (e.g., cyanobacteria, fungi, algae), deposits of organic and mineral particles, and to the accumulation of flyash, hydrocarbons and soot from combustion.

1. Introduction

Roofing materials are exposed to the elements, namely wind, sunlight, rain, hail, snow, atmospheric pollution, and temperature variations and consequently degrade over time. Even the most durable materials are modified by deposition of ambient dust and debris, and may provide an opportunity for colonization by biological organisms such as cyanobacteria, fungi and algae. In this paper, we broadly review how weathering occurs and discuss several engineering strategies that are employed for improving the performance of roofing materials.

We have been engaged in a multi-year project to develop and commercialize cooler, solar-reflective roofing in conjunction with a number of industrial partners. These materials can save energy used for air conditioning and improve occupant comfort. Since reflective white materials are sometimes not suitable from an architectural standpoint, the work has included materials with specified visual colors but with high near-infrared reflectance [1]. This paper is a summary of what we have learned concerning the weathering of roofing materials.

In Section 2 we list the various environmental stresses experienced by roofing, followed in Sec. 3 by a discussion of damage to polymeric materials (plastics, wood) and other organic materials (asphalts, pigments) initiated by the energetic ultraviolet photons in sunlight. Sec. 4 treats effects of high temperatures on roofing materials. Sec. 5 considers effects of moisture, and Sec. 6 discusses soiling by soot and biological growth.

2. Environmental stresses on roofing

a) Sunlight and temperature variations

The energy content of full direct sunlight normally incident on a roof is about 1 kW m^{-2} (1 kilowatt per square meter). There is a compensating longwave radiative cooling effect of about 60 W m^{-2}, because the effective radiant sky temperature is below air temperature. If the roof is insulated on the underside, the heat dissipation by the roof proceeds mainly by convection to the ambient outside air and by emission of thermal radiation. The convection coefficient for heat transfer is *roughly* 12 to 20 W m^{-2} K^{-1}, with the larger values occurring during windy conditions, and the radiative transfer coefficient for a surface with high thermal emittance is about 6 W m^{-2} K^{-1}. Thus the total heat transfer coefficient ranges from about 18 to 26 W m^{-2} K^{-1}. From these numbers we infer that the temperature rise of a black roof (reflectance 0.05) in full sunlight will be about 34 to 50 K (ºC), [61 to 90 ºF] warmer than the ambient air. For example, our field data show a temperature rise of 35 K (ºC) [64 ºF] at solar noon for home demonstrations with asphalt shingles exposed during August in Redding CA.

The temperature rise in sunlight can directly lead to materials degradation. Increased temperature can accelerate deleterious chemical reactions, cause loss of volatile constituents, and soften some polymers. Temperature changes, either gradual or sudden (rain shower on a hot day), cause stresses due to differential thermal expansion.. In fact even a monolithic material such as a sheet of glass experiences stress that can lead to fracture if it is heated to a non-uniform temperature [2].

The photons of which sunlight is composed vary in energy from about 0.5 to 4 electron volts (eV). About 5 % of the energy is in the form of ultraviolet photons with energies larger than 3 eV. These energetic photons can break many chemical bonds, especially in organic materials. For example, plastics, wood and asphalt are all organic materials composed largely of carbon and hydrogen atoms linked into chains, rings, and more complex structures. Most such materials are altered by ultraviolet radiation, usually followed by oxidation.

b) Wind

Wind exerts forces on roofing. Taller structures and more exposed roofing surfaces experience more force. Since the kinetic energy of wind and the resulting pressures scale as the square of the wind velocity, high-wind areas such as the U. S. Florida coastline require particularly careful attention. Beyond the concern for catastrophic failure of

roofing due to wind, periodic vibrations of roofing materials due to wind can lead to material fatigue and crack formation.

c) Moisture: rain, hail, snow, frost, and dew

Rain tends to clean the roof surface. Some roofing materials are formulated to avoid soil adherence and enhance the cleansing effect of rain. Hail is common in some locations. Large size hail causes mechanical roof damage. Where snowfall is important, the roof must be engineered to support the weight of the snow. Hence in some mountain areas highly sloping roofs that shed snow are employed. Freeze thaw cycles are an additional environmental stress. Water expands when it freezes and can therefore enlarge cracks. Dew and/or frost are a nightly occurrence in many climates. The roof temperature falls below the ambient air temperature on clear nights due to the radiative cooling effect. If the relative humidity is high, dew or frost is formed. Water vapor is absorbed by some building materials, particularly wood. Changes in humidity lead to changes in equilibrium water content. As moisture increases, wood swells; drying is accompanied by shrinkage.

d) Atmospheric gases and pollutants

The nitrogen making up most of the atmosphere (78% by volume) is not very reactive chemically. However reaction with oxygen (21%) and water vapor (~ 0.3 - 3%) can cause the formation of various oxides and hydroxides. For example, corrosion products of iron metal include FeO, Fe_2O_3, Fe_3O_4 and FeOOH. Several other important minor atmospheric constituents include oxides of carbon, sulfur, and nitrogen, for example CO_2, SO_2, and NO_2, formed by combustion. When these gases dissolve in water, acids are formed. These acids can promote corrosive chemical reactions. Another pollutant is soot from combustion. Soot is relatively unreactive but is a strong absorber of sunlight. The presence of soot on roofing darkens the color and leads to undesirable solar heating in warm climates.

e) Biological growth

Cyanobacteria, primitive single-cell organisms, are common on roofing in humid areas such as the southeastern and northwestern parts of the United States. The accumulation of dead colonies of these cyanobacteria (sometimes called algae, but now recognized as a distinct group of microorganisms) is visually evident as dark stains on light colored roofing. One reference [3] indicates that the species Gloeocapsa is prevalent on damp rocks. Research by a roofing granule company [4] has identified Gloeocapsa Magma as the most frequent cause of staining of roofing granules. Doubtless many other species can be present on roofing, including other cyanobacteria, algae, lichens, mildew, moss, etc. A lichen is a symbiotic combination of algae with a fungus; a fungus is a primitive plant-like organism that lacks chlorophyll. Mildew (e.g., on wood) is due to various species of fungus. Other examples of fungi are mushrooms, yeasts, rusts, and molds. Generally, a useful test for identifying biological growth is the application of a fresh bleach solution.

Inorganic stains such as soot and iron oxide are little affected by bleach, but most biological stains are lightened by bleach [5].

3. Photodegradation of polymeric and other organic materials

Many polymeric materials are subject to photodegradation. Energetic UV photons have sufficient energy to disrupt chemical bonds in many materials. Polymers consist of long chains of similar subunits. The absorption of UV energy can cause the breaking and/or crosslinking of the polymer chains, leading to altered chemical and mechanical properties. After disruption of the initial chemical state, the polymers are likely to react with oxygen and/or water vapor causing additional changes. Another type of photodegradation can occur due to photoabsorption by inorganic pigment particles such as TiO_2. An electron-hole pair is formed in the pigment particle. A photo-excited hole then, for example, can migrate to the particle's surface and cause a deleterious chemical reaction in the polymer. For this reason, white TiO_2 pigment particles intended for outdoor use are usually given thin coatings of passivating layers such as aluminum hydroxide.

Many polymer materials are too readily degraded by UV energy to be used in outdoor applications. Typically, photo-oxidation can be monitored by measuring the infrared absorption near 6 micrometers caused by oxygen-containing carbonyl (C=O) groups or the absorption near 3 micrometers due to the hydroxyl (OH) group. One strategy for extending polymer lifetimes is to add UV absorbers to scavenge the UV photons. Two common inorganic UV absorber pigments are carbon black and titanium dioxide white. (Both common forms of TiO_2, rutile and anatase, switch abruptly from non-absorptive to absorptive near 400 nm and therefore, while they are white in the visible spectrum. they are "black" in the UV. Nano-particles of TiO_2, with particle size much less than 200 nm, are small enough to be transparent in the visible but are still strong UV absorbers.) Another option is to choose particularly durable polymers.

While TiO_2 particles are effective UV absorbers, it should be mentioned in passing that organic tinted colors (mixtures with TiO_2 white) often fade more readily than "mass tones" (colorant without white). Extensive tables documenting this fading of organic pigments may be found in the Pigment Handbook [6]. This observation suggests that the short wavelength part of the visible spectrum (violet, blue) can sometimes be damaging as well.

For polymer coatings on metal roofing, three durable materials are polyester, silcone-modified polyester, and PVDF (polyvinylidene fluoride) [7]. Polyester is inexpensive, and can be used to form hard, scratch-resistant coatings. However, exposure to UV does cause some chalking. (Chalking is due to surface erosion, which produces small particles of polymer, and thereby causes a dark surface to look whiter. An empirical scale of 0 to 10 is sometimes used to characterize chalking [8].). Polyester formulations with longer polymer chains (higher molecular weight) are more UV resistant than shorter chains. Polyester fabrics are also used in roofing (and, in sails for sailboats). Single-ply roofing

membranes include a polyester fabric for mechanical strength. Silicone-modified polyesters can provide somewhat improved chalking resistance and gloss retention relative to unmodified formulations. For factory coating of metal materials (coil coating), PVDF polymers occupy a premium place in the marketplace. Pure PVDF powder is mixed with about 30% acrylic copolymer to aid in dispersion during the coating process. Product specifications [9,10] indicate the weathering performance expected with 10 years 45º south facing Florida exposure: less than 5 ΔE color change (1 ΔE is the threshold for visual discrimination of differences in lightness or color), 50% minimum gloss retention, 8 maximum chalk, 10% maximum film erosion. Fence post exposures in Florida confirm that PVDF-based metal roof coatings are highly durable [11]. The palette of colors exposed by several manufacturers in south Florida prove that the PVDF-based coatings are very resistant to climatic soiling because of the marginal loss in solar reflectance (less that 5%) incurred for 15 to 35 year exposures (Figure 1). Since the PVDF-based metal roof coatings are among the most durable polymeric materials, the above specifications are a good indication of the present day state of the art. The same specifications [9] indicate that accelerated testing procedures do not correlate well with actual outdoor exposure tests.

In most PVDF coating systems a primer coat of a urethane-based polymer is used to ensure good adhesion. As urethanes are readily degraded by UV radiation, it is necessary to ensure that the PVDF topcoat system is a good UV absorber, as can be accomplished with suitable pigments. This is an example of a general strategy. If outer coatings are sufficiently UV absorbing, more UV sensitive materials can be used underneath. For example, the use of high chroma colors in automotive finishes can be enabled with a UV absorbing clear topcoat. Another example is the asphalt shingle. The color bearing roofing granules must absorb UV efficiently so that UV damage to the asphalt is minimized.

Single-ply roofing membranes are usually based on polymer coatings on a polyester fabric. Polymers used include EPDM, PVC, and TPO. EPDM is a synthetic rubber termed ethylene propylene diene monomer. That is, it is three monomers (E, P, and D) polymerized together. PVC is the ubiquitous polymer polyvinyl chloride. TPO is the industry designation for thermoplastic polyolefin. Polyethylene and polypropylene are examples of TPOs. Three types of additives are used to enhance the outdoor stability of single-ply roofing membranes. First, UV absorbing pigments such as carbon black or titanium dioxide white can be added. Also designated as UVA (UV absorber) are special organic compounds such as benzophenone and hydroxyphenyl triazine [12]. The use of UV absorbers, of course, does not protect the surface region of the polymers, because a certain thickness is required to effect absorption. Important additional types of additive that can help protect the polymer including the surface region are hindered amine light stabilizers (HALS). HALS molecules do not themselves absorb UV light, but they react with free radicals (molecular groups with unpaired electrons) formed by UV absorption and thereby interfere with the photo-oxidation process.

One study of accelerated weathering of polypropylene is prototypical of how many polymeric materials change as they weather [13]. The surface region of the polymer

oxidizes during exposure to UV light in air. Infrared spectroscopy on microtomed slices of the polymer quantifies the presence of carbonyl (C=O) groups. While the reaction with oxygen requires the presence of UV light, the extent of oxidation is limited by oxygen diffusion from the surface into the interior. Figure 2 shows how the oxidation proceeded as a function of accelerated testing exposure time. Results for samples containing a UV absorbing additive were similar, but the depth of the penetration of oxygen is diminished. The oxidized surface region is brittle and cracks readily when the polypropylene film is stretched. After longer exposures, the surface region cracks spontaneously, indicating that the oxidized region is both brittle and under tensile stress.

Wood shakes and shingles are popular as roofing in some parts of the world. Wood is largely composed of cellulose, a biopolymer. The cellulose fibers provide strength, and lignin, another biopolymer, acts like an adhesive to bind the fibers into a matrix. Exposure to UV radiation from the sun changes the wood's color, with light colored wood becoming darker, and some darker woods becoming lighter. This color change is attributed to minor components of wood termed (water soluble) extractives [5]. Lignin also yellows on UV exposure [14], which indicates that it absorbs short visible wavelengths, i.e., blue. Exposure to UV also causes damage to the lignin binder, thus leading to detachment of cellulose fibers, and to erosion of the wood surface. Erosion of a number of bare wood samples mounted vertically with south facing exposure was in the range of to 0.2 – 1.3 mm over a ten-year period [5]. Thus the erosion process is slow, although it is somewhat faster for the near-horizontal exposure of wood roofing [15].

An explicit example of the changing reflectance of wood with environmental exposure is shown in Fig. 3 (from our unpublished measurements). The unweathered sample is a reddish brown, as can be inferred from the spectrum. The near-infrared reflectance is quite high. After weathering the reflectance drops (except at short wavelengths), and the resulting color is less reddish, nearly gray.

Asphalt is the key adhesive (binder) material in asphalt shingles. These roofing materials consist of a fiberglass or felt cloth that is saturated with asphalt and additives, and coated with colored roof granules [16,17]. Asphalt serves as an adhesive and as a hydrophobic water proofing agent. Asphalt itself is a complex mixture of hydrocarbons that is a byproduct of the refinement of crude oil into gasoline. In addition to the predominant hydrogen and carbon atoms, some heteroatoms such as nitrogen, oxygen, and sulfur are present. The ease of photo-oxidation of asphalt was illustrated in a study of oxygen uptake in 20 micrometer thick asphalt films [18]. Infrared absorption at 1700 cm^{-1} (5.9 micrometers wavelength) by the carbonyl group (C=O) increased rapidly in just a few hours of full sun exposure. This study also used filters to show that short wavelength UV solar photons (320 nm), while few in number, were much more damaging than longer wavelength UV photons (350 nm). At wavelengths in the visible range (>400 nm), no photo-oxidation was detected. In addition to increased concentrations of C=O groups, photo-oxidation also leads to the increased presence of several types of sulfur-oxygen groups including the sulfate (SO_4) group [19]. As a result of oxidation, asphalt becomes harder and embrittled [19.20]. In order to achieve acceptable weathering lifetimes for asphalt shingles, therefore, it is essential that the roofing granules absorb the UV

component of sunlight. Manufacturers test granules to ensure that they are efficient UV absorbers. Then, if good coverage of the asphalt substrate is achieved by the roofing granules, the photo-oxidation process is largely prevented.

Organic pigments often have high chroma (color intensity) and are desirable for product color formulation. Unfortunately rooftop exposure rules out all but the most durable organics. Application to roof tiles and roof granules, for example, not only exposes pigments to UV, but also to moisture and reactive pollutants such as SO_2 and NO_x. Even some inorganic pigments cannot withstand this weathering. For example ultramarine blue, cadmium sulfide and cadmium selenide react with oxygen; even carbon black fades to some extent. Durability is enhanced if the pigment can be isolated from gases in the environment and, particularly, if the pigment is shielded from the UV. One example of a durable organic pigment in use to color roofing granules is phthalocyanine ("phthalo") green. The Pigment Handbook [21] assigns phthalo green an exterior durability rating of 4-5 on a scale of 1 to 5 (based on 18 months exposure in Florida) and lightfastness ratings of various formulations in polymer coatings in the range of 6-8 on a scale of 1-8. It is used in roofing granules together with a durable chromium oxide green to produce a brighter color. After time, some fading of the phthalo green occurs, and the roof assumes a more muted color. The Pigment Handbook [6] and the monograph Industrial Organic Pigments [22] are useful references on the durability of organic pigments. And, of course, the pigment manufacturers are an excellent source of information of the applicability of pigments for the various specific applications.

The preceding few paragraphs are a very broad overview of the photodegradation of organic materials. This is a mature and complex subject, covered in monographs [23-26] and journals such as *Progress in Organic Coatings*, *Polymer Testing*, and *Polymer Degradation and Stability*. An additional interesting reference is the United Nations' assessment [27] of effects of increased UV exposure on building materials due to a decrease in ozone levels in the upper atmosphere.

4. Effects of increased temperatures on roofing materials

Usually, the increased temperatures experienced by roofing due to absorption of solar radiation are undesirable from a materials lifetime point of view. Furthermore, roofing materials are commonly believed to be less durable in hotter climates [28]. In this section, we discuss some of the mechanisms by which higher temperatures hasten material degradation. At the outset, however, we must acknowledge that in some cases elevated temperatures are irrelevant or beneficial. Ceramics like clay tile are fired at a high temperature in air during the manufacturing process. If free of reactive and water soluble impurities, these materials are extremely stable and understandably immune to moderate changes in temperature. Pigments that are metal oxides and mixed metal oxides are likewise rather inert. Polymeric materials often have the advantage of flexibility and elasticity, which helps them resist tearing. Exposure to cold temperatures reduces this elasticity and thus can lead to brittle failure. The failure of an O-ring in the space shuttle was a catastrophic example of this problem.

Materials degradation usually involves chemical reactions, and most chemical reactions progress more rapidly at higher temperatures. The phenomenological law describing the temperature dependence of chemical reactions is often attributed to the Swedish chemist Arrhenius [rate proportional to $\exp(-A/T)$, with A a constant and T the absolute temperature]. It is not unusual for reaction rates to double with as small a temperature increase as 10 K (10 ºC, 18 ºF).

In addition to an inherent temperature dependence of chemical reactions, many degradation processes involve in- or out-diffusion of low-molecular-weight components. Diffusion usually proceeds more rapidly at higher temperature, often with an Arrhenius temperature dependence.

Asphalt shingles

The thermal aging of asphalt roofing shingles provides a good example of effects of oxygen diffusion and reaction with oxygen. For a well-designed shingle, UV photo-oxidation is not likely to be very important since the granules absorb most of the incident UV radiation. For oxidation to occur, atmospheric oxygen must diffuse through the asphalt matrix in order to react in the interior.

Terrenzio *et* al. [29] discuss the thermal aging of the asphalt in roofing shingles as follows: In the diffusional model of asphalt aging, heat first promotes the diffusion of (lower molecular weight) oils out of the bulk of the asphalt. Then, some of the oils evaporate, and others are washed away because of photo-oxidation and subsequent solubility in water. Finally, oxygen diffuses into the system, resulting in the formation of more heptane-insoluble, polar molecules known as asphaltenes. As the aging progresses, these diffusion processes may lead to final failure of the system (typically cracking) as the asphalt becomes harder and stiffer. Further details are provided in a recent publication [30].

The Asphalt Roofing Manufacturer's Association (ARMA) recommends that asphalt shingles not be applied directly over thermal insulation [31]. The basic reason is that (solar) heat build up, which is typically a result of inadequate ventilation, may accelerate weathering and reduce the anticipated life of the asphalt shingles. Thus it is clear that excessively high shingle temperatures are detrimental. Roof venting is useful, and not merely for heat dissipation. It can also avoid moisture build up [32], which is important for many types of roofing. Excessive water vapor and/or condensation lead to swelling and rotting of wood and faster corrosion of metal. Wood shake and tile roofs often incorporate roof underside ventilation as an integral part of the design.

In a study of the aging of paving asphalts [33], the authors concluded that oxidation is a key factor in asphalt hardening in hot climates, and cited further evidence that the rate of thermal oxidation is approximately doubled for every 10 K rise in temperature.

Since photodegradation is a complex process that depends upon material type, including additives and impurities, it is difficult to generalize about how photodegradation should be altered by increased temperatures. Generally, we expect that higher temperatures may assist photodegradation. Here, we will simply cite one example, a study that investigated the durability of unprotected polyethylene [14]. Two sets of samples were exposed to sunlight in Dharhan, Saudi Arabia. One set was maintained at 25 ºC, while the other was exposed in outdoor air at higher temperatures. The sample extensibility was measured as a function of time. Extensibility is the extent of elongation before tearing. Samples maintained at 25 ºC lost 50% of their original extensibility after 6 mo. Corresponding samples at higher outdoor temperatures reached 50% extensibility after only 2 mo. Thus, in this specific case, photodegradation proceeded more rapidly at highly temperatures.

Thermoplastics such as polyvinyl chloride, polyethylene, and polypropylene become soft and can deform at high temperatures. In hot sunny climates dark colored roofing reaches temperatures approaching the boiling point of water. Manufacturers formulate roofing materials with the maximum roof temperatures in mind, and may restrict the application of certain dark colored materials in hot climates.

5. Effects of moisture

Moisture can cause decay of wood and hasten corrosion of metal. Two other deleterious effects of moisture are efflorescence, a sort of surface staining, and freeze-thaw damage.

“Dry-rot” of wood requires the presence of significant quantities of water. The fiber saturation point, the maximum moisture content reached by wood in humid air but no liquid water, is usually about 25 to 30% by weight. Wood with less than about 20% moisture is considered immune from dry rot [34]. Rot is the result of fungal infection. There are several types of fungi that stain and infect wood, and fungal spores are usually widely dispersed in ambient air. Surfaces infected with actively growing fungi show thread-like features (hyphae) under microscopic examination. Some species of fungi consume just the cellulose portion of wood, some the lignin, still others both primary wood components. After decay, the wood is much less dense and fractures readily. After sufficient fungal growth, fruiting bodies such as toadstools form that release new spores into the air.

Corrosion of metals is caused by chemical reactions with environmental substances, particularly the formation of metal oxides. Rusting of steel is a prototypical example. Modern steel used in roofing generally has a protective, sacrificial coating of zinc or a zinc-aluminum alloy to prevent rust. Then the metal alloy is further protected from chemical reactions with a polymeric coating. Nevertheless, most metals occur in mineral form only as combinations such as metal oxides, hydroxides, sulfides, carbonates, etc., and tend to revert to their mineral forms over time. Many of the corrosive reactions involved are electrochemical in nature and require the presence of an aqueous electrolyte – a solution of salts in water. Liquid water may be in direct contact with the metal in question or may be extracted from moist air due to the presence of hygroscopic dust. Thus it is not surprising that metallic corrosion proceeds more rapidly in humid climates

in which moisture is readily available [35]. Also, it is noteworthy that dissolved salts increase the electrical conductivity of water, making it a more effective electrolyte. This may be the primary reason that seaside salt air promotes corrosion.

Efflorescence is the occurrence of light colored stains on the surface of a porous material. It is caused by water seepage/diffusion through the material. Dissolved salts are transported along with the water, and are deposited on the surface when the water evaporates. A test for potential efflorescence of clay roof tiles is to immerse one end of the tile in distilled water for seven days in a drying room [36], and then inspect for staining. Efflorescence is a common issue for concrete items, particularly if they are dark in color. Water transports calcium hydroxide to the surface, and calcium carbonate is then formed by reaction with the CO_2 in air [37]. These white deposits can be prevented by the use of a polymeric coating that seals the surface [38]. Alternatively, the deposits can be removed by washing with dilute acid. If left in place, the calcium carbonate stains often weather in about 2 years, restoring the original appearance.

Freeze-thaw cycles are associated with the spallation of concrete and the premature failure of clay tiles. For this reason, ASTM standards for clay roof tile limit the permissible water absorption by the tiles [36]. For grade 1 tile, that provides resistance to severe frost action, maximum cold water absorption is limited to 8 % in any one tile and to 6 % average in a sample of 5 tiles. For grade 3 tile, that provides negligible resistance to any frost action, the permissible water absorption values are about twice as large.

6. Soiling of Roofing

Deposits on roofing originate with dry and wet (rainwater) deposition from the atmosphere. Clearly, one expects crustal dust (soil) to be present. Products of combustion such as soot, unburned hydrocarbons, and fly ash are expected as well. Sea salt is expected (in coastal areas) as are organic compounds emitted by vegetation (such as terpenes) and spores produced by plants and fungi. Due to the cleansing effects of rainwater, one expects that deposits on roofing may be depleted of water-soluble components. Of course rainwater can also transport small insoluble particles as well.

Suppose a substrate has a clean reflectance denoted R_o, which is coated with a thin uniform soil layer with absorptance a and reflectance r. In view of the assumption that the layer is thin, we take both a and r as small compared to unity. (The extension to thicker soil layers is straightforward, for example, by recursion.) Then, it is not difficult to show that the change in reflectance R of the soiled substrate is given, to first order in r and a, by $R - R_o = -2 R_o a + (1- R_o)^2 r$. Thus soil absorptance reduces R and soil reflectance increases R. Here we can also see that a will be more important if R_o is large and r will be more important if R_o is close to zero. Thus we expect that highly reflective materials tend to lose their reflectance as they are soiled, with the reflectance loss determined by absorption of the soil. Very dark materials tend to become lighter as they are soiled, with the reflectance increase caused by light scattering by soil. Finally, if the ratio r/a is such that $2 R_o a = (1- R_o)^2 r$, then $R - R_o = 0$ and soil deposits do not change the reflectance.

M. Ebert *et al*. [39] studied airborne aerosols in the size range of 0.1 to 25 micrometers, collected in Germany, by means of high resolution scanning electron microscopy and energy-dispersive X-ray microanalysis. By combining particle morphology data with chemical microanalysis, they recognized several characteristic particle types. Particles of silica and mixed oxides of silicon and aluminum were common, and appeared to have two distinct origins. Large irregular fractured particles were thought to be crustal in nature, whereas spherical particles in the sub-micron and micron size range were identified as fly ash. Particles were classified as metal oxides/metal hydroxides if they were low in silicon content and contained additional metals such as Fe, Mn, Zn, Al, Ti, Cu, Ni, and Pb. These particles could likewise be spherical fly ash or irregular dust particles. Calcium sulfate particles could be identified by the high Ca and S content and a plate-like morphology. Soot particles were identified by their fractal-like morphology: branched chains of ~ 50 nm spheres. Some biological particles had recognizable morphologies, such as fungal spores. Other biological particles were identified by >25% C, plus characteristic signatures of the minor elements Na, Mg, P, S, Cl, K, and Ca. Two further particle types were sea salt and ammonium sulfate, both of which are water soluble and will not be discussed further here.

Overall, of the elements heavier than sodium (Na), the most abundant elements were Al, Si, and S. Elements present in roughly ten times lower concentration were Na, Mg, P, Cl, K, Ca and Fe. Other elements were even less abundant. If the lighter elements had been detectable in this particular analysis, we would expect to see large contributions from H, C, N, and O as well.

The optical properties of the aerosols in the particle size range 0.1 to 3 μm were compiled based on an analysis of the phase composition of the particles. The complex refractive index thus derived is useful in computing light scattering and absorption in the atmosphere, and by extension may be useful in the optical properties of deposits on roofing. They found that the real part ranged from 1.54 to 1.72 and the imaginary part from 0.001 to 0.086. The lower values were associated with unpolluted rural air masses, and the higher values, with polluted urban air. The higher values of the real part are identified with higher concentrations of the metal oxide/hydroxide particles, and the higher values of the imaginary part are identified with increased concentrations of soot. If the imaginary part is zero, optical absorption is absent; only scattering occurs. Thus soot is the primary absorber in atmospheric aerosols.

As part of our present ongoing investigation on solar-reflective roofing, we have examined deposits that have formed on exposed roofing samples at several locations in California [40]. Selected results are shown in Table 1. Since the samples were taken in the spring, after California's winter rainfall, the deposits were affected by rainfall and are less extensive than would have been the case if the samples were obtained in September, after the dry California summer. Thus the observed solar reflectance values were about the same as for unsoiled samples. For example, three samples with initial solar reflectance of 0.57 had reflectance of 0.54 ± 0.02 after 19 months. Sulfur is not found in high abundance, which may be attributed to the absence of coal-fired power plants in

California. Calcium is found in rather high abundance, except for the remote McArthur site in northeastern California. Due to the small amount of sulfur present, the calcium is likely to be in the form of carbonate (rather than sulfate). The first five metals in Table 1 all have white oxides, and are unlikely to reduce the reflectance of highly reflective roofing. (They are, of course, expected to raise the reflectance of black roofing.) The relatively abundant transition metals Fe, Mn, Cu, Cr, have colored or black oxides and other compounds and therefore may reduce roof reflectance slightly. Of these elements, iron is the most abundant. To obtain a semi-quantitative estimate of the maximum possible optical absorption of the iron, we can assume that ~ 60 mg m^{-2} are present in the form of strongly absorbing small (0.27 μm diameter) hematite (Fe_2O_3) pigment particles. Hematite is a strong absorber of the short wavelength part of the solar spectrum (300 to 550 nm) with a coefficient of roughly 4 m^2/gm [41]. Thus such a hematite layer could absorb a measurable portion (~20 %) of the short wavelength component. Most likely, however, the iron mineral particles present are in the form of larger particles that are less efficient than the sub-micrometer particles of our example.

The role of elemental carbon (i.e., soot) is potentially more dramatic. Figure 4 shows the expected [42] solar reflectance and visible reflectance as a function of soot concentration, as a fraction of the high initial reflectance R_o. The sample exposed at Richmond has the most elemental carbon (1.3 mg m^{-2}), but this amount is insufficient to markedly reduce its reflectance.

Like hematite, the effect of organic carbon is expected to be largest at shorter wavelengths, but published absorption coefficients (roughly 0.6 m^2 g^{-1} at 550 nm) [43] suggest that it is less important than elemental carbon (~ 14 m^2 g^{-1} at 550 nm) [43] for equivalent masses per unit area.

As far as biological growth on roofing surfaces is concerned, it is clear that a large variety of species is expected to be present. For example, some of the species of fungi that occur in soil may be expected to be present. However, the ultraviolet radiation incident on roofing can kill many organisms. We have noted earlier that the cyanobacteria Gloeocapsa infests mineral roofing granules, leading to black colored stains. In a study of biomass accumulation on single ply roofing membranes exposed in Oak Ridge, Tennessee [44], it was found by phospholipid fatty acid analysis that the biological growth was in this case primarily fungal in nature.

C. C. and P. M. Gaylarde [45] recently published a study of 230 biofilms found on the exterior of buildings in Europe and in Latin America. They classified the biofilms according to the predominant microscopic organisms found, of which the most important were various cyanobacteria, algae, and fungi. The substrate was important with, for example, fungi rarely found on mineral substrates and often on paint. Climate was believed to be important as well, with algae more prevalent at cool damp European sites and dark-colored cyanobacteria frequently found in tropical locations at elevations above 1000 m.

Dupuy [46], as cited by Ortega-Calvo [47], investigated the cyanobacteria that grew on monuments exposed to strong solar radiation and that could tolerate long dry periods. They include *Calothti parietina* and *Chroococcus montanus* as pioneer species, which are followed by species of *Gloeocapsa, Nostoc* and *Scytonema*.

In a detailed study of the fungal colonization of plasticized PVC outdoors in Manchester, United Kingdom, Webb *et al*.[48] used gene sequencing to definitively identify several of the species involved. The fungus *Aureobasidium pullulans* had the ability to extract metabolic carbon from the plasticiser in the intact PVC formulation, and was thereby able to initially colonize the surface after 25 – 40 weeks. Subsequently, a group of yeasts and yeast-like fungi, including *Rhodotorula aurantiaca* and *Kluyveromyces* spp., established themselves on the PVC after 80 weeks of exposure. In addition to *A. pullulans*, many of the observed fungi, e.g., *Alternaria* spp., *Aspergillus* spp., *Paecilomyces* sp., and *Cladosporium* sp., have previously been isolated from deteriorated PVC and are common colonizers of painted surfaces and building materials.

In the roofing industry it is often not known exactly what species make up the biomass deposits on roofing. In fact, the terms algae and fungi are sometimes used interchangeably. However, it is well known that in humid climates, such as the southeastern United States, the growth of biomass on roofing leads to visible stains. In some cases, it has been noted that staining does not occur near copper and galvanized (zinc) flashings. In a patent by Narayan *et al*., [49] reviewing prior art, it is noted that algae growth on asphalt shingles can be inhibited by metal Zn particles, ZnO, ZnS, and cuprous oxide (Cu_2O). Thus it appears that zinc and copper ions can inhibit biological growth. A more recent patent [50] likewise discloses that Cu_2O, either alone or with zinc compounds, is effective in roof granules, to prevent growth of cyanobacteria (such as Gloeocapsa) and also fungi.

Levinson et al. [51] investigated a number of light-colored PVC roof membranes that had been exposed for a number of years and that had obvious biological growth, presumably fungal in nature. The spectral reflectance was measured both before and after a number of cleaning procedures. In this way inferences could be made concerning the spectral absorptance of the substances removed. Three different types of spectra were observed. First, optically thick black spots of biomass were found. Second, “organic carbon” with a spectrum similar to that in [43] was found. Third, “soot” with a broadband spectrum similar to that shown in [42,43] was found. In this study of PVC roof membranes, it was found that only partial cleaning can be performed by the use of soap and water, but that bleach is effective in removing residual stains.

Biocides are often included in the formulation of polymeric materials such as PVC. As just one example, the compound OIT (2-n-octyl-4-isothiazolin-3-one) is used commercially for this purpose. Concentrations on the order of 10 ppm inhibit the growth of a number of common fungi [52]. However, premature leaching is an issue that must be addressed in material formulation.

7. Summary

We have presented an overview of the weathering of roofing materials. Emphasis has been placed on chemical changes and changes in visible and solar reflectances. Photodegradation is very important for organic materials: plastics, wood, asphalt and organic pigments. Photodegradation is initiated by energetic UV photons in sunlight and generally involves chemical reactions with atmospheric oxygen and/or water vapor, leading to brittleness. Elevated temperatures, for example as provided by solar absorption in dark materials, lead to acceleration of deleterious chemical reactions and can hasten the diffusion of low molecular weight components. Moisture is also a key factor in many degradation processes. For example, corrosion of metals is accelerated by high humidity. Deposits that form on roofing include the various atmospheric aerosols such as crustal dust, soot and hydrocarbons from incomplete combustion, and organic particles including spores. Biological growths on roofing include cyanobacteria on roofing granules, algae on mineral materials in cool damp climates, and fungi on polymeric materials.

8. Acknowledgments

M. D. Cheng of Oak Ridge National Laboratory (ORNL) kindly provided results for Table 1 in advance of publication [40]. A. Desjarlais of ORNL, S. Wiel of Lawrence Berkeley National Laboratory and C. Scruton of the California Energy Commission provided technical and management advice. Many individuals in the roofing materials industry provided us with expert advice including C. Gross, J. Jacobs, P. Fleming, 3M Corp.; J. Reilly, R. Sypowics, American Rooftile Coatings; R. Scichili, BASF and now as a consultant to Custom-Bilt Metals, M. Shiao, L. Terrenzio, CertainTeed Corp; T. Chiovare, Custom-Bilt Metals ; L. Hahn, K. Tellman, Elk Manufacturing, Corp.; R. Abrams, R. Blonsky, J. Dunn, I. Joyce, K. Loye, D. Swiler, Ferro Corp.; M. Desouto, K. Srinivasan, GAF Materials Corp.; I. Joedicke, ISP Minerals Corp.; Y. Suzuki, MCA Clay Tile; J. Vanderwater, MonierLifetile; S. Graveline, K. Foley, Sarnafil Corp.; C. Manning, J. Nixon, T. Steger, Shepherd Color Co.;M. Vondran, Steelscape: and K. Watkins, Watkins Sawmills Ltd.

This work was supported by the California Energy Commission through its Public Interest Energy Research Program. Lawrence Berkeley National Laboratory is managed by the University of California for the U. S. Dept. of Energy under Contract No. DE-AC02-05CH11231. Oak Ridge National Laboratory is managed by UT-Battelle, LLC, for the U.S. Dept. of Energy under contract DE-AC05-00OR22725.

References

[1] R. Levinson, P. Berdahl, H. Akbari, W. Miller, I. Joedicke, J. Reilly, Y. Suzuki, and M. Vondran, Methods of creating solar-reflective nonwhite surfaces and their Application to residential roofing materials, *Sol. Energy Mater. Sol. Cells*, in press (2006).

[2] A. A. Joshi and P. J. Pagni, Fire-induced thermal fields in window glass. II – Experiments, *Fire Safefy Journal 22*, 45-65 (1994).

[3] Web page of T. Futcher, Columbia Union College, Takoma Park, Maryland, http://www.cs.cuc.edu/~tfutcher/Cyanophyta.html.

[4] Web page for 3M roofing granules, http://solutions.3m.com/wps/portal/_l/en_US/_s.155/115625/_s.155/117267.

[5] R. S. Williams, The finishing of wood, Chapter 15 of Wood handbook-Wood as an engineering material, Forest Products Laboratory, Madison, Wisconsin (1999; available online). http://woodworking.about.com/gi/dynamic/offsite.htm?site=http://www.fpl.fs.fed.us/

[6] *Pigment Handbook, Vol. I, Properties and Economics*, 2nd Ed., P. A. Lewis, Editor, John Wiley & Sons, New York (1988).

[7] R. Reed, Painted metal: From fluoropolymers to polyesters, sorting out the issues in coil coatings, in *Metal Roofing* (August-Sept. 2003).

[8] ASTM Standard D 4214 – 98, Standard test methods for evaluating the degree of chalking of exterior paint films, published by ASTM International, West Conshohocken, PA 19428-2959, United States (1998).

[9] ASCA 96 specification as listed at http://www.products.arkemagroup.com/pdf/techpoly/ASCA_96.pdf. See also Arkema, ATOFINA Chemicals, Inc., Philadelphia, product brochure on Kynar 500 PVDF resin-based metal coatings. Cited ASTM standards are Hunter color change D 2244, chalking D 4214 and D 659, and gloss D 523.

[10] P. P. Greigger and P. Wilson, High-performance fluoropolymers coatings, PPG Industries, Springdale, PA, article on website at corporate.ppg.com/ppg/paf/documents/corwhite.doc

[11] W. A. Miller, S. Kriner, and D. S. Parker, Cool metal roofing is topping the building envelope with energy efficiency and sustainability. *RCI Foundation conference, "Cool Roofs: Cutting through the glare."* (Atlanta, CA, May 12-13, 2005).

[12] Website of Ciba Specialty Chemicals (http://www.cibasc.com/), subject of Light Stabilizers.

[13] G. E. Schoolenberg and P. Vink, Ultraviolet degradation of polypropylene: 1. degradation profile and thickness of the embrittled surface layer, *Polymer 32*, 432-437 (1991).

[14] A. L. Andrady, S. H. Hamid, X. Hu, and A. Torikai, Effects of increased solar ultraviolet radiation on materials, *J. of Photochemistry and Photobiology B: Biology 46*, 96-103 (1998).

[15] M. Knaebe and C. Carll, Wood shakes and shingles for roof applications; tips for longer life, Forest Products Laboratory finishing factsheet, US Dept. of Agriculture Forest Service (January, 1998).

[16] H. Akbari, R. Levinson and P. Berdahl, Review of residential roofing materials, Part I: a review of methods for the manufacture of residential roofing materials. *Western Roofing Insulation and Siding*, 54-57 (Jan/Feb, 2005).

[17] H.Akbari, R. Levinson, and P. Berdahl, Review of residential roofing materials, Part II: a review of methods for the manufacture of residential roofing materials. *Western Roofing Insulation and Siding*, 52-58 (Mar/Apr, 2005).

[18] Y. Tropsha and A. Andrady, Photodegradation of asphalt and its sensitivity to the different wavelengths of the sunlight spectrum, in Polymeric Materials Science and Engineering, Vol. 66, Spring Mtg. of the Amer. Chem. Soc. Division of Polymeric Materials, p. 305 (1992).

[19] J. Huang, R. Yuro, and G. A. Romeo, Jr., Photooxidation of Corbett fractions of asphalt, in *Fuel Science and Technology Int'l*., 13, 1121-1134 (1995).

[20] J. C. Petersen, A dual, sequential mechanism for the oxidation of petroleum asphalts, Petroleum Science and Technology 16, 1023-1059 (1998).

[21] R. Pascoe, Phthalocyanine green pigments, Chapter I-D-1-2, Table 5, in *Pigment Handbook, Vol. I, Properties and Economics*, 2nd Ed., P. A. Lewis, Editor, John Wiley & Sons, New York, 1988.

[22] W. Herbst and K. Hunger, *Industrial Organic Pigments*, Wiley-VCH, Weinheim, Germany, 1998.

[23] *Handbook of Polymer Degradation*, Hamid, S.H., Amin, M.B. and Maadhah A.G. (eds), Marcel Dekker Inc. New York. (1995).

[24] Rabek, J.F., *Polymer Photodegradation*, Chapman and Hall, London, England. (1995).

[25] Scott, G.. *Polymer Degradation and Stabilization*, Elsevier Applied Science Publishers, London (1990).

[26] Wypych, J., *Weathering Handbook*, 2nd edition, Chemtec Publishing, Toronto, Canada (1995). Despite the title, this reference is exclusively concerned with polymers.

[27] Andrady, A. L., S.H. Hamid, X. Hu, and A. Torikai, Effects of increased solar ultraviolet radiation on materials, Chapter 7 in Environmental Effects of Ozone Depletion, 1998 Assessment of the United Nations Environmental Programme. Available online at http://www.gcrio.org/UNEP1998/.

[28] C. G. Cash, "Estimating the durability of roofing systems," in *Durability 2000: Accelerated and Outdoor Weathering Testin*g, STP 1385, W. D. Ketola and J. D. Evans, eds., American Society for Testing and Materials, Philadelphia, Pa., 165–169 (2000).

[29] L. A. Terrenzio, J. W. Harrison, D. A. Nester, and M. L. Shiao, Natural vs. artificial aging: use of diffusion theory to model asphalt and fiberglass-reinforced shingle performance, Proc. 4th Int. Symp. on Roofing Technol. 66-74 (Gaithersburg, Sept. 1997).

[30] M. L. Shiao, D. A. Nester, and L. A. Terrenzio, On the kinetics of thermal loads for accelerated aging, Roofing Research and Standards Development, 5th Volume, ASTM STP 1451, W. J. Rossiter and T. J. Wallace, Eds. (ASTM International, West Conshohocken, PA, 2003).

[31] ARMA Technical Bulletin, Application of asphalt shingles over insulation or insulated decks, ARMA Form No. 209-RR-86. Revised July, 1996.

[32] ARMA Technical Bulletin, Ventilation and moisture control for residential roofing, ARMA Form No. 211-RR-94. Revised Nov., 1997.

[33] G. R. Kemp and N. H. Predoehl, A comparison of field and laboratory environments on asphalt durability, *Asphalt Paving Technology 50*, 492-555 (1981).

[34] M. C. Baker, Decay of wood, Canadian Building Digest, CBD-111, originally published in 1969, http://irc.nrc-cnrc.gc.ca/cbd/cbd111e.html.

[35] Corrosion of zinc, "Knowledge Article" from www.Key-to-Metals.com

[36] ASTM Standard C 1167-03, Standard specification for clay roof tiles.

[37] G. Buchner and U. Kundgen, Bayer AG, An anniversary - 25 years of outdoor weathering of pigmented building materials, Betonwerk + Fertigteil Technik (July, 1996).

[38] Bayer Chemicals, Inorganic Pigments Group, Reduction of efflorescence on concrete paving blocks by impregnation with a plastic emulsion, Technical Information from Bayer AG (May, 2002). Also, Removing efflorescence and soil from the surface of concrete pavers (May, 2002).

[39] M. Ebert, S. Weinbruch, P. Hoffmann, and H. M. Ortner, The chemical composition and complex refractive index of rural and urban influenced aerosols determined by individual particle analysis, *Atmospheric Environment 38*, 6531-6535 (2004).

[40] M. D. Cheng, W. A. Miller, P. Berdahl, and S. Pfiffner, Composition and effects of atmospheric particles on the performance of steep-slope roofing materials, in preparation.

[41] R. Levinson, P. Berdahl, and H. Akbari, Solar spectral optical properties of pigments – part II: survey of common colorants, *Sol. Energy Mater. Sol. Cells 89*, 351-389 (2005), Fig. 1, Film R03.

[42] P. Berdahl, H. Akbari, and L. S. Rose, Aging of reflective roofs: soot deposition, *Appl. Optics 41*, 2355-2360 (2002).

[43] Thomas W. Kirchstetter, T. Novakov, and P. V. Hobbs, Evidence that the spectral dependence of light absorption by aerosols is affected by organic carbon, *J. Geophysical Research-Atmospheres 109,* (D21): Art. No. D21208 (NOV 12, 2004).

[44] W. A. Miller, M. D. Cheng, S. Pfiffner, and N. Byars, The field performance of high-reflectance single-ply membranes exposed to three years of weathering in various U. S. climates, Oak Ridge National Laboratory report prepared for, and available from, the Single-Ply Roofing Institute, Needham, MA (2002).

[45] C. C. Gaylarde and P. M. Gaylarde, A comparative study of the major microbial biomass of biofilms on exteriors of buildings in Europe and Latin America, *Int. Biodeterioration & Biodegradation* 55,131–139 (2005).

[46] P. Dupuy, G. Trotet and F. Grossin, Protection des monuments contre les cyanophycees en milieu abrite et humide, in R. Rossi-Manaressi (Ed.), The Conservation of Stone I, Centro per la Conservazione delle Sculture all'Aperto, Bologna, 205-219 (1976).

[47] J.J. Ortega-Calvo, X. Ariiio, M. Hernandez-Marineb, and C. Saiz-Jimenez, Factors affecting the weathering and colonization of monuments by phototrophic microorganisms, *Science of the Total Environment 167,* 329-341 (1995).

[48] J. S. Webb, M. Nixon, I. M. Eastwood, M. Greenhalgh, G. D. Robson, and P. S. Handley, Fungal colonization and biodeterioration of plasticized polyvinyl chloride, *Applied And Environmental Microbiology* 66, 3194–3200 (2000).

[49] S. B. Narayan et al., Method of inhibiting algae growth on asphalt shingles, U. S. Patent No. 5,356,664 (1994).

[50] I. B. Joedicke, U. S. Patent Application 2004110639 A1 (June 10, 2004}.

[51] M. R. Levinson, P. Berdahl, A. A. Berhe, and H. Akbari, Effects of soiling and cleaning on the reflectance and solar heat gain of a light-colored roofing membrane, *Atmospheric Environment 39*, 7807–7824 (2005).

[52] L. Coulthwaite, K. Bayley, C. Liauw, G. Craig, J. Verran, The effect of free and encapsulated OIT on the biodeterioration of plasticised PVC during burial in soil for 20 months, *Int. Biodeterioration & Biodegradation 56*, 86–93 (2005).

California location	*Shafter*	*McArthur*	*Sacramento*	*El Centro*	*Corona*	*Colton*	*Richmond*
Coordinates	35.50N 119.27W	41.02N 121.65W	38.59N 121.51W	32.79N 115.56W	33.88N 117.56W	34.07N 117.31W	37.94N 122.34W
Aluminum	16.	5.3	50.	21.	41.	39.	27.
Calcium	17.	1.0	5.6	87.	55.	96.	146.
Silicon	6.8	2.3	9.8	20.	19.	14.	9.7
Magnesium	9.0	0.51	6.1	20.	20.	20.	16.
Zinc	7.3	3.2	52.	1.8	4.4	1.3	1.1
Sulfur	1.4	<1	7.3	<2	1.8	1.2	1.7
Iron	32.	5.0	42.	33.	68.	67.	44.
Manganese	0.28	0.03	0.35	0.6	1.5	3.3	0.9
Copper	0.8	0.3	0.76	1.4	1.4	1.1	0.9
Chromium	1.3	0.7	7.7	0.15	0.6	0.7	0.8
Organic carbon	5.6	1.3	4.5	8.3	5.4	6.1	11.
Elemental Carbon	0.4	~ 0.02	0.22	0.24	0.24	0.16	1.3

Table 1. Concentration of several abundant elements and organic/elemental carbon in mg m^{-2}, collected on samples of roofing materials exposed for 19 months (until April, 2005) at several California locations [40].

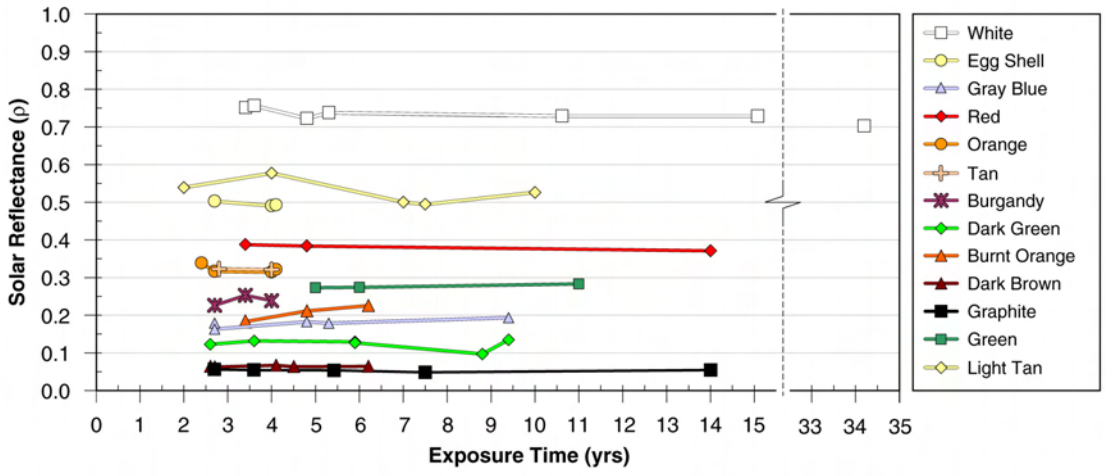

Fig. 1. Solar reflectance of PVDF painted metals acquired from south Florida field exposures for BASF, Atofina, Akzo Nobel and Solvay Solexis.

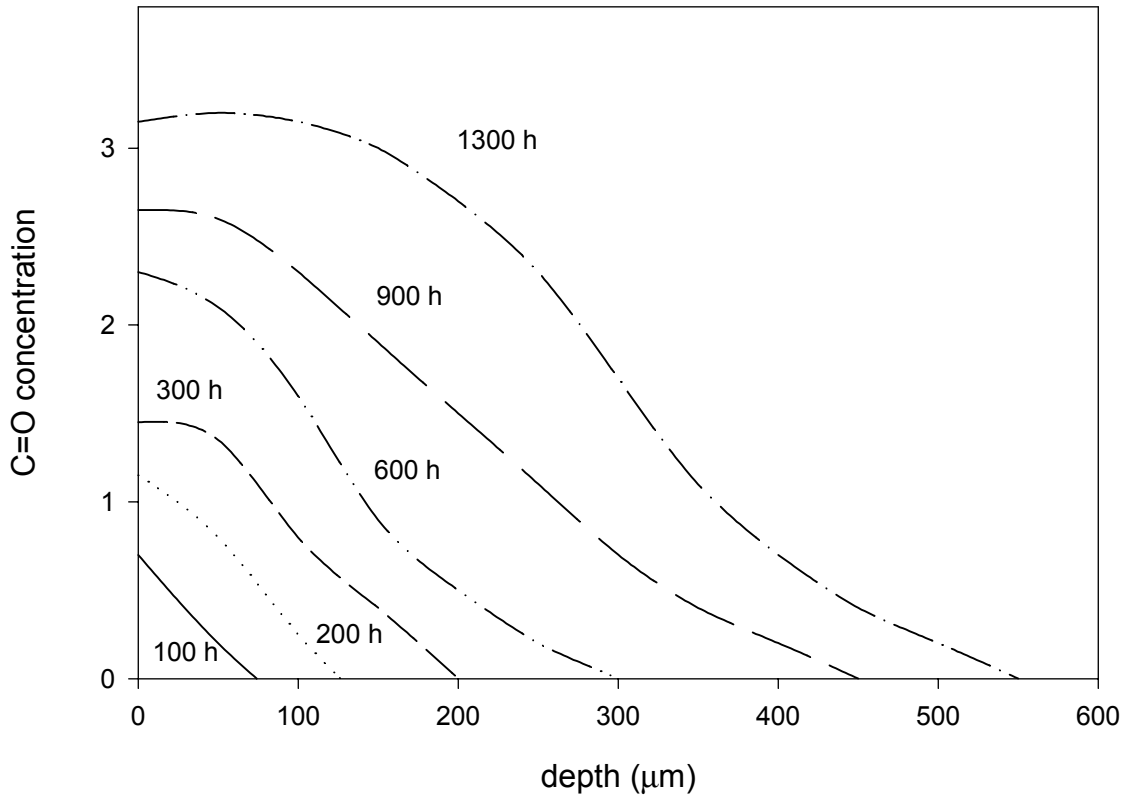

Fig. 2. Oxidation (carbonyl) profiles measured during accelerated UV aging of polypropylene, after [13].

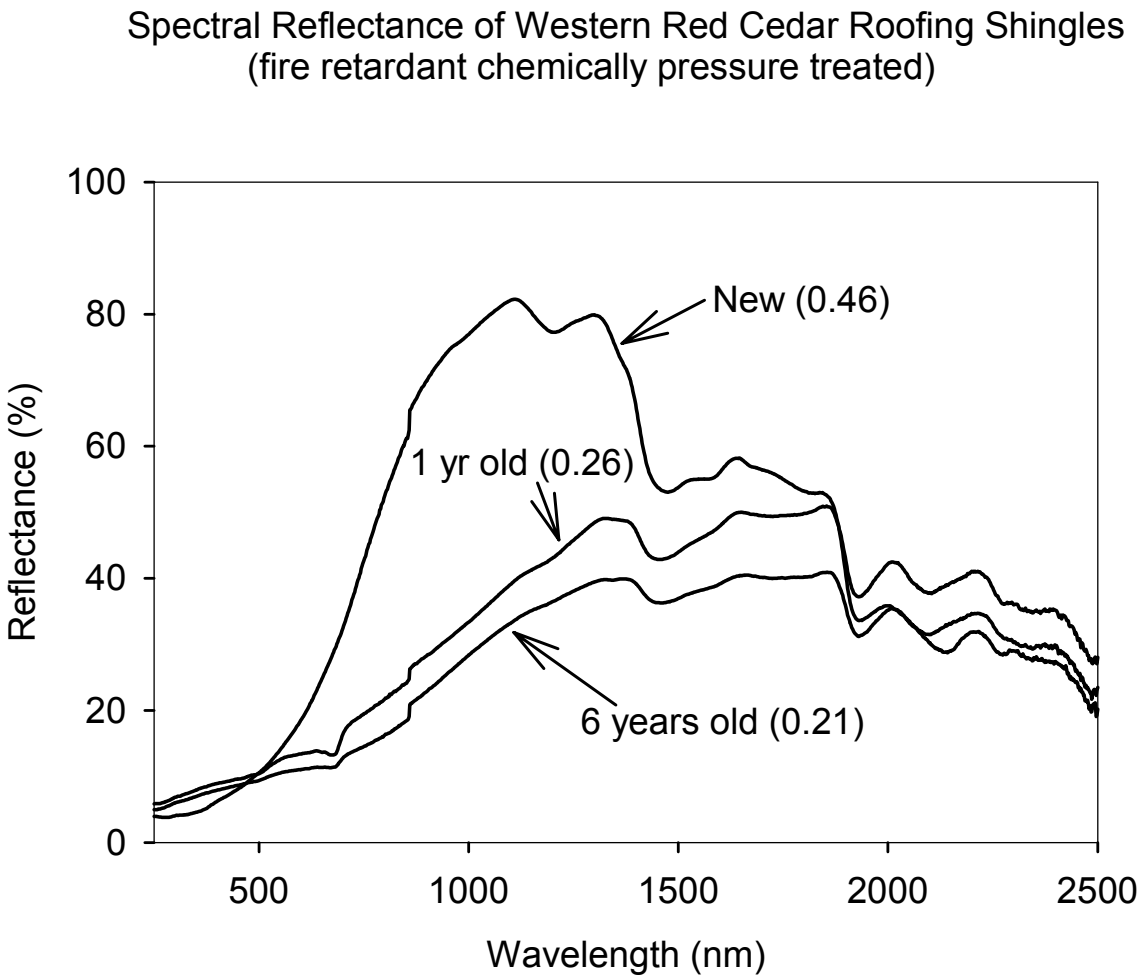

Fig. 3. Spectral reflectance of western red cedar roofing shingles. The solar reflectance is 0.46 when new, and declines to 0.21 after 6 years exposure.

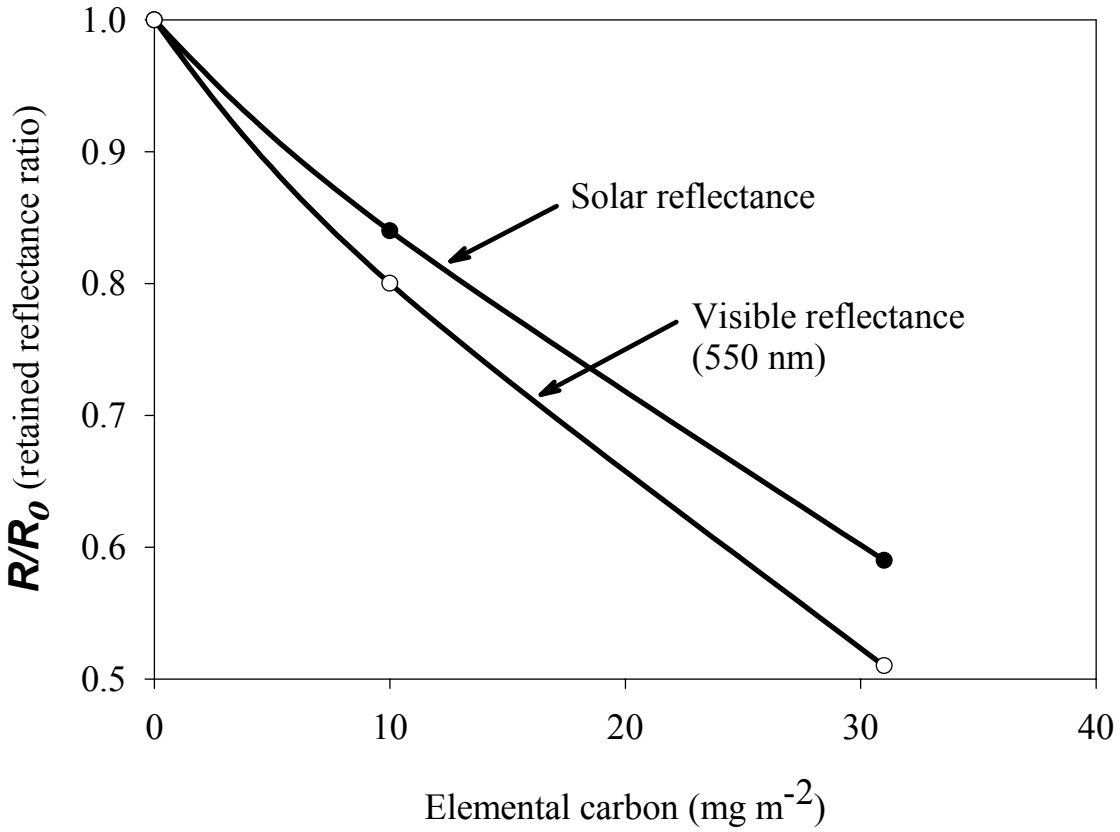

Fig. 4. Expected values for the soiled roof reflectance, divided by the unsoiled reflectance, as a function of elemental carbon (soot) concentration. After [42].

Arnold Schwarzenegger
Governor

COOL-COLOR ROOFING MATERIAL ATTACHMENT 11: TASK 2.7.1 REPORTS - TECHNOLOGY TRANSFER

PIER FINAL PROJECT REPORT

Prepared For:
California Energy Commission
Public Interest Energy Research Program

Prepared By:
Lawrence Berkeley National Laboratory and Oak Ridge National Laboratory

ERNEST ORLANDO LAWRENCE
BERKELEY NATIONAL LABORATORY

June 2006
CEC-500-2006-067-AT11

Prepared By:
Lawrence Berkeley National Laboratory
Hashem Akbari
Berkeley, California
Contract No. 500-01-021

Oak Ridge National Laboratory
William Miller
Oak Ridge, Tennessee

Prepared For:
California Energy Commission
Public Interest Energy Research (PIER) Program

Chris Scruton
Contract Manager

Ann Peterson
Building End-Use Energy Efficiency Team Leader

Nancy Jenkins
PIER Energy Efficiency Research Office Manager

Martha Krebs, Ph.D.
Deputy Director
ENERGY RESEARCH AND DEVELOPMENT DIVISION

B. B. Blevins
Executive Director

DISCLAIMER

This report was prepared as the result of work sponsored by the California Energy Commission. It does not necessarily represent the views of the Energy Commission, its employees or the State of California. The Energy Commission, the State of California, its employees, contractors and subcontractors make no warrant, express or implied, and assume no legal liability for the information in this report; nor does any party represent that the uses of this information will not infringe upon privately owned rights. This report has not been approved or disapproved by the California Energy Commission nor has the California Energy Commission passed upon the accuracy or adequacy of the information in this report.

Reports included in this attachment:

- Effects of soiling and cleaning on the reflectance and solar heat gain of a light-colored roofing membrane
- Experimental analysis of the natural convection effects observed within the closed cavity of tile roof systems
- Cool metal roofing is topping the building envelope with energy efficiency and sustainability
- Special infrared reflective pigments make a dark roof reflect almost like a white roof
- Cool colored materials for roofs
- Cool colored roofs to save energy and improve air quality
- Cool metal roofing tested for energy efficiency and sustainability
- PVDF coatings with special IR reflective pigments
- Cool color roofs with complex inorganic color pigments
- Potentials of urban heat island mitigation
- Aging and weathering of cool roofing membranes
- Cooler tile-roofed buildings with near-infrared-reflective nonwhite coatings
- Cooling down the house: residential roofing products will soon boast "cool" surfaces
- Solar spectral optical properties of pigments
- Cool colors: a roofing study is developing cool products for residential roofs

Available online at www.sciencedirect.com
SCIENCE DIRECT®
Atmospheric Environment 39 (2005) 7807–7824
ATMOSPHERIC ENVIRONMENT
www.elsevier.com/locate/atmosenv

Effects of soiling and cleaning on the reflectance and solar heat gain of a light-colored roofing membrane

Ronnen Levinson[a,*], Paul Berdahl[a], Asmeret Asefaw Berhe[b], Hashem Akbari[a]

[a]*Heat Island Group, Lawrence Berkeley National Laboratory, 1 Cyclotron Road, Berkeley, CA 94720, USA*
[b]*Ecosystem Sciences Division, University of California at Berkeley, Berkeley, CA 94720, USA*

Received 24 May 2005; received in revised form 24 August 2005; accepted 24 August 2005

Abstract

A roof with high solar reflectance and high thermal emittance (e.g., a white roof) stays cool in the sun, reducing cooling power demand in a conditioned building and increasing summertime comfort in an unconditioned building. The high initial solar reflectance of a white membrane roof (circa 0.8) can be lowered by deposition of soot, dust, and/or biomass (e.g., fungi or algae) to about 0.6; degraded solar reflectances range from 0.3 to 0.8, depending on exposure. We investigate the effects of soiling and cleaning on the solar spectral reflectances and solar absorptances of 15 initially white or light-gray polyvinyl chloride membrane samples taken from roofs across the United States. Black carbon and organic carbon were the two identifiable strongly absorbing contaminants on the membranes. Wiping was effective at removing black carbon, and less so at removing organic carbon. Rinsing and/or washing removed nearly all of the remaining soil layer, with the exception of (a) thin layers of organic carbon and (b) isolated dark spots of biomass. Bleach was required to clear these last two features. At the most soiled location on each membrane, the ratio of solar reflectance to unsoiled solar reflectance (a measure of cleanliness) ranged from 0.41 to 0.89 for the soiled samples; 0.53 to 0.95 for the wiped samples; 0.74 to 0.98 for the rinsed samples; 0.79 to 1.00 for the washed samples; and 0.94 to 1.02 for the bleached samples. However, the influences of membrane soiling and cleaning on roof heat gain are better gauged by fractional variations in solar absorptance. Solar absorptance ratios (indicating solar heat gain relative to that of an unsoiled membrane) ranged from 1.4 to 3.5 for the soiled samples; 1.1 to 3.1 for the wiped samples; 1.0 to 2.0 for the rinsed samples; 1.0 to 1.9 for the washed samples; and 0.9 to 1.3 for the bleached samples.
© 2005 Elsevier Ltd. All rights reserved.

Keywords: Roofing; Single-ply membrane; Polyvinyl chloride (PVC); Black carbon; Organic carbon; Biomass; Fungi; Algae; Solar spectral reflectance; Solar reflectance; Solar absorptance; Absorption; Optical depth; Soiling; Cleaning; Wiping; Washing; Rinsing; Bleaching

1. Introduction

A roof with high solar reflectance and high thermal emittance (e.g., a white roof) stays cool in the sun, reducing cooling energy use in a conditioned building and increasing comfort in an unconditioned building. Prior research has indicated that savings are greatest for buildings located in climates with long cooling seasons and short heating seasons, particularly those buildings that have distribution ducts in the plenum, distribution ducts on the roof, and/or low rates of plenum

*Corresponding author. Tel.: +1 510 486 7494; fax: +1 510 486 6658.
E-mail address: RMLevinson@LBL.gov (R. Levinson).

1352-2310/$ - see front matter © 2005 Elsevier Ltd. All rights reserved.
doi:10.1016/j.atmosenv.2005.08.037

Nomenclature

English symbols

A	solar absorptance of membrane
c	coefficient
f	fraction of membrane area covered by soil layer
r	spectral reflectance of membrane
R	solar reflectance of membrane
t	spectral transmittance of soil layer
z	position in soil layer (height above membrane's surface)
Z	soil layer thickness

Greek symbols

α	spectral absorption coefficient
γ	fraction remaining of initial spectral optical depth of soil layer
δZ	variation in thickness of soil layer
$\delta\tau$	absolute decrease in spectral optical depth of soil layer
η	average pathlength parameter
λ	wavelength of light (in air)
τ	spectral optical depth of soil layer

Subscripts and superscripts

0	unsoiled
n	state n, or cleaning process that begins from state n states: 5 = soiled, 4 = wiped, 3 = rinsed, 2 = washed, 1 = bleached, 0 = unsoiled
N	soiled (state 5)
$'$	of nonuniform thickness

ventilation (Abkari, 1998; Akbari et al., 1999; Konopacki and Akbari, 1998). Widespread use of cool roofs can also reduce summertime urban air temperatures by 1 to 2K (Akbari and Konopacki, 1998; Young, 1998; Pomerantz et al., 1999; Akbari et al., 1999).

The high initial solar reflectance of a white roof (not less than 0.7 for products meeting California's Title-24 energy code for nonresidential buildings with low-slope roofs (CEC, 2005)) can be degraded by deposition of soot, dust, and/or biomass (e.g., fungi or algae) to about 0.6, depending on exposure. Some materials have higher initial solar reflectance; white polyvinyl chloride (PVC) membranes, for example, typically have initial solar reflectances exceeding 0.8. Simulations indicate that replacing a roof of solar reflectance 0.20 (e.g., a weathered medium-gray roof) on a typical California commercial building by a roof of solar reflectance 0.55 (e.g., a weathered white roof) can yield net energy savings (cooling energy savings − heating energy penalties) with a 15-year net present value (NPV) of about \$1 to \$7/m^2 of roof area (Levinson et al., 2005a). The energy savings achieved by replacing a less reflective roof with a more reflective roof are linearly proportional to the change in the solar reflectance (Konopacki et al., 1997). Hence, a cleaning regimen that maintains the solar reflectance of a white roof at its initial value of 0.70 can increase the 15-year NPV of net energy savings by over 40%, worth an additional \$0.5 to \$3/m^2.

Slightly over two years of exposure at an outdoor test facility in eastern Tennessee reduced the typical solar reflectance of eight white latex coatings applied to low-slope roofing to 0.56 from 0.84 (Wilkes et al., 2000). Three and a half years of exposure at the same facility decreased the average solar reflectance of four low-slope, single-ply, white PVC roofing membranes to 0.49 from 0.86, and reduced the solar reflectance of a low-slope metal roofing panel with a white polyvinylidene fluoride (PVDF) coating to 0.62 from 0.64 (Roodvoets et al., 2004a). Solar reflectances stabilized after about two years in both studies.

A simple gauge of the cleanliness of an initially reflective surface bearing contaminants that absorb but do not scatter light is the ratio of its solar reflectance after exposure to its solar reflectance before exposure. This value approaches zero for heavily soiled surfaces and is one for clean surfaces. The solar reflectance ratios for the PVC membranes and the adjacent PDVF-coated metal panel were 0.57 and 0.97, respectively, indicating that the PVC was much more soiled.

Thermal cycling can drive liquid plasticizers to the surface of a PVC membrane, rendering it tacky (Griffin, 2002) and hence prone to collect contaminants. Roodvoets et al. (2004a) detected significant

growth of biomass (primarily fungi) on the PVC membranes exposed at the test facility. They hypothesized that airborne microorganisms attached to and possibly fed on the leached plasticizers, establishing a net-like growth on the surface that accelerated soiling by trapping dirt. The cleanliness of the PVDF-coated metal panel was attributed to its smoother and thus more difficult to colonize surface (Miller et al., 2002).

Washing the soiled PVC membranes with water or with one of several commercially available cleaning agents—trisodium phosphate, a household cleaner/degreaser, or a chlorine solution—removed most of the contaminants, raising typical solar reflectance to 0.80–0.85 (Roodvoets et al., 2004b) and typical solar reflectance ratio to 0.93–0.99.

Our earlier investigation of the effects of weathering on the solar spectral reflectances of two roofing surfaces—a light-gray PVC roofing membrane and a steel panel with a zinc-aluminum coating—concluded that their reflectances were decreased primarily by the deposition of soot (Berdahl et al., 2002). Washing with a mild soap solution removed the carbon from the PVC membrane, but not from the steel panel.

In North America, visible light (400–700 nm) conveys 43% of the power in the air-mass 1.5 global solar irradiance spectrum (300–2500 nm); the remainder arrives as near-infrared (700–2500 nm, 52%) or ultraviolet (300–400 nm, 5%) radiation (ASTM, 2003) (Fig. 1). We noted in our earlier study that most of the minerals found in atmospheric dust and soil are either nonabsorbing in the visible and near infrared ranges (quartz, ammonium sulfate, sodium chloride) or have a definite absorption spectrum (hematite [iron oxide red], hydrated clays). Soot—particulate matter emitted from fossil fuel combustion—is a notable exception. Soot is primarily "black carbon," though it can also include "organic carbon" (Kirchstetter and Novakov, 2004). Black carbon is refractory, elemental in composition (i.e., presents with a low ratio of hydrogen to carbon), and is insoluble in water (and other solvents); organic carbon is that contained in a typically complex mixture of organic compounds, and is generally taken to be the difference between total carbon and black carbon (Turpin and Lim, 2001; Turpin et al., 2000; Kirchstetter et al., 2005). Black carbon has strong absorption with a nearly featureless spectrum. The strong optical absorption by black carbon also means that it can be a minor component of the accumulated dust but still be the dominant source of reflectance change.

Spectral features in absorption by the "soil" layer on a roofing surface can identify contaminants. Fig. 2 shows typical spectral absorption coefficients

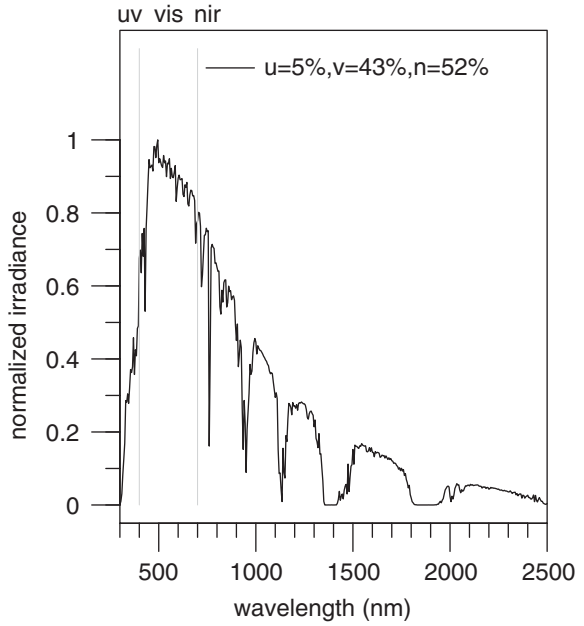

Fig. 1. Air-mass 1.5 global solar spectral irradiance typical of North American insolation (5% ultraviolet, 43% visible, 52% near-infrared) (ASTM, 2003).

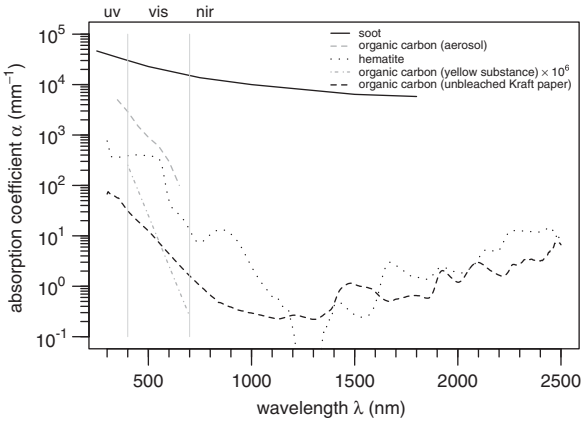

Fig. 2. Typical spectral absorption coefficients $\alpha(\lambda)$ of propane soot (Lindberg et al., 1993), hematite (Levinson et al., 2005c), and three sources of organic carbon: vehicle-exhaust and wood-smoke aerosols (Kirchstetter and Novakov, 2004), organic matter dissolved in seawater ("yellow substance") (Kirchstetter and Novakov, 2004), and unbleached brown Kraft paper. Absorption coefficient values for the yellow substance are multiplied by 10^6 to fit the scale.

of propane soot (Lindberg et al., 1993), an acrylic paint film pigmented with hematite (red iron oxide; mean particle size 0.3 μm; pigment volume concentration 3%) (Levinson et al., 2005c), and three samples of organic carbon. The first specimen of organic carbon was extracted from aerosols, namely vehicle exhaust and wood smoke (Kirchstetter and Novakov, 2004); we converted the absorption efficiency ($m^2\,g^{-1}$) presented in this reference to an absorption coefficient (mm^{-1}) by assuming a nominal density of $1\,g\,cm^{-3}$ for organic carbon. The second specimen was organic matter dissolved in seawater, commonly referred to as "yellow substance" (Kirchstetter and Novakov, 2004). The third specimen was a sheet of unbleached, brown Kraft paper, characterized following the methodology of Levinson et al. (2005b). We obtained a spectral reflectance curve similar to that of the brown Kraft paper when we characterized a brown dead leaf.

Featureless absorption wherein magnitude is inversely proportional to wavelength (declining by about half an order of magnitude between 400 and 1500 nm) signifies the presence of black carbon. Rapid, exponential decay of about two to three orders of magnitude across the visible spectrum is characteristic of absorption by organic carbon. Hematite has strong, uniform absorption in the blue and green spectra (400–600 nm); rapid, roughly exponential decay of absorption between 600 and 1200 nm; and an absorption peak between 800 and 900 nm. The absorption features in the 1300–2500 nm range shown for paper-derived organic carbon and for hematite may originate from vibrations of hydrogen atoms (in groups such as C–H, H_2O, and OH) in the paper and in the polymer binder of the red paint.

The current study examines the effects of exposure and cleaning on the solar spectral reflectances and solar absorptances of 15 initially white or light-gray membrane samples taken from roofs across the United States. Particular attention is paid to spectral characterization of the extents to which various laboratory representations of roof cleaning processes (e.g., rinsing to simulate rain) can reduce light absorption by surface contaminants and thereby increase roof reflectance. Specifically, we seek to answer the following questions:

1. What contaminants reduce the reflectance of the membranes, and by what processes are they removed?
2. To what extent does soiling degrade and cleaning improve the reflectance of a light-colored membrane?
3. How do soiling and cleaning affect the solar heat gain of a light-colored membrane roof?

2. Theory

2.1. Spectral optical depth of soil layer

We consider a very simple optical model for the soil layer. Our goal is to define "spectral optical depth," a parameter that can be used to examine spectral absorption features in soil layers. Since the light-colored membrane substrate is highly reflective (at wavelengths longer than 400 nm), the scattering by the soil layer itself is not expected to have a large effect on the reflectance of the soil/membrane composite. We therefore neglect soil scattering, and focus on the effect of soil absorptance. A more sophisticated optical model, while desirable, would introduce a level of complexity that we wish to avoid in this study.

Consider a flat, uniform, and opaque membrane. An absorbing and nonscattering soil layer of uniform thickness Z_n will have spectral optical depth

$$\tau_n(\lambda) \equiv \int_0^{Z_n} \alpha(z,\lambda)\,dz, \tag{1}$$

where $\alpha(z,\lambda)$ is the soil's spectral absorption coefficient (assumed cross-section invariant) at height z above the membrane's surface. Applying Beer's law (Incropera and DeWitt, 1985), the soil layer has spectral transmittance

$$t_n(\lambda) = \exp[-\eta\,\tau_n(\lambda)], \tag{2}$$

where the average pathlength parameter η, or ratio of light pathlength to layer thickness, is 1 for surface-normal collimated light and 2 for perfectly diffuse light.

The soil layer reduces the spectral reflectance of the membrane by the square of its spectral transmittance. That is, the spectral reflectance of the soiled membrane is

$$r_n(\lambda) = r_0(\lambda)\,\exp[-2\eta\,\tau_n(\lambda)], \tag{3}$$

where $r_0(\lambda)$ is the spectral reflectance of the unsoiled membrane. Rearranging, the spectral optical depth of the soil layer can be estimated from the ratio of the spectral reflectance of the soiled membrane to

that of the unsoiled membrane as

$$\tau_n(\lambda) = -\frac{1}{2\eta} \ln\left[\frac{r_n(\lambda)}{r_0(\lambda)}\right]. \quad (4)$$

If the soil layer is normally illuminated with collimated light and the membrane reflects diffusely, the effective value of η in Eqs. (3) and (4) is $\frac{3}{2}$.

We compute the spectral optical depth $\tau_n(\lambda)$ of the soil layer in each state n to identify soil constituents, and to determine the extents to which these contaminants are removed by each cleaning process. The values of spectral optical depth $\tau_n(\lambda)$ measured in this study should be typical of any light-colored PVC membranes exposed to similar soiling and cleaning processes. However, our assumption that the soil layer is nonscattering may be unsuited to describing the effects of soiling on the spectral and solar reflectances of an initially dark surface. For example, a scattering-induced reflectance rise of several hundredths may represent a large *fractional* increase in the reflectance of a black membrane whose initial reflectance is about 0.05 across the entire solar spectrum. Hence, any model of the effect of soiling on the reflectance of a dark membrane should consider both absorption and scattering in the soil layer.

Nonuniformities in the thickness of the soil layer (e.g., bare patches alternating with heavily soiled spots) tend to attenuate peaks in the spectral optical depth curve (Appendix A; see also Berdahl et al. (2002)). This can mask spectral features that would otherwise identify contaminants. For simplicity, we will not try to quantify the magnitudes of these nonuniformities and their effects on spectral optical depth. However, we will note in our analysis when a soil layer appears particularly nonuniform.

2.2. Effects of cleaning on spectral optical depth

The effects of cleaning on spectral absorption can be gauged by changes in spectral optical depth. Let $n = N$ denote the state of the membrane after soiling, but before cleaning. Consider a sequence of cleaning processes—in this study, wiping, rinsing, washing, and bleaching—that raise the spectral reflectance of the soiled membrane from $r_N(\lambda)$ to $r_{N-1}(\lambda)$, $r_{N-2}(\lambda), \ldots$, and finally $r_1(\lambda)$. We model the cleaning process n that increases the membrane's spectral reflectance from $r_n(\lambda)$ to $r_{n-1}(\lambda)$ as removing a soil sublayer of spectral optical depth

$$\delta\tau_n(\lambda) \equiv \tau_n(\lambda) - \tau_{n-1}(\lambda) = -\frac{1}{2\eta} \ln\left[\frac{r_n(\lambda)}{r_{n-1}(\lambda)}\right]. \quad (5)$$

Spectral features in $\delta\tau_n(\lambda)$ can indicate the removal of specific contaminants, such as black carbon, hematite or organic carbon.

The fraction of the spectral optical depth of the initial soil layer $\tau_N(\lambda)$ remaining in state n is

$$\gamma_n(\lambda) \equiv \tau_n(\lambda)/\tau_N(\lambda). \quad (6)$$

2.3. Effects of soiling and cleaning on solar reflectance and solar heat gain

One measure of the influences of soiling and cleaning on solar reflectance is R_n/R_0, the ratio of a membrane's solar reflectance in state n to that in its unsoiled state 0. The geometric relationship among the spectral reflectances of the unsoiled, soiled, and cleaned membranes generally precludes any simple theoretical relationship among their solar reflectances (Appendix B). Hence, the solar reflectance ratio R_n/R_0 is just an empirical measure of cleanliness, equalling one when the membrane is unsoiled, and approaching zero when the membrane is covered with an opaque, nonscattering soil layer. (We note that the first-surface reflectance induced by the passage of light from air [real refractive index 1] to the soil layer [real refractive index >1] will prevent R_n and hence the ratio R_n/R_0 from equalling zero (Levinson et al., 2005b).)

Since the solar heat gain of an opaque surface is proportional to its solar absorptance (1 − solar reflectance), the influence of membrane cleaning on building heat gain is better gauged by fractional variations in solar absorptance than by those in solar reflectance. For example, a cleaning process that raises solar reflectance from 0.8 to 0.9 increases solar reflectance by only one part in eight, but decreases solar absorptance and hence solar heat gain by a factor of two. Two particularly useful metrics for evaluating the influences of soiling and cleaning on building energetics are (a) solar absorptance, A_n; and (b) the ratio A_n/A_0 of solar absorptance in state n to solar absorptance in the unsoiled state. The latter indicates the factor by which the roof's solar heat gain has increased.

3. Experiment

3.1. Roofing membrane samples

Soiled and unsoiled light-colored, single-ply PVC membrane samples were taken from 15 five-to-eight-year-old low-slope roofs, all in good

Table 1
Sources and ages of 15 membrane samples taken from light-colored, low-slope PVC membrane roofs in 10 US cities

Sample	City	Building	Years exposed
1	Springfield, MA	Building a	5
2	Springfield, MA	Building b	6
3	Lancaster, OH	Building c	6
4	Heath, OH	Building d	6
5	West Hampton, NJ	Building e	6
6	West Hampton, NJ	Building f	8
7	Plantation, FL	Building g	6
8	Plantation, FL	Building g	6
9	Gardena, CA	Building h	5
10	Gardena, CA	Building h	6
11	Solano Beach, CA	Building i	8
12	Solano Beach, CA	Building i	8
13	Alpharetta, GA	Building j	6
14	Bethesda, MD	Building k	6
15	Fredericksburg, VA	Building l	5

mechanical condition, covering 12 buildings in 10 US cities in eight states (Table 1). Since roofs were chosen based on availability for sampling, the soiling experienced by these samples may or may not be representative of that experienced by any larger population of roofs. All membranes were manufactured by the same firm. At least one 0.5 m^2 membrane sample containing a membrane seam (hot-air welded overlap) was removed from each roof. The non-welded area of the flap on the underside of a seam served as the unexposed, ''unsoiled'' surface (Fig. 3).

3.2. Reflectance measurements

Small coupons (4 cm × 4 cm) were extracted from a representative portion of each unsoiled sample and a heavily soiled portion of each soiled sample. The near-normal-hemispherical solar spectral reflectance (300–2500 nm @ 5-nm intervals; hereafter, simply ''spectral reflectance'') and corresponding reflectance to air-mass 1.5 global solar radiation (ASTM, 2003) (hereafter, simply ''solar reflectance'') of a 10 mm^2 area at the center of each coupon were measured via ASTM Standard E903 (ASTM, 1996) using a PerkinElmer Lambda 900 UV/Visible/NIR Spectrometer with Labsphere 150-mm Integrating Sphere. The surface-average solar reflectance of each membrane was estimated as the mean of ASTM Standard C1549 air-mass 1.5 solar reflectances (ASTM, 2002) measured with a Devices & Services Solar Spectrum Reflectometer (model SSR-ER) at several 2.5-cm diameter spots (five per soiled membrane, three per unsoiled membrane) over a 17 cm × 17 cm area.

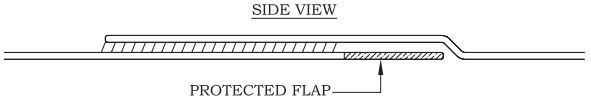

Fig. 3. Side view of a membrane sample containing a seam. The ''soiled'' coupon was extracted from the exposed top layer, while the ''unsoiled'' coupon was taken from the unexposed underside of the seam.

3.3. Cleaning

The spectral reflectance of each soiled coupon was remeasured followed each of four sequential laboratory processes—wiping, rinsing, washing, and bleaching—intended to simulate various natural and artificial cleaning mechanisms (Table 2). Each cleaning technique was applied vigorously until the appearance of the membrane stabilized. This yielded six states of exposure for each membrane: (5) soiled; (4) soiled and wiped; (3) soiled, wiped, and rinsed; (2) soiled, wiped, rinsed, and washed; (1) soiled, wiped, rinsed, washed, and bleached; and (0) unsoiled. For brevity, each state is named by its final condition—i.e., soiled, wiped, rinsed, washed, bleached, or unsoiled.

We note again that the unsoiled sample was extracted from the underside of the seam and was neither exposed nor cleaned.

4. Results

4.1. Presence and removal of soil-layer contaminants

The sample images in Fig. 4a,b suggest that the soil layer includes (a) loosely bound material that can be wiped off, as seen on soiled sample 13; (b) tightly bound material (possibly the same) that can be removed by rinsing or washing, such as that remaining on wiped sample 13; and (c) biological growth, possibly fungi or dead algae, that is especially visible on samples 7, 8, and 11, and that disappears entirely only after the application of bleach.

The measured spectral reflectances $r_n(\lambda)$ of the 15 samples in each of the six states—soiled, wiped, rinsed, washed, bleached, and unsoiled—are charted

Table 2
Laboratory simulations of roof cleaning processes

Procedure	Laboratory technique	Mechanism(s) simulated
Wiping	Wiping with dry cloth	Wind, sweeping
Rinsing	Rinsing with running water; air drying	Rain
Washing	Scrubbing with phosphate-free dishwashing detergent and water; air drying	Washing with detergent
Bleaching	Scrubbing with bleach-based algae cleaner (solution of sodium hypochlorite and sodium hydroxide) and water; air drying	Washing with algae cleaner

in Fig. 5. Analogous graphs of spectral reflectance ratio $r_n(\lambda)/r_0(\lambda)$, spectral optical depth $\tau_n(\lambda)$, and optical depth fraction $\gamma_n(\lambda) \equiv \tau_n(\lambda)/\tau_N(\lambda)$ are shown in Figs. 6–8. The spectral optical depths $\delta\tau_n(\lambda) \equiv \tau_n(\lambda) - \tau_{n-1}(\lambda)$ of sublayers removed by each process are shown in Fig. 9.

In their soiled states, the optical depth curves of all samples except 5 and 6 exhibit the broad, slowly declining absorption spectrum characteristic of black carbon, decreasing by a factor of about two from 400 to 1500 nm (Fig. 7). The swifter spectral decline in the optical depths of soiled samples 5 and 6 (decreasing by a factor of 20 over the same range), coupled with the presence of dark spots (biomass) on their surfaces, suggests that they are coated primarily with organic carbon. We rule out hematite as the dominant contaminant on samples 5 and 6 because no strong absorption peak is seen in the range 800–900 nm.

Again excepting samples 5 and 6, wiping removed a sublayer of black carbon from each membrane, as indicated by the broad, slowly declining spectra of the optical depth reductions induced by wiping (Fig. 9). However, black carbon remained on all wiped samples except 3, 10, 5, and 6. Wiping appears to have removed the black carbon from samples 3 and 10, leaving behind only organic carbon (compare to the optical depth spectra of soiled samples 5 and 6).

Rinsing removed much of the remaining black carbon from samples 7, 8, 9, 11, and 15, but little black carbon from samples 1, 2, 4, 12, 13, and 14. Very weak absorption at wavelengths longer than 1500 nm indicate that washing removed the remaining black carbon from all samples but 2, 4, 7 and 12. The optical depths of washed samples 12, 14, and 15 increased with wavelength in the near-infrared, suggesting that the washing process may have left a residue.

Samples 5–12 are each covered to various extents by biomass. The images indicate that wiping and rinsing each removed some of the growth. While wiping was not particularly effective, rinsing removed about half of the biomass present on wiped samples 7, 8, 11, and 12, and washing removed nearly all of the biomass remaining on those samples. Bleaching was required to clear isolated dark spots of growth remaining on samples 5–9 and 11–12. We note that bleach does not actually remove biomass, but instead renders colorless the light-absorbing chromophores in organic material.

4.2. Effects of soiling and cleaning on reflectance

Soiling attenuated the reflectance of membranes more strongly at shorter wavelengths, consistent with the absorption spectra of black carbon and organic carbon (Fig. 2). The reflectance ratios $r_n(\lambda)/r_0(\lambda)$ of soiled samples covered with biomass (e.g., 7, 8, and 11) were about 0.3 in the visible spectrum, and 0.3–0.8 in the near-infrared. The ratios for samples not covered with biomass were typically 0.6–0.8 in the visible, and 0.8–0.9 in the near-infrared (Fig. 6).

Gauging by the optical depth fractions $\gamma_n(\lambda)$ shown in Fig. 8, wiping was a highly effective cleaning process on biomass-free membranes. In the 300–1500 nm spectrum bearing 90% of the power in ground-level sunlight (Fig. 1), wiping removed about 50–80% of the initial optical depth $\tau_N(\lambda)$ on biomass-free samples. Wiping removed about 20–40% of the initial optical depth in that spectrum on biomass-covered samples 7, 8, and 11, and only about 10% on samples 5 and 6, which appear to

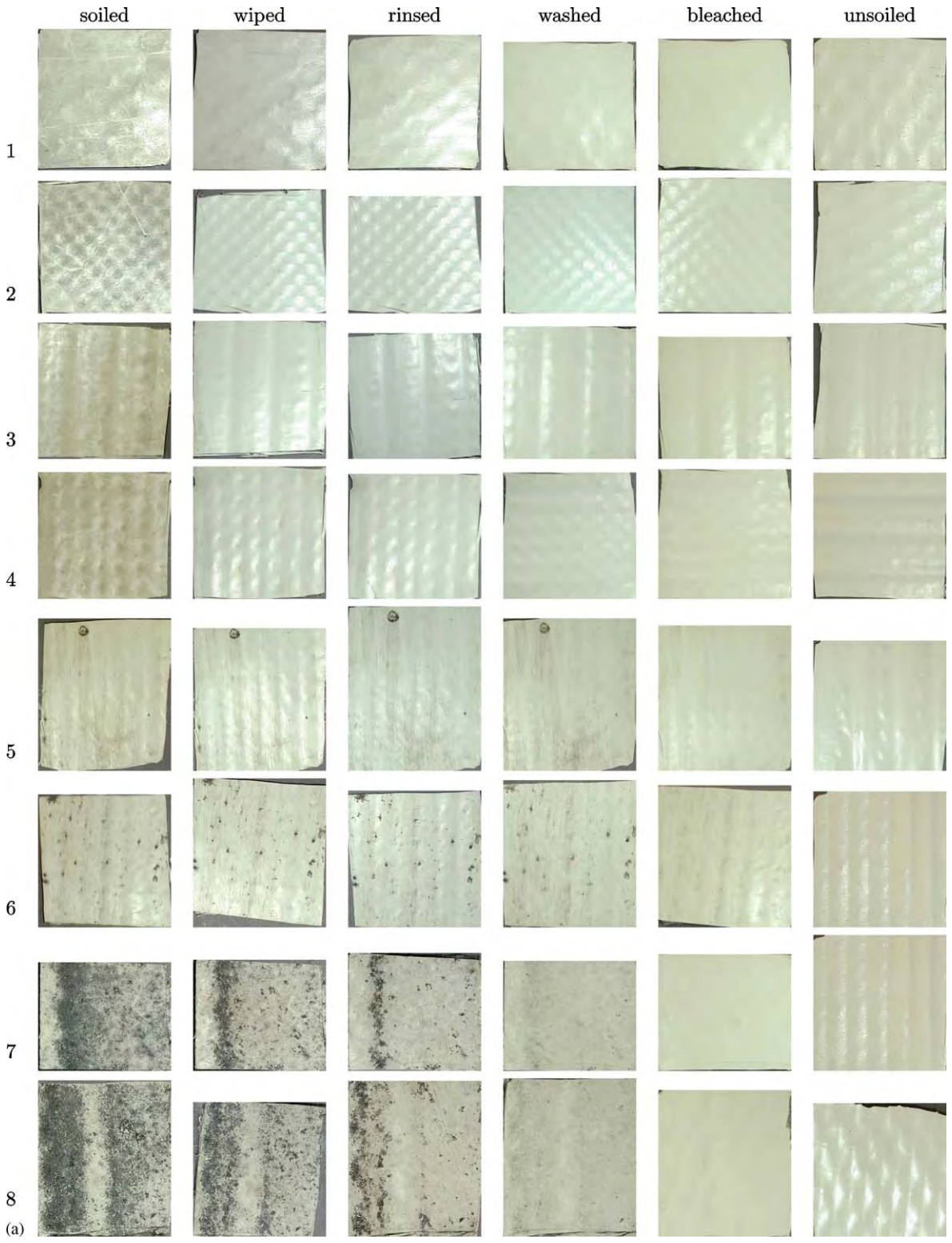

Fig. 4. Images of coupons from (a) membranes 1–8 and (b) membranes 9–15 in their soiled, wiped, rinsed, washed, bleached, and unsoiled states.

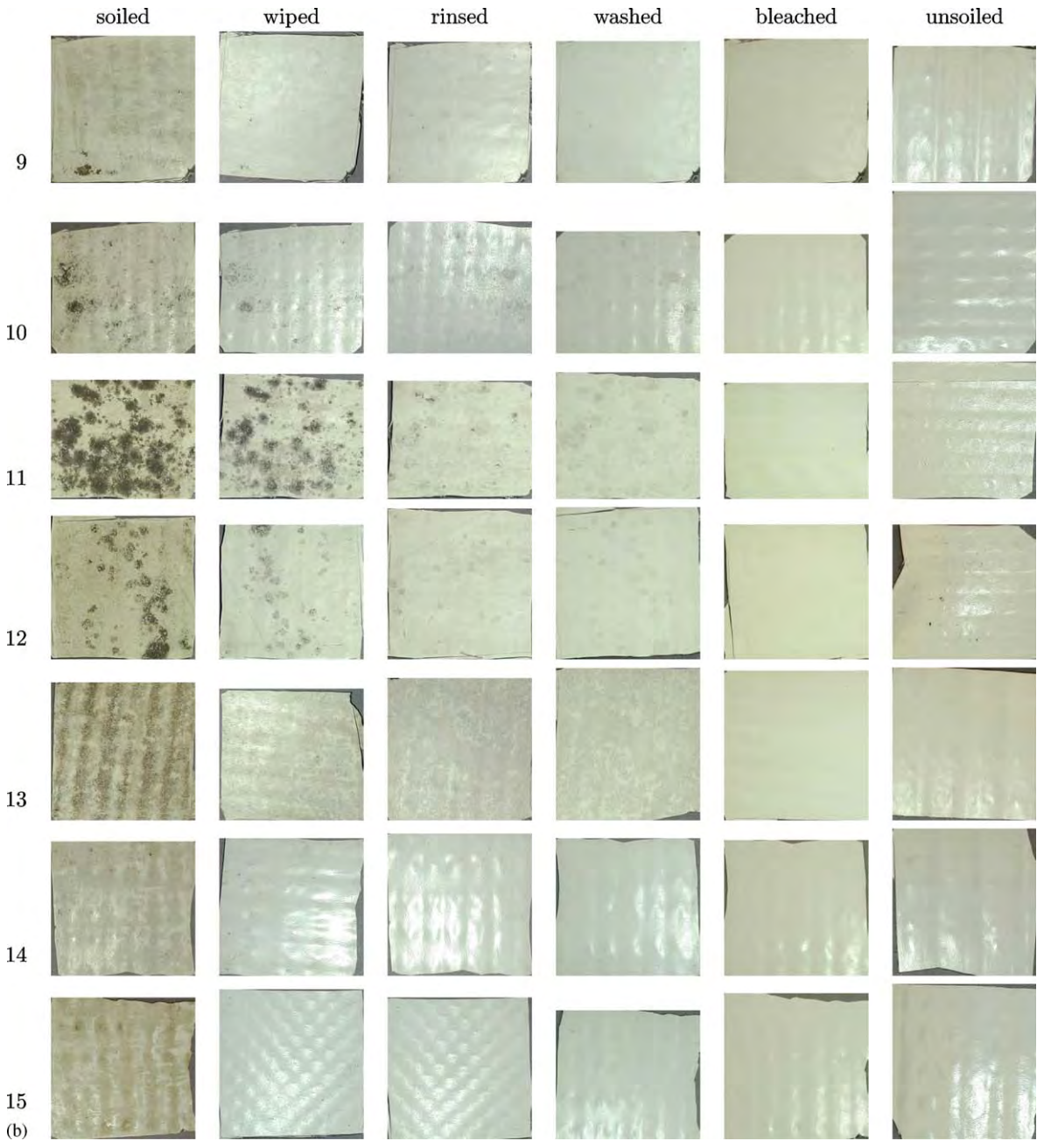

Fig. 4. (*Continued*)

have been covered with a thin layer of organic carbon.

Rinsing and washing were very effective on biomass-covered samples 7, 8, and 11, removing another 10–50% and 10–25% (respectively) of the initial optical depth $\tau_N(\lambda)$ in the 300–1500 nm spectrum. Washing and/or rinsing removed most of the remaining soil on all samples other than 5 and 6. On these two lightly soiled samples, bleaching was much more effective than wiping, rinsing, or washing.

The effect of bleaching on reflectance is largest at short wavelengths (like the effect of the black carbon), diminishing at wavelengths greater than

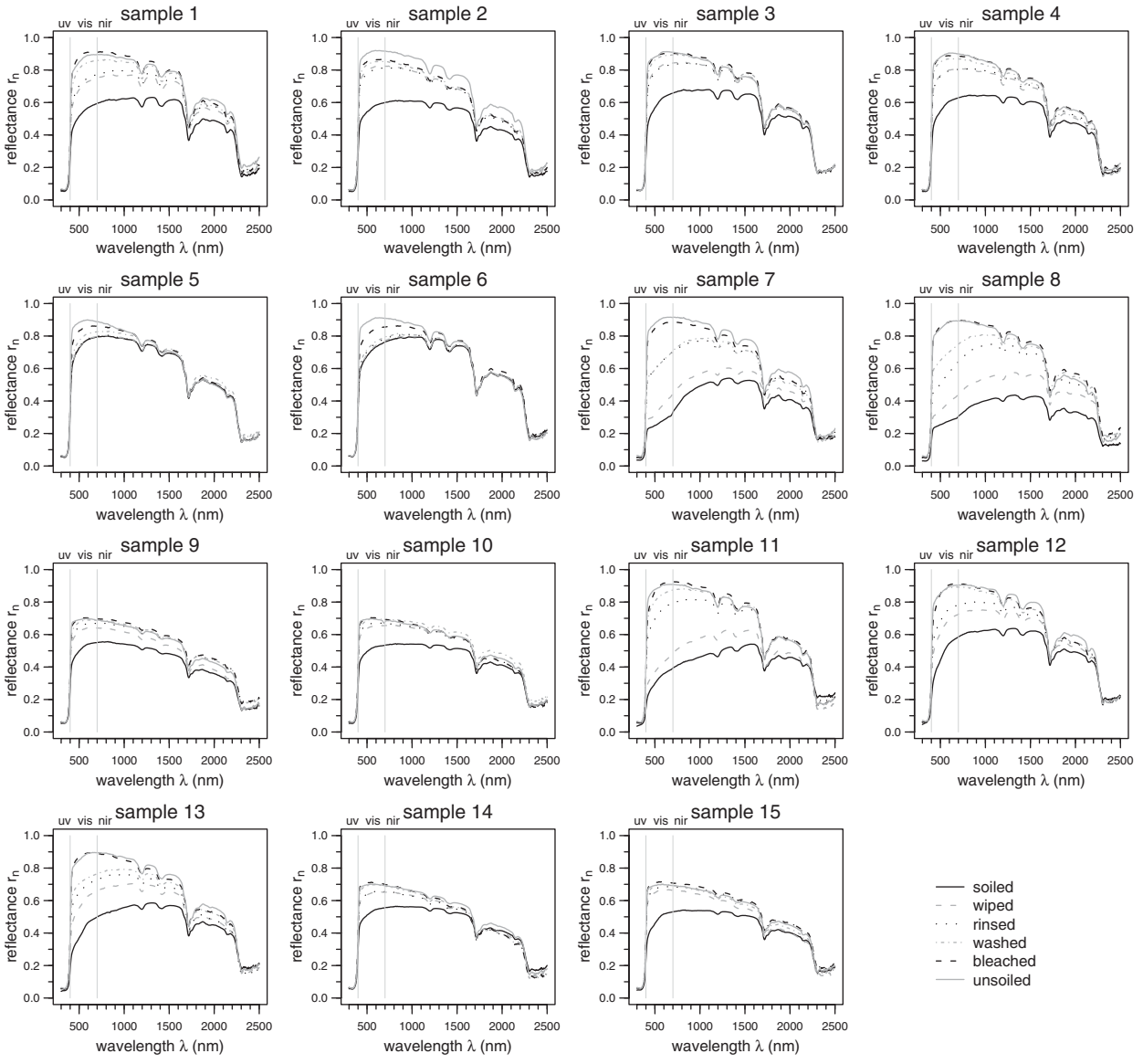

Fig. 5. Spectral reflectances $r_n(\lambda)$ of 15 membranes in their soiled, wiped, rinsed, washed, bleached, and unsoiled states.

1200 nm. After wiping, rinsing, washing, and bleaching, the optical depth of the remaining soil layer was negligible on all samples.

The ratio of solar reflectance to unsoiled solar reflectance, R_n/R_0, ranged from 0.41 to 0.89 for the soiled samples; 0.53 to 0.95 for the wiped samples; 0.74 to 0.98 for the rinsed samples; 0.79 to 1.00 for the washed samples; and 0.94 to 1.02 for the bleached samples (Table 3). In the soiled and wiped states, the solar reflectance ratios of the biomass-covered samples (7, 8, and 11) were significantly lower than those of the other samples. Washing closed most of the gap; after bleaching, the influence of the initial biomass cover vanished.

4.3. Effects of soiling and cleaning on solar heat gain

The solar absorptances A_n and ratios A_n/A_0 of solar absorptance to unsoiled solar absorptance of the 15 samples in each state are presented in Tables 4 and 5, respectively. The latter metric, indicating solar heat gain relative to that of an

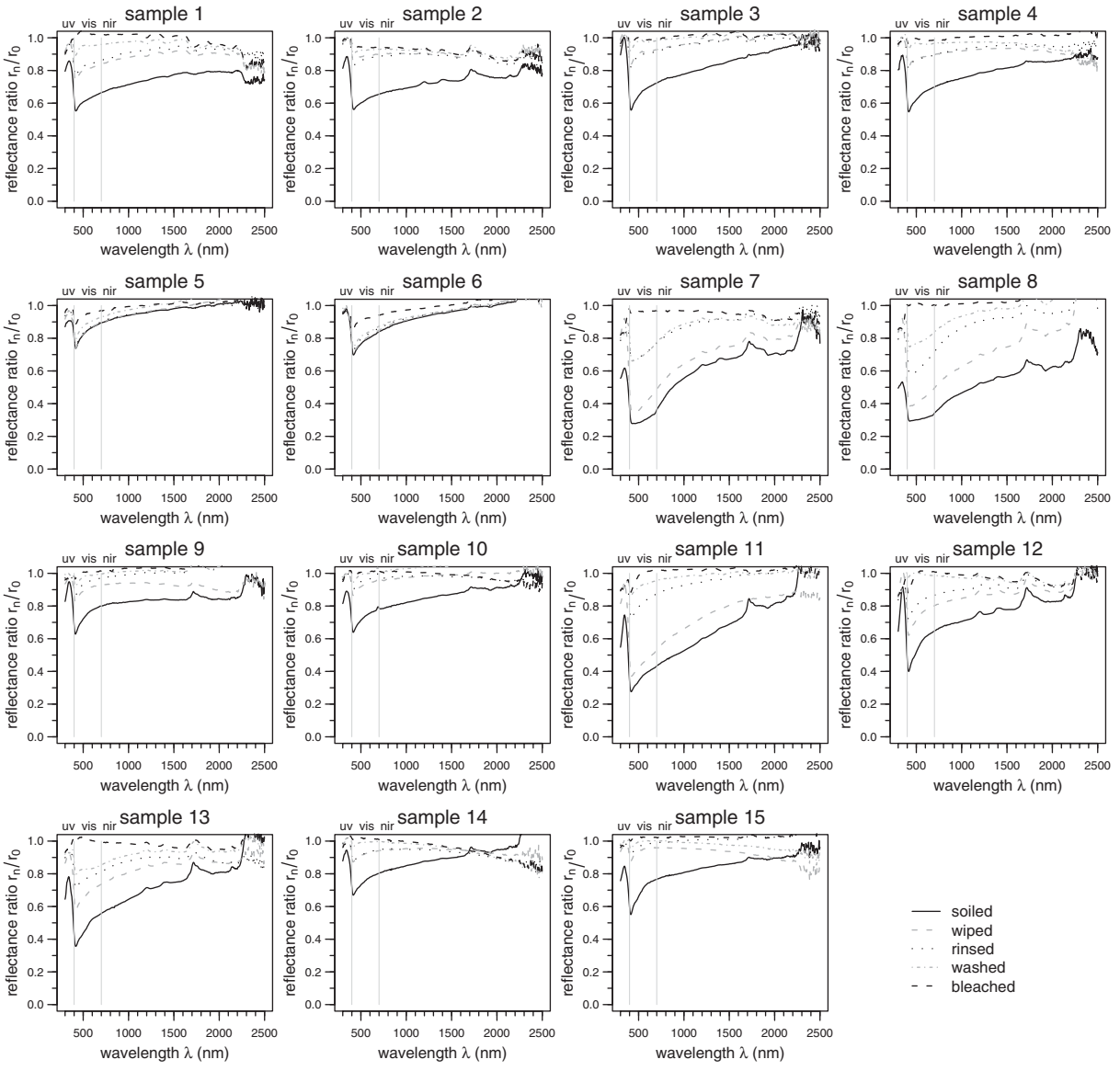

Fig. 6. Ratios $r_n(\lambda)/r_0(\lambda)$ of the spectral reflectances of 15 membranes in their soiled, wiped, rinsed, washed, and bleached states to their spectral reflectances in their unsoiled states.

unsoiled membrane, ranged from 1.4 to 3.5 for the soiled samples; 1.1 to 3.1 for the wiped samples; 1.0 to 2.0 for the rinsed samples; 1.0 to 1.9 for the washed samples; and 0.9 to 1.3 for the bleached samples.

5. Discussion

Black carbon and organic carbon were the two identifiable absorbing contaminants on the membranes. Wiping was effective at removing black carbon (a strong absorber) and less so at removing organic carbon (a weaker absorber). Rinsing and/or washing removed nearly all of the remaining soil layer, with the exceptions of (a) thin layers of organic carbon and (b) isolated dark spots of biomass. Bleach was required to clear the last two features.

Peaks in the measured spectral optical depth of a soil layer may be attenuated by variations in the

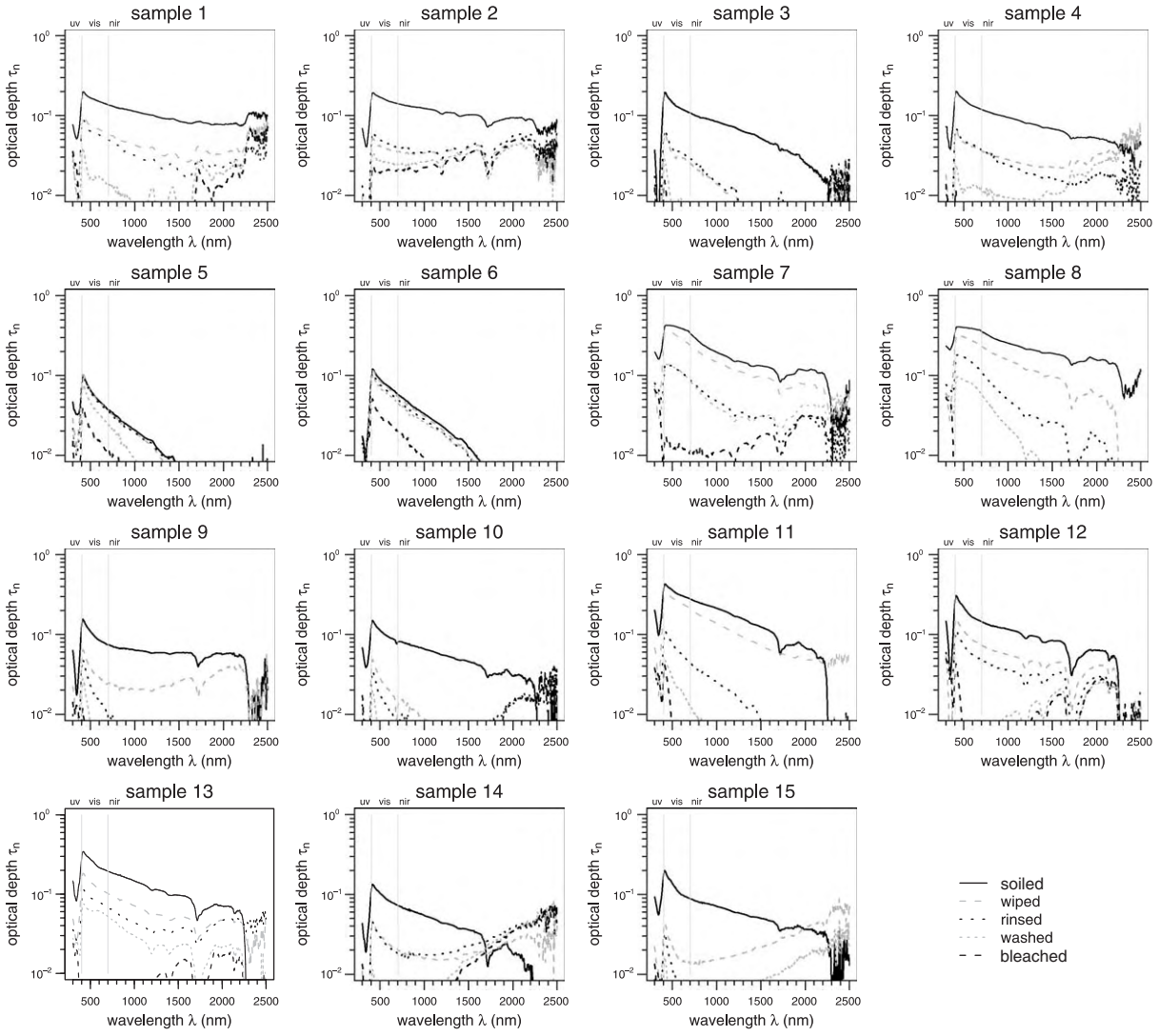

Fig. 7. Spectral optical depths $\tau_n(\lambda)$ of soil layers present on the 15 membranes in their soiled, wiped, rinsed, washed, and bleached states.

layer thickness (Appendix A). However, with the exception of a few visible-spectrum optical depths of up to 0.3 for the most heavily (but non-uniformly) soiled samples (7, 8, and 11), the measured optical depths in the visible and near-infrared spectra were generally too small (typically not exceeding order 0.1) to be significantly affected by this phenomenon (cf. Fig. A.1).

The solar reflectance of a light-colored membrane thickly coated with black carbon and/or biomass to the point where it appears brown or black can drop to about half that of the unsoiled membrane. Wiping restores some of the initial reflectance, but rinsing and/or washing are more effective. Bleaching can remove aesthetically undesirable dark spots, but in most cases does not greatly increase the solar reflectance of a washed roof.

The spectral optical depth fractions $\gamma(\lambda)$ in each state varied too much from sample to sample (e.g., compare wiped samples 1, 6, 7 and 10 in Fig. 8) to expect this property to have a particular spectral shape for each cleaning technique. This is unsurprising, since the efficacy of a cleaning process depends on the nature of the contaminants, and on how tightly they are bound to the membrane. Hence, we do not expect to be able to

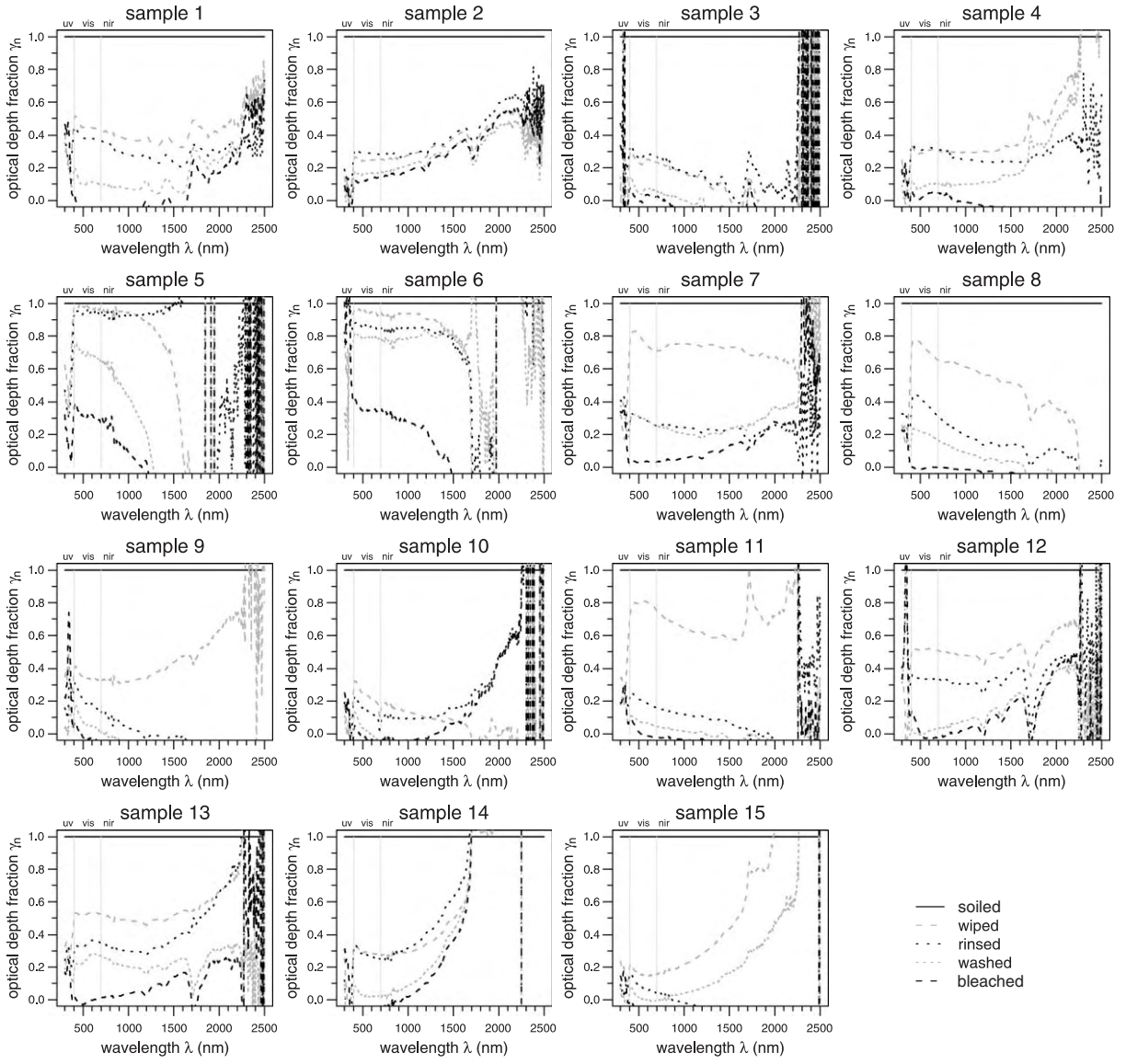

Fig. 8. Fractions $\gamma_n(\lambda)$ of the initial soil layer's spectral optical depth remaining on each of the 15 membranes in their soiled, wiped, rinsed, washed, and bleached states.

predict the spectral reflectance of a cleaned membrane from its spectral reflectances in its soiled and unsoiled states.

Solar absorptance ratio, rather than solar reflectance ratio, is the proper indicator of the effects of soiling and cleaning on roof heat gain. Since the solar absorptance of an unsoiled white roof is typically about 0.2, heavy soiling can easily triple its solar absorptance, and hence triple its solar gain. For example, the soiled, wiped, rinsed, washed, and bleached solar absorptance ratios of biomass-laden sample 7 (unsoiled solar absorptance 0.18) are 3.5, 3.1, 2.0, 1.9, and 1.2, respectively. Thus even after washing, the membrane's solar gain is 90% higher than in its unsoiled state.

We note that the solar absorptance of the most heavily soiled membrane (sample 8; soiled solar absorptance 0.68) is still much lower than that of a clean black membrane (about 0.95).

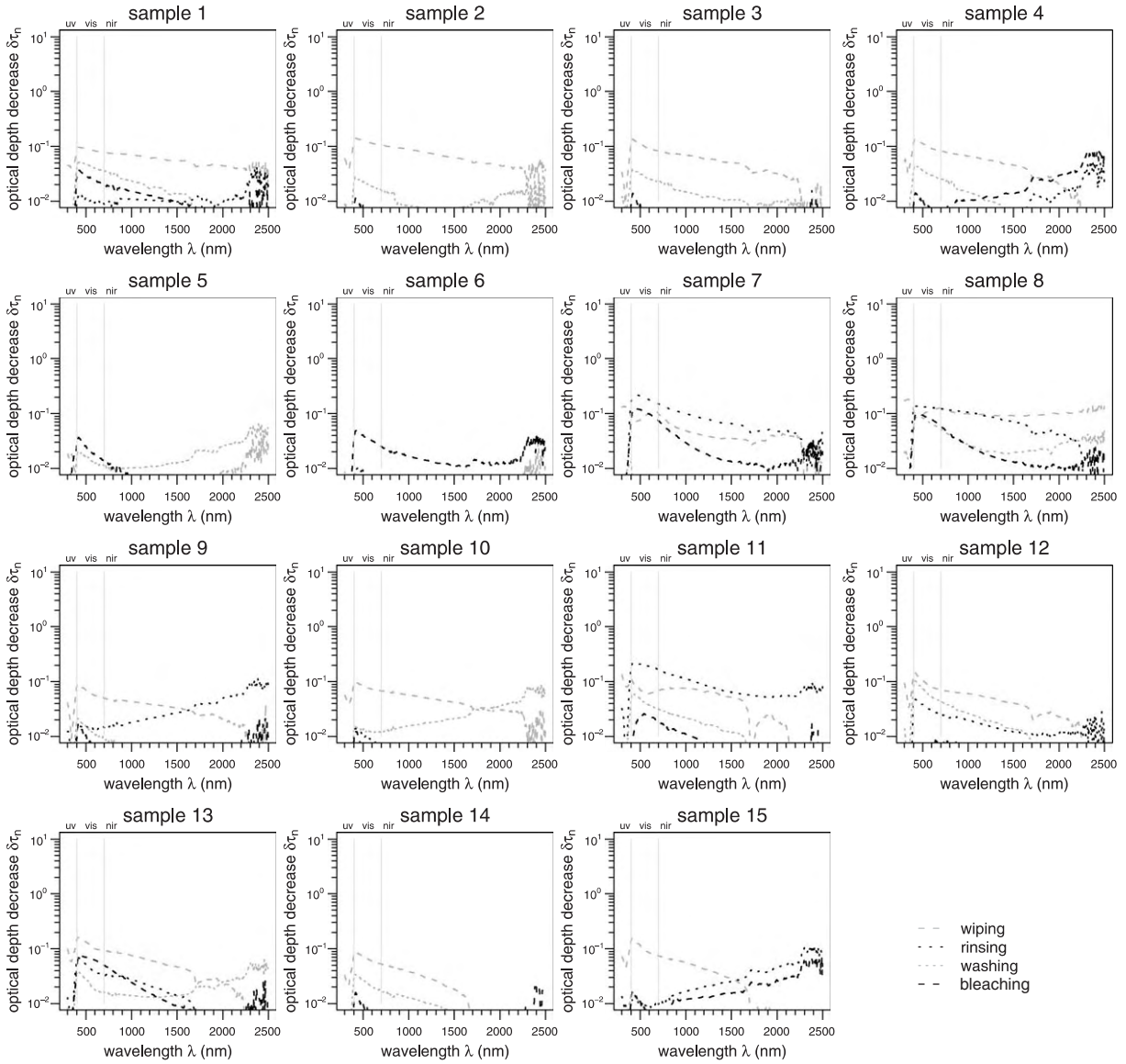

Fig. 9. Absolute reductions $\delta\tau_n(\lambda)$ in soil-layer spectral optical depth on the 15 membranes achieved by wiping, rinsing, washing, and bleaching.

6. Conclusions

Black carbon and to a lesser extent organic carbon significantly reduced the solar spectral reflectances of 15 light-colored PVC membrane samples taken from roofs across the United States. Wiping removed much of the black carbon, but was less effective at removing the (relatively weakly absorbing) organic carbon. Rinsing and/or washing removed nearly all of the remaining soil layer, though bleach was required to clear isolated dark spots of biomass. The ratio of solar reflectance to unsoiled solar reflectance (a measure of cleanliness) ranged from 0.41 to 0.89 for the soiled samples; 0.53 to 0.95 for the wiped samples; 0.74 to 0.98 for the rinsed samples; 0.79 to 1.00 for the washed samples; and 0.94 to 1.02 for the bleached samples.

The influences of membrane soiling and cleaning on roof heat gain are better gauged by fractional

Table 3
Solar reflectance R_0 of unsoiled membranes and solar reflectance ratio R_n/R_0 of membranes in each exposure state n. All solar reflectances in this table were measured via ASTM Standard E903

Sample	Solar reflectance R_0	Solar reflectance ratio R_n/R_0					
	Unsoiled	Soiled	Wiped	Rinsed	Washed	Bleached	Unsoiled
1	0.80	0.68	0.85	0.87	0.96	1.02	1.00
2	0.82	0.67	0.90	0.88	0.93	0.94	1.00
3	0.81	0.73	0.93	0.92	0.99	1.00	1.00
4	0.80	0.71	0.90	0.90	0.97	0.99	1.00
5	0.79	0.89	0.89	0.89	0.93	0.97	1.00
6	0.81	0.85	0.85	0.87	0.88	0.94	1.00
7	0.82	0.43	0.53	0.79	0.79	0.96	1.00
8	0.79	0.41	0.53	0.74	0.86	1.01	1.00
9	0.63	0.79	0.92	0.95	0.98	1.00	1.00
10	0.63	0.78	0.95	0.97	1.00	1.01	1.00
11	0.81	0.46	0.58	0.88	0.96	1.00	1.00
12	0.81	0.64	0.80	0.86	0.99	0.99	1.00
13	0.80	0.57	0.75	0.83	0.87	0.99	1.00
14	0.63	0.79	0.94	0.94	0.99	1.01	1.00
15	0.63	0.76	0.95	0.98	1.00	1.02	1.00

Table 4
Membrane solar absorptances A_n in each exposure state n based on solar reflectances measured via ASTM Standards E903 and C1549. E903 absorptances were measured at the dirtiest spot on the membrane and were thus generally higher than the C1549 values, which are averages of measurements made at three to five locations

Sample	C1549 Unsoiled	±	C1549 Soiled	±	E903 Soiled	E903 Wiped	E903 Rinsed	E903 Washed	E903 Bleached	E903 Unsoiled
1	0.19	0.01	0.39	0.05	0.46	0.32	0.30	0.23	0.18	0.20
2	0.16	0.00	0.37	0.04	0.45	0.27	0.28	0.24	0.23	0.18
3	0.16	0.00	0.39	0.00	0.41	0.24	0.25	0.20	0.19	0.19
4	0.19	0.01	0.39	0.04	0.43	0.28	0.28	0.22	0.21	0.20
5	0.19	0.00	0.23	0.02	0.29	0.29	0.29	0.27	0.23	0.21
6	0.16	0.00	0.21	0.04	0.31	0.31	0.29	0.28	0.23	0.19
7	0.17	0.00	0.48	0.12	0.65	0.57	0.36	0.35	0.21	0.18
8	0.17	0.01	0.46	0.11	0.68	0.58	0.41	0.32	0.20	0.21
9	0.35	0.00	0.53	0.09	0.50	0.42	0.40	0.38	0.37	0.37
10	0.34	0.00	0.47	0.01	0.51	0.40	0.39	0.37	0.37	0.37
11	0.17	0.00	0.52	0.05	0.62	0.53	0.29	0.22	0.18	0.19
12	0.16	0.01	0.47	0.09	0.48	0.35	0.31	0.20	0.20	0.19
13	0.17	0.00	0.52	0.04	0.55	0.41	0.34	0.31	0.21	0.20
14	0.34	0.00	0.49	0.03	0.50	0.41	0.41	0.37	0.36	0.37
15	0.34	0.00	0.51	0.03	0.52	0.40	0.38	0.37	0.36	0.37

variations in solar absorptance. Solar absorptance ratios (indicating solar heat gain relative to that of an unsoiled membrane) ranged from 1.4 to 3.5 for the soiled samples; 1.1 to 3.1 for the wiped samples; 1.0 to 2.0 for the rinsed samples; 1.0 to 1.9 for the washed samples; and 0.9 to 1.3 for the bleached samples.

Further research is required to quantify the effects of soiling and cleaning on the solar spectral reflectances of *dark* roofing surfaces.

Table 5
Ratio A_n/A_0 of solar absorptance in exposure state n to unsoiled solar absorptance, based on membrane solar reflectances measured via ASTM Standard E903

Sample	Soiled	Wiped	Rinsed	Washed	Bleached	Unsoiled
1	2.3	1.6	1.5	1.2	0.9	1.0
2	2.5	1.5	1.5	1.3	1.3	1.0
3	2.2	1.3	1.3	1.1	1.0	1.0
4	2.2	1.4	1.4	1.1	1.0	1.0
5	1.4	1.4	1.4	1.3	1.1	1.0
6	1.7	1.6	1.6	1.5	1.2	1.0
7	3.5	3.1	2.0	1.9	1.2	1.0
8	3.3	2.8	2.0	1.5	1.0	1.0
9	1.4	1.1	1.1	1.0	1.0	1.0
10	1.4	1.1	1.1	1.0	1.0	1.0
11	3.3	2.8	1.5	1.2	1.0	1.0
12	2.5	1.8	1.6	1.1	1.0	1.0
13	2.7	2.0	1.7	1.5	1.0	1.0
14	1.4	1.1	1.1	1.0	1.0	1.0
15	1.4	1.1	1.0	1.0	1.0	1.0

Acknowledgements

This work was supported by Sarnafil Incorporated, and by the Assistant Secretary for Renewable Energy under Contract No. DE-AC03-76SF00098. We would like to thank Stanley Graveline and Kevin Foley of Sarnafil and Thomas Kirchstetter of Lawrence Berkeley National Laboratory for their technical assistance.

Appendix A. Attenuation of features in spectral optical depth of soil layer by spatial variations in thickness

The spatial mean reflectance of a membrane soiled by a layer with nonuniform thickness of mean value Z_n will always exceed than that of the same membrane soiled by a layer of uniform thickness Z_n. To see this, consider a membrane half covered by a soil layer of thickness $Z_n - \delta Z$, and half covered by a soil layer of thickness $Z_n + \delta Z$. If the soil has a spatially invariant spectral absorption coefficient $\alpha(\lambda)$, the spatial mean reflectance of the nonuniformly soiled membrane (superscript prime) will be

$$r'_n(\lambda) = r_0(\lambda)\,(0.5\,\exp[-2\eta\,\alpha\,(\lambda)\,(Z_n - \delta Z)] + 0.5\,\exp[-2\eta\alpha(\lambda)\,(Z_n + \delta Z)]). \quad (A.1)$$

The reflectance of a membrane soiled with a layer of uniform thickness Z_n is

$$r_n(\lambda) = r_0\,(\lambda)\,\exp[-2\eta\,\alpha\,(\lambda)\,Z_n]. \quad (A.2)$$

For any $\delta Z > 0$,

$$\frac{r'_n(\lambda)}{r_n(\lambda)} = \cosh\,[2\eta\,\alpha\,(\lambda)\,\delta Z] > 1. \quad (A.3)$$

Applying Eq. (4), the change in optical depth induced by nonuniformity is

$$\tau'_n(\lambda) - \tau_n(\lambda) = -\frac{1}{2\eta}\ln\left[\frac{r'_n(\lambda)}{r_n(\lambda)}\right] = -\frac{1}{2\eta}\ln\cosh[2\eta\,\alpha\,(\lambda)\,\delta Z] < 0. \quad (A.4)$$

Hence, nonuniform soil layer thickness decreases spectral optical depth. This effect grows stronger as the spectral absorption coefficient $\alpha(\lambda)$ rises, attenuating peaks in the spectral absorption curve.

One particularly interesting case is that of an otherwise uniform soil layer with holes. Consider a nonuniform layer of mean thickness Z_n that covers a fraction f of the membrane with thickness Z_n/f and leaves the rest of the membrane bare. If the spectral optical depth of a soil layer of the same composition and uniform thickness Z_n is $\tau_n(\lambda)$, the spectral optical depth of the nonuniform layer—i.e, that computed from its spectral mean reflectance via Eq. (4)—will be

$$\tau'_n(\lambda) = -\frac{1}{2\eta}\ln([1-f] + f\,\exp[-2\eta\,\tau_n\,(\lambda)/f]). \quad (A.5)$$

The holes in the soil layer act as a low-pass filter on spectral optical depth. That is, when the spectral optical depth $\tau_n(\lambda)$ of the uniform layer is small, the spectral optical depth $\tau'_n(\lambda)$ of the nonuniform layer is close to that of the uniform layer; when $\tau_n(\lambda)$ is large, $\tau'_n(\lambda)$ saturates at a much lower value (Fig. A.1).

Appendix B. Predicting solar reflectance of a cleaned membrane

The solar reflectance R of a surface with spectral reflectance $r(\lambda)$ is

$$R = I^{-1}\int_{\infty}^{0} i(\lambda)\,r(\lambda)\,\mathrm{d}\lambda, \quad (B.1)$$

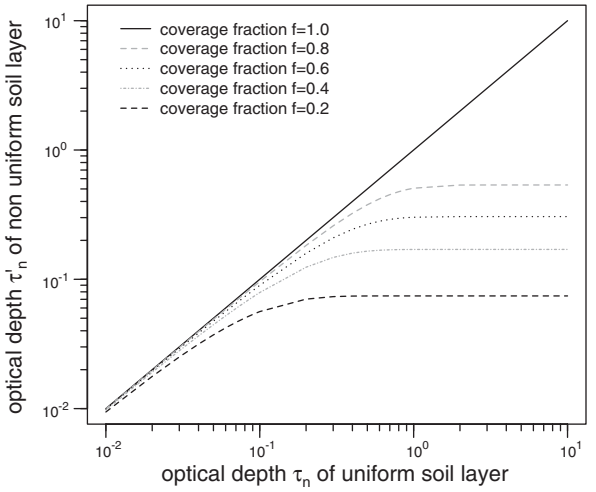

Fig. A.1. Variation with coverage fraction f of the optical depth τ'_n of a nonuniform soil layer vs. optical depth τ_n of a uniform soil layer of the same composition and equal mean thickness.

where $i(\lambda)$ is solar spectral irradiance (power per unit area per unit wavelength; see Fig. 1), and

$$I \equiv \int_{\infty}^{0} i(\lambda)\,\mathrm{d}\lambda \tag{B.2}$$

is solar irradiance (power per unit area). A *linear* relationship among the observed spectral reflectances of the cleaned, soiled, and unsoiled membranes will propagate to their solar reflectances. That is, if

$$r_n(\lambda) = c_1 r_0(\lambda) + c_2 r_N(\lambda), \tag{B.3}$$

then it follows from Eq. (B.1) that

$$R_n = c_1 R_0 + c_2 R_N. \tag{B.4}$$

However, should the observed spectral reflectances of the cleaned, soiled, and unsoiled samples exhibit a *nonlinear* relationship, their corresponding solar reflectances will lack any obvious closed-form relationship unless the spectral reflectances are constant. The relationship among the spectral reflectances derived from a Beer's law model of exponential light attenuation [cf. Eq. (3)] is geometric:

$$r_n(\lambda) = [r_0(\lambda)]^{\{1-\gamma_n(\lambda)\}} \times [r_N(\lambda)]^{\gamma_n(\lambda)}, \tag{B.5}$$

where spectral optical depth fraction $\gamma_n(\lambda) \equiv \tau_n(\lambda)/\tau_N(\lambda)$. Hence, we do not expect to find a closed-form relationship among the *solar* reflectances of the cleaned, soiled, and unsoiled membranes.

References

Abkari, H., 1998. Cool roofs save energy. ASHRAE Transactions 104 (1B), 783–788.

Akbari, H., Konopacki, S.J., 1998. The impact of reflectivity and emissivity of roofs on building cooling and heating energy use. In: Proceedings of the Thermal Performance of the Exterior Envelopes of Building, vol. VII, Clearwater Beach, FL, 6–8 December.

Akbari, H., Konopacki, S., Pomerantz, M., 1999. Cooling energy savings potential of reflective roofs for residential and commercial buildings in the United States. Energy 24, 391–407.

ASTM, 1996. ASTM E 903-96: standard test method for solar absorptance, reflectance, and transmittance of materials using integrating spheres. Technical Report, American Society for Testing and Materials.

ASTM, 2002. ASTM C 1549-02: standard test method for determination of solar reflectance near ambient temperature using a portable solar reflectometer. Technical Report, American Society for Testing and Materials.

ASTM, 2003. ASTM G 173-03: standard tables for reference solar spectral irradiance at air mass 1.5: direct normal and hemispherical on 37° tilted surface. Technical Report, American Society for Testing and Materials.

Berdahl, P., Akbari, H., Rose, L.S., 2002. Aging of reflective roofs: soot deposition. Applied Optics 41 (12), 2355–2360.

CEC, 2005. Building Energy Efficiency Standards for Residential and Nonresidential Buildings. Publication P400-03-001F, California Energy Commission, Sacramento, CA, September 2004.

Griffin, E.R., 2002. Building a better PVC: introducing stability at the molecular level. Roofing Technology Magazine 2 (2), 19–21.

Incropera, F.P., DeWitt, D.P., 1985. Fundamentals of Mass and Heat Transfer. Wiley, New York.

Kirchstetter, T.W., Novakov, T., 2004. Evidence that the spectral dependence of light absorption by aerosols is affected by organic carbon. Journal of Geophysical Research 109, D21208.

Kirchstetter, T.W., Novakov, T., Aguiar, J., Haesloop, O., Boone, A.A., 2005. Evaluation of the aethalometer for measuring real-time black carbon concentrations, in preparation.

Konopacki, S., Akbari, H., 1998. Simulated impact of roof surface solar absorptance, attic, and duct insulation on cooling and heating energy use in single-family new residential buildings. Technical Report LBNL-41834, Lawrence Berkeley National Laboratory, Berkeley, CA.

Konopacki, S., Akbari, H., Pomerantz, M., Gabersek, S., Gartland, L., 1997. Cooling energy savings potential of light-colored roofs for residential and commercial buildings in 11 U.S. metropolitan areas. Technical Report LBNL-39433, Lawrence Berkeley National Laboratory, Berkeley, CA.

Levinson, R., Akbari, H., Konopacki, S., Bretz, S., 2005a. Inclusion of cool roofs in nonresidential Title 24 prescriptive requirements. Energy Policy 33, 151–171.

Levinson, R., Berdahl, P., Akbari, H., 2005b. Solar spectral optical properties of pigments—Part I: model for deriving scattering and absorption coefficients from transmittance and

reflectance measurements. Solar Energy Materials & Solar Cells 89 (4), 319–349.

Levinson, R., Berdahl, P., Akbari, H., 2005c. Solar spectral optical properties of pigments—Part II: survey of common colorants. Solar Energy Materials and Solar Cells 89 (4), 351–389.

Lindberg, J.D., Douglass, R.E., Garvey, D.M., 1993. Carbon and the optical properties of atmospheric dust. Applied Optics 32, 6077–6081.

Miller, W.A. Cheng, M.-D., Pfiffner, S., Byars, N., 2002. The field performance of high-reflectance single-ply membranes exposed to three years of weathering in various U.S. climates. Technical Report, Single-Ply Roofing Institute, Needham, MA.

Pomerantz, M., Akbari, H., Konopacki, S.J., Taha, H., Rosenfeld, A.H., 1999. Reflective surfaces for cooler buildings and cities. Philosophical Magazine B 79 (9), 1457–1476.

Roodvoets, D., Miller, W.A., Desjarlais, A.O., 2004a. Long term reflective performance of roof membranes. In: Proceedings of the 19th International RCI Convention and Trade Show, Reno, NV.

Roodvoets, D., Miller, W.A., Desjarlais, A.O., 2004b. Saving energy by cleaning reflective thermoplastic low-slope roofs. In: Proceedings of Thermal Performance of the Exterior Envelopes of Buildings, vol. IX, Clearwater, FL.

Turpin, B.J., Lim, H.-J., 2001. Species contributions to PM2.5 mass concentrations: revisiting common assumptions for estimating organic mass. Aerosol Science and Technology 35, 602–610.

Turpin, B.J., Saxena, P., Andrews, E., 2000. Measuring and simulating particulate organics in the atmosphere: problems and prospects. Atmospheric Environment 34, 2983–3013.

Wilkes, K.E., Petrie, T.W., Atchley, J.A., Childs, P.W., 2000. Roof heating and cooling loads in various climates for the range of solar reflectances and infrared emittances observed for weathered coatings. In: Proceedings of the 2000 ACEEE Summer Study on Energy Efficiency in Buildings, American Council for an Energy-Efficient Economy, vol. 3, Washington, DC, pp. 3.361–3.372.

Young, R., 1998. Cool roofs: light-colored coverings reflect energy savings and environmental benefits. Building Design and Construction 39 (2), 62–64.

Experimental Analysis of the Natural Convection Effects Observed within the Closed Cavity of Tile Roof Systems

by

William A. Miller, Ph.D., P.E. André Desjarlais, P.E Jerry Atchley	Majid Keyhani, Ph.D. Wes MacDonald	Rick Olson Jerry Vandewater
Oak Ridge National Laboratory	*University of Tennessee*	*Tile Roofing Institute*

"Cool Roofing… Cutting through the Glare"
Atlanta, GA
May 12-13, 2005

ABSTRACT

High reflectance roof tile formulated with infrared reflective color pigments and bouyancy driven airflow on the underside of roof tile are key strategies for providing cool roof products that reduce both the heat transfer across the roof and the whole house energy consumption.

A field study is in progress to demonstrate and document the thermal benefits of clay and concrete tile roofs. The reflectance and emittance of the roof tiles, the bulk air temperatures underneath the tiles, the deck temperatures and the deck heat flux at specific distances from the roof's soffit to its ridge are being measured on an outdoor attic test assembly. The attic assembly has asphalt shingles and roof tiles directly nailed to the roof deck, and roof tile attached to batten and counter-batten systems adhered to the deck. Field data are reviewed to better understand the synergism observed from the tile's solar reflectance and the venting occurring between the roof deck and the underside of the tile.

INTRODUCTION

The Tile Roofing Institute (TRI) and the Oak Ridge National Laboratory (ORNL) are working together to quantify and report the potential energy savings for concrete and clay tile roofs. The TRI and its affiliate members are very interested in specifying tile roofs as cool roof products and they want to know the effect of the tile's solar reflectance and the effect of venting the underside of a roof tile. Parker et al., (2002) demonstrated that a Florida home with a "white reflective" barrel-shaped concrete tile roof reduced the annual cooling energy by 22% of the energy consumed by an identical and adjacent home having an asphalt shingle roof. The cost savings due to the reduced use of comfort cooling energy was about US $120 or about 6.7¢ per square foot per year.

The venting of the underside of a roof tile covering also provides thermal benefits for comfort cooling. Residential roof tests by Beal and Chandra (1995) demonstrated a 45% reduction in the daytime heat flux penetrating a counter-batten tile roof as compared to a direct nailed shingle roof. Parker et al., (2002) observed that a moderate solar reflectance

terra cotta barrel-shaped tile reduced the home's annual cooling load by about 8% of the base load measured for an identical home with an asphalt shingle roof that was adjacent to the home with terra cotta tile. These reported energy savings are in part attributed to the venting that occurs on the underside of the roof tile although it is difficult to quantify this benefit.

The reduced heat flow occurs because of a thermally driven airflow within the air gap formed between the tile and the roof deck. Wood furring strips, counter-battens, are laid vertically (soffit-to-ridge) against the roof deck, and a second batten running parallel to the roof's ridge is laid horizontally across the vertical counter-battens (Figure 1). The bottom surface of the inclined channel is formed by the roof deck and 30# felt and is relatively in-plane and smooth. The underside of the roof tiles establish the upper surface of the inclined vent, and the tile overlaps are designed to be air porous to allow pressure equalization and reduce the wind uplift on the tiles (Figure 1). The design may further complicate a solution of the heat transfer, because an accurate prediction of the airflow is required to predict the heat transfer crossing the roof boundary.

Figure 1. Batten and Counter-Batten Assembly Showing Inclined Air Cavity for the Slate Tile Roof.

The airflow in the inclined vent is driven by both buoyancy and wind-driven forces. The air gap also provides an improvement in the insulating effect of the roof system. However, measuring and correctly describing the heat flow within the vent cavity of a tile roof is a key hurdle for predicting the roof's thermal performance. The heat transfer within the channel can switch from conduction to single-cell convection to Bénard cell convection dependent on the channel's aspect ratio, the roof slope and the season of the year. The co-existence and competition of the various modes of heat transfer requires experimental measurements and numerical simulations.

Therefore, a combined experimental and analytical approach is in progress with field data just coming available, some of which we are reporting to show the potential energy savings for residential homes having concrete and clay tile roofs.

FIELD DEMONSTRATION

Members of the TRI installed clay and concrete tile on a fully instrumented attic test assembly at the ORNL campus (Figure 2). High-profile clay and concrete tile, medium-profile concrete and a concrete slate tile are directly nailed to the roof deck, installed on batten or on batten and counter-batten systems. The sixth lane (see furthermost left lane in Figure 2) has a standard production asphalt shingle roof for comparing energy savings. The tile roofs are approximately 4 feet wide with 16 feet of footprint. Table 1 lists the salient features of the concrete and clay tiles being field tested on the Envelope Systems Research Apparatus (ESRA). All tiles, whether direct nailed or installed on battens, have a venting occurring from the soffitt to the ridge and transversely along the width of the

test roofs. Parapet partitions with channel flashing were installed between lanes to restrict transverse airflows between test roofs (Figure 1). The ridge vent for each test roof was closed to mimick conventional construction.

Table 1: Clay and Concrete Tile Placed on the ESRA

Roof Cover	Roof System	Reflectance Emittance
		SR*xx*E*yy*[1]
S-Mission Clay	Direct to Deck	SR54E90
Medium-Profile Concrete	Direct to Deck	SR10E93
S-Mission Concrete	Spot Adhered to Deck using Foam	SR26E86
Slate Concrete	Counter-Batten/Batten	SR13E83
S-Mission Concrete	Batten	SR34E83
Asphalt Shingle	Direct to Deck	SR10E89

[1]SR*xx* states the solar reflectance of a new sample. E*yy* defines the thermal emittance of the new sample. As an example, the asphalt-shingle roof is labeled SR10E89; its freshly manufactured surface properties are therefore 0.10-reflectance and 0.89-emittance.

Each test roof has its own attic cavity with 11 inches of expanded polystyrene insulation installed between adjacent cavities. This reduces the heat leakage between cavities to less than 0.5% of the solar flux incident at solar noon on a test roof. Therefore, each lane can be tested as a stand-alone entity. Salient features of the ESRA facility are fully discussed by Miller et al., (2002).

Roof surface temperature, oriented strand board (OSB) temperature on both the upper and lower surfaces, and the heat flux transmitted through the roof deck are directly measured. Prior to installing the heat flux transducers, they were placed in a guard made of the same material used in construction, and calibrated using a FOX 670 Heat Flow Meter Apparatus to correct for shunting effects (i.e., distortion due to three-dimensional heat flow). Thermocouples are also stationed from the soffitt to the ridge to measure the bulk air temperatures in the air channel. The attic cavities also have an instrumented area in the ceiling for measuring the heat flows into the conditioned space. The ceiling consists of a metal deck, a 1 inch thick piece of wood fiberboard lying on the metal deck, and a ½ inch thick piece of wood fiberboard placed atop the 1 inch thick piece. The heat flux transducer for measuring ceiling heat flow is embedded between the two pieces of wood fiberboard. It too was calibrated in a guard made of wood fiberboard before put in field service.

REFLECTANCE AND EMITTANCE OF TILE

The solar reflectance and the thermal emittance of a roof surface are important surface properties affecting the roof temperature which, in turn, drives the heat flow through the roof. The solar reflectance (ρ) determines the fraction of radiation incident from all directions that is diffusely reflected by the surface. The thermal emittance (ε)

describes how well the surface radiates energy away from itself as compared to a blackbody operating at the same roof temperature.

Solar reflectance measures of the clay and concrete tile roofs exposed at ORNL are collected quarterly; these data are shown in Figure 3. Each tile roof is identified by the SR*xx*E*yy* nomenclature described in Table 1. After two years of exposure, the S-Mission tiles (SR54E90, SR26E86 and SR34E83) show little drop in solar reflectance. The medium-profile concrete (SR10E93) and the slate (SR13E83) tiles actually show slight increases in solar reflectance as does the asphalt shingle roof due to the accumulation of airborne contaminants. Dust tend to lighten these darker colors. Data for clay tile are also shown for field exposure testing in three of the sixteen climatic zones of California. The clay samples are identical to those tested at ORNL. They show a loss of solar reflectance that occurs, because of climatic soiling. The worst soiling observed occurs in the urban area of Colton and the desert area of El Centro (Figure 4). However, the crisp and clear alpine climate of McArthur shows the lowest loss of solar reflectance, because less contaminants pollute the air. Roof slope appears to affect the loss of solar reflectance (Figure 4). Testing at the slope of 8 inches of rise per 12 inches of run (33.7º slope) has less reflectance loss compared to testing at 2 inches of rise per 12 inches of run (9.5º) for all three exposure sites (Figure 4). Precipitation is not believed to be the dominant player, especially when one considers that El Centro has less than 3 inches of annual rainfall! Rather, wind may be causing the differences in loss of solar reflectance as roof slope changes from 9.5º to 33.7º. The results in Figures 3 and 4 also show that exposure testing differed between the western and mid-eastern climates of the United States. Samples from the two regions show California has more airborne dust than does Tennessee, which causes the greater loss of reflectance in California.

The clay tile (SR54E90) tested at ORNL and California exceeds the solar reflectance of all the other tile (Figure 3), because it contains complex inorganic color pigments that boost its reflectance in the infrared spectrum. A slurry coating process is used to add color to the surface of a clay tile. Once coated, the clay is kiln-fired, and the firing temperature, the atmosphere and the pigments affect the final color and solar reflectance Akbari, et al., (2004a). The complex inorganic color pigments, termed here as cool roof color materials (CRCMs), are of paramount importance and will literally revolutionize the roofing industry. The energy and cost savings reported by Parker et al., (2002) for white reflective concrete tile are promising; however, in the residential market, the issues of aesthetics and durability will limit the acceptance of “white” residential roofing. To homeowners, dark roofs simply blend better with the surroundings than their counterpart, a highly reflective “white” roof. What the public is not aware of, however, is that the aesthetically pleasing dark roof can be made to reflect like a “white” roof in the near infrared spectrum. Miller et al., (2004), Akbari et al., (2004b) and Levinson et al., (2004a and 2004b) provide further details about the potential energy benefits and identification, and characterization of dark yet highly reflective color pigments.

Coating tile with CRCMs has been successfully demonstrated by American Rooftile Coatings which applied its COOL TILE IR COATING™ to several samples of concrete tiles of different colors (Figure 5). The solar reflectance for all colors tested exceeded 0.40. Most dramatic is the effect of the dark colors. The black coating increased the solar reflectance from 0.04 to 0.41, while the chocolate brown coating increased from 0.12 to 0.41, a 250% increase in solar reflectance! Because solar heat gain is

proportional to solar absorptance, the COOL TILE IR COATING™ reduces the solar heat gain by roughly 33%, of the standard color, which is very promising. The coating application is a significant advancement for concrete tile, because the alternative is to add the CRCMs to the cement and sand mixture, which requires too much pigment and makes the product too expensive. The coating can certainly help tile roof products pass California's Title 24 and the Environmental Protection Agency's Energy Star 0.25 solar reflectance criterions for steep-slope roofing.

The thermal emittance of the clay and concrete tile has not changed much after two years of exposure in California. It remains relative constant at about 0.85.

EXPERIMENTAL RESULTS

The multiple hazard protection provided by concrete and clay tile from fire and wind and the superior aesthetics and durability of tile are making these roof materials the preference of homeowners in the western and some southern states. Thermal performance data collected from the attic test assembly at ORNL show tile to be an energy-efficient roof product. The clay S-Mission tile (SR54E90), the S-Mission tile spot adhered with foam (SR26E86) and the S-Mission tile on battens (SR34E83) had the least amount of heat penetrating into their respective roof decks (Figure 6). The roof heat flux data are for two consecutive days of exposure during August 2004 in East Tennessee's hot and humid climate. All three tiles have venting occurring along the underside of the tile's barrel from soffitt to ridge. Of these three roof systems, the clay tile (SR54E90) had the lowest heat flux through the deck due primarily to the tile's high solar reflectance. The clay tile reduced the peak heat transfer penetrating the roof deck at solar noon by about 70% of the energy penetrating through the deck of the attic covered with an asphalt shingle roof. Subsequently, the heat penetrating the ceiling of the attic assembly was reduced by about 60% of that entering through the ceiling of the attic assembly with asphalt shingles.

The solar reflectance and thermal emittance of the slate roof (SR13E83) and the medium-profile tile (SR10E93) are very similar to that of the asphalt shingle (SR10E89) but the heat transfer through the roof and ceiling of the attic with the slate roof and the medium-profile tile roof are only half that measured for the asphalt shingle roof. The reduction must be due to buoyancy and wind force effects occurring in the inclined air channel that dissipates heat away from the deck. The slate tiles are attached to batten and counter-batten strips, which form a vent cavity that is about 1½ inches deep. The medium-profile tile forms its own half-cylindrical channel of about 0.5 inch radius. It is very interesting that these two dark tile systems (SR13E83 and SR10E91) as compared to the shingle roof (SR10E89) significantly reduce the heat penetrating their respective ceilings. The data in Figure 6 clearly show the benefit derived from venting the roof deck based solely on the direct comparison of the percent reduction of peak loads (i.e., ~45% reduction for the SR13E83 or SR10E93 and a 70% reduction for the SR54E90 tile as compared to the shingle roof). By proportioning the heat reduction due solely to venting (SR10E93 vs SR10E89) to the heat reduction due to solar reflectance and venting (R54E90 vs SR10E89):

$$\overbrace{\frac{45\%\ \text{due to venting}}{70\%\ \text{due to venting and SR}}}^{\text{heat reduction}} \cdot \left[SR54_{\text{Clay Tile}} - SR10_{\text{Shingle}} \right]$$

The benefit of venting at solar noon is equivalent to roughly 30 points of surface reflectance! Hence, the data at peak loading imply that "cool roofing" credits are obtainable through venting the underside of a tile or similarly constructed roof system. The data also clearly show the synergism gained by both the solar reflectance of CRCMs (Figure 6) and the deck venting used by all tile roofs.

Demonstration homes located in Fair Oaks, California are also under field study to further document the effects of CRCMs and roof venting (Akbari et al., 2004). A pair of homes are adjacent to one another, and have the same identical floor plan and roof orientation. Both homes have the same medium-profile tile with chocolate brown color (SR10E93) as being tested on the ESRA at ORNL; however, one of the two homes was coated with CRCMs and has a measured solar reflectance of about 0.41 (see the chocolate brown color tile in Figure 5). The field data show that the higher reflectance roof reduced the attic temperature about 5°F to 15ºF around solar noon. The reduction in attic temperature is a direct result of the reduction in heat penetrating the roof. Heat flux transducers embedded in the west facing roofs of both homes show that the roof with Cool Tile IR Coating™ had less heat penetrating the roof compared to the roof with standard color tile. As result, there is a lower temperature driving force from attic to the conditioned space and, therefore, the heat penetrating the ceiling at solar noon is reduced about 70% of that measured for the standard production tile roof (Figure 7). Integrating the heat flows over the three-day daytime period shows a 25% reduction in the heat load that is due solely to the higher reflectance of the medium-profile tile. Therefore, CRCMs and roof venting are key strategies for providing cool roof products that can reduce whole house energy consumption.

PHYSICS OF THE HEAT FLOW IN THE INCLINED CHANNEL

The transfer of heat across the roof tile and roof deck has similar physics to the problem associated with the heat transfer across the inclined air channel formed by roof-mounted solar collectors. Comprehensive reviews of both experimental and theoretical results are available in the literature, Hollands et al., (1976), Arnold et al., (1976) and most recently Brinkworth (2000) studied this situation as applied to flat-plate photovoltaic cladding.

All residential roofs are sloped and make an angle θ with the horizontal plane that ranges from 2 inches of rise per 12 inches of run (9.5º slope) to a steep-sloped roof of 45º. During winter exposure, a roof deck is warmer than the tile and in the inclined air channel the heated surface is positioned below the cooler tile surface much like the solar panel application studied by Hollands et al. (1976). Here, a more dense air layer near the tile overlays a lighter air adjacent the roof deck (see θ = 0, Figure 8). Hollands observed that the heat transfer across the air channel can switch from conduction to single-cell convection to Bénard cell convection depending on the strength of a non-dimensional parameter called the Rayleigh (Ra) Number. For Rayleigh numbers less than

1708/Cos(θ), there is no naturally induced airflow within the cavity, and the heat transfer occurs exclusively by conduction. However, a flow of air occurs if buoyancy forces

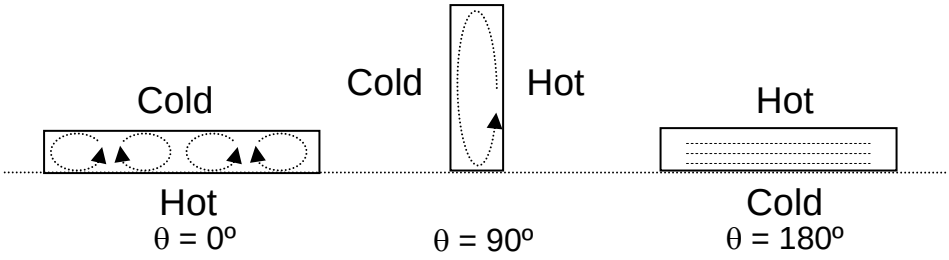

Figure 8. Heat Transfer Phenomena Occurring on the Underside of Roof Tile.

overcome the resistance imposed by the viscous or frictional forces. As the flow increases due to buoyancy, the heat transfer within the channel switches to Bénard cell convection, which has hexagonal cells with flow ascending in the center and descending along the sides of the air channel (see θ = 0, Figure 8). Arnold et al., (1976) observed that the channel's aspect ratio and the slope of the solar panel (for our application a roof) had a major impact on the flow and heat transfer within the air channel. They observed that if the channel was rotated from θ = 180º (summer exposure for a roof) all the way to θ = 0º (winter exposure), the heat transfer rises to a maximum at θ = 90º and then as θ decreases below 90º the heat transfer rate first decreases and passes through a local minimum at θ* (Bejan 1984). However, as θ decreases below θ*, the heat transfer rate again rises because of the inception of Bénard cell convection. Arnold et al., (1976) also observed that the aspect ratio of the channel changed the critical angle θ* where the heat transfer across the channel was minimal. The information may be very useful for designing tile to limit ice daming in predominantly cold climates.

During summer exposure, the tile is hotter than the roof deck and Bénard cell convection does not occur within the inclined channel, because the lighter air layer is now atop the denser air layer near the roof deck. The air heated by the underside of the tile tends to rise, and natural convection begins within a boundary layer formed along the underside of the tile (θ = 180, Figure 8). Brinkworth (2000) studied this situation as applied to flat-plate photovoltaic cladding, and it is this configuration and heat transfer mechanism that is evident in the field experiments shown for the ESRA tile roof systems.

NUMERICAL SIMULATIONS

Computer simulations for thermally induced airflow and heat transfer across an inclined air channel were conducted for several different constant temperature wall boundary conditions and several different inclinations with the horizontal plane to better understand the strength of natural convection forces occurring within the heated channel. The channel was modeled for three conditions (Table 2) with the top plate always held at a higher temperature than the bottom plate to simulate summer exposure of the tile roof. The bottom and the two side surfaces of the channel were held at 68°F, and the top surface was held at 68°F + ΔT listed in Table 2. All channel surfaces were assumed smooth and solid. The aspect ratio of the duct was fixed at 0.01.

Table 2: Channel Inclinations and Temperature Gradients used in Simulations.

Channel Inclination	Top Plate to Bottom Plate ΔT (ºF)
0°	27
5°	1.8
35°	27

The simulations in Figures 9 and 10 are plotted in terms of the isotherms (constant temperature lines shown in color) and streamlines (lines of constant velocity). The results depicted in Figure 9a show that with no inclination, natural convection flow does not occur within the channel. Rather, a plume of heated air forms above the heated top surface. Because no net airflow occurs within the channel, the heat transfer across the two plates is conduction dominated. In Figure 9b with only five degrees of inclination and the top plate held just 1.8ºF above the lower plate, there is a distinct flow moving within a boundary layer on the underside of the top plate. The flow field is laminar, which is most probably the same flow occurring in the inclined air channels of the tiles being field tested on the ESRA. These simulations indicate that naturally induced flow can be expected at very low inclination angles and very low temperature differences, well below those experienced in roofing systems. The induced flow causes a net flow from soffitt to ridge that carries heat away from the attic. Parker et al., (2001) tested the white tile roof at 5 inches of rise per 12 inches of run (35º slope). They measured during July exposure a temperature gradient from the tile to the roof deck of about 14ºF, (Figure 10). A numerical simulation is superimposed onto the roof for the roof slope studied by Parker et al., (2001) to help show the strength of the natural convection flows. The flow patterns are similar to those described in Figure 9; however, the exit jet is more in line with the duct axis indicating the momentum of the flow has increased (see Figure 10). Hence, the numerical results help to show qualitatively that the venting occurring on the underside of the roof tile can be very significant for dissipating heat away from the roof deck, making the tile roof system cooler than conventional direct nailed systems.

The numerical results do not take into account the effect of a forced flow component, which may aid or oppose the naturally induced flow nor is air leakage between the tile overlaps considered. Mixed convection (forced convection driven by wind effects that are accompanied by buoyancy effects) is an additional confounding variable that must be mathematically described a priory the prediction of the heat transfer across the roof deck. The key to the problem is to predict accurately the airflow within the cavity. Once known, the portions of heat penetrating the roof deck and that convected away through the ridge vent can be derived from energy balances.

CONCLUSION

The tile roofs exposed to East Tennessee's climate have maintained their solar reflectance after two full years of exposure. Dust and urban pollution in California's urban areas soil the materials more so than in the less populated sections of the state, and the loss of reflectance is most severe for samples exposed at the slope of 2 inches of rise

per 12 inches of run. Increasing the slope reduced the soiling because the dust is probably blown away by the strong California winds.

The addition of complex inorganic pigments to clay and concrete tile significantly increased the solar reflectance and reduced the heat penetrating into the conditioned space. Applying a coating with CRCMs to medium-profile concrete tile reduced the heat penetrating the ceiling of a demonstration home by about 70% of that measured for an identical home with the same standard production medium-profile tile.

The venting occurring beneath a roof tile and the addition of CRCMs yields a synergistic improvement in the thermal performance of clay and concrete tile roofs. Field data collected at peak solar loading for clay and concrete tile roofs at ORNL demonstrate that venting is roughly equivalent to about 30 points of solar reflectance. Therefore, venting offers a significant 50% reduction in the heat penetrating the conditioned space compared to direct nailed roof systems that are in direct contact with the roof deck.

The combination of tile venting and improved solar reflectance offers excellent credits that clay and concrete tile can claim for cool roof steep-slope roof products as specified by the EPA and many state energy offices.

Numerical simulations of the inclined air channel formed by tile roof systems demonstrated that naturally induced flow can be expected at very low roof slopes and very low temperature differences, well below those experienced in roofing systems.

ACKNOWLEDGEMENTS

Funding for this project was provided by the California Energy Commission's Public Interest Energy Research program through through the U. S. Department of Energy under contract DE-AC03-76SF00098.The PIER project "Cool Roofs" has team players Steve Weil, Hashem Akbari, Ronnen Levinson and Paul Berdahl from LBNL and André Desjarlais and William Miller from ORNL working together to make CRCMs a market reality in tile, metal and shingles by 2006.

REFERENCES

Akbari,H., R. Levinson, P. Berdahl. 2004a. "A Review of Methods for the Manufacture of Residential Roofing Materials." Report to the California Energy Commission. To be published.

Akbari,H., P. Berdahl, R. Levinson, R. Wiel, A. Desjarlais, W. Miller, N. Jenkins, A. Rosenfeld, C. Scruton. 2004b. "Cool Colored Materials for Roofs," *ACEEE Summer Study on Energy Efficiency in Buildings.* Proceedings of American Council for an Energy Efficient Economy, Asilomar Conference Center in Pacific Grove, CA, August.

Arnold, J.N., I. Catton, D.K. Edwards. 1976. "Experimental Investigation of Natural Convection in Inclined Rectangular Regions of Differing Aspect ratios." *Journal of Heat Transfer.* (February) 67-71.

Beal, D. and S. Chandra. 1995. "The Measured Summer Performance of Tile Roof Systems and Attic Ventilation Strategies in Hot Humid Climates." *Thermal Performance of the Exterior Envelopes of Buildings VI*, U.S. DOE/ORNL/BETEC, December 4-8, Clearwater, FL.

Bejan A. 1984. *Convection Heat Transfer*. New York: John Wiley & Sons, Inc.

Brinkworth, B.J. 2000. "A Procedure for the Routine Calculation of Laminar Free and Mixed Convection in Inclined Ducts." *International Journal of Heat and Fluid Flow* 21: 456-462.

Hollands K.G.T., T.E. Unny, G.D. Raithby and L. Konicek. 1976. "Free Convection Heat Transfer Across Inclined Air Layers." *Journal of Heat Transfer.* (May) 189-193.

Levinson R., P. Berdahl and H. Akbari. 2004a. "Solar spectral optical properties of pigments, Part I: model for deriving scattering and absorption coefficients from transmittance and reflectance measurements." Submitted to Solar Energy Materials & Solar Cells.

——. 2004b. "Solar spectral optical properties of pigments, Part II: survey of common colorants." Submitted to Solar Energy Materials & Solar Cells.

Miller, W.A., M-D. Cheng, S. Pfiffner and N. Byars. 2002. "The Field Performance of High-Reflectance Single-Ply Membranes Exposed to Three Years of Weathering in Various U.S. Climates." Final Report to SPRI, Inc., August.

Miller W. A., K.T. Loyle, A.O. Desjarlais, H. Akbari, R. Levenson, P. Berdahl, S. Kriner, S. Weil, and R.G. Scichile. 2004. "Special IR Reflective Pigments Make a Dark Roof Reflect Almost Like a White Roof." *Thermal Performance of the Exterior Envelopes of Buildings, IX*. Proceedings of ASHRAE THERM IX, December, Clearwater, FL.

Parker, D.S., J.K. Sonne, and J.R. Sherwin. 2002. "Comparative Evaluation of the Impact of Roofing Systems on Residential Cooling Energy Demand in Florida." *ACEEE Summer Study on Energy Efficiency in Buildings.* Proceedings of American Council for an Energy Efficient Economy, Asilomar Conference Center in Pacific Grove, CA, August.

Parker, D.S., J.K. Sonne, J.R. Sherwin and N. Moyer. 2001. "Comparative Evaluation of the Impact of Roofing Systems on Residential Cooling Energy Demand in Florida." Final Report FSEC-CR-1220-00, prepared for the Florida Power and Light Company, May.

Figure 2: Clay and Concrete Tile being Field Tested on the Steep-Slope Attic Assembly at ORNL. (From right-to-left the test roofs are: direct nailed S-Mission Clay, direct nailed Medium-Profile Concrete, spot adhered foam S-Mission Concrete, batten and counter-batten Flat Concrete Slate, batten S-Mission Concrete and the direct nailed asphalt shingle roof.)

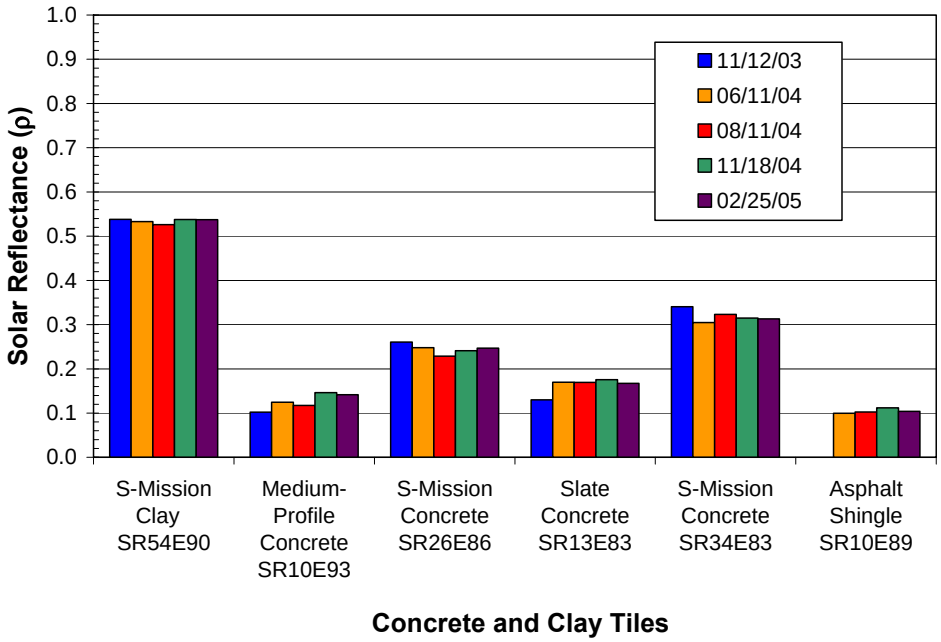

Figure 3: Solar Reflectance Measurements for the Tile Exposed on the Attic Assembly at ORNL. SRxxEyy values are solar reflectance and thermal emittance measures taken 11/12/03.

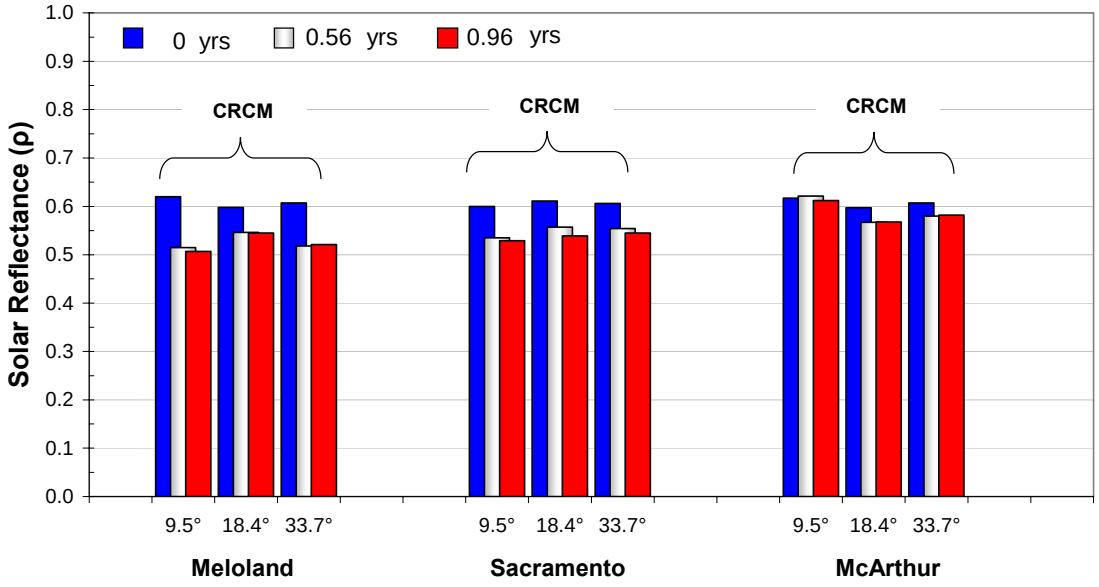

Figure 4: Clay Tile Field Tested on Exposure Racks in California at the slopes of 9.5º, 18.4º, and 33.7º which Represent Roof Slope Settings of 2, 4, and 8 inches of Rise per 12 inches of Run.

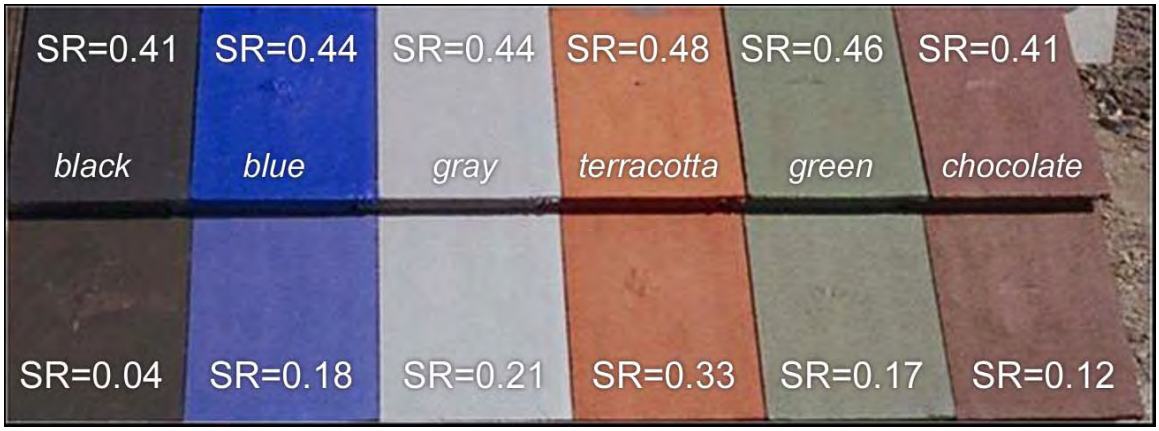

Figure 5: Solar Reflectance of Concrete Tile Roofs with CRCMs (top row) and Without CRCMs (bottom row). (The COOL TILE IR COATING™ technology was developed by Joe Reilly of American Rooftile Coating).

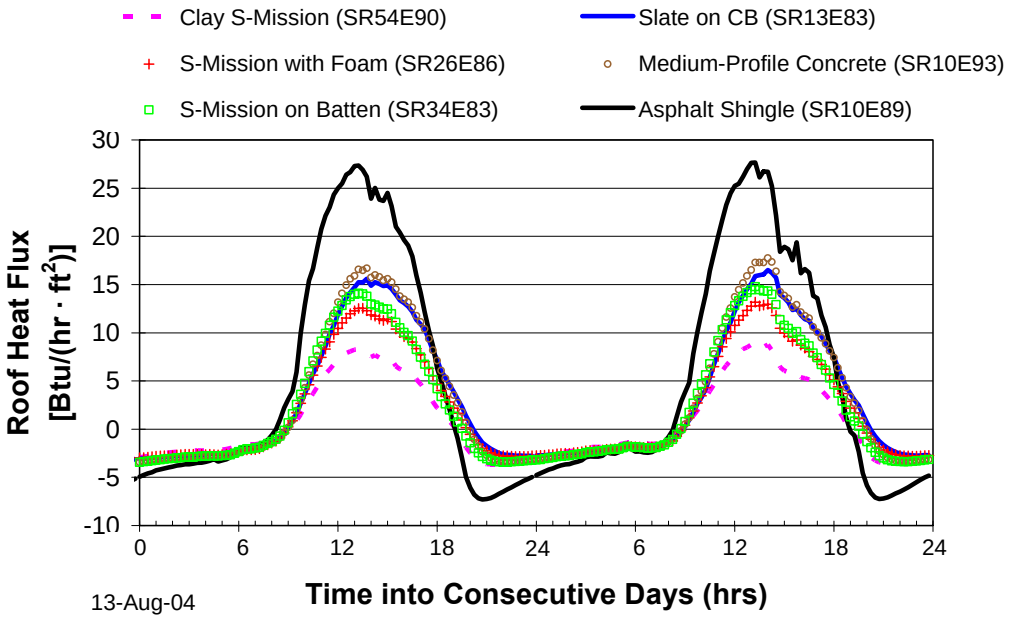

Figure 6: Heat Penetrating the Roof of each Attic Assembly being Field Tested on the ESRA.

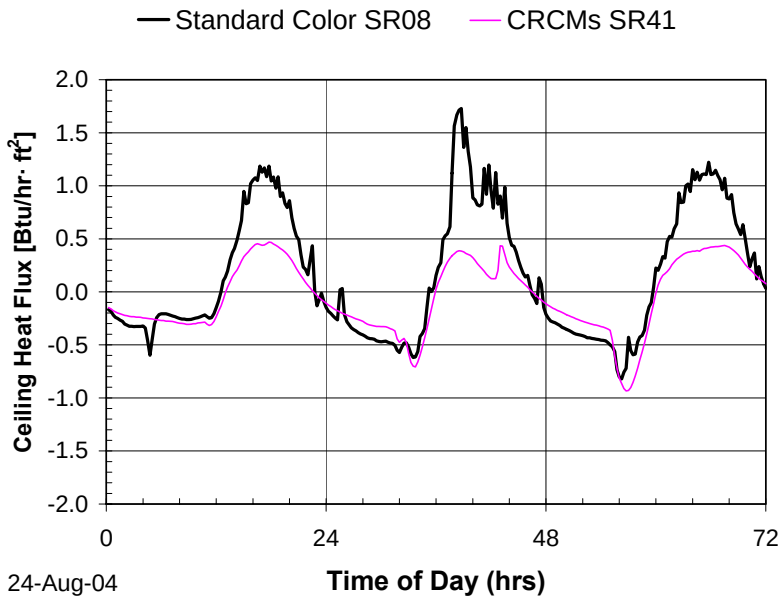

Figure 7: The Heat Penetrating the Ceiling of Two Homes Having Identical Footprint and Orientation in Fair Oaks, CA. (Roofs Are the Same as the Medium-Profile Concrete Tile Tested at ORNL.)

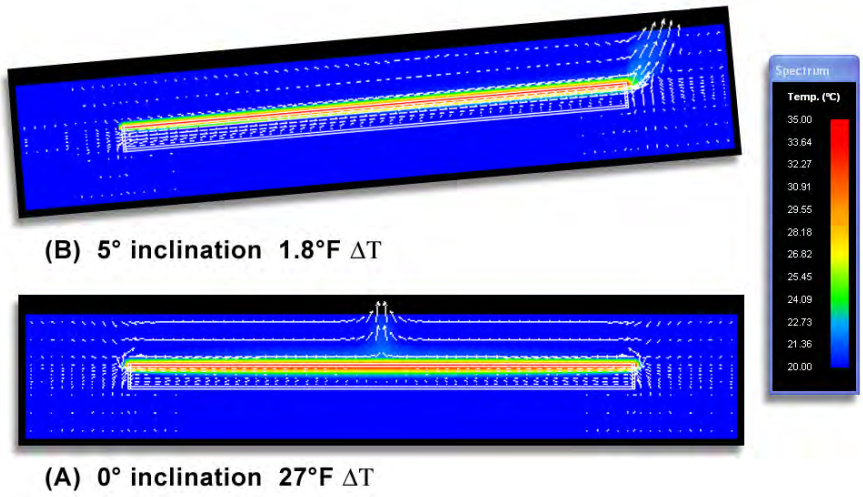

Figure 9: Naturally Induced Flow Observed at Low Inclinations and at Low Temperature Gradients from the Top Plate to the Lower Plate.

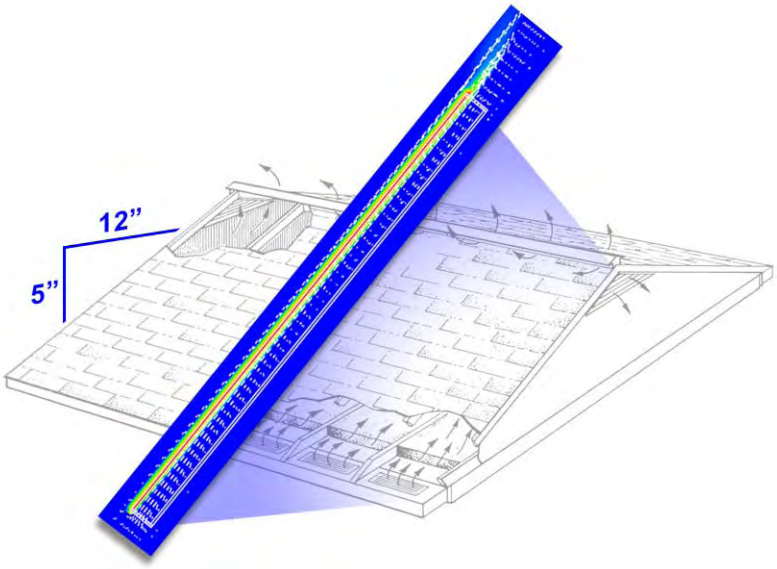

Figure 10: Naturally Induced Flow Observed at Typical Roof Slope and Temperature Gradients Observed in the work of Parker et al., (2002).

PROFESSIONAL ROOFING

Cooling down the house

Residential roofing products soon will boast "cool" surfaces

by ***Hashem Akbari and André Desjarlais***

Energy-efficient roofing materials are becoming more popular, but most commercially available products are geared toward the low-slope sector. However, research and development are taking place to produce "cool" residential roofing materials.

In 2002, the California Energy Commission asked Lawrence Berkeley National Laboratories (LBNL), Berkeley, Calif., and Oak Ridge National Laboratories (ORNL), Oak Ridge,Tenn., to collaborate with a consortium of 16 manufacturing partners and develop "cool" non-white roofing products that could revolutionize the residential roofing industry.

The commission's goal is to create dark shingles with solar reflectances of at least 0.25 and other nonwhite roofing products—including tile and painted metal—with solar reflectances not less than 0.45. The manufacturing partners have raised the maximum solar reflectance of commercially available dark products to 0.25-0.45 from 0.05-0.25 by reformulating their pigmented coatings. (For a list of the manufacturers, see "Manufacturing partners," page 36.)

Because coatings colored with conventional pigments tend to absorb invisible "near-infrared" (NIR) radiation that bears more than half the power of sunlight (see Figure 1), replacing conventional pigments with "cool" pigments that absorb less NIR radiation can yield similarly colored coatings with higher solar reflectances. These cool coatings lower roof surface temperatures, reducing the need for cooling energy in conditioned buildings and making unconditioned buildings more comfortable.

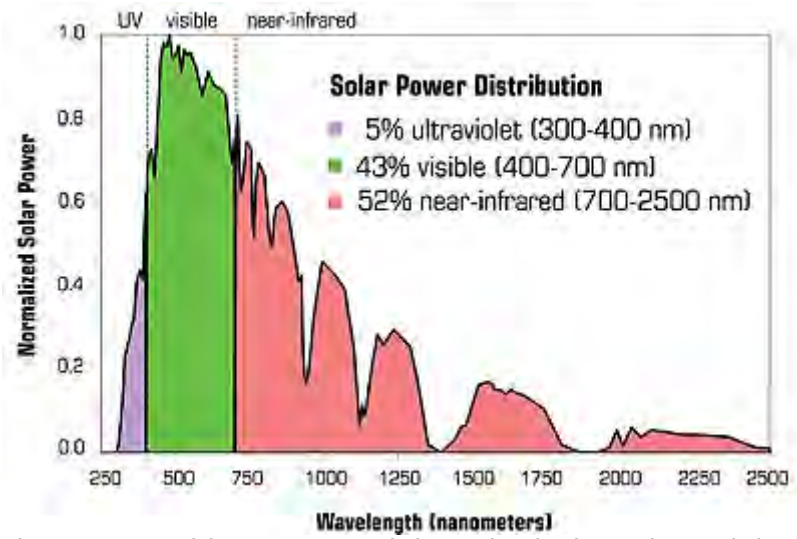

Figure courtesy of the Lawrence Berkeley National Laboratories, Berkeley, Calif.

Figure 1: Peak-normalized solar spectral power—more than half of all solar power arrives as invisible, "near-infrared" radiation

Cool, nonwhite roofing materials are expected to penetrate the roofing market within the next three years to five years. Preliminary analysis by LBNL and ORNL suggests the materials may cost up to $1 per square meter more than conventionally colored roofing materials. However, this would raise the total cost of a new roof system only 2 percent to 5 percent.

Cool, nonwhite colors

Developing the colors to achieve the desired solar reflectances involves much research and development. So far, LBNL has characterized the optical properties of 87 common and specialty pigments that may be used to color architectural surfaces. Pigment analysis begins with measurement of the reflectance—r—and transmittance—t—of a thin coating, such as paint film, containing a single pigment, such as iron oxide red. These "spectral," or wavelength-dependent, properties of the pigmented coating are measured at 441 evenly spaced wavelengths spanning the solar spectrum (300 nanometers to 2,500 nanometers).

Inspection of the film's spectral absorptance (calculated as 1-r-t) reveals whether a pigmented coating is "cool" (has low NIR

absorptance) or "hot" (has high NIR absorptance). The spectral reflectance and transmittance measurements also are used to compute spectral rates of light absorption and backscattering (reflection) per unit depth of film. The spectral reflectance of a coating colored with a mixture of pigments then can be estimated from the spectral absorption and backscattering rates of its components.

LBNL has produced a database detailing the optical properties of the 87 characterized pigmented coatings (see Figure 2). Its researchers are developing coating formulation software intended to minimize NIR absorptance (and maximize the solar reflectance) of a color-matched pigmented coating. The database and software will be shared with the consortium manufacturers later this year.

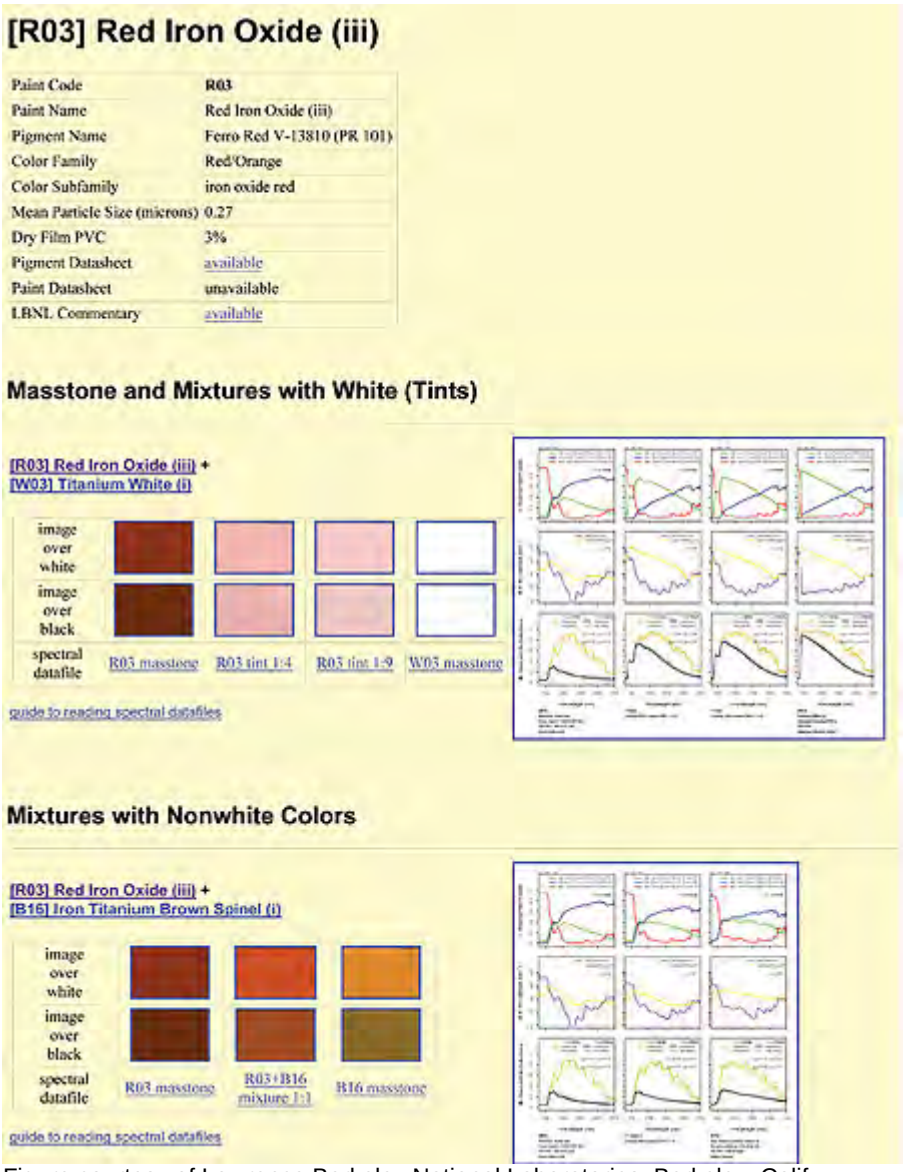

Figure courtesy of Lawrence Berkeley National Laboratories, Berkeley, Calif.

Figure 2: Description of a red iron oxide pigment in the Lawrence Berkeley National Laboratory pigment database

Shingles

A new shingle's solar reflectance is dominated by the solar reflectance of its granules, which cover more than 97 percent of its surface. Until recently, the way to produce granules with high solar reflectance has been to use a coating pigmented with titanium dioxide (TiO_2) white. Because a thin TiO_2-pigmented coating is reflective but not opaque in NIR, multiple layers are needed to obtain high solar reflectance. Thin coatings colored with cool, nonwhite pigments also transmit NIR radiation. Any NIR light transmitted through the pigmented coating will strike the granule aggregate where it will be absorbed (typical dark rock) or reflected (typical white rock).

Multiple color layers, a reflective undercoating and/or reflective aggregate can increase granules' solar reflectances, thereby increasing shingles' solar reflectances.

Figure 3 shows the iterative development of a cool black shingle prototype by ISP Minerals Inc., Hagerstown, Md. A conventional black roof shingle has a reflectance of about 0.04. Replacing the granule's standard black pigment with a cool NIR-scattering black pigment (prototype 1) increases the solar reflectance of the shingle to 0.12. Incorporating a thin white sublayer (prototype 2) raises the shingle's solar reflectance to 0.16; using a thicker white sublayer (prototype 3) increases the shingle's reflectance to 0.18. The figure also shows an approximate performance limit (solar reflectance 0.25) obtained by applying 25-micron NIR-reflective black topcoat over an opaque white background.

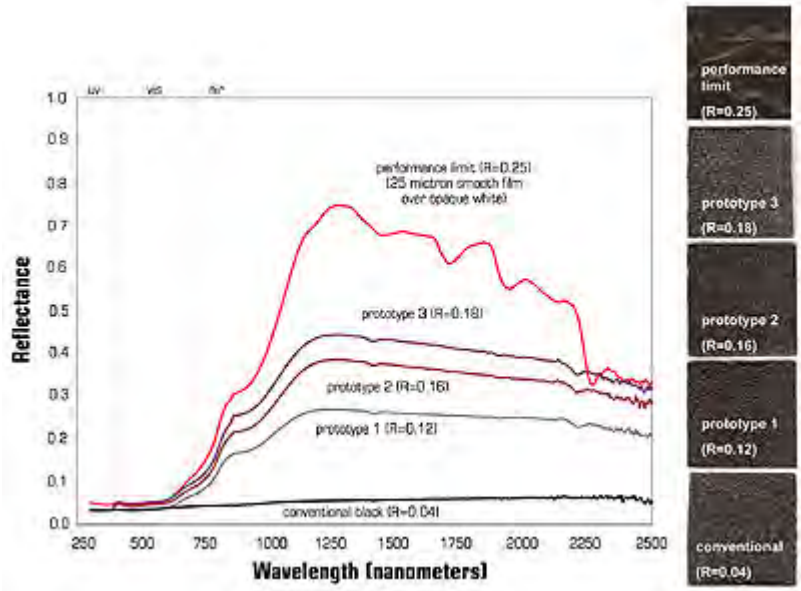

Figure courtesy of Lawrence Berkeley National Laboratories, Berkeley, Calif.

Figure 3: ISP Minerals Inc., Hagerstown, Md., is developing a cool, black shingle. Shown are the solar spectral reflectances, images and solar reflectances (R) of a conventional black shingle; three prototype cool, black shingles; and smooth, cool, black film over an opaque white background.

Tile

There are three ways to improve solar reflectances of colored tiles: use clay or concrete with low concentrations of light-absorbing impurities, such as iron oxides and elemental carbon; color tile with cool pigments contained in a surface coating or mixed integrally; and/or include an NIR-reflective sublayer, such as a white sublayer, beneath an NIR-transmitting colored topcoat.

American Rooftile Coatings, Fullerton, Calif., has developed a palette of cool, nonwhite coatings for concrete tiles. Each of its COOL TILE IR COATINGS™ shown in Figure 4 has a solar reflectance greater than 0.40. The solar reflectance of each cool coating exceeds that of a color-matched, conventionally pigmented coating by 0.15 (terra cotta) to 0.37 (black).

Metal

Cool, nonwhite pigments can be applied to metal with or without a white sublayer. If a metal is highly reflective, the sublayer may be omitted. The polymer coatings on metal panels are kept thin to withstand bending. This restriction on coating thickness limits pigment loading (pigment mass per unit surface area).

Performance research

ORNL naturally is weathering various types of conventionally pigmented and cool-pigmented roofing products at seven California sites. Each "weathering farm" has three south-facing racks for exposing samples of roofing products at typical roof slopes. Sample weathering began in August 2003 and will continue for three years—until October 2006. Solar reflectance and thermal emittance are measured twice per year; weather data are available continuously. Solar spectral reflectance is measured annually to gauge soiling and document imperceptible color changes.

ORNL and the consortium manufacturers also are exposing roof samples to 5,000 hours of xenon-arc light in a weatherometer, a laboratory device that accelerates aging via exposure to ultraviolet radiation and/or water spray. ORNL will examine the naturally weathered samples for contaminants and biomass to identify the agents responsible for soiling. This may help manufacturers produce roofing materials that better resist soiling and retain high solar reflectance. Changes in reflectance will be correlated to exposure.

The labs and manufacturing partners also have established residential demonstration sites in California. The first, in Fair Oaks

(near Sacramento), includes two pairs of single-family, detached homes. One pair is roofed with color-matched conventional and cool-painted metal shakes supplied by Custom-Bilt Metals, South El Monte, Calif., and the other features color-matched conventional and cool low-profile concrete tiles supplied by Hanson Roof Tile, Charlotte, N.C. The second site, in Redding, is under construction and by summer will have a pair of homes roofed with color-matched conventional and cool asphalt shingles.

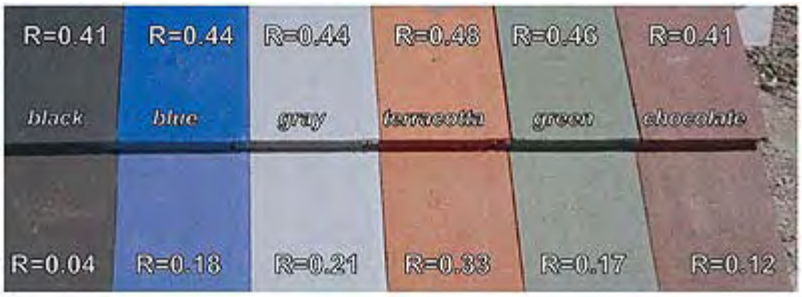

Figure courtesy of American Rooftile Coatings.

Figure 4: This is a palette of color-matched cool (top row) and conventional (bottom row) roof tile coatings developed by American Rooftile Coatings, Fullerton, Calif. Shown on each coated tile is its solar reflectance.

The homes in Fair Oaks are adjacent and share the same floor plan, roof orientation and level of blown ceiling insulation (19 hr•ft²•ºF/Btu). The homes in Fair Oaks and Redding will be monitored through at least summer 2006.

One of the Fair Oaks homes roofed with low-profile concrete tile was colored with a conventional chocolate brown coating (solar reflectance 0.10), and the other was colored with a matching cool chocolate brown (an American Rooftile Coatings COOL TILE IR COATING™ with solar reflectance 0.41). The attic air temperature beneath the cool brown tile roof has been measured to be 3 K to 5 K cooler than that below the conventional brown tile roof during a typical hot summer afternoon (273.15 K equals 0 C).

The results for the pair of Fair Oaks homes roofed with painted metal shakes are just as promising. There, the attic air temperature beneath the cool brown metal shake roof (solar reflectance 0.31) was measured to be 5 K to 7 K cooler than that below the conventional brown metal shake roof.

These reductions in attic temperature are solely the result of the application of cool, colored coatings. The use of these cool, colored coatings also decreased the total daytime heat influx (solar hours are from 8 a.m.-5 p.m.) through the west-facing concrete tile roof by 4 percent and the south-facing metal shake roof by 31 percent (see Figure 5).

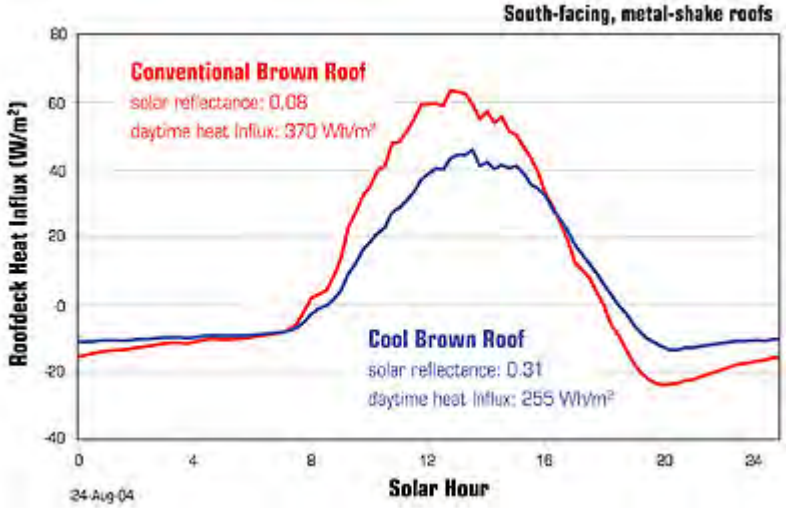

Figure courtesy of Oak Ridge National Laboratory, Oak Ridge, Tenn.

Figure 5: Heat flows through the roof decks of an adjacent pair of homes during the course of a hot summer day. The total daily heat influx through the cool brown metal shake roof (solar reflectance 0.31) between the solar hours of 8 a.m. and 5 p.m.is 31 percent lower than through the conventional brown metal shake roof (solar reflectance 0.08).

ORNL also is testing several varieties of concrete and clay tile on a steep-slope roof to further investigate the individual and combined effects of cool, colored coatings and subtile ventilation on the thermal performance of a cool roof system.

Results to date

The two laboratories and their industrial partners have achieved significant success in developing cool, colored materials for

concrete tile, clay tile and metal roofs.

Since the inception of this program, the maximum solar reflectances of commercially available dark roofing products has increased to 0.25-0.45 from 0.05-0.25. Bi-layer coating technology (a color topcoat over a white or other highly reflective undercoat) is expected to soon yield several cost-effective cool, colored shingle products with solar reflectances in excess of the U.S. Environmental Protection Agency's ENERGY STAR® threshold of 0.25. Early monitoring results indicate using cool, colored roofing products measurably reduces heat flow into conditioned homes with code-level ceiling insulation.

As homeowners continue to seek energy-efficient products, the roofing industry's research into residential roofing products that offer energy-efficient features naturally will continue to evolve.

Provided energy-efficient products continue to perform satisfactorily, we expect cool, nonwhite metal, tile and shingle products to penetrate the roofing market within the next three to five years.

Hashem Akbari leads LBNL's Heat Island Group. André Desjarlais leads ORNL's Building Envelope Group.

Editor's note: *Ronnen Levinson, scientist, Paul Berdahl, staff scientist, and Stephen Wiel, staff scientist, of LBNL; William Miller senior research engineer of ORNL; and Nancy Jenkins, program manager, Arthur Rosenfeld, commissioner, and Chris Scruton, project manager, of the California Energy Commission contributed to this article.*

Manufacturing partners

3M
St. Paul, Minn.
www.scotchgard.com/roofinggranules

Akzo Nobel
Felling, United Kingdom
www.akzonobel.com

American Rooftile Coatings
Fullerton, Calif.
www.americanrooftilecoatings.com

BASF Industrial Coatings
Florham Park, N.J.
www.ultra-cool.basf.com

CertainTeed Corp.
Valley Forge, Pa.
www.certainteed.com

Custom-Bilt Metals
South El Monte, Calif.
www.custombiltmetals.com

Elk Corp.
Dallas
www.elkcorp.com

Ferro Corp.
Cleveland
www.ferro.com

GAF Materials Corp.
Wayne, N.J.
www.gaf.com

Hanson Roof Tile
Charlotte, N.C.
www.hansonrooftile.com

ISP Minerals Inc.
Hagerstown, Md.

MCA Tile
Corona, Calif.

www.mca-tile.com

MonierLifetile LLC
Irvine, Calif.
www.monierlifetile.com

Owens Corning
Toledo, Ohio
www.owenscorning.com/around/roofing/Roofhome.asp

Shepherd Color Co.
Cincinnati
www.shepherdcolor.com

Steelscape Inc.
Kalama, Wash.
www.steelscape-inc.com

Web-exclusive information — Study about the development of cool, colored roofing materials

© Copyright 2006 National Roofing Contractors Association

COOL METAL ROOFING IS TOPPING THE BUILDING ENVELOPE WITH ENERGY EFFICIENCY AND SUSTAINABILITY

by

Scott Kriner, Akzo Nobel Coatings, Inc.
William A. Miller, Ph.D., P.E., Oak Ridge National Laboratory
Danny S. Parker, Florida Solar Energy Center

"Cool Roofing…Cutting through the Glare"
Atlanta, GA
May 12-13, 2005

INTRODUCTION

Evaluating the weathering effects on solar reflectance and thermal emittance of metal roofing is important in determining the cooling and heating energy loads on a building. Akbari and Konopacki (1998) found that annually about $0.75 billion can be saved by widespread implementation of light-colored roofs in cooling dominant climates. Their simulations based on both old and new residential and commercial construction having respectively R-11 and R-19 levels of ceiling insulation also showed that thermal emittance affects both cooling and heating energy use. In cooling dominant climates, a low-emittance roof yields a higher roof temperature and in turn, increases the cooling load imposed on the building. Their simulations showed that changing the thermal emittance from 0.90 to 0.25 caused a 10% increase in the annual utility bill. However, in cold climates, a low-emittance roof adds resistance to the passage of heat leaving the roof, which results in savings in heating energy. Akbari and Konopacki (1998) showed that in very cold climates with little or no summertime cooling, the heating energy savings resulting from decreasing the roof emittance almost reached 3% of the buildings annual energy consumption.

The durability or retention of the solar reflectance and thermal emittance is of paramount importance for sustained thermal performance of a roof. Painted metal roofing is commonly offered with 30 year product warranties because field exposures have shown it retains almost 95% of its initial solar reflectance even after 30 years of climatic exposure (Miller and Rudolph 2004). Hence, the aged radiative properties are very similar to initial values, and therefore should be considered when sizing the comfort conditioning equipment or projecting the energy cost savings as compared to other roofing products that soil and lose reflectance.

METAL ROOFING

According to 2004 F.W. Dodge reports, metal's share of the residential steep-slope roofing market has reached 8%. This is a three-fold increase in the past six years, and

more and more residential and steep-slope architectural roofing projects are demanding pre-painted metal roofing. Ducker Worldwide study (2002) showed that metal's overall share of the commercial roofing market is 15%, and in steep-slope commercial applications, metal has a 33% market share. Its finishes are colorful, inert, and do not pose a health risk. Metal roofing is code compliant and tested for fire, wind, hail resistance and is non-combustible which reduces the spread of fire in and among buildings.

Metal roofing is available in a wide variety of textures, colors, surface finishes, and formed profiles. Linear roll-formed panels as well as modular press-formed shingle, shake or tile facsimiles are possible with unpainted or pre-painted metal. Given the diversity of the family of metal roofing products, the material can be engineered for optimum energy efficiency depending on the climate and microenvironment. For example, unpainted metal roofing such as 55% Al-Zn coated steel[1] sheet or hot dip galvanized steel[2] has a relatively high solar reflectance but a low thermal emittance. In cold climates where heating loads dominate, this type of roofing product is desirable to minimize annual energy consumption, because the low thermal emittance retains heat that would otherwise radiate to the night-sky. In contrast, a light-colored, or specially a pre-painted metal roof can have a high solar reflectance and a high thermal emittance. In warmer climates where cooling loads dominate, that type of roof is desirable for reducing annual energy costs. In both cases, metal can be chosen as an energy-efficient roof product.

PRE-PAINTED METAL ROOFING

Premium industrial paint finishes are applied to metal substrates using a controlled continuous coil coating process at speeds of up to 700 feet per minute. Paint systems are oven-baked in this process and are warranted for up to 30 years for chalk and fade resistance. Paint suppliers who offer these warranties do so based on real-time outdoor performance data obtained from weathering farms. Polyvinylidene fluoride (PVDF) paint resin systems have become the premier metal roofing finish owing to its superior resistance to color fade. Color fade is measured in ΔE Hunter units per ASTM D 2244-02 (ASTM 2002). One ΔE unit is the slightest color difference perceptible to the human eye. PVDF-painted metal roofing material typically displays no more than 5 ΔE units of fade over 20 years.

The PVDF resin chemistry was patented and licensed by Pennwalt Corp. in the 1960's and is now available from Arkema under the Kynar 500® trademark and from Solvay Solexis under the Hylar 5000® trademark. The chemistry is from the same organic film bonding that is responsible for Teflon®, making it extremely chemical resistant and

[1] This steel is exposed to a molten bath composed of 55% Al-43.5% Zn -1.5% Si at a temperature of 1100°F (593°C). The coating is solidified rapidly to enhance both the microstructure and the corrosion resistance.

[2] A zinc-coated steel sheet manufactured by the steel being dipped in continuous coil form through a molten bath of zinc.

dirt shedding. Years of testing show that PVDF resin is most durable when it comprises 70% of the total resin component in a paint film. The Kynar or Hylar type coatings have superior resistance to color fade, chalk, gloss change and corrosion.

Table 1 shows examples of some typical radiative properties of different types of metal roof products that are listed on the Energy Star® roof products directory. Metal and metal paint finishes comprise 65% of the products on the Energy Star® roofing directory.

Table 1: Energy Star® Radiative Properties of Listed Metal Roofing

Surface	Initial Solar Reflectance	3-year Aged Solar Reflectance
Unpainted 55% Al-Zn	0.78	0.58
Acrylic coated 55% Al-Zn	0.68	0.57
Painted White	0.77	0.74
Painted Beige	0.67	0.67
Painted Off-White	0.56	0.52
Painted Almond	0.51	0.52
Painted Silver	0.45	0.43
Painted Copper	0.42	0.39
Painted Green	0.32	0.31
Painted Red	0.31	0.31
Note: Thermal emittance of unpainted metal surfaces is 0.08 – 0.10. Thermal emittance of painted surfaces is typically 0.84 - 0.87		

FSEC EXPERIMENTAL PROGRAMS

In the summer of 2000, the Florida Solar Energy Center (FSEC), in co-operation with Florida Power and Light (FPL) and Habitat for Humanity (HFH), instrumented seven side-by-side homes in Fort Myers, Florida with identical floor plans, construction, and orientation, but with different roofing systems designed to reduce attic heat gain (Parker et al., 2002). Six houses had R-19 ceiling insulation, and the seventh house had an unvented attic with insulation on the underside of the roof deck rather than the ceiling. Identical two-ton split system air conditioners with 5 kW strip heaters were installed in each of the seven homes. The houses underwent a series of tests to ensure that the construction and mechanical systems performed similarly.

A three-letter identification code is used to identify each roof product, and the initial solar reflectance and thermal emittance of new material are shown below.

Description of Test Roof on each HFH House	**Label**	**Solar Reflectance**	**Thermal Emittance**
• Dark Gray Fiberglass Shingles	RGS	0.082	0.89
• White Barrel-Shaped Tile	RWB	0.742	0.89
• White Fiberglass Shingle	RWS	0.240	0.91

Description of Test Roof on each HFH House	Label	Solar Reflectance	Thermal Emittance
• Flat White Tile	RWF	0.773	0.89
• Terra Cotta Barrel-Shaped Tile	RTB	0.346	0.88
• White 5-Vee Metal	RWM	0.662	0.86
• Dark Gray Fiberglass Shingles on a Sealed Attic having Insulation on the Roof Plane	RSL	0.082	0.89

The relative performance of the seven homes was evaluated for one month in the summer of 2000 under unoccupied and carefully controlled conditions. Parker et al., (2001) set the temperature controls on the air conditioning thermostats of all the houses at a constant 77º F (25°C). Table 2 summarizes the measured attic temperatures, cooling loads and savings for the seven homes over the unoccupied monitoring period; the data are ranked in descending order of total daily energy consumption. The average interior air temperature near the thermostat in all homes was within 1°F (0.56°C) of each other. However, because of the large influence of the thermostat temperature, the monitored cooling results in Table 1 are adjusted to account for set point differences among houses, (Parker et al., 2001). All thermostats were adjusted up 1°F (0.56°C) for four consecutive days and the data was used to map correction factors for power consumption by the air conditioner as effected by the variation in thermostat setpoint.

Not surprisingly, the control home (RGS) had the highest consumption (17.0 kWh/day). The true white roofing types (> 60% reflectance) had the lowest energy use. Both the white barrel (RWB) and white flat tile (RWF) roofs averaged a consumption of 13.3 kWh/day for respectively a 18.5% and 21.5% cooling energy reduction. The white metal roof (RWM) showed the largest impact with a 12.0 kWh/day July consumption, yielding a 24% reduction in cooling energy consumption.

TABLE 2: Cooling Performance* During Unoccupied Period: July 8 – 31, 2000

Site	Total kWh/d	Savings kWh/d	Thermostat (°F)	Thermostat (°C)	Mean Attic (°F)	Mean Attic (°C)	Max Attic (°F)	Max Attic (°C)	Temp. Adjust %	Field EER	Final Saving %
RGS	17.0	0.00	77.2	25.11	90.8	32.7	135.6	57.5	0.0	8.30	0.0
RTB	16.0	1.01	77.0	25.0	87.2	30.7	110.5	43.6	-1.6	8.12	7.7
RWS	15.3	1.74	77.0	25.0	88.0	31.1	123.5	50.8	-1.2	9.06	10.6
RSL	14.7	2.30	77.7	25.4	79.0	26.1	87.5	30.8	5.4	8.52	7.8
RWB	13.3	3.71	77.4	25.2	82.7	28.2	95.6	35.3	2.8	8.49	18.5
RWF	13.2	3.83	77.4	25.2	82.2	27.9	93.3	34.1	2.1	7.92	21.5
RWM	12.0	5.00	77.6	25.3	82.9	28.3	100.7	38.2	4.9	8.42	24.0

Note:
* Final savings are corrected for the differences in the interior temperature and the performance of the air conditioner among houses.

It is noteworthy that the average July outdoor ambient air temperature during the monitoring period (82.6°F [28.1°C]) was very similar to the 30-year average for Fort Myers (82°F [27.7°C]). Thus, the current data are representative of typical South Florida weather conditions. Relative to the standard control home, the data show two distinct groups in terms of performance.

- Terra Cotta tile, white shingle and sealed attic constructions produced approximately an 8% to 11% cooling energy reduction.
- Reflective white roofing yielded a 19% to 24% reduction in the consumed cooling energy.

White flat tile performed slightly better than the white barrel due to its higher solar reflectance. The better performance of white metal is believed due to the effect of thermal mass. The metal roof incurred lower nighttime and early morning attic temperatures than did the tile or shingles, leading to lower nighttime cooling demand. According to FPL, this study showed that a white painted galvanized metal roof should save a customer who lives in an average-size 1,770 square foot home approximately $128 or 23% to 24% annually in cooling costs, compared with a dark gray shingle roof on the same home. It should be noted, however, that this estimation is based on the assumption that the initial reflectance performance remains unchanged over time.

Peak Day Performance

July 26 was one of the hottest and brightest days in the data collection period and was used to view the effects of maximum solar irradiance on the candidate roofing systems and to also evaluate peak influences on utility demand (Table 3). The average solar irradiance was 371 W/m^2 and the maximum outdoor ambient air temperature was 93.0°F (33.8°C).

The roof decking temperature (Figure 1), measured just underneath the respective roof covers, were highest for the sealed attic construction (RSL) since the insulation under the decking forced much of the collected solar heat to migrate back out through the shingles. The sealed attic construction experienced measured deck temperatures that were 20ºF (11.1°C) higher than the control house during the sunlight hours. The (RGS) dark gray shingle had the next highest deck temperature; it reaching a peak high of 143.5°F (62°C). Increasing the solar reflectance of the (RGS) shingle from 0.082 to 0.24 for the white fiberglass shingle (RWS) dropped the peak deck temperature about 14°F (7.9°C). The white roofing systems (RWM, RWB and RWF) experienced peak deck temperatures approximately 40ºF (22°C) cooler than the darker shingles on the control house (RGS in Figure 1). The terra cotta barrel tile was about 29°F (16ºC) cooler on this July 26 day of peak solar irradiance.

The measured mid-attic air temperatures above the ceiling insulation further revealed the impact of the white reflective roofs with max attic temperatures about 35 to 40°F (19.2 to 22.2ºC) cooler than the control home (RGS), with the exception of white fiberglass shingles (Table 2). The white metal, white clay tile and the white shingle roofs did better at controlling demand than did the sealed attic on this very hot day. However,

the white metal roof performed best showing peak savings of 33% over the RGS control (Table 3).

TABLE 3: Summer Peak Day Cooling Performance for July 26, 2000

Site	Cooling Energy	Savings		Peak Period*		
		kWh	Percent	Demand (kW)	Savings (kW)	Percent
RGS	18.5 kWh		----	1.631	0.000	----
RTB	17.2 kWh	1.3	7%	1.570	0.061	3.7
RSL	16.5 kWh	2.0	11%	1.626	0.005	0.3
RWS	16.5 kWh	2.0	11%	1.439	0.192	11.8
RWF	14.2 kWh	4.3	23%	1.019	0.612	37.5
RWB	13.4 kWh	5.1	28%	1.073	0.558	34.2
RWM	12.4 kWh	6.1	33%	0.984	0.647	39.7
* Peak utility load occurred from 4 to 6 PM						

ORNL EXPERIMENTAL PROGRAMS

The Buildings Technology Center (BTC) of ORNL evaluated pre-painted and unpainted metal roof systems for the Cool Metal Roof Coalition (CMRC), a consortium of metal roofing industries. The American Iron and Steel Institute (AISI), the GALVALUME Sheet Producers of North America (NamZAC), the Metal Building Manufacturers Association (MBMA), the Metal Construction Association (MCA), and the National Coil Coaters Association (NCCA) are keenly interested in documenting whether their products can reduce the energy used for comfort cooling and heating of both residential and commercial buildings.

The study found that PVDF painted metal sheds dirt, retains its initial solar reflectance very well, resists the growth of biomass, resists corrosion, and performs similarly in different climates. Compared to some non-metallic roofing products, such as single-ply membrane which showed a drop in solar reflectance of 40% in a three-year period, painted metal retained 95% of its initial solar reflectance over the same time period (Miller, et al., 2004).

The BTC instrumented and field tested steep-slope and low-slope roof test sections of pre-painted and unpainted metals for three years on a test building called the Envelope Systems Research Apparatus (ESRA). The test assembly included white-painted PVDF galvanized steel, off-white polyester, 55% Al-Zn coated steel painted with a clear acrylic dichromate layer, unpainted galvanized steel, and unpainted 55% Al-Zn-coated steel. Five painted metal panels were tested on a steep-slope assembly. Three panels of white-painted PVDF galvanized steel, three panels of 55% Al-Zn-coated steel painted with a clear acrylic dichromate layer, six panels of bronze-painted PVDF aluminum, and three panels of black-painted PVDF galvanized steel were also exposed to East Tennessee's weather. An asphalt-shingle roof section was included as the base of comparison. It is warranted for a 15-year lifetime and has both Underwriter Laboratory and American

Society for Testing Materials (ASTM) approval for residential roofing. Salient features of the ESRA facility are fully discussed by Miller and Kriner (2001).

Reflectance measurements were made every three months on the ESRA's steep- and low-slope metal roofs. Each metal roof was described generically using an SR*xx*E*yy* designation. SR*xx* states the solar reflectance of a new sample, 1.0 being a perfect reflector. E*yy* defines the thermal emittance of the new sample, 1.0 being blackbody radiation. For example, the asphalt-shingle roof is labeled SR09E91 in Figure 2. Its freshly manufactured surface properties are therefore 0.09-solar reflectance and 0.91-thermal emittance. Miller and Kriner (2001) identify the SR*xx*E*yy* designations for the different painted and unpainted test metals tested at ORNL.

After 3.5 years of exposure, the white and bronze painted PVDF metal roofs, SR64E83 and SR07E87 respectively, lost less than 5% of their original reflectance. The coated steel painted with a clear acrylic dichromate layer, SR64E08, showed a 12% loss in reflectance. In comparison the asphalt shingle roof, SR09E91, had a measured reflectance of about 10% (Figure 2). The reflectance comparison is very important, because both SR64E83 and SR64E08 roofs reflected about 50% more solar energy away from these test roofs than did the asphalt shingle. Even more promising is the observed durability of the surface of the painted metals; reflectance remaind fairly level. Less heat is therefore absorbed by the "cool" painted metal roofs and the building load and the peak utility load are reduced as compared to darker more absorptive roofs (i.e., SR09E91). The urban heat content is also reduced because the "cool" painted metal roofs would not convect as much heat to the ambient wind blowing across the "cool" roof.

Testing conducted at the roof slopes of 4 inches of rise per 12 inches of run (i.e., steep slope-roof [SSR] in Figure 2) and at ¼ inch of rise per 12 inches of run (i.e., low-slope roof [LSR] in Figure 2) further show that the slope of the roof has little effect on the loss of reflectance for the painted metal roofing having the PVDF finish. The painted metal appears to have excellent corrosion resistance. Its surface opacity have limited any photochemical degradation caused by ultraviolet light present in sunlight over the three years of testing. All painted metal roofs have maintained their original manufactured appearance. After 3.5 years of exposure, acid rains with a measured pH of 4.3 in East Tennessee (National Atmospheric Deposition Program) have not etched the metal finish. ORNL scientists detected evidence of biological growth on some of the test roofs (Miller et al., 2002); however, the PVDF surface finish does not appear to allow the growth to attach itself and atmospheric pollution is washed off by rain.

Most dramatic are the trends observed in the solar reflectance and the thermal emittance of the painted metal roofs tested at different exposure sites across the country. Similar reflectance was measured in the hot, moist climate of Florida as compared to the predominantly cold climate of Nova Scotia (Figure 3). Solar reflectance and thermal emittance measures collected from the test fence exposure sites in Florida, Nova Scotia, Pennsylvania and also at Oak Ridge (Figure 3) are very similar to the reflectance and emittance measures recorded for the test roofs exposed on the ESRA in Oak Ridge (Figure 1). The changes in solar reflectance and thermal emittance of the painted PVDF metals are independent of climate. The results show that fence exposure data are a viable alternative for certifiying the painted PVDF metal roofs as Energy Star® compliant,

because they yielded very similar trends as the identical roofs exposed on the ESRA steep-slope assembly.

The emittance of the painted metal roofs did not change much after 3.5 years of weathering. In fact, the data in Figure 3 show that the emittance increased slightly over time.

AGED REFLECTANCE PERFORMANCE

Codes and standards organizations often specify only initial solar reflectance and thermal emittance values but no specific aged criteria. Instead, a standard rate of degradation is commonly assumed and applied to the initial values to predict aged values. For example, in the California state energy code Title 24, 2005 version, the prescriptive criteria for a "cool roof" specifies a minimum initial solar reflectance of 0.70 and thermal emittance of 0.75. The aged solar reflectance (ρ_{Aged}) value is calculated using the following equation:

$$\rho_{Aged} = 0.2 + 0.7 * [\rho_{initial} - 0.2]$$

Using the minimum initial solar reflectance $(\rho_{initial})$ of 0.70 prescribed by the 2005 version of Title 24, the calculation yields an assumed aged reflectance value of 0.55 or a 21.4% drop in initial solar reflectance for white-painted PVDF metal (Figure 3). Here the loss of solar reflectance is clearly overestimated. However, the prescriptive criteria fairly depict the loss of reflectance for the coated steel painted with a clear acrylic dichromate layer, SR64E08 (Figure 4).

Similarly, in the ASHRAE 90.1 commercial roofing standard, the insulation credits apply to cool roofs defined as having an initial solar reflectance of 0.70. The insulation adjustment factors are based on an aged solar reflectance value of 0.55 for the calculations. The white-painted PVDF metal appears to be unduly penalized because it retains its solar reflectance based on the three year results of the ORNL study. To further prove metal's superior retention of reflectance the metal industry collected data from the thousands of pre-painted metal samples routinely tested by suppliers for outdoor weathering. Outdoor exposure data from over a variety of time periods showed that PVDF paint systems, exposed in a variety of southern Florida weathering farms, retained approximately 95% of its initial solar reflectance (Figure 5). The data clearly demonstrates that the initial solar reflectance of pre-painted metal drops less than 5% from aging even after 30 years of exposure.

Therefore present codes and standards are unduly penalizing pre-painted metal roof systems. As an example, a light-colored painted metal roof product with a solar reflectance of 0.68 would not qualify as a "cool roof" in Title 24 or in the ASHRAE 90.1 standard even though its aged solar reflectance drops to only 0.65. In comparison, other types of non-metallic roofing that meet the initial "cool roof" solar reflectance criteria of 0.70, would be expected to degrade to a solar reflectance of about 0.55 after three years of climatic exposure. Hence, a painted metal roof may not be classed as a cool roof initially by some standards, but over time it could actually display a higher solar reflectance and provide greater energy efficiency than some "cool roofs" that meet the initial requirements but show significant degradation over time. In situations like these,

the painted metal roofing is actually disadvantaged in some code and standards with regard to the expected degradation over time.

Much of the cool roof initiative to date has focused on low-slope, large commercial roofing applications. This is true in Title 24, ASHRAE, IECC, and other codes or standards. As regulatory bodies begin to consider similar cool roof incentives for steep-slope and residential roofing applications, metal is poised to capitalize on its attractive surface properties. In steep-slope and residential roofing the aesthetics of color durability and retention of solar reflectance are expected to become more important in the selection of energy-efficient roofing materials. Codes and standards bodies should therefore take into consideration painted metal's excellent retention of solar reflectance when predicting energy savings beyond the three-year mark.

CONCLUSION

Cool metal roofing is durable in its appearance and properties, which includes its retention of initial solar reflectance. The initial value solar reflectance for pre-painted metal may not be as important as the aged value given the excellent retention of this property. This is due to the fact that the surface of this roofing material does not retain dirt or support growth of biomass. The tight tenacious bonding of the paint resin makes for a tough yet resistant surface. It has become a favorite choice of architects designing for a long lasting product with energy-efficient properties. Due to its demonstrated retention of initial solar reflectance, the standard rates of degradation cited in some codes and standards should be reconsidered for painted metal roofing products.

REFERENCES

Akbari, H. and S.J. Konopacki. 1998. "The Impact of Reflectivity and Emissivity of Roofs on Building Cooling and Heating Energy Use." *Thermal Performance of the Exterior Envelopes of Buildings*. Proceedings of ASHRAE THERM VII, Clearwater, FL, December.

American Society for Testing and Materials (ASTM). 2002. Designation D2244-02: Standard Practice for Calculation of Color Tolerances and Color Differences from Instrumentally Measured Color Coordinates. West Conshohocken, PA.: American Society for Testing and Materials.

Ducker Worldwide. 2002. "*2002 Metal Roofing Industry Profile and Analysis.*" Ducker Research Company Inc. and Metal Construction Association.

Miller, W. and B. Rudolph. 2004 "Exposure Testing Of Painted PVDF Metal Roofing." Report prepared for the Cool Metal Roof Coalition.

Miller, W.A. and S. Kriner. 2001. "The Thermal Performance of Painted and Unpainted Structural Standing Seam Metal Roofing Systems Exposed to One Year of Weathering." *Thermal Performance of the Exterior Envelopes of Buildings*. Proceedings of ASHRAE THERM VIII, Clearwater, FL, December.

Miller, W.A., A. Desjarlais, D.S. Parker and S. Kriner. 2004. “Cool Metal Roofing Tested for Energy Efficiency and Sustainability.” Proceedings of CIB World Building Congress, Toronto, Ontario, May 1-7, 2004.

Parker, D.S., J.K. Sonne, J.R. Sherwin, and N. Moyer. 2001, “Comparative Evaluation of the Impact of Roofing Systems on Residential Cooling Energy Demand in Florida.” Final Report FSEC-CR-1220-00, prepared for the Florida Power and Light Company, May.

Parker, D.S., J.K, Sonne, J.R. Sherwin. 2002, “Comparative Evaluation of the Impact of Roofing Systems on Residential Cooling Energy Demand in Florida.” *ACEEE Summer Study on Energy Efficiency in Buildings.* Proceedings of American Council for an Energy Efficient Economy, Asilomar Conference Center in Pacific Grove, CA, August.

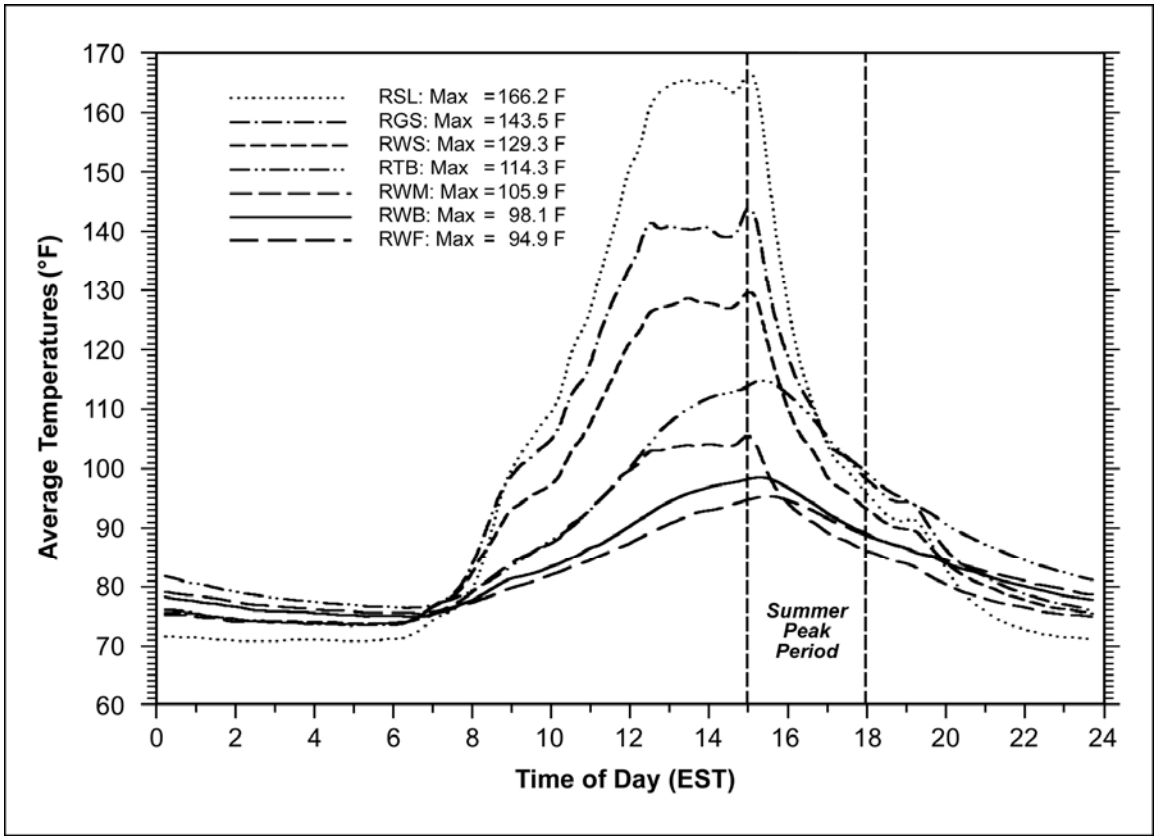

Figure 1. Roof surface temperatures for the demonstration homes tested by FSEC in Ft. Myers, FL.

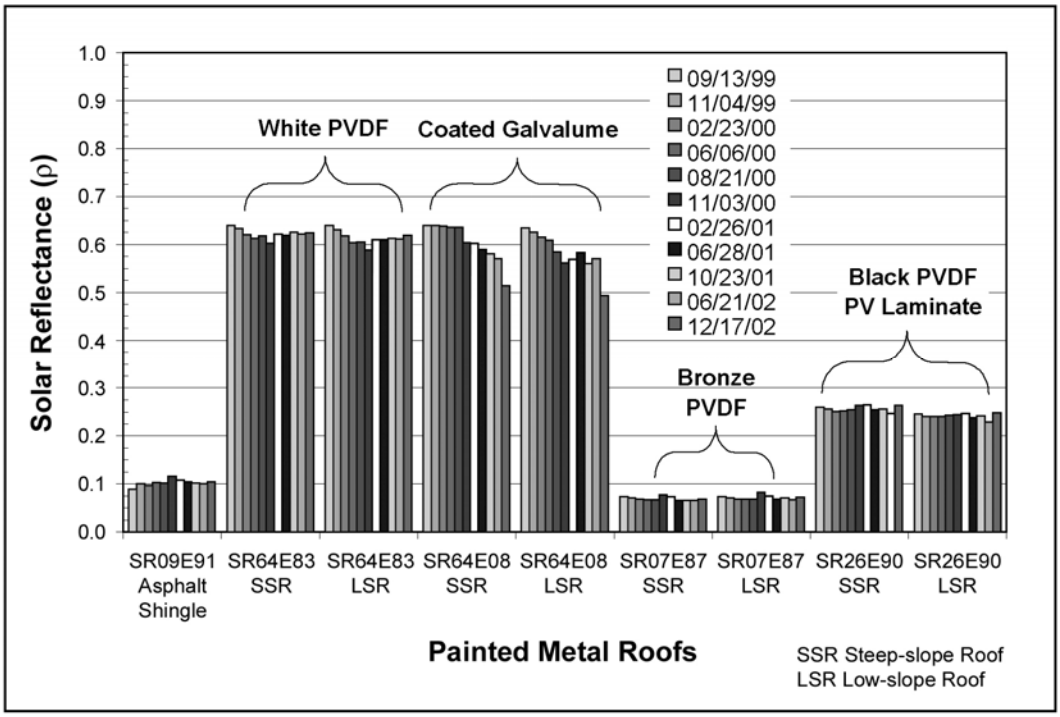

Figure 2. Solar reflectance of painted metal exposed to weathering on ESRA at Oak Ridge, TN.

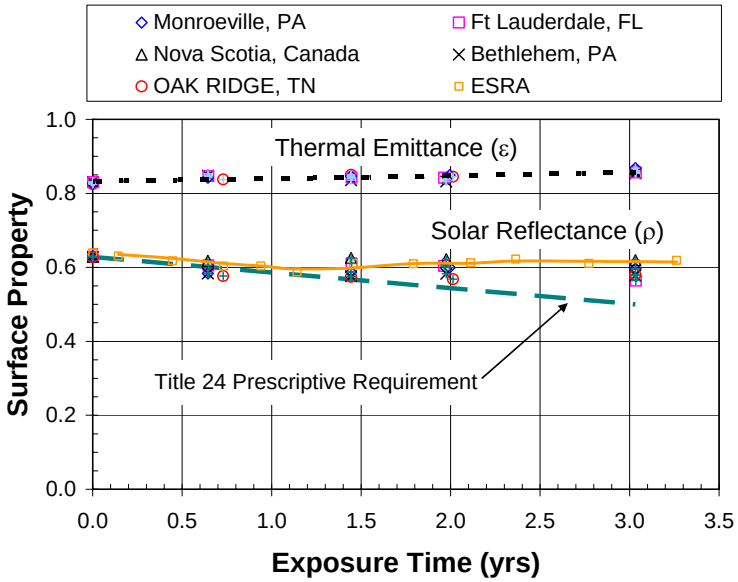

Figure 3. Solar reflectance and emittance of white PVDF painted metal (SR64E83) exposed at weathering sites and on the low-slope assembly at ORNL

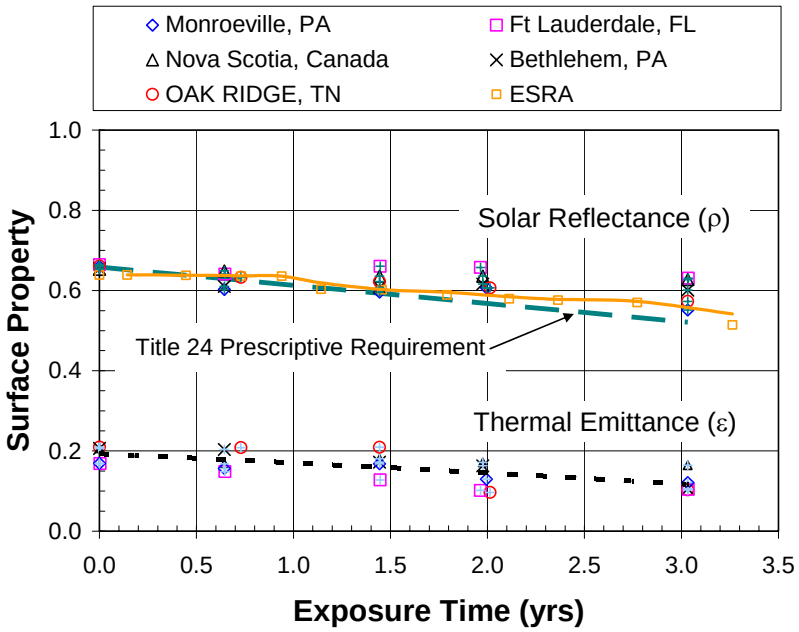

Figure 4. Solar reflectance and thermal emittance of 55% Al-Zn-coated steel with a clear acrylic dichromate layer exposed at weathering sites and on the low-slope assembly at ORNL.

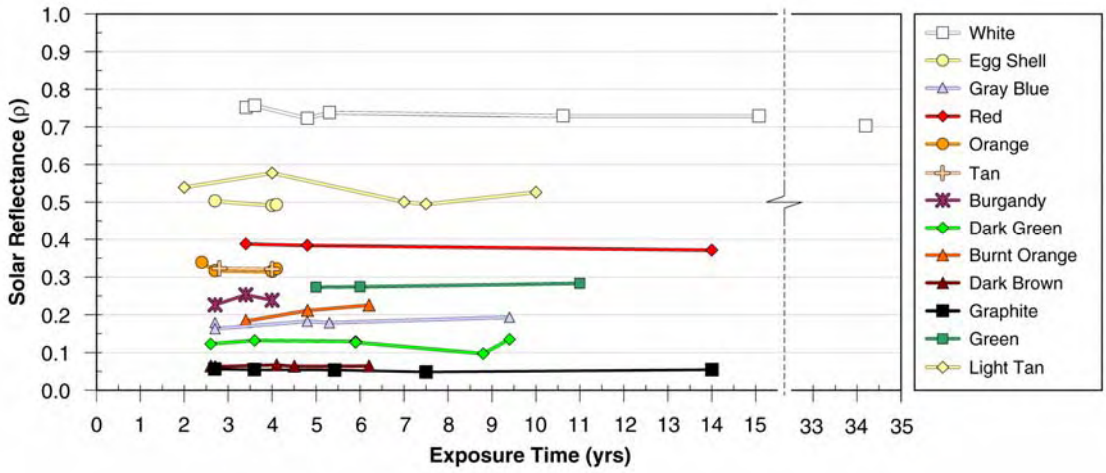

Figure 5. Solar reflectance of PVDF pre-painted metals from BASF, Atofina, Akzo Nobel and Solvay Solexis.

Special Infrared Reflective Pigments Make a Dark Roof Reflect Almost Like a White Roof

William (Bill) Miller[1], Ph.D.
Oak Ridge National Laboratory
Member ASHRAE

Kenneth T. Loye
FERRO Corporation

Andre Desjarlais
Oak Ridge National Laboratory
Member ASHRAE

Hashem Akbari, Ph.D.
Lawrence Berkeley National Laboratory
Member ASHRAE

Scott Kriner
Metal Construction Association

Stephen Wiel, Ph.D.
Lawrence Berkeley National Laboratory

Ronnen Levinson, Ph.D.
Lawrence Berkeley National Laboratory

Robert G. Scichili
BASF Corp

Paul Berdahl, Ph.D.
Lawrence Berkeley National Laboratory

ABSTRACT

Pigment colorant researchers are developing new complex inorganic color pigments that exhibit dark color in the visible spectrum and high reflectance in the near-infrared portion of the electromagnetic spectrum. The new pigments increase the near infrared reflectance of exterior finishes and paints thereby dropping the surface temperatures of roofs and walls, which in turn reduces the cooling-energy demand of the building. However, determining the effects of climate and solar exposure on the reflectance and the variability in color over time is of paramount importance for promoting these energy efficiency benefits and for accelerating the market penetration of products using the new color pigments.

INTRODUCTION

A new roofing product is about to revolutionize the building industry, bringing relief to homeowners and utilities alike. Cool Roof Color Materials (CRCMs) made from complex inorganic color pigments (CICPs) will reduce the amount of energy needed to cool buildings, helping the power utilities reduce hot-weather strain on the electrical grids. The new technology will help mitigate carbon dioxide emissions, reduce the impacts of metropolitan heat buildups and urban smog, and support conservation of water resources otherwise used to clean and process fuel consumed by fossil-fuel driven power plants Gipe (1995).

The California Energy Commission (CEC) has two sister laboratories' Oak Ridge (ORNL) and Lawrence Berkeley (LBNL) working collaboratively on a 3-year, $2 million project with the roofing industry to develop and produce new reflective, colored roofing products. The CEC aims to make CRCMs a market reality in the California homebuilding industry within 3 to 5 years. For tile, painted metal, and wood shake, the CEC's goal is products with about 0.50 solar reflectance. For residential shingles, the goal is a solar reflectance of at least 0.30.

The Florida Power & Light Company sponsored a field project in Fort Myers, FL that compared the energy performance of six identically constructed, side-by-side homes built with various reflective roof products. Parker, Sonne and Sherwin (2002) showed that a white galvanized metal roof and a white S-

[1] Dr. William Miller is a research scientist working at the Oak Ridge National Laboratory (ORNL). Kenneth Loye is the Technical Manager of the Pigments Group at FERRO Corporation. André Desjarlais is manager of ORNL's Building Envelope Group. Scott Kriner is Chairman of the Metal Construction Association. Robert Scichili is the Industrial Coatings Manager at BASF. Dr. Hashem Akbari, Dr. Ronnen Levinson and Dr. Paul Berdahl are research scientists working at Lawrence Berkeley National Laboratory. Steve Weil is retired from LBNL and serves as acting Director of the Cool Roof Project sponsored by the CEC.

shaped cement tile roof caused the respective Fort Myers' homes to use 4.2 to 3.0 kilowatt-hours per day less air-conditioning energy than an otherwise identical home with a dark gray asphalt shingle roof. The measurements showed that the white reflective roofs reduced cooling energy consumption by 18-26% and peak demand by 28-35%. The resultant annual savings for comfort cooling the two homes with white reflective roofs was reported at roughly $120 or about 6.7¢ per square foot per year, which is very promising. However, in the residential market, the issues of aesthetics and durability are more important to the homeowner than are the potentials for reduced air-conditioning loads and reduced utility bills. To homeowners, dark roofs simply look better than their counterpart, a highly reflective "white" roof. What the public does not know, however, is that the aesthetically pleasing dark roof can be made to reflect like a "white" roof in the near infrared spectrum.

Therefore a combined experimental and analytical approach is in progress with field data just coming available, some of which we are reporting along with preliminary results of computer simulations showing the potential energy savings throughout the U.S. for residential homes having CRCMs roofs. A roof covered with CRCMs absorbs less solar energy and we believe can reduce home air-conditioning energy ~20%, which in turn reduces the national primary energy consumption by ~0.5 quads per year.

COOL ROOF COLORED MATERIALS (CRCMs)

Dark roofing can be formulated to reflect like a highly reflective "white" roof in the near infrared (NIR) portion of the solar spectrum (700 to 2,500 nm). For years the vinyl siding industry has formulated different colors in the same polyvinyl chloride base by incorporating titantium dioxide (TiO_2) and black NIR-reflective paint pigments to produce dark siding that is cool in temperature (Ravinovitch and Summers 1984). Researchers discovered that a dark color is not necessarily dark in the infrared. Brady and Wake (1992) found that 10 μm particles of TiO_2 when combined with colorants such as red and yellow iron oxides, phthalocyanine blue, and paliogen black, could be used to formulate fairly dark colors with near-infrared reflectances of 0.3 and higher. Researchers working with the Department of Defense added complex inorganic color pigments (CICPs) to paints used for military camouflage and matched the reflectance of background foliage in the visible and NIR spectra. At 750 nm the chlorophyll[2] in foliage naturally boosts the reflectance of a plant leaf from 0.1 to about 0.9, which explains why a dark green leaf remains cool on a hot summer day. Tailoring CICPs for high NIR reflectance similar to that of chlorophyll provides an excellent passive energy saving opportunity for exterior residential surfaces such as walls and roofs. A CICP consisting of a mixture of the black pigments chromic oxide (Cr_2O_3) and ferric oxide (Fe_2O_3) increases the solar reflectance of a standard black pigment from 0.05 to 0.26 (Sliwinski, Pipoly & Blonski 2001).

Identification and Characterization of Pigments

We are working with pigment manufacturers to optimize the solar reflectance of a pigmented surface by identifying and characterizing pigments with optical properties suitable for cool roof color materials (CRCMs). LBNL characterized some 83 single-pigment paints as reported by Levinson, Berdahl and Akbari (2004b), and used the data to formulate and validate an algorithm for predicting the spectral irradiative properties Levinson, Berdahl and Akbari (2004a). LBNL also characterized various coating additives such as "transparent" mineral fillers (e.g., mica, clay, silica, talc) and binders (e.g., polymeric resins, silicates) to identify deleterious absorptions in the near infrared. The maximum amount of each material is then determined so that it will not impair the near-infrared reflectance of the pigmented surface. The spectral solar reflectance and transmittance; pigment chemistry, name, and measured film thickness; computed absorption and backscattering coefficients; and many ancillary values are planned for public dissemination for the 83 single-pigment paints from the Cool Roof web site (http://coolcolors.lbl.gov). Futher discussion of the pigment identification and characterization work is reported by Akbari et al. 2004.

Application of Pigments to Roof Products

Identifying, characterizing and then optimizing the reflectance of a pigmented coating is only part of the job for making dark yet highly reflective roof products. The application of the CRCMs varies among the different roof products, and we are working with industry to develop enginering methods for successfully applying them to the sundry roof systems. Each roofing type has its own specific challenges.

[2] Chlorophyll, the photosynthetic coloring material in plants, naturally reflects near-IR radiation.

For composition shingles, the application of pigmented coatings to roofing granules appears to be the critical process because the solar reflectance is predominately determined by the granules, which cover ~97% of a shingle's surface. Coating the granules with CRCMs helps increase reflectance, but some pigments are partly transparent to NIR light and therefore any NIR light not reflected by the cool pigment is transmitted to the dark substrate, where it is absorbed as heat. Multiple layers of coatings can be applied to increase reflectance; however, each additional coating increases cost. A two-step, two-layer process has proven more cost effective. In the first step, the granule is pre-coated with an inexpensive white pigment that is highly reflective to NIR light. In the second step, the cool-colored pigment is applied to the pre-coated granules.

A slurry coating process is used to add color to the surface of a clay tile. Once coated the clay is kiln-fired, and the firing temperature, the atmosphere and the pigments affect the final color and solar reflectance. However, for concrete tile the colorants are included throughout the bulk of the tile or are applied as a slurry coat to the surface. The addition of CRCMs to the material bulk requires too much pigment and makes the process too expensive. Coating the tile has been successfully demonstrated by American Rooftile Coatings who applied their COOL TILE IR COATING™ to several samples of concrete tiles of different colors (Fig. 1). The solar reflectance for all colors tested exceeded 0.40. Most dramatic is the effect of the dark colors. The black coating increased the solar reflectance from 0.04 to 0.41, while the chocolate brown coating increased from 0.12 to 0.41, a 250% increase in solar reflectance! Because solar heat gain is proportional to solar absorptance, the COOL TILE IR COATING™ reduces the solar heat gain roughly 33% of the standard color, which is very promising. The coating can certainly help tile roof products pass the Environmental Protection Agency's Energy Star 0.25 solar reflectance criterion as well as California's Title 24 pending criterion[3] for steep-slope roofing.

Premium coil coated metal roofing probably has the best opportunity for applying CRCMs because the paint coating is reasonably thick (~25 micron) and because the substrate has high NIR reflectance (ρ_{nir} ~ 0.55 to 0.7). The coatings for metal shingles are durable polymer materials, and many metal roof manufacturers have introduced the CRCM pigments in their complete line of painted metal roof products. The additional cost of the pigments is only about 5¢ per square foot of finished metal product (Chiovare 2002). Success of the new CRCM metal products is evident in the market share recently captured by the metal roof industry. Historically metal roofs have had a smaller share of only about 4% in the residential market. The architectural appeal, flexibility, and durability, due in part to the CICPs pigments, has steadily increased the sales of painted metal roofing, and as of 2002 its sales volume has doubled since 1999 to 8% of the residential market, making it the fastest growing residential roofing product (F. W. Dodge 2002).

FADE RESISTANCE OF ROOF PRODUCTS WITH CRCMs

The color of a roof product must remain fade resistant or the product will not sell. Industry judges fade resistance by measuring the spectral reflectance and transmittance of a painted surface and converting the measures to color-scale values based on the procedures in ASTM E308-02 (ASTM 2001). The color-scale values are compared to standard colors and the color differences (ΔL, Δa, and Δb), which represent the luminance of color, are calculated from:

- $\Delta L = L_{Batch} - L_{Standard}$, where $\Delta L > 0$ is lighter and a $\Delta L < 0$ is darker;
- $\Delta a = a_{Batch} - a_{Standard}$, where $\Delta a > 0$ is redder and a $\Delta a < 0$ is greener; and
- $\Delta b = b_{Batch} - b_{Standard}$, where $\Delta b > 0$ is more yellow and $\Delta b < 0$ is bluer.

Manufacturers of premium coil coated metal use a total color difference (ΔE) to specify the permissible color change between a test specimen and a known standard. The total color difference value is described in ASTM D 2244-02 (ASTM 2002), and is a method adopted by the paint industry to numerically identify variability in color over periods of time; it is calculated by the formula:

$$\Delta E = \left[(\Delta L)^2 + (\Delta a)^2 + (\Delta b)^2 \right]^{1/2} \qquad (1)$$

[3] Title 24 has legislation pending approval that will require new steep-slope roofs to have a reflectance exceeding the 0.25 Energy Star threshold after 2008.

Typically, premium coil-coated metal roofing is warranted for 20 years or more to have a ΔE of 5 units or less for that period. ΔE color changes of 1 unit or less are almost indistinguishable from the original color, and depending on the hue of color, ΔE of 5 or less is considered very good.

Fade Resistance Results for Painted PVDF Roofing

To evaluate color changes of CRCMs as compared to standard colors, we used a three-year exposure test to natural sunlight in Florida following ASTM G7-97 (ASTM 1997). Test data showed excellent light fastness of the CRCM masstones[4] exposed in the field (Fig. 2). The three color pairs labeled in Figure 2 are identified with their respective unweathered solar reflectance values (e.g., SR40 designation represents a solar reflectance of 0.40 for the CRCM green-painted PVDF metal). Differences in the masstone discoloration occur after two years of exposure for the green and brown CRCM coil-coated metals. However, both the green and brown CRCM colors have faded less than their counterpart standard colors. After three years of exposure the standard black has a ΔE~3.5 as compared to the CRCM black with only a 0.5 ΔE. Four years of exposure were also available for the standard colors, and the green and brown masstones were stable, while the black showed a ΔE of 21 (Fig. 2). The Florida exposure data is promising and shows that over the three-year test period the CRCMs fade less than do the standard masstone colors with known performance characteristics. For the CRCM black masstone the fade resistance is much improved over the standard color. Tints, expecially the blue tints are well known to fade; however, 50/50 tints of the CRCMs field tested in Florida also show excellent fade resistance (Table 1). The highest total color change was observed for the CRCM black tint, which is still indistinguishable from the original color.

Table 1. Color Difference for 50/50 tints of the CRCMs exposed to natural sunlight for three years in Florida. (ΔE based on International Commission on Illumination (CIE L*A*B) Index)

	Total color difference (ΔE)				
Years	Green	Yellow	Brown	Black	Marine Blue
1	0.55	0.21	0.47	0.19	0.46
2	0.42	0.25	0.70	0.67	0.50
3	0.53	0.14	0.99	1.51	0.76

The xenon-arc accelerated weathering tests were previously reported by Miller et al. (2002) and showed that after 5000 hours of xenon-arc exposure all CRCMs were clustered together with ΔE<1.5, which is considered a very good result.

FIELD TESTING OF ROOFS WITH CRCMs

Experimental field studies are in progress to catalog temperature, heat transmission, solar reflectance, thermal emittance and color fastness data for CRCMs applied to tile, metal, wood shake and composition shingle roofs. We are using the data to formulate and validate design tools for predicting the roof energy load during the cooling and heating seasons for residential buildings that use CRCM roof products. A demonstration site in Sacramento, California has two pair of identical homes, one pair roofed with concrete tile with and without the CRCMs and the other pair roofed with painted metal shakes with and without CRCMs. All roofs have the same visible dark brown color. A coating was applied to one of the two homes having concrete tile roofs; solar reflectance for the coated roof was a measured 0.41 as compared to the other base house with tile reflectance of only 0.08. Solar reflectance of the painted metal roof with CRCMs was 0.31 versus the roof with standard color metal shingles having 0.08 reflectance.

We are also exposing samples of metal, clay and concrete tile materials at weathering farms in seven different climate zones of California and are conducting thermal performance testing of several tile roofs of different profile on a fully instrumented roof assembly to help quantify the potential energy savings as compared to asphalt shingles. The Tile Roof Institute (TRI) and its affiliate members are keenly interested in specifying tile roofs as cool roof products using CRCMs. TRI is also keenly interested in knowing the effect of venting the underside of concrete and clay roof tiles. Beal and Chandra (1995) demonstrated a 45% daytime reduction in heat flux for a counter-batten tile roof as compared to a direct nailed shingle roof. The reduced heat flow occurs because of a thermally driven airflow within a channel that is formed by the tile nailed to a counter-batten roof deck. Typically, stone-coated metal and tile coverings are placed on

[4] Masstones represents the full color of the pigment while tints are blends of colors.

batten and counter batten supports, yielding complex air flow patterns through the supports. Correctly modeling the heat flow across the air channel is a key hurdle for predicting the thermal performance of tile roofs.

The data for these field studies are just coming online and will be reported in future publications. However, for the present work the results of simulations are presented for quantifying the potential energy savings for residential roofs with CRCMs. The data acquired from the demonstration homes and from the tile roof assemblies will be used to further formulate and validate our simulation tool, AtticSim.

THERMAL PERFORMANCE OF ROOFS WITH CRCMs

The ultimate goal of the pigment identification, characterization and application work is to increase the solar reflectance of roofing materials upwards of 0.50. Present CRCMs pose an excellent opportunity for raising roof reflectance from a typical value of 0.1 – 0.2 to an achievable 0.4 without compromising the home's exterior décor. The adoption of CRCMs into the roofing market can therefore significantly reduce the 2.0 quadrillion BTUs (quads) of primary electrical energy consumed for the comfort cooling of residential homes (Kelso and Kinzey 2000). To estimate these energy savings we conducted simulations using AtticSim based on two senarios:

1. energy savings for CRCM metal products already on the open market, and
2. energy savings for dark roof products achieving the 0.50 solar reflectance goal.

The Cool Metal Roof Coalition (CMRC) provided measurements of solar reflectance and thermal emittance of painted PVDF metal products. These values are used by AtticSim to answer the first question regarding potential energy savings for available CRCM products. The surface properties are as follow:

Table 2. Reflectance and emittance values* for PVDF metal roofs with and without CRCMs.

	Regal White	Surrey Beige	Colonial Red	Chocolate Brown
CRCM	SR75E80	SR65E80	SR45E80	SR30E80
Standard	SR70E80	SR52E80	SR27E80	SR08E80

*The roof colors are described generically using a SRxxEyy designation. "SRxx" states the solar reflectance; "Eyy" defines the thermal emittance. Thus, labeling the standard regal white color as SR70E80 indicates that it has a solar reflectance of 0.70 and an emittance of 0.80.

The Table 2 reflectance data were verified by a coatings manufacturer (Scichili 2004), and show that the darker the color the greater is the increase in reflectance induced by the CRCMs. ORNL used an emissometer to measure the emittance for several samples of the Table 2 colors and found the emittance to be 0.82 ± 0.02. The pigments in the CRCMs do not affect the emittance and at the request of the CMRC, we fixed emittance at 0.80 for all the simulations.

AtticSim SIMULATIONS

AtticSim is a computer tool for predicting the thermal performance of residential attics. It mathematically describes the conduction through the gables, eaves, roof deck and ceiling; the convection at the exterior and interior surfaces; the radiosity heat exchange between surfaces within the attic enclosure; the heat transfer to the ventilation air stream; and the latent heat effects due to sorption and desorption of moisture at the wood surfaces. Solar reflectance, thermal emittance and water vapor permeance of the sundry surfaces are input. The model can account for different insulation R-values and/or radiant barriers attached to the various attic surfaces. It also has an algorithm for predicting the effect of air-conditioning ducts placed in the attic (Petrie et al. 2004). The code reads the roof pitch, length and width and the ridge orientation (azimuth angle with respect to north) and calculates the solar irradiance incident on the roof. Conduction heat transfer through the two roof decks, two gables and vertical eaves are modeled using the thermal response factor technique (Kusuda 1969), which requires the thermal conductivity, specific heat, density and thickness of each attic section for calculating conduction transfer functions.

Heat balances at the interior surfaces (facing the attic space) include the conduction, the radiation exchange with other surfaces, the convection and the latent load contributions. Heat balances at the exterior

surfaces balance the heat conducted through the attic surface to the heat convected to the air, the heat radiated to the surroundings and the heat stored by the surface. Iterative solution of the simultaneous equations describing the heat balances yields the interior and exterior surface temperatures and the attic air temperature at one-hour time steps. The heat flows at the attic's ceiling, roof sections, gables and eaves are calculated using the conduction transfer function equations. The tool was validated by Wilkes (1991) against field experiments, and is capable of predicting the ceiling heat flows integrated over time to within 10% of the field measurement. AtticSim can predict the thermal performance of attics having direct nailed roof products but it has not been used to predict the heat flow across a tile roof having a venting occurring on the underside of the roof, between the roof deck and exterior roof cover.

Ventilation In Attic Space. An important issue in our study is the effect of venting the attic. CRCMs are best suited to hot and moderate climates and in hot climates the primary reason for ventilating an attic is to keep it cool and lessen the burden on the comfort cooling system. Ledger (1996) reported that some roof warranties insist on attic ventilation to protect their roof products against excessive temperatures. CRCMs can help improve the durability and extend the longevity of certain roof products, and the CRCMs will help lower the attic air temperature thereby reducing the heat penetrating the house.

The AtticSim simulations assumed equal soffit and ridge vent openings with a net free vent area of 1:300[5]. Using a constant ventilation rate is the simple approach to simulating the attic convective heat flows; however, thermal buoyancy affects the surface temperatures of the attic enclosure, which in turn causes error in the calculated attic heat flows. This is especially true in climates where there is little to no wind to force air in and out of the vents. Buoyancy, termed by many as stack effects, then becomes the sole driving force for attic ventilation.

AtticSim was exercised for a moderately insulated (R-19 h•ft²•°F/Btu) attic exposed in both hot and cold climates in the U.S. Roof pitch was set at 4-in of rise per 12-in of run and the ridge vent was oriented east–west. The soffitt and ridge vent areas were made equal and yielded a net free vent area of 1:300. We conducted a regression analysis to derive a correlation of AtticSim's computed attic ventilation air changes per hour (ACH) as function of the wind velocity and the computed attic-air-to-outdoor ambient air temperature gradient; results depicted in Figure 3. Summer (June, July and August) and winter (December, January and February) seasonal averages were used to fit the correlation. The regression coefficients for the correlation show a stronger dependence on stack effect than on the wind driven forces. Note that the correlation was not used for computing ACH, rather it was derived to better view both stack and wind effects in a simple two-dimensional plot and for comparing AtticSim's computations to published literature data. The ordinate of Figure 3 is scaled by the regression paramenter $1.1\{V^{0.04}\}$. The curve fit $\{\Delta T\}^{0.33}$ is superimposed onto AtticSim's computed ACH values, which as stated are scaled by $1.1\{V^{0.04}\}$. The resultant graph allows direct comparison of the data by Burch and Treado (1979) and by Walker (1993) to AtticSim's output. Burch and Treado (1979) listed field data for soffit and ridge venting of a Houston, Texas house. A tracer gas technique using sulfur-hexafluoride was released at six-inch levels above the ceiling insulation at eight different attic locations. Sixteen air samples were collected at different attic locations and the dilution of the gas yielded the ACH. They stated the attic ventilation measurements were probably somewhat on the high side; however, their field data for soffitt and ridge venting compares well to the results computed by AtticSim. Walker (1993) studied attic ventilation in Alberta, Canada. His results showed large variations in ventilation rates. We culled his data by selecting some of the measured ACH values for wind speeds not exceeding 4.5 mph (2 m/s). Further, Parker, Fairey and Gu (1991) also measured attic ventilation rates using short term sulfur hexafluoride tracer gas. Their results under normal summer wind and thermal conditions in Cape Canaveral, Florida yielded an average of 2.7 ACH over a three-day period with variation from 0.5 to 4.5 ACH. The AtticSim simulations yielded an annual average of 2.9 ACH with variation from 0.2 to 10 ACH. Therefore, the AtticSim code appears consistent with literature data, and yields reasonable values of attic ventilation for the soffit and ridge venting being exercised in this report.

SIMULATION PROCEDURE. Simulations generated the heat flux entering or leaving the conditioned space for a range of roof insulation levels, exterior roof radiation properties, and climates derived from the TMY2 database (NREL 1995). Roof insulation levels ranged from no ceiling insulation

[5] Ventilation area is defined as the ratio of the net free vent area to the footprint of the attic floor area.

through R-49. Simulations assumed painted PVDF metal roofs with and without CRCMs. The roof's solar reflectance and thermal emittance were chosen based on the state-of-the art CRCMs on the open market and also based on our ultimate goal for optimizing solar reflectance (see Table 2). The roofs are assumed direct nailed to the roof deck having only a direct conduction path through the material of the roof deck. The hourly averages of the outdoor ambient dry bulb and specific humidity, the cloud amount and type, the wind speed and direction and the total horizontal and direct beam solar irradiance were read from the TMY2 database for the climates of Miami, FL; Dallas, TX; Burlington, VT; and Boulder, CO. The hourly ceiling heat flux predicted by AtticSim was used to generate annual cooling and heating loads for the attic and roof combinations. An annual cooling load $[Q_{Cool}]$ was defined as the time integrated heat flux entering the conditioned space through the ceiling when the outdoor air temperature exceeded 75°F (24°C). Similarly, the annual heating load $[Q_{Heat}]$ was defined as the time integrated heat flux moving upward through the ceiling if the outdoor air temperature dropped below 60°F (16°C).

The output from AtticSim can be coupled to the DOE-2.1E program to model the effect of the ceiling heat flux from the perspective of the whole house energy consumption. However, the multiplicity of residential homes, the diversity of occupant habits, the broad range of exterior surface area-to-house volume, and the internal loading can confound the interpretation of results developed for reflective roofing. Therefore, the reported results center on the heat flows entering and leaving the ceiling of the house. Further analysis of the whole house will be conducted as the data become available from the demonstrations sites to validate our results.

SIMULATION RESULTS The annual energy savings due to the change in heat penetrating the ceiling is displayed in Figure 4 for the various painted PVDF metals whose solar reflectance and thermal emittance properties are listed in Table 2. The reductions in energy (cooling savings) are based on the difference in ceiling heat flux for the same color roof with and without CRCMs. Potential savings are also shown for a popular chocolate brown roof whose solar reflectance is increased from 0.08 to our ultimate reflectance goal of 0.50.

A chocolate brown color roof with 30% reflective CRCMs decreased the consumed cooling energy by 15% of that used for a roof with standard colors exposed in Miami and Dallas; the cooling savings are respectively 623 and 884 Btu per yr per square foot of ceiling for an attic having R-19 insulation[6] (Fig. 4). We believe the pigment optimizations can increase reflectance to the 0.50 mark. In that case, the heat penetrating the ceiling would drop by 30% of that computed for the same standard color roof exposed in Miami and Dallas.

Notice that as the roof color lightens, the CRCMs produce less energy savings as compared to the same standard pigmented color because the lighter colored standard materials have higher solar reflectance to start with (Fig. 4). The increase in solar reflectance caused by CRCMs diminishes as the visible color of the roof lightens from black to brown to a white painted PVDF metal (Fig. 4). The CRCMs induce about a 0.05 reflectance point increase for white-painted metal (SR70E80) while a darker chocolate brown roof (SR08E80) increases 0.22 points (Table 2), which is the benefit of the CRCMs. People prefer the darker color roof and the dark colors yield the higher gain in reflectance. The data in Figure 4 therefore show the level of achievable energy savings with roof color for existing CRCMs being marketed as cool roof products. However further improvements are achievable! We have successfully demonstrated concrete tile coatings (Fig. 1) with reflectances slightly above 0.40 and continue to develope prototype coatings to achieve our solar reflectance goal of 0.50, a ~0.40 increase in solar reflectance over a standard brown color!

Figure 4 compares materials of the same color. However, the lighter the color of the roof, the greater are the energy savings due to less heat penetrating the roof. If the comparison is made between different colors, one can judge the thermal advantage gained by selecting a lighter roof décor. As example, if the surrey biege with CRCM (SR65E80) is compared to the standard chocolate brown (SR08E80), then the surrey beige reduces the ceiling heat flux 42% of that predicted for the standard brown SR08E80 roof exposed in Dallas with R-19 attic insulation. In comparison the same chocolate brown color (SR30E80) saved 15% as compared to the same color SR08E80.

[6] The International Energy Conservation Code's recommended ceiling R-value for Dallas is R-19 and for Miami it is R-13 for a home having windows covering 12% of the exterior walls.

CRCMs IN VARIOUS CLIMATES Simulations for attics with R-19 insulation (Fig. 5) show the tradeoffs between the heating and cooling season. In the more moderate climates there is a heating load penalty that offsets the cooling energy savings and because higher levels of insulation are required in moderate to cold climates CRCMs do not yield an energy savings. Burlington VT is a cold climate and incurs an annual penalty for roofs with CRCMs (Fig. 5) regardless of the level of attic insulation. A slight benefit is observed for the climate of Boulder exposing brown and surry biege colored roofs having CRCMs (Fig. 5). Obviously the hotter the climate the better is the performance of the CRCMs. In Miami, the net savings are almost 900 Btu per year per square foot for a chocolate brown CRCM covering an attic with R-19 ceiling insulation (Fig. 5).

CEILING INSULATION EFFECTS The most obvious trend shown in Figure 4 is the effect of the ceiling insulation on the reduction of heat penetrating into the conditioned space. The level of attic insulation directly affects the ceiling's thermal load. As example, for Dallas TX, a chocolate brown metal roof (SR30E80) saves about 4902 Btu per year per square foot for an attic having no ceiling insulation (Fig. 4). Increasing the insulation to R-19 drops the savings to 623 Btu per year per square foot. R-49 further drops the savings to only 250 Btu per year per square foot. Table 3 lists the International Energy Conservation Code's recommended attic R-value based on the number of heating degree-days (HDD_{65}). The number of cooling degree days (CDD_{65}) and the average daily solar flux are also listed in Table 3. We included our predictions of the attic heat penetrating the ceiling of a house having the chocolate brown painted PVDF metal roof with and without CRCM. The calculations used the recommended attic insulations from the IECC (2000) for each city (Table 3).

In Burlington, VT a house with R-49 attic insulation does not yield enough cooling benefit from the CRCMs to merit their use. In Bolder the cooling benefit is about 164 Btu per year per square ft, and it exceeds the heating penalty by only 23 Btu per yr per square ft. In Dallas, TX the recommended R-19 attic with SR30E80 chocolate brown CRCM dropped the heat flux entering the ceiling by 623 Btu per yr per square ft of ceiling. In the still hotter climate of Miami, the CRCM SR30E80 incurrs 15% less energy penetrating the ceiling for an R-13 attic. Using the SR60E80 CRCM the performance improves and about 31% less energy penetrated from the attic into the house.

Table 3. Ceiling insulation minimum R-values recommended by the International Energy Conservation Code (IECC, 2000) for homes with windows covering 12% of the exterior wall.

	Burlington, VT	Boulder, CO	Dallas, TX	Miami, FL
Recommended R-Value	**R-49**	**R-38**	**R-19**	**R-13**
HDD_{65}	7903	6012	2304	141
CDD_{65}	407	623	2415	4127
Solar flux[1] [Btu/(h·ft^2)]	1194	1467	1559	1557
SR08 Annual Cooling [Btu/yr·ft^2]	335	920	4017	8450
SR50 Annual Cooling [Btu/yr·ft^2]	215	596	2798	5860

[1]Average daily global flux incident on a horizontal surface.

[2]Annual cooling represents the annual energy transfer by attic heat penetrating through the ceiling into the living space.

It is interesting that both Burlington and Boulder, which have moderate cooling demands also have incident solar irradiance that is almost as much as that for Dallas and Miami (Table 3). Despite the low energy savings in Boulder or Burlington as compared to the hotter climates, the high summer irradiance affects peak demand loads on the electric utility seen in urban areas. CRCMs will help alleviate the demand load as homeowners replace their roof, which they are more apt to do than adding attic insulation.

THE ECONOMICS OF ROOFS WITH CRCMs

We estimated the value of energy savings using the electric and natural gas prices published at the Energy Information Administration's web site http://www.eia.doe.gov/. An electricity cost of $0.10 per

kWh and natural gas cost of \$10.00 per 1000 ft^3 (about 10^6 Btu or 10 Therm) are slightly above the 2001 national average for these energy sources and are assumed for estimating the value of energy savings.

ALGORITHM FOR ESTIMATING SAVINGS The coefficient of performance (COP) describes the performance of the HVAC system in terms of the ratio of the machine's cooling capacity to the power needed to produce the cooling effect. To estimate the value of the electrical energy savings requires systems performance data for the HVAC unit:

$$\mathrm{COP}_{\mathrm{HVAC}} = \frac{\mathrm{Cooling\ Capacity}}{\mathrm{Power}_{\mathrm{HVAC}}} \qquad (2)$$

Because the HVAC unit meets the house load, the heat penetrating the ceiling $[Q_{Cool}]$ can substitute for the "Cooling Capacity" term of Eq. 2 to estimate the power needed to meet the attic's portion of the building load. Cost savings (\$cool) follow from the formula:

$$\$\mathrm{cool} = \frac{Q_{cool} \cdot \$\mathrm{elec}}{\mathrm{COP}_{\mathrm{HVAC}}} \qquad (3)$$

The annual heating energy cost savings (\$heat) require the efficiency of the furnace and are calculated by the formula:

$$\$\mathrm{heat} = \frac{Q_{heat} \cdot \$\mathrm{fuel}}{\eta_{heat}} \qquad (4)$$

The efficiency of the furnace (η) was set at 0.85 and is relatively constant; however, the cooling COP of HVAC equipment typically drops as the outdoor air temperature increases, as the heat exchangers foul, as mechanical wear occurs on the compressor valves and especially as the unit leaks refrigerant charge. Hence what COP should one use to fairly judge cost savings? A conservative approach would be to use the average COP of 2.5 for new HVAC equipment reported by Kelso and Kinzey (2000).

PREDICTED SAVINGS FOR CRCMS AND INSULATION The more insulation in the attic the lower is the ceiling heat flow, and the less is the benefit of more reflective roofing. Conversely, it is also true that the higher the solar reflectance of the roof the lower is the ceiling heat flow, and the less is the benefit of additional ceiling insulation in cooling dominant climates. There can therefore be a tradeoff between the level of ceiling insulation and the solar reflectance of the roof, and the tradeoff is constrained by material costs and the value of energy saved by the CRCMs and by the ceiling insulation.

In Miami the recommended ceiling insulation for a house with about 12% exterior window coverage is R-13 (IECC 2000). Dallas requires R-19 ceiling insulation. Typically a dark residential roof has a solar reflectance of about 0.08. We therefore assumed these recommended insulations levels and used SR08E80 as the base for computing the savings in operating energy for incremental increases in both CRCMs and additional insulation for roofs exposed in Miami and Dallas.

We looked at the energy savings from the perspective of increasing the amount of blanket insulation in the ceiling while holding the solar reflectance constant at 0.08 and also at the higher value of 0.45 (plots SR08 and SR45 in Figure 6). R-values 19, 30, 38 and 49 are displayed to help the reader pick off the savings data listed on the abcissa of Figure 6. The savings are based on the incremental gains over an SR08E80 roof with R13 insulation in Miami and R-19 insulation in Dallas. An SR08E80 roof in Miami saves ~5 cents per year per square ft if blanket insulation is increased from R13 to R19 (see SR08 plot for Miami). For CRCMs having 0.45 solar reflectance, the savings are ~4 cents per year per square ft. The installed cost for R-19 insulation is about \$0.36 per square ft in new construction and is \$0.41 for existing construction (R.S. Means 2002). From these data, the additional insulation (R-13 to R-19) is paid for in

about 7 years for new construction and in about 8 years for existing construction for an SR08 roof. In Dallas going from the recommended R-19 to R-38 yields savings of ~$0.05 per year per square ft, which for new construction pays for itself in ~7 years.

Figure 6 also shows the energy savings from the perspective of increasing roof reflectance while holding the ceiling insulation constant at the recommended code level and at the higher level of R-38. The R-13 plot for Miami (Fig. 6) shows the cost savings for CRCMs on an attic with R-13 ceiling insulation (SR values are labeled from 0.08 to 0.75). Results show that CRCMs yield savings of about 2.2 cents per year per square foot for the identical color SR30E80 roof as compared to the SR08E80 roof with R-13 insulation. As stated earlier, the incremental cost for adding CRCMs to coil-applied metal roofing is ~5 cents per square foot. Hence, the savings in Miami pay for the CRCM technology in about 2½ years. Increasing solar reflectance to 0.50 increases the cost premium and the CRCMs pay for themselves in just 1 year! In Dallas with R-19 recommended insulation, the SR30E80 roof pays for the added cost of the CRCMs in about 5 years; at 0.50 solar reflectance the premium shortens to ~2½ years. If the ceiling insulation is increased to R-38, the incremental increases in solar reflectance are not as economically effective as seen by the slopes of the R-13 vs R-38 plots for Miami (Fig. 6). The savings in Miami are ~$0.10 per year per square ft for the SR08E80 roof (R-13 vs R-38) and diminish to about $0.06 per year per square ft for a SR75E80 roof (again, R-13 vs R-38). The comparable savings in Dallas are about half those predicted for Miami (Fig. 6).

For the earlier stated fuel prices and the energy savings, the annual cost savings per square foot of ceiling can be as high as $0.07 per year per square ft in Miami, FL for a house with R-13 ceiling insulation. In Dallas the savings can be as high as $0.03 per year per square ft for a house with R-19 ceiling insulation. Therefore the CRCMs have an affordable premium; energy savings easily pay for the roughly 5¢ added expense of the pigments in a CRCM metal roof.

SUMMARY

We have identified and characterized some 83 different complex inorganic pigments and are developing engineering methods to apply them with optimum solar reflectance for the various roof products. Coatings have been developed and demonstrated that match a tile's color and increase the solar reflectance from about 0.08 to over 0.40, a 5-fold jump in reflectance. The solar reflectance of painted PVDF metals available on the open market are about 3 times better with the addition of CRCMs, and we expect further gains as more pigments are identified and new engineering applications are adopted for the production of the metal roof products. Work continues to improve the solar reflectance to our 0.50 goal for tile and painted PVDF metal roofing.

Accelerated weather testing using natural sunlight and xenon-arc weatherometer exposure are proving the CRCMs retain their color. After three years of natural sunlight exposure in southern Florida, the CRCMs show excellent fade-resistance and remain colorfast. The CRCMs have excellent discoloration resistance, as proven by the three-years of field exposure and the 5000 hours of xenon-arc exposure. Their measure of total color difference was an ΔE value less than 1.5. CRCM 50/50 tints field tested in Florida also showed excellent fade reisitance. The highest total color change was observed for the CRCM black tint, which is still indistinguishable from the original color. Therefore, color changes in many of the CRCMs are indistinguishable from their original color.

CRCMs reflect much of the NIR heat and therefore reduce the surface temperature of the roof. The lower exterior temperature leads to energy savings. A chocolate brown color roof with 30% reflective CRCMs decreases the consumed cooling energy by 15% of that used for a roof with standard chocolate brown color exposed in Miami and Dallas. If we achieve reflectance measures of 0.50 the energy savings increase to ~30% of the heat flow through an attic having recommended ceiling insulation and the same color roof. The CRCMs also provide an ancillary benefit in older existing houses that have little or no attic insulation and poorly insulated ducts in the attic because the cooler attic temperature in turn leads to reduced heat gains to the air-conditioning ductwork.

The cost to the homeowner to achieve this efficiency improvement for coil-applied metal roofing is the incremental cost of about 5¢ per square foot. The CRCMs being sold in coil-applied metal roofing yield

savings of about 2.2¢ per year per square foot for the identical color SR30E80 roof as compared to the SR08E80 roof with R-13 insulation. Hence, the savings in Miami pay for the CRCM technology in about 2½ years. Increasing solar reflectance to 0.50 increases the cost premium and the CRCMs would pay for themselves in just 1 year!

REFERENCES

Akbari, H., Berdahl, P., Levinson, R., Wiel, S., Desjarlais, A., Miller, W., Jenkins, N., Rosenfeld, A., Scruton, C. 2004. "Cool Colored Materials for Roofs," in ACEEE Summer Study on Energy Efficiency in Buildings, proceedings of American Council for an Energy Efficient Economy, Asilomar Conference Center in Pacific Grove, CA., Aug. 2004.

American Society for Testing and Materials (ASTM). 2002. Designation D2244-02: Standard Practice for Calculation of Color Tolerances and Color Differences from Instrumentally Measured Color Coordinates. West Conshohocken, Pa.: American Society for Testing and Materials.

———. 1997b. Designation G7-97: Standard Practice for Atmospheric Environmental Exposure Testing of Nonmetallic Materials. West Conshohocken, Pa.: American Society for Testing and Materials.

———.2001. Designation E 308-02: Standard Practice for Computing the Colors of Objects by using the CIE System. West Conshohocken, Pa.: American Society for Testing and Materials.

Beal, D. and Chandra, S., 1995. "The Measured Summer Performance of Tile Roof Systems and Attic Ventilation Strategies in Hot Humid Climates," Thermal Performance of the Exterior Envelopes of Buildings VI, U.S. DOE/ORNL/BETEC, December 4-8, 1995, Clearwater, FL.

Brady, R. F., and L. V. Wake. 1992. "Principles and Formulations for Organic Coatings with Tailored Infrared Properties." Progress in Organic Coatings 20:1–25.

Burch, D.M. and Treado, S.J. 1979. "Ventilating Residences and Their Attics for Energy Conservation—An Experimental Study." NBS Special Publication 548: Summer Attic and Whole House Ventilation. Washington, D.C.: National Bureau of Standards.

Chiovare, Tony CEO of Custom-Bilt Metals, personal communications with ORNL and LBNL on cost premiums for painted metal roofs having CRCMs.

Gipe, P. 1995. Wind Energy Comes of Age, John Wiley & Sons.

F.W. Dodge. 2002. Construction Outlook Forecast, F.W. Dodge Markert Analysis Group, 24 Hartwell Avenue, Lexington, MA 02421. Telephone 800-591-4462, FAX 781-860-6884, URL:www.FWDodge.com.

International Energy Conservation Code, 2000, p. 81.

Kelso, J., and Kinzey, B., 2000, "BTS Core Data Book," DOE's Office of Building Technology, State and Community Programs, U.S. Department of Energy, Washington, DC.

Kusuda, T. 1969. "Thermal Response Factors for Multi-Layer Structures of Various Heat Conduction Systems," ASHRAE Transactions, Vol. 75, Part 1, pp. 246-271.

Ledger, G. 1996. "Building Hot Roofs." House Magazine, Patric Gass and Company, Inc.

Levinson, R., and Berdahl, P., and and Akbari, H. 2004a. "Solar Spectral Optical Properties of Pigments, Part II: Survey of Common Colorants." in review at LBNL.

Levinson, R., and Berdahl, P., and and Akbari, H. 2004b. "Solar Spectral Optical Properties of Pigments, Part I: Model for Deriving Scattering and Absorption Coefficients from Transmittance and Reflectance Measurements." in review at LBNL.

Miller, W.A., Loye, K. T., Desjarlais, A. O., and Blonski, R.P. 2002. "Cool Color Roofs with Complex Inorganic Color Pigments," in ACEEE Summer Study on Energy Efficiency in Buildings, proceedings of American Council for an Energy Efficient Economy, Asilomar Conference Center in Pacific Grove, CA., Aug. 2002.

NREL, 1995, "TMY2s. Typical Meteorological Years Derived from the 1961–1990 National Solar Radiation Database," Data Compact Disk. National Renewable Energy Laboratory, Golden, CO.

Parker, D.S., Fairey, P.W., and Gu, L. 1991. "A Stratified Air Model for Simulation of Attic Thermal Performance," pp. 44-69, Insulation Materials: Testing and Applications, 2nd Volume, ASTM STP 1116, R.S. Graves and D.C. Wysocki, Eds. Philadelphia, PA: American Society for Testing and Materials.

Parker, D.S., Sonne, J. K., Sherwin, J. R. 2002. “Comparative Evaluation of the Impact of Roofing Systems on Residential Cooling Energy Demand in Florida,” in ACEEE Summer Study on Energy Efficiency in Buildings, proceedings of American Council for an Energy Efficient Economy, Asilomar Conference Center in Pacific Grove, CA., Aug. 2002.

Petrie, T.W., Stovall, T.K., Wilkes, K.E. and Desjarlais, A.O. 2004. “Comparison of Cathedralized Attics to Conventional Attics: Where and When Do Cathedralized Attics Save Energy and Operating Costs?,” to be published in Thermal Performance of the Exterior Envelopes of Buildings, IX, proceedings of ASHRAE THERM VIII, Clearwater, FL., Dec. 2004.

Ravinovitch, E. B., and J. W. Summers. 1984. “Infrared Reflecting Vinyl Polymer Compositions.” U.S. Patent 4,424,292. January 3.

R. S. Means Company, Means CostWorks 2002, R. S. Means Company, Inc., Kingston, MA, Version 6.0

Robert G. Scichili, BASF Industrial Coatings, personal communications with ORNL on reflectance of painted PVDF metals containing CRCMs, April 2004.

Sliwinski, T. R., R. A. Pipoly, and R. P. Blonski. 2001. “Infrared Reflective Color Pigment.” U.S. Patent 6,174,360, January 16.

Walker, I. S. May 1993. “Prediction of Ventilation, Heat Transfera nd Moisture Transport in Attics.” Ph.D. dissertation, Edmonton, Alberta, Canada.

Wilkes, K.E. 1991.*Thermal Model of Attic Systems with Radiant Barriers.* ORNL/CON-262. Oak Ridge, Tenn.: Oak Ridge National Laboratory.

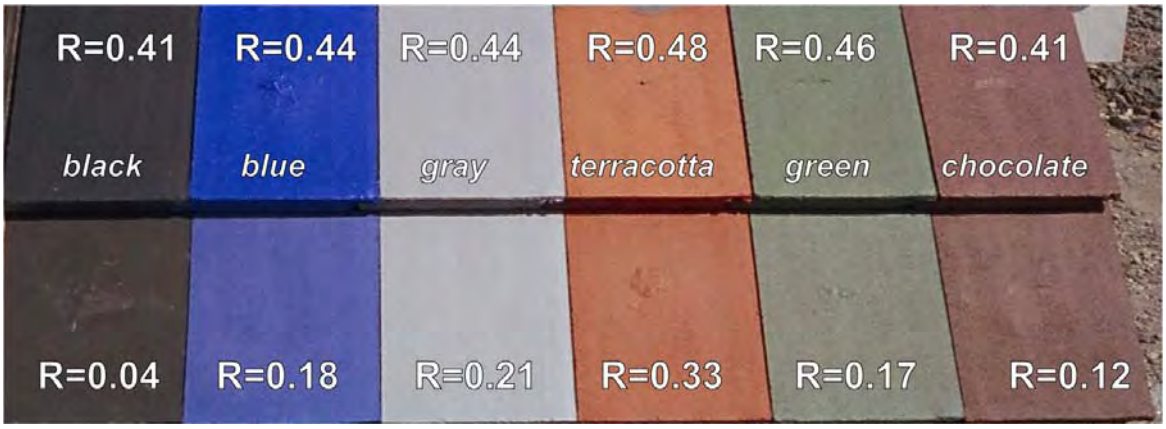

Figure 1. Solar reflectance of concrete tile roofs with CRCMs (top row) and without CRCMs (bottom row). The COOL TILE IR COATING™ technology was developed by Joe Riley of American Rooftile Coating.

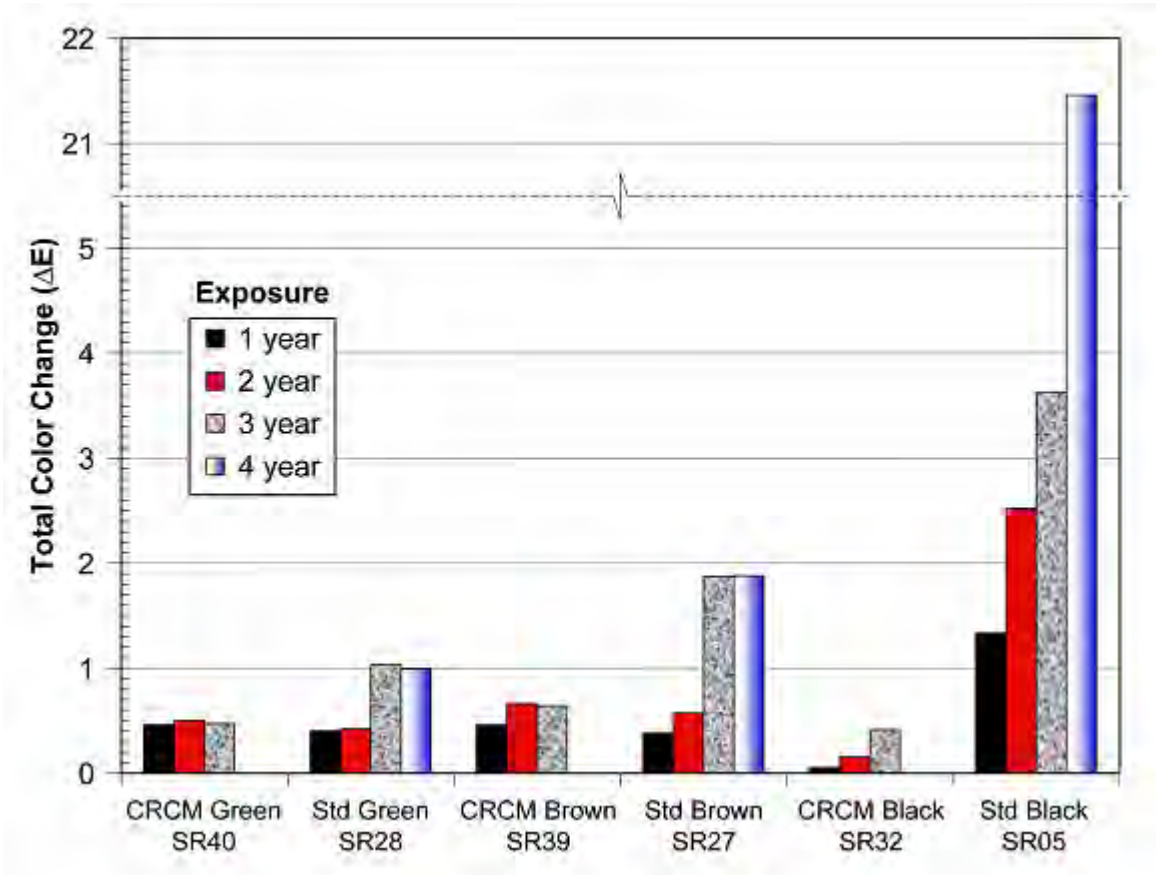

Figure 2. Three years of natural sunlight exposure in Florida shows that the CRCMs have improved the fade resistance of the painted PVDF metals.

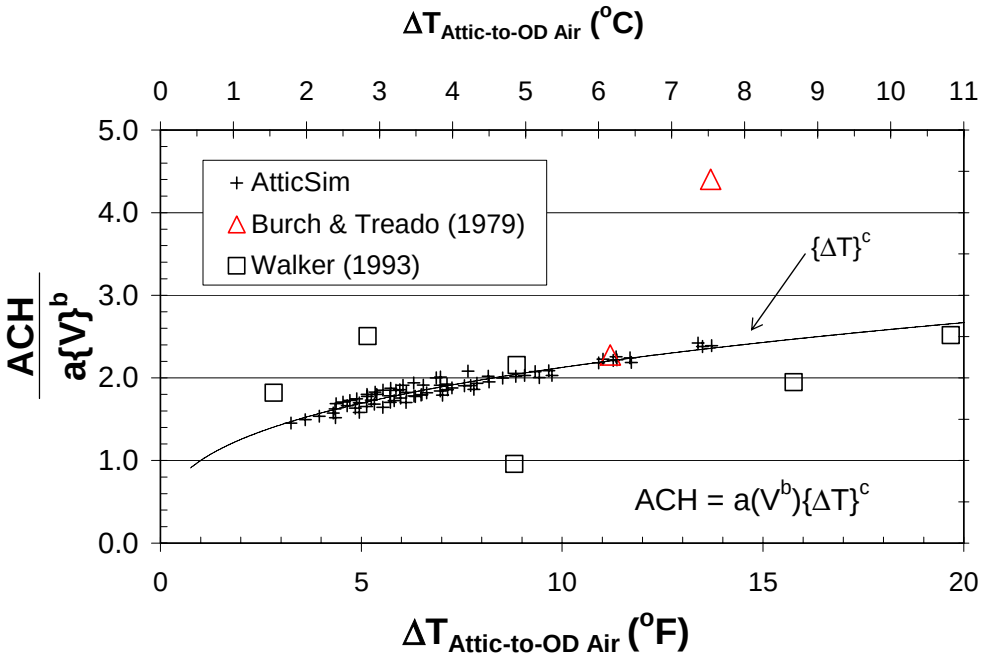

Figure 3. The air changes per hour (ACH) computed by AtticSim are compared to literature data and show the reasonableness of the predicted ventilation rate.

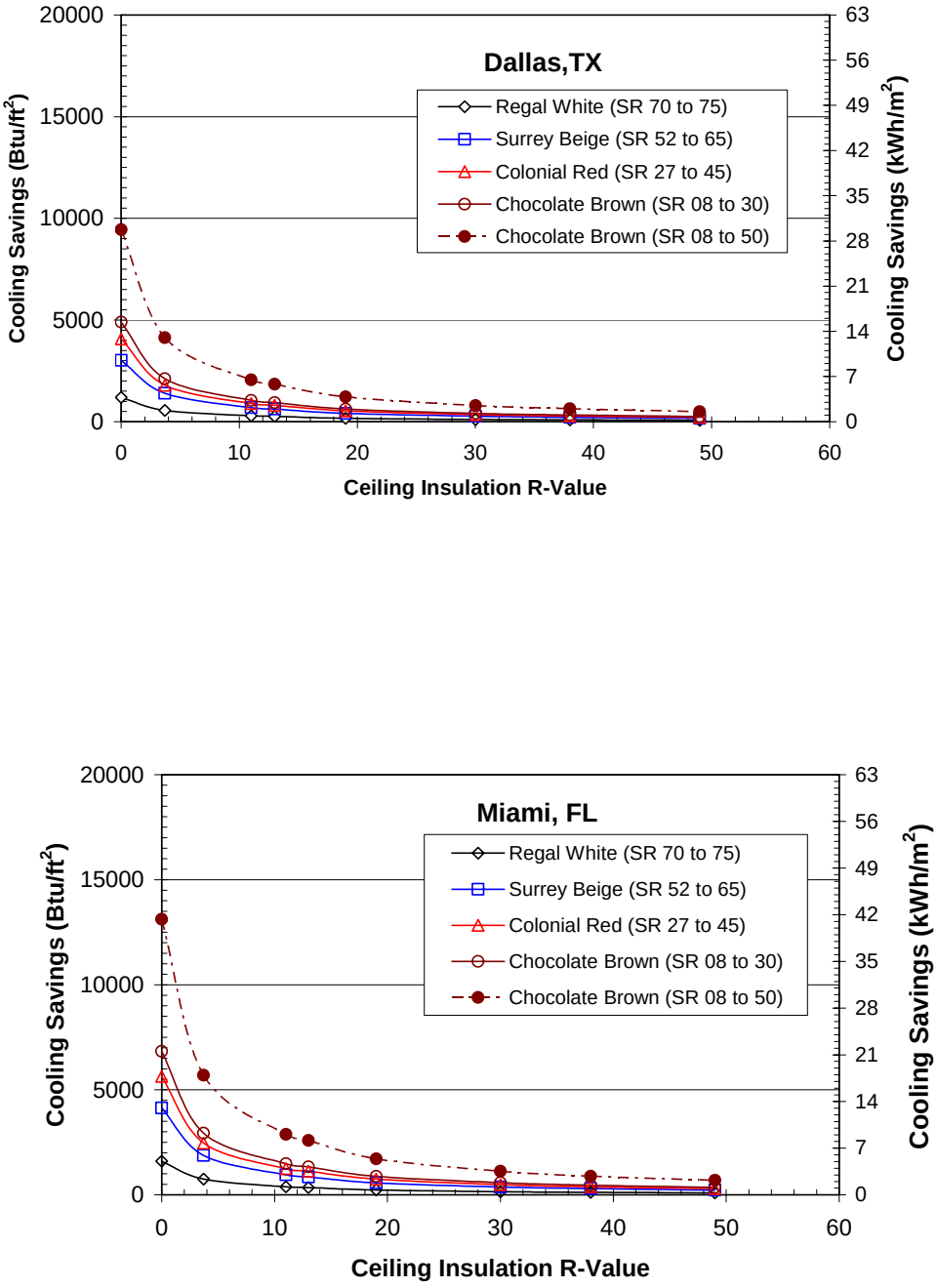

Figure 4. The reduction in the ceiling heat produced by CRCMs as compared to the same standard color roof.

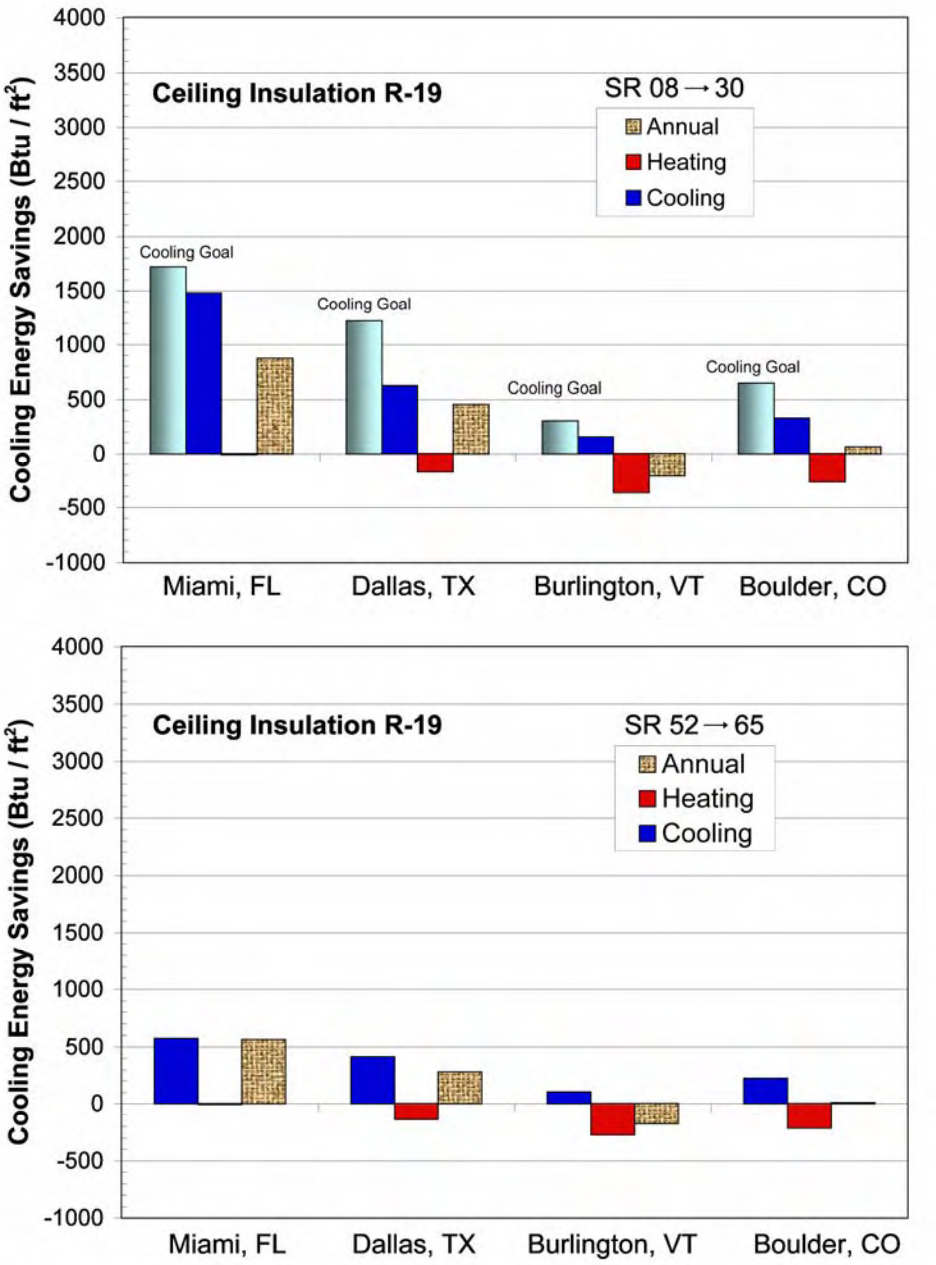

Figure 5. The cooling, heating and net annual energy savings achieved by CRCMs as compared to the same standard color roof with R-19 attic insulation. kWh = 0.00315∗[Btu /ft^2]

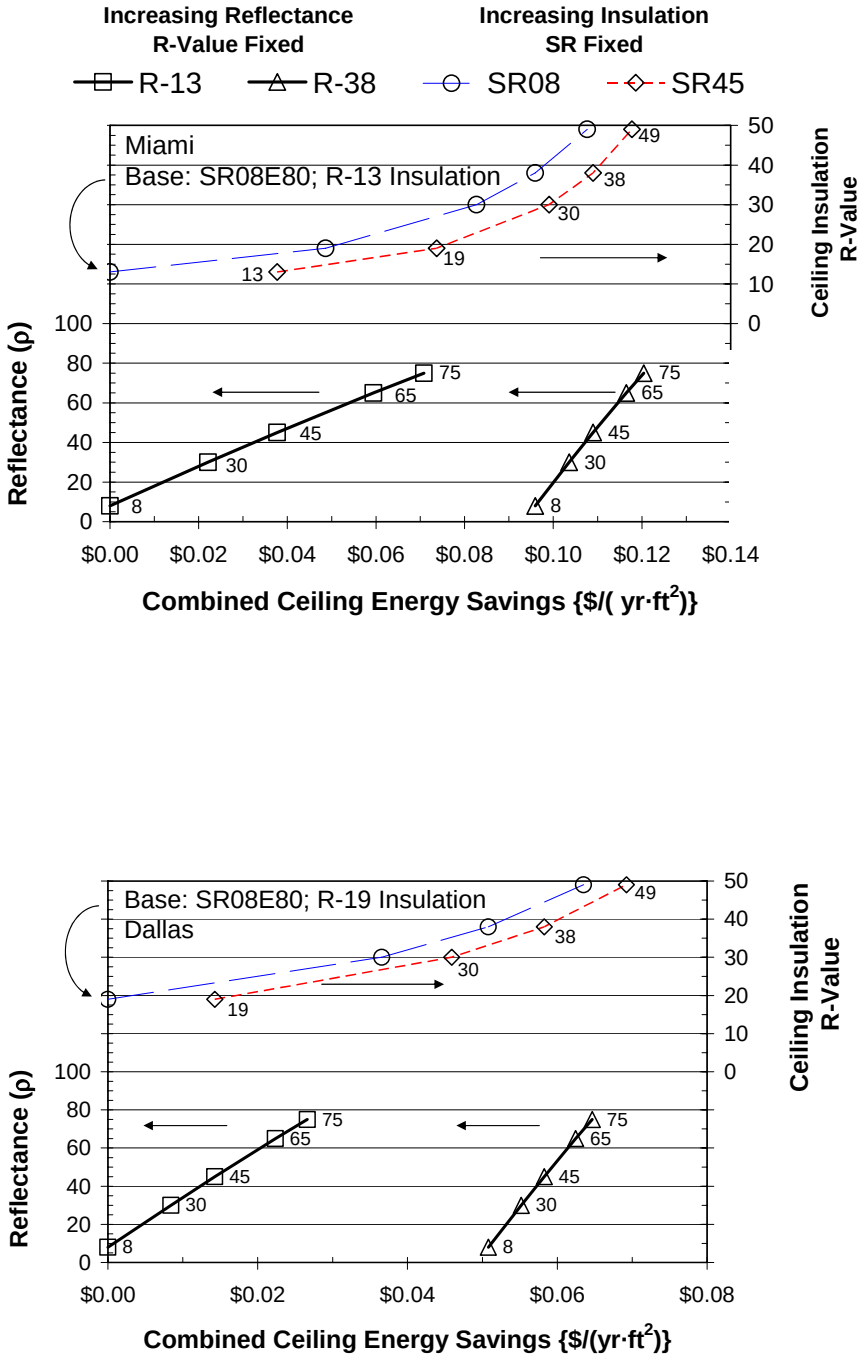

Figure 6. The energy savings estimates for the combined effects of CRCMs and ceiling insulation. Base of comparisons based on recommended insulation levels and a roof having SR08E80 radiation properties.
$/(yr·m^2) = 10.764∗$/(yr·ft^2)

Cool Colored Materials for Roofs

H. Akbari, P. Berdahl, R. Levinson, and S. Wiel, Lawrence Berkeley National Laboratory
A. Desjarlais and W. Miller, Oak Ridge National Laboratory
N. Jenkins, A. Rosenfeld, and C. Scruton, California Energy Commission

ABSTRACT

Raising the solar reflectance of a roof from a typical value of 0.1 – 0.2 to an achievable 0.6 can reduce cooling-energy use in buildings by more than 20%. Cool roofs also reduce ambient outside air temperature, thus further decreasing the need for air conditioning and retarding smog formation.

We are collaborating with pigment manufacturers to characterize colorants, and with manufacturers of roofing materials to produce cool colored products, including asphalt shingles, tiles, metal roofing, wood shakes, membranes, and coatings. Significant efforts are being devoted to the identification and characterization of pigments suitable for cool-colored coatings, and to the development of engineering methods for applying cool coatings to roofing materials. We are also measuring and documenting the laboratory and in-situ performances of roofing products. Demonstration of energy savings can accelerate the market penetration of cool-colored roofing materials. Early results from this program have yielded colored concrete, clay, and metal roofing products with solar reflectances exceeding 0.4. Obtaining equally high reflectances for roofing shingles is more challenging, but we expect manufacturers to soon have several cost-effective colored shingles with reflectances of at least 0.25.

Introduction

Benefits of Cool Roofs

Building-energy monitoring studies in California and Florida have demonstrated cooling-energy savings in excess of 20% upon raising the solar reflectance of a roof to 0.6 from a prior value of 0.1 - 0.2 (Konopacki and Akbari, 2001; Konopacki *et al.*, 1998; Parker *et al.*, 2002). Energy savings are particularly pronounced in older houses that have little or no attic insulation, especially if the attic contains the air distribution ducts. Our research estimates U.S. potential energy savings in excess of $750 million per year in net annual energy bills (cooling-energy savings minus heating-energy penalties) (Akbari *et al.*, 1999). Cool roofs also significantly reduce peak electric demand in summer (Akbari *et al.*, 1996; Levinson *et al.*, 2004a). The widespread installation of cool roofs can lower the ambient air temperature in a neighborhood or city, decreasing the need for air conditioning, retarding smog formation, and improving environmental comfort. These "indirect" benefits of reduced ambient air temperatures have roughly the same economic value as the direct energy savings (Rosenfeld *et al.*, 1997).

Lower surface temperatures may also increase the lifetime of roofing products (particularly asphalt shingles), reducing replacement and disposal costs. Our preliminary analysis suggests that there may be a surcost of up to $1 per square meter for cool roofing materials. This represents 2 to 5% of the cost of installing a new residential roof.

Availability of Cool Roofing Materials

Cool (solar-reflective) roofing products currently available in the market, such as single-ply membranes and elastomeric coatings, are applied almost exclusively to commercial buildings with low-sloped roofs. Cool products for pitched residential roofs are generally limited to tile and metal. Asphalt shingles dominate the residential roofing market, comprising 47% of 2004 sales in the western state residential market (Western Roofing, 2004). Assuming that the cost per unit roof area of asphalt shingles is about half that of other residential roofing products, we estimate the fraction by surface area is over 60%. Most commercially available asphalt shingles are optically dark, with solar reflectance ranging from 0.05 to 0.25, depending on color. With the exception of one "ultra-white" product, even nominally "white" shingles appear gray, and have a solar reflectance of about 0.25—much lower than the solar reflectance of 0.7 achieved by a white tile or a white metal panel. It is possible to produce a truly white shingle with a solar reflectance of about 0.55 by increasing the amount of white pigment (titanium dioxide rutile) on its granules. However, since many homeowners desire nonwhite roofs, we seek to develop and promote cool colored roofing products, especially shingles.

Development of Nonwhite Cool Roofing Materials

Currently, suitable cool *white* materials are available for most roofing products, with the notable exception of asphalt shingles. Cool nonwhite materials are needed for all types of roofing. Industry researchers have developed complex inorganic color pigments that are dark in color but highly reflective in the infrared portion of the solar spectrum. The high near-infrared reflectance of coatings formulated with these and other "cool" pigments—e.g., chromium oxide green, cobalt blue, phthalocyanine blue, Hansa yellow—can be exploited to manufacture roofing materials that reflect more sunlight than conventionally pigmented roofing products.

The California Energy Commission (CEC) has engaged Lawrence Berkeley National Laboratory (LBNL) and Oak Ridge National Laboratory (ORNL) on a three-year project to (a) work with the roofing industry to develop and produce colored roofing products with high solar reflectance, and (b) encourage the homebuilding industry to use these products. The intended outcome of this project is to make nonwhite cool roofing materials commercially available within three to five years. Specifically, we aim to produce nonwhite shingles with solar reflectances not less than 0.3, and other types of nonwhite roofing products (e.g., tiles) with solar reflectances not less than 0.45. The reflectance goal for shingles is lower than that for other products because (a) the roughness of a shingle's surface reduces its reflectance, and (b) manufacturing constraints typically limit the reflectance of coatings applied to granules.

We are collaborating with pigment manufacturers to characterize colorants, and with manufacturers of roofing materials to produce cool colored products, including asphalt shingles, tiles, metal roofing, wood shakes, membranes, and coatings. Significant efforts are being devoted to the identification and characterization of pigments suitable for cool-colored coatings, and to the development of engineering methods for applying cool coatings to roofing materials. We are also measuring and documenting the laboratory and in-situ performance of roofing products. The latter, including demonstrations of building energy savings, can accelerate the market penetration of cool-colored roofing materials.

Research & Marketing Issues

Our activities are designed to address the following six topics.

1. *Formulation of Cool Colored Coatings.* How can we maximize the total solar reflectance of a pigmented coating while matching a desired color?
2. *Development of Cool Colored Roofing Prototypes.* What is the relationship between the optical properties of a simple pigmented coating and the optical properties of a pigmented coating applied to roofing materials (e.g., granules, tiles)?
3. *Durability of Cool Colored Coatings.* How do cool colored coatings weather and age?
4. *Longevity of Cool Colored Roofing Materials.* Does higher solar reflectance increase the lifetime of cool colored roofing materials?
5. *Demonstration of Energy Savings.* What are the building-energy savings yielded by use of cool colored roofing materials?
6. *Market Introduction.* How can we promote the use of cool colored roofing materials?

Formulation of Cool Colored Coatings

In order to determine how to optimize the solar reflectance of a pigmented coating matching a particular color, and how the performance of cool-colored roofing products compares to that of a standard material, we (a) have identified and characterized the optical properties of over 100 pigmented coatings; (b) have created a preliminary database of pigment characteristics; and (c) are developing a computer model to maximize the solar reflectance of roofing materials for a choice of visible color.

Pigment Characterization

We have measured the spectral optical properties of many individual pigments and have used these data to develop a method to predict the spectral radiative properties of materials fabricated with these pigments (Levinson *et al.*, 2004b,c).

We illustrate our characterization efforts by presenting results for four blue pigments (see Figure 1). Each pigment is described by a column of three solar spectral charts. The first chart shows the measured transmittance, measured reflectance, and calculated absorptance of a pigmented film; the second, its computed absorption coefficient K and backscattering coefficient S; and the third, its measured and computed reflectances over black and white backgrounds, which serve as checks on the mathematical consistency of the results. The absorption coefficient K should be large in parts of the visible spectral range, to permit the attainment of desired colors, and should be small in the near infrared (NIR). The backscattering coefficient S should be small (or large) in the visible spectral range for formulating dark (or light) colors, and is preferably large in the NIR.

Cobalt aluminate blue ($CoAl_2O_4$; U01) derives its appearance from modest scattering ($S \sim 30$ mm^{-1}) in the blue (400 - 500 nm) and strong absorption ($K \sim 150$ mm^{-1}) in the rest of the visible spectrum. It has very low absorption in the short NIR (700 - 1000 nm, containing 50% of the NIR energy), but exhibits an undesirable absorption band in the 1200 - 1600 nm range, which contains 17% of the NIR energy. A white background dramatically increases NIR reflectance but makes it lighter in color.

Figure 1. Characterizations of Several Blue Pigments

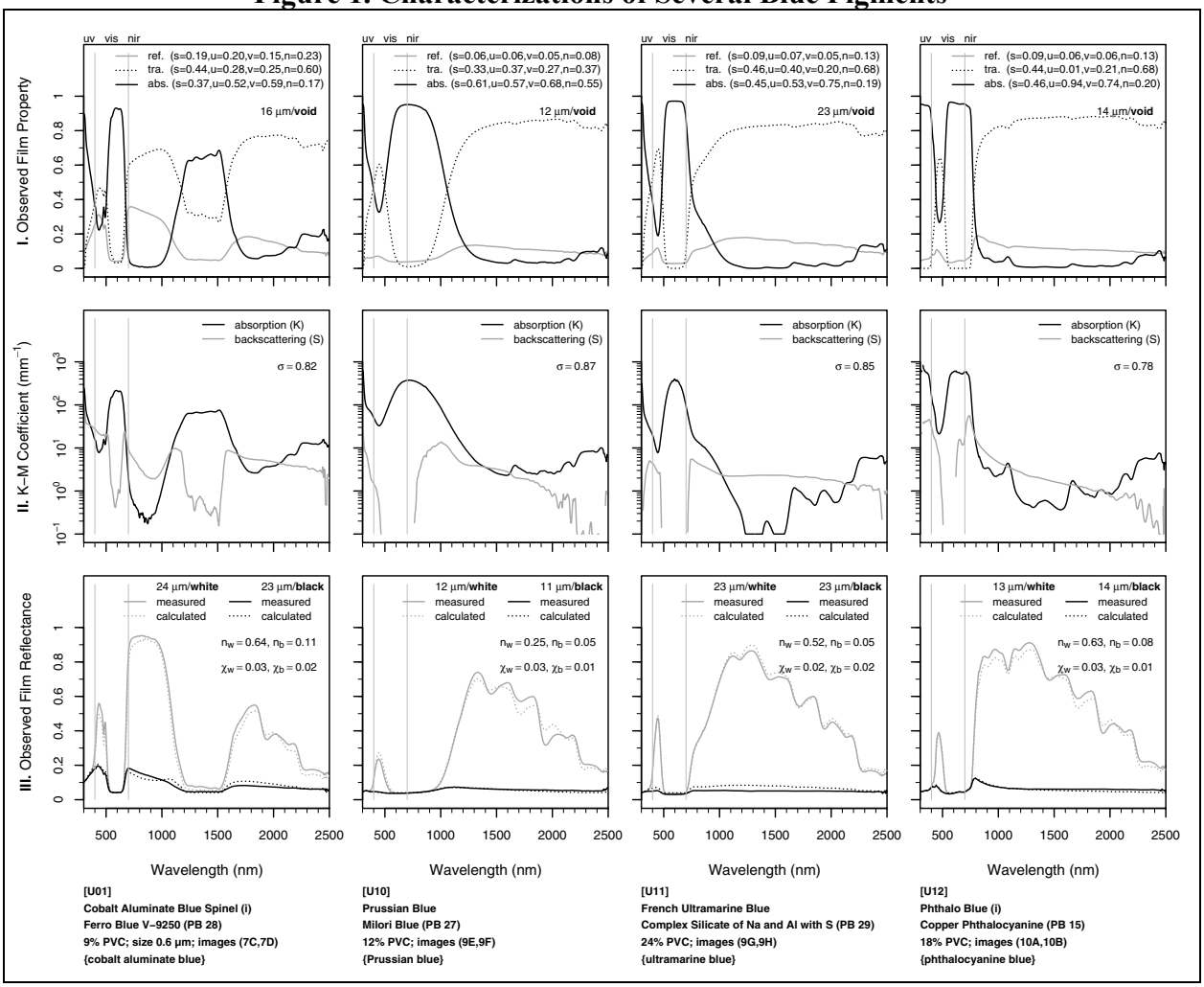

Each pigment is described by a column of three solar spectral charts. The first chart shows the transmittance, reflectance, and absorptance of a pigmented film; the second, its absorption coefficient *K* and backscattering coefficient *S*; and the third, its measured and computed reflectances over black and white backgrounds, which serve as checks on the mathematical consistency of the results.

Iron (a.k.a. Prussian or Milori) blue (U10) is a weakly scattering pigment with strong absorption in the visible and short NIR, and weak absorption at longer wavelengths. It appears black and has little NIR reflectance over a black background, but looks blue and achieves a modest NIR reflectance (0.25) over a white background. It should be avoided in cool coatings.

Ultramarine blue (U11), a complex silicate of sodium and aluminum with sulfur, is a weakly scattering pigment with some absorption in the short NIR. If sparingly used, it can impart absorption in the yellow spectral region without introducing a great deal of NIR absorption. This is a durable inorganic pigment with some sensitivity to acid. While most colored inorganic pigments contain a transition metal such as Fe, Cr, Ni, Mn, and Co, ultramarine blue is unusual. It is a mixed oxide of Na, Si, and Al, with a small amount of sulfur. The metal oxide skeleton forms an open clathrate structure that stabilizes S_3 ions in cages to form the chromophores. Thus isolated S_3 molecules with an attached unpaired electron cause the light absorption in the 500-700 nm range, producing the blue color.

Copper phthalocyanine blue ("phthalo" blue) (U12) is a weakly scattering, dyelike pigment with strong absorption in the 500 - 800 nm range and weak absorption in the rest of the visible and NIR. Phthalo blue appears black and has minimal NIR reflectance over a black background, but looks blue and achieves a high NIR reflectance (0.63) over a white background. It is durable and lightfast, but as an organic pigment it is less chemically stable than (high temperature) calcined mixed metal oxides such as cobalt aluminate.

Pigment Property Database

We have developed a preliminary database summarizing our characterizations of about 100 pigments. The database describes each pigment with a tab-delimited plaintext file that includes identification (name, color, and chemistry); mechanical properties (film thicknesses); spectral optical properties (measured reflectance, transmittance, and absorptance; derived absorption and backscattering coefficients; predicted reflectances over various backgrounds); and ancillary parameters generated in the derivation of absorption and backscattering coefficients. We have shared this database with our industrial partners to help them develop cool colored coatings and roofing products.

Cool-Color Formulation Software

We are developing a model that estimates the spectral solar reflectance of coatings from (a) pigment properties (spectral absorption and backscattering coefficients); (b) coating composition (pigments, vehicle, and filler); and (c) coating geometry (thickness and roughness). This model will be implemented in software that suggests recipes to maximize the solar reflectance of a colored coating. The software will be available to pigment, coating, and roofing manufacturers.

Development of Cool Colored Roofing Prototypes

We have surveyed methods of manufacturing various roofing materials, and are working with roofing manufacturers to design innovative techniques for producing cool-colored materials.

Survey of Manufacturing Methods

We estimate that roofing shingles, tiles, and metal panels comprise over 80% (by roof area) of the western state residential roofing market. We contacted representative manufacturers of asphalt shingles, concrete and clay tiles, metal panels, and wood shakes to obtain information on the processes used to color their products. We also reviewed patent and other literature on the fabrication and coloration of roofing materials, with particular emphasis on asphalt roofing shingles.

Shingles. The solar reflectance of a new shingle is dominated by the solar reflectance of its granules, since by design, the surface of a shingle is well covered with granules. Hence, we focus on the production of cool granules.

Until recently, the way to produce granules with high solar reflectance has been to use titanium dioxide (TiO_2) rutile, a white pigment. Since a thin layer of TiO_2 is reflective but not opaque, multiple layers are needed to obtain the desired solar reflectance. This technique has been used to produce "super-white" (meaning truly white, rather than gray) granulated shingles with solar reflectances exceeding 0.5. Manufacturers have also tried to produce colored granules with high solar reflectance by using nonwhite pigments with high NIR reflectance. However, like TiO_2, cool-colored pigments are also partly transparent to NIR light; thus, any NIR light not reflected by the cool pigment is transmitted to the (typically dark) granule underneath, where it can be absorbed. To increase the solar reflectance of colored granules with cool pigments, multiple color layers, a reflective undercoating, and/or reflective aggregate should be used. Obviously, each additional coating increases the cost of production.

The application of pigmented coatings to roofing granules appears to be the critical process step. Several layers of silicate coatings can be involved, and may include not just one or more pigments, but the use of clay additives to control viscosity, biocides to prevent staining, and process chemistry controls to avoid unreacted dust on the product.

One way to reduce the cost is to produce cool-colored granules via a two-step, two-layer process. In the first step, the granule is pre-coated with an inexpensive pigment that is highly reflective to NIR light. In the second step, the cool-colored pigment is applied to the pre-coated granules.

Tiles. For colored tiles, there are three ways to improve the solar reflectance: (1) use of raw clay materials with low concentrations of iron oxides and elemental carbon; (2) use of cool pigments in the coating; and (3) application of the two-layered coating technique using pigmented materials with high solar reflectance as an underlayer. Although all these options are in principle easy to implement, they may require changes in the current production techniques that may add to cost of the finished products. Colorants can be included throughout the body of the tile, or used in a surface coating. Both methods need to be addressed.

Metal panels. Application of cool-colored pigments in metal roofing materials may require the fewest number of changes to the existing production processes. As in the cases of tile and asphalt shingle, cool pigments can be applied to metal via a single or a double-layered technique. If the raw metal is highly reflective, a single-layered technique may suffice. The coatings for metal shingles are thin, durable polymer materials. These thin layers use materials efficiently, but limit the maximum amount of pigment present. However, the metal substrate can provide some NIR reflectance if the coating is transparent in the NIR.

Wood shakes. We will survey methods of manufacturing wood shakes in the near future.

Innovative Methods for Application of Cool Coatings to Roofing Materials

We have collaborated with 12 companies that manufacture roofing materials, including shingles, roofing granules, clay tiles, concrete tiles, tile coatings, metal panels, metal coatings, and pigments. To date, over 50 prototype cool shingles, 30 tiles or tile coatings, and 20 metal roofing prototypes have been developed and tested. The development work with our industrial partners has been iterative and has included selection of cool pigments, choice of base coats for the two-layer applications, and identification of pigments to avoid.

Figure 2 shows the iterative development of a cool black shingle. A conventional black roof shingle has a reflectance of about 0.04. On the first try to increase the solar reflectance of the shingle, we replaced the standard black pigment on the granules with one that is NIR reflective. That increased the reflectance of the granule to 0.12. On the second try, we used a two-layered technique where we first applied a layer of TiO_2 white base (increasing the solar reflectance of the base granule to 0.28) and then a layer of NIR-reflective black pigment. This increased the reflectance of the black granule to 0.16. On our third prototype, the base granule was coated in ultra-white (reflectance 0.44) and then with an NIR-reflective black pigment. This increased the solar reflectance to 0.18. Figure 2 also shows the performance limit (reflectance 0.25) where a 25-μm thick layer of NIR-reflective black coating is applied on an opaque white background.

Figure 2. Development of a Cool Black Shingle

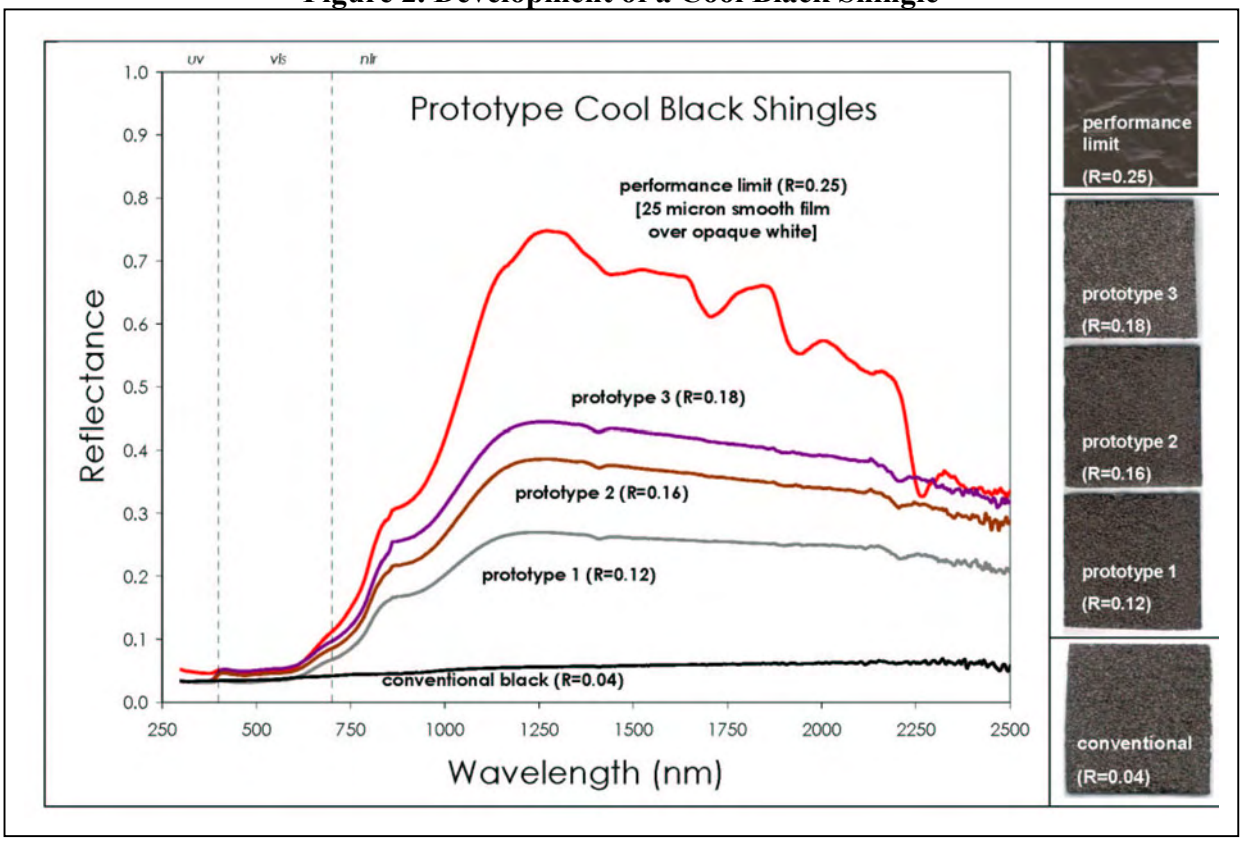

Figure 3 shows the results of similar efforts to develop coatings for concrete tile roofs, which yielded a palette of cool colors each with solar reflectance exceeding 0.4.

Durability of Cool Colored Coatings

Natural, real-time weathering, such as outdoor exposure in Florida or Arizona, and accelerated tests using weatherometers are in progress to gauge the color-stability and integrity (warranty-related properties) of prototype roofing materials. Accelerated testing is essential because the cool pigment combinations must remain fade resistant or the product will not sell.

Pigment stability and discoloration resistance will be judged using a total color difference measure as specified by ASTM D 2244-93 (ASTM 1993).

Figure 3. Solar Reflectance of Several Cool Coatings for Concrete Tile Roofs

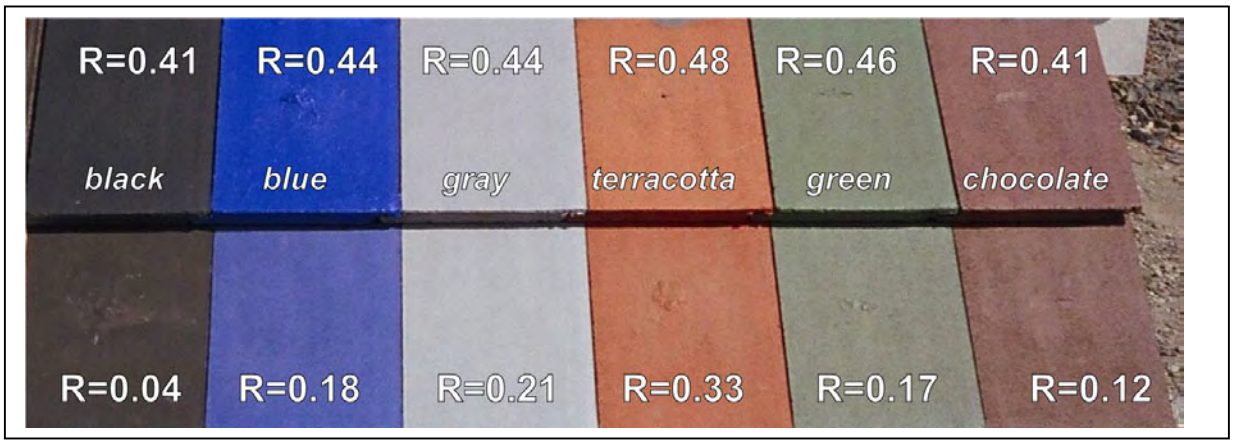

Image courtesy of American Rooftile Coatings (Fullerton, CA)

Natural Weathering

Several different styles and colors of roof samples have been placed in seven of California's 16 climate zones for exposure studies. Reflectance and emittance data are recorded quarterly the first year and twice a year thereafter (weather data are available continuously). In addition, the solar spectral reflectance of each weathered sample is measured annually to gauge soiling and to document color changes too small to perceive.

We will also examine the roof samples for contaminants and determine the elemental composition and biomass on the surface of the roof products. The surface composition studies will identify the drivers affecting the soiling of the roof samples, which in turn will provide valuable information to manufacturers for improving the sustainability of their roof products. The data will be used to formulate an algorithm that correlates changes in reflectance with exposure.

Accelerated Weathering

In collaboration with industrial partners, we are exposing samples to 5,000 hours of xenon-arc light in a weatherometer following ASTM G-155 (ASTM 2000).

Longevity of Cool Colored Roofing Materials

We will soon begin to investigate the effect of reflectance on the useful life of roofing products. There have been claims that cool roofs will last longer, although no specific data have been offered. The research team will work with industry to design and implement a test method for this purpose and use laboratory and outdoor accelerated aging techniques to gather data on the effect.

Roofing materials fail mainly because of three processes: gradual changes to physical and chemical composition induced by the absorption of ultraviolet (UV) light; aging and weathering

(e.g., loss of plasticizers in polymers and low-molecular-weight components in asphalt), which may accelerate as temperature increases; and diurnal thermal cycling, which stresses the material by expansion and contraction. Our goal is to clarify the material degradation effects due to UV absorption and those due to heating. The results will be used to quantify the effect of solar reflectance on the useful life of roofs; provide data to manufacturers to develop better materials; and support development of appropriate ASTM standards.

Demonstration of Energy Savings

Homeowners and utilities considering new rebate programs need proof that an aesthetically pleasing dark roof can be made to reflect like a white roof in the infrared spectrum, and save energy and money. Therefore, demonstrating the potential energy savings is paramount for fostering the market penetration of the cool pigment technology. Field experiments cover a range of conditions necessary to benchmark analytical tools and permit an accurate assessment of energy conservation potential over a range of climates. These experiments include measuring energy savings in pairs of homes at CA field sites, and thermal testing of tile roofs on a steep-slope attic assembly.

Building Energy Use Measurements at California Demonstration Sites

We have set up a residential demonstration site in Fair Oaks, CA (near Sacramento) consisting of two pairs of single-family, detached houses roofed with metal and concrete tile. We are planning for another two pair of houses to demonstrate asphalt shingles and cedar shakes. The monitoring period will last at least through summer of 2005. The demonstration pairs each include one building roofed with a cool-pigmented product and a second building roofed with a conventionally (warmer) pigmented product of nearly the same color.

Solar reflectance and thermal emittance are measured twice a year. Temperatures at the roof surface, on the underside of the roof deck, in the mid-attic air, at the top of the insulation, on the interior ceiling's sheet rock surface, and inside the building are logged continuously by a data acquisition system. Relative humidity in the attic air and the residence are also measured. Heat flux transducers are embedded in the sloped roofs and the attic floor to measure the roof heat flows and the building heat leakage. We have instrumented the building to measure the total house and air-conditioning power demands. A fully instrumented meteorological weather station is set up to collect the ambient dry bulb temperature, the relative humidity, the solar irradiance, and the wind speed and wind direction.

Thermal Testing on Steep-slope Assembly at Oak Ridge National Laboratory

The multiple hazard protection provided by concrete and clay tile from fire, wind and earthquake are making tile the preference of upper income residences in western and some southern states. The typical reflectance of tile is about 0.1; however, applying the cool pigments increases reflectance beyond 0.4 (Fig. 3). The thermal analysis of tile roofing is an interesting challenge because of the air gap formed between the tile and the roof deck. Yet that air gap poses significant energy savings as proved by Beal and Chandra (1999) who demonstrated a 45% daytime reduction in heat flux for a counter-batten tile roof (the reduction over a 24 hour cycle was much less due to differing rates of nocturnal cooling) as compared to a direct nailed shingle

roof. Quantifying the effect of the cool pigments on tile roofs requires testing and analysis to correctly model the heat flow across the air channel.

We are testing several concrete and clay tile on a steep-slope roof to further learn and document the effect of reflectance and emittance weathering on the thermal performance of the cool pigment roof systems. The Roof Tile Institute and its affiliate members are keenly interested in specifying tile roofs as cool roof products and they want to know the individual and combined effects of cool pigments and of venting the underside of concrete and clay roof tile. The data will help better formulate the simulation program, AtticSim, for predicting the thermal performance of the cool colored tile systems.

Market Introduction of Cool Colored Roofing Products

Through close coordination with industry, utilities and code developers, this project is expected to have near-term success facilitating the deployment of cool colored roofing products, particularly in California. In addition to its ongoing close working relationship with coating manufacturers and roofing manufacturers, the team is working closely with California utilities and California codes-and-standards programs.

In April 2004, the research team and several roofing manufacturer representatives introduced emerging cool colored roofing products to the Emerging Technology Coordinating Council (ETCC). Members of the ETCC are responsible for emerging technology programs at each of the investor owned utilities. The emerging technology programs at the utilities are also a critical validation step that can lead to product incentives through the utilities' energy efficiency programs.

Many products developed as a result of this research will be able to meet the residential cool roof credit requirements contained in the 2005 Title 24 California Building Energy Efficiency Standards and the research team will work with the standards program staff to provide input on possible future code enhancements.

Conclusion

The early results from this program indicate significant success in developing cool-colored materials for concrete tile, clay tile, and metal roofs. Since the inception of this program, the solar reflectance of commercially available products has increased to 0.30-0.45 from 0.05-0.25. To be cost effective, shingle manufacturers apply a very thin layer of pigments on the roofing granules. Use of a reflective undercoated (two-layered coating) is expected to soon yield several cost-effective cool-colored shingle products, with solar reflectances in excess of 0.25 (the EPA threshold for EnergyStar roofs). Our ongoing collaboration with granule and shingle manufacturers may yield shingles with solar reflectances exceeding 0.3.

Acknowledgements

This work was supported by the California Energy Commission (CEC) through its Public Interest Energy Research Program (PIER), by the Laboratory Directed Research and Development (LDRD) program at Lawrence Berkeley National Laboratory (LBNL), and by the Assistant Secretary for Renewable Energy under Contract No. DE-AC03-76SF00098.

References

Akbari, H., S. Konopacki, and M. Pomerantz. 1999. "Cooling energy savings potential of reflective roofs for residential and commercial buildings in the United States," *Energy*, **24**, 391-407.

Akbari, H., S. Bretz, H. Taha, D. Kurn, and J. Hanford. 1997. "Peak Power and Cooling Energy Savings of High-albedo Roofs," *Energy and Buildings* — Special Issue on Urban Heat Islands and Cool Communities, **25**(2);117–126.

American Society for Testing and Materials (ASTM). 2000. Designation G155-00ae1: Standard Practice for Operating Xenon Arc Light Apparatus for Exposure of Non-Metallic Materials. West Conshohocken, Pa.: American Society for Testing and Materials.

-------. 1993. Designation D2244-93: Standard Test Method for Calculation of Color Differences from Instrumentally Measured Color. West Conshohocken, Pa.: American Society for Testing and Materials.

Beal, D. and S. Chandra. 1995. "The Measured Summer Performance of Tile Roof Systems and Attic Ventilation Strategies in Hot Humid Climates," Thermal Performance of the Exterior Envelopes of Buildings VI, U.S. DOE/ORNL/BETEC, December 4-8, 1995, Clearwater, FL.

Konopacki, S., and H. Akbari. 2001. "Measured Energy Savings and Demand Reduction from a Reflective Roof Membrane on a Large Retail Store in Austin." Lawrence Berkeley National Laboratory Report No. LBNL-47149, Berkeley, CA.

Konopacki, S., L. Gartland, H. Akbari, and L. Rainer. 1998. "Demonstration of Energy Savings of Cool Roofs." Lawrence Berkeley National Laboratory Report No. LBNL-40673, Berkeley, CA.

Levinson, R., H. Akbari, S. Konopacki, and S. Bretz. 2004a. "Inclusion of cool roofs in nonresidential Title 24 prescriptive requirements," In Press. *Energy Policy*.

Levinson, R., P. Berdahl, and H. Akbari. 2004b. "Spectral Solar Optical Properties of Pigments Part I: Model for Deriving Scattering and Absorption Coefficients from Transmittance and Reflectance Measurements." Draft

-------. 2004c. "Spectral Solar Optical Properties of Pigments Part II: Survey of Common Colorants." Draft

Miller, W.A., H. Akbari, R. Levinson, K.T. Loye, S. Kriner, R.G. Scichili, A.O. Desjarlais, S. Weil, and P. Berdahl. 2004. "Special Infrared Reflective Pigments Make a Dark Roof Reflect Almost Like a White Roof," to be published in Thermal Performance of the Exterior Envelopes of Buildings, IX, proceedings of ASHRAE THERM VIII, Clearwater, FL., Dec.

Parker, D.S., J.K. Sonne, and J.R. Sherwin. 2002. "Comparative Evaluation of the Impact of Roofing Systems on Residential Cooling Energy Demand in Florida," Proceedings of the 2002 ACEEE Summer Study on Energy Efficiency in Buildings, Vol. 1, p. 219, Pacific Grove, CA.

Petrie, T.W., T.K. Stovall, K.E. Wilkes, and A.O. Desjarlais. 2004. "Comparison of Cathedralized Attics to Conventional Attics: Where and When Do Cathedralized Attics Save Energy and Operating Costs?," to be published in Thermal Performance of the Exterior Envelopes of Buildings, IX, proceedings of ASHRAE THERM VIII, Clearwater, FL., Dec.

Rosenfeld, A. H., J. J. Romm, H. Akbari, and M. Pomerantz. 1998. "Cool Communities: Strategies for Heat Islands Mitigation and Smog Reduction," *Energy and Buildings,* **28**(1);51–62.

Western Roofing. 2004. Online at http://WesternRoofing.net .

Cool Colored Roofs to Save Energy and Improve Air Quality*

Hashem Akbari, Ronnen Levinson, William Miller†, and Paul Berdahl
Heat Island Group
Lawrence Berkeley National Laboratory
(510) 486-4287
H_Akbari@lbl.gov
http://HeatIsland.LBL.gov/

ABSTRACT

Raising the solar reflectance of a roof from a typical value of 0.1–0.2 to an achievable 0.6 can reduce cooling-energy use in buildings by more than 20%. Cool roofs also reduce ambient outside air temperature, thus further decreasing the need for air conditioning and retarding smog formation.

We are collaborating with pigment manufacturers to characterize colorants, and with manufacturers of roofing materials to produce cool colored products, including asphalt shingles, concrete and clay tiles, metal roofing, wood shakes, and coatings. In this collaboration, we have identified and characterized pigments suitable for cool-colored coatings, and developed engineering methods for applying cool coatings to roofing materials. We are also measuring and documenting the laboratory and *in-situ* performances of roofing products. Demonstration of energy savings can accelerate the market penetration of cool-colored roofing materials. Early results from this effort have yielded colored concrete, clay, and metal roofing products with solar reflectances exceeding 0.4. Obtaining equally high reflectances for roofing shingles is more challenging, but some manufacturers have already developed several cost-effective colored shingles with solar reflectances of at least 0.25.

Introduction

Coatings colored with conventional pigments tend to absorb the invisible "near-infrared" (NIR) radiation that bears more than half of the power in sunlight (Figure 1). Replacing conventional pigments with "cool" pigments that absorb less NIR radiation can yield similarly colored coatings with higher solar reflectance. These cool coatings lower roof surface temperature, reducing the need for cooling energy in conditioned buildings and making unconditioned buildings more comfortable.

Field studies in California and Florida have demonstrated cooling-energy savings in excess of 20% upon raising the solar reflectance of a roof to 0.6 from a prior value of 0.1–0.2 (Konopacki and Akbari, 2001; Konopacki *et al.*, 1998; Parker *et al.*, 2002). Energy savings are particularly pronounced in older houses that have little or no attic insulation, especially if the attic contains the air distribution ducts. At 8¢/kWh, the value of U.S. potential nationwide net commercial and residential energy savings (cooling savings minus heating penalties) exceeds $750 million per year (Akbari *et al.*, 1999). Cool roofs also significantly reduce peak electric demand in summer (Akbari *et al.*, 1997; Levinson *et al.*, 2005a). The widespread installation of cool roofs can lower the ambient air temperature in a neighborhood or city, decreasing the need

* Parts of this paper have been presented in an earlier conference publication (Akbari *et al*. 2004).
† Oak Ridge National Laboratory, Oak Ridge, Tennessee.

for air conditioning, retarding smog formation, and improving environmental comfort. These "indirect" benefits of reduced ambient air temperatures have roughly the same economic value as the direct energy savings (Rosenfeld *et al.*, 1998). Lower surface temperatures may also increase the lifetime of roofing products (particularly asphalt shingles), reducing replacement and disposal costs.

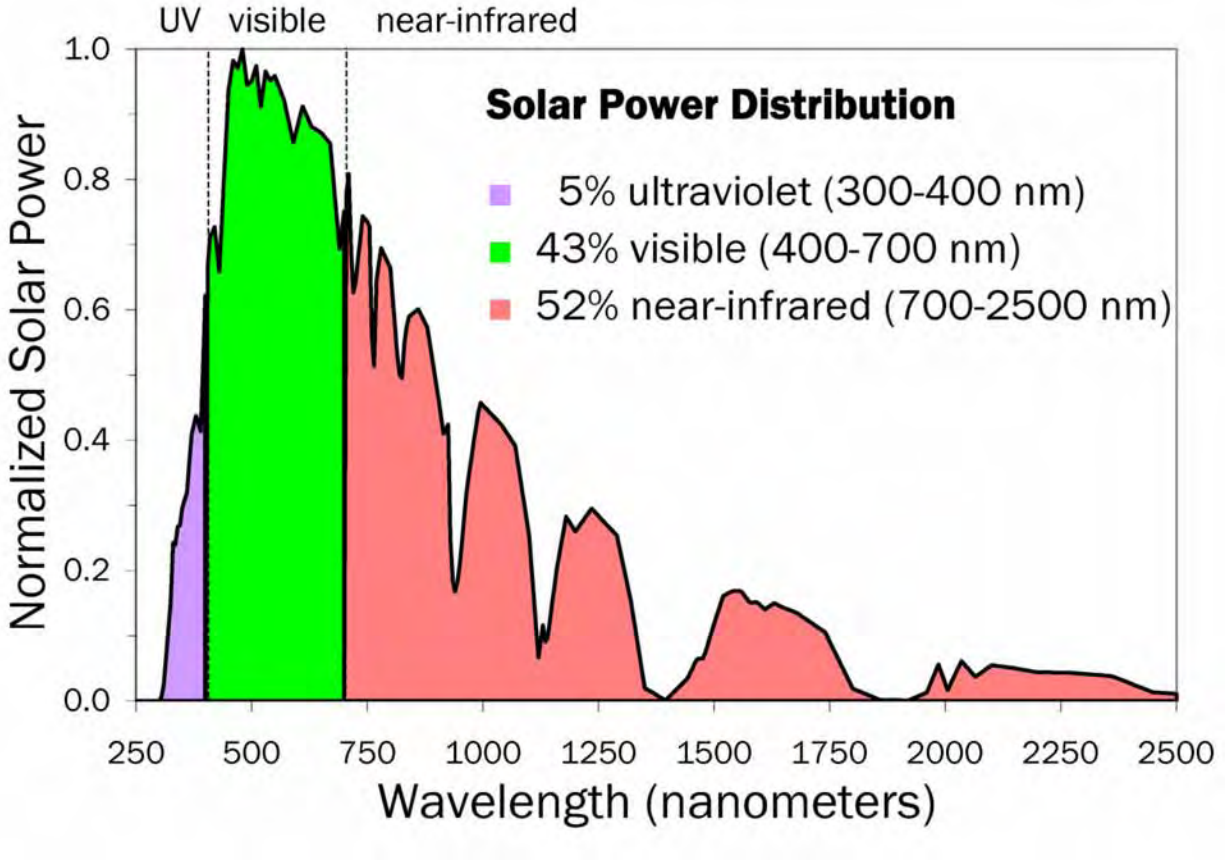

Figure 1. Peak-normalized solar spectral power; over half of all solar power arrives as invisible, "near-infrared" radiation

According to *Western Roofing Insulation and Siding* magazine (2002), the total value of the 2002 projected residential roofing market in 14 western U.S. states (AK, AZ, CA, CO, HI, ID, MT, NV, NM, OR, TX, UT, WA, and WY) was about $3.6 billion (B). We estimate that 40% ($1.4B) of that amount was spent in California. The lion's share of residential roofing expenditure was for fiberglass shingle, which accounted for $1.7B, or 47% of sales. Concrete and clay roof tiles made up $0.95B (27%), while wood, metal, and slate roofing collectively represented another $0.55B (15%). The value of all other roofing projects was about $0.41B (11%). We estimate that the roofing market area distribution was 54–58% fiberglass shingle, 8–10% concrete tile, 8–10% clay tile, 7% metal, 3% wood shake, and 3% slate (Table 1).

Suitable cool *white* materials are available for most roofing products, with the notable exception (prior to March 2005*) of asphalt shingles. Cool nonwhite materials are needed for all types of roofing. Industry researchers have developed complex inorganic color pigments that are dark in color but highly reflective in the near infrared (NIR) portion of the solar spectrum. The high near-infrared reflectance of coatings formulated with these and other "cool" pigments—e.g., chromium oxide green, cobalt blue, phthalocyanine blue, Hansa yellow—can be exploited to manufacture roofing materials that reflect more sunlight than conventionally pigmented roofing products.

Roofing Type	Market share by $		Estimated market share by roofing area
	$B	%	%
Fiberglass Shingle	1.70	47.2	53.6-57.5
Concrete Tile	0.50	13.8	8.4-10.4
Clay Tile	0.45	12.6	7.7-9.5
Wood Shingle/Shake	0.17	4.7	2.9-3.6
Metal/Architectural	0.21	5.9	6.7-7.2
Slate	0.17	4.7	2.9-3.6
Other	0.13	3.6	4.1-4.4
SBC Modified	0.08	2.1	2.4-2.6
APP Modified	0.07	1.9	2.2-2.3
Metal/Structural	0.07	1.9	2.2-2.3
Cementitious	0.04	1.1	1.2-1.3
Organic Shingles	0.02	0.5	0.6
Total	**3.60**	**100**	**100**

Table 1. Project residential roofing market in the U.S. western region surveyed by Western Roofing (2002). The 14 states included in the U.S. western region are AK, AZ, CA, CO, HI, ID, MT, NV, NM, OR, TX, UT, WA, and WY

Cool colored roofing materials are expected to penetrate the roofing market within the next few years. Preliminary analysis suggests that they may cost up to $\$1/m^2$ more than conventionally colored roofing materials. However, this would raise the total cost of a new roof (material plus labor) by only 2 to 5%.

We have collaborated with 12 companies that manufacture roofing materials, including shingles, roofing granules, clay tiles, concrete tiles, tile coatings, metal panels, metal coatings, and pigments. The development work with our industrial partners has been iterative and has included selection of cool pigments, choice of base coats for the two-layer applications (discussed later in this paper), and identification of pigments to avoid.

Creating Cool Nonwhite Coatings

In order to determine how to optimize the solar reflectance of a pigmented coating matching a particular color, and how the performance of cool-colored roofing products compares to those of a standard materials, we (a) have identified and characterized the optical properties of

* In March 2005, a major manufacturer of roofing shingles in California announced availability of cool colored shingles in four popular colors.

over 100 pigmented coatings; (b) have created a database of pigment characteristics; and (c) are developing a computer model to maximize the solar reflectance of roofing materials for a choice of visible color.

Pigment analysis begins with measurement of the reflectance *r* and transmittance *t* of a thin coating containing single pigment or binary mix of pigments (Levinson *et al.*, 2005b,c). These "spectral", or wavelength-dependent, properties of the pigmented coating are measured at 441 evenly spaced wavelengths spanning the solar spectrum (300 – 2,500 nanometers). In addition, each sample is characterized by its computed spectral absorption coefficient *K* and backscattering coefficient *S*. A cool color is defined by a large absorption coefficient *K* in parts of the visible spectral range, to permit the attainment of desired colors, and a small absorption coefficient *K* in the near infrared (NIR). For cool colors, the backscattering coefficient *S* is small (or large) in the visible spectral range for formulating dark (or light) colors, and large in the NIR.

Inspection of the film's spectral absorptance (calculated as 1-*r*-*t*) reveals whether a pigmented coating is cool (has low NIR absorptance) or hot (has high NIR absorptance). The spectral reflectance and transmittance measurements are also used to compute spectral rates of light absorption and backscattering (reflection) per unit depth of film. The spectral reflectance of a coating colored with a mixture of pigments can then be estimated from the spectral absorption and backscattering rates of its components.

We have produced a database detailing the optical properties of the characterized pigmented coatings (Figure 2). We are currently developing coating formulation software intended to minimize the NIR absorptance (and hence maximize the solar reflectance) of a color-matched pigmented coating.

Creating Cool Nonwhite Roofing Products

We estimate that roofing shingles, tiles, and metal panels comprise more than 80% (by roof area) of the residential roofing market in the western United States. In this project, we have collaborated with manufacturers of many roofing materials in order to evaluate the best ways to increase the solar reflectance of these products. The results of our research have been utilized by the manufacturers to produce cool roofing materials. To date and as the direct result of this collaborative effort, manufactures of roofing materials have introduced cool shingles, clay tiles, concrete tiles, metal roofs, and concrete tile coatings.

In addition to using NIR reflective pigments in manufacturing of cool roofing materials, application of novel engineering techniques can further economically enhance the solar reflectance of colored roofing materials. Cool-colored pigments are partly transparent to NIR light; thus, any NIR light not reflected by the cool pigment is transmitted to the underneath layer, where it can be absorbed. To increase the solar reflectance of colored materials with cool pigments, multiple color layers, a reflective undercoating can be used. This method is referred as a two-layered technique.

Figure 3 demonstrates the application of the two-layered technique to manufacture cool colored materials. A thin layer of dioxazine purple (14–27 μm) is applied on four substrates: (a) aluminum foil (~ 25 μm), (b) opaque white paint (~1000 μm), (c) non-opaque white paint (~ 25 μm), and (d) opaque black paint (~ 25 μm). As it can be seen (and is confirmed by visible reflectance spectrum), the color of the material is black. However, the solar reflectance of the sample exceeds 0.4 when applied to an opaque white or aluminum foil substrate; while its solar reflectance over a black substrate is only 0.05.

[R03] Red Iron Oxide (iii)

Paint Code	**R03**
Paint Name	Red Iron Oxide (iii)
Pigment Name	Ferro Red V-13810 (PR 101)
Color Family	Red/Orange
Color Subfamily	iron oxide red
Mean Particle Size (microns)	0.27
Dry Film PVC	3%
Pigment Datasheet	available
Paint Datasheet	unavailable
LBNL Commentary	available

Masstone and Mixtures with White (Tints)

[R03] Red Iron Oxide (iii) +
[W03] Titanium White (i)

image over white				
image over black				
spectral datafile	R03 masstone	R03 tint 1:4	R03 tint 1:9	W03 masstone

guide to reading spectral datafiles

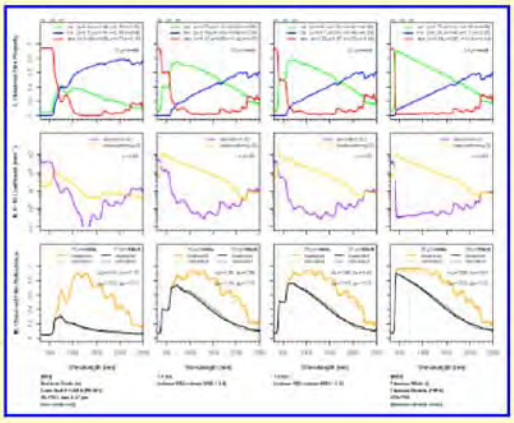

Mixtures with Nonwhite Colors

[R03] Red Iron Oxide (iii) +
[B16] Iron Titanium Brown Spinel (i)

image over white			
image over black			
spectral datafile	R03 masstone	R03+B16 mixture 1:1	B16 masstone

guide to reading spectral datafiles

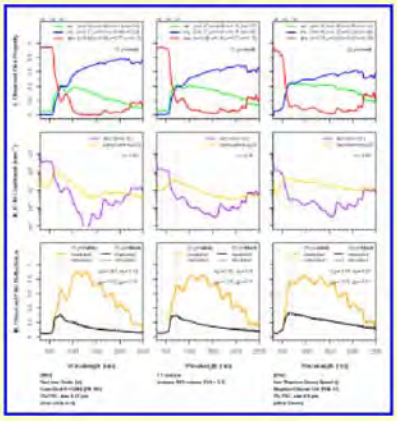

Figure 2. Description of an iron oxide red pigment in the Lawrence Berkeley National Lab pigment database

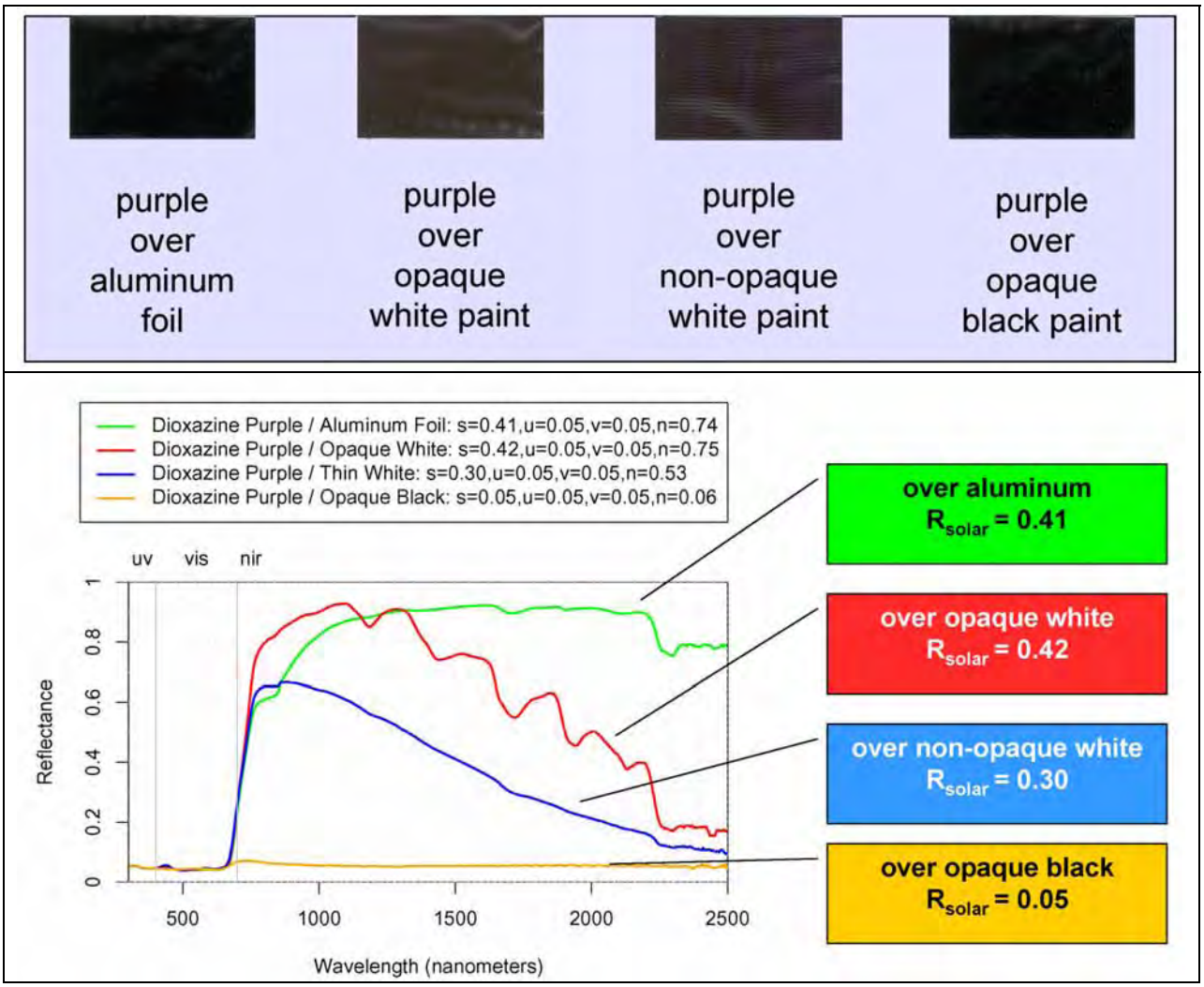

Figure 3. Application of the two-layered technique to manufacture cool colored materials

Shingles

The solar reflectance of a new shingle, by design, is dominated by the solar reflectance of its granules, which cover over 97% of its surface. Until recently, the way to produce granules with high solar reflectance has been to use a coating pigmented with titanium dioxide (TiO_2) rutile white. Because a thin TiO_2-pigmented coating is reflective but not opaque in the NIR, multiple layers are needed to obtain high solar reflectance. This technique has been used to produce "super-white" (meaning truly white, rather than gray) granulated shingles with solar reflectances exceeding 0.5 (see Figure 4).

Although white roofing materials are popular in some areas (e.g., Greece, Bermuda; see Figure 5), many consumers aesthetically prefer non-white roofs. Manufacturers have also tried to produce colored granules with high solar reflectance by using nonwhite pigments with high NIR reflectance. To increase the solar reflectance of colored granules with cool pigments, multiple color layers, a reflective undercoating, and/or reflective aggregate should be used. Obviously, each additional coating increases the cost of production.

Several cool shingles have been developed within the last year. Figure 6 shows examples of prototype cool shingles and compares their solar reflectances with those of the standard colors. Recently, a major manufacturer of roofing shingles in California announced availability of cool colored shingles in four popular colors. Figure 7 shows two houses with cool colored roofing shingles.

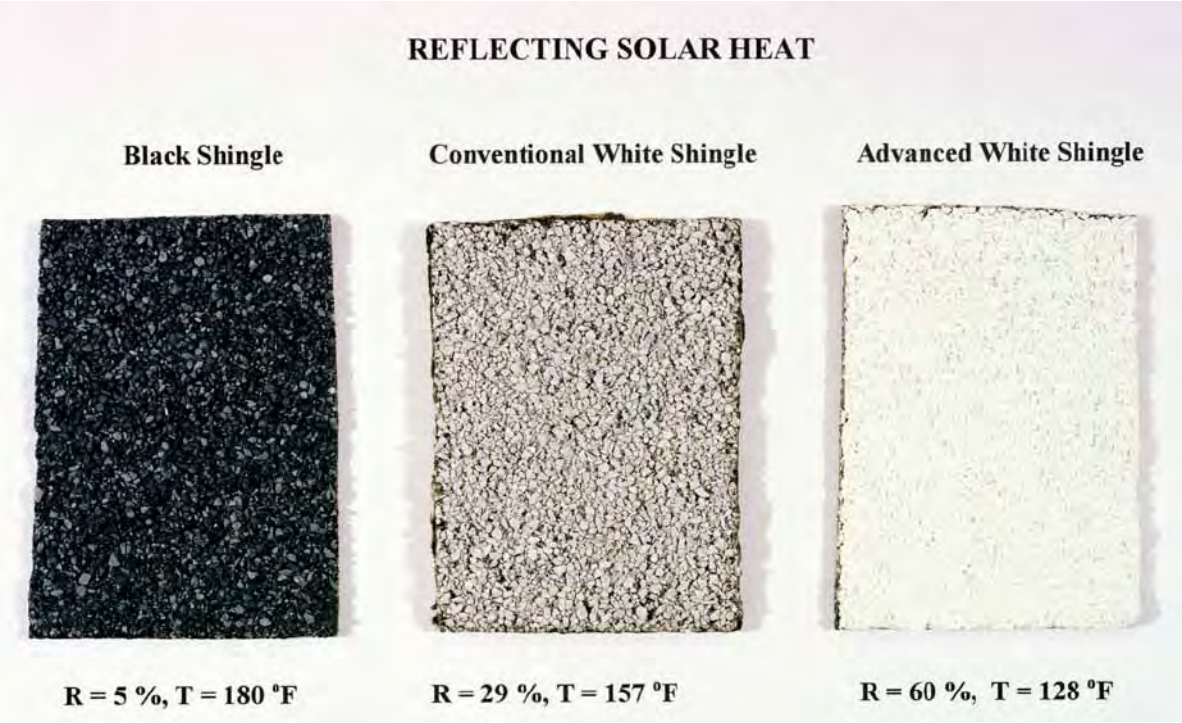

Figure 4. Development of super white shingles

Bermuda

Santorini (Greece)

Figure 5. White roofs and walls are used in Bermuda and Santorini (Greece)

Figure 6. Examples of prototype cool shingles

Figure 7. Test application of cool colored roofing shingles on two houses

Tiles and Tile Coatings

Clay and concrete tiles are used in many areas around the world. In the U.S., clay and concrete tiles are more popular in the hot climate regions. There are three ways to improve the solar reflectance of colored tiles: (1) use clay or concrete with low concentrations of light-absorbing impurities, such as iron oxides and elemental carbon; (2) color the tile with cool pigments contained in a surface coating or mixed integrally; and/or (3) include an NIR-reflective (e.g., white) sublayer beneath an NIR-transmitting colored topcoat. Although all these options

are in principle easy to implement, they may require changes in the current production techniques that may add to cost of the finished products. Colorants can be included throughout the body of the tile, or used in a surface coating. Both methods need to be addressed.

One of our industrial partners has developed a palette of cool nonwhite coatings for concrete tiles. Each of the cool colored coatings shown in Figure 8 has a solar reflectance better than 0.40. The solar reflectance of each cool coating exceeds that of a color-matched, conventionally pigmented coating by 0.15 (terracotta) to 0.37 (black). Another industrial partner also manufactures clay tiles in many colors (glazed and unglazed) with solar reflectance greater than 0.4 (See Table 1).

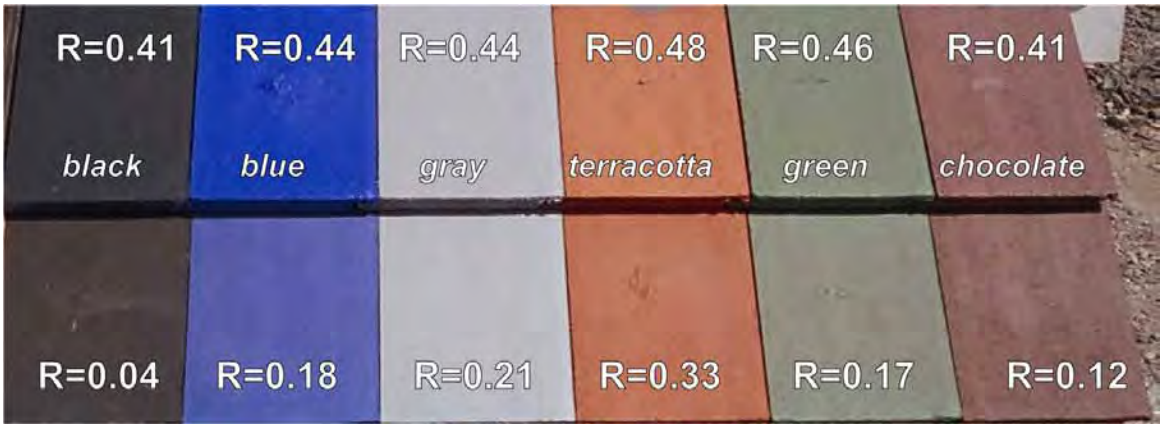

Figure 8. Palette of color-matched cool (top row) and conventional (bottom row) rooftile coatings developed by industrial partner American Rooftile Coatings. Shown on each coated tile is its solar reflectance R

Metal Panels

Metal roofing materials are installed on a small (but growing) fraction of the U.S. residential roofs. Historically metal roofs have had only about 3% of the residential market. However, the architectural appeal, flexibility, and durability, due in part to the cool-colored pigments, has steadily increased the sales of painted metal roofing, and as of 2003 its sales volume has increased to 8% of the residential market, making it the fastest growing residential roofing product (F.W. Dodge 2003). Metal roofs are available in many colors and can simulate the shape and form of many other roofing materials (see Figure 9). Application of cool-colored pigments in metal roofing materials may require the fewest number of changes to the existing production processes. As in the cases of tile and asphalt shingle, cool pigments can be applied to metal via a single or two-layered technique. If the metal substrate is highly reflective, a single-layered technique may suffice. The coatings for metal shingles are thin, durable polymer materials. These thin layers use materials efficiently, but limit the maximum amount of pigment present. However, the metal substrate can provide some NIR reflectance if the coating is transparent in the NIR. Several manufactures develop cool colored metal roofs.

Model	Color	Initial solar reflectance	Solar reflectance after 3 years
Weathered Green Blend		0.43	0.49
Natural Red		0.43	0.38
Brick Red		0.42	0.40
White Buff		0.68	0.56
Tobacco		0.43	0.41
Peach Buff		0.61	0.48
Regency Blue		0.38	0.34
Light Cactus Green		0.51	0.52

Table 2. Sample cool colored clay tiles and their solar reflectances (Source: http://www.MCA-Tile.com)

Durability of Cool Nonwhite Coatings

Roofing materials fail mainly because of three processes: (1) gradual changes to physical and chemical composition induced by the absorption of ultraviolet (UV) light; (2) aging and weathering (e.g., loss of plasticizers in polymers and low-molecular-weight components in asphalt), which may accelerate as temperature increases; and (3) diurnal thermal cycling, which stresses the material by expansion and contraction. Our goal is to clarify the material degradation effects due to UV absorption and those due to heating. The results will be used to quantify the

effect of solar reflectance on the useful life of roofs, provide data to manufacturers to develop better materials, and support development of appropriate ASTM standards.

We are naturally weathering various types of conventionally- and cool-pigmented roofing products at seven California sites. Solar reflectance and thermal emittance are measured twice per year; weather data are available continuously. Solar spectral reflectance is measured annually to gauge soiling and to document imperceptible color changes.

We have also exposed roofing samples to 5,000 hours of xenon-arc light and to about 10,000 hours of fluorescent light in weatherometers, laboratory devices for accelerated aging. Figure 10 compares the total color change and reduction in gloss of cool roofing colored metals (CRCM) and standard colored metals exposed to accelerated fluorescent UV light. In almost all cases cool materials have performed better than standard materials.

Measurement of Energy Savings

Demonstration Homes

We have set up a residential demonstration site in Fair Oaks, CA (near Sacramento) consisting of two pairs of single-family, detached houses roofed with metal and concrete tile. We are planning for another two pairs of houses to demonstrate asphalt shingles. The demonstration pairs each include one building roofed with a cool-pigmented product and a second building roofed with a conventionally (warmer) pigmented product of nearly the same color. The paired homes are adjacent, and share the same floor plan, roof orientation, and level of blown ceiling insulation of 3.37 m^2K/W (R-19 insulation). Each home will be monitored through at least summer 2006.

Solar reflectance and thermal emittance are measured twice a year. Temperatures at the roof surface, on the underside of the roof deck, in the mid-attic air, at the top of the insulation, on the interior ceiling's sheet rock surface, and inside the building are logged continuously by a data acquisition system. Relative humidity in the attic air and the residence are also measured. Heat flux transducers are embedded in the sloped roofs and the attic floor to measure the roof heat flows and the building heat leakage. We have instrumented the building to measure the total house and air-conditioning power demands. A fully instrumented meteorological weather station is set up to collect the ambient dry bulb temperature, the relative humidity, the solar irradiance, and the wind speed and wind direction.

One of the Fair Oaks homes roofed with low-profile concrete tile was colored with a conventional chocolate brown coating (solar reflectance 0.10), while the other was colored with a matching cool chocolate brown with solar reflectance 0.41. The attic air temperature beneath the cool brown tile roof has been measured to be 3 to 5 K cooler than that below the conventional brown tile roof during a typical hot summer afternoon. The results for the pair of homes roofed with painted metal shakes are just as promising. There the attic air temperature beneath the cool brown metal shake roof (solar reflectance 0.31) was measured to be 5 to 7 K cooler than that below the conventional brown metal shake roof.

The application of cool colored coatings is solely responsible for these reductions in attic temperature. The use of these cool colored coatings also decreased the total daytime heat influx (solar hours 8AM – 5PM) through the south-facing metal shake roof by 31% (Figure 11).

(a) (b) (c)

(d) (e) (f)

(g) (h) (i)

(j) (k) (l)

Figure 9. Simulated roofing products made from metal: (a) Advanta Shingles; (b) Bermuda Shakes; (c) Castle Top; (d) Dutch Seam Panel; (e) Granutile; (f) Perma Shakes; (g) Scan Roof Tile; (h) Snap Seam Tile; (i) Techo Tile; (j) Verona Tile; (k) Oxford Shingles; and (l) Timbercreek Shakes. Products a-j are manufactured by ATAS International, Inc., while products k and l are manufactured by Classic Products, Inc. (Photos courtesy of ATAS International and Classic Products)

Estimates of Energy and Peak Demand Savings

To estimate the effect of cool-colored roofing materials, we calculated the annual cooling energy use of a prototypical house for most cooling dominant cities around the world. We used a simplified model that correlates the cool energy savings to annual cooling degree days (base

18°C) (CDD18*). The model is developed by regression of simulated cooling energy use against CDD18. We performed parametric analysis and simulated the cooling- and heating-energy use of a prototypical house with varying level of roof insulation (R-0, R-1, R-3, R-5, R-7, R-11, R-19, R-30, R-38, and R-49) and roof reflectance (0.05, 0.1, 0.2, 0.4, 0.6, and 0.8) in more than 250 climate regions, using the DOE-2 building energy use simulation program. For each prototypical analysis, the parametric analysis led to 15,000 DOE-2 simulations. Then the resulting cooling- and heating-energy use was correlated to CDD18.

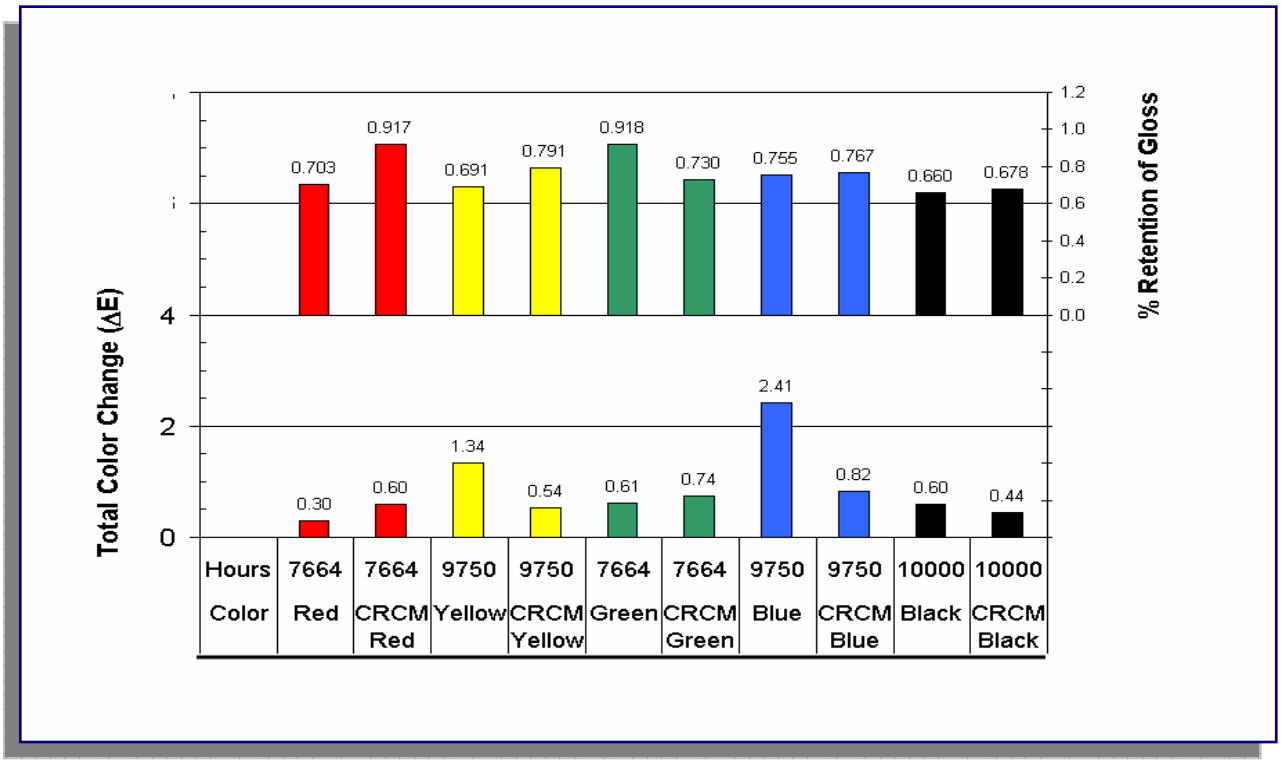

Figure 10. Fade resistance and gloss retention of painted metals (data courtesy of BASF)

The prototypical house used in this paper is assumed to have roofing insulation of 1.94 m^2K/W (R-11 insulation). The coefficient of performance (COP) of the prototype house air conditioner is assumed to be 2.3. The estimates of savings are for an increase in roof solar reflectance from a typical dark roof of 0.1 to a cool-colored roof of 0.4. These calculations present the variation in energy savings in different climates around the world. The typical building may not necessarily be representative of the stock of house in all countries. Here, we only report of cooling energy savings; potential wintertime heating energy penalties are not accounted for in these results.

Table 3 shows CDD18 and potential cooling energy savings in kWh per year for a house with $100m^2$ of roof area. The savings can be linearly adjusted for houses with larger or smaller roof areas. The savings range from approximately 250 kWh per year for mild climates to over

* To calculate the cooling degree days for a particular day, find the day's average temperature by adding the day's high and low temperatures and dividing by two. If the number is below 18°C, there are no cooling degree days that day. If the number is more than 18°C, subtract 18°C from it to find the number of cooling degree days. The annual cooling degree days is simply the sum of all daily cooling degree days.

1000 kWh per year for very hot climates. For houses that are not air conditioned, cool-colored roofing materials offer comfort, typically at very reasonable costs.

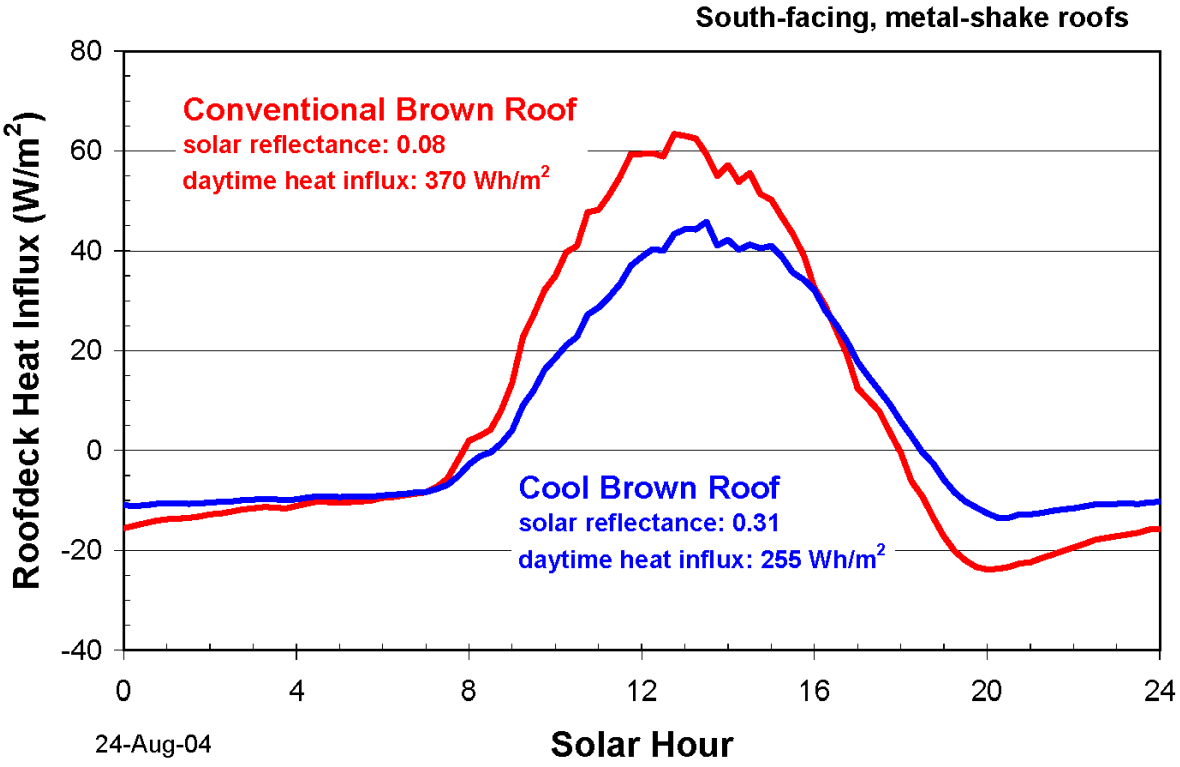

Figure 11. Heat flows through the roof decks of an adjacent pair of homes over the course of a hot summer day. The total daily heat influx through the cool brown metal shake roof (solar reflectance 0.31) between the solar hours of 8AM and 5PM is 31% lower than that through the conventional brown metal shake roof (solar reflectance 0.08).

Conclusion

The results from this program indicate significant success in developing cool-colored materials for concrete tile, clay tile, metal roofs, and shingles. Since the inception of this program, the solar reflectance of commercially available colored roofing products has increased to 0.30–0.45 from 0.05–0.25 for all materials but shingles. To be cost effective, shingle manufacturers apply a very thin layer of pigments on the roofing granules. Use of a reflective undercoated (two-layered coating) has yielded several cost-effective cool-colored shingle products, with solar reflectances in excess of 0.25. Our ongoing collaboration with granule and shingle manufacturers may yield shingles with solar reflectances exceeding 0.3. The energy savings from the installation of cool roofs range from approximately 250 kWh per year for mild climates to over 1000 kWh per year for very hot climates. For houses that are not air conditioned, cool-colored roofing materials offer comfort, typically at very reasonable costs.

Country	City	CDD18	Savings	Country	City	CDD18	Savings
Albania	Tirana	715	312	Morocco	Rabat-Sale	606	280
Algeria	Alger/Dar-El-Beida	899	366	Mozambique	Maputo	2,085	715
Argentina	Buenos Aires/Ezeiza	693	305	Pakistan	Karachi Airport	3,136	1025
Australia	Sydney/K Smith	678	301	Panama	Howard AFB	3,638	1173
Bahamas	Nassau	2,511	841	Paraguay	Asuncion/Stroessner	2,218	755
Bermuda	St Georges/Kindley	1,802	632	Peru	Lima-Callao/Chavez	906	368
Bolivia	Trinidad	2,879	949	Philippines	Manila Airport	3,438	1114
Brazil	Belo Horizonte	1,702	603	Puerto Rico	San Juan/Isla Verde	3,369	1094
	Brasilia	1,353	500	Saudi Arabia	Dhahran	3,340	1085
	Rio de Janeiro	2,360	796		Medina	3,691	1189
	Sao Paulo	1,187	451		Riyadh	3,304	1075
Brunei	Brunei Airport	3,516	1137	Senegal	Dakar/Yoff	2,445	822
China	Beijing (Peking)	840	349	Singapore	Singapore/Changi	3,647	1176
	Shanghai/Hongqiao	1,129	434	Spain	Barcelona	533	258
Cuba	Havana/Casa Blanca	2,700	897		Madrid	886	362
Cyprus	Akrotiri	1,139	437	Syria	Damascus Airport	1,074	417
Egypt	Aswan	3,187	1040	Taiwan	Taipei	2,204	750
	Cairo	1,833	641	Tajikistan	Dusanbe	1,081	420
France	Nice	545	262	Tanzania	Dar es Salaam	2,922	962
Greece	Athenai/Hellenikon	1,030	405	Thailand	Bangkok	3,962	1269
Hong Kong	Royal Observatory	2,136	730		Chiang Mau	3,140	1026
India	Bombay/Santa Cruz	3,386	1099	Tunisia	Tunis/El Aouina	1,102	426
	Calcutta/Dum Dum	3,211	1047	Turkey	Istanbul/Yesilkoy	567	268
	New Delhi/Safdarjung	2,881	950	Turkmenistan	Ashkhabad	1,442	526
Indonesia	Djakarta/Halimperda	3,390	1100	United States	Phoenix	2,579	861
Italy	Palermo/Punta Raisi	1,058	413		Burbank/Hollywood	920	372
	Roma/Fiumicino	621	284		Sacramento	743	320
Jamaica	Kingston/Manley	3,656	1178		Washington/National	930	375
	Montego Bay/Sangster	3,112	1018		Miami	2,516	842
Japan	Kyoto	1,084	420		Atlanta	1,104	426
	Osaka	1,180	449		Honolulu, Oahu	2,651	882
	Tokyo	938	377		New Orleans/Moisant	1,627	580
Jordan	Amman	1,063	414		Memphis	1,324	491
Kenya	Nairobi Airport	566	268		Dallas-Ft Worth	1,519	549
Korea	Seoul	746	321	Uruguay	Montevideo/Carrasco	595	276
Libya	Tripoli/Idris	1,686	598	Venezuela	Caracas/Maiquetia	3,331	1083
Madagascar	Antananarivo/Ivato	701	308	Vietnam	Saigon (Ho Chi Minh)	3,745	1205
Malaysia	Kuala Lumpur	3,475	1125	Zimbabwe	Harare Airport	775	329
Mexico	Chihuahua	1,058	413				
	Mexico City	245	173				
	Acapulco/Alvarez	3,623	1169				

Table 3. Cooling degree days (base 18°C) and potential cooling energy savings (kWh per 100m^2 of roof area)

Acknowledgement

This work was supported by the California Energy Commission (CEC) through its Public Interest Energy Research Program (PIER), and by the Assistant Secretary for Renewable Energy under Contract No. DE-AC03-76SF00098.

References

Akbari. H, P. Berdahl, R. Levinson, S. Wiel, A. Desjarlais, W. Miller, N. Jenkins, A. Rosenfeld, and C. Scruton. 2004. "Cool Colored Materials for Roofs." Proceedings of the 2004 ACEEE Summer Study on Energy Efficiency in Buildings, Vol. 1, p. 1, Pacific Grove, CA.

Akbari, H., S. Konopacki, and M. Pomerantz. 1999. "Cooling energy savings potential of reflective roofs for residential and commercial buildings in the United States," *Energy*, **24**, 391-407.

Akbari, H., S. Bretz, H. Taha, D. Kurn, and J. Hanford. 1997. "Peak Power and Cooling Energy Savings of High-albedo Roofs," *Energy and Buildings* — Special Issue on Urban Heat Islands and Cool Communities, **25**(2); 117–126.

F.W. Dodge. 2003. Construction Outlook Forecast, F.W. Dodge Market Analysis Group, 24 Hartwell Avenue, Lexington, MA 02421. Telephone 800-591-4462.

Konopacki, S. and H. Akbari. 2001. "Measured Energy Savings and Demand Reduction from a Reflective Roof Membrane on a Large Retail Store in Austin." Lawrence Berkeley National Laboratory Report No. LBNL-47149, Berkeley, CA.

Konopacki, S., L. Gartland, H. Akbari, and L. Rainer. 1998. "Demonstration of Energy Savings of Cool Roofs." Lawrence Berkeley National Laboratory Report No. LBNL-40673, Berkeley, CA.

Levinson, R., H. Akbari, S. Konopacki, and S. Bretz. 2005a. "Inclusion of cool roofs in nonresidential Title 24 prescriptive requirements," *Energy Policy*, **33** (2): 151-170.

Levinson, R., P. Berdahl, and H. Akbari. 2005b. "Spectral Solar Optical Properties of Pigments Part I: Model for Deriving Scattering and Absorption Coefficients from Transmittance and Reflectance Measurements." *Solar Energy Materials & Solar Cells* (in press).

-------. 2005c. "Spectral Solar Optical Properties of Pigments Part II: Survey of Common Colorants." *Solar Energy Materials & Solar Cells* (in press).

Parker, D.S., J.K. Sonne, and J.R. Sherwin. 2002. "Comparative Evaluation of the Impact of Roofing Systems on Residential Cooling Energy Demand in Florida," Proceedings of the 2002 ACEEE Summer Study on Energy Efficiency in Buildings, Vol. 1, p. 219, Pacific Grove, CA.

Rosenfeld, A.H., J.J. Romm, H. Akbari, and M. Pomerantz. 1998. "Cool Communities: Strategies for Heat Islands Mitigation and Smog Reduction," *Energy and Buildings,* **28**(1);51–62.

Western Roofing. 2005. Online at http://WesternRoofing.net .

COOL METAL ROOFING TESTED FOR ENERGY EFFICIENCY AND SUSTAINABILITY

William A. Miller, Ph.D., P.E.
Oak Ridge National Laboratory

Andre Desjarlais
Oak Ridge National Laboratory

Danny S. Parker
Florida Solar Energy Center

Scott Kriner
Metal Construction Association

ABSTRACT

High solar reflectance and high infrared emittance roofs incur surface temperatures that are only about 5°F (3°C) warmer than the ambient air temperature, while a dark absorptive roof exceeds the ambient air temperature upwards of 75°F (40°C). In predominantly warm climates, the high solar reflectance and high infrared emittance roof drops the building's air conditioning load and reduces peak energy demands on the utility. In North American climates, being predominantly cold, a more moderate reflectance and a low (not high) emittance result in a warmer exterior roof temperature, which reduces heat loss from the building.

Temperature, heat flow, reflectance, and emittance field data have been catalogued for a full 3 years for 12 different painted and unpainted metal roofs exposed to weathering on an outdoor test facility at Oak Ridge National Laboratory (ORNL).

Habitat for Humanity homes were tested by the Florida Solar Energy Center (FSEC) for a full summer in Fort Myers, Florida. The houses were side-by-side, unoccupied and had different roofing systems designed to reduce the attic heat gain. Measurements showed that the white reflective roofs reduced cooling energy consumption by 18-26% and peak demand by 28-35%.

Results show that a judicious selection of the roof surface properties of reflectance and emittance represent the most significant energy and cost saving options available to homeowners and builders in predominantly hot climates.

INTRODUCTION

Determining how weathering affects the solar reflectance and infrared emittance of metal roofs is of paramount importance for documenting the magnitude of the comfort cooling and heating energy load consumed by a building. The building's load, is directly related to the solar irradiance incident on the building; to the exterior temperature; to the level of roof, wall and foundation insulation; to the amount of fenestration; and to the building's tightness against unwanted air and moisture infiltration. The solar reflectance and infrared emittance and the airside convective currents strongly affect the envelope's exterior temperature. Our data show that in moderate to predominantly hot climates, an exterior roof surface with a high solar reflectance and high infrared emittance will reduce the exterior temperature and produce savings in comfort cooling. For predominantly heating-load climates, surfaces with moderate reflectance but low infrared emittance will save in comfort heating, although field data documenting the trade-off between reflectance and emittance are sparse.

Full building field tests in Florida and California using before-after experiments have examined the impact of reflective roofing on air conditioning (AC) energy use. In Florida tests measured air conditioning electrical savings averaged 19% (7.7 kWh/Day) (Parker et al., 1998). Even greater fractional savings have been reported for similar experiments in California (Akbari, et al., 1997).

Author Note:
W. Miller, Specialist, Engineering Science and Technology Division, Oak Ridge National Laboratory, Oak Ridge, TN; A. Desjarlais, Program Leader, Building Envelope and Materials Research Program, Oak Ridge National Laboratory, Oak Ridge, TN; D. Parker, Principal Research Scientist, Florida Solar Energy Center, Cocoa, FL; S. Kriner, Technical Director, Metal Construction Association, Glenview, IL.

Experimental Initiatives

The Buildings Technology Center (BTC) of ORNL has instrumented and field tested steep-slope- and low-slope-roof test sections of painted and unpainted metals for the past three years on a test building called the Envelope Systems Research Apparatus (ESRA). The low-slope assembly (Figure 1) consists of white-painted polyvinylidene fluoride (PVDF) galvanized steel[1]; off-white polyester; 55% Al-Zn coated steel[2] painted with a clear acrylic dichromate layer; unpainted galvanized steel; and unpainted 55% Al-Zn-coated steel. Five painted metal panels are being tested on the steep-slope assembly (Figure 1). Three panels of white-painted PVDF galvanized steel; three panels of 55% Al-Zn-coated steel painted with a clear acrylic dichromate layer; six panels of bronze-painted PVDF aluminum; and three panels of black-painted PVDF galvanized steel[3] were exposed to weather in east Tennessee. An asphalt-shingle roof section was included as the base of comparison. Salient features of the ESRA facility are fully discussed by Kriner and Miller (2001). Exposure sites were also setup to field test the identical painted and unpainted metal samples at Monroeville, PA, Fort Lauderdale, FL, Nova Scotia, Canada and Bethlehem, PA.

Florida Solar Energy Center (FSEC) instrumented seven side-by-side Habitat for Humanity (HFH) homes in Fort Myers, Florida with identical floor plans and orientation, but with different roofing systems designed to reduce attic heat gain (Figure 2). Six houses had R-19 ceiling insulation, and the seventh house had an unvented attic with insulation on the underside of the roof deck rather than the ceiling. All seven residences have a three bedroom, one bath floor plan and are of identical construction and exposure. Identical two-ton split system air conditioners with 5 kW strip heaters were installed in each of the seven homes. The houses underwent a series of tests in order to ensure that the construction and mechanical systems performed similarly. The following three-letter identification codes are used in the text, and the solar reflectance and infrared emittance of new material are also provided each roofing system :

Description of Test Roof on each HFH House	Label	Solar Reflectance	Infrared Emittance
• Dark gray fiberglass shingles	RGS	0.082	0.89
• White barrel-shaped tile	RWB	0.742	0.89
• White fiberglass shingle	RWS	0.240	0.91
• Flat white tile	RWF	0.773	0.89
• Terra cotta barrel-shaped tile	RTB	0.346	0.88
• White 5-vee metal	RWM	0.662	0.86
• Sealed attic with insulation on the roof plane	RSL	0.082	0.89

The salient features of the Habitat for Humanity homes and their respective roofs field tested in Fort Myers, Florida are fully described by Parker et al. (2001).

DISCUSSION

Reflectance and Emittance Surface Properties

The solar reflectance and the infrared emittance of a roof surface are important surface properties affecting the roof temperature, which in turn drives the heat flow through the roof. The reflectance and emittance are phenomenon occurring just a fraction of a micrometer within the irradiated surface. The solar reflectance gages the percentage of the sun's energy that a roof deflects off the building, and the infrared emittance is the percentage of infrared heat that a roof releases from the building. Reflectance and emittance are expressed as mathematical ratios. The reflectance (ρ) determines the fraction of radiation incident from all directions that is diffusely reflected by the surface. The emittance (ε) describes how well the surface radiates energy away from itself as compared to a blackbody operating at the same roof temperature. The emittance of painted metal is about 0.90 while unpainted metal has values of about 0.10. The impact of emmittance on roof temperature is just as important as that of reflectance.

Reflectivity measurements were made every 3 months on the ESRA's steep- and low-slope metal roofs; these measurements are shown in Figure 3. Each metal roof is described generically using an R*xx*E*yy* designation. R*xx* states the solar reflectance of a new sample, 1.0 being a perfect reflector. E*yy* defines the

[1] A zinc-coated steel sheet dipped in continuous coil form through a molten bath of zinc.

[2] This steel is exposed to a molten bath composed of 55% Al-43.5% Zn -1.5% Si at a temperature of 1100°F (593°C). The coating is solidified rapidly to enhance both the microstructure and the corrosion resistance.

[3] Black-painted polyvinylidene fluoride (PVDF) laminated with amorphous photovoltaic cells.

infrared emittance of the new sample, 1.0 being blackbody radiation. For example, the asphalt-shingle roof is labeled R09E91 in Figure 3. Its freshly manufactured surface properties are therefore 0.09-reflectance and 0.91-emittance. Kriner and Miller (2001) identify the R*xx*E*yy* designations for the different painted and unpainted test metals tested at ORNL.

After 3½ years of exposure, the white and bronze painted PVDF metal roofs, R64E83 and R07E87 respectively, have lost less than 5% of their original reflectance. The coated steel painted with a clear acrylic dichromate layer, R64E08, shows only a 12% loss in reflectance. In comparison the asphalt shingle roof, R09E91, increased a percentage point in reflectance after the 3½ years of exposure (Figure 3). The reflectance comparison is very important, because both R64E83 and R64E08 roofs reflected about 50% more solar energy away from these test roofs than did the asphalt shingle roof. Even more promising is the observed durability of the surface of the painted metals; reflectance remained fairly level. Less heat is therefore absorbed by the "cool" painted metal roofs and the building load and the peak utility load are reduced as compared to darker more absorptive roofs (i.e.,R09E91).

Testing conducted at the roof slopes of 4-in of rise per 12-in of run (i.e., Steep Slope Roof [SSR] in Figure 3) and at ¼-in of rise per 12-in of run (i.e., Low Slope Roof [LSR] in Figure 3) further show that the slope of the roof has little effect on the loss of reflectance for the painted metal roofing having the PVDF finish. The painted metal appears to have excellent corrosion resistance. Their surface opacity have limited any photochemical degradation caused by ultraviolet light present in sunlight over the 3-years of testing. All painted metal roofs have maintained their original manufactured appearance. After 3½ years of exposure, rains with a measured ph of 4.3 in East Tennessee (National Atmospheric Deposition Program) have not etched the metal finish. ORNL scientists detected evidence of biological growth on some of the test roofs (Miller et al. 2002); however, the PVDF surface finish does not appear to allow the growth to attach itself and atmospheric pollution is washed off by rain.

Most dramatic are the trends observed in the solar reflectance and the infrared emittance of the painted metal roofs tested at different exposure sites across the country. Similar reflectance was measured in the hot, moist climate of Florida as compared to the predominantly cold climate of Nova Scotia (Figure 4). The Environmental Protection Agency's Energy Star® Program requires field testing at three different building sites; however, the results for painted metal show the reflectance to be very similar whether exposed in Florida, Nova Scotia or Pennsylvania. Also solar reflectance and infrared emittance measures collected from the test fence exposure sites in Florida, Nova Scotia, Pennsylvania and also at Oak Ridge (Figure 4) are very similar to the reflectance and emittance measures recorded for the test roofs exposed on the ESRA in Oak Ridge (Figure 3). For this 3½ year time limited study, the changes in solar reflectance and infrared emittance of the painted PVDF metals is independent of climate! The results show that fence exposure data are a viable alternative for certifiying the painted PVDF metal roofs as Energy Star compliant, because they yielded very similar trends as the identical roofs exposed on the ESRA.

The emittance of the painted metal roofs did not change much after 3½ years of weathering. In fact, the data in Figure 4 shows that the emittance increased slightly over time. The coated steel painted with a clear acrylic dichromate layer, R64E08, has a much lower emittance than the white PVDF (R64E83) roof. Note however that the emittance of several of the freshly manufactured coated steel samples painted with the clear acrylic dichromate layer varied from a low of 0.08 to a high of 0.20, probably because of the coating. Emittance trends of the low-slope coated and unpainted steel increased while those of the painted metal remained relatively flat, Kriner and Miller (2001).

Thermal Performance of Painted Metal Roofing at ORNL

Increasing the solar reflectance or infrared emittance of a roof will reduce the exterior temperature, which in turn results in reduced building load. Solar reflectance effects naturally occur during the sunlight hours, while the effects of emittance occur continuously as long as there is a temperature difference between the metal and the radiant sky[4].

Temperature data for metal roof surfaces on the steep-slope assembly of the ESRA are shown in Figure 5. These data are for a week of summer and winter weather having clear skies. Note that each label on the abscissa in Figure 5 is for midnight. The maximum daily ambient air temperature ranged from about 85°F to 95°F (29°C to 36°C) over the week in August. In February, the daily maximum air temperature ranged from 40°F to 60°F (4°C to 16°C). Peak air temperature usually occurs at about 4 P.M. with the peak roof temperature occurring slightly earlier at about 2 P.M.

The summer roof temperature for the R07E87, R26E90, and R09E91 (asphalt-shingle) sections all exceeded 160°F (71°C) and on some days reached a peak temperature of 165°F (74°C). The more reflective

[4] Measures of the global infrared irradiance made by the BTC's field pyrgeometer used to calculate the radiant sky temperature from the equation for blackbody radiation: $q_{IR} = \sigma T_{sky}^4$.

R64E83 and R64E08 test sections had peak temperatures of about 115°F and 135°F (46°C to 57°C), respectively. The lower temperatures in turn imply less heat transmission into the building. On Aug 11, 2000, however, the R64E83 roof emittance was 0.826 as compared to 0.176 for the R64E08 test roof. Therefore, the 20°F (11°C) difference in roof temperature for the white PVDF versus the steel with clear acrylic layer is driven predominantly by the effect of emittance. The effect is even better depicted for the February data (Figure 5). During the evening hours, the lower emittance test roof (R64E08) maintains a temperature that exceeds the dew point temperature of the ambient air. Therefore, during the evening hours, less heat leaks to the outdoor ambient from the less emissive of the two metal roofs.

The temperature data of Figure 5 for the painted metals roofs were cast in terms of the average roof temperature averaged over the sunlight hours between 6 A.M. and 6 P.M. The averaged data were then fit using the solar reflectance and infrared emittance as independent variables, and the regression fits to these averaged roof temperature data are shown in Figure 6. Fixing the reflectance and decreasing the emittance causes the roof temperaturee to increase during August exposure. The hotter roof temperature in turn increases the heat entering the roof, which reveals why a low emittance is not thermally efficient on a hot summer day. For the August data one can see that a high solar reflectance and a high infrared emittance yields the coolest roof surface (Figure 6). The August data also reveals the interdependence of the infrared emittance and solar reflectance on roof heat flow. The lower the solar reflectance the greater is the effect of the infrared emittance on the roof temperature. Conversely the lower the infrared emittance the greater is the effect of the solar reflectance.

However, the effects of the infrared emittance observed in February are not as strong as those observed for the August data. Decreasing the infrared emittance caused less than a 5°F (3°C) increase in the average roof temperature; its effect is relatively flat in the winter. Decreasing the reflectance from 0.60 to 0.40 caused the average roof temperature to increase about 11°F (6°C). The results imply that the lowest heat loss from the roof occurs when the solar reflectance and the infrared emittance are low, and the effect of reflectance is more pronounced than is the effect of the emittance during this cold winter day.

Akbari and Konopacki (1998) performed DOE2.1e parametric simulations to estimate the impact of reflectance and emittance on the heating and cooling energy consumption for eleven metropolitan U.S. cities. Simulations were based on both old and new residential and commercial construction having respectively R-11 and R-19 levels of ceiling insulation. Nationwide, Akbari and Konopacki (1998) found that annually about $0.75 billion can be saved by widespread implementation of light-colored roofs in cooling dominant climates.

Their simulations also showed that the infrared emittance effects both cooling and heating energy use. In cooling dominant climates, a low emittance roof yields a higher roof temperature and in turn increases the cooling load imposed on the building. Akbari and Konopacki (1998) simulations showed that changing the infrared emittance from 0.90 (typical emittance of most nonmetallic surfaces) to 0.25 (emittance of a shiny metallic surface) caused a 10% increase in the annual utility bill. However, in cold climates, a low emittance roof adds resistance to the passage of heat leaving the roof, which results in savings in heating energy. Akbari and Konopacki (1998) showed that in very cold climates with little or no summertime cooling, the heating energy savings resulting from decreasing the roof emittance almost reached 3% of the building's annual energy consumption.

Therefore, the design of a metal roof should focus on the both the solar reflectance and infrared emittance of the surface. High solar reflectance and high infrared emittance yield significant thermal benefits in predominantly cooling climates, while a modest solar reflectance and low infrared emittance produce modest thermal performance gains in predominantly heating load climates. During winter exposure, moisture problems with icings and ice dams may possibly be reduced by a low emittance roof because the lower emittance retains heat and has an exterior temperature during the evening hours that may exceed the dew point temperature of the outdoor air (see Figure 5 for R64E83 and R64E08 during the hours around midnight).

Thermal Performance of Painted Metal Roofing at FSEC

While previous research efforts have investigated the thermal performance of various roofing systems, this particular study conducted by the FSEC and the Florida Power and Light Company represents the first time an attempt has been made to quantify roofing influence on cooling performance on identical, unoccupied, side-by-side residences. The project consisted of seven, single-family residential homes located in Fort Myers, Florida. The focus of the study was to investigate how various roofing systems impact air conditioning electrical demand. The houses underwent a series of tests in order to ensure that the construction and mechanical systems performed similarly. Details are not described here but can be found in the works by Parker, Sonne and Sherwin (2002).

The relative performance of the seven Habitat for Humanity (HFH) homes was evaluated for one month in the summer of 2000 under unoccupied and carefully controlled conditions. Table 1 summarizes the measured attic temperatures, cooling loads and savings for the seven homes over the unoccupied monitoring period; the data are ranked in descending order of total daily energy consumption. The average interior air temperature

near the thermostat in all homes was within 1°F of each other. However, because of the large influence of the thermostat temperature, we adjusted the monitored cooling results in Table 1 to account for set point differences among houses, (Parker et al. 2001).

Not surprisingly, the control home (RGS) has the highest consumption (17.0 kWh/day). The home with the terra cotta barrel tile (RTB) has a slightly lower use (16.0 kWh/day) for a 7.7% cooling energy reduction. Next is the home with the white shingles (15.3 kWh/day) – an 10.6% reduction. The sealed attic (RSL) comes in with a 7.8% cooling energy reduction (14.7 kWh/day). The true white roofing types (> 60% reflectance) had the lowest energy use. Both the white barrel (RWB) and white flat tile (RWF) roofs averaged a consumption of 13.3 kWh/day for respectively a 18.5% and 21.5% cooling energy reduction. The white metal roof (RWM) showed the largest impact with a 12.0 kWh/day July consumption, yielding a 24% reduction in cooling energy consumption.

TABLE 1. Cooling Performance* During Unoccupied Period: July 8th – 31st, 2000

Site	Total kWh/day	Savings kWh/day	Thermo-stat (F)	Thermo-stat (C)	Mean Attic (F)	Mean Attic (C)	Max Attic (F)	Max Attic C)	Temp. Adjust. %	Field EER	Final Saving %
RGS	17.0	0.00	77.2	25.11	90.8	32.7	135.6	57.5	0.0	8.30	0.0
RTB	16.0	1.01	77.0	25.0	87.2	30.7	110.5	43.6	-1.6	8.12	7.7
RWS	15.3	1.74	77.0	25.0	88.0	31.1	123.5	50.8	-1.2	9.06	10.6
RSL	14.7	2.30	77.7	25.4	79.0	26.1	87.5	30.8	5.4	8.52	7.8
RWB	13.3	3.71	77.4	25.2	82.7	28.2	95.6	35.3	2.8	8.49	18.5
RWF	13.2	3.83	77.4	25.2	82.2	27.9	93.3	34.1	2.1	7.92	21.5
RWM	12.0	5.00	77.6	25.3	82.9	28.3	100.7	38.2	4.9	8.42	24.0

* Final savings are corrected for differences in interior temperature and AC performance among houses.

It is noteworthy that the average July outdoor ambient air temperature during the monitoring period (82.6°F [28.1°C]) was very similar to the 30-year average for Fort Myers (82°F [27.7°C]). Thus, the current data are representative of typical South Florida weather conditions. Relative to the standard control home, the data show two distinct groups in terms of performance:

- Terra Cotta tile, white shingle and sealed attic constructions produced approximately an 8-11% cooling energy reduction
- Reflective white roofing yielded a 19-24% reduction in the consumed cooling energy.

White flat tile performed slightly better than the white barrel due to its greater solar reflectance. The better performance of white metal is believed due to the effect of thermal mass. The metal roof incurred lower nighttime and early morning attic temperatures than did the tile or shingles, leading to lower nighttime cooling demand.

Peak Day Performance

July 26th was one of the hottest and brightest days in the data collection period and was used to view the effects of maximum solar irradiance on the candidate roofing systems and to also evaluate peak influences on utility demand (Table 2). The average solar irradiance was 371 W/m^2 and the maximum outdoor ambient air temperature was 93.0°F (33.8°C).

The roof decking temperature (Figure 7) and subsequently the surface temperature were highest for the sealed attic construction (RSL) since the insulation under the decking forced much of the collected solar heat to migrate back out through the shingles. The sealed attic construction experienced measured deck temperatures that were 20°F (11.1°C) higher each sunny day than the control house. The white roofing systems (RWM, RWF and RWB) experienced peak deck temperatures approximately 40°F (22°C) cooler than the darker shingles on the control house (RGS in Figure 7). The terra cotta barrel tile was about 29°F (16°C) cooler on this July 26th day of peak solar irradiance.

The measured mid attic air temperatures above the ceiling insulation further revealed the impact of the white reflective roofs with max attic temperatures about 35 to 40 °F cooler than the control home (RGS). As expected, the home with the sealed attic had the lowest attic temperatures reaching a maximum of 87.5°F (30.8°C) compared with the 77°F (25°C) being maintained inside. However, the sealed attic case has no

insulation on the ceiling floor with only studs and sheet rock. Thus, from a cooling loads perspective, the low attic temperature with this construction is deceptive. Since ½ inch sheet rock has a thermal resistance $R \leq 1$, a significant level of heat transfer takes place across the uninsulated ceiling. While this construction method reduced attic air temperatures, it did not reduce ceiling heat transfer as well as other options. Ceiling heat fluxes are actually higher. In this case, the ceiling and duct system is unintentionally cooling the attic space, which can lead to the false impression that roof/attic loads are lower.

These data show that during periods of high solar irradiance the performance of the sealed attic case (RSL) suffers significantly. The tile and white shingle roofs did better at controlling demand than did the sealed attic on this very hot day. However, the white metal roof performed best showing peak savings of about 35% over the RGS control.

TABLE 2.
Summer Peak Day Cooling Performance: July 26th, 2000

		Savings		Peak Period*		
Site	Cooling Energy	KWh	Percent	Demand (kW)	Savings (KW)	Percent
RGS	18.5 kWh		----	1.631	0.000	----
RTB	17.2 kWh	1.3	7%	1.570	0.061	3.7%
RSL	16.5 kWh	2.0	11%	1.626	0.005	0.3%
RWS	16.5 kWh	2.0	11%	1.439	0.192	11.8%
RWF	14.2 kWh	4.3	23%	1.019	0.612	37.5%
RWB	13.4 kWh	5.1	28%	1.073	0.558	34.2%
RWM	12.4 kWh	6.1	33%	0.984	0.647	39.7%
* Peak utility load occurred from 4 to 6 PM						

CONCLUSIONS

The painted metal roofs have maintained their reflective surface; drops in reflectance are only about 5% after 3½ years of exposure. They appear to have an excellent corrosion-resistant surface whose opacity limits photochemical degradation caused by ultraviolet light present in sunlight. After 3½ years of exposure, rain has not etched the metal finish, and there is no evidence of any effects due to biological growth on the test roofs. Drops in solar reflectance are due more to airborne pollution than to any effect of the sun. Therefore, as roof slope increases, the washing action of precipitation increases, which helps to refresh the reflectance.

Exposure data for the more reflective painted metal roofs show the roofs qualify for the Energy Star® label for both steep-slope and low-slope roofing. In low-slope applications, the initial reflectance are boaderline; however, the painted PVDF metal roofs maintain their reflectance above 0.5 after the required 3 years of exposure.

The design of a metal roof for predominantly heating-load application should focus first on the level of roof insulation, secondly on the surface reflectance and finally on the emittance of the surface. A moderate solar reflectance with a low infrared emittance showed the least heat leakage from the test roofs during the winter. In predominantly cooling-load climates, the high solar reflectance and high infrared emittance of white-painted metal roofs yielded the best thermal performance. Here, design should focus on increasing both the emittance and reflectance to decrease the exterior roof temperature, which in turn decreases the heat leakage into the building.

The FSEC field study demonstrated that the roof and attic exert a powerful influence on the cooling energy used in the seven side-by-side Habitat for Humanity homes tested in South Florida. Each of the examined alternative roofing systems were found to be thermally superior to standard dark shingles, both in providing lower attic temperatures and lower AC energy use. The sealed attic construction provided modest savings to cooling energy, but no real peak reduction due to its sensitivity to periods with high solar irradiance. The HFH field study points to the need for reflective roofing materials or lightcolored tile roofing for good energy performance with sealed attics.

The HFH project revealed essentially two classes of performance for the 1,144 square foot homes. Analysis showed the white highly reflective roofing systems (RWF, RWB and RWM) provide annual cooling energy reductions of 600 to 1,100 kWh in South Florida (18-26%). Savings of terra cotta tile roofs are modest at 3-9% (100-300 kWh), while shingles provide savings of 3-5% (110-210 kWh). Sealed attic construction produced savings of 6-11% (220-400 kWh). The highly reflective roofing systems showed peak demand impacts of 28-35% (0.8-1.0 kW). White metal had the best cooling related performance. Its high conductivity coupled with nocturnal radiation resulted in lower nighttime and early morning attic temperatures that lead to a reduced cooling demand during evening hours.

REFERENCES

Akbari, H., S., Bretz, H. Taha, D. Kurn, and J. Hanford. 1997. “Peak Power and Cooling Energy Savings of High-albedo Roofs,” Energy and Buildings — Special Issue on Urban Heat Islands and Cool Communities, 25(2);117-126.

Akbari, H., Konopacki, S.J. 1998. “The Impact of Reflectivity and Emissivity of Roofs on Building Cooling and Heating Energy Use,” in Thermal Performance of the Exterior Envelopes of Buildings, VII, proceedings of ASHRAE THERM VIII, Clearwater, FL., Dec. 1998.

Miller, W. A., and Kriner, S. 2001. “The Thermal Performance of Painted and Unpainted Structural Standing Seam Metal Roofing Systems Exposed to One Year of Weathering,” in Thermal Performance of the Exterior Envelopes of Buildings, VIII, proceedings of ASHRAE THERM VIII, Clearwater, FL., Dec. 2001.

Miller, W.A., Cheng, M-D., Pfiffner, S., and Byars, N. 2002. “The Field Performance of High-Reflectance Single-Ply Membranes Exposed to Three Years of Weathering in Various U.S. Climates,” Final Report to SPRI, Inc., Aug., 2002.

Parker, D. S., Sherwin, J. R. 1998. “Comparative summer attic thermal performance of six roof constructions.” *ASHRAE Trans*., Vol. 104, pt. 2, 1084–1092.

Parker, D.S., Sonne, J. K., Sherwin, J. R. 2002. “Comparative Evaluation of the Impact of Roofing Systems on Residential Cooling Energy Demand in Florida,” in ACEEE Summer Study on Energy Efficiency in Buildings, proceedings of American Council for an Energy Efficient Economy, Asilomar Conference Center in Pacific Grove, CA., Aug. 2002.

Parker, D.S., Sonne, J.K., Sherwin, J.R. and Moyer N. 2001. “Comparative Evaluation of the Impact of Rofing Systems on Residential Cooling Energy Demand in Florida,” Final Report FSEC-CR-1220-00, prepared for the Florida Power and Light Company, May 2001.

Figure 1. The Envelope Systems Research Apparatus used for testing painted and unpainted metal roofing.

Figure 2. Habitat for Humanity homes tested by the FSEC in Fort Myers, Florida.

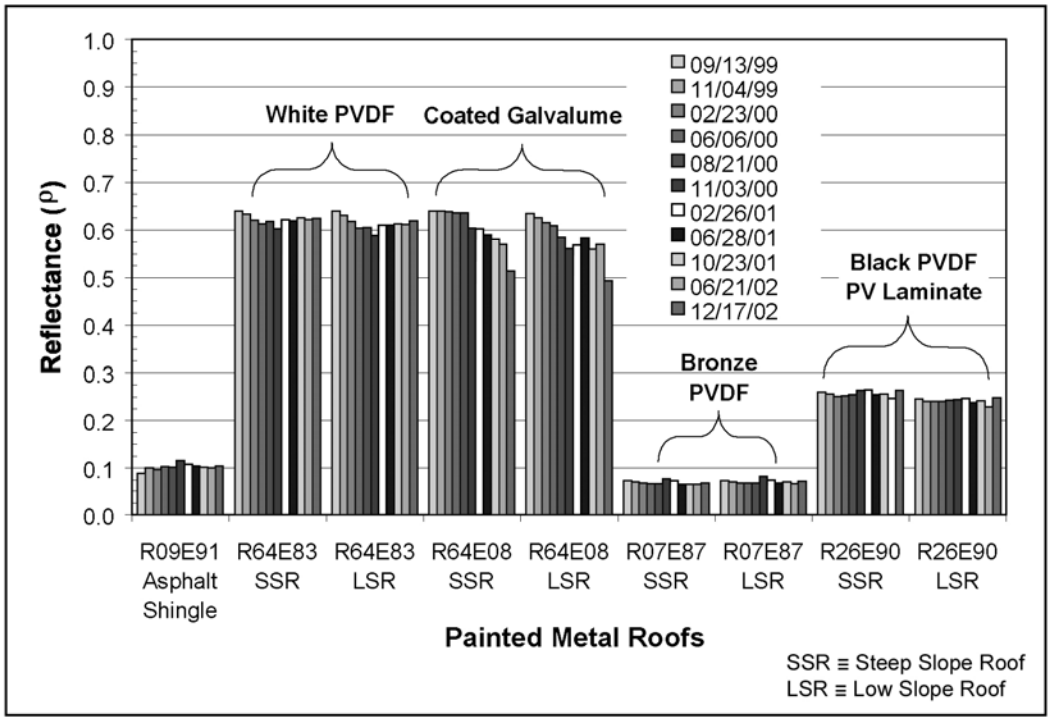

Figure 3. Solar reflectance of the painted metals exposed to weathering on the ESRA.

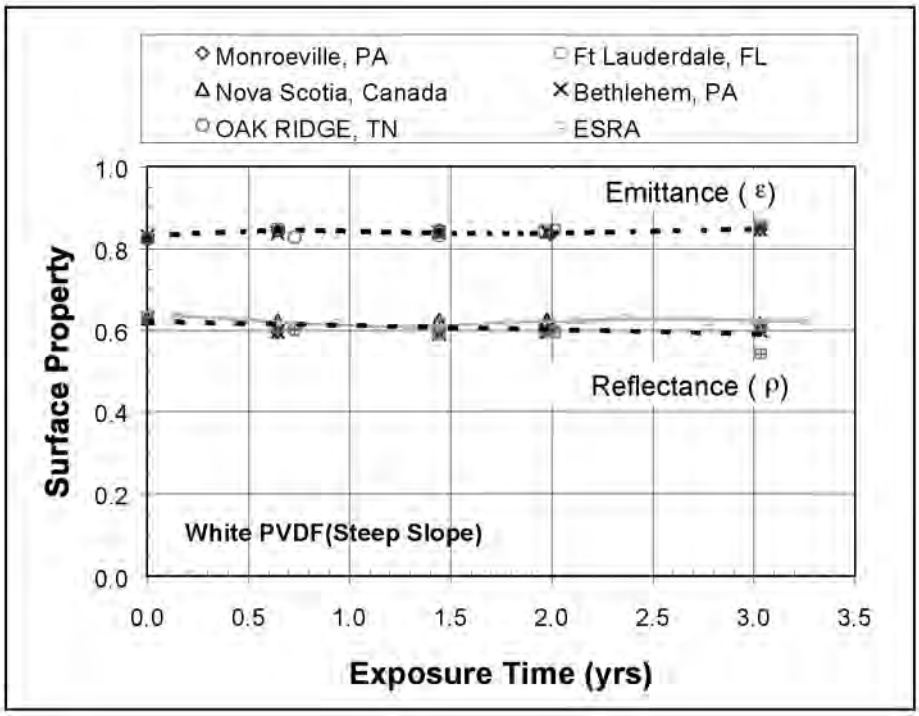

Figure 4. Solar reflectance and infrared emittance of white PVDF painted metal (R64E83).

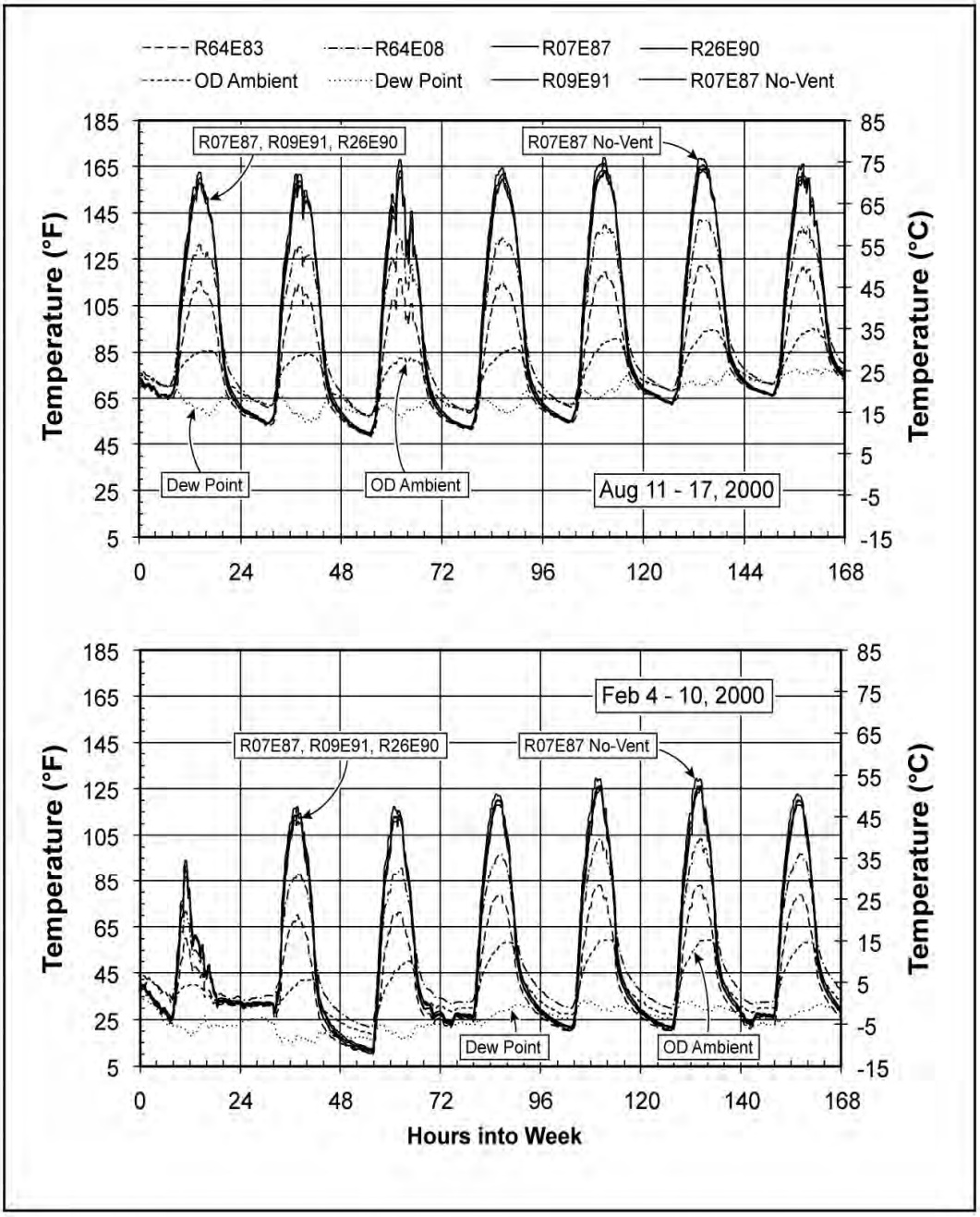

Figure 5. Field data collected for the steep-slope metal roof assembly for one week of summer and one week of winter data.

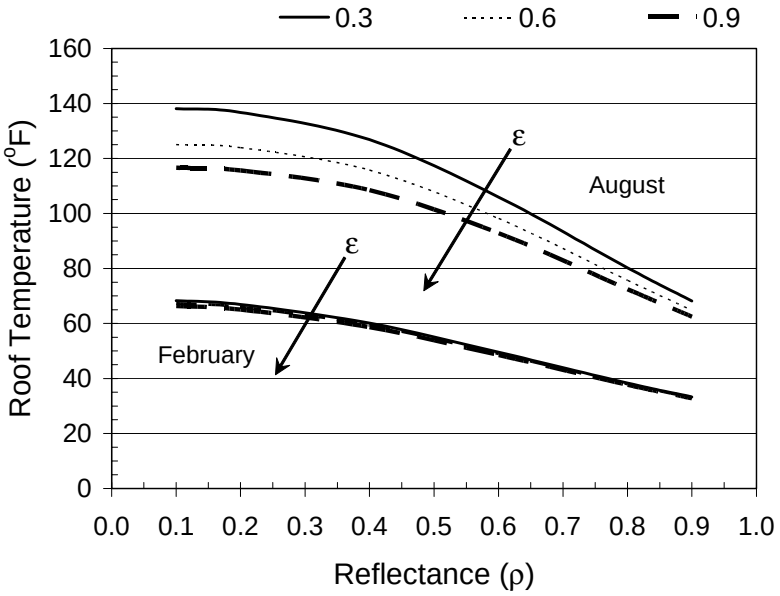

Figure 6. Roof temperature for painted metal roofs averaged over the sunlit hours.

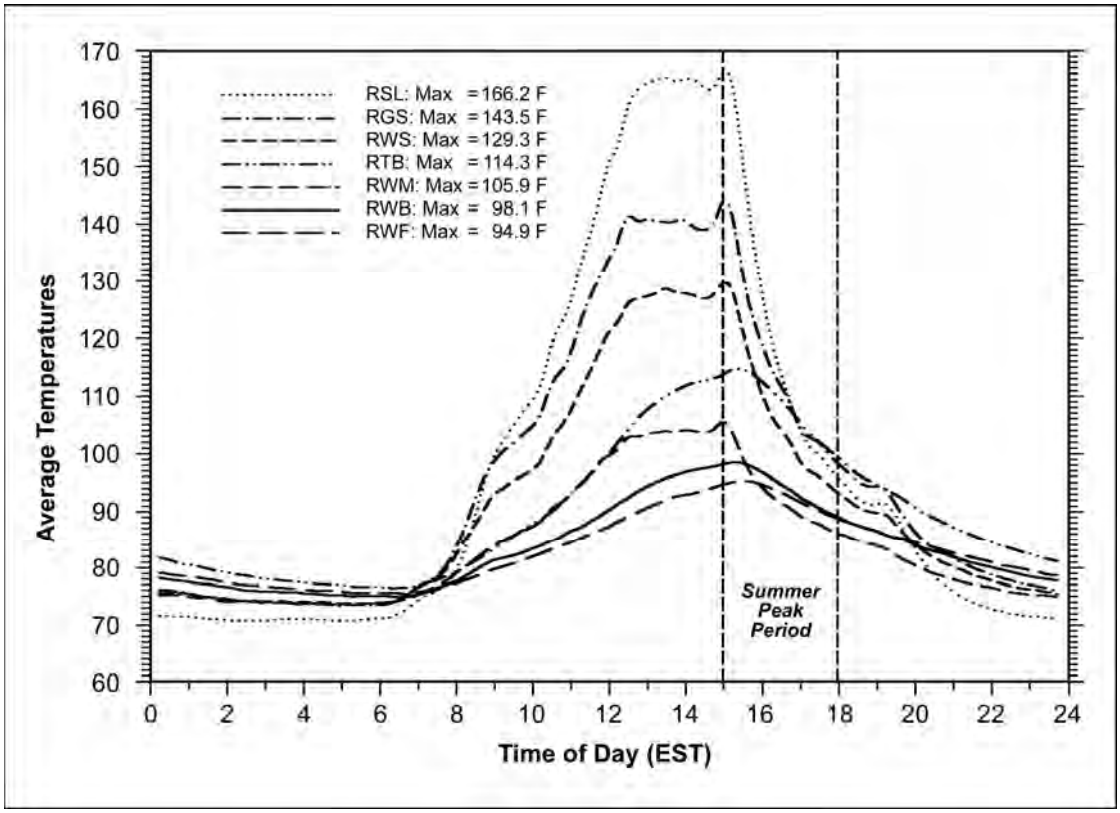

Figure 7. Deck temperatures measured on July 26, 2000.

PVDF Coatings with Special IR Reflective Pigments

William A. Miller,[1] Oak Ridge National Laboratory
Kenneth T. Loye, FERRO Corporation
André O. Desjarlais, Oak Ridge National Laboratory
Robert P. Blonski, FERRO Corporation

ABSTRACT

Pigment colorant researchers have developed new complex inorganic color pigments (CICPs) that exhibit dark color in the visible spectrum and high reflectance in the near-infrared portion of the electromagnetic spectrum. CICPs can increase the infrared reflectance of building paints thereby droping the surface temperatures of the roof and exterior walls. The lower temperatures in turn reduce the cooling-energy demand of the building. However, determining the effects of climate and solar exposure on the reflectance and the variability in color over time is of paramount importance for promoting the energy efficiency and for accelerating the market penetration of products using CICPs.

CICPs consisting of a mixture of infrared reflective pigments, chromic oxide (Cr_2O_3) and ferric oxide (Fe_2O_3) boosts the total hemispherical reflectance of a black polyvinylidene fluoride paint finish from 0.05 to 0.26. The increase in reflectance reduces the temperature of the painted surface, and as result xenon-arc exposure testing and two-years of field exposure testing show the CICPs have improved the fade resistance of polyvinylidene fluoride paints.

Introduction

High-reflectance single-ply membranes, painted and unpainted metal, and spray-on roof coatings are reducing energy use in the commercial market as building contractors substitute these high-reflectance roofs for bitumen-based built-up roofing (BUR) and ethylene propylene diene monomer (EPDM). Since a high-reflectance low-slope roof cannot be seen from the ground, the roof's functionality is far more important than its looks. However, in steep-slope residential roofing the issues of appearance, cost, and then durability typically drive the selection of the roofing material because the homeowner wants the roof to complement the décor of the house while protecting the underlying residential structure for a long period of time at an affordable cost.

To homeowners, dark roofs simply look better than a highly reflective "white" roof. Yet the aesthetically pleasing dark roof can be made to reflect light like a "white" roof in the infrared portion of the solar energy spectrum. Researchers working with the Department of Defense developed new complex inorganic color pigments (CICPs) that exhibit dark color in the visible spectrum and high reflectance in the near-IR portion of the electromagnetic spectrum (Sliwinski, Pipoly & Blonski 2001).

---

[1]Dr. William A. Miller is a research engineer in the Buildings Technology Center of Oak Ridge National Laboratory (ORNL), Oak Ridge, Tennessee. Kenneth T. Loye is the Technical Manager of the Pigments Group at FERRO Corporation, Cleveland, Ohio. André O. Desjarlais is the manager of ORNL's Building Thermal Envelope Systems & Materials Program. Robert P. Blonski is a research chemist working in the Pigments Group at FERRO Corporation.

The opportunity exists for a significant impact on energy use in commercial buildings and residential housing, both in new construction and for re-roofing existing homes. The total sales volume for roofing and re-roofing is booming and nearly doubled between 1997 and 2000, from $20 billion to $36 billion (Good 2001). Of the sales volume in 2000, low-slope roofing accounted for 64% ($21.7 billion), while steep-slope roofing comprised about 35.6% ($12 billion) (Good 2001).

Our research estimates U.S. potential savings in excess of $750 million per year in net annual energy bills (cooling-energy savings minus heating-energy penalties). These savings account for only the direct impact of cool roofs; savings would double once the indirect benefits (cooling of the ambient air) and smog reductions are included. The decrease in electric demand translates to a decrease of approximately 30.4 million tons in CO_2 emissions per year.

Surface Properties Affecting Reflectance

Titanium dioxide (TiO_2) is currently the most important white pigment used in the manufacture of paints and plastics. TiO_2 is chemically inert, insoluble, and very heat-resistant. It has been commercially processed from rutile since as early as 1941 (Du Pont Ti-Pure 1999). Rutile TiO_2 increases surface reflectance through refraction and diffraction of the light. As a light ray passes through a TiO_2 particle, the ray bends, or refracts, because light travels more slowly through the pigments than it does through the resin or binder. This occurs because TiO_2 has a much larger refractive index than the resin. This phenomenon is depicted in Figure 1 for two pigmented films. The film containing the pigment with higher refractive index bends the light more than does the film containing the lower refractive index pigment.

Figure 1. Path of Light as It Penetrates Two Different Coatings, One Having Pigments with a Higher Refractive Index Than the Other

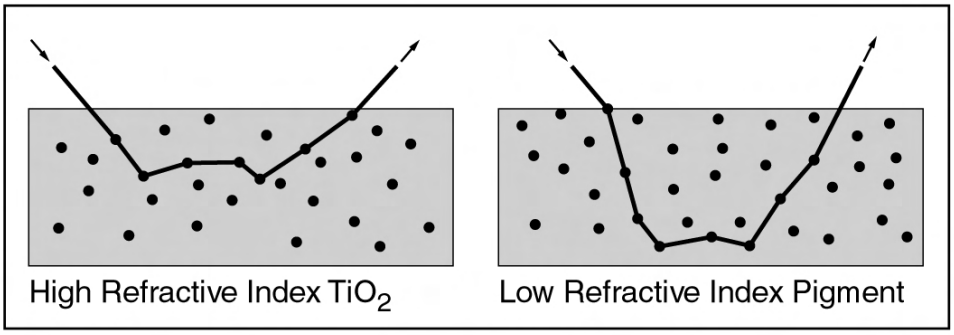

The light travels a shorter path and does not penetrate as deeply into the film; therefore, less heat is absorbed. The reflectance of the surface increases because the surface opacity increases through refraction induced by the TiO_2 particles. In general, the greater the difference between the refractive index of the pigment and that of the resin or filler in which it is dispersed, the greater will be the light scattering and therefore the increase in surface reflectance, Martin and Pezzuto (1998).

Diffraction is another physical factor affecting a pigment's ability to scatter light. As a light ray passes by a TiO_2 particle, the ray bends, or diffracts, around the pigment (Fig. 2). Maximum diffraction occurs when the diameter of the pigment is slightly less than one-half the wavelength of the light to be scattered. Physical modifications of the size, the distribution, and the shape of pigment particles will therefore affect the light scattering. If particles are too large or too closely spaced, little diffraction occurs. Conversely, if the pigment particles are too small, the light will not "see" the particles. Commercially processed rutile TiO_2 has particle diameters ranging from about 200 to 300 nm and is highly reflective in the visible spectrum (yellow-green light at about 550 nm). However, as the wavelength of light increases, the reflectance of TiO_2 drops in the infrared spectrum especially for wavelengths beyond 1250 nm.

Figure 2. Light Diffraction as a Light Ray Travels near a Pigment Particle

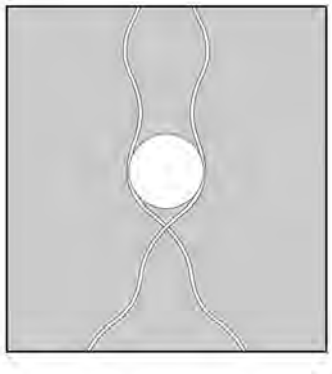

The "Optical" Properties of Pigments

Pigments are typically thought of in terms of their "color", that is, their reflectance spectrum in the 400 to 700 nm range. The performance of pigments, however, actually covers a much broader spectral region from the ultraviolet through the near infrared and beyond. A pigment interacts with electromagnetic radiation by either absorbing it, or scattering it as mathematically described by the Kubelka-Munk formalism. The equation relating the pigments absorption (K) and scattering (S) properties to the reflectance (ρ) of an infinitly thick sample is given by:

$$\frac{K}{S} = \frac{(1-\rho)^2}{2\rho} \qquad \textbf{(1)}$$

The pigment industry uses the Kubelka-Munk equation to parameterize the reflectance (ρ) of a pigment by the two wavelength dependent parameters, the pigments absorption coefficient (K) and its scattering coefficient (S), Billmeyer and Saltzman (2000). Laboratories and local paint and hardware stores custom match paints and coatings using Eq. 1 by color matching the mixture of pigments needed to match a target reflectance. The interaction of the absorption and scattering components of a pigment is of paramount importance to the response of the pigment to electromagnetic radiation, especially in wavelengths beyond the visible. And the engineering of pigment properties beyond the visible is well known to those involved with "radiation signature tailoring", which is becoming increasingly important in both military and domestic applications.

Scattering

The scattering characteristics of a pigment particle in a medium can be calculated using Mie Scattering Theory, Bohren and Huffman (1983). Figure 3

contains a curve of the scattering cross section of a TiO_2 particle, index of refraction equal 2.7, versus particle size, in a medium of index of refraction of 1.5, calculated for a wavelength of 550 nm. The human eye sensitivity peaks at about 550 nm. According to this graph, the maximum scattering of a TiO_2 particle for a wavelength of 550 nm occurs in a particle size range of about 200 to 300 nm, which is the particle size range of commercial white TiO_2 pigments. TiO_2 pigments in this size range scatter, that is, reflect, 550 nm electromagnetic radiation most efficiently and therefore yield optimum opacity at this wavelength. Particles of TiO_2 below about 50 nm in size do not scatter 550 nm electromagnetic radiation at all; in fact, the particles are transparent. TiO_2 pigment in the 50 nm particle size range is used in the topcoat of automobile finishes to increase the effective index of refraction of the topcoat making it look thicker.

Figure 3. Mie Scattering Cross-section of TiO_2, having an index of refraction of 2.7, in a media of index 1.5 for wavelengths of a) 550 nm and b) 1500 nm. [1000 nm = 1 μm]

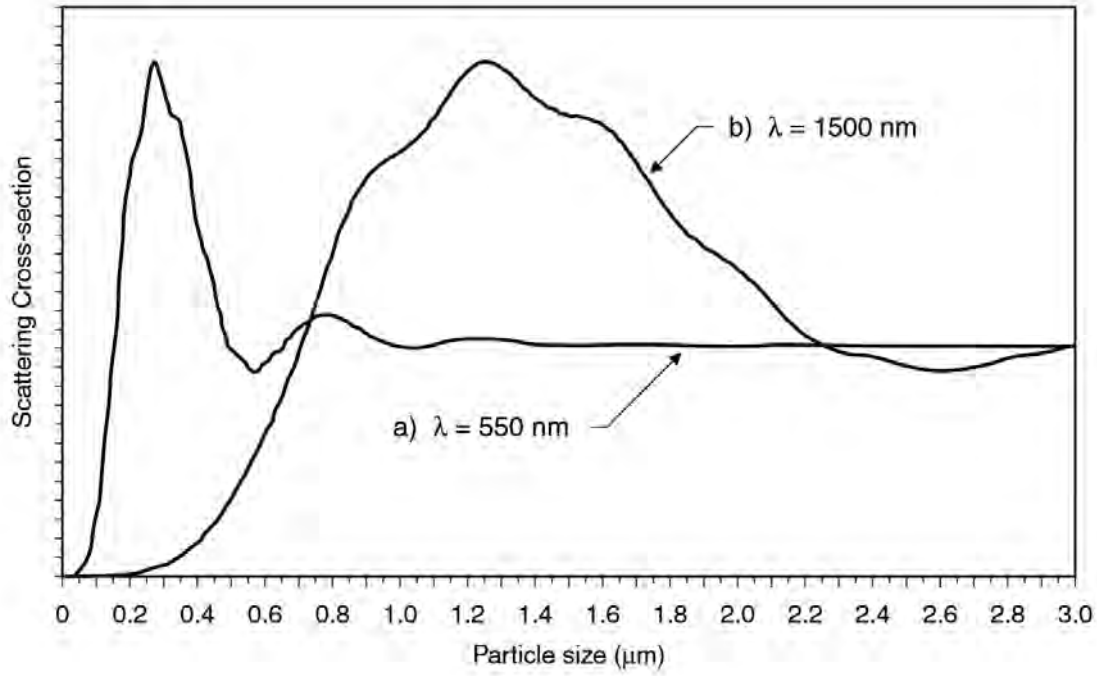

Figure 3 contains a second curve of the same scattering cross section claculation of a TiO_2 particle at a wavelength of 1500 nm. For this wavelength the maximum scattering occurs at a particle size of about 1200 nm, and the particle becomes transparent at about 200 nm, that is, just about the size for maximum scattering of 550 nm electromagnetic radiation. The distribution of infrared radiation from a wood fire peaks at about 1500 nm, Berdahl (1998). If you wanted a coated surface that would reflect the infrared from a fire and protect the underlying surface, you would not use a standard white TiO_2 pigment. Although this pigment is very white in the visible, it is effectively transparent to the infrared of a wood fire. Thus, whether a pigment particle scatters electromagnetic radiation at a given wavelength, or is transparent at that wavelength, depends primarily on its size.

Absorption

The absorption of a pigment throughout the entire electromagnetic spectra is sensitive to the pigments chemical composition, to the valence state of its constituents, and to the arrangement of the atoms in the crystal structure of the pigment. Human eyes are sensitivity to electromagnetic radiation in the wavelength range from 400 to 700 nm, and the absorption of a pigment in this range gives it the “color” we see. As example, the “white color” property of TiO_2, used in porcelain enamel coatings for microwave ovens, is effectively “white” only in the visible spectrum (Fig. 4).

Figure 4. Reflectance versus wavelength curves for a) a typical white porecelain enamel surface and b) a high infrared reflecting porcelain enamel surface.

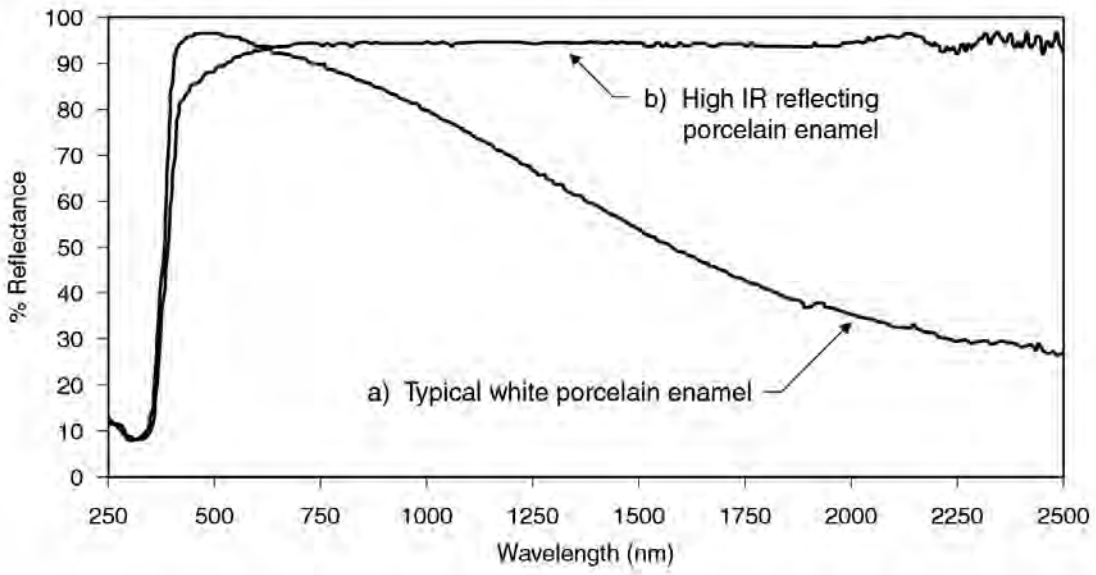

The first microwave ovens cooked food that was not as appealing as food cooked in a standard convection oven. A source of infrared radiation was needed to improve the browning of food and to quicken cooking time. The standard “white” porcelain enamel surface absorbs electromagnetic radiation for $\lambda \geq 1000$ nm, that is, it will get hot (Fig. 4). Porcelain enamel is a glass coating that is manufactured by smelting titantia and grinding the subsequent glass into a fine powder, known as a frit. Firing is done to melt the glass frit into a smooth layer. During the firing process, the TiO_2 precipitates out of the enamel, giving the enamel its bright white color. The enamel contains iron contaminants, and if the valence charge of the iron ions is Fe^{2+} the enamel will strongly absorb infrared radiation (Fig. 4). To improve microwave cooking, researchers added an oxidizing agent to increase the valence of iron ions to Fe^{3+} or Fe^{4+}, which does not absorb infrared radiation, Faust and Evele (1999). Figure 4 contains the reflectance curve for an “infrared reflecting” porcelain enamel surface. The improved porcelain enamel coating is effectively "white" in the visible and also in the near infrared spectral regimes (Fig. 4). Therefore, chemistry can be used to alter the absorption and therefore the reflectance of a pigment. By blending metal oxides or oxide precursors and calcining them, the solids themselves become reactive.

Metal and oxygen ions in the solids rearrange to a form a new, more stable structure, termed a complex inorganic color pigment that is ideal for high-temperature coatings.

Infrared Reflecting Complex Inorganic Color Pigments (CICPs)

The characteristics of CICPs being marketed as “infrared reflecting” are controlled over the range of wavelengths from 300 to 2500 nm. In order to control the optical properties of a pigment over this wide of a wavelength range requires great care in all aspects of the manufacturing process starting with the selection of raw materials and going all of the way through to the milling and finishing of the pigment, Sliwinski, Pipoly and Blonski (2001).

For years the vinyl siding industry has formulated different colors in the same polyvinyl chloride base by altering the content of TiO_2 and black IR-reflective (IRR) paint pigments to produce “dark” siding that is “cool” in temperature (Ravinovitch and Summers 1984). Researchers discovered that a dark color is not necessarily dark in the infrared. Brady and Wake (1992) found that 1-μm particles of TiO_2 when combined with red iron, or ferric, oxide effectively scattered IR radiation at a wavelength of 2300 nm.

The new CICPs are used in paints for military camouflage to match the reflectance of background foliage in the visible and IR spectrum. At 750 nm the chlorophyll in foliage naturally boosts the reflectance of a plant leaf from 0.1 to about 0.9 (Fig. 5), which explains why a dark green leaf remains cool on a hot summer day.[2]

Figure 5. Spectral Solar Reflectance of TiO_2, a Green Leaf, Standard Carbon Black and a Complex Inorganic Color Pigment Containing Infrared Reflective $(Fe,Cr)_2O_3$ Pigment (Normalized Solar Irradiance Shown for Reference)

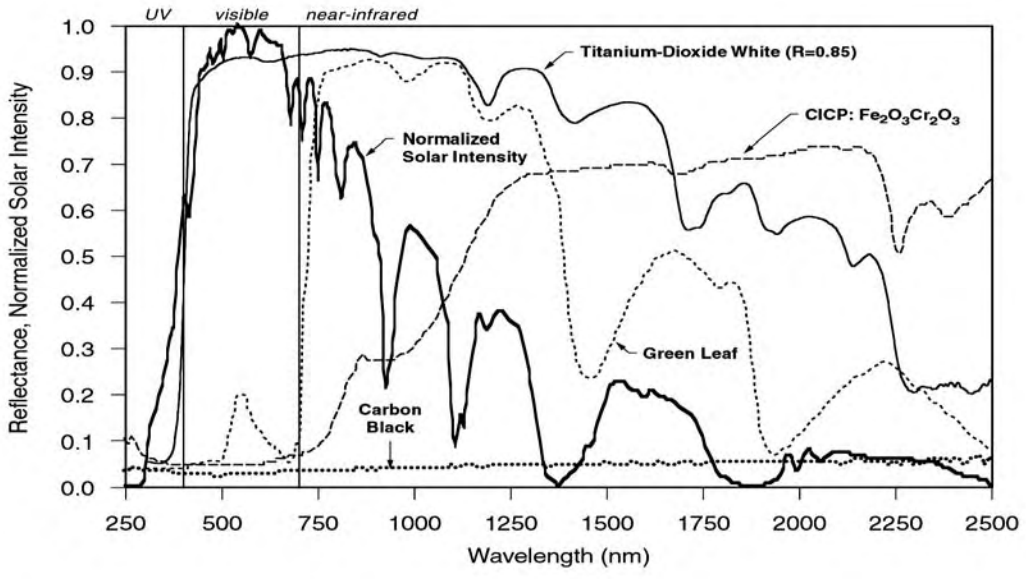

[2]Chlorophyll, the photosynthetic coloring material in plants, naturally reflects near-IR radiation.

CICPs, having been tailored for high IR reflectance similar to that of chlorophyll, are very suitable for roof applications where increased IR reflectance is desirable. CICPs consisting of a mixture of black IRR pigments, chromic oxide (Cr_2O_3) and ferric oxide (Fe_2O_3) boosts the total hemispherical reflectance of carbon black from 0.05 to 0.26 (see CICP:Fe_2O_3·Cr_2O_3 in Fig. 5). Typically, a black asphalt shingle or a black Kynar®[3] metal roof has a reflectance of only about 0.05. The CICPs therefore boosts the reflectance by a factor of 5, and in the infrared spectrum CICPs boost the reflectance to almost 0.70 (Fig. 5).

CICPs are formed by calcinating blends of metal oxides or oxide precursors at temperatures over 1600°F (870°C). The calcination causes the metal and oxygen ions in the solids to rearrange in a new structure that is very heat-stable. The inherent heat stability of CICPs makes them ideal for high-temperature coatings in roofing applications. Because of their small particle size and high index of refraction, CICPs will effectively backscatter a significant amount of ultraviolet (UV) and IR light away from a surface.

Thermal Performance of CICPs

CICPs offer excellent opportunities for improving the thermal performance of roofs. About 44% of the sun's total energy is visible to the eye (Fig. 5). Absorbing this 44% is what makes a black appear black. The absorbed light energy is however converted to heat energy and the temperature of the surface rises. Sunlight also emits another 51% of its energy in the invisible IR spectrum. Adding CICPs to roof materials will make the black roof absorb less light by reflecting near IR energy, which in turn results in a lower roof surface temperature.

Temperature measurements taken on a highly reflective roof show the surface as only about 5°F (3°C) warmer than the ambient air temperature, while a dark absorptive roof exceeds the ambient air temperature by more than 75°F (40°C). Lowering the exterior roof temperature will reduce the heat leakage into the building, which in turn, reduces the air conditioning load.

Light-Color CICPs

The authors tested several IRR pigments against standard pigments using the ASTM D4803 test procedure (ASTM 1997a). This procedure has long been used by the vinyl siding industry to quantify the heat buildup properties of vinyl siding, even though it overstates the sample's properties in the near IR at the expense of visible portion of the spectrum (Ravinovitch and Summers 1984). Table 1 shows the temperatures for both CICPs and standard light-gray, mid-tone bronze, and dark-tone bronze colors when exposed to a flux of 484 Btu/(hr·ft^2) [550 J/(hr·cm^2)] emitted from an infrared heat lamp. These colors are very popular for low-slope roofing in commercial and academic applications where bronze Kynar® metal roofing is commonly used.

The colors containing CICPs show a significant drop in temperature as compared to the temperatures of standard light-gray, mid-tone bronze, and dark bronze colors. The temperature is 55°F (30.5°C) cooler for the light gray color if

[3]Kynar, the registered trademark for polyvinylidene fluoride (PVDF) paint finish, has excellent corrosion and abrasion resistance.

CICPs are contained in the pigment mixture. Similarly, a mid-tone bronze showed a 63°F (35°C) reduction in surface temperature. Even the dark-tone bronze had a measured 54°F (30°C) drop in temperature because the IRR pigments absorb less electromagnetic energy near the cutoff between the visible and infrared wavelengths. They have a more selective absorption band and reflect much of the infrared.

Table 1. CICP Color Matches vs. Standard Pigmentation Exposed to ASTM D4803 Heat Lamp Protocol [a]

Pigment	Pigment Constituents		Maximum Temperature	Temperature Difference (ΔT)
Light gray				
Standard	Carbon black TiO_2 Fe_2O_3	1.5% 96.8% 1.7%	202°F (94.4°C)	
CICP	IRR black TiO_2	10% 90%	147°F (63.9°C)	55°F (30.5°C)
Mid-tone bronze				
Standard	Carbon black TiO_2 Fe_2O_3	11.8% 75.0% 13.2%	225°F (107.2°C)	
CICP	IRR black TiO_2	50% 50%	162°F (72.2°C)	63°F (35°C)
Dark-tone bronze				
Standard	Carbon black TiO_2 Fe_2O_3	33% 29% 38%	220°F (104.4°C)	
CICP	IRR black TiO_2	90% 10%	166°F (74.4°C)	54°F (30°C)

[a] A flux of 484 Btu/(hr·ft^2) [550 J/(hr·cm^2)] emitted from an infrared heat lamp.

Dark-Color CICPs

We also exposed dark colors containing the IRR pigments to the infrared heat lamp. Again, the increased reflectance in the near-IR spectrum (Fig. 6) significantly reduced the surface temperature as compared to carbon black. An IRR green was a measured 54°F (30°C) cooler than carbon black, an IRR dark brown was ~48.6°F (27°C) cooler, and an IRR black was a measured 46.8°F (26°C) cooler.

For our test site at Oak Ridge National Laboratory (ORNL), Oak Ridge, Tennessee, the maximum irradiance from the sun, at solar noon, is about 308 Btu/(hr·ft^2) [350 J/(hr·cm^2)]. ASTM procedure D4803 (ASTM 1997a) relates the intensity of solar irradiance to the intensity derived from the infrared lamp via a ratio of the temperature rises above the ambient air temperature (i.e., the ΔT for IRR black to the ΔT for standard carbon black, see the right side of Eq. 2) to predict the specimen's solar temperature rise by:

$$\left[\frac{\Delta T_{\text{IRR Black}}}{\Delta T_{\text{black Kynar}}}\right]_{\text{solar}} = \left[\frac{\Delta T_{\text{IRR Black}}}{\Delta T_{\text{black Kynar}}}\right]_{\text{ASTM D4803}} \quad \textbf{(2)}$$

where

$\Delta T_{IRR\ Black}$ = "predicted" temperature rise above the ambient air temperature for IRR black when exposed to solar irradiance

$\Delta T_{\ black\ Kynar}$ = "experimentally measured" temperature rise above the air temperature for a black Kynar® (~40°C above ambient as field-tested at ORNL)

Figure 6. Heat Buildup of High-IRR Pigments vs. Standard Carbon Black and Reflectance of IRR Black vs. Standard Carbon Black

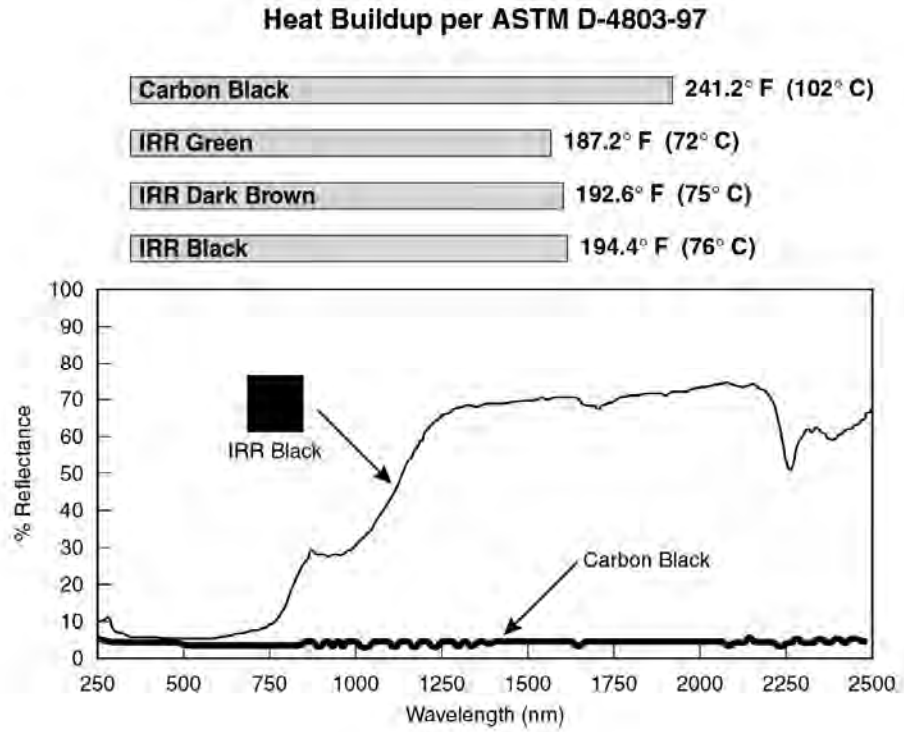

Based on Equation (2) and summertime field data for a black Kynar® metal roof tested by Miller and Kriner (2001), the IRR black sample would be about 25°F (14°C) cooler at solar noon than a conventional dark roof.

Durability and Weathering of CICPs

Testing protocols to determine the resistance to weathering of paints and coating systems designed for outdoor use include both natural, real-time weathering, such as outdoor exposure in Florida or Arizona, and accelerated tests using a weatherometer equipped with carbon-arc, fluorescent UV, and xenon-arc light sources. To evaluate color changes in roof samples with CICPs as compared to samples with standard colors, we used a two-year exposure test to natural sunlight in Florida and also a 5000-hour xenon-arc accelerated exposure test, following ASTM G-155 (ASTM 2000). Test data showed excellent light fastness for all the CICPs. Pigment stability and discoloration resistance were judged using a total color difference measure (ΔE) as specified by ASTM D 2244-

93 (ASTM 1993). The ΔE value for all the colors tested was a color change of approximately 1.0 or less (Figs. 7 and 8).

The total color difference value, ΔE, is a method adopted by the paint industry to numerically identify variability in color over periods of time. This value shows the difference in color between a standard and a batch and includes the three following values computed in the formula:

- lightness (*L*), where a +*L* value is lighter and a –*L* value is darker;
- redness/greenness (*a*), where a +*a* value is redder and a –*a* value is greener; and
- yellowness/blueness (*b*) where a +*b* value is yellower and a –*b* value is bluer.

$$\Delta E = \left[(\Delta L)^2 + (\Delta a)^2 + (\Delta b)^2\right]^{1/2}, \quad \textbf{(3)}$$

where

$\Delta L = L_{batch} - L_{standard}$
$\Delta a = a_{batch} - a_{standard}$
$\Delta b = b_{batch} - b_{standard}$

Typically, coil-coated metal roofing panels are warranted for 20 years or more and specify a ΔE of 5 units or less for that period. ΔE color changes of 1 unit or less are almost indistinguishable from the original color, and depending on the hue of color, ΔE of 5 or less is considered very good.

Figure 7. Total Color Difference (ΔE) Values for Color Samples in Xenon-Arc Accelerated Weathering Test

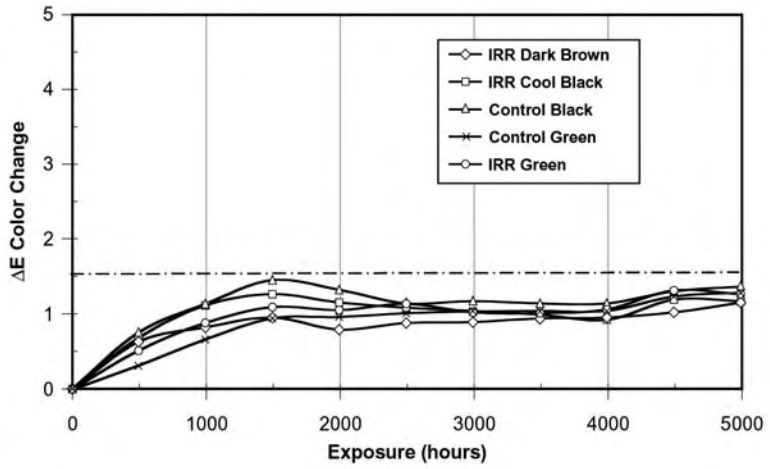

The xenon-arc accelerated weathering initially saw most of the colors rise in ΔE up to about 1500 hours of exposure and then level off; at the end of 5000 hours all are clustered together at less than 1.5 ΔE, which is considered excellent results (Fig. 7). Control products with known performance characteristics were included in the testing to compare results with the new products.

The Florida exposure data in Figure 8 are just as promising, indicating that over the two-year test period the CICPs do not fade in the presence of ozone,

acid rain, SO_x, NO_x, or other airborne pollutants. Tests have shown that CICPs remain colorfast in the presence of strong acids, bases, and oxidizing or reducing agents. They are non-migratory and showed no dissolving or bleeding in contact with airborne solvents. Most important, CICPs retain their color when mixed with TiO_2 to produce light pastel shades which possess improved lightfast characteristics as compared to previously tried and proven standard colors.

Figure 8. Total Color Difference (ΔE) Values for Color Samples in One-Year Florida Weathering Test

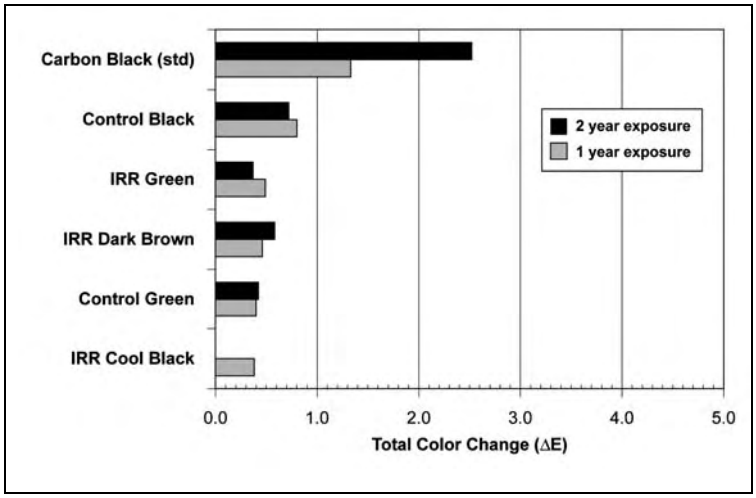

Conclusions

Accelerated weather testing using natural sunlight and xenon-arc weatherometer exposure proved that CICPs retain their color. After two years of natural sunlight exposure in south Florida the CICPs show excellent fade-resistance and remain colorfast. CICPs are very stable pigments and have excellent discoloration resistance, as also proven by the 5000 hours of xenon-arc exposure; their measure of total color difference was a ΔE value less than 1.5. Therefore, color changes in the CICPs were indistinguishable from their original color.

CICPs have a selective light absorption band in the infrared spectrum. They reflect much of the near-IR heat and therefore reduce the surface temperature upwards of 50°F (28°C) as compared to carbon black pigments when exposed to irradiance from an infrared lamp. For a steep-slope roof in the field, an IRR black would be about 25°F (14°C) cooler at solar noon than would a conventional dark roof. The lower exterior temperature leads to energy savings and provides an ancillary benefit in older existing houses with little or no attic insulation and poorly insulated ducts in the attic because the cooler attic temperature in turn leads to reduced heat gains to the air-conditioning ductwork.

References

American Society for Testing and Materials (ASTM). 1993. *Designation D2244-93: Standard Test Method for Calculation of Color Differences from*

Instrumentally Measured Color. West Conshohocken, Pa.: American Society for Testing and Materials.

———. 1997a. *Designation D4803-97: Heat Build-Up Apparatus Standard Test Procedure*. West Conshohocken, Pa.: American Society for Testing and Materials.

———. 2000. *Designation G155-00a: Standard Practice for Arc Operating Xenon Arc Light Apparatus for Exposure on Non-metallic Materials*. West Conshohocken, Pa.: American Society for Testing and Materials.

Brady, R. F., and L. V. Wake. 1992. “Principles and Formulations for Organic Coatings with Tailored Infrared Properties.” *Progress in Organic Coatings* 20:1–25.

Du Pont Ti-Pure. 1999. *Titanium Dioxide for Plastics*. Wilmington, Del.: Du Pont Corporation.

Good, C. 2001. “Eyeing the Industry: NRCA’s Annual Market Survey Provides Interesting Industry Analyses.” In *NRCA 2000–2001 Annual Market Survey,* 116–20. Rosemont, Ill.: National Roofing Contractors Association.

Martin, P., and H. L. Pezzuto. 1998. “Pigments Which Reflect Infrared Radiation from Fire.” U.S. Patent 5,811,180, September 22.

Miller, W. A., and S. Kriner. 2001. “The Thermal Performance of Painted and Unpainted Structural Standing Seam Metal Roofing Systems Exposed to One Year of Weathering.” In *Thermal Performance of the Exterior Envelopes of Buildings, VIII: Proceedings of ASHRAE THERM VIII.* Clearwater, Fla.: American Society of Heating, Refrigerating, and Air-Conditioning Engineers, Dec. 2–7.

Ravinovitch, E. B., and J. W. Summers. 1984. “Infrared Reflecting Vinyl Polymer Compositions.” U.S. Patent 4,424,292. January 3.

Sliwinski, T. R., R. A. Pipoly, and R. P. Blonski. 2001. “Infrared Reflective Color Pigment.” U.S. Patent 6,174,360, January 16.

Billmeyer and Saltzman's Principles of Color Technology, 3rd Edition , R.S. Berns, John Wiley, New York, 2000

Absorption and Scattering of Light by Small Particles , C.F. Bohren, D.R. Huffman, John Wiley, New York, 1983

“Pigments Which Reflect Infrared Radiation from Fire”, P.H. Berdahl, US Patent 5,811,180, issued September 22, 1998

“Reflective Porcelain Enamel Coating Compositions”, W.D. Faust, H.F. Evele, US Patent 6,004,894, issued December 21, 1999

“Infrared Reflecting Colored Pigment”, T.R. Sliwinski, R.A. Pipoly, R.P. Blonski, US Patents 6,174,360, issued 1/16/2001 and 6,454,848, issued 9/24/2002

Cool Colors

A Roofing Study is Developing Cool Products for Residential Roofs

By Hashem Akbari, Paul Berdahl, Andre Desjarlais, Nancy Jenkins, Ronnen Levinson, William Miller, Arthur Rosenfeld, Chris Scruton and Stephen Wiel

Raising the solar reflectance of a residential roof from a typical value of 0.1 or 0.2 to an achievable 0.5 can reduce cooling-nergy use in buildings by more than 15 percent. nergy savings are particularly pronounced in lder houses with minimal attic insulation, espe-ially if the attic contains air distribution ducts.

Research conducted by Lawrence Berkeley lational Laboratory (LBNL), Berkeley, Calif., esti-ıates U.S. potential energy savings in excess of 750 million per year in net annual residential ıd commercial energy bills (cooling-energy sav-gs minus heating-energy penalties) simply by stalling "cool roofs"—that is, roofs that reflect a rge fraction of incident sunlight. Cool roofs also gnificantly reduce peak electric demand in sum-er. Although preliminary analysis suggests there ay be a surcharge of up to $1 per square meter r cool roofing materials, this represents only 2 ercent to 5 percent of the cost of installing a new sidential roof.

The widespread installation of cool roofs can wer the ambient air temperature in a neighbor-od or city, further decreasing the need for air nditioning. Lower ambient air temperatures ard smog formation, increase environmental mfort and improve human health. Lower surface mperatures also may increase the lifetime of roofing products (particularly asphalt shingles), reducing replacement and disposal costs. The collective benefits resulting from reduced ambient air temperature have roughly the same economic value as that of the energy savings achieved by reducing building heat gain through the roof

The California Energy Commission, Sacramento, Calif., has engaged LBNL and Oak Ridge National Laboratory (ORNL), Oak Ridge, Tenn., in a three-year project to work with the roofing industry to develop and produce colored roofing products with high solar reflectance and encourage the home-building industry to use these products. LBNL and ORNL's goal is to make nonwhite cool roofing materials commercially available within three to five years. About two years into the study, researchers already have interesting findings to report.

Nonwhite Cool Roofing Materials

Cool white materials are available for most roofing products with the notable exception of asphalt shingles. Cool nonwhite materials are needed for all types of roofing. Industry researchers have developed durable complex inorganic color pigments that are highly reflective to "near-infrared" (NIR) solar radiation. This invisible spectrum contains more than 50 percent of the power in sunlight. The high NIR reflectance of coatings formulated with complex inorganic and other "cool" pigments—chromium oxide green, cobalt blue, phthalocyanine blue, Hansa yellow—can be exploited to manufacture colored roofing materials that reflect more sunlight than do conventionally pigmented roofing products.

Specifically, LBNL and ORNL aim to produce nonwhite shingles with solar reflectances not less than 0.3 and other types of nonwhite roofing products (tiles) with solar reflectances not less than 0.45. The reflectance goal for shingles is lower than that for other products because the roughness of a shingle's surface reduces its reflectance and because manufacturing constraints typically limit the reflectance of coatings applied to granules.

Research activities are designed to address the following five topics:

Formulation of Cool-colored Coatings: How can the total solar reflectance of a pigmented coating be maximized while matching a desired color?

Development of Cool-colored Roofing Prototypes: What is the relationship between the optical properties of a simple pigmented coating and those of a pigmented coating applied to roofing materials (granules, tiles)?

Durability of Cool-colored Coatings: How do ɔol-colored coatings weather and age?

Longevity of Cool-colored Roofing Materials: oes higher solar reflectance increase the lifetime : cool-colored roofing materials?

Demonstration of Energy Savings: What is the ıilding-energy savings yielded by use of cool-ılored roofing materials?

ormulation of Cool-olored Coatings

maximize the solar reflectance of a pigmented ating matching a particular color, LBNL has aracterized the optical properties of more than)0 common and specialty pigments and is devel-ıing a computer model for design of lor-matched cool pigmented coatings.

Each pigment initially is characterized by the ɔlar spectral" reflectance and transmittance of a ɜmented coating (a free film of paint), measured 5-nanometer (nm) intervals across the solar ɛctrum (300 to 2,500 nm). Solar spectral sorptance (1-reflectance-transmittance) is an ɛellent indicator of whether a pigment is cool ıs low NIR absorptance) or hot (has high NIR sorptance). (See Figure 1a.)

The measured reflectance and transmittance ɜ used to compute solar spectral absorption and ɛkscattering coefficients, which indicate in the ɔular "Kubelka-Munk" (K-M) light-flux theory rates at which pigment particles absorb and ɛkscatter light in a pigmented coating. (See ure 1b.) Finally, the film reflectances over black d white backgrounds predicted by the K-M the-are compared with measured reflectances to ɛk the validity of the computed absorption and ɛkscattering coefficients. (See Figure 1c.)

Cool nonwhite pigments must have absorption fficients that are large in parts of the visible ctrum (to produce the desired color) and small he NIR spectrum (to minimize absorption of sible solar radiation). The backscattering coef-ɜnt of a cool pigment ideally should be large in NIR to maximize reflectance in that spectrum, ıgh weak NIR backscattering is acceptable if coating has an NIR-reflective background.

LBNL has developed a preliminary database marizing characterizations of about 100 pig-ıts and have shared this database with ıstrial partners to help them develop cool-colored coatings and roofing products.

The researchers also are developing a model that estimates the solar spectral reflectance of coatings from pigment properties, including absorption and backscattering coefficients; coating composition, such as pigments, vehicle and filler; and coating geometry, including thickness, roughness and background. This model will be implemented in software that suggests recipes to maximize the solar reflectance of a colored coating. The software will be available to pigment, coating and roofing manufacturers.

Development of Cool-colored Roofing Prototypes

Researchers at LBNL and ORNL estimate that roofing shingles, tiles and metal panels comprise more

Characterization of a Near-infrared-reflecting Cool Black Pigment

(About 25-micron- [1-mil-] thick film of chromium green-black hematite modified in clear binder of refractive index 1.5; 7 percent pigment volume concentration)

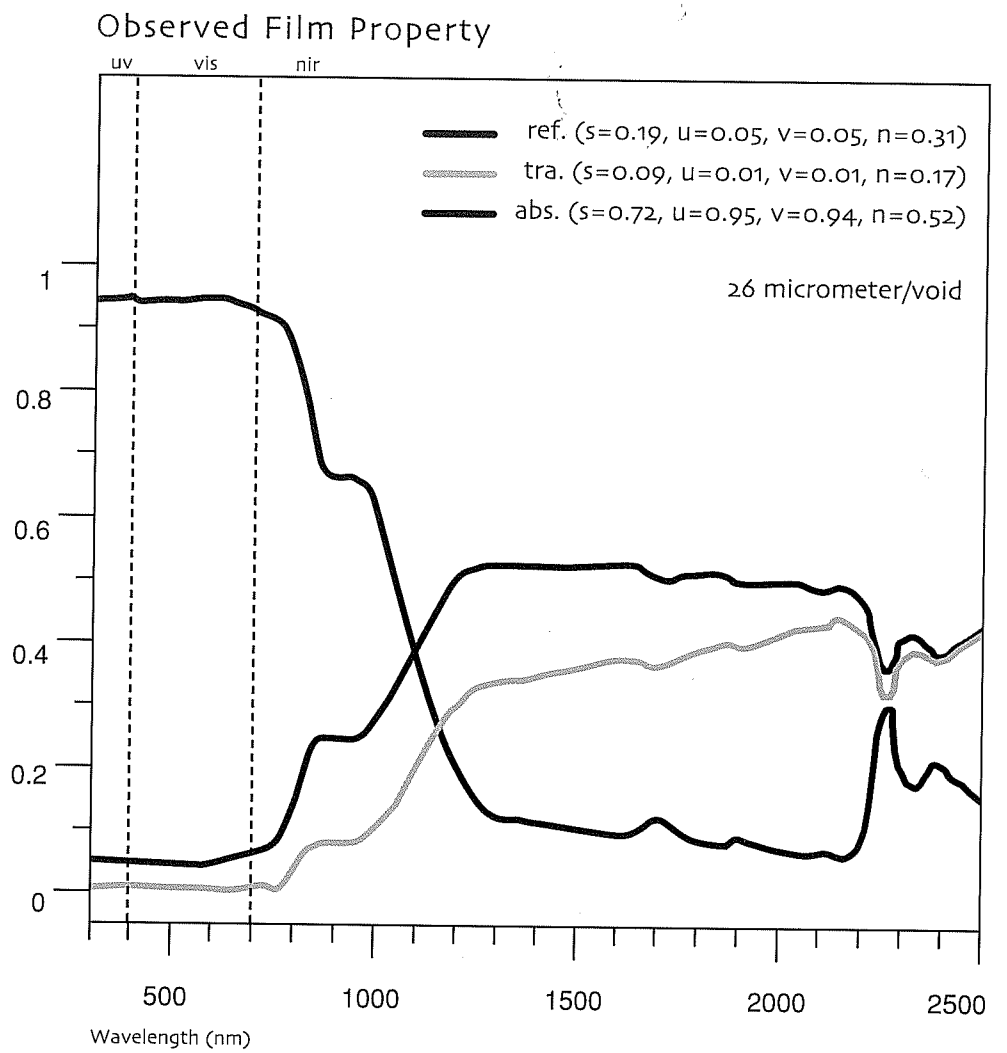

Figure 1a: Measured reflectance, measured transmittance and computed absorptance of a free film. Parenthetical values are irradiance-weighted averages over the solar (s), ultraviolet (u), visible (v) and near-infrared (n) spectra.

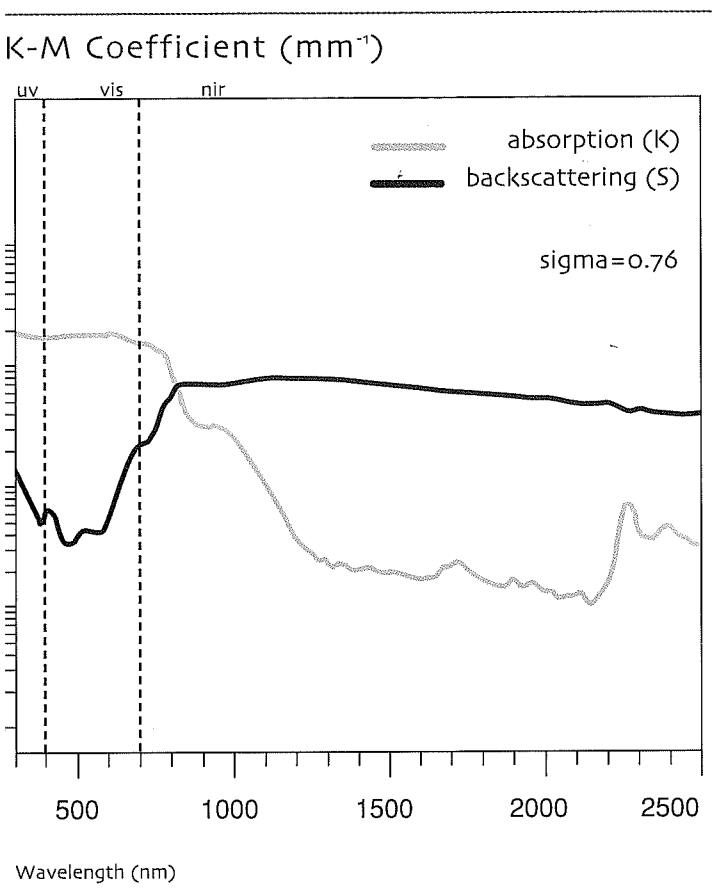

Figure 1b: "Kubelka-Munk" (K-M) absorption coefficient K and backscattering coefficient S

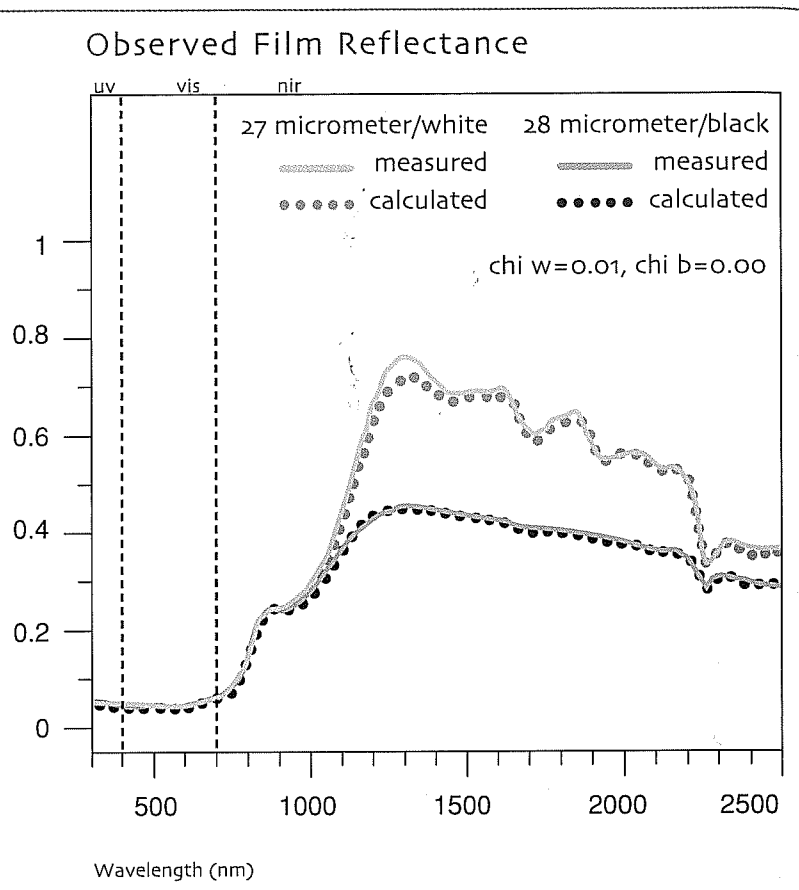

Figure 1c: Comparison of measured reflectances of the film over opaque white and opaque black backgrounds with values calculated from computed absorption and backscattering coefficients

80 percent (by roof area) of the residential ng market in the western United States. The archers interviewed manufacturers of asphalt gles, concrete and clay tiles, and metal panels otain information about the processes used to their products. Patent and other literature it the fabrication and coloration of roofing rials, especially asphalt roofing shingles, also been reviewed.

ngles

olar reflectance of a new shingle is dominated ne solar reflectance of its granules because—lesign—the shingle's surface is well covered granules. Until recently, the way to produce ules with high solar reflectance has been to itanium dioxide (TiO_2) rutile, a white pigment. use a thin layer of TiO_2 is reflective but not opaque, multiple layers are needed to attain the desired solar reflectance. This technique has been used to produce "super-white" (meaning truly white, rather than gray) granulated shingles with solar reflectances exceeding 0.5.

Manufacturers also have tried to produce colored granules with high solar reflectance by using nonwhite pigments with high NIR reflectance. However, similar to TiO_2, cool-colored pigments are partly transparent to NIR light. Thus, any NIR light not reflected by the cool pigment is transmitted to the (typically dark) granule underneath, where it can be absorbed. To increase the solar reflectance of granules colored with cool pigments, multiple color layers, a reflective undercoating and/or reflective aggregate should be used. Obviously, each additional coating increases production cost.

The application of pigmented coatings to roofing granules appears to be the critical process step. Several layers of silicate coatings can be involved and may include not just one or more pigments but the use of clay additives to control viscosity, biocides to prevent staining and process chemistry controls to avoid residual dust on the product.

One way to reduce the cost is to produce cool-colored granules via a two-step, two-layer process. In the first step, the granule is precoated with an inexpensive pigment, such as TiO_2, that is highly reflective to NIR light. In the second step, the cool-colored pigment is applied to the precoated granules.

Tiles

There are three ways to improve the solar reflectance of colored tiles: use clay or concrete with low concentrations of light-absorbing impurities, such as iron oxides and elemental carbon;

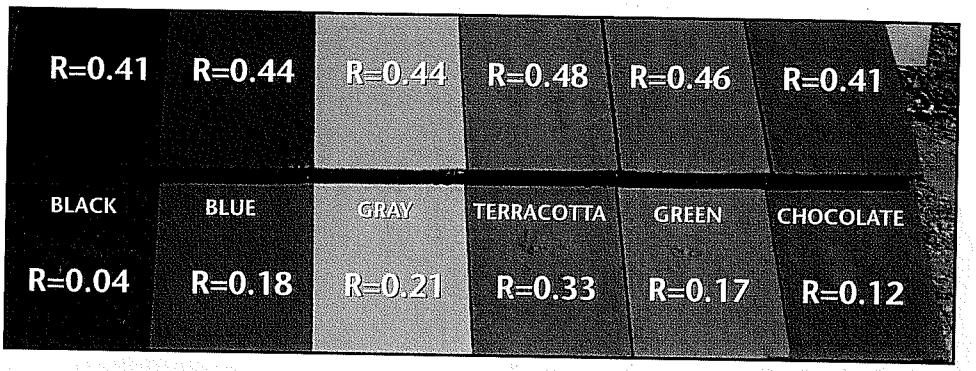

Figure 3: Cool coatings developed for concrete roof tiles. The upper row shows six cool-colored coatings, each with solar reflectance R exceeding 0.4, which match conventionally pigmented coatings in the lower row.

Photo courtesy of American Rooftile Coatings, Fullerton, Calif.

olor the tile with cool pigments contained in a urface coating or mixed integrally; and/or clude an NIR-reflective underlayer, such as hite, beneath an NIR-transmitting colored top- oat. Although these options are in principle easy implement, they may require changes in current oduction techniques that could add to the cost of ished products.

Metal Panels

corporation of cool-colored pigments in metal ofing products may require the fewest number of anges to existing production processes. Cool gments can be applied to metal via a single- or uble-layered technique; if the raw metal is high- reflective, a single-layered technique may fice. The coatings for metal shingles are thin, rable polymer materials. These thin layers use terials efficiently but limit the maximum amount pigment present. The metal substrate can pro- e significant NIR reflectance if the coating is nsparent in the NIR.

Wood Shakes

the near future, LBNL and ORNL will survey thods of manufacturing wood shakes.

ample Prototypes

NL and ORNL have collaborated with 14 com- nies that manufacture roofing materials, uding shingles, roofing granules, clay tiles, crete tiles, tile coatings, metal panels, metal tings and pigments. The development work been iterative and included selection of cool ments, choice of base coats for the two-layer lications and identification of pigments void.

ol Black Shingle

re 2 shows the iterative development of a cool

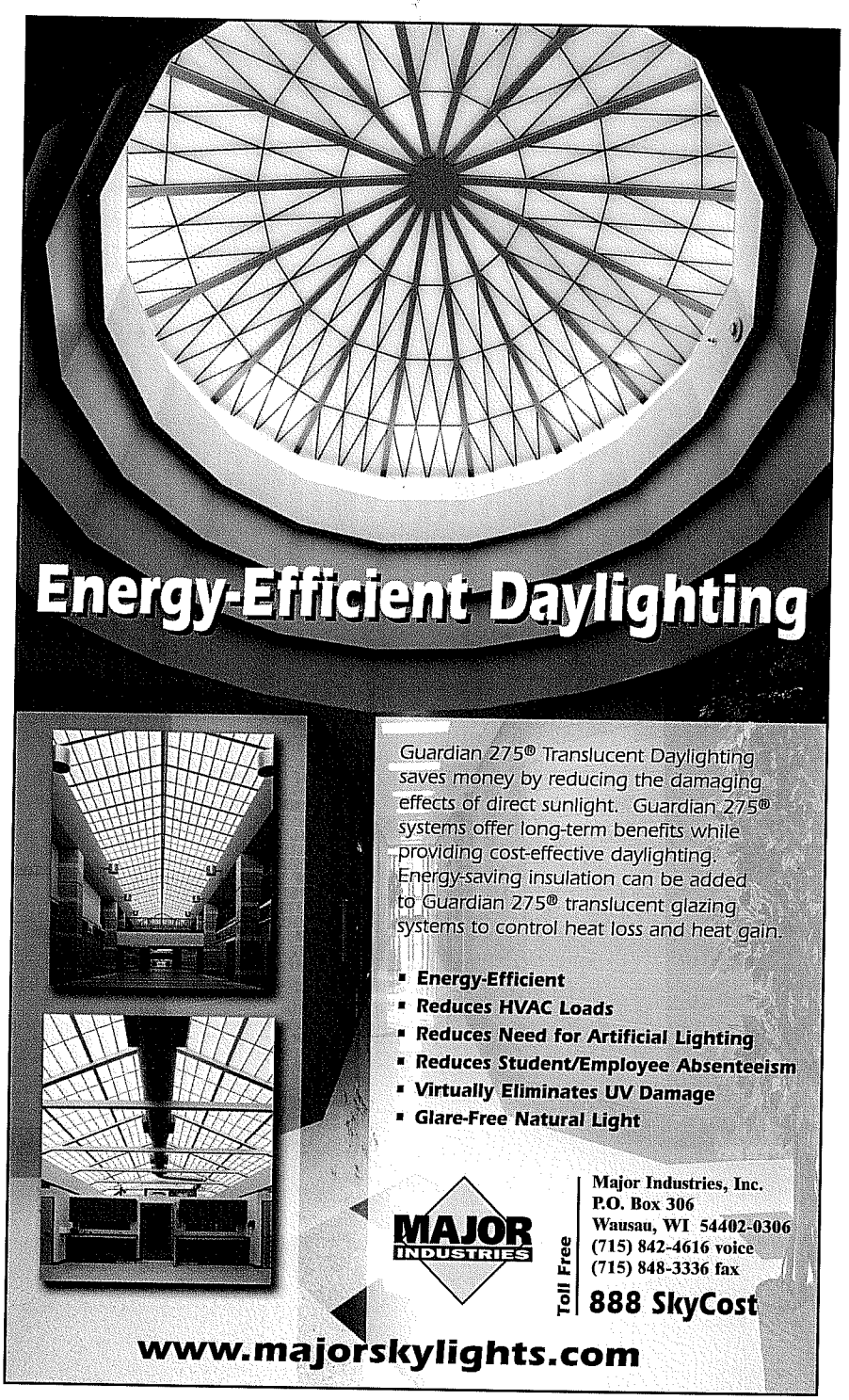

CIRCLE NO. 20

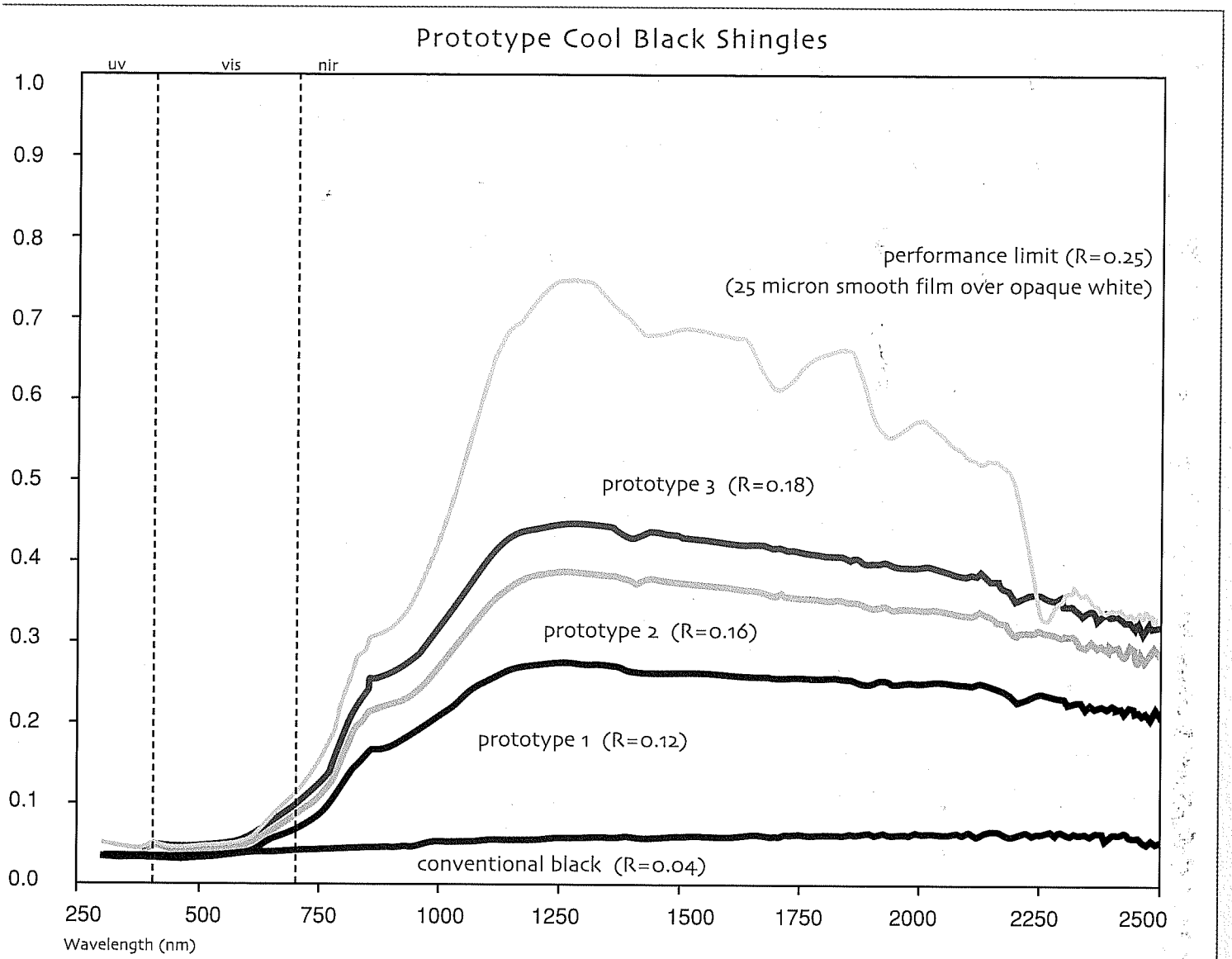

Figure 2: Development of a cool black shingle, showing effects of incorporating cool pigments and adding near-infrared reflecting underlayers

black shingle. A conventional black roof shingle has a reflectance of about 0.04. The researchers initially replaced the granule's standard black pigment with an NIR-reflecting black, increasing the solar reflectance of the shingle to 0.12. Next, an NIR-transmitting black was applied over a thin TiO_2 white underlayer, increasing the shingle's solar reflectance to 0.16. Finally, the thickness of the white underlayer was increased, raising the shingle's reflectance to 0.18. Figure 2 also shows an approximate performance limit (reflectance 0.25), which was obtained when a 25-micron- (about 1-mil-) thick NIR-reflective black topcoat is applied over an opaque white background.

Cool Concrete Tiles

Figure 3 shows the results of similar efforts to develop coatings for concrete tile roofs, which yielded a palette of cool colors each with solar reflectance exceeding 0.4.

Durability of Cool-colored Coatings

Samples of several roofing product styles and colors have been placed in seven of California's 16 climate zones for exposure studies. Solar reflectance and thermal emittance are measured twice per year, and weather data are available continuously. Solar spectral reflectance is measured annually to gauge soiling and document color changes too small to perceive.

LBNL and ORNL also will examine the roof samples for contaminants and biomass. The surface composition studies will identify the drivers affecting the soiling of the roof samples, which will provide valuable information to manufacturers for improving the sustainability of their roofing products. The data will be used to formulate an algorithm correlating changes in reflectance with exposure.

In collaboration with industrial partners, the researchers are exposing samples to 5,000 hours of xenon-arc light in a weatherometer following ASTM Standard G155-00ae1, "Standard Practice for Operating Xenon Arc Light Apparatus for Exposure of Non-Metallic Materials."

Longevity of Cool-colored Roofing Materials

Roofing materials fail mainly because of three processes: gradual changes to physical and chemical composition induced by the absorption of

olet (UV) light; aging and weathering (loss
isticizers in polymers and low-molecular-
t components in asphalt), which may
rate as temperature increases; and diurnal
al cycling, which stresses the material by
sion and contraction. The researchers soon
egin to investigate reflectance effects on the
life of roofing products to evaluate claims
ool roofs will last longer.
NL and ORNL's goal is to clarify the material
dation effects caused by UV absorption and
ig. The results will be used to quantify the
of solar reflectance on the useful life of roofs,
de data to manufacturers to develop better
ials and support development of appropriate
\ standards.

monstration of Energy vings

researchers have established a residential
onstration site in Fair Oaks, Calif., that
des two pairs of single-family, detached hous-
ofed with metal and concrete tile. Two more
of houses will be added to demonstrate
alt shingles and cedar shakes. The monitoring
d will last at least through summer 2005. The
onstration pairs include one building roofed
a cool-pigmented product and a second
ling roofed with a conventionally (warmer)
ented product of nearly the same color.
olar reflectance and thermal emittance are
sured twice per year. Temperatures at the roof
ace, on the underside of the roof deck, in the
attic air, at the top of the insulation, on the
ior ceiling's Sheetrock surface and inside the
ding are logged continuously by a data acqui-
n system. Relative humidity in the attic and
dence also are measured. Heat-flux transduc-
embedded in the sloped roof and attic floor
sure roof heat flow and building heat leak-
. Researchers have instrumented the building
neasure the total house and air-conditioning
ver demands. A weather station collects the
oient dry bulb temperature, relative humidity,
ar irradiance, and wind speed and direction.
ORNL is testing several varieties of concrete and
tile on a steep-slope roof to further investigate
effect of weathering-induced changes to solar
ectance and thermal emittance on the thermal
formance of a cool roof system. The Roof Tile Institute and its affiliate members are keenly interested in specifying tile roofs as cool roof products and want to know the individual and combined effects of cool pigments and subtile ventilation. The data will help better formulate the institute's simulation program, AtticSim, to predict the thermal performance of the cool-colored tile systems.

Early Results

The early results from this program indicate significant success in developing cool-colored materials for concrete tile, clay tile and metal roofs.

Since the inception of this program, the solar reflectance of commercially available products has increased from 0.05 - 0.25 to 0.30 - 0.45. Use of a reflective undercoated (two-layered) coating is expected to soon yield several cost-effective cool-colored shingle products with solar reflectances in excess of the ENERGY-STAR threshold for roofs of 0.25. LBNL and ORNL's ongoing collaboration with granule and shingle manufacturers may yield shingles with solar reflectances exceeding 0.3.

For more information about the study, visit the project Web site, http://coolcolors.lbl.gov, or contact Hashem Akbari at (510) 486-4287 or h_akbari@lbl.gov.

Hashem Akbari is a group leader, staff scientist and principal investigator in the Environmental Energy Technologies Division of Lawrence Berkeley National Laboratory (LBNL), Berkeley, Calif. Paul Berdahl is an applied solid-state physicist whose interests include optical properties of semiconductors and complex materials, such as practical roofing materials. Andre Desjarlais is group leader of the Building Envelope Group of the Engineering Science and Technology Division at Oak Ridge National Laboratory (ORNL), Oak Ridge, Tenn. Nancy Jenkins is the PIER buildings program manager at the California Energy Commission (CEC), Sacramento, Calif. Ronnen Levinson is a scientist in the Heat Island Group at LBNL whose recent research has focused on the development of cool materials for roofs and pavements with emphasis on the optical characterization of pigments. William Miller is a research engineer in the Engineering Science and Technology Division of ORNL. Arthur Rosenfeld currently serves as commissioner of CEC. Chris Scruton is a program manager at CEC and oversees scientific research and development of projects focused on technologies applied to commercial and residential buildings. Stephen Wiel leads the Collaborative Labeling and Appliance Standards Program at LBNL, a program that stimulates the use of energy-efficiency standards and labels worldwide.

Manufacturing Partners

3M Industrial Minerals, Pittsboro, N.C.
www.scotchgard.com/roofinggranules

American Rooftile Coatings, Fullerton, Calif.
www.americanrooftilecoatings.com

BASF, Mount Olive, N.J.
www.basf.com

CertainTeed Corp., Valley Forge, Pa.
www.certainteed.com

Custom-Bilt Metals, South El Monte, Calif.
www.custombiltmetals.com

Elk Corp., Dallas
www.elkcorp.com

Ferro Corp., Cleveland
www.ferro.com

GAF Materials Corp., Wayne, N.J.
www.gaf.com

Hanson Roof Tile, Fontana, Calif.
www.hansonrooftile.com

ISP Minerals Inc., Hagerstown, Md.
(301) 733-4000

MCA Tile, Corona, Calif.
www.mca-tile.com

MonierLifetile LLC, Irvine, Calif.
www.monierlifetile.com

Shepherd Color Co., Cincinnati
www.shepherdcolor.com

Steelscape Inc., Kalama, Wash.
www.steelscape-inc.com

Cool Color Roofs with Complex Inorganic Color Pigments

William A. Miller,[1] Oak Ridge National Laboratory
Kenneth T. Loye, FERRO Corporation
André O. Desjarlais, Oak Ridge National Laboratory
Robert P. Blonski, FERRO Corporation

ABSTRACT

Temperature measurements taken on a highly reflective roof show the surface as only about 5°F (3°C) warmer than the ambient air temperature, while a dark absorptive roof exceeds the ambient air temperature by more than 75°F (40°C). Lowering the exterior roof temperature reduces the heat leakage into the building, which in turn, reduces the air conditioning load. In the residential market, however, the issues of aesthetics and durability are more important to the homeowner than are the potentials for reduced air-conditioning loads and reduced utility bills. Dark roofs simply look better than highly reflective "white" roofs. Yet the aesthetically pleasing dark roof can be made to reflect light like a "white" roof in the infrared portion of the solar energy spectrum. Researchers have formulated new complex inorganic color pigments (CICPs) that exhibit high reflectance in the near-infrared portion of the electromagnetic spectrum and boost the total hemispherical reflectance by a factor of 5 over that of conventional dark roofing.

Introduction

A building's required comfort cooling and heating energy, termed *load*, is directly related to several factors: the solar insolation absorbed by the building; the level of roof, wall, and foundation insulation; the amount of fenestration; and the building's tightness against unwanted air and moisture infiltration. The solar reflectance and long-wave infrared (IR) emittance and the airside convective currents strongly affect the envelope's exterior roof temperature, which in turn drives the load.

In the summer, the higher the roof temperature, the greater the potential for heat leakage into the building, and the greater the burden on the comfort cooling system. In winter, the lower the temperature, the greater the potential for heat leakage from the building, and the greater the energy consumed for comfort heating. In moderate to predominantly hot climates, an exterior roof surface with a high reflectance and high IR emittance will reduce the exterior temperature and produce savings in comfort cooling (Miller and Kriner 2001). For climates predominated by heating loads, surfaces with moderate reflectance and low IR emittance will save in comfort heating.

Field measurements of ten homes by Parker and Barkaszi (1997) showed that reflective white roofing reduced space-cooling energy use an average of 19% as compared to dark asphalt shingles. Measurements made during the summer by Parker and Sherwin (1998)

---

[1]Dr. William A. Miller is a research engineer in the Buildings Technology Center of Oak Ridge National Laboratory (ORNL), Oak Ridge, Tennessee. Kenneth T. Loye is the Technical Manager of the Pigments Group at FERRO Corporation, Cleveland, Ohio. André O. Desjarlais is the manager of ORNL's Building Thermal Envelope Systems & Materials Program. Robert P. Blonski is a research chemist working in the Pigments Group at FERRO Corporation.

showed that white tile roofing caused a 76% reduction in the ceiling heat flux into the house relative to a black shingle roof; the second-best performer in this study, a white-painted metal surface, showed a 61% reduction. Field studies conducted by Parker et al. (1998) on several homes in Fort Myers, Florida, showed that the roof, attic, and air-conditioning ductwork accounted for about 25% of the total cooling load in residences. Highly reflective roofs yielded cooling energy savings upwards of 23% of the annual load.

Each field study documented energy savings by simply raising the reflectance of the roof from a value of about 5% to about 60%. The opportunity therefore exists for a significant impact on energy use in commercial buildings and residential housing, both in new construction and reroofing work. The total sales volume for roofing and reroofing is booming and nearly doubled between 1997 and 2000, from $20 billion to $36 billion (Good 2001). Of the sales volume in 2000, low-slope roofing accounted for 64% ($21.7 billion), while steep-slope roofing comprised about 35.6% ($12 billion) (Good 2001).

High-reflectance single-ply membranes, painted and unpainted metal, and spray-on roof coatings are reducing energy use in the commercial market as building contractors substitute these high-reflectance roofs for bitumen-based built-up roofing (BUR) and ethylene propylene diene monomer (EPDM). Since a high-reflectance low-slope roof cannot be seen from the ground, the roof's functionality is far more important than its looks. However, in steep-slope roofing the issues of appearance, cost, and then durability typically drive the selection of the roofing material because the homeowner wants the roof to complement the décor of the house while protecting the underlying residential structure for a long period of time at an affordable cost. To homeowners, dark roofs simply look better than a highly reflective "white" roof. With the new CICPs, however, an aesthetically pleasing dark roof can be made to reflect like a "white" roof in the infrared portion of the solar spectrum and save energy for both homeowners and utilities.

Surface Properties Affecting Reflectance

Titanium dioxide (TiO_2) is currently the most important white pigment used in the manufacture of paints and plastics. TiO_2 is chemically inert, insoluble, and very heat-resistant. It has been commercially processed from rutile since as early as 1941 (Du Pont Ti-Pure 1999). Rutile TiO_2 increases surface reflectance through refraction and diffraction of the light. As a light ray passes through a TiO_2 particle, the ray bends, or refracts, because light travels more slowly through the pigments than it does through the resin or binder. This occurs because TiO_2 has a much larger refractive index than the resin. This phenomenon is depicted in Figure 1 for two pigmented films. The film containing the pigment with higher refractive index bends the light more than does the film containing the lower refractive index pigment. The light travels a shorter path and does not penetrate as deeply into the film; therefore, less heat is absorbed. The reflectance of the surface increases because the surface opacity increases through refraction induced by the TiO_2 particles. In general, the greater the difference between the refractive index of the pigment and that of the resin or filler in which it is dispersed, the greater will be the light scattering and therefore the increase in surface reflectance.

Diffraction is another physical factor affecting a pigment's ability to scatter light. As a light ray passes by a TiO_2 particle, the ray bends, or diffracts, around the pigment (Fig. 2). Maximum diffraction occurs when the diameter of the pigment is slightly less than one-half

Figure 1. Path of Light as It Penetrates Two Different Coatings, One Having Pigments with a Higher Refractive Index Than the Other

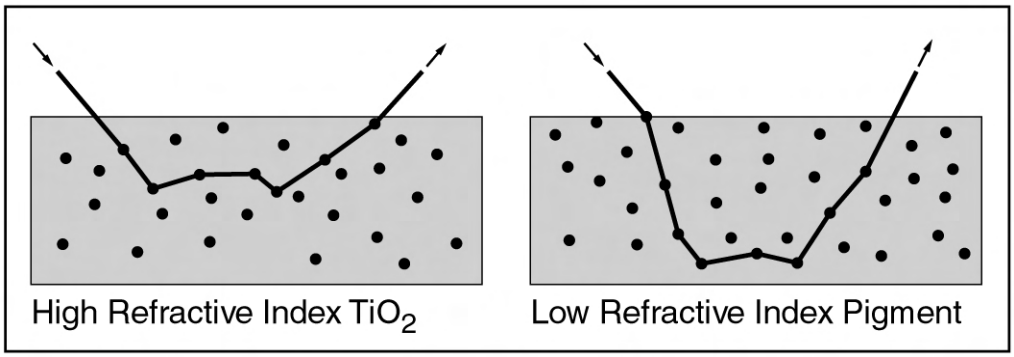

Figure 2. Light Diffraction as a Light Ray Travels near a Pigment Particle

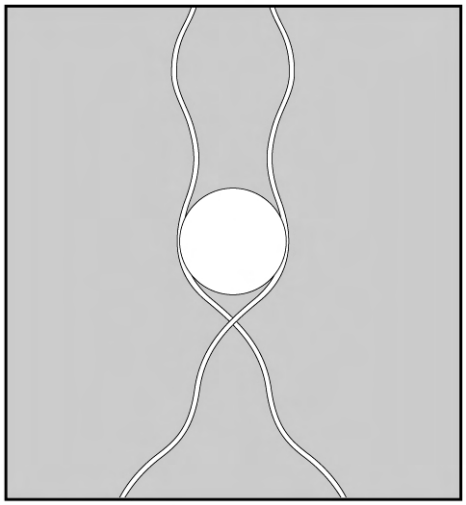

the wavelength of the light to be scattered. Physical modifications of the size, the distribution, and the shape of pigment particles will therefore affect the light scattering. If particles are too large or too closely spaced, little diffraction occurs. Conversely, if the pigment particles are too small, the light will not "see" the particles. Commercially processed rutile TiO_2 has particle diameters ranging from about 200 to 300 nm and is highly reflective in the visible spectrum (yellow-green light at about 550 nm; see Fig. 3). However, as the wavelength of light increases, the reflectance of TiO_2 drops in the infrared spectrum, especially for wavelengths exceeding 1250 nm (Fig. 3).

Complex Inorganic Color Pigments (CICPs)

Aesthetically pleasing dark roofing can be formulated to reflect like a highly reflective "white" roof in the IR portion of the solar spectrum. For years the vinyl siding

Figure 3. Spectral Solar Reflectance of TiO_2, a Green Leaf, Standard Carbon Black and a Complex Inorganic Color Pigment Containing Infrared Reflective $(Fe,Cr)_2O_3$ Pigment (Normalized Solar Irradiance Shown for Reference)

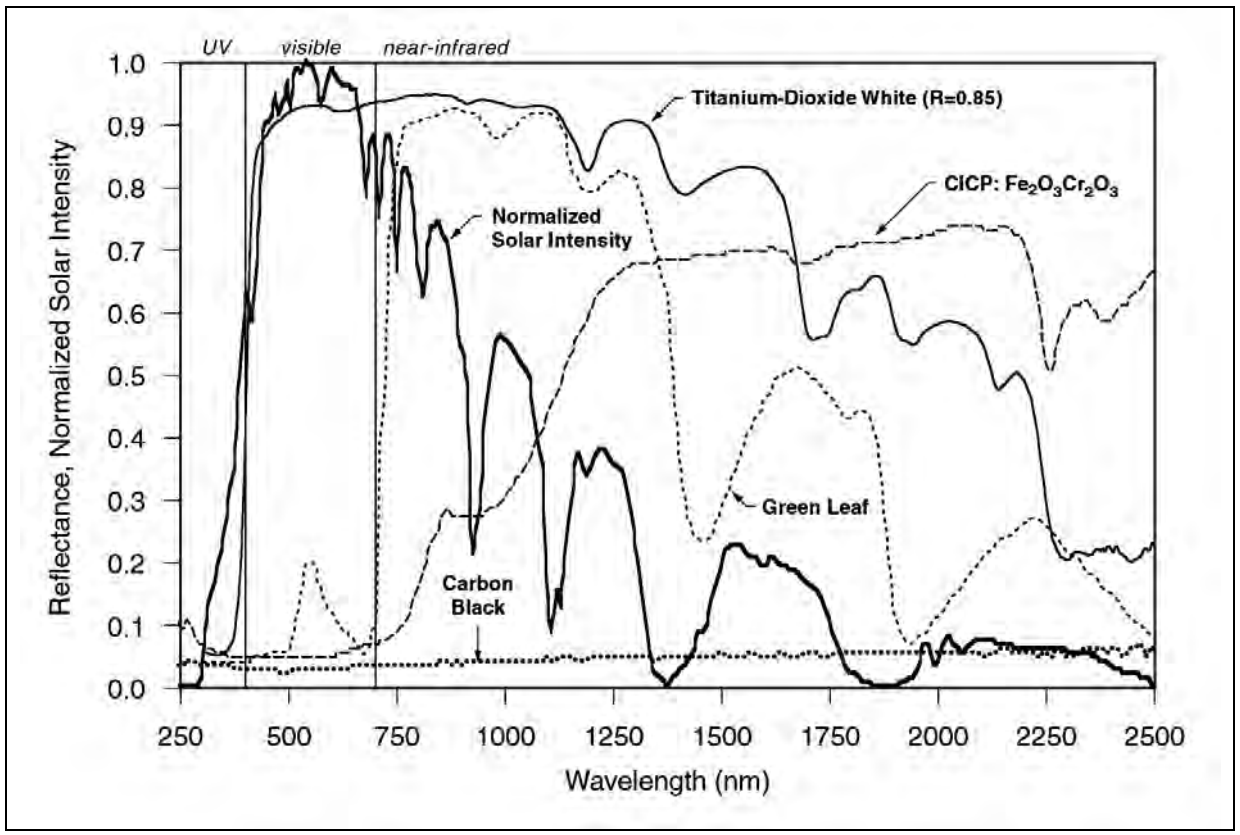

industry has formulated different colors in the same polyvinyl chloride base by altering the content of TiO_2 and black IR-reflective (IRR) paint pigments to produce "dark" siding that is "cool" in temperature (Ravinovitch and Summers 1984). Researchers discovered that a dark color is not necessarily dark in the infrared. Brady and Wake (1992) found that 1-μm particles of TiO_2 when combined with red iron, or ferric, oxide effectively scattered IR radiation at a wavelength of 2300 nm. Researchers working with the Department of Defense developed new complex inorganic color pigments (CICPs) that exhibit dark color in the visible spectrum and high reflectance in the near-IR portion of the electromagnetic spectrum (Sliwinski, Pipoly & Blonski 2001). The new CICPs are used in paints for military camouflage to match the reflectance of background foliage in the visible and IR spectrum. At 750 nm the chlorophyll in foliage naturally boosts the reflectance of a plant leaf from 0.1 to about 0.9 (Fig. 3), which explains why a dark green leaf remains cool on a hot summer day.[2]

CICPs, having been tailored for high IR reflectance similar to that of chlorophyll, are very suitable for roof applications where increased IR reflectance is desirable. A CICP consisting of a mixture of black IRR pigments, chromic oxide (Cr_2O_3) and ferric oxide (Fe_2O_3) boosts the total hemispherical reflectance of carbon black from 0.05 to 0.26 (see

[2]Chlorophyll, the photosynthetic coloring material in plants, naturally reflects near-IR radiation.

CICP:$Fe_2O_3 \cdot Cr_2O_3$ in Fig. 3). Typically, a black asphalt shingle or a black Kynar®[3] metal roof has a reflectance of only about 0.05. The CICP therefore boosts the reflectance by a factor of 5, and in the infrared spectrum CICPs boost the reflectance to almost 0.70 (Fig. 3).

CICPs are formed by calcinating blends of metal oxides or oxide precursors at temperatures over 1600°F (870°C). The calcination causes the metal and oxygen ions in the solids to rearrange in a new structure that is very heat-stable. The inherent heat stability of CICPs makes them ideal for high-temperature coatings in roofing applications. Because of their small particle size and high index of refraction, CICPs will effectively backscatter a significant amount of ultraviolet (UV) and IR light away from a surface. Martin and Pezzuto (1998) observed that pigments that are transparent in the required spectral range and that have a refractive index substantially different from that of the binder work well as IRR pigments.

Thermal Performance of CICPs

CICPs offer excellent opportunities for improving the thermal performance of roofs. About 44% of the sun's total energy is visible to the eye (Fig. 3). Absorbing this 44% is what makes a black appear black. Sunlight emits another 51% of its energy in the invisible IR spectrum. Adding CICPs to roof material can make a black roof reflect near IR energy and therefore maintain a lower roof surface temperature. Using a heat buildup test procedure described by Hardcastle (1979), Ravinovitch and Summers (1984) measured a 23.4°F (13°C) lowering of temperature when a mixture of Cr_2O_3 and Fe_2O_3 was used in place of carbon black.

Light-Color CICPs

The authors tested several IRR pigments against standard pigments using the ASTM D4803 test procedure (ASTM 1997a). This procedure has long been used by the vinyl siding industry to quantify the heat buildup properties of vinyl siding, even though it overstates the sample's properties in the near IR at the expense of visible portion of the spectrum (Ravinovitch and Summers 1984). Table 1 shows the temperatures for both CICPs and standard light-gray, mid-tone bronze, and dark-tone bronze colors when exposed to a flux of 484 Btu/(hr·ft^2) [550 J/(hr·cm^2)] emitted from an infrared heat lamp. These colors are very popular for low-slope roofing in commercial and academic applications where bronze Kynar metal roofing is commonly used.

The colors containing CICPs show a significant drop in temperature as compared to the temperatures of standard light-gray, mid-tone bronze, and dark bronze colors. The temperature is 55°F (30.5°C) cooler for the light gray color if CICPs are contained in the pigment mixture. Similarly, a mid-tone bronze showed a 63°F (35°C) reduction in surface temperature. Even the dark-tone bronze had a measured 54°F (30°C) drop in temperature because the IRR pigments absorb less electromagnetic energy near the cutoff between the visible and infrared wavelengths. They have a more selective absorption band and reflect much of the infrared.

---

[3]Kynar, the registered trademark for polyvinylidene fluoride (PVDF) paint finish, has excellent corrosion and abrasion resistance.

Table 1. CICP Color Matches vs. Standard Pigmentation Exposed to ASTM D4803 Heat Lamp Protocol [a]

Pigment	Pigment Constituents		Maximum Temperature	Temperature Difference (ΔT)
Light gray				
Standard	Carbon black TiO_2 Fe_2O_3	1.5% 96.8% 1.7%	202°F (94.4°C)	
CICP	IRR black TiO_2	10% 90%	147°F (63.9°C)	55°F (30.5°C)
Mid-tone bronze				
Standard	Carbon black TiO_2 Fe_2O_3	11.8% 75.0% 13.2%	225°F (107.2°C)	
CICP	IRR black TiO_2	50% 50%	162°F (72.2°C)	63°F (35°C)
Dark-tone bronze				
Standard	Carbon black TiO_2 Fe_2O_3	33% 29% 38%	220°F (104.4°C)	
CICP	IRR black TiO_2	90% 10%	166°F (74.4°C)	54°F (30°C)

[a] A flux of 484 Btu/(hr·ft^2) [550 J/(hr·cm^2)] emitted from an infrared heat lamp.

Dark-Color CICPs

We also exposed dark colors containing the IRR pigments to the infrared heat lamp. Again, the increased reflectance in the near-IR spectrum (Fig. 4) significantly reduced the surface temperature as compared to carbon black. An IRR green was a measured 54°F (30°C) cooler than carbon black, an IRR dark brown was ~48.6°F (27°C) cooler, and an IRR black was a measured 46.8°F (26°C) cooler.

For our test site at Oak Ridge National Laboratory (ORNL), Oak Ridge, Tennessee, the maximum irradiance from the sun, at solar noon, is about 308 Btu/(hr·ft^2) [350 J/(hr·cm^2)]. ASTM procedure D4803 (ASTM 1997a) relates the intensity of solar irradiance to the intensity derived from the infrared lamp via a ratio of the temperature rises above the ambient air temperature (i.e., the ΔT for IRR black to the ΔT for standard carbon black, see the right side of Eq. 1) to predict the specimen's solar temperature rise by:

$$\left[\frac{\Delta T_{\text{IRR Black}}}{\Delta T_{\text{black Kynar}}}\right]_{\text{solar}} = \left[\frac{\Delta T_{\text{IRR Black}}}{\Delta T_{\text{carbon black}}}\right]_{\text{ASTM D4803}} \quad (1)$$

where

$\Delta T_{\text{IRR Black}}$ = "predicted" temperature rise above ambient air temperature for IRR black when exposed to solar irradiance

$\Delta T_{\text{black Kynar}}$ = "experimentally measured" temperature rise above ambient temperature for a black Kynar roof (~40°C above ambient as field-tested at ORNL)

Figure 4. Heat Buildup of High-IRR Pigments vs. Standard Carbon Black and Reflectance of IRR Black vs. Standard Carbon Black

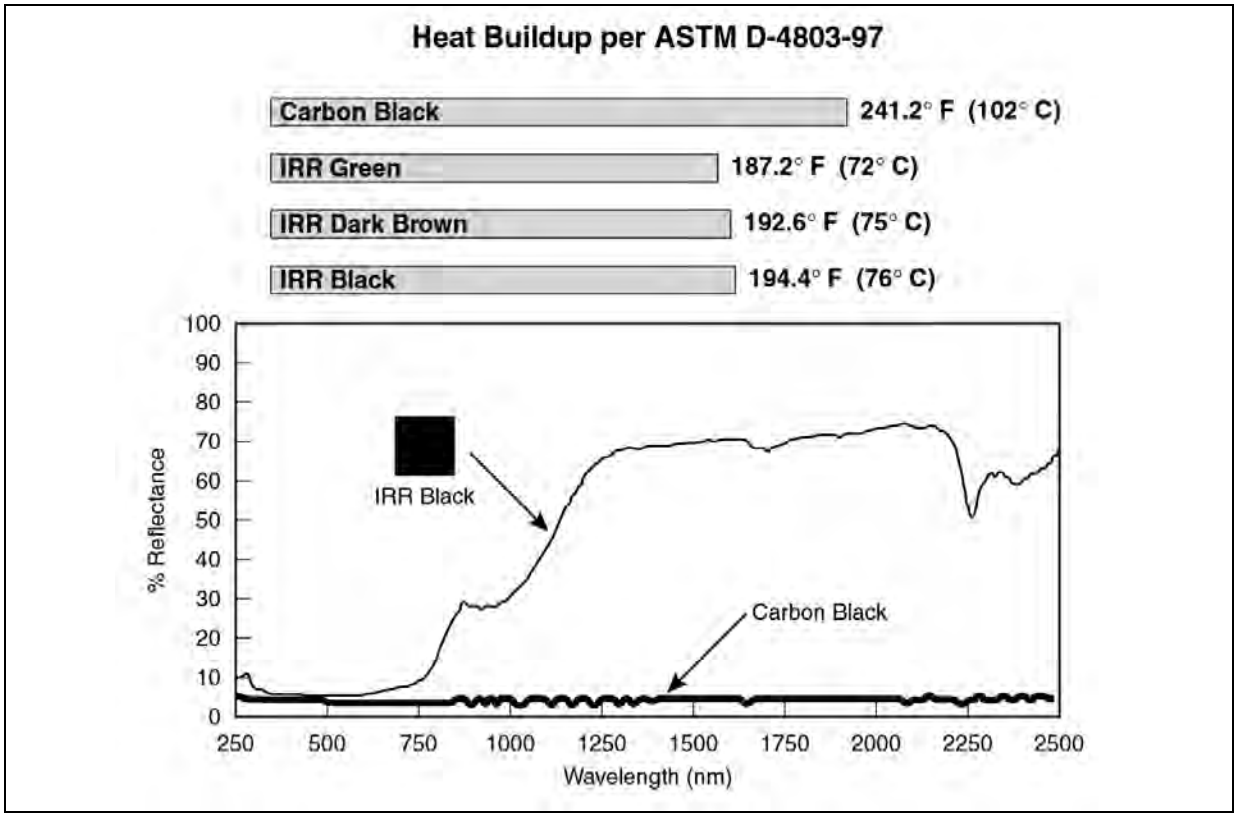

Based on Equation (1) and summertime field data for a black Kynar metal roof tested at ORNL, the IRR black sample would be about 25°F (14°C) cooler at solar noon than a conventional dark roof.

Durability and Weathering of CICPs

Testing protocols to determine the resistance to weathering of paints and coating systems designed for outdoor use include both natural, real-time weathering, such as outdoor exposure in Florida or Arizona, and accelerated tests using a weatherometer equipped with carbon-arc, fluorescent UV, and xenon-arc light sources. To evaluate color changes in roof samples with CICPs as compared to samples with standard colors, we used a one-year exposure test to natural sunlight in Florida and also a 5000-hour xenon-arc accelerated exposure test, following ASTM G-155 (ASTM 2000). Test data showed excellent light fastness for all the CICPs. Pigment stability and discoloration resistance were judged using a total color difference measure (ΔE) as specified by ASTM D 2244-93 (ASTM 1993). The ΔE value for all the colors tested was a color change of approximately 1.0 or less (Figs. 5 and 6).

The total color difference value, ΔE, is a method adopted by the paint industry to numerically identify variability in color over periods of time. This value shows the difference in color between a standard and a batch and includes the three following values computed in the formula:

- lightness (L), where a $+L$ value is lighter and a $-L$ value is darker;
- redness/greenness (a), where a $+a$ value is redder and a $-a$ value is greener; and
- yellowness/blueness (b) where a $+b$ value is yellower and a $-b$ value is bluer.

$$\Delta E = \left[(\Delta L)^2 + (\Delta a)^2 + (\Delta b)^2\right]^{1/2}, \quad (2)$$

where

$\Delta L = L_{batch} - L_{standard}$
$\Delta a = a_{batch} - a_{standard}$
$\Delta b = b_{batch} - b_{standard}$

Typically, coil-coated metal roofing panels are warranted for 20 years or more and specify ΔE of 5 units or less for that period. ΔE color changes of 1 unit or less are almost indistinguishable from the original color, and depending on the hue of color, ΔE of 5 or less is considered very good.

The xenon-arc accelerated weathering initially saw most of the colors rise in ΔE up to about 1500 hours of exposure and then level off; at the end of 5000 hours all are clustered together at less than 1.5 ΔE, which is considered a very good result (Fig. 5). Control products with known performance characteristics were included in the testing to compare results with the new products. The Florida exposure data in Figure 6 is just as promising, indicating that over the one-year test period the CICPs do not fade in the presence of ozone, acid rain, SO_x, NO_x, or other airborne pollutants. Tests have shown that CICPs remain colorfast in the presence of strong acids, bases, and oxidizing or reducing agents. They are non-migratory and showed no dissolving or bleeding in contact with airborne solvents.

Conclusions

Accelerated weather testing using natural sunlight and xenon-arc weatherometer exposure proved that CICPs retain their color. After one year of natural sunlight exposure in south Florida the CICPs show excellent fade-resistance and remain colorfast. CICPs are very stable pigments and have excellent discoloration resistance, as proven by the 5000 hours of xenon-arc exposure; their measure of total color difference was a ΔE value less than 1.5. Therefore, color changes in the CICPs were indistinguishable from their original color.

CICPs have a selective light absorption band in the infrared spectrum. They reflect much of the near-IR heat and therefore reduce the surface temperature upwards of 50°F (28°C) as compared to carbon black pigments when exposed to irradiance from an infrared lamp. For a steep-slope roof in the field, an IRR black would be about 25°F (14°C) cooler at solar noon than would a conventional dark roof. The lower exterior temperature leads to energy savings and provides an ancillary benefit in older existing houses with little or no attic

Figure 5. Total Color Difference (ΔE) Values for Color Samples in Xenon-Arc Accelerated Weathering Test

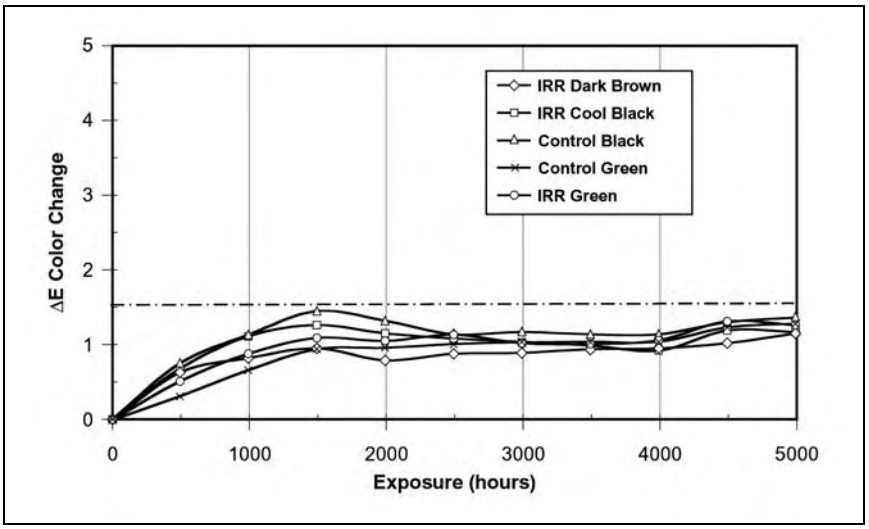

Figure 6. Total Color Difference (ΔE) Values for Color Samples in One-Year Florida Weathering Test

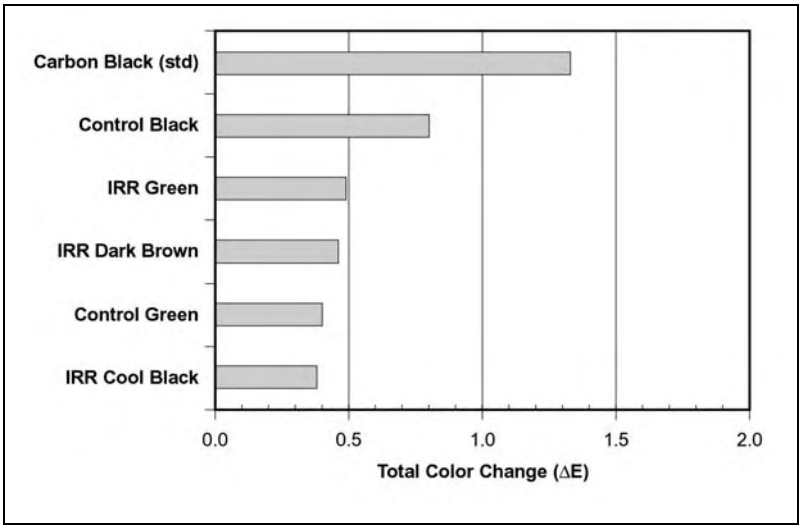

insulation and poorly insulated ducts in the attic because the cooler attic temperature in turn leads to reduced heat gains to the air-conditioning ductwork.

Recommendations

The United States has about 102 million residential homes, with more than 1 million new homes being added each year (Kelso and Kinzey 2000). The space conditioning of these homes accounts for 5.78 quadrillion BTUs (quads) of site energy use per year (EIA 1995); of this amount of energy use, heat leakage through roofs contributes about 14% (Huang, Hanford & Yang 1999). The net national residential cooling load is about 1 quad, and

electrically driven air-conditioning is used in about 66 million U.S. residences (Census Bureau 1987).

Improving energy savings in residential housing for both new housing and existing homes can reduce utility loading significantly. The adoption of CICPs in roof manufacturers' products has the potential to save the nation about 0.1 quad per year. This decrease in electric demand would translate to a decrease of approximately 30.4 million tons in CO_2 emissions per year from utilities powered by coal. Hence, both air quality and quality of life would be improved if measures were enacted to implement the use of CICPs in tile, metal, wood shake, and asphalt shingle roofing products.

Therefore, Lawrence Berkeley National Laboratory (LBNL) and ORNL have initiated a collaborative research and development project in conjunction with pigment (colorant) manufacturers. LBNL and ORNL will work with roofing materials manufacturers to reduce the sunlit temperatures of asphalt shingles, roofing tiles, metal roofing, wood shakes, roofing membranes, and roof coatings.

The addition of CICPs to roofing products will reduce the exterior roof temperature and produce energy savings in space cooling. Moreover, in the case of asphalt shingles, durability and life expectancy should improve, helping to reduce the replacement and disposal costs of solid asphalt shingle roofing (asphalt shingles are typically replaced every 15 years).

The cost to the homeowner to achieve this efficiency improvement when replacing an asphalt roof is estimated to be an incremental cost of about 10¢ per square foot for the CICP reflective roof (Akbari, Berdahl & Levinson 2002). However, only prototypes have been developed in asphalt roofing. In coil-applied metal roofing, which is already painted, the cost could be anywhere from no additional cost to approximately 2¢ per square foot.

References

Akbari, H., P. Berdahl, and R. Levinson (Lawrence Berkeley National Laboratory). 2002. Personal communications.

American Society for Testing and Materials (ASTM). 1993. *Designation D2244-93: Standard Test Method for Calculation of Color Differences from Instrumentally Measured Color*. West Conshohocken, Pa.: American Society for Testing and Materials.

———. 1997a. *Designation D4803-97: Heat Build-Up Apparatus Standard Test Procedure*. West Conshohocken, Pa.: American Society for Testing and Materials.

———. 1997b. *Designation G7-97: Standard Practice for Atmospheric Environmental Exposure Testing of Nonmetallic Materials*. West Conshohocken, Pa.: American Society for Testing and Materials.

———. 2000. *Designation G155-00a: Standard Practice for Arc Operating Xenon Arc Light Apparatus for Exposure on Non-metallic Materials*. West Conshohocken, Pa.: American Society for Testing and Materials.

Brady, R. F., and L. V. Wake. 1992. "Principles and Formulations for Organic Coatings with Tailored Infrared Properties." *Progress in Organic Coatings* 20:1–25.

Du Pont Ti-Pure. 1999. *Titanium Dioxide for Plastics*. Wilmington, Del.: Du Pont Corporation.

Energy Information Administration (EIA). 1995. *1993 Residential Energy Consumption Survey (RECS).* Washington, D.C.: U.S. Department of Energy.

Good, C. 2001. “Eyeing the Industry: NRCA’s Annual Market Survey Provides Interesting Industry Analyses.” In *NRCA 2000–2001 Annual Market Survey*, 116–20. Rosemont, Ill.: National Roofing Contractors Association.

Hardcastle, H. K. 1979. “The Cooling and Sizing Requirements of Vinyl House Siding.” In *Coloring Technology for Plastics*. Ed. Ronald M. Harris. Norwich, N.Y.: William Andrew Publishing.

Huang, J., J. Hanford, and F. Yang. 1999. *Residential Heating and Cooling Loads Component Analysis*. LBNL-44636. Berkeley, Calif.: Lawrence Berkeley National Laboratory.

Kelso, J., and B. Kinzey. 2000. *BTS Core Data Book.* Silver Spring, Md: D&R International, and Richland, Wash.: Pacific Northwest National Laboratory.

Martin, P., and H. L. Pezzuto. 1998. “Pigments Which Reflect Infrared Radiation from Fire.” U.S. Patent 5,811,180, September 22.

Miller, W. A., and S. Kriner. 2001. “The Thermal Performance of Painted and Unpainted Structural Standing Seam Metal Roofing Systems Exposed to One Year of Weathering.” In *Thermal Performance of the Exterior Envelopes of Buildings, VIII: Proceedings of ASHRAE THERM VIII.* Clearwater, Fla.: American Society of Heating, Refrigerating, and Air-Conditioning Engineers, Dec. 2–7.

Parker, D. S., and S. F. Barkaszi. 1997. “Roof Solar Reflectance and Cooling Energy Use: Field Research Results for Florida.” *Energy and Buildings* 25 (2): 105–15.

Parker, D. S., Y. J. Huang, S. J. Konopacki, L. M. Gartland, J. R. Sherwin, and L. Gu. 1998. “Measured and Simulated Performance of Reflective Roofing Systems in Residential Buildings.” *ASHRAE Transactions* 104 (pt. 1B): 963–75.

Parker, D. S., and J. R. Sherwin. 1998. “Comparative Summer Attic Thermal Performance of Six Roof Constructions.” *ASHRAE Transactions* 104 (pt. 2): 1084–92.

Ravinovitch, E. B., and J. W. Summers. 1984. “Infrared Reflecting Vinyl Polymer Compositions.” U.S. Patent 4,424,292. January 3.

Sliwinski, T. R., R. A. Pipoly, and R. P. Blonski. 2001. “Infrared Reflective Color Pigment.” U.S. Patent 6,174,360, January 16.

U.S. Bureau of the Census. 1987. *American Housing Survey: National Core and Supplement 1985–1987*. Washington, D.C.: Government Printing Office.

Potentials of Urban Heat Island Mitigation*

Hashem Akbari
Heat Island Group
Lawrence Berkeley National Laboratory
(510) 486-4287
H_Akbari@lbl.gov
http://HeatIsland.LBL.gov/

ABSTRACT

Urban areas tend to have higher air temperatures than their rural surroundings as a result of gradual surface modifications that include replacing the natural vegetation with buildings and roads. The term "Urban Heat Island" describes this phenomenon. The surfaces of buildings and pavements absorb solar radiation and become extremely hot, which in turn warm the surrounding air. Cities that have been "paved over" do not receive the benefit of the natural cooling effect of vegetation. As the air temperature rises, so does the demand for air-conditioning (a/c). This leads to higher emissions from power plants, as well as increased smog formation as a result of warmer temperatures. In the United States, we have found that this increase in air temperature is responsible for 5–10% of urban peak electric demand for *a/c* use, and as much as 20% of population-weighted smog concentrations in urban areas.

Simple ways to cool the cities are the use of reflective surfaces (rooftops and pavements) and planting of urban vegetation. On a large scale, the evapotranspiration from vegetation and increased reflection of incoming solar radiation by reflective surfaces will cool a community a few degrees in the summer. As an example, computer simulations for Los Angeles, CA show that resurfacing about two-third of the pavements and rooftops with reflective surfaces and planting three trees per house can cool down LA by an average of 2–3K. This reduction in air temperature will reduce urban smog exposure in the LA basin by roughly the same amount as removing the basin entire on-road vehicle exhaust. Heat island mitigation is an effective air pollution control strategy, more than paying for itself in cooling energy cost savings. We estimate that the cooling energy savings in U.S. from cool surfaces and shade trees, when fully implemented, is about $5 billion per year (about $100 per air-conditioned house).

Introduction

Across the world, urban temperatures have increased faster than temperatures in rural areas. For example, from 1930 to 1990, downtown Los Angeles recorded a growth of 0.5 degrees C per decade (Akbari *et al*. 2001). Every degree increase adds about 500 megawatts (MW) to the air conditioning load in the Los Angeles Basin (Akbari *et al*. 2001). Similar increases are taxing the ability of developing countries to meet urban electricity demand, while increasing global GHG emissions. Local air pollution (e.g., particulates, volatile organics, and nitrogen oxides, which are precursors to ozone formation) are already a problem in most cities in developing countries. Higher temperatures mean increased ozone formation, with accompanying health impacts. LBNL has conducted research on both the electricity and air pollution effects of higher temperatures, and devised methods to reduce both effects. We have tested reflective coatings on building roofs and pavements, and tree-planting schemes, to demonstrate potential cost-effective reductions of

* This paper is an abridged and updated version of an earlier paper published in *Solar Energy* (Akbari et al 2001).

energy use—between 10 and 40 percent. Among energy-efficiency solutions, cool roofs and cool pavements are ideally suited to hot climates that prevail in much of the developing world. Cool (light-colored) pavements also increase nighttime visibility and pavement durability.

Urban areas have typically darker surfaces and less vegetation than their surroundings (HIG 2005). These differences affect climate, energy use, and habitability of cities. At the building scale, dark roofs heat up more and thus raise the summertime cooling demands of buildings. Collectively, dark surfaces and reduced vegetation warm the air over urban areas, leading to the creation of urban "heat islands." On a clear summer afternoon, the air temperature in a typical city is as much as 2.5K higher than in the surrounding rural areas. Research shows that peak urban electric demand rises by 2–4% for each 1K rise in daily maximum temperature above a threshold of 15–20°C. Thus, the additional air-conditioning use caused by this urban air temperature increase is responsible for 5–10% of urban peak electric demand.

In California, Goodridge (1987, 1989) shows that, before 1940, the average urban-rural temperature differences for 31 urban and 31 rural stations in California were always negative, i.e., cities were cooler than their surroundings. After 1940, when built-up areas began to replace vegetation, the urban centers became as warm or warmer than the suburbs. From 1965 to 1989, urban temperatures increased by about 1K.

Regardless of whether there is an urban-rural temperature difference, data suggest that temperatures in cities are increasing. For example, the maximum temperatures in downtown Los Angeles are now about 2.5K higher than they were in 1930. The minimum temperatures are about 4K higher than they were in 1880 (Akbari *et al*. 2001). In Washington, DC, temperatures increased by about 2K between 1871 and 1987. The data indicate that this recent warming trend is typical of most U.S. metropolitan areas, and exacerbates demand for energy. Limited available data also show this increasing trend in urban temperatures in major cities of other countries (**Figure 1.**)

Not only do summer heat islands increase system-wide cooling loads, they also increase smog production because of higher urban air temperatures (Taha *et al*. 1994). Smog is created by photochemical reactions of pollutants in the air; and these reactions are more likely to intensify at higher temperatures. For example, in Los Angeles, for every 1°C the temperature rise above 22°C, incident of smog increases by 5%.

Heat Islands Mitigation Technologies

Use of high-albedo[†] urban surfaces and planting of urban trees are inexpensive measures that can reduce summertime temperatures. The effects of modifying the urban environment by planting trees and increasing albedo are best quantified in terms of "direct" and "indirect" contributions. The direct effect of planting trees around a building or using reflective materials on roofs or walls is to alter the energy balance and cooling requirements of that particular building. However, when trees are planted and albedo is modified throughout an entire city, the energy balance of the whole city is modified, producing city-wide changes in climate. Phenomena associated with city-wide changes in climate are referred to as indirect effects, because they indirectly affect the energy use in an individual building. Direct effects give immediate benefits to the building that applies them. Indirect effects achieve benefits only with widespread deployment.

[†] When sunlight hits an opaque surface, some of the sunlight is reflected (this fraction is called the albedo = a), and the rest is absorbed (the absorbed fraction is 1-a). Low-a surfaces of course become much hotter than high-a surfaces.

Figure 1. Increasing urban temperature trends over the last 3–8 decades in selected cities

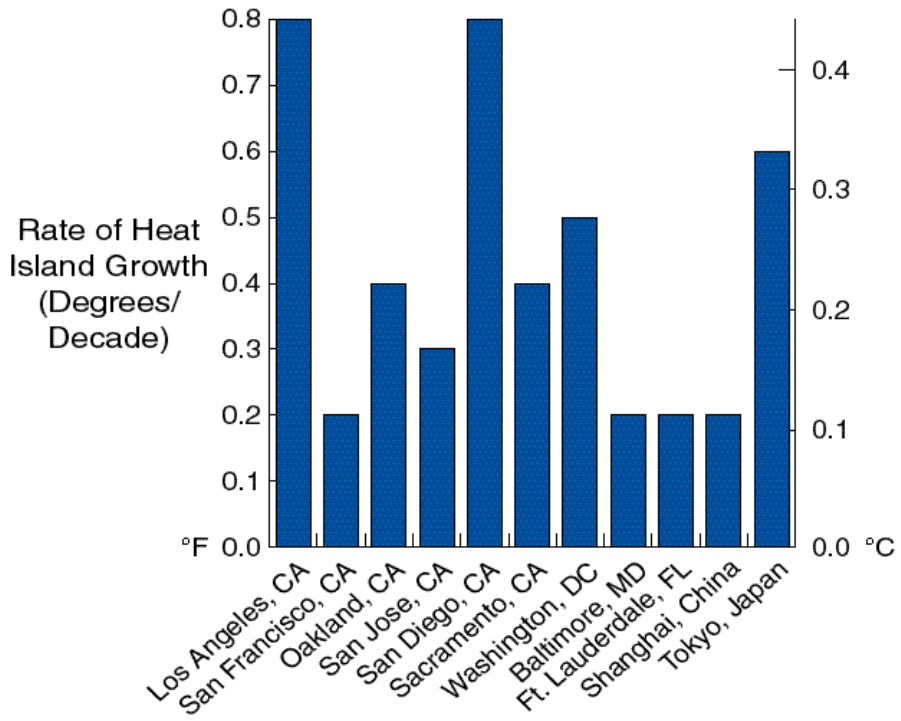

The issue of direct and indirect effects also enters into our discussion of atmospheric pollutants. Planting trees has the direct effect of reducing atmospheric CO_2 because each individual tree directly sequesters carbon from the atmosphere through photosynthesis. However, planting trees in cities also has an indirect effect on CO_2. By reducing the demand for cooling energy, urban trees indirectly reduce emission of CO_2 from power plants. Akbari *et al*. (1990) showed that the amount of CO_2 avoided via the indirect effect is considerably greater than the amount sequestered directly. Similarly, trees directly trap ozone precursors (by dry-deposition, a process in which ozone is directly absorbed by tree leaves), and indirectly reduce the emission of these precursors from power plants (by reducing combustion of fossil fuels and hence reducing NOx emissions from power plants) (Taha 1996).

Over the past two decades, LBNL has been studying the energy savings and air-quality benefits of heat-island mitigation measures. The approaches used for analysis included direct measurements of the energy savings for cool roofs and shade trees, simulations of direct and indirect energy savings of the mitigation measures (cool roofs, cool pavements, and vegetation), and meteorological and air-quality simulations of the mitigation measures. **Figure 2** depicts the overall methodology used in analyzing the impact of heat-island mitigation measures on energy use and urban air pollution.

To understand the impacts of large-scale increases in albedo and vegetation on urban climate and ozone air quality, mesoscale meteorological and photochemical models are used (Taha *et al*. 1997). For example, Taha *et al*. (1995) and Taha (1996, 1997) used the Colorado State University Mesoscale Model (CSUMM) to simulate the Los Angeles Basin's meteorology and its sensitivity to changes in surface properties. More recently, we have utilized the PSU/NCAR mesoscale model (known as MM5) to simulate the meteorology. The Urban Airshed Model (UAM) was used to simulate the impact of the changes in meteorology and emissions on ozone

air quality. The CSUMM, MM5, and the UAM essentially solve a set of coupled governing conservation equations representing the conservation of mass (continuity), potential temperature (heat), momentum, water vapor, and chemical species continuity to obtain prognostic meteorological fields and pollutant species concentrations.

Figure 2: Methodology for energy and air-quality

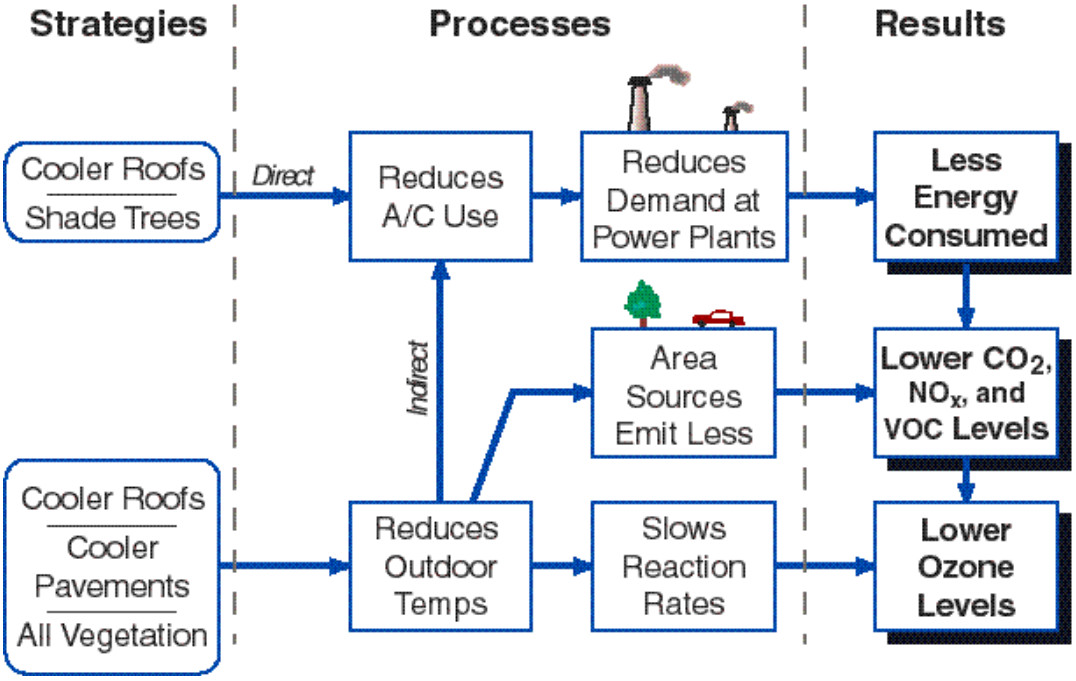

Cool Roofs

At the building scale, a dark roof is heated by the sun and thus directly raises the summertime cooling demand of the building beneath it. For highly absorptive (low-albedo) roofs, the difference between the surface and ambient air temperatures may be as high as 50K, while for less absorptive (high-albedo) surfaces with similar insulative properties, such as roofs covered with a white coating, the difference is only about 10K (Berdahl and Bretz 1997). For this reason, "cool" surfaces (which absorb little "insolation") can be effective in reducing cooling-energy use. Highly absorptive surfaces contribute to the heating of the air, and thus indirectly increase the cooling demand of (in principle) all buildings. In most applications, cool roofs incur no additional cost if color changes are incorporated into routine re-roofing and resurfacing schedules (Bretz *et al*. 1997 and Rosenfeld *et al*. 1992).

Most high-albedo roofing materials are light colored, although selective surfaces that reflect a large portion of the infrared solar radiation but absorb some visible light can be dark colored and yet have relatively high albedos (Levinson et al 2005a,b, Berdahl and Bretz 1997).

1. Energy and Smog Benefits of Cool Roofs

Direct Energy Savings

Several field studies have documented measured energy savings that result from increasing roof solar reflectance (see **Table 1**). Akbari *et al.* (1997) reported monitored cooling-energy

savings of 46% and peak power savings of 20% achieved by increasing the roof reflectance of two identical portable classrooms in Sacramento, California. Konopacki *et al.* (1998) documented measured energy savings of 12–18% in two commercial buildings in California. Konopacki and Akbari (2001) documented measured energy savings of 12% in a large retail store in Austin, Texas. Akbari (2003) documented energy savings of 31–39 $Wh/m^2/day$ in two small commercial buildings with very high internal loads, by coating roofs with a white elastomer with a reflectivity of 0.70. Parker *et al.* (1998) measured an average of 19% energy savings in eleven Florida residences by applying reflective coatings on roofs. Parker *et al.* (1997) also monitored seven retail stores in a strip mall in Florida before and after applying a high-albedo coating to the roof and measured a 25% drop in seasonal cooling energy use. Hildebrandt *et al*. (1998) observed daily energy savings of 17%, 26%, and 39% in an office, a museum and a hospice, respectively, retrofitted with high-albedo roofs in Sacramento. Akridge (1998) reported energy savings of 28% for a school building in Georgia which had an unpainted galvanized roof that was coated with white acrylic. Boutwell and Salinas (1986) showed that an office building in southern Mississippi saved 22% after the application of a high-reflectance coating. Simpson and McPherson (1997) measured energy savings in the range of 5–28% in several quarter-scale models in Tucson AZ.

In addition to these building monitoring studies, computer simulations of cooling energy savings from increased roof albedo have been documented in residential and commercial buildings by many studies, including Konopacki and Akbari (1998), Akbari *et al*. (1998a), Parker *et al*. (1998), and Gartland *et al.* (1996). Konopacki *et al*. (1997) estimated the direct energy savings potential from high-albedo roofs in eleven U.S. metropolitan areas. The results showed that four major building types account for over 90% of the annual electricity and monetary savings: pre-1980 residences (55%), post-1980 residences (15%), and office buildings and retail stores together (25%). Furthermore, these four building types account for 93% of the total air-conditioned roof area. Regional savings were found to be a function of three factors: energy savings in the air-conditioned residential and commercial building stock; the percentage of buildings that were air-conditioned; and the aggregate regional roof area. Metropolitan-wide annual savings from the application of cool roofs on residential and commercial buildings were as much as $37M for Phoenix and $35M in Los Angeles and as low as $3M in the heating-dominated climate of Philadelphia. Analysis of the scale of urban energy savings potential was further refined for five cities: Baton Rouge, LA; Chicago, IL; Houston, TX; Sacramento, CA; and Salt Lake City, UT by Konopacki and Akbari (2002, 2000).

The results for the 11 Metropolitan Statistical Areas (MSAs) were extrapolated to estimate the savings in the entire United States. The study estimates that nationally light-colored roofing could produce savings of about 10 TWh/yr (about 3.0% of the national cooling-electricity use in residential and commercial buildings), an increase in natural gas use by 26 GBtu/yr (1.6%), a decrease in peak electrical demand of 7 GW (2.5%) (equivalent to 14 power plants each with a capacity of 0.5 GW), and a decrease in net annual energy bills for the rate-payers of $750M.

Indirect Energy and Smog Benefits

Using the Los Angeles Basin as a case study, Taha (1996, 1997) examined the impacts of using cool surfaces (cool roofs and pavements) on urban air temperature and thus on cooling-energy use and smog. In these simulations, Taha estimates that about 50% of the urbanized area in the L.A. Basin is covered by roofs and roads, the albedos of which can realistically be raised by 0.30 when they undergo normal repairs. This results in a 2K cooling at 3 p.m. during an

August episode. This summertime temperature reduction has a significant effect on further reducing building cooling-energy use. The annual savings in Los Angeles are estimated at $21M (Rosenfeld *et al*. 1998).

We have also simulated the impact of urban-wide cooling in Los Angeles on smog; the results show a significant reduction in ozone concentration. The simulations predict a reduction of 10–20% in population-weighted smog (ozone). In L.A., where smog is especially serious, the potential savings were valued at $104M/year (Rosenfeld *et al*. 1998).

Table 1. Comparison of measured summertime air-conditioning daily energy savings from application of reflective roofs. Δρ is change in roof reflectivity, RB is radiant barrier, duct is the location of air-conditioning ducts, and R-val is roof insulation in Km^2/W.

Location	Building type	Roof area	Roof system			Savings
		[m^2]	R-val	duct	Δρ	[$Wh/m^2/day$]
California						
Davis	Medical Office	2,945	1.4	Interior	0.36	68
Gilroy	Medical Office	2,211	3.3	Plenum	0.35	39
San Jose	Retail Store	3,056	RB	Plenum	0.44	4.3
Sacramento	School Bungalow	89	3.3	Ceiling	0.60	47
Sacramento	Office	2,285	3.3	Plenum	0.40	14
Sacramento	Museum	455	0	Interior	0.40	20
Sacramento	Hospice	557	1.9	Attic	0.40	11
Sacramento	Retail Store	1600	RB	None	0.61	72
San Marcus	Elementary School	570	5.3	None	0.54	45
Reedley	Cold Storage Facility					
	Cold storage	4900	5.1	None	0.61	69
	Fruit conditioning	1300	4.4	None	0.33	
	Packing area	3400	1.7	None	0.33	Nil (open to outdoor)
Florida						
Cocoa Beach	Strip Mall	1,161	1.9	Plenum	0.46	7.5
Cocoa Beach	School	929	3.3	Plenum	0.46	43
Georgia						
Atlanta	Education	1,115	1.9	Plenum	N/A	75
Nevada						
Battle Mountain	Regeneration	14.9	3.2	None	0.45	31
Carlin	Regeneration	14.9	3.2	None	0.45	39
Texas						
Austin	Retail Store	9,300	2.1	Plenum	0.70	39

2. Other Benefits of Cool Roofs

Another benefit of a light-colored roof is a potential increase in its useful life. The diurnal temperature fluctuation and concomitant expansion and contraction of a light-colored roof is smaller than that of a dark one. Also, the degradation of materials resulting from the absorption of ultra-violet light is a temperature-dependent process. For these reasons, cooler roofs may last longer than hot roofs of the same material.

3. Potential Problems with Cool Roofs

Several possible problems may arise from the use of reflective roofing materials (Bretz and Akbari 1994, 1997). A drastic increase in the overall albedo of the many roofs in a city has the potential to create glare and visual discomfort if not kept to a reasonable level. Fortunately, the glare for flat roofs is not a major problem for those who are at street level. For sloped roofs, the problem of glare should be studied in detail before proceeding with a full-scale implementation of this measure.

In addition, many types of building materials, such as tar roofing, are not well adapted to painting. Although such materials could be specially designed to have a higher albedo, this would entail a greater expense than painting. Additionally, to maintain a high albedo, roofs may need to be recoated or rewashed on a regular basis. The cost of a regular maintenance program could be significant.

A possible conflict of great concern is the fact that building owners and architects like to have the choice as to what color to select for their rooftops. This is particularly a concern for sloped roofs.

4. Cost of Cool Roofs

To change the albedo, the rooftops of buildings may be painted or covered with a new material. Since most roofs have regular maintenance schedules or need to be re-roofed or recoated periodically, the change in albedo should be done then to minimize the costs.

High-albedo alternatives to conventional roofing materials are usually available, often at little or no additional cost. For example, a built-up roof typically has a coating or a protective layer of mineral granules or gravel. In such conditions, it is expected that choosing a reflective material at the time of installation should not add to the cost of the roof. Also, roofing shingles are available in a variety of colors, including white, at the same price. The incremental price premium for choosing a white rather than a black single-ply membrane roofing material is less than 10%. Cool roofing materials that require an initial investment may turn out to be more attractive in terms of life-cycle cost than conventional dark alternatives. Usually, the lower life-cycle cost results from longer roof life and/or energy savings.

Cool Pavements

The practice of widespread paving of city streets with asphalt began only within the past century. The advantages of this smooth and all-weather surface for the movement of bicycles and automobiles are obvious, but some of the associated problems are perhaps not so well appreciated. One consequence of covering streets with dark asphalt surfaces is the increased heating of the city by sunlight. The pavements in turn heat the air. LBNL has conducted studies to measure the effect of albedo on pavement temperature. The data clearly indicate that significant modification of the pavement surface temperature can be achieved: a 10K decrease in temperature for a 0.25 increase in albedo. If urban surfaces were lighter in color, more of the incoming light would be reflected back into space and the surfaces and the air would be cooler. This tends to reduce the need for air conditioning. Pomerantz *et al*. (1997) present an overview of cool paving materials for urban heat island mitigation.

1. Energy and Smog Benefits of Cool Pavements

Cool pavements provide only indirect effects through lowered ambient temperatures. Lower temperature has two effects: 1) reduced demand for electricity for air conditioning and 2) decreased production of smog (ozone). Rosenfeld *et al*. (1998) estimated the cost savings of

reduced demand for electricity and of the externalities of lower ozone concentrations in the Los Angeles Basin.

Simulations for Los Angeles (L.A.) basin indicate that a reasonable change in the albedo of the city could cause a noticeable decrease in temperature. Taha (1997) predicted a 1.5K decrease in temperature of the downtown area. The lower temperatures in the city are calculated based on the assumption that all roads and roofs are improved. From the meteorological simulations of three days in each season, the temperature changes for every day in a typical year were estimated for Burbank, typical of the hottest 1/3 of L.A. basin. The energy consumptions of typical buildings were then simulated for the original weather and also for the modified weather. The differences are the annual energy changes due to the decrease in ambient temperature. The result is a city-wide annual saving of about $71M, due to combined albedo and vegetation changes. The kWh savings attributable to the pavement are $15M/yr, or $0.012/m^2-yr. Analysis of the hourly demand indicates that cooler pavements could save an estimated 100 MW of peak power in L.A.

The simulations of the effects of higher albedo on smog formation indicate that an albedo change of 0.3 throughout the developed 25% of the city would yield a 12% decrease in the population-weighted ozone exceedance of the California air-quality standard (Taha 1997). It has been estimated (Hall *et al*. 1992) that residents of L.A. would be willing to pay about $10 billion per year to avoid the medical costs and lost work time due to air pollution. The greater part of pollution is particulates, but the ozone contribution averages about $3 billion/yr. Assuming a proportional relationship of the cost with the amount of smog exceedance, the cooler-surfaced city would save 12% of $3 billion/yr, or $360M/yr. As above, we attribute about 21% of the saving to pavements. Rosenfeld *et al.* (1998) value the benefits from smog improvement by altering the albedo of all 1250km^2 of pavements by 0.25 saves about $76M/year (about $0.06/m^2 per year).

2. Other Benefits of Cool Pavements

It has long been known that the temperature of a pavement affects its performance (Yoder & Witzak 1975). This has been emphasized by the new system of binder specification advocated by the Strategic Highway Research Program (SHRP). Beginning in 1987, this program led pavement experts to carry out the task of researching and then recommending the best methods of making asphalt concrete pavements. A result of this study was the issuance of specifications for the asphalt binder. The temperature range which the pavement will endure is a primary consideration (Cominsky *et al*. 1994). The performance grade (PG) is specified by two temperatures: (1) the average 7-day maximum temperature that the pavement will likely encounter, and (2) the minimum temperature the pavement will likely attain.

Reflectivity of pavements is also a safety factor in visibility at night and in wet weather, affecting the demand for electric street lighting. Street lighting is more effective if pavements are more reflective, which can lead to greater safety; or, alternatively, less lighting could be used to obtain the same visibility. These benefits have not yet been monetized.

3. Potential Problems with Cool Pavements

A practical drawback of high reflectivity is glare, but this does not appear to be a problem. We suggest a change in resurfacing using not black asphalt, with an albedo of about 0.05–0.12, but the application of a product with an albedo of about 0.35, similar to that of cement concrete. The experiment to test whether this will be a problem has already been performed: every day

millions of people drive on cement concrete roads, and we rarely hear of accidents caused by glare, or of people even complaining about the glare on such roads.

There is also a concern that, after some time, light-colored pavement will darken because of dirt. This tends to be true, but again, experience with cement concrete roads suggests that the light color of the pavement persists after long usage. Most drivers can see the difference in reflection between an asphalt and a cement concrete road when they drive over them, even when the roads are old.

4. Cost of Cool Pavements

It is clear that cooler pavements will have energy, environmental, and engineering benefits. The issue is then whether there are ways to construct pavements that are feasible, economical, and cooler. The economic question is whether the savings generated by a cool pavement over its lifetime are greater than its extra cost. Properly, one should distinguish between initial cost and lifetime costs (including maintenance, repair time, and length of service of the road). Often the initial cost is decisive.

A typical asphalt concrete contains about 7% of asphalt by weight, or about 17% by volume; the remainder is rock aggregate, except for a few percent of voids. In one ton of mixed asphalt concrete the cost of materials only is about $28/ton, of which about $9 is in the binder and $19 is in the aggregate. For a pavement about 10 cm thick (4 inches), with a density of 2.1 ton/m^3, the cost of the binder is about $2 per m^2 and aggregate costs about $4.2 per m^2.

Using the assumptions for Los Angeles, a cooler pavement would generate a stream of savings of $0.07/$m^2$ per year for the lifetime of the road—about 20 years. The present value of potential savings at a real discount rate of 3% is $1.1/$m^2$. This saving would allow for purchase of a binder costing $3/$m^2$, instead of $2/$m^2$—or 50% more. Alternatively, one could buy aggregate; instead of spending $4.2/$m^2$, one can now afford $5.2/$m^2$ (a 20% more expensive, whiter aggregate). It is doubtful that such modest increases in costs can buy much whiter pavements.

At some times in its life, a pavement needs to be maintained, i.e., resurfaced. This offers an opportunity to get cooler pavements economically. Good maintenance practice calls for resurfacing a new road after about 10 years (Dunn 1996) and the lifetime of resurfacing is only about 5 years. Hence, within 10 years, all the asphalt concrete surfaces in a city can be made light colored. As part of this regular maintenance, any additional cost of the whiter material will be minimized.

For pavements, the energy and smog savings may not pay for whiter roads. However, if the lighter-colored road leads to substantially longer lifetime, the initial higher cost may be offset by lifetime savings.

Shade trees and urban vegetation

Akbari 2002 provides an overview of benefits and cost associated with planting urban trees. Shade trees intercept sunlight before it warms a building. The urban forest cools the air by evapotranspiration. Trees also decrease the wind speed under their canopy and shield buildings from cold winter breezes. Urban shade trees offer significant benefits by both reducing building air conditioning and lowering air temperature, and thus improving urban air quality by reducing smog. Over the life of a tree, the savings associated with these benefits vary by climate region and can be up to $200 per tree. The cost of planting trees and maintaining them can vary from $10 to $500 per tree. Tree planting programs can be designed to be low cost, so they can offer

savings to communities that plant trees.

1. Energy and Smog Benefits of Shade Trees

Direct Energy Savings

Data on measured energy savings from urban trees are scarce. In one experiment, Parker (1981) measured the cooling-energy consumption of a temporary building in Florida before and after adding trees and shrubs and found cooling-electricity savings of up to 50%. In the summer of 1992, Akbari *et al*. (1997) monitored peak-power and cooling-energy savings from shade trees in two houses in Sacramento, California. The collected data included air-conditioning electricity use, indoor and outdoor dry-bulb temperatures and humidities, roof and ceiling surface temperatures, inside and outside wall temperatures, insolation, and wind speed and direction. The shading and microclimate effects of the trees at the two monitored houses yielded seasonal cooling-energy savings of 30%, corresponding to average savings of 3.6 and 4.8 kWh/day. Peak-demand savings for the same houses were 0.6 and 0.8 kW (about 27% savings in one house and 42% in the other).

DeWalle *et al*. (1983), Heisler (1989), and Huang *et al*. (1990) have focused on measuring and simulating the wind-shielding effects of tree on heating- and cooling-energy use. Their analysis indicated that a reduction in infiltration because of trees would save heating-energy use. However, in climates with cooling-energy demand, the impact of windbreak on cooling is fairly small compared to the shading effects of trees and, depending on climate, it could decrease or increase cooling-energy use. In cold climates, the wind-shielding effect of trees can reduce heat-energy use in buildings. However, using strategically placed deciduous trees can decrease winter heating penalties. Akbari and Taha (1992) simulated the wind-shielding impact of trees on heating-energy use in four Canadian cities. For several prototypical residential buildings, they estimated heating-energy savings in the range of 10–15%.

Taha *et al*. (1996) simulated the meteorological impact of large-scale tree-planting programs in 10 U.S. metropolitan areas: Atlanta GA, Chicago IL, Dallas TX, Houston TX, Los Angeles CA, Miami FL, New York NY, Philadelphia PA, Phoenix AZ, and Washington, DC. The DOE-2 building simulation program was then used to estimate the direct and indirect impacts of trees on saving cooling-energy use for two building prototypes: a single-family residence and an office. The calculations accounted for a potential increase in winter heating-energy use, and showed that in most hot cities, shading a building can save annually \$5 to \$25 per $100m^2$ of roof area of residential and commercial buildings.

Indirect Energy and Smog Benefits

Taha *et al*. (1996) estimated the impact on ambient temperature resulting from a large-scale tree-planting program in the selected 10 cities. They used a three-dimensional meteorological model to simulate the potential impact of trees on ambient temperature for each region. The mesoscale simulations showed that, on average, trees can cool down cities by about 0.3K to 1K at 2 pm.; in some simulation cells the temperature was decreased by up to 3K. The corresponding air-conditioning savings resulting from ambient cooling by trees in hot climates ranges from \$5 to \$10 per year per $100m^2$ of roof area of residential and commercial buildings. Indirect effects are smaller than the direct effects of shading, and, moreover, require that the entire city be planted.

Rosenfeld *et al*. (1998) studied the potential benefits of planting 11M trees in the Los Angeles Basin. They estimate an annual total savings of \$270 million from direct and indirect

energy savings and smog benefit; about 2/3 of the savings resulted from the reduction in smog concentration resulting from meteorological changes due to the evapotranspiration of trees. It also has been suggested that trees improve air quality by dry-depositing NO_X, O_3, and PM10 particulates. Rosenfeld *et al*. (1998) estimate that 11M trees in LA will reduce PM10 by less than 0.1%, worth only $7M, which is disappointingly smaller than the benefits of $180M from smog reduction.

The present value (PV) of savings is calculated to find out how much a homeowner can afford to pay for shade trees. Rosenfeld *et al*. (1998) estimate that, on this basis, the direct savings to a homeowner who plants three shade trees would have a present value of about $200 per home ($68/tree). The present value of indirect savings was smaller, about $72/home ($24/tree). The PV of smog savings was about $120/tree. Total PV of all benefits from trees was thus $210/tree.

2. Other Benefits of Shade Trees

There are other benefits associated with urban trees. Some of these include improvement in the quality of life, increased value of properties, decreased rain run-off water and hence a protection against floods (McPherson *et al*. 1994). Trees also directly sequester atmospheric carbon dioxide, but Rosenfeld *et al*. (1998) estimate that the direct sequestration of CO_2 is less than one-fourth of the emission reduction resulting from savings in cooling-energy use. These other benefits of trees are not considered in the cost benefit analysis shown in this paper.

3. Potential Problems with Shade Trees

There are some potential problems associated with trees. Some trees emit volatile organic compounds (VOCs) that exacerbate the smog problem. Obviously, selection of low-emitting trees should be considered in a large-scale tree-planting program. Benjamin *et al*. (1996) have prepared a list of several hundred tree species with their average emission rate.

In dry climates and areas with a serious water shortage, drought-resistant trees are recommended. Some trees need significant maintenance that may entail high costs over the life of the trees. Tree roots can damage underground pipes, pavements and foundations. Proper design is needed to minimize these effects. Also, trees are a fuel source for fire; selection of appropriate tree species and planting them strategically to minimize the fire hazard should be an integral component of a tree-planting program.

4. Cost of Trees

The cost of a citywide tree-planting program depends on the type of program offered and the types of trees recommended. At the low end, a promotional planting of trees 5–10 feet high costs about $10 per tree, whereas a professional tree-planting program using fairly large trees could amount to $150–470 a tree (McPherson 1994). McPherson has collected data on the cost of tree planting and maintenance from several cities. The cost elements include planting, pruning, removal of dead trees, stump removal, waste disposal, infrastructure repair, litigation and liability, inspection, and program administration. The data provide details of the cost for trees located in parks, in yards, and along streets, highways, and houses. The present value of all these life-cycle costs (including planting) is $300–500 per tree. Over 90% of the cost is associated with professional planting, pruning, tree and stump removal. On the other hand, a program administered by the Sacramento Municipal Utility District (SMUD) and Sacramento Tree Foundation in 1992–1996 planted 20-foot tall trees at an average cost of $45 per tree. This only

includes the cost of a tree and its planting; it does not include pruning, removal of dead trees, and removal of stumps. With this wide range of costs associated with trees, in our opinion, tree costs should be justified by other amenities they provide beyond air-conditioning and smog benefits. The best programs are probably the information programs that provide data on energy and smog savings of trees to the communities and homeowners that are considering planting trees for other reasons.

5. Conclusions

Cool surfaces (cool roofs and cool pavements) and urban trees can have a substantial effect on urban air temperature and hence can reduce cooling-energy use and smog. We estimate that about 20% of the national cooling demand can be avoided through a large-scale implementation of heat-island mitigation measures. This amounts to 40 TWh/year savings, worth over $4B per year by 2015 in cooling-electricity savings alone. Once the benefits of smog reduction are accounted for, the total savings could add up to over $10B per year.

Achieving these potential savings is conditional on receiving the necessary federal, state, and local community support. Scattered programs for planting trees and increasing surface albedo already exist, but to start an effective and comprehensive campaign would require an aggressive agenda. We are collaborating with the American Society for Testing of Materials (ASTM), the Cool Roof Rating Council (CRRC), and the industry, to create test procedures, ratings, and labels for cool materials. The cool roofs criteria and standards are incorporated into the Building Energy Performance Standards of ASHRAE (American Society of Heating Refrigeration, and Airconditioning Engineers), California Title 24, and the California South Coast's Air Quality Management Plans. Many field projects have demonstrated the energy benefits of cool roofs and shade trees. The South Coast Air Quality Management District and the United States Environmental Protection Agency (EPA) now recognize that air temperature is as much a cause of smog as NO_X or volatile organic compounds. In 1992, the EPA published a milestone guideline for tree planting and light-colored surfacing (Akbari *et al.* 1992). Many countries have joined efforts in developing heat-island-reduction programs to improve urban air quality. The efforts in Japan are of notable interest.

6. Acknowledgement

This work was supported by the Assistant Secretary for Conservation and Renewable Energy, Office of Building Technologies of the U. S. Department of Energy and the California Energy Commission under contract No. DE-AC0376SF00098.

7. References

Akbari, H. 2003. “Measured energy savings from the application of reflective roofs in 2 small non-residential buildings,” *Energy,* **28**:953-967.

Akbari, H., 2002. “Shade trees reduce building energy use and CO_2 emissions from power plants,” *Environmental Pollution,* **116**:S119-S126.

Akbari, H., M. Pomerantz, and H. Taha. 2001. "Cool surfaces and shade trees to reduce energy use and improve air quality in urban areas," *Solar Energy*, **70**(3):295-310.

Akbari, H., S. Konopacki, C. Eley, B. Wilcox, M. Van Geem and D. Parker. 1998a. “Calculations for Reflective Roofs in Support of Standard 90.1,” *ASHRAE Transactions*

104(1):984-995.

Akbari, H., L. Gartland, and S. Konopacki. 1998b. "Measured Energy Savings of Light-colored Roofs: Results from Three California Demonstration Sites," *Proceedings of the 1998 ACEEE Summer Study on Energy Efficiency in Buildings*, Vol. 3, p. 1.

Akbari, H., S. Bretz, D. Kurn, and J. Hanford. 1997. "Peak Power and Cooling Energy Savings of High-Albedo Roofs," *Energy and Buildings* **25**:117-126.

Akbari, H., S. Bretz, H. Taha, D. Kurn, and J. Hanford. 1997. "Peak Power and Cooling Energy Savings of High-albedo Roofs," *Energy and Buildings - Special Issue on Urban Heat Islands and Cool Communities*, **25**(2):117-126.

Akbari, H., S. Davis, S. Dorsano, J. Huang, and S. Winnett (editors). 1992. *Cooling Our Communities: A Guidebook on Tree Planting and Light-Colored Surfacing*, U. S. Environmental Protection Agency, Office of Policy Analysis, Climate Change Division.

Akbari, H., A. Rosenfeld, and H. Taha. 1990. "Summer Heat Islands, Urban Trees, and White Surfaces," *ASHRAE Transactions*, **96**(1), American Society for Heating, Refrigeration, and Air Conditioning Engineers, Atlanta, Georgia.

Akbari, H. and H. Taha. 1992. "The Impact of Trees and White Surfaces on Residential Heating and Cooling Energy Use in Four Canadian Cities," *Energy, the International Journal*, **17**(2):141-149.

Akridge, J. 1998. "High-Albedo Roof Coatings - Impact on Energy Consumption," *ASHRAE Technical Data Bulletin* **14**(2).

Benjamin, M.T., M. Sudol, L. Bloch, and A.M. Winer. 1996. "Low-emitting urban forests: A taxonomic methodology for assigning isoprene and monoterpene emission rates," *Atmospheric Environment*, **30**(9):1437-1452.

Berdahl, P. and S. Bretz. 1997. "Preliminary Survey of the Solar Reflectance of Cool Roofing Materials," *Energy and Buildings - Special Issue on Urban Heat Islands and Cool Communities*, **25**(2):149-158.

Boutwell, C. and Y. Salinas. 1986. "Building for the Future—Phase I: An Energy Saving Materials Research Project," Oxford: Mississippi Power Co., Rohm and Haas Co. and the University of Mississippi.

Bretz, S., H. Akbari, and A. Rosenfeld. 1997. "Practical Issues for Using High-Albedo Materials to Mitigate Urban Heat Islands," *Atmospheric Environment*, **32**(1):95-101.

Bretz, S. and H. Akbari. 1997. "Long-term Performance of High-Albedo Roof Coatings," *Energy and Buildings - Special Issue on Urban Heat Islands and Cool Communities*, **25**(2):159-167.

Bretz, S. and H. Akbari. 1994. "Durability of High-Albedo Roof Coatings," *Proceedings of the ACEEE 1994 Summer Study on Energy Efficiency in Buildings*, Vol. 9, p. 65.

Cominsky, R.J., G.A. Huber, T.W. Kennedy, and M. Anderson. 1994. The Superpave Mix Design Manual for New Construction and Overlays. SHRP-A-407. Washington, DC: National Research Council.

DeWalle D.R., G.M. Heisler, R.E. Jacobs. 1983. "Forest home sites influence heating and cooling energy," *Journal of Forestry*, **81**(2):84-87.

Dunn, B.H. 1996. "What you need to know about slurry seal," Better Roads March 1996: 21-25.

Gartland, L., S. Konopacki, and H. Akbari. 1996. "Modeling the Effects of Reflective Roofing," *Proceedings of the ACEEE 1996 Summer Study on Energy Efficiency in Buildings* **4**:117-124. Pacific Grove, CA.

Goodridge, J. 1989. "Air temperature trends in California, 1916 to 1987," J. Goodridge, 31 Rondo Ct., Chico CA 95928.

Goodridge, J. 1987. "Population and temperature trends in California," *Proceedings of the Pacific Climate Workshop*, Pacific Grove CA, March 22-26.

Hall, J.V., A.M. Winer, M.T. Kleinman, F.M. Lurmann, V. Brajer and S.D. Colome. 1992. "Valuing the Health Benefits of Clean Air," *Science*, **255**: 812-817.

HIG. 2005. Heat Island Group world-wide web: http://HeatIsland.LBL.gov . Lawrence Berkeley National Laboratory, Berkeley, CA.

Heisler, G.M. 1989. "Effects of trees on wind and solar radiation in residential neighborhoods," Final report on site design and microclimate research, ANL No. 058719, Argonne National Laboratory, Argonne, IL.

Hildebrandt, E., W. Bos and R. Moore. 1998. "Assessing the Impacts of White Roofs on Building Energy Loads," *ASHRAE Technical Data Bulletin* **14**(2).

Huang, Y.J., H. Akbari, H. Taha. 1990. "The wind-shielding and shading effects of trees on residential heating and cooling requirements," *ASHRAE Transactions*, **96**(1), American Society of Heating, Refrigeration, and Air conditioning Engineers, Atlanta, Georgia, (February).

Konopacki, S. and H. Akbari. 2002 "Energy savings of heat-island-reduction strategies in Chicago and Houston (including updates for Baton Rouge, Sacramento, and Salt Lake City," Lawrence Berkeley National Laboratory Report LBL-49638, Berkeley, CA.

Konopacki, S. and H. Akbari. 2001. "Measured Energy Savings and Demand Reduction from a Reflective Roof Membrane on a Large Retail Store in Austin," Report number LBNL-47149. Berkeley, CA: Lawrence Berkeley National Laboratory, 2001.

Konopacki, S. and H. Akbari. 2000. "Energy Savings Calculations for Heat Island Reduction Strategies in Baton Rouge, Sacramento and Salt Lake City," Lawrence Berkeley National Laboratory Report LBNL-42890. Berkeley, CA.

Konopacki, S. and H. Akbari. 1998. "Simulated Impact of Roof Surface Solar Absorptance, Attic, and Duct Insulation on Cooling and Heating Energy Use in Single-Family New Residential Buildings," Lawrence Berkeley National Laboratory Report LBNL-41834. Berkeley, CA.

Konopacki, S., H. Akbari, L. Gartland, and L. Rainer. 1998. "Demonstration of Energy Savings of Cool Roofs," Lawrence Berkeley National Laboratory Report LBNL-40673. Berkeley, CA.

Konopacki, S., H. Akbari, S. Gabersek, M. Pomerantz, and L. Gartland. 1997. "Cooling Energy Saving Potentials of Light-Colored Roofs for Residential and Commercial Buildings in 11 U.S. Metropolitan Areas," Lawrence Berkeley National Laboratory Report LBNL-39433,

Berkeley, CA.

Levinson, R., P. Berdahl, and H. Akbari. 2005a. “Solar spectral optical properties of pigments, part I: Model for deriving scattering and absorption coefficients from transmittance and reflectance measurements,” *Solar Energy Materials & Solar Cells* (in press).

------. 2005b. “Solar spectral optical properties of pigments, part II: Survey of common colorants,” *Solar Energy Materials & Solar Cells* (in press).

McPherson, E.G., D.J. Nowak, and R.A. Rowntree. 1994. "Chicago's urban forest ecosystem: results of the Chicago Urban Forest Climate Project," Forest Service, U. S. Dept. of Agriculture. NE-186.

Milford, J.B., G.R. Armistead, and G.J. McRae. 1989. "A New Approach to Photochemical Pollution Control: Implications of Spatial Patterns in Pollutant Responses to Reduction in Nitrogen Oxides and Reactive Organic Emissions," *Environmental Science and Technology*, **23**, pp. 1290-1301.

Parker, D., J. Huang, S. Konopacki, L. Gartland, J. Sherwin, and L. Gu. 1998. “Measured and Simulated Performance of Reflective Roofing Systems in Residential Buildings,” *ASHRAE Transactions* **104**(1):963-975.

Parker, D., J. Sonne, and J. Sherwin. 1997. “Demonstration of Cooling Savings of Light Colored Roof Surfacing in Florida Commercial Buildings: Retail Strip Mall,” Florida Solar Energy Center Report FSEC-CR-964-97. Cocoa, FL.

Parker, J. H. 1981. "Use of landscaping for energy conservation," Department of Physical Sciences, Florida International University, Miami, Florida.

Pomerantz, M., H. Akbari, A. Chen, H. Taha, and A.H. Rosenfeld. 1997. "Paving Materials for Heat Island Mitigation," Lawrence Berkeley National Laboratory Report LBNL-38074. Berkeley, CA

Rosenfeld, A.H., J.J. Romm, H. Akbari, and M. Pomerantz. 1998. "Cool Communities: Strategies for Heat Islands Mitigation and Smog Reduction," *Energy and Buildings*, **28**, pp. 51-62.

Rosenfeld A., H. Akbari, H. Taha, and S. Bretz. 1992. "Implementation of Light-Colored Surfaces: Profits for Utilities and Labels for Paints," *Proceedings of the ACEEE 1992 Summer Study on Energy Efficiency in Buildings*, Vol. 9, p. 141.

Simpson J.R. and E.G. McPherson. 1997. “The Effect of Roof Albedo Modification on Cooling Loads of Scale Residences in Tucson, Arizona,” *Energy and Buildings*; **25**:127–137.

Taha, H. 1997. "Modeling the impacts of large-scale albedo changes on ozone air quality in the South Coast Air Basin," *Atmospheric Environment*, **31**(11):1667-1676.

Taha, H. 1996. "Modeling the Impacts of Increased Urban Vegetation on the Ozone Air Quality in the South Coast Air Basin," *Atmospheric Environment*, **30**(20):3423-3430.

Taha, H., S. Douglas, and J. Haney. 1994. "The UAM Sensitivity Analysis: The August 26-28 1987 Oxidant Episode," Chapter 1 in "Analysis of Energy Efficiency and Air Quality in the South Coast Air Basin - Phase II", by H. Taha *et al*., Lawrence Berkeley Laboratory Report LBL-35728, Berkeley, CA.

Taha, H., S. Douglas, J. Haney, A. Winer, M. Benjamin, D. Hall, J. Hall, X. Liu, and B. Fishman. 1995. "Modeling the ozone air quality impacts of increased albedo and urban forest in the South Coast Air Basin," Lawrence Berkeley Laboratory Report LBL-37316, Berkeley, CA.

Taha, H., S. Konopacki, and S. Gabersek. 1996. "Modeling the Meteorological and Energy Effects of Urban Heat Islands and their Mitigation: A 10-Region Study," Lawrence Berkeley Laboratory Report LBL-38667, Berkeley, CA.

Taha, H., S. Douglas, and J. Haney. 1997. "Mesoscale meteorological and air quality impacts of increased urban albedo and vegetation," *Energy and Buildings - Special Issue on Urban Heat Islands and Cool Communities*, **25**(2):169-177.

Yoder, E.J. and M.W. Witzak. 1975. *Principles of Pavement Design*, New York, NY: Wiley and Sons.

Solar Spectral Optical Properties of Pigments

Ronnen Levinson, Ph.D.

Paul Berdahl, Ph.D.

Hashem Akbari, Ph.D.

Owners of homes with pitched roofs visible from ground level often prefer non-white roofing products for aesthetic considerations. This paper reports on a collaborative research between a U.S. national laboratory and the industry for developing cool colored materials for sloped roofs. The suitability of a pigment for inclusion in “cool” colored coatings with high solar reflectance can be determined from its solar spectral backscattering and absorption coefficients. Pigment characterization is performed by dispersing the pigment into a transparent film and then measuring spectral transmittance and reflectance. Measurements of the reflectance of film samples on black and white substrates are also used. Various pigments are characterized by determination of absorption and backscattering coefficients as functions of wavelength in the solar spectral range of 300 to 2500 nanometers. Pigments in widespread use are examined, with particular emphasis on those that may be useful for formulating non-white materials that can reflect the near-infrared (NIR) portion of sunlight, such as the complex inorganic color pigments (mixed metal oxides). These materials remain cooler in sunlight than comparable colors. NIR-absorptive pigments are to be avoided. High NIR reflectance can be produced by a reflective metal substrate, an NIR-reflective underlayer, or directly by using of a pigment that scatters strongly in the NIR.

Solar Spectral Optical Properties of Pigments[1]

Owners of homes with pitched roofs visible from ground level often prefer non-white roofing products for aesthetic considerations. This paper reports on a collaborative research between a U.S. national laboratory and the industry for developing cool colored materials for sloped roofs. The suitability of a pigment for inclusion in "cool" colored coatings with high solar reflectance can be determined from its solar spectral backscattering and absorption coefficients. Pigment characterization is performed by dispersing the pigment into a transparent film and then measuring spectral transmittance and reflectance. Measurements of the reflectance of film samples on black and white substrates are also used. Various pigments are characterized by determination of absorption and backscattering coefficients as functions of wavelength in the solar spectral range of 300 to 2500 nanometers. Pigments in widespread use are examined, with particular emphasis on those that may be useful for formulating non-white materials that can reflect the near-infrared (NIR) portion of sunlight, such as the complex inorganic color pigments (mixed metal oxides). These materials remain cooler in sunlight than comparable colors. NIR-absorptive pigments are to be avoided. High NIR reflectance can be produced by a reflective metal substrate, an NIR-reflective underlayer, or directly by using of a pigment that scatters strongly in the NIR.

INTRODUCTION

Nonwhite pigments with high near-infrared (NIR) reflectance historically have been used to camouflage military surfaces (by mimicking foliage) and to minimize solar heating of dark exterior architectural surfaces, such as colored vinyl siding and gray battleship hulls (Brade and Wake, 1992; Burkhart et al., 2001;Sliwinski et al., 2001). In recent years roofing manufacturers have incorporated NIR-reflecting pigments in coatings applied to a variety of nonwhite roofing products, such as metal panels and clay tiles (Nixon, 2003; Ferro, 2004; Shepherd, 2004; BASF, 2004; Custom-Bilt, 2004; MCA, 2004). In this paper we compute the solar spectral absorption and backscattering coefficients of a wide variety of pigments that may be used in architectural coatings.

Visible light (400 to 700 nanometers) accounts for only 43% of the energy in the air-mass 1.5 global solar irradiance spectrum (300 to 2500 nm) typical of North-American insolation (ASTM, 2003); the remainder arrives as near-infrared (700 to 2500 nm, 52%) or ultraviolet (300 to 400 nm, 5%) radiation (Figure). Hence, replacing NIR-absorbing ("conventional") roofing with visually similar, infrared-reflecting ("cool") roofing can significantly reduce building heat gain.

A cool coating must have low visible transmittance to hide its background and low NIR absorptance to minimize NIR heat gain. Cool films may be subclassified as either "NIR-reflecting" or "NIR-transmitting." An NIR-reflecting film is always cool, while an NIR-transmitting film requires an NIR-reflecting background (e.g., a shiny metal or a white coating) to form a colored NIR-reflecting composite (Brady and Wake, 1992; Genjima and Mockizuki, 2003).

A paint is a dispersion of pigment particles (e.g., titania) in a clear binder, such as acrylic. The propagation of light through pigmented coatings is of natural interest to the coating and colorant industries and has been extensively studied over the past century. One of the simplest and most popular continuum models is the two-flux theory introduced by Schuster in 1905 and popularized by Kubelka and Munk (Kubelka, 1948; Kortum, 1969; Bohren, 1987; Judd, 1952; Johnson, 1988). The Kubelka-Munk (K-M)

[1] Ronnen Levinson, Ph.D. is scientist, Environmental Energy Technologies Division, Lawrence Berkeley National Laboratory. Paul Berdahl, Ph.D. is applied solid-state physicist, Environmental Energy Technologies Division, Lawrence Berkeley National Laboratory. Hashem Akbari, Ph.D. is staff scientist and Heat Island Group leader, Environmental Energy Technologies Division, Lawrence Berkeley National Laboratory.

model describes the one-dimensional, bidirectional propagation of diffuse light through a film by parameterizing the rates at which the film absorbs and/or backscatters light.

We compute absorption and backscattering coefficients from spectrometer measurements of film reflectance and transmittance. We examine 87 pigmented coatings, identifying both cool pigments — i.e., those that can be used to make NIR-reflecting or NIR-transmitting cool coatings — and pigments that should be excluded from cool coatings. Our goal is to provide complete solar spectral absorption and backscattering coefficients describing a large palette of pigments potentially usable for architectural coatings.

This summary paper highlights major results of our pigment characterization research. The theory, experimental procedure, and the measured and computed spectral properties of the pigments are fully detailed in Levinson et al. (2005a,b).

We note that our study concerns only the solar radiative properties of roof coatings. Thermal radiative properties, mechanical durability, and lightfastness are generally outside its scope.

THEORY

The purpose of our measurements and model of radiant transfer in single-pigment coatings is to obtain backscattering and absorption coefficients *S* and *K* that approximately characterize the pigment. High precision is not the goal, but a reliable general characterization of each individual pigment is. We cover the solar spectral region from 300 to 2500 nm at 5-nm intervals. Each wavelength is treated independently of all others except for the use of the forward scattering ratio. Since the K-M model applies to diffuse illumination, whereas we are using collimated radiation, the treatment may be expected to be more accurate in strongly scattering films in which a fully diffuse radiation field quickly develops. However, we have used a formulation in which a non-scattering pigment (e.g., a dye) is assigned a *K* value approximating Beer's law for diffuse radiation traversing a slab. In summary, we are not expecting precise characterization, but expect to extract consistent, reliable and practical information for each pigment.

The one-dimensional propagation of light through a coating is approximated by the two-flux Kubelka-Munk (K-M) theory, in which downward and upward beams can be absorbed and/or backscattered as they traverse the film. All light in the film is assumed to be diffuse (subscript *d*), either because the film is diffusely illuminated, or because the film is strongly scattering. The downward diffuse flux $i_d(z)$ and upward diffuse flux $j_d(z)$ within the film are modelled by

$$-\frac{di_d}{dz} = -(K+S)\,i_d + S\,j_d \tag{1}$$

$$-\frac{dj_d}{dz} = -(K+S)\,j_d + S\,i_d \tag{2}$$

where *K* and *S* are coefficients of absorption and backscattering, respectively. The fluxes and coefficients are wavelength specific.

Our theory and algorithm for computing the coefficients *K* and *S* from measurements of the reflectance and transmittance of pigmented coatings in contact with air (i.e., paint films in a spectrometer) are detailed in Levinson et al. (2005a).

EXPERIMENT

The optical properties of 87 pigment films — 4 white, 21 black or brown, 14 blue or purple, 11 green, 9 red or orange, 14 yellow and 14 pearlescent — were characterized by computing spectral K-M coefficients and non-spectral forward scattering ratios from spectral measurements of film reflectance and transmittance. Our methodology is detailed in Levinson et al. (2005a).

PIGMENT CLASSIFICATION

For convenience in presentation, the pigments were grouped by color "family" (e.g., green) and then categorized by chemistry (e.g., chromium oxide green). Some families span two colors (e.g., black/brown) because it is difficult to consistently identify color based on pigment name and color index (convention for identifying colorants (Society of Dyers and Colorists and American Association of Textile Chemists and Colorists, 2004). For example, a dark pigment may be marketed as "black," but carry a "pigment brown" color index designation and exhibit red tones more characteristic of brown than of black. Pigment categories are presented in the order of simpler inorganics, more complex inorganics and then finally organics. Each member of a color family is assigned an identification code X*nn*, where X is the color family abbreviation and *nn* is a serial number. For example, the 11 members of the green color family ("G") have identification codes G01 through G11.

The same pigment may be present in more than one pigmented film. For example, our survey includes four titanium dioxide white films (W01-W04). However, the concentration of pigment, pigment particle size and/or source of the pigment (manufacturer) may vary from film to film.

PIGMENT PROPERTIES BY COLOR AND CATEGORY

Table 1 summarizes some relevant bulk properties of the pigmented films in each category, such as NIR reflectances over black and white backgrounds. The measured and computed spectral properties of each pigmented film (reflectance, transmittance, absorptance, absorption coefficient and scattering coefficient) are charted in Levinson et al. (2005b). Space limitations preclude the presentation of spectral charts in te current paper.

When examining spectral optical properties, it is worth noting that most of the NIR radiation in sunlight arrives at the shorter NIR wavelengths. Of the 52% of solar energy delivered in the NIR spectrum (700 - 2500 nm), 50% lies within 700 - 1000 nm; 30% lies within 1000 - 1500 nm; and 20% lies within 1500 - 2500 nm (Figure 1). We refer to the 700 - 1000 nm region containing half the NIR solar energy (and a quarter of the total solar energy) as the "short" NIR.

In the discussions below, black and white *backgrounds* are assumed to be opaque, with observed NIR reflectances of 0.04 and 0.87, respectively. Note that in the absence of the air-film interface, the continuous refractive index (CRI) NIR reflectances of the black and white backgrounds are 0.00 and 0.94, respectively.

Note that the descriptions of pigments as "hot" or "cool" in the following are only qualitative, in the sense that a pigmented coating with a high NIR absorptance (approaching 1) is hot, and a pigmented coating with a low NIR absorptance (approaching 0) is cool. We are not aware of any official standards by which pigments can be designed cool or hot.

The NIR absorptances of the various pigmented coatings are quantitatively compared at the end of this section.

White

All four whites were titanium dioxide (TiO_2) rutile. Other white pigments (not characterized in this study) include zinc oxide, zinc sulfide, antimony oxide, zirconium oxide, zirconium silicate (zircon) and the anatase phase of TiO_2.

TiO_2 rutile is a strongly scattering, weakly absorbing, stable, inert, nontoxic, inexpensive and hence extremely popular white pigment(Lewis, 1998). TiO_2 whites W01 - W04 exhibit similar curves of strong backscattering and weak absorption in the visible and NIR, except for drops in backscattering around 1500-2000 nm seen for W03 and W04. These last two samples are undiluted and 12:1 diluted versions of the same artist color.

Physically, the light scattering is due to the difference between the refractive index of the rutile particles (2.7) and that of the surrounding transparent medium (1.5). At high pigment volume concentrations, the presence of numerous nearby rutile particles raises the effective refractive index of the surrounding medium and thereby reduces the efficiency of scattering. This fall in scattering efficiency is termed pigment crowding (Blakey and Hall, 1998).

Rutile is a direct bandgap semiconductor and therefore has a very abrupt transition from low absorption to high absorption that occurs at 400 nm, the boundary between the visible and ultraviolet regions. For wavelengths below 400 nm (photon energies above 3.1 eV), the absorption is so strong that our data saturate, except in the case of the highly dilute (2% PVC) sample W04. At wavelengths above 400 nm, absorption is weak; most of the spectral features may be attributed to the binders used. One of the four white pigments (W01) has a slightly less abrupt transition at 400 nm — there is an absorption “tail” near the band edge. This type of behavior is likely due to impurities in the TiO_2.

The sharp rise in absorptance near 300 nm shown for some films, such as W04, is an artifact due to the use of a polyester substrate.

Black/Brown

Carbon Black, Other Non-Selective Black.

Carbon black, bone black (10% carbon black + 84% calcium phosphate), copper chromite black ($CuCr_2O_4$) and synthetic iron oxide black (Fe_3O_4 magnetite) (B01 - B04) are weakly scattering pigments with strong absorption across the entire solar spectrum. Carbon black B01 is the most strongly absorbing, but all four are “hot” pigments.

Most non-selective blacks are metallic in nature, with free electrons permitting many different allowed electronic transitions and therefore broad absorption spectra. Carbon black is a semi-metal that has many free electrons, but not as many as present in highly conductive metals. Both the iron oxide (magnetite) and copper chromite blacks are (electrically conducting) metals.

Chromium Iron Oxide Selective Black.

Chromium iron oxide selective blacks (B05 - B11) are mixed metal oxides (chromium green-black hematite, chromium green-black hematite modified, chromium iron oxide, or chromium iron nickel black spinel) formulated to have NIR reflectance significantly higher than carbon and other non-selective blacks. Some, such as chromium green-black hematite B06, appear more brown than black. While these pigments have good scattering in the NIR, with a backscattering coefficient at 1000 nm about half that of TiO_2 white, they are also quite absorbing ($K \sim 50$ mm^{-1}) in the short NIR. These pigments are visibly hiding (opaque to visible radiation) and NIR transmitting, so use of a white background improves their NIR reflectances without significantly changing their appearances.

Pure chromium oxide green (Cr_2O_3), pigment green 17, has the hematite crystal structure and will be discussed further together with other green pigments. When some of the chromium atoms are replaced by iron, a dark brownish black with the same crystal structure is obtained — i.e., a traditional cool black pigment (e.g., B06-B11; B05 differs because it contains nickel and has a spinel structure). It is sometimes designated as Cr-Fe hematite (Swiler, 2002) or chromium green-black hematite (DCMA, 1991) and has been used to formulate infrared-reflective vinyl siding since about 1984 (Rabonovitch and Summers, 1984). A number of modern recipes for modified versions of this basic cool black incorporate minor amounts of a variety of other metal oxides. One example is the use of a mixture of 93.5 g of chromium oxide, 0.94 g of iron oxide, 2.38 g of aluminum oxide and 1.88 g of titanium oxide (Sliwinski et al., 2001). The mixture is calcined at about 1100°C to form hematite-structure crystallites of the resulting mixed metal oxide.

Organic Selective Black.

Perylene black (B12) is a weakly scattering, dyelike organic pigment that absorbs strongly in the visible and very weakly in the NIR. Its sharp absorption decrease at 700 nm gives this pigment a jet black appearance and an exceptionally high NIR reflectance (0.85) when applied over white. Perylene pigments exhibit excellent lightfastness and weatherfastness, but their basic compound (dianhydride of tetracarboxylic acid) may or may not be fast to alkali; Herbst and Hunger (1993) and Lewis (1988) disagree on the latter point.

Iron Oxide Brown.

Iron oxide browns (B13 - B15) such as burnt sienna, raw sienna and raw umber exhibit strong absorption in part of the visible spectrum and low absorption in the NIR. These can provide effective cool brown coatings if given a white background, though this will make some (e.g., burnt sienna B13) appear reddish. These browns are “natural” and can be expected to contain various impurities.

Other Brown.

Other browns characterized (B16 - B21) include iron titanium (Fe-Ti) brown spinel, manganese antimony titanium buff rutile and zinc iron chromite brown spinel. These mixed-metal oxides have strong absorption in most or all of the visible spectrum, plus weak absorption and modest scattering in the NIR. A white undercoating improves the NIR reflectance of all browns, but brings out red tones in iron titanium brown spinels B16 and B17.

The cool Fe-Ti browns (B16 - B18) have spinel crystal structure and basic formula Fe_2TiO_4 (DCMA, 1991; Brabers, 1995). Despite the presence of Fe^{2+} ions, the infrared absorption of this material is weak. (In many materials, the Fe^{2+} ion is associated with infrared absorption (Glebov and Boulos, 1998; Clark, 1999); see also our data for Fe_3O_4 in Levinson et al. (2005b). The current data demonstrate that the absorption spectra also depend on the environment of the Fe^{2+} ion.) We also note that while B17 and B18 are nominally the same material, the details of the absorption are different.

We have not yet characterized a synthetic iron oxide hydrate brown (e.g., FeOOH).

Blue/Purple

Cobalt Aluminate Blue, Cobalt Chromite Blue.

Cobalt aluminate blue (nominally $CoAl_2O_4$, but usually deficient in Co (Buxbaum, 1998) U01 - U05) and cobalt chromite blue ($Co[Al,Cr]_2O_4$; U06 - U09) derive their appearances from modest scattering (S ~ 30 mm^{-1}) in the blue (400 - 500 nm) and strong absorption (K ~ 150 mm^{-1}) in the rest of the visible spectrum. They have very low absorption in the short NIR, but exhibit an undesirable absorption band in

the 1200 - 1600 nm range, which contains 17% of the NIR energy. A white background dramatically increases NIR reflectance but makes some (e.g., cobalt aluminum blue spinel U02) much lighter in color.

Iron Blue.

Iron (a.k.a. Prussian or Milori) blue (U10) is a weakly scattering pigment with strong absorption in the visible and short NIR and weak absorption at longer wavelengths. It appears black and has little NIR reflectance over a black background, but looks blue and achieves a modest NIR reflectance (0.25) over a white background. It is not ideal for cool coating formulation.

Ultramarine Blue.

Ultramarine blue (U11), a complex silicate of sodium and aluminum with sulfur, is a weakly scattering pigment with some absorption in the short NIR. If sparingly used, it can impart absorption in the yellow spectral region without introducing a great deal of NIR absorption. This is a durable inorganic pigment with some sensitivity to acid (Lewis, 1988).

While most colored inorganic pigments contain a transition metal such as Fe, Cr, Ni, Mn, or Co, ultramarine blue is unusual. It is a mixed oxide of Na, Si and Al, with a small amount of sulfur ($Na_{\{7.5\}}Si_6Al_6O_{\{24\}}S_{\{4.5\}}$). The metal oxide skeleton forms an open clathrate sodalite structure that stabilizes $S_{3^{\wedge}-}$ ions in cages to form the chromophores (Buxbaum, 1998: s. 3.5; Clark and Cobbold, 1978). Thus isolated S_3 molecules with an attached unpaired electron cause the light absorption in the 500-700 nm range, producing the blue color. The refractive index of ultramarine blue is not very different from the typical matrix value of 1.5 (Buxbaum, 1998: s. 3.5), so the pigment causes little scattering.

Phthalocyanine Blue.

Copper phthalocyanine blue (U12 - U13) is a weakly scattering, dyelike pigment with strong absorption in the 500 - 800 nm range and weak absorption in the rest of the visible and NIR. Phthalo blue appears black and has minimal NIR reflectance over a black background, but looks blue and achieves a high NIR reflectance (0.63) over a white background (U12). It is durable and lightfast, but as an organic pigment it is less chemically stable than (high temperature) calcined mixed metal oxides such as the cobalt aluminates and chromites.

General information on the structure and properties of phthalocyanines is available in Mckeown (1998). The refractive index varies with wavelength and exceeds 2 in the short wavelength part of the infrared spectrum (Wilbrandt et al., 1996). Therefore the weak scattering we observe in our samples indicates that the particle size is quite small. The pigment handbook indicates a typical particle diameter of 120 nm (Lewis, 1988), which is consistent with our data.

Dioxazine Purple.

Dioxazine purple (U14) is an organic optically similar to phthalo blue, but even more absorbing in the visible and less absorbing in the NIR. It is nearly ideal for formulation of dark NIR-transparent layers, but is subject to the chemical stability considerations noted above for phthalo blue.

Green

Chromium Oxide Green, Modified Chromium Oxide Green.

Chromium oxide green Cr_2O_3 (G01 - G02) exhibits strong scattering alternating with strong absorption across the visible spectrum and strong scattering and mild absorption in the NIR. Since the pigment is almost opaque in the visible, a thin layer of chromium oxide green over a white background yields a medium-green coating with good NIR reflectance (0.57 for 13-µm thick film G02). The modified chromium

oxide green (G03) is mostly chromium oxide, with small amounts of iron oxide, titanium dioxide and aluminum oxide (Sliwinski et al., 2001). A layer of the modified chromium oxide green over a white background produces a medium green with excellent NIR reflectance (0.71).

Cr_2O_3 green is often mentioned as an infrared-reflective pigment that is useful for simulating the high infrared reflectance of plant leaves. Indeed, a high NIR reflectance is observed. However, our data for sample films G01 and G02 do show that there is a broadband absorption of about 10 mm^{-1} in the near-infrared. While our measurements of absorptance coefficient are not precise for low absorptances (Levinson et al., 2005a), this value is clearly distinct from zero. Pure Cr_2O_3, fired in air, tends to become slightly rich in oxygen, which results in p-type semiconducting behavior (de Cogan and Lonergan, 1974; Goodenough, 1984). Thus it is possible that the broadband IR absorption of Cr_2O_3 is due to free carrier absorption by mobile holes. de Cogan and Lonergan (1974) also report that doping with Al can reduce the p-type conductivity in Cr_2O_3, so it seems likely that doping with Al and/or certain other metals can also reduce the IR absorption.

The modified chromium oxide green G03 is similar to G01 and G02 Cr_2O_3. However its green reflectance peak at 550 nm is somewhat smaller and its infrared absorption is clearly much smaller than those of samples G01 and G02.

Cobalt Chromite Green.

Cobalt chromite green (G04 - G06) is similar to cobalt chromite blue and is commonly used for military camouflage.

Cobalt Titanate Green.

Cobalt titanate green (G07 - G09) is similar to cobalt chromite green, but scatters more strongly across the entire solar spectrum and has a pronounced absorption trough around 500 nm. A white background makes cobalt teal G07 very NIR reflective (0.73) but also appear light blue (hence, the name teal). The other two cobalt titanate greens (G08, G09) have respectable NIR reflectances (0.47, 0.37) over white and appear medium green.

Phthalocyanine Green.

Phthalocyanine green (G10 - G11) is similar to phthalocyanine blue, but absorbs more strongly in the short NIR. Hence, the NIR reflectance of a thin phthalo green film over white, while respectable, is only 70% of that achieved by a thin layer of phthalo blue over white (0.45 for G10 vs. 0.63 for U12).

Red/Orange

Iron Oxide Red.

Iron oxide red (R01 - R04) derives its appearance from weak scattering and very strong absorption in the 400 - 600 nm band. One of the iron oxide reds (R01) exhibits moderate absorption across the NIR that may be due to doping of the Fe_2O_3 hematite crystals with impurities or result from broadband absorbing impurity phases such as Fe_3O_4; it is not a cool pigment. However, the remaining three iron oxide reds weakly absorb in the NIR and present both a dark red appearance and good NIR reflectance (0.53 - 0.67) over a white background. R02 also has a respectable NIR reflectance (0.38) over a black background and has backscattering *S* comparable with TiO_2 white in the NIR.

Cadmium Orange.

Cadmium orange (R05) has weak scattering and very strong absorption in the 400 - 600 nm band, followed by strong scattering and virtually no absorption at longer wavelengths. Applied over a white

background, it appears bright orange and has very high NIR reflectance (0.87) — essentially the same as that of the white background. Cadmium orange (and cadmium yellow, below) are Cd(S,Se) direct bandgap semiconductors. They exhibit sharp transitions between absorbing and non-absorbing regions and have high refractive indices (e.g., 2.5 for CdS) that lead to large scattering coefficients. However, sensitivity to acid and the toxicity of cadmium limit their applications.

Organic Red.

Organic red pigments (R06 - R09) such as acra burnt orange, acra red, monastral red and naphthol red light have weak scattering and strong (sometimes very strong) absorption up to 600 nm, followed by very weak absorption and moderate-to-weak scattering at longer wavelengths. As a result they yield a medium-red color and a very high NIR reflectance (0.83 - 0.87) when applied over a white background. Masstones of acra burnt orange, acra red and naphthol red light are all lightfast; their tints are slightly less so (Lewis, 1988}.

Yellow

Iron Oxide Yellow.

Iron oxide yellow FeOOH (Y01) is a brownish yellow similar to iron oxide red. It appears tan and has a high NIR reflectance (0.70) when applied over a white background.

Cadmium Yellow.

Cadmium yellow (Y02) is similar to cadmium orange. It appears bright yellow and has very high NIR reflectance (0.87) over white.

Chrome Yellow.

Chrome yellow $PbCrO_4$ (Y03) is optically similar to cadmium yellow but exhibits a more gradual reduction in absorptance. It appears bright yellow and achieves a high NIR reflectance (0.83) over white. In some applications, the presence of lead and/or the Cr(VI) ion impose limitations.

Chrome Titanate Yellow.

Chrome titanate yellow (Y04 - Y07) is similar to chrome yellow, but scatters more strongly in the NIR. Its scattering coefficient can exceed 100 mm^{-1} in the short NIR, suggesting that this pigment might be used in place of titanium dioxide white to provide a background of high NIR reflectance. Over a black background, chrome titanate yellow appears brown to green and has moderate to high NIR reflectance (0.26 - 0.62). Over white, it appears orange to yellow and has very high NIR reflectance (0.80 - 0.86). Y07 over black produces a medium brown with NIR reflectance 0.62.

The curves for Y04 and Y05 illustrate how the backscattering coefficient *S* varies with particle size (manufacturer data). For smaller particles, the decrease in *S* with increasing wavelength is more dramatic.

Nickel Titanate Yellow.

Nickel titanate yellow (Y08 - Y11) is similar to chrome titanate yellow. Note that these compounds usually also contain antimony in their formulation. Over white, it appears a muted yellow and yields very high NIR reflectance (0.77-0.87); over black, it appears yellowish green and achieves moderate to high NIR reflectance (0.22 - 0.64). Y11 is a particularly good candidate to use over black.

Strontium Chromate Yellow + Titanium Dioxide.

Strontium chromate yellow (solids mass fraction 11%) mixed with titanium dioxide (solids mass fraction 9%) in a paint primer (Y12) appears greenish brown over a black background and pale yellow over a white background. It has very low absorption (order 1 mm^{-1}) and strong scattering (order 100 mm^{-1}) at 1000 nm, giving it a good NIR reflectance over black (0.38) and a very high NIR reflectance over white (0.86).

Hansa Yellow, Diarylide Yellow.

Hansa yellow (Y13) and diarylide yellow (Y14) are weakly scattering, dyelike organic pigments with high absorption below 500 nm and very weak absorption elsewhere. Over white, they appear bright yellow and orange-yellow, respectively and yield very high NIR reflectance (0.87).

Pearlescents

Mica + Titanium Dioxide.

Mica flakes coated with titanium dioxide (P01 - P09) exhibit strong scattering and weak absorption, producing their colors (e.g., gold, blue, green, orange, red, violet, or bright white) via thin-film interference. Some have scattering coefficients exceeding 100 mm^{-1} in the near infrared. Over white, they appear white and have very high NIR reflectance (0.88 - 0.90); over black, they achieve their named colors and have high NIR reflectance (0.35 - 0.54). The NIR reflectance of a pearlescent film over an opaque white background can exceed that of the background.

Mica + Titanium Dioxide + Iron Oxide.

Mica flakes coated with titanium dioxide and iron oxide (P10 - P14) are in most cases similar to mica flakes coated with only titanium dioxide, but are more absorbing, less scattering, darker and somewhat less reflecting in the NIR. The exception is rich bronze P13, which has very high absorption and would not make a suitable cool pigment.

Aluminum + Iron Oxide + Silicon Oxide

While not characterized in the current study, the solar spectral reflectances of single-layer (iron oxide Fe_2O_3) or double layer (Fe_2O_3 on silicon dioxide SiO_2) interference coatings on aluminum flakes are presented in Smith et al. (2003a,b).

Cool and Hot Pigments

A simple way to evaluate the utility of a pigmented coating for “cool” applications is to consider its NIR absorptance and NIR transmittance. If the NIR absorptance is low, the pigment is cool. However, a cool pigment that has high NIR transmittance will require an NIR-reflective background (typically white or metallic) to produce an NIR-reflecting coating. Charts of the NIR absorptance and transmittance of the members of each color family are shown in Figure 2. An ideal cool pigment would appear near the lower left corner of the chart, indicating that it is weakly absorbing, weakly transmitting and thus strongly reflecting in the NIR. Pigments appearing higher on the left side of the chart will form a cool coating if given an NIR-reflective background. Use of pigments appearing toward the right side of the chart (i.e., those with strong NIR absorption) should be avoided in cool applications. It should be noted that these charts do not provide perfect comparisons of “cool” performance because they show the NIR properties of films of varying thickness (10 – 37 μm) and visible hiding (visible transmittance 0 - 0.43 for non-pearlescents and 0.02 - 0.54 for the pearlescents). Black-filled circles indicate visible transmittance less than 0.1; gray-filled circles, between 0.1 and 0.3; and white-filled circles, above 0.3.

There are cool films in the white, yellow, brown/black, red/orange, blue/purple and pearlescent families with NIR absorptance less than 0.1. These films have moderate to high NIR transmittances (0.25 - 0.85), indicating than they would require an NIR-reflective background to perform well. There are also other slightly less cool black/brown, blue/purple, green, red/orange, yellow and pearlescent films with NIR absorptance less than 0.2. These have somewhat lower NIR transmittances (0.20 - 0.70), but are still far from NIR-opaque. A handful of pearlescent, blue/purple and red/orange films, along with half a dozen brown/black films, have NIR absorptances exceeding 0.5 and may considered warm. A few nonselective blacks with NIR absorptance approaching unity may be considered hot.

Other useful metrics for “coolness” are NIR reflectances over white and black backgrounds (Table 1). Over a white background, the coolest pigments — i.e., those with NIR reflectances of at least 0.7 — include members of the pearlescent, white, yellow, black/brown, red/orange and blue/purple color families: mica coated w/titanium dioxide (0.88-0.90), titanium dioxide white (0.87-0.88), cadmium yellow (0.87), cadmium orange (0.87), Hansa yellow (0.87), diarylide yellow (0.87), organic selective black (0.85), organic red (0.83-0.87), dioxazine purple (0.82), chrome titanate yellow (0.80-0.86), nickel titanate yellow (0.77-0.87), modified chromium oxide green (0.71) and iron oxide yellow (0.70). Other pigments with NIR reflectances of at least 0.5 include members of the blue/purple, black/brown and green color families: cobalt aluminum blue (0.62-0.70), cobalt chromite blue (0.55-0.70), phthalo blue (0.55-0.63), cobalt chromite green (0.58-0.64), ultramarine blue (0.52), chromium oxide green (0.50-0.57) and other brown (0.50-0.74). Over a black background, the coolest pigments — in this case, those with NIR reflectances of at least 0.3 — include members of the white, yellow, black/brown, red/orange, pearlescent and green color families: titanium dioxide white (0.24-0.65), nickel titanate yellow (0.22-0.64), chrome titanate yellow (0.26 - 0.62), mica coated w/titanium dioxide (0.35-0.54), mica + titanium dioxide + iron oxide, chromium oxide green (0.33-0.40), other brown (0.22-0.40), strontium chromate yellow + titanium dioxide (0.38), iron oxide red (0.19-0.38), chromium iron oxide selective black (0.11-0.35) and cobalt titanate green (0.21-0.30).

CONCLUSIONS

Our characterizations of the solar spectral optical properties of 87 predominately single-pigment paint films with thicknesses ranging from 10 to 37 μm have identified cool pigments in the white, yellow, brown/black, red/orange, blue/purple and pearlescent color groupings with NIR absorptances less than 0.1, as well as other pigments in the black/brown, blue/purple, green, red/orange, yellow and pearlescent groupings with NIR absorptances less than 0.2. Most are NIR transmitting and require an NIR-reflecting background to form a cool coating. Over an opaque white background, some pigments in the pearlescent, white, yellow, red/orange, green and blue/purple families offer NIR reflectances of at least 0.7, while other pigments in the blue/purple, black/brown and green color families have NIR reflectances of at least 0.5. A few members of the white, yellow, pearlescent and green color families have NIR scattering sufficiently strong to yield NIR reflectances of at least 0.3 (and up to 0.64) over a black background.

Use of pigments with NIR absorptances approaching unity (e.g., nonselective blacks) should be minimized in cool coatings, as might be the use of certain pearlescent, blue/purple, green and red/orange and brown/black pigments with NIR absorptances exceeding 0.5.

ACKNOWLEDGEMENTS

This work was supported by the California Energy Commission (CEC) through its Public Interest Energy Research Program (PIER), by the Laboratory Directed Research and Development (LDRD) program at Lawrence Berkeley National Laboratory (LBNL), and by the Assistant Secretary for Renewable Energy under Contract No. DE-AC03-76SF00098. The authors wish to thank CEC Commissioner Arthur Rosenfeld and PIER program managers Nancy Jenkins and Chris Scruton for their support and advice. Special thanks go also to Mark Levine, director of the Environmental Energy Technologies Division at LBNL, and Stephen Wiel, head of the Energy Analysis Department at LBNL, for their encouragement and support in the initiation of this project. We also wish to thank the following people for their assistance: Kevin Stone and Melvin Pomerantz, LBNL; Michelle Vondran, John Buchko, and Robert Scichili, BASF

Corporation; Richard Abrams, Robert Blonski, Ivan Joyce, Ken Loye, and Ray Wing, Ferro Corporation; Tom Steger and Jeffrey Nixon, Shepherd Color Company; and Robert Anderson, Liquitex Artist Materials.

REFERENCES

ASTM (American Society for Testing and Materials). 2003. "ASTM G 173-03: Standard Tables for Reference Solar Spectral Irradiance at Air Mass 1.5: Direct Normal and Hemispherical on 37° Tilted Surface." Technical report, American Society for Testing and Materials.

BASF Industrial Coatings. 2004. "Ultra-Cool™: The New Heat Reflective Coatings from BASF." <http://www.ultra-cool.basf.com>.

Blakey, R.R. and J.E. Hall. 1988. "Titanium Dioxide." Chapter A in *Pigment Handbook, Volume I*. John Wiley and Sons, pp.1-42.

Bohren, Craig F. 1987. "Multiple Scattering of Light and Some of Its Observable Consequences." *American Journal of Physics*, vol 55, no. 6 (June): 524-533.

Brabers, V.A.M. 1995."The Electrical Conduction of Titanomagnetites." *Physica B*, vol. 205: 143–152.

Brady, R.F. and L.V. Wake. 1992. "Principles and Formulations for Organic Coatings with Tailored Infrared Properties." *Progress in Organic Coatings*, vol. 20, no. 1: 1-25.

Burkhart, Gil, Terry Detrie, and Dan Swiler. 2001. "When Black Is White." *Paint and Coatings Industry Magazine.* (January).

Buxbaun, Gunter. 1998. *Industrial Inorganic Pigments*. Wiley-VCH, 2nd edition.

Clark, R.J.H. and D.G. Cobbold. 1978. "Characterization of Sulfur Radical Anions in Solutions of Alkali Polysulfides in Dimethylformamide and Hexamethylphosphoramide and in the Solid State in Ultramarine Blue, Green, and Red." *Inorganic Chemistry*, vol. 17: 3169–3174.

Clark, R.N. 1999. "Spectroscopy of Rocks and Minerals, and Principles of Spectroscopy." Chapter 1 in *Manual of Remote Sensing, volume 3: Remote Sensing for the Earth Sciences,* pp. 3-58. John Wiley and Sons, <http://speclab.cr.usgs.gov>, Fig. 5.

Custom-Bilt Metals. 2004. "Ultra-Cool™ Coating Saves Energy and Money on Custom-Bilt Metals Roofing Systems." <http://www.custombiltmetals.com>.

DCMA (Dry Color Manufacturer's Association). 1991. *Classification and Chemical Description of the Complex Inorganic Color Pigments*. Dry Color Manufacturer's Association, P.O. Box 20839, Alexandria, VA 22320.

de Cogan, D. and G.A. Lonergan. 1974. "Electrical conduction in Fe_2O_3 and Cr_2O_3." *Solid State Communications*, vol. 15: 1517-1519.

Ferro Corporation. 2004. "Cool Colors™ and Eclipse™ Pigments." <http://ferro.com>.

Genjima, Yasuhiro and Haruhiko Mochizuki. 2002. "Infrared Radiation Reflector and Infrared Radiation Transmitting Composition." U.S. Patent 6,366,397 B1, April 16.

Glebov, L.B. and E.N. Boulos. 1998. "Absorption of Iron and Water in the Na_2O-CaO-MgO-SiO_2 Glasses, II. Selection of Intrinsic, Ferric, and Ferrous Spectra in the Visible and UV Regions." *J. Non-Crystalline Solids*, vol. 242: 49-62.

Goodenough, Hamnett. 1984. “Oxides of Chromium.” Chapter 9.15.2.5.1 in *Landolt-Bornstein Numerical Data and Functional Relationships in Science and Technology, New Series, Group III: Crystal and Solid-State Physics, Volume 17g (Semiconductors: Physics of Non-Tetrahedrally Bonded Binary Compounds III)*. Berlin: Springer-Verlag.

Herbst, Willy and Klaus Hunger. 1993. *Industrial Organic Pigments.* VCH.

Johnston, Ruth M. 1988. “Color Theory.” Chapter D-b in *Pigment Handbook, Volume III*. John Wiley and Sons.

Judd, Deane B. 1952. *Color in Business, Science, and Industry.* John Wiley and Sons.

Kortum, Gustav. 1969. *Reflectance Spectroscopy: Principles, Methods, Applications.* Springer.

Kubelka, P. 1948. “New Contributions to the Optics of Intensely Light-Scattering Materials, Part I.” Journal of the Optical Society of America, vol. 38: 448.

Levinson, Ronnen, Paul Berdahl, and Hashem Akbari. 2005a. “Solar Spectral Optical Properties of Pigments, Part I: Model for Deriving Scattering and Absorption Coefficents from Transmittance and Reflectance Measurements.” *Solar Energy Materials & Solar Cells* (in press).

———. 2005b. “Solar Spectral Optical Properties of Pigments, Part II: Survey of Common Colorants.” *Solar Energy Materials & Solar Cells* (in press).

Lewis, Peter A. 1988. *Pigment Handbook, Volume I.* John Wiley and Sons.

MCA Tile. 2004. “MCA Tile ENERGY STAR Roof Products.” <http://www.mcatile.com>.

McKeown, N.B. 1998. *Phthalocyanine Materials: Synthesis, Structure and Function.* Cambridge: Cambridge University Press.

Nixon, Jeffrey D. 2003. “The Chemistry Behind ‘Cool Roofs’.” *eco-structure*, vol. 1, no. 1: 63–65.

Rabinovitch, E. B. and J. W. Summers. 1984. “Infrared Reflecting Vinyl Polymer Compositions.” U.S. Patent 4,424,292.

Schuster, A. 1905. “Radiation through a Foggy Atmosphere.” *Astrophys. J.*, vol. 21, no. 1.

Shepherd Color Company. 2004. “Arctic Infrared-Reflecting Pigments.” <http://shepherdcolor.com>.

Sliwinski, Terrence R., Richard A. Pipoly, and Robert P. Blonski. 2001. “Infrared Reflective Color Pigment.” U.S. Patent 6,174,360 B1, January 16.

Smith, G.B., A. Gentle, P. Swift, A. Earp, and N. Mronga. 2003a. “Coloured Paints Based on Coated Flakes of Metal as the Pigment, for Enhanced Solar Reflectance and Cooler Interiors: Description and Theory.” S*olar Energy Materials & Solar Cells*, vol. 79, no. 2: 163-177.

———. 2003b. “Coloured Paints Based on Iron Oxide and Silicon Oxide Coated Flakes of Aluminium as the Pigment, for Energy Efficient Paint: Optical and Thermal Experiments.” Solar Energy Materials & Solar Cells, vol. 79, no. 2: 179-197.

Society of Dyers and Colourists and American Association of Textile Chemists and Colorists. 2004. *Colour Index International: Fourth Online Edition.* <http://www.colour-index.org>.

Swiler, Daniel Russell. 2002. “Manganese Vanadium Oxide Pigments.” U.S. Patent 6,485,557 B1, November 26.

Wilbrandt, S., O. Stenzel, A. Stendal, U. Beckers, and C. von Borczyskowski. 1996. “The Linear Optical Constants of Thin Phthalocyanine and Fullerite Films from the Near Infrared to the UV Spectral Regions: Estimation of Electronic Oscillator Strength Values.” *J. Phys. B*, vol. 29: 2589-2595.

Table 1. Ranges of NIR Reflectance Over White (ROW_{NIR}), NIR reflectance over black (ROB_{NIR}), Visible Transmittance (T_{vis}) and Thickness (δ) Measured for Pigmented Films in Each Pigment Category.

Category	ROW_{NIR}	ROB_{NIR}	T_{vis}	δ (μm)	Film Codes
titanium dioxide white	0.87-0.88	0.24-0.65	0.10-0.42	17-29	W01-W04
carbon black	0.05-0.06	0.04-0.04	0.03-0.07	16-19	B01-B02
other non-selective black	0.04-0.05	0.04-0.05	0.00-0.07	20-24	B03-B04
chromium iron oxide selective black	0.23-0.48	0.11-0.35	0.00-0.15	19-26	B05-B11
organic selective black	0.85	0.10	0.01	23	B12
iron oxide brown	0.47-0.61	0.06-0.27	0.03-0.24	14-26	B13-B15
other brown	0.50-0.74	0.22-0.40	0.01-0.24	17-28	B16-B21
cobalt aluminate blue	0.62-0.71	0.09-0.20	0.16-0.28	16-23	U01-U05
cobalt chromite blue	0.55-0.70	0.10-0.25	0.05-0.28	16-26	U06-U09
iron blue	0.25	0.05	0.27	12	U10
ultramarine blue	0.52	0.05	0.20	23	U11
phthalocyanine blue	0.55-0.63	0.06-0.08	0.21-0.22	14-26	U12-U13
dioxazine purple	0.82	0.05	0.21	10	U14
chromium oxide green	0.50-0.57	0.33-0.40	0.00-0.01	12-26	G01-G02
modified chromium oxide green	0.71	0.22	0.22	23	G03
cobalt chromite green	0.58-0.64	0.14-0.18	0.17-0.28	13-23	G04-G06
cobalt titanate green	0.37-0.73	0.21-0.30	0.04-0.22	10-24	G07-G09
phthalocyanine green	0.42-0.45	0.06-0.07	0.10-0.20	13-25	G10-G11
iron oxide red	0.31-0.67	0.19-0.38	0.00-0.08	13-26	R01-R04
cadmium orange	0.87	0.26	0.18	10	R05
organic red	0.83-0.87	0.06-0.14	0.15-0.32	11-27	R06-R09
iron oxide yellow	0.70	0.21	0.16	19	Y01
cadmium yellow	0.87	0.29	0.25	11	Y02
chrome yellow	0.83	0.34	0.18	24	Y03
chrome titanate yellow	0.80-0.86	0.26-0.62	0.05-0.23	17-26	Y04-Y07
nickel titanate yellow	0.77-0.87	0.22-0.64	0.09-0.51	17-27	Y08-Y11
strontium chromate yellow + titanium dioxide	0.86	0.38	0.21	19	Y12
Hansa yellow	0.87	0.06	0.43	11	Y13
diarylide yellow	0.87	0.08	0.35	12	Y14
mica + titanium dioxide	0.88-0.90	0.35-0.54	0.31-0.54	17-37	P01-P09
mica + titanium dioxide + iron oxide	0.27-0.85	0.25-0.44	0.02-0.42	20-24	P10-P14

Figure 1. Air Mass 1.5 Hemispherical Solar Spectral Irradiance Typical of North American Insolation (5% Ultraviolet, 43% Visible, 52% Near-Infrared) (ASTM, 2003}.}

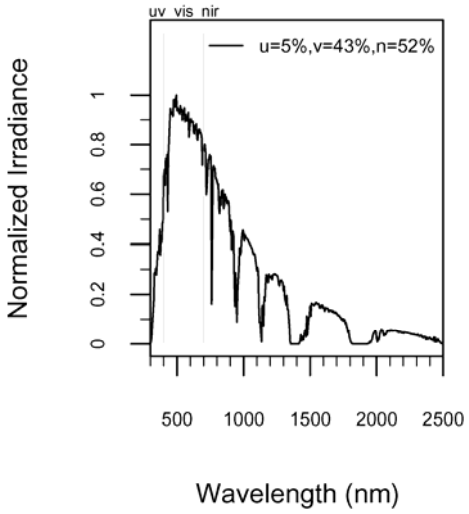

Figure 2. NIR Absorptances and Transmittances of 87 Pigmented Films.
A pigment with low NIR-absorptance is cool, but a cool pigment with high NIR transmittance requires an NIR-reflecting background. The color of each circle's interior indicates visible transmittance: black, less than 0.1; gray, between 0.1 and 0.3; white, over 0.3.

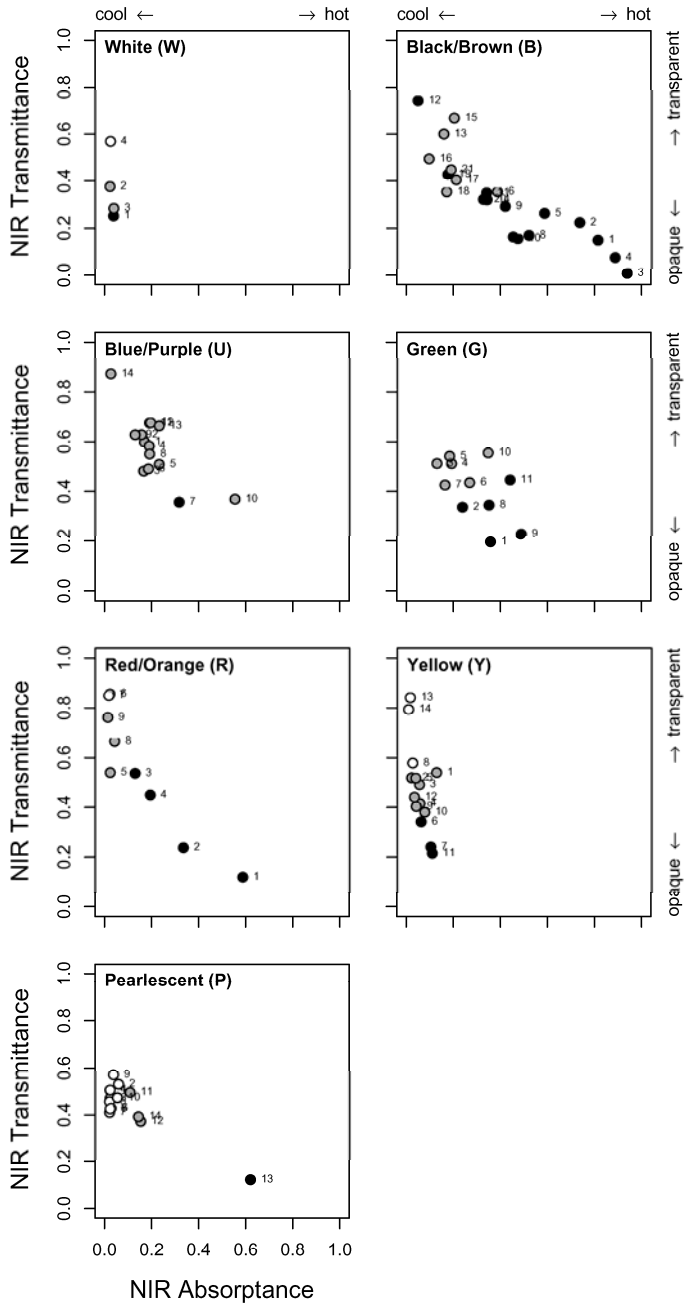

Aging and Weathering of Cool Roofing Membranes

Hashem Akbari, Asmeret A. Berhe, and Ronnen Levinson, Heat Island Group, Lawrence Berkeley National Laboratory (LBNL)
Stanley Graveline and Kevin Foley, Sarnafil
Ana H. Delgado and Ralph M. Paroli, Institute for Research in Construction, National Research Council (NRC), Canada

ABSTRACT

Aging and weathering can reduce the solar reflectance of cool roofing materials. This paper summarizes laboratory measurements of the solar spectral reflectance of unweathered, weathered, and cleaned samples collected from single-ply roofing membranes at various sites across the United States. Fifteen samples were examined in each of the following six conditions: unweathered; weathered; weathered and brushed; weathered, brushed and then rinsed with water; weathered, brushed, rinsed with water, and then washed with soap and water; and weathered, brushed, rinsed with water, washed with soap and water, and then washed with an algaecide. Another 25 samples from 25 roofs across the United States and Canada were measured in their unweathered state, weathered, and weathered and wiped.

We document reduction in reflectivity resulted from various soiling mechanisms and provide data on the effectiveness of various cleaning approaches. Results indicate that although the majority of samples after being washed with detergent could be brought to within 90% of their unweathered reflectivity, in some instances an algaecide was required to restore this level of reflectivity.

Aging and Weathering of Cool Roofing Membranes*

ABSTRACT

Aging and weathering can reduce the solar reflectance of cool roofing materials. This paper summarizes laboratory measurements of the solar spectral reflectance of unweathered, weathered, and cleaned samples collected from single-ply roofing membranes at various sites across the United States. Fifteen samples were examined in each of the following six conditions: unweathered; weathered; weathered and brushed; weathered, brushed and then rinsed with water; weathered, brushed, rinsed with water, and then washed with soap and water; and weathered, brushed, rinsed with water, washed with soap and water, and then washed with an algaecide. Another 25 samples from 25 roofs across the United States and Canada were measured in their unweathered state, weathered, and weathered and wiped.

We document reduction in reflectivity resulted from various soiling mechanisms and provide data on the effectiveness of various cleaning approaches. Results indicate that although the majority of samples after being washed with detergent could be brought to within 90% of their unweathered reflectivity, in some instances an algaecide was required to restore this level of reflectivity.

Introduction

The solar reflectance or albedo of a roof's surface affects roof temperature, air temperature above the roof, and the heating and cooling energy use in buildings (Akbari and Konopacki, 1998). Lighter colored roofing membranes, including those covered with high-albedo, low-absorptance, white coating materials, reflect incident solar energy, enabling them to stay cooler in the sun than low-albedo roofing materials. Young (1998) and Akbari and Konopacki (1998) found that cool roofing membranes can reduce building cooling energy use by 10% to 50%, that can result in savings of $10 to $100 per year per 100 m^2 roof surface. In cities, cool roofs can reduce summertime air temperature of their surroundings by 1-2 K (Akbari and Konopacki, 1998; Young, 1998; Pomerantz et al., 1999 and Akbari et al., 1999).

Cool materials for low-sloped roofs are characteristically white with smooth surfaces (Eilert, 2000). But the albedo of light-colored roofing materials changes, because of aging, weathering, and discoloration—which results from weathering. In this paper, we present data from two independent series of tests carried out at Lawrence Berkeley National Laboratory (LBNL) and National Research Council (NRC) in Canada. The LBNL study included measuring the spectral solar reflectance of 15 weathered roofing membranes from eight cities across the United States. The study also investigated the effect of four cleaning treatments in restoring the reflectance relative to its original levels. The NRC study also included measuring the solar reflectance of 25 weathered roofing membranes from 25 cities across the United States and Canada. But only the effects of two cumulative cleaning processes in restoring the solar reflectance were measured. All membranes were produced by the same manufacturer.

Effects of Light Colored Roofs

Roof temperature strongly influences air temperature inside and outside of buildings. Solar absorptance, thermal emittance, convection coefficient, and heat conduction through a roofing membrane, all affect the roof surface temperature (Pomerantz et al., 1999). Consequently, lighter colored (reflective), cool roofs reduce the demand for indoor cooling by controlling the temperature from the outside and therefore heat flow into buildings.

The reduction in annual electricity use resulting from the application of cool roofs is greatest for buildings in areas with short cold seasons, because cool roofs have the potential to increase heating energy demand during extended cold periods (Levinson et al., 2005). However, significant annual net energy savings have been calculated for northern locations such as Chicago, Salt Lake City, and Toronto, through the implementation of heat island reduction strategies (Akbari and Konopacki, 2004; Konopacki and Akbari, 2002).

---

* Hashem Akbari, Asmeret A. Berhe, and Ronnen Levinson, Heat Island Group, Lawrence Berkeley National Laboratory (LBNL); Stanley Graveline and Kevin Foley, Sarnafil; Ana H. Delgado and Ralph M. Paroli, Institute for Research in Construction, National Research Council (NRC), Canada

Recognizing the potential energy savings that could be achieved through the use of reflective roofing materials, the US Environmental Protection Agency (EPA) and the US Department of Energy (DOE) introduced the Energy Star Roof Products Program in 1999. Energy Star labeled membranes must meet defined minimum reflectivity levels according to their intended applications (low and high slope). Looking to curb energy demand, beginning in 2005, the State of California will prescribe the use of cool roofs on low-sloped non-residential buildings in their Title 24 Energy Code.

The reduced temperatures of reflective roofing surfaces, in turn, keeps air blowing over the roof and downwind from the buildings cooler (Taha, 1996). In large metropolitan areas, this contributes to a reduction in the urban heat island which reduces smog formation and the greenhouse effect (Akbari et al, 1990, 1999, 2001; Akbari and Konopacki, 1998; Pomerantz et al., 1999).

The United States Green Building Council's (USGBC) Leadership in Energy and Environmental Design (LEED) recognizes these benefits by awarding a point for the use of highly reflective and emissive roof materials in their green building rating system. The City of Chicago is looking to introduce an urban heat island ordinance that would call for the use of high reflectance roof materials beginning in 2008.

Typically, all non-metallic materials absorb the sun energy in the ultraviolet (UV) band (0.30-0.40 μm). Ultraviolet light is characterized as the major factor in aging and material degradation. Although the aging is primarily caused by UV absorption, the degradation process is highly temperature dependent. For the same UV absorption, the higher the temperature and temperature fluctuations through a day, the faster the material degrades. Reflective surfaces, by keeping the surface temperature low during the sunlit hours that result in less diurnal thermal expansion and contraction, may have a longer useful life.

Cooler roof surface temperatures have also been found to improve the performance of roof insulation. The thermal resistance of insulation materials installed immediately below a black membrane has been found to be up to 30% lower than advertised, when measured at peak summertime temperatures in Austin, Texas (Konopacki and Akbari, 2001).

Effect of Aging and Weathering

The durability and solar reflectance of high albedo, cool roofs is affected by weathering (Paroli et al., 1993). Precipitation, dust and air pollutant depositions can degrade the solar reflectance of cool roof materials (Eilert, 2000). Over a period of several years, light colored roofing surfaces are typically expected to lose about 20% of their initial solar reflectance. Aged roofing membranes show a greater increase in absorptance on short wavelengths than long wavelengths (Berdahl et al., 2002).

Berdahl et al. (2002) indicated that the soil deposited on the surface of roofing membranes is made up of elemental carbon, hydrocarbons and other deposits that along with the soil further reduce the reflectivity of the membranes. Soiling and accumulation of carbonaceous particles is a serious problem in or around urban centers that are exposed to higher levels of fossil fuel combustion. Since carbonaceous aerosols can travel fast in the mixing atmosphere, they can spread to both urban and rural places to create a similar effect.

Methodology

To investigate these and other related phenomena, this study was carried out on 15 membranes from eight locations that have been weathered for five to eight years and additional membranes from 25 other locations (Whelan et al., 2004), exposed 15 to 22 years. Solar (0.3 – 2.5 μm), UV (0.3 – 0.4 μm), visible (0.4 – 0.7 μm), and near-infrared (0.7 – 2.5 μm) reflectances were analyzed.

Sample Description

The LBNL received weathered membranes (about 30-cm square) from 15 roofs while the NRC received membranes from 25 roofs. All samples contained at least one hot air welded seam. The bottom flap of material within the overlap was protected from weathering (but may still have been exposed to some elevated temperatures) and is thus labeled "unweathered." The roofing membranes were made of about 1.2-mm to 1.5-mm thick polyvinyl chloride (PVC). The top half of most of the samples was white from the use of a rutile-phase titanium dioxide (TiO_2) pigment, while a few were very light gray in color. The 15 LBNL roof membrane samples were collected from eight locations where they had been installed for five to eight years (see **Table 1**). The 25 NRC roof membrane samples were from various locations in the United States and Canada, and had a top surface which was light gray in color. Buildings selected for

sampling were chosen based on owner willingness to allow sample removal, and geographic and climate location.

Table 1: Location, Length of Time Since Installation, and Solar Reflectance of Weathered and Cleaned Samples, Studied at the LBNL

Sample			Solar Reflectance					
Sample No.	Location	Date of Installation	Uncleaned	Wiped	Rinsed	Detergent-Washed	Algae-Cleaner Washed	Unweathered
Group A (white)								
1	Springfield, MA	09/22/1995	0.54	0.68	0.70	0.77	0.82	0.80
2	Springfield, MA	05/31/1995	0.55	0.73	0.72	0.76	0.77	0.82
3	Lancaster, OH	03/28/1995	0.59	0.76	0.75	0.80	0.81	0.81
4	Heath, OH	04/01/1995	0.57	0.72	0.72	0.78	0.79	0.80
5	West Hampton, NJ	05/01/1995	0.71	0.71	0.71	0.73	0.77	0.79
6	West Hampton, NJ	02/04/1993	0.69	0.69	0.71	0.72	0.77	0.81
7	Plantation, FL	11/04/1994	0.35	0.43	0.64	0.65	0.79	0.82
8	Plantation, FL	11/04/1994	0.32	0.42	0.59	0.68	0.80	0.79
11	Solano Beach, CA	09/20/1992	0.38	0.47	0.71	0.78	0.82	0.81
12	Solano Beach, CA	09/20/1992	0.52	0.65	0.69	0.80	0.80	0.81
13	Alpharetta, GA	04/01/1995	0.45	0.59	0.66	0.69	0.79	0.80
Group B (very light gray)								
9	Gardena, CA	10/25/1995	0.50	0.58	0.60	0.62	0.63	0.63
10	Gardena, CA	10/25/1995	0.49	0.60	0.61	0.63	0.63	0.63
14	Bethesda, MD	04/28/1995	0.50	0.59	0.59	0.63	0.64	0.63
15	Fredericksburg, VA	11/06/1995	0.48	0.60	0.62	0.63	0.64	0.63

Note: The cleaning process was cumulative. All samples went through a cleaning process progression of dry wiping, rinsing with water, washing with detergent, and washing with algae cleaners.

Measurement Protocols

Although some membranes received at LBNL were more soiled than others, all the samples appeared to be in good mechanical condition when the measurements were taken. For each sample, the most heavily soiled spot of each membrane was exposed to the different cleaning treatments.

The cleaning process was made to replicate natural and professional cleaning of the roofs, as given in **Table 2**. The unweathered samples refer to the part of the sample that was underneath the weathered part (i.e., in the overlap) and was assumed to have the optical properties of new membrane. The weathered samples were the soiled exposed samples. On each sample, we carried out a progression of four cleaning processes. First, each sample was dry wiped to simulate the effect of the dust removal by wind. After the measurements of the dry wiped samples, they were rinsed with running water to simulate the effect of rain. Samples were also washed with detergent and sodium hypochlorite (NaClO) and sodium hydroxide (NaOH) solution (algae cleaners) to simulate the effect of professional cleaning. The unweathered and uncleaned samples were handled in such a way so as not to alter the conditions under which they were collected. For each of the wet cleaning treatments, the sample was allowed to dry before the spectral reflectance measurements were taken.

For the samples received at the NRC, specimens taken from two different areas (1 and 2) of the "as received" top (weathered) sheet were analyzed before and after cleaning (see **Table 3**). Cleaning was

achieved by using water and a cloth to wipe off the dirt. No detergent or algaecide was used. One to two specimens from the bottom sheet (underlap) without cleaning were analyzed. In some cases, two specimens were analyzed before and after cleaning. This was done to check for differences in the solar reflectivity values between the two areas or between the dirty and clean top surface of the bottom sheet.

Table 2: Cleaning Processes

Sample	Cleaning Process	To Replicate
Unexposed	None	Unweathered, aged condition
Uncleaned	None	Weathered, aged condition
Wiped	Wiped with dry cloth	Effect of wind and sweeping
Rinsed	Rinsed with running water	Effect of rain
Detergent-Washed	Phosphate-free household detergent with brush	Professional cleaning
Algae-Cleaner Washed	Sodium Hypochlorite (NaClO) and Sodium Hydroxide (NaOH) solution, with brush	Professional cleaning

Table 3: Weighted Average Solar Reflectance of Samples Studied at the NRC

Sample			Solar reflectance		
Sample ID	Location	Year Installed	Top: Uncleaned	Top: Washed and Wiped	Bottom: Unweathered
1D	Canton, MA	1979	0.48	0.50	0.52
2A	Wenham, MA	1984	0.32	0.41	0.55
2D	Wenham, MA	1984	0.39	0.44	0.51
3A	Woburn, MA	1983	0.39	0.41	0.48
4B	Dickson, TX	1984	0.40	0.45	0.49
5B	Tyler, TX	1981	0.41	0.46	0.50
6A	Euless, TX	1984	0.42	0.49	0.51
7A	City of Industry, CA	1979	0.44	0.50	0.53
8A	El Segundo, CA	1982	0.39	0.43	0.50
9B	Mountain View, CA	1983	0.40	0.45	0.52
10B	Lacey, WA	1982	0.40	0.43	0.51
11B	Ft. Steilacoom, WA	1983	0.45	0.47	0.52
12A	Atlanta, GA	1986	0.42	0.48	0.50
13A	Jacksonville, FL	1982	0.41	0.47	0.52
14A	Appleton, WI	1985	0.38	0.44	0.49
15B	Mt. Prospect, IL	1981	0.33	0.39	0.49
15D	Mt. Prospect, IL	1981	0.50	0.52	0.54
16A	Park Ridge, IL	1984	0.35	0.42	0.50
17B	Hackensack, NJ	1986	0.35	0.41	0.50
18A	Englewood, NJ	1985	0.39	0.43	0.48
18C	Englewood, NJ	1985	0.32	0.37	0.48
19A	Iowa, IA	1982	0.34	0.4	0.49
20B	Davis, CA	1981	0.47	0.49	0.52
21A	Haileybury, ON	1981	0.48	0.49	0.55
21C	Haileybury, ON	1981	0.44	0.47	0.51
22A	Hamilton, ON	1984	0.34	0.38	0.51
24A	Oakville, ON	1977	0.43	0.46	0.48
25A	Sarnia, ON	1984	0.37	0.43	0.50

All samples were analyzed using a Varian Cary-5 UV-Vis-NIR spectrophotometer equipped with a total integrating sphere (ASTM, 1996). Spectral reflectance measurements were weighted according to

the ASTM G 159-98 to obtain the overall solar reflectance (ASTM, 1998). This standard is a combination of an editorial revision of tables E 891 and E 892 to make the reference solar spectral energy standard harmonious with ISO 9845-11992. The ASTM G 159 states that the conditions chosen for these tables "are representative of average conditions in the 48 contiguous states of the United States. In real life, a large range of atmospheric conditions can be encountered, resulting in more or less important variations in the atmospheric extinction. Thus, considerable departure from the present reference spectra might be observed depending on time of the day, geographical location, and other fluctuating conditions in the atmosphere."

Results

The results of the LBNL measurements are summarized in Table 1 and **Figures 1** and **2**. The samples can be divided in two groups: Group A with the unweathered solar reflectance of about 0.80 (see Figure 1) and Group B with unweathered solar reflectance of about 0.63 (see Figure 2).

The solar reflectance of the weathered samples in Group A ranged from 0.32 to 0.71 with a median of 0.55 (see **Figure 3**). With wiping, the solar reflectance improved to 0.42 to 0.75 with a median of 0.69. Rinsing with water improved the solar reflectance to 0.59 to 0.75 with a median of 0.71. Further washing with detergent improved the solar reflectance to 0.65 to 0.80 with a median of 0.77. And washing with an algae cleaner practically restored the solar reflectance of the samples to their unweathered values (the range was 0.77 to 0.82 with a median of 0.80). The solar reflectance of the unweathered samples ranged from 0.79 to 0.82 with a median of 0.80.

There were only four samples in Group B. The solar reflectance of these unweathered samples was 0.63 (see **Figure 4**). The solar reflectance of the weathered samples in Group B ranged from 0.48 to 50. Wiping and rinsing with water improved the solar reflectance to 0.59 to 0.62, practically approaching the solar reflectance of the unweathered samples.

The results of the NRC measurements are summarized in Table 3 (see also **Figure 5**). The weighted average solar reflectance for the unweathered (bottom) and weathered (top) surfaces of the gray colored samples ranges from 0.29 to 0.55. As should be expected, surfaces display a higher reflectance value after cleaning. The top side of the bottom (unweathered) sheet also showed higher solar reflectance than the weathered side of the top sheet. Only 10 surfaces (bottom and/or top) out of the 25 tested have slightly over 0.5 solar reflectance. Based on previous work done at the NRC, bottom flaps can be used as a reference material when no original material is available. In most cases, the bottom flap retains most, if not all, of the original properties. It was decided that this would also be done for the reflectivity data. However, in some cases, the bottom flap was found to be dirty and had to be cleaned. It is speculated that the bottom flap may have picked up dirt at the time of installation simply from the environment.

In summary, it is interesting to note that a simple cleaning with water and cloth allowed the samples to regain a substantial part of their original reflectivity. Furthermore, it appears that the roofing materials evaluated in this study did not lose *any* inherent reflectivity with aging, but rather, in-situ reflectivity diminishment was because of obfuscation by atmospheric deposition (primarily by soot) and other "local" environmental factors.

Conclusion

The experiments conducted at the LBNL suggest that for the PVC roofing materials studied that are not covered with algae, wiping and rinsing with water (simulating the annual cleaning by rain) have restored the solar reflectance of the sample to at least 80% of the solar reflectance of the unweathered samples. For samples with algae, washing with detergent and algae-cleaners has practically restored the solar reflectance of the weathered roofing membranes to the solar reflectance of the unweathered membranes.

The solar reflectance measurements from the NRC indicated that with a few exceptions, all roofs have a weighted averaged solar reflectance of less than 0.6. There was no unweathered material available at the time of the analysis. Hence, no final conclusions can be drawn about the effect of weathering on solar reflectance of the roof material analyzed. However, as in the case of the samples analyzed by the LBNL, at least 70%, and as much as 100%, of the initial reflectivity was regained by simply washing the PVC membranes with water (no cleaning detergent).

Thus, if high reflectivity is critical to the roof owner, then it would be recommended that the regular maintenance protocol include power washing the membrane (for cases with no significant potentials for algae growth) on a frequency to be determined according to the roof's requirements.

Figure 1: Solar Reflectance of Samples 1-8 and 11-13

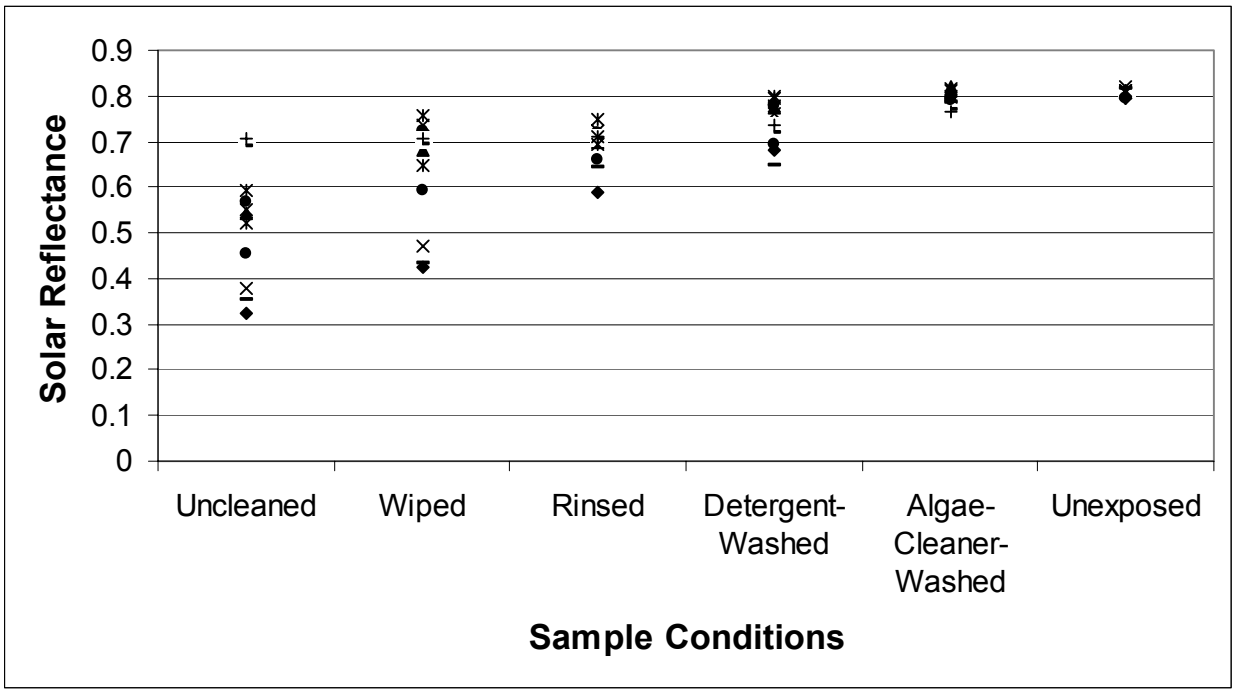

Note: Values are Hemispherical Solar reflectance calculated with air mass 1.5

Figure 2: Solar Reflectance of Samples 9-10 and 14-15

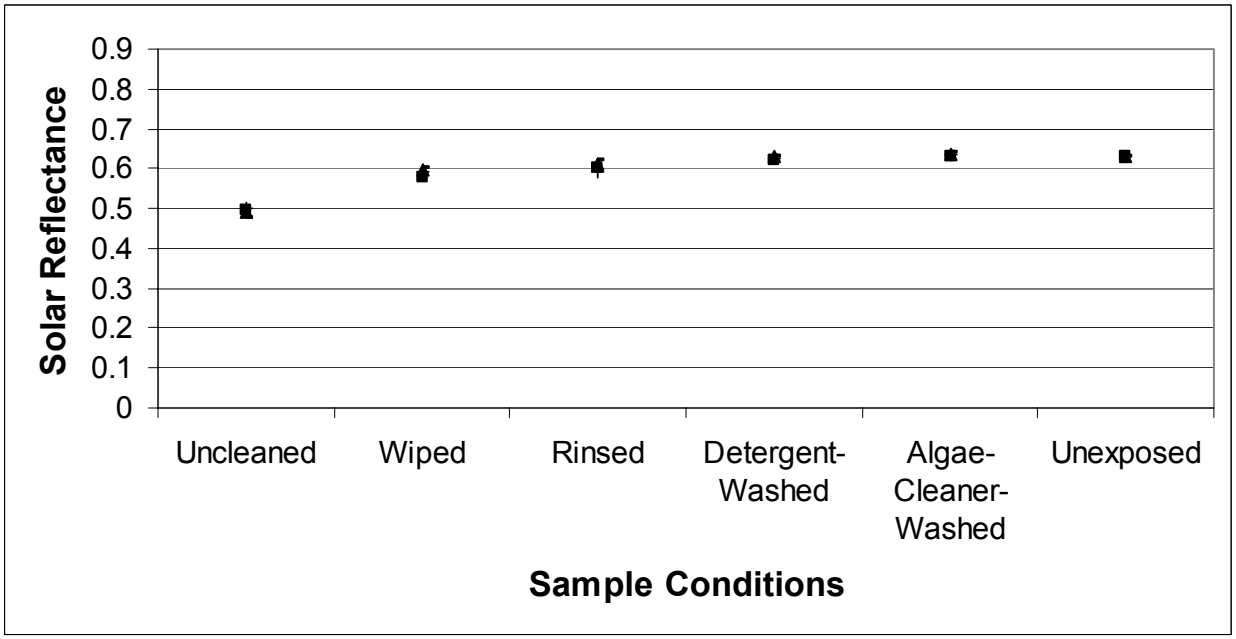

Note: Values are hemispherical solar reflectance calculated with an air mass of 1.5

Figure 3: Solar Reflectance of Samples 1-8 and 11-13

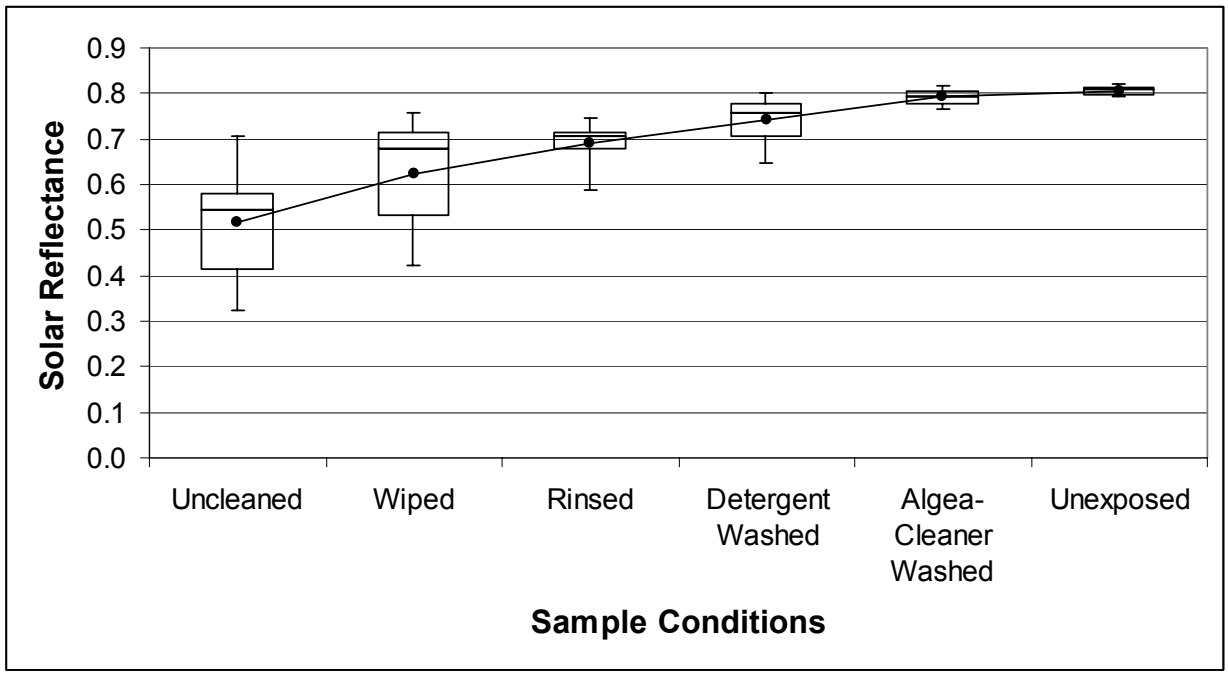

Note: The data show the minimum, 25th quartile, 50th quartile (median), 75th quartile, and maximum solar reflectance of the samples. The solid line shows the average reflectance of all samples.

Figure 4: Solar Reflectance of Samples 9-10 and 14-15

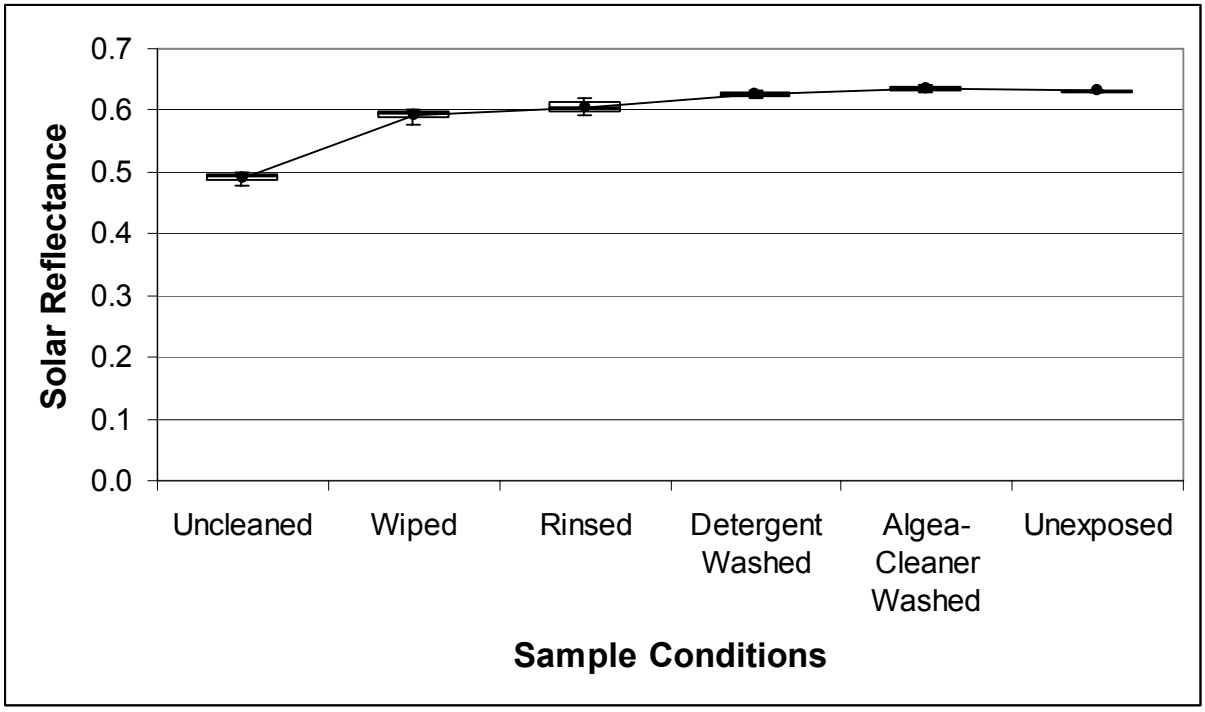

Figure 5: Solar Reflectance of Samples Analyzed at the NRC

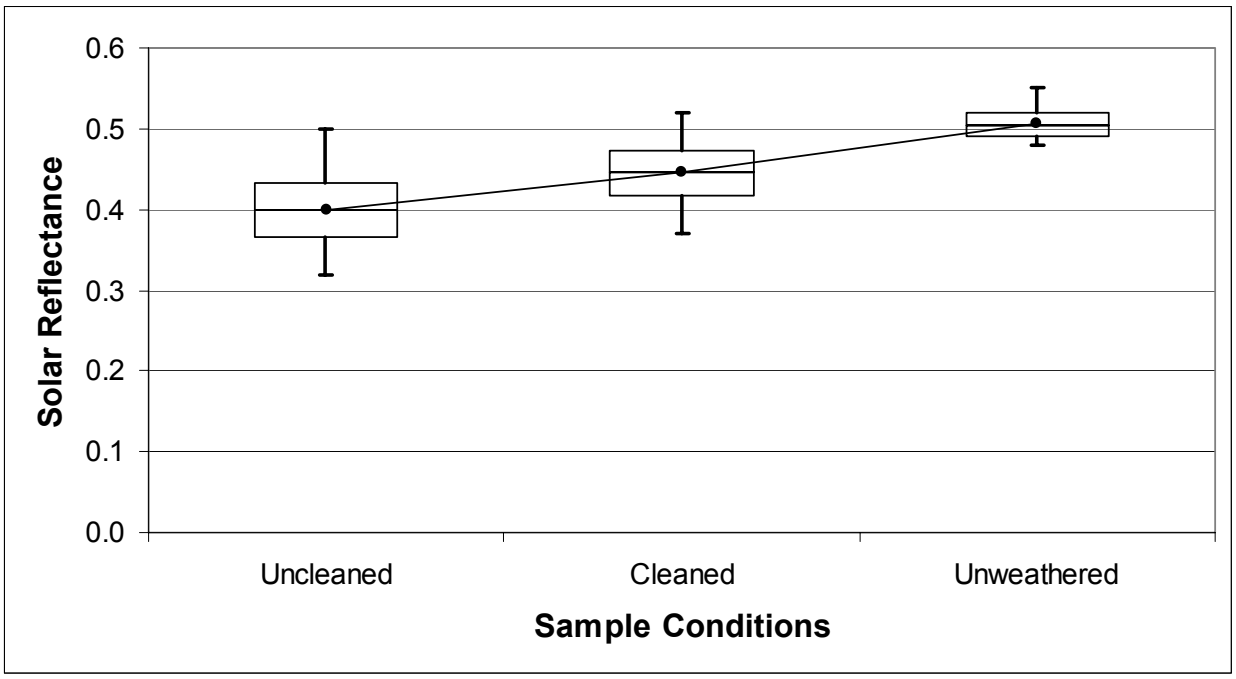

Note: The data show the minimum, 25th quartile, 50th quartile (median), 75th quartile, and maximum solar reflectance of the samples. The solid line shows the average reflectance of all samples.

Acknowledgements

This work was supported by the U.S. Environmental Protection Agency under IAG DW89938442-01-2 and by the Assistant Secretary for Energy Efficiency and Renewable Energy, Building Technologies, of the U.S. Department of Energy, under Contract No. DE-AC03-76SF00098. We thank Sarnafil US Inc. for providing us with the samples and treatments for this study and also for supplying the necessary information.

References

Akbari, H. and S.J. Konopacki 1998. “The Impact of Reflectivity and Emissivity of Roofs on Building Cooling and Heating Energy Use.” *Proceedings of the Thermal Performance of The Exterior Envelopes of Building VII.* December 6-10, 1998. Clearwater Beach, FL.

———. 2004. “Energy Impacts of Heat Island Reduction Strategies in Toronto, Canada.” *Energy* 29: 191-210.

Akbari, H., S. Konopacki and M. Pomerantz. 1999. “Cooling Energy Saving Potential for Reflective Roofs for Residential and Commercial Buildings in the United States.” *Energy* 24: 391-407.

Akbari, H., M. Pomerantz, and H. Taha. 2001. "Cool surfaces and shade trees to reduce energy use and improve air quality in urban areas." *Solar Energy* 70, no 3: 295-310.

Akbari, H., A.H. Rosenfeld and H. Taha. 1990. “Summer Heat Islands, Urban Trees and White Surfaces.” *ASHRAE Transactions* 96, no. 1.

ASTM (American Society for Testing and Materials). 1996. Standard Test Method for Solar Absorptance, Reflectance, and Transmittance of Materials Using Integrating Spheres. Technical report, ASTM E 903-96.

———. 1998. Standard Tables for References Solar Spectral Irradiance at Air Mass 1.5: Direct Normal and Hemispherical for a 370 Tilted Surface. Technical report, G 159-98. (Hemispherical values were used.)

Berdahl, P., H. Akbari, and L.S. Rose. 2002. “Aging of reflective roofs: soot deposition,” *Applied Optics* 41, no. 12: 2355-2360.

Eilert, P. 2000. High Albedo (Cool) Roofs: Codes and Standards Enhancement (CASE) Study. Pacific Gas and Electric Company.

Konopacki, S.J., and H. Akbari. 2001. *Measured Energy Savings and Demand Reduction from a Reflective Roof Membrane on a Large Retail Store in Austin*. Lawrence Berkeley National Laboratory Report No. LBNL-47149, Berkeley, CA.

———. 2002. Energy Savings for Heat Island Reduction Strategies in Chicago and Houston (Including Updates for Baton Rouge, Sacramento, and Salt Lake City. Lawrence Berkeley National Laboratory Report No. LBNL-49638, Berkeley, CA.

Levinson, R., H. Akbari, S.J. Konopacki, and S. Bretz. 2005. “Inclusion of cool roofs in nonresidential Title 24 prescriptive requirements,” *Energy Policy* 33, no. 2: 151-170.

Paroli, R.M., O. Dutt, A.H. Delgado and H.K. Stenman. 1993. “Ranking PVC Roofing Membranes Using Thermal Analysis.” *Journal of Materials and Civil Engineering* 5, no. 1: 83-95.

Pomerantz, M., H. Akbari, P. Berdahl, S.J. Konopacki, H. Taha and A.H. Rosenfeld. 1999. “Reflective Surfaces for Cooler Buildings and Cities.” *Philosophical Magazine B* 79, no. 9: 1457-1476.

Taha, H. 1996. “Modeling the Impacts of Large-Scale Albedo Changes on Ozone Air Quality in the South Coast Air Basin.” *Atmospheric Environment 31*, no. 11: 1667-1676.

Whelan, B.J., S.P. Graveline, A.H. Delgado, K. Liu, R.M. Paroli. 2004. “Field Investigation and Laboratory Testing of Exposed Poly (Vinyl Chloride) Roof Systems.” CIB World Building Congress.

Young, R. 1998. “Cool Roofs: light –colored coverings reflect energy savings and environmental benefits.” *Building Design and Construction* 39, no. 2: 62-64.

Cooler Tile-Roofed Buildings with Near-Infrared-Reflective Nonwhite Coatings

Ronnen Levinson, Lawrence Berkeley National Laboratory (contact)[1]
Hashem Akbari, Lawrence Berkeley National Laboratory[2]
Joe Reilly, American Rooftile Coatings[3]

Abstract

Owners of homes with pitched roofs visible from ground level often prefer non-white roofing products for aesthetic considerations. Non-white, near-infrared-reflective architectural coatings can be applied in-situ to pitched concrete or clay tile roofs to reduce tile temperature, building heat gain, and cooling power demand, while simultaneously improving the roof's appearance. Scale model measurements of building temperatures and heat-flux were combined with solar and cooling energy use data to estimate the effects of such cool roof coatings in various California data. Under typical conditions—e.g., 1 kW m^{-2} summer afternoon insolation, R-11 attic insulation, no radiant barrier, and a 0.3 reduction in solar absorptance—absolute reductions in roof surface temperature, attic air temperature, and ceiling heat flux are about 12 K, 6.2 K, and 3.7 W m^{-2}, respectively. For a typical 1,500 ft^2 (139 m^2) house with R-11 attic insulation and no radiant barrier, reducing roof absorptance by 0.3 yields whole-house peak power savings of 230, 210, and 210 W in Fresno, San Bernardino, and San Diego, respectively. The corresponding absolute and fractional cooling energy savings are 92 kWh yr^{-1} (5%), 67 kWh yr^{-1} (6%), and 8 kWh yr^{-1} (1%), respectively. These savings are about half those previously reported for houses with non-tile roofs. With these assumptions, the statewide peak cooling power and annual cooling energy reductions would be 240 MW and 63 GWh yr^{-1}, respectively. These energy savings would reduce annual emissions from California power plants by 35 kilotonnes CO_2, 11 tonnes NO_x, and 0.86 tonnes SO_x. The economic value of cooling energy savings is well below the cost of coating a tile roof, but the simple payback times for using cool pigments in a rooftile coating are modest (5-7 years) in the hot climates of Fresno and San Bernardino.

[1] 1 Cyclotron Road, MS 90R2000, Berkeley, CA 94720; tel. 510/486-7494; RMLevinson@LBL.gov
[2] 1 Cyclotron Road, MS 90R2000, Berkeley, CA 94720; tel. 510/486-4287; H_Akbari@LBL.gov
[3] 432 Cienaga Drive, Fullerton, CA 92835; tel. (714) 680-6436; jcreilly@adelphia.net

Key Words: tile roof, cool coating, near-infrared reflective, building simulation, cooling energy, cooling power, California, cool roof, COOLTILE IR COATINGS™

Introduction

Owners of homes with pitched roofs visible from ground level often prefer non-white roofing products for aesthetic considerations. American Rooftile Coatings [ARC; Fullerton, CA] has developed non-white, near-infrared (NIR)-reflective architectural coatings that can be applied in-situ to pitched concrete or clay tile roofs. These coatings can reduce tile temperature, building heat gain, and cooling power demand, while simultaneously improving the roof's appearance. Such NIR-reflective roof coatings can cool tiles while allowing choice of color by reflecting a significant fraction of the 52% of solar energy that arrives as invisible, NIR radiation[4] (Levinson *et. al* 2004a, 2004b).

Previous studies have measured and/or simulated reductions in cooling energy use and/or peak cooling power demand achieved by retrofitting houses with *white* roofs. For example, Parker *et al.* (1998) measured energy savings averaging 19% for eleven Florida homes, while Akbari *et al.* (1997), measured cool-roof energy savings exceeding 80% at a house in Sacramento. (The Sacramento house was unusual in that its walls were well-shaded by trees, making its roof the primary source of solar heat gain.) Konopacki and Akbari (2000), Konopacki et al. (1997), and Akbari and Konopacki (2004) have simulated residential cooling energy and peak demand savings in many North American cities and estimate savings of about 10-20%, depending on the house construction and roof insulation. Cool-roof simulations have been used to develop the EPA EnergyStar Roofing Comparison Calculator (EPA 2004) and the DOE Cool Roof Calculator (DOE 2004), online tools that calculate cool-roof savings as a function of reflectance increase, building characteristics, cooling equipment, and climate.

Since cooling power and energy savings are proportional to increase in roof reflectance (Konopacki *et al.* 1997), white-roof savings can be scaled down to estimated savings achievable

[4] In the air-mass 1.5 hemispherical solar irradiance considered typical of North American ground-level insolation, 52% of the energy arrives as near-infrared radiation (0.7 – 2.5 microns). The remainder arrives in the ultraviolet (0.3 – 0.4 microns, 5%) and visible (0.4 – 0.7 microns, 43%) spectra.

by (typically less reflective) nonwhite cool roofs. However, these savings are not directly applicable to tile-roofed homes, because the flow of heat from roof to building can be significantly decreased by the well-ventilated gap between tile and roofdeck.

The current study uses measurements from scale models to quantify the reductions in roof surface temperature, attic air temperature, and ceiling heat flux that are achieved by finishing roof tiles with NIR-reflective coatings. This data is then used to predict the energy savings that would accrue in various climates to full-scale homes roofed with NIR-reflective tiles.

We have monitored the interior and exterior temperatures of four adjacent, 1:10 scale, air-conditioned model houses sited in the hot, inland Southern California city of Riverside. The four buildings were roofed with concrete tiles finished with black, white, cool color (NIR reflecting), and standard color (NIR absorbing) coatings, respectively. The thermal performances of the buildings with matching cool and standard color roofs were compared to each other and to those of the black- and white-roofed reference buildings. From this comparison we characterized the thermal performance of the cool roof tile coating, and extrapolated the results to estimate potential reductions in peak cooling power demand and annual cooling energy consumption by homes in various California climates.

Theory

Reductions in Roof Surface Temperature, Attic Air Temperature, and Ceiling Heat Flux

Neglecting thermal storage and linearizing the exchange of thermal radiation between the roof and its environment, reductions in roof surface temperature T_s, attic air temperature T_a, and ceiling heat flux q are proportional to the reduction $\Delta\alpha$ in the solar absorptance of the roof. That is,

$$\Delta x = k_x \times I \Delta\alpha \qquad (1)$$

where I is insolation [W m^{-2}]; x is a building property (T_s, T_a, or q); and the property-specific sensitivity (coefficient) k_x depends on the thermal resistances (hereafter, simply "resistances"; m^2 K W^{-1}) to convection of heat from the roof to the outside air, radiation of heat from the roof to its radiative exchange surface, and transfer of heat from the roof to the air-conditioned interior

(Appendix). This simplified model of building heat transfer can be used to determine k_x by regressing measurements of building property reduction Δx to reduction in absorbed insolation, $I\,\Delta\alpha$.

Cooling Power Savings

If a house is cooled by an air-conditioner with coefficient of performance COP, reducing ceiling heat flux by Δq [W m^{-2}] decreases cooling power demand per unit ceiling area P [W m^{-2}] by

$$\Delta P = \mathrm{COP}^{-1}\,\Delta q = \mathrm{COP}^{-1}\,k_q\,I\,\Delta\alpha \tag{2}$$

Cooling Energy Savings

The annual cooling energy savings per unit ceiling area [kWh m^{-2}] will be

$$\Delta E = \tfrac{1}{\mathrm{COP}} \times \int_{\tau_{\mathrm{load}}} \Delta q(\tau)\,d\tau = \tfrac{1}{\mathrm{COP}} \times k_q\,\Delta\alpha \int_{\tau_{\mathrm{load}}} I(\tau)\,d\tau \tag{3}$$

where COP is the air conditioner's coefficient of performance (output cooling power / input electrical power), assumed constant; τ is time; and $\int_{\tau_{\mathrm{load}}} I(\tau)\,d\tau$ is the annual global horizontal insolation [kWh m^{-2}] incident on the roof during those hours in which there is a positive ceiling heat flux into the interior of the house that is then removed by air conditioning. This insolation load may be estimated as $\phi \times d_{\mathrm{annual}} \times \bar{J}$, where $\bar{J}$ is the annual average daily insolation [kWh day^{-1}] weighted according to monthly distribution of cooling degree days, d_{annual} is the number of days per year on which the building is air-conditioned, and ϕ represents the fraction of daily insolation that generates a ceiling heat flux that must be removed by the air conditioner. The weighted daily insolation can be estimated from historical weather and solar data, while the number of operating days can be estimated from simulations of annual cooling energy consumption.

Since the fraction of daily insolation that generates a ceiling heat flux that must be removed by the air conditioner depends on both the thermal mass of the roof and on the operating schedule of a building's cooling equipment, a proper estimation of the fraction ϕ requires modeling outside

the scope of the current study. Hence, we arbitrarily set ϕ to its midrange value of 0.5, with the observation that our estimates of energy savings can be linearly rescaled to another value of ϕ.

Statewide Savings

Cooling Power

If the reduction in cooling power demand per unit ceiling area per unit decrease in solar absorptance of a house in California climate i is $\left(\Delta P/\Delta\alpha\right)_i$ [W m^{-2}], the potential reduction in peak cooling power demand $\Delta\tilde{P}_{\mathrm{CA}}$ [W] for the state of California (assuming that building cooling demand peaks at the same time as overall power demand) may be estimated as

$$\Delta\tilde{P}_{\mathrm{CA}} = \Delta\alpha_{\mathrm{avg}} \sum_i \left(\Delta P/\Delta\alpha\right)_i A_i \tag{4}$$

where $\Delta\alpha_{\mathrm{avg}}$ is the average expected reduction in solar absorptance, and A_i is the aggregate ceiling area of air-conditioned, potentially coatable tile-roofed houses in regions of California whose weather we can characterize by that of climate i (Fresno, San Bernardino, or San Diego). We further assume that in each climate, some fraction f of houses are roofed with coatable tiles, and that the average ceiling area of a house is A_{ceiling}. If the number of air-conditioned houses in each climate is N_i, then $A_i = f\, A_{\mathrm{ceiling}}\, N_i$, yielding statewide power savings

$$\Delta\tilde{P}_{\mathrm{CA}} = f\, \Delta\alpha_{\mathrm{avg}}\, A_{\mathrm{ceiling}} \sum_i \left(\Delta P/\Delta\alpha\right)_i N_i \tag{5}$$

The California Energy Commission has published yearly estimates of the number of air-conditioned houses in each of its 16 demand forecasting climate zones[5] (Figure 9, p.32). We estimate N_i by assigning the houses located in each of the forecasting climate zones to one of the three simulation climates (Table 6, p.26).

Cooling Energy

The statewide reduction in annual cooling energy consumption, $\Delta\tilde{E}_{\mathrm{CA}}$ [kWh yr^{-1}] may be estimated from the analogous expression

[5] Note that the Forecasting Climate Zones are not the same as the California Thermal Zones used in building simulations.

$$\Delta\tilde{E}_{\mathrm{CA}} = f\,\Delta\alpha_{\mathrm{avg}}\,A_{\mathrm{ceiling}}\sum_i \left(\Delta E/\Delta\alpha\right)_i\,N_i \qquad (6)$$

Emissions

Energy savings reduce emissions of carbon dioxide (CO_2), nitrogen oxides (NO_x), and sulfur oxides (SO_x) from California power plants at the rates of 563 kg CO_2, 17 g NO_x , and 14 g SO_x per MWh (ICF Consulting, 1999).

Experiment

Construction, Installation, and Instrumentation of the Scale Models

We tested four identical, 1:10 scale, single-room wooden houses modeled after desert homes. Each building had

- a concrete tile roof mounted on a pitched deck;
- a naturally ventilated attic;
- R-11 (1.9 m^2 K W^{-1}) foam-board insulation constituting the room's ceiling and lining the inside of the room's floor and walls;
- an aluminum foil facing on the top of the ceiling;
- white exterior walls;
- a thermoelectric air conditioner with a cooling output of 120 W (400 BTU h^{-1}), controlled by an electronic thermostat capable of regulating the air temperature inside the room to within 0.2K; and
- a resistive heating element in the center of the room available to supply a known heat load during calibration of the air conditioner.

The attic's natural ventilation was provided by two pairs of 5-cm diameter holes in its gable equipped with removable plugs. One pair of holes was closed, while each member of the other pair was half-closed (i.e., fitted with half-circle plugs).

The scale models (denoted *A*, *B*, *C*, and *D*) were installed in a courtyard on the grounds of the Riverside Public Utilities (RPU) facility in Riverside, CA (Figure 1, p.28). Each building was set

on temporary concrete footers, and oriented to align the ridge of its roof along an east-west line. The goal was to provide each building's roof with full southern solar exposure free from shading by local mountains, surrounding structures and neighboring scale models. The courtyard was modestly windy, with mid-afternoon peak windspeeds of 1.5 to 2 m s^{-1} (3.4 – 4.5 mph).

Each building was instrumented with precision thermistors (accuracy ±0.2K, response time 15s) to measure the temperatures of the tile upper surface, tile lower surface, deck upper surface, deck lower surface, attic air, ceiling upper surface, ceiling lower surface, and room air. Heat fluxes (W m^{-2}) through the tile, deck, and ceiling were determined by dividing the temperature difference across each structural element (K) by the element's thermal resistance (m^2 K W^{-1}). The input power drawn by each air conditioner was determined from voltage and current transducers (power = voltage × current).

An on-site weather station was erected to measure ambient air temperature, horizontal insolation, relative humidity, wind speed, and wind direction. A pair of dataloggers were programmed to record 1-minute averages of all measurements, and connected to a dedicated phone line. We periodically downloaded these results via modem. The one-minute measurements were averaged over 15-minute intervals to reduce noise and compact the data set.

Uniformity of building construction and orientation was increased by coating the roofs of all 4 buildings black, then rotating buildings and sealing leaks to reduce building-to-building variations in measured temperatures.

Coating Formulation, Tile Preparation, and Reflectance Measurement

Six experimental NIR reflective coatings—terracotta (red), chocolate (brown), gray, green, blue, and black—were prepared, each similar in appearance to a conventional coating (Figure 2, p.29). These formulations provide a reasonably full color palette. The first four NIR-reflective coatings were single-layer systems (i.e., color on gray tile), while the blue and black NIR-reflective coatings were formed by applying a NIR-transmitting layer of color over an opaque, highly-reflective white undercoating.

The solar reflectances of 25-cm^2 tile chips finished with each standard and cool coating were measured in the lab according to ASTM Test Method C 1549 (Devices & Services Solar

Spectrum Reflectometer) (ASTM 2003a). All coatings had thermal emittance circa 0.9, and each each cool coating had a solar reflectance ρ exceeding 0.4 (Table 1, p.24).

Standard and cool versions of each of the six color coatings were airlessly sprayed onto tiles and trim pieces, preparing 20 tiles per coating.

Trials

The roof of building *C* was left black (ρ=0.04), and building *B* reroofed with white tiles (ρ=0.85). Over the course of a summer, building *D* was reroofed with a series of standard color tiles, while building *A* was reroofed with a series of matching cool colors tiles. Hence, at any given time building *C* had a black roof, building *B* had a white roof, building *D* had a standard color roof, and building *A* had a cool color roof matching that of building *D*.

Each color-pair trial included several days during which the air conditioners were turned off, and several more during which they were turned on (Table 1, p.24). Two days of clear-weather data were selected for each color-pair trial: one on which the buildings were air conditioned, and another on which they were not (Table 1, p.24).

On any given day, all thermostats were programmed to the same setpoint, which was typically about 5K below the expected daily peak outside air temperature. It would have been preferable to use a constant setpoint typical of real-house operation (e.g., 24ºC), but the device in the black-roofed house tended to saturate (fail to meet cooling load) when the outside air temperature exceeded the setpoint by more than 5K. Our budget did not permit the installation of additional or higher-capacity cooling units.

Results

Thermal Performance of Tile Coatings on the Scale Models

Measured Reductions in Temperature, Heat Flux

The performance of each cool roof tile coating was gauged by measured reductions (standard color value – matching cool color value) in the daily peak values of roof surface temperature T_s, attic air temperature T_a, interior air temperature T_i of an unconditioned building, and heat flux q

into the ceiling of an air-conditioned building (Table 2, p.24). The coatings reduced roof surface temperature by 5-10 K and ceiling heat flux by about 10 to 20%.

Note that the ceiling heat flux was computed assuming a ceiling undersurface temperature of 24ºC to make the flux values relevant to real-house performance.[6] Also, noise originating from transient building-to-building differences in incident solar radiation was decreased by basing these peak reductions on full days of data from all four buildings (Appendix).

We note that the reductions in peak roof surface temperature, attic air temperature, unconditioned interior air temperature, and ceiling heat flux each decrease as the roof-level windspeed increases. Hence, reductions may be smaller for peak daily windspeeds greater than the 1.5 – 2 m s^{-1} observed at the experimental site.

Regressed Sensitivities of Temperature, Heat Flux to Reduction in Absorbed Insolation

Reductions in peak temperature (ΔT_s, ΔT_a, ΔT_i) and peak heat flux (Δq) were linearly regressed to the reduction in absorbed insolation $I\,\Delta\alpha$ to yield sensitivities k_x, where $x = T_s, T_a, T_i,$ or q (Figure 3 - Figure 6, pp.29-31).

The top of the foam board insulation that comprised the ceiling was faced with aluminum foil (thermal emittance about 0.07). This foil acted as a radiant barrier, increasing the radiative resistance between ceiling and roofdeck from about R-1 (what would be observed if both ceiling and roofdeck had emittance of 0.9) to about R-14. The radiative resistance in a house without a radiant barrier would be much lower, and the heat flux through the ceiling much higher. Since the sensitivities determined from the measured data apply only to a building with (a) R-11 aggregate resistance of the ceiling plus attic insulation and (b) a radiant barrier, heat transfer theory (Appendix) was used to extrapolate sensitivities for a building that (a) does not have a radiant barrier; (b) has ceiling resistance R-2; and (c) has attic insulation varying from R-0 to R-30 (Table 3, p.25).

[6] Ceiling heat flux is the ratio of the temperature difference across the ceiling to the thermal resistance of the ceiling. Since the ceiling was formed by a slab of R-11 insulation, the temperature of the ceiling's upper surface was minimally affected by the temperature of its underside. Hence, the "standardized" ceiling heat flux was computed as $(T_{\text{top of ceiling}} - 24ºC) / R_{\text{ceiling}}$.

Typical sensitivities (reduction in temperature or flux per reduction in absorbed insolation) extrapolated for an air-conditioned house with R-11 attic insulation, an R-2 ceiling, and no radiant barrier are approximately 41 K / (kW m^{-2}) for roof surface temperature, 21 K / (kW m^{-2}) for attic temperature, and 12 W m^{-2} / (kW m^{-2}) for ceiling heat flux per unit ceiling area. Hence, under typical conditions—e.g., R-11 attic insulation, 1 kW m^{-2} insolation, 0.3 reduction in solar absorptance—absolute reductions in roof surface temperature, attic air temperature, and ceiling heat flux would be about 12 K (21 ºF), 6.2 K (8.0 ºF), and 3.7 W m^{-2}, respectively.

Cooling Power and Energy Savings of the Scale Models

The instantaneous cooling power demand $\tilde{P}$ [W] of each scale model was calculated as the total power drawn by its thermoelectric air conditioner minus the constant power demand of the device's always-on fans. Building cooling power demand can be used to determine the reduction (standard color building value – cool color building value) in each of four quantities:

- building cooling power demand per unit ceiling area, P [W m^{-2}];
- building cooling load per unit ceiling area, $\mathrm{COP}^{-1} P$ [W m^{-2}];
- daily building cooling energy use per unit ceiling area, $E = \int_{\text{day}} P \, d\tau$ [kWh m^{-2}], and
- daily building cooling load per unit ceiling area, $\mathrm{COP}^{-1} E$ [kWh m^{-2}].

Here τ is time, and COP is the coefficient of performance of each thermoelectric air conditioner, measured in nighttime's calibration trials as the ratio of cooling power demand [W] to known resistive heat flux [W].

After a great deal of analysis, it was determined that direct determination of scale-model cooling power and energy savings was impractical, because

- the cooling load of each building was dominated by heat gains through the walls, making the ceiling contribution difficult to measure;
- wall thermal resistance varied building to building, primarily because of infiltration around and/or conduction through the wall-mounted air conditioner; and

- the COP of each thermoelectric device was temperature dependent, meaning that COP values determined during nighttime calibrations of the devices were not necessarily applicable to operation at higher daytime temperatures.

Hence, we decided to base estimates of real-house cooling power savings on reduction in ceiling heat flux, which was easier to measure.

Estimated Cooling Power Savings for Full-Scale Houses

Figure 7 (p.31) charts the peak cooling power savings per unit decrease in solar absorptance, $\Delta P/\Delta\alpha$, versus ceiling insulation, estimated via Eq. (2) for full-scale houses (without radiant barriers) in three California climates: Fresno (Central Valley), San Bernardino, and San Diego (coastal). Results for common levels of attic insulation are also presented in Table 4 (p.25). Whole-house peak cooling power savings $\Delta\tilde{P}$ [W] may be computed by multiplying the tabulated value of $\Delta P/\Delta\alpha$ (5.5, 5.1, and 5.0 W m^{-2} for Fresno, San Bernardino, and San Diego, respectively, assuming R-11 ceiling insulation) by ceiling area (e.g., $A = 139$ m^2 [1,500 ft^2]) and decrease in solar absorptance (e.g., $\Delta\alpha = 0.3$). Whole-house peak power savings are 230, 210, and 210 W in Fresno, San Bernardino, and San Diego, respectively.

Estimated Cooling Energy Savings for Full-Scale Houses

Figure 8 (p.32) charts the annual cooling energy savings per unit decrease in solar absorptance, $\Delta E/\Delta\alpha$, versus ceiling insulation, for the same three climates—Fresno, San Bernardino, and San Diego. Results for common levels of attic insulation are also presented in Table 4 (p.25). Whole-house cooling energy savings $\Delta\tilde{E}$ [kWh yr^{-1}] may be computed by multiplying the tabulated value of $\Delta E/\Delta\alpha$ (2.2, 1.6, and 0.2 kWh m^{-2} yr^{-1} for Fresno, San Bernardino, and San Diego, respectively, assuming R-11 attic insulation) by ceiling area and decrease in solar absorptance. The whole-house energy savings are 92, 67, and 8 kWh yr^{-1} in Fresno, San Bernardino, and San Diego, respectively.

For a typical ceiling area of 1,500 ft^2 (139 m^2) and a typical reduction in roof absorptance of 0.3, the whole-house peak power savings were 230, 210, and 210 W, respectively, while the whole-

house energy savings were 92, 67, and 8 kWh yr^{-1}, respectively. At 0.12 \$/kWh, the values of energy savings in Fresno, San Bernardino, and San Diego are 11, 8, and 1 \$/yr.

If the area of the sloped tile roof is about 1.5 times the ceiling area, or 209 m^2, the cost of coating the roof (at 15 \$/m^2) about \$3100. Of this, the premium for using cool pigments in place of standard pigments(at 0.27 \$/m^2) is about \$56. Hence, while the economic value of the energy savings derived from a cool colored rooftile coating is far below than cost of the coating, the simple payback times for the cost *premium* associated with using cool pigments in the coating are about 5 and 7 years in the hot climates of Fresno and San Bernardino, respectively.

These energy savings can be cast as fractions of cooling energy use by using California Energy Commission projections of average annual residential cooling energy use in each climate. Assuming a typical house flat roof area of 1,500 ft^2 (139 m^2), average cooling energy uses in Fresno, San Bernardino, and San Diego in the year 2000 were 12.1, 8.2, and 4.3 kWh m^{-2} yr^{-1}, respectively (CEC 2000). Hence, fractional savings were 5%, 6%, and 1% in these three climates.

Statewide Reductions in Power Demand, Energy Consumption, and Emissions

There are about 2.41, 1.01 and 3.01 million air-conditioned California homes in climates characterizable by those of Fresno, San Bernardino, and San Diego, respectively (Table 6). If $f = 20\%$ of California houses were roofed with coatable tiles, and all had R-11 attic insulation and an average ceiling area of 139 m^2 (1,500 ft^2), rooftile coatings that lower solar absorptance by 0.3 would yield statewide peak demand savings of

$$0.20 \times 0.3 \times 139 \times \left(5.5 \times 2{,}410{,}000 + 5.1 \times 1{,}010{,}000 + 5.0 \times 3{,}010{,}000\right) = 280 \text{ MW}$$

The aggregate cooling energy use reduction would be

$$0.20 \times 0.3 \times 139 \times \left(2.2 \times 2{,}410{,}000 + 1.6 \times 1{,}010{,}000 + 0.2 \times 3{,}010{,}000\right) = 63 \text{ GWh yr}^{-1}$$

which at \$0.12 kWh^{-1} is worth about \$7.5 M yr^{-1}.

These energy savings would reduce annual emissions from California power plants by 35 kilotonnes CO_2, 11 tonnes NO_x, and 0.86 tonnes SO_x.

Discussion

Power savings (per unit ceiling area) were about half those reported for Florida houses with R-11 attic insulation (Parker *et al.* 1998). This may result from

- the high thermal resistance between the roof tiles and roofdeck, which adds about R-2 to the roof-to-interior thermal resistance (Appendix);
- convective roofdeck cooling by air flowing between tile and deck; and/or
- natural attic ventilation in the model houses.

It should be also noted that there is additional uncertainty in the energy savings because of the arbitrary assumption that half of the daily insolation incident on a house results in ceiling heat flux that must be removed by air conditioning. However, our results can be linearly rescaled to another value of this fraction ϕ. Similarly, our estimates of statewide savings are proportional to the fraction of California homes roofed with coatable tiles, assumed to be $f = 0.2$. These savings can be linearly rescaled to another value of the fraction f.

Peak power demand reductions in cooler climates (e.g., San Diego) may eliminate the need for air conditioning in some homes by keeping the interior air temperature of a house below the thermostatic setpoint. This would permit homeowners to avoid the purchase of air-conditioning equipment.

Conclusions

Application of NIR-reflective rooftile coatings yielded measurable reductions in roof surface temperature, attic air temperature, unconditioned interior air temperature, and ceiling heat flux. The coatings reduced roof surface temperature by about 5 to 10 K and ceiling heat flux by about 10 to 20%.

The coatings are predicted to save about 230 W (1.7 W m^{-2}) in peak cooling power and 92 kWh yr^{-1} (0.7 kWh m^{-2} yr^{-1}) in cooling energy for a 1,500 ft^2 (139 m^2) Fresno house with R-11 attic insulation. The economic value of annual energy savings is much less than the total cost of a tile coating, but in the hot Fresno climate, the simple payback time for the cost premium of using

cool pigments in a rooftile coating is only 5 years. Savings can be about 3 times higher for houses with minimal ceiling insulation. The peak power demand reductions in cooler climates (e.g., San Diego) may eliminate the need to purchase an air conditioner.

Statewide reductions in peak cooling power demand and annual cooling energy consumption would be 240 MW and 63 GWh yr^{-1}, respectively. These energy savings would reduce annual emissions from California power plants by 35 kilotonnes CO_2, 11 tonnes NO_x, and 0.86 tonnes SO_x.

A survey and analysis of the California new construction and retrofit markets for cool tile coatings should be conducted to better quantify the potential savings that these coatings may afford, as well as their market acceptability.

Acknowledgements

This work was supported by the California Energy Commission (CEC) through its Public Interest Energy Research Program (PIER) / Energy Innovation Small Grant Program (EISG), and by the Assistant Secretary for Renewable Energy under Contract No. DE-AC03-76SF00098.

We would like to acknowledge the valuable assistance of David Wright, Atoya Mendez, Steven Lafund and especially Klaus Meister of Riverside Public Utilities; Dennis DeBartolomeo and Paul Berdahl of Lawrence Berkeley National Laboratory; and Glen Sharp of the Energy Commission. We thank Jerry Vandewater and Chris Dodge from Monier-Lifetile for supplying the tile. We also thank various other contributors who helped to make this project a success, including Phil Bremenstuhl of C. T. Consultants; Bob Sypowicz and John Wauchope of MCC, Inc.; Dave Getty, Steve Aprea, Bernie Cunningham, and Peter Croft for blueprint drawings, construction, installation and Visio drawings; Jim Dunn and Ken Loye of Ferro Company; Phil Avery and Craig Blockfelter of BASF; and Dana Harding and Mike Muldown of Consolidated Color Corporation.

References

Akbari, H., S. Bretz, D. Kurn and J. Hanford. 1997. Peak power and cooling energy savings of high-albedo roofs. *Energy and Buildings* **25**:117-126.

Akbari, H. and S. Konopacki. 2004. Energy impacts of heat island reduction strategies in Toronto, Canada. *Energy,* **29**, 191-210. Also Lawrence Berkeley National Laboratory Report LBNL-49172, Berkeley, CA, November 2001.

ASTM. 2003a. C1549-02: Standard test method for determination of solar reflectance near ambient temperature using a portable solar reflectometer. Annual Book of ASTM Standards 04.06. Philadelphia, PA: American Society for Testing and Materials.

California Energy Commission (CEC). 2000. California energy demand, 2000-2010. P200-00—002. Sacramento, CA: California Energy Commission.

DOE. 2004. DOE Cool Roof Calculator. Online at http://www.ornl.gov/sci/roofs+walls/facts/CoolCalcEnergy.htm .

EPA. 2004. EnergyStar Roofing Comparison Calculator. Online at http://roofcalc.com .

ICF Consulting. 1999. Emissions factors, global warming potentials, unit conversions, emissions, and related facts. Online at http://www.epa.gov/appdstar/pdf/brochure.pdf .

Konopacki, S. and H. Akbari. 2000. Energy savings calculations for heat island reduction strategies in Baton Rouge, Sacramento and Salt Lake City. Lawrence Berkeley National Laboratory Report LBNL-42890. Berkeley, CA.

Konopacki, S. and H. Akbari. 2001. Measured energy savings and demand reduction from a reflective roof membrane on a large retail store in Austin. LBNL-47149. Berkeley, CA: Lawrence Berkeley National Laboratory.

Konopacki, S. and H. Akbari. 2002. Energy savings of heat-island-reduction strategies in Chicago and Houston (including updates for Baton Rouge, Sacramento, and Salt Lake City). Lawrence Berkeley National Laboratory Report LBL-49638, Berkeley, CA.

Konopacki, S., H. Akbari, M. Pomerantz, S. Gabersek and L. Gartland. 1997. Cooling energy savings potential of light-colored roofs for residential and commercial buildings in 11 U.S. metropolitan areas". Lawrence Berkeley National Laboratory Report LBNL-39433. Berkeley, CA.

Levinson, R., P. Berdahl, and H. Akbari. 2004a. Solar spectral optical properties of pigments, part I: model for deriving scattering and absorption coefficients from transmittance and reflectance measurements. Submitted to *Solar Energy Materials & Solar Cells*.

Levinson, R., P. Berdahl, and H. Akbari. 2004b. Solar spectral optical properties of pigments, part II: survey of common colorants. Submitted to *Solar Energy Materials & Solar Cells*.

Parker, D., J. Huang, S. Konopacki, L. Gartland, J. Sherwin and L. Gu. 1998. Measured and simulated performance of reflective roofing systems in residential buildings. *ASHRAE Transactions* **104**(1):963-975.

Schultz, Don. 1983. Measurement and evaluation of the energy conservation potential in California's residential sector. Publication 400-83-026. Sacramento, CA: California Energy Commission.

Appendix

Building Heat Transfer

Roof Energy Balance

We can obtain approximate but highly useful relations for the thermal properties of a building by neglecting thermal storage and linearizing the exchange of thermal radiation. With these assumptions, the quasi-steady energy balance on the surface of a roof may be written

$$\alpha I = R_o^{-1}\left(T_s - T_o\right) + R_r^{-1}\left(T_s - T_r\right) + R_i^{-1}\left(T_s - T_i\right) \quad \text{(A1)}$$

where α is the roof's solar absorptance (1-solar reflectance); I is insolation [W m^{-2}]; T_s, T_o, T_r, and T_i are the temperatures [K] of the roof surface, outside air, radiative exchange surface seen by the roof (e.g., the sky), and the air inside the room, respectively; and R_o, R_r, and R_i are the thermal resistances (hereafter, simply "resistances"; m^2 K W^{-1}) to convection of heat from the roof to the outside air, radiation of heat from the roof to the its radiative exchange surface, and transfer of heat from the roof's surface to the air-conditioned interior, respectively.

Absolute Roof Surface Temperature, Attic Air Temperature, and Ceiling Heat Flux

Eq. (A1) can be solved to find the roof's surface temperature,

$$T_s = \frac{\alpha I R_o R_r R_i + R_i R_r T_o + R_o R_r T_i + R_o R_i T_r}{R_o R_r + \left(R_o + R_r\right) R_i} \quad \text{(A2)}$$

and the roof-to-interior, or "ceiling," heat flux [W m^{-2}]

$$q = R_i^{-1}\left(T_s - T_i\right) \quad \text{(A3)}$$

If the resistance of the ceiling plus the attic insulation is R_c, and the resistance between the top of the roof and the bottom of the roofdeck is R_d, the temperatures of the insulation top and roofdeck bottom will be

$$T_{\text{insulation top}} = T_i + q\,R_c \quad \text{(A4)}$$

and

$$T_{\text{roofdeck bottom}} = T_s - q\,R_d \quad \text{(A5)}$$

respectively. The attic air temperature, T_a, will be approximately the average of these two surface temperatures:

$$T_a = \frac{T_{\text{insulation top}} + T_{\text{roofdeck bottom}}}{2} = \frac{\left(T_s + T_i\right) + q\left(R_c - R_d\right)}{2} \tag{A6}$$

Normalized Roof Surface Temperature, Attic Air Temperature, and Ceiling Heat Flux

Any thermal property x of a building with a colored roof can be compared to the corresponding properties of an otherwise-identical white-roofed building, x_w, and an otherwise-identical black-roofed building, x_b, using the normalization

$$\hat{x} \equiv \frac{x - x_w}{x_b - x_w} \tag{A7}$$

If all roofs are good thermal emitters, and colored roofs have solar absorptances between those of the white and black roofs, the normalized thermal properties have expected values between 0 (white) and 1 (black). Inspection of Eqs. (A2) through (A6) shows that the normalized roof surface temperature, attic air temperature, and ceiling heat flux are all equal, constant, and dependent only on the solar absorptances of the roofs:

$$\hat{T}_s = \hat{T}_a = \hat{q} = \frac{\alpha - \alpha_w}{\alpha_b - \alpha_w} \tag{A8}$$

Averaging Normalized Properties to Eliminate Transients

In practice, the tendency of dark, thermally-massive surfaces to heat more rapidly than light, thermally-massive surfaces, combined with minor, solar-angle-related differences among buildings in incident insolation and radiative cooling, will make these normalized properties vary somewhat over the course of the day. One way to characterize the thermal performance of a colored-roof building is to use a daytime-averaged value of each normalized property, $\hat{x}_{\text{avg}}$, and invert the normalization definition [Eq. (A7)] to express the absolute colored-roof building property x in terms of the absolute white- and black-roofed building properties x_w and w_b:

$$x \approx x_w + \left(x_b - x_w\right)\hat{x}_{\text{avg}} \tag{A9}$$

This characteristic is particularly useful when comparing the thermal properties of two colored-roof buildings (e.g., a cool red and a standard red) for which the difference in their absolute values might be comparable in magnitude to solar-angle-dependent noise. For example, this technique may be used to evaluate the absolute difference between the daily peak properties of a cool roof and a standard roof as

$$\Delta x_{\text{peak}} \approx \left(x_{b,\text{peak}} - x_{w,\text{peak}}\right)\left(\hat{x}_{\text{standard,avg}} - \hat{x}_{\text{cool,avg}}\right) \tag{A10}$$

Absolute Reductions in Roof Surface Temperature, Attic Air Temperature, and Ceiling Heat Flux

Further inspection of Eqs. (A2) through (A6) indicates that reducing roof solar absorptance by $\Delta\alpha$ (say, by switching from a standard color coating to a cool color coating) will lower the roof surface temperature, attic air temperature, and ceiling heat flux by

$$\Delta T_s = \frac{R_o R_r R_i}{R_o R_r + \left(R_o + R_r\right) R_i} \times I\,\Delta\alpha \tag{A11}$$

$$\Delta T_a = \frac{R_i + R_c - R_d}{2\,R_i}\,\Delta T_s \tag{A12}$$

and

$$\Delta q = R_i^{-1}\,\Delta T_s \tag{A13}$$

respectively. Since the reductions in roof surface temperature, attic air temperature, and ceiling heat flux are all proportional to the decrease in absorbed solar radiation (or increase in reflected solar radiation), $I\,\Delta\alpha$, this suggests that measured reductions in each property x should be regressed to $I\,\Delta\alpha$ to yield an empirical relation of the form

$$\Delta x = k_x \times I\Delta\alpha \tag{A14}$$

where k_x is a fitted sensitivity.

Variation of Ceiling Heat Flux With Thermal Resistances

The reduction in ceiling heat flux, Δq, and hence the sensitivity k_q measured in a scale model, depend on its various thermal resistances. The sensitivity k_q' applicable to another building whose resistances are denoted with primes may be extrapolated from the measured k_q via the relation

$$\frac{k_q'}{k_q} = \frac{\Delta q'}{\Delta q} = \frac{\left(R_o + R_r\right) R_i + R_o R_r}{\left(R_o + R_r\right) R_i' + R_o R_r} \tag{A15}$$

The roof surface and attic air temperature sensitivities may similarly be extrapolated via the relations

$$\frac{k'_{T_s}}{k_{T_s}} = \frac{\Delta T'_s}{\Delta T_s} = \frac{R'_i}{R_i} \times \frac{\Delta q'}{\Delta q} \tag{A16}$$

and

$$\frac{k'_{T_a}}{k_{T_a}} = \frac{\Delta T'_a}{\Delta T_a} = \frac{R'_i + R'_c - R'_d}{R_i + R_c - R_d} \times \frac{\Delta q'}{\Delta q} \tag{A17}$$

respectively.

Example. Δq and k_q are measured using a model house whose concrete roof tiles are painted with a high-emittance coating [$R_r \approx 0.17$ m^2 K W^{-1}] and situated in a moderate wind [$R_o \approx 0.08$ m^2 K W^{-1}]. The ceiling of the model house is an R-11 rigid foam board [$R_c = 1.9$ m^2 K W^{-1}] with an aluminum foil upper face (average thermal emittance 0.06). Assuming the only mode of heat transfer between the tile and deck and between the deck and ceiling is radiative, the thermal resistance from the roof to the ceiling is the sum of the conductive resistance of the tile [$R \approx 0.03$ m^2 K W^{-1}], the radiative resistance between the tile and deck [$R \approx 0.2$ m^2 K W^{-1}], the conductive resistance of the wooden deck [$R \approx 0.08$ m^2 K W^{-1}], and the radiative resistance between the deck and ceiling [$R \approx 2.8$ m^2 K W^{-1}].[7] That is, $R_s \approx 3.1$ m^2 K W^{-1}, and $R_i = R_s + R_c \approx 4.7$ m^2 K W^{-1}. We can use Eq. (A15) to estimate $\Delta q'$ and k'_q for a similarly tiled and situated real house that has an R-2 ceiling (0.35 m^2 K W^{-1}) topped with R-11 attic insulation (1.9 m^2 K W^{-1}), but does not have a radiant barrier:

$$\frac{k'_q}{k_q} = \frac{\Delta q'}{\Delta q} = \frac{(0.08+0.17)(4.7)+(0.08)(0.17)}{(0.08+0.17)(2.8)+(0.08)(0.17)} = 1.7 \tag{A18}$$

Hence, the absolute increase in ceiling heat flux for the real house would be 1.7 times greater than that measured for the model house. In the limiting case of a real house with no attic

[7] The high thermal resistance between the lower surface of the roofdeck and the upper surface of the scale-model house ceiling results from the low thermal emittance of the foil facing on the top of the insulation board that serves as the ceiling. The expression for radiative thermal resistance R between two parallel surfaces of emittances ε_1 and ε_2 is $R = h_r^{-1}\left(\varepsilon_1^{-1} + \varepsilon_2^{-1} - 1\right)$. The radiation coefficient $h_r \approx 4\sigma\overline{T}^3$, where σ is the Stefan-Boltzmann constant and $\overline{T}$ is a temperature characteristic of the surfaces.

insulation [$R_c' = 0.35$ and $R_i' = 0.85$], the absolute increase in ceiling heat flux would be about 3 times greater than that for a real house with R-11 attic insulation.

Estimated Energy Savings for Full-Scale House

Estimating Annual Energy Savings from Annual Load-Hour Insolation

Assume that reducing roof solar absorptance by $\Delta\alpha$ decreases ceiling heat flux [W m^{-2}] by $\Delta q = k_q \times I \Delta\alpha$, where I is global horizontal insolation [kW m^{-2}] and k_q is an experimentally determined sensitivity. The annual cooling energy savings [kWh] accrued to a house of ceiling area A will be

$$\Delta E = \frac{1}{\text{COP}} \times A \int_{\tau_{\text{load}}} \Delta q(\tau)\, d\tau = \frac{1}{\text{COP}} \times A\, k_q\, \Delta\alpha \int_{\tau_{\text{load}}} I(\tau)\, d\tau \qquad \text{(A19)}$$

where COP is the air conditioner's coefficient of performance (output cooling power / input electrical power), τ is time, and $\int_{\tau_{\text{load}}} I(\tau)\, d\tau$ is the annual global horizontal insolation [kWh m^{-2}] incident on the roof during those hours in which there is a positive ceiling heat flux into the interior of the house that is then removed by air conditioning.

Estimating Annual Load-Hour Insolation from Annual Operating Days and Monthly Cooling Degree Days

The number of operating days in month m can be estimated by apportioning the number of annual operating days d_{annual} according to the fraction of annual cooling degree days (say, CDD24C) contained in each month, $f_m \equiv \frac{\text{CDD24C}_m}{\text{CDD24C}_{\text{annual}}}$:

$$d_m = f_m \times d_{\text{annual}} \qquad \text{(A20)}$$

The average daily insolation [kWh day^{-1}] in month m is

$$J_m = \frac{1}{\text{calendar days in month } m} \times \int_{\text{month } m} I(\tau)\, d\tau \qquad \text{(A21)}$$

A residential air conditioner is typically scheduled to activate in late afternoon; hence, it has to remove heat that has built up in the structure over the course of the day, as well as remove the flux coming through the ceiling during its hours of operation. We assume that some fraction ϕ (say, half) of all insolation received during a day on which the air conditioner runs results in

ceiling heat flux that must ultimately be removed from the building interior by the air conditioner. This yields

$$\int_{\tau_{\text{load}}} I(\tau)\, d\tau = \phi \sum_m d_m J_m = \phi\, d_{\text{annual}} \sum_m f_m J_m = \phi\, d_{\text{annual}}\, \bar{J} \tag{A22}$$

where $\bar{J}$ is the CDD24C-weighted average of daily insolation [kWh m^{-2} day^{-1}] (Table 7, p.27).

Estimating Annual Operating Days

Consider a typical 1,500 ft^2 ($A = 139$ m^2), single-family house cooled by a 3-ton (36 kBTU h^{-1}), EER-8 unit drawing 4.5 kW. If the air conditioner typically runs n hours/day (say, $n = 6$) when the weather is warm enough to require operation, the annual number of operating days d_{annual} is

$$d_{\text{annual}} = \frac{\tilde{E}}{\tilde{P} \times n} \tag{A23}$$

where $\tilde{E} = A \times E$ is annual cooling energy consumption [kWh] and $\tilde{P} = A \times P$ is cooling power demand [kW]. We obtain $\tilde{E}$ from prior simulations of annual cooling energy consumption versus level of ceiling insulation R_c for houses in three California climates: hot Central-Valley city Fresno; temperate Inland-Empire city San Bernardino; and cool, coastal San Diego (Schultz 1983). Regression of the simulated data yields climate-specific functions of the form

$$\tilde{E} = \tilde{E}_0 + bU_i \tag{A24}$$

where $\tilde{E}_0$ is the annual cooling energy consumption due to heat sources other than the ceiling (e.g., wall and internal loads), $U_i \equiv R_i^{-1}$ is the thermal conductance from roof to interior [W m^{-2} K^{-1}], and bU_i is the annual cooling energy consumption due to heat gain through the ceiling (Figure 10, p.33). The roof-to-interior resistance is the sum of the roof assembly resistance (R-1.8), attic insulation (R-0 to R-30), and ceiling resistance (R-1.8). The number of operating hours, $\tilde{E}/\tilde{P}$, versus ceiling resistance in each climate is shown in Table 8 (p.27).

Tables

Table 1. Color-pair trial solar reflectances and schedule (summer 2003). Note that since the roof surface is opaque, solar reflectance increase $\Delta\rho$ is equivalent to solar absorptance decrease $\Delta\alpha$.

Color	$\rho_{standard}$	ρ_{cool}	$\Delta\rho$	Trial Dates	Clear-Weather Day, A/C On	Clear-Weather Day, A/C Off
TERRACOTTA	0.33	0.48	0.15	Jun 6 – Jul 1	Jun 15	Jun 30
CHOCOLATE	0.12	0.41	0.29	Jul 6 – 15	Jul 6	Jul 10
GRAY	0.21	0.44	0.23	Jul 17 – Aug 6	Jul 27	Jul 31
GREEN	0.17	0.46	0.29	Aug 8 - 19	Aug 16	Aug 8
BLUE	0.19	0.44	0.25	Aug 21– Sep 3	Aug 22	Aug 31
BLACK	0.04	0.41	0.37	Sep 4- Oct 6	Sep 14	Sep 5

Table 2. Reductions in scale-model peak tile surface temperature, peak attic air temperature, peak ceiling heat flux (A/C on only), and peak interior air temperature (A/C off only) measured in each of six color-pair trials.

decrease in solar absorptance ($\Delta\alpha = \Delta\rho$)	terracotta 0.15	chocolate 0.29	gray 0.23	green 0.29	blue 0.25	black 0.37
AC on						
trial date	2003-6-15	2003-7-10	2003-7-27	2003-8-16	2003-8-22	2003-9-14
peak horizontal insolation (kW m^{-2})	873	778	817	834	822	734
reduction of peak tile surface temperature (K)	4.6	8.6	6.7	9.6	8.2	13.8
reduction of peak attic air temperature (K)	1.9	3.7	2.8	3.9	2.3	5.5
reduction of peak ceiling heat flux (W m^{-2})	1.0 (13%)	1.7 (17%)	1.4 (15%)	2.0 (17%)	1.1 (13%)	2.1 (21%)
AC off						
trial date	2003-6-30	2003-7-6	2003-7-31	2003-8-8	2003-8-31	2003-9-5
peak horizontal insolation (W m^{-2})	863	847	848	856	794	766
reduction of peak tile surface temperature (K)	5.5	9.4	6.8	11.0	8.2	13.5
reduction of peak attic air temperature (K)	3.0	4.0	2.8	4.5	2.4	7.2
reduction of peak interior air temperature (K)	0.8	1.0	1.1	1.1	0.7	1.8

Table 3. Sensitivities of the peak roof surface temperature, attic air temperature, and ceiling heat flux in an air-conditioned house to peak decrease in absorbed insolation. Values are extrapolated from the scale-model results and assume a real house with an R-2 ceiling and no radiant barrier.

Attic Insulation (ft^2 h F BTU^{-1})	Roof Surface Temperature Sensitivity $k_{T_s} = \Delta T_s / I\Delta\alpha$ [K / (kW m^{-2})]	Attic Air Temperature Sensitivity $k_{T_a} = \Delta T_a / I\Delta\alpha$ [K / (kW m^{-2})]	Ceiling Heat Flux Sensitivity $k_q = \Delta q / I\Delta\alpha$ [(W m^{-2}) / (kW m^{-2})]
0	39.4	12.1	38.9
7	40.9	19.2	16.5
11	41.2	20.5	12.4
19	41.4	21.8	8.3
30	41.6	22.7	5.7

Table 4. Reductions in each of three climates in peak tile surface temperature, attic air temperature, ceiling heat flux, cooling power demand, and cooling energy use of an air-conditioned house per unit reduction in solar absorptance, tabulated versus ceiling insulation. Note that all figures must be multiplied by the reduction in solar absorptance (e.g., $\Delta\alpha = 0.3$).

	Attic Insulation (ft^2 h F BTU^{-1})	0	7	11	19	30
Fresno	Tile Surface Temperature Reduction $\Delta T_s / \Delta\alpha$ (K)	40.9	42.4	42.7	43.0	43.2
	Attic Air Temperature Reduction $\Delta T_a / \Delta\alpha$ (K)	12.5	20.0	21.3	22.7	23.5
	Ceiling Heat Flux Reduction $\Delta q / \Delta\alpha$ (W m^{-2})	40.4	17.1	12.9	8.6	5.9
	Cooling Power Demand Reduction $\Delta P / \Delta\alpha$ (W m^{-2})	17.2	7.3	5.5	3.7	2.5
	Cooling Energy Use Reduction $\Delta E / \Delta\alpha$ (kWh m^{-2} yr^{-1})	9.0	3.0	2.2	1.4	0.9
San Bernardino	Tile Surface Temperature Reduction $\Delta T_s / \Delta\alpha$ (K)	38.0	39.5	39.7	40.0	40.2
	Attic Air Temperature Reduction $\Delta T_a / \Delta\alpha$ (K)	11.6	18.6	19.8	21.1	21.9
	Ceiling Heat Flux Reduction $\Delta q / \Delta\alpha$ (W m^{-2})	37.6	15.9	12.0	8.0	5.5
	Cooling Power Demand Reduction $\Delta P / \Delta\alpha$ (W m^{-2})	16.0	6.8	5.1	3.4	2.3
	Cooling Energy Use Reduction $\Delta E / \Delta\alpha$ (kWh m^{-2} yr^{-1})	6.8	2.2	1.6	1.0	0.7
San Diego	Tile Surface Temperature Reduction $\Delta T_s / \Delta\alpha$ (K)	37.0	38.4	38.7	38.9	39.1
	Attic Air Temperature Reduction $\Delta T_a / \Delta\alpha$ (K)	11.3	18.1	19.3	20.5	21.3
	Ceiling Heat Flux Reduction $\Delta q / \Delta\alpha$ (W m^{-2})	36.6	15.5	11.7	7.8	5.4
	Cooling Power Demand Reduction $\Delta P / \Delta\alpha$ (W m^{-2})	15.6	6.6	5.0	3.3	2.3
	Cooling Energy Use Reduction $\Delta E / \Delta\alpha$ (kWh m^{-2} yr^{-1})	0.7	0.2	0.2	0.1	0.1

Table 5. Annual cooling energy savings per unit decrease in roof solar absorptance vs. ceiling insulation. Shown in each three climates are absolute savings, savings as a fraction of cooling energy required to dissipate the roof heat load, and savings as a fraction of whole-house cooling energy. Note that all figures must be multiplied by the reduction in solar absorptance (e.g., $\Delta\alpha = 0.3$).

	FRESNO			SAN BERNARDINO			SAN DIEGO		
Attic Insulation (ft^2 h F BTU^{-1})	absolute (kWh m^{-2} yr^{-1})	roof fraction	house fraction	absolute (kWh m^{-2} yr^{-1})	roof fraction	house fraction	absolute (kWh m^{-2} yr^{-1})	roof fraction	house fraction
0	9.0	97%	33%	6.8	74%	29%	0.7	64%	26%
7	3.0	80%	14%	2.2	60%	12%	0.2	51%	11%
11	2.2	77%	11%	1.6	57%	9%	0.2	48%	8%
19	1.4	74%	7%	1.0	54%	6%	0.1	46%	6%
30	0.9	72%	5%	0.7	53%	4%	0.1	44%	4%

Table 6. Year-2003 number of air-conditioned houses in each Energy Commission demand forecasting climate zone (FCZ), and the fraction assigned to each simulation climate (Fresno, San Bernardino, or San Diego).

Forecasting Climate Zone	Houses (thousands)	Fresno	San Bernardino	San Diego
FCZ01	147			100%
FCZ02	314	100%		
FCZ03	907	100%		
FCZ04	660			100%
FCZ05	70			100%
FCZ06	435	100%		
FCZ07	176	100%		
FCZ08	820			100%
FCZ09	616	50%		50%
FCZ10	1007		100%	
FCZ11	279			100%
FCZ12	394	50%		50%
FCZ13	460			100%
FCZ14	0		100%	
FCZ15	0		100%	
FCZ16	145	50%		50%
Total Houses (thousands)	**6,430**	**2,410**	**1,010**	**3,010**

Table 7. Monthly cooling degree days at 24ºC (CDD24C), average daily insolation (energy/area), and average peak insolation (power/area) in three climates. Shown also is each climate's CDD24C-weighted annual average daily insolation, $\overline{J}$.

	FRESNO				SAN BERNARDINO				SAN DIEGO			
month	CDD24C (days)	CDD24C fraction	average daily sun (kWh m^{-2})	average peak sun (W m^{-2})	CDD24C (days)	CDD24C fraction	average daily sun (kWh m^{-2})	average peak sun (W m^{-2})	CDD24C (days)	CDD24C fraction	average daily sun (kWh m^{-2})	average peak sun (W m^{-2})
January	0	0.00	2.33	419	0	0%	3.03	532	0	0%	2.33	428
February	0	0.00	3.60	599	0	0%	3.77	624	0	0%	3.18	543
March	0	0.00	4.95	746	0	0%	4.51	738	0	0%	4.45	700
April	0	0.00	6.47	900	0	0%	5.52	816	0	0%	5.44	786
May	20	0.04	7.55	967	0	0%	6.96	956	0	0%	6.28	841
June	92	0.18	8.66	1038	38	10%	7.37	946	0	0%	7.42	939
July	180	0.35	8.22	994	127	34%	7.50	965	0	0%	7.22	928
August	150	0.29	7.28	934	130	35%	6.22	891	10	67%	6.21	861
September	72	0.14	6.05	851	75	20%	5.76	831	5	33%	5.74	817
October	0	0.00	4.58	712	3	1%	4.52	713	0	0%	4.35	682
November	0	0.00	3.18	543	0	0%	3.59	600	0	0%	2.88	491
December	0	0.00	2.35	438	0	0%	2.89	516	0	0%	2.41	435
$\overline{J}$			***7.70***				***6.67***				***6.05***	

Table 8. Annual hours of residential air-conditioner operation versus attic insulation, simulated in each of 3 climates.

Attic Insulation (ft^2 h F BTU^{-1})	Fresno (h yr^{-1})	San Bernardino (h yr^{-1})	San Diego (h yr^{-1})
0	841	735	84
7	671	568	64
11	642	539	60
19	612	510	57
30	594	492	55

Figures

Figure 1. Four identical 1:10-scale model houses sited in a courtyard at the Riverside Public Utilities facility in Riverside, CA. Counterclockwise from left (east), the four buildings are shown with (A) cool chocolate, (B) white, (C) black, and (D) standard chocolate roof tile coatings. An instrument shed lies in the center, while a weather tower stands in the foreground.

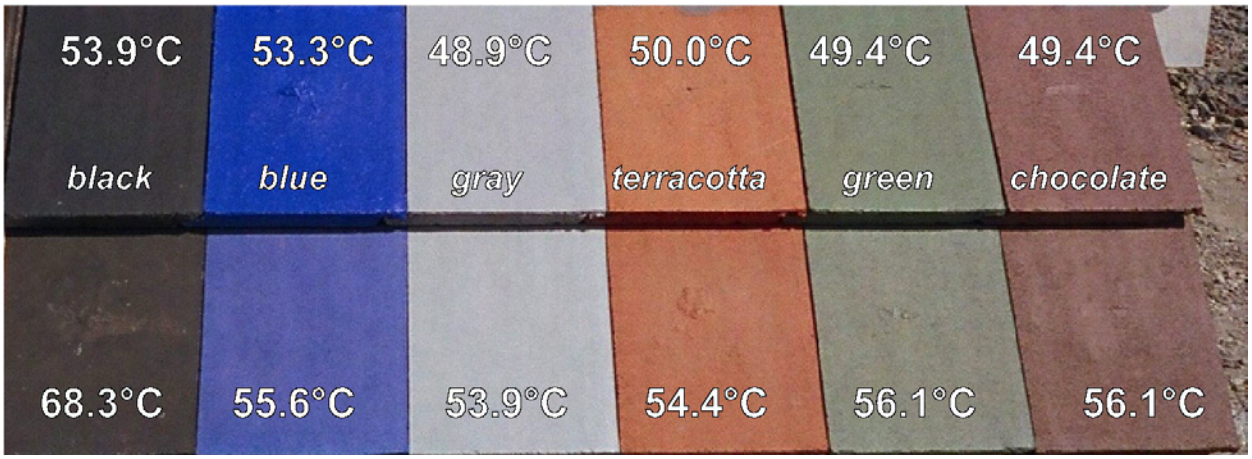

Figure 2. Appearance and surface temperatures of cool tile coatings (top row) formulated to match standard color coatings (bottom row). Surface temperatures were measured from 11:20 – 11:30AM solar on 17 September 2003 (outside air temperature 27ºC, horizontal global insolation 820 W m^{-2}).

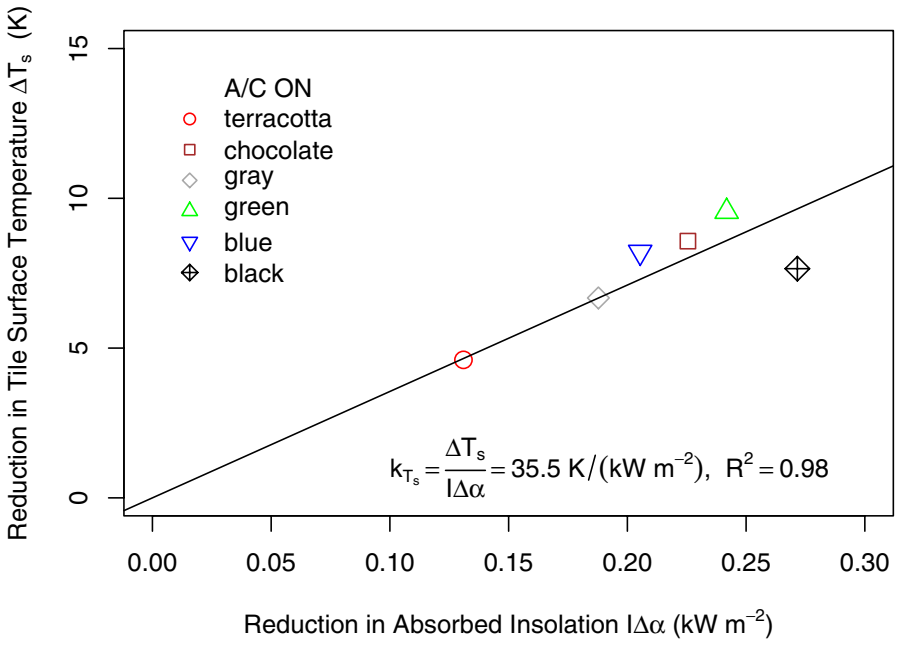

Figure 3. Measured reduction in peak roof tile surface temperature of an air-conditioned scale model vs. reduction in peak absorbed insolation achieved by switching from a standard color coating to a cool color coating.

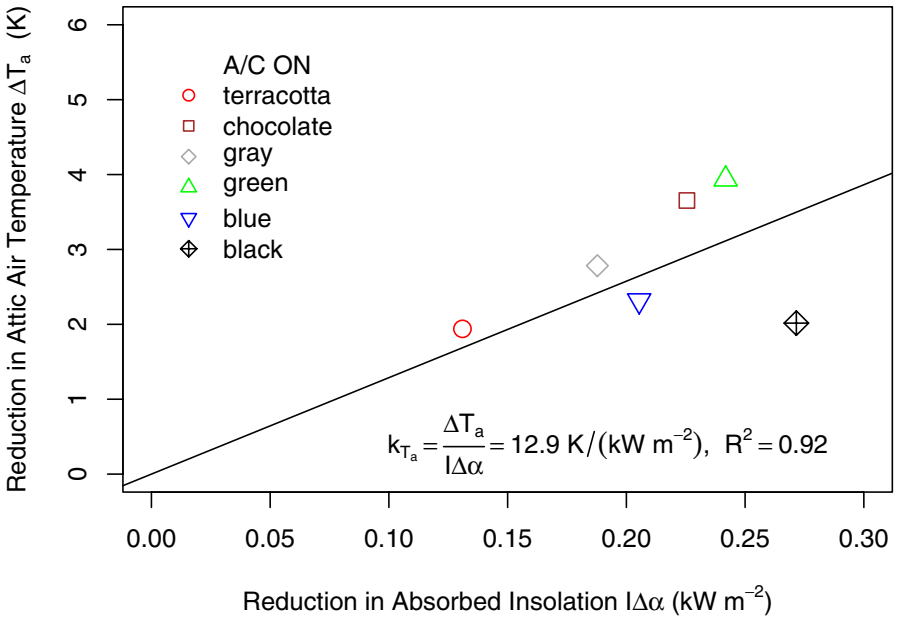

Figure 4. Measured reduction in peak attic air temperature of an air-conditioned scale model vs. reduction in peak absorbed insolation achieved by switching from a standard color coating to a cool color coating.

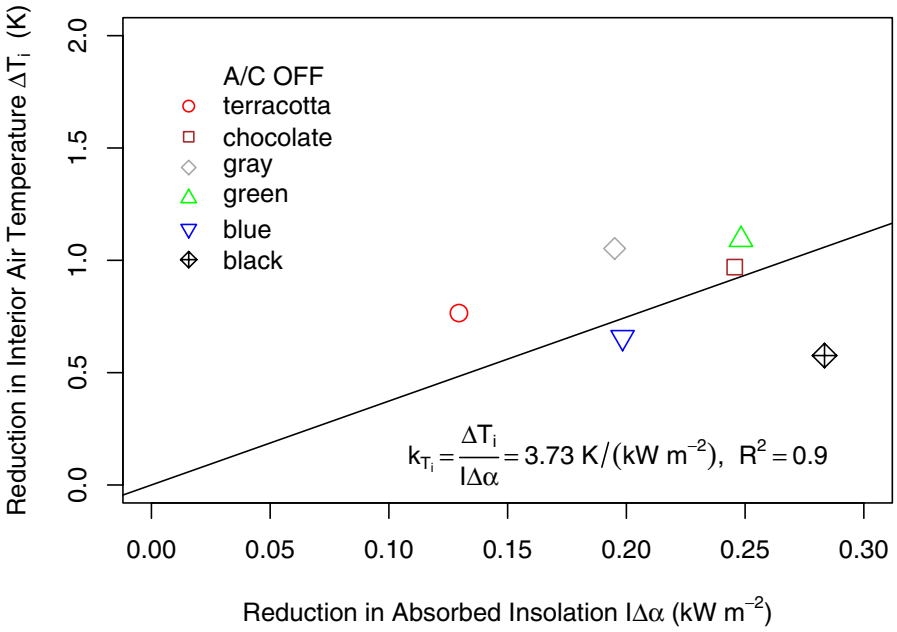

Figure 5. Measured reduction in peak interior air temperature of an unconditioned scale model vs. reduction in peak absorbed insolation achieved by switching from a standard color coating to a cool color coating.

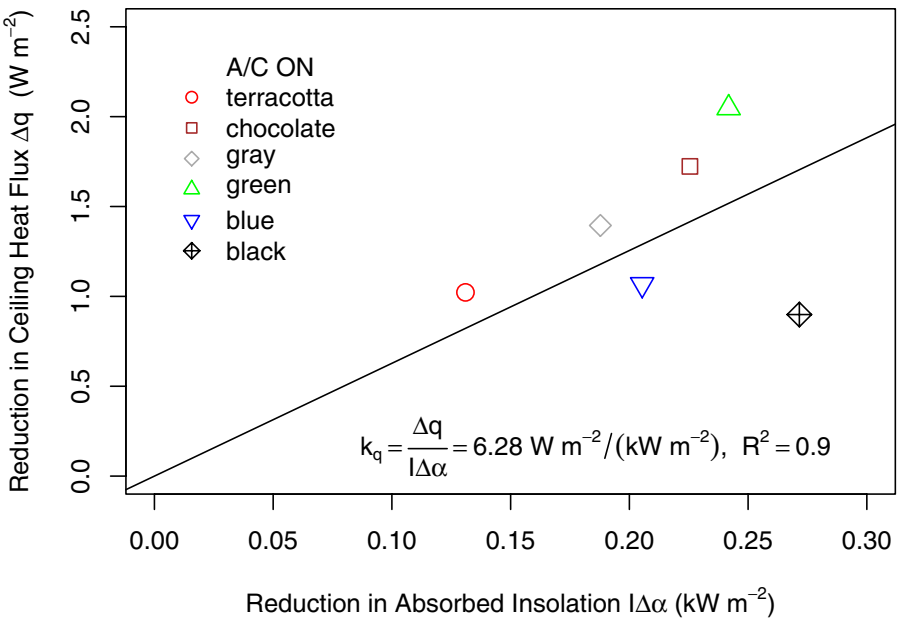

Figure 6. Measured reduction in peak ceiling heat flux into an air-conditioned scale model vs. reduction in peak absorbed insolation achieved by switching from a standard color coating to a cool color coating. Note that heat flux values have been adjusted to assume a common interior air temperature of 24ºC.

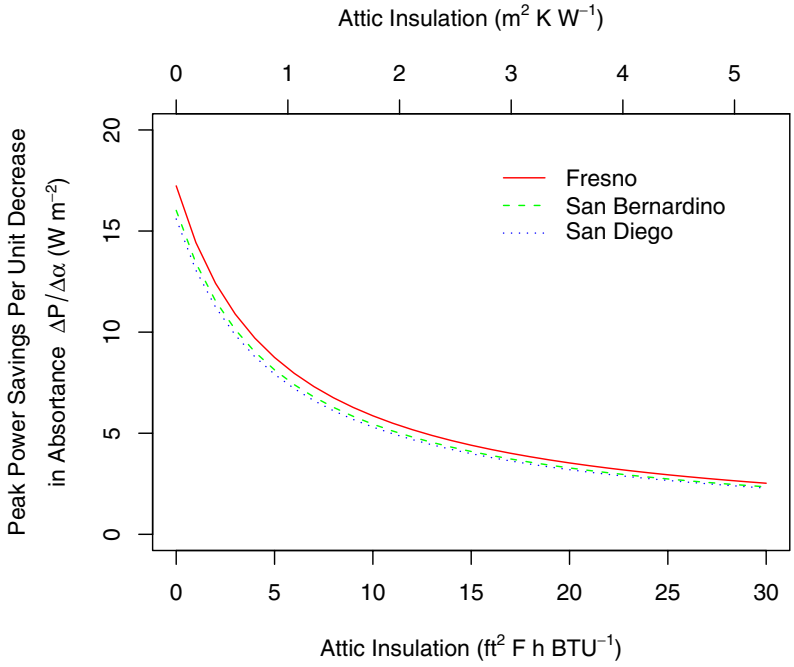

Figure 7. Estimated savings in real-house peak cooling power demand (per unit ceiling area) per unit decrease in solar absorptance versus ceiling insulation. Note that this curve must be multiplied by reduction in roof solar absorptance (e.g., $\Delta\alpha = 0.3$) to obtain actual savings.

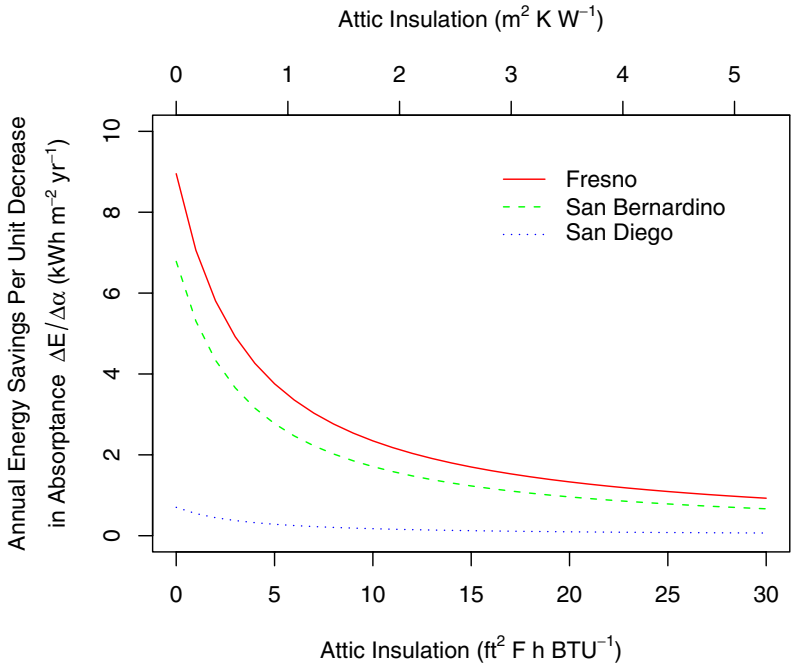

Figure 8. Estimated savings in real-house annual cooling energy consumption (per unit ceiling area) per unit decrease in solar absorptance versus ceiling insulation. Note that this curve must be multiplied by reduction in roof solar absorptance (e.g., $\Delta\alpha = 0.3$) to obtain actual savings.

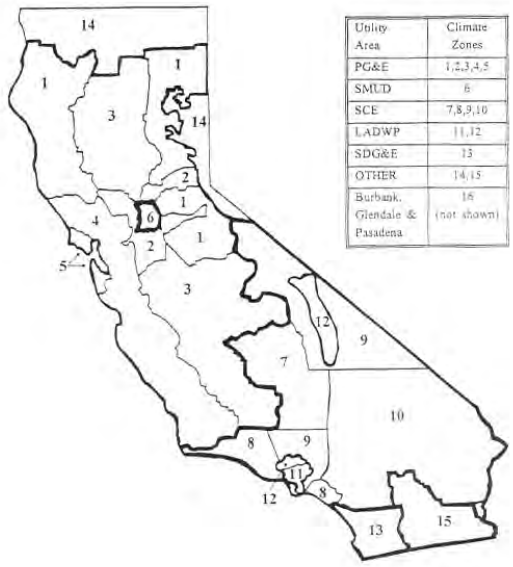

Figure 9. The Energy Commission's 16 demand forecasting climate zones in California. Note that these differ from the California Thermal Zones commonly used in building simulations.

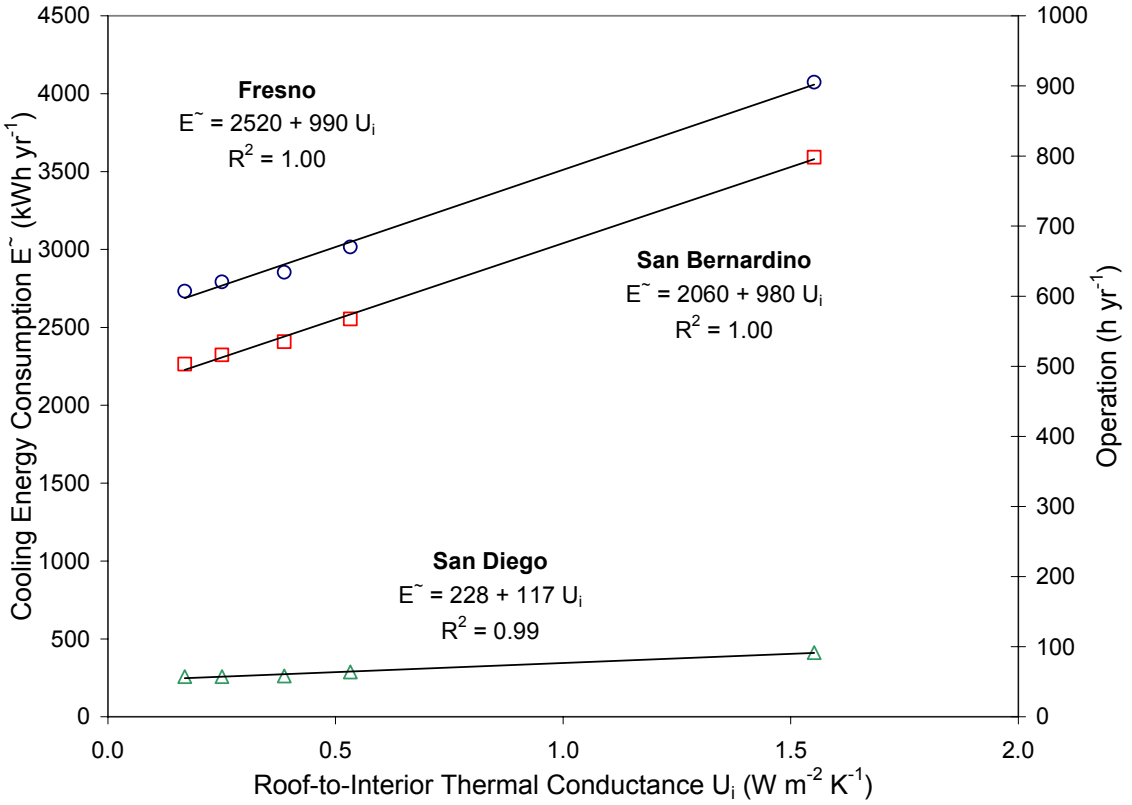

Figure 10. Annual cooling energy consumed by a 1,500 ft^2 (139 m^2) single-family house versus roof-to-interior thermal conductance, simulated in each of three climates. Annual hours of operation assume a 3-ton, EER-8 air conditioner (power demand 4.5 kW).

PROFESSIONAL ROOFING

Cooling down the house

Residential roofing products soon will boast "cool" surfaces

by ***Hashem Akbari and André Desjarlais***

Energy-efficient roofing materials are becoming more popular, but most commercially available products are geared toward the low-slope sector. However, research and development are taking place to produce "cool" residential roofing materials.

In 2002, the California Energy Commission asked Lawrence Berkeley National Laboratories (LBNL), Berkeley, Calif., and Oak Ridge National Laboratories (ORNL), Oak Ridge,Tenn., to collaborate with a consortium of 16 manufacturing partners and develop "cool" non-white roofing products that could revolutionize the residential roofing industry.

The commission's goal is to create dark shingles with solar reflectances of at least 0.25 and other nonwhite roofing products—including tile and painted metal—with solar reflectances not less than 0.45. The manufacturing partners have raised the maximum solar reflectance of commercially available dark products to 0.25-0.45 from 0.05-0.25 by reformulating their pigmented coatings. (For a list of the manufacturers, see "Manufacturing partners," page 36.)

Because coatings colored with conventional pigments tend to absorb invisible "near-infrared" (NIR) radiation that bears more than half the power of sunlight (see Figure 1), replacing conventional pigments with "cool" pigments that absorb less NIR radiation can yield similarly colored coatings with higher solar reflectances. These cool coatings lower roof surface temperatures, reducing the need for cooling energy in conditioned buildings and making unconditioned buildings more comfortable.

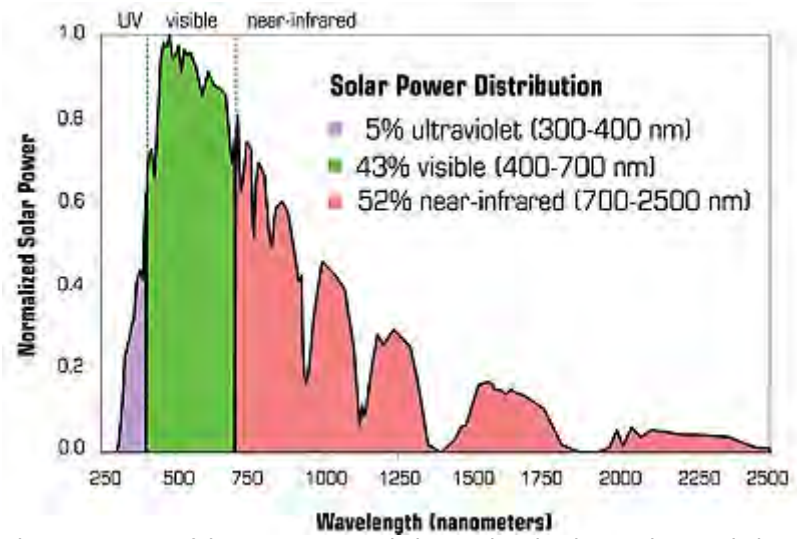

Figure courtesy of the Lawrence Berkeley National Laboratories, Berkeley, Calif.

Figure 1: Peak-normalized solar spectral power—more than half of all solar power arrives as invisible, "near-infrared" radiation

Cool, nonwhite roofing materials are expected to penetrate the roofing market within the next three years to five years. Preliminary analysis by LBNL and ORNL suggests the materials may cost up to $1 per square meter more than conventionally colored roofing materials. However, this would raise the total cost of a new roof system only 2 percent to 5 percent.

Cool, nonwhite colors

Developing the colors to achieve the desired solar reflectances involves much research and development. So far, LBNL has characterized the optical properties of 87 common and specialty pigments that may be used to color architectural surfaces. Pigment analysis begins with measurement of the reflectance—r—and transmittance—t—of a thin coating, such as paint film, containing a single pigment, such as iron oxide red. These "spectral," or wavelength-dependent, properties of the pigmented coating are measured at 441 evenly spaced wavelengths spanning the solar spectrum (300 nanometers to 2,500 nanometers).

Inspection of the film's spectral absorptance (calculated as 1-r-t) reveals whether a pigmented coating is "cool" (has low NIR

absorptance) or "hot" (has high NIR absorptance). The spectral reflectance and transmittance measurements also are used to compute spectral rates of light absorption and backscattering (reflection) per unit depth of film. The spectral reflectance of a coating colored with a mixture of pigments then can be estimated from the spectral absorption and backscattering rates of its components.

LBNL has produced a database detailing the optical properties of the 87 characterized pigmented coatings (see Figure 2). Its researchers are developing coating formulation software intended to minimize NIR absorptance (and maximize the solar reflectance) of a color-matched pigmented coating. The database and software will be shared with the consortium manufacturers later this year.

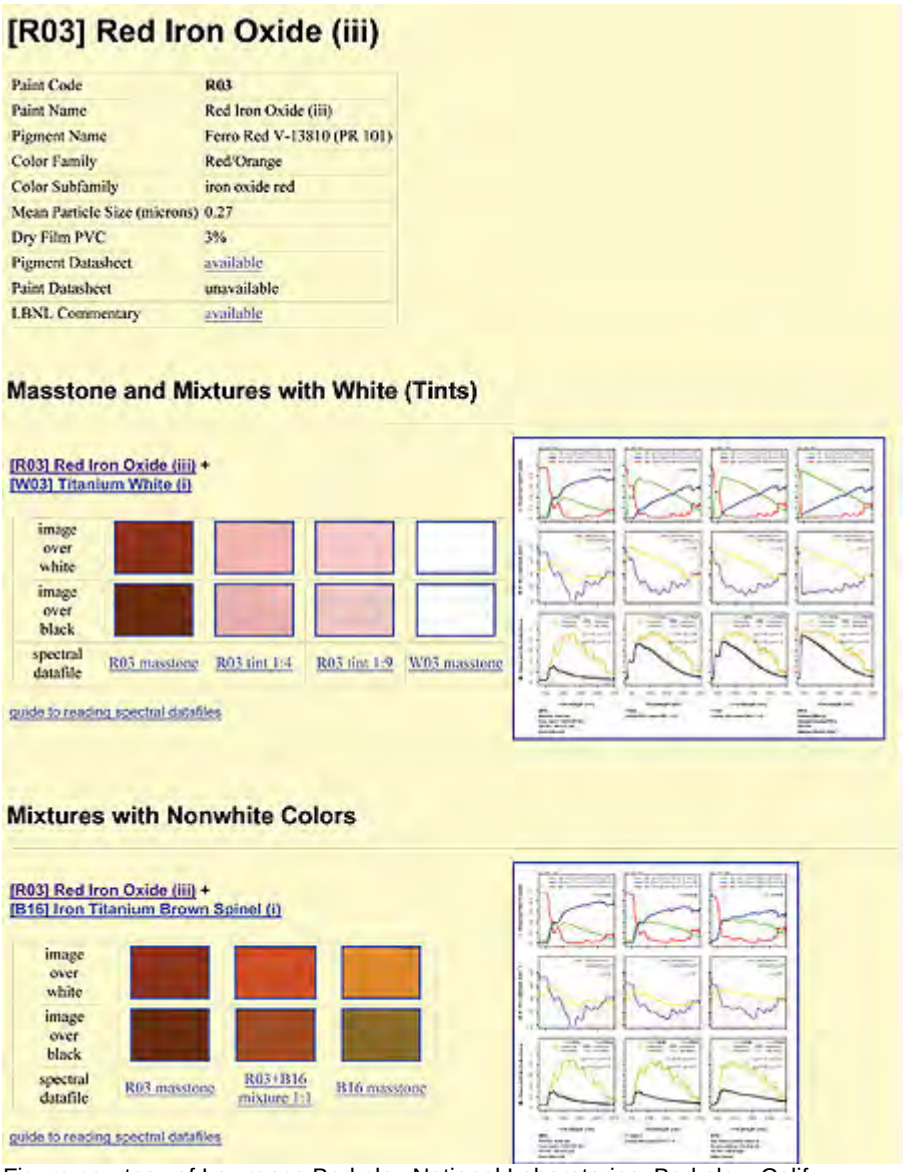

Figure courtesy of Lawrence Berkeley National Laboratories, Berkeley, Calif.

Figure 2: Description of a red iron oxide pigment in the Lawrence Berkeley National Laboratory pigment database

Shingles

A new shingle's solar reflectance is dominated by the solar reflectance of its granules, which cover more than 97 percent of its surface. Until recently, the way to produce granules with high solar reflectance has been to use a coating pigmented with titanium dioxide (TiO_2) white. Because a thin TiO_2-pigmented coating is reflective but not opaque in NIR, multiple layers are needed to obtain high solar reflectance. Thin coatings colored with cool, nonwhite pigments also transmit NIR radiation. Any NIR light transmitted through the pigmented coating will strike the granule aggregate where it will be absorbed (typical dark rock) or reflected (typical white rock).

Multiple color layers, a reflective undercoating and/or reflective aggregate can increase granules' solar reflectances, thereby increasing shingles' solar reflectances.

Figure 3 shows the iterative development of a cool black shingle prototype by ISP Minerals Inc., Hagerstown, Md. A conventional black roof shingle has a reflectance of about 0.04. Replacing the granule's standard black pigment with a cool NIR-scattering black pigment (prototype 1) increases the solar reflectance of the shingle to 0.12. Incorporating a thin white sublayer (prototype 2) raises the shingle's solar reflectance to 0.16; using a thicker white sublayer (prototype 3) increases the shingle's reflectance to 0.18. The figure also shows an approximate performance limit (solar reflectance 0.25) obtained by applying 25-micron NIR-reflective black topcoat over an opaque white background.

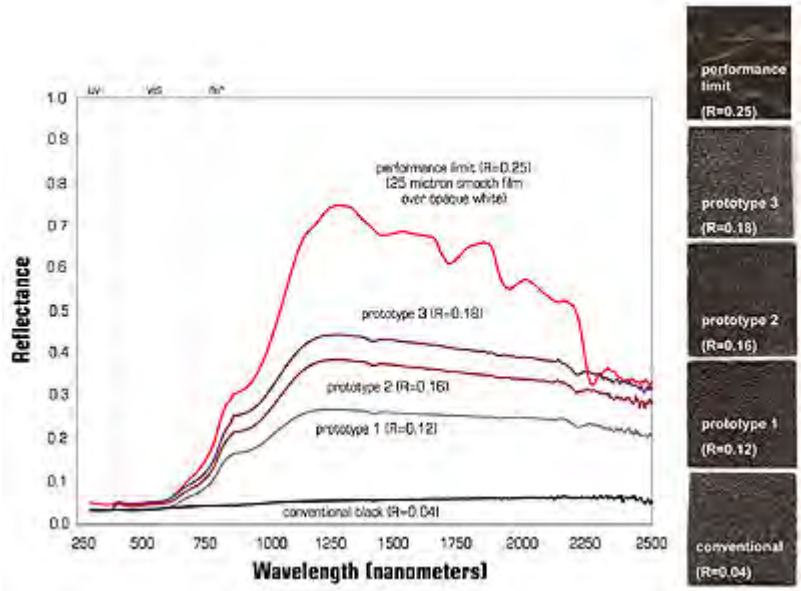

Figure courtesy of Lawrence Berkeley National Laboratories, Berkeley, Calif.

Figure 3: ISP Minerals Inc., Hagerstown, Md., is developing a cool, black shingle. Shown are the solar spectral reflectances, images and solar reflectances (R) of a conventional black shingle; three prototype cool, black shingles; and smooth, cool, black film over an opaque white background.

Tile

There are three ways to improve solar reflectances of colored tiles: use clay or concrete with low concentrations of light-absorbing impurities, such as iron oxides and elemental carbon; color tile with cool pigments contained in a surface coating or mixed integrally; and/or include an NIR-reflective sublayer, such as a white sublayer, beneath an NIR-transmitting colored topcoat.

American Rooftile Coatings, Fullerton, Calif., has developed a palette of cool, nonwhite coatings for concrete tiles. Each of its COOL TILE IR COATINGS™ shown in Figure 4 has a solar reflectance greater than 0.40. The solar reflectance of each cool coating exceeds that of a color-matched, conventionally pigmented coating by 0.15 (terra cotta) to 0.37 (black).

Metal

Cool, nonwhite pigments can be applied to metal with or without a white sublayer. If a metal is highly reflective, the sublayer may be omitted. The polymer coatings on metal panels are kept thin to withstand bending. This restriction on coating thickness limits pigment loading (pigment mass per unit surface area).

Performance research

ORNL naturally is weathering various types of conventionally pigmented and cool-pigmented roofing products at seven California sites. Each "weathering farm" has three south-facing racks for exposing samples of roofing products at typical roof slopes. Sample weathering began in August 2003 and will continue for three years—until October 2006. Solar reflectance and thermal emittance are measured twice per year; weather data are available continuously. Solar spectral reflectance is measured annually to gauge soiling and document imperceptible color changes.

ORNL and the consortium manufacturers also are exposing roof samples to 5,000 hours of xenon-arc light in a weatherometer, a laboratory device that accelerates aging via exposure to ultraviolet radiation and/or water spray. ORNL will examine the naturally weathered samples for contaminants and biomass to identify the agents responsible for soiling. This may help manufacturers produce roofing materials that better resist soiling and retain high solar reflectance. Changes in reflectance will be correlated to exposure.

The labs and manufacturing partners also have established residential demonstration sites in California. The first, in Fair Oaks

(near Sacramento), includes two pairs of single-family, detached homes. One pair is roofed with color-matched conventional and cool-painted metal shakes supplied by Custom-Bilt Metals, South El Monte, Calif., and the other features color-matched conventional and cool low-profile concrete tiles supplied by Hanson Roof Tile, Charlotte, N.C. The second site, in Redding, is under construction and by summer will have a pair of homes roofed with color-matched conventional and cool asphalt shingles.

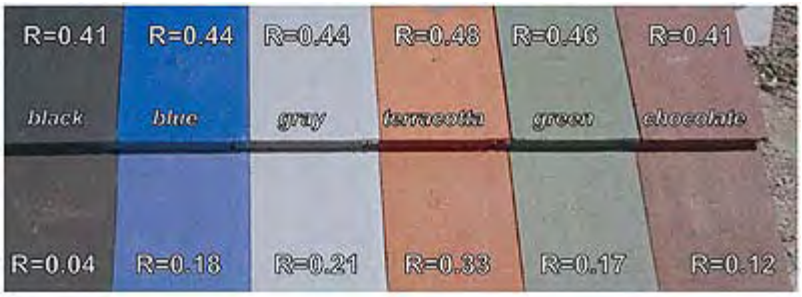

Figure courtesy of American Rooftile Coatings.

Figure 4: This is a palette of color-matched cool (top row) and conventional (bottom row) roof tile coatings developed by American Rooftile Coatings, Fullerton, Calif. Shown on each coated tile is its solar reflectance.

The homes in Fair Oaks are adjacent and share the same floor plan, roof orientation and level of blown ceiling insulation (19 hr•ft²•ºF/Btu). The homes in Fair Oaks and Redding will be monitored through at least summer 2006.

One of the Fair Oaks homes roofed with low-profile concrete tile was colored with a conventional chocolate brown coating (solar reflectance 0.10), and the other was colored with a matching cool chocolate brown (an American Rooftile Coatings COOL TILE IR COATING™ with solar reflectance 0.41). The attic air temperature beneath the cool brown tile roof has been measured to be 3 K to 5 K cooler than that below the conventional brown tile roof during a typical hot summer afternoon (273.15 K equals 0 C).

The results for the pair of Fair Oaks homes roofed with painted metal shakes are just as promising. There, the attic air temperature beneath the cool brown metal shake roof (solar reflectance 0.31) was measured to be 5 K to 7 K cooler than that below the conventional brown metal shake roof.

These reductions in attic temperature are solely the result of the application of cool, colored coatings. The use of these cool, colored coatings also decreased the total daytime heat influx (solar hours are from 8 a.m.-5 p.m.) through the west-facing concrete tile roof by 4 percent and the south-facing metal shake roof by 31 percent (see Figure 5).

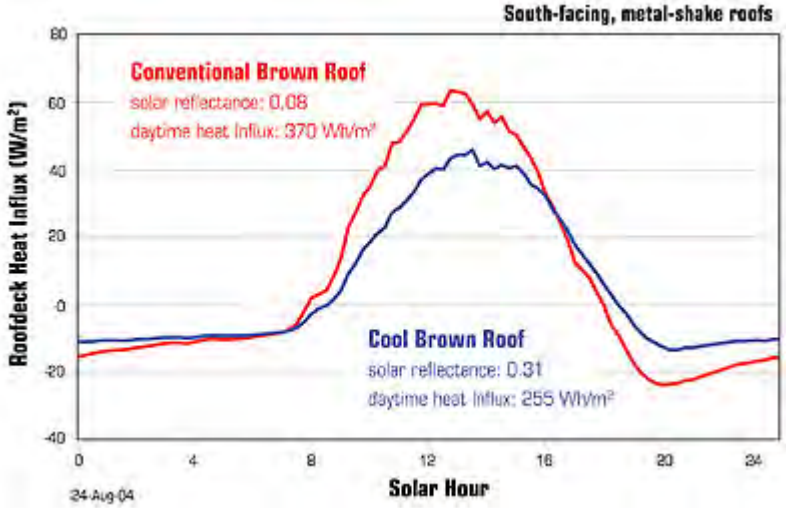

Figure courtesy of Oak Ridge National Laboratory, Oak Ridge, Tenn.

Figure 5: Heat flows through the roof decks of an adjacent pair of homes during the course of a hot summer day. The total daily heat influx through the cool brown metal shake roof (solar reflectance 0.31) between the solar hours of 8 a.m. and 5 p.m.is 31 percent lower than through the conventional brown metal shake roof (solar reflectance 0.08).

ORNL also is testing several varieties of concrete and clay tile on a steep-slope roof to further investigate the individual and combined effects of cool, colored coatings and subtile ventilation on the thermal performance of a cool roof system.

Results to date

The two laboratories and their industrial partners have achieved significant success in developing cool, colored materials for

concrete tile, clay tile and metal roofs.

Since the inception of this program, the maximum solar reflectances of commercially available dark roofing products has increased to 0.25-0.45 from 0.05-0.25. Bi-layer coating technology (a color topcoat over a white or other highly reflective undercoat) is expected to soon yield several cost-effective cool, colored shingle products with solar reflectances in excess of the U.S. Environmental Protection Agency's ENERGY STAR® threshold of 0.25. Early monitoring results indicate using cool, colored roofing products measurably reduces heat flow into conditioned homes with code-level ceiling insulation.

As homeowners continue to seek energy-efficient products, the roofing industry's research into residential roofing products that offer energy-efficient features naturally will continue to evolve.

Provided energy-efficient products continue to perform satisfactorily, we expect cool, nonwhite metal, tile and shingle products to penetrate the roofing market within the next three to five years.

Hashem Akbari leads LBNL's Heat Island Group. André Desjarlais leads ORNL's Building Envelope Group.

Editor's note: *Ronnen Levinson, scientist, Paul Berdahl, staff scientist, and Stephen Wiel, staff scientist, of LBNL; William Miller senior research engineer of ORNL; and Nancy Jenkins, program manager, Arthur Rosenfeld, commissioner, and Chris Scruton, project manager, of the California Energy Commission contributed to this article.*

Manufacturing partners

3M
St. Paul, Minn.
www.scotchgard.com/roofinggranules

Akzo Nobel
Felling, United Kingdom
www.akzonobel.com

American Rooftile Coatings
Fullerton, Calif.
www.americanrooftilecoatings.com

BASF Industrial Coatings
Florham Park, N.J.
www.ultra-cool.basf.com

CertainTeed Corp.
Valley Forge, Pa.
www.certainteed.com

Custom-Bilt Metals
South El Monte, Calif.
www.custombiltmetals.com

Elk Corp.
Dallas
www.elkcorp.com

Ferro Corp.
Cleveland
www.ferro.com

GAF Materials Corp.
Wayne, N.J.
www.gaf.com

Hanson Roof Tile
Charlotte, N.C.
www.hansonrooftile.com

ISP Minerals Inc.
Hagerstown, Md.

MCA Tile
Corona, Calif.

www.mca-tile.com

MonierLifetile LLC
Irvine, Calif.
www.monierlifetile.com

Owens Corning
Toledo, Ohio
www.owenscorning.com/around/roofing/Roofhome.asp

Shepherd Color Co.
Cincinnati
www.shepherdcolor.com

Steelscape Inc.
Kalama, Wash.
www.steelscape-inc.com

Web-exclusive information — Study about the development of cool, colored roofing materials

© Copyright 2006 National Roofing Contractors Association

Arnold Schwarzenegger
Governor

COOL-COLOR ROOFING MATERIAL ATTACHMENT 12: TASK 2.7.2 REPORTS - MARKET PLAN

PIER FINAL PROJECT REPORT

Prepared For:
California Energy Commission
Public Interest Energy Research Program

Prepared By:
Lawrence Berkeley National Laboratory and Oak Ridge National Laboratory

ERNEST ORLANDO LAWRENCE
BERKELEY NATIONAL LABORATORY

June 2006
CEC-500-2006-067-AT12

Prepared By:
Lawrence Berkeley National Laboratory
Hashem Akbari
Berkeley, California
Contract No. 500-01-021

Oak Ridge National Laboratory
William Miller
Oak Ridge, Tennessee

Prepared For:
California Energy Commission
Public Interest Energy Research (PIER) Program

Chris Scruton
Contract Manager

Ann Peterson
Building End-Use Energy Efficiency Team Leader

Nancy Jenkins
PIER Energy Efficiency Research Office Manager

Martha Krebs, Ph.D.
Deputy Director
ENERGY RESEARCH AND DEVELOPMENT DIVISION

B. B. Blevins
Executive Director

DISCLAIMER

This report was prepared as the result of work sponsored by the California Energy Commission. It does not necessarily represent the views of the Energy Commission, its employees or the State of California. The Energy Commission, the State of California, its employees, contractors and subcontractors make no warrant, express or implied, and assume no legal liability for the information in this report; nor does any party represent that the uses of this information will not infringe upon privately owned rights. This report has not been approved or disapproved by the California Energy Commission nor has the California Energy Commission passed upon the accuracy or adequacy of the information in this report.

A Proposed Marketing Plan:
Deployment of Cool-Colored Roofing Materials

An Industry, LBNL and ORNL Collaborative Effort

Hashem Akbari and William (Bill) Miller

July 25, 2005

Executive Summary

The California Energy Commission (CEC) has dramatically advanced the technology of non-white "Cool Roofs" that exploit complex inorganic paint pigments to boost the solar reflectance of clay and concrete tile, painted metal, and asphalt shingle roofing. The project has successfully developed several non-white cool-colored roof products for sloped roofs over the past three years and has shown positive energy savings in residential field tests demonstrating pairs of homes roofed in concrete tile, painted metal and asphalt shingles with and without cool pigmented materials. Without further efforts, the accomplishments achieved by the CEC in its "Cool Roofs" Public Interest Energy Research (PIER) project will creep into the marketplace over the next several decades, slowly bringing the significant energy, cost, smog and carbon savings that the technology promises.

Near the end of the CEC project, the project's 16 industrial partners discussed their needs to further develop and successfully market their residential cool roofing products. Their recommendations and requests are summarized in Table 1.

The opportunity exists to rapidly accelerate the uptake of cool roofing materials. First and foremost, residential cool roofs need to be credited and recommended in the state's Title 24 standards that primarily determine what products are used in the construction of new houses and major remodels. Second, more cool materials for all residential (and commercial) sloped roofing systems must be available and appropriately labeled. Third, the application of appropriate labels on roofing products must become universal. Fourth, architects, designers, builders, roofing material distributors and retailers, and consumers need to learn of the availability and benefits of using cool roofing materials. Fourth, California utilities and the state government can further influence the selection of cool roofs through innovative incentive and rebate programs to accelerate their market penetration. Finally, market penetration can also be accelerated by enhancing the credibility of retailer and utility marketing claims through large-scale demonstrations of cool roofs to consumers, developer, designers, and roofing contractors.

We therefore define a market plan for industry/national labs collaborative efforts to help the CEC in deploying cool-colored roofing. The plan focuses on six parallel initiatives: 1) regulate, 2) increase product selection, 3) label, 4) educate, 5) provide incentives and, 6) demonstrate performance.

Table 1: Industry needs to successfully market their cool roof product

Assistance requested in marketing cool roofs	**Industry partner requesting assistance**
Continuing education for design build firms, architects, utility consumers, construction professionals and homeowners integrated into seminars offered by the CABEC.	Steelscape, BASF, Custom-Bilt, Shepherd
Software to estimate the cooling energy savings and peak demand reduction achieved by installing cool roofs on specific buildings	Steelscape, BASF, Custom-Bilt, Ferro, Elk, ARC
Monitoring solar reflectance and color change of the materials installed at the California weathering sites	Steelscape, BASF, Custom-Bilt, ISP, Ferro, Elk, ARC
Monitoring solar reflectance, color change, and thermal performance of materials at ORNL test facilities and the Sacramento test homes	Steelscape, BASF, Custom-Bilt, ISP, Elk, Ferro, ARC
Expanding the cool coating database	Steelscape, BASF, Custom-Bilt, ISP, Ferro, Shepherd, 3M
Large-scale demonstration of cool roofs	Steelscape, BASF, Custom-Bilt, ISP, Ferro, Elk, ARC
Predictive software for design of cool coatings	Steelscape, BASF, Custom-Bilt, ISP, Ferro, 3M
Research to increase reflectivity and reduce costs	ISP, Ferro, Elk, 3M, Shepherd, ARC
Tools to accurately measure solar reflectance	ISP, Elk, 3M, ARC
Calculations of weathering benefits of cool roofing	ISP
Identification of new materials and techniques	ISP, Ferro, 3M
Determination of the relationship between granule and ultimate shingle reflectances	3M
Acceleration of cool roof rating criteria by CRRC and Energy Star	3M

1. REGULATE: Modify California Title 24 Standards (2008) for non-residential sloped roofs and residential low-sloped/sloped cool roofs

California Title 24 standards have been an effective way to promote and market cool roofing materials. In January 2001, the California Title 24 adopted a measure to credit buildings that install cool roofs. In November 2003, the Energy Commission approved a proposal to upgrade Title 24 standards by making cool roofs a prescriptive requirement for low-sloped roof non-

residential buildings. This revision to the standards will be effective on October 2005. During the 2005 cycle of Title 24 upgrades, cool materials for steep-sloped roofs were scarce. Thanks to the current effort and leadership of the Energy Commission, now several manufacturers have developed cool colored materials for steep-sloped roofs. The California utilities, the PAC, industry partners, and the national labs (both LBNL and ORNL) are in full agreement that we shall proceed with efforts to develop proposals to upgrade Title 24 standards to adopt cool roofs as prescriptive requirements for sloped-roof non-residential, low-sloped-roof residential, and steep-sloped roof residential buildings.

With the Pacific Gas and Electric Company's (PG&E) and the Energy Commission leaderships, efforts are well underway to perform the required analyses to upgrade the Title 24 standards. PG&E is sponsoring work to upgrade the non-residential (both low-sloped and steep-sloped roof) buildings. The Energy Commission is sponsoring the work to upgrade the residential (both low-sloped and steep-sloped roof) buildings. The work plans for the non-residential and residential cool roof Title 24 upgrade is provided in Attachments B and C.

It has been claimed that municipalities (cities, towns, villages, and boroughs) do not require permits for residential re-roofing projects. Since the re-roofing market is typically four times larger than the new-construction roofing market, programs developed for California should have a strong component to address the re-roofing of existing homes. Hence, there is a need to work with the municipalities to ensure that ordinances are in place for compliance with California Title 24 standards in retrofit applications.

2. INCREASE PRODUCT SELECTION: Continue development work with manufacturers of cool-colored materials to deploy their products

The ongoing CEC-sponsored project has brought 16 roofing industry partners together to develop cool-colored roofing materials. Several other leading manufacturers of cool roofing products would also like to join this CEC-sponsored collaborative research. The project has made significant advances in developing cool colored concrete tiles, clay tiles, and metal products. Development of cool shingles has proved to be more challenging and requires continued support to bring cool shingles to market. The following are some activities that manufacturers have asked for help from the national labs in developing and marketing new cool materials.

Development and marketing of improved cool materials

During the course of the current CEC-sponsored project, the granule manufacturers have developed cool colored granules with solar reflectance of 0.10 to 0.15 higher than standard products of the same color. Furthermore, many of these products are not yet economically viable. The granule manufacturing partners (ISP Mineral, 3M, and CertainTeed) have asked for continued support from the Energy Commission and national labs to improve the reflectance of their granules using the bilayer technique in such methods that the production cost is further reduced. The granules from these manufacturers will be available to Elk, GAF and others to produce cool shingles at competitive prices. Other industry partners (specifically MonierLifetile and Hanson Tile) have asked for similar support for improving the reflectance of concrete tiles using the bilayer technique.

Measurement of solar reflectance at manufacturing plant

The manufacturing partners, particularly Elk, GAF, 3M, ISP Minerals, CertainTeed, MonierLifetile, Hanson Tile, and MCA Tile, on many occasions have stated that the current ASTM standards have serious limitations for measuring solar reflectance of variegated roof materials or roofing materials with three-dimensional geometry. While ASTM standards E903 and C1549 allow measuring reflectance of small roof areas (areas of less than 1" in diameter), ASTM standard E1918 is for measuring solar reflectance of larger surfaces (areas larger than 10' in diameter). Hence, measurements by E903 and C1549 are not suitable for variegated and corrugated suitable and performing measurements for large samples can be cumbersome. Our industry partners, for quality control of their products, need to have instruments with which can measure the solar reflectance of roofing materials at their production plants. This would accelerate product development, and facilitate quality control in future production lines.

Correlation between the reflectance of granules to that of the shingles

Roofing granules cover at least 97% of area of roofing shingles. Hence, the optical properties of roofing shingles are primarily defined by those of the granules. The granule industry partners (ISP Minerals, 3M, and CertainTeed) would like to develop a method to relate the solar reflectance of a roofing shingle to that of its granules. A strong correlation between granule and shingle solar reflectance may be acceptable to Cool Roof Rating Council (CRRC), potentially allowing the granule manufacturers to obtain CRRC labels for their products, then transfer the labels to shingle products.

Cool roof energy saving calculator for contractors

Our industry partners have repeated mentioned that a "cool-roof saving calculator" will be extremely useful to the manufacturers, distributors, and roofing contractors in their marketing of cool roofing products. Currently, there are two models available that predict different saving potentials: DOE model (developed by ORNL) and EPA model (developed by LBNL). The national labs (ORNL and LBNL) need to work together to develop an integrated calculator for estimating the effect of the roof solar reflectance on heating and cooling energy use. The algorithm developed for the calculations of savings need to be utilized in a web-based calculator (and a PC-based version) with which roofing contractors and distributors can estimate the cooling energy savings and peak demand reduction achieved by installing cool roofing on specific buildings. This would allow the manufacturers of cool roofing materials to use the benefit of cool roofs to help market their products.

Aging and evaluation of cool roofing products in California weathering site

Manufacturers are constantly developing new and improved cool roofing materials. To characterize the long-term performance of the cool materials, we need to continue to monitor the solar reflectance and color change of the roofing materials installed at the California weathering sites in order to accommodate new products as they are developed. A database of the optical performance of the cool roofing materials will be extremely useful to both manufacturers, consumers, policy makers, and the Cool Roof Rating Council.

Cool roof product monitoring and evaluation at labs

As new products are becoming available, the characterization of their performances is necessary for ultimate deployment and marketing of the products. The manufacturers have submitted many samples for performance monitoring at the ORNL test facilities. The manufacturers would like to continue monitoring the solar reflectance, color change, and thermal performance of roofing materials installed and new materials to be installed at ORNL test facilities. The results of these characterizations can be integrated in the cool materials database.

Assist manufacturers of cool roofing products with CRRC labeling

Many roofing manufacturers have not applied for CRRC labels. The manufacturers would like to join CRRC, and CRRC is anxious to expand their manufacturing members. In a fully coordinated effort, we need to work with the industry and CRRC to understand technical reasons for the manufacturers' delays and provide them technical assistance needed to obtain CRRC labels.

This task will build on the simulation efforts outlined in Task 1 by developing detailed and customized estimates of energy savings and peak demand reductions for several detailed prototypical residential and high-sloped commercial buildings. In this task, we will

- perform detailed and calibrated DOE-2 simulations of several residential, commercial, and industrial buildings for all climate regions in California,
- develop a database of savings and perform cost/benefit analyses for various cool roofing types, customized for California utilities' rebate applications,
- work with Southern California Edison and PG&E in designing innovative and effective consumer incentive and emerging technologies programs.

3. LABEL: Facilitate labeling of cool roofs through CRRC

The manufacturing partners consider the Cool Roof Rating Council (CRRC) organization and labeling as an effective method for marketing cool roofing materials. They would like the national labs to support the CRRC in its effort to accelerate market penetration of cool roofing materials via the following activities:

- Help CRRC and roofing manufacturers to overcome and resolve technical issues that arise in implementation of the CRRC label program.
- Provide technical information that helps manufacturers develop brochures and educational kits for distribution at trade shows and roofing materials distribution centers (see Attachment D as an example).
- Develop a web site which manufacturers can educate their customers, contractors, and designers

4. EDUCATE: Tell the California Building Community and Homeowners about "Cool Roof" Benefits

This task will be accomplished primarily through the California Association of Building Energy Consultants (CABEC) (http://www.cabec.org/). CABEC currently hosts classes and seminars on the latest technologies in heating, ventilation and air-conditioning, windows and air distribution

systems, but offers little training that addresses "Cool Roofs" because of the dearth of information. We propose to enhance the roofing component of CABEC's training program with emphasis on the benefits of cool roofs.

The CEC should integrate "Cool Roof" training into building efficiency seminars already hosted by the public utilities and taught through the existing framework of the California Association of Building Energy Consultants (http://www.cabec.org/). The CABEC hosts training seminars on the Energy Efficiency Standards for Residential and Nonresidential Buildings (Title 24, Part 6 of the California Code of Regulations) that communicate the new 2005 building compliance rules, which take effect October 1, 2005. Part of the new compliance rules call out prescriptive requirements for the minimum solar reflectance and thermal emittance for commercial low-slope roofs, and 2008 rules will focus on steep-slope roofs. Therefore, "Cool Roof" training must be directly integrated into these seminars and address Title 24 roof legislation that architects and design build firms[1] must know. Some of the class topics presently taught through the CABEC includes high performance glazing and radiant barrier roof sheathing, duct testing and procedures that verify home energy usage (an example, the Home Energy Rating System). However, training materials are sparse on the advantages of "Cool Roofs." Several one-day training courses are needed for contractors and designers in the application of cool roofing products in California, and can be offered at the energy centers of PG&E, San Diego Gas and Electric, Southern California Gas, Southern California Edison and Sacramento Municipal Utility District.

Additional training is needed to explain the implications of cool roofs on time of demand metering. Seminars should be offered explaining potential rebate incentives for the builder. Mortgage incentives for the homeowner choosing a cool roof should be offered and information provided on the impact of sustainable cool roofs on the resale value of homes. Training is also needed to help builders and construction crews improve installation practices, which will cut construction costs, especially for tile and painted metal roofing. Success of the educational program requires the complete buy-in by the public utilities and a commitment to communicate through articles published in trade association magazines[2], newspaper articles and each respective utilities newsletter that they broadcast to the community of California builders within their region. Large-scale demonstrations of cool roofs would certainly help demonstrate to utilities, architects, builders and homeowners the energy saving potentials from which the California utilities and the state government can confidently offer incentives appropriate to the level of savings afforded by cool roofs.

5. PROVIDE INCENTIVES: Develop incentive programs for cool colored roofs

Utility-sponsored programs have been a proven and an effective approach in introducing innovative energy technology products to California markets. The rebates are payments for acquiring larger public benefits that aren't captured by the private marketplace. To develop rebate programs, utilities require accurate and customized estimates of energy savings and peak demand reductions for all roofing systems and building types in all climate regions within their service territories. To develop and market roofing products that comply with utility rebate

[1] Metal Constructions census revealed that 67% of metal roof projects are done by design build firms and 52% of metal roof projects involve architects.

[2] California Builders magazine, Professional Roofing, Western Roofing, Metal Roofing, RCI Interface, Metal Architecture, Metal Construction News, Metal Home Digest, etc.

programs, manufacturers need this same information. The utilities are offering rebates for home improvements that include insulation, improved water heaters and higher performance windows. Cool roofs should be a part of the utilities rebate program. A hypothetical rebate of $0.10 per square foot of roof may represent only about 5% of the total installed cost of the roof to the consumer (about $2 per square foot of roof). However, the same rebate of $0.10 per square foot might increase the net profit to the contractor by about 50%. Also, the production of cool roofing materials can be encouraged by offering incentives to manufacturers so that they can market cool roofing materials competitively.

Countrywide Home Mortgage Loans, PHH Mortgage Services and Chase Manhattan offer Energy Star mortgages for Energy Star compliant homes. The mortgages include discounted interest rates, cash back after closing and higher appraisal values on the resale value of homes that can demonstrate lower utility bills. The Appraisal Journal (Oct. 1998 & 1999) reported that "the market value of a home increases $20 for every $1 decrease in annual utility cost." Offering mortgage incentives to homeowners would also foster the selection of cool roof products.

It is important to note that an Energy Star labeled roof is not part of the requirements for an Energy Star home (Kriner private conversation with Rachel Schmeltz and Steve Ryan of the EPA), because the EPA believes there are no Energy Star labeled products available for steep slope roofing. Implementing our market strategy will correct this misconception and open the opportunity for including cool roof incentive in Energy Star mortgages.

6. DEMONSTRATE PERFORMANCE: Arrange large-scale demonstrations in each utility service area to showcase cool-colored roofing materials

Demonstrations of new products can be a powerful tool to showcase the performance of cool roofs to consumers, developer, designers, and roofing contractors. The manufacturers would benefit from a community-wide demonstration by publicizing their products to the market (consumers, developers, designers, utilities). Proving product performance will reduce consumer risk and uncertainty. The utilities will benefit by validating the performance of the products which will make cool roofs more attractive to developers and homeowners.

We have been discussing and planning development of large-scale demonstrations with many of our partners to showcase cool roofing materials in communities with hundreds of homes. Attachment E presents a recent plan developed for demonstrations in Southern California. The materials to be demonstrated are painted metal. Similar demonstrations are needed for cool shingles or clay and concrete tiles. The goal is to initiate two demonstration projects, one in northern and one in southern California. The monitoring cost of the demonstrations will be cost-shared with utilities. The developers would pay for the roofing, which the manufacturers would make offer at costs comparable to those of their standard products.

Conclusion — Market Potential

California's ability to meet peak electricity demand in the future is one of the primary electrical issues confronting its public utility companies. The CEC has stated that hot summer temperatures can drive up peak electrical demand as much as forty-five percent, and California is increasingly relying on out-of-state electrical supplies. Residential air-conditioning loads represent almost 14

percent of the summer peak demand; the equivalent of over 7,000 MW of peak capacity during a hot California summer day. To exacerbate the problem, significant new housing growth in both the near and long term will occur in California's urban areas and hot inland regions. "Cool Roofs" can provide a significant part of the solution to California's dilemma. The market opportunity therefore exists for a "cool roofs" business venture. What is needed is the reasoned faith derived from the research and the fortitude to act upon the results.

This report outlines six market interventions available to the CEC to reduce or eliminate barriers that slow the market penetration of cool roofing products into the residential housing market. These interventions reach manufacturers, distributors, retailers, architects, designers, builders, utilities, and consumers. All are useful in accelerating the use of cool roofing materials in California's residences. If they are implemented, California will benefit by reducing cooling energy use (by about 1 TWh per year; worth about $100 M per year) and peak air conditioning demand (by about 1-2 GW), and improve ozone air quality (estimated at about $200 M per year).[3]

Acknowledgement

This work was supported by the California Energy Commission (CEC) through its Public Interest Energy Research Program (PIER), and by the U.S. Department of Energy's Assistant Secretary for Energy Efficiency and Renewable Energy under Contract No. DE-AC03-76SF00098. We acknowledge the contributions of John McCaskill of Elk, Bob Scichili of Custom Bilt, Scott Kriner of Akzo Nobel, Ken Loye of Ferro, Tom Steger of Shepherd, Yoshihiro Suzuki of MCA Tiles, Ingo Joedicke of ISP Minerals, and Jerry Vandewater of Monierlifetile for preparation of this document. The authors would like to acknowledge the support and guidance of the CEC/PIER project and program managers Chris Scruton and Nancy Jenkins. We also acknowledge the contributions of Steve Wiel, Paul Berdahl, Ronnen Levinson form LBNL and Andre Desjarlais from ORNL.

[3] We estimate that over 70% of the residential buildings in California have colored shingle roofs with reflectivities of about 10% - 20%. We estimate that about 50% of the approximately 12 million single-family residences are air-conditioned. The average AC peak demand for each house is about 1.5 kW; hence, the contribution of residential AC demand to total utility demand is about 8 GW. The air-conditioning systems of many of these houses (particularly those located in coastal areas) usually do not operate except on a few extremely hot days. Application of cool colored roofs in residential sector can significantly reduce this peak demand (we estimate on the average by 15%-30%, or 1.2GW to 2.4GW). The annual energy savings is estimated at about 1 TWh.

Attachment A

In May 2002, the California Energy Commission (Energy Commission) sponsored a research project to develop "cool" nonwhite roofing products that could revolutionize the residential roofing industry. An initial collaboration between Lawrence Berkeley National Laboratory, Oak Ridge National Laboratory, and eight roofing manufacturing rapidly grew to include 16 industrial partners (see Table A.1). Seven other manufacturers and roofing organizations have joined the project's advisory committee (see TableA.2).

Table A.1. List of manufacturing industry partners

1. 3M Industrial Minerals, Pittsboro, NC; www.scotchgard.com/roofinggranules
2. Akzo-Nobel, Macungie, PA; www.akzonobel.com
3. American Rooftile Coatings, Fullerton, CA; www.americanrooftilecoatings.com
4. BASF Industrial Coatings, Mount Olive, NJ; www.ultra-cool.basf.com
5. CertainTeed, Valley Forge, PA; www.certainteed.com
6. Custom-Bilt Metals, South El Monte, CA; www.custombiltmetals.com
7. Elk Corporation, Dallas, TX; www.elkcorp.com
8. Ferro Corporation, Cleveland, OH; www.ferro.com
9. GAF Materials Corporation, Wayne, NJ; www.gaf.com
10. Hanson Roof Tile, Fontana, CA; www.hansonrooftile.com
11. ISP Minerals Incorporated, Hagerstown, MD; Tel. (301) 733-4000
12. MCA Tile, Corona, CA; www.mca-tile.com
13. MonierLifetile LLC, Irvine, CA; www.monierlifetile.com
14. Owens Corning, Granville, OH; http://www.owenscorning.com/around/roofing/Roofhome.asp
15. Shepherd Color Company, Cincinnati, OH; www.shepherdcolor.com
16. Steelscape Incorporated, Kalama, WA; www.steelscape-inc.com

Table A.2. Industry Representation on the Project Advisory Committee

1. DuPont Titanium Technologies
2. National Roofing Contractors Association
3. Cedar Shake and Shingle Bureau (CSSB)
4. Cool Roof Rating Council (CRRC)
5. Cool Metal Roofing Coalition
6. Roof Tile Institute
7. Asphalt Roofing Manufacturers Association

Cool Roofs for non-Residential Steep- and Low-Sloped Roofs Buildings

Background:

In 2003, the Pacific Gas and Electricity Company (PG&E) submitted a proposal to California Energy Commission (CEC) to amend the existing Title 24 standards by requiring cool roofs for California low-sloped non-residential buildings. With the sponsorship of PG&E, LBNL prepared the technical document (CASE study) to support the modifications to Title 24 standards. In November 2003, CEC approved the CASE proposal and amended the Title 24 to adopt "cool roofs" as prescriptive requirement for low-slope roofs in non-residential buildings. CEC has also shown a strong interest to expand the current scope of the proposal to cover low- and steep-sloped roofs residential buildings.

PG&E reviews existing codes in the California Code of Regulations, Building Energy Efficiency Standards, Title 24, Part 6 (hereinafter Title 24) typically every three years. It reviews current practices with the latest and/or promising design and technological advances in residential and nonresidential construction while ensuring cost effectiveness for consumer. PG&E is conducting the following activities in developing and supporting a Title 24 code enhancement proposal for steep-slope nonresidential cool roofs, for California's 2008 building code upgrade cycle. The main objectives of this proposal are to develop a CASE study for application of cool roof on non-residential sloped Roofs and conduct research on incorporating degradation of cool roofing materials into Title 24.

Scope of Work:

The Work to be performed by LBNL under the Contract shall consist of the following:

- developing Codes and Standards Enhancement studies (hereinafter "CASE Studies")
- conducting market research and consensus-building workshops
- conducting research on incorporating degradation of cool roofing materials into Title 24
- advocating adoption of the CASE study proposals during CEC's public rulemaking process
- ensuring that PG&E's Code amendment proposals are correctly incorporated into the CEC Title 24 documents.

LBNL will perform all the Work necessary to complete each task under the Contract as defined below and shall provide deliverables as required and on the due dates.

CASE Studies for Cool Roofs:

LBNL shall collaborate with PG&E Project Manager to develop the following code enhancement proposal for California's 2008 building code upgrade cycle: the application of cool roofs to non-

residential steep-sloped roof buildings. The CASE study, as described in the workplan, will recommend adoption of specific revisions to the California Code of Regulations, Building Energy Efficiency Standards, Title 24, Part 6 (hereinafter "Code**"**).

Task 1. Kickoff meeting:

LBNL shall conduct a Kick-off Meeting with the PG&E Project Manager within ten (10) business days of receiving a signed Contract. At the meeting, LBNL shall present a brief review of CASE study technical, market and stakeholder issues as they relate to the potential for future adoptability. Adoptability criteria shall include a general assessment of technical and economic feasibility, market readiness by 2008, and stakeholder support. LBNL's presentation shall be an overview of issues pertinent to the CASE Study. Following the meeting, LBNL shall produce an e-mail summary of the meeting including significant issues discussed and action items.

DELIVERABLE/DUE DATE:

1) Kick-off meeting presentation two business days prior to the kick-off meeting
2) E-mail summary three days after the kick-off meeting

Task 2. CASE Study Work Plan:

Following the kickoff meeting, LBNL shall develop a work plan that address the requirements defined in Task 3.1. The work plan shall include, but not be limited to:

- Identification of issues or barriers unique to development of the CASE Study and/or implementation of the proposed measure
- Establishment of deliverables (tasks and subtasks), that ensure all items in Task 3 are adequately addressed. The number of tasks and subtasks shall reflect the Work needed to be performed and clearly convey the status of each Case Study.
- Budget and schedule for each task or subtask
- The number of anticipated stakeholder meetings to review the progress of each CASE Study.

DELIVERABLES/DUE DATES:

1. DRAFT WORK PLAN: LBNL shall submit a draft work plan to PG&E Project Manager for review, comments and approval. Submittal of draft work plans to be scheduled by PG&E Project Manager and Consultant.
2. FINAL SUMMARY REPORT: LBNL shall incorporate PG&E Project Manager's comments and resubmit the final work plans to PG&E Project Manager five (5) business days after receipt of comments.

Task 3. Develop CASE study:

LBNL shall coordinate the development of the CASE Studies with PG&E, CEC, industry representatives, and other stakeholders.

Task 3.1. CASE study for steep-sloped nonresidential roofs.

LBNL shall develop a CASE report for sloped-roof nonresidential buildings. The elements of this task include:

A. Development of prototype buildings for sloped-roof nonresidential buildings. In this subtask, we will use the CEC existing residential prototypes. We will modify and revise the prototypes as necessary.

B. Collecting market share data and reviewing cool roofs application on sloped-roof nonresidential buildings.

C. Incorporating the effects of ageing on cool roof materials into Title 24.

D. Performing energy simulations to estimate savings for all California climate regions. We are planning to use DOE2 software for these calculations. The calculations will be performed for both existing and new nonresidential buildings.

E. Performing a cost/benefit analysis (both TDV and non-TDV). The analysis will be carried out for both existing and new nonresidential buildings.

F. Estimating state-wide savings. The state-wide savings will be estimated for both existing and new nonresidential buildings.

G. Preparing proposals to change the relevant sections of Title 24

H. Presenting the results and responding to comments.

DELIVERABLES/DUE DATES:

1. PRELIMINARY DRAFT CASE STUDY: LBNL will submit preliminary draft report for each CASE Study for PG&E Project Manager's review and comments as set forth in each CASE Study work plan, but not later than 180 days after Contract execution.
2. FIRST REVISION OF DRAFT CASE STUDY: LBNL will incorporate comments and resubmit draft CASE Study to PG&E Project Manager seven (7) business days after receipt of comments.

Task 3.2. Modification to Title 24 standards for ageing of low-sloped nonresidential roofs.

Currently, the Title 24 standard in its prescriptive requirements specifies the solar reflectance of new cool materials. A cool roof is defined having an initial solar reflectance of at least 0.70. In the "performance" and "over-all envelop" sections, the calculations are performed for aged solar reflectance of 0.55. The objective of this task is to perform the required research on degradation of cool roofing materials and incorporate the results into Title 24. The elements of this task include:

1. Collect field data on the solar reflectance of aged cool materials. In 2003, the Cool Roof Rating Council (CRRC) initiated a program to measure the three year solar reflectance of roofing materials in Arizona and Florida. By the summer of 2005, some of the samples have been weathered for about two years. We will visit the weathering site in Arizona and measure the solar reflectance of the 2-year old specimen. We will

analyze the data and produce a short report of the aged reflectance *vs.* initial reflectance, categorized by type of roofing materials.
2. Share the aging data with experts and solicit comments. The data will be shared with CEC and CRRC and comments will be gathered.
3. Prepare a proposal for Title 24 modification. We will incorporate received comments and prepare a proposal to modify Title 24 standards of the aged reflectance.

Task 3.3. Project update meetings and reporting:

LBNL project team members shall attend a maximum of six (6) - 2-hour meetings to present progress and issues that arise during the development of the CASE study. Meetings shall be held at PG&E facilities in San Francisco or Davis. LBNL shall prepare a memorandum after each project update meeting to address issues and concerns discussed at the meetings. LBNL shall also submit a Monthly Status Report to the PG&E Manager. The Monthly Status Report shall include work progress and comparison of budget and actual expenditures for all tasks/subtasks in the work plan, status of key deliverables, and other items as requested by the PG&E ProjectManager.

DELIVERABLES/DUE DATES:

1. MEMORANDUM: LBNL will submit Issues Memorandum to PG&E Project Manager (5) business days after each project update meeting.
2. MONTHLY STATUS REPORT: At the end of each month, LBNL shall issue a Monthly Status Report to PG&E.

Task 4. Stakeholder workshop:

LBNL shall assist the PG&E Manager with planning and conducting an industry stakeholder (consensus-making) workshop to present CASE Study findings and solicit comments from the stakeholders. The workshop shall be held at a PG&E facility in San Francisco or Davis.

Task 4.1. Workshop agenda:

LBNL shall develop the following meeting materials for review and approval by the PG&E Project Manager.

a) An agenda and a proposed list of stakeholders

b) Presentation materials than include an outline and summary of the CASE Study report

Following the workshop, LBNL shall prepare a workshop report summarizing the workshop proceedings. The workshop report shall include a list of attendees, workshop agenda and handouts, meeting minutes, outstanding issues not resolved at the workshop, and recommended actions to take with respect to issues raised. LBNL shall revise the draft workshop report based on comments provided by the PG&E Project Manager.

DELIVERABLES/DUE DATES:

1. LBNL shall submit draft workshop agenda and list of stakeholders to PG&E Project Manager at a mutually agreed schedule for review. LBNL will incorporate the PG&E Project Manager's comments, if any, and submit revised agenda three (3) business

days prior to the workshop. In addition, LBNL shall distribute agenda and Draft CASE Studies to all meeting attendees via email at least two (2) business days prior to the workshop.

2. LBNL shall develop and submit presentation materials for each CASE study to the PG&E Project Manager for review and comment at a mutually agreed upon schedule. LBNL shall incorporate the PG&E Project Manager's comments and issue presentation materials to the PG&E Project Manager two (2) business days prior to the workshop. Consultant shall provide up to 30 printed copies of the presentation materials at the workshop.
3. LBNL will prepare draft report for the PG&E Project Managers' review and approval five (5) business days after the workshop, and shall incorporate PG&E Project Managers' comments into the final workshop summary report five (5) business days after receipt of comments.

Task 4.2. Final draft case study:

LBNL will produce a Final Draft CASE Study report. The final draft report shall incorporate input including, but not limited to, outstanding issues and recommended actions identified by workshop attendees and PG&E and CEC Project Managers.

DELIVERABLES/DUE DATES: LBNL shall revise the draft CASE Study report for the PG&E Project Managers' review and comment for each CASE Study within fifteen (15) business days after CASE Study was presented at a PG&E workshop and shall incorporate PG&E Managers' comments into the Final Draft CASE Study no more than five (5) business days after receipt of PG&E Project Manager's comments.

Task 5. Support for PG&E CASE study proposals during CEC rulemaking:

LBNL shall participate in a maximum of four (4) CEC workshops or adoption hearings, and six (6) teleconferences, as requested by the PG&E Project Manager, to assist with advocacy of proposed code enhancements and to gather comments. The scope of these activities shall include both PG&E's nonresidential code change proposals and related code change proposals submitted by others.

Task 5.1. Presentation materials:

Prior to each CEC workshop, hearing, or teleconference call, LBNL shall prepare support materials as requested by the PG&E and CEC Project Managers. Support materials shall include, but not be limited to:

- CASE studies and summary presentations; and
- Ongoing research, analyses and status summary presentations.

DELIVERABLES/DUE DATES: LBNL shall prepare draft presentation materials for review and approval by the PG&E Project Manager, ten (10) business days before each CEC workshop or hearing, and shall incorporate PG&E Project Managers' comments into the final presentation

materials five (5) business days before each CEC workshop or hearing. LBNL will provide up to 50 print copies of support materials on the day of each CEC workshop or hearing.

Task 5.2 CEC workshop and summary report:

During each workshop, hearing, or teleconference, LBNL shall present materials, participate in discussions and record significant issues presented by each stakeholder, significant questions, and outstanding issues. Following each CEC workshop, hearing or teleconference, LBNL will provide a written summary report to the PG&E Project Manager. The summary report shall include, but is not limited to, links to the CEC web site where the workshop agenda and presentations are posted, information recorded (significant issues and questions) during the meetings, and recommended actions in response to questions and outstanding issues.

LBNL shall prepare draft responses to questions and issues under the direction of the PG&E Project Manager. Responses shall include, but are not limited to:

- Performing additional analysis;
- Conducting additional market research;
- Developing alternative code revision language;
- Preparing communications memoranda, e-mail comments, or other materials;
- Conducting teleconferences or stakeholder meetings;
- Revising the CASE Study; and
- Gathering or developing other materials as needed.

DELIVERABLES/DUE DATES

1. SUMMARY REPORT: LBNL will provide summary report three (3) business days after each CEC workshop.
2. RESPONSES TO QUESTIONS AND ISSUES: LBNL shall prepare draft responses for PG&E Project Managers' review and approval, and incorporate PG&E Project Managers' comments into the final responses to questions and issues. Schedule to be determined by the PG&E Project Manager and LBNL.

Task 6. Review of Title 24 documents:

LBNL shall review drafts of CEC Title 24 documents to ensure that PG&E Code amendment proposals are correctly incorporated in:

- 2008 Building Energy Efficiency Standards for Nonresidential Buildings (and related appendices);
- 2008 Nonresidential and Alternative Calculations Methods Manual (and related appendices)
- Nonresidential Manual for Compliance with 2008 Energy Efficiency Standards for Nonresidential Buildings, High-Rise Residential Buildings, and Hotels/Motels (and related appendices).

Under the direction of the PG&E Project Manager, LBNL will report the status of and describe needed changes to draft documents by performing the following:

- Conducting a detailed review of Title 24 documents focusing on text and diagrams related to code enhancements for which PG&E has made significant contributions;
- Identifying and documenting inconsistencies between Title 24 documents and PG&E's goals, as established in PG&E CASE studies;
- Proposing edits in the CEC-required format;
- Attending up to five conference calls to discuss proposed edits with PG&E and CEC staff;
- Providing edits to Title 24 documents that resolve inconsistencies; and
- Gathering or developing other materials as needed.

DELIVERABLES/DUE DATES: As requested by the PG&E Project Manager, LBNL will prepare proposed edits to Title 24 documents for review. LBNL will incorporate comments by the PG&E Project Manager to prepare final proposed edits, and submit to PG&E Project Manager and CEC staff. Schedule to be determined by PG&E Project Manager based on CEC rulemaking schedule and other deadlines.

Task 7. Final CASE studies and estimated overall impacts:

Following adoption of the 2008 standards, LBNL shall prepare a final CASE Study report documenting the initial proposal, any modifications throughout the process, and the final status of the proposal. LBNL shall review the CEC's impact analysis for 2008 standards and identify significant differences between the CEC's and PG&E's savings estimates. For each CASE study for which savings differ significantly, LBNL shall analyze differences in methodology and assumptions and either: a) recommend changes to revise PG&E CASE Study savings, or b) explain why revisions are not necessary.

LBNL shall update all sections of each Final Draft CASE Study to reflect all changes (for example, code language or savings estimates) resulting from stakeholder input during the CEC rulemaking process and differences in impact analyses.

DELIVERABLE/DUE DATE: LBNL will submit each Final 2008 CASE Study to the PG&E Project Manager for review and comment and shall incorporate comments into final document. Schedule to be determined by PG&E Project Manager and LBNL.

Cool Roofs for Residential Low- and Steep-Sloped Roofs

Background:

In 2003, the Pacific Gas and Electricity Company (PG&E) submitted a proposal to California Energy Commission (CEC) to amend the existing Title 24 standards by requiring cool roofs for California low-sloped non-residential buildings. With the sponsorship of PG&E, LBNL prepared the technical document (CASE study) to support the modifications to Title 24 standards. In November 2003, CEC approved the CASE proposal and amended the Title 24 to adopt "cool roofs" as prescriptive requirement for low-slope roofs in non-residential buildings. CEC has also shown a strong interest to expand the current scope of the proposal to cover sloped-roof non-residential buildings and low- and steep-sloped roofs residential buildings. This proposal is to develop CASE studies for application of cool roof on (1) residential low-sloped roofs and (2) residential steep-sloped roofs. A companion study sponsored by the PG&E will develop a CASE study for non-residential steep-sloped roofs.

Scope of Work:

The Work to be performed by LBNL under the Contract shall consist of the following:

- developing Codes and Standards Enhancement studies (hereinafter "CASE Studies")
- conducting market research and consensus-building workshops
- advocating adoption of the CASE study proposals during CEC's public rulemaking process
- ensuring that the Code amendment proposals are correctly incorporated into the CEC Title 24 documents.

LBNL will perform all the Work necessary to complete each task under the Contract as defined below and shall provide deliverables as required and on the due dates as agreed upon by CEC Project Manager and LBNL. A companion study sponsored by the PG&E will develop a CASE study for non-residential steep-sloped roofs. This project will closely coordinate the efforts between the projects sponsored by CEC and PG&E.

CASE Studies for Cool Roofs:

LBNL will develop two code enhancement proposals for California's 2008 building code upgrade cycle: (1) application of cool roofs for sloped-roofs residential buildings (2) application of cool roofs for low-sloped-roofs residential buildings. The CASE study, as described in the workplan, will recommend adoption of specific revisions to the California Code of Regulations, Building Energy Efficiency Standards, Title 24, Part 6 (hereinafter "Code").

Task 1. Organize a Project Advisory Committee:

The project will be carried out in direct collaboration with the industry and other national laboratories interested in cool roofs. LBNL will organize a Project Advisory Committee for the studies. The initial list of participants will include:

- Oak Ridge National Laboratory
- Florida Solar Energy Center
- Cool Roof Rating Council
- Pacific Gas and Electric Company
- Southern California Edison Company
- San Diego Gas and Electric Company and Southern California Gas Company
- California Energy Commission
- Berkeley Solar Group

DELIVERABLE/DUE DATE: **List of PAC members**.

Task 2. Kickoff meeting:

LBNL will conduct a Kick-off Meeting with the CEC Project Manager and PAC members. At the meeting, LBNL will present a brief review of two CASE Study topics for consideration of the potential for future adoptability. Adoptability criteria shall include a general assessment of technical and economic feasibility, market readiness by 2008, and stakeholder support. LBNL's presentation shall be an overview of issues pertinent to each CASE Study.

DELIVERABLE/DUE DATE: LBNL will conduct a kickoff meeting within ten (10) business days of receiving a signed Contract.

Task 3. CASE studies workplan:

Following the kickoff meeting, LBNL shall develop a work plan that address the requirements defined in Task 4. The work plan shall include, but not be limited to:

- Identification of issues or barriers unique to development of the CASE Study and/or implementation of the proposed measure
- Establishment of deliverables (tasks and subtasks), that ensure all items in Task 3 are adequately addressed. The number of tasks and subtasks shall reflect the Work needed to be performed and clearly convey the status of each Case Study.

DELIVERABLES/DUE DATES: **DRAFT WORK PLAN**.

Task 4. Develop CASE study:

LBNL will coordinate the development of the CASE Studies with California utilities, CEC, industry representatives, and other stakeholders.

Task 4.1. Development of a CASE study for steep-sloped-roof new and existing residential buildings.

In this task, we will develop a CASE report for steep-sloped-roof residential buildings. This task will include both existing and new steep-sloped-roof residential buildings. The elements of this task include:

A. Development of prototype buildings for steep-sloped-roof new and existing residential buildings. In this subtask, we will use the CEC existing residential prototypes. We will modify and revise the prototypes as necessary.

B. Coordinating activities with CEC PIER project analyzing attic performance and modeling assumptions to ensure the results of the PIER project are incorporated into the CASE studies.

C. Collecting market share data and reviewing cool roofs application on steep-sloped-roof new and existing residential buildings.

D. Performing energy simulations to estimate savings for all California climate regions. We are planning to use EnergyPro software for these calculations. The calculations will be performed for both existing and new residential buildings.

E. Performing a cost/benefit analysis (both TDV and non-TDV). The analysis will be carried out for both existing and new residential buildings.

F. Estimating state-wide savings. The state-wide savings will be estimated for both existing and new residential buildings.

G. Preparing proposals to change the relevant sections of Title 24

H. Presenting the results and responding to comments.

DELIVERABLES/DUE DATES:

1. **PRELIMINARY DRAFT CASE STUDY**: LBNL will submit preliminary draft report for the CASE Study for CEC Project Manager's review and comments.
2. **FIRST REVISION OF DRAFT CASE STUDY**: LBNL will incorporate comments and resubmit draft CASE Study to CEC Project Manager

Task 4.2. Development of a CASE study for low-sloped-roof new and existing residential buildings.

In this task, we will develop a CASE report for low-sloped-roof residential buildings. This task will include both existing and new low-sloped-roof residential buildings. The elements of this task include:

A. Development of prototype buildings for low-sloped-roof new and existing residential buildings. In this subtask, we will use the CEC existing residential prototypes. We will modify and revise the prototypes as necessary.

B. Coordinating activities with CEC PIER project analyzing attic/roof performance and modeling assumptions to ensure the results of the PIER project are incorporated into the CASE studies.

C. Collecting market share data and reviewing cool roofs application on low-sloped-roof new and existing residential buildings.

D. Performing energy simulations to estimate savings for all California climate regions. We are planning to use EnergyPro software for these calculations. The calculations will be performed for both existing and new residential buildings.

E. Performing a cost/benefit analysis (both TDV and non-TDV). The analysis will be carried out for both existing and new residential buildings.

F. Estimating state-wide savings. The state-wide savings will be estimated for both existing and new residential buildings.

G. Preparing proposals to change the relevant sections of Title 24

H. Presenting the results and responding to comments.

DELIVERABLES/DUE DATES:

1. **PRELIMINARY DRAFT CASE STUDY**: LBNL will submit preliminary draft report for the CASE Study for CEC Project Manager's review and comments.
2. **FIRST REVISION OF DRAFT CASE STUDY**: LBNL will incorporate comments and resubmit draft CASE Study to CEC Project Manager

Task 4.3. Project update meetings and reporting:

This task will be carried out in collaboration with PG&E. LBNL project team members will attend a maximum of six (4) - 2-hour and two (2) - half-day project update meetings with the CEC Project Manager and stakeholders. LBNL will present progress of each CASE Study and issues that arise during the development of each CASE Study. LBNL will prepare a memorandum after each project update meeting to address issues and concerns discussed at the meetings. LBNL will also submit Quarterly Status Report to the CEC Project Manager for review, comment, and approval. Quarterly Status Report shall include but is not limited to a brief description of the proposed standards change and objective, Work progress and comparison of budget and actual expenditures for all tasks/subtasks in the work plan for each CASE Study, and status of key deliverables.

DELIVERABLES/DUE DATES:

1. **ISSUES MEMORANDUM**: LBNL will submit Issues Memorandum to CEC Project Manager.
2. **QUARTERLY STATUS REPORT**: At the end of each quarter, LBNL will issue a Quarterly Status Report to CEC Project Manager

Task 5. CEC Stakeholder workshop:

This task will be collaborated between CEC- and PG&E-sponsored projects. LBNL will assist the CEC Project Managers with planning and conducting one (1) industry stakeholder (consensus-making) workshop to present CASE Studies findings and solicit comments from the stakeholders.

Task 5.1. Workshop agenda:

LBNL will develop a meeting agenda and a proposed list of stakeholders for review and approval by the CEC Project Managers.

DELIVERABLES/DUE DATES: **WORKSHOP AGENDA**. LBNL will submit draft workshop agenda and list of stakeholders to CEC Project Manager for review. LBNL will incorporate CEC Project Manager's comments, if any, and submit revised agenda. In addition, LBNL will distribute agenda and Draft CASE Studies to all meeting attendees prior to each scheduled workshop.

Task 5.2. Presentation material:

For each CASE Study to be presented at the workshops, LBNL will prepare draft presentation materials for CEC Project Manager's review and approval. Presentation materials shall include an outline and summary of the CASE Study report and be presented in a format agreed to or provided by CEC Project Manager.

DELIVERABLES/DUE DATES: **PRESENTATION MATERIALS**. LBNL will develop and submit presentation materials for each CASE study to CEC Project Manager. LBNL will incorporate CEC Project Manager comments and finalize presentation materials.

Task 5.3. Workshop summary report:

LBNL will prepare a workshop report summarizing the workshop proceedings. The workshop report shall include a list of attendees, workshop agenda and handouts, meeting minutes, outstanding issues not resolved at the workshop, and recommended actions to take with respect to issues raised regarding each CASE Study. LBNL will revise the draft workshop report based on comments provided by the CEC Project Manager.

DELIVERABLES/DUE DATES: **WORKSHOP SUMMARY REPORT**. LBNL will prepare draft report for CEC Project Manager's review and approval, and will incorporate CEC Project Manager's comments into the final workshop summary report.

Task 5.4. Final draft case study:

LBNL will produce Final Draft CASE Study reports. The final draft report shall incorporate input including, but not limited to, outstanding issues and recommended actions identified by workshop attendees and CEC Project Manager.

DELIVERABLES/DUE DATES: **FINAL DRAFT CASE STUDY REPORTS**. LBNL will revise the draft CASE Study reports for CEC Project Manager's review and comment and will incorporate CEC Project Manager's comments into the Final Draft CASE Study reports.

Task 6. Support for CEC CASE study proposals during CEC rulemaking:

LBNL will participate in a maximum of eight (4) CEC workshops or adoption hearings, and twenty (6) teleconferences, as requested by the CEC Project Manager, to assist with advocacy of proposed code enhancements and to gather comments on CEC Code change proposals.

Task 6.1. Presentation materials:

Prior to each CEC workshop, hearing, or teleconference call, LBNL will prepare support materials as requested by the CEC Project Manager. Support materials shall include, but not be limited to:

- CASE studies and summary presentations; and
- Ongoing research, analyses and status summary presentations.

DELIVERABLES/DUE DATES: **PRESENTATION MATERIALS**. LBNL will prepare draft presentation materials for CEC Project Manager's review and approval and will incorporate CEC Project Manager's comments into the final presentation materials.

Task 6.2 CEC workshop and summary report:

During the workshop, LBNL will present materials, participate in discussions and record significant issues presented by each stakeholder, significant questions, and outstanding issues. Following each CEC workshop, hearing or teleconference, LBNL will provide a written summary report to the CEC Project Manager. Summary report shall include, but is not limited to, links to the CEC web site where the workshop agenda and presentations are posted, information recorded (significant issues and questions) during the meetings, and recommended actions in response to questions and outstanding issues. LBNL will prepare draft responses to questions and issues under the direction of the CEC Project Manager. Responses shall include, but are not limited to:

- Performing additional analysis;
- Conducting additional market research;
- Developing alternative code revision language;
- Preparing communications memoranda, e-mail comments, or other materials;
- Conducting teleconferences or stakeholder meetings;
- Revising CASE Studies; and
- Gathering or developing other materials as needed.

DELIVERABLES/DUE DATES

1. **SUMMARY REPORT**: LBNL will provide summary report after each CEC workshop.
2. **RESPONSES TO QUESTIONS AND ISSUES**: LBNL will prepare draft responses for CEC Project Manager's review and approval, and incorporate CEC Project Manager's comments into the final responses to questions and issues.

Task 7. Review of Title 24 documents:

LBNL will review drafts of CEC Title 24 documents to ensure that CEC Code amendment proposals are correctly incorporated:

- 2008 Building Energy Efficiency Standards for Residential and Nonresidential Buildings (and related appendices);
- 2008 Nonresidential and Residential Alternative Calculations Methods Manual (and related appendices); and
- Residential Manual for Compliance with 2008 Energy Efficiency Standards for Low-Rise Residential Buildings (and related appendices).

Under the direction of the CEC Project Manager, LBNL will report the status of and describe needed changes to draft documents by performing the following:

- Conducting a detailed review of Title 24 documents focusing on text and diagrams related to code enhancements;
- Identifying and documenting inconsistencies between Title 24 documents and CEC CASE studies;
- Proposing edits in the CEC-required format;
- Attending up to five conference calls to discuss proposed edits with CEC staff;
- Providing edits to Title 24 documents that resolve inconsistencies; and
- Gathering or developing other materials as needed.

DELIVERABLES/DUE DATES: **PROPOSED REVISIONS TO TITLE 24**. LBNL will prepare proposed edits to Title 24 documents for review. LBNL will incorporate comments by the CEC Project Manager to prepare final proposed edits, and submit to CEC Project Manager and CEC staff. Schedule to be determined by CEC Project Manager based on CEC rulemaking schedule and other deadlines.

Task 8. Final CASE studies and estimated overall impacts:

Following adoption of the 2008 standards, LBNL will prepare a final CASE Study report documenting the initial proposal, any modifications throughout the process, and the final status of the proposal.

LBNL will update all sections of each Final Draft CASE Study to reflect all changes (for example, code language or savings estimates) resulting from stakeholder input during the CEC rulemaking process and differences in impact analyses.

DELIVERABLE/DUE DATE: **FINAL CASE REPORTS**. LBNL will submit each Final 2008 CASE Study to the CEC Project Manager for review and comment and shall incorporate comments into final document. Schedule to be determined by CEC Project Manager and LBNL.

Custom-Bilt Energy Efficient Sustainable and Durable Roofs

CUSTOM-BILT METALS
13950 Magnolia Avenue
S. El Monte CA 91733
Phone (626) 454 4850
Fax (626) 454 4785

COOL ROOF COLOR MATERIALS (CRCMs)

Most painted roofs today have a reflectance of about 5% to 20%, but special paint made using cool pigmented colors can give you a much higher reflectance of almost 60%. A roof covered by this special paint absorbs less solar energy and can save nearly 20% of your air conditioning costs.

BASF, FERRO Corp. and the Shepherd Color Company have developed a palette of Cool Roof Color Materials CRCMs that look dark in color even though they reflect most of the sun's energy. How can these dark roofs reflect as much or more energy than a white roof? The sun's radiation consists of ultraviolet, visible, and infrared energy. Our eyes can only see the visible region. The visible light that is reflected from an object determines the color of that object. White roofs reflect most of the visible light (which mixes together to look white to our eyes), but over half of the sun's energy is contained in the infrared region, which isn't visible to our eyes. Because we can't see this energy, we can reflect it away from the roof without changing the roof's color.

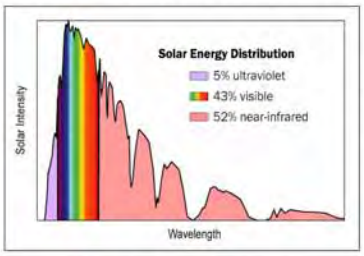

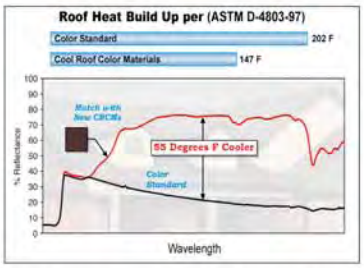

Advantages of Cool Roof Color Materials

- Architectural appeal and durability
- Reflect more sunlight and stay cooler
- Lower utility bill for cooling the house
- Better fade resistance than standard colors

Architectural appeal and Durability

The national demand for painted metal roofs for homes increased three-fold over the past six years. Painted metal roofing is available in a wide variety of textures, colors, surface finishes, and formed profiles, See Custom-Bilt's photo gallery at their web site: (http://www.custombiltmetals.com/). Its finishes are colorful, inert, and do not pose a health risk. It is code compliant and tested for fire, wind, hail resistance and is non-combustible which reduces the spread of fire in and among buildings. CRCMs further protect the residence from external forest fires by reflecting the infrared energy away from the roof.

Reflect more sunlight and stay cooler

A demonstration site in Fair Oaks, California (suburb of Sacramento) has two pairs of identical homes being evaluated by LBNL and ORNL. Custom-Bilt had the one pair of homes of identical footprint roofed with painted metal shakes of the same color, one roof with CRCMs the other roof having standard color pigments. The field study continues to show the positive energy benefits of painted metal roofs. Measurements for September, 04 show the heat penetrating the south facing painted metal roof dropped 36% of that crossing the metal shake with conventional pigmented colors.

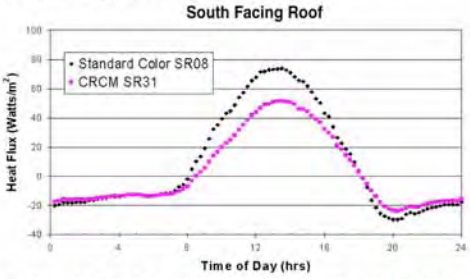

Painted Metal Shakes with and without CRCMs.

Lower utility bill for cooling the house

Because less heat penetrates the roof, the attic remains cooler and, in turn, the heat leaking into your air-conditioned home drops. A chocolate brown color roof with 30% reflective CRCMs decreases the consumed cooling energy by 15% of that used for a roof with standard chocolate brown color exposed in hot climates.

Better Fade Resistance

Over 10,000 hours of accelerated fluorescent (UV) exposure has proven the CRCMs more fade resistant simply because they reflect more light and are cooler than conventional pigmented products.

ORNL · Dr. William Miller · (865) 574-2013
LBNL · Dr. Hashem Akbari · (510) 486-4287

Attachment E

A Twenty-Seven Home Large-Scale Demonstration Showcasing Painted Metal Roofs with Cool-Pigmented Colors

Contact Persons: Tony Chiovare, Owner and CEO of Custom-Bilt Metals,
13940 Magnolia Avenue, Chino, CA 91710, Phone (909) 664-1500,
FAX (909) 664-1520, Email: Conniec@custombiltmetals.com

Robert Scichili, Color Specialist and Consultant for Custom-Bilt Metals,
1120 Dumont Dr, Richardson, TX 75080, Phone (972) 234-0180,
FAX (972) 231-2523, Email: RGScichili@AOL.com

William A. Miller, Ph.D., Buildings Technology Center,
Energy Science and Technology Division,
One Bethel Valley Road, Oak Ridge, TN 37831-6070, Phone (865) 574-2013,
FAX (865) 574-9354, Email: wml@ornl.gov

Hashem Akbari, Heat Island Group,
Lawrence Berkeley National Laboratory, Berkeley, CA 94720, Phone (510) 486-4287,
FAX (270) 638-2814, Email: H_Akbari@lbl.gov

Technology: Industry researchers, including those working with the Department of Defense, have developed novel complex inorganic color pigments that are dark in color but highly reflective in the infrared portions of the solar spectrum. Originally, paints with these pigments were used for military camouflage to match the visible and infrared reflectance of background foliage. However, the painted metal industry observed through testing that cool-pigments consisting of a mixture of chromic oxide (Cr_2O_3), ferric oxide (Fe_2O_3) and titanium dioxide would boost the solar reflectance of black polyvinylidene fluoride painted metal by a factor of 5 over that of conventional dark roofing. The increase in reflectance reduces the temperature of the painted surface, and the aesthetically pleasing dark roof reduces the cooling-energy demand of the building, which saves money.

Subsequently, Custom-Bilt Metals of El Monte, CA, Classic Products of Piqua, OH and other metal roof manufacturers have introduced several lines of painted metal roof products that take advantage of the cool-pigment technology. Tony Chiovare, CEO of Custom-Bilt Metals, stated that the additional cost of the cool-pigments is only about 5¢ per square foot of finished product, which researchers have shown will pay for itself easily within three years because of the building energy savings.

Goals: The California Energy Commission (CEC) wants the cool-pigment technology fully integrated in all roof products. However, rebates and or energy credits are needed to accelerate the market adoption of cool-pigmented metal, tile and asphalt shingles. The California utility companies want to see demonstrated the electrical energy savings per ton of air-conditioning capacity from which each utility can best determine realistic and fair rebates for consumers purchasing cool-pigmented roof products. Our primary objective then is to demonstrate in a large-scale residential subdivision the benefits of cool-pigmented roofs and the subsequent beneficial impact on the urban environment. The large-scale demonstration is more statistically significant than a one or two pair home demonstration and will provide the information needed for establishing rebates. Therefore our specific goals are to:

- Develop several large-scale demonstrations that show-case cool-pigmented painted metal, asphalt shingle, clay tile and concrete tile roofs.
- Collect whole house and air-conditioning power measurements for all homes participating in the large-scale demonstrations.
- Select a pair of homes at each demonstration site for collecting more detailed temperature and thermal measurements of the roof, attic, air-conditioner and living space. Collect high spatial resolution thermal infrared and visible reflectance data obtained from aircraft equipped with special scanners and map the surface temperature and reflectance characteristics of the large-scale demonstration to further assess the effectiveness of cool-pigmented roofs in mitigating heat island buildup.

Project: The California Energy Commission's Public Interest Energy Research program has two sister labs, Oak Ridge National Laboratory (ORNL) and the Lawrence Berkeley National Laboratory (LBNL) working with pigment colorant researchers and roof manufacturers to make cool-pigmented roof products a market reality by 2006. LBNL has developed a cool-pigment database containing a palette of visibly dark yet highly reflective colors. ORNL is demonstrating the potential energy savings of existing cool-pigment technology at two- and four-house demonstrations in Fair Oaks, Redding and Martinez, California. The CEC and industry are very encouraged by the collaborative work and now want to go the next step to fully implement the cool-pigment technology in the state of California.

Walt Ferguson Construction has asked Custom-Bilt Metals to supply painted metal roofs for a new subdivision being built in Yucaipa, California. Some twenty-seven homes are proposed for the new subdivision, and each house has a footprint of about 2,500 square feet. We propose to install energy management systems (EMSs) on an exterior wall of each home, and monitor the whole- house and air-conditioning power consumed by the twenty-seven homes. The EMSs will also control the thermostat settings in a pair of fully instrumented homes. We will instrument the one pair to measure the temperatures at the roof surface, on the underside of the attic deck, in the mid-attic air, at the top of the insulation, on the interior ceiling sheet rock surface, and inside the building. Relative humidity in the attic air and the residence will also be measured. Heat flux transducers will be embedded in the sloped roofs and the attic floor to measure the roof heat flows and the building heat leakage. The air-conditioner and ancillary building power demands will also be recorded to document whole building services and help gauge the cost

savings for reflective roofing. A fully instrumented meteorological weather station will be setup at one of the two pair of homes, and will collect the ambient dry bulb temperature, the relative humidity, the solar irradiance, and the wind speed and wind direction. The weather stations will also serve as a command center acquiring power measurements for all twenty-seven homes using wireless technology.

The services of NASA's Stennis Space Center shall be acquired for obtaining thermal infrared and visible data from their Advanced Thermal and Land Applications Sensor (ATLAS) scanner flown aboard a Lear 23 jet aircraft. The ATLAS can collect data ranging from 2 to 20 meters in resolution, and will provide mapping of the surface temperature and reflectance of the large-scale demonstration. The data can then be used for surface parameterization of meteorological and air quality models for assessing the effect of cool-pigments in mitigating urban heat which in turn reduces carbon dioxide emissions and smog.

Roles: Custom-Bilt Metals will contract with Walt Ferguson Construction to sell and install panted metal roofs for the new subdivision in Yucaipa, California. ORNL will provide and install the EMSs on an exterior wall of each home. ORNL will also provide a central station for collecting the weather data as well as power measurements from the twenty-seven homes using wireless setup. LBNL will use the urban surface temperature and reflectance mapping in models to better quantify the ancillary energy savings derived for cool-pigmented roofs.

Arnold Schwarzenegger
Governor

COOL-COLOR ROOFING MATERIAL ATTACHMENT 13: TASK 2.7.3 REPORTS - CODE REVISIONS

PIER FINAL PROJECT REPORT

Prepared For:
California Energy Commission
Public Interest Energy Research Program

Prepared By:
Lawrence Berkeley National Laboratory and Oak Ridge National Laboratory

ERNEST ORLANDO LAWRENCE BERKELEY NATIONAL LABORATORY

June 2006
CEC-500-2006-067-AT13

Prepared By:
Lawrence Berkeley National Laboratory
Hashem Akbari
Berkeley, California
Contract No. 500-01-021

Oak Ridge National Laboratory
William Miller
Oak Ridge, Tennessee

Prepared For:
California Energy Commission
Public Interest Energy Research (PIER) Program

Chris Scruton
Contract Manager

Ann Peterson
Building End-Use Energy Efficiency Team Leader

Nancy Jenkins
PIER Energy Efficiency Research Office Manager

Martha Krebs, Ph.D.
Deputy Director
ENERGY RESEARCH AND DEVELOPMENT DIVISION

B. B. Blevins
Executive Director

DISCLAIMER

This report was prepared as the result of work sponsored by the California Energy Commission. It does not necessarily represent the views of the Energy Commission, its employees or the State of California. The Energy Commission, the State of California, its employees, contractors and subcontractors make no warrant, express or implied, and assume no legal liability for the information in this report; nor does any party represent that the uses of this information will not infringe upon privately owned rights. This report has not been approved or disapproved by the California Energy Commission nor has the California Energy Commission passed upon the accuracy or adequacy of the information in this report.

Technical Note:
HIG-TN01-0505

Estimates of Energy-Savings for Cool Colored Residential Roofs in California

Hashem Akbari
Heat Island Group
Lawrence Berkeley National Laboratory
Berkeley, California 94720

May 2005

This work was supported by the California Energy Commission (CEC) through its Public Interest Energy Research Program (PIER), and by the Assistant Secretary for Renewable Energy under Contract No. DE-AC03-76SF00098.

Estimates of Energy-Savings for Cool Colored Residential Roofs in California

H. Akbari
Heat Island Group
Environmental Energy Technologies Division
Lawrence Berkeley National Laboratory

1. Introduction

Raising the solar reflectance of a roof from a typical value of 0.1–0.2 to an achievable 0.6 can reduce cooling-energy use in buildings by more than 20%. Cool roofs also reduce ambient outside air temperature, thus further decreasing the need for air conditioning and retarding smog formation.

We are collaborating with pigment manufacturers to characterize colorants, and with manufacturers of roofing materials to produce cool colored products, including asphalt shingles, concrete and clay tiles, metal roofing, wood shakes, and coatings. In this collaboration, we have identified and characterized pigments suitable for cool-colored coatings, and developed engineering methods for applying cool coatings to roofing materials. We are also measuring and documenting the laboratory and *in-situ* performances of roofing products. Demonstration of energy savings can accelerate the market penetration of cool-colored roofing materials. Early results from this effort have yielded colored concrete, clay, and metal roofing products with solar reflectances exceeding 0.4. Obtaining equally high reflectances for roofing shingles is more challenging, but some manufacturers have already developed several cost-effective colored shingles with solar reflectances of at least 0.25.

One of the project tasks (Task 2.7.3) was to develop preliminary estimates of cooling electricity savings and potential heating energy penalties resulting from the installation of cool colored roofing materials on residential buildings in California. To accomplish this objective, we simulated the cooling and heating energy use of a prototypical building for 16 California climate zones. This brief report highlights the characteristics of the prototype buildings and summarizes the results of the simulations.

2. Residential Building Descriptions

The prototype residential building was modeled as a single-story single-family detached structure. Changing the reflectance of the roof affects the heat transfer through the roof structure. Therefore, we focused on prototypical simulations of the upper floor, which captures the effects of changes in roof reflectance. The average roof area selected for these prototypical simulations was 1600 ft^2.

The roof was constructed with asphalt shingles on a 20° sloped plywood deck, over a naturally ventilated and unconditioned attic, above a studded ceiling frame with fiberglass insulation (varying by vintage), and with a sheet of drywall beneath. The fractional-leakage-area of the attic and living quarters depended on vintage. Variable air infiltration was modeled by the

Sherman-Grimsrud algorithm (Sherman 1986). The existing solar reflectance of the roof was selected to be 0.1, typical for dark asphalt shingles, and the albedo of the reflective roof was taken to be 0.3. The thermal emittance of each roof was 0.9.

The residence was cooled and heated by a central air-conditioning system with ducts located in the attic space, with a constant volume fan, and without an economizer. Heating was modeled once with a gas furnace and again with an electric heat pump. Cooling by natural ventilation was available by window operation. The systems were sized based on peak cooling and heating loads as determined by DOE-2. System component efficiencies were selected for each vintage. A Seasonal Energy Efficiency Ratio (SEER) of 8.5 and 10 was assumed for the central air-conditioner of the pre-1980 and 1980^{+} buildings, respectively. Also a Heating Season Performance Factor (HSPF) of 5 and 7 was assumed for the stock of old and new residential central electric heat pumps.

Modified part-load-ratio curves for a typical air-conditioner, heat pump, and gas furnace were used in place of the standard DOE-2 curves, as they have been shown to model low-energy use more accurately (Henderson 1998). Duct loads were simulated with a validated residential duct function (Parker *et al*. 1998) implemented into DOE-2 to better estimate the thermal interactions between the ducts and space. The function was designed for the residential central system type (RESYS) in DOE-2 and for a single air-conditioned living space with an attic and basement. Since this function greatly improves cooling- and heating-energy use estimates, and the top story of a building receives the bulk of the benefits of a reflective roof, the single-story residential structure was modeled.

Building data for residences are shown in **Table 1** and were obtained from several sources. We used existing data to characterize the existing stock of pre-1980 buildings (Konopacki *et al*., 1997). Characteristics for 1980^{+} construction homes were identified from DOE national appliance energy standards (NAECA 1987), California Energy Commission prototypes (CEC 1994), and Energy Star® (USDOE 2001).

3. Solar-Reflectance of Cool Colored Roofs

To simulate the effect of cool colored materials, the values of roof albedo were chosen to be 0.1 for the base case (representing dark colored fiberglass asphalt shingles) and 0.3 for the cool case (representing colored cool shingles). The thermal emittance of each material was 0.9. In DOE-2 the *ABSORPTANCE* keyword for roof construction was 0.9 (solar reflectance 0.1) for the basecase and was changed to 0.7 (solar reflectance 0.3). To estimate savings from increased roof reflectance ($\Delta\rho$) other than the differential specified in the tables, multiply the savings by the ratio $\Delta\rho/0.2$[*].

We estimated the cooling electricity savings and heating energy penalties for various levels of roof insulation: R-5, R-7, R-11, R-19, and R-30 for pre-1980 prototypes; and R-11, R-19, R-30, R38, and R-49 for 1980^{+} prototypes.

[*] Linear interpolation can be used to estimate savings or penalties for net changes in roof solar reflectance ($\Delta\rho_2$) other than that used in the simulations ($\Delta\rho_1$) (Konopacki *et al*. 1997). Therefore, these results can be simply multiplied by the ratio $\Delta\rho_2/\Delta\rho_1$ to obtain estimates for other roof reflectance scenarios.

3. Weather Data

We used the California Energy Commission CTZ (California Thermal Zone) climate descriptions to simulate the cool-roof savings from in each of 16 zones. **Table 2** shows the number of cooling and heating degree days in each zone.

4. Simulation results

Tables 3-6 summarize the results of the simulations. For most California climates, the application of cool colored roof yields net savings in the range of 100-400 kWh per 1000 ft^2 per year. The savings are obviously smaller for buildings with higher roof insulation.

The results presented in Tables 3-6 also apply to flat cool colored concrete and clay tiles. For most clay tiles, the base-case solar reflectance is about 0.2 and the cool-case solar reflectance is 0.4.

5. Summary

We have performed building energy simulations for a prototype residential building in 16 California Climate zones. Cool colored roofing materials can increase the solar reflectance of the roofs by about 0.2. Such an increase in solar reflectance of the roof will result in cooling energy savings in the range of 100-400 kWh per 1000 ft^2 per year.

6. Acknowledgement

This work was supported by the California Energy Commission (CEC) through its Public Interest Energy Research Program (PIER), by the Laboratory Directed Research and Development (LDRD) program at Lawrence Berkeley National Laboratory (LBNL), and by the Assistant Secretary for Renewable Energy under Contract No. DE-AC03-76SF00098. The authors wish to thank CEC Commissioner Arthur Rosenfeld and PIER managers Nancy Jenkins and Chris Scruton for their support and advice.

5. References

Building Energy Simulation Group (BESG). 1990. "Overview of the DOE-2 Building Energy Analysis Program, Version 2.1D." Lawrence Berkeley National Laboratory Report LBL-19735, Rev. 1. Berkeley, CA.

California Energy Commission (CEC). 1994. “Technology Energy Savings Volume II: Building Prototypes,” California Energy Commission Report P300-94-007, Sacramento, CA.

Henderson, H. 1998. "Part Load Curves for Use in DOE-2." Draft report prepared for Lawrence Berkeley National Laboratory and Florida Solar Energy Center. CDH Energy Corp. Cazenovia, NY. January 16, 1998.

Konopacki, S., H. Akbari, M. Pomerantz, S. Gabersek and L. Gartland. 1997. "Cooling Energy Savings Potential of Light-Colored Roofs for Residential and Commercial Buildings in 11 US Metropolitan Areas." Lawrence Berkeley National Laboratory Report LBNL-39433. Berkeley, CA.

National Appliance Energy Conservation Act of 1987 (NAECA). 1987.

Parker, D., J. Huang, S. Konopacki, L. Gartland, J. Sherwin and L. Gu. 1998. "Measured and Simulated Performance of Reflective Roofing Systems in Residential Buildings." *ASHRAE Transactions* **104**(1):963-975.

Sherman, M., D. Wilson and D. Kiel. 1986. "Variability in Residential Air Leakage." Measured Air Leakage in Buildings ASTM STP-904. Philadelphia, PA.

US Department of Energy (USDOE). 2001. "Choosing or Upgrading Your Central Air Conditioner." Office of Building Technology, State and Community Programs". http://www.eren.doe.gov/buildings/heatcool_cenair.html.

Winklemann, F., B. Birdsall, W. Buhl, K. Ellington and A. Erdem. 1993. "DOE-2 Supplement Version 2.1E." Lawrence Berkeley National Laboratory Report LBNL-34947. Berkeley, CA.

Table 1. Prototypical building description for single-family residence.

Single-Family Residence	**Pre-1980**	**1980$^+$**
single-story, non-directional		
roof & floor area (ft^2)	1,600	
Zones		
living (conditioned)		
attic (unconditioned)		
basement (unconditioned)		
Roof Construction		
20^o slope		
¼" asphalt shingle		
¾" plywood deck w/ 2" x 6" rafters		
naturally ventilated attic		
¾" plywood deck w/ 2" x 6" rafters (15%)		
fiberglass insulation (85%)	parametric	parametric
½" drywall		
Roof Solar Reflectance		
pre	0.1	
post	0.3	
Roof Thermal Emittance	0.9	
Wall Construction		
brick exterior		
wood frame (15%)		
fiberglass insulation (85%)	R-5	R-13
½" drywall interior		
Windows		
clear with operable shades		
number of panes	1	2
window to wall ratio	0.18	
Fractional Leakage Area ($in^2/100\ ft^2$)		
living	4	2
attic	8	4
Air-conditioning equipment		
central a/c, direct expansion, air-cooled		
seasonal energy efficiency ratio (SEER)	8.5	10
coefficient of performance (COP)	2.5	2.9
cooling setpoint (^{o}F)	78	
natural ventilation available		
Heating Equipment		
1) central forced air gas furnace		
efficiency (%)	70	78
heating setpoint (^{o}F)	70	
11pm - 7am setback (^{o}F)	60	
2) central electric heat pump		
heating season performance factor (HSFP)	5	7
Duct Air Leakage (%)	20	10

Table 2. Heating and Cooling Degree Days (base 65) for each California Thermal Zone (CTZ).

Climate Zone	City	HDD65	CDD65
CTZ1	Arcata	3933	0
CTZ2	Santa Rosa	3073	482
CTZ3	Oakland	2588	50
CTZ4	Sunnyvale	2367	351
CTZ5	Santa Maria	2504	49
CTZ6	Los Angeles	1521	389
CTZ7	San Diego	1292	547
CTZ8	El Toro	1424	808
CTZ9	Pasadena	1361	1035
CTZ10	Riverside	1674	1363
CTZ11	Red Bluff	2709	1408
CTZ12	Sacramento	2675	871
CTZ13	Fresno	2237	2029
CTZ14	China Lake	2979	1858
CTZ15	El Centro	875	4156
CTZ16	Mount Shasta	5414	292

Table 3. Estimates of annual cooling electricity savings (kWh) and heating energy penalties (therms) from installation of cool-colored roofs on pre-1980 single-family detached homes with gas furnace heating systems. All savings and penalties are per 1000 ft^2 of roof area. Solar reflectance change is 0.2 (for fiber glass asphalt shingles: change of the roof reflectance from 0.1 to 0.3; for clay and concrete tiles: change of the roof reflectance from 0.2 to 0.4). The savings and penalties can be linearly adjusted for other values of changes in solar reflectance.

Roof Insulation	R-5		R-7		R-11		R-19		R-30	
Climate Zone	Cooling (kWh)	Heating (therms)	Cooling (kWh)	Heating (therms)	Cooling (kWh)	Heating (therms)	Cooling (kWh)	Heating (therms)	Cooling (kWh)	Heating (therms)
CTZ1	110	-11	90	-9	67	-7	47	-5	35	-5
CTZ2	172	-9	149	-7	120	-6	93	-4	76	-3
CTZ3	117	-8	97	-6	73	-5	52	-4	39	-3
CTZ4	155	-7	133	-6	106	-5	80	-3	65	-3
CTZ5	116	-8	96	-6	73	-5	51	-3	39	-3
CTZ6	160	-5	137	-4	110	-3	84	-2	68	-2
CTZ7	181	-5	157	-4	127	-3	99	-2	82	-1
CTZ8	214	-5	188	-4	156	-3	124	-2	104	-1
CTZ9	244	-5	215	-4	180	-3	146	-2	124	-1
CTZ10	286	-6	255	-5	216	-3	177	-2	152	-2
CTZ11	292	-8	260	-7	221	-5	182	-4	156	-3
CTZ12	223	-8	196	-7	162	-5	130	-4	110	-3
CTZ13	372	-7	336	-6	289	-4	241	-3	209	-2
CTZ14	350	-9	315	-7	270	-6	225	-4	195	-3
CTZ15	646	-4	593	-3	521	-2	445	-1	393	-1
CTZ16	148	-14	126	-12	99	-10	75	-8	60	-6

Table 4. Estimates of annual cooling electricity savings (kWh) and heating energy penalties (therms) from installation of cool-colored roofs on 1980^{+} single-family detached homes with gas furnace heating systems. All savings and penalties are per 1000 ft^2 of roof area. Solar reflectance change is 0.2 (for fiber glass asphalt shingles: change of the roof reflectance from 0.1 to 0.3; for clay and concrete tiles: change of the roof reflectance from 0.2 to 0.4). The savings and penalties can be linearly adjusted for other values of changes in solar reflectance.

Roof Insulation	R-11		R-19		R-30		R-38		R-49	
Climate Zone	Cooling (kWh)	Heating (therms)	Cooling (kWh)	Heating (therms)	Cooling (kWh)	Heating (therms)	Cooling (kWh)	Heating (therms)	Cooling (kWh)	Heating (therms)
CTZ1	43	-4	29	-3	21	-2	18	-2	15	-2
CTZ2	73	-3	54	-2	42	-2	38	-2	34	-1
CTZ3	46	-3	32	-2	23	-1	20	-1	17	-1
CTZ4	65	-3	47	-2	36	-1	33	-1	29	-1
CTZ5	46	-3	32	-2	23	-1	20	-1	17	-1
CTZ6	67	-2	49	-1	38	-1	34	-1	30	0
CTZ7	77	-2	58	-1	45	-1	41	0	37	0
CTZ8	93	-2	71	-1	57	-1	51	-1	47	0
CTZ9	107	-2	83	-1	67	-1	61	0	55	0
CTZ10	127	-2	100	-1	81	-1	74	-1	68	-1
CTZ11	130	-3	102	-2	83	-1	76	-1	70	-1
CTZ12	97	-3	74	-2	59	-1	54	-1	49	-1
CTZ13	168	-2	134	-2	111	-1	102	-1	94	-1
CTZ14	158	-3	125	-2	103	-2	95	-1	87	-1
CTZ15	300	-1	244	-1	206	0	190	0	176	0
CTZ16	61	-6	44	-4	34	-3	30	-3	27	-3

Table 5. Estimates of annual cooling electricity savings (kWh) from installation of cool-colored roofs on pre-1980 single-family detached homes with electric heat pump heating systems. All savings and penalties are per 1000 ft^2 of roof area. Solar reflectance change is 0.2 (for fiber glass asphalt shingles: change of the roof reflectance from 0.1 to 0.3; for clay and concrete tiles: change of the roof reflectance from 0.2 to 0.4). The savings and penalties can be linearly adjusted for other values of changes in solar reflectance.

Roof Insulation	R-5	R-7	R-11	R-19	R-30
Climate Zone	(kWh)	(kWh)	(kWh)	(kWh)	(kWh)
CTZ1	-178	-184	-189	-185	-181
CTZ2	-79	-90	-100	-105	-108
CTZ3	-168	-174	-179	-177	-174
CTZ4	-106	-115	-124	-127	-128
CTZ5	-168	-175	-180	-177	-174
CTZ6	-98	-108	-118	-121	-122
CTZ7	-66	-77	-89	-95	-98
CTZ8	-12	-26	-41	-51	-58
CTZ9	34	19	1	-14	-23
CTZ10	102	83	61	40	28
CTZ11	111	92	69	48	34
CTZ12	1	-13	-29	-41	-48
CTZ13	239	214	183	150	130
CTZ14	203	180	151	122	103
CTZ15	676	631	572	502	456
CTZ16	-118	-127	-135	-137	-137

Table 6. Estimates of annual cooling electricity savings (kWh) from installation of cool-colored roofs on 1980^{+} single-family detached homes with electric heat pump heating systems. All savings and penalties are per 1000 ft^2 of roof area. Solar reflectance change is 0.2 (for fiber glass asphalt shingles: change of the roof reflectance from 0.1 to 0.3; for clay and concrete tiles: change of the roof reflectance from 0.2 to 0.4). The savings and penalties can be linearly adjusted for other values of changes in solar reflectance.

Roof Insulation	R-11	R-19	R-30	R-38	R-49
Climate Zone	(kWh)	(kWh)	(kWh)	(kWh)	(kWh)
CTZ1	-75	-70	-64	-62	-59
CTZ2	-28	-30	-30	-29	-28
CTZ3	-70	-66	-61	-58	-55
CTZ4	-41	-41	-39	-38	-36
CTZ5	-70	-66	-61	-58	-56
CTZ6	-37	-38	-36	-35	-34
CTZ7	-22	-24	-25	-25	-24
CTZ8	4	-3	-6	-7	-7
CTZ9	26	16	10	8	7
CTZ10	57	43	34	30	28
CTZ11	62	47	37	33	30
CTZ12	10	2	-2	-3	-4
CTZ13	122	98	82	75	70
CTZ14	105	84	69	64	59
CTZ15	328	274	235	219	204
CTZ16	-47	-46	-43	-42	-40